DOE/METC/84-7
(DE84003052)
CONF-830827--

Proceedings of the Ninth Annual UNDERGROUND COAL GASIFICATION SYMPOSIUM

December 1983

U. S. Department of Energy
Office of Fossil Energy
Morgantown Energy Technology Center
Morgantown, West Virginia

FOSSIL ENERGY

TECHNICAL INFORMATION CENTER
U. S. DEPARTMENT OF ENERGY

DO NOT MICROFILM COVER

DISCLAIMER

Available from the National Technical Information Service, U. S. Department of Commerce, Springfield, VA 22161.

Price: Printed copy A25
Microfiche AO1

Codes are used for pricing all publications. The code is determined by the number of pages in the publication. Information pertaining to the pricing codes can be found in the current issues of the following publications, which are generally available in most libraries: *Energy Research Abstracts (ERA), Government Reports Announcements* and Index (*GRA* and I); *Scientific and Technical Abstract Reports (STAR)*; and publication NTIS-PR- 360 available from NTIS at the above address.

DISCLAIMER

DOE/METC--84-7

DE84 003052

PROCEEDINGS OF THE NINTH ANNUAL ***UNDERGROUND COAL GASIFICATION SYMPOSIUM***

P. R. Wieber, J. W. Martin, and C. W. Byrer, Editors

Sponsored by
U. S. Department of Energy
Office of Fossil Energy
Morgantown Energy Technology Center
Morgantown, West Virginia

Held at
Indian Lakes Resort Conference Center
Bloomingdale, Illinois
August 7-10, 1983

Proceedings Coordination and Compilation Assistance by L. B. Schaeffer
EG&G, Washington Analytical Services Center, Inc., Morgantown Operations

December 1983

TABLE OF CONTENTS

TABLE OF CONTENTS
(Continued)

TABLE OF CONTENTS
(Continued)

TABLE OF CONTENTS
(Continued)

TABLE OF CONTENTS
(Continued)

1.0 INTRODUCTION

1.1 FORWARD

The Ninth Underground Coal Gasification Symposium was held August 7-10, 1983 at the Indian Lakes Resort and Conference Center in Bloomingdale, Illinois. This symposium was sponsored and hosted by the Morgantown Energy Technology Center (METC) of the U. S. Department of Energy (DOE). The papers printed in the Proceedings have been reproduced from camera ready manuscripts furnished by the authors. They have not been refereed nor have they been edited extensively.

Over one-hundred attendees from industry, academia, National Laboratories, State Government, and the U. S. Government participated in the exchange of ideas, results and future research plans. Representatives from six countries including France, Belgium, United Kingdom, The Netherlands, West Germany, and Brazil also participated by presenting papers. Fifty papers were presented and discussed in four formal sessions and two informal poster sessions. The presentations described current and future field testing plans, interpretation of field test data, environmental research, laboratory studies, modeling, and economics.

The information obtained from the research activities over the last decade has resulted in a level of maturity which is both gratifying and surprising for the relatively low research funds invested. Successful field tests have been operated continuously for up to sixty days in both flat-lying and steeply-dipping seams of low ranked coals, and the feasiblity of gasifying bituminous coal seams in situ has been shown. These tests, which produced both low- and medium-BTU gas, usually shut down voluntarily without any significant major equipment failures. As a result of these experiences, several announcements of future large scale tests and even commercialization prospects have been made, but these may be delayed by the currently depressed economy and apparent "oil glut," requiring further reductions in technical risk to initiate new ventures that might yield less revenue in the near term.

Although significant progress has been made, many uncertainties in the technology remain to be resolved. Primary among these are the reliable establishment of linkage paths between process wells under varying overburden and coal seam conditions, and the environmental effects resulting from subsidence, aquifer disruption, and possible groundwater contamination. Future research activities should address these problems, and also continue the development of instrumentation and process control techniques to ensure a stable product gas quality and quantity with varying coal seam conditions.

My sincere appreciation is extended to Mr. Cleve Benedict, Deputy Assistant Secretary for Oil, Gas, Shale, and Coal Liquids, U. S. DOE, for providing the opening remarks for the symposium. I also extend my sincere appreciation to Dr. Bernard S. Lee, President, Institute of Gas Technology for his address, "World Energy Perspective."

My gratitude and special thanks go to the symposium coordinator, Bernie Ervin, and her dedicated staff - Annette Ahart, Tammie Allbritton, and Laura Cowell - of Morgantown Operations, EG&G, Washington Analytical Service Center, Incorporated. Their professional and able handling of the many details involved in arranging and conducting the symposium and in printing the Proceedings ensured a pleasant, timely and complete exchange of current information on Underground Coal Gasification.

Further, our thanks are extended to the session chairmen for their skillful handling of the sessions and to the authors for their contributions to the information exchange.

Finally, recognition is given to Messrs. Charlie Byrer, Allen Brummert, and especially Joe Martin, of the METC technical professional staff, for their assistance, and often leadership, that assured the successful planning and execution of this symposium.

P. R. Wieber
Symposium Chairman

2.0 FIELD WORK

SESSION I: ORAL PRESENTATIONS

2.1 THE DOE UCG PROGRAM

by

Edward L. Burwell

ABSTRACT

In the decade from 1973 to 1983, underground coal gasification (UCG) in the United States has moved from a doubtful concept to the point of commercial development. Over a dozen field tests have been conducted during the development of UCG technologies with gasification of over 30,000 tons of coal. An extensive data base has been established relative to UCG describing various operational and control parameters, and those problems remaining which are hindering commercial development have been identified and are described.

INTRODUCTION

Underground coal gasification (UCG) R&D in the Department of Energy has evolved from 1972 to the present time to one of the more promising synthetic fuel technologies. The program basically moved through three phases. Under the Bureau of Mines (USBM), from 1972 to 1975, the basic feasibility of UCG was established. From 1975 to 1978, under the Energy Research and Development Administration (ERDA), seven major field tests were conducted to investigate operational and control parameters and to establish the data base relative to UCG technology. The Department of Energy (DOE) work is primarily focused of filling the remaining gaps in the data base relative to the coal types addressed and in extending UCG technologies to coal types and geologic settings not previously addressed.

While major work still remains to be accomplished, the technical feasibility of UCG has been demonstrated for subbituminous coals in both flat lying and steeply dipping coal seams. Industry interest in UCG, both domestic and foreign, appears high, and it is expected that one or more industry-funded commercial demonstrations will be initialed by 1985.

EVOLUTION OF THE DOE UCG PROGRAM

The DOE UCG program over the past decade reflects both the research needs of an emerging technology and the political and philosophical changes that have occurred in the area of Government research during that period. Each of the three major phases of the program, to date, has served to advance the technology, but because of the differing thrust of each, each probably deserves separate mention.

Phase 1 USBM -- (1972-1975)

In 1972, the USBM was directed to initiate planning for UCG research and development. Since a usable data base for design and operation of a UCG field test was virtually nonexistant, the program managers first task was to assemble a research team which was accomplished by drawing from Government scientists previously engaged in thermal in site recovery from oil sands or oil shale, USBM employees who had been assigned to the Gorgas, Alabama UCG effort in the 1950's, and some outside hires in selected areas. This team from LETC and METC were joined by LLNL and SNL

researchers and began the arduous tasks of researching all relevant foreign and domestic literature and developing a rough test plan which led to the first UCG field tests of the current program -- Hanna 1 and 2. These tests conducted with primarily borrowed people and much surplus or, otherwise, hastily appropriated equipment were surprisingly successful, and the data from these tests and from concurrent basic laboratory studies clearly confirmed the feasibility of the UCG concept and laid the groundwork for the next phase during which most of the major field tests, to date, were either conducted or planned.

Phase 2 -- ERDA (1975-1978)

In the nearly 1,000 days that ERDA existed, seven major field tests were completed and three others were planned or fielded. These tests were: Hann 2-1, 2-2, 2-3, 3, 4; Hoe Creek 1 and 2 with Hoe Creek 3 planned; Rawlins 1 fielded; and Pricetown 1 started.

The data provided by these tests provided the early inputs for the current United States data base relative to UCG. Basic models and computer codes were developed at LETC, LLNL, SNL, and at several universities to assist in the understanding of UCG, in design of future test, or for technology transfer to the growing number of groups outside the Government who were beginning to actively study the promise of UCG.

Major progress in many areas during this period include direct and remote sensing techniques and hardware, better control parameters, and delineation of many of the major problems and promises. The technical feasibility of UCG was clearly confirmed, and the overriding importance of site selecting and characterization was defined. The problems identified during the field tests, also, gave a much clearer direction to the DOE phase of the program.

Phase 3 -- (1978-1983)

Many major accomplishments have occurred during the DOE R&D efforts in UCG. Basically, the major thrust has been directed toward filling holes in the data base by addressing major process problems. These include problems associated with hydrology and subsidence, relationship of the process to geology, site characterization, better process control, process well linking and prevention of override of burns, and the ability to predict process performances within acceptable limits. Actual accomplishments include the demonstration during Rawlins II of long-term production of good quality medium-Btu gas with reasonable process control and promising economics, the demonstration of the safe use of oxygen as an injection gas during Rawlins II and Hoe Creek 3, and that a UCG burn can be accomplished in a high-swelling bituminous coal was demonstrated during Pricetown 1. In addition, past burn coring and evaluation of most of the past tests along with laboratory studies at various sites, including a coal outcrop, gave a much better understanding of early cavity growth and reaction zone expansion. Replacement of economic and process models have been a continuing process, and a wide variety are nonavailable addressing most parts of the UCG technology.

CURRENT PROGRAM

A major policy shift in DOE was accompanied by several actions that have put extreme pressure on nearly all fossil energy programs. These include major funding cuts (an order of magnitude overall), the demise of the demonstration program, the defederalization of the lead center for UCG (LETC), a major reduction in force at DOE headquarters, the existing temporary gas glut, and the gross inflation with the resulting severe negative impact on available capital.

All of the above have required a very severe focusing of the program to allow completion of the steps which must be accomplished to allow industrial groups to do credible assessment of the technical, economic, and environmental risks preceding a decision to test the commercial value of the technology.

The current DOE UCG program is addressing such problems as improved linking procedures, process thermal and recovery efficiency improvements, refinement of process models, and environmental impact mitigation procedures. In addition, an agressive technology transfer program is underway in attempts to involve outside groups in the program and to make all past data available to potential developers. During the next 2 years, it is expected that the potential of a unique operational technique, the controlled retracting injection point (CRIP), will be tested. The next logical step in a program addressing bituminous coal will be accomplished, preliminary results of aquifer restoration studies will be available, and a cooperative program with a domestic or foreign industry will be underway on a commercial demonstration of the process.

CURRENT STATUS AND NEEDS

Process and technology developments addressing the different geologic settings and coal types are not at equal stages of development. It is felt that UCG technology addressing steeply dipping coal beds (SDB) has shown sufficient technical and economic promise to warrant commercial testing by industry. Flat seam UCG is within 2 to 4 years (1-3 tests addressing specific parameters) of the same stage of development, and UCG in bituminous coal is the research challenge still facing the program. In all areas, the proof of ability to handle water problems must be demonstrated, but no "show-stoppers" appear likely to preclude UCG from making its contribution to the nations need for viable alternatives to imported energy.

CONCLUSION

1. UCG in the past decade has moved from a doubtful concept to a clearly established concept with an extensive data base and a credibly demonstrated ability to produce low- or medium-Btu gas.

2. The need for a commercialization test in at least one coal type with non-Government funds appears the next essential step.

3. The promise of UCG is extremely strong, good economics, no show stoppers, and high domestic and foreign industry interest.

2.2 THE CENTRALIA PARTIAL-SEAM CRIP TEST

by

R. W. Hill [1/]
C. B. Thorsness [1/]
D. S. Thompson [1/]

ABSTRACT

The controlled retracting injection point (CRIP) concept for underground coal gasification was successfully tested on a small scale in early 1982 in the large block tests, near Centralia, Washington. The basic idea of the CRIP concept is to start a new burn in fresh coal, upstream of the old burn, whenever the quality of the product gas from the old burn falls to an uneconomic level. To start the new burn, a section of the injection pipe is burned off so as to establish a new injection point.

The Centralia partial-seam CRIP test, described here, will be a larger scale test of the concept--the first of several tests in a commercialization program designed to develop the CRIP concept of underground coal gasification as applied to a high-wall geometry. The test will be carried out jointly by Lawrence Livermore National Laboratory (LLNL) and Washington Irrigation and Development Company (WIDCO), whose open-pit coal mine is the site of the test. Sponsors of the test are the Department of Energy, the Gas Research Institute, and two northwestern utilities: the Washington Water Power Company and Pacific Power and Light.

The Centralia partial-seam test is designed to use half the coal seam thickness and to allow for four or five injection point withdrawals. The main test objectives are (1) to determine the appropriate spacing and timing for injection point withdrawal, and (2) to study the gas composition and burn width. Steam-oxygen injection is planned, the expected coal consumption is 2000 tons during 30 days of gasification, and the dry-product-gas heating value is estimated to be 270 Btu/scf.

INTRODUCTION

One of the most economical methods of gasifying coal underground is through the use of the high wall left at the worked-out boundary of a surface mine. Access to the coal seam through the high wall eliminates some of the most expensive preparatory drilling that is required when the coal seam is entirely underground and accessible only from the ground surface above. If, in addition, a nearby electric power plant provides a potential customer for the UCG gas produced, the economic situation improves even further.

The Centralia partial-seam CRIP test described here will be the first step in the realization of such an idea. This test, together with the full-seam CRIP test designed to follow it, will provide the basic technical data needed to make a realistic evaluation of the economic potential of *in situ* coal gasification at the Centralia site. These experiments, which are part of the Tono Basin test series, are designed to take every possible advantage of the particular high-wall location in the WIDCO mine and to utilize the equipment still available from the large block experiments recently completed at that site. By restricting the scale, we are able to keep the costs low compared to some of the larger scale tests done in the past.

The design for the partial-seam test is based on the controlled retracting injection point or CRIP[1] concept of *in situ* coal gasification. Normally, there

[1/]Lawrence Livermore National Laboratory, Livermore, CA 94550.

are only three parameters that can be used to control in situ coal gasification: i.e., injection-gas flow rate, injection gas composition, and system operating pressure. The CRIP concept adds one more control parameter, the position of the injection point. This is important for the following reasons. As a burn cavity progresses, inevitably roof collapse brings inert material into contact with the burning coal. The heat lost to this material is subtracted from the total available for useful reactions, and the result is a lowering of the heating value of the product gas. With the CRIP system, when the product-gas heating value has declined to an unacceptable level, the injection point is moved back upstream along the horizontal injection well into a region of fresh coal, where a new burn cavity is begun. The heating value of the product gas rises again, reflecting the return to conditions of low heat loss. The product gas travels to the production well through the previous cavity. This process can be repeated at any desired interval until the entire useful length of the injection well is used up.

The CRIP concept is illustrated in the drawing shown in Fig. 1. For this first test, only the upper half of the coal seam will be gasified, to allow significant roof interaction and consequent heat loss to take place with modest burn times. The goal is to be able to try a number of CRIP injection-point retractions and still stay within a 30-day period of forward burn, so as not to exceed our budget.

Although an injection well drilled in the coal seam along the dip is a necessary part of the CRIP idea, the position of the production well is not so constrained. We have shown a vertical production well intersecting the end of the injection well in Fig. 1, to be used as a backup production well. The CRIP idea does imply advantages to be gained by keeping the burn geometry compact and of a fairly constant size; in order to achieve that goal we have shown as the primary production well one that slants in from the coal face at a slight angle to the injection well. Thus as the injection point is moved back toward the face, the production point will tend to move back also, keeping the burn cavity more or less constant in size, with a rubble-filled zone left behind downstream. Depending on the flow rates used and the details of the burn geometry, there will be a horizontal distance between injection and production wells over which all of the coal will be consumed. We will try to determine that distance for the conditions of this test by angling in the production well so that the horizontal distance to the injection well constantly increases as the injection point moves back. Also, we plan to bring the slant production well in through the overburden above the coal to reduce the possibility of the hot gases causing leaks by shrinking the coal along the casing.

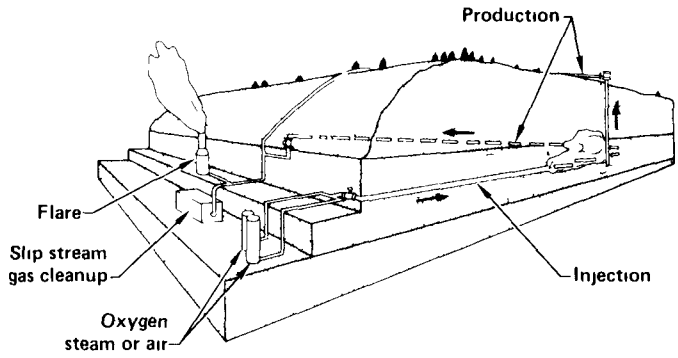

Fig. 1. Planned layout of the Centralia partial-seam CRIP test.

The primary goals and objectives of the Centralia partial-seam CRIP test are as follows:

1. Determine the relationship between coal recovery, product-gas heating value, and injection-point retracting distance for the CRIP system.

2. Investigate the effect of roof interaction on gas quality over the 30-day burn period, using the CRIP system.

3. Investigate long-term gas production with a slant production well.

4. Confirm the design and operational parameter relationships determined during the large block experiments.[2]

5. Provide design data for the 90-day full-seam CRIP test.

6. Provide the basis for preliminary design and cost analysis of a commercial-scale high wall UCG application at the site.

7. Identify gas-cleanup design parameters.

8. Provide for technology transfer to industry partners.

EXPERIMENTAL PLAN[3]

The major technical goal of this experiment is to provide as complete a test of in situ gasification of the coal at the Centralia field site with as much contingency coverage as possible within the budgetary constraints imposed for the experiment. The highest priority is given to testing the CRIP system, which we believe will give the best chance for economical gas production. The design is conservative in that redundant gas production and injection points are built in to allow operational changes to be made if it becomes necessary to counter possible failure modes.

The backup production well is included in the design because of the lack of any previous field data on gas production through long, nearly horizontal holes and because of the large amount of rubbling and subsequent pressure buildup that occurred during the LBK experiments. The two tests done in a steeply dipping coal seam at Rawlins, Wyoming, by Gulf[4,5] for DOE are strong evidence in favor of long, slanting production wells, since in those tests no production well problems were encountered. However, the dip angle at Rawlins was four times greater than the 15° at the Centralia site, and the coal at Rawlins, although also subbituminous, was different from the WIDCO coal. We do not expect to have any problems with the slant well, but, in case our expectations are wrong, the vertical well will allow us to take remedial action without shutting down.

The slant production well has been designed so that its intersection point with the burn cavity will move upstream as the cavity grows larger. Not only does the intersection point move upstream, but it also moves away from the injection channel as both cavity growth and CRIP retraction move the injection point upstream. Thus the exhaust part of the channel will move more and more at right angles to the injection channel. This will produce a comma-shaped burn cavity, with the main combustion zone in the head, more or less symmetrical with the injection point, and the tail curving away toward the production channel.

The separation of the two slant casing points will be about 60 ft, so this design should provide a good test of effective sweep width for use in future designs.

This angled intersection design was not intended as a potential commercial-scale design. (For commercial use the injection and production slant wells would most likely be parallel and joined at the ends by a common directionally drilled linking well.) This design was the most easily linked and least costly configuration that would allow us to meet the goals of the test. The sideways separation minimizes the possibility of short-circuiting through collapse, and the entry of the product well in the overburden above the coal should significantly reduce gas leak problems due to shrinking caused by hot gas.

The proposed well pattern is shown in Fig. 2. The main production well, Prod-1, is drilled on a slant from a point on the face about 20 ft above the coal seam and displaced laterally about 200 ft. The drilled hole intersects the roof of the coal seam on a line perpendicular to the injection well at the final injection point.

Prod-1 crosses the injection well at a point about 25 ft in front of the vertical pump well P-1. The backup production well, Prod-2, is drilled to intersect both Prod-1 and the injection well at this point.

The injection system will supply steam, oxygen, argon, and air, all with individual flow control and measuring stations. Air will be used only for ignition and linking, and as emergency standby supply in case of oxygen loss during the burn.

Both production wells will be connected to the system with valves so that the gas stream flow from either one can be measured and burned in the flare.

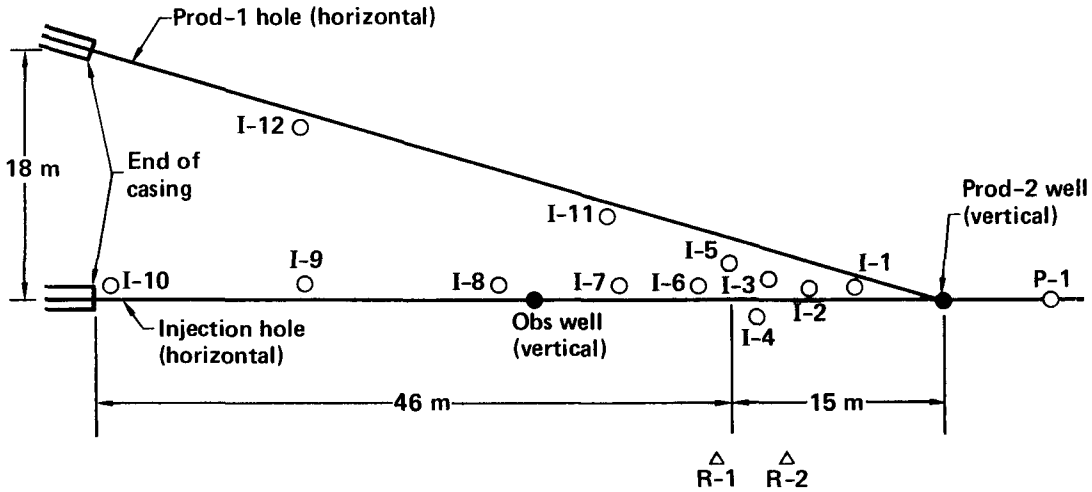

Fig. 2. Plan view of the Centralia partial-seam CRIP test, showing locations of the process wells and the instrument wells.

A slipstream port will be provided for gas utilization experiments. Back-pressure control will be provided via a remote control valve. Water cooling with flow control will be needed for both production wells and the injection well.

A cyclone separator will be placed in the production line to provide for some gas cleanup before flaring the gas.

Burn Cavity Diagnostics

The plan view in Fig. 2 shows the 12 instrument wells (I-wells). These wells each contain a number of thermocouples. Several of the site characterization wells (not shown) will be equipped with downhole water samplers, placed at appropriate levels in the coal and overburden as determined from the hydrology measurements. The instrument wells have a crushable coaxial cable included to indicate subsurface ground motion by measuring changes in cable length due to collapse-induced breakage. The stemming for these wells will alternate sections of bentonite and cement grout, with the cement sections placed at levels of interest in the overburden. The bentonite sections will not support much tensile stress and thus should allow the cement sections and cable to move with the collapsing strata. Wells I-3, I-4, and I-5 will be equipped with Sandia's inverted thermocouple strings, and wells R-1 and R-2 will be the receiver wells for these instruments.

In addition to the thermocouple wells, a backup injection or production well is shown in Fig. 2, labeled Obs. This well will be drilled and cased to a point 3 ft above the injection channel and will have thermocouples fastened to the casing. It will be equipped with a fused quartz window and nitrogen purge system so that it can be used as an observation well with an optical pyrometer when it is not needed for its backup role. This well will have valves suitable for either injection or production but will not be connected to the UCG system unless needed.

Thermocouples will also be fastened to the casing of the vertical production well, Prod-2, to the injection well liner, and to the pump well casing. Four thermocouples will be included with the igniters, which will be placed in each slant well to serve as movable temperature probes in both the injection and production channels.

Sandia National Laboratories, Albuquerque, is also planning to field the controlled-source audio magneto-telluric (CSAMT) system,[6] which is under development, in a test of its ability to define the shape of an underground cavity from surface field measurements.

Several other means of obtaining information on cavity shape also figure in

the plan. A high-resolution seismic survey of the site will be carried out by Laramie Energy Technology Center, both before and after the burn, to obtain data on the cavity shape. Surface subsidence will be measured by means of survey monuments, of a design suitable for the area, which are to be installed and surveyed before the test starts at about 50-ft intervals along the injection and Prod-1 lines. These lines should extend 100 ft toward the coal face from the casing points and the same distance beyond Prod-2. Accurate level surveys will be made before the test and a few weeks after the completion of the test as a minimum requirement.

Finally, a postburn coring and drilling program is included in the plan for this test, to accurately determine the final cavity boundaries.

Environmental Monitoring

Three or four of the site hydrology wells will be used for routine sampling of any groundwater present before, during, and after the burn. The water samplers will make it possible to sample low rates of water influx since only a small sample is needed.

The water from the pump well P-1 will be monitored also. If we have to pump P-1 to dewater the burn zone during the burn, the water will be held and monitored for contaminants before disposal.

OPERATIONAL PLAN

Final Linking Procedure

The final linking procedure will depend on how successful the drilling program has been. If the link well has intersected both slant holes, then no further step will be necessary. However, if a good link (low pressure drop, high conductance) has not been achieved, reverse combustion may be used to improve the connection between the two slant wells.

If Prod-1 crosses below the injection well or too far above it to be quickly linked by hot gas flow, reverse combustion will be initiated by igniting the coal close to the intersection point, using the igniter in Prod-1. Oxygen-enriched air will be injected into the injection well to draw the fire zone in Prod-1 through the intervening coal to the injection well. The igniter in the injection well (with its attached thermocouple) will be used to detect the arrival of the flame front at the injection well and to help control the reverse burn rate up the injection channel. Once the burn front has reached the injection liner, forward combustion will be started with oxygen/steam injection, and the gas produced will be drawn out through Prod-1.

Forward Combustion

Forward combustion will be started by igniting the coal at the end of the injection liner. This will be accomplished with the silane igniter in the injection liner if no reverse-burn step has been used. Otherwise, the reverse burn itself will be used to bring the burn front back to the end of the liner to start the forward burn. The burn will be started with an oxygen-enriched air mixture at a low flow rate, and a gradual transition will be made to 3/1 steam/oxygen injection over the first few hours. The steam/oxygen flow rate will be increased on a schedule proportional to the square of the elapsed time, as was done in the LBK experiments. The time scale for the increase to the full oxygen flow rate of 15 mol/s will be about five days; the actual flow schedule will be chosen when the final operating instructions are drawn up.

Forward burn will be continued at the 15-mol/s oxygen injection rate, with continuous monitoring of gas compositions and other operating parameters. The information from the instrument wells will be considered, along with the product gas composition, to determine the degree of roof interaction and the extent of cavity development. The heating value of the gas will be allowed to drop to a lower value than might be optimum for economic operation, in order to study the way the interaction with the roof occurs. When the heating value has declined to the appropriate minimum level, the first CRIP retraction will be carried out.

CRIP Retraction Procedure

The present plan calls for four to five CRIP retractions, the first one to

be 30 ft upstream of the original injection point, and each of the succeeding ones to be an additional 46 ft farther upstream. The actual schedule of retractions will be decided on during the experiment and will depend on the results previously achieved. Although we have made some calculations to show what we expect to accomplish in the way of gas composition and coal consumption, they are based on assumptions which can only be verified by doing the experiment.

Prior to a CRIP retraction, the injection flow will be switched to a low flow of oxygen-enriched air suitable for ignition, and the igniter will be placed at the desired location for the new injection point. After the igniter has been lighted, the fuel/oxygen ratio will be adjusted to that previously determined to be correct for melting the stainless steel liner. After the liner has been cut (as determined by one of the thermocouples on the liner), the flame will be maintained long enough to ignite the coal at the new location. The igniter will be extinguished and pulled back to its next location, the injection flow will be returned to steam/oxygen, and a new burn cavity will be started by increasing the flow rate on a new schedule.

Shutdown

We will continue the burn for 30 days and try to complete as many retractions as possible within that time. When the decision is made to end the experiment, the injection flow will be stopped and the production flow will be monitored for a few days as the system shuts down. Groundwater will be allowed to enter the burn zone and cool the cavity.

SYSTEM PERFORMANCE ESTIMATES

Assumptions

We have made performance estimates for the partial-seam CRIP test based on the results of the LBK experiments. The estimates are premised on the following assumptions:

- The coal is similar to that at the LBK site.
- No significant leakage or mobile water influx will occur.
- Cavities will develop roughly as cylinders having an elliptical transverse cross section.
- Initial product-gas composition will be similar to that of LBK-1.
- Product-gas degradation will begin when the roof begins to fall into the system.

The coal composition assumed in making the performance estimates is given in Table 1. This represents a partial-seam average (the top 22 ft of the seam) of the Big Dirty coal obtained from cores at the LBK site. The averaging does not include the major parting (1 or 2 ft thick) located in the bottom third of the seam, shown in Fig. 3. The estimates of system performance are not a strong function of the assumed coal composition.

From a preliminary analysis of the LBK results, it appears to us that a reasonable approximation of the main cavity growth can be obtained on the basis of the following assumptions:

- The bottom of the cavity remains fixed near the original drilled link.
- The transverse cross section of the cavity boundary can be approximated by an ellipse with major (vertical) and minor (horizontal) axes in the ratio of 1.5.
- The developing cavity is roughly three times as long as it is wide.

Gas Composition

Degradation of the product gas is assumed to begin when the top of the developing cavity reaches the roof of the seam. The resulting change in system performance is estimated using our water-gas-shift equilibrium model.[2] In developing the estimates, we first obtained initial model parameters by fitting the results of the LBK-1 experiment. Then subsequent calculations were performed with increasing amounts of water input to, and sensible heat loss from, the reaction zone. For simplicity, we assumed that the reaction zone would have to absorb all the heat loss from drying and heating the overburden material as it fell in. For these initial estimates we assumed that the roof material had a density of 1.5 Mg/m^3 (or g/cm^3), a

Table 1. Coal composition assumed in making performance estimates for the Centralia partial-seam CRIP test.

Wet basis:	
Moisture- and ash-free coal	64.0%
Moisture	21.6%
Ash	14.4%
Density	1.384 Mg/m^3 (or g/cm^3)
Dry basis:	
Hydrogen/carbon ratio	0.95
Oxygen/carbon ratio	0.19
Heat of combustion	494 kJ per gram-atom of carbon

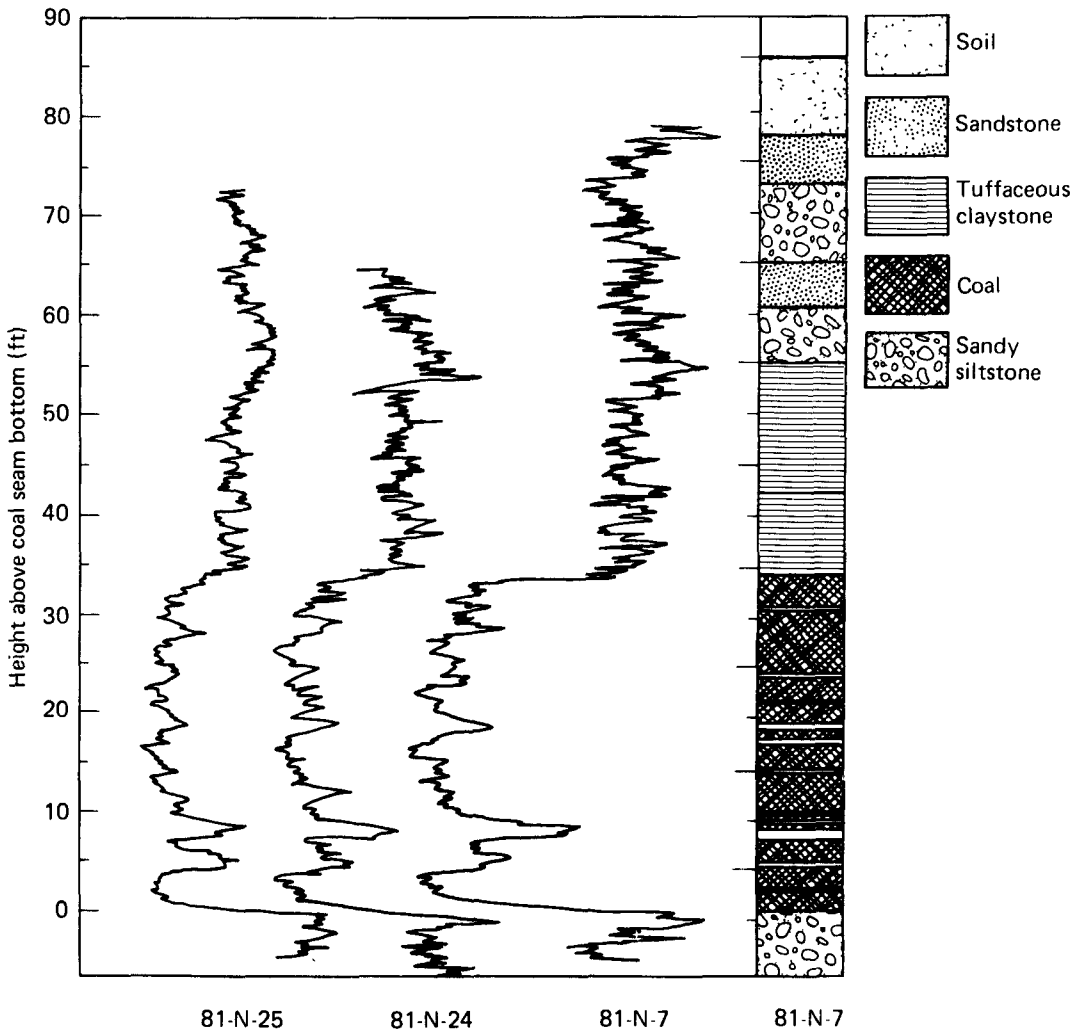

Fig. 3. Lithology and well logs for three test wells at the LBK test site, near the partial-seam CRIP test site.

water content of 20%, and a heat capacity of 0.35 kJ/kg-°C.

Figure 4 shows the decline in dry-gas heat of combustion, H_c, and dry-gas heat of combustion per mole of injected oxygen, H_0, as functions of coal affected. This figure was used to estimate the termination point of a standard module experiment, which is defined as that period between ignition at a given location and reignition at a new point. We chose a drop of 25% in H_0 as our target termination point. From Fig. 4 we see that this corresponds to a total coal consumption of 317 m^3. At this point our model cavity is 7.1 m high, 4.7 m wide, and 14 m long. In addition to the 317 m^3 of coal affected, 50 m^3 of overburden would also be included in the cavity region.

The estimated gas composition as a function of time is given in Fig. 5. Only the major constituents are shown. We expect all other components to be less than 0.005 mole fraction. The tar loading is very difficult to estimate but should be small.

Flow Rate

We propose to use a flow rate schedule similar to that used on the LBK experiments: a 3/1 steam/oxygen ratio, with the rate of oxygen injection given by

$$g(O_2) = 8.61 \times 10^{-11} t^2 \text{ mol/s} \quad \text{for } t < 4.17 \times 10^5 \text{ s}$$

$$= 15 \text{ mol/s for } t > 4.17 \times 10^5 \text{ s}$$

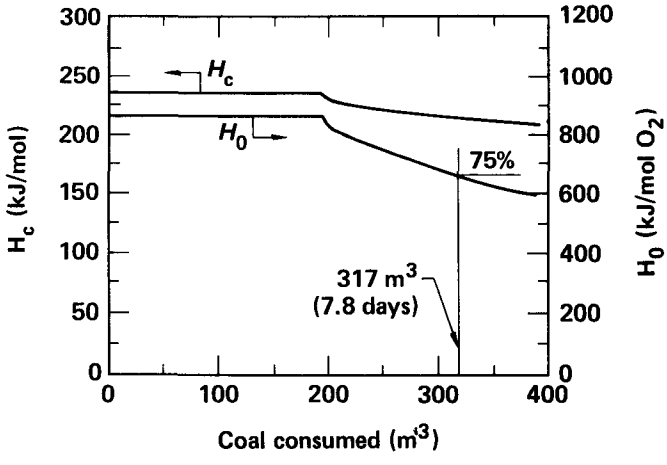

Fig. 4. Calculated product-gas heat of combustion (H_c) and product-gas energy per mole of oxygen injected (H_0) vs coal consumption for the Centralia test. The vertical line marks the 25% decline point in H_0, which gives the time (7.8 days) planned for the initial forward burn before making the first CRIP retraction.

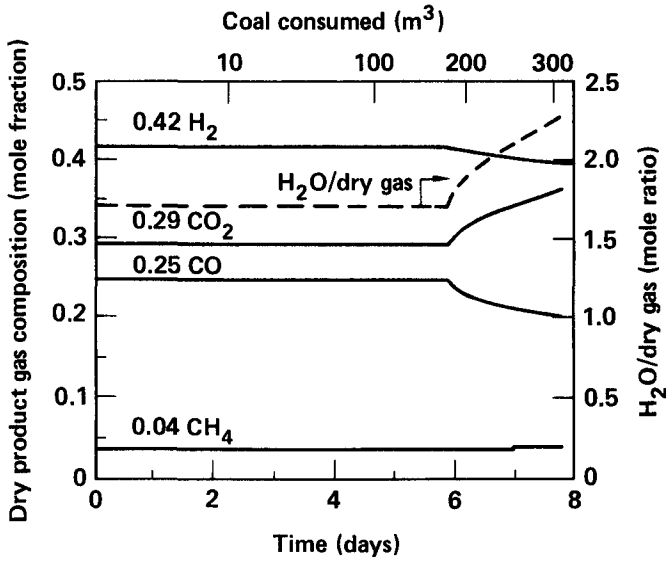

Fig. 5. Calculated ratio of water to dry gas in product gas, and composition of the dry gas.

(4.17×10^5 s = 4.83 days). Using this schedule and the estimated gas composition, we calculate that a standard module affecting 317 m^3 of coal will take 7.8 days to complete.

To maintain a product temperature near 300°C, we plan to inject cooling water into the base of the production well. The cooling-water injection rates (upper limits) as well as the calculated injection and production flow rates are shown in Figs. 6 and 7 as functions of time and volume of coal affected.

Pressure Buildup

During the LBK experiments, we observed a pressure buildup between the injection and production wells which was due partly to increasing flow rates (following the t^2 flow schedule) and partly to increasing flow resistance. The flow resistance contribution to the pressure drop is believed to be from rubble filling the exit borehole connecting the cavity and the production well. The excavation results showed rubble-filled exit channels in all but one of the LBK experiments.

Analysis of the LBK data based on simple packed-bed theory indicates that after the channel fills, gradual enlargement takes place due to thermal and mechanical interaction with the product gas. An enlargement rate proportional to the integral of the product flow was found to match the data from LBK-4 and LBK-5, the two tests which resulted in the largest pressure drops.

Because of the larger borehole and geometry being proposed for the Centralia partial-seam CRIP test, we are uncertain whether rubble filling of the exit borehole will take place. However, in case rubble filling does occur, we have proceeded to estimate the resultant pressure drop vs time. Solving the compressible-packed-bed pressure equation, with the area changing according to

$$A = A_0 + 1.0 \times 10^{-7} \left(\frac{m^2}{mol}\right) \times \int_0^{t(s)} \text{flow (mol/s)}\, dt ,$$

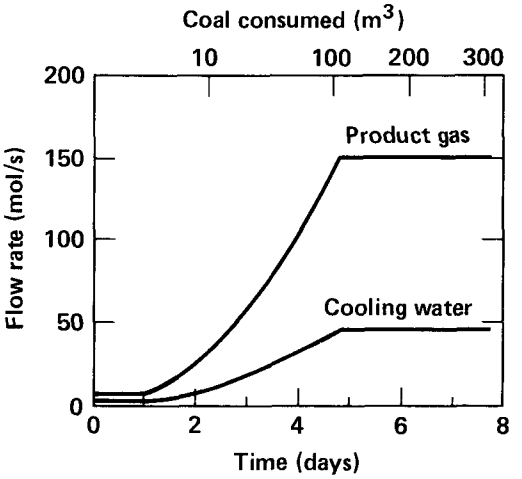

Fig. 6. Calculated flow rates of product gas and product cooling water as a function of time for the first cavity of the Centralia test.

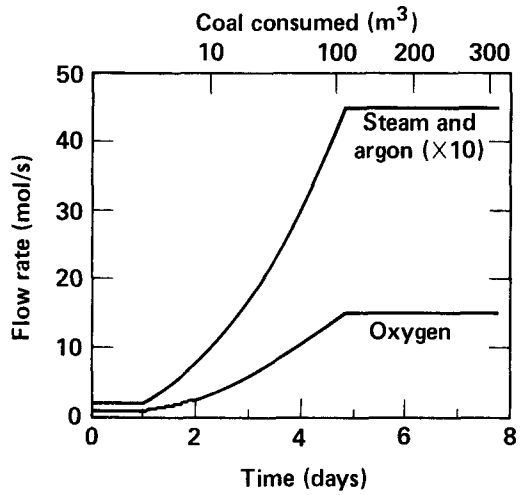

Fig. 7. Calculated injection flow rates of oxygen, steam, and argon tracer for the first cavity of the Centralia test.

where

$$A_0 = 0.2\ m^2,$$

we determine the pressure drop vs time in an uncased exit borehole 150 ft long. To this pressure drop we add that of the piping in the production and injection wells. Finally, assuming a production

wellhead pressure of 30 psia (207 kPa), we arrive at the estimated injection pressure vs time shown in Fig. 8. We see that the maximum injection pressure is 95 psia (655 kPa), which is near the hydrostatic pressure at the experiment site.

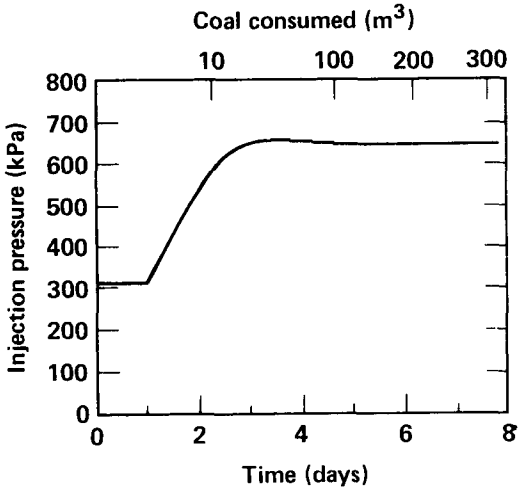

Fig. 8. Calculated injection pressure as a function of time for the first cavity of the Centralia test.

CRIP Criteria

If the test performs exactly as predicted in the above estimates, the 200 ft of uncased injection well will give room for 4.26 standard modules fitted end to end. However, we plan to perform one initial ignition and four CRIP maneuvers. We will place the first ignition point at a distance from the production point equal to the standard module length of 46 ft, and follow it up with two partial modules each initiated by moving the ignition point back only 30 ft. These partial modules are planned to obtain data useful in estimating the optimum distance for CRIP retractions. The two 30-ft modules will be followed by two more 46-ft standard modules, so that the total distance is exactly 200 ft. The time required for each partial module should be 6.1 days, giving an estimated total time for the entire experiment of about 36 days. The total coal affected would be about 2000 tons (1350 m^3).

It must be stressed that the flow rate, coal volume, and time estimates made here are primarily for planning purposes. We do not expect the system to perform exactly as outlined, and our operating strategy will be modified as needed. In particular, the number and duration of each module will undoubtedly be modified as actual performance data becomes available.

DESIGN SPECIFICATIONS

Injection and Production Flow Rates and Pressures

The estimated injection and production flow rates and delivery pressures are given in Table 2.

Process Well Intersection

Although the details of the drilling program will be developed in consultation with the drilling contractor, one possible program is outlined here.

The injection well was drilled parallel to the dip of the coal seam from a point on the coal face. A pilot hole was drilled first, using nonmagnetic material for the surface conductor, to allow an accurate downhole directional survey to be made. The directional survey data will enable the slant production well, Prod-1, to be drilled so as to cross a foot or two above the injection well and about 25 ft upstream from the end of the well. This well will also be directionally logged.

We can use either a gamma-ray source and counter or a three-axis magnetometer and solenoid to measure hole separations by signal attenuation. The magnetic field produced by the current in the solenoid is proportional to $1/r^3$ at distances large compared to the dimensions of the solenoid. By using the earth's magnetic field to determine the orientation of the magnetometer, we can measure the distance between magnetometer and solenoid by measuring the field strength with the current on. The gamma-ray source and counter can be used in much the same way to determine distance, but the effective range is only about 5 ft, compared to 25-30 ft for the magnetometer.

Inserting the solenoid into one hole and the magnetometer into the other, we can find the distance of closest approach of the two holes and the downhole distance to that point. With this information and

Table 2. Estimated injection and production flow rates and pressures required for the Centralia partial-seam CRIP test.

Injection requirements	
Flow rates:	
Air	0.1 to 25 mol/s (5 to 1250 scfm)
Oxygen	0.1 to 15 mol/s (5 to 750 scfm)
Steam	1.0 to 45 mol/s (50 to 2260 scfm)
Argon	0.01 to 0.5 mol/s (0.5 to 25 scfm)
Steam/oxygen ratio	1/1 to 3/1
Pressure at end of injection liner at full flow	310 to 1035 kPa (45 to 150 psia)
Cooling water in annulus	0 to 50 mol/s (0 to 15 gpm) at 1380 kPa (200 psia)
Production requirements	
Flow rates	0.2 to 160 mol/s (10 to 8000 scfm)
Pressure at base of production well	210 to 450 kPa (30 to 65 psia)
Maximum cooled gas temperature	300°C
Cooling water flow	0 to 50 mol/s (0 to 15 gpm) at 1380 kPa (200 psia)

the directional survey information, we can establish a location for the pump well P-1. Then, drilling a pilot hole, we can use the magnetometer to measure the actual separation between the vertical pilot hole and the slant injection well (assuming intersection is not achieved on the first try). By shifting the drilling point as indicated by the measurement, actual intersection should be possible with two or three trials. This technique worked quite well during the construction of the LBK experiments.

Once the pump well has been located, we should be able to drill the vertical production well, Prod-2, to intersect both slant wells. The diameter of the vertical hole in the intersection region can be increased by underreaming to aid in the intersection process.

Process Well Design

The injection well liner will be 600 to 700 ft (185 to 215 m) long, depending on final site location. It will be stainless steel, and sized so as to allow full flow of 3000 scfm (60 mol/s) of steam/oxygen over a possible burn-cavity pressure range of 45 to 150 psia. This liner, complete with thermocouples at 10-ft intervals over the last 180 ft, will be inserted through a grout-sealed casing that extends from the face to a point 200

ft from the vertical production well. The liner will be centralized within this casing to provide maximum thermal insulation between liner and casing. Provision will be made to inject water into the annulus or liner if necessary for cooling or to replace some of the steam later in the test. We want to have the option of injecting nitrogen into the annulus to prevent burnback along the injection channel by flushing out the accumulated oxygen and air. This will be done before the start of the burn, and perhaps a few times during the burn.

The product wells will be sized to handle the expected maximum flow rate of 160 mol/s. For both wells, it is important to have solidly grouted casings to prevent excessive gas leaks. Water cooling lines will be used to provide spray cooling of the product gas at the base of each product well to hold the product gas temperature in the 200-300°C range. These lines should be provided with overpressure rupture disks so that flow can be restored if the nozzles become plugged with tars. Computer readout and remote control of injection flow and production backpressure are required.

The Igniter System

The igniter will be an improved version of the one used for the LBK experiments. It will be a silane/propane (or silane/methane) system in which the pyrophoric gas silane is used to ignite the propane, which is then used to ignite the coal or to melt off the injection liner for the CRIP retractions.

The silane is supplied as a mixture of 93.5% argon and 6.5% silane in bottles pressurized to 2000 psia (14 MPa). This mixture was found to give smoother ignitions than pure silane. The igniter tube is simply a long, 1/2-in.-diam stainless steel tube with four thermocouples spaced along it at 50-ft intervals for diagnostic purposes. The tube is overfilled with the silane/argon mixture, and the flow is then stopped to allow ignition to take place as the silane flows out the end of the tube and into the airstream. Then propane flow is started, and as the propane/silane interface leaves the tube, the already burning silane ignites the propane. The propane flow and the air flow in the channel are then adjusted to levels suitable for igniting the coal or for cutting the stainless steel liner, whichever is required. When the desired goal has been achieved, the propane flow is shut off and the igniter is retracted back into the liner until needed again.

The end thermocouple in the igniter protrudes a few inches beyond the end of the tube to give a direct indication of successful ignition.

Pump Well

A pump will be required, capable of pumping 15-20 gpm at 200-ft head and provided with an automatic water-level control to hold the water level constant within ±1 ft. If pumping is needed during the burn, some water-storage facility will be required for the possibly contaminated water that will be produced.

Surface Plant

The surface plant will be similar in design to that used for the LBK experiments. Much of the same valving and piping can be used.

The injection system will consist of steam, oxygen, argon, and air supplies, all with individual flow control and measuring stations. Air will be used only for ignition and linking, and as emergency standby supply in case of oxygen loss during the burn. Instrument air should be supplied to the injection system through a check valve or automatic solenoid valve to prevent loss of pressure in case of oxygen loss.

Both production wells will be connected to the system with valves so that the gas stream flow from either one can be measured and burned in the flare.

A particulate knockout vessel equipped with a bypass line will be used to provide some cleanup of the gas stream before disposing of it in the flare.

A slipstream port will be provided for gas utilization experiments. Backpressure will be controlled by a remote control valve. Water cooling with flow control will be needed for both of the production wells and for the injection well.

All pressure and temperature transducers will be connected to the data acquisition system for permanent recording

and real-time process monitoring. Mechanical gauges will be provided to read pressures and temperatures at important points in the system. All flow-monitoring stations will be provided with appropriate valves to allow isolation and easy calibration of the transducers and to provide a low-pressure-drop shunt for the ΔP transducer across the orifice plate.

FUTURE PLANS

A full-seam CRIP test is planned for 1984 at the Centralia site, in partnership with Washington Water Power Company and Pacific Power and Light. The steam-oxygen test is projected to consume 6000 tons of coal over a 90-day period. Following this test, a large-scale pilot test is planned for 1985-86.

ACKNOWLEDGMENT

This work was done under the auspices of the U.S. Department of Energy by Lawrence Livermore National Laboratory under Contract No. W-7405-Eng-48.

REFERENCES

1. R. W. Hill and M. J. Shannon, "The Controlled Retracting Injection Point (CRIP) System: A Modified Stream Method for In Situ Coal Gasification," Proc. Seventh Underground Coal Conversion Symposium (Fallen Leaf Lake, Calif., Sept 8-11, 1981), CONF-810923 (1981), pp. 730-739. Also UCRL-85852 (1981).

2. C. B. Thorsness and R. W. Hill, "The Large Block Tests," Proc. Eighth Underground Coal Conversion Symposium (Keystone, Colorado, August 15-19, 1982), SAND82-2355 (1982), pp. 365-375. Also UCRL-87611 (1982).

3. R. W. Hill and C. B. Thorsness, The Centralia Partial Seam CRIP Test: Preliminary Design, Lawrence Livermore National Laboratory, Livermore, Calif., UCID-19610 (1982).

4. A. H. Singleton, N. L. Noll, and J. M. Allen, "Summary Report of the Rawlins T-1 for Gasification of Steeply Dipping Coal Beds," Proc. Sixth UCC Symposium (Afton, Oklahoma, July 13-17, 1980).

5. B. E. Davis et al., Underground Gasification for Steeply Dipping Coal Beds--Phase III Report: Results of Rawlins Test No. 2, Laramie Energy Technology Center, Laramie, Wyo., LETC-13108-94 (1982).

6. R. E. Glass, Ed., Instrumentation and Process Control Development for In Situ Coal Gasification, Quarterly Report: April-June, 1980, Sandia National Laboratories, Albuquerque, N. Mex., SAND-80-1921 (1980).

2.3 AN INDUSTRIAL PERSPECTIVE FOR UCG

by

Burl E. Davis [1/]
Jerry H. Daniel [1/]
Alan H. Singleton [1/]

ABSTRACT

During the last decade, UCG technology has been developed that is capable of producing low- and medium-Btu gas from low-rank coals and lignites. The technical feasibility has been demonstrated in subbituminous coals and lignite in both horizontal and steeply dipping seams. Although improvements are needed, the technology appears adequate for commercialization in selected resources. As in development of any new technology, the scale of the early operations must be kept small to minimize capital requirements. Also, the product slate for the early-on operations may differ significantly from the long-term products. This paper will discuss priorities for the initial facilities and how they could influence choice of resources, products, and scale of operations.

INTRODUCTION/BACKGROUND

In 1972, the Laramie Energy Technology Center began the first[1] of a series of UCG tests at a site near Hanna, Wyoming. The results of this initial effort served as the basis for the federal program in UCG technology development. The program has supported 14 field tests at four different sites, as well as development of supporting technology.[2] The results of the federally funded tests are summarized in Table 1. Highlights of the DOE program include:

Demonstration of UCG in horizontal seams of western subbituminous coals.

Development of UCG process models relating gas composition to coal chemistry and blast composition.

Demonstration of thermal efficiencies comparable to surface gasifiers.

Definition of process effects on groundwater at several sites.

Economic estimates for a commercial-scale UCG facility.

Development of predictive models for subsidence.

Demonstration of directional drilling in three different geologic domains.

Estimates of resources amenable to in situ gasification.

Demonstration of UCG in steeply dipping coal seams.

Promotion of significant industrial interest in the technology through their field tests and annual symposium.

Support of industrial field tests with technical support and consultation.

The promising results in the federal program spurred significant efforts in the

1/ Gulf Research & Development Company
P. O. Drawer 2038
Pittsburgh, PA 15230

private sector with a total of six field tests, primarily with private funds, which are summarized in Table 2. Although the work was performed in the private sector, the DOE, and its predecessor ERDA, provided technical support to many of these programs.

The in situ conversion of coal to a gas that can either be utilized directly as a fuel or as a feedstock for higher value products has significant advantages over surface processes using mined coal. The fact that it combines an extraction process with a conversion process offers an opportunity for significant reduction in capital costs. This, along with the ability of the process to utilize coal resources that are not recoverable by conventional technology, it provides a strong economic and resource-related incentive for commercializing the technology.

The technology required to install and operate a UCG reactor has been demonstrated more than 20 times in this country alone. The major issues are: Can the process be operated reliably, economically, and within the regulatory considerations that will be required for commercial operations? The results of the Rawlins program clearly suggest that this can be done.

A commercial UCG facility would utilize a well field that would consist of several reactors operated simultaneously to produce the product gas. The individual reactors would operate at gasification rates similar to those used for the field tests. This suggests that scale-up from field tests to commercial operations will be simpler than for conventional surface processes. The scale-up problems will be more related to logistics and operations rather than changes in the operating characteristices of the process.

All these factors combine to suggest that UCG has significant advantages over competing synthetic fuel processes. The major barriers to commercialization are related to the lack of large-scale operating experiences and also to the environmental problems encountered during some of the field tests.

BASIS FOR COMMERCIALIZATION

We normally think of commercial-scale energy plants as being of the five-to-ten thousand tons/day size to benefit from the economy of scale. The UCG process not only has inherently lower capital costs, but also has a smaller economy of scale. In Figure 1, when return on investment is plotted against plant size, the ROI increases with plant size reaching a plateau with a plant size of 3000 tons. Although these calculations are based upon a specific case, the shape of the curve is quite similar for most cases for UCG. Reasonable profits can be projected for UCG plants producing fuel gas for a local market at gasification rates of 1000 tons coal/day. The capital costs for such a facility would be in the range of 60-80 million dollars (Figure 2).

The resource size required to support a plant of this size for 20 years would be in the range of 10-15 million tons of in-place subbituminous coal. Published results suggest that the seam thicknesses should be in the range of 20-30 ft, with no aquifers in the coal seam or in the overburden. Both the efficency and resource recovery costs become unacceptable as seam thicknesses decrease to 10 feet and smaller.[4] The seam should be dipping at an angle of greater than 50° to optimize oxygen utilization and gas quality[5] since the proposed plant size is less than optimum. Operation of a plant of this size would demonstrate the logistics and performance required for long-term operations. Although some of the technical data would be site-specific, most of the information would be applicable to other UCG facilities. Additionally, it would increase private industry's confidence in the readiness of the technology for commercialization.

LONG-TERM POTENTIAL

Although the first UCG plants may be developed to meet local markets for fuel gas, the real potential for the technology lies in the ability to produce low-cost synthesis gas at $3.50-$4.00/mm Btu. Our in-house estimates indicate that these costs are 50 to 65% of that produced from new natural gas. That is; synthesis gas produced from reforming new gas ($5.00/mm Btu) would cost $8.00/mm Btu. Although well-defined markets for synthesis gas do not presently exist in the Rockies, there are several potential markets that could develop once the ability to produce the

gas is demonstrated (Figure 3).

WHERE IS THE TECHNOLOGY HEADED?

The present UCG technology, i.e., linked vertical wells and footwall entry for UCG-SDB, appears to be adequate for most of the western subbituminous coals. Texas lignites could also be considered as amenable to the technology.[6] However, there is considerable room for advancement in the technology required to deal with operations in very wet seams or where aquifers can be affected.[7,8] Without these advancements, it is unlikely that regulatory agencies would permit commercial operations in resources where aquifers could be affected.[9] Transfer of the technology to eastern coal reserves will require additional advances in the technology as well as a considerable change in the price of competitive fuels. UCG in eastern coals must not only deal with the effects of agglomeration and swelling but the higher recovery costs inherent for operations in thin seams (<8 ft) will be a significant factor. Agglomeration and swelling of the bituminous coals created severe operational problems during the METC field test at Pricetown and the Bureau of Mines program at Gorgas.[10] Special linking and seam treatments will be needed to minimize these problems. However, the more serious barrier to commercialization is probably the inherently poorer economics of thin-seam gasification. This is not only due to the increased drilling costs for each ton of coal gasified, but it is also due to the poorer efficiencies of thin seam operations. This causes added expense not only in the oxygen supply requirements, but it also increases the size of the product processing system to deal with the poorer quality product.

SUMMARY

Underground Coal Gasification technology has made significant advances in the last decade and, in some cases, has reached a level of maturity to warrant commercialization on a small scale. The most mature and lowest cost technology appears to be that related to gasification of the steeply dipping reserves in the Rockies. Opportunities can be found for small-scale commercial plants producing fuel gas for local markets. These plants would make a profit while demonstrating long-term operations that would provide a basis for larger, more profitable, plants producing higher value products. Before the technology can be applied to the bulk of the U.S. subbituminous coals and lignites, improved process reliability and the ability to mitigate the process effects on aquifers must be demonstrated. To date, there has been little done in the development of aquifer protection and restoration technology for these systems. Regulatory agencies are justifiably concerned over the lack of demonstrated techniques in this area.[10] Commercialization of bituminous coals in the Eastern U.S. will require additional developments of technology related to the coal swelling and thin-seam operations. Its inherently poorer economics will require that prices of competitive fuels, primarily natural gas, exceed $10.00/mm Btu before UCG operations will be commercially attractive. Obviously, if the price of energy increases twofold, or the U.S. government takes position of high subsidies for domestic fuels, commercialization of eastern bituminous coals could come much faster.

REFERENCES

1. L. A. Schrider, J. W. Jennings, C. F. Brandenberg, and D. D. Fischer, "An Underground Coal Gasification Experiment, Hanna, Wyoming," presented at the SPE Fall meeting of AIME, Houston, Texas, October 6-9, 1974.

2. D. R. Stephens, "Underground Coal Gasificaton--Leading Contender in the Synfuels Industry," Lawrence Livermore Report UCRL53216, October 27, 1981.

3. B. E. Davis and P. F. Ahner "UCG-SDB, A Second Generation Synthetic Fuels Process," presented at SPE meeting, New Orleans, September 1982.

4. W. Gregg and D. U. Olness, "Basic Principles of Underground Coal Gasification," Lawrence Livermore Laboratory, Preprint UCGL- 52107, August 18, 1976.

5. P. F. Ahner, J. M. Avasthi, B. E. Davis, M. E. Dolde, C. A. Greenman, and J. E. Miranda, "A Site Qualification Study of the UCG Site at North

Knobs, Presented at the 6th Annual UCC Symp. Afton, Ok., July 1980.

6. J. W. Jennings, R. F. Strickland, and W. D. Von Gonten, "Texas A&M Project Status: Underground Lignite Gasification," 3rd Annual Undergound Coal Conversion Symposium, Fallen Leaf Lake, California, June 6-9, 1977.

7. C. A. Salotti and J. M. Avasthi, "Subsidence as a Technical Hazard to Underground Coal Gasification," Presented at the 6th Annual UCC Symp. Afton, Ok., July 1980.

8. A. C. Riese and B. E. Davis, "Aquifer Restoration and Groundwater Rehabilitation: Application to Underground Coal Gasification Sites," to be presented at the 9th UCC Symposium, Bloomingdale, Ill., August 1983.

9. P. M. Schmittdiel, "Groundwater Quality in Underground Coal Gasification--A Regulatory Outlook," Proceedings of the 8th Underground Coal Conversion Symposium, Keystone, Co., August 1982, pp. 535-542.

10 M. M.Siegel, et al., "An Assessment of Underground Coal Gasification in Bituminous Coals," Proceedings of the 8th Underground Coal Conversion Symposium," Keystone, Co., August 1982, pp. 245-260.

Table 1. Summary of U.S. DOE-Sponsored UCG field tests

Test	Year	Duration (days)	Coal consumed (tons)	Gas quality (Btu/scf)	Coal gas efficiency (%)
Laramie Energy Technology Center--Hanna, Wyoming, site					
I	1973-1974	168	2720	126	77
II-1A	1975	37	962	137	85
II-1B	1975	38	780	143	86
II-II	1976	26	2201	168	92
II-III	1976	39	3414	132	77
III	1977	38	2663	138	77
IV-A (a)	1978	7	294	109	78
IV-A (b)	1978	48	3184	102	73
IV-B (a)	1979	7	468	149	95
IV-B (b)	1979	16	663	122	83
Lawrence Livermore National Laboratory--Hoe Creek, Wyoming, site					
I	1976	11	123	101	82
II (air)	1977	13	286	108	80
II (O_2)	1977	2	47	263	88
II (air)	1977	43	1155	104	74
III (air)	1979	7	256	113	81
III (O_2)	1979	47	3251	212	73
Morgantown Energy Technology Center--Pricetown, West Virginia, site					
I	1979	17	234	149	97
Gulf Research & Development Company--Rawlins, Wyoming, site					
I (air)	1979	30	1207	151	91
I (O_2)	1979	5	125	212	74
II	1981	66	8560	329	88

Table 2. Privately sponsored UCG field tests

Test	Year	Duration (days)	Gas quality (Btu/scf)	dry gas production (million scf/day)	Coal gasified (tons)	Coal Gas thermal efficiency (%)
Basic Resources, Inc.						
Fairfield, TX	1976	26	126	--	--	--
Tennessee Colony, TX:						
Air Injection	1978-1979	197	81	2.5	4000-5000	--
Oxygen Injection		10	230	1.0	212	--
ARCO Coal Co.						
Reno Junction, WY	1978	60	200	4.5	3600	94
Texas A&M University (with Industrial Consortium)						
College Station, TX	1977	1	35-114	0.3	2	--
Bastrop County, Tx	1979	2	85	1.4	--	--
Bastrop County, Tx	1980	--	35-150	--	--	--

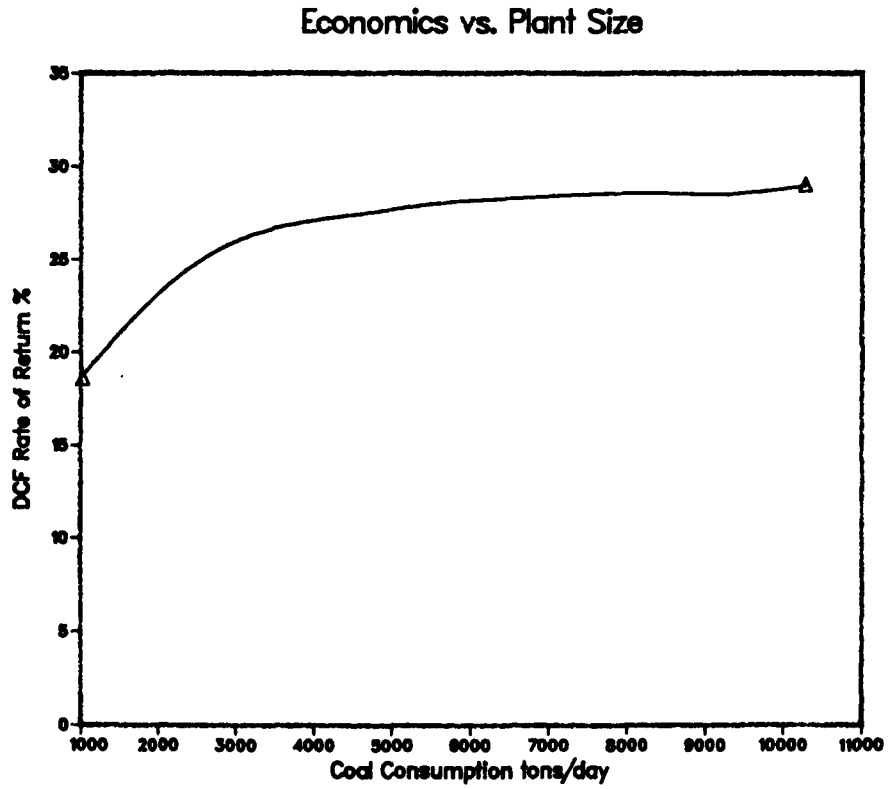

Figure 1

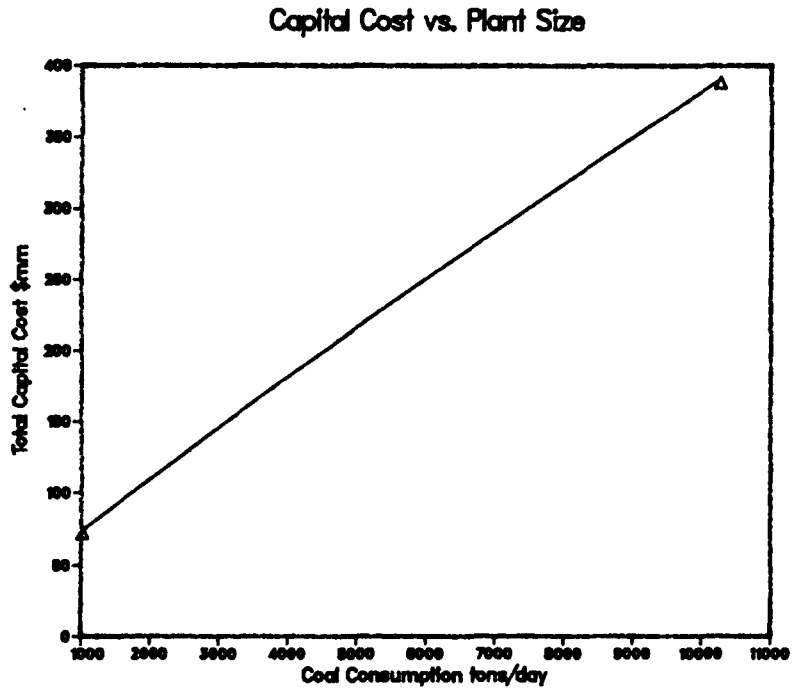

Figure 2

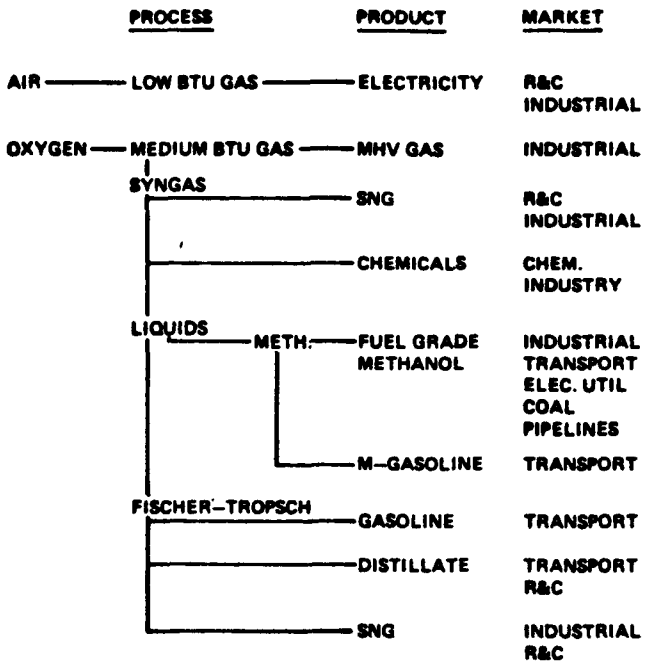

Figure 3. UCG Product Options

2.4 FIRST RESULTS OF THE BELGIAN-GERMAN UCG-TEST AT GREAT DEPTH

by

P. LEDENT, T.K. LI, V. CHANDELLE, R. FABRY, M. KURTH and C. SONNTAG (*)

Institution pour le Développement de la Gazéification Souterraine,
rue du Chéra, 200, B-4000, Liége, BELGIQUE.

ABSTRACT

A first trial of reverse combustion linking was carried out from April until November 1982.

Even though the combustion of coal was kept continuously for a period of more than six months, with air injections at pressures ranging between 250 and 300 bar, the trial has not led to the creation of a channel, but only to the formation of two zones of increased permeability in the vicinity of the wells I and II.

The failure of this first trial is to be ascribed to three factors : the self-ignition of the coal in the vicinity of the injection well, the system of ignition and the high level of the back pressure at the recovery well.

A second linking trial has started in July 1983.

Taking into account the experience that has been gathered, some elements of the experimental equipment have been modified; these modifications mainly concern :

- replacement of air injection by injection of a cold mixture air + CO_2;
- use of a new system of ignition, by means of a fuel-oil torch;
- reduction of the back pressure and continuous drainage of the water at the bottom of the recovery well.

1. Equipment of the wells

A first reverse combustion linking test was carried out at Thulin between the wells I and II in the period from April until November 1982.

Figure 1 shows the arrangement of both wells at the point of intersection with the Léopold-Charles sequence.

The casing of well I stops at the roof of the first coal-band.

The casing of well II was extended to about fifteen metres below the seams; it was cut away for a length of 2.5 metres at the level of the upper belt of the seam Charles.

Perforated liners with an external diameter of 5 1/2" were installed at the bottom of the wells, in order to reduce the risks of coal creep.

Well I was used for air injection. This injection was carried out through a 1 3/4" tubing which ends at the level of the upper belt of the seam Charles.

---

* Director, Deputy Director and Members of the Project Management.

Well II was used as recovery well, the product gases being recovered through a 1 3/4" tubing, which ends 9 or 10 metres above the upper belt of the seam Charles.

This tubing was also used for the ignition operation at the bottom of well II; this operation was carried out by injection of hot air heated to a temperature between 100 and 400°C by means of an electrical igniter, installed some thirty metres above the seam.

2. Start of the reverse combustion test

The first ignition was established on 1st April 1982, with injection of a flow of 285 m^3_N/h of air, preheated at a temperature of 115°C, at 208 bar pressure. Self-ignition of the coal occurred after 3 hours and 36 minutes.

New injections of hot air were carried out on 5 and 7 April, and gas analyses carried out after partial pressure release of the well confirmed the presence of a very active fire.

The first phase of reverse combustion went on from 11 until 15 May.

The injected air flow ranged from 580 to 440 m^3_N/h, with an injection pressure of 224 bar.

The recovery rate on well II increased from 7.5 to 15 %; analysis of the gases recovered during the last two days oscillated around the following values :

O_2 : 18.5 %
CO_2 : 1.8 %
CH_4 : 2.1 %
H_2 : 0.3 %

3. Problems related with the self-ignition of the coal at the bottom of the injection well

On 15 May, at 8.40 a.m., a sudden temperature increase at the bottom of well I, as well as a very strong decrease of the permeability of the seam were observed; the pressure inside well I increased rapidly, and the volume of air injected into the seam dropped to about zero.

Air injection into the well was continued for 1 h 55 up to maximum pressure of 280 bar, without any gas penetration through the wall of incandescent coal being noticed.

Self-ignition of the coal in the vicinity of the injection well brings about two major disadvantages : it reduces the possibility of further injection into the seam, and it consumes the oxygen of the air, thus making it unsuitable for the feeding of a reverse combustion fire.

Three attempts were made to overcome these difficulties :

At first we tried to dislocate the coal zone affected by the self-ignition, by carrying out a partial pressure release, and by extinguishing the fire, filling the bottom of the well with water.

This process was repeated about ten times, and each time we managed to recover a rather satisfying permeability in the seam, which brought the injection pressure back to its normal value of 220 to 230 bar.

However, these extinction operations had only a temporary efficiency. The water does not allow the temperature of the coal to recover its original value and, after each new pressure build-up in the well, the fire resumes after a relatively short time. The periods that were observed varied between 1 hour and 60 hours.

A trial of reversing the gas flow direction between both wells was abandoned after some ten days, the gas recovery rate in the direction II → I being too small.

In a third period we tried to eliminate the clogging at the bottom of the injection well by an

extension of the fire zone. We first applied alternatively pressurizations and pressure releases; later on we applied a continuous injection.

After some eight days, we managed to stabilize the injected air flow at 195 m^3_N/h, and the injection pressure slowly decreased from 280 to 220 bar.

Figure 2 shows the evolution of analysis of the gases recovered through well II. After a short period, during which the CO_2-content reached about 20 %, we noticed a gradual decrease of the contents of CO_2, methane and hydrogen, as well as a simultaneous increase of the oxygen content.

The results obtained during this period could be explained as follows :

After the first self-ignition has led to a general ignition of the coal walls at the bottom of the well, combustion resulting from the injection of a small air flow at very high pressure in a very compact coal seam develops towards the formation of several small fires, shifting along the fissures of the coal.

The air flow feeding all these fires has a tendency to be reduced gradually, as the passage of the combustion products through the fissures causes a partial clogging of these fissures.

The injected air is seeking new flow paths, and the flow is split up into an increasing number of circuits developing in a dendritic way.

The ratio between the flow passing through each of these circuits and the surrounding coal volume is evermore decreasing, and in an increasing number of circuits it drops below the limit value needed to keep combustion going on.

Consequently, a phenomenon of gradual self-extinction and a reduction of the amount of oxygen consumed in the zone surrounding the injection well are noticed.

Owing to these results, we decided to continue the linking test between the wells, accepting the simultaneous presence of direct combustion fires around well I and reverse combustion fires around well II.

4. Continuation of the reverse combustion test

The new tests went on for three months (July, August, September) with an interruption of 15 days in the second half of July. The main results are given in table I.

The first two weeks of July and the first four weeks of August appeared to be rather positive as far as the recovery rate and the amount of consumed coal are concerned.

This period ended with a sudden increase of the injection pressure, which was a tangible sign of a reactivation of the fires of combustion in the vicinity of the injection well.

During the period from 27/8 until 6/9 we still had a high recovery rate, but the injected flow remained very small, as a result of the resistance of the deposit.

The results obtained during the period from 7 until 27 September confirmed the deterioration of the experimental conditions. The injection pressure remained very high, the recovery rate dropped to 6.3 %, and the presence of high methane and hydrogen contents in the product gas made us think that the combustion fires in the vicinity of well II had practically disappeared.

5. Tracer tests

When the tests were going on, we periodically made tracer injections (radioactive Xenon) in order

to control the evolution of the gas flow conditions between the wells I and II.

Three data are particularly significant for interpretation of the results :

- the tracer "recovery rate";
- the "active volume", which can be defined as the volume of a reactor providing the same residence time when the same gas flow is passing through it;
- the "variance", measuring the dispersion of the residence times.

Figure 3 shows the evolution of the first two parameters :

Three periods are characterized by a rapid increase of the "recovery rate" :

- the first two weeks of July;
- the first four weeks of August and
- the period in November during which nitrogen was injected after extinction of the combustion fires in the vicinity of well I. However, the recovery rate never reached a value which was perceptibly higher than the one obtained in January and in May, before the first self-ignition of the coal.

Referring to the curve of variation of the "active volume", one can find out that the gas flow between the wells I and II in the period July-August was located in a zone with a rather small volume; however, this evolution was not accompanied by a systematic decrease of the "variance", which characterizes the dispersion of the residence times.

This leads us to conclude that the positive results obtained during the period July-August did not result from the development of a channel, but that they evidenced the regrouping of the gas flow through a large number of fissures, connecting two zones in the vicinity of the wells I and II, the permeability of which strongly increased by the development of the combustion phenomena.

6. Analysis of the results

Three factors seem to have played a part in the failure of this first linking trial :

- The self-ignition of the coal at the bottom of the injection well has lead to a decrease of the oxygen content of the air in the vicinity of the gas recovery well. It has also caused a decrease of the permeability of the seam, which forced us to reduce the injected air flows.
- The technique of ignition by injection, at high pressure, of an air flow, preheated between 100 and 400°C, did not lead to the forming of a large fire, but resulted in the dispersion of the fire into a large number of fires with a small volume. This led to the development, around the recovery well, of a strongly permeable zone, kind of a sponge, comprising a large number of holes with a very small diameter, without bringing about a real channel likely to establish a linking between both wells.

  Several coal samples, taken in April 1983 in the vicinity of well II, when the liner was being replaced, confirmed this interpretation. They showed small channels with a diameter of 3 or 4 mm, obtained by the progression of the fire. These channels had developed in the direction of the cleavages.
- The high back pressure (30 to 40 bar), kept at the bottom of well II during the reverse combustion operations, also had a negative influence in two respects :
  - by favouring the progression of the fire into holes with a small diameter
  - by transforming the recovery well into a real condenser, which prevented the removal of the steam and caused the accumulation of water at the bottom

of the well, below the tubing for gas removal.

7. Second reverse combustion trial

In November 1982, we extinguished the fire by water and nitrogen injections.

The operations were resumed in July 1983, after we had modified some elements of the equipments; these modifications aimed at solving the problems we had met during our first trial. They concern three points :

1. In order to reduce the risks of self-ignition of the coal in the vicinity of well I, we decided to cool the bottom of the well to a temperature of about 0°C. This cooling is obtained by simultaneous injection of an air flow of about 500 m^3_N/h and a liquid CO_2 flow of 120 kg/h.

   After evaporation of the CO_2, we obtain a mixture of 89 % air and 11 % CO_2, the temperature of which has decreased with about 30°C.

   According to Arrhenius' law, the velocity of the oxydation reactions is dependent upon the absolute temperature, according to the relation :

   $$V = e^{\frac{-E}{RT}} \cong e^{\frac{-5000}{T}}$$

   The temperature decrease from 303 to 273°K should reduce the heat emissions in a ratio 5 to 1.

2. The system of ignition by injection of hot air, requiring the use of very high pressures (> 220 bar) causing the dispersion of the fire, was replaced by an ignition system which can function at a back pressure of 2 or 3 bar, and which is capable of heating the liner to a temperature of 700 to 800°C.

   This device, a sketch of which is given in fig. 4, consists of a porous ceramic torch, through which a liquid combustible is distributed and ignited by injection of a small quantity of TEB (triethylborane).

3. The back pressure at the bottom of the recovery well is kept as low as possible for the whole duration of the reverse combustion operation, and possible water inrushes are continuously eliminated by an air-lift system, the principle of which is shown in fig. 5.

8. References

P. Ledent, Ch. Beckervordersandforth, V. Chandelle, T.K. Li, R. Fabry and C. Sonntag

- Planning and state of the Belgian-German experiment of underground gasification, 7th U.C.C. Symposium - Fallen Leaf Lake, California - September 1981.
- State of the Belgian-German experiment of underground gasification, 8th U.C.C. Symposium - Keystone, Colorado - August 1982.

Table I. Reverse Combustion Test - July-September

PERIOD		2-15/7	4-21/8	21-27/8	27/8-6/9	7-27/9
Injection pressure	(bars)	232	242-230	230-280	280-254	254-277
Injection rate	(m^3_N/h)	306	207	380	154	207
Back pressure in Borehole II	(bars)	40	30	30	30	30-15
Average recovery rate	(m^3_N/h)	34.6	21.6	60	23	13.4
Percentage recovery	(%)	11.3	10.4	15.8	14.8	6.3
Gas analysis :						
O_2	(%)	13.1	13.7	14.9	10.7	10.1
CO_2	(%)	5.4	4.9	4.3	7.1	5.7
CH_4	(%)	1.1	2.7	< 0.1	1.3	5.2
H_2	(%)	< 0.1	0.3	0.0	0.3	0.8
Coal consumption between I and II	(kg/h)	0.98	0.56	1.38	0.88	0.40

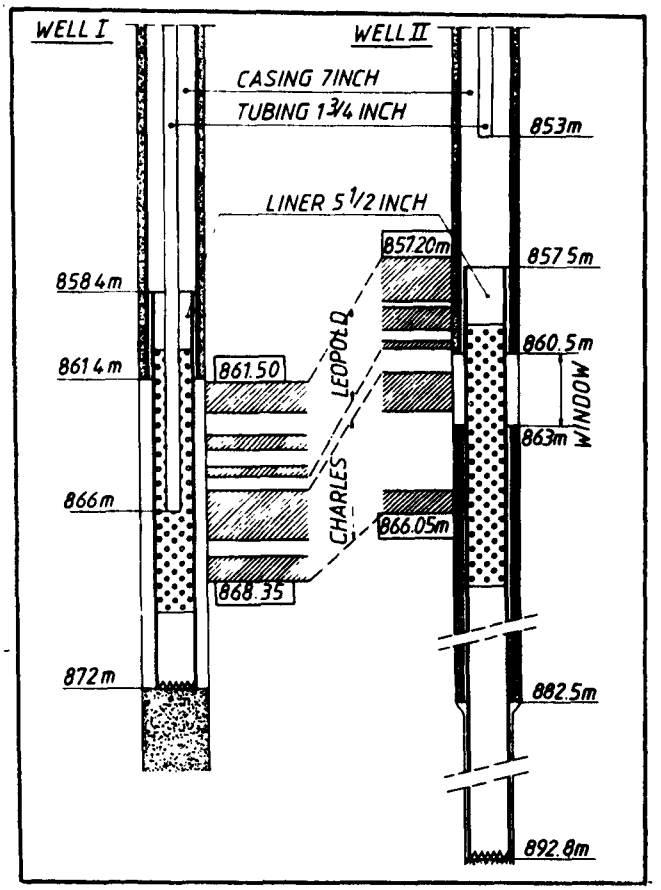

Figure 1. Lay-out of the wells.

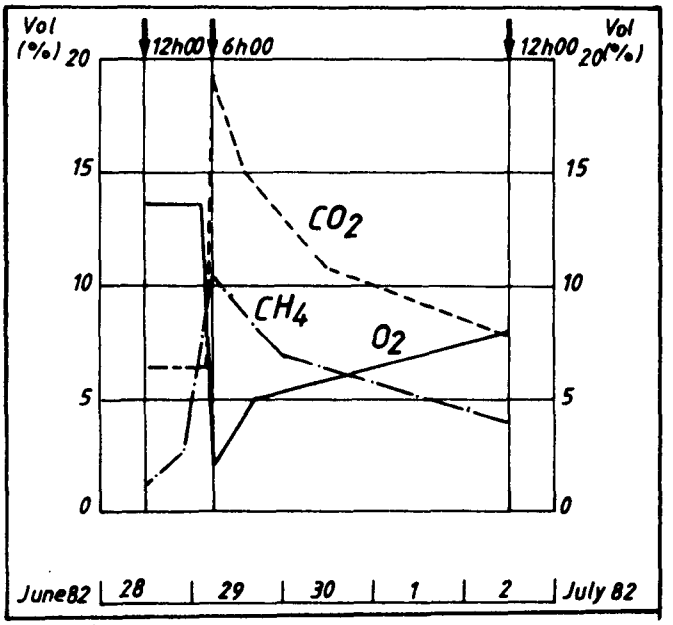

Figure 2. Analysis of the gas recovered during the period of extension of the combustion zone.

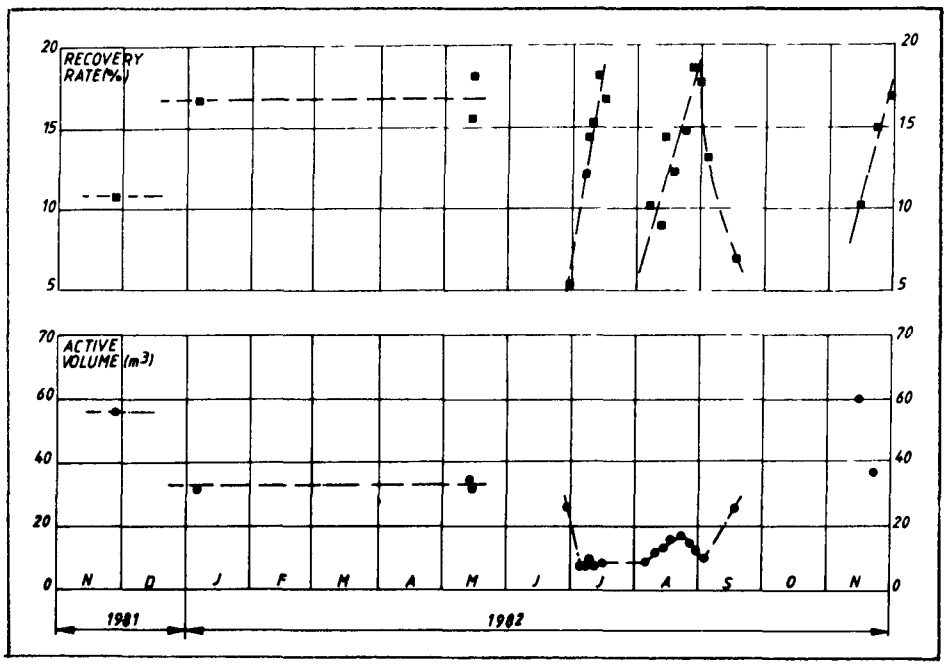

Figure 3. Tracer-tests : Evolution of the "Recovery Rate" and of the "Active volume".

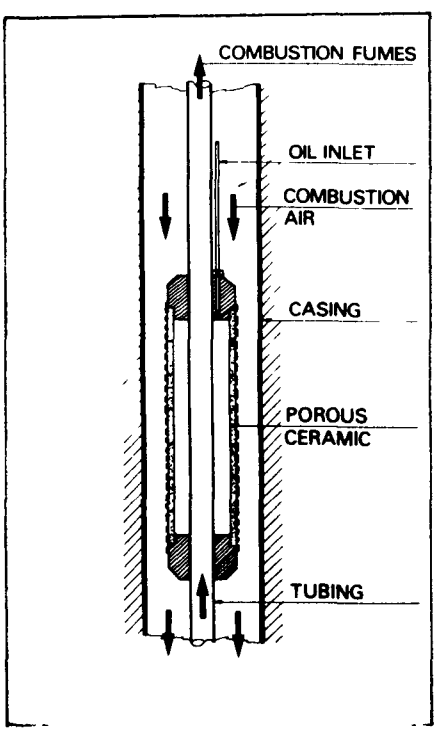

Figure 4. Ignition device.

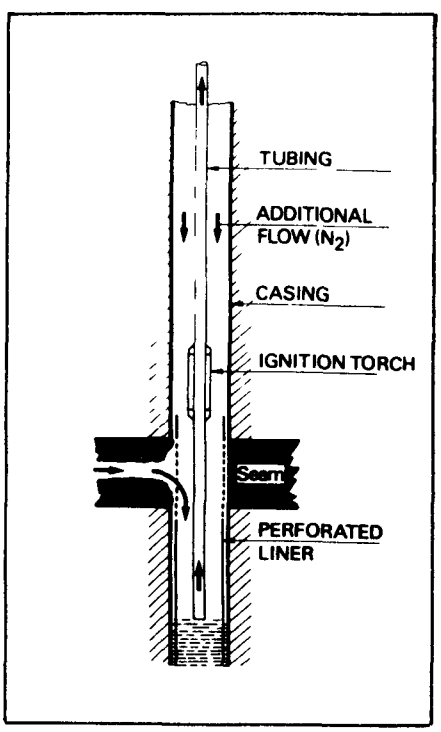

Figure 5. Device for extraction of water

2.5 UNDERGROUND GASIFICATION OF DEEP COAL ELECTROLINKING EXPERIMENTS*

J. LESSI, J. MARRAST, P. PERREAU
Institut Français du Pétrole
RUEIL MALMAISON, FRANCE 92506
R. SIMAND
- Charbonnage de France -
Houillères de la Loire
42000 SAINT ETIENNE - FRANCE

ABSTRACT.

In France, the Groupe d'Etudes de la Gazéification Souterraine du Charbon (G.E.G.S.)** is interested in the possibility of extracting deep coals (depth greater than 800 meters) by the mean of in situ gasification.***

A major property of coals at this depth is their very low permeability. So the main problem encountered in the gasification process is the need, before any other operation, of a hydraulic prelinking between two wells. Among the methods considered for prelinking (particularly hydraulic fracturing and monitored drilling) electrolinking has been studied and tested through several experiments for two years.

The electrolinking method consists in creating between the two wells a coke channel by injecting a strong electric current. When this is possible, the method has the major advantage of realizing a prelinking which remains inside the coal seam.

The main problem of this technique is the level of the necessary electric power when the distance between two wells is large (about 60 meters).

Laboratory tests on blocks of decimetrical size and small scale tests (1,2 and 3 meters) on a coal outcrop have been achieved, these experiments enabled extrapolating the parameters of a test between two wells, their mutual distance being 10 meters and the depth of the coal seam being 30 meters.

A first test was made in March 1982, 14.5 hours and a peak power of 2 MW were necessary to establish a channel.

A second experiment has been made at the end of May 1983, and it was possible to obtain the electrolinking under better conditions, particularly by reducing the maximum necessary electric power. The permeability of the coke channel reaches several darcy.

* Communication presented on behalf of the Technical Committee of Groupe d'Etude de la Gazéification Souterraine (G.E.G.S.).

** The G.E.G.S. (Groupe d'Etude de la Gazéification Souterraine du Charbon) is formed by : Bureau de Recherches Géologiques et Minières, Charbonnages de France, Gaz de France, Institut Français du Pétrole.

*** This project is supported by the E.E.C. (Communauté Economique Européenne), the French Department of Industry and Research (Ministère de l'Industrie et de la Recherche).

INTRODUCTION

The underground gasification of coal implies the possibility of circulating a gas between two bore-holes with adequate pressure and flow rate.

In the case of deep coal deposits which present very low permeability i.e 10^{-6} to 10^{-5} Darcy, a preliminary linkage of the holes by a hydraulic process is required before the final linkage is made for example by applying reverse combustion ; this process requires to inject adequate quantities of oxygen in more or less deluted form and at sufficiently low pressure to avoid any risk of self-ignition into the injection bore-hole (1).

An alternative method of linking bore-holes, other than reverse combustion, was tested in the nineteen fifties in the U.S.A., UK and RUSSIA ie electrocarbonization. This process consists in developing a channel of coke between two bore-holes by applying a relatively high voltage electric current (several thousands of volts) ; the coke channel presents sufficient permeability to make possible the circulation of gas flow rates which are necessary for coal gasification around the channel.

The electrocarbonization process which is based on the electric properties of coal and their evolution with temperature, presents the advantage of not being sensitive to the very low permeability of deep coal deposits.

The French Research group on coal gasification (G.E.G.S.), has undertaken for the past 2 years several studies and experimental trials on the electrocarbonization process, with a view to developing this technology either for achieving a hydraulic prelinkage of bore-holes prior to enlarging the communication by reserve combustion, or for achieving directly a hydraulic linkage which would permit counter-current gasification of coal.

I. PREVIOUS EXPERIENCE WITH ELECTROCARBONIZATION.

Electrocarbonization tests were conducted between 1947 and 1955 in the U.S.A., UK and USSR.

The first studies on the subject were carried out in the laboratory at the Missouri School of Mines ; this research work enabled to identify the characteristic evolution of the electric resistance of coal under the influence of an electric current. The work was followed by a site trial at Hume, Missouri in a 60 cm thick bituminous coal seam lying at a depth of 10m. Electrode distances varied from 7 to 20 meters (2).

Site experiments were also conducted after 1951 at Gorgas, Alabama by the US Bureau of Mines and the Alabama Power Company. The trials were made in a 1 m thick bituminous coal seam lying at a depth of 60 m. Electrode distances varied from 25 to 55 meters. Three trials enabled to develop a linkage between two electrodes separated by a distance of 50 m. However, except for the first test the channels that were obtained presented an unexpected path as they did not link two electrodes used during a given trial but one of the electrodes to a channel which was already formed (3).

The above trials made it possible to establish the following results (2) :

- The electrical resistance between the electrodes when the electric linkage is obtained is practically the same for the 3 trials at 50 m distance between electrodes.

- The electric voltage which is necessary to develop a channel in the coal varies little with the distance between electrodes.

- No determination of the maximum distance at which a linkage could be obtained was made.

Practically at the same time, the US Bureau of Mines conducted a series of laboratory tests and small scale site trials (4). This research work enabled to investigate the form of coke channels as a function of coal stratigraphy i.e. zonal distribution. It should be noted here that no coke channel was obtained for a distance between electrodes greater than 2.3 m, probally due to the insufficient electrical equipment i.e. the electric power available was too small.

In view of the promising results obtained at Gorgas Alabama, electrocarbonization tests were conducted in the UK in 1953 and 1955 at the test sites of Baytor and Newman spinney (5).

Distance between electrodes varied from 10 to 50 m. A great number of problems associated with the technology of bore-holes equipment and electrodes were solved during these tests.

The trials that were successful, were characterised by a low value of electrical resistance, a satisfactory hydraulic linkage and a bore hole distance no greater than 15 m. The electric power available (1500 KVA) appears to have been to small for greater distances between bore-holes. Although the site was subsequently mined out, very little data were obtained on the form of the coke channels, because when a hydraulic linkage was successfully completed, a gasification test was conducted afterwards.

The results of the tests that were conducted in the UK led to abandonning the concept of electrocarbonization for underground gasification of coal because the technology was found to be unreliable, in its place it was deemed preferable to adopt a method of hydraulic linkage based on directional drilling.

Very little information is available on research work conducted in the USSR (6-7) but it seems that the results obtained were more successful that in the UK. Electrocarbonization, as a method for developing a hydraulic linkage between 2 bore-holes was applied at least until the mid nineteen sixties.

Little work has been carried out until recently (8) to understand the processes involved in electrocarbonization. Two phases are generally distinguished i.e. a first phase which is characterized by a high electrical resistance and a high voltage ; this is identified as the electrolinking phase ; a second phase characterized by a lower resistance between electrodes and during which the voltage must gradually be decreased. This second phase is generally identified as the electrocarbonization phase ; this phase will hereafter be referred to as the coke channel development phase, the term electrocarbonization being reserved to the process considered as a whole.

This bibliographical study outlines the two main factors at play in an electrocarbonization test i.e. the electric power available and the reliable performance of the electrodes and equipment in the bore-holes.

It seems,indeed , that there are 2 main causes of failure to complete a coke channel between two bore-holes i.e. the thermal destruction of the electrodes or power cables on the one hand, and the insufficient electric power available for a given distance between electrodes on the other hand.

In view of these findings,the research programme that has been established by G.E.G.S. for investigating on the electrocarbonization process comprises different types of tests :

- laboratory tests on coal blocks of decimetrical size with a view to better understanding the processes involved during the development of a coke channel, and determining the electrical power required.

- small scale trials conducted on a coal outcrop with varying distances between electrodes of the order of one meter The purpose of these trials is to determine the physical laws which govern electrical power required.

- two trials at a decametrical scale of electrode distance, using parameters extrapolated from the previous trials

with a view to possibly preparing full scale trials with bore-holes spaced at 60 m, at a depth of 1000 m which is the goal assigned to G.E.G.S.. The 2 trials described above should also enable to develop technology for manufacturing electrodes and bore-hole equipment.

II LABORATORY TESTS

Laboratory tests were conducted on blocks of coal of different origins i.e. Nord-Pas-de-Calais,Centre Midi and Lorraine. The coal blocks of parallelepiped form have an average dimension of 30 cm. The electrodes are placed in the middle of the coal block at a distance of approximately 10 cm.

The tests have enabled to establish a number of results regarding the level of voltage required to achieve electrocarbonization, and to improve the understanding of the process before and during the completion of the coke channel.

II.1 Difference of voltage between electrodes required to develop electrocarbonization.

The level of voltage differential that is required to develop a process of electrocarbonization is highly variable from one block to another depending on the origin of coal, on the difference of nature of the coal between two blocks from the same seam, and on the degree of saturation of the block.However, it can be noted that a voltage of 2000 volts was required in most cases.

Tests were also conducted with deliberately lower values ; these led to the following results :

- under a certain value of voltage, no electro-linkage is obtained.

- the voltage that must be applied to the electrodes to develop subsequently a coke channel is then greater than the voltage that would have been required if the low voltage phase had not been applied. The resistance between the electrodes before the electrolinking occurs is also higher, possibly due to a substantial effect of drying up. However this dessication is probably greater in the laboratory because of the small dimensions of the test blocks.

II.2 The electrolinking-phase

The electrolinking- phase is characterized by a high value of resistance at least in the case of laboratory tests or trials in which the electrodes are placed at a short distance. During this phase, a high voltage (approximately 2000 V) must be applied between the electrodes ; a more or less regular decrease of resistance between electrodes can be noted. The completion of this phase of the process is obtained, in the laboratory, when a brutal short-circuit occurs. The phase of channel development is thereafter conducted, with a lower voltage. Maximum power is consumed at the end of the electrolinking phase when the voltage applied is still high and the resistance between the electrodes is the smallest. Because this phase of the electrocarbonization process is believed to be critical, it was decided to conduct a series of tests in which the process would be interrupted immediately after electrolinking was completed in order to make observations on what had happened.

Figure 1 shows the result of one of these tests. The test block has been sectioned along the center plane of the segment joining the two electrodes. The value of the resistance measured with an ohmmeter between the surface of the block and the corresponding electrode has been indicated on the photography of each block section. The resistance between any point of the block and the electrode is in principle infinite.However it is possible to delimit several zones of least resistance (figure 1).

These zones are distributed over each section of the block and are often located nearly preexisting fissures in the coal.

Moreover it can be noted that the zones of least resistance do not correspond on both sections of the block except in one case. The electrical continuity from one electrode to the other could therefore only be completed through this particular zone and this is probably where the coke channel would have developed if the test had not been

interrupted for observations.

The development of the coke channel appears to result from the random correspondance of two electrically conductive paths having developed around each of the electrodes. The others paths are then abandoned due to the decrease of voltage and one unique channel will develop during the second phase of the process.

II.3 The phase of development of a coke channel.

The size of the coke channel obtained during the phase of development directly depends on the time this period lasts. The electrical resistance between the electrodes is smallest when the time of development of the coke channel is great.

However in the case of the laboratory tests, the development of a coke channel is limited due to the dimensions of the test block.

Coke swelling provokes, indeed, the breakage of the test block.

Fig. 2 shows a coke channel obtained after a short time of development. The almost constant cross-section of this channel suggests a radial development in a plane transverse to current intensity which is principally concentrated in the channel during this phase of the process.

In some cases where the phase of channel development was carried out during a longer period of time, an accumulation of coke around the electrodes can be noted . This effect was never noticed when the phase of development extended only over a short period of time.

III SMALL SCALE TRIALS

III.1 Introduction

The bibliographical study and laboratory tests lead to formulating the two following conclusions :

- a voltage of several thousand volts is necessary to obtain an electrolinking.

- The electrical power required appears to be strongly related to the distance over which it is desired to obtain electrolinking. The electrical power applied in the laboratory tests was approximately 100 W.In order to improve on the reliability of extrapolating the electrical power required for an electrocarbonization linkage of 2 bore-holes separated by a distance of the order of 10 m, several small scale tests were first conducted on the outcrop of a coal seam

Distances between electrodes were respectively 1, 2 and 3 meters.

The electrodes were constituted by a steel cylinder of 30 mm diameter and 10 cm long, fitted at the end of a steel tube of 22 mm diameter and 2 m long. This tube was used to supply the current and enabled to introduce a thermocouple inside until contact was made with the electrode.

An outer concentric mica tube isolated the steel tube from the coal (fig. 3).

The electrodes were placed loosely in the holes of 1,70 m length, 40 mm diameter; they were then forced into the coal by hammering them in, on a depth of several centimeters.

A certain number of electrodes for monitoring purposes, identical to those described above, were used to monitor the evolution of voltage and temperature (fig. 4).

Electrical power was supplied through a transformer of 20 KVA which gave a maximum voltage of 5000 V and a maximum current intensity of 100 Amps under 180 Volts.

III.2 The electrolinking phase

Electrolinking was obtained during the tests having electrodes placed at a distance of 1 and 2 meters. No electrolinking was obtained when the electrodes were placed at 3 m distance (2 trials).

Figures 5 , 6 and 7 show the evolution of voltage and electrical power VS time for trials n°2 (distance between

electrodes of 1 m), n°4 (distance 2 m) and 5 (3 meters). Figures 5 bis- 6bis and 7 bis show for the same trials the evolution of resistance between the electrodes.

In the case of trials n°2 and n°4, electrolinking was completed with a voltage of 2500 V. The power dissipated just before the channel occurred was respectively 6 KW and 22 KW. The resistance between electrodes at this moment was respectively 945 ohm and 285 ohm. The initial values of resistance were 2000 ohm and 2500 ohm respectively.

During trial n°5, the 2500 volts voltage was insufficient. At this value, the resistance between electrodes increased in 4 hours time from 375 ohm to 590 ohm. At the next voltage increment (3000 volts), the transformer was saturated and the level of power dissipated was approximately 24 KW (fig. 10 and 10 bis).

During this phase, no significant increase of electrode temperature was noted; electrode temperature stabilizes at approximately 100°C. The thermocouples fitted to the monitoring electrodes indicated no temperature variation.

The subsequent mining out of the site of trial n°5, as well as of the site of trial n°3 (with a distance of 3 m between electrodes for which electrolinking did not succeed), shows no evidence of coke accumulating around the electrode.Nor was there any evidence of modification of the environment either by visual observations or by measuring with an ohmmeter. However, the coal around the electrodes was necessarily modified as the resistance between electrodes which was initially 1700 ohm decreased to an ultimate value of 370 ohm (trial n°5 - figure 7 bis).

III.3 Phase of coke channel development.

When electrolinking was obtained, the coke channel developed while continuing to dissipate energy under gradually lower values of voltage.

In the case of trial n°2, channel resistance fell from 14 ohm to in 6 hours 45 minutes time. The voltages applied varied from 200 V to 38 Volts. A total energy of 80000 KJ was dissipated during this phase.

During trial n°4, the resistance between electrodes fell from 40 ohm to 0,53 ohm during 11 hours time while voltage decreased from 130 volt to 57 volt and total energy dissipated was 275000 KJ.

Mining out of the site of trial n°2, showed a coke channel of almost cylindrical form with an elliptical cross section. The small axis of the ellipse was transverse to stratification and was 14 cm long ; the grand axis was 15 to 26 cm long. The volume of coke formed was estimated to be 37 dm^3.

The coke channel obtained during trial n°4 presented a more complicated path (fig. 8).

Total path length was 3.20 m -its cross section was also elliptical, with the small axis transverse to stratification and a length of 7 to 10 cm ; the grand axis was 14 cm long. The volume of this second channel was estimated to be 60 dm^3.

By comparing the quantity of energy dissipated to obtain these coke channels, it can be seen that for trial n°2 2000 KJ/dm^3 were used instead of 4600 KJ/dm^3 in the case of trial n°4. It seems probable that in this latter trial the dimensions of the channel were stabilised before the trial was interrupted ; the additional power received was therefore used to compensate for heat losses by leakage without producing any more coke.

Channel cross-sections show an elliptical concentric form suggesting a radial process of channel development and radial contraction fissures (fig. 9). Reflectance measurements along a radius, show an evolution of maximum temperatures varying from 400°C to 1000°C from the periphery of the channel to its core.

IV ELECTROCARBONIZATION TRIALS BETWEEN BORE-HOLES SEPARATED BY A DISTANCE OF 10 M.

IV.1 Introduction

Two trials were conducted to obtain

electrocarbonization between 2 bore-holes separated by a distance of 10 m; these trials were carried out at the site of Echaux near Saint-Etienne in the center of France. The coal seam which is approximately 2 m thick lies at an average depth of 35 m at the test site (fig. 10). Coal quality is 25 to 55% ash and 18% volatile matter.

Petrography analysis, shows the macerals contained are 95.5% vitrinite 4.5% inertinite and the average reflectance is 1.7% (9).

The objectives of these two trials were the following :

- to verify the possibility of achieving an electrocarbonization channel over a relatively long distance, near to the distance considered as economically viable (60 m).

- to verify the extrapolation of requisite electric power.

- to improve on bore-hole equipment

- to quantify the hydraulic parameters of the channel.

- to provide direct observation of the results obtained by mining out coal within a short time.

The extrapolation of the electric power required from the small scale trials leads to a value of 700 KW. In view of the uncertainty of this estimate, due in particular to the influence of the seam walls that present a lower resistivity than the coal (120 ohm meter instead of 800 ohm meter), a maximum power of 2000 KW was adopted for a distance between the bore-holes of 10 m.

The monophased transformer that was installed on the site enables to modify voltage applied by increments of 150 volts up to a maximum of 6400 volts. Maximum intensity is 1000 amps, under voltages lower or equal to 1000 volts.

IV.2 Trial Echaux n°1

Trial Echaux n°1 took place in the southern part of the site of Echaux (fig. 10). The 3 bore-holes F3, F4 and F5 were sheathed with a fiberglass casing agglomerated with an epoxy resin. This casing provides electrical isolation between the bore-hole and the strata up to a voltage of 10 KV.

Bore-holes F3 and F5 were fitted with an electrode of 1 m height, whose diameter could be expanded from 125 to 150 mm. This electrode fitted to the coal wall left open and permitted the passage of a current of 1000 amps. Current was supplied by 3 copper wire cables.

The electrode is mechanically connected to a tubing of 2" 7/8 diameter. The circulation at the bottom of the bore-hole is made possible between the annular space left between the 2" 7/8 tubing and the 7" fiberglass tube and the inside of the tubing (fig. 11).

Bore-hole F4, located at 2 m from bore-hole F5, was used to measure the voltage at the level of the coal seam.

The equipment available at the surface made it possible for this trial to maintain the bore-hole under nitrogen atmosphere, the two phase production (liquid-gas) under counter pressure, the separation liquid-gas with separate counting of the volumes produced, and gas analysis by gas chromophotography.

Figures 12 and 12 bis show the evolution of voltage, calculated power and resistance between electrodes, as a function of time.

The bore-holes, as well as monitoring bore-hole F4 started producing pyrolysis gas under a back pressure of 4 bar, 8 hours after the trial was initiated. The gases produced was made up of a mixture of carbon dioxide, carbon monoxide, hydrogen and methane (table 1).

During the entire period of electrolinking, the voltage of bore-hole F4 increased steadily until it reached after 11 hours, the voltage of electrode F5. The electrical resistance between the 2 electrodes was then 30 ohm.

The electrolinking was obtained after a time of 14,5 hours under a voltage of 5600 volts. The power dissipated was at that moment 1.9 megawatt and the resistance between the electrodes 16.5.

ohm.

The phase of coke channel development then started. The resistance of the channel after one hour was 1 ohm (800 amps with a voltage between electrodes of 800 volts). This phase could not be continued due to the destruction of the electrodes.

On dismantling the bore-hole after the trial, it was noted that the electrode of bore-hole F3 had effectively been destroyed ; the 2 " 7/8 diameter tubing had melted 4 m above the bottom of the hole.

However, the electrode of bore-hole F5 had remained unaltered although the state of bore-hole F4 proves that a very high temperature was reached as evidenced by melting of the steel tube.

All this evidence points out that the destruction of the electrode of bore-hole F3 was caused by extremely hot gases (steam and pyrolysis gases) rather than by electrical problems.

The poor condition of bore-hole F3 as well as the insufficient time of the carbonization phase did not permit to carry out any quantitative trial for testing the hydraulic flow between the bore-holes.

The main conclusions that can be drawn from these results are the following :

- the electrical parameters which were extrapolated from the laboratory tests and from the small scale trials, were roughly confirmed. The maximum power and total energy used are however greater than were expected. An explanation for this may be that the seam roof and floor are more conductive than the coal itself. Another possible explanation might be the fact that higher voltages were used during this trial than during the small scale trials.

- it seems that by monitoring the electrical tension in monitor holes placed near an electrode, it is possible to obtain data on the way the process develops during the electrolinking phase.

- the level of temperature attained is very high at least during the phase of coke channel development (approximately 1500°C).

These conclusion enabled to formulate recommendations for conducting the next trial Echaux n°2. These recommendations were the following :

- modification of bore-hole equipment as well as surface equipment in order to protect against the effect of excessive heat.

- utilisation of several monitoring bore-holes.

- attempt to reduce the level of voltage to be applied with a view first to decreasing maximum power used at the end of the electrolinking phase and also possibly to reduce the temperatures attained.

IV.3 Trial Echaux n°2

In this trial, the electrodes were slightly modified in order to permit fluid circulation between the annular space and the inside of the tubing under the electrode (fig. 13).

The surface equipment was designed to permit a continuous scavenging of the electrodes by a nitrogen gas flow that was as high as 50 NM^3/h.

The equipment also provided a discontinuous injection of water in order to cool the electrodes if necessary. Also the effluent gases were cooled down by means of an aerorefrigerator which totally condensed the water vapour.

As these equipments were to operate even when the electrodes were under tension, an auxiliary low voltage supply unit, provided by isolation transformers had to be installed (fig. 14).

Twelve monitoring bore-holes each fitted with an electrode for measuring the voltage, and having a thermocouple were drilled upon the test site mainly around the electrode F6 (fig. 15).

The complete set of measurements can be processed in real time by a minicomputer which produces an image of the voltage field during the electrolinking phase.

Trial Echaux n°2 took place from 25 to 27 may 1983 ; the full quantity of data obtained has not yet been processed particularly the measurements of temperature and of voltage fields.

Figures 16 and 16 bis show the evolution of Voltage between electrodes, power dissipated and resistance between electrodes vs time during the electrolinking phase.

An increase of voltage in the monitoring bore-holes was noted during this phase; this is characterized by a dilation of the iso-tension lines around the electrodes and their deformation towards the other electrode (fig. 17).

Two hours after the trial was initiated, bore-hole M4 had reached the same voltage as electrode F6 ; at the same time, bore-hole M9 was at the same voltage as electrode F8. Bore-hole M12 increased in voltage after 4.5 hours but a lack of isolation at the wellhead led to interrupt the trial during almost 24 hours.

The electrolinking was finally completed after the voltage was applied during a total time of 10 hours.

The voltage used was 4200 volts while power dissipated, just before the linking was completed, was approximately 1.4 megawatt and the resistance between electrodes was 13 ohm.

Electrode temperature was kept at approximately 150°C. The analysis of effluent gases is given in table 2.

The coke channel was then developed under voltage decreasing gradually from 1900 V to 220 V (fig. 18). The final resistance attained during the trial was 0.25 ohm. Total energy received during this phase of channel development was 2 megawatt hour or $7.2\ 10^9$ Joules.

These electrical data make it possible to give a preliminary estimate of channel dimensions based on the extrapolation of coke channels obtained during the small scale tests.

Assuming a channel of cylindrical form 10 m long, by extrapolating from the values of resistance, the diameter of coke channel would be between 35 and 60 cm.

If we consider the total energy used during channel development, the volume of coke yielded by the progess would be between 1.5 m^3 and 3.3 m^3 ; therefore if the same form as above is assumed, the diameter of the channel would be between 40 and 65 cm.

Nitrogen flow tests between boreholes F6 and F8 were undertaken immediately after switching off the electrical tension ; the permeability evidenced by these tests was poor. But the same tests repeated after one week of cooling down showed a conductivity between bore-hole of approximately $7,10^{-2}$ Darcy meter (table 3) i.e. a permeability of 5 Darcy if it is assumed that the channel is a cylinder of 10 m length and 40 cm diameter.

V CONCLUSIONS

This comprehensive series of electrocarbonization tests has permitted to attain the objectives that were assigned i.e. :

- to demonstrate the feasibility of producing a coke channel between 2 boreholes separated by a distance of 10 m. It was possible to protect the equipment of the bore-holes from the destroying effect of heat by subjecting the holes to a circulation of nitrogen and water.

- to demonstrate the possibility of reducing the maximum power required to produce a coke channel by decreasing the voltage differential between the electrodes.

- to verify the quality of the hydraulic link achieved. The results obtained during trial Echaux n°2 enabled to extrapolate in the case of 2 bore-holes separated by a distance of 60 m, a hydraulic linkage which would be at least sufficient to permit reverse combustion.

This research has also enabled to verify experimentally the process of electrocarbonization i.e. :

- a phase of steady development of zones where electrocarbonization reactions occur at a more or less microscopic scale. These zones which are characterized by a low value of macroscopic reactivity, develop in a pseudo-radial man-

ner around each electrode, with increasing deformation towards the other electrode.

- a phase which is superimposed on the latter and which is characterized by the development, in increasing numbers, of zones of instabilities and paths which are caused by the random development of cokefied zones.

- when two of these paths connect together, a coke channel is obtained.

The level of power dissipated when the coke channel is completed is a function of the dimensions of the carbonized zones (these dimensions in turn , depend on the distance between the electrodes), and of the voltage used. The voltage level affects the process in two ways :

-first a higher voltage accelerates the development of a coke channel (below a certain minimum value of voltage, the development of a channel is impossible);

-Second, a high voltage accelerates reaction kinetics and enables to obtain higher value of thermal gredients locally which reduces consequently the influence of dried up areas. This result in a lower value of resistance before the coke channel develops which means a higher value of power consumption.

The problem which is emphasized at this stage of the research programme concerns the possibility of obtaining reliably a coke channel over a distance between electrodes of 60 m.

By extrapolating the values of power obtained during the small scale tests and during trial Echaux n°2, the power required would be 40 to 50 MW. However it should be noted that if the power used was reduced during trial Echaux n°2, it has not yet reached optimum value. If one considers 700 KW as the minimum value of power required for a distance of 10 m between electrodes (which results from extrapolating the small scale tests to a distance of 10 m), one obtains for 60 m a minimum power of 25 MW.

On the other hand , the application of decreased power, implies using a lower voltage, with the risk of not achieving a coke channel. The random character of successful tests which was noted previously is perhaps due to insufficient electrical power available on the test site.

It is therefore necessary to overcome the difficulties presented by the availability and utilisation of electrical power at site of the order of several tens of megawatt (which corresponds at the levels of voltage used, to current intensities of the order of 10.000 amps). Future research work will therefore concentrate on the following aspects :

- small scale characterization in the laboratory of the carbonized zones which correspond to the phase of steady development of the process and which are responsible for the high power consumption.

- study of these zones on the site by mean of the open-pit mining out after trials Echaux n°1 and n°2.

- investigation on the possibility of combining hydraulic fracturing and electrocarbonization. A combination of these 2 technologies, as already applied in the USSR (7), should be favourable to the development of instable zones and should accelerate the development of a coke channel developing from smaller carbonized zones, with a corresponding reduction of the electrical power required.

REFERENCES

(1) MAJOR PROBLEMS, FIRST RESULTS AND PROJECTS OF UNDERGROUND GASIFICATION OF DEEP COALS IN FRANCE

C. GADELLE and al.

8th Underground coal Conversion Symposium, August 1982.

(2) ASSESSMENT OF UNDERGROUND COAL GASIFICATION IN BITUMINOUS COAL

Process Division of Williams Brothers Engineering Company.

(3) U.S. BUREAU OF MINES TESTS AT GORGAS ALABAMA (1947 - 1959)

D.R. STEPHENS

LLNL Underground Coal Gasification Project

Quaterly Progress Report - July - September 1980.

(4) SIMULATED UNDERGROUND GASIFICATION OF COAL AND ELECTROLINKING - CARBONIZATION METHOD OF PREPARING PATH IN A COAL BED

M.W. WILSON and al.

USBM report n° 5605

(5) BRITISH TRIALS IN UNDERGROUND GASIFICATION (1954-1955)

Ministry of fuel and power

London - Her Majesty's Stationnery Office - 1956.

(6) APPLICATION OF ELECTRIC CURRENT FOR DIRECT ACTION ON A SEAM OF FUEL IN SHAFTLESS UNDERGROUND GASIFICATION

S.T. BONDARENDKO and al.

Academy of Sciences of the USSR Moscou 1959.

(7) COMBINED METHOD OF LINKING BOREHOLES AT THE SHATSKII PODZEMGAS STATION

G.F. KREIN N.S. MIRINGOF

Moscou 1965.

(8) MATHEMATICAL MODELING OF ELECTROLINKING

R.K. TRIDBALL, W.B. KRANTZ, R.D. GUNN

International Gas Research Conference

London June 1983.

(9) LA MICROSCOPIE OPTIQUE QUANTIFIEE DE LA PHASE CARBONE DES COKES

H.G. QIU

Thesis - Université d'Orléans -

May 1983.

Table 1

Experiment ECHAUX 1 : Gas composition

Experiment start : 8h30

WELL F3

Time	N2	H2	CO	CH_4	CO_2
17h10	12	30	7.6	25	20
18h40	4.2	35	10.7	25	20
20h55	8	34	14.7	13.5	20.7

WELL F5

Time	N2	H2	CO	CH_4	CO_2
17h10	5	35	4.5	42	8
18h40	5.7	37	7	35	9
20h55	2.2	40.5	9.7	33	6.7

Table 2

Experiment ECHAUX 2 : Gas composition

WELL F6

Time	N2	H2	CH_4	CO_2
25th May				
12h00	99.3	0.8	-	-
13h15	99	1.25	-	-
14h30	76.3	11.9	5.2	-
16h30	81.1	8.8	4.1	-
18h00	100	0.3	-	-
26th May				
17h30	100	-	-	-
18h00	81.2	8.6	-	-
19h15	76.3	10.0	2.7	2.7
20h15	64.8	14.3	5.6	4.2
21h15	65.1	14.8	3.2	3.5
22h30	43.5	23.6	8.7	7.0

Experiment was stopped at 17h45.

Table 2

Experiment ECHAUX 2 : Gas composition

WELL F8

Time	N2	H2	CH_4	CO_2
25th May				
11h40	98	0.7	-	-
13h00	95.2	1.2	-	-
14h20	89.3	4.0	2.5	-
16h15	98.2	1.1	-	-
18h02	99.4	0.2	-	-
26th May				
17h26	98.4	1	-	-
18h06	92	3.3	0.2	0.9
19h30	77.7	12.8	-	-
20h50	66.9	15.1	2.8	4.6
21h55	44.4	25.2	9	3.5
23h30	27.0	32.9	8.1	5.2

Table 3

Linking permeability

(permeability before linking = 0)

From well F8 to well F6

Pressure F8 (bar)	Pressure F6 (bar)	Flow rate (Nm^3/h)	Permeability $\frac{kS}{L}$ (D.m)	k(D)*
5.5	1.8	14.8	$4.1\ 10^{-2}$	5.8
6	2	18	$4.5\ 10^{-2}$	6.3
7.4	2.7	24	$4.2\ 10^{-2}$	5.9

From well F6 to well F8

Pressure F6 (bar)	Pressure F8 (bar)	Flow rate (Nm^3/h)	Permeability $\frac{kS}{L}$ (D.m)	k(D)*
5.4	0.7	19.3	$5.0\ 10^{-2}$	7.1
6.4	0.7	24	$4.6\ 10^{-2}$	6.5
7.6	0.8	32.8	$4.6\ 10^{-2}$	6.5

* channel diameter 0.3 m
channel length 10.0 m

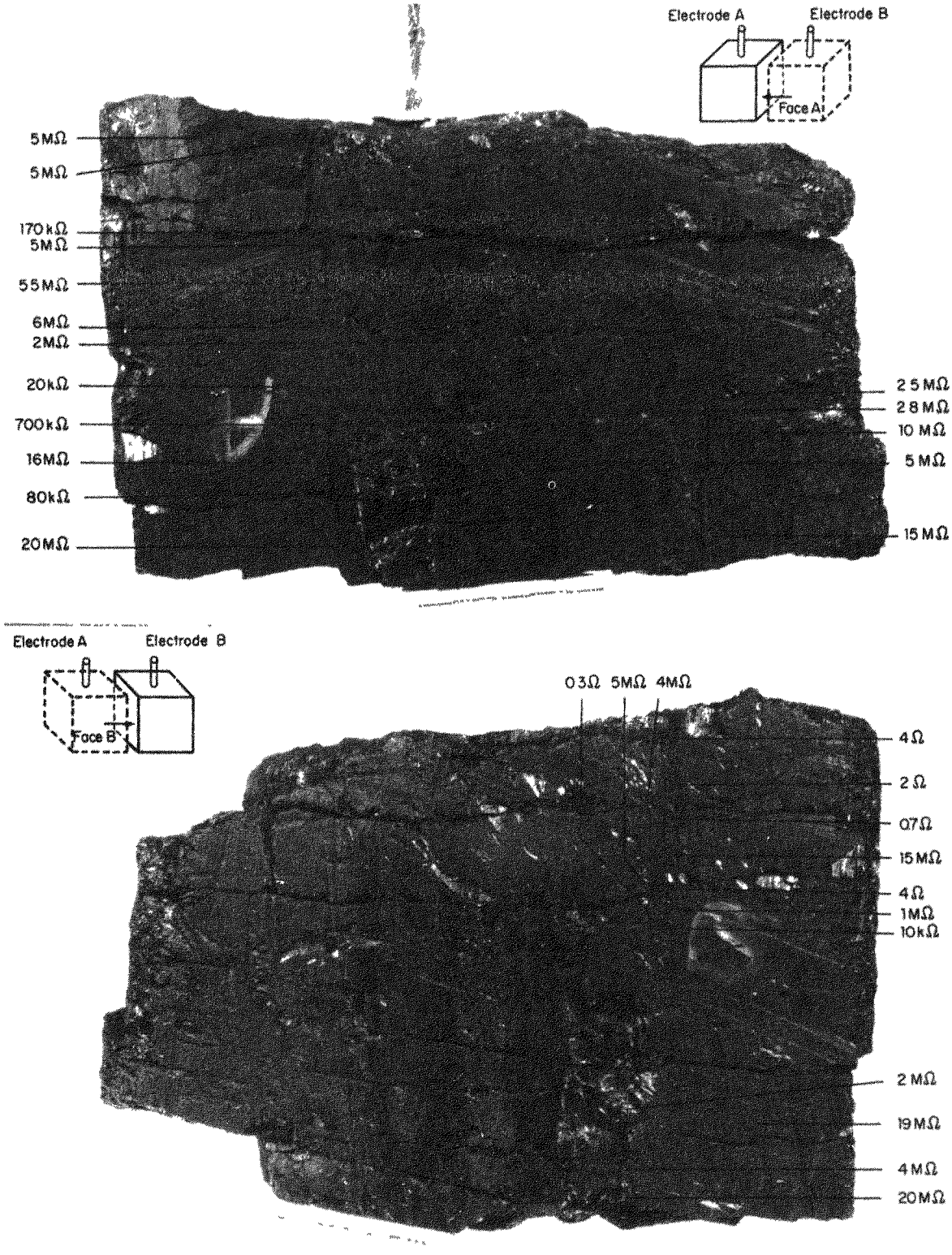

Figure 1 - Laboratory test
Low resistance areas after electrolinking

Figure 2 - Laboratory test
Coke channel

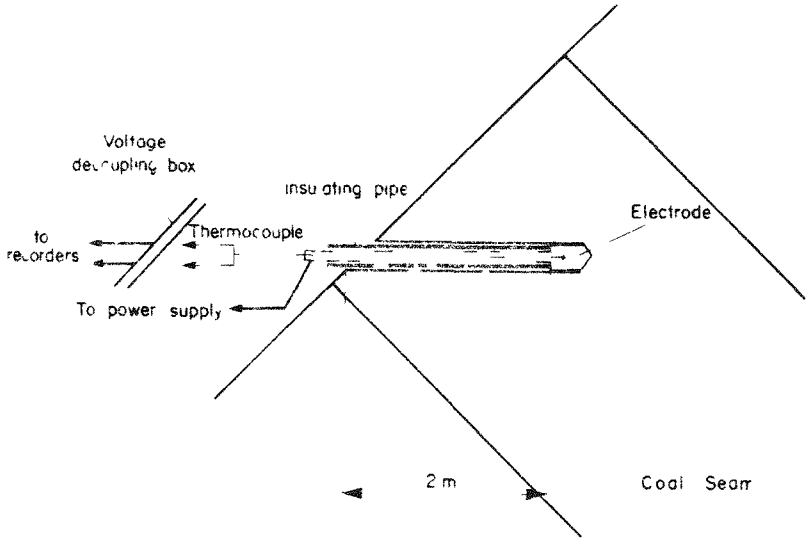

Figure 3 - Small scale experiments
Electrode design

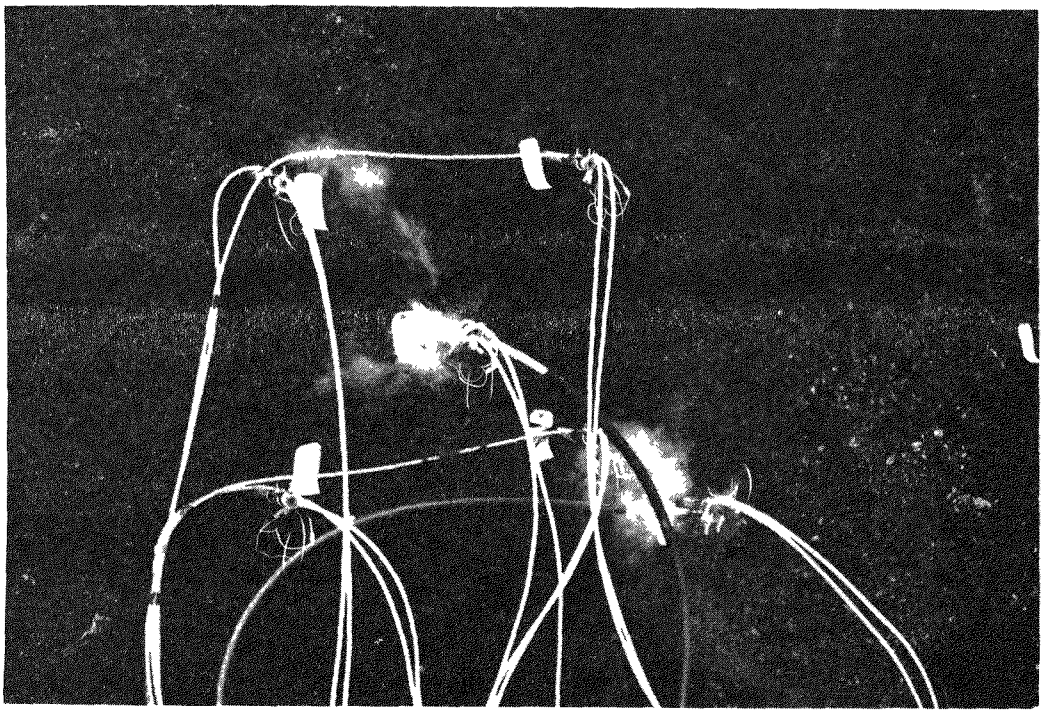

Figure 4 - Small scale experiments
Trial n°2

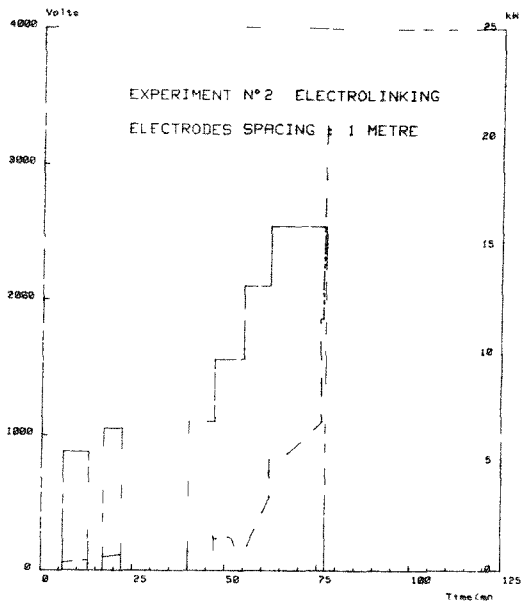

Figure 5 - Trial N°2
Voltage and power v s time

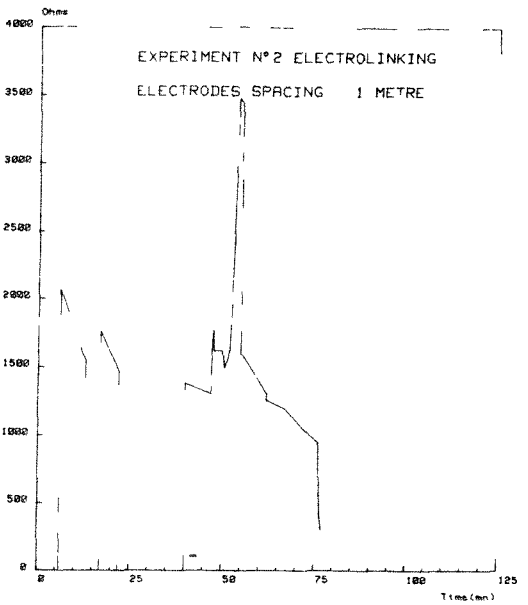

figure 5 bis - Trial N°2
Resistance v s time

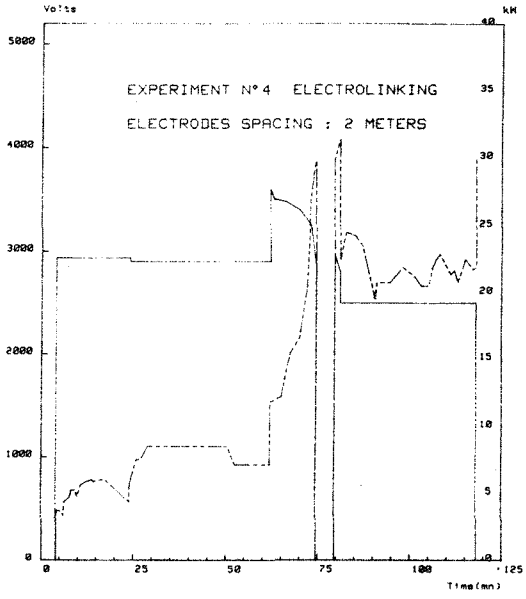

Figure 6 - Trial N°4
Voltage and power v s time

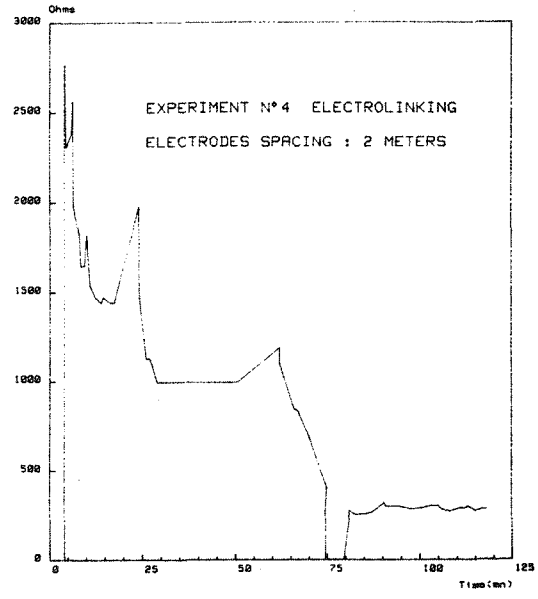

Figure 6 bis - Trial n°4
Resistance between electrodes vs time

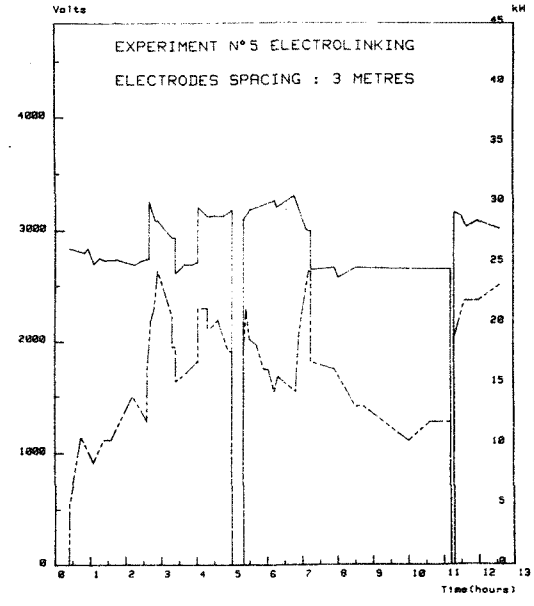

Figure 7 - Trial n°5
Voltage and power vs time

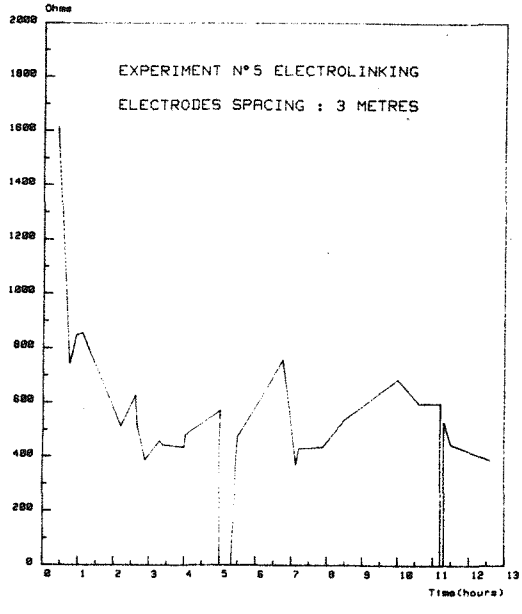

Figure 7 bis - Trial n°5
Resistance between electrodes vs time

Figure 8 - Trial n°4 Coke channel

Figure 9 - Channel cross-section

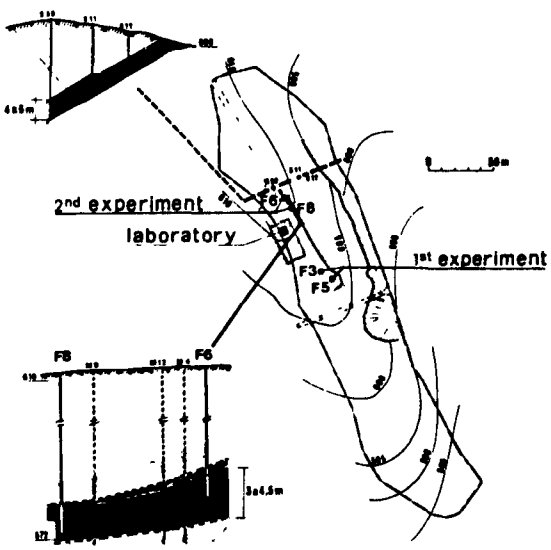

Figure 10 - ECHAUX site

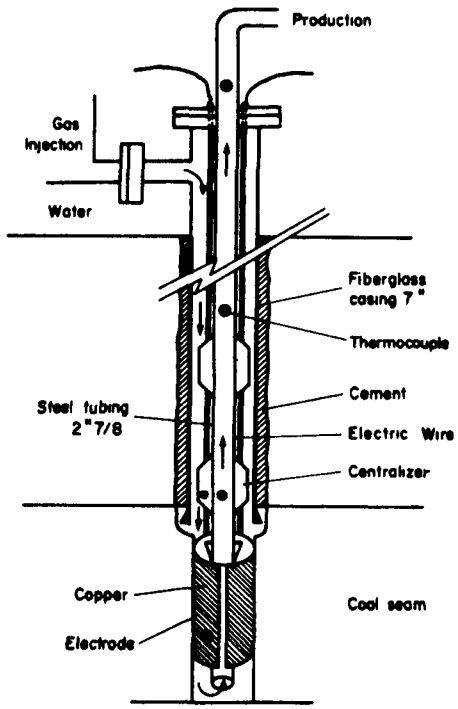

Figure 11 - Well completion

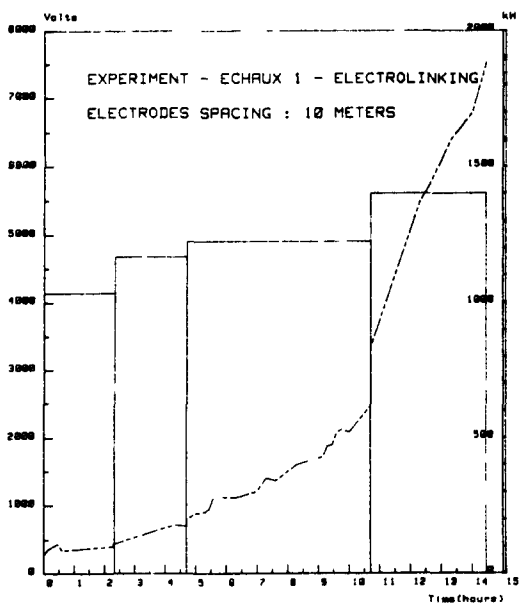

Figure 12 - ECHAUX 1
Voltage and power vs time

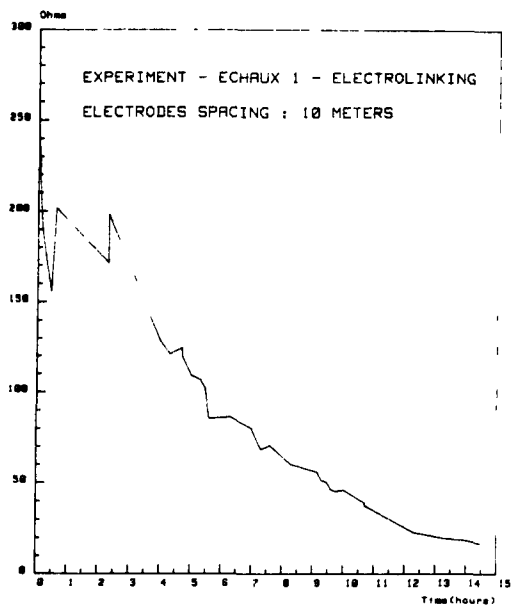

Figure 12 bis - ECHAUX 1
Resistance between electrodes vs time

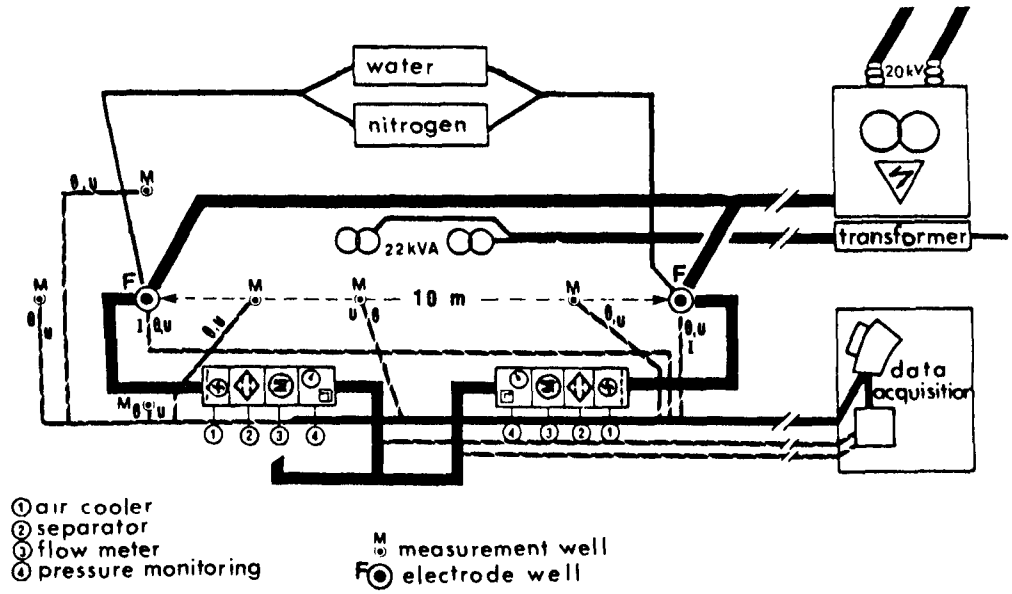

Figure 13 - ECHAUX 2
Surface equipment

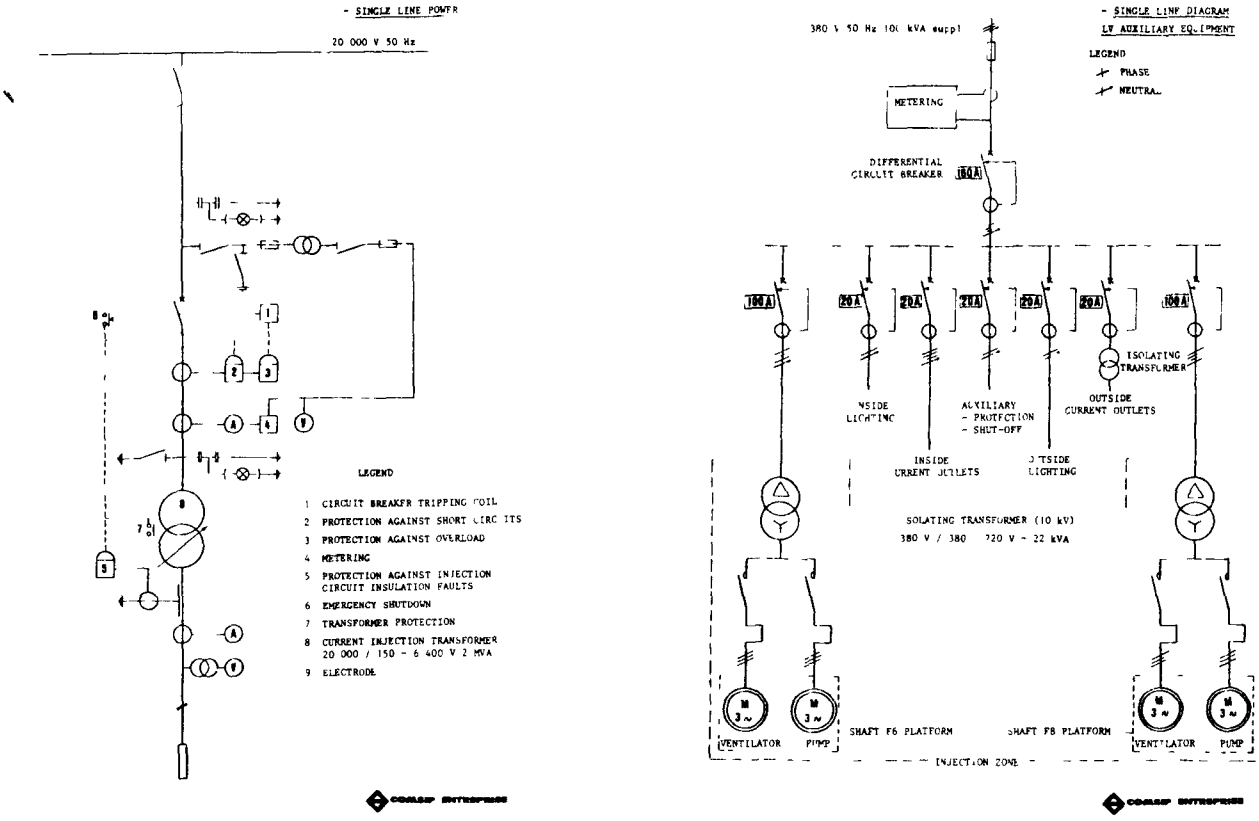

Figure 14 - ECHAUX 2
Electrical equipment

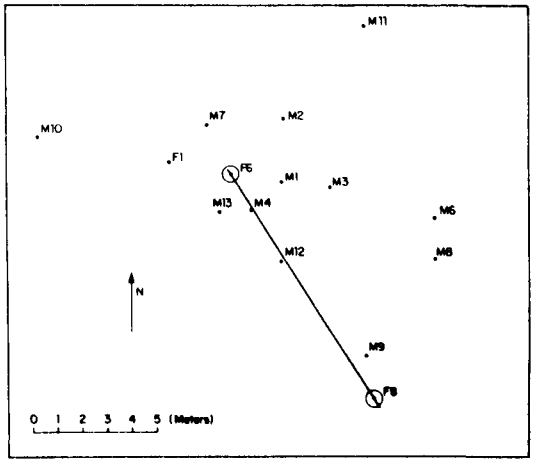

Figure 15 - ECHAUX 2
Wells location

Figure 16
ECHAUX 2
Voltage and power
vs time

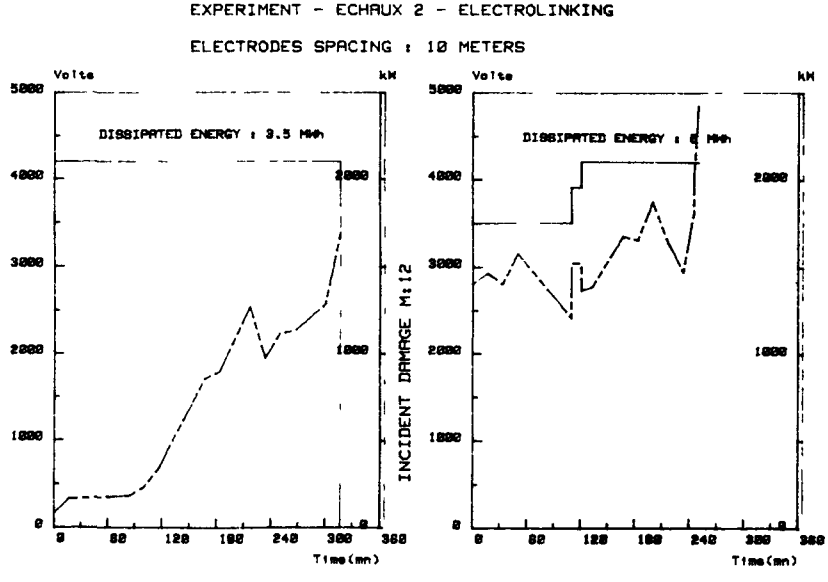

Figure 16 bis
ECHAUX 2
Resistance between
electrodes vs time

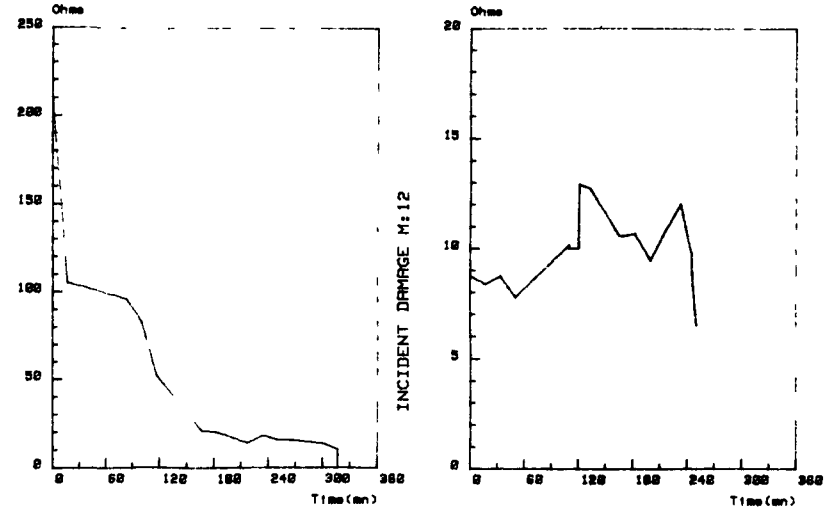

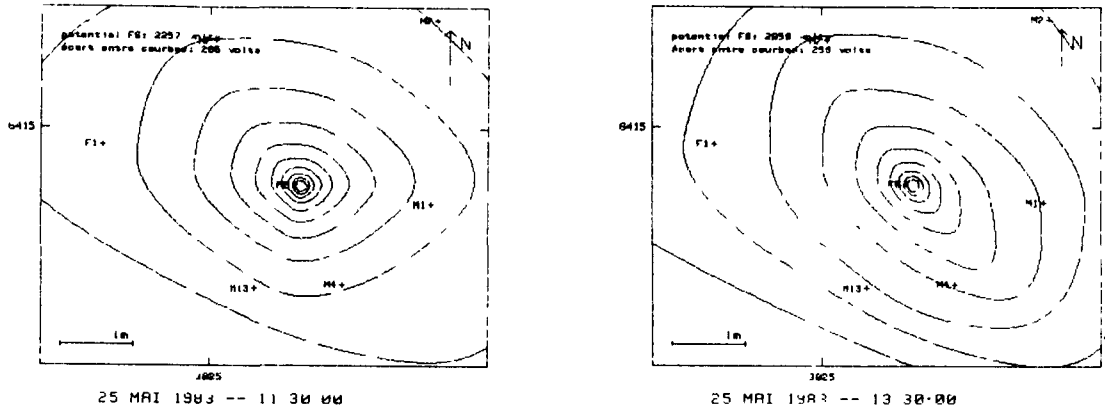

Figure 17 - Equipotential curves during ECHAUX 2 Trial

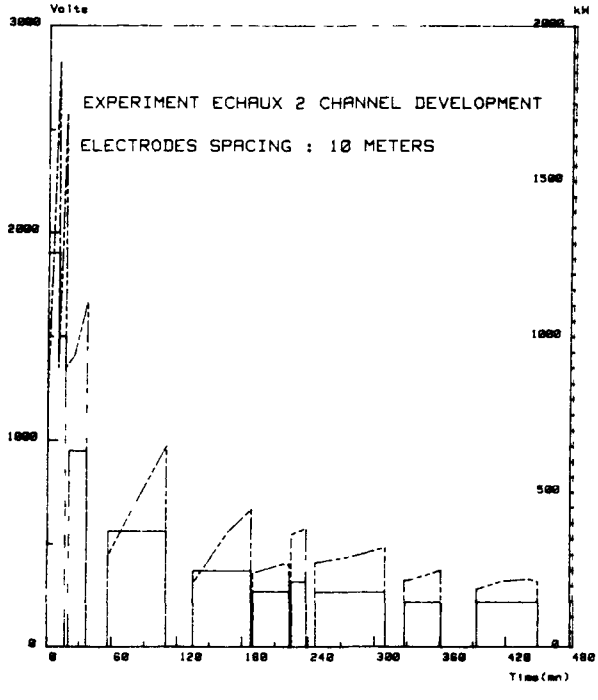

Figure 18 - ECHAUX 2
Voltage and power vs time

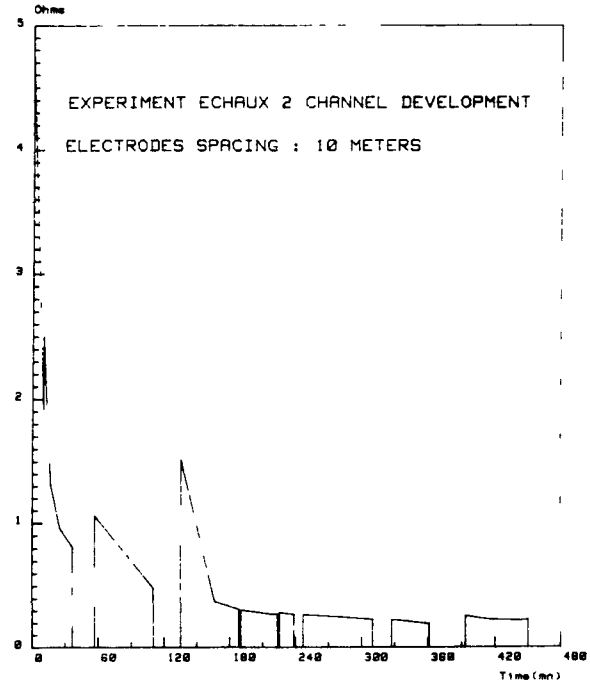

Figure 18 bis - ECHAUX 2
Resistance between electrodes vs time

2.6 A REVIEW OF PRODUCED GAS COMPOSITIONS IN UNDERGROUND COAL GASIFICATION FIELD TESTS IN THE UNITED STATES

by

B. W. Gash[1/]
E. B. Hunt[1/]

ABSTRACT

The data on produced gas compositions from the recent UCG field tests in the U.S. have been studied on a dry N_2-free basis using a ternary diagram to determine the range over which UCG produced gas compositions vary. All the U.S. UCG field test data fall into a very limited area on the CO_2-CH_4-synthesis gas (H_2+CO) ternary diagram. Except for Rawlins T2 and Pricetown, the CH_4 content in UCG field tests has not varied appreciably. The largest variation in UCG produced gas composition occurs in the amount of synthesis gas. Synthesis gas content in the produced gas is inversely correlated with water influx during gasification.

INTRODUCTION

In designing the surface processing facility for a commercial scale UCG operation, one of the important parameters is the produced gas composition. In the single-well pair UCG field tests which have been conducted recently in the U.S., the produced gas composition has varied with time and different well pairs in the same coal seam have had different average produced gas compositions. Because no long-term, multiwell pair UCG tests have been conducted in the U.S., the data on produced gas compositions available from all recent U.S. UCG field tests have been reviewed in this study to determine possible long-term UCG produced gas compositions.

1/ Amoco Production Company, P. O. Box 591, Tulsa, OK 74102

DISCUSSION

Underground coal gasification involves the partial oxidation of coal with air or O_2 to produce synthesis gas, (H_2+CO). The produced gas compositions from air and O_2-blown UCG tests are compared on a N_2-free basis throughout this paper. On a dry, N_2-free basis, UCG product gas consists mainly of four components: CO, H_2, CO_2 and CH_4. (Trace components such as H_2S and C_2 hydrocarbons usually present in UCG produced gas are not considered in this paper.) Considering UCG produced gas as a four-component mixture, all compositions fall within the tetrahedron shown in Figure 1. If, however, H_2 and CO are considered as a pseudocomponent; i.e., synthesis gas; then the UCG produced gas can be treated as a three-component mixture and all possible compositions occur within the ternary diagram shown in Figure 1. It is reasonable to consider synthesis gas as a single component because H_2 and CO are of equal value as products; i.e., they have essentially the same heating value and are easily interconverted using the water-gas shift reaction.

On a dry N_2-free basis, all the UCG produced gas compositions observed in recent field tests in the U.S. fall into the small triangle shown on the CO_2-CH_4-synthesis gas ternary diagram in Figure 2. Figure 3 is an enlargement of the small triangle in Figure 2 bounded by (0.9 synthesis gas, 0.1 CO_2), (0.6 CO_2, 0.4 synthesis gas) and (0.5 CH_4, 0.4 synthesis gas, 0.1 CO_2). Figure 3 also contains a contour plot of the heating value (Btu/SCF) as a function of the dry N_2-free gas composition.

H_2 and CO have nearly the same heating value (324 and 321 Btu/SCF, respectively). The average of these two values was assigned to synthesis gas in making the contour plot. The contours are a series of straight lines because the synthesis gas and the CH_4 heating values blend linearly and CO_2 merely acts as a diluent.

Figure 4 is a plot of gas compositions from the recent U.S. UCG field tests on a dry, N_2-free basis. The compositions for the Hanna, Hoe Creek, Pricetown and Rawlins tests are from the Lawrence Livermore (LLNL) UCG data base.[1] These data are overall average produced gas compositions. That is, each composition is that which would result from mixing all the gas produced during the complete test, including the small amount produced during linking. The WIDCO data are from Reference 2. The WIDCO compositions do not include the gas produced during linking because the link gas was a significant part of the total produced gas in the WIDCO tests. (Figure 4 includes both the Pre-CRIP and Post-CRIP compositions for LBK-1. Only the Pre-CRIP composition is considered in the remaining discussion.) The Tennessee Colony composition is the average of the typical compositions given in Reference 3. As can be seen, most of the UCG produced gas compositions observed in recent field tests in the U.S. fall into a very limited area bounded by 0 and 10% CH_4 on the ternary diagram of Figure 4. Only two UCG pilots in the U.S. have had significantly greater than 10% CH_4 and fall outside the limited area: Rawlins T2 conducted by Gulf and the Pricetown test conducted by the Morgantown Energy Technology Center (METC).

With the Rawlins T2 and Pricetown data excluded, the arithmetic average of the produced gas compositions of the other 18 recent UCG field tests in the United States is 60.8% synthesis gas, 6.7% CH_4 and 32.5% CO_2. The arithmetic average gives equal weight to the compositions from all the other 18 field tests. The average composition represents a composition that would result if all the other 18 U.S. field tests had been conducted simultaneously and the produced gas blended (this assumes each test produced gas at the same rate). The average UCG produced gas composition is more what might be expected in a commercial operation with many well pairs operating than any of the individual tests which usually involved only a single-well pair. (If the WIDCO series of tests are excluded, since the intent of these tests was to study early time cavity growth, the average composition of the other 13 tests is 57.9% synthesis gas, 7.4% CH_4, and 34.7% CO_2.) It is interesting that the average produced gas composition for Angren, the largest scale and longest duration Russian UCG project, falls near the average of the recent U.S. UCG results on the CO_2-CH_4-synthesis gas ternary diagram. At Angren[4], as many as 20 well pairs were operated at one time and the operation lasted around 20 years. The average gas composition for Angren was 59.5% synthesis gas, 2.4% methane and 38.1% CO_2 (Figure 4).

The average U.S. UCG produced gas composition is very close to the produced gas composition for Sasol, the commercial South African surface gasification facility. The produced gas composition for Sasol[5] is 60.8% synthesis gas, 9.7% CH_4, and 29.3% CO_2. UCG produced gas is, therefore, in a compositional range that can be used commercially.

Synthesis Gas-CO_2 Content in UCG Produced Gas

As can be seen in Figure 4, the largest variation in UCG produced gas composition has occurred in the ratio of synthesis gas to CO_2. The lowest ratio was 1.0 (46% synthesis gas and 46% CO_2) reported in the Tennessee Colony test.[3] The highest was 3.2 (71% synthesis gas and 22% CO_2) in the WIDCO LBK-2 test.[2]

A factored economic sensitivity study based on the Williams Brothers Engineering Company (WBEC) data[6] has been made to determine the effect of variations in synthesis gas and CO_2 in the produced gas on the economics of producing SNG from UCG (Figure 5). CH_4 was held constant at 5.7%. The WBEC base case composition, which is very close to the average value of the U.S. UCG field tests, has a "levelized constant dollar" (LCD) price[6] of $4.74/MMBtu. At the highest CO_2 (lowest synthesis gas composition) observed in the U.S. UCG field tests, the LCD price for SNG production is $5.36/MMBtu. At

the highest synthesis gas composition (lowest CO_2 content) the LCD price is \$3.95/MMBtu. Increasing synthesis gas content in the produced gas improves the economics of SNG production from UCG. The economics of liquid fuel production (e.g., methanol and gasoline) from UCG will also improve with increased synthesis gas content in the produced gas.

High CO_2 content in the produced gas correlates with high water content in the produced gas and with high water influx during gasification. As shown in Figure 6, the high CO_2 content produced gas compositions have the highest water-to-dry-gas ratio. Figure 7 shows that high CO_2 content correlates with high water influx into the coal seams during gasification. The data points in Figure 6 are from Reference 1. The data points in Figure 7 were calculated from values given in Reference 1 using the "Balance Results without Char." In Hoe Creek II and III, water influx was the largest source of water, although some water was introduced to cool the product gas.[1] In Hoe Creek III some water was injected with the oxygen. The WIDCO data are not included in Figure 6 or Figure 7 because these were small block tests intended to study early time cavity growth. Water content of the produced gas and water influx data are not available for the Tennessee Colony test. The Russian literature also contains a correlation similar to Figure 7 showing that as water influx increases, the CO_2 content of the produced gas increases.[7] The Russian data are consistent with equilibrium calculations which predict higher CO_2 content at lower reaction temperatures.

Figure 8 is a ternary diagram for coal gasification products with gaseous water as one component and the two pseudocomponents: H_2+CO and CO_2+CH_4. The components used in the ternary diagram in Figure 8 are suggested by the chemical reactions which occur during the UCG process.

After the coal is gasified in the cavity, the gas is cooled during its trip to the surface. The water-gas shift reaction

$$CO + H_2O \rightleftarrows H_2 + CO_2$$

is the only reaction which proceeds at a significant rate during the cooling of the gas.[7] In this reaction the total amount of H_2+CO (synthesis gas) remains the same. Since water and CO_2 are involved in this reaction, the percent of synthesis gas on a dry gas basis would be affected by the water-gas shift. The ternary diagram in Figure 8 is constructed so that water is explicitly included as a component of the mixture. CH_4 is included with CO_2, since both these components reflect low reaction temperatures.

The isotherms drawn in Figure 8 are for thermodynamic equilibrium compositions reported by Stephens and Miller[8] for gasification of a typical Wyoming coal with a pseudomolecule of $CH_{0.858}$ $O_{0.208}$ and various O_2/H_2O ratios at 10 atm pressure. In varying the O_2/H_2O ratio, O_2 was held constant at 0.2221 mole. As can be seen, the percentage of the desirable product, synthesis gas, increases rapidly with increasing temperature.

Such an improved synthesis gas content at a higher operating temperature is observed in surface gasifiers. The Lurgi dry-bottom surface gasifier produces a gas containing about 60% synthesis gas on a dry-gas basis.[9] The produced gas from the Lurgi slagging surface gasifier, however, contains about 85% synthesis gas due to the higher operating temperature of this gasifier.[9]

The U.S. UCG field-test results from Reference 1 are also shown in Figure 8. The data indicate low gasification temperatures during UCG (even though temperatures in the range of 2500°F have been reported[10] during UCG tests), nonequilibrium at a high gasification temperature and/or additional oxidation of the product gas subsequent to gasification. A similar observation was made by Stevens and Miller[11] concerning the Russian UCG produced gas compositions and equilibrium thermodynamic calculations.

In any event, excess water above that required for gasification has been present in all recent U.S. UCG field tests. This excess water reduces the efficiency of the process. Dewatering wells which were used by the Russians

could be used to reduce the amount of water influx. However, in single-cavity (i.e., single-well pair) field tests, a major portion of the water influx is probably due to water contained in pieces of the rock falling into the cavity from the collapsing roof.[12] Dewatering wells would not be useful in this instance. In the Hanna II field test, which involved two linked cavities, a significant part of the water influx in the third phase of the test probably came from the adjacent cavity used in the second phase of the test.[12] In a full field UCG development where many cavities could become water filled after gasification and then affect water influx in adjacent cavities being gasified, dewatering wells might prove useful.

CH_4 Content in UCG Produced Gas

Usually, the CH_4 content of UCG produced gas is less than 10% (Figure 4), and results from pyrolysis of the coal.[7] Only two U.S. UCG field tests have had significantly more than 10% CH_4: Rawlins T2 and Pricetown. The Pricetown results should probably not be considered representative of UCG tests in general because of the swelling bituminous coal at that site and difficulties encountered during the test. No satisfactory explanation has been given for the high CH_4 content observed during Rawlins T2. Rawlins T1 (carried out in the same coal seam) had a CH_4 content consistent with pyrolysis.[13]

Assuming pyrolysis produced the same amount of CH_4 per cubic foot of coal in both Rawlins tests, the high CH_4 content in Module #1 of Rawlins T2 would require the pyrolysis of 164 thousand ft^3 of coal. Preliminary estimates for Rawlins T2, Module #1, show that approximately 350 thousand ft^3 of coal was affected (caved in). Only half of this affected coal would have to be pyrolyzed to account for the CH_4 content produced during Module #1 of Rawlins T_2. Thus with the presently available data, pyrolysis cannot be ruled out as a source of the high CH_4 content during Rawlins T2. (Details of this calculation are included in the appendix of this paper.)

CONCLUSIONS

1. On a dry N_2-free basis, UCG product gas compositions obtained in recent U.S. field tests show little variation. The average gas composition, 60.8% synthesis gas (H_2 + CO), 6.7% CH_4, and 32.5% CO_2, is very close to the produced gas composition observed at Angren, a long-term, commercial scale, Soviet UCG operation. This suggests that in a commercial scale UCG operation with many well pairs operating simultaneously, the average gas composition will be close to the average value of the U.S. UCG field tests.

2. The largest variation in UCG produced gas composition occurs in the amount of CO_2 and synthesis gas. The UCG field tests with high CO_2 content also have the highest water content in the produced gas due to high water influx during gasification. In a commercial scale UCG development, dewatering adjacent cavities may help increase synthesis gas content in the produced gas.

3. A factored sensitivity study based on a Williams Brothers Engineering Company economic study of SNG production from UCG shows that increasing the synthesis gas content in the produced gas improves the economics of SNG production from UCG.

4. Except for Rawlins T2 and Pricetown, the CH_4 content in recent U.S. UCG field tests has not varied appreciably.

REFERENCES

1. Cena, R. J., Thorness, C. B., and Ott, L. L., Underground Coal Gasification Data Base, UCID -19169 Rev. 1, November 24, 1982, Table 19.1, p. 267.

2. Hill, R. W. and Thorness, C. B., "Summary Report on Large Block Experiments in Underground Coal Gasification, Tono Basin, Washington, Vol. 1, Experimental Description and Data Analysis," UCRL 53305 Vol. 1, July 9, 1982, Table 5, p. 29.

3. Grant, J. F. and Fernbacher, J. M., "Tennessee Colony Steam-Oxygen In Situ Lignite Gasification Test," 5th UCC Symposium Proceedings, Alexandria, Virginia, June 1979, Table 1, p. 113.

4. Olness, D., "The Angrenskaya Underground Coal Gasification Station," UCRL 53300, July 17, 1982, Table 13, p. 21.

5. Hebden, D. and Stroud, H. J. F., "Coal Gasification Processes," in Chemistry of Coal Utilization, 2nd Supplementary Vol., M. A. Elliott, ed., Wiley Interscience, 1981, p. 1624.

6. Siegel, M. M., Neinaber, J. H., Gash, B. W., Hill, V. L., and Rosenberg, J. I., "Comparative Economics of Substitute Natural Gas Production by Underground Coal Gasification and Surface Gasification of Western Coal," 9th UCC Symposium, Bloomingdale, Illinois, August, 1983.

7. Edgar, T. F. and Greg, D. W., "Underground Gasification of Coal," in Chemistry of Coal Utilization, 2nd Supplementary Vol., M. A. Elliott, ed., Wiley Interscience, 1981, p. 1810-1811, p. 1807, p. 1804.

8. Stephens, D. R. and Miller, D. G., "Thermodynamic Equilibrium for Wyoming Coal: New Calculations," UCID 17044, February 24, 1976.

9. Schad, M. K. and Hafke, C. F., "Recent Developments in Coal Gasification," Chemical Engineering Progress, May 1983, p. 45.

10. Burns, L. K., Craig, G. N., II, Alexander, W. G., Etheridge, F. G., Laughter, T. and Youngberg, A. D., "The Application of Geological and Mineralogical Studies to Underground Coal Gasification Technology," 8th UCC Symposium Proceedings, Keystone, Colorado, August, 1982, p. 553.

11. Stephens, D. R. and Miller, D. G., "Soviet-Bloc Underground Coal Gasification Results Using Enriched Air and Steam," UCID 17245, August 26, 1976.

12. Levie, B. E., Krantz, W. E., Gunn, R. D., and Youngberg, D., "A Model for Roof Spalling and Its Application to Predicting Cavity Shape for the Hanna III UCG Field Test," 8th UCG Symposium Proceeding, Keystone, Colorado, August 1982, p. 321.

13. Singleton, A. H., Noll, W. L., and Allen, J. M., "Summary Report of the Rawlins Test 1 for Gasification of Steeply Dipping Coal Beds," 6th UCG Proceeding, Afton, Oklahoma, July 1980, Table 1, p. I-31.

14. Davis, B. E., Ahner, P. F., Avasthi, J. M., Bencini, J. F., Bloomstran, M. A., Bebout, R. A., and Garon, A. M., "Underground Gasification for Steeply Dipping Coal Beds Phase III Report Results of Rawlins Test No. 2," LETC 13108-94, July 1982, Fig. 4.4-11, p. 105; Table 6.1-1, p. 123; p. 103.

APPENDIX

Calculation of CH_4 from Pyrolysis during Rawlins T1 (Reference 13)

30-Day Air Injection

Avg. Dry Gas Production	4.7	MMSCF/D
Fraction CH_4	x 0.047	
Avg. CH_4 Production	0.22	MMSCF/D

$$\frac{\text{Avg. } CH_4 \text{ Production}}{\text{Avg. Coal Consumption}} = \frac{0.22 \text{ MMSCF/D}}{37.4 \text{ T/D}}$$

$$= 5.9 \text{ MSCF } CH_4/\text{T of Coal}$$

Calculation of CH_4 Volume Produced during Rawlins T2 Module #1 (Reference 14)

Total Dry Gas Production	272	MMSCF
Fraction CH_4	x 0.16	
Total CH_4 Production	43.5	MMSCF

Calculation of Amount of Coal Necessary to Produce 43.5 MMSCF of CH_4 from Pyrolysis of Coal which Yields 5.9 MSCF CH_4/T

$$\frac{43.5 \text{ MMSCF } CH_4}{5.9 \text{ MSCF } CH_4/\text{T of Coal}} = 7.4 \times 10^3 \text{ T of Coal}$$

$$\frac{7.4 \times 10^3 \times 2000 \text{ lb/T}}{90 \text{ lb/ft}^3} = 164 \times 10^3 \text{ ft}^3$$

Coal Density of 90 lb/ft^2 from Reference 14.

Figure 4.4-11 in Reference 14 shows more than 350×10^3 ft^3 of coal was affected during Rawlins T2 Module #1.

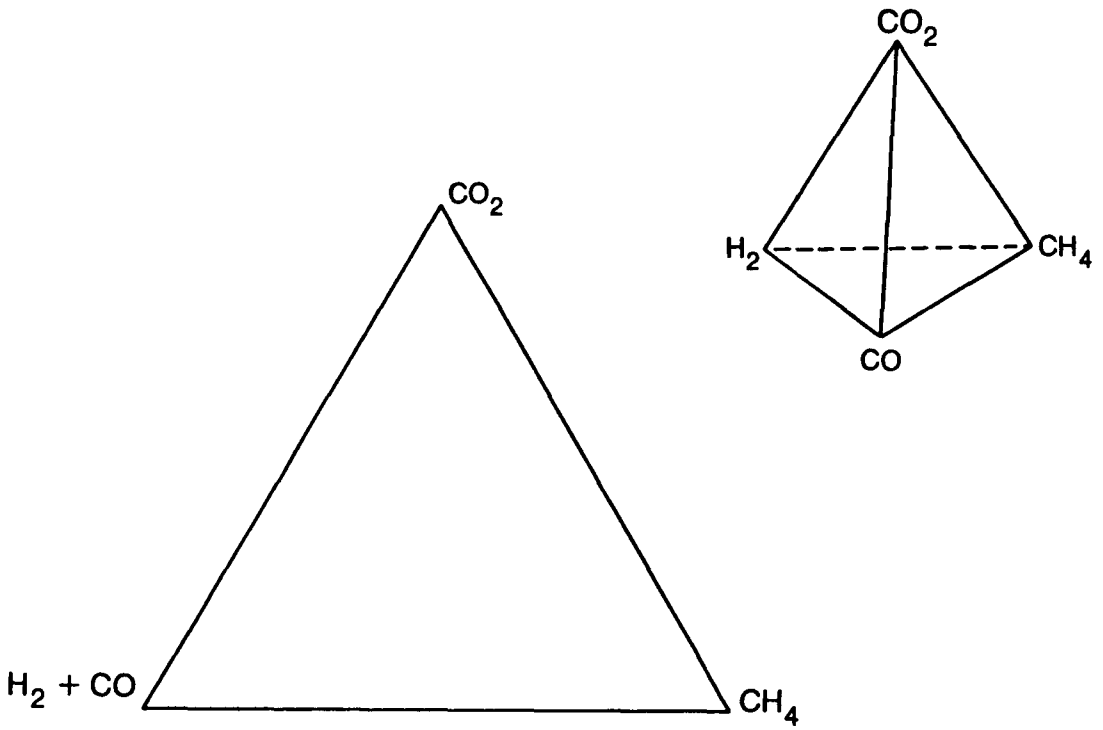

Figure 1. UCG Produced Gas Compositions on a Dry N_2-Free Basis Can Be Plotted on a Ternary Diagram if H_2+CO, Synthesis Gas, is Considered a Pseudo-component.

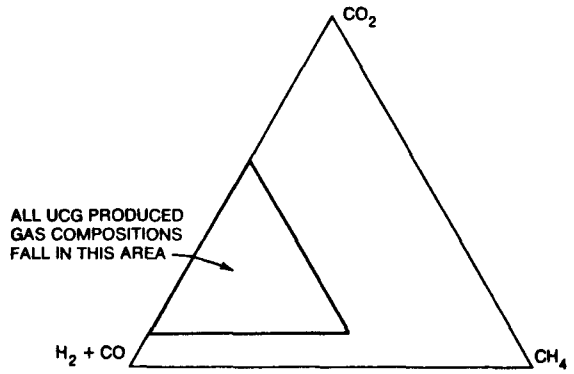

Figure 2. Synthesis Gas-CO_2-CH_4 Ternary Diagram Showing the Triangular Area Containing UCG Produced Gas Compositions.

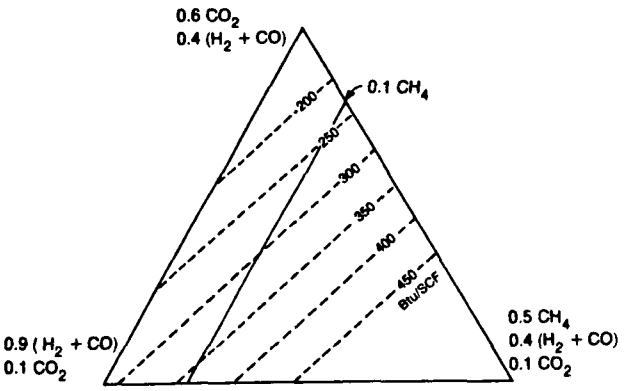

Figure 3. Enlargement of the Triangular Region Containing UCG Produced Gas Compositions with Iso-Heating Value Contours and the Constant CH_4 Composition Line.

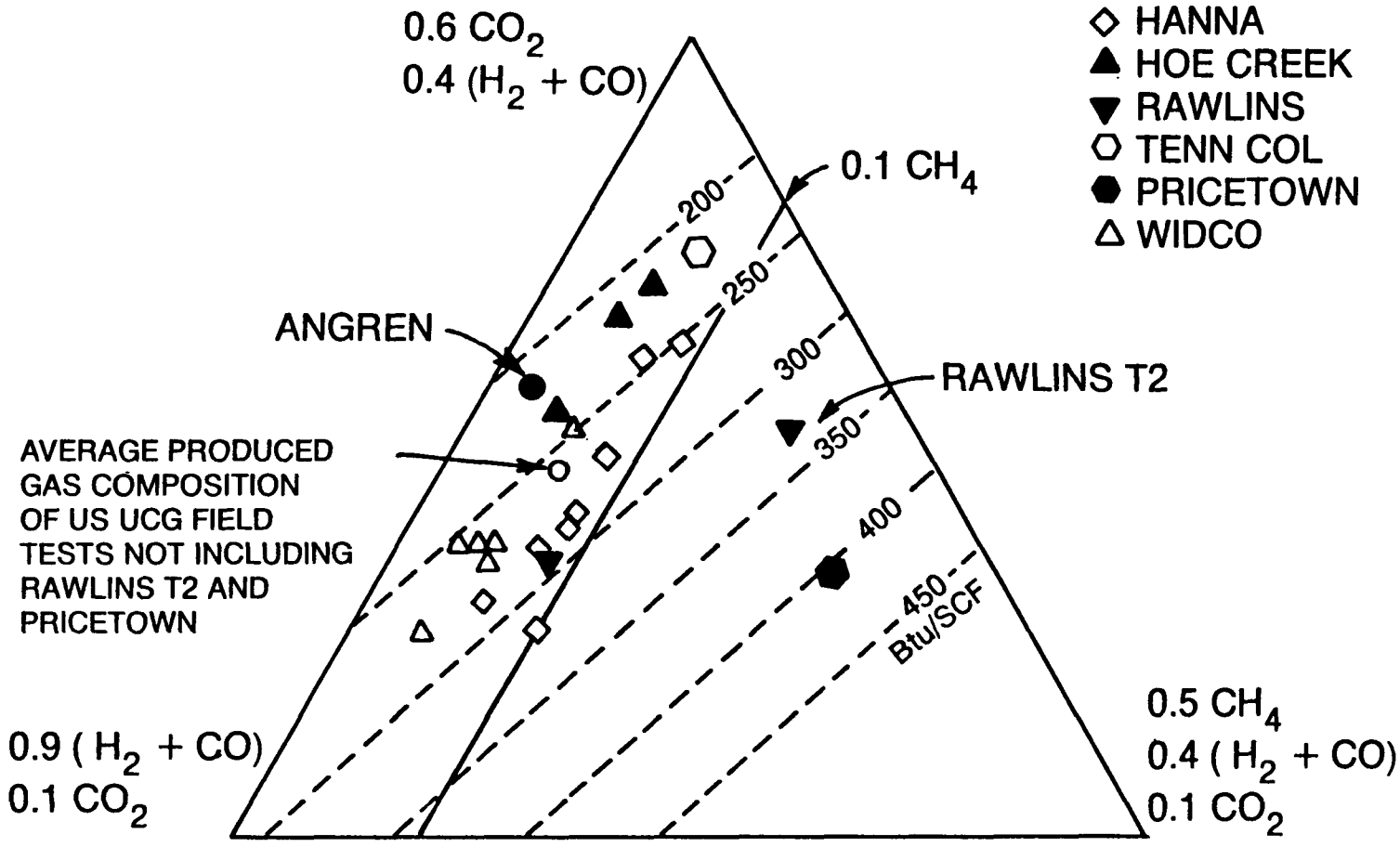

Figure 4. Recent US UCG Product Gas Compositions on a Dry N_2-Free Basis. Angren, a long term Soviet UCG test, is also included.

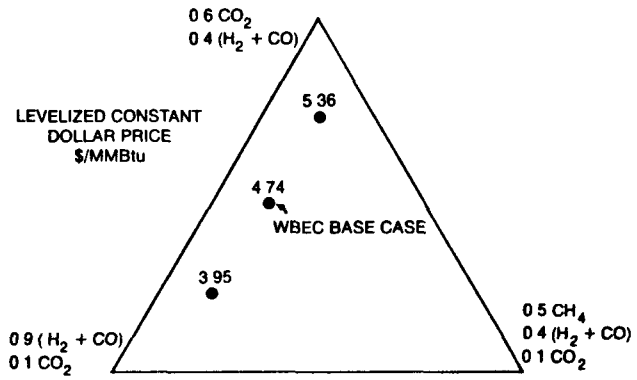

Figure 5. Levelized Constant Dollar Price for Surface Conversion of UCG Produced Gas to SNG as a Function of Synthesis Gas Content of the UCG Produced Gas on a Dry N_2-Free Basis.

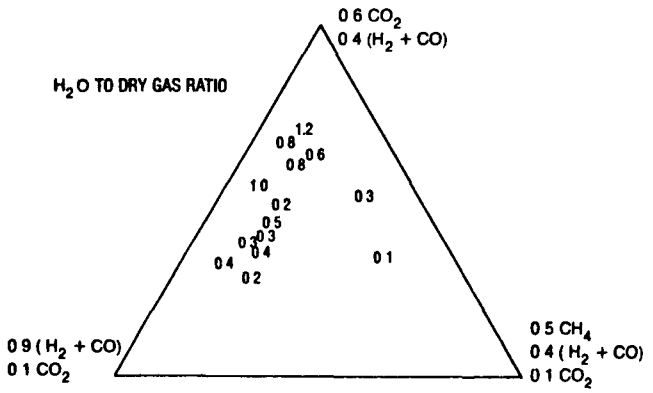

Figure 6. Water to Dry Gas Ratio in Recent US UCG Field Tests as a Function of Produced Gas Composition on a Dry N_2-Free Basis.

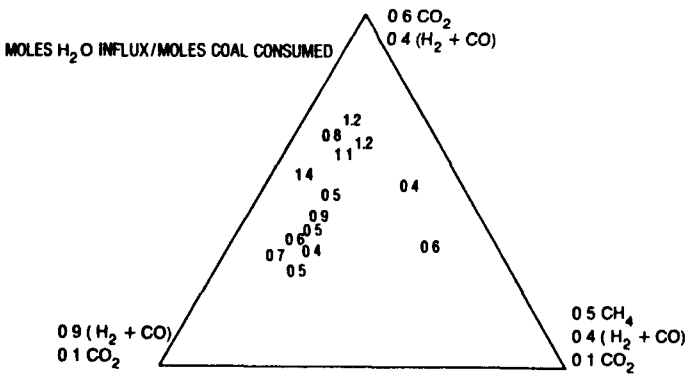

Figure 7. Moles of Water Influx per Mole of Coal Consumed in Recent US UCG Field Tests as a Function of Produced Gas Composition on a Dry N_2-Free Basis.

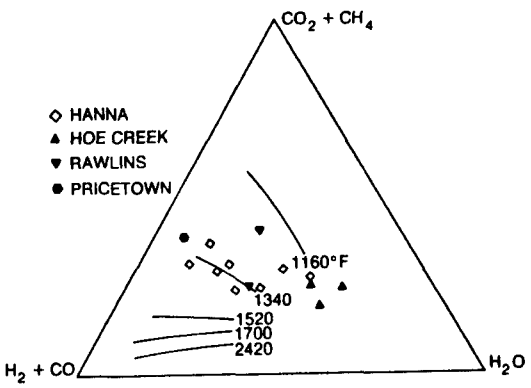

Figure 8. Equilibrium Isotherms at 10 atm Pressure and Produced Gas Compositions from Recent US UCG Field Tests on a N_2-Free Basis.

2.7 UNDERGROUND COAL GASIFICATION: THE LEADING SOURCE FOR LOWER-PRICED GAS

by

Frederic W. Hammesfahr
Patricia L. Winter

ABSTRACT

Among the various synthetic fuel technologies, underground coal gasification is the leading third generation contender as a source of low cost clean fuel and synthesis gas.

The progress that has been made is outstanding. It has opened to the program two opportunities, each with its own set of needs.

The first is that of securing a pioneering multi-module facility based on the technology developed on Western coal seams. For that, a project must be developed that incorporates surface clean-up and a surface application. To do this at reasonable cost, the use of existing local market demand to avoid the need for expensive high volume chemical upgrading appears one attractive approach. The possibilities for this approach will be discussed in some typical Western states with UCG potential.

For the second opportunity, broadening to the Eastern bituminous seams, the technology is much less developed. Here, the problem is more one of developing the necessary funding and industrial support of a program on these coals. Possibilities here will be discussed.

A Task Force of a leading professional society studied the underground coal gasification technology to see if it warranted support against the Administration's criteria of long range, high risk, and high potential pay-out. The Task Force concluded the technology did. The approach the Task Force followed and the results of their efforts will be briefly treated.

1/ Hammesfahr, Winter & Assoc., Inc.
2/ P.O. Box 536
Bernardsville, N.J. 07924

DISCUSSION

The synthetic fuel field is in trouble today. Under the combined weight of huge capital costs and uncertain fuel prices, the major projects have been falling by the wayside at fast rate. While this has been happening, underground coal gasification (UCG) has been proceeding forward to an extent not generally appreciated. Its capital costs are low; its price forecasts are very attractive.

In Table I,there are compared the capital costs of the same sized plants for producing synthetic natural gas (SNG) via surface and underground gasification technologies. The data show the capital cost via underground coal gasification to be 25% to 50% less than the capital required for an equivalent surface facility. Actually, the advantage is even greater for the underground coal

gasification as it requires no supporting mining investment, whereas the surface facility must have such an investment.

Capital costs using UCG technology can be held down even further by making a product requiring less surface processing. For such a plant producing 24 billion Btu/day (4,100 bbl oil equivalent/day), capital costs fall within the range of $95 to $170 million dollars. (MBG gas)

The advantage of low capital costs carries through even with more sophisticated products requiring more surface processing. Comparison of a surface plant producing methanol with similar plants using underground coal gasification technology shows the UCG plant to be from 22% to 30% lower in capital costs. (Table II) Once again, this is without charging the surface project for the cost of its associated coal mines.

This capital cost reduction brings the funding required for a synthetic fuel facility down into the range which most large companies would consider large but, nevertheless, within their financing capability. With UCG, the multi-billion and the high hundred million dollar type of project are replaced by projects whose costs can be discussed reasonably in the corporate board room.

This advantage in capital cost is reflected in the projected product prices.

The price support levels proposed by the Synthetic Fuels Corporation (SFC) reflect their appraisal of the revenues required by surface projects if the projects are to show minimal acceptable financial returns. The currently proposed support levels are $10/million Btu for medium Btu gas, $11.55/million Btu for synthetic natural gas, $1/gallon for methanol, and $1.95/gallon for gasoline. (Table III)

Estimates of the revenues required for the production of products using UCG technology are given in Table IV. Against the $10/million Btu estimated required for medium Btu gas from a surface facility, an underground coal gasification plant requires only $3.50 to $5.50 per million Btu. SNG, estimated to need a price support bringing revenues to $11.55/ million Btu from a surface plant, requires from UCG revenues of $6.50 to $9.00/million Btu. M-gasoline is projected to require revenues of $.95/gallon. The currently contemplated support level for surface plants is $1.95/gallon.

The SFC supports were projected based on plants producing 10,000 boe/day (58 billion Btu/day) or more. Required revenues increase as plant size decreases. Keeping this in mind, methanol, from a UCG plant of 31 billion Btu/day output is estimated to require revenues of $.55/ gallon rather than the $1/gallon needed for larger surface facilities.

Clearly, all of the available indicators show UCG technology to be one which projects lower product prices and which requires less capital investment. Where applicable, it is a highly competitive technology.

The progress that has been made to date has opened to UCG two program opportunities, each requiring its own strategy.

The Western coal program has been extensive. Of the approximately 37,800 tons of coal that have been converted in UCG programs, 37,200 were Western coals. The balance, 560 tons, is distributed approximately evenly between programs on Texas lignite and programs on Appalachian coals. (Table V)

With that substantial data base on Western coals, this program appears ready to move forward to a larger pre- commercial, multi-module test.

Previous attempts to move the Western UCG program forward to pre-commercial scale have contemplated, because of the remote location of Western UCG reserves, building dedicated surface facilities to use the substantial volume of gas and energy produced. Pragmatically, this approach is unappealing. The surface investment is at risk to the success of the underground program. As a result, it attracted no support. Therefore,

in late 1981, DOE funded Hammesfahr, Winter & Associates, Inc. under contract number DE-AC20-81LC10703 to determine whether there were existing surface facilities in the area of UCG amenable reserves that could provide an industrial application and revenues for the gases produced in a pre-commercialization, multi-well field test.

To confine the study effort to manageable proportions, limiting parameters were established. The review was confined to five states. New Mexico, Washington, and Wyoming were included because of the broad data base on Western coals. Texas was included because of local interest in UCG, and Illinois was included because of its important coal reserves and its proximity to major markets. The production rate for the pre-commercialization test was estimated at 4.8 billion Btu/day. This is the energy required for 20 megawatts of power production. Attention was focused on three industries, all major fuel consumers. They were the utility industry, the refinery industry, and natural gas processors. Since the purpose was to minimize new dedicated surface investment, fuel applications were targeted. In an exception to this, the production of transportation grade methanol for local use was also considered.

The three industries have approximately 680 facilities within these five states. Many of these are were too distant from the UCG coal resources amenable to underground coal gasification to be viable candidates for the program. Limiting the search for users to those within fifty miles of the coal resources reduced the number to forty-two facilities. This was still a large number, and, in addition, the distance of fifty miles brings in excessive pipelining costs. The distribution of these forty-two facilities by distance from the nearest coal resource was then determined. Twenty-three, or 55%, of these were found to be within three miles of the coal resource. Within ten miles of the coal resource, 79% were located. (Table VI)

Contact was made with a significant percentage of the 55% found within three miles of a coal resource. From these contacts, we would conclude that the utility industry is a potential market for a pre-commercialization program, The Western refinery industry is a poor prospect. Western refineries are small, and 4.8 billion Btu's of new fuel upsets their refinery balance and marketing strategies. Size is not a problem in Illinois, while Texas has no refineries near UCG amenable coal. The natural gas processing industry of the West can use the fuel without incurring the marketing problems, but 4.8 billion Btu's is large relative to their fuel demand.

By contrast, size near UCG amenable coal reserves is much less of a problem in Illinois.

Prospective users had interest only in medium Btu gas. The derating that occurs firing low Btu gas was held unacceptable. At energy levels of 350 Btu/scf or more, concern over derating dropped. Many facilities have used gas of 400 to 450 Btu/scf with little or no derating. They, therefore, felt they could use gas of 350 Btu/scf successfully, blending in a small amount of natural gas if necessary to raise the Btu level to the 400-450 level.

No prospective user was willing to bear the cost of retrofitting furnaces or boilers so that they could change from natural gas or from a liquid fuel oil to medium Btu gas. This would become a project expense. Estimates for this change-over from one refinery were in the range of $4 million dollars.

All users were willing to pay a competitive price for the fuel taken.

In summary, the concept of using existing facilities to take gas from a pre-commercialization project appears sound. The number of facilities at any coal resource is limited but adequate for this purpose.

In the West, production of methanol for local or regional markets is impractical. The minimum size plant is large relative to these markets and requires capturing

unrealistic market shares. In the East, again, this would be less of a problem.

The opportunity in the East is quite different. The access of Eastern seams to more and larger surface facilities will make commercialization easier. Because of this and because the study team believed that much of the technology developed on Western coals could be used in an Eastern program, it recommended that the UCG program be broadened to include development of an Eastern coal UCG technology. Reflecting inputs from this study and other sources, DOE is now studying the possibilities for developing such a program.

During the course of the past year, the American Institute of Chemical Engineers (AIChE) became interested in the contrast between the very favorable cost estimates that had been produced by a variety of contractors working for both DOE and non-DOE clients and the relatively low budget that had been planned for underground coal gasification in fiscal 1983. With the historic involvement of the chemical engineering profession in the National synfuel program, the AIChE established a Task Force for the purposes of assessing the status of UCG technology and seeing if this technology warranted support. The criteria for support were taken from the Administration's view that only long-term, high risk, and high promise technology qualified for Federal support.

The Task Force studied and assessed the status of UCG over a period of about six months. It unanimously concluded that UCG technology met the Administration's criteria of long term, high risk, and high promise research. The Task Force further agreed both in recommending a multi-module, long term field test as the necessary next technical step and in recommending that appropriate funding for such be included in the Federal Government's fossil fuel research budget.

The Task Force observed that the budgets for underground coal gasification had been relatively small. The progress made on these limited budgets indicated to the Task Force that the management of this program had been highly professional, and they complimented the project on that basis.

After the AIChE's internal peer review, augmented by outside inputs from an umbrella engineering society, distribution of the Task Force report was authorized. A summary was printed in Chemical Engineering Progress, the senior journal of the American Institute of Chemical Engineers. It has a circulation of 55,000. Energy Progress, a more specialized journal of the Institute with a circulation of 6,000, printed the entire report. Copies were given to members of the press, and a summary was reproduced in many of the trade publications devoted to energy matters. Copies were also sent to nineteen Congressional committees and agencies, to six executive agencies and departments, to two independent agencies, and to over 200 energy companies and interested entities.

In summary, the progress made on the UCG program is reaching an expanding audience. Within the program itself, increasing attention is being successfully given both to finding low capital routes to get through the pre-commercialization stages and to broadening the technology to handle new important coal resources. The successes of the program are developing new opportunities for UCG technology.

TABLE I

24,000 million Btu/day at MBG level

Product	SNG	SNG	SNG	MBG	MBG
Type of gasification	Surface	UCG	UCG	UCG	UCG
Type of bed		Horiz.	SD*	Horiz.	SD*
Plant cost, million $ **	$350	$270	$165	$170	$95

* SD-Steeply Dipping Bed
** UCG data from 8th UCG Symposium paper by P. R. Bruggink and B. E. Davis of Gulf. Surface data from unpublished sources. Surface investment does not include cost of supporting coal mines.

TABLE II

1,000 tons methanol/day

Type of gasification	Surface	UCG	UCG
Type of bed		Horizontal	SD*
Plant cost, million $ **	$400	$316	$280

* SD-Steeply Dipping Bed
** UCG data from 8th UCG Symposium paper by P. R. Bruggink and B. E. Davis of Gulf. Surface data from unpublished sources. Surface investment does not include cost of supporting coal mines.

TABLE III

Proposed SFC Price Support Levels

	Proposed Maximums
Medium Btu Gas	$10.00/million Btu
SNG	$11.55/million Btu
Methanol	$ 1.00/gallon
Gasoline	$ 1.95/gallon

TABLE IV

UCG Price Forecasts

Product	Type Coal Resource	
	Horizontal	Steeply Dipping
	Required Product Price, dollars	
MBG		
Plant Size-60 billion Btu/day		
Product price, per MM Btu	$5.50	$3.50-$4.00
SNG		
Plant Size-55 billion Btu/day		
Product price, per MM Btu	$9.00	$6.50
M-Gasoline		
Plant Size-9,600 bbl/day		
Product price, $/gallon	$0.95	
Methanol		
Plant Size-1,600 tons/day (31,000 billion Btu/day)		
Product price, $/gallon	$0.55	

Sources: 8th UCG Symposium paper by P. R. Bruggink and B. E. Davis of Gulf
The UCG study for Lawrence Livermore National Laboratory by the Pritchard Corporation, June, 1982

TABLE V

Experience Base in UCG Program

Type Coal		Tons coal processed in UCG programs
Western:		
Horizontal	27,400	
Steeply dipping	9,820	
Total Western		37,220
Texas lignite, approximate		280
Appalachian, approximate		280
Total coal processed		37,780

TABLE VI

Distribution of Potential Users by State
(By distance from coal resource)

	Within 3 miles	Within 10 miles	Within 50 miles
Illinois	4	8	12
New Mexico	7	7	7
Texas	3	3	3
Washington	2	6	11
Wyoming	7	9	9
Total	23	33	42
Percent	55%	79%	100%

SESSION II: POSTER PRESENTATIONS

2.8 NUMERICAL MODELING: A SITE SELECTION TOOL FOR IN-SITU GASIFICATION OF TEXAS LIGNITE

by

James E. Russell [1/]
Yih-Ji Wang [2/]
Earl R. Hoskins [3/]

ABSTRACT

Texas lignite occurs in several combinations of geologic groups (or formations) and facies that reflect respectively the age of the deposit and the environment of deposition. It is well known that lignite samples from these groups (or formations) and facies classifications have different properties. In this paper, we present the preliminary results of a systematic parameter study of the influence of proximate analysis data on the quality of the product gas.

Proximate analysis results in dry basis form are presented on a ternary diagram for 356 Texas lignite samples without regard to geologic age or environment of deposition. Similar figures are shown with the data classified into appropriate subsets reflecting geologic age and environment of deposition. Isopleths of the heating value of the simulated produced gas are plotted on a ternary diagram at the mean moisture content along with a window enclosing 70 percent of the data points. Regions on ternary diagrams where there is inadequate heat for the char-steam reaction are shown.

1/ Departments of Petroleum Engineering and Geophysics
Texas A&M University
College Station, TX 77843
2/ Department of Geophysics
Texas A&M University
College Station, TX 77843
3/ Departments of Geophysics and Petroleum Engineering
Texas A&M University
College Station, TX 77843

BACKGROUND AND INTRODUCTION

Site Selection

Site selection for in-situ gasification projects normally involves application of site screening criteria, often in two or more stages, beginning with consideration of rather large geographic areas and progressing to smaller and smaller areas where conditions for in-situ gasification are progressively more favorable. Table 1 shows preliminary screening criteria modified from Bartel and Love (1981) for Washington State. Table 2 shows second stage screening factors again modified from Bartel and Love (1981). Other recent examples of site selection criteria, in more detail, may be found in Ahner, et al. (1980) and Wilkerson and Jepsen (1981).

In this paper, we focus on the role of the lignite composition in determining the quality of the product gas. For our purposes, the quality of the gas will be measured by its energy content (high heating value) in Btu/scf. Also, in this study, the composition of the lignite is assumed to be adequately represented by the proximate analysis parameters and the energy content of the solid fuel. Furthermore, this paper considers only Texas lignite which, however, is somewhat variable, as discussed below.

Variability of Texas Lignite

Texas lignite deposits exhibit considerably more variability than coal deposits in other provinces. Table 3 is modified from Russell and Wang (1983) and contains data from Kaiser (1974), U.S. Bureau of Mines (1948), and unpublished sources. Note that the heating values of the lignite are from about 15 to 40 percent higher than those commonly reported for mine-run Texas lignite, and by Luppens (1979).

As shown on Figure 3, Russell and Wang (1983) have classified Texas lignite deposits into six categories representing geologic group or formation (representing age) and facies (representing environment of deposition) in preparation for the current study. Table 4, also modified from Russell and Wang (1983) shows the rank of each of the group (or formation)-facies categories in moisture, volatiles, fixed carbon, ash, and heating value. This ranking is based on the same data set as Table 3.

Objective

In view of the inherent variability of the proximate analysis data for Texas lignite, a parameter study of the influence of this variability on the quality of the product gas was desirable. Because of the relationship between the proximate analysis values (their sum must be one hundred percent), it was not apparent how these values should be systematically changed and still be representative of actual Texas lignite, i.e., if ash is increased, which of the other values should be decreased. Russell and Wang (1983) developed the required methodology which was used in the current study as input to a slightly modified version of an existing numerical model from Jennings, et al. (1977).

The objective of this paper is to illustrate the use of numerical models in preliminary siting studies for future in-situ gasification projects in Texas. In particular, this paper is concerned with numerical modeling of the influence of lignite composition (as represented by proximate analysis data) on product gas heating value. Numerical modeling is used to study these questions and it becomes, then, a site selection tool.

Numerical Model

Numerical models are representations of reality based on apppropriate physical and chemical principles along with a number of assumptions and a conceptual idea of the process to be modeled. A successful numerical model captures the essence of the process and allows us to study the influence of changes in the process variables and parameters.

The model used herein was slightly modified from that described by Jennings, et al. (1977) which followed from an earlier model described by Gunn and Whitman (1976). This model uses overall energy-balance relationships which predict product gas composition and flame-front velocity. Energy and material balances were written for a constant control volume moving through the system with the velocity of the flame front which is governed by the consumption of char by the combustion and steam-char reactions.

Conceptually, the control volume contains a leading devolatilization zone, followed by a steam-char reaction zone, which in turn is followed by the combustion zone. The control volume includes that portion of the lignite from a point in the ash behind the flame front to a point ahead of the flame front where devolatilization ceases. Therefore, the model includes the endothermic devolatilization reaction, the endothermic steam-char reaction, and the exothermic partial combustion reaction which is controlled by the ratio (CR) of CO to CO_2 produced by the oxidation of carbon. Inclusion of the CR ratio allows the inclusion of competing combustion reactions without specifically describing reaction kinetics. The other adjustable parameters in the model are the fraction of tars in the lignite which are cracked and converted to gas, and the heat loss to the surroundings.

Additional assumptions included in the model involve the extent and priority of the reactions that take place. The partial combustion reaction is assumed to have no competition and goes to completion controlled by the molar flux of oxygen into the system. Of the two competing endothermic reactions, the model assumes that the devolatilization reaction has priority over the steam-char

reaction because the devolatilization is complete at 1700°F, as shown by experiment, whereas the steam-char reaction requires a higher temperature in order for its reaction rate to be significant.

This model has been validated by simulating combustion tube tests on Texas lignite reported by Marable (1975).

The above described model was judged to be adequate for comparison of the combustion tube performance of the various categories of Texas lignite using the rather extensive data base described above. We say that our comparison is combustion-tube performance because this model has only been validated against combustion-tube data and conditions in a combustion tube are different than those in situ. However, the quality and composition of the product gas from the laboratory experiments does appear to be similar to that produced during the early part of the field tests, Hoskins, et al. (1982).

METHODOLOGY

Classification of Texas Lignite

The first step in accomplishing the parameter study was the classification of Texas lignite occurrences by age and environment of deposition, both of which can affect the composition of the lignite. In general, the older lignite deposits have a higher fraction of fixed carbon and lower volatile and moisture fractions. The environment of deposition influences the ash fraction as noted by Kaiser (1974) and this is apparent in the lagoonal and deltaic facies categories shown on Tables 3 and 4.

The numerical model described above requires the as-received proximate analysis data for the lignite. Therefore, classification by age and depositional environment, which influence the proximate analysis values, is appropriate.

Ranges of Proximate Analysis Data

The next step in the parameter study was to decide over what ranges it is appropriate to vary moisture (M), ash (A), fixed carbon (FC), and volatiles (V) in keeping with the requirements that their sum remain one hundred percent and that the combination chosen represents one that is known to exist in Texas lignite. A procedure for accomplishing these ends has been discussed by Russell and Wang (1983).

If the proximate analysis data are reduced to the dry-basis form, only V, FC, and A remain. These three values must now sum to one hundred percent and may appropriately be plotted on a ternary diagram, as shown on Figure 1. The inset triangles or "windows" contain 90% of the respected data and were selected by the program WINDOW described by Russell and Wang (1983). Note that the window for Yegua-Jackson Lagoonal (YJL) and Jackson Deltaic (JD) is shifted toward the ash apex. Further note that the fewer number of samples in these categories still allows the 90% window for all data to be very similar to the window for the remaining four categories.

If sample points are within the appropriate window, we are reasonably certain that the resulting combination of dry-basis A, FC, and V is an appropriate one for the group (or formation)-facies category under consideration. In order to restrict the ranges of the variables further toward the region of highest density of data points (see Russell and Wang (1983)), we chose the 70% dry-basis windows for use in this study as shown on Figures 2 and 3.

The numerical model requires as-received data and consequently the dry-basis windows shown on Figures 1 through 3 must be shifted to some non-zero moisture plane before analysis. Figure 4 shows a frequency diagram for each of the lignite categories under consideration. Note that the moisture contents are extremely variable. Nevertheless, the mean values of moisture content should be the most representative values and were used in the analysis. Note that the sum of A, FC, and V must now equal 100% minus M. A preliminary study indicated that moisture did not correlate strongly with any of the other proximate analysis values. Therefore, it appeared to be reasonable to choose moisture independently for this study.

Calculations

Calculation of the product gas composition and heating value using this model requires as-received proximate analysis values, the composition of the tars in the lignite, and an estimate of

the heating value of the solid lignite. The composition of the volatiles (gases and tars) and the fraction of tars cracked during the process were taken from Jennings, et al. (1977). A multivariable linear model of the heating value of the solid lignite was available from Russell and Wang (1983) and used in this study.

Calculations could then be made for a regular array of points in the ternary diagram for each appropriate mean moisture content. Isopleths of constant gas heating value can then be prepared and the average heating value within the 70% windows calculated, if desired.

RESULTS

Heating value of the product gas does depend on the relative values of the proximate analysis values, although not as strongly as one might expect. Figure 5 shows isopleths of constant heating values for data from all categories. As expected, the heating value of the produced gas declines as ash increases. The heating values are highest when as-received volatiles are in the 40 to 50% range, ash is about 6%, and fixed carbon in the 15 to 25% range when the mean moisture is about 26%. Heating value declines as the fixed carbon apex is approached.

These observations are explained as follows. The decline in heating value as ash increases is explained by the relative lack of carbon and volatiles and the fact that the ash that is left behind contains heat that would have been available for the steam-char reaction which produces combustible gases. Thus high ash content is associated with lower heating values of the produced gas.

The association of higher heating values with high volatile content when ash is low demonstrates the importance of the gases driven off during devolatilization and of those cracked from the tar. The devolatilization gases also explain the decline in heating value as the fixed carbon apex is approached and ash is low. For points near the fixed carbon apex, the combustible gases produced contain a higher fraction of CO and H_2 which have lower heating values than the devolatilization gases, such as methane.

A zone near the right side of Figure 5 is labeled as "Inadequate Heat for the Char-Steam Reaction." Recall that in this model the heat is produced by the exothermic combusion reaction and consumed by the endothermic devolatilization and steam-char reactions with the devolatilization reaction having priority because it occurs at a lower temperature. As the right side of the diagram is approached, there is less carbon available for combustion. At the boundary of the inadequate heat zone, all of the heat generated by oxidizing the carbon is consumed in the devolatilization reaction. Further into this zone, there would be inadequate heat to drive even the devolatilization.

Figures 6 through 11 depict ternary diagrams for the six categories given in Table 1 at the mean moisture contents. Values shown at the points are the heating value of the produced gas in Btu/scf. The size of the encompassing ternary diagrams was chosen to be large enough to include the 70% window and a portion of the inadequate heat zone. Each diagram also shows the window containing 70% of the data and the zone where there is inadequate heat to allow the steam-char reaction. Figure 12 presents the same information for data from all categories together. Figure 11 indicates that a portion of the 70% window for the Jackson-Deltaic category overlaps with the inadequate heat zone. Note that, in general, the 70% windows are biased toward the fixed carbon apex.

Table 5 presents a summary of the highest, central, and lowest points within the 70% windows of Figures 6 through 12. The consistency of these values indicates that the composition of the lignite as represented by proximate analysis data has only a minor effect on the heating value of the simulated product gas.

CONCLUSIONS

The Wilcox Deltaic and Yegua Deltaic categories have the smallest 70% inclusive data windows and are probably the most consistent lignite for siting in-situ gasification projects. However, it appears that there is little or no correlation between the heating value of the simulated produced gas and the heating value of the solid lignite.

High ash content in the lignite appears to be undesirable. From this point of view, the Jackson Deltaic and the Yegua-Jackson Lagoonal categories appear to be the least desirable.

The 70% inclusive window of the Jackson Deltaic overlaps the inadequate heat zone. This fact, along with the variance in the data, make the JD category the least desirable.

A systematic study of the influence of moisture content has not been made at this time. Lignite composition, as represented by the proximate analysis data and the lignite heating value, appear to be poor screening tools in choosing potential sites for in-situ gasification projects in Texas lignite.

LIMITATIONS

Care should be exercised in using the conclusions of this study because the samples were not chosen randomly from the respective geologic categories. Consequently, data may be biased toward local area(s) in the category. Also, insufficient data were available to use geostatistical methods.

The number of data in the various categories varied considerably.

The composition of the volatiles was held constant for all categories.

Moisture content was held at the mean value for each category and specified independently of the other proximate analysis values.

ACKNOWLEDGEMENTS

This work was supported, in part, by the U. S. Department of Energy under Grant No. DE-FG22-80PC30221 to the Texas A&M Research Foundation. The Texas Municipal Power Agency and the San Miguel Electric Power Cooperative supplied data that aided this study greatly.

REFERENCES

Ahner, P. F., et al., (1980), "A Site Qualification Study of the UCG Site at North Knobs," Proc.-Sixth Underground Coal Conversion Symposium, Shangri-La, OK, LETC CONF. No. 800716, pp. VIII-24 to VIII-31.

Bartel, L. C. and Love, S. L., (1981), "Final Report - Site Selection and Characterization for an Underground Coal Gasification Test in Washington State," Vol. 1. Project Summary, Sandia Report SAND 81-2051/1.

Gunn, R. D. and Whitman, D. L., (1976), "An Insitu Coal Gasification Model (Forward Mode) for Feasibility Studies and Design," LERC/RI-76/2.

Hoskins, E. R., Russell, J. E., and Brimhall, R. M., (1982), "Results of the Texas A&M In-Situ Gasification Project," Sixth Annual Uranium Seminar, Published by Soc. of Mining Engineers of AIME, pp. 1-16.

Jennings, J. W., Strickland, R. F., and Von Gonten, W. D., (1977), "Texas A&M Project Status, Underground Lignite Gasification," Proc. Third Annual Underground Coal Conversion Symposium, US DOE-LLL Conf.-770652, pp. 83-91.

Kaiser, W. R., (1974), "Texas Lignite: Near-Surface and Deep-Basin Resources," RI-79, Bureau of Economic Geology, University of Texas at Austin, 70 pp.

Marable, M. (1975), "Some Effects of Pressure and Temperature on Combustion of Lignite," M.S. Thesis, Texas A&M University, College Station, TX.

Russell, J. E. and Wang, Y. J., (1983), "Characterization of Texas Lignite Based on Proximate Analysis Data," First Conf. on Use of Computers in the Coal Industry, West Virginia University, Aug. 1-3, Paper No. A-085-2.

U. S. Bureau of Mines, (1948), "Analyses of Michigan, North Dakota, South Dakota, and Texas Coals," Technical Paper 700, U. S. Bureau of Mines, 106 pp.

TABLE 1
PRELIMINARY SCREENING CRITERIA FOR SITE SELECTION
AFTER BARTEL AND LOVE (1981)

Criterion	Range or Desirable Attributes
Seam Thickness	> 6 ft
Seam Depth	300 to 1000 ft
Size of Deposit	> 50 million tons
Geologic Structure	Simple - No Major Faults
Roof and Floor Rocks	Competent, Relatively Impermeable* and Dry
Physical Access	Easy*
Proximity to Market	Close*

*Not presently quantified

TABLE 2
SECOND STAGE SCREENING FACTORS FOR SITE SELECTION

Factors	Desirable Attributes
Lignite Composition	Low Ash, High Fixed Carbon
Homogeneity	High
Directional Permeability of the Seam	*
Local and Regional Hydraulic Gradients and Flow Rates	*
Potential for Groundwater Contamination	Low
Potential for Air Quality Degredation	Low
Potential for Surface Subsidence and/or Caving	Low

*Currently under study

TABLE 3
STATISTICS BASED ON PROXIMATE ANALYSIS AND ENERGY CONTENT DATA FOR TEXAS LIGNITE FROM KAISER (1974), U. S. BUREAU OF MINES (1948), AND UNPUBLISHED SOURCES MODIFIED FROM RUSSELL AND WANG (1983)

Group or Formation Facies Class.	Prox. Anal. Var.	As-Received Basis Mean	Stand. Dev.	Coef. of Var.	Dry-Basis Mean	Stand. Dev.	Coef. of Var.	No. of Samples n
	M	25.6	9.14	0.357	-	-	-	
	V	33.9	7.09	0.209	45.7	8.21	0.180	
All	FC	26.7	8.23	0.308	35.8	10.0	0.280	356
	A	13.8	8.75	0.637	18.5	11.3	0.612	
	Btu/lb	7383	1379	0.187	10067	3124	0.310	278
	M	20.9	11.2	0.533	-	-	-	
Wilcox-	V	35.3	8.49	0.240	44.7	10.8	0.241	
Lagoonal	FC	31.2	9.17	0.294	38.8	8.68	0.224	23
	A	13.4	6.71	0.501	16.6	7.10	0.429	
	Btu/lb	7454	488	0.065	10260	3055	0.298	12
	M	26.1	7.46	0.286	-	-	-	
Wilcox-	V	33.9	5.30	0.156	46.0	6.65	0.144	
Deltaic	FC	30.0	5.45	0.182	40.6	6.52	0.161	102
	A	9.99	3.88	0.388	13.4	4.44	0.332	
	Btu/lb	8095	907	0.112	10885	2917	0.268	91
	M	25.3	8.28	0.328	-	-	-	
Wilcox-	V	35.6	7.46	0.209	47.7	7.99	0.168	
Fluvial	FC	28.8	6.92	0.240	38.6	8.24	0.214	136
	A	10.2	4.66	0.455	13.8	6.06	0.441	
	Btu/lb	7912	799	0.101	10760	2922	0.272	95
	M	23.7	9.96	0.420	-	-	-	
Yegua-	V	29.1	6.83	0.234	38.2	6.55	0.171	
Jackson-	FC	19.4	4.86	0.250	25.7	5.91	0.230	47
Lagoonal	A	27.5	9.53	0.346	36.1	10.8	0.298	
	Btu/lb	5932	1224	0.206	7810	2333	0.299	47
	M	23.1	11.0	0.478	-	-	-	
Yegua-	V	37.5	5.56	0.148	49.4	6.51	0.132	
Deltaic	FC	25.5	5.62	0.221	33.5	6.53	0.195	21
	A	13.6	8.12	0.599	17.1	7.74	0.452	
	Btu/lb	7462	782	0.105	10678	3280	0.307	12
	M	34.5	7.85	0.228	-	-	-	
Jackson-	V	29.8	5.22	0.175	45.9	8.06	0.176	
Deltaic	FC	13.5	7.29	0.540	20.4	10.3	0.509	27
	A	22.1	8.91	0.403	33.8	12.2	0.363	
	Btu/lb	5069	1157	0.228	7982	3286	0.412	21

TABLE 4
RANK OF GROUP(OR FORMATION)-FACIES CATEGORY FOR EACH PROXIMATE ANALYSIS VARIABLE AND ENERGY CONTENT. NUMBERS ARE MEAN VALUES IN PERCENT, EXCEPT FOR ENERGY CONTENT IN Btu/lb

Rank High to Low	As-Received Basis					Dry Basis			
	M	V	FC	A	Btu/lb	V	FC	A	Btu/lb
1=High	JD	YD	WL	Y-JL	WD	YD	WD	Y-JL	WD
	34	38	31	28	8095	49	41	36	10885
2	WD	WF	WD	JD	WF	WF	WF	JD	WF
	26	36	30	22	7912	48	39	34	10760
3	WF	WL	WF	YD	YD	WD	WL	YD	YD
	25	35	29	14	7462	46	39	17	10678
4	Y-JL	WD	YD	WL	WL	JD	YD	WL	WL
	24	34	26	13	7454	46	34	17	10260
5	YD	JD	Y-JL	WD	Y-JL	WL	Y-JL	WF	JD
	23	30	19	10	5932	45	26	14	7982
6=Low	WL	Y-JL	JD	WF	JD	Y-JL	JD	WD	Y-JL
	21	29	14	10	5069	38	20	13	7810

TABLE 5
HIGHEST, CENTRAL, AND LOWEST HEATING VALUE OF SIMULATED PRODUCED GAS IN THE 70% WINDOW

Category	Highest (Btu/scf)	Central (Btu/scf)	Lowest (Btu/scf)
WL	162.8	161.1	142.1
WD	162.3	154.5	142.0
WF	162.8	159.3	146.1
YD	162.3	161.3	150.0
YJL	161.5	159.5	135.8
JD*	161.4	159.2	142.1
All	163.2	161.5	138.7

* Overlaps inadequate heat zone

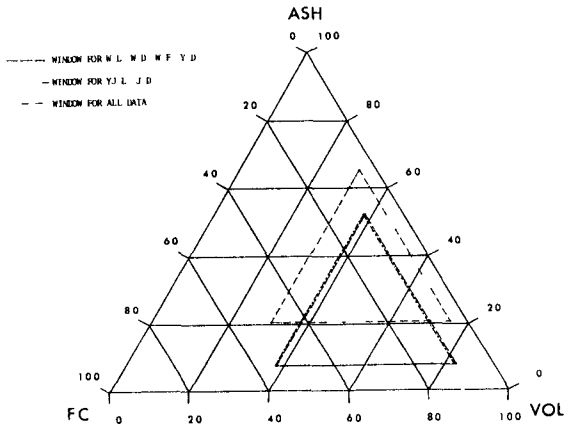

Figure 1. Dry-Basis Ternary Diagram for Texas Lignite with 90% Windows for Group (or Formation) and Facies Categories.

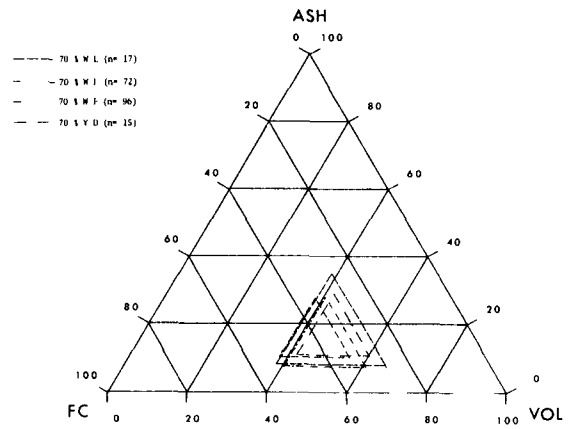

Figure 2. Dry-Basis Ternary Diagram for Texas Lignite from the Wilcox Group and the Yegua Formation with 70% Windows.

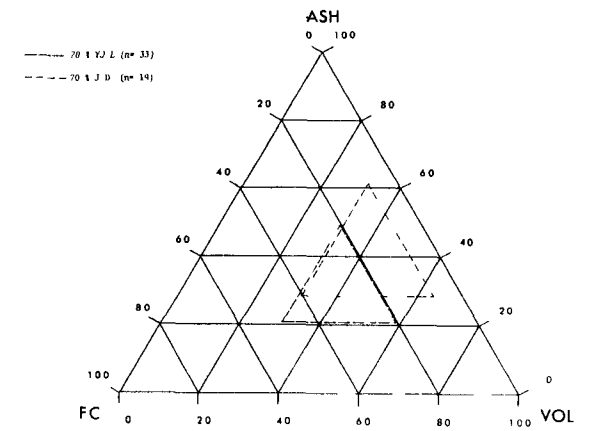

Figure 3. Dry-Basis Ternary Diagram for Texas Lignite from the Yegua-Jackson and Jackson Categories with 70% Windows.

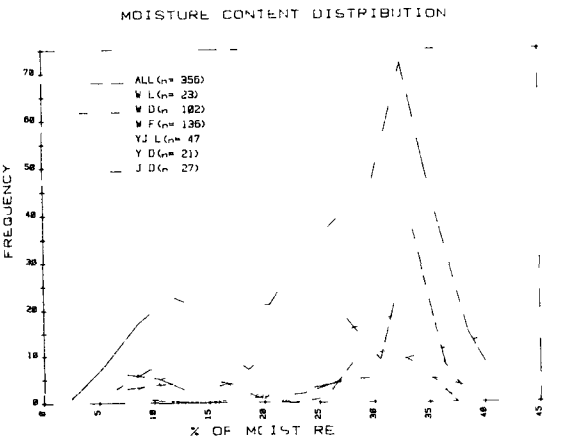

Figure 4. Frequency Plot of Moisture Distribution by Texas Lignite Category.

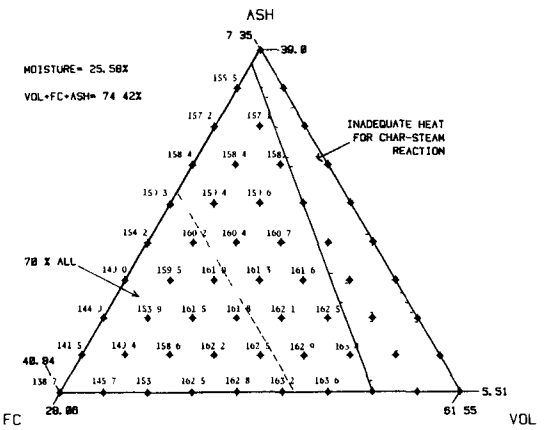

Figure 5. Isopleths of Constant Heating Values for Data from All Categories.

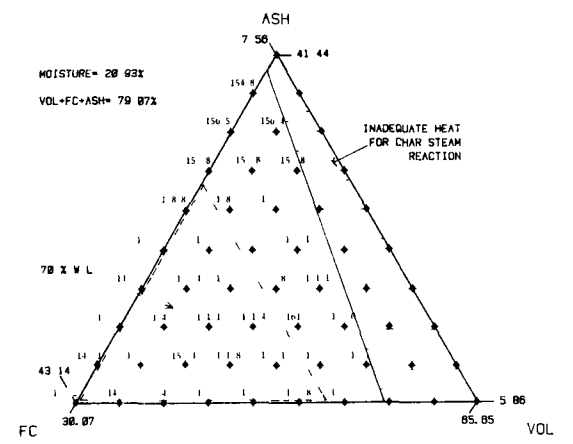

Figure 6. Ternary Diagram for Wilcox-Lagoonal Category at 20.93% Moisture.

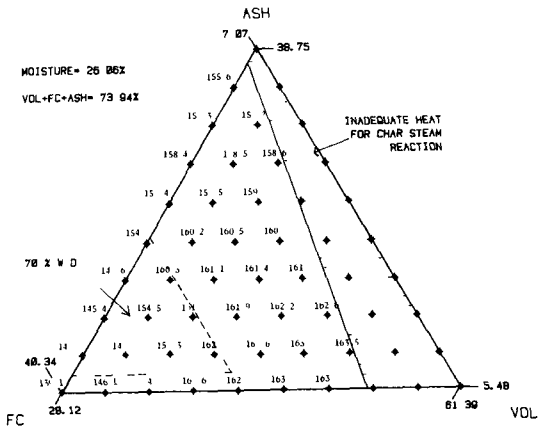

Figure 7. Ternary Diagram for Wilcox-Deltaic Category at 26.06% Moisture.

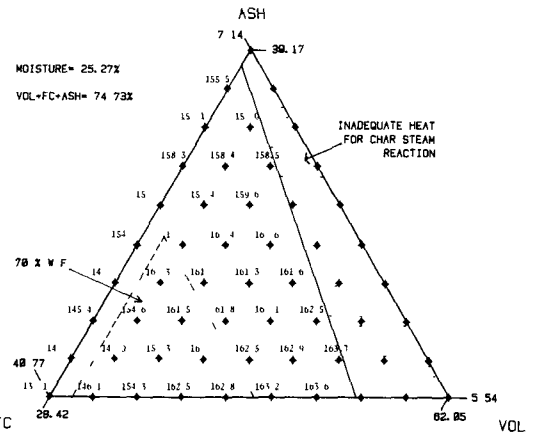

Figure 8. Ternary Diagram for Wilcox-Fluvial Category at 25.27% Moisture.

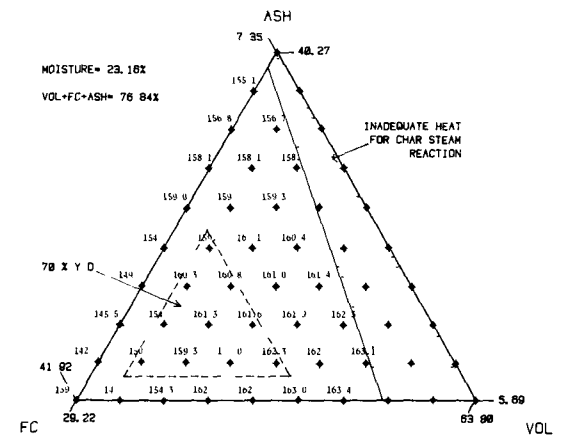

Figure 9. Ternary Diagram for Yegua-Deltaic Category at 23.16% Moisture.

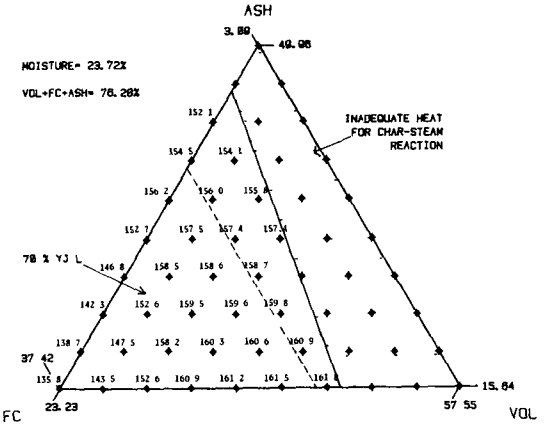

Figure 10. Ternary Diagram for Yegua-Jackson Lagoonal Category at 23.72% Moisture.

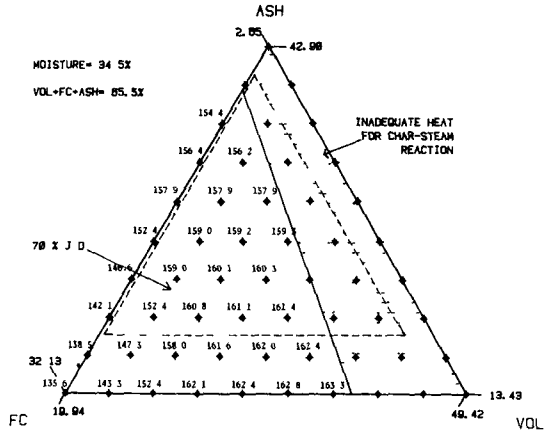

Figure 11. Ternary Diagram for Jackson-Deltaic Category at 34.5% Moisture.

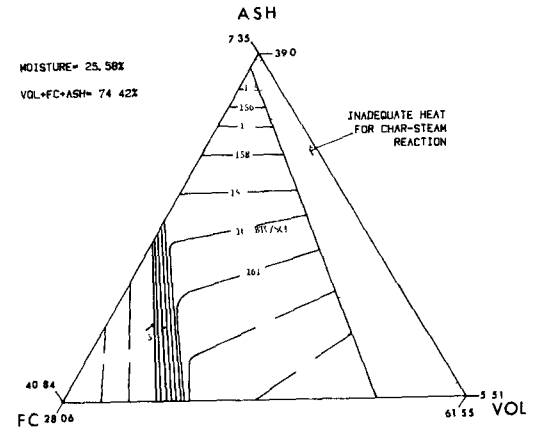

Figure 12. Ternary Diagram for All Data at 25.58% Moisture.

2.9 UNDERGROUND COAL GASIFICATION CAVITY DEFINITION FOR RAWLINS TEST 2

J. M. AVASTHI [1/]

ABSTRACT

The cavity definition study of the first test of the DOE-sponsored underground coal gasification program in steeply dipping beds, provided results to plan, install, instrument, and monitor the second test at Rawlins, Wyoming. The successfully completed test met all its objectives and set the stage for future multi-module tests. The cavity definition field work for the second test was conducted by the Laramie Energy Technology Center with input from the Gulf Research & Development Company. The results of this work indicate that the firepit mechanism was operative for Test 2, and a void space similar to that observed in Test 1 also exists for Test 2. The present study estimates the dimensions and volume of the affected area, updip extent and bulking factor of the affected rock, based on the field work performed by LETC.

INTRODUCTION

Gulf Research & Development Company (GR&DC) has successfully completed a DOE-sponsored (Contract No. DE-AC20-77ET13108) underground coal gasification project in steeply dipping coal beds (UCG/SDB), in order to assess the technical and economic viability of the process. The first test in the program was completed in December 1979. The experiment included a 28-day air injection test followed by a 5-day steam/oxygen test, and gasified approximately 1200 tons of coal over that period.(1) A program to characterize the reactor cavity was implemented in the Fall of 1980.(2) The data collected during the post-burn characterization program of Test 1 aided in defining the process, the gasification cavity, and resource recovery. It also helped in the design of the process module and monitoring wells for Test 2.

The second and last test in the UCG/SDB program was completed in November 1981. This test included 65 days of oxygen/steam injection and gasified aproximately 8560 tons of coal (~200 000 cu ft).(3,4) The test activities during Test 2 are summarized in Table 1, and the major differences between Test 1 and 2 are summarized in Table 2. A program to characterize the reactor cavity was implemented by the Laramie Energy Technology Center in the Summer of 1982. The objectives of the post-burn characterization program for Test 2 were:

- to determine the extent, shape and dimensions of the gasified area.
- to confirm the firepit mechanism observed in Test 1.
- to determine the volume of the overall affected region.

RAWLINS TEST 2 DESCRIPTION

The Test 2 process module consisted of a slant production well (SPW), a vertical linking well (VLW), a slant injection well (SIW), and a vertical injection well (VIW) as shown in Figures 1 and 2. The plan view of the module (Figure 1) shows the arrangement of wells along the strike

1/ Gulf Research & Development Company
P. O. Drawer 2038
Pittsburgh, PA 15230

TABLE 1

SUMMARY OF ACTIVITIES DURING TEST 2

Julian Day	Greg Day	Activity
219	August 7	Facility construction complete
226	August 14	System checkout complete.
229	August 17	Test operations began.
229	August 17	Repeated attempts to ignite the coal in the VLW failed.
235	August 23	Successful ignition of the coal seam at the base of the slant injection well (SIW) was completed.
237	August 25	HFEM Well 2-6 was converted to a linking well to help draw the link from SIW ===> SPW.
247	September 4	The link between the slant injection well and the product well was completed.
249	September 6	The SIW was converted from air to steam/oxygen injection.
250	September 7	The oxygen flow was increased to 400 scfm and the experimental schedule for Module 1 (SIW ===> SPW) was begun.
275	October 3	Linking to the vertical injection well was begun.
284	October 11	The link to the vertical injection well (VIW ===> SPW) was completed.
290	October 17	Steam/oxygen injection into the VIW was begun with the SIW on standby. Experiments for the second module began (VIW ===> SPW).
304	October 31	Module 1 (SIW ===> SPW) restored and simultaneous operations in both modules began.
314	November 10	Deliberate, cyclic oxygen flow was begun at the SIW.
315	November 11	Steam/oxygen flow terminated and shutdown began.
317	November 13	SPW vented through portable flare and post-test operations began.

TABLE 2

MAJOR DIFFERENCES BETWEEN TESTS 1 AND 2

	Test 1		Test 2
True Vertical Depth of Test (ft)	400		600
Open Drilled Link Length (ft)	60		250
Injectant	Air	Steam/O_2	Steam/O_2
Steam/O_2 Ratio	--	0.2 to 2.7	1 to 5
Test Duration	28	5	65
Operating Pressure (psi)	20-80	<20	60 to 150
Coal Gasified (tons)			
Daily	30*	33	130*
Total	1035	165	8562
Dry Gas Production (MMSCF)			
Daily	4.0*	2.5	6.9*
Total	112	12.5	455
Dry Gas Heating Value (Btu/scf)	146	227	326
Combustion Energy of Coal in Product Gas (%)	76		86

* Denotes average for the total test.

of the seam. The SPW formed the centerline of the module with the VLW drilled to intersect (within 2 ft) the SPW uncased length. The VIW was drilled to the same depth as the VLW but was displaced 23 ft site south from the SPW along strike. The SIW was drilled 25 ft site north of the centerline. Figure 2 shows the three dimensional view of the process module. The SPW extends to 600 ft true vertical depth (with the last 250 ft of uncased drilled "link" zone in the coal seam). This well penetrated the footwall of the main G seam at a true vertical depth (TVD) of 200 ft to minimize potential leakage problems along the product well casing and the outcrop zone. The SIW entered the footwall of the main G seam at approximately the depth of the SPW and was cased into the G seam approximately 5 ft. About 50 ft of uncased hole extended beyond the casing shoe. The VIW and VLW were cased to the top of the main G seam. The uncased length of the VLW and VIW was 42 and 41 ft, respectively.

The 250-ft long open drill link in the SPW was designed to provide a main burn path for Test 2. However, there was no indication from test data that hot gases had flowed through the bottom two-thirds of the drilled link. Apparently, an alternate link was created by injecting high pressure air into the SIW after ignition with gas production through the SPW. The apparent location of this link path was formed at the beginning of operations in module 1, as shown in Figure 3. This link path was derived from the leading points of contours of the affected region[4] which was based on the times of failures of the wells, the HFEM data and mass balance calculations. The direction of the link path (or fracture) is consistent with the geologic and structural features of the test site.[4]

The test activities during Rawlins Test 2 are summarized in Table 1, and the major differences between Tests 1 and 2 are summarized in Table 2.

REACTOR GROWTH MONITORING IN TEST 2

The growth of the gasification reactor in steeply dipping coals is believed to be explained by the "fire pit" concept. The process gases are injected at the bottom of the reactor. Coal is consumed by the oxidation and gasification reactions. The hot product gases pass through fresh coal which then dries and falls to form a rubblized bed. In a stabilized reactor, oxidation occurs just above the ash and slag zone. The gasification and pyrolysis reactions occur further updip in the coal and char rubble. Drying of rubblized coal and fresh coal occurs further updip. As coal char is consumed from below, the rubble pile continues to shift downward. However, new coal falling at the top bulks to minimize the void space. This concept was supported by the results from Test 1.[2]

The Test 2 reactor growth was monitored in real time by nine High Frequency Electromagnetic Mapping (HFEM) wells, three Multiple Point Borehole Extensometer (MPBX) wells, and one multiple thermocouple well (Figure 4). The most conclusive information was obtained through thermal logs taken in the HFEM wells and the HFEM well failures.[4] Five HFEM wells failed during the test operations period. The locations and Julian date of the well failures are shown in Figure 5. It is believed that the wells failed due to shifting of the coal as the affected zone approached. Small initial cracks in the cement and fiberglass casing resulted in water drainage from the wells. The times of the well failures provided useful information for determining the growth of the affected region.[4] HFEM 2-3 failed soon after the beginning of oxygen injection, suggesting that the initial growth was in that direction. The sequence of the next well failures suggested expansion of the region to the south along with the updip growth. The failure of HFEM 2-7 during VIW linking indicated that VIW-SPW communication was attained by linking and not through growth of the reactor. The fact that the three updip wells (HFEM 2-8, 2-10, and H-21) did not fail provides evidence of the limit of the affected region. All of the data confirmed the firepit theory which is discussed in later sections.

POST-TEST OBSERVATIONS

The cavity growth monitoring conducted during Test 2 continued in the form of post-burn observations which consisted of monitoring the surface and subsurface strata movement and changes in the cavity and surrounding area temperatures. The observation of strata movement above the resulting UCG cavity was divided into two parts. The surface movement was observed

through the subsidence monuments and subsurface strata movement and roof fall was observed by the borehole extensometers. Surface subsidence monuments which were located along and perpendicular to the Test 2 reactor center line have not recorded any surface movement to date. A maximum surface subsidence of the order of 2.6 in. was predicted using British National Coal Board[5] calculation procedures.

During Test 2, there was no definite indication of any major roof fall or strata movement, except circumstantial observation of events in the flare emissions (i.e., sudden short bursts of particulates). Following the termination of the burn on November 15, 1981, a data logger on the test site was programmed to collect the strata movement and temperature data. Prior to February 1982, the extensometer anchors and TDR observations did not indicate any major strata movement or disturbance. During February and March 1982 the TDR data from extensometer well EX-2 indicated strata disturbances between the depths of 492 and 521 ft, and 446 and 471 ft. Since there was no corresponding movement in the anchor readings, the TDR disturbances were assumed to be evidence of lateral strata movement with subsequent pinching and shorting out of the TDR cable. A manual inspection of the extensometer wellheads confirmed that none of the anchors had been lost, so extensive roof fall at the anchor locations probably did not occur.

The subsurface temperatures were monitored in a thermocouple well and in the extensometer wells at each of the anchor depths. Due to the malfunctioning of the data acquisition system, no temperature changes in the extensometer wells were indicated during the test. After the termination of the test when the data acquisition system was rewired and reprogrammed, temperature observations in the extensometer wells were recorded for the first time. Some thermocouples have shown a steady temperature decrease since the termination of the test. It is not possible to determine when these temperatures began to increase or their maximum values. Other thermocouples showed a steady temperature increase.

Six out of the seven thermocouples in the extensometer well (EX-2) had experienced temperature increase. The thermocouples at the anchors 1 and 2 were most affected due to their close proximity (56 and 116 ft) to the burn zone. Only one of the seven thermocouples in extensometer well EX-1 showed any noticeable thermal effects. Two other thermocouples in well EX-1 and three thermocouples in well EX-3 showed only slight increase in temperatures.

POST-BURN CAVITY DEFINITION PROGRAM

The cavity definition program which included the real-time monitoring, post-burn monitoring, and post-test characterization* phases was designed to meet the following objectives:

- to determine whether the "firepit mechanism" postulated for UCG-SDB is valid for Test 2.
- to compare the cavities formed by footwall vs roofwall injection.
- to obtain resource recovery and sweep data.
- to obtain and characterize cores taken from various parts of the cavity to determine the effects of UCG on the surrounding rock strata.
- to obtain void volume and packed volume data to determine bulking factors and their effect on surface subsidence.
- to obtain data for predictive modeling efforts.

In order to meet the cavity definition objectives, it was necessary to determine the location and shape of the UCG reactor, the affected area, and the void space above the reactor in Test 2. The cavity definition program for Test 2, as established by the LETC and GR&DC, consisted of the following:

1. Drilling and logging of the failed HFEM wells.
2. Drilling and logging of five new post-burn wells.
3. Sonar caliper survey of the appropriate HFEM and post-burn wells.

* conducted by the Laramie Energy Technology Center.

4. CSAMT survey of the UCG reactor to delineate the char boundary.
5. High resolution seismic survey of the UCG reactor.
6. Core analyses to determine the thermal history of the burn.

The following paragraphs describe the above activities to define the cavity volume, shape, and post-burn characterization.

HFEM Wells

As a first step towards the post-burn characterization, the use of existing HFEM wells was made. These HFEM wells, besides providing the HFEM data during the UCG test, also provided the well failure data (Figure 5) which was a valuable source for extrapolating the burn volume as well as the extent of the affected area. During the early part of the post-burn investigation the access depth in each well was determined by lowering the caliper logging tool. The results of this investigation were as follows:

Well	TVD	Access Depth	Remarks
HFEM 2-3	568 ft	142 ft	In steel casing
HFEM 2-4	563 ft	442 ft	In steel casing
HFEM 2-7	608 ft	393 ft	In fiberglass casing
HFEM 2-9	517 ft	336 ft	In fiberglass casing

The access depth of the logging tool in these wells is indicative of either the pinching of casing pipe or some sort of blockage in the well, caused by ground disturbance. Due to the possible drilling problems associated with drilling through damaged steel casing, drilling HFEM wells 2-3 and 2-4 was avoided. The drilling and logging observations in each of the HFEM wells drilled, cored, and logged are given below.

HFEM 2-7

After clearing the blockage in this well the drill string moved freely in the borehole and hit the bottom at a depth of 473 ft, where coring was commenced. No void space was encountered in this well. The cores obtained showed the thermal effects on the coal seam and overlying rocks. Apparently the burn was limited to the upper 10 ft of the main G coal seam, whereas the lower part of the seam was unaffected. This was confirmed by the density and gamma ray logs (Figure 6), which clearly show the difference between the thermally altered and unaffected coal and rocks. The overlying rocks containing the upper coal stringer up to 45 ft above the main G coal seam were also thermally affected. The coring was carried to below main G coal seam, up to 589-ft depth.

HFEM 2-9

The blockage in this well was cleared by drilling at the depth of 336 ft. The drill string immediately entered a void space, which continued to the depth of 364 ft where a rubble pile was hit. Coring was continued through the rubble to the depth of 484 ft, until drilling was out of the burn zone, the main G seam coal, and thermally unaltered strata. The rubble core showed distinctly thermal alteration of sandstone and shale. The caliper log of the HFEM 2-9 showed expansion of the borehole diameter at the depth of 336 ft, thus confirming the existence of the void space at that depth.

Post-Burn Wells

Five post-burn coring wells were drilled in the Test 2 burn area. The location of these wells was decided by discussion and consultaion between the LETC and GR&DC personnel. The location of the five wells is shown in Figure 7. These wells were drilled with a noncoring bit to a depth of 250 ft, and were then cored through the burn area. The results of the drilling and logging of these boreholes is discussed individually in the following paragraphs.

Post-Burn Well PB 2-1

The purpose of this borehole was to locate the burn area at the base of the VIW, which constituted module 2. Between the coring depth of 250 ft and 491 ft, only the unaltered rock strata was encountered. The first indication of thermal alteration of rock by UCG was noticed at the coring interval of 491 to 501 ft. From this interval onward the core recovery dropped sharply from 80-90% to 25-50%, and it was hard to determine, from what depth the core was recovered. This apparently was due to the crumbling nature of the rock caused by thermal alteration. No

void space was encountered in this well, but altered sandstone, paralava, and thermally altered coal cores were obtained from the burn cavity. In this well also, as in the HFEM 2-7, a zone of thermally unaffected coal was observed. The borehole was drilled to the final true vertical depth of 596 ft, into the lower coal stringer.

Post-Burn Well PB 2-2

This well was drilled to locate the slag pit at the base of the SIW (module 1), and to collect samples of the ash and slag. Between the coring point (i.e., 250-ft depth) and 406-ft depth, unaltered rock strata were encountered. The first indication that the corehole was nearing the burn cavity came from the sandstone core (coring interval 406 to 416 ft) which was hot but thermally unaltered. From this core interval onward, thermally altered rock samples were obtained, and the core recovery was poor. From 486-ft depth onward the corehole seemed to be in the burn cavity. The core samples showed evidence of extreme thermal effects on rock, coal, and ash samples. The samples obtained were of varied colors, textures, and vesicular nature, and included paralava, fused, and baked shale. The borehole was drilled to a depth of 586 ft into the shaly siltstone which underlies the main G seam. The extent of the thermal effects observed in this well and core samples are evidence of the firepit postulated in Test 1.

Post-Burn Well PB 2-3

Since HFEM 2-3 and HFEM 2-4 could only be accessed into the steel casing, and the decision not to drill through steel casing was made, a post-burn well between these two HFEM wells was drilled. Moreover, it could provide information in the mid-section of the UCG cavity. From the coring point at 250-ft depth, unaltered rocks were encountered up to a depth of 416 ft. Beyond this depth thermal alteration of rocks was noticed, and the core recovery became low. This indicated that the core came from either the thermally altered zone or the rubble zone. In this borehole only thermally altered rock cores and coal were obtained; there were no ash samples. This borehole was drilled to the depth of 546 ft into the unaltered siltstone below the main G seam.

Post-Burn Well PB 2-4

This well was drilled to locate the updip extent of the burn zone along the SPW. The CSAMT survey conducted by the Sandia Laboratories indicated the presence of fingering in the upper part of the burn zone. This well did not show any thermal alteration, void space, or burn zone up to the depth of 416 ft. The bottom part of the borehole ended in the unaltered G coal seam.

Post-Burn Well PB 2-5

This borehole was located in the middle of HFEM 2-3 and HFEM 2-5 towards north. The purpose of this hole was to confirm the width of the UCG affected area. From the coring point at 258 ft to the 456-ft depth, only unaltered rock was cored. The first evidence of thermal alteration in this well came from the coring interval of 456-466 ft, where slightly altered shale was recovered. Beyond this point the corehole was in the rubble zone. The coring in this well was continued to a depth of 566 ft, till it was out of the main G seam.

Sonar Caliper Survey

LETC contracted to conduct the sonar caliper survey in one well as a part of the Test 2 post-burn cavity definition program. The well chosen for this purpose was HFEM 2-9. The contractor was able to lower the sonar equipment into the cased well, but was unable to make any observation due to the presence of high humidity in the post-burn cavity.

CSAMT Survey

Sandia National Laboratories conducted mapping of the Rawlins Test 2 area using the CSAMT (Controlled Source Audio-frequency Magnetotelluric) technique.[6] The plan view of the interpreted "char" boundary is shown in Figure 8. The "char" boundary as shown in Figure 8 for Test 2 agrees with observations made in HFEM wells. The partial CSAMT results for Test 2[7] were extrapolated to obtain the extent of the char boundary for the rest of Test 2 cavity, and is also shown in Figure 8.

High Resolution Seismic Survey

LETC conducted the high resolution seismic survey of the Test 2 burn area. A rubble-filled cavity was detected,[8] but it failed to detect any water- or air-filled voids at Test sites 1 and 2, the presence of which had been confirmed by other means. The results of the seismic study could not adequately outline the UCG affected area; therefore, these results could not be used to substantiate the observations made by post-burn drilling and CSAMT survey.

Core Analyses

The cores obtained from the post-burn wells are being analyzed by the Colorado State University, Ft. Collins, under a contract with LETC. The purpose of these analyses is to obtain the thermal history of the burn and thermal effects on the overburden. These results will be available in the near future in a separate report.

CAVITY DEFINITION DATA ANALYSIS

The data from the drilling and logging of the HFEM and post-burn wells were combined with the results of the CSAMT survey to obtain a three-dimensional conceptual picture of the UCG affected area and cavity. It should be stated that the data used for this purpose are not complete. A significant amount of cavity definition data from the sonar and high resolution survey could not be obtained. In the absence of these data a number of assumptions were made to obtain the cavity configuration, volume estimates of the Test 2 UCG burn area and the resulting cavity. The following assumptions were made regarding the cavity shape and dimensions:

- The char boundary predicted by the CSAMT survey is the maximum limit of the UCG burn area.
- The UCG cavity is symmetric in shape.
- The cavity has a dome shape as would be expected in an unsupported mined-out area.
- The cavity has stabilized and no more changes in its configuration are expected.
- The volume of coal consumed in the burn, calculated from the mass balance calculations is 200 000 cu ft.

The information obtained from the geologist's field logs and geophysical logs for the HFEM and post-burn wells was put together to prepare a physical model of the UCG burn cavity. Using the width at the point of intersection of the boreholes with the plane of the main G coal seam floor as a guide, cross sections of the cavity were made for those boreholes which intersected the cavity. These cross sections were put together on the coal seam floor along its dip. This outlined a cavity approximately 200 ft along its axis, about 100 ft wide along most of its 200-ft length, and about 50 ft high (perpendicular to the plane of the coal seam). The shape of the UCG affected area can be visualized as a half cylinder (100 ft long and 50-ft radius), with a quarter sphere (50-ft radius) on each end (Figure 9). The volume of this shape can be calculated easily, as follows:

The volume of the UCG affected area
$= (\pi \times 50 \times 50 \times 100)/2 + 2/3 \times (\pi \times 50 \times 50 \times 50)$
$= 654\ 762$ cu ft

Since the actual affected shape will not be as regular as visualized, therefore, the actual volume of such area is assumed to be 600 000 cu ft for the convenience of following calculation:

According to the mass balance calculations the volume of coal consumed in Test 2 = 200 000 cu ft
Assuming 5% ash content by volume, the volume of ash left in the rubble form =10 000 cu ft
Therefore, void volume caused by the burnt coal = 190 000 cu ft
Total volume of rock affected by UCG in Test 2 = 600 000 cu ft
Total volume of rock (now in rubble form) = (total volume of rock affected - void volume caused by the coal consumed)
= (600 000 - 190 000) = 410 000 cu ft
Assuming, the volume of the void space in the affected area = V cu ft
The volume of rubble in the affected area = (600 000 - V) cu ft
Therefore, the bulking factor for Test 2 = (600 000-V)/410 000

Assuming different values of V, we get the following results:

V = 7 400*cu ft, bulking factor = 1.445
V = 10 000 cu ft, bulking factor = 1.439
V = 15 000 cu ft, bulking factor = 1.427
V = 20 000 cu ft, bulking factor = 1.414
V = 30 000 cu ft, bulking factor = 1.390

DISCUSSION

Analysis of data gathered during Test 2 have led to the development of a "conceptual" model of the process. The major growth of the reactor was updip along the fractures created during the initial stages of the Test 2, between the casing shoes of the SIW and SPW. This was indicated by the early failure of the HFEM wells between the SIW and the SPW during the test. Apparently, the reactor grew via periodic dropping of large chunks of coal into the base of the reactor. A rubble bed was established over the base of the SIW and served as a firepit. The firepit was confirmed in post-burn well PB 2-1 in which large amounts of slag were found. Presumably there was a constant feeding of the coal in rubble form from the coal seam in the updip region. This rubblized coal was observed in HFEM 2-9 taken through the upper 1/3 of the reactor. In the process of gasification and cavity growth the overlying rocks were also thermally affected, weakened, and ultimately failed and formed the part of the overall cavity. The failure of roof rocks and its extent is limited only by the overall stabilization process governed by rock properties, strength parameters, and the in situ stresses.

Although, the above discussion basically explains the "fire pit" cavity growth concept for the SDB cases, it does not explain the differences observed between the Tests 1 and 2. The major difference is in the type of cavity resulting from two tests. The explanation of this difference is mainly in the manner in which the cavity growth took place in the two cases. In Test 1 a drilled borehole link formed the basis of the cavity growth, which initially formed a cigar-shaped cavity. Half way through the burn it had to be stimulated by injecting diesel fuel, because it seemed that the coal was no longer being fed to firepit and the char bed was being depleted. This stimulation probably did help to increase the duration of test, but its exact effect on the cavity growth is hard to explain. Apparently in Test 2, the bottom two-thirds or so of the drilled link never played any active role, presumably due to its collapse and/or plugging during the idle period before the start of the test. The postulated plugged borehole link and the plugged vertical link well (see schedule of events in Table 1) required multiple pressurizations during start-up, creating the formation of the fractured link between the SIW casing shoe and the SPW drilled link. The fractured link may have helped create a compact reactor, as compared to Test 1. The fractured coal seam and the following drying process provided a continuous feed into the firepit. This probably also provided a continuous support to the immediate roof due to its bulking, which ultimately did not produce any major roof fall or sudden movement of the overlying strata. The roof rocks which finally formed the part of the overall UCG cavity resulted due to the thermal effects on them, thus causing weakening and fracturing. The consistency of the test and product gas quality support this form of cavity growth. Moreover, the entire reactor was not consumed by the time of test termination and could have lasted significantly longer.

The bulking factor calculated for Test 2 is an approximation. In the absence of accurate void space volume, only a range of bulking factor values can be obtained by assuming different values of the void space. This range of values so obtained for Test 2 (1.39-1.445) is lower than that of the Test 1 (1.84 to 2.04). The explanation of this difference lies in the earlier discussion. The extensive fracturing discussed earlier caused the coal to feed the firepit at a more constant rate than Test 1 and therefore did not provide the opportunity to the overlying rocks and the falling coal to bulk as much as in Test 1. This may have resulted in the lower bulking factor values. This is further supported by the in situ thermal alteration of the overlying rocks, as observed in the cores from the post-burn coreholes. It should be pointed out that the bulking factor calculated on the basis of volumes of coal burned and affected region within the coal seam also projected a bulking factor of 1.4.[4]

All of the available data indicate that the thermal alteration was limited

* The volume of void space in Test 1, as observed by the sonar caliper survey.

only to the overburden rocks. The rocks underlying the main G coal seam did not show any evidence of thermal alteration. This observation is similar to that of Test 1.

CONCLUSIONS

The following conclusions can be made based upon the results of the cavity definition study:

- The post-burn coring data, along with operational data, indicate that the firepit mechanism of reactor growth was operative for all of Test 2.
- There is a slag pit at the bottom of the reactor near slant injection well (SIW) casing shoe in Test 2.
- Although core analysis is yet to be conducted, a visual inspection of the cores indicates similarity with the cores from the post-burn wells of Test 1. This may indicate a similar temperature range (i.e., 1000-1500°C) for Test 2.
- The shale above the G coal seam fused with coal ash to form slag at the bottom of the UCG cavity.
- The reactor did not grow beyond the slant production well (SPW) casing shoe, as was observed in the case of Test 1 reactor.
- Thermally altered sandstone, shale, and siltstone rocks were found in the reactor cavity. The in situ thermal alteration of overlying rocks was also evident in Test 2.
- Void space was only observed in HFEM 2-9 well and its height as measured by the drill string was approximately 30 ft. The volume of this void space is yet to be determined.
- The bulking factor for Test 2 is approximately 1.4, as compared to 1.84-2.04 in Test 1.

ACKNOWLEDGMENT

The author would like to acknowledge the help of the Laramie Energy Technology Center, especially Mr. Dan Youngberg, for providing the information and data used in preparation of this paper.

REFERENCES

1. Singleton, A.H., Noll, W.L., and Allen, J.M., "Summary Report of the Rawlins Test 1 for Gasification of Steeply Dipping Coal Beds," Proceedings of the Sixth Underground Coal Conversion Symposium, Shangri-La, Oklahoma, 1980, pp. I-30 to I-40.

2. Davis, B.E., Avasthi, J.M., Reid, C.S., Slater, G.E., and LaBerge, G.L., "Rawlins Test #1 Cavity Definition Study," Proceedings of the Seventh Underground Coal Conversion Symposium," Fallen Leaf Lake, California, 1981, pp. 66-81.

3. GR&DC--"Phase III Report: Results of Rawlins Test No. 2," March 1, 1980-April 15, 1982, Vol. 1, Report Prepared for the Division of Oil, Gas and In Situ Technology, U.S. Department of Energy, Contract No. DE-AC20-77ET13108, 1982.

4. Garon, A.M., Cala, G.C., and Avasthi, J.M., "Rawlins Test 2 Cavity Growth," Proceedings of the 8th Underground Coal Conversion Symposium, Keystone, Colorado, 1982, pp. 103-114.

5. National Coal Board, "Subsidence Engineers Handbook," Mining Department, London, England, 1975.

6. Bartel, L.C., "Potential Use of the CSAMT Geophysical Technique to Map UCG Processes," Proceedings of the 8th Underground Coal Conversion Symposium, Keystone, Colorado, 1982, pp. 59-70.

7. Bartel, L.C., Personal Communication with J. M. Avasthi regarding the CSAMT Survey of Rawlins Tests 1 and 2, September 1982.

8. Youngberg, A.D., Berkman, E., and Orange, A.S., "High Resolution Seismic Survey of the Rawlins, Wyoming, Underground Coal Gasification Area," Report by the Emerald Exploration Consultants, Inc., January 1983.

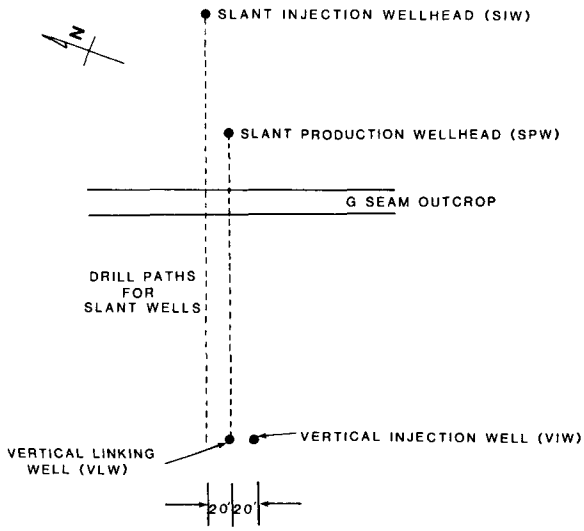

FIGURE 1. PLAN VIEW OF THE UCG MODULE FOR TEST 2

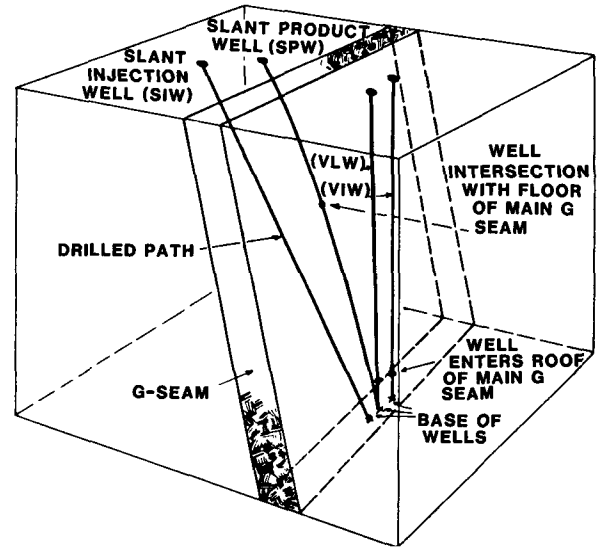

FIGURE 2. THREE-DIMENSIONAL VIEW OF THE UCG MODULE FOR TEST 2

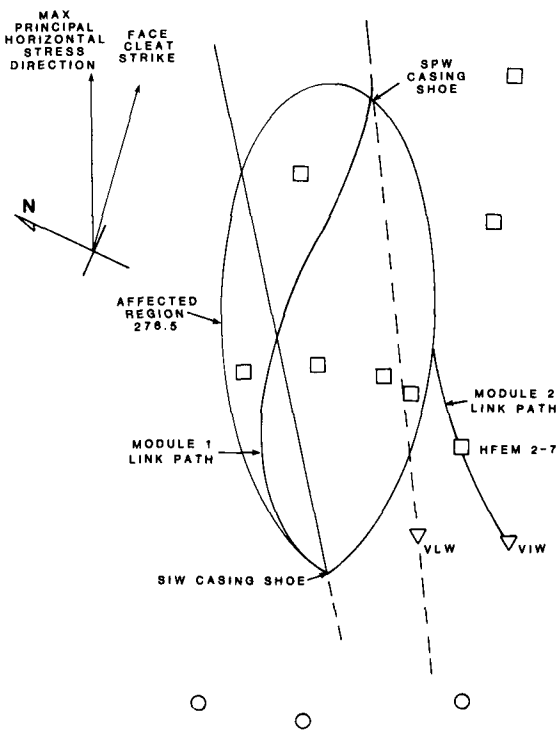

FIGURE 3. LINK PATHS FOR MODULES 1 AND 2 [FROM GARON, et al.[4]]

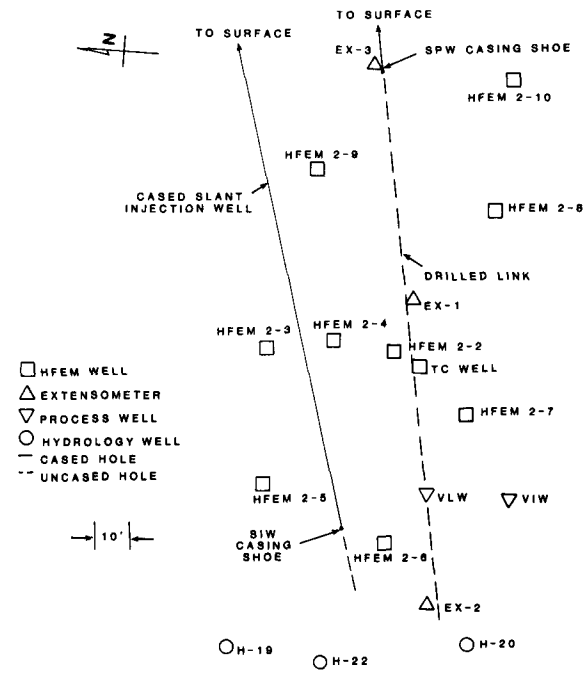

FIGURE 4. DOWNHOLE LOCATION OF DEEP INSTRUMENT WELLS IN TEST 2

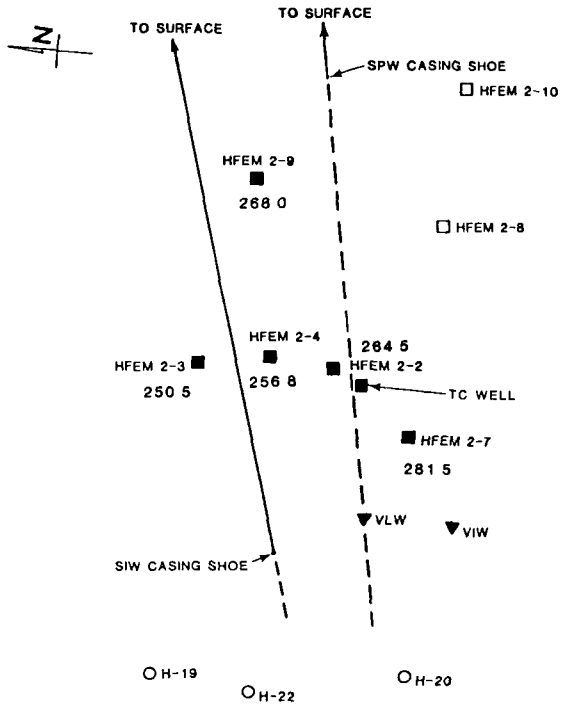

FIGURE 5. HFEM WELL FAILURES (IN JULIAN DAYS) OBSERVED IN TEST 2 [FROM GARON, et al.(4)]

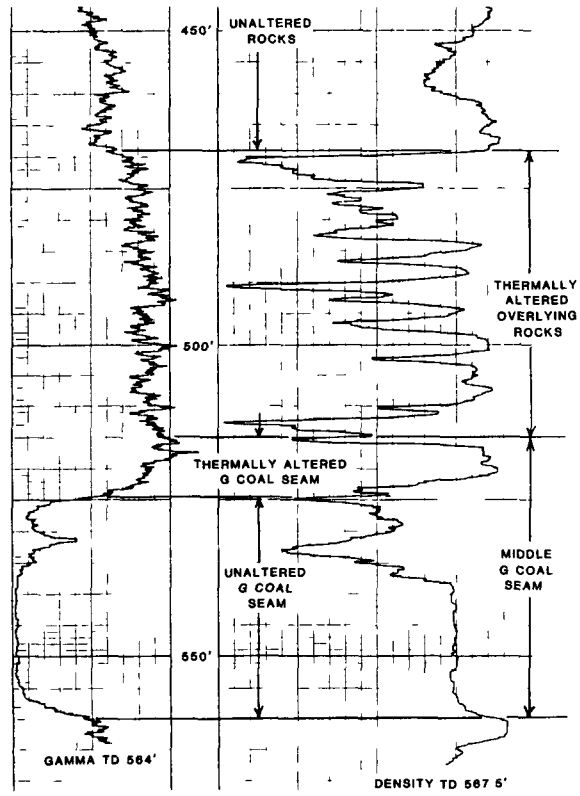

FIGURE 6. DENSITY AND GAMMA RAY LOGS IN HFEM 2-7 WELL, SHOWING DIFFERENCE BETWEEN THE AFFECTED AND UNAFFECTED ROCK AND COAL STRATA

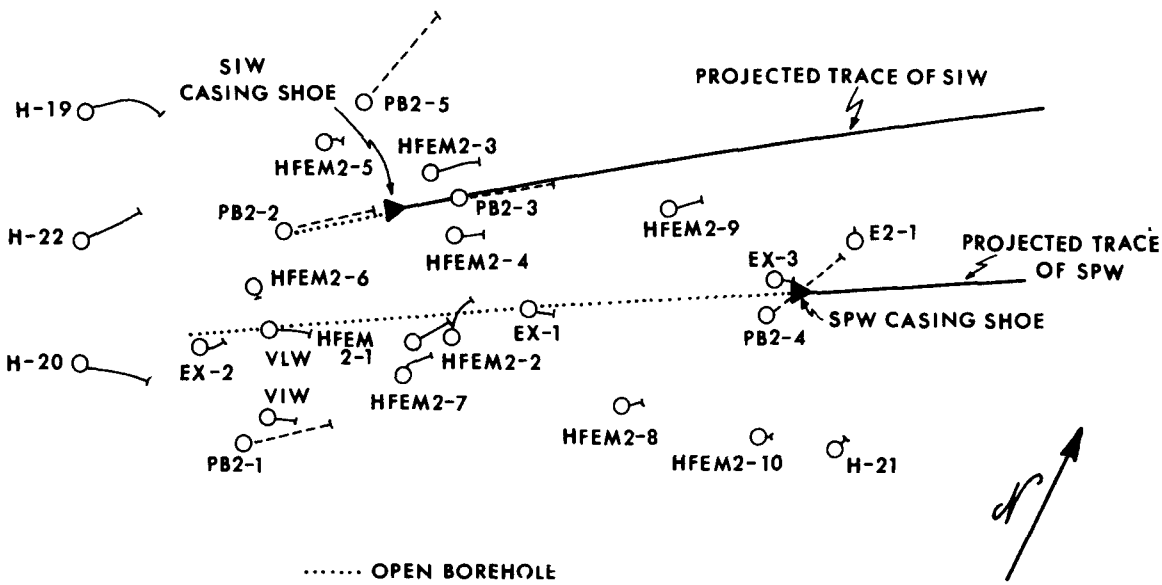

FIGURE 7. LOCATION OF THE POSTBURN AND OTHER WELLS FOR TEST 2

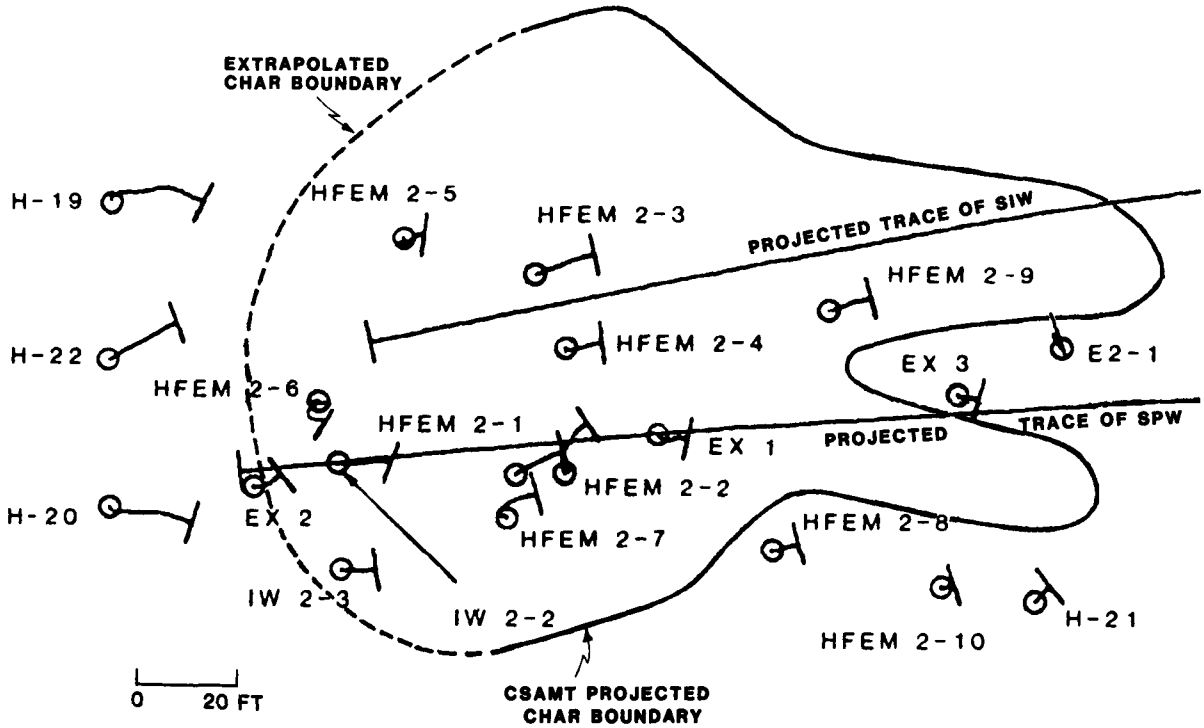

FIGURE 8. PLAN VIEW OF THE CSAMT INTERPRETED CHAR BOUNDARY FOR TEST 2

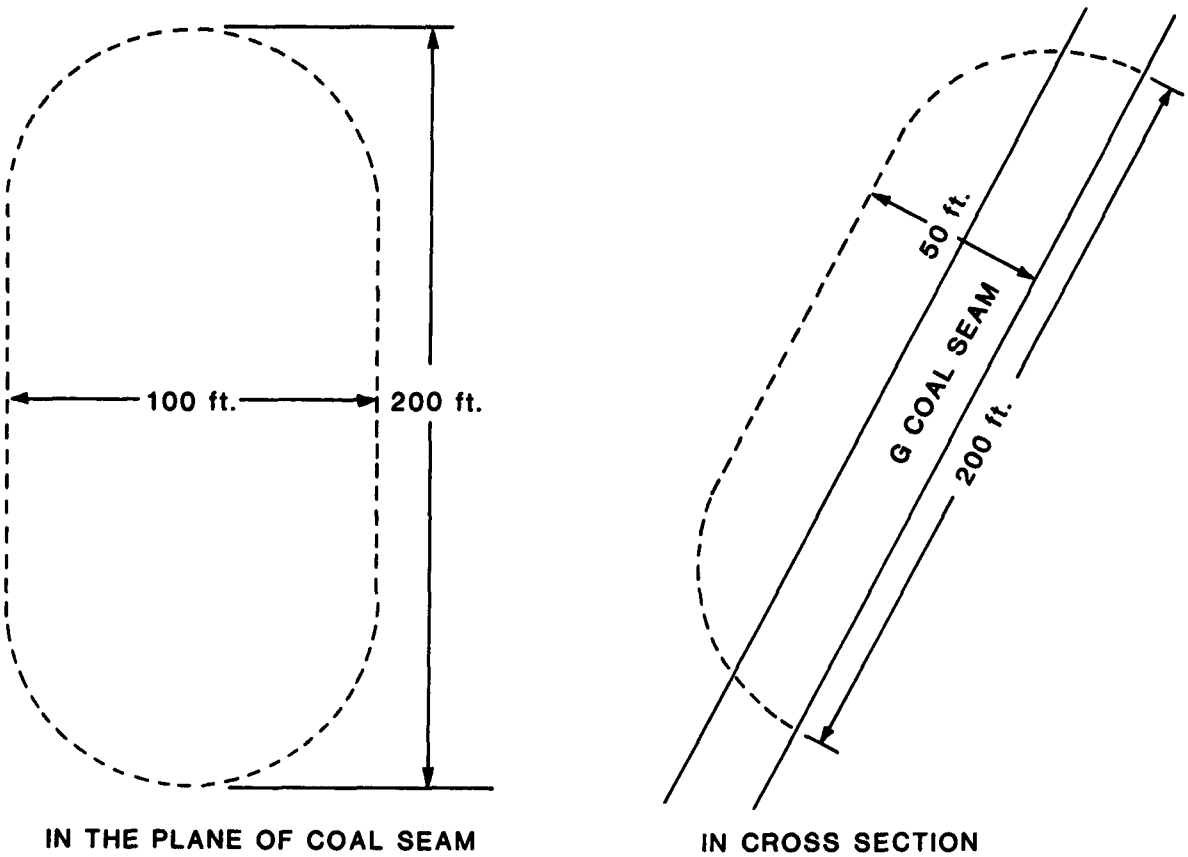

FIGURE 9. PROJECTED CAVITY AND AFFECTED AREA FOR RAWLINS TEST 2

2.10 SUBSIDENCE PREDICTION FOR THE FORTHCOMING TONO UCG PROJECT

by

Herbert R. Sutherland 1/
Paul J. Hommert 1/
Lee M. Taylor 1/
Steve E. Benzley 2/

ABSTRACT

The motion of the strata that overlie the TONO UCG Project partial seam test is calculated using the analyses that have been developed for the prediction of subsidence above coal mines. This purely mechanical analysis of the overburden response to the formation of a void in the underlying coal seam is based on the analysis of two codes. The first is a finite element code that uses a nonlinear "rubble" model to describe both the kinematics of roof fall and the continuum behavior of broken and unbroken strata. The second is a "block" code that treats the overburden as an assemblage of blocks. The equations of motion are solved for each block using an explicit integration operator. As both of these calculations are two dimensional in nature, they are used to calibrate the semi-empirical, complementary influence function model. This model permits the extension of the two dimensional analyses to three dimensions by using computationally efficient algorithms. These techniques are calibrated to UCG projects by analyzing the Hoe Creek 3 burn. Their application to the TONO project required the estimation of the lateral extent of the cavity for the partial seam test. The estimates utilized the projected tons of coal to be removed and two scenarios for the burn sequence. The subsidence analytical techniques were combined with the expected pattern of coal removal to place an upper bound on the surface subsidence that can be anticipated at the TONO UCG site.

1/ Sandia National Laboratories, Albuquerque, New Mexico 87185
2/ Brigham Young University Provo, Utah 84602

This work supported by the U.S. Dept. of Energy under Contract DE-AC04-76P00789.

INTRODUCTION

Modeling the failure and settlement of strata above mine openings requires a knowledge of several different geomechanical processes such as the failure of the rock mass above the mine opening, the fall of this mass into the opening, the associated bulking of the rock rubble, and the recompaction of the rubble under subsequent loading. These processes have been studied at Sandia National Laboratories over the past several years in an effort to develop a predictive model for the subsidence above coal mines.[1] This effort has led to the development of several models which describe the mechanical response of the overburden to the formation of a void in an underlying coal seam.

In this manuscript, the motion of the strata that overlie the TONO UCG Project partial seam test is calculated using the analyses that were developed in the coal mine subsidence R&D program. The manuscript starts with the descriptions of the three models that will be used in the analysis. The first two models, the rubble model and the block model, are then calibrated against the Hoe Creek 3 data. Finally, all three models are used to place an upper bound on the subsidence at the TONO site. The TONO predictions are based on two estimates of the lateral extent of the burn cavity. It should be emphasized that

these calculations describe only the purely mechanical response of the overburden, i.e., no thermal response is considered.

ANALYSIS TECHNIQUES

Rubble Model

The special feature of this numerical approach to the prediction of subsidence is the incorporation of a continuum description of the "rubblization" process that occurs as the roof material fails and falls into the cavity below it.[2] A graphical representation of this process is shown in Figure 1. Initially the model characterizes a geological material in its original state (Figure 1a). In this particular formulation, a typical rock material may be characterized as either elastic or elastic plastic with a pressure dependent yield surface. After failure (under tension), the strata breaks apart to form rubble that falls under the influence of gravity (Figure 1b). The rubble collects at the bottom of the void to form a stable pile of material with a void space above it (Figure 1c). Note that the rubble pile may increase in volume, i.e., bulked, when compared to its original state. As subsequent layers fail and fall, the rubble pile begins to compress and responds as a low shear material (Figure 1d). This process is also described in the volumetric strain-hydrostatic pressure plane of Figure 2. Rubble formation is introduced into the calculations via the volumetric strain and is activated when a critical tensile stress is reached. The initially solid material in compression behaves in a normal manner but, in tension, when the critical failure condition is attained (point 1), the material loses all stiffness and is allowed to deform freely within the physical confines of the system. This expansion is equivalent to free fall of the material. During recompression, the material again deforms freely until a redefined bulked state is reached (point 2). From this point, the material again supports a load. As described above, this model treats the elastic-plastic response of a continuum, the kinematics of rubble fall, and the post failed response of the rubble.

Block Model

The block motion model is intended for modeling the planer motions of highly jointed or layered geologic media where the deformations of the intact rock are negligible compared to the displacements which occur across the preexisting joint systems. The model divides the rock into a collection of discrete, individual blocks and monitors all the collisions which occur between them. This type of model was first proposed and developed by Cundall[3,4] and has been extended and used by several investigators for a number of geological investigations.[5,6,7]

The rigid body motions of each block are integrated using an explicit integration operator. Collisions between adjacent blocks are detected when a corner of one block attempts to penetrate the edge of another. A normal contact force is calculated for each corner/edge contact based on the distance that the corner penetrates the edge and the normal velocity of the corner with respect to the edge. A simple spring and dashpot model is used to calculate the resulting normal force. The shear (tangential) forces are calculated in the same manner using the same spring and dashpot model in conjunction with a Coulomb friction law.

The blocks can be treated as either rigid blocks or be endowed with the ability to deform. In the deformable case, each block has degrees of freedom associated with the strains in the block (in addition to the rigid body motions). An elastic constitutive relation is used to calculate average stresses in each block from the strains. The deformable blocks are analogous to constant strain elements in the finite element method. The blocks are deformable in all the examples shown here.

Complementary Influence Functions

Early considerations of subsidence before the advent of computer analysis led to the development of empirical formulations for the description of subsidence. In a recent paper, Sutherland and Munson[8] examined the motivating concepts for the influence function formulation of these models. Their analysis illustrated that the material

remaining in the seam is as influential on the surface subsidence as that of the void left by the extraction. This realization leads to an influence function concept that is based on two elements: the mined element and the unmined element. As shown in Figure 3, this concept, called complementary influence functions, assigns a surface response function for each element. The surface response is then determined by integrating (appropriately summing) the response for each element over all of the elements in the area of interest. This approach has the important property that it eliminates the computational difficulties normally associated with influence function formulations; that it can handle two and three dimensional calculations with equal ease; and that it can be used to examine the implications of changing stratigraphy on surface subsidence.

For the analysis described in this manuscript, this model offers a computationally efficient algorithm for extending the two dimensional calculations of the rubble model and the block model to the three dimensional geometry that will be encountered at the TONO site. The procedure for the three dimensional analysis is to "calibrate" the model using the two dimensional analyses of the other two models (i.e., determine the parameter set for this semi-empirical model) and then use the predicted cavity sizes to determine the surface subsidence.

SIMULATION OF HOE CREEK 3

Before a numerical model prediction of a rubblization can be attempted, some documented verification of the model(s) must be made. In this section the data from the Hoe Creek 3 coal gasification experiment are used to calibrate the input parameters for the TONO calculations. Hoe Creek 3 was an experiment conducted in the fall of 1979 near the town of Gillette, Wyoming (e.g., see Reference 9). A numerical model of this experiment has been done by Advani et al[10] in which a thermo-viscoelastic calculation was performed. An interpretation of the collapsed region of Hoe Creek 3 as given in Reference 9 is shown in Figure 4d. Note the complete rubblization above the burn cavity. The surface profile from Reference 9 and a description of the current maximum subsidence[11] are shown in Figure 5.

Rubble Simulation

The finite element grid used to model the Hoe Creek 3 experiment is given in Figure 4b. Note that this cross section represents a longitudinal model of this problem. Here the coal elements were assumed to gasify and were completely eliminated (ash remaining from the burn was not considered) and the claystone and sand elements were assumed to rubblize. Shown in Figure 4a is a description of the stratigraphy at this site. The material properties for the individual geologic layers are listed in Table I. As stated in Reference 9, "all the earth materials are poorly indurated. They are generally weak or friable, with strength characteristics very similar to those expected from soil materials, and are likely to be unstable if they form the roof and sides of an underground cavity." Consequently, all the overburden materials were assumed to fail at a tensile stress of 2.0 KPa.

Several calculations were done on the Hoe Creek 3 model to establish realistic bulking factors and failure conditions to simulate the subsidence condition. As reported in Reference 9, "gradual collapse of the roof occurred during the course of the burn and later, as a result, much of the material fell into the cavity as blocks and numerous voids were formed..." Thus, this field experiment provided an excellent source for determining the value of a "bulking factor" needed for the kinematics of rubblization calculations. This factor is defined here as the ratio of the initial volume of the material to the bulked volume of the material after it has failed and fallen. A bulking factor of 0.88 was required to match the field measured subsidence. A graphical plot of the rubble calculation is given in Figure 4e. A comparison of the measured and computed subsidence is shown in Figure 5.

Block Simulation

The Hoe Creek 3 experiment was analyzed using the same material properties as that used in the rubble model (i.e., Table I). The original configur-

ation of the blocks is shown in Figure 4c. The solid region in the figure represents the burned volume in the two coal seams. The asymmetry of the burned volumes was chosen to match the burned volume shown in Figure 4d.[9] There are 611 blocks in the model. Along each layer the block spacing was generated randomly.

In the original configuration, the blocks are unstable and begin to fall into the burned void. The final configuration is shown in Figure 4f and the surface subsidence trough is shown in Figure 5. As can be seen, the model gives a conservative prediction of the subsidence.

There are several explanations for the overestimate of subsidence. The fact that the model does not include any strength across the joints leads to a complete collapse if arching does not occur. The actual rock mass does have some strength and should behave as a continuum before failure. Also, there should be at least a 20 percent ash from the burn which was not included here in the burn volume. The burning of the coal would result in a gradual removal of the coal and a resultant sequential collapse of the rock mass which would reduce the total ground subsidence.

In addition to the physical explanations given above for the overestimate of the subsidence, the model has some features which lead to these over predictions. First, the contact law used to model the collisions between blocks relies upon a spring force to develop the contact force. As a result, the corners of the blocks penetrate the sides of the adjacent blocks a small amount. This results in a compaction of the total block mass and a resultant volumetric reduction. Second, the use of the deforming block option results in straining the blocks under their own weight. Since the blocks start from an undeformed, unstrained configuration this contributes to the total surface subsidence.

SIMULATION OF THE TONO PROJECT

Cavity Prediction

The first step in predicting subsidence for the TONO test is to estimate the shape and extent of the cavity that will be formed during the gasification process. Unfortunately for the TONO test, this prediction is especially difficult to do a priori. The TONO test will be the first at depth application of the Controlled Retracting Injection Point (CRIP) method of Underground Coal Gasification. This approach to gasification involves moving the injection back from the active gasification cavity into fresh coal when gas quality deteriorates as a result of roof interaction. The effect that this gasification technique will have on sweep and cavity shape is unknown and, in fact, determining cavity shape using CRIP is one of the primary complicating objectives of the TONO Partial Seam Test. Another complicating factor for predicting cavity shape on this test is the use of a horizontal production well at an angle to the injection line.

Because of the difficulties in making a priori estimates of cavity shape at TONO, two scenarios were adopted for making subsidence predictions. For both cases the expected tonnage to be gasified (2000 tons, 1350 m^3) was used.[12] For the first case shown in Figure 6a, an attempt was made to have the cavity reflect the various CRIP retractions. The CRIP retractions will have the overall effect of producing a cavity that is longer and narrower than has been seen in most field tests where linked vertical wells have been used. Figure 6a reflects this showing a cavity that is 71 m long with a maximum width of 12 m. For this cavity the average thickness of the coal removed is 2.16 m. This thickness is less than the expected nominal thickness of the coal above the injection hole. A thinner average thickness was selected because it is assumed that the cavity will progress in much the same fashion as it did at Hoe Creek where the cavity progressed quickly to the roof of the seam and then grew laterally along the top of the seam removing less than the full seam thickness. The long, thin cavity of Figure 6a (although even this cavity is probably wider than will be produced) represents a condition that will lead to the maximum subsidence.

In order to test the subsidence calculation under more severe conditions, a second cavity shape is postulated. This

gasification was performed using linked vertical wells, as opposed to the CRIP approach. This cavity is shorter and wider with a maximum width of 20 m and a length of 40 m.

In developing the shapes in both Figures 6a and 6b, the asymmetry that will be introduced by the horizontal production well was ignored since it is impossible at this time to predict what effect this will have on the cavity shape. The shapes in Figure 6 were used as the basic configurations for a series of calculations examining the effect of cavity width on subsidence. In some cases, larger than expected cavity widths were used so as to give conditions likely to lead to maximum subsidence. Once the field test has been run and the actual cavity shape is defined, the calculations can be repeated using the exact same set of assumptions to give estimates of subsurface strata movement that can be directly compared with that measured in the field.

Two Dimensional Calculations

The results of the Hoe Creek analyses were used to help select the input parameters for the analysis of the TONO UCG Project. The stratigraphy charts for the site were obtained from core hole 83N24 data that was logged on April 22, 1983.[13]

Several calculations were conducted with each simulation model. For the rubble model and the block model, the calculations were conducted for three cavity widths that ranged to 80 m. These variations were used to determine the cavity width necessary to produce surface collapse. The assumed height of the burn was a constant 5.5 m across the cavity. This assumption was used to insure that the predictions would be conservative (see discussion of the cavity size prediction above). Unlike the Hoe Creek 3 experiment only one coal seam will be burned and therefore symmetric models were used.

Rubble Model Prediction: The cavity widths analyzed using the rubble model were 16 m, 40 m, and 80 m.

The strata of this problem are significantly more competent than those of Hoe Creek 3; consequently, the maximum failure stress criteria used previously must be modified for the rubble simulation of this site. A maximum tensile stress criteria that degrades with temperature (see Table II) was used. The size of the assumed temperature degraded region is shown for the 40 m cavity in Figure 7a (the cross hatched area).

The rubblization associated with these calculations is shown in Figures 7b, 7c, and 7d. The maximum subsidence calculated for the 40 m cavity was 1.38 m. This figure clearly demonstrates the transition from essentially elastic to a catastrophic plug failure as a function of cavity width.

Block Model Predictions: Figure 8 shows the block model used to predict the subsidence for cavity widths of 12 m, 40 m, and 80 m.

The material properties used are the same as those used in the Hoe Creek 3 analysis, i.e., Table I. A symmetric model with 698 blocks was used. Here we used a cavity height of 4.4 m to include the approximately 20 percent of ash which will remain after the burn.

The final rubblized configurations of the blocks are shown in Figure 8. As expected, the 80 m width shows a total collapse of the overlying strata. The 40 m cavity shows a much smaller surface subsidence because of arching of the blocks. The 12 m width shows very little surface subsidence. The maximum subsidence predicted for the 40 m cavity was 2.5 m.

Three Dimensional Calculations

The profiles predicted by the two dimensional analyses were used to determine the surface subsidence contours using the complementary influence function. As this technique used a square element, the cavities had to be idealized as shown in Figure 6. For both two dimensional calculations, the influence functions were fit to the predicted surface profile and then computationally extended to the predicted cavity shape.

Both techniques produced similar results, with the calculations based on the block model producing the greatest subsidence. These calculations are shown in Figure 9 for both predicted

cavity shapes. As can be seen in this figure, for the CRIP sequence (Figure 6a) the maximum subsidence will be 4 percent of the maximum subsidence parameter and 8 percent for the larger cavity shape (Figure 6b). The best estimate of this maximum subsidence parameter is 1.38 m based on the rubble calculations and 2.5 m for the block model calculation.

CONCLUDING REMARKS

In this manuscript we have developed a prediction of the surface subsidence for the forthcoming TONO UCG Project partial seam test. This prediction is based on the purely mechanical analysis of the overburden strata. The analysis shows that the "plug failure" subsidence observed at Hoe Creek 3 will not be observed at TONO, and that the surface subsidence will be little more than the "elastic" deflection of the strata above the cavity. It should be emphasized that these predictions do not consider any large roof falls that could be created by thermal gradients introduced into them by burning the coal.

REFERENCES

1. H. J. Sutherland and K. W. Schuler, "A Review of Subsidence Prediction Research Conducted at Sandia National Laboratories," Proceedings: Workshop on Surface Subsidence Due to Underground Mining, S. S. Peng and M. Harthill, eds., West Virginia University, Morgantown, March 1982, pp 1-14.

2. S. E. Benzley and R. D. Krieg, "A Continuum Finite Element Approach for Rock Failure and Rubble Formation," Int. J. Numerical and Analytical Methods in Geomechanics, Vol. 6, 1982, pp 277-286.

3. P. A. Cundall, "A Computer Model for Simulating Progressive Large Scale Movements in Blocking Rock Systems," Proceedings of the Symposium on Rock Fracture (IRSM), paper ii-8,1971.

4. P. A. Cundall, "Rational Design of Tunnel Supports: A Computer Model for Rock Mass Behavior Using Interactive Graphics for the Input and Output of Geometrical Data," U.S. Corps of Engineers Technical Report, MRD-2-74, 1974.

5. L. M. Taylor, BLOCKS, a Block Motion Code for Geomechanics Studies, SAND-82-2373, Sandia National Laboratories, Albuquerque, NM.

6. P. A. Cundall, J. Marti, P. Beresford, N. Last, M. Asgain, and T. Maini, Computer Modeling of Jointed Rock Masses, Dames and Moore Technical Report N-78-4, Los Angeles, 1978.

7. O. R. Walton, Particle Dynamics Modeling of Geological Materials, PhD Thesis, University of California, Davis, 1980.

8. H. J. Sutherland and D. E. Munson, "Prediction of Mine Subsidence Using Complementary Influence Functions," submitted for publication.

9. A Ramirez, H. C. Ganow, and D. G. Wilder, "Postburn Core Drilling Results for Hoe Creek 3," Seventh Underground Coal Conversion Symposium, Fallen Leaf Lake, CA, Sept. 8-11, 1981, pp 29-40.3.

10. S. H. Advani, J. K. Lee, O. K. Min, and S. Lee, "Status of Technology Associated with Cavity and Subsidence Response Prediction Associated with Underground Coal Conversion," Proc. 8th Underground Coal Conversion Symposium, August 1982.

11. H. C. Ganow, personal communication.

12. LINL Underground Coal Gasification Project, Quarterly Progress Report - October Through December 1982, D. R. Stephens and W. Clements, eds., UCRL-50026-82-4, March 17, 1983, 26 pp.

13. R. Paul, personal communication.

TABLE I. Material Properties for Hoe Creek 3 Finite Element Analysis

Property	Units	Seam Number 1	2	3	4	5
Mass Density	kg/m^3	2731.	2290.	1394.	2195.	1394.
Youngs Modulus	Mpa	40.	43.	94.	62.	94.
Poisson's Ratio		0.36	0.37	0.32	0.37	0.32
Failure Stress	Mpa	0.002	0.002	0.002	0.002	0.002

TABLE II. Material Properties for Tono Finite Element Analysis

Property	Units	Seam Number 1	2	3	4	5	6
Mass Density	kg/m^3	2090.	2360.	2360.	2300.	2500.	1390.
Youngs Modulus	Mpa	89.6	171.7	171.7	156.2	171.7	113.6
Poisson's Ratio		0.37	0.36	0.36	0.37	0.36	0.32
Failure Stress	Mpa	0.07	0.07	0.07	0.07	0.07	0.07
Temp. Degraded Failure Stress	Mpa	0.00	0.00	0.00	0.00	0.00	0.00

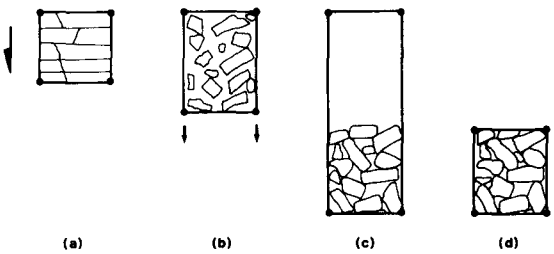

1. (a) Continuum element under gravity load. (b) Rubble element in free fall. (c) Unloaded, bulked rubble element. (d) Loaded, bulked rubble element.

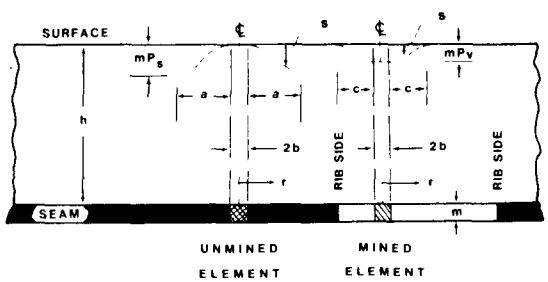

3. Complementary elements for a mine with P_S and P_V the maximum nondimensional subsidence of the respective elements, a and c the radial influence of the respective elements, b the radius of each element, m the mined height, h the depth of the void, and r the radial coordinate from the element.

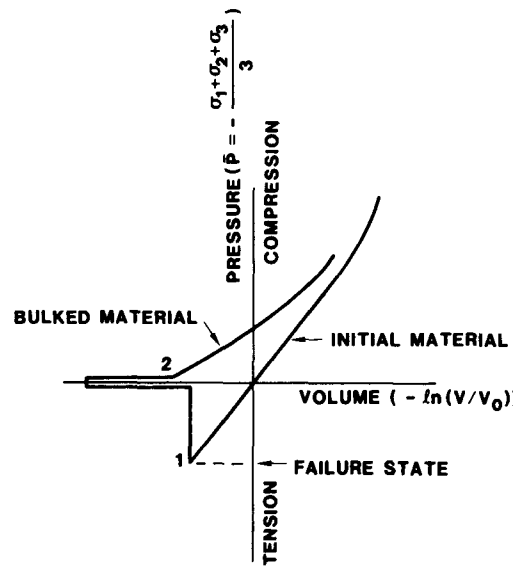

2. Pressure versus volumetric strain behavior for rock, rock failure, and rubble.

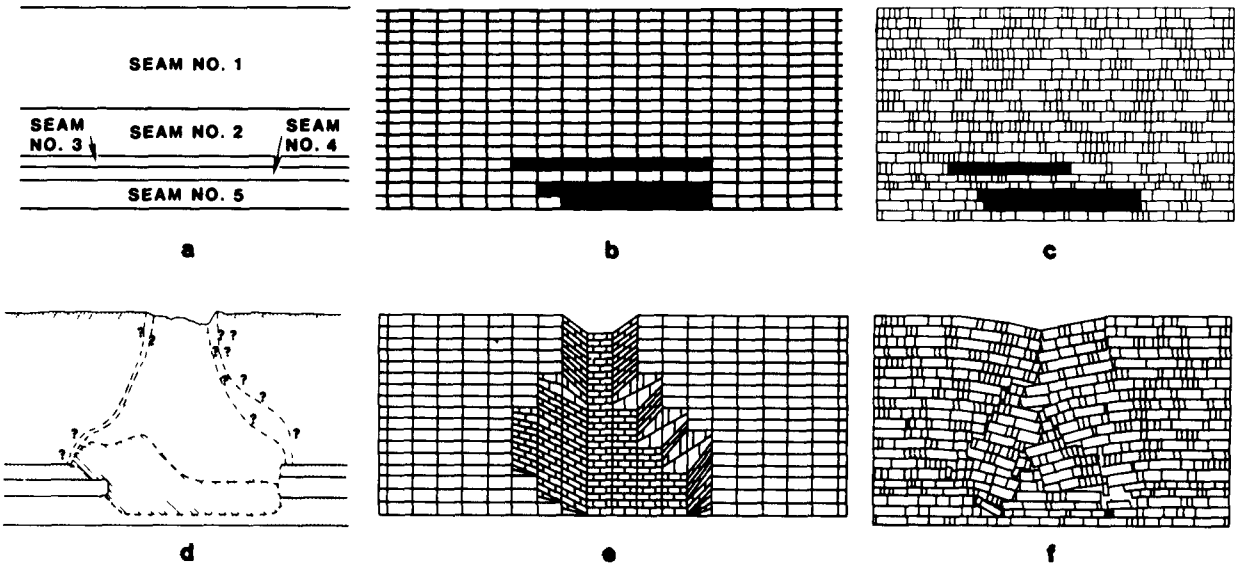

4. Subsidence predictions for Hoe Creek 3.
   (a) Idealized stratigraphy. (b) Finite element model.
   (c) Block motion model. (d) Measured collapse zone and subsidence trough.
   (e) Finite element prediction. (f) Block prediction.

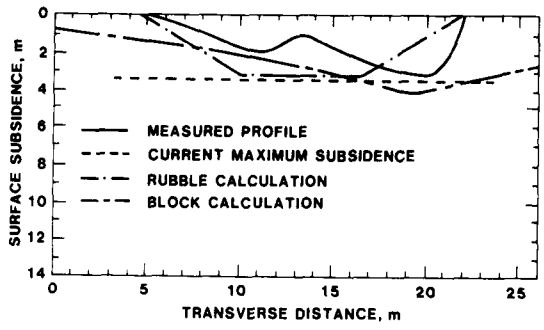

5. Subsidence trough for Hoe Creek 3.

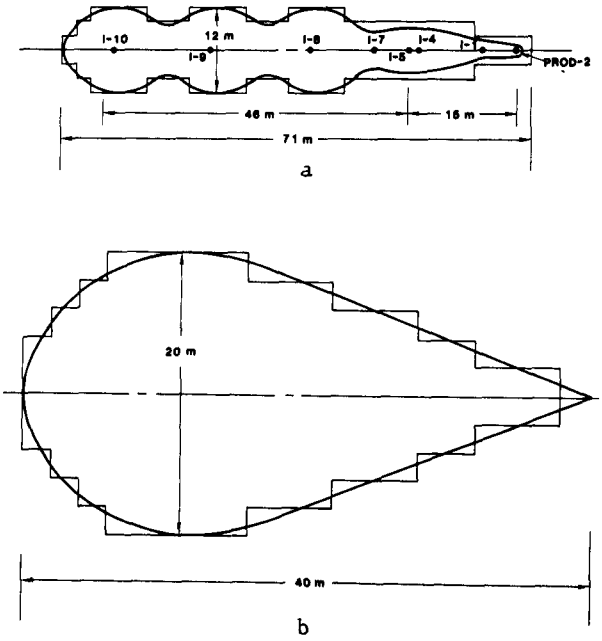

6. Plan view of the burn cavity showing the calculated shape of the cavity (smooth contour) and its influence function representation (square corner contour). (a) CRIP sequence. (b) Linked vertical wells sequence.

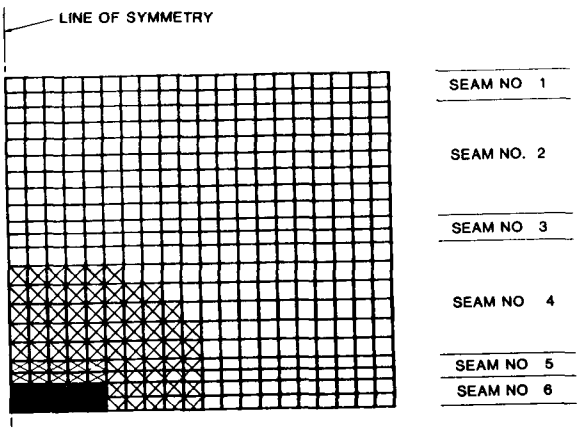

a

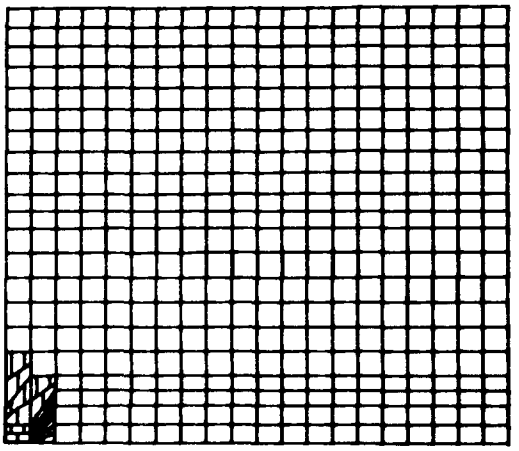

b

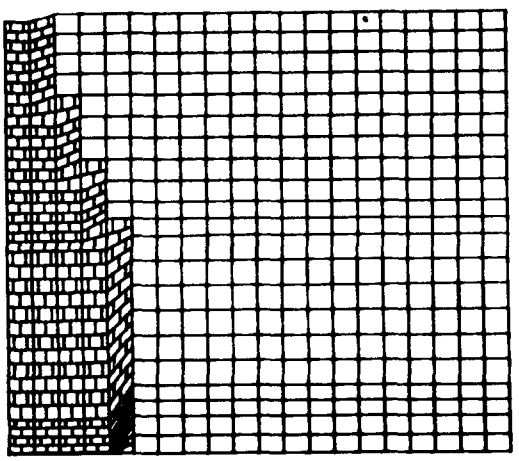

c

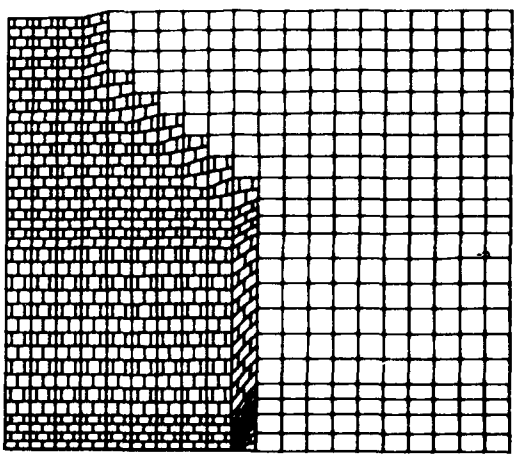

d

7. Rubble model predictions for the TONO experiment. (a) Finite element grid. (b) 16 m cavity. (c) 40 m cavity. (d) 80 m cavity.

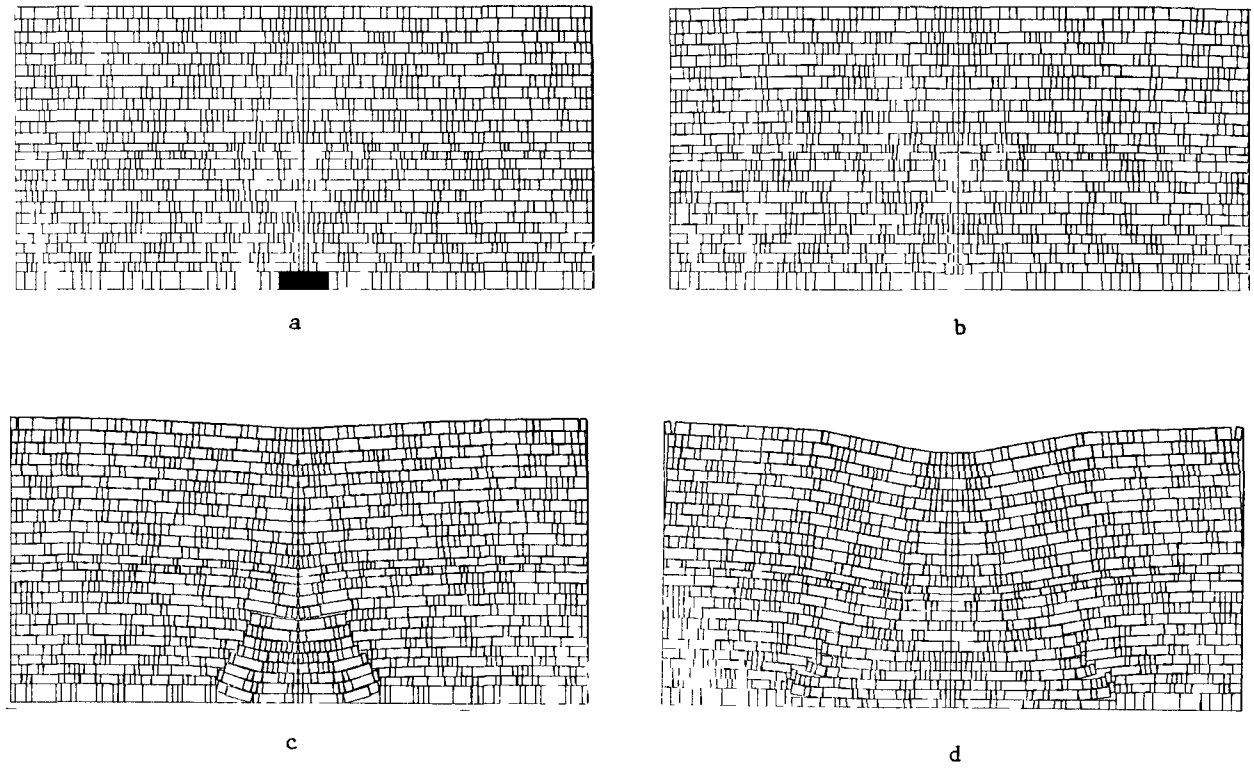

8. Block motion model predictions for the TONO experiment. (a) Original configuration. (b) 12 m cavity. (c) 40 m cavity. (d) 80 m cavity.

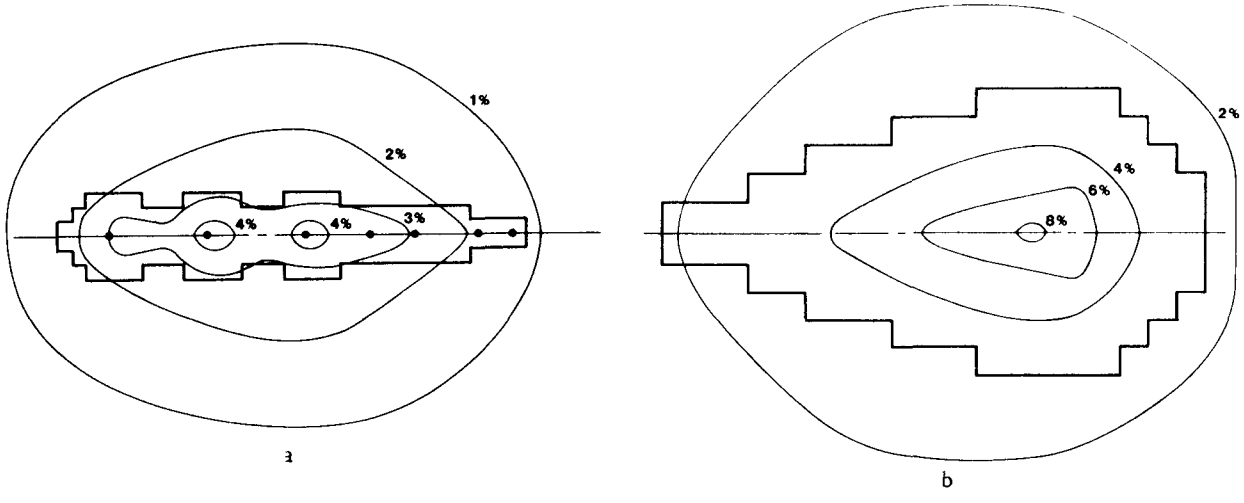

9. Subsidence contours for the TONO experiment. Contours are expressed in terms of percentage of the maximum subsidence. (a) CRIP sequence. (b) Linked vertical wells sequence

Proceedings of the Ninth Annual Underground Coal Gasification Symposium, August, 1983

2.11 MONITORING OF THE TONO PROJECT PARTIAL SEAM CRIP UCG EXPERIMENT USING THE CSAMT TECHNIQUE

by

Lewis C. Bartel
George S. Davidson
Ronald D. Jacobson

ABSTRACT

The controlled source audio-frequency magnetotelluric (CSAMT) technique will be used to monitor an underground coal gasification (UCG) experiment. The UCG experiment will be conducted in late summer of 1983 at the Washington Irrigation and Development Co. (WIDCO) property near Centralia, WA. Previous field experiments, mapping the Hanna II, Phases 2 and 3 and the Rawlins T-2 UCG cavities, indicate that the CSAMT technique is capable of mapping an active UCG process. It is expected that a CSAMT monitoring system will give one meter resolution of the width of the process. The data acquisition system (hardware and software), measurement philosophy, model calculations of expected results, pre-test CSAMT data, and overall system design will be discussed.

INTRODUCTION

Sandia National Laboratories is developing geophysical techniques to map and monitor the underground coal gasification (UCG) process. The techniques which have been used to monitor the UCG process include a passive seismic technique,[1,2] an induced seismic technique,[2] and galvanic electrical potential techniques.[1,3,4] A brief discussion of these techniques, their successes and limitations, was given in a previous paper.[5] In that previous paper,[5] the potential use was discussed of the controlled source audio-frequency magnetotelluric (CSAMT) geophysical technique to map the UCG process.

Sandia has used the CSAMT geophysical technique to map a steamflood tar sand oil recovery experiment conducted by the Laramie Energy Technology Center at a site near Vernal, Utah and a fireflood heavy oil recovery experiment conducted by the Bartlesville Energy Technology Center at a site near Bartlett, Kansas.[6,7] For both floods, the progress of the processes has been successfully monitored using the CSAMT technique. In particular, the asymmetry of the steamflood process, the direction of steam flow, and oil production records agreed with the CSAMT results.[7] Further, three post-test core holes (one behind the combustion front, one in the front, and one ahead of the front) were successfully spotted for the heavy oil fireflood test from the CSAMT data.[7]

The CSAMT technique is being evaluated for mapping coal mine fires; a coal mine fire is essentially a UCG process.[5,8-10] Recently, a CSAMT survey was performed over an abandoned coal mine fire near Uniontown, Pennsylvania. Several borehole locations

*This work performed at Sandia National Laboratories supported by the U.S. Department of Energy.

Sandia National Laboratories
Albuquerque, New Mexico 87185

were spotted in areas where the CSAMT results suggested there was active fire and/or coked coal. Subsequent drilling of these boreholes confirmed the results indicated by the CSAMT data.[10]

There are large changes in the electrical resistivity of coal during the UCG process. Water-saturated virgin coal may have a resistivity of 150-300 ohm-m, and dry unaltered coal at ambient temperature has a resistivity in excess of 10^5-10^6 ohm-m. Upon devolatization and reaction, the resistivity decreases continuously so that hot (~650°C) carbonized coal has a resistivity of approximately 1 ohm-m.[11] It is noteworthy that coke has a resistivity of approximately 1 ohm-m even at ambient temperature.[10] Because of these drastic changes in the electrical resistivity, electrical and/or electromagnetic (EM) geophysical techniques seem appropriate to map the UCG process.

Based upon the success of using the CSAMT technique to map enhanced oil recovery processes,[6,7] shale oil recovery process,[12] and the coal mine fires,[5,8-10] the CSAMT technique will be fielded to map the UCG process of the test to be conducted at the Washington Irrigation and Development Company (WIDCO) surface coal mine near Centralia, Washington. This experiment will test the Lawrence Livermore National Laboratory (LLNL) controlled retracting injection point (CRIP) concept.[13] In this paper the experimental design of a CSAMT monitoring technique will be discussed. In the following sections, the CSAMT technique will be discussed, layered earth model calculations of expected results will be given, results of a pre-test survey will be given, and the experimental arrangement for the monitoring system along with a discussion of hardware and software will be presented.

THE CSAMT TECHNIQUE

The CSAMT geophysical technique is an EM technique in which the primary EM field is usually produced by a long electric dipole laid out on the surface of the earth and grounded at both ends. A transmitter operating at selected frequencies (2-4096 Hz) is located at the center of the dipole. The transmitting antenna is located a distance from the area of investigation three-to-five times the depth to be interrogated. The receiving antenna consists of a relatively short dipole (approximately 2-100 m) in contact with the earth at both ends to measure the electric field (E) parallel to the transmitting antenna (x-direction) and a magnetometer to measure the magnetic field (H) perpendicular to the transmitting antenna (y-direction) and in the plane of the earth (Fig. 1). In addition, E_y and H_x are often measured. Measurements are made of E and H at various locations over the area to be interrogated.

The wave impedance is equal to the ratio of orthogonal components of E and H, and for plane waves the wave impedance is given by[14,15]

$$z = \frac{E_x}{H_y} = \frac{i\omega\mu}{k} \qquad (1)$$

where $\omega = 2\pi f$ (f is the frequency), μ the magnetic permeability (for free space $\mu_o = 4\pi \times 10^{-7}$ henrys/m), and k is the magnitude of the wave vector. Here

$$k = (\varepsilon\mu\omega^2 - i\omega\mu\sigma)^{1/2} \qquad (2)$$

where ε is the electric permeability for free space, $\varepsilon_o = 1/(36\pi \times 10^9)$ farads/m and σ is the apparent conductivity of the earth; the resistivity is the inverse of the conductivity. At low frequencies, the displacement current ($\varepsilon\mu\omega^2$) term can generally be neglected; thus, at low frequencies, such as the audio-frequencies, apparent resistivity ρ_a can be determined from Equations (1) and (2)[14]

$$\rho_a = \frac{1}{\mu\omega}\left|\frac{E_x}{H_y}\right|^2 \qquad (3)$$

$$= \frac{1.2666 \times 10^5}{f}\left|\frac{E_x}{H_y}\right|^2$$

The resistivity given by Equation (3) is called the Cagniard resistivity.

The skin depth for the EM waves is given by[14]

$$\delta = (2\rho_a/\omega\mu)^{1/2} \qquad (4)$$

$$= 503.3\,(\rho_a/f)^{1/2}$$

The skin depth for an EM wave is the distance the wave penetrates before its magnitude decreases e^{-1} (37 percent) of the original magnitude. The depth of interrogation depends upon the frequency; the lower the frequency, the deeper the penetration of the EM wave. The resistivities of the various formations as a function of depth are determined by measuring the apparent resistivity as a function of frequency. The apparent resistivity ρ_a determined at a given frequency, Equation (3), depends upon the resistivities of all the formations penetrated by the EM wave.

If the area to be interrogated is at least three skin depths (3δ) away from the transmitting antenna and within a 45° angle off the perpendicular bisector (Fig. 1) of the transmitting antenna, then Goldstein and Strangway[15] and Sandberg and Hohmann[16] have shown that plane wave solutions are appropriate for a layered earth and resistivities calculated from Equation (3) are within 10 percent of the true apparent resistivities for E_x and H_y. This region, which is at least 3δ from the transmitting antenna is referred to as the far-field (plane wave) regime. The region which is less than 3δ from the transmitting antenna is referred to as the near-field regime. Sandberg and Hohmann[16] suggest that far-field conditions may only truly be met when the transmitter is 5δ away. Since the skin depth depends upon the frequency, the near-field far-field demarcation depends upon the frequency, and a given location may be in the far-field regime for the higher frequencies and in the near-field regime for the lower frequencies.

In the near field regime resistivities calculated using Equation (3) may not represent the true apparent resistivities and plane wave solutions are not appropriate. Calculations of the fields in the near-field region must include the geometry and location of the transmitting antenna. If the distance to the transmitting antenna is on the order of the depth to be interrogated, then calculations show that it is difficult to distinguish between a subsurface insulating layer and a conducting layer.[15] From the work of Goldstein and Strangway[15] it is obvious the distance to the transmitting antenna should be at least three times the depth to be interrogated to properly interpret subsurface layer resistivities. In the next section, results from some layered earth model calculations will be discussed which support the calculations of Goldstein and Strangway.[15]

MODEL CALCULATIONS

Even though the UCG process is a three-dimensional conducting anomaly buried in a layered earth, insight can be gained by examining the results of layered earth CSAMT calculations. Model calculations were performed using the EMFIN4* code which numerically computes all Cartesian components of both electric and magnetic fields about a grounded electric dipole or finite wire source of arbitrary length for the quasi-static case over an isotropic horizontally stratified earth.[17] The basic theory developed by Wait[18] for a stratified

*The EMFIN4 code was obtained from W. L. Anderson, USGS, Denver.

anisotropic half-space, by Bannister[19] for quasi-static fields of dipole antennas, and by Wait[20] for EM fields about a horizontal dipole became a starting point for Anderson's[17] work.

Calculated resistivity versus frequency results are shown in Figures 2 and 3 where the layered earth models are given in Table 1. The results shown in Figure 2 are for a perpendicular distance (y-direction in Fig. 1) to the transmitter of 732 m (2400 ft) and off the center line of the transmitting antenna (x-direction in Fig. 1) 414 m (1360 ft). The results shown in Figure 3 are for a y-distance of 1766 m (5795 ft) and an x-distance off center line of 689 m (2260 ft). These transmitting antenna locations, with respect to the area interrogated, were chosen to correspond in two potential antenna locations for the CRIP test. Figures 2 and 3 show results with no conducting layer and with the bottom half, top half, and full seam a conducting layer; the layer thicknesses and resistivities are given in Table 1. The solid lines with solid dots show results for no conducting layer (virgin coal seam), the short dashed lines with open circles show results for the bottom half of the seam a conducting layer, the "pluses" represent results for the top half of the seam a conducting layer, and the long dashed lines with the "x's" show results for the full seam thickness a conducting layer.

For the transmitting antenna distance of 732 m, the transmitting antenna is greater than or equal to three skin depths away if the resistivity and frequency satisfy $\rho_a \leq 0.235 \times f$ and is greater than or equal to five skin depths away if the resistivity and frequency satisfy $\rho_a \leq 0.0846 \times f$. For the transmitting antenna distance of 1766 m, the transmitting antenna is greater than or equal to three and five skin depths away if the resistivity and frequency satisfy $\rho_a \leq 1.368 \times f$ and $\rho_a \leq 0.493 \times f$, respectively. The two diagonal long and short dashed lines in Figures 2 and 3 show the near-field far-field demarcation based upon the three and five skin depth criteria; regions to the right of the lines are in the far-field regimes.

An examination of the calculated results shown in Figures 2 and 3 show that the resistivities for decreasing frequency display the following behavior. As the frequency decreases the calculated resistivity, for no conducting layer, decreases slightly and then flattens until the near-field effects take over. When conducting layers are present at a depth of approximately 60-75 m, the resistivities are greater than the resistivity for no conducting layer for frequencies greater than approximately 800 Hz demonstrating the typical "overshoot" phenomenon. For frequencies less than 800 Hz, the calculated resistivities for conducting layers at a depth of approximately 60-75 m are all less than the calculated resistivity for no conducting layer. The decreasing resistivity for decreasing frequency persists to low frequencies well below a frequency necessary to significantly penetrate the conducting layer. Note that for half the seam a conductor, the maximum percentage change for the transmitting distance of 732 m is 46% and for the transmitting distance 1766 m the percentage change is 39%. These calculated changes in resistivity represent significant changes that should be readily detected. It is anticipated that the transmitting antenna 732 m away will be the one used in the test.

Sandberg and Hohmann[16] show results of resistivity calculations for both two- and three-dimensional (2- and 3-D) subsurface conducting structures. Results of their calculations of resistivities over 2- and 3-D structures show the same resistivity as a function of frequency behavior as the layered earth calculations except that the behavior is accentuated; i.e., the "overshoots" and "undershoots" are more pronounced and the low resistivity persists to even lower frequencies than the layered earth calculations predict. In addition, their results show that resistivities, calculated on the surface adjacent to the conductor for the electric field perpendicular to the strike of the conductor, are larger than the back-

ground value; this phenomena is also called a resistivity "overshoot."

PRE-TEST SURVEY RESULTS

The proposed test is to take place in the "Big Seam" in the area where the test is to take place, the seam is at a depth of approximately 61-76 m (200-250 ft). The "Big Seam" is approximately 15 m (50 ft) thick and is characterized by numerous partings.[21] The UCG test is to take place in the upper 4.6-6.1 m (15-20 ft) of the "Big Seam".

In order to aid in the evaluation of the suitability of the proposed site, aid in the design of the monitoring system, and provide pre-test data, a limited pre-test CSAMT survey was performed at the proposed UCG test site. This survey was conducted in March 1983 and provided the opportunity to obtain pre-test data before any facilities had been constructed.

The CSAMT pre-test survey consisted of several lines of data using a 2 m electric field receiver dipole spacing. With this receiver dipole spacing, the subsurface resolution is 1 m. The locations of the lines of data stations relative to exploratory boreholes and permanent monuments are shown in Figure 4. Approximately 120 stations of CSAMT data were taken. The transmitting antenna for this survey was located approximately 1766 m (5795 ft) away from the area interrogated in the direction indicated in the figure.

The CSAMT obtained apparent resistivities as a function of frequency were analyzed using the Bostick "delta resistivity" inversion scheme[22] and approximate resistivities at approximate depths were obtained. Samples of the Bostick inversion results for selected lines are shown in Figures 5 and 6. These figures show contours of "interpreted" equal resistivity. The "interpreted" depths of 60, 80, and 100 m were selected to "bracket" the depth of the proposed process which is approximately 70 m.

The results for Line 101, Figure 5, show various areas of low resistivity. These areas are at Stations 13-15, 17, 23 and 28-31. The low resistivity areas, Stations 13-15, and 17 may be associated with a near surface condition; namely, the water saturated dirt piles. The low resistivity anomalies at Stations 23 and 28-31 are associated with deeper lying regions of increased electrical conductivity. This increased electrical conductivity may be associated with natural fractures. The deep lying conductors evident for Line 402, Figure 6, Stations 16-17 and 38-39 may also be associated with natural fractures. Line 402 crosses the area of the proposed UCG test, and Line 101 is outside the area to be gasified. Note that the depths in Figures 5 and 6, along with the resistivities, represent a reasonable "first-order" approximation.

MEASUREMENT GRID

The overall goal of the monitoring is to obtain a daily "snapshot" of the UCG process with a resolution of 1 m in the subsurface. This goal will be achieved by measuring the electric field using 2 m receiver dipole spacing along individual lines. The resolving power of the CSAMT technique is in the variation of the electric field across a subsurface anomaly. The magnetic field generally varies gradually across the subsurface anomaly. In order to accelerate the data acquisition process, the electric field will be measured over a relatively fine grid for a fixed transmitting antenna location. The magnetic field will be measured at selected locations. The exact locations will be determined during the collection of background data. Using the appropriate values of the magnetic field, the apparent resistivity will be determined over the entire area of interest.

The truncated measurement field (TMF) is shown in Figure 7. The location of the instrumentation wells are also shown in Figure 7. The electric field will be measured along the individual lines with a receiver dipole separation of 2 m. Note that at various locations, lines of data stations are separated by 4 m; e.g., Lines 1 and 3, Lines 20 and 22, etc.

For this measuring grid, there are 569 electric field measurement data stations. It is anticipated that the magnetic field will be measured at no more than 10% of these data stations. The result is that approximately 600 separate data points need to be taken to get a complete picture of the process; however, only a portion of these data points will be measured on any given day.

This represents a monumental geophysical survey project, which must be completed daily. To make it feasible, a semi-automatic data collection system had to be designed. This computer based system will also be used to provide data reduction and support analysis, in the field, of the process induced changes in the data. With the semi-automatic data collection system discussed below, it is anticipated that approximately 300 data points can be collected daily. Those data stations where the process is inactive will not be collected on a daily basis.

THE DATA ACQUISITION AND ANALYSIS SYSTEM

As a completely automatic data collection system proved to be too costly and because daily manual field surveys of the required magnitude were not feasible, a combination of automatic scanning and manual surveying has been selected for the Tono CRIP test.

As shown in Figure 7, the survey stations are arranged in lines with varying numbers of sample stations per line. Figure 8 shows how these stations will be connected to the data system. Each sample station consists of a set of three contiguous probes in the same line. These three probes are connected to a field pre-amplifier to make a differential voltage measurement. The output of this amplifier is sent to the input side of the multiplexer. The GDP-12* geophysical data processor, handles two stations at a time, so the multiplexer will be set to select a station from a line and also the corresponding station in the subsequent line. Four field pre-amplifiers are available. This will allow the system to be collecting data from the stations on two lines while the other two amplifiers are being connected to the next stations on a third and fourth line. In this way, the survey moves alternately along four lines. A fifth multiplexer input pair will be connected to a coil which will periodically measure the magnetic field at various locations while the other pairs are used to sample the electrical field.

Figure 9 shows the data collection system including the signal multiplexer, the control computer, and the GDP-12 geophysical instrument. As discussed above, a set of sample stations will be connected to the multiplexer which will connect two pair (or the coil pair) to the GDP-12 when commanded to do so by the computer. The GDP-12 will make the voltage readings while controlling the current transmitter to sweep the desired range of frequencies. The results are accumulated and then transmitted to the control computer. After storing the results on disk, this computer selects the other pair of input lines, which were manually repositioned while the other readings were being made, and restarts the GDP-12. This will be continued until the daily survey has been completed.

This same data control computer, the PDP 11/23,** will also be available for data reduction and field analysis. Data listings, line plots, contour plots and modeling programs will be available to allow interpretations of the process motion. As an example of the capabilty that will be available in the field, consider Figure 10 which shows a typical psuedosection resistivity profile, one of the types of plots to be produced for daily interpretation.

SUMMARY

The "real-time" monitoring of the UCG process will allow the operator to

*Trade name of Zonge Engineering and Research Organization.

**Trade name of Digital Equipment Corp.

determine the progress of the process and allow "corrective" action if necessary. The purpose of testing the CSAMT technique on the partial seam CRIP experiment is to determine if this technique can map the process with the desired resolution. The CSAMT results will be compared to thermal results to determine resolution. If the CSAMT technique, deployed at the surface, does provide the necessary temporal and spatial resolution, then the cost of monitoring the UCG process can be reduced by eliminating or decreasing the number of monitoring instrumentation wells. Additionally, the CSAMT technique will give broader coverage than can be obtained from a limited number of instrumentation wells.

The CSAMT monitoring system to be fielded at the UCG test is a semi-automatic system for evaluation of the technique. This system was selected because of time and cost constraints, both hardware and software development time and costs. If the technique successfully monitors the UCG test, then it may be desirable to develop the necessary hardware and software to fully automate the system to make the monitoring less labor intensive.

REFERENCES

1. L. C. Bartel, S. G. Beard, L. W. Beckham, R. P. Reed and R. W. Seavey, "Instrumentation Results From an In Situ Coal Gasification Experiment", presented at the 51st Annual Fall Tech. Conf. and Exhib. of the Soc. of Petroleum Engineers, New Orleans, LA, Oct. 3-6, 1976, paper no. SPE 6151.

2. L. W. Beckham, H. D. Garbin and D. A. Northrop, "Instrumentation for In Situ Coal Gasification: IV. Seismic and Acoustic Techniques for Remote Monitoring", In Situ, Vol. 3, No. 1, 1979, pp 1-31.

3. L. C. Bartel, R. W. Seavey and D. A. Northrop, "Instrumentation for In Situ Coal Gasification: III. Electrical Techniques for Remote Monitoring", In Situ, Vol. 2, No. 4, 1978, pp 247-269.

4. L. C. Bartel, "Analysis of the Electrical Potential Data for the Hanna IV Underground Coal Gasification Test", proceedings of the Fourth Underground Coal Conversion Symposium, Steamboat Springs, CO, July 17-20, 1978, pp 305-315.

5. L. C. Bartel, "Potential Use of the CSAMT Geophysical Technique to Map UCG Processes, "proceedings of the Eighth Underground Coal Conversion Symposium, Keystone, CO, August 1982, pp 59-70.

6. L. C. Bartel and J. R. Wayland, "Results from Using the CSAMT Geophysical Technique to Map Oil Recovery Processes", presented at the 56th Annual Tech. Conf. and Exhib. of the Soc. of Petroleum Engineers, San Antonio, TX, Oct. 5-7, 1981, paper no. SPE 10230.

7. L. C. Bartel, "Modeling and Analysis of the CSAMT Geophysical Technique Results to Map Oil Recovery Processes", presented at the 57th Annual Fall Tech. Conf. and Exhib. of the Soc. of Petroleum Engineers, New Orleans, LA, Sept. 26-29, 1982, paper no. SPE 11192.

8. L. C. Bartel, S. L. Love and R. D. Jacobson, "Results of Using the CSAMT Geophysical Technique to Map Coal Mine Fires: Part I - Case Histories", Sandia National Laboratories report, SAND 82-0196, 1982.

9. L. C. Bartel, "Evaluation of the CSAMT Geophysical Technique to Map Abandoned Coal Mine Fires", presented at the Society of Exploration Geophysicists 52nd Annual International Mtg. and Exhib., Dallas, TX, Oct. 17-21, 1982; an extended abstract appears in the Technical Program Abstracts and Biographies of that meeting, pp 419-421.

10. L. C. Bartel and R. D. Jacobson, to be published.

11. D. A. Northrop, editor, "Instrumentation and Process Control Development for In Situ Coal Gasification, Second Quarterly Report", Sandia National Laborato-

ries report, SAND 76-0366, June 1976 and from electrical geophysical logs from the Hanna site.

12. L. C. Bartel and R. D. Jacobson, to be published.

13. R. W. Hill and M. J. Shannon, "The Controlled Retracting Injection Point (CRIP) System: A Modified Stream Method for In Situ Coal Gasification", proceedings of the Seventh Underground Coal Conversion Symposium, Fallen Leaf Lake, CA, Sept. 8-11, 1981, LLNL Report CONF-810923, pp 730-739 (also UCRL-85052, 1981).

14. W. M. Telford, L. P. Geldart, R. E. Sheriff, and D. A. Keys, Applied Geophysics, Cambridge University Press, Cambridge, MA, 1976, pp 446-477.

15. M. A. Goldstein and D. W. Strangway, "Audio-Frequency Magnetotellurics with a Grounded Dipole Source", Geophysics, Vol. 40, August 1975, pp 609-683.

16. S. K.Sandberg and G. W. Hohmann, "Controlled-Source Audio-Frequency Magnetotellurics in Geothermal Exploration", Geophysics, Vol. 47, January 1982, pp 101-116.

17. W. L. Anderson, "Electromagnetic Fields About a Finite Electric Wire Source", U.S. Geological Survey Report, USGS-6D-74-04, 1974.

18. J. R. Wait, "The Electromagnetic Fields of a Horizontal Dipole in the Presence of a Conducting Half-Space", Canadian Journal of Physics, Vol. 39, 1961, pp 1017-1028.

19. P. R. Bannister, "Quasi-static Fields of Dipole Antennas at the Earth Surface", Radio Science, Vol. 1, No. 11, 1966, pp 1321-1370.

20. J. R. Wait, "Fields of a Horizontal Dipole Over a Stratified Anisotropic Half-Space, "IEEE Trans on Antennas and Propagation, Vol. AP-14, No. 6, 1966, pp 790-792.

21. R. A. Paul, Washington Irrigation and Development Co, private communication.

22. F. X. Bostick, "A Simple Almost Exact Method of MT Analysis", in S. H. Ward, ed., Workshop on Electrical Methods in Geothermal Exploration, University of Utah, Salt Lake City, UT, 1977, pp 175-183.

TABLE 1. LAYERS AND RESISTIVITIES FOR LAYERED EARTH CSAMT MODEL CALCULATIONS.

MODEL	LAYERS IN METERS	RESISTIVITIES IN OHM-M
Unaffected coal seam	0 - 10	50
	10 - 61	10
	61 - 76	150
	76 → ∞	10
Top half of coal seam affected	0 - 10	50
	10 - 61	10
	61 - 68.5	1
	68.5 - 76	150
	76 → ∞	10
Bottom half of coal seam affected	0 - 10	50
	10 - 61	10
	61 - 68.5	150
	68.5 - 76	1
	76 → ∞	10
Full coal seam affected	0 - 10	50
	10 - 61	10
	61 - 76	1
	76 → ∞	10

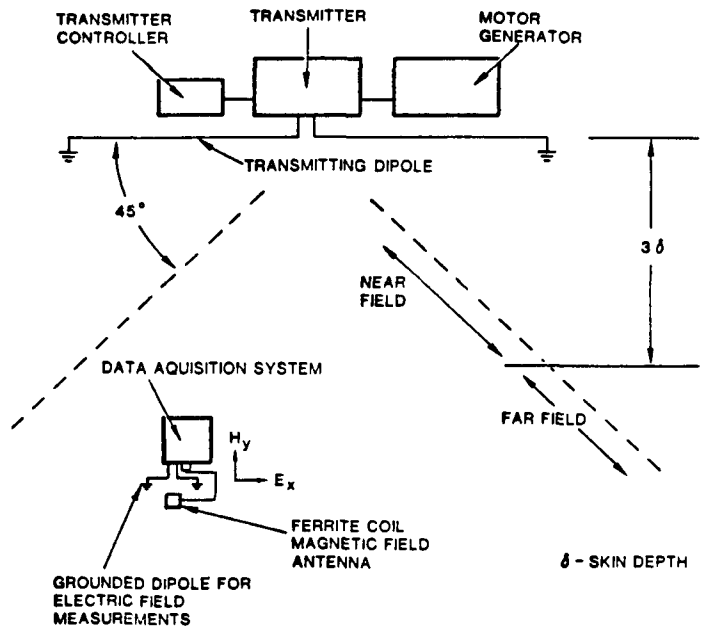

FIGURE 1. Schematic of CSAMT technique.

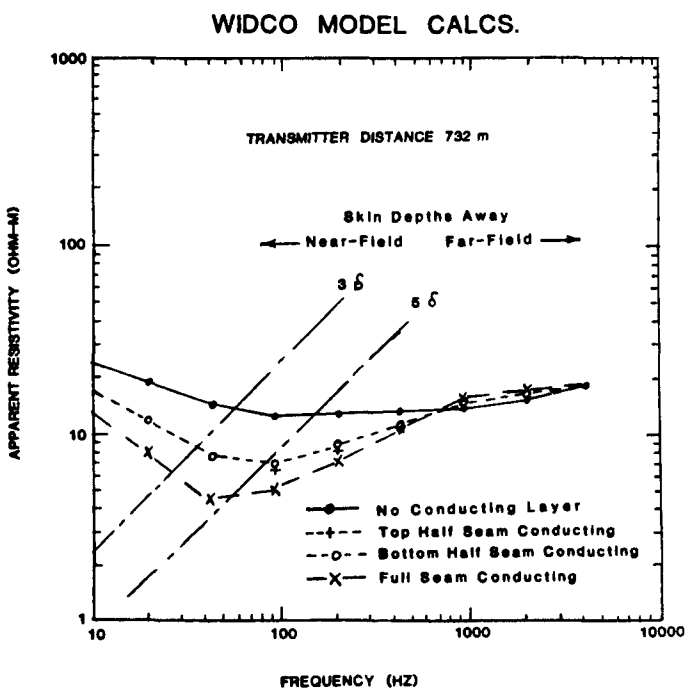

FIGURE 2. Layered earth CSAMT model calculations for y = 732 m (perpendicular distance to the transmitting antenna) and x = 414 m (distance off centerline of antenna). Layers and resistivities are given in Table 1.

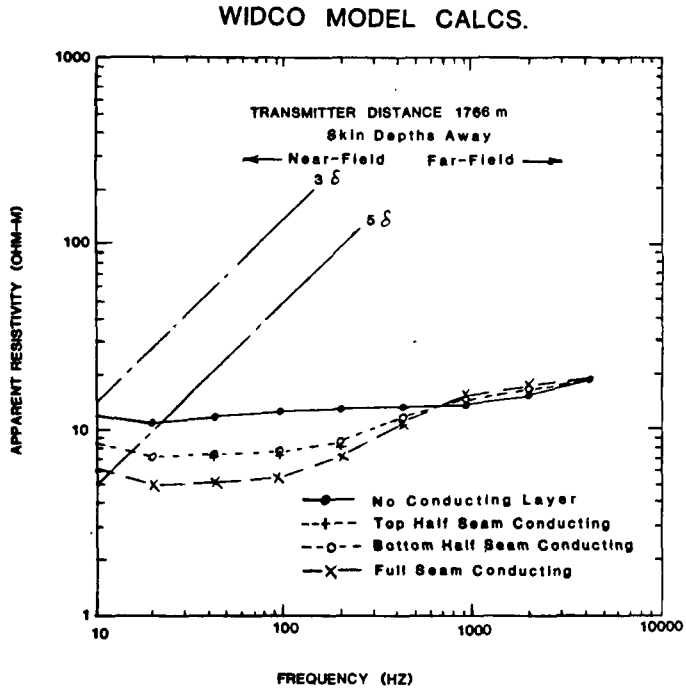

FIGURE 3. Layered earth CSAMT model calculations for y = 1766 m (perpendicular distance to the transmitting antenna) and x = 689 m distance off centerline of antenna). Layers and resistivities are given in Table 1.

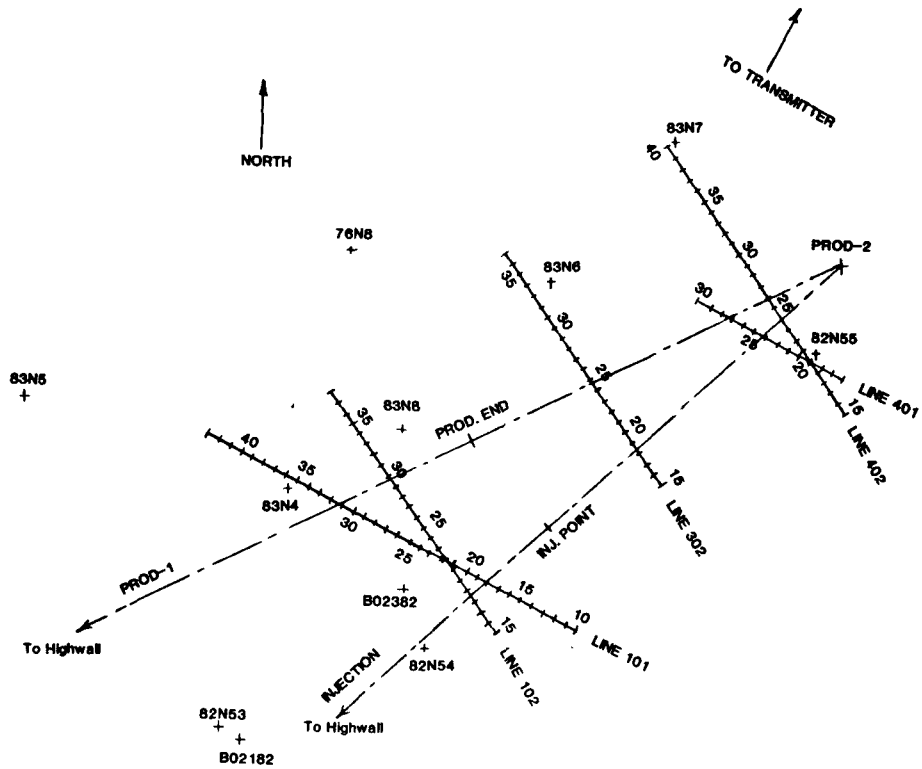

FIGURE 4. Location of the pretest CSAMT survey lines for the partial seam CRIP test, Centralia, WA. The individual stations are separated by 2 m. Locations of boreholes and permanent markers are also shown.

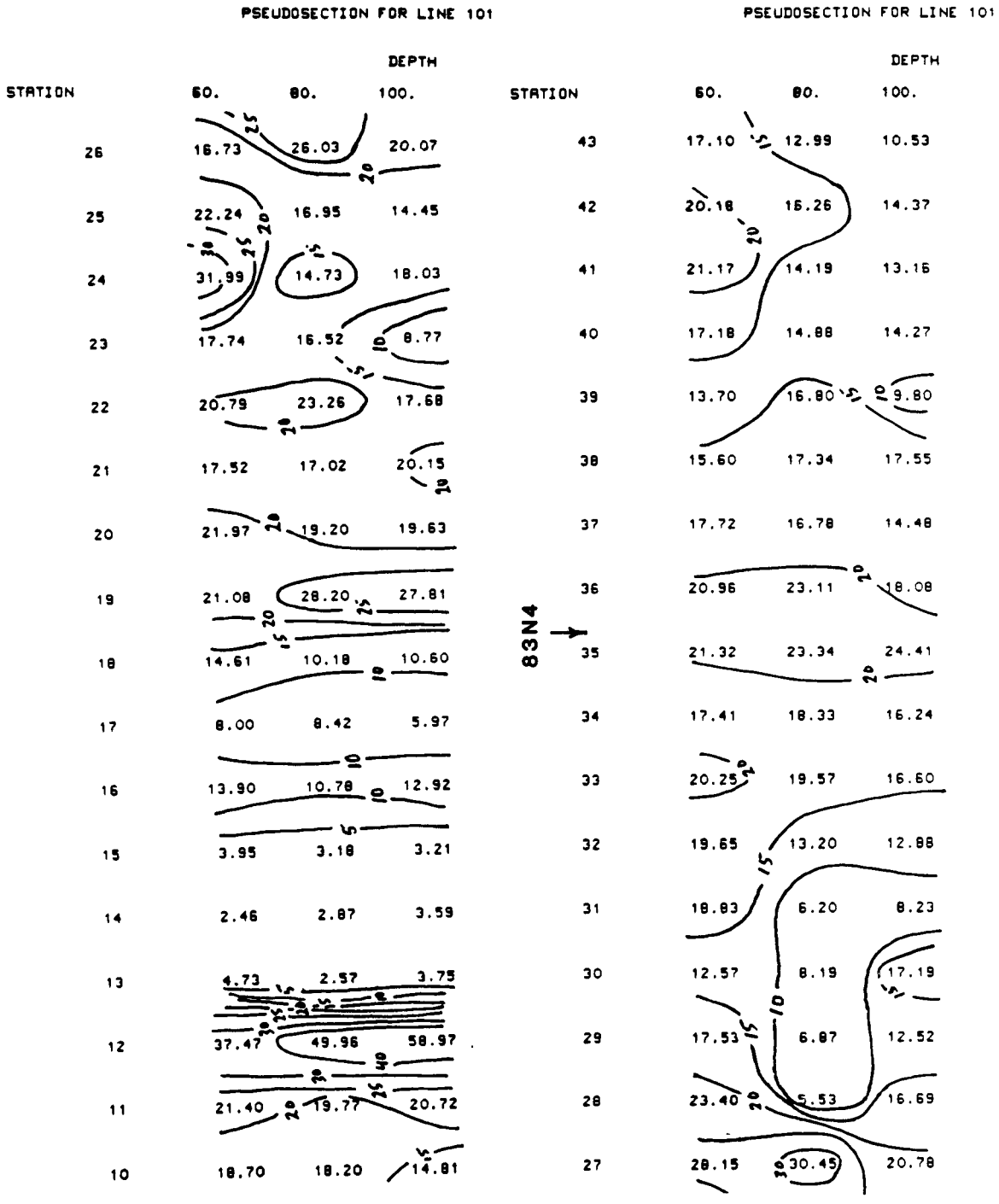

FIGURE 5. "Interpreted" resistivities as a function of depth for Line 101. The location of borehole 83N4 is also shown.

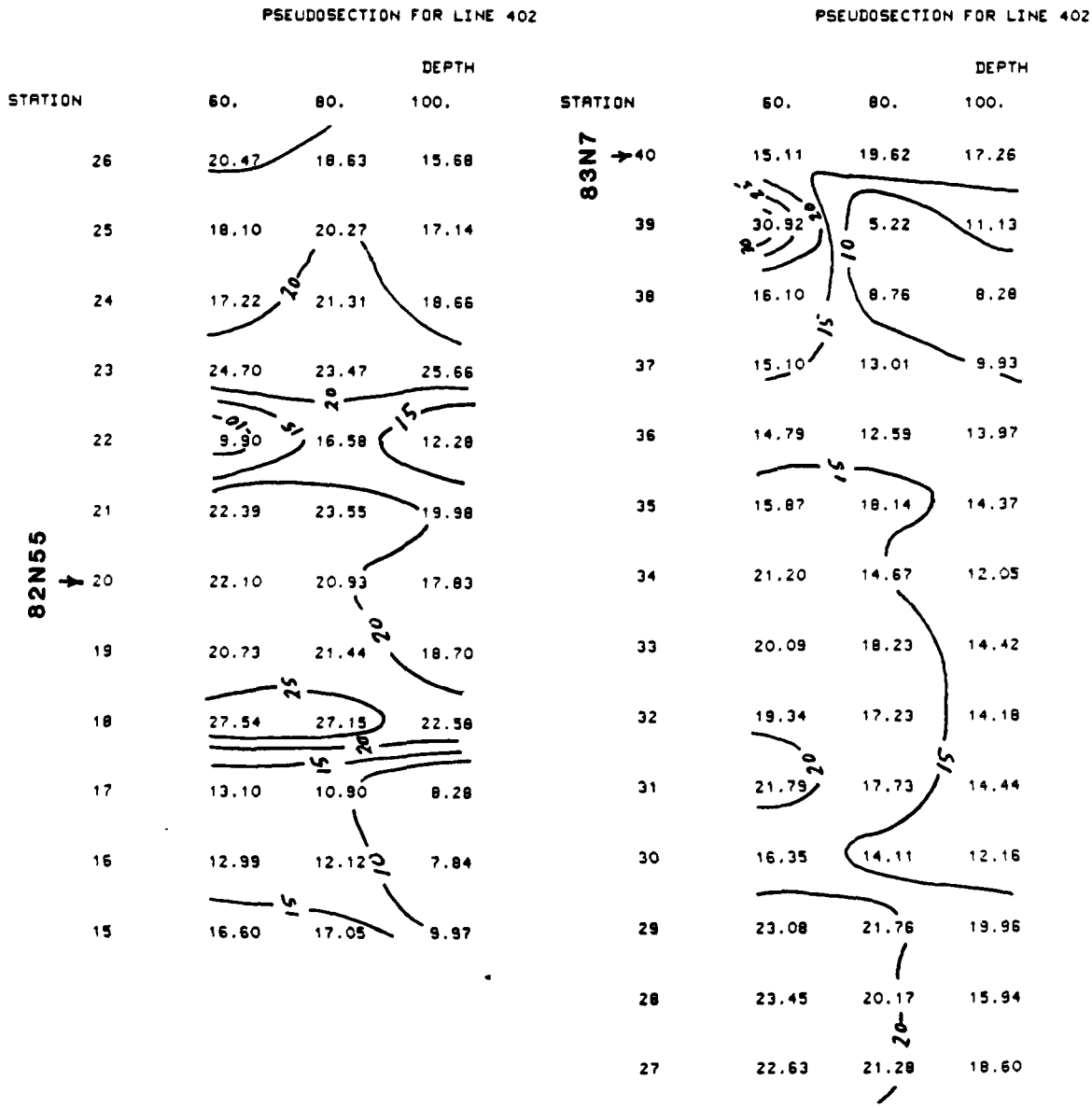

FIGURE 6. "Interpreted" resistivities as a function of depth for Line 402. The locations of boreholes 82N55 and 83N7 are also shown.

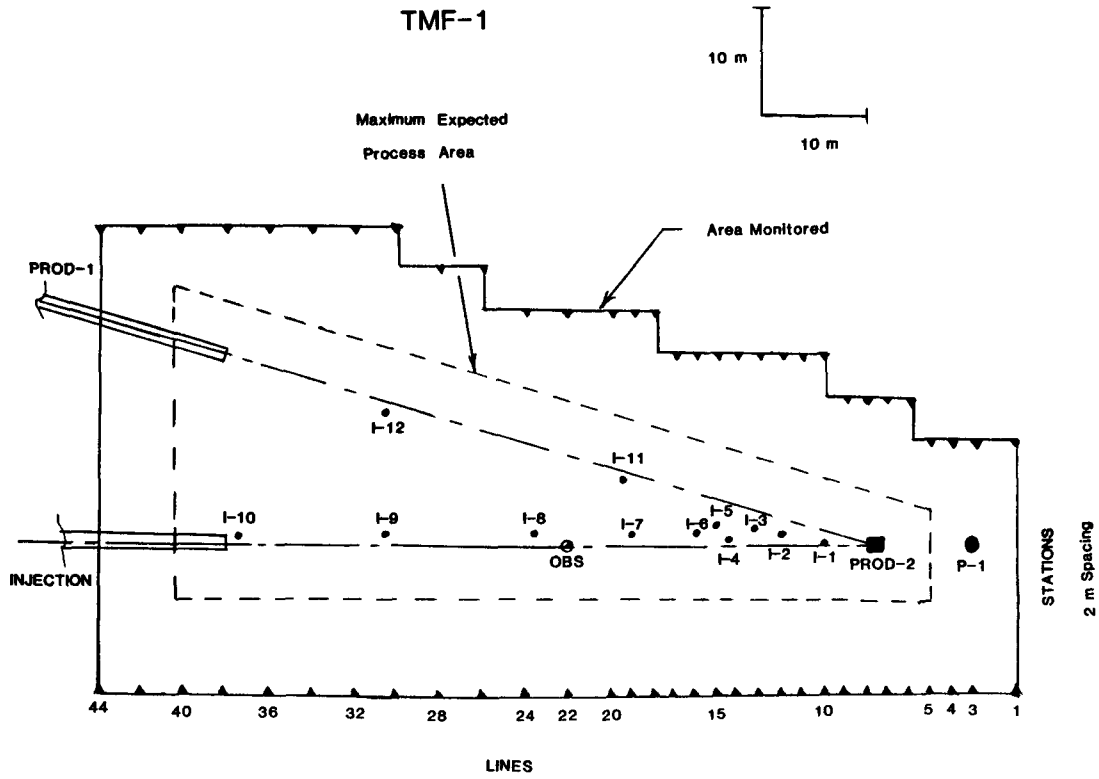

FIGURE 7. Schematic layout of the truncated measurement field (TMF). The station spacing along individual lines is 2 m.

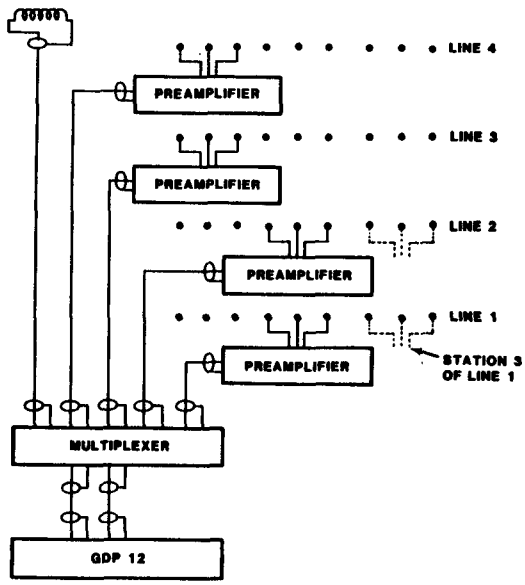

FIGURE 8. A schematic showing how the four amplifiers will be used to survey the process.

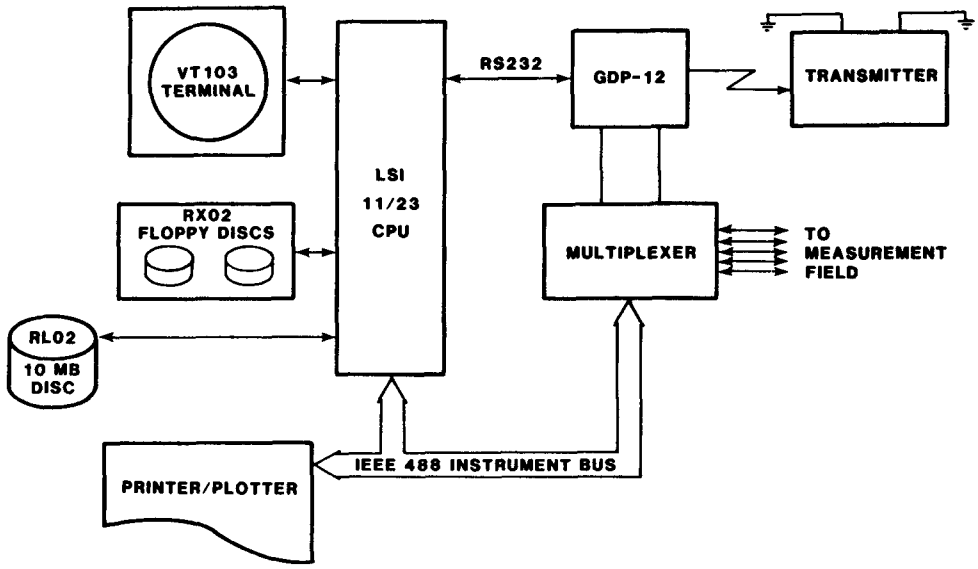

FIGURE 9. The major components of the data collection system.

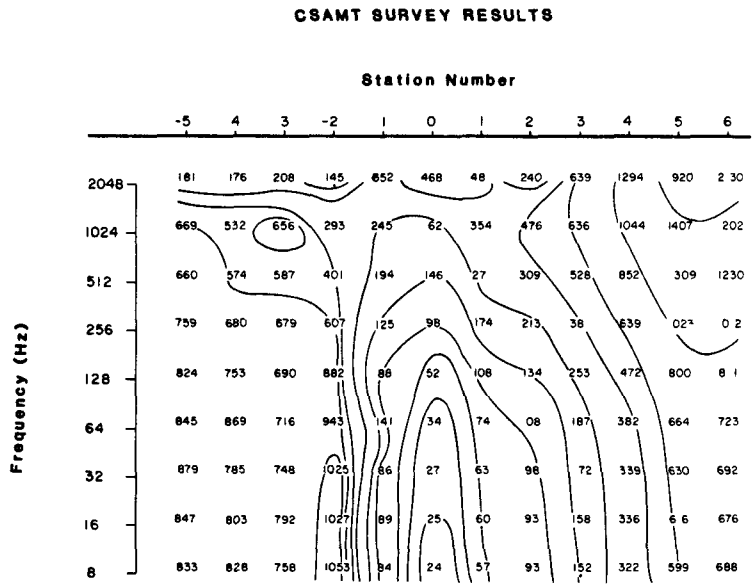

FIGURE 10. Illustration of typical pseudo-section plots to be used for data analysis.

Proceedings of the Ninth Annual Underground Coal Gasification Symposium, August, 1983

2.12 APPLICATION OF REMANENT AND ROCK MAGNETIC PROPERTIES TO THERMAL ALTERNATION OF OVERBURDEN AT THE HANNA, WYOMING, UCG SITE

by

John Wm. Geissman[1/]
James T. Callian [2/]
Alv D. Youngberg [3/]

ABSTRACT

Studies of the remanence and rock magnetic properties of host-rock Early Tertiary Hanna Formation at the Hanna II, Phases 2 and 3 underground coal gasification (UCG) experiment, Hanna, Wyoming, have determined the nature of the remanent magnetism of unaltered Hanna Formation and changes in the remanence and magnetic mineralogy attending the UCG tests. Core holes 2HP-174 and 2HP-176, located in the center of ther burn cavity, contain intervals approximately 10 m thick immediately above the burn cavity in which the natural remanent magnetization(NRM) intensity (greater than 1.0 A/m), NRM dispersion (k values exceeding 1000), NRM mean inclination(very close to +69°, the ambient field inclination during burning), initial susceptibility (greater than 1.0×10^{-4}), and demagnetization properties(distributed blocking temperatures and moderate coercivity spectra, suggesting significant coarse magnetite) all are anomalous in comparison to the "background" properties of fresh Hanna Formation. Post-burn core holes located near the edge of the burn cavity do not contain such intervals of anomalous magnetization properties. As well, Hanna Formation beneath the burn cavity is not remagnetized.

The origin of the remagnetized zone is due to the production of 1-5 volume percent secondary magnetite from detrital ferromagnesian silicates and, possibly, hematite. Thermal demagnetization experiments on fresh Hanna Formation show that magnetite production occurs in air at temperatures above about 300°C. The magnetic data have significant application toward better understanding UCG experiments and attending thermal anomalies. Thermal perturbations on surrounding Hanna Formation units must have been funnelled vertically upward from the center of the burn cavity, not radially away from it. Assuming that magnetite production is solely temperature dependent, the thermal gradient above the burn cavity is estimated to be approximately 70C°/m.

[1/]Department of Geology, Colorado School of Mines, Golden, CO 80401

[2/]Department of Geology, Colorado School of Mines, Golden, CO 80401

[3/]U.S. Department of Energy, Laramie Project Office, Laramie, Wyoming 82071

INTRODUCTION

Several underground coal gasification (UCG) experiments have been conducted in the Hanna No. 1 coal seam of the Hanna Basin in southeast Wyoming. During the Fall, 1980, the Laramie Energy Technology Center performed a post-burn field study of the Hanna II, Phases 2 and 3 experiment at the Hanna UCG site. The field work consisted of high resolution seismic, drilling, coring, and geophysical logging. The Paleomagnetism Laboratory, Department of Geology, Colorado School of Mines, contributed to the post-burn study by doing remanent and rock-magnetic measurement laboratory work on the core material. Funding was provided by the Laramie Energy Technology Center. The purpose of the study was to determine the nature of the remanent magnetism of the overburden

Hanna Formation and changes in the remanence and magnetic mineralogy attending underground coal gasification experiments. With this information, further estimates of the thermal and chemical conditions reached during the conversion experiment could be made.

RESULTS

The core holes investigated (2HP-133, 172, 173, 174, 175, 176, 178, and 182) are shown in Figure 1 with respect to the burn cavity. Unaltered overburden in the burn area, consisting of non-marine mudstones, sandstones, coals, and conglomerates, is characterized by very low intensities of natural remanent magnetization (10^{-3} to 10^{-4} A/m). Demagnetization experiments suggest that the magnetization in these lithologies resides largely in rare detrital magnetite of variable grain size. Dispersion of magnetization directions is generally very high in unaltered overburden material and is probably due to depositional and post-depositional (diagenetic) processes. Figure 2 gives typical remanence and rock magnetic data from pre-burn core hole 2HP-133 and illustrates the magnetization properties described above

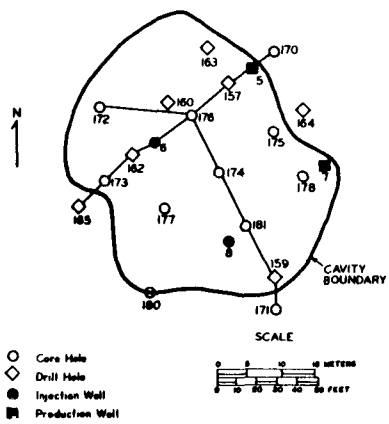

Figure 1. Plan view and well locations for the Hanna II, Phases 2 and 3 UCG sites. The approximate burn cavity boundary is also shown. Modified from Craig, et al.(1982).

In the vicinity of the burn cavity (Figure 1), overburden units immediately above the Hanna No. 1 coal seam have been subjected to high temperature pyrometamorphism during Hanna II UCG experiments. This activity caused significant changes in the magnetic mineralogy and the associated remanence characteristics of the overburden sediments. Core holes 2HP-174 and 2HP-176, drilled in the center of the burn cavity (Figure 1), best display the magnetization changes. For each hole, a zone approximately 10 m thick immediately above the void space created during collapse exhibits anomalous magnetization properties (e.g., natural remanent magnetization intensities between 10^{-1} and 1.0 A/m; k(dispersion parameter) values exceeding 500 (meaning excellent grouping of directions); initial susceptibilities exceeding 10^{-4}; and anomalous demagnetization characteristics (distributed blocking temperatures and moderate coercivity spectra, suggesting an abundance of coarse-grained, relatively pure magnetite as the major remanence carrier)). Figure 3 gives typical remanence and rock magnetic data from post-burn core hole 2HP-174 and illustrates the dramatic change in magnetization properties with respect to the geometry of the burn cavity.

Core holes at the dege of the burn chamber (e.g., 2HP-173, Figure 1) show very little change in magnetization properties as the chamber is approached. As well, Hanna Formation beneath the burn cavity is not remagnetized (e.g., Figure 3, data from intervals below 300').

The origin of the "remagnetized" zone immediately above the burn cavity of Hanna II, Phases 2 and 3, is attributed to the formation of 1-5 +/- volume per cent magnetite from detrital ferromagnesian silicates and hematite in overburden Hanna Formation. Stephenson(1969) and Dunlop(1971) have observed the formation of such quantities of magnetite during laboratory heating of red sandstones and siltstones. Thermal demagnetization studies, in which samples are heated at a given temperature in a zero magnetic field, then cooled in a zero magnetic field, then measured, support this hypothesis. For example, Figure 4 shows the response by several fresh Hanna Formation samples to thermal demagnetization. Mag-

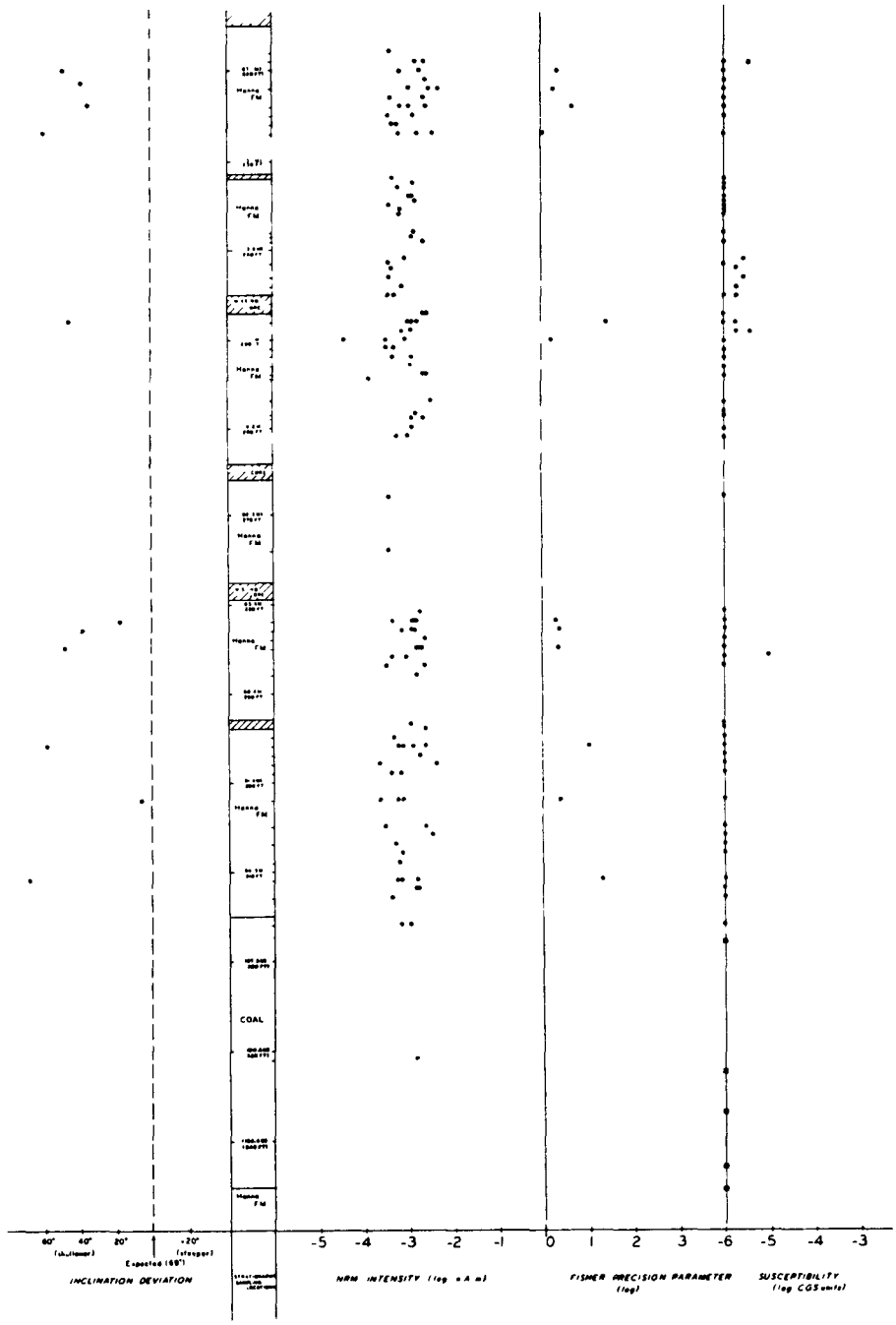

Figure 2. Remanence and rock magnetic data plotted vs. core depth, Hanna II site, core 2HP-133. In the first column, the deviation from the expected inclination ($+69^0$, see text) of the mean inclination of the natural remanent magnetization is plotted for stratigraphic levels where three or more specimens were measured and mena NRM directions and associated statistics could be calculated. In the second column, the rock type and core nature is summarized. In the third column, the intensity of the NRM is plotted. The fourth column displays the Fisher precision parameter (Fisher, 1953). The fifth column gives the initial susceptibility. Susceptibility data given in circles refer to Hanna Formation rock specimens; squares refer to fragmented char or rubble samples. The maximum sensitivity of the Bison unit used for measurements is 1.0×10^{-6} cgs units. All values less than this are plotted as 1.0×10^{-6}.

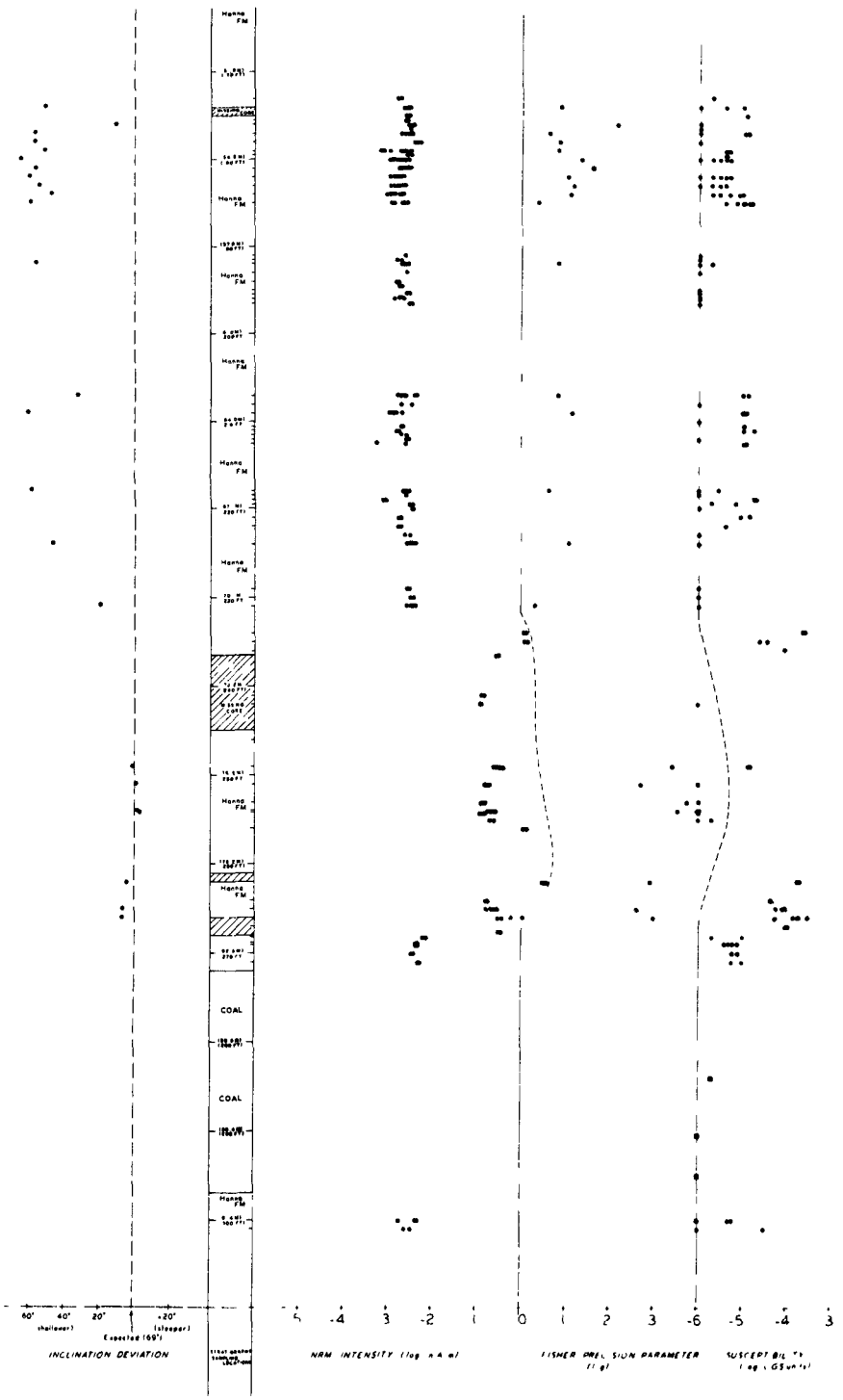

Figure 3. Remanence and rock magnetic data plotted vs. core depth, Hanna II site, core 2HP-174. The location of this core hole is given in Figure 1. The presentation of the data is as in Figure 2.

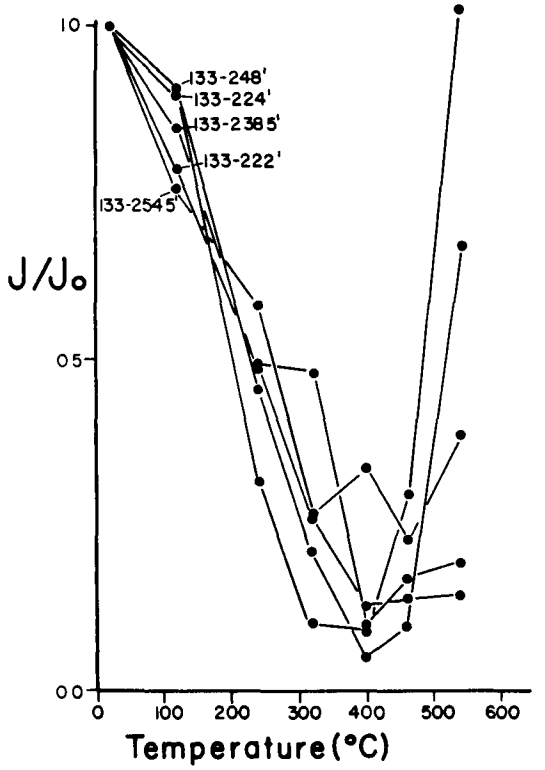

Figure 4. Normalized magnetization intensity vs. temperature; thermal demagnetization, unaltered Hanna Formation. Specimens from core hole 2HP-133, at different depths.

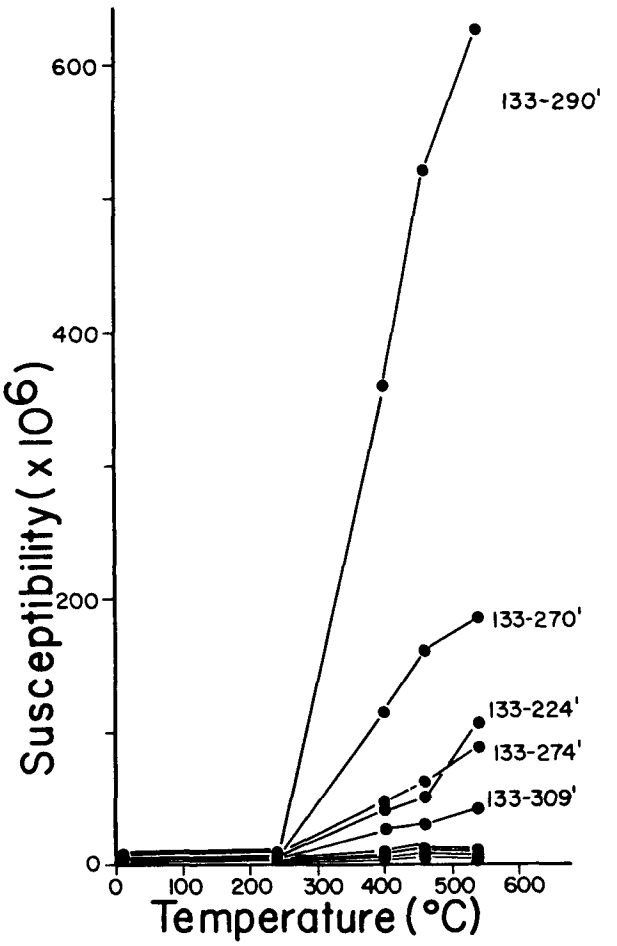

Figure 5. Plot of susceptibility vs. temperature; thermal demagnetization, unaltered Hanna Formation. Specimens from core hole 2HP-133, at different depths.

netization intensities decrease during heating to about 300°C, but drastically increase above that temperature. The formation of magnetite in air must be kinetically activated at approximately this temperature. Figure 5 illustrates the corresponding increase in susceptibility, proving magnetite formation, at approximately this temperature. Figure 6, on the other hand, shows that remagnetized Hanna Formation is thermodynamically stable during thermal demagnetization; a simple decrease in the magnetization intensity up to 585°C, the maximum blocking temperature of pure magnetite is seen. As well, the susceptibility of remagnetized Hanna Formation changes very little during thermal treatment(Figure 7).

The magnetization data from the core holes at Hanna II, Phases 2 and 3, have significant application toward better understanding UCG experiments and attending thermal anomalies. Thermal perturbations must have been funnelled vertically upward through surrounding Hanna Formation units from the center of the burn cavity and not radially away from it. Assuming that magnetite production is solely temperature-dependent, the thermal gradient above the burn cavity is estimated to be approximately 70°C/m. Magnetization data may be more useful in determining thermal environments around UCG test sites and more simple to interpret than data from other presently incorporated techniques.

The surface magnetic expression of the burn cavity should be able to be modelled as being due to a thin magnetic slab overlying the cavity. Pyrometamor-

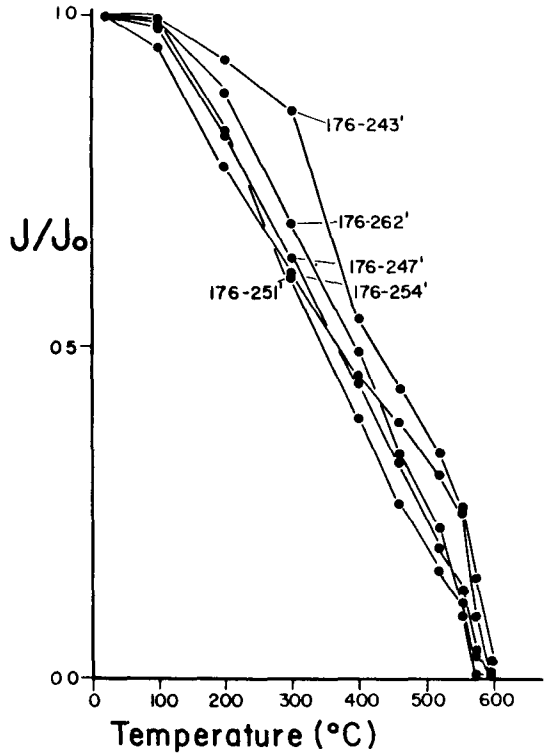

Figure 6. Normalized intensity vs. temperature; thermal demagnetization, remagnetized Hanna Formation. Specimens from core hole 2HP-174, at different depths.

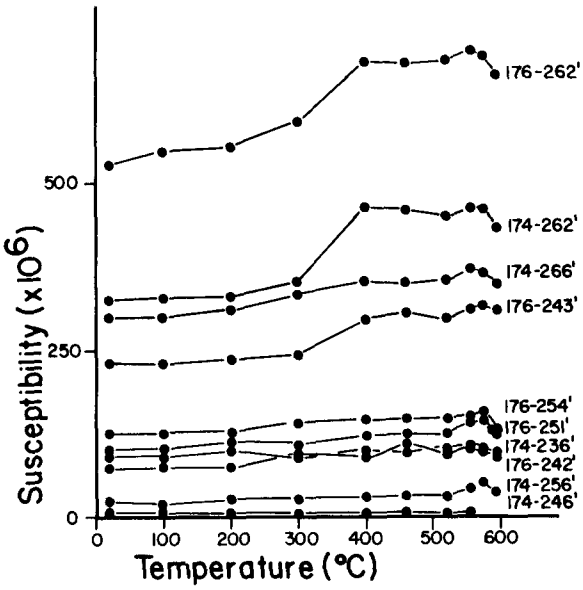

Figure 7. Plot of susceptibility vs. temperature; thermal demagnetization, remagnetized Hanna Formation. Specimens from core hole 2HP-174, at different depths.

phosed material that has collapsed into the cavity should have any magnetization essentially randomized due to collapse and therefore should be able to be incorporated into a magnetic anomaly model.

A more complete discussion of this study may be found in Geissman et al. (1983).

ACKNOWLEDGEMENTS

This project was funded by the U.S. Department of Energy, Laramie Energy Technology Center, under contract number DE-AS2081LC10694. Theodore C. Barke made this study possible by providing funding from the LETC Underground Coal Gasification Project. Mark Hudson, Bill Oppenheimer, Ken Shonk, and Edmond Suher aided the authors in various aspects of the project.

REFERENCES

Craig, G. N., II, Burns, L. K., Ethridge, F. G., Laughter, T. F., and Youngberg, A. D., 1982, Overburden characterization and post-burn study at the Hanna, Wyoming, Underground Coal Gasification Site: stratigraphy, depositional environments and mineralogy, Hanna Formation: U.S. Department of Energy, Technical Information Center, 10496-T1, 188 p.

Dunlop, D. J., 1971, Magnetic mineralogy of unheated and heated red sediments by coercivity spectrum analysis: Geophys. Jour. Roy. Astr. Soc., v. 27, p. 37-55.

Fisher, R. A., 1953, Dispersion on a sphere: Proc. Roy. Soc. London, A217, p. 295-305.

Geissman, J. W., Callian, J. T., and Youngberg, A. D., 1983, Remanent and rock magnetic properties at the Hanna, Wyoming, Underground Coal Gasification Site: Hanna

II, Phases 2 and 3, Experiment: U.S. Department of Energy, Technical Information Center.

Stephenson, A., 1968, The effect of heat treatment on the magnetic properties of the Old Red Sandstone: Geophys. Jour. Roy. Astr. Soc., v. 13, p. 424-440.

2.13 GEOTECHNICAL STUDIES ON THE OVERBURDEN ROCK FROM THE RAWLINS, T-2 UCG SITE

by

Lary K. Burns [1/]
Thomas R. Marks [1/]
Frank G. Ethridge [1/]
Alv D. Youngberg [2/]

ABSTRACT

Mechanical properties, specifically uniaxial compressive strength, tensile strength, propagation velocities for compressional (P) and shear (S) waves and dynamic elastic moduli, measured for rock types from the Rawlins, Wyoming T-2 underground coal gasification (UCG) site correlate well with mean grain size, volume percent cement, types of cement and percent porosity. Mechanical properties show the strongest relationship with the amount of calcite cement present. Mean grain size, percent porosity and percent clay cement show less pronounced relationships with mechanical properties when the amount of calcite cement present is small. Mechanical wave velocities and uniaxial compressive strength are related, but the relationship is not linear. Recommendations are given for routine sampling, testing and analysis procedures to assess mechanical and lithological parameters at UCG sites.

INTRODUCTION

The UCG site in steeply dipping beds (UCG-SDB) near Rawlins, Wyoming (Fig. 1) was one of the most successful of the UCG experiments in terms of gas recovery and in terms of sustaining the UCG burn. The strength and stability of the overburden host rock, as well as the steep dip of the beds (65^{o}) were contributing factors in the success of this experiment.

The purpose of this paper is to summarize the mechanical and lithological properties determined from rocks taken from cores drilled at the Rawlins T-2 site. A further objective is to determine the relationships between mechanical and lithological properties of the overburden rocks. Specifically, this report provides the following data on 42 overburden samples: tensile strength and unconfined compressive strength determined by the point load test [1,2,3], compressional wave velocity (V_p), shear wave velocity (V_s), and density (ℓ); and dynamic elastic constants such as Young's modulus (E), bulk modulus (K), shear modulus (G), and Poisson's ratio (ν), derived from the velocities and rock densities.

METHODOLOGY

MECHANICAL TESTS

Point Load Test

The static geotechnical test used was the point load test which has gained considerable international approval [1,2,3, 4,5] in the past decade and is now considered one of the most reliable geotechnical rock strength tests. It was selected because it is reliable, simple to perform and gives a measure of both tensile strength and unconfined compressive strength [1,2,3] of the rock specimen. The test is performed by compressing a rock between two rounded points. Although several specimen shapes including

1/ Department of Earth Resources, Colorado State University, Fort Collins, Colorado.

2/ U. S. Dept. of Energy, Laramie Energy Technology Center, Laramie Wyoming.

cylinders, spheres and irregularly-shaped rocks have been used, the most consistent results have been obtained by applying the point load perpendicular to the axis of a cylinder that is at least 1.5 times as long as the diameter of the cylinder ($L/D > 1.5$) [1,3]. For this reason, the point load test is especially suited for testing rock core. Figure 2 shows the experimental setup used in the diametrally applied point load test that was used in this study. Two standard point load test platens were made from oil-hardened steel with the dimensions and specifications given by Broch and Franklin [1] and Bieniawski [2] (Fig. 3). The pressure on the point load platens was applied using a 60 KIP hydraulic universal testing machine. Pressure was measured with a fluid filled pressure cell driving a Bourdon tube whose motion was magnified on the dial readout face. This pressure measurement system had a sensitivity of ±0.1 percent. An additional error of ±10-20 pounds was introduced due to human error in reading the dial face.

Dynamic (Ultrasonic) Testing

The dynamic geotechnical testing was done using a Model 1007H Seismic Analyzer ultrasonic testing device (Fig. 4). The mechanical (ultrasonic) pulses are generated by a piezoelectric crystal at frequencies of 1000 KHz.

Sample preparation involved cutting the rock core into a disk shape with the ends cut perpendicular to the axis of the core sample. This was done using a lapidary saw with a diamond saw blade. The ends of each sample were ground smooth with #400 silicon carbide grit to remove any irregularities and to insure good contact between the testing platens and the rock sample. Each sample was cemented between the wave generating platens using phenyl salicyclate. This crystalline material is heated to the melting point and the liquid is applied to the contact surface. Upon cooling, the material bonds to the metal and rock surfaces.

The compressional wave travel time ranged from 21.4 μs (microseconds) to 99.8 μs. The compressional wave delay time* was 12.5 μs. Travel time for shear waves ranged from 46.0 μs to 191.7 μs. The shear wave delay time was 19.5 μs. Compressional wave velocities ranged from 955.4 meters per second (m/s) to 5007.9 m/s. Shear wave velocites ranged from 484.3 m/s to 1802.9 m/s.

ROCK CHARACTERIZATION

The core samples used in the study were taken from core holes CH3, CH4 and CH231. Sample numbers used in this report give the core hole from which the sample is taken and the depth from which the sample is taken in feet. For core pieces a few tenths of a foot long used in the mechanical testing, the depth to the approximate center of the sample is given. The vertical distribution of the samples tested is given in cross sections through the T-2 site (Figs. 5 and 6).

The lithologic aspects of overburden material that are reported here are those parameters which have a relationship to the mechanical properties. These parameters are grain size, rock density, pore space colume (porosity), amount and type of cement and volume of framework grains (Table 1).

Grain size of overburden sandstones was determined from thin sections by using a calibrated micrometer eyepiece on a polarizing microscope. A minimum of 40 grains were measured for each thin section sample. Twenty-five samples for which thin sections were not available were assigned the median grain size for each rock based on Folk's [6] grain-size scale for sediments.

Rock densities were measured for forty-two core samples by weighing air-dried samples and the volume was determined by measuring the amount of water displaced upon immersion of the sample.

The pore space volume was determined for 17 sandstones by point counting a minimum of 200 points per section. The amount and type of cement, and the amount of each mineral component were also determined by the point counting procedures. Percentages reported are volume percents.

---

* Delay time is the time it takes the mechanical wave to pass from the generating crystal in the platen to the sample, plus the time it takes for this wave to get from the other end of the sample to the receiver.

RESULTS

MECHANICAL TESTS

In their extensive investigation of the application of the point load test to an extremely wide variety of rock types, Broch and Franklin [1] show that a rock strength index for virtually any specimen can be given as a function of the pressure required on the standard point load platen (Fig. 3) to break the rock divided by the square of the distance between the contact points of the two platens,

$$I_s = \frac{P}{D^2} \qquad (1)$$

A nomogram relating the rock strength point-load index to core of different diameters was developed by Broch and Franklin [1]. The data and approach used by Broch and Franklin have been supplemented by tests done by Hassani and others [3] who have refined the nomogram and presented the correction equations in an exponential form [3],

$$\log_{10} I_{s(50)} = 0.256 + \log_{10} I_s - 1.008^{e^{-0.027}} \qquad (2)$$

This allows the uniaxial compressive strength and the tensile strength to be calculated directly using the following expressions:

uniaxial compressive strength-

$$q_u = 29.07\ I_{s(50)}, \qquad (3)$$

tensile strength-

$$T_s = 2.77\ I_{s(50)}, \qquad (4)$$

where $I_{s(50)}$ is the point-load index of strength corrected for cores of various diameters to a standard 50mm diameter. The correction is given in Equation 2, or may be obtained from the modified nomogram of Hassani and others [3] (Fig. 7).

The results of the point load tests of this study are presented in Table 2. The sample numbers give the core hole from which the sample came and the depth in feet to the center of the segment of core tested. Core diameters are given as the cores were not all the same size. The rock type, point load index, tensile strength and uniaxial compressive strength are also given for each sample. All of the strength values are derived from the point load test.

Table 3 gives the compressional or P-wave velocities (V_p) and the shear or S-wave velocities (V_s) for the 42 samples tested. Figure 8A gives a typical P-wave trace with a sharp arrival of the compressional P-wave at point P, 22.5 μs after the sweep and ultrasonic wave were triggered. Since the instrument used has a P-wave delay time of 12.5 μs, the actual travel time is 10.0 μs for the P-wave. Point S marks the arrival of the S-wave on Figure 8B. It is obvious that the shear wave is not the first wave to arrive even though the crystal wave generator is oriented to produce only a shear wave. This problem is, unfortunately, not confined to our experiment, but is almost invariably seen in ultrasonic tests [7,8]. These early-arriving waves are undoubtedly P-waves, generated at non-penetrative boundaries within the sample or at the sample walls. This phenomenon, known as mode conversion, is a constant problem for not only laboratory ultrasonic tests, but also for field tests [9]. The problem is to identify the arrival of the first shear wave in the train of incoming waves. In attempting to identify that arrival, several properties of the shear wave generated in such a manner should be noted.

The shear wave will have more energy than the P-waves it generates by mode conversion and this will be reflected as an increased magnitude in the wave on the trace. Compare the amplitude of the wave on Figure 8B for the secondary P-waves, i.e., those arriving before point S, with the amplitude of the S-wave train which is seen after the arrival (point S).

Another check on the determination of the S-wave arrival time is to use the chosen arrival time to calculate the value of Poisson's ratio for the rock (Equation 8). Since the calculated Poisson's ratio is very sensitive to the S-wave velocity, a 10 percent change in the S-wave velocity can give a 100 percent change in Poisson's ratio. Selection of the wrong wave perturbation for the arrival time for the S-wave usually gives Poisson's ratios outside the normal range of 0.0 to 0.5.

Elastic properties or dynamic elastic constants can be expressed as a function of the compressional wave velocity (V_p), the shear wave velocity (V_s) and the mass density (ρ).

Dynamic Elastic Modulus

Shear Modulus

$$G = \rho V_s^2 \quad (5)$$

Young's Modulus

$$E = \rho V_s^2 \frac{3V_p^2 - 4V_s^2}{V_p^2 - V_s^2} \quad (6)$$

Bulk Modulus

$$K = \rho (V_p^2 - 4/3 V_s^2) \quad (7)$$

Poisson's Ratio (8)

$$\nu = \frac{V_p^2 - 2V_s^2}{2(V_p^2 - V_s^2)} = \frac{1 - 1/2 (V_p/V_s)^2}{1 - (V_p/V_s)^2}$$

Where: V_s = shear wave velocity
V_p = compression wave velocity
ρ = mass density

Only one of these relations, the shear modulus, is not dependent on all three of the measured properties. The measured wave velocities (V_p and V_s), mass density (ρ) and the dynamically derived elastic constants, (G, E, K and ν) are given in Table 3.

CORRELATIONS

One of the primary objectives of this study, in addition to determination of the mechanical and lithological properties of the rocks at the Rawlins UCG site, is to determine the relationship between these two sets of parameters. This was done through linear regression when a linear relationship was suggested. When the relationship between two parameters appeared non-linear, a visual best-fit curve was drawn.

Uniaxial Compressive Strength

The unconfined compressive strength of samples tested is plotted against mean grain size for calcite-cemented samples and for samples with dominantly clay cement (those with less than 10 percent total calcite) in Figure 9. Figure 9 shows that calcite-cemented siltstones and sandstones are significantly stronger than clay-cemented overburden samples. Further, the plot indicates that uniaxial compressive strength (q_u) is significantly more dependent on the type of cement than on grain size. For the clay-dominant cement overburden rocks (Fig. 10), there is a tendency for rocks of a mean grain size of ~.044mm (siltstone) to have a greater uniaxial compressive strength than either finer or coarser-grained sedimentary rocks. This plot includes 46 samples ranging in grain size from claystones, whose average grain size is less than .02mm, to coarse-grained sandstones, whose average grain size is ~.71mm.

The amount of calcite cement in the sandstones is the most significant factor in controlling the rock strength of the overburden material. The uniaxial compressive strength of sandstones derived from the point load test is linearly related to the amount of calcite cement (Fig. 11). One sample(CH4 448-449) has 65 percent calcite and is not included in the graph for sandstones since it is a limestone rather than a sandstone. The calcite grains are large in this sample and enclose the detrital sand grains present; therefore, the strength of the rock is that of crystalline sandy limestone. Since calcite has excellent rhombohedral cleavage, the rock strength of this type of limestone will be directionally dependent. The amount of clay minerals as a cementing agent in the sandstones has a non-linear relation with the rock strength (Fig. 11). There is considerable scatter in the data points for this curve. However, the reason for the relationship is that the percentages of clay cement and calcite cement are inversely related to each other in these rocks.

Figure 12 shows that as porosity decreases, strength increases in a non-linear fashion. This is due to an inverse relationship of percent cement to percent porosity and direct relationship between percent cement and strength (Fig. 11).

Mechanical Wave Velocity

The compressional wave (P-wave) and shear wave(S-wave) velocities are dynamic constants that are measured directly. Therefore, they have been selected as the dynamic parameters to relate to lithologic and strength parameters. The other dynamic constants given in this report are derived from these velocities, and, if the velocities are related to a lithologic or strength parameter, the derived constants should be related in a similar fashion as well. In addition, direct field measurements of the seismic wave velocities may be done either in situ [7,9,10,11] or directly on core material using an ultrasonic testing device [7].

The P- and S-wave velocities for all the sedimentary samples tested are plotted against the mean grain size in Figures 13 and 14. Samples that are cemented with greater than 10 percent calcite are shown as open circles, and overburden samples that have clay minerals as the dominant cement are shown as black dots. The mechanical wave velocity is more dependent on type of cementing material than on mean grain size. Samples with greater than 10 percent calcite cement (open circles) have a tendency to have higher mechanical wave velocities (P-wave and S-wave) than samples with less than 10 percent calcite cement (black dots). There is a general tendency for wave velocity to decrease as grain size increases up to approximately .28mm. For coarser-grained rocks, mean grain size no longer appears to effect wave velocity (Figs. 13 and 14). The probable reason for this relationship is that as grain size increases, porosity also increases, thus decreasing wave propagation velocity (Fig. 15).

Just as was shown for uniaxial compressive strength, seismic wave velocities (V_p and V_s) are strongly controlled by the amount of calcite cement in the rock. Further, as the amount of clay mineral cement is inversely related to the amount of calcite cement, the amount of clay cement will be inversely related to the seismic wave velocities (Fig. 16). This figure shows that the P-wave and S-wave velocity curves have a good linear fit with volume percent calcite. There is less scatter for the P-wave curve ($r^2 = .81$) than with the S-wave curve ($r^2 = .75$). However, both of the r^2 values are significant considering the many factors other than amount of calcite cement that are influencing these velocities. It appears that the calcite cement is the overriding factor in controlling these wave velocities.

It should be noted that the scatter is much greater for points of the curves of wave velocity vs. clay mineral cement in Figure 16. The curves are a visually drawn best fit, and the r^2 values were not calculated. The apparent relationship in Figure 16 between percent clay cement and seismic wave velocities (V_p and V_s) is primarily due to the previously discussed inverse relationship between percent clay cement and percent calcite cement.

Figure 17 shows a non-linear direct relationship between uniaxial compressive strength and mechanical wave velocities for the 42 samples tested. It should be noted that the actual data points have been removed for clarity and that considerable scatter was present. This relationship is due to the fact that uniaxial compressive strength and wave velocities are both strongly dependent on the same lithologic parameters.

SUMMARY

This study characterizes certain geotechnical rock parameters and descriptive lithological parameters of overburden samples taken from the Rawlins, Wyoming UCG site. The point load test was used to determine the point load strength index, tensile strength, and the uniaxial compressive strength of the samples. The velocities of compressional waves (V_p) and shear waves (V_s) were determined using a Model 1007H Seismic Analyzer ultrasonic testing device.

Lithologic properties that are related to the geotechnical parameters are given. These lithologic properties were quantified for samples coarse-grained enough for detailed petrographic studies (i.e.,coarse siltstones and sandstones) and related to the mechanical properties of the rocks.

The results of the study show that the type and amount of the cementing mineral in the rocks is the most important lithologic parameter in determining rock strength and P- and S-wave velocities

(Figs. 11 and 16). Grain size has an effect on rock strength (Fig. 10) and P- and S-wave velocities (Figs. 13 and 14) when clay cement is the dominant cement type.

Porosity shows a non-linear inverse relationship to both rock strength and ultrasonic wave velocities (Figs. 12 and 15). As porosity increases, strength and wave velocity tend to decrease. This is probably due to an inverse relationship between percent porosity and percent cement.

Uniaxial compressive strength displays a non-linear direct relationship to P- and S-wave velocities for all rock types tested at the Rawlins T-2 UCG site (Fig. 17). This relationship is potentially useful in estimating rock strengths at UCG sites where only down-hole wireline logs and/or seismic data are available.

In overburden rocks of the Rawlins UCG site, the amount of calcite present as a cementing agent is the most important single factor in controlling both rock strength and P- and S-wave velocities (Figs. 9, 11 and 16). The amount of clay as a cementing agent seems to be inversely related to rock strength and P- and S-wave velocity, but this relationship may be a function of an inverse relationship between percent calcite and percent clay cement. In conclusion, it has been shown that the variation in rock strength and propagation velocities of mechanical waves through rock material is not random, but controlled by lithologic parameters of the rocks.

RECOMMENDATIONS

If the relationships between mechanical and lithologic parameters are to be useful in investigations such as those required for UCG site characterization and experiment evaluation, the parameters must be of the type that are reproducible and that can be reasonably determined without a significant increase in technical personnel or specialized equipment. In other words, the methods must be cost effective. All of the measurements described in this paper are either already being routinely made at UCG sites or could be made with fairly inexpensive equipment and existing personnel. The lithologic parameters are all routinely determined in both site characterization and experiment evaluation studies currently conducted at UCG sites. The mechanical tests could be made by a geologist or geotechnician when the original core is being logged. The point load tests could be reliably done in the field on each lithologic type found in the core samples, and the dynamic (ultrasonic) tests could be done at the same time the lithologic core descriptions are made in the laboratory.

It is recommended that the following tests and precedures be carried out routinely at UCG sites.

1) Point load tests should be done on rock core for every lithologic type in the overburden. This can be done with a portable point load testing machine which meets the specifications of Broch and Franklin [1].
2) Strength values should be recorded for all rock types in the core.
3) Ultrasonic mechanical wave tests (P- and S-wave) should be completed on at least two samples of each lithologic type either at the site or later in a laboratory setting to facilitate sample preparation. Photographs should be taken of each wave trace and retained as a permanent record.
4) Lithologic parameters should be measured for each sedimentary rock type. These should include density, grain size, sorting, type and relative percentage of cement(s), percent porosity and percent framework (detrital grains).
5) The measured values of seismic velocities for rock types in a given UCG site should be used for seismic surveys of overburden material in that site. The use of these values rather than other assumed values should result in more accurate seismic data.
6) P- and S-wave crosshole and downhole measurements would give valuable data on velocities, especially for horizontal beds and a geophysical experiment to measure these velocities is advised.

ACKNOWLEDGMENTS

This work was funded by the U. S. Department of Energy, Laramie Energy Technology Center. Terri Bostedt typed the manuscript and aided in all parts of the completion of the paper. The figures were drafted by Melanie Keenan.

REFERENCES

[1] E. Broch and J. A. Franklin, "The Point Load Strength Test", Int. Jour. of Rock Mech. Min. Sci., Vol. 9, 1972, p. 669-697.

[2] Z. T. Bieniawski, "The Point Load Test in Geotechnical Practice", Engineering Geology, Vol. 9, 1975, p. 1-11.

[3] F. P. Hassani, J. J. Scoble and B. N. Whittaker, "Application of the Point Load Index Test of Strength Determination of Rock and Proposals for a New Size Correlation Chart", Rock Mechanics, A State of the Art, Proc. 21st Symp. on Rock Mech., Univ. of Missouri, Rolla, 1982, p. 241-246.

[4] M. Greminger, "Technical Note: Experimental Studies of the Influence of Rock Anisotropy in Size and Shape effects in Point Load Testing", Int. Jour. Rock Mech. Min. Sci., and Geomech. Abst., Vol. 19, 1982, p. 241-246.

[5] E. Z. Lajtai, "Tensile Strength and its Anisotropy Measured by Point and Line Loading of Sandstone", Engineering Geology, Vol. 15, 1980, p. 163-171.

[6] R. L. Folk, "Petrology of Sedimentary Rocks", Hemphill Publishing Co., Austin, Texas, 1965, p. 25.

[7] R. W. Stepehenson, "Ultrasonic Testing for Determining Dynamic Soil Moduli", Dynamic Geotechnical Testing, ASTM-SPG 654, M. L. Silver and Drew Tiedemann, (eds.), 1978, p. 179-195.

[8] Jackson Odum, U. S. Geological Survey, personal communication, 1983.

[9] R. J. Hoar and K. H. Stokoe, II, "Generation and Measurement of Shear Waves in Situ", Dynamic Geotechnical Testing, ASTM-STP 654, M. L. Silver and Drew Tiedemann, (eds.), 1978, p. 3-29.

[10] Andy Viksne, "Evaluation of In Situ Shear Wave Velocity Measurement Techniques", U. S. Bur. Reclamation Tech. Rept. REC-ERC-76-6, 1976, p. 40.

[11] V. R. McLamore, D. G. Anderson and C. Espana, "Crosshole Testing Using Explosive Mechanical Energy Sources", Dynamic Geotechnical Testing, ASTM-STP 654, M. L. Silver and Drew Tiedemann (eds.), 1978, p. 30-65.

Table 1 Lithologic parameters of sandstones from the Rawlins UCG site, Wyoming Values are in percent of total constituents, except for grain size, which is mean diameter of the framework grains in mm

Sample Number	Lithology	Grain Size	Framework Grains	Total Cement	Clay Cement	Fex-oxide Cement	Siderite Cement	Calcite Cement	Porosity	Density Glow
CH3 212 5	mgss	388	59 0	39 0	3 0	5	1 0	34 5	2 0	2 44
CH3 18 3	mgss	413	90 0	6 5	6 5	0	0	0	3 5	2 04
CH3 238 5	mgss	284	75 0	18 5	14 0	0	3 0	1 5	6 5	2 13
CH3 343 5	mgss	279	67 5	14 5	14 0	0	5	0	18 0	2 06
CH3 386 5	fgss	244	72 0	18 5	13 0	1 5	3 0	5	9 5	2 11
CH3 467 5	fgss	148	70 5	23 5	2 5	0	14 5	6 5	6 0	2 15
CH4 73 3	cgss	522	76 0	17 5	12 0	5 0	0	5	6 5	2 39
CH4 165 5	vfgss	120	69 5	15 5	9 0	5 5	0	1 0	15 0	2 22
CH4 190 5	fgss	238	60 5	39 5	0	3 0	0	36 5	0	2 52
CH4 407 5	vfgss	082	74 5	23 0	6 5	5	3 5	12 5	2 5	2 14
CH4 446 9	fgss	139	62 5	37 5	0	0	0	37 5	0	2 59
CH4 448 5	vfgss	088	34 5	65 5	0	1 0	1 5	64 0	0	2 68
CH4 457 7	fgss	180	64 0	36 0	0	0	5 0	31 0	0	2 59
CH4 458 5	fgss	170	55 0	44 5	5 5	5	3 5	35 0	5	2 58
CH4 496 7	sltstn	043	49 0	48 0	10 5	17 0	10 0	10 5	3 0	2 25
CH231 402 4	fgss	243	85 0	9 5	6 5	0	1 0	2 0	5 5	2 10
CH231 403 8	mgss	284	86 0	8 0	3 5	0	2 0	2 5	6 0	2 14

ABBREVIATIONS cgss - coarse-grained sandstone (1/2 to 1mm) mgss - medium-grained sandstone (1/4 to 1/2mm) fgss - fine(to medium)grained sandstone (2^{-3} to 2^{-1}mm) vfgss-very fine-grained sandstone (2^{-4} to 2^{-3}mm) sltstn - siltstone ($2^{-9}$to 2^{-4}mm)

Table 2 Results of point load tests on rock samples from Rawlins T-2 UCG site, Wyoming

Sample * Number	Core Diameter (mm)	Rock Type	Point Load Index $I_{s(50)}$	Tensile Strength (Ts) (MPa)	Uniaxial Compressive Strength (q_u) (MPa)
CH3 40 6	88 1	sltstn	1 861	5 14	53 97
CH3 41 9	88 1	sltstn	2 183	6 03	63 31
CH3 43 6	88 1	sltstn	2 031	5 61	58 90
CH3 212 5	88 1	mgss	1 461	4 04	42 37
CH3 218 3	88 1	mgss	342	0 94	9 92
CH3 238 5	88 1	mgss	513	1 42	14 87
CH3 294 5	88 1	mgss	513	1 42	14 87
CH3 343 5	88 1	mgss	493	1 36	14 30
CH3 386 5	88 1	mgss	816	2 25	23 66
CH3 467 5	88 1	fgss	1 538	4 25	44 60
CH4 49 8	88 1	fmgss	910	2 51	26 39
CH4 73 3	88 1	cgss	607	1 68	17 60
CH4 165 5	88 1	vfgss	500	1 38	14 50
CH4 190 5	88 1	fgss	5 068	14 0	146 97
CH4 241 5	75 4	fgss	1 000	2 76	29 00
CH4 363 5	75 4	Intbd sltstn & mstn	1 465	4 05	42 49
CH4 385 1	75 4	mstn	1 832	5 06	53 13
CH4 405 3	75 4	vfgss	1 499	4 14	43 47
CH4 407 5	75 4	vfgss	1 405	3 88	40 75
CH4 415 2	75 4	muddy sltstn	1 428	3 94	41 41
CH4 416 4	75 4	vfgss	1 380	3 81	40 02
CH4 426 8	75 4	intbd sltstn&mstn	1 928	5 33	55 91
CH4 428 3	75 4	intbd sltstn&mstn	1 023	2 83	29 67
CH4 431 5	75 4	sltstn	2 321	6 41	67 30
CH4 441 6	75 4	sltstn	1 976	5 46	57 30
CH4 445 0	75 4	sltstn-vfgss	1 738	4 80	50 40
CH4 446 9	75 4	fgss	9 949	27 48	288 52
CH4 448 5	75 4	vfgss	7 022	19 38	203 63
CH4 451 4	75 4	vfgss	1 452	4 01	42 11
CH4 457 7	75 4	fgss	6 570	18 15	190 53
CH4 458 5	75 4	fgss	4 617	12 75	133 89
CH4 476 7	75 4	mstn	499	1 38	14 48
CH4 479 4	75 4	clstn	762	2 10	22 10
CH4 479 4	75 4	clstn	452	1 25	13 11
CH4 481 4	75 4	clstn	405	1 12	11 75
CH4 483 8	75 4	mstn	1 904	5 26	55 22
CH4 485 7	75 4	sltstn	1 214	3 35	35 21
CH4 488 9	75 4	mdstn	1 238	3 42	35 90
CH4 494 9	75 4	sltstn	2 880	7 95	83 5
CH4 496 7	75 4	sltstn	2 904	8 02	84 22
CH231 402 4	58 9	mgss	364	1 01	10 56
CH231 403 8	58 9	mgss	364	1 00	10 54

* The depths given are to the center of the core length tested, rounded to the nearest tenth of a foot

ABBREVIATIONS

cgss - coarse-grained sandstone (1/2 to 1mm)
mgss - medium-grained sandstone (1/4 to 1/2mm)
fmgss - fine to medium grained sandstone (2^{-3} to 2^{-1}mm)
vfgss - very fine-grained sandstone (2^{-4} to 2^{-3}mm)
sltstn - siltstone (2^{-9} to 2^{-4}mm)
Intbd - interbedded
mstn - mudstone
clstn - claystone

Table 3. Results of Dynamic (ultrasonic) tests on rock samples from the Rawlins T-2 UCG site, Wyoming.

Sample Number	V_p Ms^{-1}	V_s Ms^{-1}	ρ	G	E	K	ν
CH3 -40.6	2581.7	1307.9	2.26	3.87	10.3	9.92	.327
CH3 -41.9	2609.0	1287.5	2.24	3.71	9.95	10.3	.339
CH3 -43.6	2694.5	1347.3	2.16	3.92	10.5	10.5	.333
CH3 -212.5	2556.0	1330.8	2.44	4.32	11.4	10.2	.314
CH3 -218.3	131317	702.2	2.04	1.01	2.62	2.18	.300
CH3 -238.5	1270.9	811.0	2.13	1.4	3.24	1.57	.157
CH3 -294.5	1325.5	621.4	2.21	.85	2.32	2.74	.359
CH3 -343.5	1348.1	661.0	2.06	.90	2.42	2.55	.342
CH3 -385.5	1929.6	1118.7	2.11	2.64	6.59	4.34	.247
CH3 -467.5	2278.9	1225.3	2.15	3.23	8.38	6.88	.297
CH4 -49.8	1757.0	712.3	2.08	1.06	2.96	5.03	.402
CH4 73.3	1758.9	1067.8	2.39	2.73	6.59	3.76	.208
CH4 165.5	1894.5	1104.8	2.22	2.71	6.74	4.35	.242
CH4 190.5	5007.9	1802.9	2.52	8.19	23.4	52.3	.426
CH4 241.5	2691.3	1382.6	2.41	4.61	12.2	11.4	.321
CH4 363.5	2672.3	1373.3	2.30	4.34	11.5	10.7	.321
CH4 -385.1	2412.3	1221.7	2.20	3.28	8.72	8.45	.328
CH4 -405.3	2477.4	1287.7	2.23	3.70	9.73	8.77	.315
CH4 -407.5	2398.1	1258.4	2.14	3.30	8.88	7.79	.310
CH4 -415.2	2840.2	1396.7	2.34	4.56	12.2	12.8	.341
CH4 -416.4	2683.3	1093.0	2.32	2.77	7.77	13.1	.401
CH4 -426.8	3060.2	1489.7	2.34	5.19	14.0	15.1	.345
CH4 -428.3	2694.5	1362.1	2.31	4.29	11.3	10.9	.328
CH4 -431.5	3157.7	1593.7	2.45	6.22	16.6	16.2	.329
CH4 -441.6	2902.8	1040.8	2.46	2.66	7.61	17.1	.426
CH4 -445.0	2330.3	1361.9	2.16	4.01	9.95	6.4	.241
CH4 -446.9	4280.1	1752.9	2.59	7.96	22.3	36.8	.399
CH4 -448.5	4794.8	1610.3	2.68	6.95	20.0	52.1	.436
CH4 -451.4	2679.9	1389.0	2.23	4.30	40.8	37.0	.316
CH4 -457.7	3770.3	1592.7	2.59	6.57	18.3	28.0	.391
CH4 -458.5	3913.5	1700.3	2.58	7.46	20.7	20.7	.384
CH4 -476.7	2709.3	1451.4	2.39	5.03	13.1	10.9	.299
CH4 -479.4	2927.8	1274.6	2.37	3.85	10.7	15.2	.383
CH4--479.4	2748.0	1219.2	2.46	4.00	10.1	13.7	.377
CH4 -481.4	2585.7	797.3	2.41	1.53	4.44	14.0	.447
CH4 -483.8	2417.1	1311.4	2.26	3.89	10.0	7.97	.291
CH4 -485.7	2720.8	1260.3	2.26	3.59	9.79	11.9	.363
CH4 -488.9	2781.3	1151.3	2.13	2.82	7.89	12.8	.397
CH4 -494.9	2866.8	1408.8	2.44	4.84	13.0	13.6	.341
CH4 496.7	2686.4	392.9	2.25	4.37	11.5	10.4	.316
CH231 -402.4	1410.5	858.0	2.10	1.55	3.73	2.11	.206
CH231 - 403.8	1148.8	684.8	2.14	1.00	3.46	1.49	.224

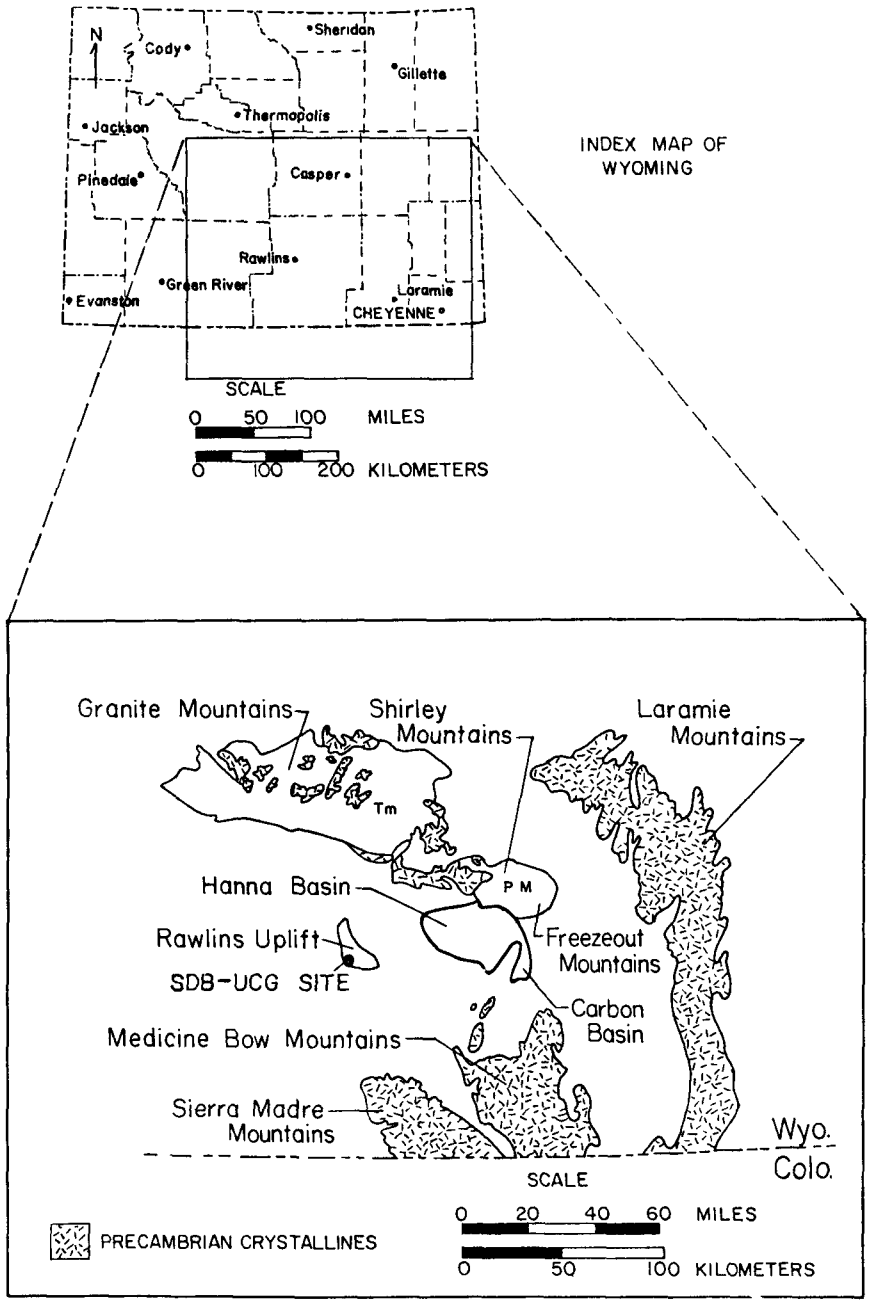

Figure 1. Location map, steeply dipping bed-underground coal gasification site, (SDB-UCG) North Knobs, Carbon County, Wyoming.

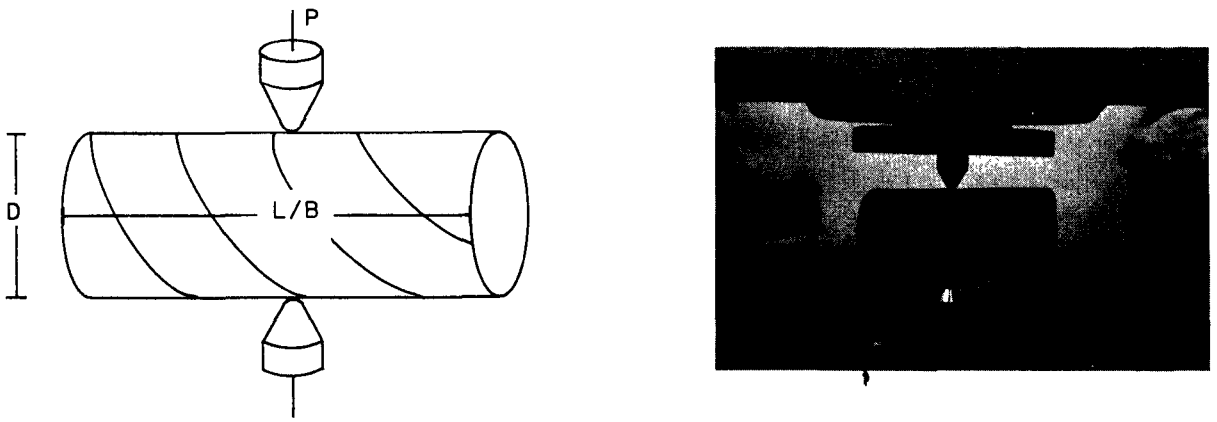

Figure 2. Diametral point load test showing relation of point loading to the typical dip of bedding of the Rawlins T-2 UCG core samples.

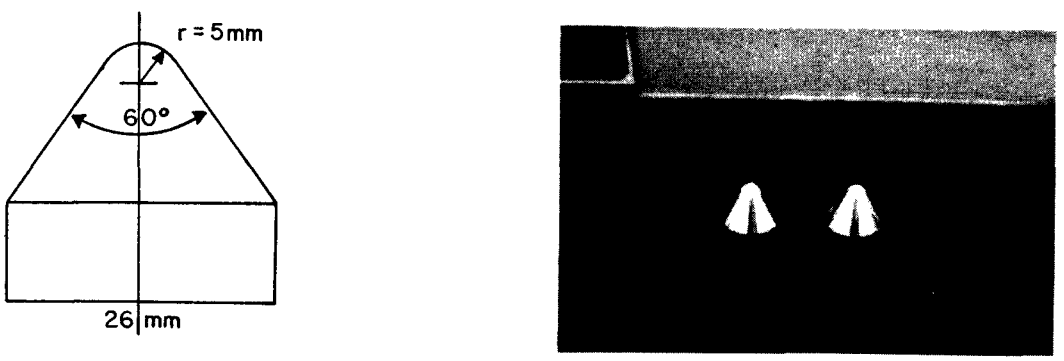

Figure 3. Platen design and dimensions for the point load test.

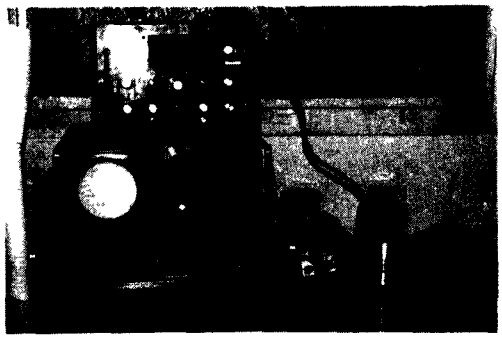

A

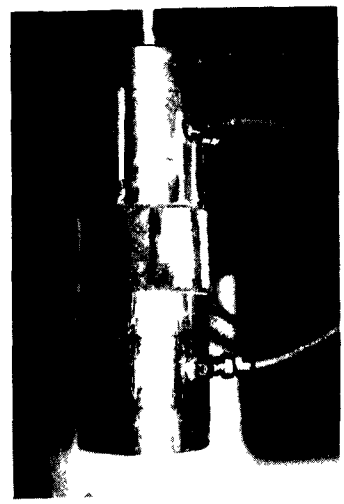

B

Figure 4. Photos of ultrasonic testing device. Detail of core sample used shown in B.

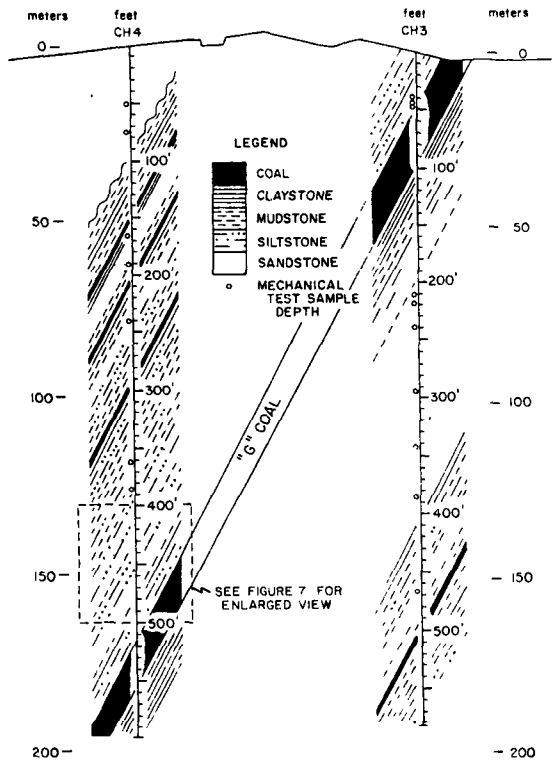

Figure 5. Cross section of area drawn through holes CH3 CH4 showing general lithologies present and location of preburn mechanical test samples.

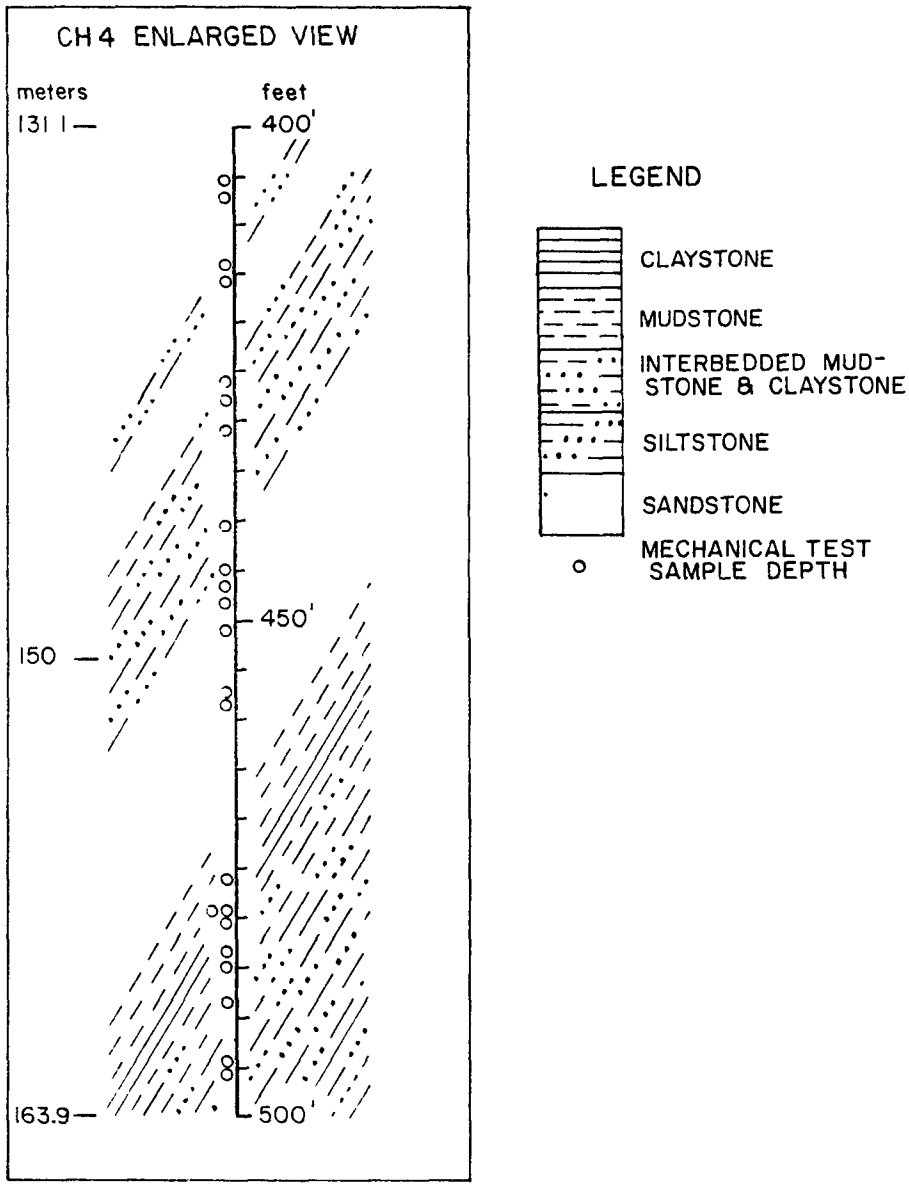

Figure 6. Section interval of well CH4 between depths of 400 and 500 feet expanded to show detail of lithology and mechanical test sample locations.

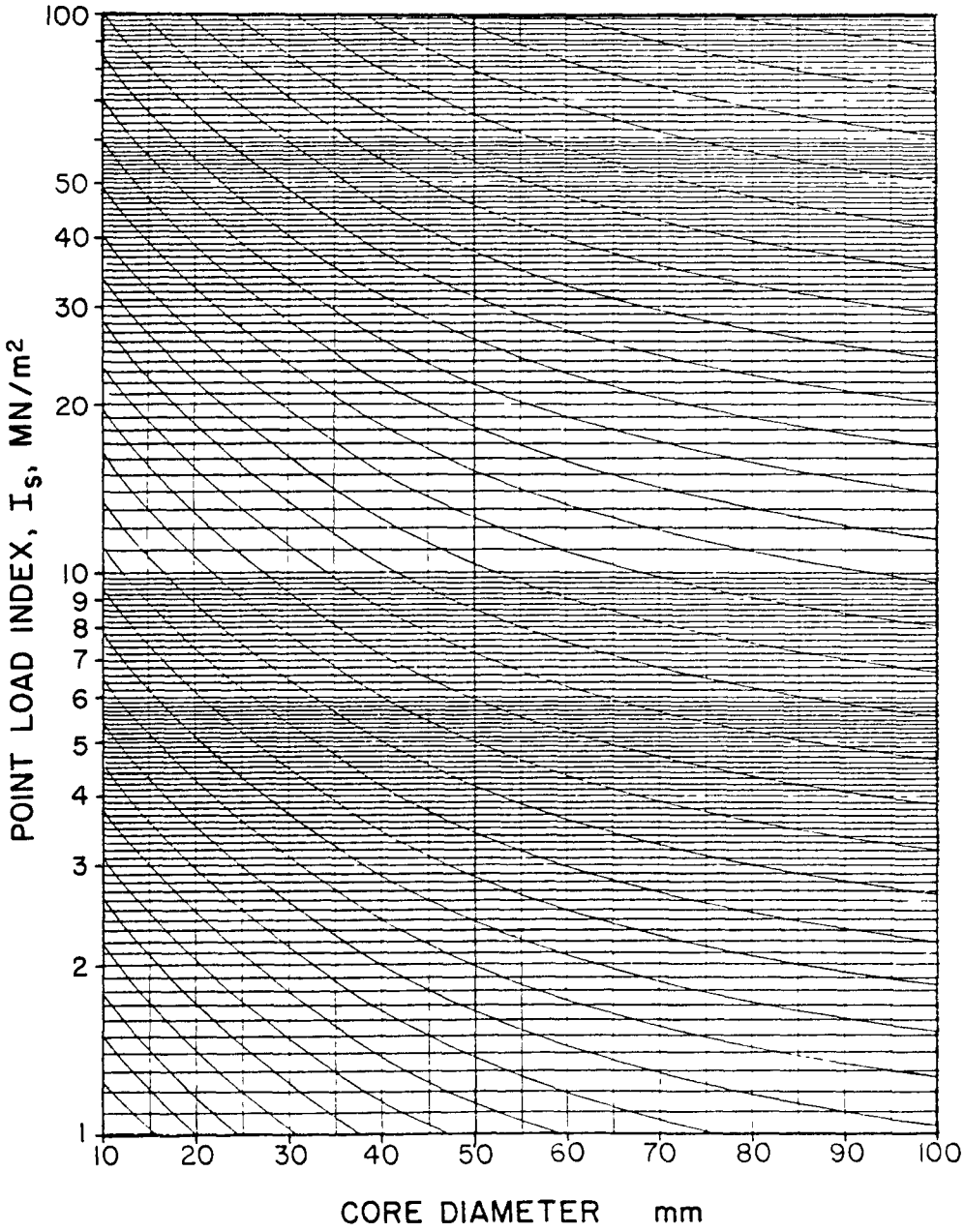

Figure 7. Modified point load index size correlation chart (from Hassani, Scoble, and Whittaker (3)).

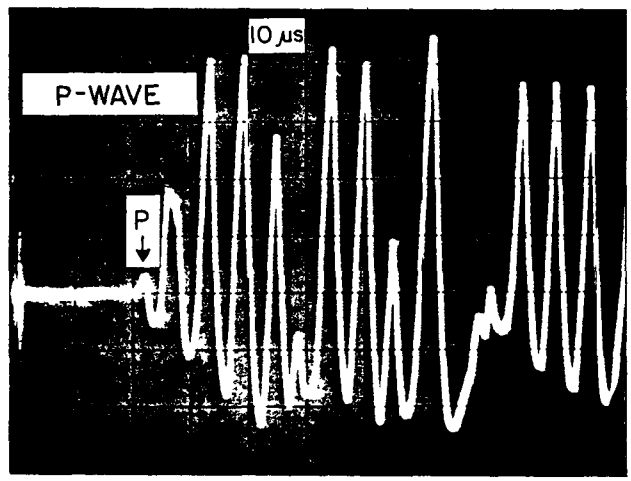

A.

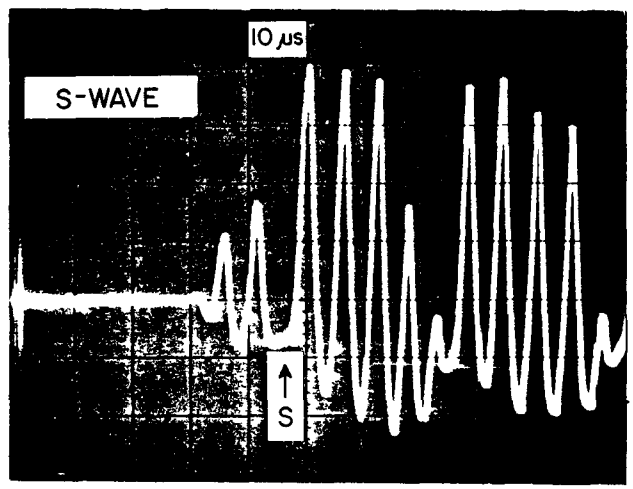

B.

Figure 8. Typical ultrasonic wave traces showing (A) P-wave test; (B) S-wave test. The P-wave arrival (P) and the S-wave arrival (S) are marked on the patterns. Sweep time = 10 µs/division.

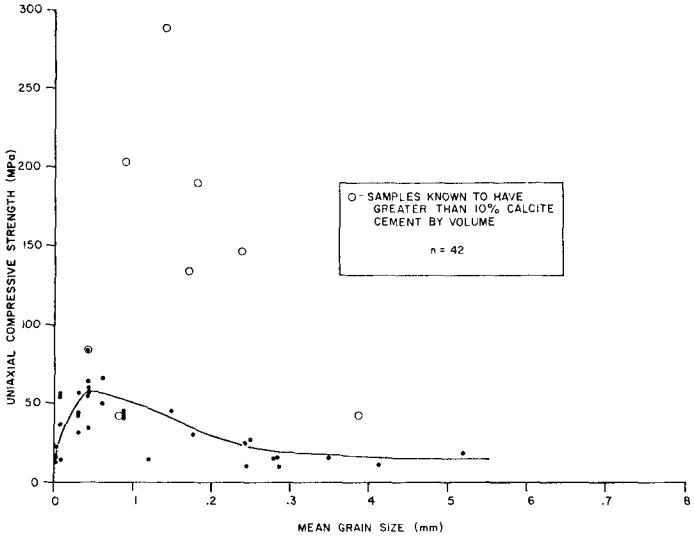

Figure 9. Uniaxial compressive strength vs. mean grain size for sedimentary rock samples from Rawlins, Wyoming UCG site. (note 1: curve visually fitted for non-calcite cemented samples only. Note 2: one sample with greater than 50 percent calcite has been omitted from this graph).

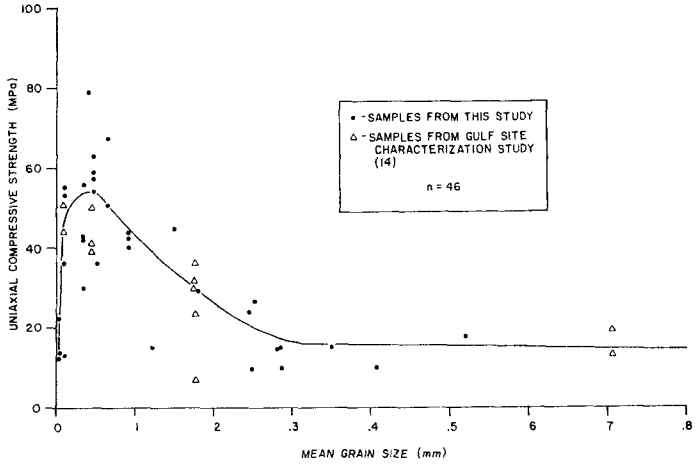

Figure 10. Uniaxial compressive strength vs. mean grain size for sedimentary rock samples from Rawlins UCG site, Wyoming. Sandstones with greater than 10 percent calcite cement shown on Figure 9 (note: curve visually fitted).

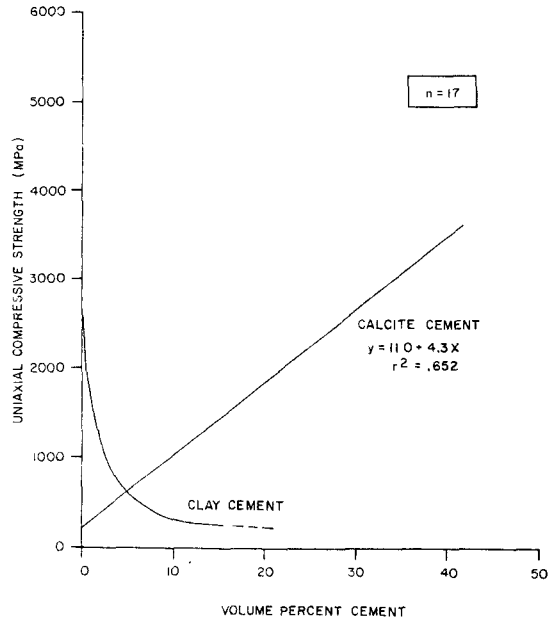

Figure 11. Uniaxial compressive strength vs. volume percent of calcite cement and clay-mineral cement for sandstones from the Rawlins, Wyoming UCG site. (Note: clay cement curve visually fitted).

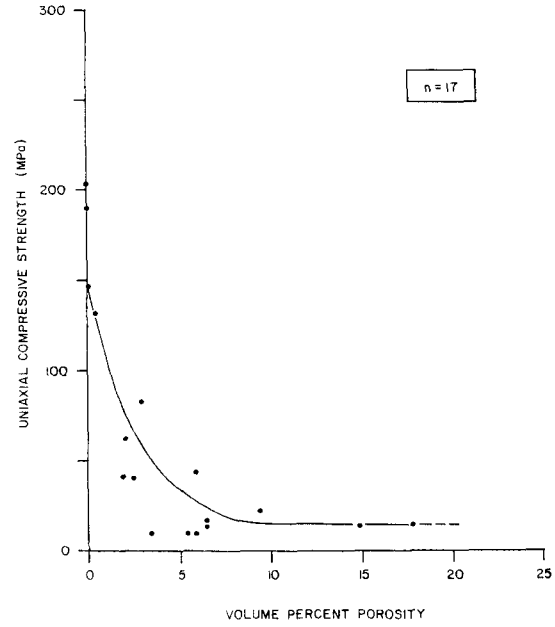

Figure 12. Uniaxial compressive strength vs. percent porosity for sandstones from the Rawlins, Wyoming UCG site (Note: curve visually fitted).

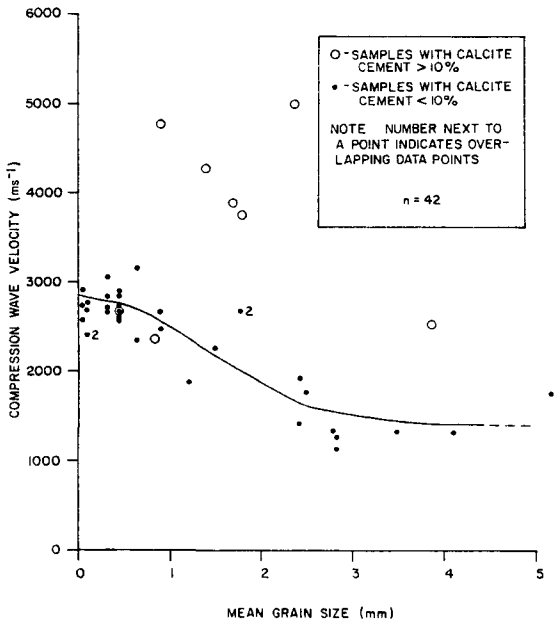

Figure 13. Compressional wave velocity vs. mean grain size for sedimentary rock samples from the Rawlins, Wyoming UCG site (Note: curve visually fitted).

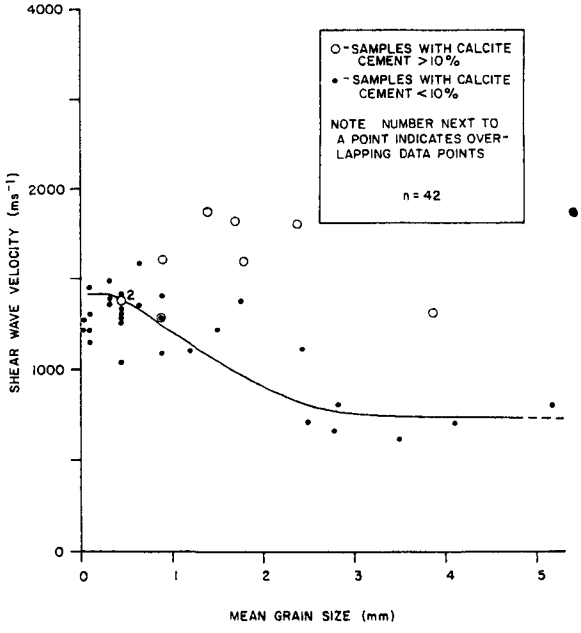

Figure 14. S-wave velocity vs. mean grain size for sedimentary rock samples from the Rawlins, Wyoming UCG site (Note: curve visually fitted).

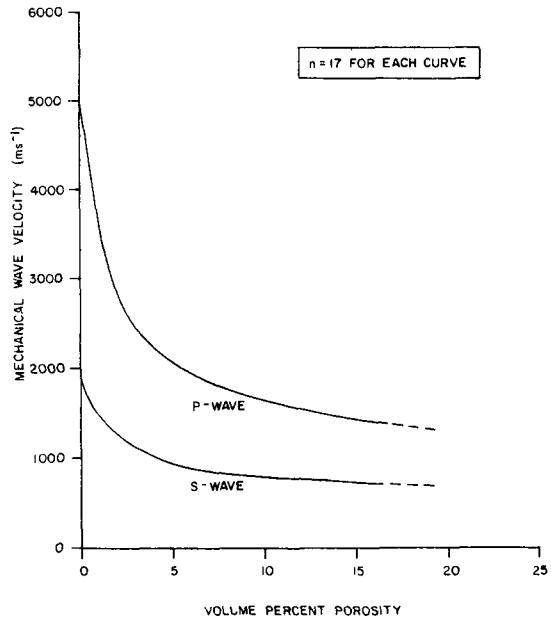

Figure 15. P- and S-wave velocities vs. percent porosity for sandstone samples from the Rawlins, Wyoming UCG site (Note: curves visually fitted).

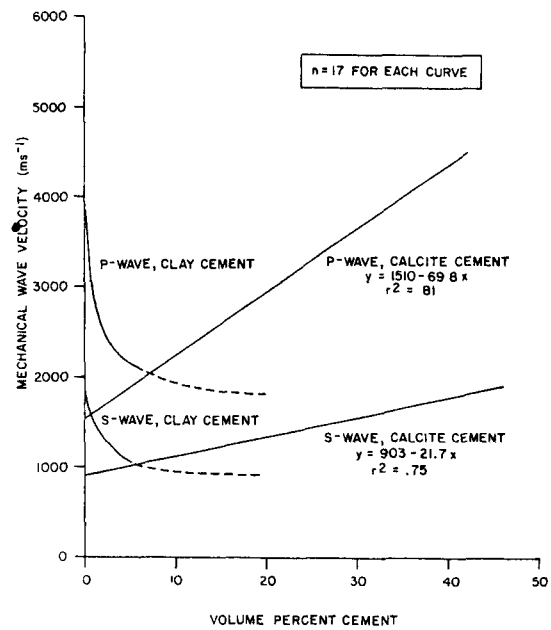

Figure 16. P-wave and S-wave velocities vs. two different cements in sandstones from the Rawlins, Wyoming UCG site (Note: clay cement curves visually fitted.)

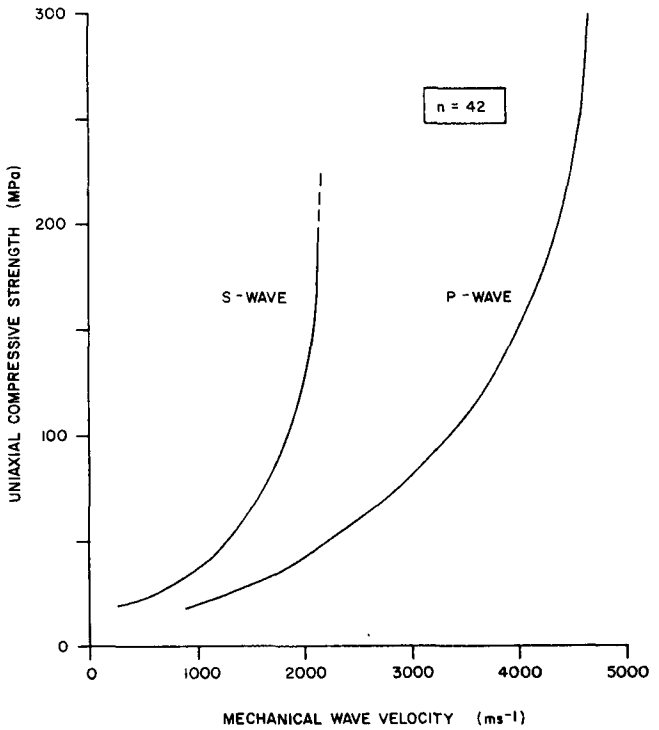

Figure 17. Uniaxial compressive strength vs.ultrasonic P- and S-wave velocities in all samples tested from the Rawlins, Wyoming UCG site (Note: curves visually fitted).

2.14 POTENTIAL FOR DEVELOPMENT OF UNDERGROUND COAL GASIFICATION IN THE BITUMINOUS COAL RESOURCE

by

J. W. Martin[1]
C. W. Byrer[2]
A. C. Brummert[3]
P. R. Wieber[4]

ABSTRACT

The Morgantown Energy Technology Center of the U.S. Department of Energy is conducting a research and development (R&D) project to develop the technology leading to the extraction of energy from bituminous coal by underground coal gasification. The process will produce a combustible gas of low-to-medium heating value which can be treated and cleaned for end use through methods similar to those utilized in surface gasification processes. This resource is located within regions of high population and high energy use centers with the infrastructure for potential commercialization currently in place. Three states -- Illinois, Kentucky, and Ohio -- have been recommended as having the best potential sites. Outcrop and deep seam field test sites will be chosen in one of these states using stringent site selection criteria. In relation to the potential sites, linking techniques and gasification concepts will be discussed. The need for supporting research involving laboratory studies and modeling activities will be related to known and potential field problems. A timetable and cost estimate for project development will be presented to integrate the various elements of the project.

[1] Project Manager, Underground Coal Gasification

[2] Project Manager, Coalbed Methane

[3] Petroleum Engineer, Extraction Projects Management Division

[4] Director, Extraction Projects Management Division
Morgantown Energy Technology Center
P.O. Box 880
Morgantown, WV 26505

INTRODUCTION

Background

The Morgantown Energy Technology Center is initiating R&D activities to assess the potential of using underground coal gasification to provide fuels for energy from eastern bituminous coal. The overall R&D goal is to establish a data base for recovery of energy from deep, thin seam, swelling, high-sulfur bituminous coals that are presently uneconomical to mine, clean, transport, and convert to usable energy by conventional methods.

During the last decade, many successful field tests and supporting research experiments have been conducted in the lower-ranked subbituminous and lignite coals of the western United States. The Soviet Union also has conducted extensive research in similar coals and, in addition, has operated small commercial installations. However, much less field-based R&D has been done with higher-ranked bituminous coals and, therefore, increased emphasis is being placed on research in this resource in an attempt to develop a data base comparable to that developed in the lower ranked resources.

An initial field test data base was established during 1979, when METC conducted a small-scale field test using the linked vertical well (LVW) concept

that had been applied successfully in the lower-ranked coals. This air-blown test was conducted near Pricetown, Wetzel County, West Virginia, in the 900-foot deep, 6-foot thick, highly swelling bituminous Pittsburgh coal seam. The results [1], which demonstrated that UCG in bituminous coals is technically feasible, revealed many of the problems and technical risks that must be investigated. In general, solutions to these problems are not available since the differences between the lower- and higher-ranked coals preclude the complete transfer of current UCG technology to the bituminous coal resource. Therefore, new and innovative linking and gasification concepts and methods must be investigated.

Issues of Concern

Accessing viable quantities of coal in an economically and environmentally acceptable manner must be considered thoroughly. A large area will be required for the commercial gasification of deep, thin, low permeability bituminous coal seams. This issue is important because such a large area may extend under rough terrain or regions of high population density.

Establishing and maintaining a permeable channel between process wells must be evaluated also. Of prime interest is the application of directional drilling techniques to establish long horizontal boreholes within the coal seam. By investigating various borehole channel length-to-diameter ratios, a viable channel may be established to permit continuous gasification with tar condensation in this swelling resource. Stabilizing the link through reverse combustion or electrolinking techniques may also be required.

Another issue concerns the production of a combustible gas of stable quality and quantity. The gas quality and/or quantity will change with coal reactivity, carbon conversion, injection pressure, flow rate, and oxygen/steam concentration. Cavity growth may require ramping of the injection flow rate to maintain propagation of the reaction front. Subsidence and local roof collapse will expose unheated material which will result in increased heat losses. These heat losses may shift equilibrium points to produce more carbon dioxide or cause an increase in condensation of the tar-laden gases, both of which may change gas quality adversely.

The delineation of UCG technology-related environmental effects, which includes the evaluation of air, ground and surface water, and land quality prior to, during, and subsequent to UCG, is a necessity. Air quality will be monitored closely throughout the tests. The product gas will be evaluated thoroughly to define environmental effects and to provide data to design gas treatment requirements for subsequent end users. Particular emphasis will be given to removal of the sulfur species and particulates. Surface and subsurface water quality will be monitored using samples collected from surface streams and hydrology wells. The effects on land quality will be monitored to define restoration requirements appropriate to state and Federal regulations.

Approach

In 1982, the results of a study performed by Williams Brothers Engineering Company [2] revealed UCG amenable bituminous coal resources as shown in Figure 1. Figure 1 also shows the projected target resources in the states of Illinois, Kentucky, and Ohio which were evaluated as having desirable potential test sites for continued R&D in bituminous coal.

The approach for the development of a bituminous coal UCG R&D data base revolves around establishing a cooperatively supported R&D program. The program will involve cooperation between the Federal Government, one state, and local governments, industry, and universities within the state.

The data base will be developed through a coordinated program consisting of (1) supporting research involving laboratory studies and modeling and (2) field tests involving open seam outcrop or highwall tests and deep seam tests. A strong initial Federal role is planned; however, as the technical risks are reduced, a decreasing Federal role with an increasing role by the state and industrial participants is anticipated.

SITE SELECTION FOR OUTCROP/ HIGHWALL TESTS

The site selection effort involves the initial evaluation of prospective sites for both the UCG outcrop/highwall and deep seam tests. Initial screening of these sites will include the assessment of geologic and geographic data available for each proposed site. Background information on surface and subsurface features will aid in determining those sites best suited for the bituminous UCG project.

The site selection criteria for the planned UCG outcrop/highwall test(s) include categories of amenable coal characteristics, geological constraints, and geographical considerations. Amenable coal characteristics for the test include the following: (1) a bituminous coal seam greater than 4 feet in thickness, (2) an adequate extent of coal at the proposed site, (3) a coal seam which is accessible by an outcrop or a highwall, (4) an overburden of at least 50 feet and no more than 125 feet, and (5) the preference of competent roof and floor rock.

The geological constraints include (1) the possibility of having the outcrop/highwall test site near the projected deep seam test site; (2) very little, if any, faulting or fracturing within the test area; and (3) no major aquifers in or above the target coal seam.

The geographical considerations include (1) total acreage of an outcrop/highwall site is approximately 20 acres; (2) site location should be in a low population area; (3) no known unplugged oil or gas wells in area; and (4) no known surface buildings, pipelines, or other structures nearby.

SITE SELECTION FOR DEEP SEAM TEST(S)

The criteria for the UCG deep bituminous coal seam site(s) include these factors: (1) a coal seam greater than 4 feet in thickness, (2) located within a commercially viable quantity of coal, (3) a target coal seam at least 300 feet below the water table, (4) a competent roof and floor structure, and (5) initial coal properties amenable to UCG testing.

The geological constraints for the deep seam test(s) may include proximity to the outcrop/highwall test, no major faults in the test area, and a preference for stratigraphic uniformity and continuity.

Geographical considerations include (1) a site area of 50-60 acres; (2) an adequate distance from surface features and activities (this would include a distance of 1 mile from populated areas, major rivers, and lakes and 1/4 mile from major highways and railroads); (3) very little, if any, oil and gas development; (4) an absence of underground mining; and (5) an industrial infrastructure in the area containing consuming industries, supporting industries, and a transportation network.

SITE CHARACTERIZATION

Once proposed sites have been selected for both the outcrop/high wall and deep seam tests, an in-depth site characterization study, shown in Figure 2, is to be performed on each site. The evaluation of both sites will include surface mapping, subsurface mapping, and a hydrologic assessment of the local area.

The surface mapping of a test site will include the topography of the site, surface hydrology, soil formation, surface lineaments, oil/gas wells, active/ abandoned mines, highways, pipelines, buildings/dwellings, and other significant features which are located in the local area. Subsurface mapping would include a stratigraphic cross section of all major rock units, a hydrogeologic section of all known aquifers, an isopach (thickness) map of coal, and an isopach of the floor and roof rock units. The hydrology assessment includes the type and location of aquifers, various aquifer productivity results, an assessment of groundwater quality, and regional/local groundwater flow direction.

OPEN SEAM OUTCROP/HIGHWALL TEST(S)

The objectives of the various UCG tests to be performed at the outcrop/ high wall site are to establish an initial field-scale data base by conducting

a series of well-instrumented, low-pressure experiments. The data base and test data correlations will be enhanced by excavating, analyzing, and mapping individual test zones.

Research needs relative to the in situ gasification of thin, swelling, bituminous coals are centered around linking concepts and techniques and, also, the actual gasification process as illustrated in Figure 3. Specific borehole linking experiments will be focused upon ignition, channel stabilization, injection flow velocities, diameter-to-length ratios, swelling effects, tar condensation, and innovative geometries.

Electrolinking experiments will be conducted to assess electrode configuration, power requirements, linking rate, link path geometry, and channel permeability.

Gasification experiments will focus on swelling of the coal, tar condensation, system pressures, flow rates, heat losses, roof subsidence, coal extraction rate, coal conversion efficiency, sweep width, coal seam residue, product gas composition, enhanced oxygen injection, and innovative geometries.

DEEP SEAM TEST(S)

The purpose of the deep seam test(s) is to investigate various UCG concept designs at depth. Specific deep seam objectives include tests at pressure with emphasis on borehole and electrocarbonization linkage techniques. This will subsequently lead to the design, construction, and operation of a proof-of-concept test in a thin bituminous coal seam. It is anticipated that, upon completion, the data base will be used to evaluate the potential for future operations at or near the UCG test site facility.

The deep coal tests will be designed to evaluate high potential concepts as determined during the highwall experiments. Concepts under consideration, for example, include single-borehole, multiple-borehole such as "REVERSE FLOW," as shown in Figure 4, "CO-FLOW," electrolinking-carbonization, and hydrofracturing. Some of the problems to be investigated in the deep coal test include the control of directional drilling, borehole stability, sweep efficiency, heat loss effects, and electrolinking control.

The various stages of the testing program include site characterization, test plan development incorporating previous test results, site construction, environmental monitoring (air quality, groundwater/surface quality, subsidence, by-product disposal, socioeconomic factors, test control, drilling waste/mud disposal), test operations, post-burn coring and core analyses, evaluation of deep UCG testing results, and test site restoration.

SUPPORTING RESEARCH

Laboratory Studies

Laboratory process parameter studies include the investigation of process parameters in electrolinking/carbonization, open borehole linking, and gasification. Process parameters to be investigated in electrolinking/carbonization are power requirements during the electrolinking process and power requirements after the electrolinking process, during carbonization. Process parameters to be investigated in open borehole linking are sweep efficiency and drilling accuracy as a function of cleat direction and borehole diameter-to-length ratio. Process parameters to be investigated in gasification are ignition temperature and injected oxygen concentrations, flow rates, and pressures.

Laboratory studies may also include the investigation of innovative concepts. These concepts include gasification with unsteady injection flow rates to expose unburned coal, multiple borehole, and formation pretreatment with catalysts.

Modeling Studies

Initially, modeling efforts will revolve around the evaluation and, where applicable, the modification of existing models. Six models [3] have been obtained. Five of the six models were originally developed for subbituminous coal and may need to be modified. The sixth model was developed for bituminous coals. The model types include equilibrium models and steady- and unsteady-state models ranging from one to three dimensions.

Modeling studies will include model development of innovative concepts. These concepts include single borehole linking; multiple borehole linking, such as "REVERSE FLOW" and "CO-FLOW;" electrolinking; and unsteady flow gasification.

Modeling studies will also include the provision of economic models. The economic models will contain the costs of field development, process operation, gas surface treatment, end use retrofitting, and site restoration for the various linking and gasification concepts.

CONCLUSION

The Morgantown Energy Technology Center has initiated activities to develop a comprehensive data base for UCG in the deep, thin-seamed bituminous coal resource. The data base will be derived from field testing which will include both deep seam and highwall experiments and supporting research which includes laboratory experiments and modeling/data correlation studies.

Project development has been emphasized in the states of Ohio, Illinois, and Kentucky as a result of the WBEC study and responses to a request for expressions of interest which was widely advertised. All three states indicated high interest in cooperatively supporting this proposed project. In addition, several industrial and private concerns also expressed interest.

Currently, the locations of specific potential test sites in each state are being ascertained from existing state geological survey data. Also, the surface and mineral rights owners of the potential sites are being contacted to determine interest in cooperatively supporting the project. It is DOE's intent to establish an agreement with one state to conduct field testing at one site (or two sites if the deep seam location is different from the outcrop). The agreement, in all probability, will include the surface and mineral rights owner and, perhaps, a potential end user for the gas produced during the larger, deeper seam tests.

The projected schedule and cost for this proposed project is shown in Figure 5. Both the schedule and cost are premised on R&D activities which make full utilization of UCG technology already developed in the lower ranked subbituminous coal resource, result in no or minimal major technical obstacles to the research, assumes appropriate cooperative support from the state and industry, and anticipates adequate commitment and funding from the Federal Government.

It should be emphasized that this proposed project is oriented toward research and development activities. The proposed schedule and cost of each activity represent project goals. Fulfillment of these schedule and cost goals will not be made at the risk of project research and development quality.

ACKNOWLEDGEMENT

The authors wish to thank Mr. Tom Addis for his engineering graphic designs.

REFERENCES

[1] Liberatore, A. J. and M. W. Wilson, "Field Scale Experiment in Underground Gasification of Coal at Pricetown, WV," DOE/METC-83-49 (DE83011052), 201 pp., April 1983.

[2] Williams Brothers Engineering Company, "Assessment of Underground Coal Gasification in Bituminous Coals," DOE/METC (DE-AC05-80MC 14584).

[3] Kunselman, L. V., D. W. Fausett, and C. G. Mones, "A Comparison of Forward Combustion Gasification Models," Proceedings of the Eighth Underground Coal Conversion Symposium, Keystone, CO, 335, August 15-19, 1982.

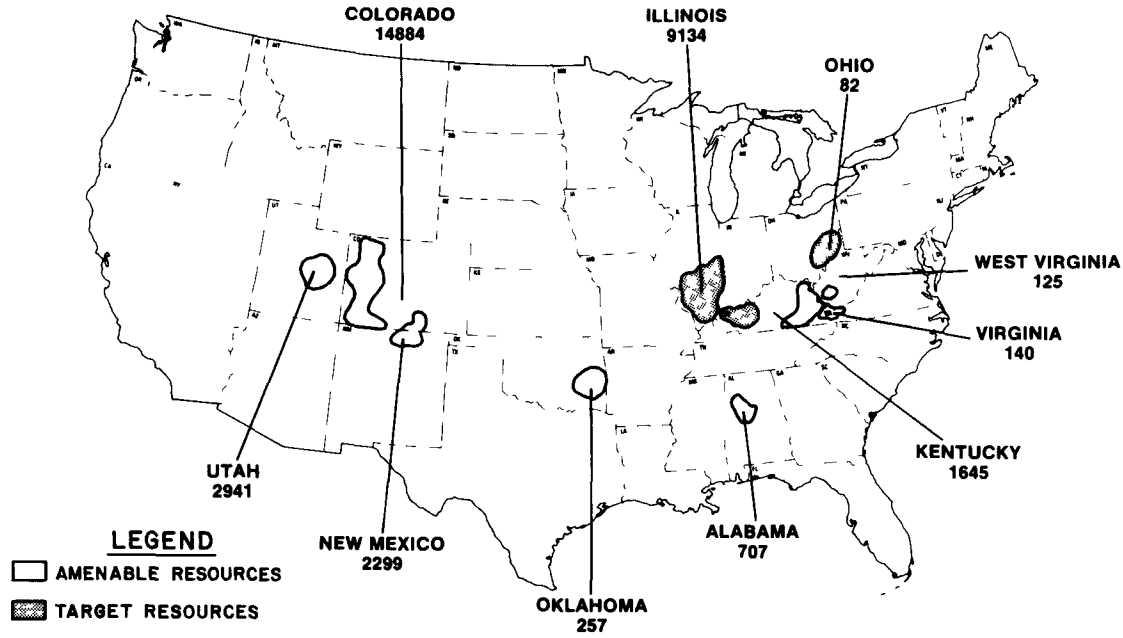

Figure 1. UCG amenable bituminous coal resources (Millions of short tons).

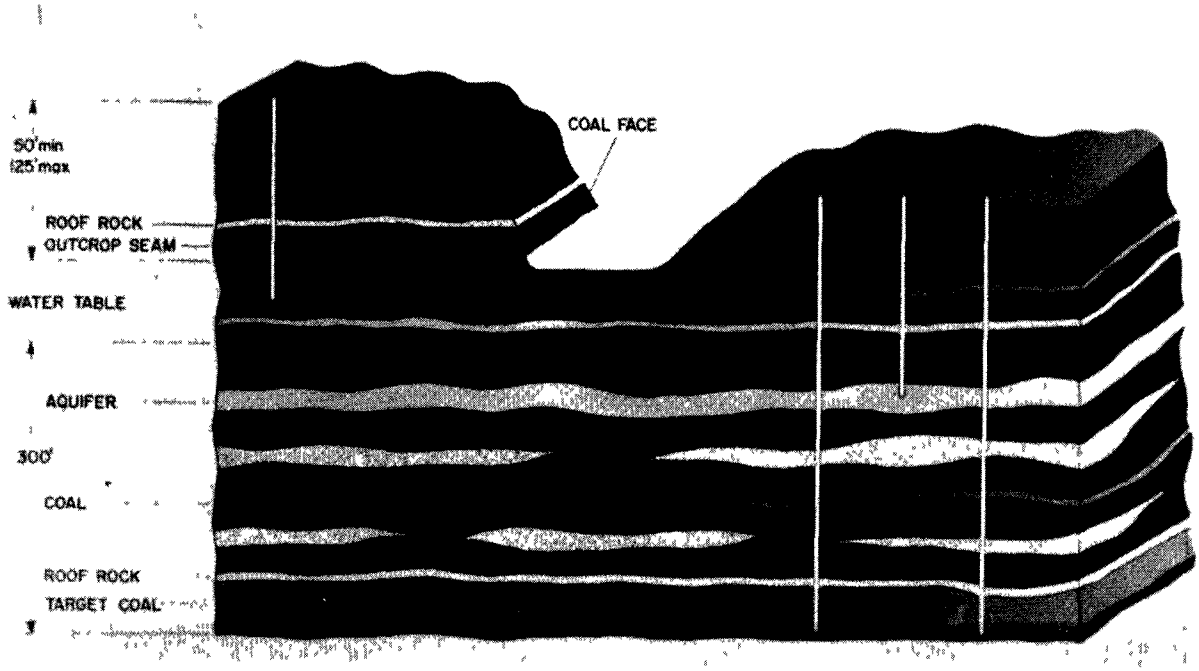

Figure 2. Test site characterization.

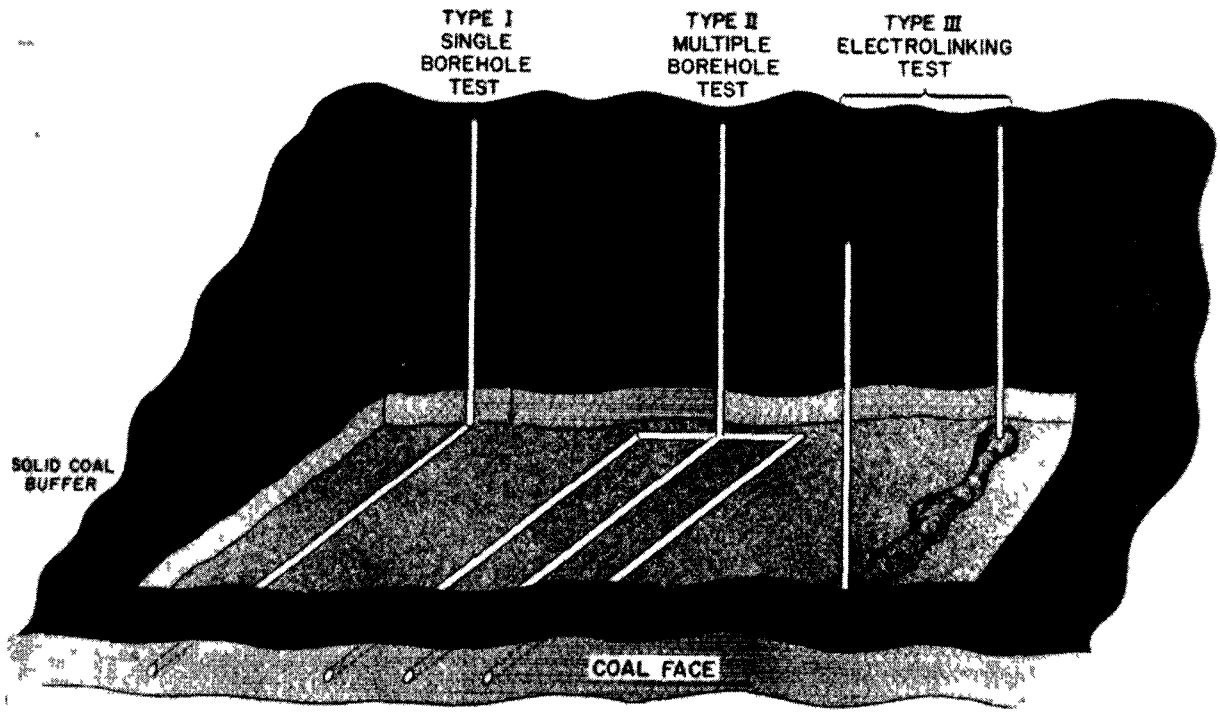

Figure 3. Proposed open seam highwall tests.

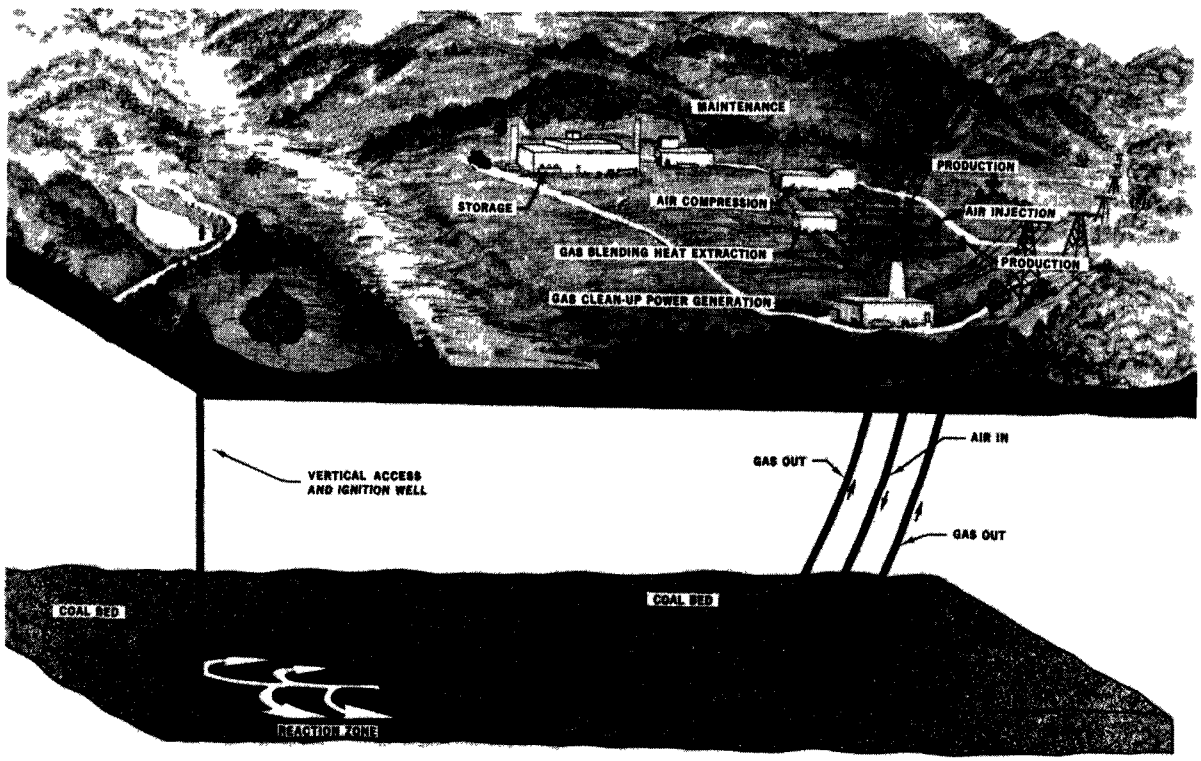

Figure 4. Reverse flow stream gasification concept.

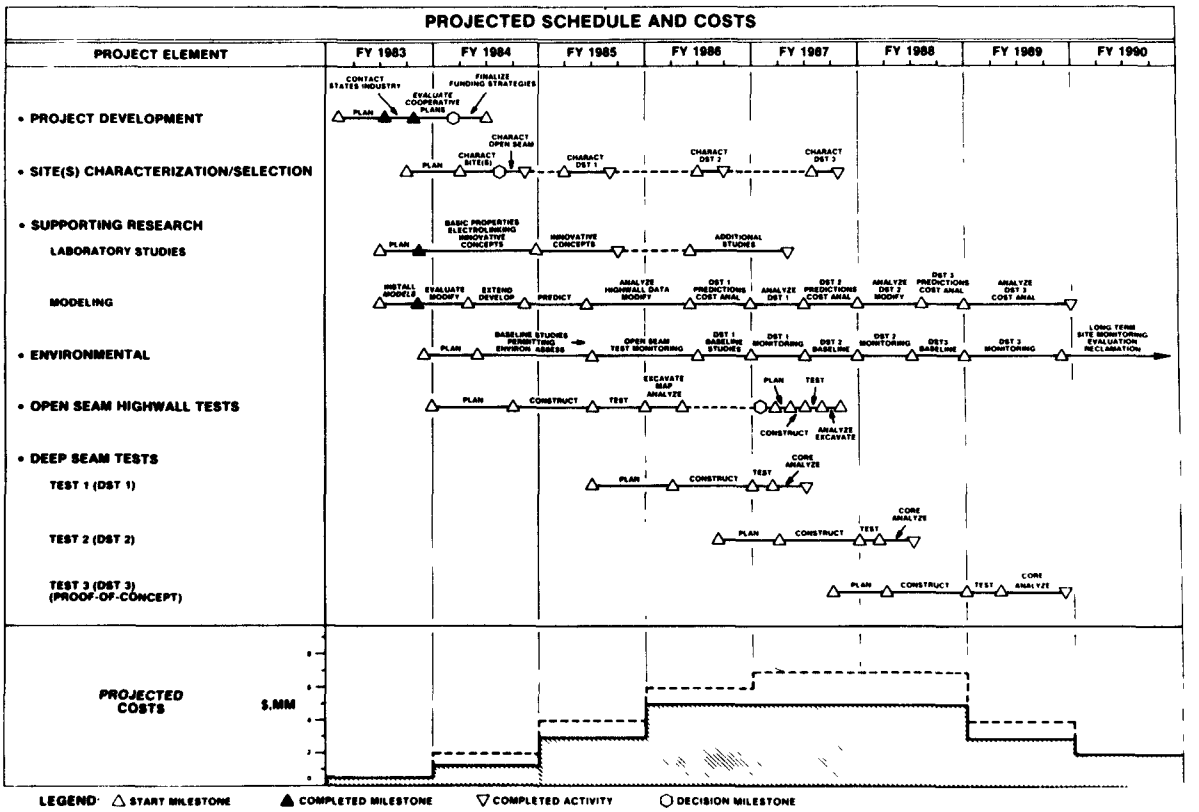

Figure 5. Projected schedule and costs.

2.15 ELECTROENHANCED UNDERGROUND COAL GASIFICATION

by

Dr. Erich Sarapuu 1/

ABSTRACT

Experimental field work has demonstrated effective techniques for underground electrogasification of coal. Numerous considerations are involved, such as electrode design and placement, the initial electrolinking step, electrocarbonization, and supporting reactions involving controlled amounts of air and oxygen, steam, and other selected materials. Geological setting, coal properties, and surrounding deposits must be considered in deriving techniques applicable to any given area.

Original field work in the United States was sponsored by Sinclair Coal Company, the University of Missouri, Alabama Power Company, and the Bureau of Mines. Continuous operation was achieved and a gas of sufficient heating value was produced for use in surface power generation. These findings are considered together with results of other related work in Belgium, England, Estonia, Germany, Italy, Russia, Sweden, and the United States. This method of deriving energy is generally applicable to a wide variety of coal deposits, as well as other carbonaceous deposits. Advantages, include the relatively low initial investment, relatively little excavating or drilling, and applicability to otherwise inaccessable deposits. Economical industrial applications can be foreseen, especially in the area of industrial fuels and power generation. Conclusions and recommendations are provided by a principle investigator who contributed fundamental concepts and employed them successfully in the field work on underground coal electrogasification at Gorgas, Alabama and Hume, Missouri.

1/ Electrofrac Corporation/ 3100 Broadway, Kansas City, MO 64111

INTRODUCTION

The United States largely owes its leading position as a world power to its wealth of natural resources. The overall combination of liquid, gaseous and solid hydrocarbons rank high among the raw materials which have contributed to this pre-eminent standing of the nation. Coal is, in turn, a very large component of the overall hydrocarbon resource, and is available in many of the conterminous United States, as is illustrated in Figure 1, and Alaska. Total coal reserves exceed 6,000 billion tons, which is ample to satisfy all of our energy needs for many hundreds of years. It is a truly abundant energy resource. However, coal remains under utilized even though one of the present day problems facing our economy is the serious shortage which is progressively developing in the supply of readily available liquid and gaseous hydrocarbons. Today, the depletion of available reserves of liquid and gaseous hydrocarbons has become pronouncedly apparent.

The energy problem can be overcome by increased use of coal for power generation and various other industrial uses. But that approach is prevented by a combination of limited accessibility to conventional mining methods and a variety of legislated restraints to both mining and quality, particularly sulfur content.

Underground coal gasification is another solution to the energy problem. It is especially attractive as a way of overcoming the conventional limitations and contraints, because it is a technology that can increase the production of gaseous energy from domestic hydrocarbon resources. Some consideration has been given to making a substitute natural pipeline gas from coal. However, an easier and more economical approach

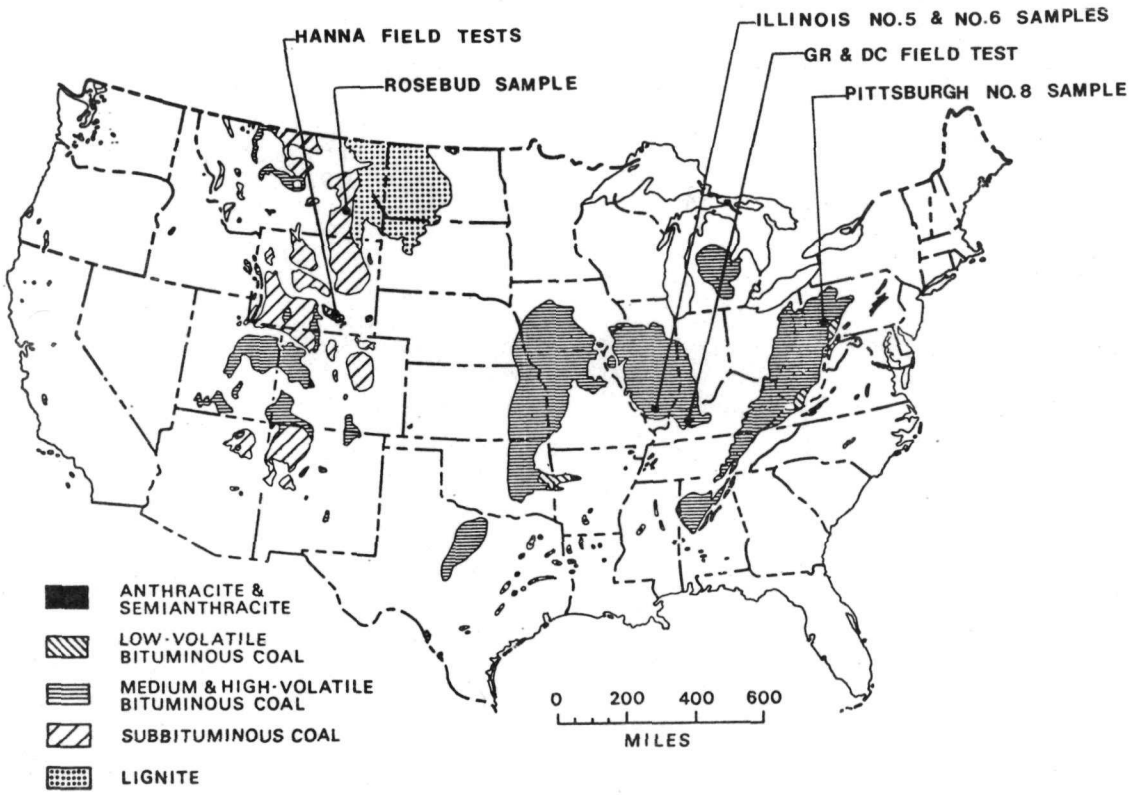

FIGURE 1 - COAL FIELDS OF THE CONTERMINOUS UNITED STATES

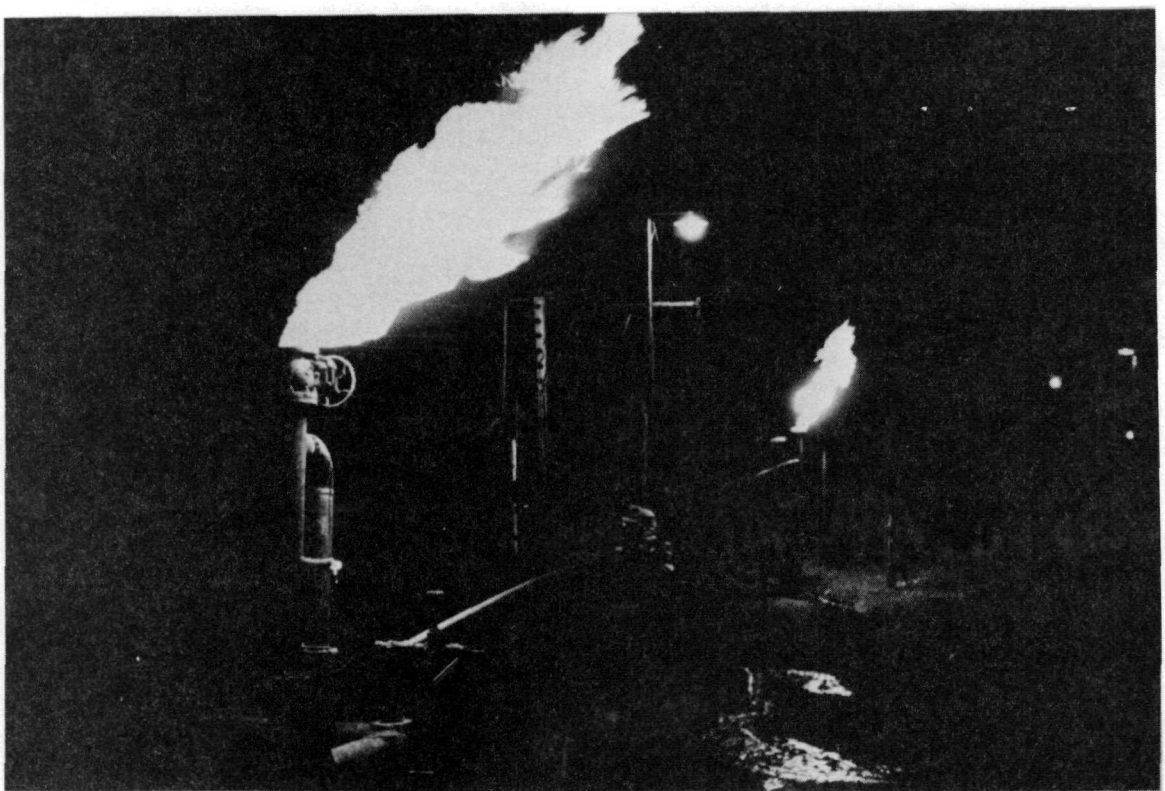

Figure 2. Electrolinking of coal at Gorgas, Alabama

is to produce gas of medium to low heating value that can well serve various industrial applications such as on-site power generation, industrial plant fuel gas, hydrocarbon synthesis, and by product carbon dioxide for enhanced oil recovery.

Thus, the principal reason for the extensive interest today in underground coal gasification program are:

- it offers an environmentally clean way to utilize coal
- it expands the range of coal deposits which can be exploited
- capital and operating costs are lower than alternative methods of gasification
- the basic technology exists

Alternative techniques for underground coal gasification have been reported at the Annual Underground Coal Gasification Symposium, and other trade media. Some of the work has been carried to advanced stages of demonstration in recent years. Primary attention has focused on various mechanical means for creating an underground path for partial combustion of the coal so as to form usable gas. But the alternative of using electrical energy has not yet received the full attention it deserves, despite significant potential advantages which have as yet undergone only a first generation of field demonstration.

HISTORICAL DEVELOPMENT

Underground gasification of coal was first proposed in 1868 by Sir William Siemens, an Englishman. In 1909 an American, A.O. Betts, obtained a British patent covering a method of gasifying coal underground.

Between the first and Second World Wars, Russia appeared to be the only nation sufficiently interested in the possibilities of underground gasification to carry out research and development. Since the close of World War II, trials have been conducted in Britain, Belgium, Italy, French Morocco, United States, Poland and Czechoslovakia.

In 1940 the Russians started experimental work in Brown Coal at Tula in the Moscow Basin. The higher permeability of the Brown Coal allowed them to develop pneumatic linkages between vertical holes. By 1957 there were around 500 scientists, engineers and technologists employed on UCG in the various agencies and a considerable program of future work was planned. Unfortunately the worldwide interest in UCG was concentrated in Russia and they shortly ceased even the publication of Podzemnoi Gazificatsii Uglei which had been useful source of information. It seems that they have been operating three different underground gasification plants since that time.

The United States has carried on extensive research and development in underground gasification of coal since 1946. This research was conducted at two centers: Hume, Missouri by Sinclair Coal Company and the University of Missouri; and, Gorgas, Alabama by Alabama Power Company and the U.S. Bureau of Mines. Dr. Erich Sarapuu, the author of this paper, conceived and initiated that original work on Electroenhanced Underground Coal Gasification more than three decades ago.

Two techniques known as "electrolinking" and "electrocarbonization" were developed and demonstrated at that time. The first of these terms, electrolinking has become popular, its use has tended to retard a full understanding of the overall concept. Thus, the more general term "Electroenhanced Underground Coal Gasification" should be applied to the overall process of producing gas from coal underground. Actually, several different concepts are applicable to the overall process in varying degrees, depending on the specific applications. They are defined as follows:

- Electrolinking. It is necessary to provide a basic link between the electrodes within the raw coal stratum to begin electrogasification of the coal. Electrical coking starts at the electrodes and advances through the formation forming a continuous carbon conductive zone between the electrodes, which becomes the final linkage. Once a conductive zone is

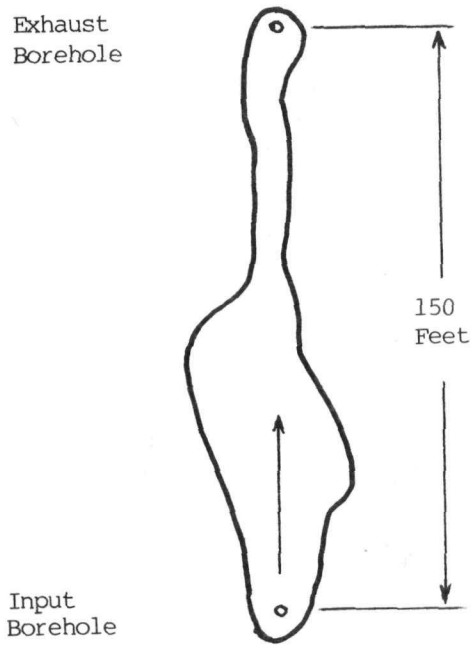

Figure 3. Sketch of gasified area at Gorgas, Alabama

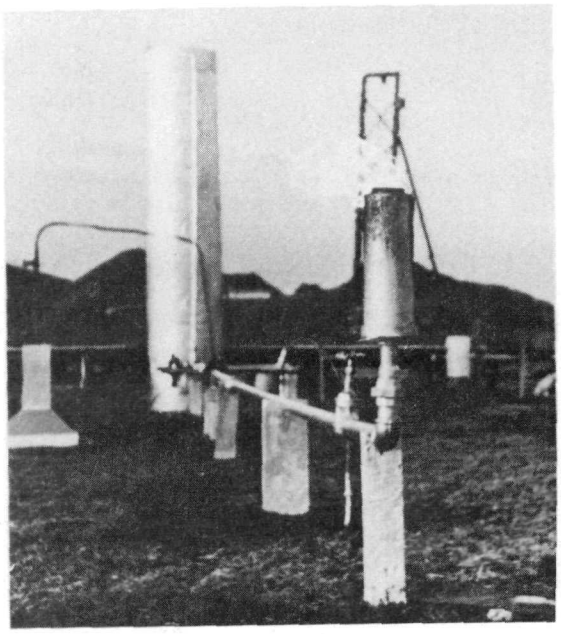

Figure 4. Electrogasification of coal at Hume, Missouri

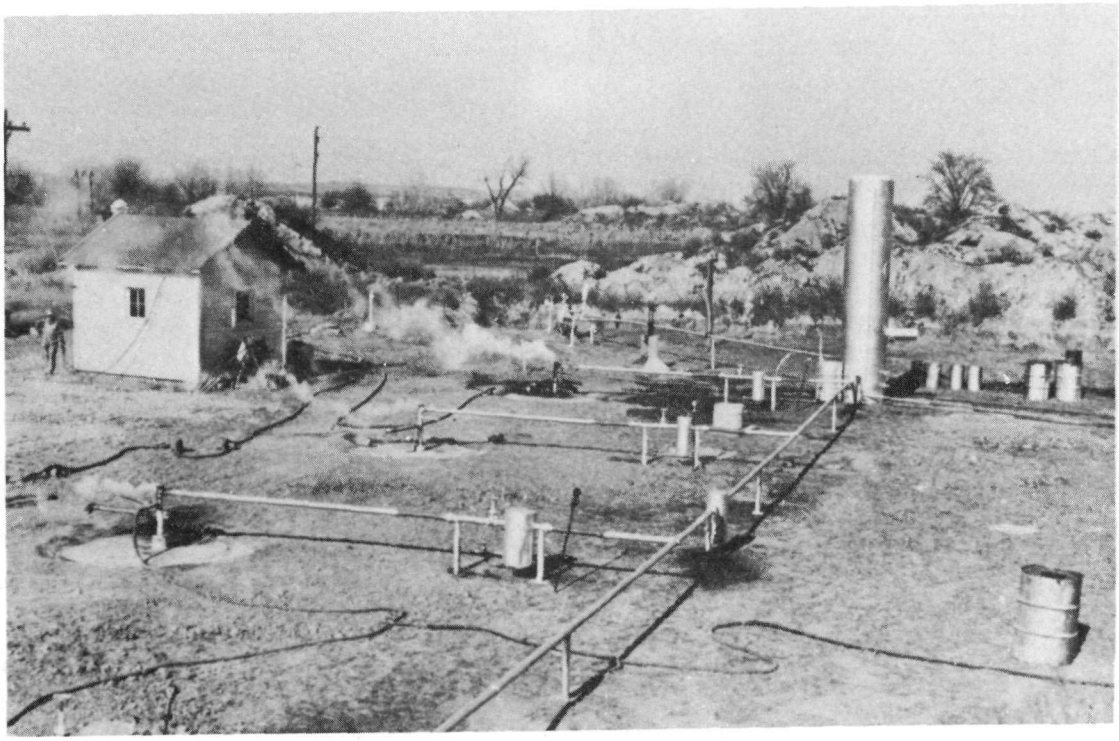

Figure 5. Electrocarbonization and gasification plant at Hume, Missouri

completed, it will allow passage of sufficient current to begin carbonization of nearby coal.

- Electrocarbonization. This term is used to designate a relatively long-duration electrical coking of coal before starting a gasification cycle. As carbonization proceeds, it may be accompanied by electrofracing, due to resulting temperatures and pressures within the formation. When properly controlled, electrofracing enhances overall permeability.

- Electrogasification. This phase of operation entails simulataneous or cyclic electrical heating and injection of reactants, typically air and/or steam in the fuel medium. The electrogasification procedure will yield a gaseous mixture from subsurface fuel deposit that is similar to enriched producer gas or water gas.

- Electropyrolysis of oil or tar within the coal deposit is another option to produce high BTU gas by electrical energy and gasification reactions.

- Electroenhanced Underground Coal Gasification. The application of one or more of the above processes as required to achieve best results for any given application.

The use of electric power for carbonization or gas generation is more economical at localities where low cost electric power is available, such as off-peak power. For that reason, processes using electricity were developed in Norway and Italy where hydro-electric power was available at a low cost to the gas manufacturer. It is often desirable to utilize electric power plant equipment during off-peak periods, and in such cases the use of electric power for gas production may well be considered.

Renewed interest of underground gasification of coal in this country started after 1973. Extensive programs have been carried out such as:

- DOE project in Wyoming

- The MERC program for in situ gasification of eastern coal

- Underground gasification of steeply dipping coal beds. This project was spearheaded by the Gulf Oil Research and Development Company

- Developments by Texas A & M University

- Tennessee Colony in situ gasification project

These studies have been conducted or sponsored largely by the Energy Research and Development Administration, followed by today's Department of Energy. Reports on findings are available in government publications which have been summarized in the various proceedings of the annual underground coal conversion symposia.

THEORETICAL CONSIDERATIONS

Coal is an aggregate consisting of hydrocarbons and minerals of various compositions and electrical conductivity. When electrodes are placed into the coal seam and electric field is applied, a relatively large electric current may flow through the coal stratum if the electric field intensity exceeds a certain threshold value. The electrically induced ionization (coking) will start acting as a partial conductor to transfer the field concentration at the electrodes to the area between vertical wells until a continuous coke layer is formed between electrodes.

The electrical conductivity of earth material has been the subject of geophysical measurements and investigation for many years. In accord with the physical concepts of the electrical conductivity in the earth, each of the following should be considered: (a) Electrolytic conductivity; (b) Electronic conductivity and (c) Dielectric conductivity. The pertinent factors affecting the ground conductivity are (a) Type of soil - petrographic composition; (b) Definite anisotrophism of flow of electric current; (c) Chemical impurities in electrolyte; (d) Temperature; (e) Chemical composition of rock-forming minerals.

In order to describe the different types of earth heating problems by ground electrodes, an attempt is made to analyze the flow of electric current in the earth. For instance, in a conductor with fixed cross-sectional area and resistivity, the current flow is normal to the imaginary cross-sectional area between two potentials. However, in the earth the current flow is distributed through a cross section of practically infinite dimensions and continual change of resistance in ground circuit.

Therefore, the current density is highest at the electrode and diminishes as the square of radial distance from the electrode. When current flows from an electrode to the ground, heat is generated in the immediate surrounding of the ground electrode. The temperature limitation of the heating of a ground electrode is given as the boiling point of the electrolyte. When the temperature exceeds the boiling point of water, the electric ground is disrupted. In underground electrocarbonization however, temperatures far above the boiling point of water are required. The coking and decomposing of hydrocarbons have been accomplished in the temperature range of 1000^{o} F. When dealing with hydrocarbons, the temperature limit (100^{o} C) of heating geological strata by electric energy has been expanded by replacing electrolytic conductivity of moisture in coal with the conductivity of hot coke which has been formed between electrode wells.

FIELD WORK

Early laboratory and field experimentation of coal was made by using bituminous coal of a Melbourn seam in Hume, Missouri. The primary purpose of this study was to ascertain basic data and secure fundamental knowledge that would later guide the development of large scale underground gasification plants. It was deemed particularly to determine the following controlling factors:

- The magnitude of electric resistivity of coal. The laboratory measurements showed that the electrical resistivity of coal was about 6 orders of magnitude higher than under its original conditions in situ. The increase of the resistivity was due to the loss of moisture of coal samples.
- It was demonstrated that the coal could be electrolinked in the laboratory and the current density to initiate electrolinking was about 0.10 to 0.15 amps/cm^2 of electrode surface ore.

The first field study of underground electrocarbonization was carried out at the Tiger Mine property of the Sinclair Coal Company where a coal seam is about 20 feet below the surface. Successful electrolinking and electrocarbonization of the coal seam was obtained with the electrode spacing of 60 feet. For instance, in an experimental program, the resistance decreased from an initial 11 ohms to approximately 7 ohms in a period of 12 hours; at the end of which time, electrolinking was accomplished and the resistance dropped very rapidly to less than 0.4 ohms. Figure 4 shows the field test facilities of underground electrocarbonization of coal in Hume, Missouri.

Following is the composition of a sample of coke gas produced during the electrocarbonization of bituminous coal at Hume, Missouri:

CO_2	3.8%
Illuminants	4.0%
0_2	0.3%
CO	12.0%
H_2	54.5%
CH_4	24.1%
N_2	1.3%

Heating value of this sample was 525 Btu/cu. ft. A laboratory electrocarbonization experiment using Texas lignite resulted in production of 69 percent of hydrogen in pyrolysis gas. This data illustrates the range of possibilities for gas composition which will respond to operating conditions when proper control is maintained.

The electrolinking data secured from Hume, Missouri and Gorgas, Alabama experimentation have been plotted comparitively in Figure 6. Graphs No. 1 and No. 2 in this illustration are of data taken at Hume and they represent results of

tests where the electrodes were spaced respectively at 20 feet and 60 feet. Graphs No. 3, 4 and 5 are from data obtained at Gorgas where in each case the electrodes were about 150 feet apart. It is felt that No. 3, which shows that electrolinking was accomplished in about 21 hours or at a rate of approximately 7 feet per hour, is the more typical expression of what might be expected from a large-scale operation. Figure 2 illustrates the production of coke gas in Gorgas after the electrolinking was completed.

Efforts were made at Gorgas to determine the size and shape of the underground gasified area which resulted from several months electrocarbonization in the field research program. Figure 3 illustrates the extent of the gasified area as defined by electrical measurements tracing the distortion of equipotential lines along the high electrical conductivity zone of the gasification channel.

Inasmuch as the field tests at Hume had been made in shallow coal, it was possible to expose the gasified area by stripping the cover with a dragline and thus ascertain the pattern of the affected zone in situ. The gasification by air was carried out for the sole purpose of studying the behavior of residual matter after the gasification of coke zone. It was found that the gasification channel was completely filled with porous fused clinker.

The need for process control in underground gasification can be appreciated when analyzing the operating differences between gasification in a retort and in situ. This control is obtained by the electrogasification process.

The gasification of coal in surface retort proceeds under controlled physical, thermal and chemical conditions. All factors which affect the results of gasification can be readily designed and selected for the operational requirements. In general, the conditions which regulate the outcome of gasification are:

- physical conditions of the fuel bed
- composition of coal
- height of the fuel bed
- heat losses through the wall of the retort
- tortuosity of gasification channels
- volume of gasification reagent and its composition
- pressure drop in the retort
- reaction temperature and pressure

A radical change of any of these factors would greatly degrade the performance of a commercial gasification retort. However, several of these conditions change continually in processing of coal in situ, and reduce the gasification efficiency unless corrective measures and techniques are developed. This is a joint responsibility of the process developer and the field operator.

The actual performance of an underground gasification unit is followed by remote control methods. The control of chemical reactions by electrical energy is one way of improving the outcome of the underground gasification of coal.

Some investigators have encountered difficulty in individual trials of electrolinking. However, a very extensive series of investigators in England and Russia have verified the original work by this author and his collaborators. The Russians have also conducted electrogasification on a large scale, but we cannot yet benefit from this because they stopped publishing results after 1959.

SUBSEQUENT DEVELOPMENTS

Knowledge gained in field trials and related work has been applied more generally to underground production of synthetic fuels mineral deposits containing hydrocarbons such as coal, tar sands, oil shale, and heavy oil, or residual unrecoverable oil remaining after enhanced oil recovery efforts have been exhausted. This generalized process is illustrated in Figure 7.

Versatile power generation equipment has been developed and has been placed in use in related applications such as electroenhanced oil recovery and electrical

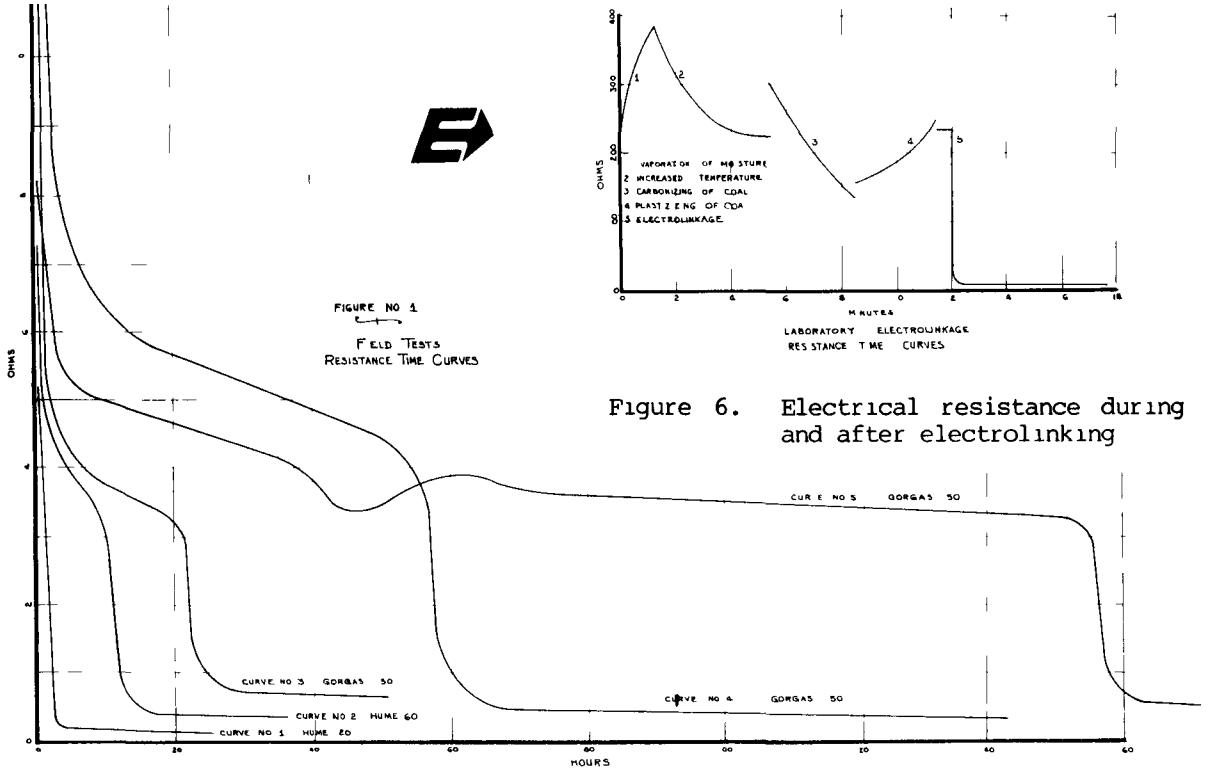

Figure 6. Electrical resistance during and after electrolinking

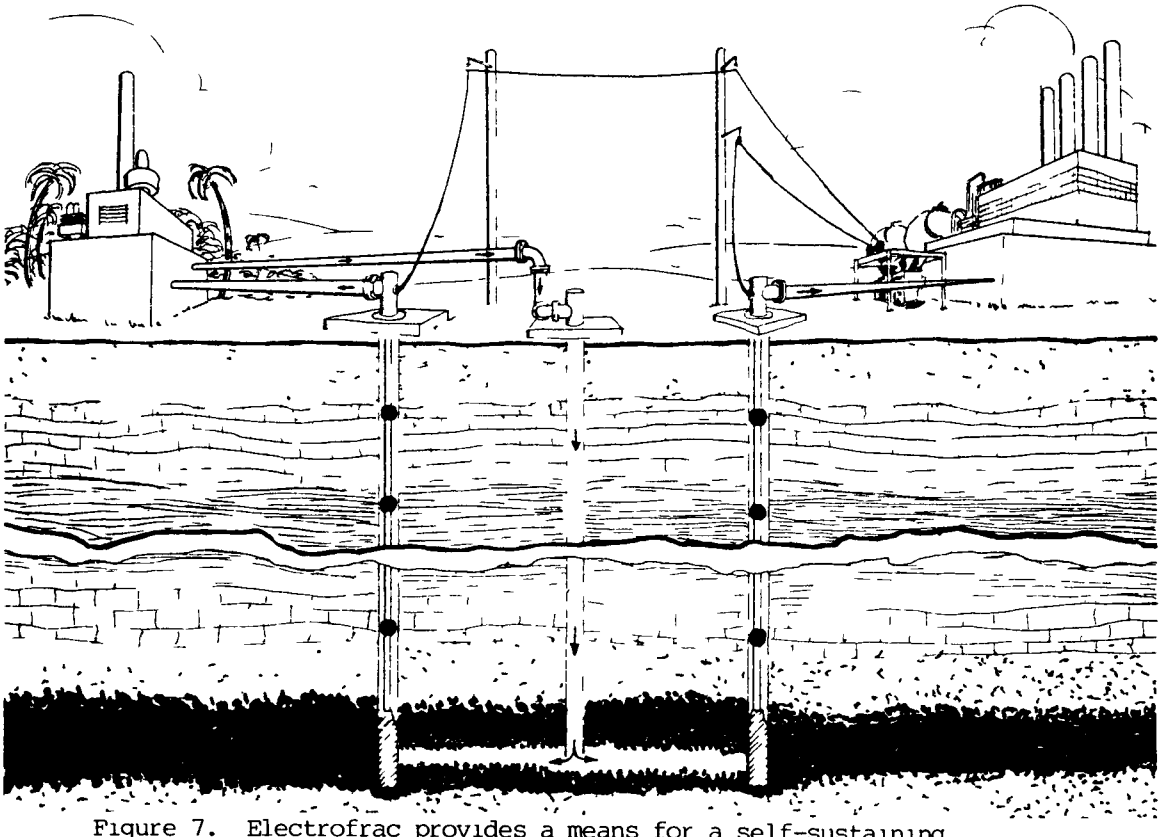

Figure 7. Electrofrac provides a means for a self-sustaining source of power & production at a coal reserve wherever needed

rock breaking. The power units are specially designed to provide a reliable source of power under widely varying current loads and voltages. They are illustrated in Figures 8 and 9. Simultaneously, specialized electrodes of proprietary design have been developed and tried under various field conditions.

Other related developments by various investigators include the following:

- Electroflood process. Electropyrolysis is employed to raise pressure by decomposing water in an oil reservoir.
- Electric well bore heating to melt paraffin deposits.
- Electric production tube heating to melt paraffin deposits.
- Electric heating (without electrolinking) to reduce viscosity in tar sands.
- High frequency (microwave) heating of oil sands or shale.
- Electrofrac Heatflood Process. Primarily employed as an enhanced oil recovery method; plus electrogasification of residual hydrocarbons.
- Ljungstrom Process. Electrical resistance "rods" are buried in oil shale to heat the formation.

Of these, the Electrofrac Heatflood Process is now undergoing demonstration on an economical scale in southeastern Kansas.

INDUSTRIAL DEVELOPMENT

Work to date has been limited to a combination of basic research work plus a first phase of industrial scale demonstration and development. A second phase is now needed to provide experience needed to guide further research and development, long range planning, and ultimate industrial applications.

This second phase of demonstration should be conducted on a larger scale than the work at Gorgas, Alabama. Primary features of this second phase of demonstration should include:

- Site selection in an industrially important area
- A bituminous coal seam at least 3 to 5 feet thick in a major coal field that is not highly attractive for conventional mining development
- A demonstration field of about 20 boreholes at about two hundred foot spacing for optimum electric power utilization without excessive gas flow resistance
- Complete auxiliary facilities including power and steam generators, air compressors, heat recovery, and gas treatment
- Either a power generator to utilize product gas or an adjoining industrial user for the gas
- Complete laboratory and service facilities
- Extended facilities as required to permit simultaneous demonstration of alternative methods of underground coal gasification

About five years would be required to complete the demonstration, but it is required to measure the full potential of procedures proven to date in this country and abroad. Concurrent research and development work should also be conducted as an adjunct, and as a supplement to evaluate alternative approaches.

Additional phases of industrial demonstration can then begin after reliability and capability have been well established.

CONCLUSIONS

The research of the process of underground electrocarbonization of coal that was conducted in the laboratory and pilot-plant tests demonstrated that the process is feasible as a method of underground gasification and it offers a means of solution of many of the problems that have attended other methods. For example, the fundamental desirable char-

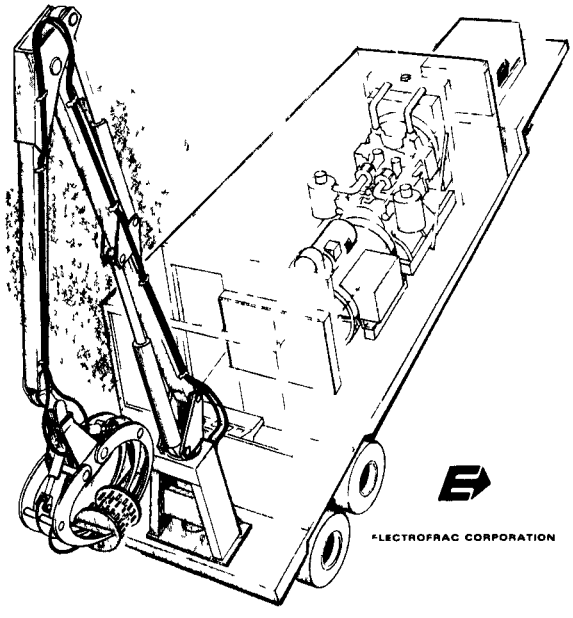

Figure 8. Mobile 500 kva power unit which has been used for rock breaking and electroenhanced oil recovery.

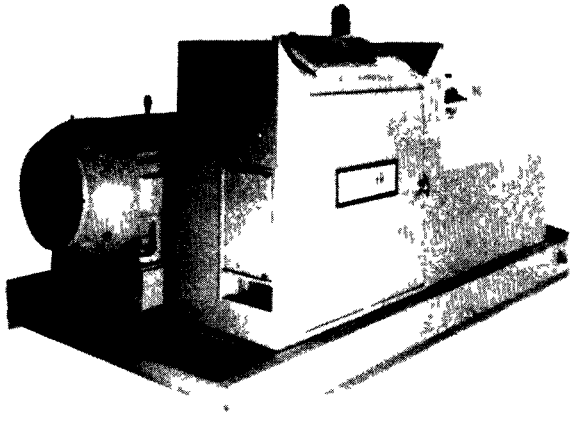

Figure 9. Skid mounted 150 kva power unit for field use.

acteristics of electrocarbonization are:

- relatively low construction and installation cost
- comparatively low cost of operation and maintenance
- simple regulation and control of gasification reactions
- high efficiency and resultant good economical yield

Though the economics of the process as a whole depends on many factors such as cost of power, depth of fuel bed, thickness of seam, proximity and character of industrial activities, the research has demonstrated that underground electrocarbonization and electrogasification may contribute significantly to the early development of underground gasification for industrial scale application.

REFERENCES

- Capp, J.P., Lowe, R.W., and Simon, D.W. Underground Gasification of Coal, 1945-60: A Biblography. BuMines information circular 8193. Published 1963.
- U.S. Department of Energy. Assessment of Underground Coal Gasification in Bituminous Coals. Four volumes. Prepared by Williams Brothers Engineering Company. Published 1982.
- Lawrence Livermore National Laboratory. Underground Coal Gasification (UCG) Gas to Methanol and MTG - Gasoline. Two reports: Tasks A and B. Prepared by the Pritchard Corporation. Published 1982.
- Gumz, W. Gas Producers and Blast Furnaces - Theory and Methods of Calculation. Copyright 1950 by John Wiley & Sons, Inc.
- Taylor, H.G., "The Current-Loading Capacity of Earth Electrodes," report (Ref. F/T81) of the British Electrical and Allied Industries.
- Siegal, M. Private communication concerning state of the art in Electrolinking and Electrocarbonization of Bituminous Coal. July 1, 1983.
- Sarapuu, E. The Underground Electrocarbnization and Gasification of Mineral Fuels. Submitted in partial fulfillment of the requirements for degree of Doctor of Philosophy. University of Missouri, May, 1951.
- Meerovich, E.A., ED., Applications of Electric Current for Direct Action on a Seam of Fuel in Shaftless Underground Gasification (G.M. Krzhiyhanovskii Power Institute Academy of Sciences, USSR, 1959) UCRL-Trans 11050, Lawrence Livermore Laboratory.
- Sarapuu, E. Wohlbier, Reinhard. Underground Gasification of Coal by the Electrical Method, UCRL-Trans 10874.
- Meerevich, E.A., "The Application of Electric Current for Purpose of Underground Gasification," Podz. Gaz. Ugley No. 2, 1957
- Gregg, D.W. "Relative Merits of Alternate Linking Techniques for Underground Coal Gasification and Their System Design Implications", Lawrence Livermore Laboratory, UCRL-82112, 1979.
- Forrester, J.D., Sarapuu, E. "The Process of Underground Electro-Carbonization", Publication of the Missouri School of Mines, No. 78, January 1952.
- Sarapuu, E. "Fundamental Aspects of In Situ Electrocarbonization and Electrogasification of Coal", Second Annual Underground Coal Gasification Symposium, Morgantown, West Virginia, August 1976,
- Cheasely, Thomas C. Electrocarbonization of Coal. Min. Cong. J., v. 36, January 1950, pp. 18-19
- Sarapuu, Erich. The Underground Electrocarbonization and Gasification of Mineral Fuels. Dissertation, Univ. of Missouri, Columbia, Mo., May 1951, 146 pp.
- Forrester, J.D., Sarapuu, E. Process of Underground Electrocarbonization. Univ. of Missouri, Sch. Mines and Met., Tech Ser. 78, Jan. 1952, 85 pp.

- Cheasley, Thomas C., Forrester, J.D., Sarapuu, Erich. Underground Electrocarbonization of Coal and Related Hydrocarbons. Min. Eng., v.6, No. 9, September 1954, pp. 908-915.

- Elder, James L., Fies, M.H., Graham, Hugh G., Capp, J.P., and Sarapuu, Erich. Field-Scale Experiments in Underground Gasification of Coal at Gorgas, Ala.: Use of Electrolinking-Carbonization as a Means of Site Preparation. BuMines Rept. of Inv. 5367, 1957, 101 pp.

- Krukovskii, V.K., Farberov, I.L., (Investigation of the Heating of Blocks of Coal by an Electric Current. Trudy Inst. Goryuchikh Iskopaemykh, Adad, Nauk S.S.S.R., Otdel. Tekh, Nauk, V.7, 1957, pp. 23-29.

- Lyandres, S.N., Reznikov, A.D. (The Use of Electric Current for Firing Underground Generators.) Podzemnaya Gazifikatsiya Uglei, No. 2, 1958, pp. 49-51; Humphreys & Glasgow Transl. by P.R. Wilson, 4 pp.

- Rauk, J. (Contacting of Electrodes With the Seam in the Underground Gasification of Coal.) Prace Glownego Inst. Gornictwa, Komun. (Katowice), ser. A, No. 244, 1960, 8 pp.

- British Trials in UG 1949-1955 by the Ministry of Fuel and Power.

- Bleakely, W.B.: Electrofrac - will it solve some of our toughest production problems? Oil and Gas Journal, February 12, 1962.

- Sarapuu, Erich: Underground Electropyrolysis of Oil Shale. Second Oil Shale Symposium, Colorado School of Mines, April 1965.

- Schoeppel, R.J. and Sarapuu E.: Laboratory Studies of Oil Recovery from Tar Sands by Electrocarbonization. Production Research Symposium, SPE, SPE-281, April 1962, Tulsa, Oklahoma.

- Sarapuu E., Calhoun, R.L., Clark, W. Electrofrac Techniques. ASME-AIME Joint Solid Fuel Conference, Birmingham, Alabama, October 1961.

PATENTS

- Electrocarbonization in situ, US #, 795,279; 7-11-57

- Electrofracing by Impulse Voltage, US # 3, 169,577; 2-16-65

- Single WEll Electrofracing, U.S. # 3, 211,220; 10-12-65

- Electrofracing Through Casing, U.S. # 3, 236,304; 2-22-65

- Electropressurization (secondary oil recovery) US # 3, 141,504; 7-21-64

- Method of Underground Electrolinking and Electrocarbonization of Mineral Fuels, Canada # 561,709; 8-12-58

- Rock Breaking Method and Apparatus (electrical rock breaking), US # 3, 460,766; 8-12-69

- Rock Breaking Method and Apparatus (electrical rock breaking), Canada #877,536; 8-3-71

- Electrical Disintegration Drilling, US # 3, 179,187; 4-29-65

Proceedings of the Ninth Annual Underground Coal Gasification Symposium, August, 1983

2.16 FIELD TESTING OF CORNERING WATER JET DRILL

by

Bruce P. Engler
David L. Shirey

ABSTRACT

Sandia National Laboratories is developing a drilling system which uses high velocity water jets to make horizontal holes in a coal seam accessed through a vertical borehole. For underground coal gasification (UCG), these horizontal holes can be drilled to create linking paths between vertical process wells.

During shake-down tests in Albuquerque, five holes were drilled in a simulated coal seam. The eight to twelve inch diameter holes deviated from their intended trajectories by less than twelve inches in twenty feet. Similar results have been produced during more recent field tests in an open pit coal mine. An exposed coal seam with undisturbed overburden was penetrated to a depth of over seventy feet with maximum deviations of less than four inches vertically and six degrees horizontally. To date, all tests have utilized an elevated platform to permit observation of the cornering mechanism during drilling operations. For all tests to date, the on board logging instrumentation has provided accurate guidance and hole location data. Test results indicate that the drilling system is capable of producing horizontal holes for UCG applications. A proof of concept test is forthcoming that will require the drill to access a coal seam from an underreamed cavity located at the bottom of a vertical borehole.

Sandia National Laboratories, Albuquerque, New Mexico 87185

INTRODUCTION

Previous publications[1-6] have described the preliminary cornering water jet drill (CWJD) designs, feasibility tests and design evaluation exercises. An improved drill head and string assembly, a previously untested cornering mechanism, and an up-dated instrumentation system underwent shake-down testing in Albuquerque during mid-1982. Described by Engler[6] and Shirey,[5] these experiments were sufficiently promising to prompt further testing at the Albuquerque test site and, later, field tests at a surface coal mine.

In Albuquerque, all system components, excluding a down-hole sump pump, were evaluated and improved while drilling five holes through the length of a four ft (1.22 m) square x 20 ft (6.1 m) long simulated coal seam. After completing the shake-down phase in September 1982, the entire operation was moved to the McKinley open pit coal mine operated by Pittsburg and Midway Mining Co., near Gallup, New Mexico.

Two holes were drilled into an exposed coal seam with over 100 ft (30.5 m) of undisturbed overburden. Exercising the complete drill system in an actual coal seam with overburden pressure was desirable prior to going

"down hole" in the proof-of-concept test. In addition, valuable field experience was gained by the test crew and several significant modifications were made to the system as a result of the exposed seam tests.

The purpose of this paper is to describe the later Albuquerque experiments and the McKinley Mine field tests. System improvements and recorded drilling data are presented and discussed.

BACKGROUND

During the early 1970's a significant effort was made to develop high velocity water jets as a means of cutting rock and coal. From 1975 to 1978, D. A. Summers, at the University of Missouri-Rolla (UMR), worked under contract with DOE to apply the concept to geothermal drilling.[7] Independent conclusions were drawn by both UMR and Sandia National Laboratories personnel that horizontal drilling might be done from the bottom of a vertical borehole. Development of a cornering water jet drill was initiated by Sandia and UMR in 1978. Two potential applications were considered: (1) methane drainage in coal mines, and (2) linking vertical process wells for underground coal gasification.

The University of Missouri-Rolla, under contract to Sandia, conducted tests to demonstrate the feasibility of drilling round-the-corner with water jets. The results were encouraging; consequently, work began on the design of an improved version. Drillhead development was undertaken by UMR while Sandia assumed the responsiblity for the drill string, rotation and advance mechanism and guidance instrumentation. During 1979 and 1980, performance of the head, string and instrumentation was tested, without the cornering device, in an exposed coal seam. In 1981, development of the entire system for the DOE was undertaken by Sandia.

Recognizing the many complex subsystems required in this drilling method, a decision was made to demonstrate the concept using full scale prototypes. Time consuming studies of nozzle optimization, reducing the vertical access hole diameter to a minimum, etc., would follow the successful demonstration.

SYSTEM OPERATION

A simplified description of the CWJD system being developed is provided for reference. More complete details may be found in References 2, 3 and 6. Figure 1 outlines the basic system configuration planned for actual use.

Coal seam access is provided by a 16 inch (40.64 cm) cased borehole terminated by a 6 ft (1.83 m) diameter underreamed area below and a special well head assembly topside. A rotation and advance assembly (R&A) is hung from the wellhead on a pair of 2-1/2 inch (6.40 cm) pipes which double as feed and discharge conduit for a slurry sump pump.

When the R&A assembly is in place, the shoe and drive gear are pivoted to a horizontal position. This manuever forms a 2 ft (.61 m) radius cam surface which guides the drill head and string through the drive gear and into the target. A hydraulic motor provides torque to the drive gear through a chain and sprocket assembly (see Fig. 2).

A drill string, composed of 17 inch (43.20 cm) long sections of 3x5 inch (7.62x12.70 cm) steel tubing hinged together at the top, is stored in 11 ft (3.35 m) sections on a special rack. Four fluid supply hoses and two electrical cables are fed through the string sections prior to drilling. The string sections are lowered through the wellhead assembly, the borehole casing and the R&A cam section into the drive gear. Advance force required to overcome reaction from the water jets and friction in the R&A assembly is provided by the gear which engages holes in the drill string boxes. Advance rate is adjusted by flow regulators which synchronize the drive gear and string support winch. Drill string retraction forces are supplied by the drive gear and supplemented by the winch.

Cutting water is supplied to the drill head by a high pressure pump capable of producing 25 GPM (91 LPM) at 10 kpsi (69,000 kPa). The water is fed through a steel reinforced rubber hose to a drill head fitted with a rotating nozzle holder (see Fig. 3). As the drill string advances, a cylindrical hole is created by the cutting action of the high velocity jets. Chips produced by the cutting action are carried to the underreamed area by the cutting jet water combined with additional flush water. The flush water is pumped from the surface at 34 GPM (123 LPM) through nozzles located 20 inches behind the drill head.

Due to the inherent stiffness of the drill string in the lateral direction, guidance control is provided for the vertical direction only. A hydraulic cylinder, controlled from the surface, sets the head pitch with respect to string pitch at either 0° or -4°. Another hydraulic cylinder and cable device is normally actuated to stiffen the leading 7 ft (2.13 m) of drill string.

At one second intervals, on board instrumentation updates a computerized data acquisition and display system located on the surface. String and head pitch data are provided by 0-1 g accelerometers. These are combined with magnetometer generated azimuth data and string depth-in-hole readings to provide a calculated drill head location. Other recorded items are cutting jet pressure, nozzle rpm and axial force on the string suspension cable. The functional diagram is shown in Figure 4.

TESTING HISTORY

The primary goal of the Albuquerque site "shakedown" test was to assure that the new equipment would perform as designed and to make the necessary modifications if it didn't. Experience gained while drilling holes 1 and 2 is described by Shirey[5] and Engler.[6]

The major goal established for holes 3, 4 and 5 was to refine the drilling technique to improve system reliability and vertical displacement control. The three holes were produced with successively greater ease with drilling rates at times exceeding 5 ft (1.52 m) per minute. Since no mechanism exists to adjust the drill string in the lateral direction, the horizontal deviation was not controlled. Due to magnetic interference, magnetometer data was not initiated until the magnetometer was 8 ft into the simulated block. A key feature of the system is the ability to map the location of the drill string underground at all times. Plots of the horizontal, vertical components of the mapped holes are shown in Figures 5-8. The intended hole shown in Figures 6-8 and 11-12, is merely a straight line extention of the initial azimuth orientation, allowing indication of the deviation that occurred in the horizontal plane. Experience gained later in the surface mine field test indicates that hole deviations could have been decreased by lower advance rates and more careful pitch cylinder adjustments.

The Albuquerque shakedown tests were completed on October 13, 1982. By October 29, 1982, the entire drill system and support equipment array was moved to the field test site in the McKinley open pit coal mine near Gallup, NM. The chosen site was in an abandoned cut possessing an exposed 5 ft (1.52 m) thick coal seam covered by over 100-130 ft (30.5-39.65 m) of shale and sandstone overburden. Mine survey data indicated that the seam was relatively uniform and pitched approximately 1° negatively away from the exposed face (see Fig. 9).

The purpose of the exposed seam field test was to study the drilling system performance, both at depths unattainable at the Albuquerque site, and in a real coal seam. Also, the effect of heavy overburden was unknown since previous testing in actual coal was done in an uncovered seam[1,3] without the cornering mechanism. For the Gallup field test, no significant changes were made to the shakedown test drilling hardware.

An initial hole was drilled to a depth of 12 ft. At this time a combination of drill head motor failures

and severe freezing weather made it logical to cease drilling for the winter months as this initial "proof-of-concept" system had not been designed for winter operation. The winter months were occupied with designing and building a new hydraulic motor driven drill head.

Drilling efforts resumed in March in the same hole begun in November. Drilling progressed nominally until a depth of 49 ft (14.94 m), whereupon progress was abruptly stopped. After repeated attempts to advance failed, a new hole was started near the first but at an angle which would cause a separation of 5 ft (1.52 m) at a 50 ft (15.24 m) depth. As with hole no. 1, the second hole was drilled with ease until approximately 40 ft (12.19 m) was reached. Drilling continued slowly to 60 ft (18.29 m) at which time the electric nozzle drive motor failed.

The new hydraulic motor drive head and a larger flush supply hose were installed before continuing the drilling tests. Progress was slow but steady to a depth of 66 ft (20.12 m) where the drill string became lodged in the hole. Repeated attempts to move the string were unsuccessful; however, after allowing the string to rest in the hole for several days, it was withdrawn easily. Possibly, the water-laden coal chips became jammed between the drill string and the hole walls until natural drainage freed them.

Since a jammed drill string would create serious problems in the downhole proof-of-concept test, studies were initiated to improve the drilling procedure. Glass[8,9] recommended lower and more uniform advance rates and a more rigorous flushing procedure. A real time vertical deviation vs. hole depth and a 5 ft interval, time at pressure vs. hole depth plotting capability was developed and added to the data acquisition system.

Drilling activity resumed with the intention of testing and learning to use the new procedures. The entire 66 ft (20.12 m) hole was reamed to increase uniformity. Drilling began at 66 ft (20.12 m) and advanced easily to 72 ft (21.95 m) when on June 15, a minor breakdown and time limitations forced an end to the exposed seam phase of testing. (For plots of horizontal/vertical components of the mapped holes, see Figs. 10-12.)

Preparations for drilling the vertical borehole from the ground level above the exposed seam test site began June 16 and to date, a 16 inch (40.64 cm) cased hole has been completed.

SYSTEM MODIFICATIONS AND IMPROVEMENTS

One of the most valuable consequences of both the Albuquerque shakedown experiments and the Gallup field tests was a series of modifications and improvements to the drilling hardware and procedures. The three most significant improvements made to the system while completing the final three holes in the simulated coal seam were:

1. Both the high pressure and the flush supply hoses were routed through the drill string segment which contained the magnetometer. Since each hose contained steel reinforcement braid, a distorted azimuth signal was being recorded. Short sections of non-metallic reinforced hoses were inserted in the magnetometer area resulting in more accurate azimuth data.

2. Regardless of the position of the pitch cylinder piston, the drill head had a tendency to pitch down under the force of the stiffener. Investigation revealed equal diameters for both the stiffener and pitch cylinders. A larger pitch cylinder was installed, assuring the ability of the operator to maintain a 0° head with-respect-to string pitch.

3. For shoe positioning, microswitches and indicator lights had been provided on the rotation and advance assembly. It was determined that accurate cam surface alignment was impossible using the indicator lights; therefore, 0-1 g accelerometers were added to the shoe and main structure. Coupled to a digital readout on the surface, these devices allow an align-

ment tolerance of ± 0.06 inch (.15 cm)

During the exposed seam field tests, many adjustments were made to the system to allow testing to proceed. The three most significant changes were:

1. Flush water flow became marginal at hole depths of over 40 ft (12.19 m). The 7/8 inch (2.22 cm) diameter flush supply hose was replaced with a 1-1/4 inch (3.18 cm) diameter hose; flush water flow increased 35%.

2. The original drill head contained a 1/12 HP (0.062 kW) electric nozzle rotation motor which produced 45 in-lbs (5.0 N-m) of torque at the output of a 50 to 1 gear set. After suffering several failures, the fragile gear motor was replaced by a submersible hydraulic motor capable of 145 in-lbs (16.4 N-m) of torque without gear reduction. In addition to added torque and durability, the hydraulic drive made accurate RPM measurements possible through a calibrated flow meter at the surface.

3. Due to anomalies in the hole diameter and trajectory plus a marginal chip flushing system, drilling became difficult at depths of over 40 ft. A new, more rigorous drilling procedure was developed to produce a straighter, more uniform hole and to force the operator to retract the string more frequently to improve flushing. Additional computer capabilities were added to aid in utilizing the new technique. Real time vertical hole deviation vs. hole depth may be plotted during the drilling process. Also, at 5 ft (1.52 m) intervals, time at cutting pressure vs. hole depth is displayed as an indication of hole diameter uniformity.

Two additional modifications are being made as a result of the testing experience.

1. To simplify, increase reliability, and minimize down hole instrumentation, the drill head high pressure transducer is being moved to the high pressure pump at the surface. Experience has taught that it's unnecessary to monitor pressure at the nozzle.

2. "Tripping" drill string in and out of the hole requires segment separation and "threading" of the cumbersome hose and cable bundle. Since this procedure takes over 50% of the man hours devoted to drilling, a significant improvement can be made by eliminating the "threading" procedure. Prior to more testing, the drill string segments will be split lengthwise and fastened together with screws. As a consequence, labor requirments should be reduced substantially.

DEVELOPMENT TEST PLANS

The ultimate goal of the CWJD project is to develop a drill capable of turning a corner at the bottom of a 300 ft (91.44 m) vertical borehole and drill 100 ft (30.50 m) horizontally into a coal seam. It has been demonstrated previously that the drill head and string are capable of creating a 100 ft (30.50 m) long hole. Also, early shakedown tests in Albuquerque proved the instrumentation system's ability to accurately map drill progress and the cornering device's effectiveness to rotate the drill string and advance it into a horizontal hole.

Additional simulated coal seam tests have indicated that, with proper technique, the drill will maintain a relatively level course. Also, a remote shoe orientation system was designed, installed and proven to be reliable.

During the exposed seam field tests, the drilling technique and equipment were improved. The effect of 100 ft of overburden appeared to be unimportant and, although difficulty increases with hole depth, the device should be capable of drilling 100 ft (30.50 m) horizontally.

To date, in preparation for the proof-of-concept test, a level working surface has been prepared approximately 100 ft (30.50 m) above the coal seam. Also, a vertical 16 inch (40.64 cm) cased hole has been created to

allow access to the seam. A 50 ft (15.25 m) deep x 19-1/2 inch (49.53 cm) diameter uncased extension was drilled below the coal to provide a reservoir for chips both during the underreaming and the proof-of-concept test.

A 6 ft (1.83 m) diameter x 10 ft (3.05 m) deep underreamed cavity will be created at the seam using an expanding arm bit and conventional drill rig. Underreaming is considered a crucial part of the proof-of-concept test since it's never been used for this specific purpose.

Following the successful preparation of the access hole, a sump pump must be chosen. Two pumps have been purchased for testing, a 7-1/2 HP (5.6 kW) submersible water well pump fitted with a large sand screen to prevent damage from the coal chips and a jet pump which is capable of passing 1/2 inch (1.27 cm) particles but requires a large water supply pumped from the surface. Either pump will be fitted underneath the R&A assembly.

The R&A assembly will be lowered to the underreamed cavity on 2-1/2 inch (6.35 cm) suspension pipes secured at the wellhead. Attempts will be made to drill 100 ft horizontally and exit the exposed coal seam face in the pit (the vertical access hole was drilled 100 ft (30.50 m) from the seam face). Forcing the drill to exit the exposed seam will make accurate hole trajectory verification possible (see Fig. 13). Successful completion of these tests will verify the soundness of the basic drilling system concept and provide the necessary experience to attempt actual UCG process well linkage.

CONCLUSIONS

The Albuquerque site shakedown experiment and the exposed face coal seam field tests have both been completed successfully. Each of the five holes created in the simulated coal seam were drilled with successively greater ease and accuracy.

Although the test goal of drilling a single 100 ft deep hole in the overburdened coal seam wasn't met, both shorter holes were drilled with little difficulty in the first 40 ft (12.19 m). The flushing and string binding problems encountered beyond that point were dealt with in a systematic manner and a procedure was developed that should improve our chances of success in the proof-of-concept test.

The drill string guidance system and on-board hole logging instrumentation have proven to be very effective in keeping the drill on its intended course. The operators should have little trouble keeping the trajectory near the coal seam floor and locating the end of the hole.

System modifications made during the field tests have proven successful. The new hydraulic motor driven drill head worked well. The benefits include ruggedness, greater available torque, and an accurate and reliable RPM indicator located conveniently on the surface.

Thirty-five percent greater flush water volume has been provided by a larger supply hose. Since greater hole depth was reached following its installation, we conclude that the modification improved the system.

Hole characteristic plots to be studied during the drilling process, a more methodical drilling procedure based upon hole diameter control and more rigorous chip flushing appear to be the greatest contributions to the successful completion of a proof-of-concept test. Due to lack of time, efforts to drill the final hole beyond 72 ft (21.95 m) were stopped; however, no other major obstacle to hole completion was encountered.

Some questions remain--for example: Can an underreamed cavity be made and will it stay intact during the drilling operation? Will either of the sump pumps be able to discharge 65-70 GPM (246-265 LPM) of water from the underreamed cavity without clogging? Is the system capable of drilling 100 ft? Assuming that these potential obstacles can be overcome, the experience gained during the

shakedown and exposed seam tests has provided confidence that the proof-of-concept test will be successful.

ACKNOWLEDGEMENTS

This project is sponsored by the Department of Energy through the Morgantown Energy Technology Center and the Laramie Project Office (formerly Laramie Energy Technology Center). Dr. Harold Shoemaker and Dr. T. C. Bartke are the respective project officers. Data analysis and procedure recommendations were supplied by test crew member R. E. Glass. Additional field test assistance was provided by D. W. Cook and C. Sifre Soto.

REFERENCES

1. H. D. Shoemaker and K. M. Timmerman, "Drilling Right Angle Drainage Holes in Coal Utilizing Water Jets", ASME Publication 82-PET-14, December 10, 1981.

2. S. L. Love and K. M. Timmerman, "Testing of a Cornering Water Jet Drilling System for Drilling Horizontal Holes in Coal", presented at the Seventh Underground Coal Symposium, Fallen Leaf, CA, September 1981.

3. C. R. Barker, "Water Jet Drilling Head Development, Phase Report, January 1980-December 1980", December 1980.

4. C. R. Barker, "Water Jet Drilling Head Development, Phase Report, June 1978-December 1979", December 1979.

5. D. L. Shirey and S. L. Love, "Development Testing of a Cornering Water Jet Drill", presented at the Eighth Underground Coal Symposium, Keystone, CO, August 1982.

6. B. P. Engler, "Instrumentation for the Cornering Water Jet Drill", presented at the Eighth Underground Coal Symposium, Keystone, CO, August 1982.

7. D. A. Summers and T. F. Lehnhoff, "The Design of a Water Jet Drill for Development of Geothermal Resources", prepared for Geothermal Div., ERDA, by the University of Missouri-Rolla, Contract No. EY-76-S02-2677, 1978.

8. R. E. Glass, "Cornering Water Jet Drill Data", internal memorandum to P. J. Hommert, 9747, Sandia National Laboratories, May 5, 1983.

9. R. E. Glass, "Drilling Procedure", internal memorandum to P. J. Hommert, 9747, Sandia National Laboratories, May 31, 1983.

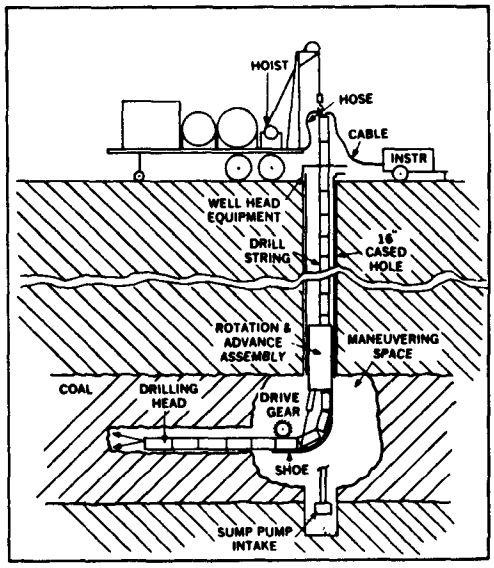

FIGURE 1. Water jet drilling system layout.

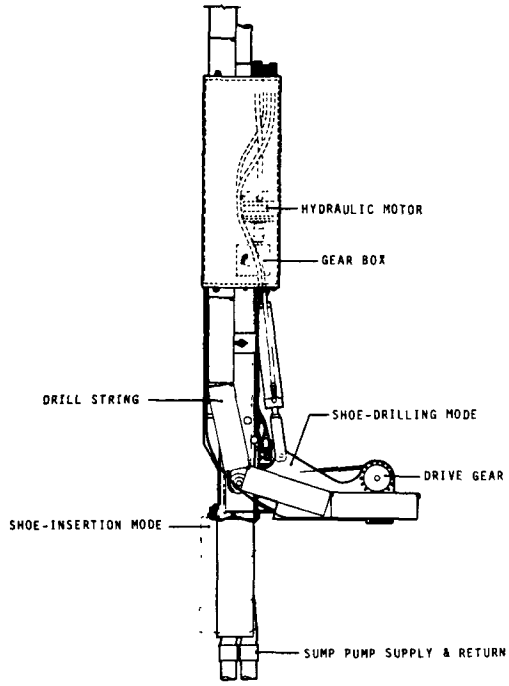

FIGURE 2. Rotation and advance assembly.

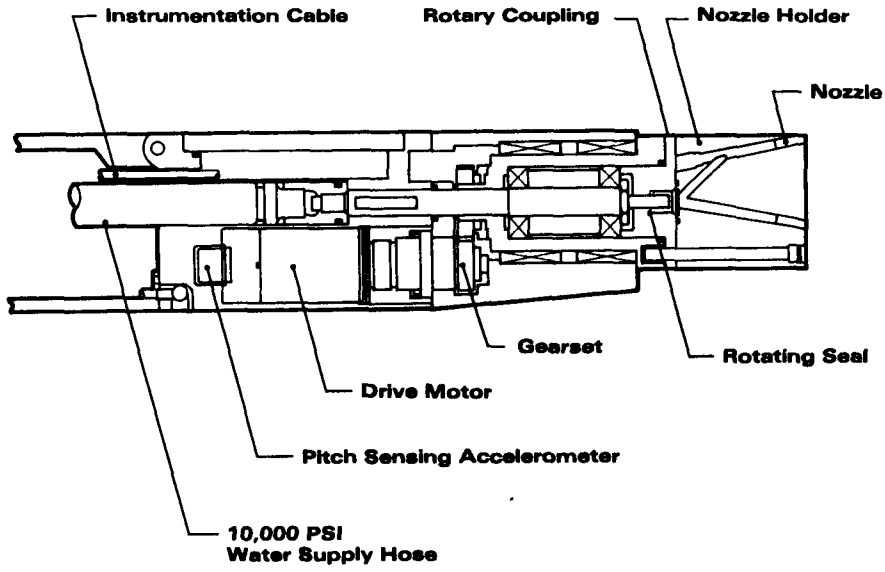

FIGURE 3. Drill head assembly.

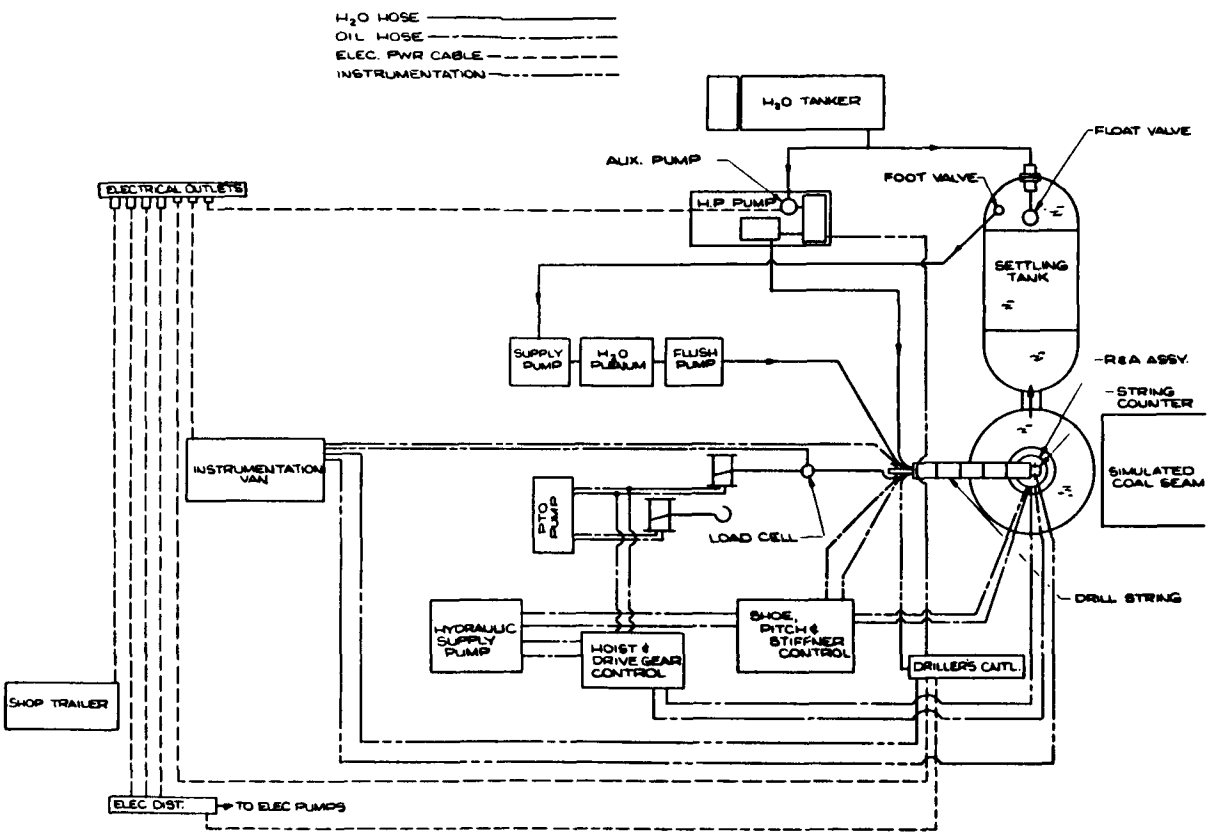

FIGURE 4. CWJD system, functional diagram.

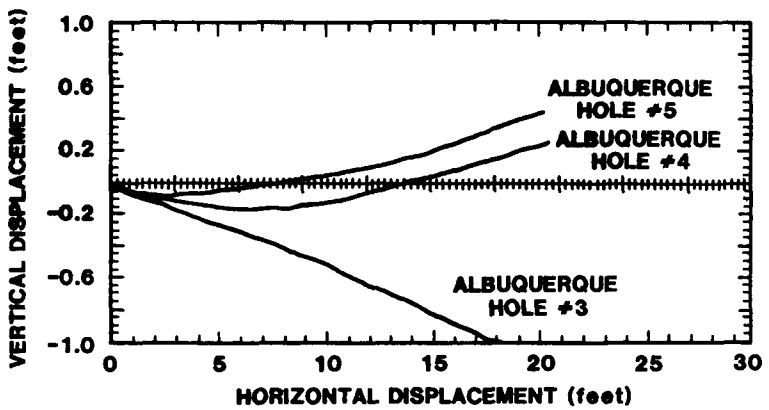

FIGURE 5. Vertical vs. horizontal displacement of shakedown test holes 3, 4 and 5.

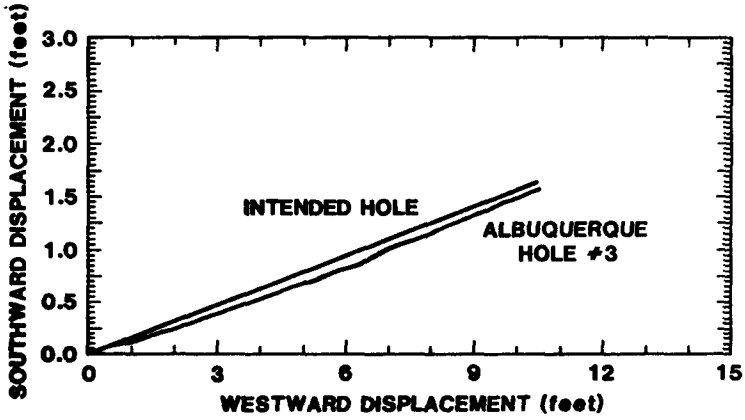

FIGURE 6. Hole displacement in the horizontal plane - shakedown test hole 3.

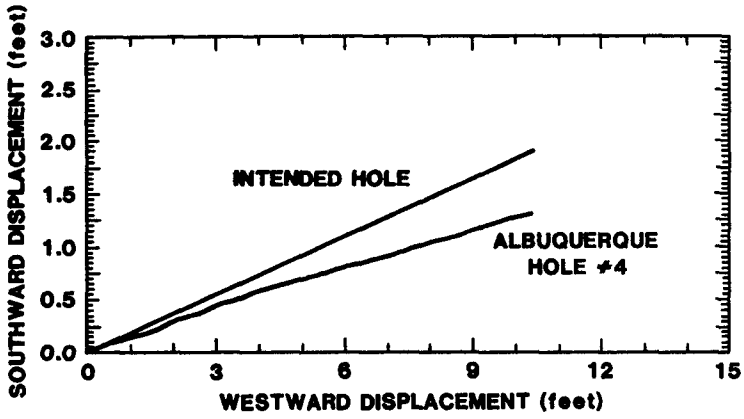

FIGURE 7. Hole displacement in the horizontal plane - shakedown test hole 4.

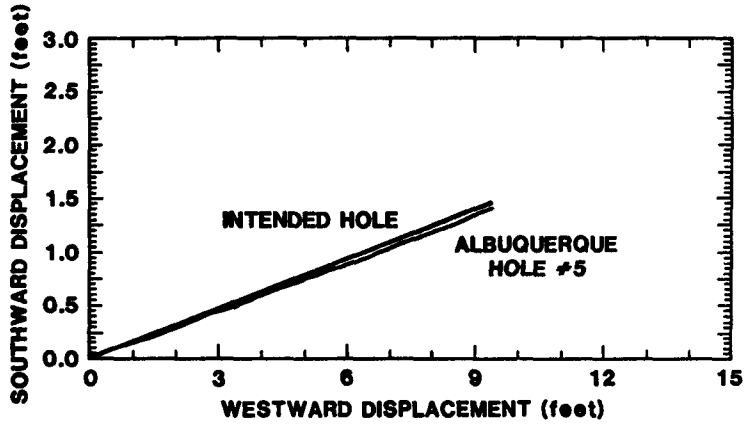

FIGURE 8. Hole displacement in the horizontal plane - shakedown test hole 5.

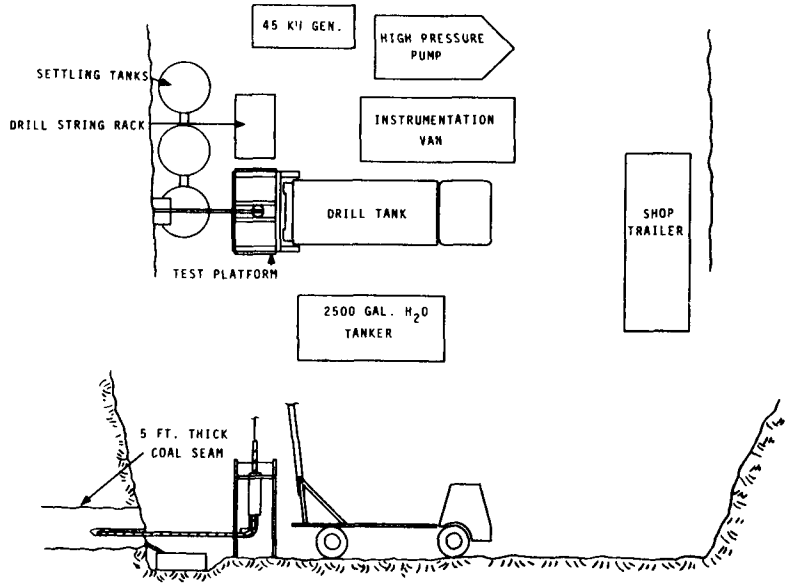

FIGURE 9. Exposed seam field test setup.

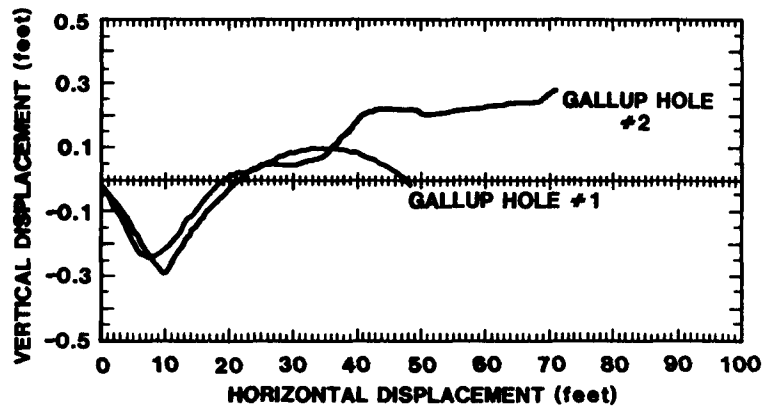

FIGURE 10. Vertical vs. horizontal displacement of field test holes 1 and 2.

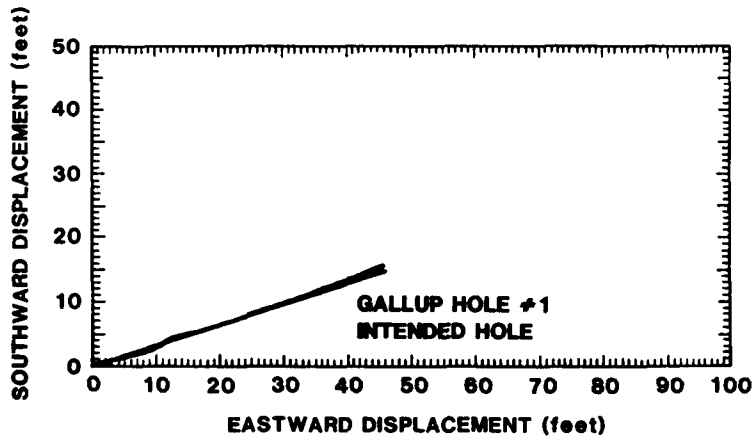

FIGURE 11. Hole displacement in the horizontal plane - field test hole 1.

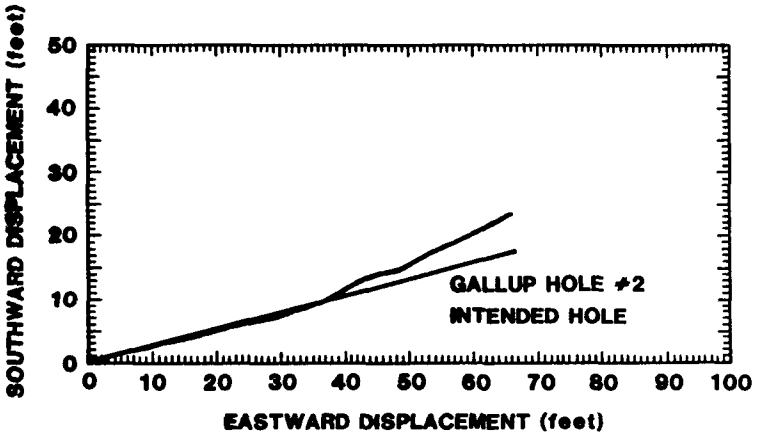

FIGURE 12. Hole displacement in the horizontal plane - field test hole 2.

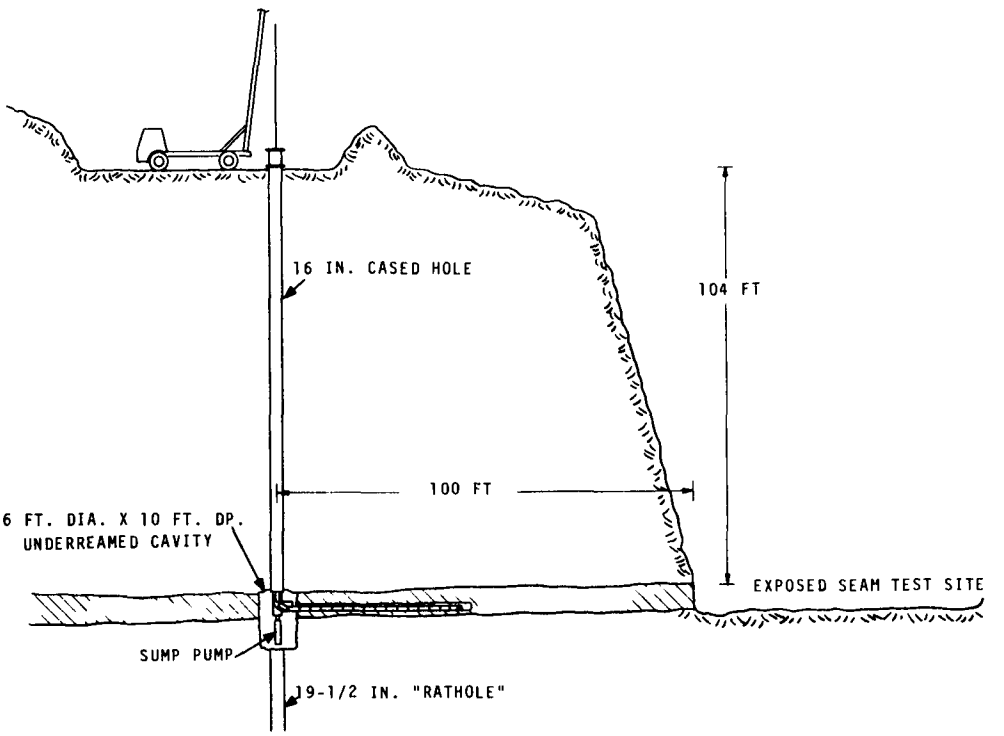

FIGURE 13. Proof-of-concept test setup (planned).

2.17 A COMPARISON OF FORWARD COMBUSTION GASIFICATION MODELS-II

by

Laurene V. Kunselman 1/
Donald W. Fausett
Charles G. Mones

ABSTRACT

The survey and comparison of forward combustion gasification models has been extended to incorporate analyses with each of the six computer programs included in the study based on data representing two oxygen/steam injection field experiments. Those experiments are the Hoe Creek III and Rawlins II field tests. This report presents the simulated results obtained with each model for those two field tests, and provides an indication of the applicability of each model to such tests. Modifications made to the computer codes to enable them to accommodate a variety of injection gas compositions are discussed. Further comparisons of the computational features of the six computer codes are given. Some revised results from the previously reported model comparisons for Hanna III, Hoe Creek II, Pricetown I, and Rawlins I field experiments are included, based on data for those tests in the revised LLNL UCG Data Base which differ in some respects from those published in the original edition. More details are provided concerning the capabilities and limitations of each model.

INTRODUCTION

In order to complete the project [1] of making a computational comparison of six forward combustion UCG models that are available in the public domain, data from two oxygen/steam injection field experiments have been selected and analyses performed with each of the models. The experiments chosen are the Hoe Creek III and Rawlins II field tests. A general description of the six models is given in the initial report [1]. The nomenclature introduced in that report is used herein to refer to the models included in the survey:

(1) TEQ - A constrained mass balance, equilibrium model developed at the University of Texas, partially funded by DOE [2];
(2) LEQ - An equilibrium model developed at Lawrence Livermore National Laboratory (LLNL) [3,4];
(3) W1 - A steady-state, one-dimensional model developed at the University of Wyoming, partially funded by DOE [5,6];
(4) L1 - An unsteady-state, one-dimensional combustion tube model developed at LLNL [7];
(5) M2 - A three-dimensional, cavity growth model developed at the University of West Virginia, funded by DOE [8];
(6) L2 - An unsteady-state, two-dimensional model developed at LLNL [4].

Additional modifications to some of the computer programs were required in order for them to be able to accommodate oxygen/steam injection data. Also some of the data for the four previously studied field experiments have been re-analyzed because of differences between the

1/University of Wyoming Research Corporation
P.O. Box 3395, University Station
Laramie, Wyoming 82071

revised UCG Data Base [9] and the original UCG Data Base [10] on which the initial report [1] was based. Furthermore, there were some corrections to models and some improvements in data preparation methods.

DATA SELECTION AND REVISIONS

The oxygen/steam injection field experiments included in this study are the Hoe Creek III (HC3) test and the slant injection well phase (module one) of the Rawlins II (R2) test. Data sets for those two tests have been prepared for the six models being compared. The primary source for the data was the revised LLNL UCG Data Base [9]. The four air injection field experiments previously studied [1] are the Hanna III (H3), Hoe Creek II (HC2), Pricetown I (P1), and Rawlins I (R1) tests. Because of some differences between the revised Data Base and the original edition [10], new data sets for those four tests have been prepared for the TEQ, L1, and M2 models. New data sets were not prepared for the other three models because they either require extensive user adjustments (LEQ, W1) or consume large amounts of computer time (L2).

The most significant changes in the revised Data Base occur in the P1 data. The last five and one-half days of forward gasification (which had a low flow rate) have been tabulated separately from the main part of the forward burn and are not included in the P1 data used in the present phase of this study. Data for R2 appear for the first time in the revised Data Base, and data for R1 are more complete. An error in the energy distribution percentages has been corrected for all cases.

A summary of input values for variables which are used in several of the models appears in Table 1.

The link zone diameter required by the M2 model has been recalculated in a more appropriate manner than in the initial report [1]. The fact that the model treats the link zone as a region of devolatilized coal rather than as a void space was overlooked in the initial study. The link diameter is now determined by setting the amount of coal consumed during reverse combustion linking equal to π times the square of the link zone radius times the distance between the injection and production wells times the mass fraction of volatile matter in the raw coal. This calculation treats the porosity of the link zone as being equivalent to the mass fraction of volatile matter in the raw coal.

Another important input parameter to M2 is the ratio of total coal consumed during forward gasification to total oxygen injected. Previously that parameter had been calculated by using the moles of coal consumed times the molecular weight of the coal to determine the amount of coal consumed. That calculation gave only the amount of dry, ash free coal consumed. The Data Base value for the amount of raw coal consumed is the proper quantity for computing the coal/oxygen ratio parameter, and it has been used in the present study. The use of this empirical parameter by M2 to determine the amount of coal consumed during each time step restricts the predictive capability of the model.

For TEQ, the insitu heat loss percentage has been assigned a fixed input value for each case rather than using it as an adjustable fitting parameter, as was done previously.

The water influx parameter in W1 has been redefined as the ratio of available water to injected oxygen instead of the ratio of available water to injected air.

MODIFICATION TO THE PROGRAMS

TEQ and M2 have been modified to read input from a data file. TEQ originally accepted data interactively from a computer terminal. M2 had statements defining data values embedded in the code. LEQ, TEQ, L1 and L2 required no modifications to accommodate oxygen/steam injection. W1 required modifications to the water influx parameter, the mass balance equations and the energy balance equation because it had been written originally for modelling of air injection only.

Some fairly simple modifications were made to M2 in order to accommodate oxygen/steam injection data. These modifications were based on the assumption that all references to air (e.g. temperature, heat capacity,

fraction of oxygen) can be replaced by references to the injection gas. This assumption is not theoretically valid for the two oxygen/steam injection cases because the oxygen in the steam is not free to react directly with coal. More extensive modifications to the model to properly account for steam injection are being performed currently by researchers at METC/WVU. In spite of the preceding comments, results from M2 for the oxygen/steam injection tests appear as reasonable as those for the air injection tests. In the course of studying the M2 model to determine the necessary modifications for steam injection, a mistake was discovered in an energy equation. The corrected equation enables M2 to analyze R1 test data, which the uncorrected version could not process. Other differences were discovered between the equations in the code and those in the published report [8], but it was determined that the coded equations were the correct ones.

RESULTS

The two equilibrium models, TEQ and LEQ, differ in terms of their ease of use and predictive capability. TEQ is the more modest in its modelling scope, but it is also much easier to use. As long as the in situ heat loss percentage and the water influx rate are known, the model predicts product gas composition. Alternatively, the heat loss percentage can be used as a fitting parameter to match a known gas composition. The HC3 and R2 data were used with an assigned value from the Data Base for the heat loss parameter. It had been used as an adjustable parameter to match Data Base values for product gas composition for the H3, HC2, P1, and R1 field tests in the initial phase of the study. Those cases have been reanalyzed using data from the revised Data Base and with an assigned value for the heat loss parameter. Predicted values for product gas composition for HC3 and R2 are shown in Figures 7 and 8. The model had no difficulty in handling oxygen/steam injection data and does not require user manipulation of any fitting parameters. The computed heating value of the product gas per mole of injected oxygen compares well with the Data Base value for HC3: 544 kJ/mol vs. 578 kJ/mol, whereas the computed value for R2 is twenty-seven percent lower than the Data Base value: 1389 kJ/mol vs. 1915 kJ/mol.

LEQ functions by dividing the UCG process into three zones: reaction, pyrolysis/drying, and mixing. Material and energy balances are performed on each zone. The products leaving the reaction zone can be determined by assuming either full thermodynamic equilibirum or water-gas shift equilibrium at a user-specified temperature. The assumption of thermodynamic equilibrium is more useful for matching laboratory tube experiments. The HC3 and R2 simulations were run assuming water-gas shift equilibrium. The HC3 case converged quickly with good agreement to values in the Data Base. R2 data caused stability problems and a protracted convergence procedure. In order to obtain convergence, it was necessary to initiate the matching procedure with a water influx rate (into the reaction zone) that was much lower than the value given in the Data Base. The water influx rate was gradually increased during the matching process intrinsic to model convergence. The final value at convergence was of the same general magnitude as the Data Base value.

The converged LEQ results were not in good agreement with Data Base values for the R2 case. Good agreement with Data Base gas analysis values could be obtained only by using a large negative value for water influx (efflux) for the mixing zone. R2 results are reported with the non-negative water influx value for physical consistency. Fitted values for gas composition for the HC3 and R2 tests are shown in Figures 7 and 8. Calculated energy distributions are shown in Figures 5 and 6.

In the initial phase of the model comparison project, the L1 model failed to execute satisfactorily with any field scale test data. The model was designed originally to simulate combustion tube coal gasification experiments. Further attempts to use L1 with field test data have produced partially successful results with HC2 and HC3 data.

The major difficulties encountered in applying L1 to field test data appear to be due to the limitations on

the stability ratio $(\Delta t/(\Delta x)^2)$, restriction on the maximum spatial increment (Δx) which can be used without loss of resolution, and the computer central memory requirements which limit the maximum array dimensions. The central memory requirements could be reduced by use of extended core storage, but that modification would entail extensive reprogramming which was not feasible as part of the present project. The maximum spatial increment for which the model executed correctly was 6 cm. By increasing the array dimensions from the original value of 401 to 1001, a total distance of 6 m could be modelled. The largest time increment (Δt) that could be used with the maximum spatial increment is 40 s. The first five hours of HC2 were simulated using the first 5 m of the cavity, during which time the combustion zone was predicted to advance 30 cm. Attempting to increase the effective particle diameter very much above the sample input data value of 1 cm caused the program to fail.

Various difficulties were encountered in the use of W1 to analyze the two oxygen/steam injection cases. The variables that are used as optimization parameters by the Powell optimization scheme are the carbon monoxide flux and the water flux at the gas exit boundary, the velocity of the combustion zone, and the relative concentration of residual char at the gas entrance boundary. The optimization scheme seeks to match the forward and reverse integration values of seven functions: carbon monoxide flux, water flux, oxygen flux, methane flux, char content of the coal, temperature slope, and temperature. Because the magnitude of the temperature slope is large ($\sim 10^5$) near the leading edge of the combustion zone and is changing rapidly in that region, it is difficult to fit the forward and reverse integration values of the slope function together smoothly. Also, because of the large magnitude of the slope, its values dominate those of the other functions in the optimization procedure, which means that the other functions tend to have discontinuities at the match point.

One of the input parameters to the W1 model specifies the number of forward integration intervals used in an analysis. The optimization procedure is very sensitive to the value of that variable, and it is a trial and error process to determine a proper value for it. Also upper and lower estimates for the temperature at the gas entrance boundary are input data to the model. Appropriate values for those estimates are determined by trial and error also.

The product gas compositions predicted by the model for HC3 and R2 data are shown in Figures 7 and 8. The combustion zone velocity computed by W1 for R2 is in very close agreement with the value calculated from the Data Base: 0.1539 ft/hr vs. 0.1536 ft/hr. The value computed for HC3 is about fifty percent larger than that calculated from the Data Base: 0.0720 ft/hr vs. 0.0462 ft/hr.

Predicted heating values for dry product gases for HC3 and R2 are presented in Table 2 for LEQ, TEQ, and W1, along with the Data Base values for those cases.

M2 results remain very dependent on the time step chosen and the diameter of the link zone, as reported in the initial phase of the project. Furthermore, the Rayleigh exponent has been used as a fitting parameter in the current analyses (as suggested by T.L. Eddy, personal communication). It was given a fixed value in the initial phase of the project. For two of the field tests (H3 and R2), link zone diameters larger than those calculated from the Data Base were required in order to obtain realistic burn-through times and gas temperatures at the production well. All field test data were analyzed first with the same specification of time increments as in the sample data set. The first day was divided into two time steps of three hours each, followed by three time steps of six hours each. After the first day, all time steps were 24 hours. When this procedure produced unreasonably fast burn times (H3, HC2, R1, and R2), uniform time steps of 24 hours were used throughout the simulation. This has the effect of slowing the burn because of constraints in the model for determination of cavity shape. Predicted cavity shapes for all six field tests are shown in Figures 9-14.

Difficulties encountered in using the L2 model result from its extensive

demands on computer resources rather than from the code's capability to process the field test data. Execution times are large which means that the program is relatively expensive to run. The program generates a large output file which can cause problems with the computer's file storage allocation system. The model requires practically all of the available central memory on the Cyber 760 computer, therefore the computer is essentially tied up when L2 is processing.

L2 has successfully analyzed all of the field test data. The only difficulties encountered in data analyses were the result of choosing a spatial grid network which was too large for the array dimensions in the code. It is not feasible to increase the array dimensions because of the central memory constraint on program size. The temperature profile evolution for R2 is less uniform than for HC3. The time steps for R2 chosen by the program during execution are approximately ten times larger than those used for HC3. The R2 computed time steps reach the upper bound on admissible time steps as specified in the sample data set and used for all field test cases.

The L2 simulation of R2 predicted a very slow burn. The maximum temperature was only one-third of the distance from the injection well to the production well after 52 days of simulation time. The elapsed time for the first module of the field test was 40 days. The HC3 simulation predicted burn-through after 39 days; the actual oxygen/steam injection test lasted for 47 days.

M2 and L2 predicted cavity shapes for HC3 and R2 are compared in Figures 1 and 2. L2 predicted gas temperature profiles for HC3 and R2 are shown in Figures 3 and 4.

CONCLUSIONS

The general conclusions presented in the initial report [1] concerning the state-of-the-art of mathematical modelling of forward combustion UCG processes remain valid a year later. The capabilities and computational features of the six models surveyed have been discussed at some length. A more comprehensive and detailed report of this project is being prepared [11]. With malice toward none, it is perhaps most useful to conclude this study with a brief summary of the input data requirements of each model that limit its predictive capacity:

(1) TEQ requires values for water influx, temperature of the production gas, and the in situ heat loss percentage;
(2) LEQ requires temperature and composition of the production gas;
(3) W1 requires injection gas flux (based on combustion cavity diameter) and an accurate initial estimate for the combustion zone velocity;
(4) L1 requires production well pressure, particle size distribution, and cavity permeability;
(5) M2 requires a ratio for coal consumed to oxygen supplied and a diameter for the link zone;
(6) L2 requires production well flow rate and pressure.

Unless the geochemistry and geophysics of the coal seam to be gasified are well known in advance of actual gasification, values for these variables will not be known with any great accuracy. Therefore the ultimate goal of UCG modelling should be to develop a model of sufficient generality that it can be incorporated into a feedback control mechanism; i.e. the model would be given real-time data during gasification (such as product gas flow rate, composition, and temperature), and the model would recommend values for control variables (such as injection gas rate and composition) to achieve efficient operation. Implementation of such a control model should be attainable at the level of laboratory combustion tube experiments without great difficulty; implementation on field scale projects poses a more formidable task.

ACKNOWLEDGMENTS

The authors gratefully acknowledge helpful discussions with Dr. T. C. Bartke, Laramie Project Office; Dr. R. J. Cena, Lawrence Livermore National Laboratory; Dr. T. L. Eddy, Georgia Institute of Technology; Dr. T. F.

Edgar, University of Texas; Dr. R. D. Gunn, University of Wyoming; and Dr. H. W. Haynes, Jr., University of Wyoming. L. J. Fahy of the University of Wyoming Research Corporation kindly assisted in the preparation of this report. Financial support was provided by DOE Cooperative Agreement No. DE-FC01-83FE60177 with the University of Wyoming.

REFERENCES

[1] L. V. Kunselman, D. W. Fausett, and C. G. Mones, "A Comparison of Forward Combustion Gasification Models", Proc. Eighth Underground Coal Conversion Symposium, Keystone, Colorado, 335, August 15-19, 1982.

[2] R. Natarajan , T. F. Edgar, and J. G. Savins, "Prediction of Product Gas Composition for UCG", Proc. Sixth Underground Coal Conversion Symposium, Shangri-La, Oklahoma, VIII-15, July 13-17, 1980.

[3] C. B. Thorsness and R. J. Cena, "A UCG Process Data Base", ibid., VIII-32.

[4] C. B. Thorsness and R. J. Cena, "In Situ Coal Gasification Models", UCRL-82269, 35 pp., February 1979.

[5] H. W. Haynes, Jr., "Steady-State Permeation Model for Underground Coal Gasification", ACS Symposium Series, v. 196, 321, 1982.

[6] H. W. Haynes, Jr., "An Analysis of Permeation Models for In Situ Coal Gasification (Forward Combustion Mode)", Spring National Meeting of AIChE, (Paper No. 36F), Anaheim, California, 32 pp., June 6-10, 1982.

[7] C. B. Thorsness, E. A. Grens, and A. Sherwood, "A One-Dimensional Model for In Situ Coal Gasification", UCRL-52523, 55 pp., August 1978.

[8] S. H. Schwartz, T. L. Eddy, and G. E. Nielsson, "A Simple UCG Cavity Model with Complex Energy Balance", Proc. Sixth Underground Coal Conversion Symposium, Shangri-La, Oklahoma, III-69, July 13-17, 1980.

[9] R. J. Cena, C. B. Thorsness, and L. L. Ott, "Underground Coal Gasification Data Base", UCID-19169 Rev. 1, 622 pp., November 24, 1982.

[10] R. J. Cena and C. B Thorsness, "Lawrence Livermore National Laboratory Underground Coal Gasification Data Base", UCID-19169, August 21, 1981.

[11] L. V. Kunselman and D. W. Fausett, "Survey and Comparison of UCG Forward Combustion Models", to appear as UWYRC Report of Investigations, 1983.

TABLE I. SUMMARY OF INPUT VALUES

	H3	HC2	HC3	P1	R1	R2
Proximate Analysis (wt %)						
Moisture	8.62	30.11	30.11	1.36	14.62	14.62
Ash	28.92	4.05	4.05	11.03	5.07	5.07
Volatile Matter	31.67	32.12	32.12	38.08	35.41	35.41
Fixed Carbon (char)	30.79	33.72	33.72	49.53	44.90	44.90
Coal density (kg/m^3)	1363.	1350.	1350.	1340.	1350.	1350.
Well spacing (m)	18.	18.	30.	17.	18.	76.
Length of test (days)	37.291	43.089	47.138	11.897	29.043	39.917
Injection gas composition						
AR	.0100	.0100	.0010	.0100	.0100	.0001
N_2	.7800	.7800	.0316	.7800	.7800	.0060
O_2	.2100	.2100	.4751	.2100	.2100	.3802
Steam	.0000	.0000	.4923	.0000	.0000	.6138
Coal consumed (m^3)	1727.89	1029.95	2184.97	145.39	776.39	3377.35
Insitu water influx (mol/s)	12.	11.	36.	3.7	9.4	25.
Pressures (kPa)						
injection	455.	297.	299.	2108.	651.	834.
production	322.	279.	296.	441.	520.	674.
Temperatures (K)						
injection	336.6	338.6	383.4	323.2	293.2	448.6
production	682.8	549.3	612.2	613.6	624.8	555.4
Gas flows (mol/s)						
injection	57.	46.	41.	24.	32.	34.
production	93.	66.	104.	39.	62.	116.

TABLE II. HEATING VALUE OF DRY PRODUCT GAS (kJ/mol)

	D.B.	LEQ	TEQ	WI
HC3	189	195	191	172
R2	303	313	233	247

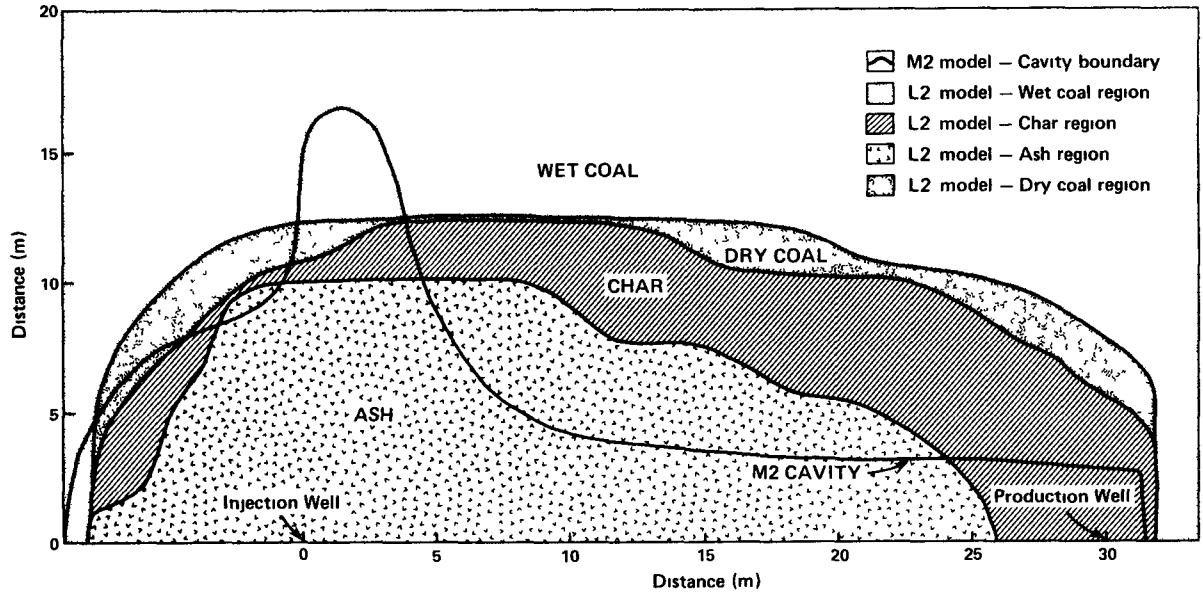

Figure 1. Hoe Creek III predicted cavity shape after 38 days

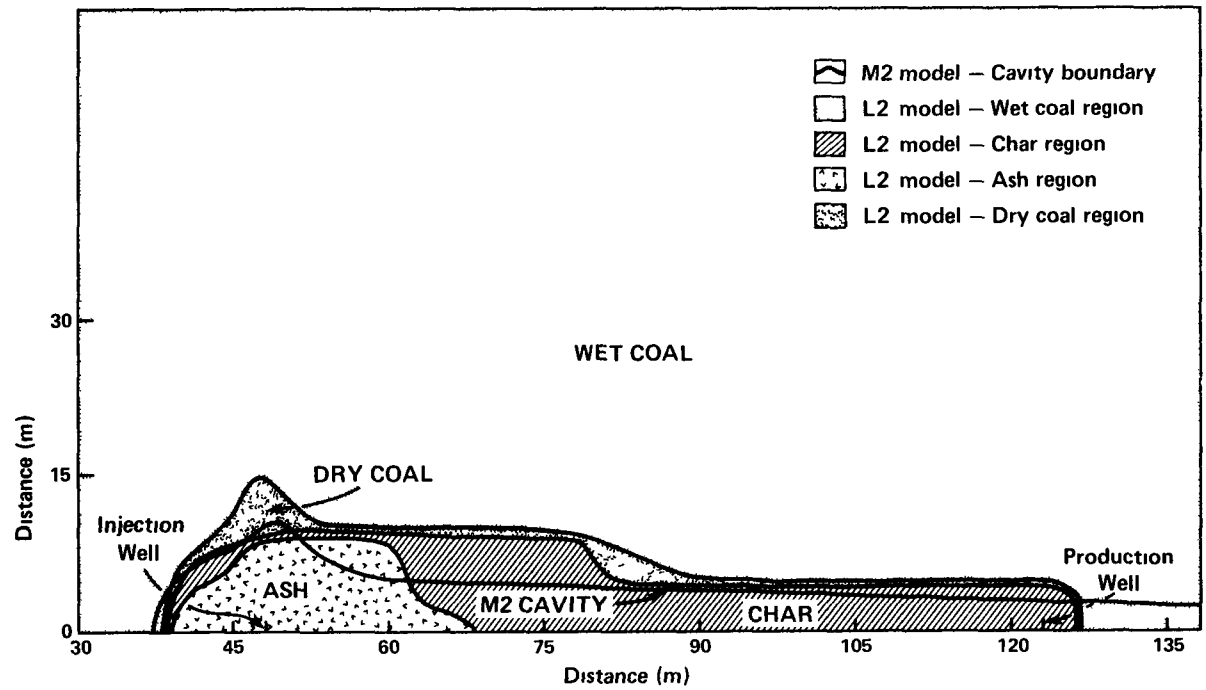

Figure 2. Rawlins II predicted cavity shape after 40 days

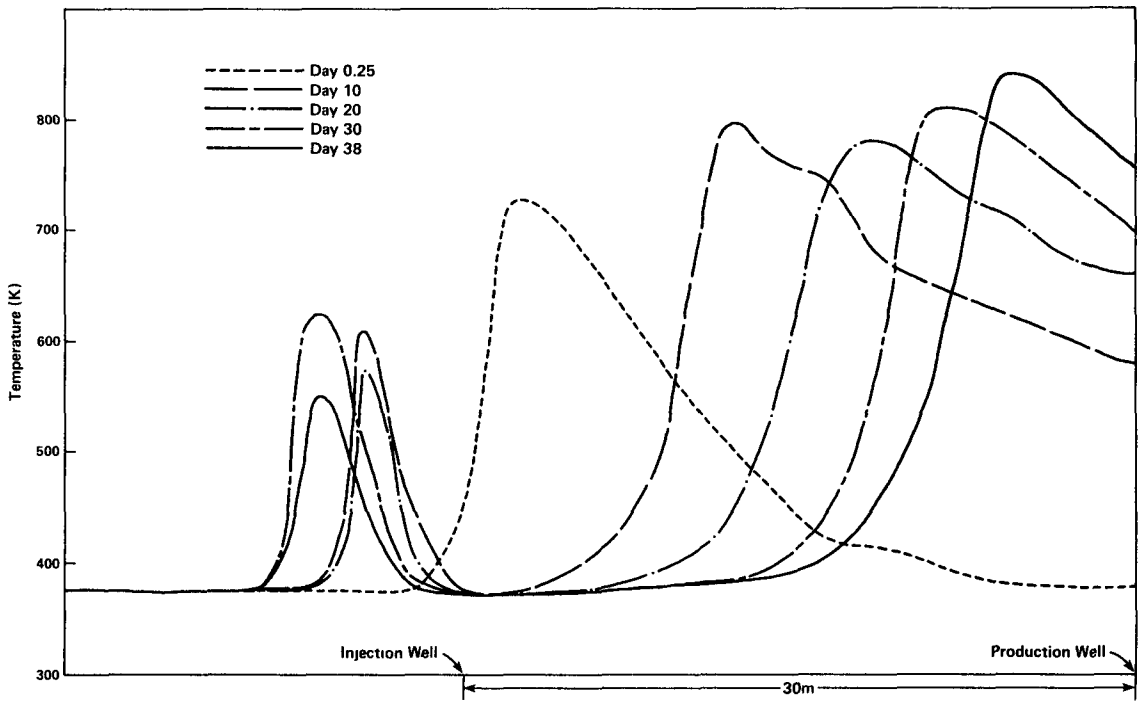

Figure 3. Hoe Creek III gas temperature profile evolution from L2 model

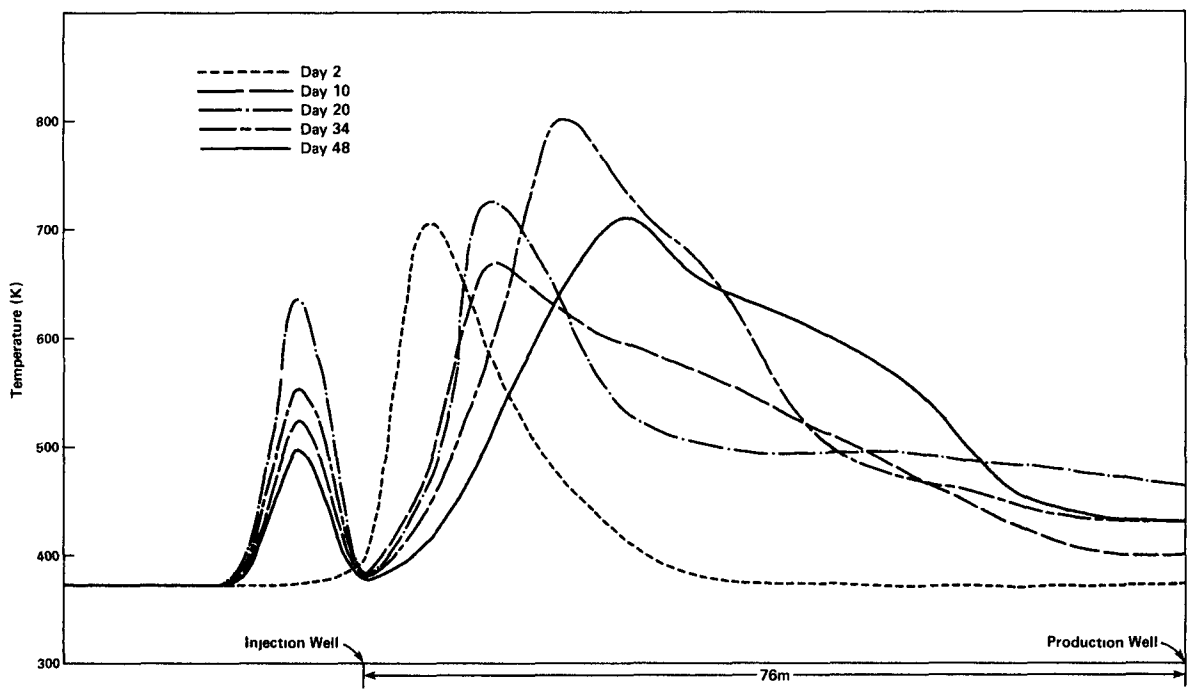

Figure 4. Rawlins II gas temperature profile evolution from L2 model

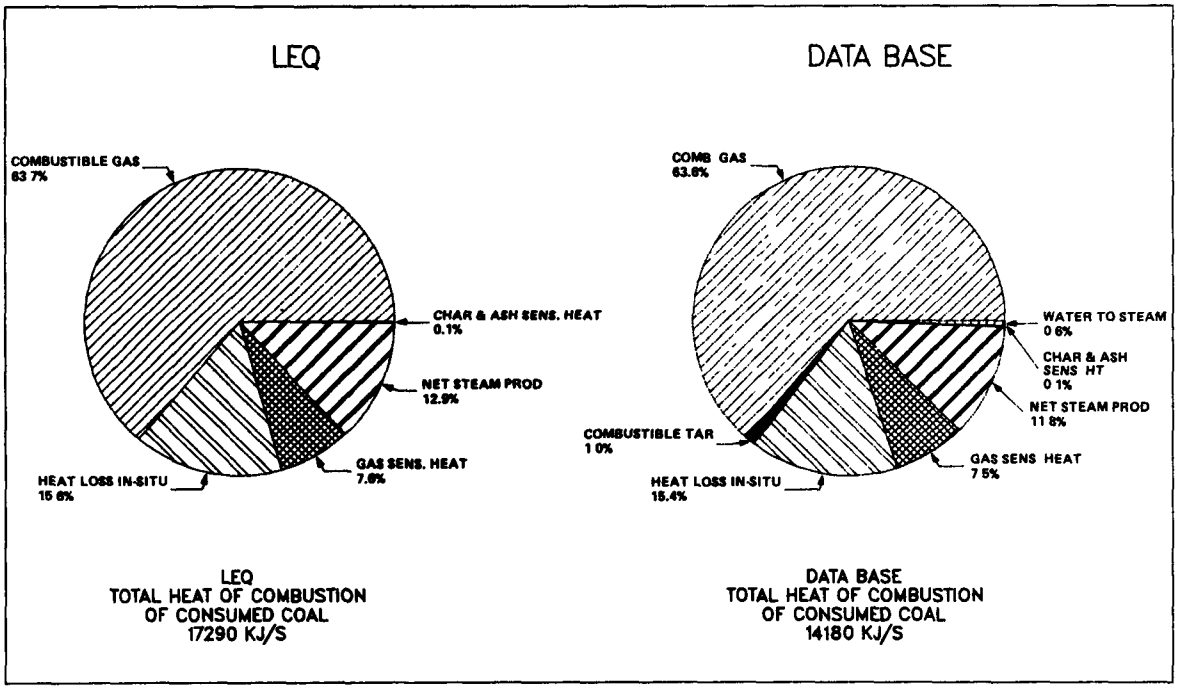

Figure 5. Hoe Creek III energy distribution

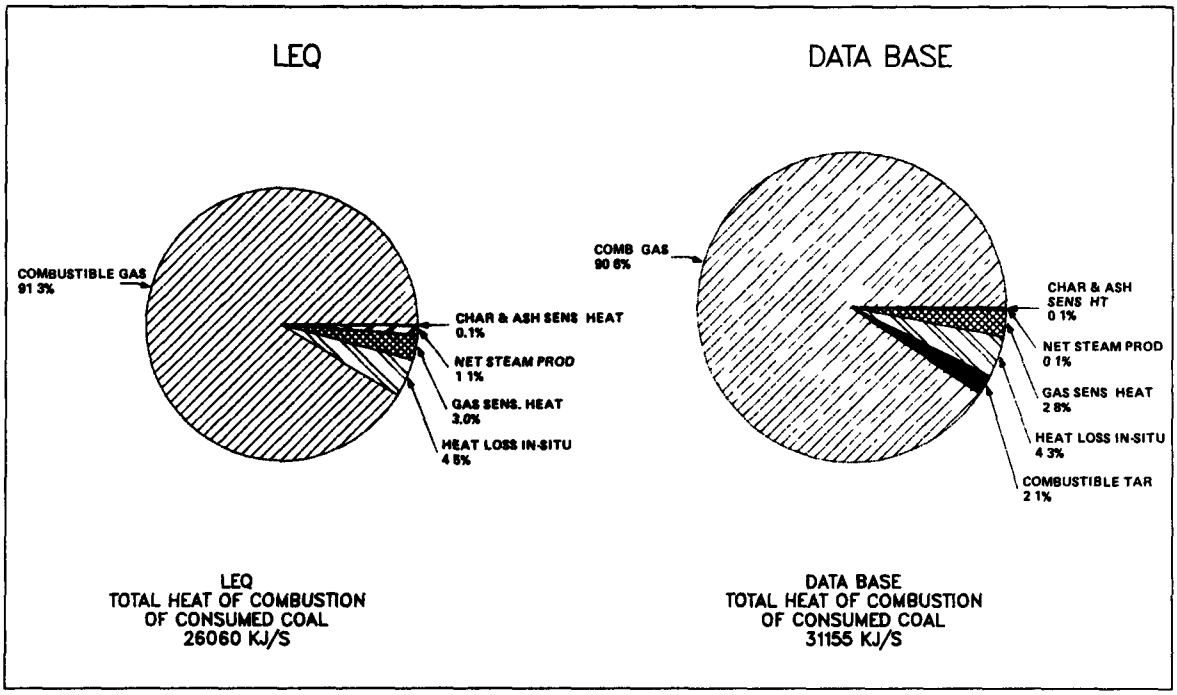

Figure 6. Rawlins II energy distribution

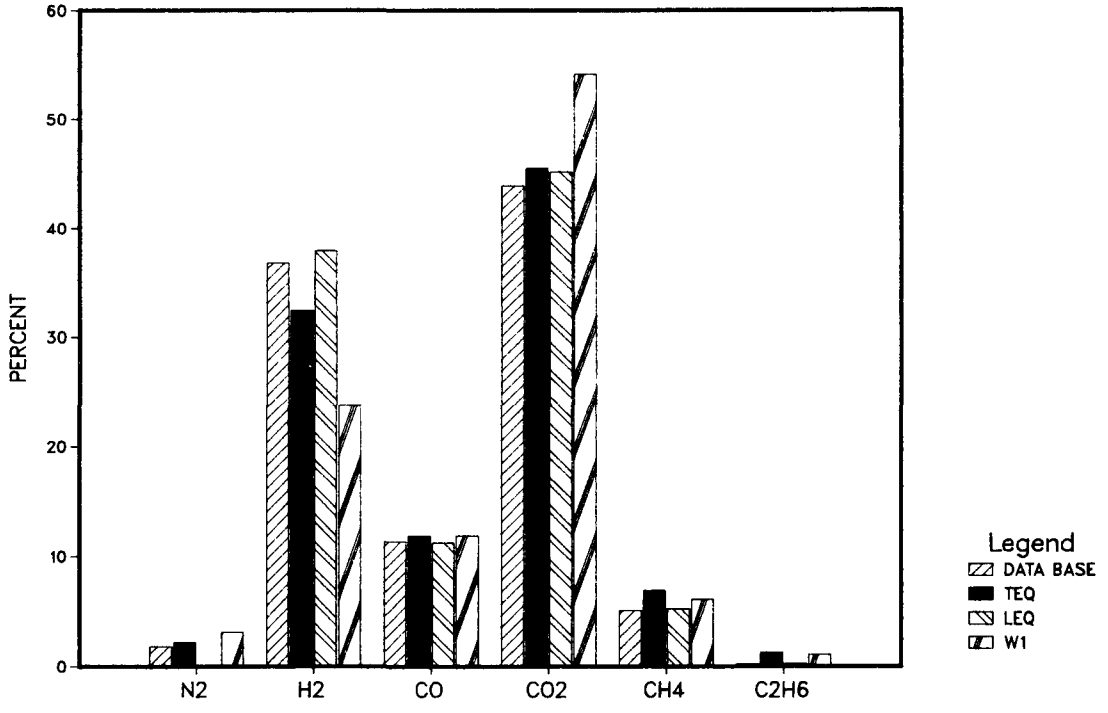

Figure 7. Hoe Creek III dry product gas composition

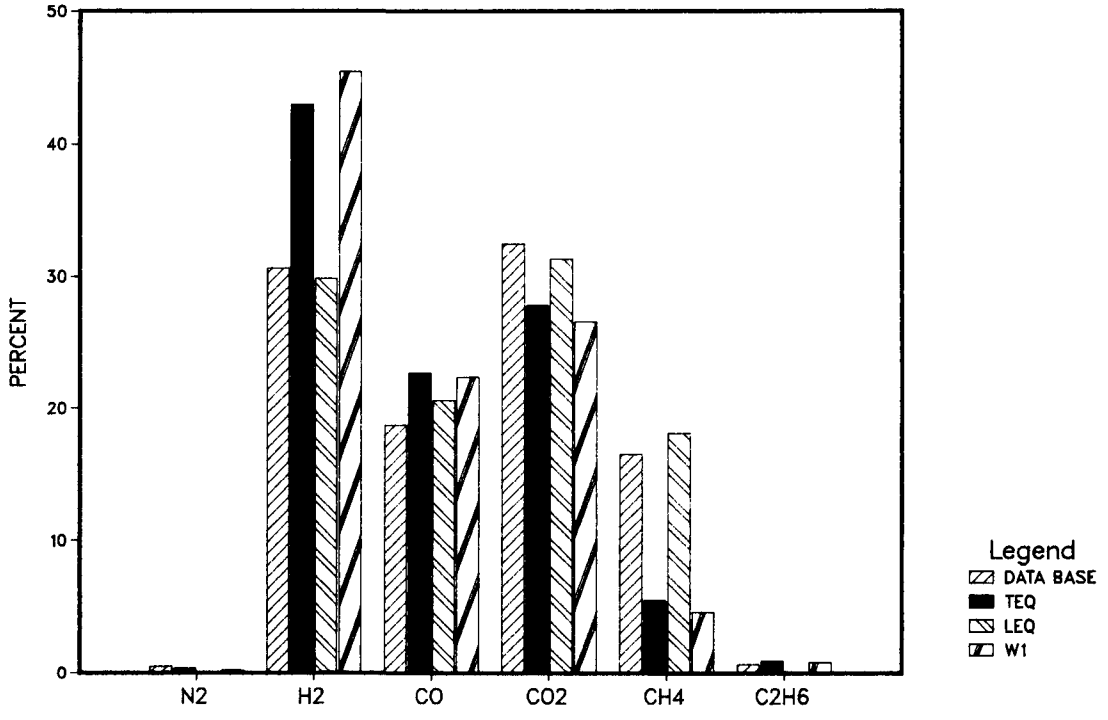

Figure 8. Rawlins II dry product gas composition

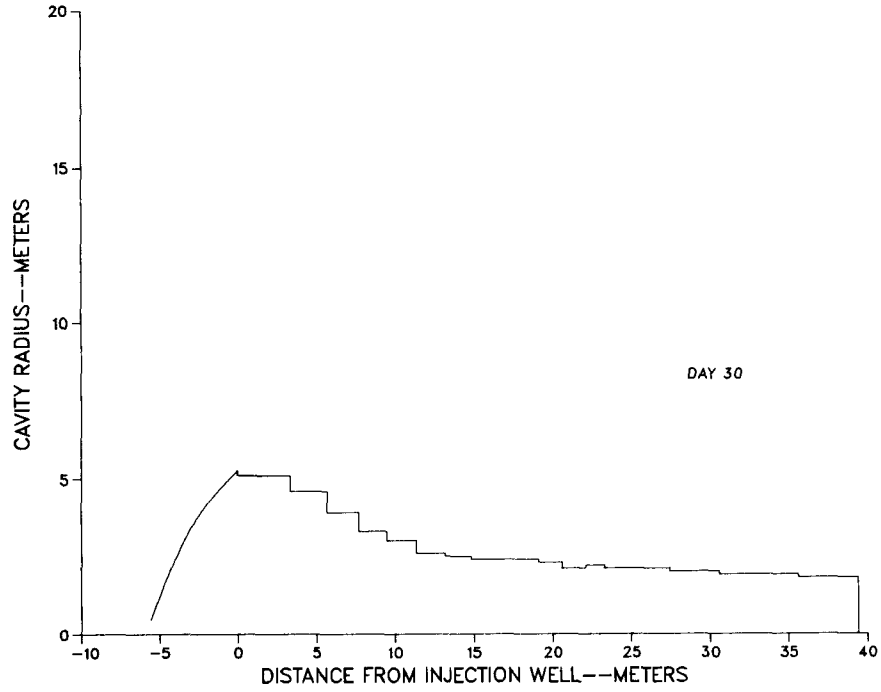

Figure 9. Rawlins I predicted cavity shape from M2 model

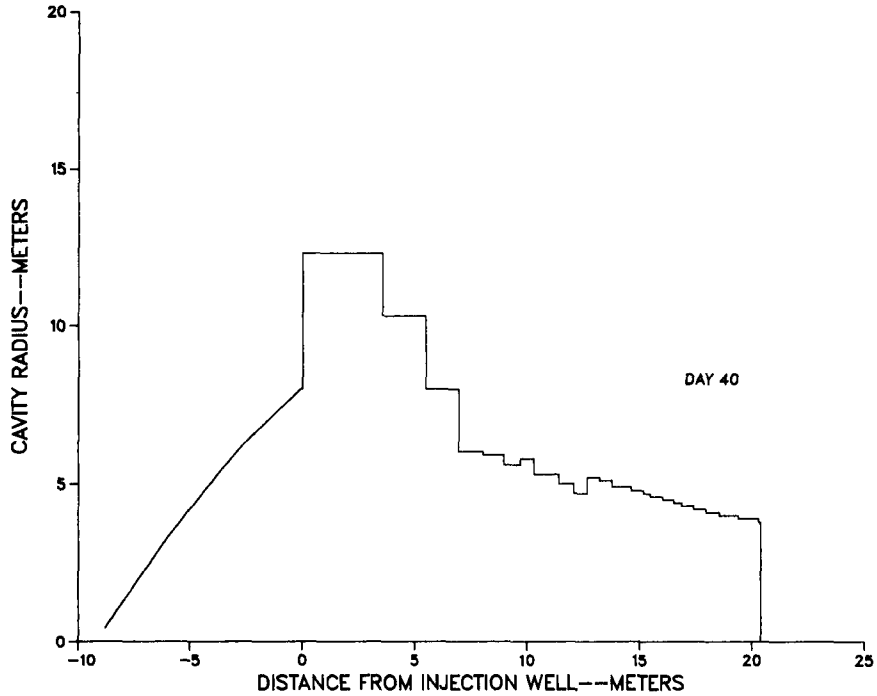

Figure 10. Hanna III predicted cavity shape from M2 model

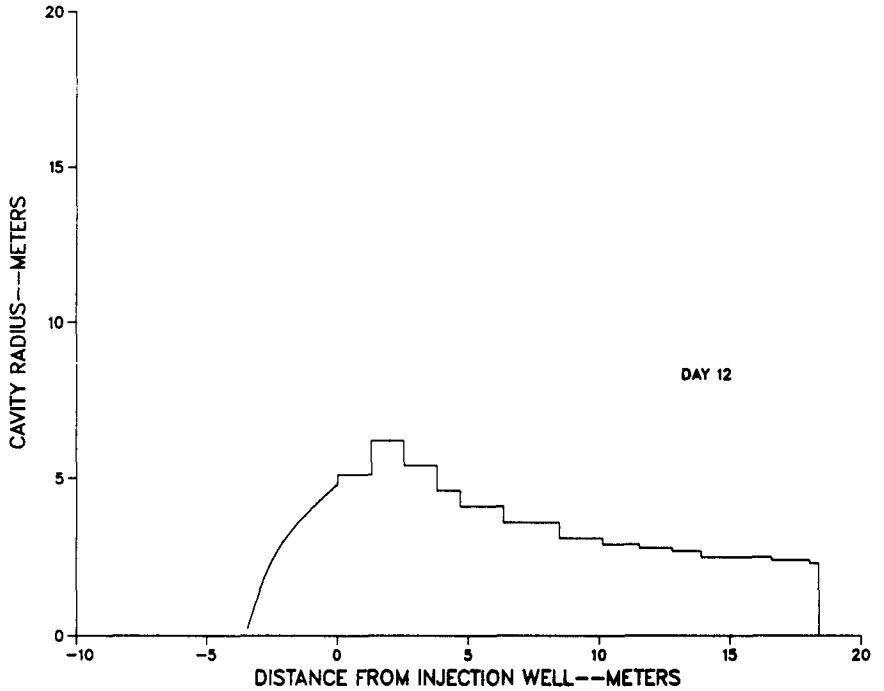

Figure 11. Pricetown I predicted cavity shape from M2 model

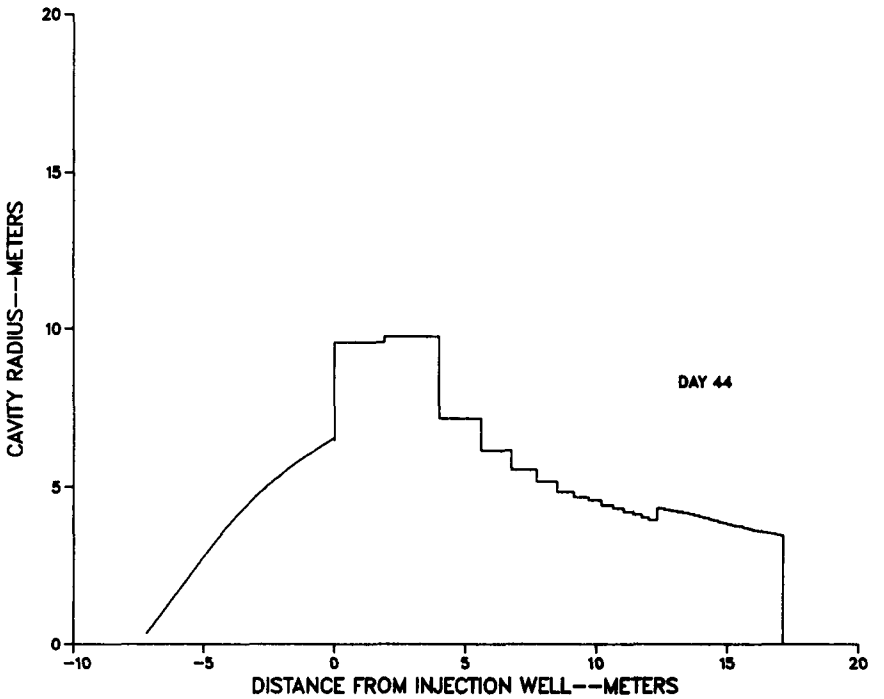

Figure 12. Hoe Creek II predicted cavity shape from M2 model

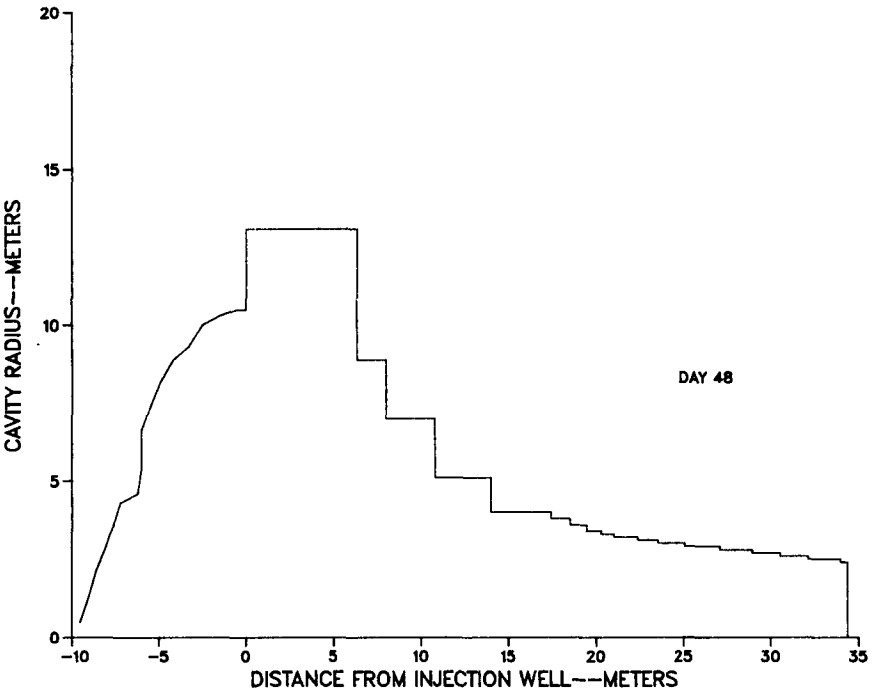

Figure 13. Hoe Creek III predicted cavity shape from M2 model

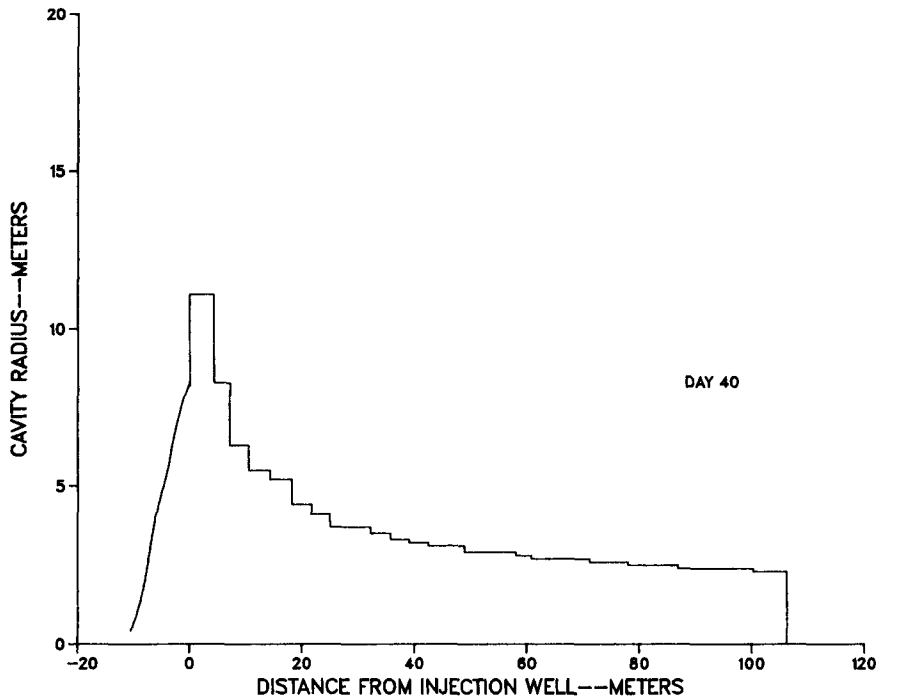

Figure 14. Rawlins II predicted cavity shape from M2 model

2.18 CONCLUSIONS FROM MODELING THE FINAL DATA OF PRICETOWN I

by

R. T. Gibbs and T. L. Eddy 1/

ABSTRACT

Modeling the Pricetown I field test using the final, corrected data has resulted in two major conclusions. First, the link enhancement phase proceeded under two different flow regimes. A "sub-laminar" flow regime during the initial period when the flow rate was less than 50 SCFM and a "laminar" flow regime when the flow rate exceeded 150 SCFM. The latter increased the pore size which increased the oxygen transport to the virgin coal/char, wall thus greatly decreasing the time necessary to get flows comensurate to gasification. Second, modeling the combined reactor and downstream gasification process resulted in the surprising conclusion that the water-gas reaction was negligible. The product gas components were apparently provided by oxidation/reduction of the char link via oxygen and carbon dioxide alone with down stream devolatilization. Most of the methane appears to come from devoltilization. Outgasing does not explain the constant percentage and significant methane supply. The gasification results appear to be due to the relatively dry seam at the site, the relatively large char link zone developed prior to gasification and to

1/ Mechanical Engineering, Georgia Institute of Technology, Atlanta, Georgia 30332

The results at Pricetown I indicate a need to understand the link enchancement mechanisms in bituminous coals and to research methods to further decrease link enchancement times. The modeling and the results show that it is imperative to utilize steam/oxygen injection to provide adequate temperatures to sustain combustion, disseminate tars and potential plugging problems, and to provide an optimum product gas for commercialization.

INTRODUCTION

The purpose of this work was to apply the underground coal gasification models previously developed [1-3] to the final Pricetown I field test computerized data as corrected by the Mound Facility [4]. Other papers and reports have discussed the general results of the field test [5], results from the mass balance analysis [6] and the post burn core analysis [7]. This paper presents the summary results of the application of two thermodynamic UCG computer models with input from references [4-7] to estimate the cavity shape, temperature profile, and coal recovery efficiency. The details of the calculations using the link enhancement and gasification models are beyond the scope of this paper and are presented elsewhere [8].

At the Pricetown I field test three veritical production/injection wells (P/I-1, 2 and 3) make up a column of two-well pairs along a generally common axis. Preliminary investigations [3] of the experimental data from the Princetown I burn suggested the following classification by four general process phases:

1. An air acceptance phase which forms an air bubble by "dewatering" region between the two wells. Flows are generally very low (about 10 SCFM or 17 m^3/hr) and pressure drops high (several tens of atmospheres).

2. An initial linking phase which increases the permeability between wells via reverse combustion linking (RCL), hydrofracking, electrolinking, drilling a borehole, or other means. Flow rates may double or triple and pressure drops decrease, but not proportionately. Once started, RCL is usually completed without interruption. "Reverse" indicates the burn front moves opposite to the flow direction, which enhances the increased product gas flow rate and oil and tar removal.

3. A link enhancement phase usually occurs next because the flow rates are not yet adequate to support combustion of the fixed carbon or char. Usually combustion link enhancement (CLE) is used. The mechanisms of the burn are much different than in the case of 2 above. The mechanism for mass transfer to the burn front in CLE is analogous to the mass transfer to the side walls in a packed bed reactor.

4. As the link grows, flow rates increase, pressure drops decrease and finally, sufficient oxygen is obtained to sustain combustion of the char/coke link itself and forward gasification commences.

Table 1. Phases of the Pricetown I field test for computer modeling.

Phase	Starting Date/Time	Burn Date	Stages	Approx. Phase[6]
1 RCL-23	6/9/79 - 12:30	0	1	RCL - 1
2 CLE-23	6/15/79 - 10:15	6.0	25	RCL - 2
3 RCL-12	7/9/79 - 14:10	30.1	2	RCL - 3
4 CLE-123A	7/23/79 - 12:30	44.0	13	LE - 1
5 CLE-123B	8/19/79 - 8:00	70.7	11	LE - 2
6 FG	9/23/79 - 14:30	106.1	11	FG
End	10/5/79 - 9:10	117.8	-	-

Table 2. Selected time - averaged values for each phase.

Phase	Flow Direction	Rounded Duration (days)	Flow (SCFM) In	Flow (SCFM) Out	Well Pres. (PSIA) Inj	Well Pres. (PSIA) Prod	$\frac{CO}{CO_2}$	$R_{C/H}$	$R_{vm/o}$	$R_{ch/o}$	$R_{c/o}$
RCL-23	3-2	6.00	35	31	829	108	0.48	3.80	3.93	---	---
CLE-23	3-2	7.75	45	56	495	170	0.58	5.61	1.26		
	2-3	16.38	25	42	367	121	0.71	4.73	2.43		
	Phase	24.13	31	46	408	137	0.67	5.01	2.05	---	---
RCL-12	1-2	13.88	14	21	773	136	0.38	3.54	1.46	---	---
CLE-123A	1-2,3	20.12	29	48	303	151	0.36	5.88	1.41		
	2-1	2.38	14	23	405	178	0.34	5.42	3.74		
	3-1,2	4.25	42	66	228	159	0.77	5.94	1.29		
	Phase	26.75	30	49	300	155	0.42	5.85	1.60	---	---
CLE-123B	1-2,3	35.38	182	303	322	55	0.69	4.78	1.62	---	---
FG	1-2,3	11.75	1203	1982	303	88	1.99	9.71	0.562	0.549	0.789

Table 3. Summary of tons of coal consumed and affected as well as mass consumption efficiency (η_m) based on product gas composition and injected air flow rates and intervals.

Phase	Volatile Matter 1/ Affected (tons)	Volatile Matter 1/ Consumed (tons)	Volatile Matter 1/ Consumed (%)	Char 2/ Consumed (tons)	Coal Affected 3/ (tons)	Coal Affected 3/ (%)	Coal Consumed 4/ (tons)	Coal Consumed 4/ η_m(%)
RCL 23	3.18	2.46	77.5	--	8.35	38.1	2.46	29.5
CLE 23	15.40	14.08	91.4	0.34	40.43	38.1	14.42	35.7
RCL 12	4.96	3.40	72.5	--	12.32	38.1	3.40	27.6
CLE 123A	11.60	10.96	94.5	1.00	30.46	38.1	11.96	39.3
CLE 123B	116.01	111.47	96.1	0.84	304.65	38.1	112.31	36.9
Sub Total	150.88	142.37	94.4	2.18	396.21	38.1	144.55	36.5
FG	101.49	96.42	95.0 5/	95.85	266.52	74.0	192.27	72.1
TOTAL	247.30	238.79	96.6	98.03	662.73	52.1	336.82	50.8

1/ The volatile matter affected is based on the available $R_{C/H}$ ratio (Eq. 2.16), for the volatile matter (f 5.00) assuming that 100% of the hydrogen in the voltile matter is released. The volatile matter consumed is based on the actual $R_{C/H}$ ratio (Eq. 2.15).

2/ The char consumed is determined from the amount of carbon consumed, over and above that obtained from the volatile matter affected.

3/ The percent of coal affected during linking is assumed to equal the voltile matter divided by Y_{vm}(=38.1% here). The coal affected during foward gasification includes the conservative assumption that 95% of the voltile matter was consumed. If downstream devoltilization is less efficient than the overall linking process than a significantly larger coal region could be effected ($\gtrsim$ 20% larger).

4/ The mass consumptionn efficiency is the total "coal-material" consumed divided by the total coal affected.

5/ Approximately 95% is assumed based on the overall linking value.

COAL CONSUMED AND AFFECTED

The data of [Ref 4] has been averaged into 63 stages over the five phases shown in Table 1. Time averaged values over the phases are presented in Table 2. Details regarding the averaging are presented elsewhere [8].

Linking (RCL and CLE)

During linking, the temperature remains below approximately 1200°F [3] and the products appear to come from devolatilization enhanced by oxidation, without any significant oxidation of fixed carbon (char or coke).

Forward Gasification

The total averages of the linking data (Table 3) show that 95% or more of the link zone has been devolatilized. Our CLE computer model (Figure 1 shows that the volatile matter in the virgin coal is 15 feet or more away from the injection well. Whole coal "gasification" is therefore improbable over much of the burn and relations to be utilized must assume local gasification of char followed by downstream devolatilization of whole coal via heat transfer from the hot product gas. When the gasification reaction comes to within a certain distance from

the virgin coal wall, it is assumed that volatile matter and fixed carbon are removed in proportion to their respective concentrations in the virgin coal. The forward gasification computer program selects either method depending upon the proximity of the virgin coal wall to the burn front. The computer model uses the value of the mass ratio of char removed to oxygen supplied ($R_{ch/o}$), calculated from the product gas composition, plus thermal devolatilization downstream (as determined by mass and energy balances on a given k-th segment) when gasifying char. When the cavity comes within an experimentally determined distance of the virgin coal, the model uses the mass ratio of coal removed to oxygen supplied ($R_{c/o}$), plus thermal devolatilization downstream.

The amount of water available is apparently insignificant, which gives further evidence of the lack of any significant steam gasification or shift conversion occuring over the burn. Just partial oxidation of the char locally and thermal devolatilization downstream apparently occurred. A summary of the coal consumed and affected for each phase is presented in Table 3 from which we conclude the following.

1. There is no significant gasification (char removal via CO_2 or water gas reduction) during any of the linking phases.

2. The volatile matter removal efficiency during reverse combustion linking was about 75%.

3. The volatile matter removal efficiency during combustion linking enhancement was about 95%.

4. The apparent "forward gasification" mass removal efficiency was 72%.

5. The apparent overall "coal" mass removal efficiency was 51%.

6. An estimated 663 tons of coal were affected by the field test. Approximately 239 tons of volatile matter and 98 tons of char (fixed carbon) were removed.

These sums do not include the affected coal providing the tars left down hole or in the knockout pot(s). Items 4) and 5) are somewhat deceiving because of the extensive size of the link prior to gasification and subsequent relatively early stoppage of the burn, as dicussed below, hence the term "apparent."

RESULTS

Linking

The CLE model is based on gas flow through a porous duct. The initial geometry is determined by the RCL burn which is closed assuming a "hemisphere" on each end. The following mechanisms are assumed to occur. Oxygen flowing through the porous duct does not react with the char during CLE. The oxygen diffuses to the link/coal wall interface by convective diffusion. Partial oxidation of the volatile matter releases thermal energy which in part devolatizes more voltile matter, in part is convected/conducted/radiated away, and in part is absorbed by the new formed char link. In the CLE model, only a simple chemical energy balance including the exothermic energy of combustion, the endothermic latent heat of the volatile matter, and the enthalpy of the char are considered. The experimental temperature histories tend to support the assumption that reactions in the bulk flow are negligible. The basic features included in the CLE model are:

1. a variable-eight sector geometry for mass and energy balances in the hemisphere,

2. lumped chemical reactions,

3. vortex mixing of product and blast flows with exponential decay,

4. restricted flow availability,

5. a combined chemical-latent-sensible energy balance,

6. specified wall and gas bulk temperatures from thermocouple measurements, and

7. the gas to wall convective mass transfer of oxygen.

The following is our interpretation of how the burn developed based on the product gas analysis, monitor well thermocouple temperatures, post-burn coring results, and the temperature-calculating/cavity-shape-determining computer models.

The initial RCL-23 phase from P/I-2 to P/I-3 proceeded smoothly and directly with an average injection flow rate of 35 SCFM. It provided a link with an effective diameter of 2.39 ft and a porosity of about 30%.

The ensuing CLE-23 phase between P/I-2 and P/I-3 alternated flow direction, and intensity, averaging about 31 SCFM. By the end of the phase the affected region should approximate the shape shown in Figure 1a as calculated by the CLE computer model. The affected region should have a porosity of approximately 38%, an approximate pore diameter of 0.00041 ft, and a terminal velocity critical length of 0.0123 ft or approximately 30 pore diameters. The natural convection correlation is found to be $Nu = 1.67\ Ra^{0.167}$, which indicates a "sub-laminar" range.

The RCL-12 phase from P/I-2 to P/I-1 proceeded smoothly and directly with an average injection flow rate of 14 SCFM. It provided a link with an effective diameter of 2.56 ft and a porosity of about 27%.

The first phase (A) of CLE-123 between P/I-1 and P/I-2 or P/I-3 alternated in flow direction and intensity which averaged about 30 SCFM. By the end of phase A the affected region should approximate the shape shown in Fig. 1.b as calculated by the CLE computer model. Most of the coal affected is between P/I-1 and P/I-2, which should have a porosity of approximately 36%, and effective pore diameter of about 0.00044 ft, and a terminal velocity characteristic length of 0.0123 ft. or 28 diameters. The natural convection correlation is again found to be $Nu = 1.67\ Ra^{0.167}$ which again incidates a "sub-laminar" flow regime.

The second phase (B) of CLE-123 was constant in flow direction. The intensity averaged about 182 SCFM. By the end of the CLE-123B the link shape formed develops as shown in Fig. 1c as calculated by the CLE computer model. The larger flow rates apparently caused a "laminar" flow regime giving a natural convection correlation of $Nu = 0.15\ Ra^{0.25}$. The porosity remains about 35% but the effective pore diameter doubled to about 0.00080 ft accompanying an increase in the terminal velocity characteristic length to 0.050 ft or about 63 diameters.

The forced convection correlation based on flow through a porous media in an entrance region is included in the CLE computer model but it contributes negligibly to the heat and mass transfer between bulk gas flow and the virgin coal wall in all the CLE phases encountered herein. The "forced" and "natural" convective flows are not coupled mathematically; hence, it appears that the only impact of the increases flow rate (other than providing more total oxygen) is to increase the effective pore size and thus the terminal velocity for the natural convective mechanism.

Forward Gasification

In the forward gasification (FG) phase, the flow of about 1203 SCFM proceeded from P/I-1 to P/I-2 and P/I-3. The large devolatilized link zone around P/I-1 (See Fig. 1c) and the apparent shortage of water (as steam) in the reacting zone contributed to a gasification process consisting mainly of the (partial?) oxidation of char and possibly and CO_2-char reduction reaction. This was followed downstream by thermal devolatilization when the hot combustion gases "contacted" the virgin coal as the gases flowed from the cavity through the link to the production well(s). The above hypothesis was validated by the chemical reaction mass balance using the final product gas compositions. Though both the water-gas and water-gas shift reactions were included, the product gas composition indicated that neither reaction was significant over the FG burn. The major basis for this result is that the methane in the product gas must come from downstream devolatilization. (The temperatures are too high for methanization).

The original calculation for the FG data was based on a coal gasification mass balance in which the coal in question was devolatilized and then gasified. Some char remained which is accounted for by calculating the "fraction of char removed". Actually the voltile matter is removed from a different piece of coal than that from which the char is being "gasified." The two processes are uncoupled except that the FG computer model must put them together in the right way to obtain tons removed corresponding to Table 3.

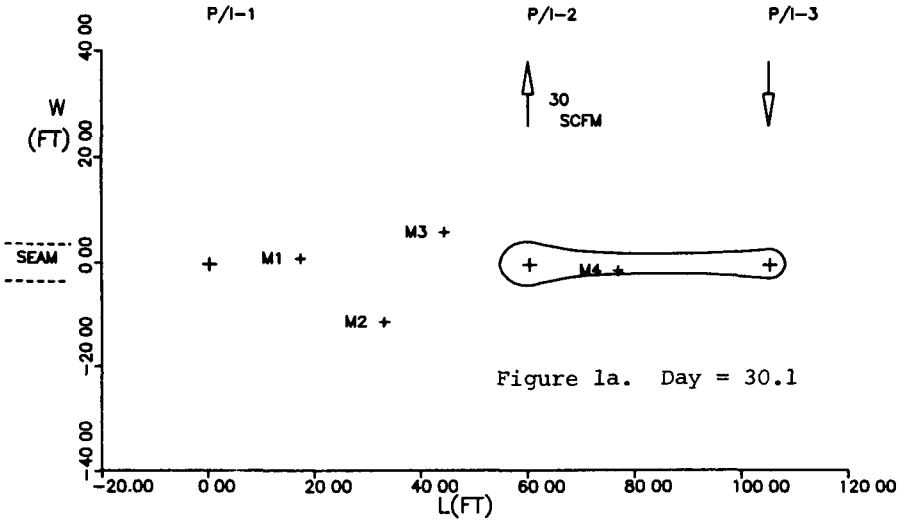

Figure 1a. Day = 30.1

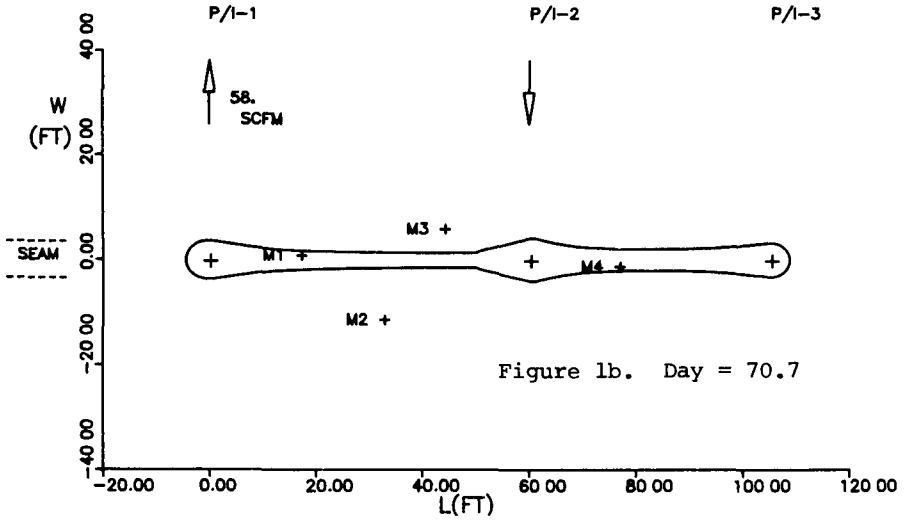

Figure 1b. Day = 70.7

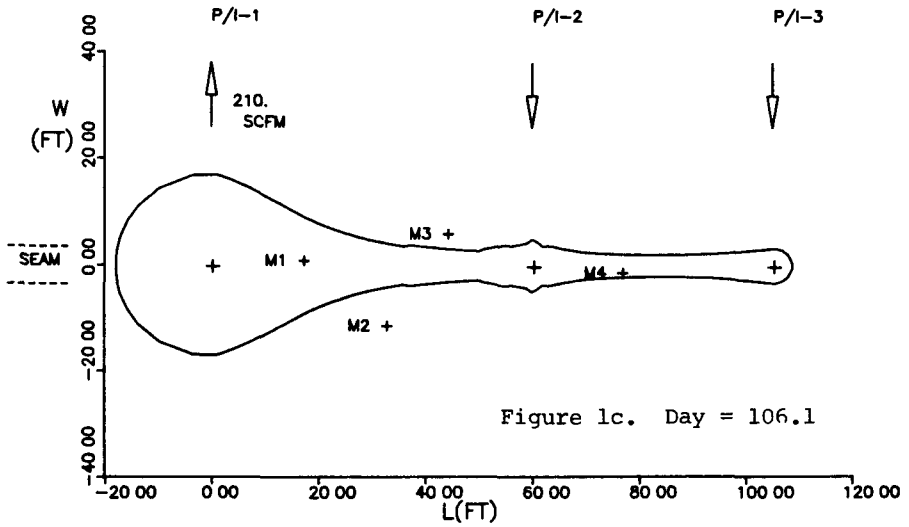

Figure 1c. Day = 106.1

Figure 1. Plan view of CLE model computed line zone geometry after a) the sub-laminar link enhancement between wells 2 and 3, b) the sub-laminar link enhancement between wells 1, 2 and 3, and c) the laminar link enhancement between wells 1, 2 and 3.

At the end of the burn, the forward gasification process had just reached monitoring well M3 and was devolatilizing at M2 as indicated by thermocouple responses [3]. The FG computer model cavity must then just reach M3 and be in the vicinity of M2 at the end of the burn. Under the present conditions that is difficult to do because the amount of gasification is low compared to the amount of oxygen supplied. It was only accomplished by assuming that 80% of the car did not react, i.e. 20% of the char did react. Based on whole coal, this means that only 49% of the coal was removed locally via RCL, CLE and FG. The effective coal seam height of Pricetown I was 7 ft; therefore, the resulting cavity averages 3,44 ft high. In the previous report [3], it had been necessary to assume that half the char was removed locally throughout the gasification process. The two methods give similar results. Figure 2 shows a 3-D projection of the calculated final cavity. The development of the FG computer model calculated cavity and affected region is shown in Fig. 3.

Figure 2 also includes the core well locations (C1, C3 and C4) that were found to intersect the cavity. The results of the electric density logs and coring appear to be the following [7]. At C1 a 1.5 to 2 ft void was found above 5 ft of ash. This completely burned out region lay above a 3 ft layer of hardened slag. There was little rubblization at this probably widest part of the cavity. The presumed ash was unrecoverable and listed as a "void" in the core reslts. At C3 the electric log again suggested a 2 ft void above a rubble filled cavity. The core results indicated a 6 ft void with 1 to 1.5 ft of coal rubble and slag at the bottom. Again there was negligible rubblization from the overburden. At C4 the electric density log indicated a 5 ft void while the coring indicated 8 ft of void. The 1 ft overlying seam of coal was in place but the 1 ft shale layer between it and the main seam was missing. Since the average cavity height is "predicted" to be 3.44 ft the cavity cross section probably slopes from about six (6) ft at the center to 1-2 ft at the edge. This result is supported by thermocouple temperature values.

Wall and gas temperatures predicted by the model (using the optically thin gas assumption) are plotted in Figs. 4

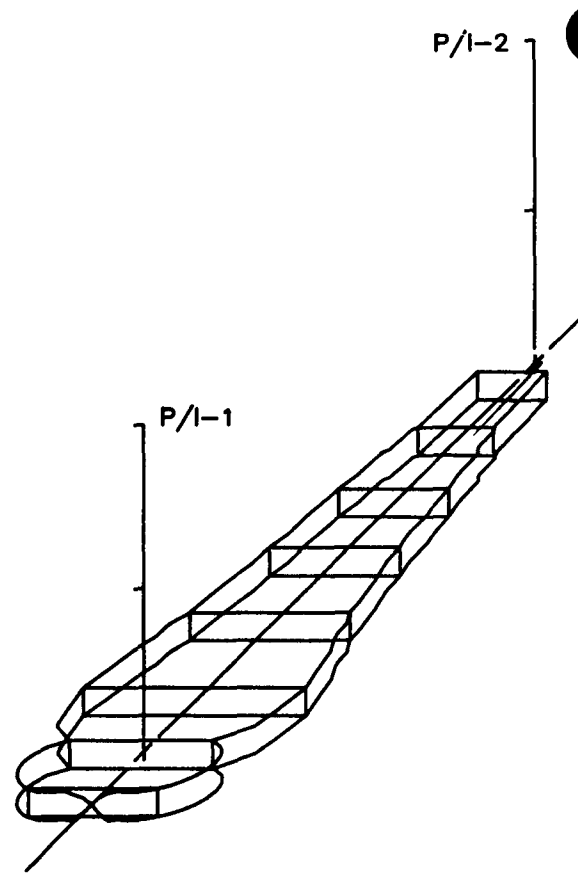

Figure 2. Three-dimensional plot of FG model computed cavity geometry at the end of forward gasification.

and 5, respectively, for various days of forward gasification. The wall temperature oscillations shown are a result of the finite difference scheme and the sensitive range of convergence with the wall radiation terms. Time limitations precluded improving the convergence scheme further. The temperatures calculated are much lower than the values obtained previously [3]. The lower temperatures are a result of the smaller energy source term with the present reactions (the partial oxidation of char), as well as a variable burden wall temperature calculation. The low temperatures predicted by the model suggest that actually a two step process (oxidation of char followed by char - CO_2 reduction) may be more appropriate than the single step (partial oxidation of the char to CO and CO_2) process assumed herein.

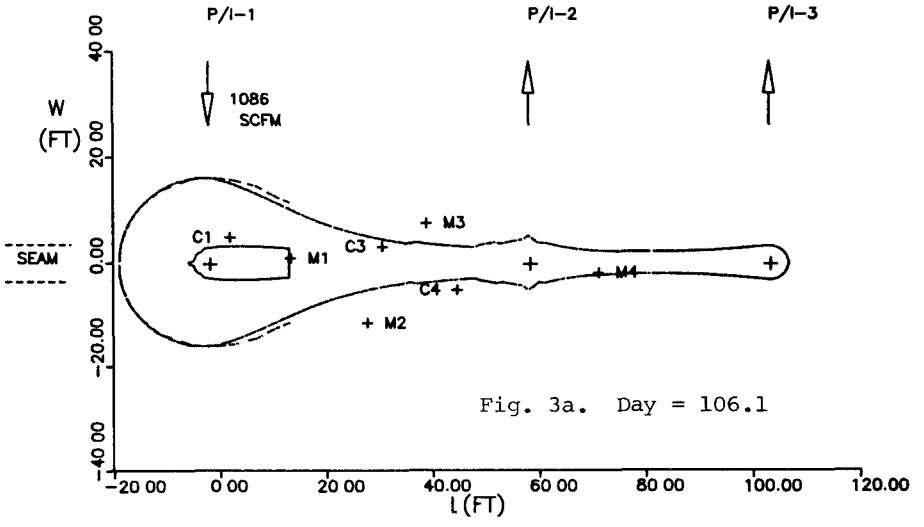

Fig. 3a. Day = 106.1

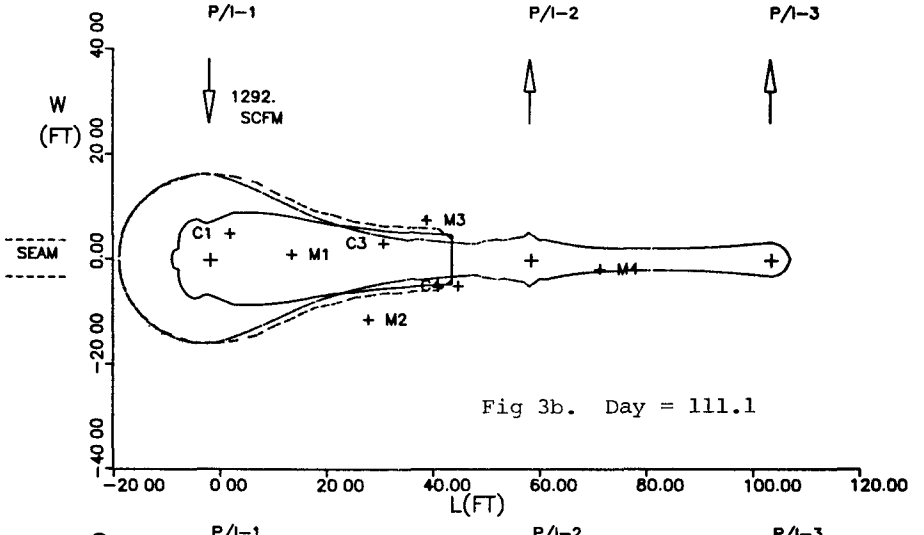

Fig 3b. Day = 111.1

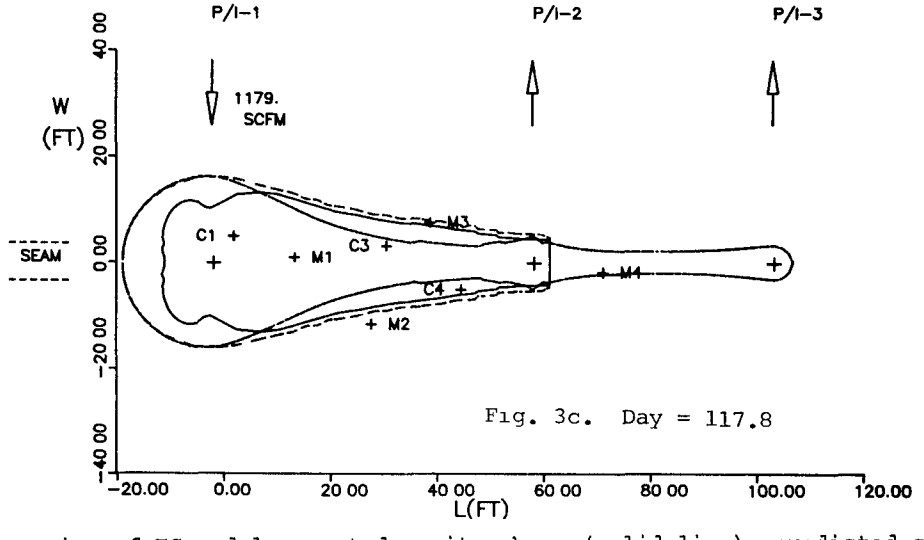

Fig. 3c. Day = 117.8

Figure 3. Plan view of FG model computed cavity shape (solid line), predicted char region (long-dashed line), and initial link zone region (short dashed line) after the a) first, b) sixth, and c) last day of forward gasification.

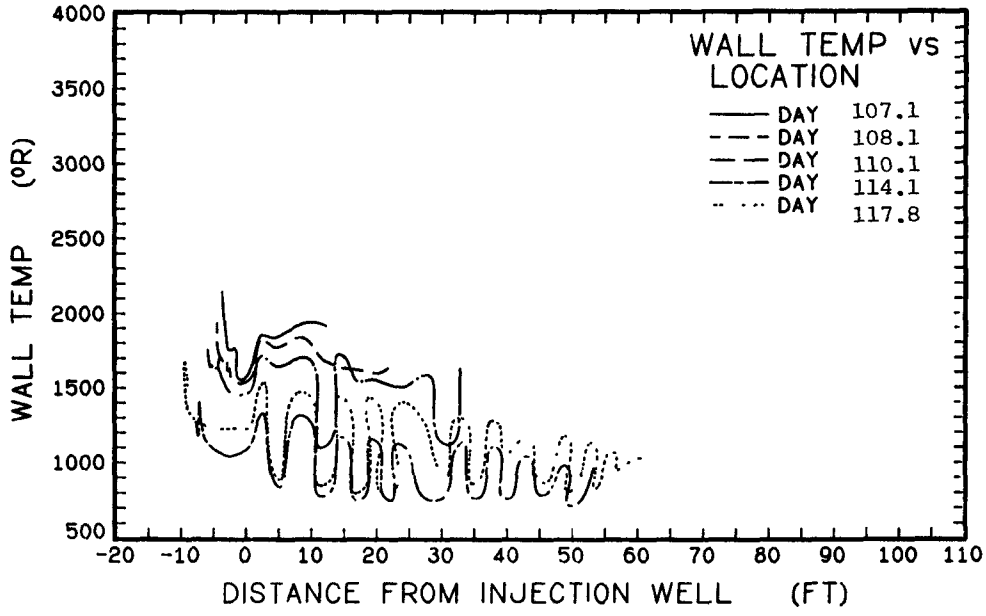

Figure 4. Wall temperatures during forward gasification assuming optically thin radiation in cavity.

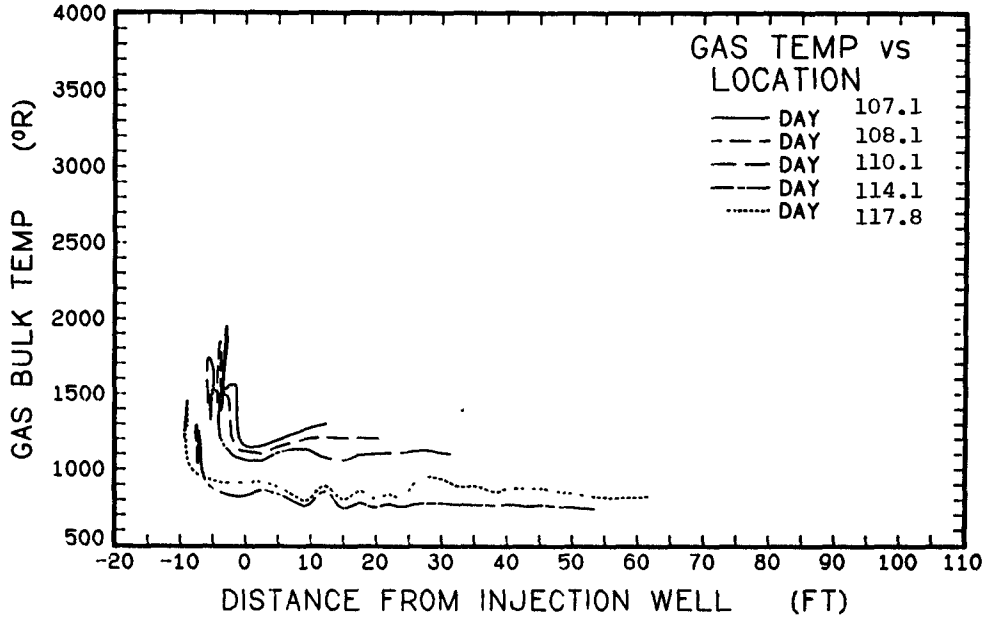

Figure 5. Gas bulk temperatures during forward gasification assuming optically thin radiation in cavity.

In this and the previous model, the temperature drops significantly after four days, when the major portion of the cavity wall area is exposed burden.

The optically thick gas option was run for the same input values. The predicted cavity shape was similar to the former but was larger near the injection well and smaller downstream near M2 and M3 monitoring wells. Predicted wall and gas teperatures indicated abnormally high values in the injection region because the radiation is absorbed immediately in the mixed gas region next to the wall. Though the optically thick program runs about 10 times faster than the optically thin program, it appears that the optically thin gas assumption gives much better results.

CONCLUSIONS

The present findings are disappointing in that a greater degree of gasification and char removal was not accomplished. The apparent reason is the extent of the link zone prior to gasification which precluded (without a steam-oxygen supply) gasification in the proximity of the virgin coal. This would have provided both moisture and pyrogenic water and additional energy required for additional gasification.

Actually the persistence of the linking process, as well as the weak gasification, could have been overcome if the METC engineers would have had the steam and oxygen capability that they had originally desired for the run. Steam and oxygen capability were unavailable because of budget limitations. It is essential to keep the reactor hot to prevent the tars from condensing or solidifying and thereby plugging or reducing flow rates. Steam helps maintain reactor temperature since it will not cool off appreciably during injection. The oxygen is needed to overcome the cooling affect of the exposed burden, as well as improve the product gas composition and heating value. The steam will also help overcome the cooling affect of the burden because of its latent energy and radiative properties. The latter will shift the radiation away from the optically thin condition, thus reducing radiation between the reacting wall and the exposed burden.

Finally, it should be noted that the FG process was maintained by burning an average of 20% of the char link zone (about one porous foot) to support the downstream devolatilization. This is a remarkable feat in itself and made the process look like a gasification process. Steam and oxygen must be added to any future burn to promote appropriate linking and ensure proper and uninterrupted gasification. Proper gasification followed by significant downstream devolatilization would make the product gas steam even more valuable than straight gasification and give higher yields prior to breakthrough.

REFERENCES

1. Schwartz, S. H., T. L. Eddy, et al., "Two-Dimensional Thermodynamic Model of the Underground Coal Gasification Process for the Linked Vertical Well Method in Eastern Thin-Seamed Coals," DOE Contract #EY-77-C-21-8087, Final Report, December 1978.

   Schwartz, S. H., T. L. Eddy, K. H. Mehta, S. A. Lutz and M. Binaie-Kondolojy, "Cavity Growth Mechanisms in UCG with Side Wall Burn Gasification," SPE Paper 7525, 1978.

2. Schwartz, S. H. and T. L. Eddy, "Two-Dimensional Thermodynamic Model (Second Stage) of In-Situ Underground Coal Gasification of Eastern Thin Seam Coals," Final Report, DOE-METC Contract EY-77-C-21-8087, Task 17, Mod. 2, December 1979.

   Eddy, T. L., S. H. Schwartz and C. L. Raju, "An Improved Side Wall Burn Model for Cavity Growth in Underground Coal Conversion," Energy-sources Technology Conference & Exhibition, New Orleans, LA, Feb. 3-7, 1980.

   Eddy, T. L. and G. E. Nielsson, "Radiation Heat Transfer in an Irregular Enclosure with Axial Flow," ASME Paper 81-HT-70, 1981.

3. Eddy, T. L., W. H. Ford, Jr., G. J. Morris and S. Thynell, "3-D Thermodynamic Model of Underground Coal Gasification in Eastern Thin Seam Coals," Final Report, DOE-METC Contract DE-AT21-79MC11284, DOE/MC/11284-1160 (DE82012525), December 1981.

4. Agarwal, A. K., P. W. Seabaugh and R. E. Zielinski, "Pricetown I Underground Coal Gasification Field Test - Operations Report," Mound Facility Report MLM-MU-81-62-0007, Miami, Ohio, 1981.

5. Martin, J. W., J. D. McClung, A. J. Liberatore, and L. D. Strickland, "Field Results from a Linked Vertical Well UCG Test in Deep, Thin Seam Bituminous Coal," Energy Sources Technology Conference and Exhibition, New Orleans, LA, Feb 3-7,. 1980.

6. Agarwal, A. K., P. W. Seabaugh and R. E. Zielinski, "Mass Balance Results from the Pricetown I Underground Coal Gasification Field Test," Mound Facility Report MLM-MU-81-72-0002, Miami, Ohio, 1981.

7. Zielinski, R. E. and J. C. Webb, "Phase I - Post Burn Core Analysis of Samples from the Pricetown I UCG Field Test," Mound Facility Report MLM-MU-81-62-0005, Miami, Ohio, 1981.

8. Eddy, T. L., R. T. Gibbs, C. M. Jong, T. X. Phouc and W. H. Ford Jr., "Evaluation of the Final Data for the Pricetown I UCG Field Test via Existing Thermodynamic Models," Final Report DOE-METC Contract DE-AC21-81MC16477, December, 1982.

ACKNOWLEDGEMENTS

The work was sponsored by the Morgantown Energy Technology Center under DOE Contract No. DE-AC21-81MC16477 with A. J. Liberatore as Technical Project Officer. The authors appreciate the assistance of C.M. Jong and T. X. Phouc in the calculations and Miss Melinda Wilson in the preparation of the manuscript.

2.19 RECLAMATION OF THE RAWLINS UCG SITE

by

Ronald W. Genser [1/]
Richard H. Evilsizor [1/]

ABSTRACT

On the site of two UCG-SDB tests near Rawlins, Wyoming, reclamation work was nearly completed during July-October 1982. Reclamation procedures had been approved by the Wyoming Department of Environmental Quality. Upon successful revegetation of the site and removal of the perimeter fence, surface restoration will be deemed complete. This site met the criteria of restorability for UCG site selection established at the start of this UCG-SDB Project. While site reclamation is the major topic of this paper, other activities comprising site restoration are described briefly. Photographs taken before construction, during UCG Test 2, and after reclamation are shown.

RECLAMATION OF THE RAWLINS UCG SITE

INTRODUCTION

Gulf Research & Development Company, with the sponsorship of the Department of Energy, conducted two underground coal gasification tests near Rawlins, Wyoming. Test 1 was conducted during October to December 1979; Test 2, August to November 1981. Reclamation of the site was initiated in April 1981 with the reclaiming of 2 acres. The remaining 18 acres of affected land were reclaimed during July-October 1982. After completion of the ongoing environmental monitoring program and successful revegetation of the reclaimed land, with permission from the DEQ, the monitor stations and the site fence will be removed.

The term "site" is used herein to indicate both the land surface and the subsurface. "Reclamation" is used to indicate actions taken in pursuit of full site restoration; and "restoration" indicates the return to pre-use value and appearance.

Restorability of the Rawlins UCG site was considered during the the site selection process in 1977-78. While the site was determined to be technically acceptable for UCG experimentation, it also had features amenable to full restoration, such as: (1) land surface would suffer only minimal disturbance, (2) facility design and orientation could accommodate surface geologic features, (3) hydrologic properties would probably contain any contaminants in their local regime, (4) no archeological or historical site had to be disturbed by any UCG activity, and (5) pre-use activities probably would resume in a short time following reclamation.

In fact, through careful emplacement of the UCG facilities and prudent use of the site, reclamation was relatively easy to accomplish. Meanwhile, a post-test environmental monitoring program is continuing in which observations are made and data are collected regarding groundwater quality, temperature, and elevation, as well as land subsidence. Presently, site restoration is progressing well. Grasses are revegetating the reclaimed area, and it appears that small wildlife species are returning to the site. Only the site perimeter fence and 38 monitoring stations (13 hydrology wells, 22 subsidence monu-

[1/] Gulf Research & Development Company
P. O. Drawer 2038
Pittsburgh, PA 15230

ments, 3 extensometer wells) remain. Groundwater quality and elevation in some wells have returned to pre-use (baseline) conditions.

PRE-CONSTRUCTION PLANNING

Long before UCG process wells and surface facilities were emplaced on the Rawlins site, reclamation and restorability were being considered. One of the site selection criteria in the Rawlins UCG Program was that a site must be easily restorable to its pre-use value. An adjunct to this was that minimal disturbance should occur as a result of any UCG activity. Through careful placement of the UCG facilities and prudent use of the Rawlins site, it was anticipated that reclamation would be accomplished easily by prescribed procedures.

Reclamation procedures were written by GR&DC with advice from consultants and others, and with guidance from the Wyoming Department of Environmental Quality (DEQ). These procedures were included in the Permit-to-Mine application (Ref. 1), and were subsequently approved by the DEQ.

Early planning for the UCG facility involved the collection of data and information on its following features: land use, wildlife, topography, soil, vegetation, geology, hydrology, archeological sites, and historical sites (Ref. 1 & 2). In 1977, the area being considered for UCG was being used for livestock grazing, wildlife habitat, and recreational hunting. Therefore, the ultimate restoration of the site--that is, resumption of these activities--was of considerable importance. GR&DC assumed that these activities would resume on the UCG site in a short time following reclamation. To this end, the plans called for minimal land disturbance. Furthermore, construction activity was planned to avoid all sites having historical or archeological significance.

Topographical features were documented both with aerial and land-based photographs and surveys. Survey maps and photos showed topographical features, namely contours, terrain, elevation and structures, such as outcropping strata. This documentation was intended for use during recontouring in order to approximately restore the natural terrain. Exhibit 1 is a photograph of the site taken in 1978 before construction.

Other planning for reclamation used the data and information obtained on vegetation, soil, wildlife, hydrology, and geology (Ref. 1). The Soil Conservation Service of the U.S. Department of Agriculture assessed vegetation and soil. Subsequently, the Wyoming DEQ specified that topsoil would be scraped and stockpiled for later replacement; and revegetation would require a seed mix for plants indigenous to this area. An environmental contractor performed the assessment of wildlife and concluded that impact of the UCG facility would be minimal. While several individual animals and birds might be displaced, their population would not be appreciably diminished. Loss of habitat would have the most significant impact on site, but would not be significant on a regional basis. Based on these studies it was anticipated that displaced wildlife would return to the site following reclamation.

Hydrologic properties were such that groundwater movement would not likely disperse the by-products of UCG; i.e., they would be contained in their local regime because movement was extremely slow (Ref. 3). Furthermore, the groundwater in the coal and its boundary strata was of very poor quality (Class IV) and was not suitable for livestock or agriculture. There was no plan to withdraw groundwater except for occasional analysis.

Some subsurface geologic features were visible on the surface as outcrops. Prominent, extended outcrops were to be avoided as much as practical by construction in order to preserve the natural terrain. Design of the UCG facility would accommodate such features by redirecting piping runs and relocating wells, buildings and other facilities (Ref. 4 & 5). Exhibit 2 is a photograph taken in 1981 of the Test 2 facility.

EXTENT OF RECLAMATION AT RAWLINS UCG SITE

At the Rawlins UCG site, reclamation consisted of:

- removal of surface facilities and roads

- abandonment and plugging of drill holes and wells
- surveying and staking disturbed land in conjunction with recontouring
- construction of sediment runoff control ponds
- disking or ripping the surface of affected land
- spreading of topsoil on disturbed land
- seeding all affected land
- mulching all seeded land

Reclamation was implemented where required; that is, wherever the land was affected or disturbed. The degree of disturbance dictated the extent of reclamation.

In the context of land use and reclamation, the terms "disturbed" and "affected" are used to indicate the degree of severity of use or disturbance. Disturbed land is that which has been graded, contoured, drilled, or otherwise altered; usually, vegetation has been destroyed and topsoil removed. In contrast, affected land was subjected to less severe use: topsoil was not removed, although vegetation may have been damaged. Typically, affected land was either used as a road or trail, or for storage of material, or equipment was set upon it.

RECLAMATION PROCEDURES USED

With guidance from the Wyoming Department of Environmental Quality and advice from consultants and others, GR&DC wrote procedures for all aspects of reclamation, and incorporated them into the application for a Permit-to-Mine. Prior to implementation, these procedures were approved by DEQ.

While working under close scrutiny of the WY-DEQ, GR&DC obtained permission to proceed with each activity of reclamation. The planned procedure was reviewed on site by the parties to ensure thorough understanding of the regulatory requirements and to guarantee appropriate treatment of the affected or disturbed areas. These procedures are described below.

A. Drilled hole and well abandonment and plugging.

At the Rawlins UCG site, approximately 60 wells and 120 holes were abandoned and plugged as described below.

For cased wells the following procedure was used:

- At the bottom of the casing an inflatable packer was set.
- Above the packer the casing was plugged with approximately 5 ft of cement, then allowed to set for 24 hours.
- The depth of the cement plug was checked to make sure it had not slipped; in fact, none did.
- The casing was filled with cement up to at least 20 ft above the hydrostatic level and not closer than 4 ft from the land surface.
- Casing was cut off 2 to 4 ft below grade.
- If a well contained a dip-tube which could not be removed, it too was plugged with cement and cut off.
- Remaining hole was filled with earthen material.
- The land was covered with topsoil, then seeded and mulched.

For uncased wells and holes, the following procedure was used:

- Any tubing was removed from the hole.
- The hole was filled with cement up to 4 ft from the land surface so that artesian flow and communication between strata is prevented.
- Remaining hole was filled with earthen material and the surface was reclaimed as stated above.

Several monitoring sites remain and will be used during the next three years for the ongoing environmental monitoring program.

B. Removal of surface facility and roads.

The UCG surface facility consisted of trailers, pipelines, compressors, tanks, oxygen storage and delivery equipment, utility poles, flare, concrete slabs, perimeter fence, equipment, and instrumentation (Ref. 4 & 5). In the summer of 1982 the facility was completely disassembled and removed from the site. All concrete from equipment pads, all debris, and scrap were removed from the site and disposed of of properly (with permission of local authorities). Everything was removed except the site perimeter fence; it will remain until revegetation is deemed successful by the WY-DEQ.

Roads were reclaimed by first removing gravel, then using the procedure for disturbed land.

C. Surveying , staking, and recontouring.

Prior to construction on the Rawlins UCG site the topography was recorded and mapped via both aerial and land-based photographs and surveys. These recordings were used during reclamation in order to approximate the shape of land surface. Based on photographs, rough grade contouring was done first. Then, maps, along with new survey data and staking, were used to indicate pre-use contours. A grid of stakes was laid out with 50 ft intervals on all disturbed areas. As a result of this effort, the final contours are within 2 ft of their original elevations.

D. Sediment run-off control ponds.

To provide containment and allow settlement of suspended solids in run-off from the reclaimed area two ponds were required by the Wyoming DEQ. Each pond is an excavated "reservoir" without a dam. They were designed and constructed in accordance with Wyoming regulations and instructions from the Wyoming State Engineer, as well as under the direction of a licensed engineer and surveyor. A permit had to be obtained for each pond from the State Engineer. Pond 1 has an "active capacity" of 0.182 acre-feet and its area of high-water line is 0.074 acres. Its source of possible runoff is 20.6 acres of the East Knobs Draw immediately above the pond. No groundwater enters this pond. It is maintained, drained, and cleaned if necessary. Pond 2 is similar, but has slightly different dimensions and capacity; its source is 17.8 acres of the West Knobs Draw.

E. Ripping/disking/scarifying.

All three terms may be used to indicate loosening of the soil a few inches deep. This was done on areas (about 8 acres) which had undergone compaction due to any cause, usually vehicular traffic or emplacement of equipment. Disking was done for two reasons: (1) to prepare the soilbed for seeding or replacement of topsoil, and (2) to hold moisture and reduce runoff.

F. Replacement of topsoil.

Topsoil replacement was necessary on all recontoured land and on some land which suffered from compaction or simply had insufficient topsoil or subsoil to provide a suitable seedbed. Topsoil from stockpiles on site was spread to obtain a layer of topsoil 2 in. to 5 in. deep, depending on the depth of subsoil. Where the loosened subsoil was thin or nonexistent, a thicker layer of topsoil was spread. If a thin layer of topsoil already existed, then it was augmented to a depth of 2 in. Raking by hand was used to assure evenness. Seeding was the next step.

G. Seeding of all affected land.

Seeding of 20 acres of prepared seedbed was accomplished during October 25-27, 1982. A permanent seed mix of grasses indigenous to this area was planted according to an approved plug-seeding method by a seeding contractor. Following seedbed preparation, 2 in. wide by 1 in. deep furrows were made with a tool behind a tractor. The tool dropped seeds into the furrow, then covered them with 1/2 in. to 1 in. of soil. Wherever the grade prevented maneuvering the tractor this seeding procedure was accomplished manually. Applied at a rate of 15 lb per acre, the seed consisted of the following DEQ-approved mix:

5 lb/acre of streambank wheatgrass
6 lb/acre of thickspike wheatgrass
2 lb/acre of Indian ricegrass
2 lb/acre of fourwing saltbush.

In April 1981 the same seed mix was applied to 1.7 acres of prepared seedbed, but with a rotary broadcast seeder. Manual raking followed, but not mulching. The result was poor germination. Consequently, interseeding the sparsely vegetated areas was necessary.

H. Mulching of seeded land.

Following the seeding process, a mulch was applied by mechanical means to the entire seeded area. Thirty-five tons of native hay were applied at a rate of nearly 2 tons per acre. Mulch increases the chances of successful revegetation because it (1) stabilizes the seedbed, (2) reduces seed and soil loss due to wind and rain, and (3) improves moisture retention.

I. Inspections by Wyoming DEQ.

GR&DC obtained approval of the reclamation procedures from the Wyoming DEQ prior to commencing the reclamation process. Then, during reclamation, permission to proceed to the next step was granted after site inspections. Occasionally, DEQ Inspectors requested additional tasks or modifications. For example, a diversion ditch was installed uphill from a topsoil pile which was reserved for reclamation of the sediment control ponds. An interceptor ditch was installed to control runoff where such runoff would not benefit from entering a pond. GR&DC complied with all of DEQ's requests and recommendations after discussions and agreements on the extent of such changes.

The cooperative efforts of the WY-DEQ and GR&DC are reflected in the success of the reclamation work, which is described below.

RESULTS OF RECLAMATION

Twenty acres of affected and disturbed land have been reclaimed with apparent success, as grass can be seen emerging on most of the site and it appears that small species of wildlife are returning to the site. Land contours and elevations are very similar to those original features. The most significant achievement at this time is that of revegetation. The wheatgrasses have emerged and, by local standards, are flourishing; while the fourwing saltbush and Indian ricegrass are slow to emerge. Grasses are growing best where the hay mulch was thickest. During the recent winter and spring seasons there was ample precipitation to promote germination.

The result of seeding 1.7 acres in 1981 was less successful; that is, grasses emerged sparsely. This was probably due to the method of seeding and covering which placed the seed too deep. Another cause, of course, could be the age of the seed. With the more recent reseeding, this acreage is undergoing successful revegetation.

No problems with the reclamation have surfaced yet. Weeds have not appeared significantly; there are no erosional problems; the sediment runoff control ponds are effective. Meanwhile, the perimeter fence is preventing full use of the site until revegetation is complete.

Exhibit 3 is a photograph of part of the reclaimed site taken in June 1983.

POST TEST ENVIRONMENTAL MONITORING

In conjunction with site reclamation, a post-test environmental monitoring program has been under way since UCG Test 1 concluded in December 1979. It expanded in 1981 to include the Test 2 environment. It is merely mentioned here and not discussed because it is the subject of other papers written by GR&DC for this UCG Symposium (Ref. 3, 6). The intent is to point out the integrated effort in pursuit of full site restoration.

One objective of this environmental monitoring program is to monitor the effects of UCG on groundwater quality and level, as well as to measure any subsidence due to UCG. To date, data have indicated that the tests have only minor impact on groundwater quality and levels, and no subsidence has occurred. A major conclusion, therefore, is that this site was an excellent choice for UCG testing because of its properties: low permeability, low groundwater yield, poor groundwater quality, and strong roof rock. From

the standpoint of site restoration the subsurface environment appears to be returning to baseline conditions (Ref. 3, 6).

SUMMARY AND CONCLUSION

The majority of reclamation at the Rawlins UCG site was accomplished in 1982. This includes removal of surface facilities and many wells, followed by land surface reclamation. All 20 affected acres of the site were prepared for revegetation. By June 1983 grasses have emerged on most of the reclaimed area and they are flourishing in some places. It appears that species of small wildlife are repopulating the site. Meanwhile, the environmental monitoring program is ongoing; data indicate that long-term effects of UCG at this site range from minimal to none. These results of reclamation are encouraging because full restoration is well under way. Much of this success is attributed to selection of a site which met a set of criteria designed to minimize environmental impact.

REFERENCES

1. "Permit-To-Mine Application," submitted to Wyoming Department of Environmental Quality, January 1981, Gulf Research & Development Company, Report No. 624RM141.

2. "A Site Qualification Study of the UCG Site at North Knobs (Rawlins)," P. F. Ahner, J. M. Avasthi, B. E. Davis, M. E. Dolde, C. A. Greenman, and J. E. Miranda, Gulf Research & Development Company, Proceedings of Sixth Underground Coal Conversion Symposium, Afton, Oklahoma, July 1980.

3. "Effects of the Rawlins UCG/SDB Tests on Groundwater Composition and Migration," P. F. Ahner and M. A. Bloomstran, Gulf Research & Development Company, Proceedings of Ninth Underground Coal Gasification Symposium, Bloomingdale, Illinois, August 1983.

4. "An Industrial Approach to UCG Facility Design, D. W. Bailey and J. L. Gregory," Proceedings of Sixth Underground Coal Conversion Symposium, Afton, Oklahoma, July 1980.

5. "UCG Test Facility Design Criteria and Evaluation," R. A. Bebout and D. G. Damin, Gulf Research & Development Company, Proceedings of Eighth Underground Coal Conversion Symposium, August 1982, Keystone, Colorado.

6. UCG Cavity Definition for Rawlins Test 2," J. M. Avasthi, Gulf Research & Development Company, Proceedings of Ninth Underground Coal Gasification Symposium, Bloomingdale Illinois, August 1983.

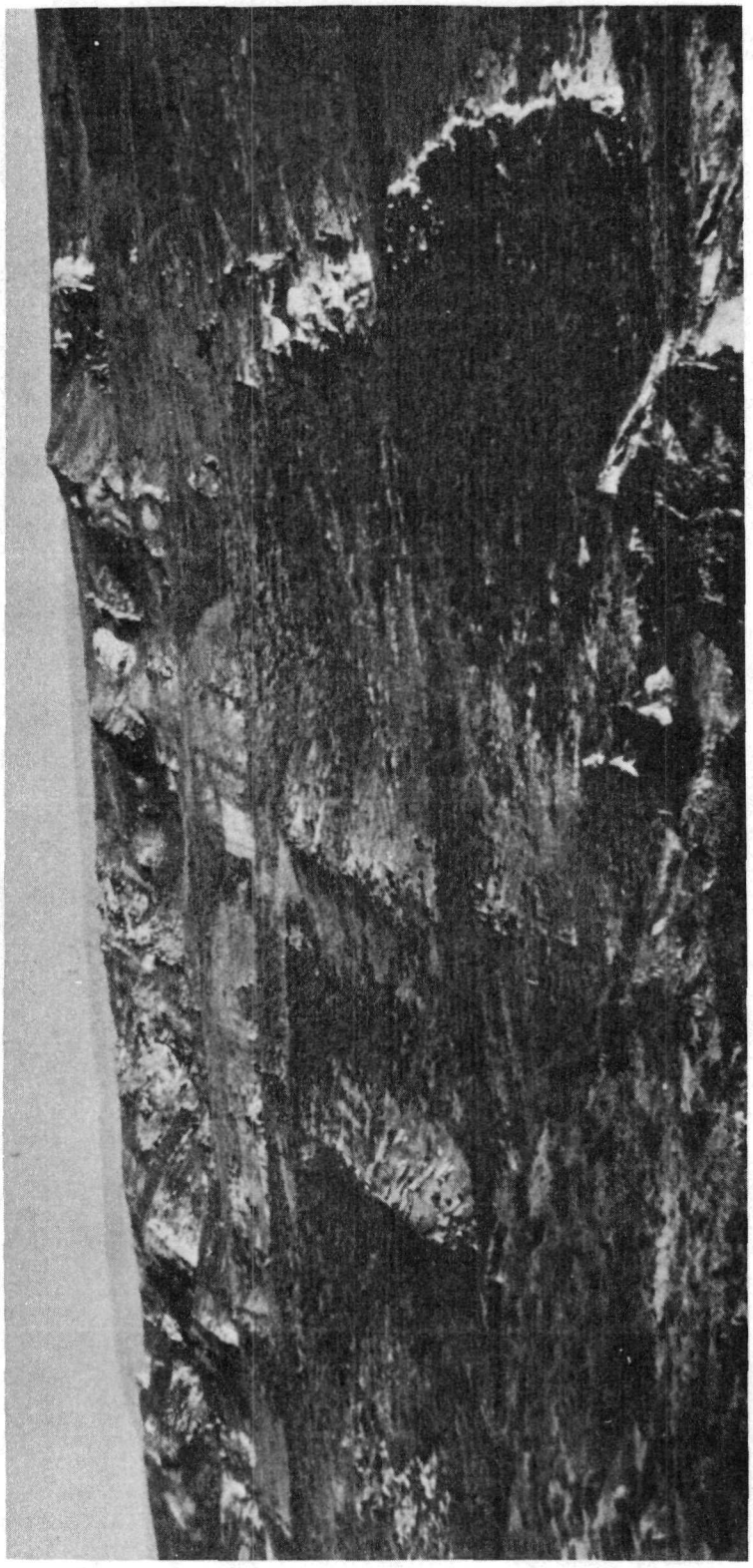

EXHIBIT 1
1978. View of Area Adjacent to UCG Site

EXHIBIT 2
UCG Test 2 facility operating in September 1981.

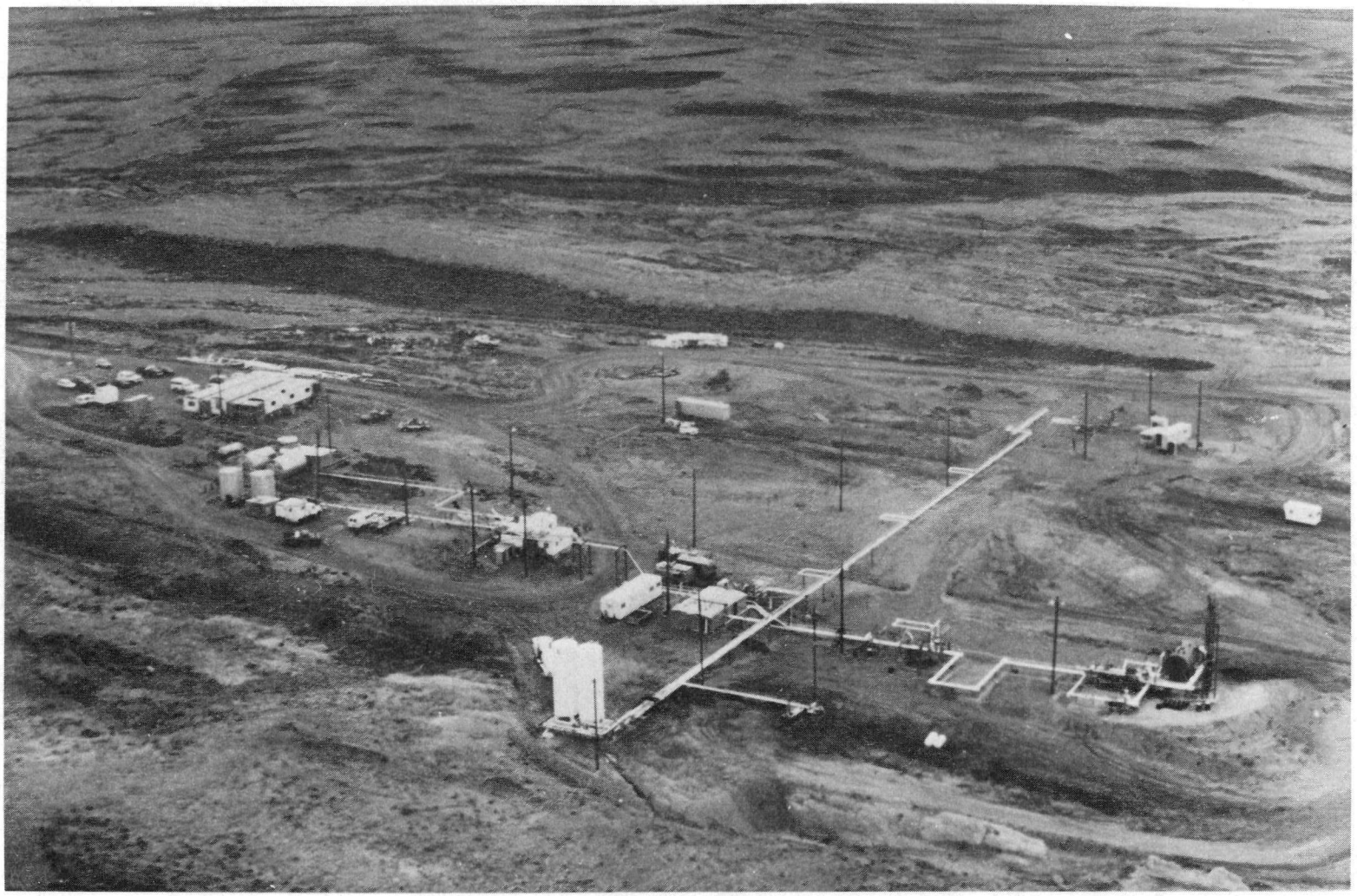

EXHIBIT 3

LOOKING NORTH. JULY 1983. RECLAIMED LAND OF UCG SITE

3.0 MODELING/EXPERIMENTAL

SESSION III: ORAL PRESENTATIONS

Proceedings of the Ninth Annual Underground Coal Gasification Symposium, August, 1983

3.1 UNEXPECTED ASPECTS OF REVERSE COMBUSTION EFFECTS OF PRESSURE, VOLATILITY, AND CHEMICAL REACTIVITY

by

Ronald R. Glaser[1]
Robert D. Gunn[2] William D. Krantz[3]
Klaus P. Breidung[4] Heinrich Gudenau[5]

ABSTRACT

The Kotowski-Gunn one dimensional model is shown to be satisfied by two solutions, not one as previously believed. Application of the Krantz-Gunn stability model indicates three modes of operation where sustained propagation of a link may be expected in the field. One mode of operation on the new solution branch indicates that much shorter linking times than previously thought possible may be achieved. This work also demonstrates the profound influence that pressure, coal volatile content and chemical reactivity have upon reverse combustion performance.

INTRODUCTION

Successful in situ coal gasification projects often employ reverse combustion as a permeability enhancement method prior to the main production phase which is forward gasification or combustion. Virgin coal seams do not exhibit sufficient permeability to permit the desired flow rate of gases from the injection to the production wells. Communication between the wells is often realized by preparing the coal seam with a reverse combustion step. The primary difference between reverse and forward combustion is the relative direction of air flow with respect to the direction of propagation of the reaction zone. The reverse combustion reaction zone, as the name implies, propagates in the opposite direction as the flow of oxidant, while in forward combustion the reaction zone propagates in the same direction. Superficially this appears to be a small difference, but it produces surprising contrasts in the results obtained. Reverse combustion is primarily a low temperature carbonization process that forms small channels that propagate rapidly toward the source of air. Forward combustion propagates much slower and hotter than reverse combustion along a much wider reaction zone that gasifies nearly all of the coal in the well pattern. The heating value of the gas produced by reverse combustion is much lower than the heating value of the gas produced by forward combustion.

Reverse combustion is an interesting option for linking wells. A highly permeable, preheated pathway is formed which provides the ideal conduit for the products of forward gasification. As in all engineering applications of physical phenomenon, a fundamental understanding of the process is required to insure the reliability of its application.

1/ Graduate Student, Department of Chemical Engineering, University of Wyoming, Laramie, Wyoming
2/ Professor, Department of Chemical Engineering, University of Wyoming, Laramie, Wyoming
3/ Professor, Department of Chemical Engineering, University of Colorado, Boulder, Colorado
4/ Doktor-Ingenieurs, Institut für Eisenhüttenkunde, Technischen Hochschüle, Aachen, West Germany
5/ Professor, Institut fur Eisenhuttenkunde, Technischen Hochschule, Aachen, West Germany

REVERSE COMBUSTION MODEL

Kotowski and Gunn (1976) developed a one dimensional model of reverse combustion with considerable success. Continuity and energy balance partial differential equations are reduced to ordinary differential equations by the employment of a spacial coordinate system that travels at the reaction front velocity. The coal is treated as two components, char and volatile matter (fuel) which reduces the continuity equations to an easily manageable number, and more importantly, reduces the model's requirement for kinetic expressions (many of which are not known) to a single Arrhenius expression. The model successfully predicts peak combustion temperature, heating value of the product gas, front velocity and thermal gradients (Lu, 1980; Okutan, 1980). The Kotowski-Gunn model also yields some unexpected predictions. The peak combustion temperature decreases if oxygen enriched air is injected in place of ordinary air if the total flux of oxygen is held constant. Intuitively, the opposite effect would be expected, especially since oxygen enrichment does lead to higher temperatures driving forward combustion. Also unexpected, is the effect of water influx on the peak combustion temperature. In forward combustion, as expected, an increase in water influx lowers the peak temperature of the process. In reverse combustion, however, the peak temperature increases with increasing water influx. These effects have been confirmed experimentally (Lu, 1980; Okutan, 1980). An examination of the model formulation provides an explanation of this and other curious behavior observed in reverse combustion. The effect of oxygen enriched air is explained by the fact that the rate of reaction, temperature gradient, and front velocity are all closely coupled. An increase in the oxygen concentration does increase the reaction rate. This in turn steepens the temperature profile, which increases the reaction zone velocity. A high frontal velocity means more coal must be heated and this results in a lowered combustion temperature.

Although the one dimensional Kotowski-Gunn model successfully explains many aspects of reverse combustion, it does not alone explain all of the phenomena observed in field test applications of reverse combustion. The model predicts increased front velocity with an increase in air flow rate. This response was not observed in the Hanna series of field tests (Krantz and Gunn, 1981); but curiously, combustion tube experiments did quantitatively confirm the theoretical prediction. The Kotowski-Gunn model provides no information concerning channel formation. Why does reverse combustion form small channels instead of the broad reaction zone observed in forward combustion? Why is reverse combustion sensitive to flow rate in the laboratory and not sensitive in the field? The use of stability theory has proven very successful in answering these questions.

STABILITY THEORY

A one dimensional stability model has been developed by Krantz and Gunn (1977) and Gunn and Krantz (1980) for reverse combustion. This model solves the perturbed Laplace and energy equations for fluid flow in porous media, but in addition two parameters must be obtained from solutions to the reverse combustion model. The stability model shows that reverse combustion is an unstable process similar to fingering observed in oil field water floods. Water floods are used to displace petroleum in oil fields to improve production. Under certain conditions, the petroleum is not displaced in the desirable piston-like manner. When these unstable conditions are present, the water petroleum interface breaks up into multiple fingers which bypass a large fraction of the reservoir. In reverse combustion, channels form instead of a broad reaction zone. The stability model not only demonstrates why reverse combustion is unstable, but provides a means for predicting channel diameters. In reverse combustion, disturbances in the broad reaction zone propagate at velocities dependent upon the size of the disturbance. The disturbance that propagates most rapidly corresponds to the observed reverse combustion channel diameter.

Reverse combustion channels formed in balsa wood have been studied by Cooney et al. (1980). Experiments by the underground coal gasification group at Aachen, West Germany on solid coal blocks have developed channels that approximately

correspond to stability theory predictions (Breidung, 1982). Calculations on the Hanna series field test data explained the observed insensitivity to injection rate. The stability model shows that with increasing injection rate, the channel diameter also increases at a rate that produces a near constant flux through the reaction zone, hence a near constant front velocity. In the laboratory, the channel diameter is limited by the size of the equipment used, so that high fluxes can be imposed on the system that cannot be realized in the field (Krantz and Gunn, 1981). The reverse combustion and stability models have not only been the source of unexpected predictions; the models are a key to a fundamental understanding of the behavior of reverse combustion. The joint application of the Kotowski-Gunn reverse combustion and the Krantz-Gunn stability models has proven successful in the interpretation of the shallow field tests conducted in the western U.S.A. What do the models tell us concerning the more severe operating conditions encountered in the deep coal gasification projects in Europe and similar projects planned for the eastern United States?

MODELLING REVERSE COMBUSTION AT EXTENDED CONDITIONS

The modelling and experimental work mentioned previously has been aimed at understanding reverse combustion in the shallow subbituminous coal beds field tested in the western coal regions of the United States. Investigations have not previously been extended to high pressures, high air fluxes, and various coal ranks. Modelling reverse combustion at great depth requires calculations over a much broader range than is required for shallow low rank coals. Deeper coal seams in the U.S. and abroad present problems that are considerably more complex than those encountered with shallow coals. Great depth requires high pressure on the injection side, and deeper coals are often higher in rank and exhibit different reactivities. Unfortunately, high operating pressures lead to troublesome spontaneous ignition of the coal on the injection side. The successful employment of reverse combustion requires a choice of operating conditions such that the link is completed prior to spontaneous ignition. This requires the maximization of the combustion front velocity and/or the use of agents on the injection side to inhibit spontaneous ignition.

The Kotowski-Gunn model is employed, with some modifications, jointly with the Krantz-Gunn stability model to predict the behavior of reverse combustion over a wider range of conditions than previously determined. The pseudo-component fuel continuity equation has been expanded to nine separate continuity equations:

1) Fixed Carbon
2) Tar
3) Ethane
4) Methane
5) Hydrogen
6) Water
7) Steam
8) Carbon Dioxide
9) Carbon Monoxide

Also, an approximate formulation of the heat loss in the radial direction is incorporated into the model. Channel diameters are calculated from the linear stability model developed by Gunn and Krantz (1980).

EFFECTS OF PRESSURE, CHEMICAL REACTIVITY AND VOLATILE CONTENT

The modified Kotowski-Gunn reverse combustion model yields the relationship between combustion front velocity and air flux shown in Figure 1. These results are based upon a first order (in oxygen) Arrhenius rate dependency with a frequency factor of 1×10^9 hr^{-1} and an activation energy of -7550 Btu/lbmole. The figure shows solutions for 10% volatile content coal at 290 and 580 psia. An interesting aspect of these results is the existence of two solutions at a given air flux. The higher velocity solutions are limited by oxygen (oxygen limited), while the lower solutions are limited by the availability of combustible pyrolysis products (fuel limited). The oxygen limited solution has been previously described in the work of Kotowski and Gunn (1976) and experimentally verified by (Lu, 1980; and Okutan, 1980). The lower branch of the curve, the fuel limited solution, has not been previously described. Figures 2A and 2B illustrate the differences between the two solutions. These figures are temperature and composition profiles through the reaction zone, with the

reaction propagating from right to left. The large and small dashes represent the mass fractions of fuel constituents and oxygen, respectively. The solid line represents the temperature profile. Figure 2A is an example of a fuel limited solution. The rate of oxidation greatly exceeds the rate of pyrolysis, so a very small concentration of combustibles is observed with excess oxygen in the product gas. Figure 2B is an example of an oxygen limited case where the rate of pyrolysis exceeds the rate of oxidation, leaving the gas phase rich in fuel. The reaction proceeds until the oxygen is nearly all consumed, leaving unburned fuel.

Although the existence of the excess oxygen branch of the velocity curve in Figure 1 was previously unknown, it can be easily justified on physical grounds. Only one air flux produces perfect stoichiometry. This flux corresponds to the maximum velocity and temperature shown on the curves of Figures 1 and 3. At any other flux, there are two possibilities, an excess of fuel (oxygen limited) or an excess of air (fuel limited). Both possibilities exist and represent multiple steady states, as is often the case in combustion phenomena. The fuel limited branch corresponds to a low peak temperature and a lower frontal velocity than the oxygen limited case at the same flux. Experimental results from the work of Ledant (1982) provide verification that the fuel limited branch exists. The experiments were performed at 30 bars and high air fluxes on solid coal blocks of various rank. The product gas consisted of very little combustible material and high oxygen fractions, which are characteristics of the fuel limited solutions indicated by the model.

It is interesting to note that at excessively high air fluxes, no solutions exist (Fig. 1), because the air flow rate becomes so high that either the fire is "blown out" or the direction of burning is reversed to forward combustion.

Effect of Pressure

Increasing pressure enlarges the envelope of possible solutions. As explained earlier, on the oxygen limited branch an increase in oxygen concentration leads to lower combustion temperatures and increased velocities as indicated by Figures 1 and 3. The fuel limited branch of the curve in these figures behave differently. The increase in pressure increases the reaction rate because the partial pressure of oxygen is raised. Consequently, the combustion reaction proceeds faster than pyrolysis, thus increasing the reaction rate of combustion. This serves to deplete the fuel sooner at a lower temperature. The net effect is both a lower velocity and lower peak temperature.

Volatile Content

Figures 4 and 5 are identical to Figures 1 and 3 except two coals of different volatile contents are compared at constant pressure. The oxygen limited solutions are nearly identical, except the more volatile coal is extended over a wider range of airflux, because the increased fuel availability requires a shift in the stoichiometric point. As one would expect, the fuel limited solutions are markedly different. For the low volatile coal, the front must advance faster in order to heat a larger volume of coal needed to provide sufficient fuel. Obviously low volatile coal contains less fuel than a high volatile coal on a volumetric basis.

Chemical Reactivity

An increase in chemical reactivity has nearly the same effect as an increase in pressure (Fig. 1). When faster kinetics are expressed by changing the frequency factor, the effects are identical to raising the pressure since the partial pressure of oxygen acts as a simple multiplier of the reaction rate term in the model. Because of the great similarity in reactivity and pressure changes, the same conclusions may be drawn from variation in either parameter; pressure or reaction rate.

REVERSE COMBUSTION STABILITY

While the one dimension model of Kotowski and Gunn is valid for constrained geometries such as combustion tube experiments, stability calculations must be performed to gain insight into what may be expected in the nearly infinite media of a coal seam. Figure 6 depicts the results of the stability model applied to the 10% and 15% volatile content coals at 290 psi. The solid lines represent the functionality between air flux and diameter of the fastest growing channel as calculated from the

stability model. The dashed lines represent the relationship between the injection rate (lb/hr) and the flux(lb/ft^2-hr) as a function of channel diameter. The value of the injection rate is expressed as mass flow of air per channel. Multiple channels may be examined on this graph by multiplying the given injection rate by the appropriate factor. Figure 7 is a simplified drawing of a stability analysis result for explanatory purposes. The solid line represents the diameter of the fastest growing channel (stable-metastable line) as a function of air flux while curves Q1, Q2, and Q3 represent constant injection rate curves of decreasing magnitude. The constant injection rate curves are simply a plot of the relationship between air injection rate and air flux as a function of channel diameter. Point B corresponds to an initial channel diameter and injection rate that will result in sustained propagation. The channel diameter will decrease, with a corresponding flux increase, until line Q2 intersects the stable-metastable line at point X. A channel of a diameter represented by X will continue to propagate without further change in diameter. At the diameter and injection rate corresponding to C, the channel diameter will increase, with a corresponding decrease in air flux as indicated by line Q2 until point X is again reached. Because point D is to the right of the stable-metastable line, the channel will decrease in size just as it did for point A until the fire is blown out. The conditions represented by point E will finally result in the channel diameter and flux indicated by point Y. A large segment of the stable-metastable line cannot be reached from any initial channel diameters and injection rates that do not coincide already with this line. This segment is represented by the portion of the stability curve below the transition point. This portion of the curve is metastable; any minute disturbance will cause permanent displacement from these operating conditions. Therefore, this potential mode of operation has no practical value. The portion of the curve above the transition point represents the channel diameters and corresponding air fluxes where continued propagation of the reverse combustion link can be expected.

In Figure 6, points B represent transition points for the fuel limited conditions, points A represent transition points for the oxygen limited conditions. Only those portions of the curves above the transition point represent stable propagating channel sizes, except for the region on the fuel limited curves to the right of the minimum. This region is very interesting for linking applications because it indicates that channel propagation may be possible at fairly high air fluxes where frontal velocities may be as much as ten times those attainable in the low flux stable regions above points A and B which are the regions used currently.

However, operation at high flux presents problems. This type of reverse combustion operates dangerously close to the blow out line. Can reverse combustion be safely operated in this region? If further work demonstrates that "blow out" of high flux combustion can be controlled, then the short linking times promised at these operating conditions has important implications especially for deep coal gasification where spontaneous ignition is a problem.

CONCLUSIONS

This and previous studies have shown that reverse combustion in coal seams is not a simple phenomenon. Model results indicate that with coals of low volatile content, the process is very sensitive and susceptible to blow out or flame front reversal. Three regions are indicated where channel propagation is possible. The two low flux regions develop large channels that propagate slowly, while the high flux region develops smaller, fast growing channels. However, operation at high flux requires operation dangerously close to the blow out point. The practicality of operating at these conditions is not known.

FUTURE WORK

Work is currently underway to prove experimentally the influence of coal types and operating conditions on reverse combustion over a wide behavior range. The experimental work is designed to verify quantitatively the theoretical solutions presented in this paper.

ACKNOWLEDGMENTS

Two of the authors gratefully

acknowledge financial support for this work through grant No. 5081-260-0570. Neither GRI, members of GRI, nor any person acting on behalf of either: (1) Make any warranty or representation, express or implied with respect to the accuracy, completeness, or usefulness of the information contained in this report; or (2) Assumes any liability with respect to the use of, or for damages resulting from the use of, any information, apparatus, method, or process disclosed in this report.

REFERENCES

1. Kotowski, M.D. and Gunn, R.D., "Theoretical Aspects of Reverse Combustion in the Underground Gasification of Coal", ERDA Report LERC/RI/4, (1976)
2. Krantz, W.B., and Gunn, R.D., "Linear Stability of Reverse Combustion for In Situ Coal Gasification", Proceedings of the Third Annual Underground Coal Conversion Symposium, Fallen Leaf Lake, Calif., (1977)
3. Gunn, R.D., and Krantz, W.B., "Reverse Combustion Instabilities in Tar Sands and Coal", SPE Journal, 20, 267 (1980)
4. Okutan, F., "Reverse Combustion During In-Situ Coal Gasification", M.S. Thesis, University of Wyoming (1980)
5. Lu, H.S., "Laboratory Simulation of Reverse Combustion for UCG", M.S. Thesis, University of Wyoming (1980)
6. Krantz, W.B., and Gunn, R.D., "Use of Stability Theory in Interpreting UCG Field Test Data", In Situ, 5(3), 199-219 (1981)
7. Ledant, P., personal communication, laboratory data to be published (1982)
8. Breidung, K.P., "Stofftransport und Erhöhung der Gasdurchlassigkeit bei der In-Situ-Vergasung tiefliegender Steinkohlenflöze", Doktor-Ingenieurs Dissertataion, Rheinisch-Westfälischen Technischen Hochschüle Aachen, Bundesrepublik Deutschland (1982)
9. Cooney, D.O., Gunn, R.D., and Puri, R., personal communication (1980)

FIGURE 1
FRONT VELOCITY VS AIR FLUX
FOR 10% VOLATILE COAL

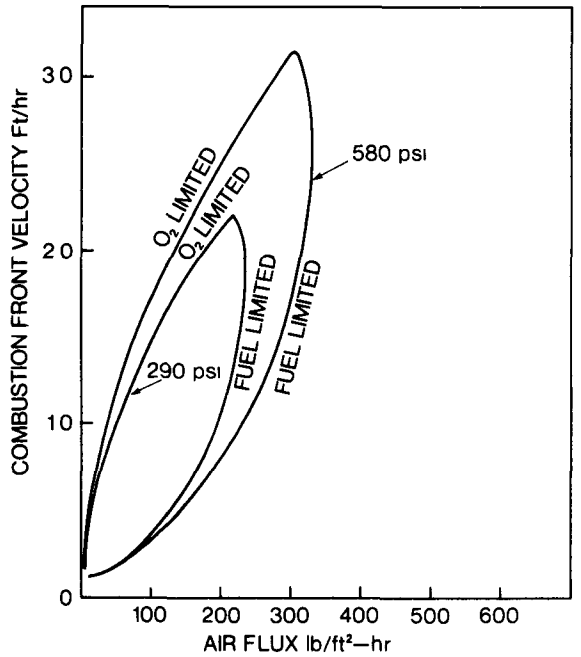

FIGURE 2B

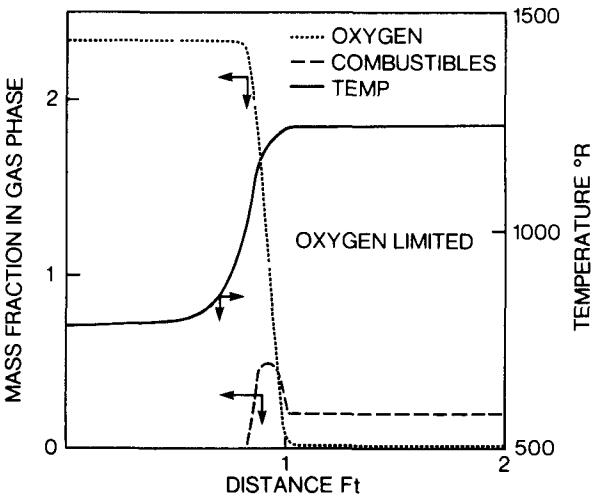

FIGURE 2A

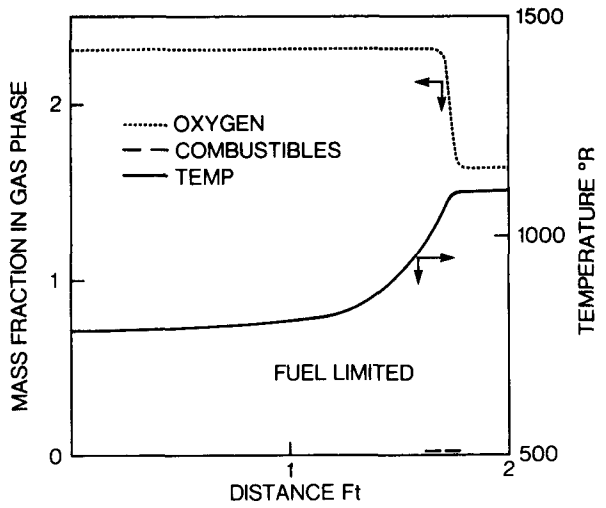

TEMPERATURE
AND COMPOSITION
PROFILES– 10%
VOLATILE COAL
AT 290 psi -
10 lb/ft²–hr
AIR FLUX

FIGURE 3
PEAK COMBUSTION TEMPERATURE VS
AIR FLUX FOR 10/% VOLATILE COAL

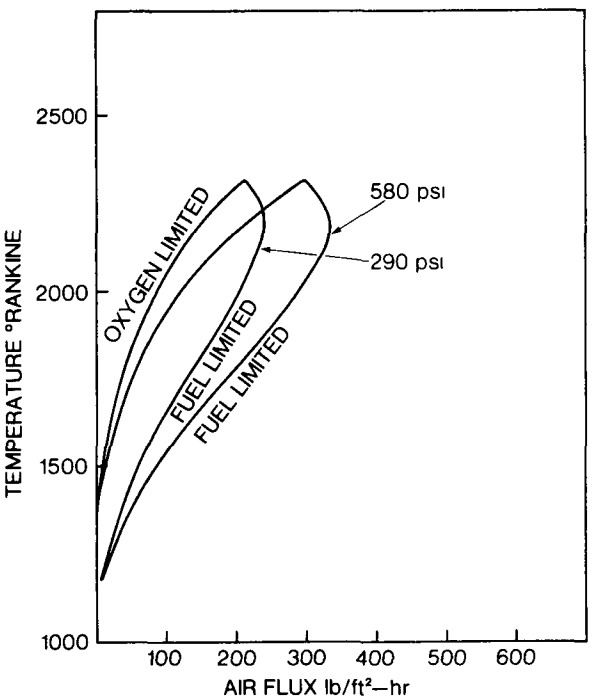

FIGURE 4
FRONT VELOCITY VS. AIR FLUX
AT 290 psi BACKPRESSURE

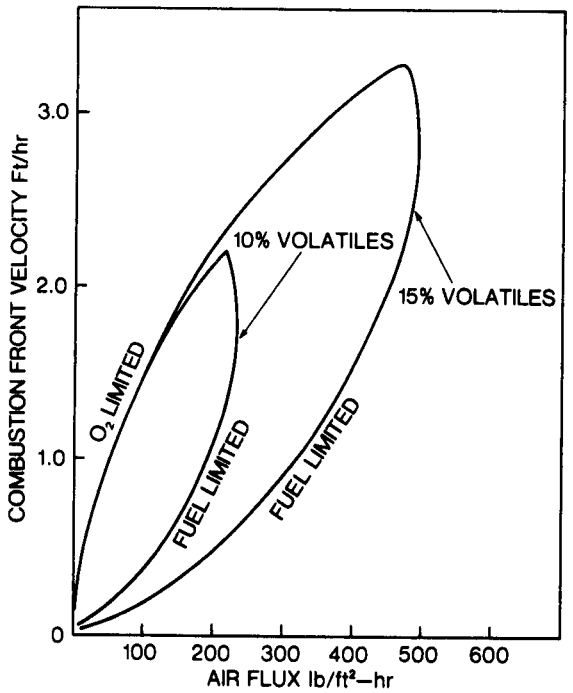

FIGURE 6
LINEAR STABILITY RESULTS AT 290 psi

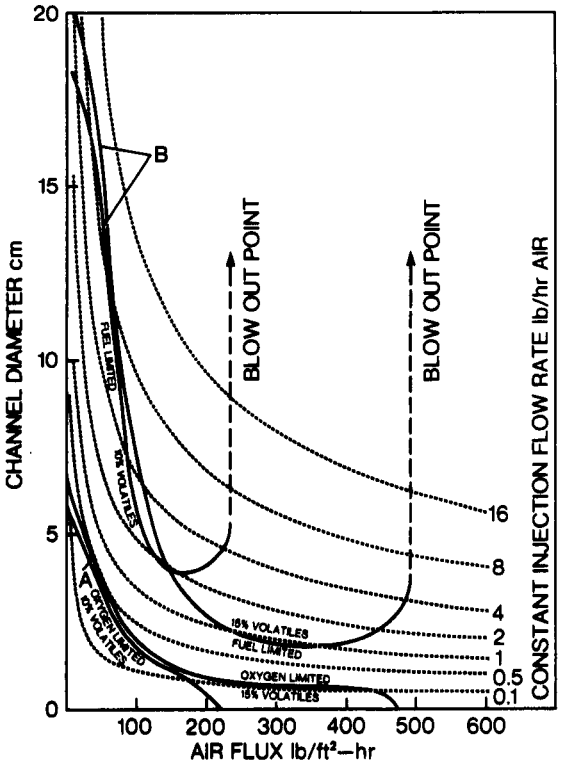

FIGURE 5
PEAK COMBUSTION TEMPERATURE VS.
AIR FLUX AT 290 psi BACKPRESSURE

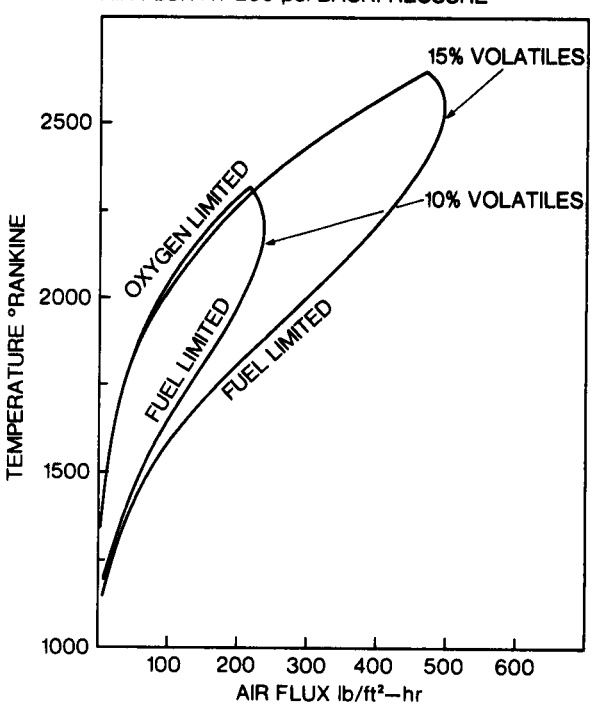

FIGURE 7

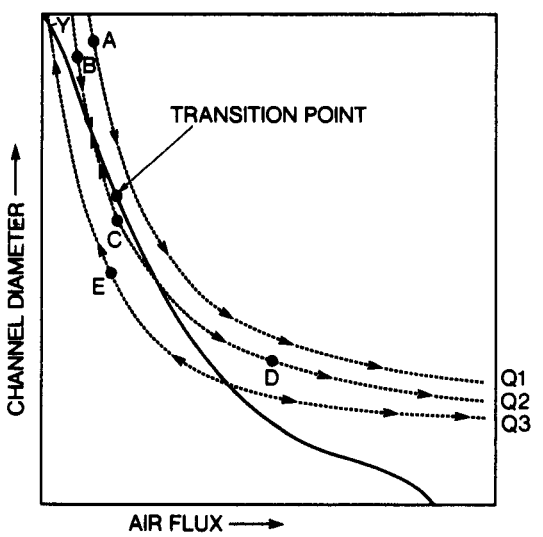

Proceedings of the Ninth Annual Underground Coal Gasification Symposium
August 1983

3.2 ASSESSMENT OF LATERAL CAVITY GROWTH MECHANISMS

by

James B. Riggs

ABSTRACT

A number of mechanisms that could contribute to the lateral growth of the cavity during underground coal gasification are identified and assessed. In addition, a cavity model based upon the conclusions from the assessment is presented.

The processes that control the lateral growth of the cavity during UCG are not well understood. In fact, there are a number of competing theories which describe methods for lateral cavity growth. From these theories, the following cavity growth mechanisms are identified: combustion, structural failure of the virgin coal, structural failure of the dried coal on the side wall, thermally driven gasification and abrasion of the side wall by the settling of the rubble pile. The assessment is based upon laboratory and field test experience, as well as, on the theoretical analysis of each mechanism. It is concluded that thermally driven gasification is the major factor affecting lateral cavity growth. That is, the hot gases produced by the combustion of coal in the rubble pile drive the gasification of the coal on the side wall.

A two-dimensional cavity growth model is proposed which is based upon the assumption that the cavity will grow symmetrically about the injection well. The model will consider two-dimensional flow through the rubble pile with bouyancy effects as the result of the combustion of the coal in the rubble pile. The model will also consider the material and energy balances for the gas as it flows through the rubble pile and into the void space above it. In addition, the dynamics of the rubble pile are considered, i.e., spalling of the overburden feeding the rubble pile, pyrolysis of the coal in the rubble pile, gasification of the char, and the production of ash or slag. And the lateral growth of the cavity is modeled as the thermal driven gasification of the side walls for which the thermal energy is provided by convection.

work done at West Virginia University. Presently at Dept. of Chemical Engineering, Texas Tech University, Lubbock, TX 79409

INTRODUCTION

Cavity growth during underground coal gasification (UCG) has long been recognized as having a major impact upon the economic viability of the process. More speicifically, economic studies (1,2) show that the amount of coal gasified for each injection/production well pair has a major impact upon the economics of the process. Therefore, it is desireable to gasify as much coal as possible for each injection/production well pair while maintaining product gas heating value.

Since the renewed interest in UCG in this country, there has been considerable effort directed at modeling the UCG cavity growth process. Unfortunately, there is not currently a physically realistic UCG cavity growth model primarily because of the lack of knowledge of the controlling factors (3), especially for the lateral cavity growth process. But recent results from laboratory (4) and field tests (5,6) have provided new insight into the controlling factors affecting cavity growth. Therefore, the purpose of this paper is to identify and assess potential mechanisms for lateral growth of a UCG cavity.

PREVIOUS WORK

There have been a number of UCG cavity growth models proposed over the past eight years. Riggs and Edgar (3) have reviewed a number of these cavity growth models and indicated areas where future work is needed. The major differences between cavity growth models lie in the geometric configuration for the cavity, the description of the gas flow behavior, and the modeling of the combustion and gasification of the coal that each model uses.

Several models (3) have assumed a void cavity in addition to using the plug flow assumption for the flow of injected gas through the cavity toward the production well. The utility of these models for cavity growth prediction is limited because of the assumption of plug flow and because of neglecting the coal rubble pile.

One of the common features of the cavity growth models to date is the way in which the coal combustion and gasification process are described. That is, most of the models (3) assume instantaneous reaction between the coal and the oxygen in the gas phase. As a result, none of the models is able to predict maximun cavity growth or is able to predict the point at which product gas heat value drops below acceptable limits or the point at which oxygen breakthrough occurs. Massquoi and Riggs (7,8) have developed a one-dimensional model of a burning coal surface under UCG conditions. This model was based upon a rigorious analysis of the physico-chemical process that determine the gasification of coal under UCG conditions including reaction kinetics. As a result, this model is able to predict the flame extinction behavior of wet coal and appears to be consistant with experimental studies on coal combustion.

CAVITY CONFIGURATIONS

In order to assess lateral cavity growth mechanisms one must first consider the environment within the cavity and its influence on the side walls. For this purpose we will consider the mode of gas injection into the cavity. Based upon field test experience (5,6,9) there appears to be two different modes of gas injection for UCG cavities: injection at the top of the cavity and injection at the bottom of the rubble pile. Failure of the injection well at the top of the cavity results in an injection configuration similar to the one shown in Figure 1. The other configuration considered is shown in Figure 2, in which the injection point is maintained near the bottom of the rubble pile.

The configuration with the injection point in the rubble pile (Figure 2) bears significant resembelance to a fixed bed gasifier. That is, there is a counter-current contacting between the injected gas and the coal: consider a chunk of coal that spalls from the roof of the cavity and falls onto the top of the rubble pile. As the rubble pile settles and more coal falls onto the rubble pile, the chunk of coal is contacted with hot gases that contain little or no oxygen; therefore, this coal will have the remainder of its pyrolysis gases driven off. As the coal chunk settles further, it will contact hotter and hotter gases resulting in the gasification of carbon by the C/steam and the C/CO_2 reactions. These reactions will

occur largely on or near the surface of the coal chunks. Finally, the coal chunk will enter the oxidzation zone where the remainder of its carbon is combusted with oxygen leaving only the ash.

This particular configuration (Figure 2) was maintained during the majority of the Rawlings II test on a steeply dipping bed. This efficient counter-current contacting between the injected gas and the coal most likely played a significant role in the success of this field test.

The configuration shown in Figure 2 differs from that of a fixed bed gasifier in that the flow for the UCG system is much more two-dimensional in nature. That is, the injected flow moves vertically through the bed and radially toward the cavity walls. It is likely that this radial flow plays a significant role in the lateral growth of the cavity.

When the injection gas is supplied to the cavity as shown in Figure 1, the contacting between the gas and coal is considerably different than for the previous case considered. For this situation, the oxidation zone would probably be less localized: at the surface of the coal rubble pile and in the void space above the rubble pile and possibly at the exposed coal surface that forms the cavity boundary above the rubble pile.

When a chunk of coal falls on to the rubble pile, it would be hit by the blast of the injection gas causing rapid combustion. But as more coal falls onto the rubble pile, it would soon be shielded from direct contact of the injected gas. Therefore, combustion would stop. However, gasification of this chunk will continue if the temperature is sufficient and adequate levels of CO_2 and H_2O are present. Obviously, the gasification of altered coal inside the rubble pile would at some point be hindered.

It is interesting to consider the effect of encountering the overburden for each of these configurations. When the injection point is inside the rubble pile, spalling of rock overburden on to the rubble pile would have a much less immediate effect upon the performance of the process than when the injection is at the top of the cavity. Moreover, spalling of roof rock on to the rubble pile would quickly hinder contacting between the injected gas and the altered coal in the rubble pile for the case shown in Figure 1. For example, at Hoe Creek III (10) the heating value of the product gas drops-off immediately when the overburden was encountered.

FACTORS AFFECTING LATERAL CAVITY GROWTH

The following factors are considered in this section with regard to their effect upon the lateral growth of the UCG cavity:

- Combustion of the side wall
- Structural failure of the virgin coal on the side wall
- Structural failure of the dried coal on the side wall
- Thermally driven gasification on the side wall
- Abrasion of the dried coal from the side wall by settling bed.

Combustion of the Side Wall

It is unlikely that combustion plays a direct role in the lateral growth of the cavity for the configuration shown in Figure 2 (injection in the rubble pile). For this situation, all the oxygen would be quickly consumed near the injection well.

But when the injection point is at the top of the cavity, it is possible that some combustin of the side wall would result. This could happen if not all the oxygen in the blast gas reacted when it encountered the rubble bed and if the flow were deflected to the side walls by the rubble pile. Note that this mechanism would only be operative for the exposed side wall above the

rubble pile.

If combustion does occur at the side wall, the gas near the side wall would be high in temperature and relatively low in oxygen concentration. Under these conditions, it is probable that the flame would be located in the gas layer adjacent to the side wall.

It is also possible that the oxygen that does not react with the coal in the rubble pile would react directly with combustible gases in the void spaces above the rubble pile. If this occurred, no oxygen would reach the side walls and combustion would not affect the lateral growth of the cavity. In conclusion, if combustion does play a role in the lateral growth of the cavity, it is a limited to the exposed side wall when the injection point is at the top of the cavity.

Structural Failure of the Virgin Coal on the Side Wall

Under this senario, the extra load on the side wall created by the formation of the cavity (see Figure 3) is sufficient to fracture sections of the virgin coal that comprise the side wall. While this mechanism is possible, finite element calculation on this geometry that have been done to date (11,12) indicate that the side wall is structurally strong enough to handle the additional load. It is expected that this type of failure of virgin coal would occur in the arch forming the roof of the cavity as the diameter of the cavity increases.

Structural Failure of the Dried Coal on the Side Wall

Livermore conducted a set of barrel tests (4) using three different types of coal: Wyodak, Widco, and Hanna coal. They found that although each coal yeilded roughly the same heating value of product gas, they had dissimilar cavity shapes. Figure 4 shows the general cross-sections observed at the end of the experiments in the three different coals with the observed fracture patterns in the dried coal. Notice that the fracture patterns for the Wyodak and Widco coal were parallel to the bedding plane while Hanna coal experienced a cylinderically symmetric radial fracture pattern.

Glass (13) analyzed the LLNL barrel tests using thermomechanical properties of the coals and concluded that the Wyodak and Widco coals were structurally weaker than the Hanna coal. Moreover, the largest internal stress for each of these coals was that caused by the shrinkage of the coal at elevated temperatures. Therefore, the weaker coals (Wyodak and Widco) fractured parallel to the bedding plane because these coals are weakest in that direction. It is not clear why the fracture pattern for the Hanna coal did not appear to be influenced by the bedding plane since the Hanna coal is also weaker along the bedding plane although considerably stronger than the Wyodak or Widco coals. In any event, these results suggest that fracture lines at a UCG cavity side wall would be horizontal in orientation and would be caused by the shrinkage of the coal as it dries and pyrolyzes on the side wall of the cavity as shown in Figure 5.

Glass (13) also found that Hanna coal went through a plastic state in the temperature range of 375-450^{o}C, but actually solidified and became structrually stronger at temperatures above 450^{o}C. Therefore, at this point it appears that structural failure of the dried coal on the side wall does not directly contribute to the lateral growth of the cavity although experimental work would be required to prove this conclusion.

Thermally Driven Gasification of the Side Wall

In the case of thermally driven gasification, thermal energy from the gas phase is transported to the altered coal to drive the endothermic C/H_2O and C/CO_2 reactions. The consumption of the

carbon from the char and the subsequent mechanical failure of the ash produce the moving boundary shown in Figure 6. Therefore, if adequate thermal energy is transported to the char surface of the side wall, thermally driven gasification would at least contribute to the lateral growth of the cavity.

Two factors affect the transport of thermal energy to the char surface of the side wall: (1) convection and radiation of thermal energy to the side wall, and (2) the formation of an ash layer on the char surface of the side wall.

Convective transport of thermal energy to the side wall is likely for the situations depicted in both Figures 1 and 2. But convection would probably be small for the side wall beneath the rubble pile for the case shown in Figure 1. It is possible that radiation could play a role for the case of injection at the top of the cavity and only then for the exposed side wall.

The presence of an ash layer on the char surface of the side wall would represent a significant resistance to thermal transport to the char. Consideration of the kinetics of the C/H_2O and C/CO_2 reactions, shows that temperature in excess of $1000^{o}K$ are required in order to provide reasonable linear gasification velocities. Therefore, even a very thin ash layer would significantly impede heat transfer to the char especially since the char surface should be in excess of $1000^{o}K$. Estimation of ash layer thickness is a relatively unknown area at present, but ash layers are quite weak structurally and for low ash content coal may not even form on the coal during gasification.

Figure 5 shows the expected configureation of altered coal on a side wall. Since at the side wall the bedding planes are essentially perpendicular to the side wall, it is expected that cracks would result along these bedding planes and crevices would be created in these cracks due to shrinkage of the coal. These crevices both enhance the surface area and provide low flow resistance paths for the steam generated at the evaporation front and the pyrolysis gases released from the coal. Note that thermally driven gasification would occur primarily along the surfaces closest to the bulk gas.

Since UCG cavities are known to maintain temperatures in excess of $1300^{o}K$ (4,6), thermally driven gasification should play a significant role in the later growth of the cavity at least for coals that do not retain significant ash layers.

Abrasion of the Dried Coal from the Side Wall by Settling of the Rubble Bed

This mechanism represents a combination of thermal drying and pyrolysis of the coal on the side wall followed by the abrasion of the dried coal by the settling rubble pile. It is also probably the most difficult of the mechanisms considered to appraise with regard to its contribution to lateral cavity growth.

This mechanism is based upon the fact that the char left after the coal has been dried and pyrolyzed has a very low structural strength. But for this method to be operative, the rubble pile must be settling next to the side wall; therefore, this mechanism would not be applicable to the cavity configuration shown in Figure 1 since the removal of coal is at the top of the rubble pile. But for the flow configuration shown in Figure 2, the coal is being consumed at the bottom of the rubble pile and as a result the rubble pile would be settling. However, the majority of the coal being consumed in the rubble pile is located near the center of the cavity so the majority of the settling would occur at the center portion of the rubble pile. Therefore, it is difficult to invision that the rubble pile near the side wall would settle enough to remove altered coal at the side wall. In any event, the proper analysis of this mechanism

would require laboratory and theoretical confirmation.

Conclusion to the Assessment of Lateral Cavity Growth Mechanisms

At this point it appears that thermally driven gasification is the dominant mechanism affecting the lateral cavity growth during UCG. It is far from conclusive and should, therefore, be verified experimentally. It is possible that for certain high ash content coals that ash layer formation would significantly supress gasification of the side walls.

Also, laboratory experiments should be conducted to study the dynamics of the rubble bed in a UCG cavity in order to evaluate the possible effects of rubble bed settling and the load of the rubble bed upon the structural integrity of the dried coal on the side wall. Also, laboratory tests should be done to see if some types of coal experience structural failure of the dried coal on the side walls.

PROPOSED MODEL FOR LATERAL CAVITY GROWTH

Even though gasification was selected as the primarly mechanism of lateral cavity growth, it is interesting to note that the other two mechanisms that are possible contributors to lateral cavity growth (abrasion of the dried coal and structural failure of the dried coal) are both dependent upon heat transfer to the side wall. Therefore, regardless of which of the mechanisms or which combination of the mechanisms controls the lateral growth process, the heat transfer to the side wall will ultimately control the lateral growth process.

For the purpose of simplicity, let us consider a cylinderically symmetric cavity with a cross-section similar to that shown in Figure 7. For the injection configuration shown in Figure 7, the assumption of cylinderical symmetry is reasonable since the major pressure drop in the system will be in the rubble bed. For LLNL's CRIP configuration, the system would be somewhat less symmetric, although this two-dimensional representation will approximate the general behavior of the system. For this approximation, the inertial effects of the injected flow are neglected in addition to the rubble zone extending toward the production well.

Since the residence time of the gas in the system is considerablely less than for a coal chunk in the rubble pile, and since solid/gas systems are generally described well using the psuedo-steady state assumption; one can assume that the rubble pile and cavity boundaries remain fixed, and that the system behaves in a psuedo-steady state manner. That is, the temperature, pressure, and composition distribution throughout the system remain fixed over a reasonable time step.

Therefore, the first task is to determine the gas flow distribution, the temperature distribution, and the local solid/gas reaction rates for the rubble bed and side wall. Then based upon these results and an appropriate time step, the consumption of the coal in the rubble pile at the side wall can be calculated. The settling in the rubble pile can then be calculated as well as the lateral growth of the cavity. Also during this time step a certain amount of roof spalling will occur; therefore, this coal must be added to the top of the rubble pile. In this manner the growth of the cavity can be predicted. If several mechanisms are operating simultaneously affecting lateral cavity growth and once these are quantified, they can be interfaced with the model to include their contribution to the lateral growth of the cavity.

In order to determine the gas flow pattern, the temperature distribution, and the local coal consumption rate, the momentum, heat and mass transfer equations must be solved simultaneously. This will require an iterative numerical

procedure. First the gas flow pattern would be solved assuming Darcy's law. The flow distribution problem as posed represents a two-dimensional boundary value problem which would require an iterative numerical solution, itself.

Then the local temperature and coal consumption rate would be calculated from the local gas velocity by neglecting heat transfer by conduction; and then the flow distribution problem would have to be solved again. And so on, until changes in each of the dependent variables diminished to an acceptable level.

The model is obviously an idealization of the processes occurring in a UCG cavity; but it represents a physically realistic picture of the system and should provide valuable insight into the factors that control the performance of the process: both site specification and operational factors.

REFERENCES

1. "UCG Gas to Methanol and MTG - Gasoline - An Economic and Sensitivity Study," by the Pritchard Corporation for LLNL June 1982.

2. Massay, N.A., B.H. Gladzer, and T.F. Edgar. "Estimated Costs of Methanol, Hydrogen, and Syngas from In Situ Gasification of Texas Lignite," Proceedings of the 7th UCC Symposium, Fallen Leaf, CA, September 1981.

3. Riggs, J.B. and T.F. Edgar. "UCG Cavity Growth Models: A Critical Assessment," AIChE National Meeting, Anaheim, CA, June 1982.

4. Thorness, C.B. and R.W. Hill. "Coal Block Gasification Experiments: Laboratory Results and Field Plans," Proceedings of the 7th UCC Symposium, Fallen Leaf, CA, September 1981.

5. Garon, A.M., G.C. Cala, and J.M. Avasthi. "Rawlings UCG Test 2 Reactor Growth," Proceedings of the 8th UCC Symposium, Keystone, CO, August 1982.

6. Thorness, C.B. and R.W. Hill. "The Large Block Tests," Proceedings of the 8th UCC Symposium, Keystone, CO, August 1982.

7. Massaquoi, J.G.M. and J.B. Riggs. "Heat and Mass Transfer in a Burning Coal Seam," Proceedings of the 7th UCC Symposium, Fallen Leaf, CA, September 1981.

8. Massaquoi, J.G.M. and J.B. Riggs. "Study of the Flame Extinction for Coal under UCG Conditions," Proceedings of the 8th UCC Symposium, Keystone, CO, August 1982.

9. Hill, R.W. "Burn Cavity Growth During the Hoe Creek No. 3 UCG Experiment," Proceedings of the 7th UCC Symposium, Fallen Leaf, CA, September 1981.

10. Hill, R.W., C.B. Thorness, R. J. Cena, W.R. Armin, and D.R. Stephens. "Results from the 3rd Underground Coal Gasification Experiment at Hoe Creek," Proceedings of the 6th UCC Symposium, Shangri-La, OK, July 1980.

11. Advanti, S.H., J.K. Lee, O.K. Min, and S. Lee. "Status of Technology Associated with Cavity and Substance Response Prediction Associated with UCC," Proceedings of the 8th UCC Symposium, Keystone, CO, August 1982.

12. Jegbefume, E.U. and T.W. Thompson, "The Use of the Finite Element Method to Predict Roof Collaspe and Subsidence Resulting from UCG," Proceedings of the 7th UCC Symposium, Fallen Leaf, CA, September 1981.

13. Glass, R.E. "Thermochemical Cavity Growth Modeling," Proceedings of the 8th UCC Symposium, Keystone, CO, August 1982.

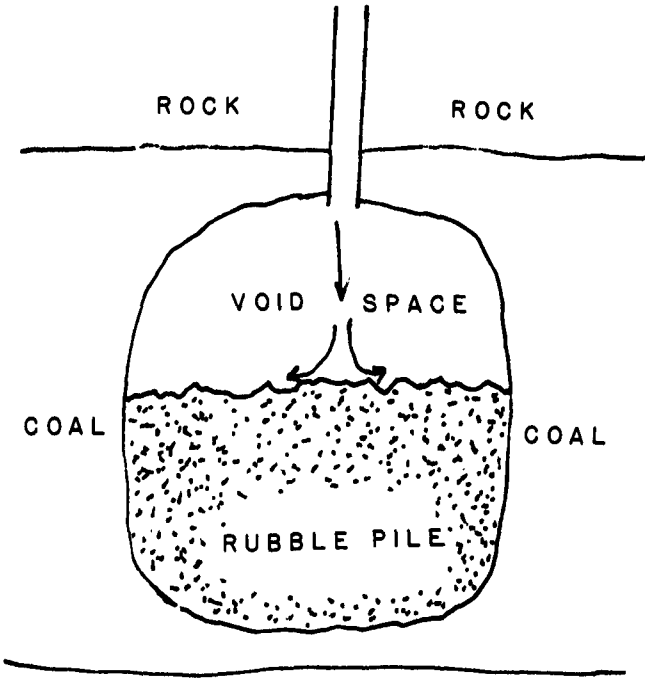

Figure 1. Cavity Configuration for Injection at the Top of the Cavity

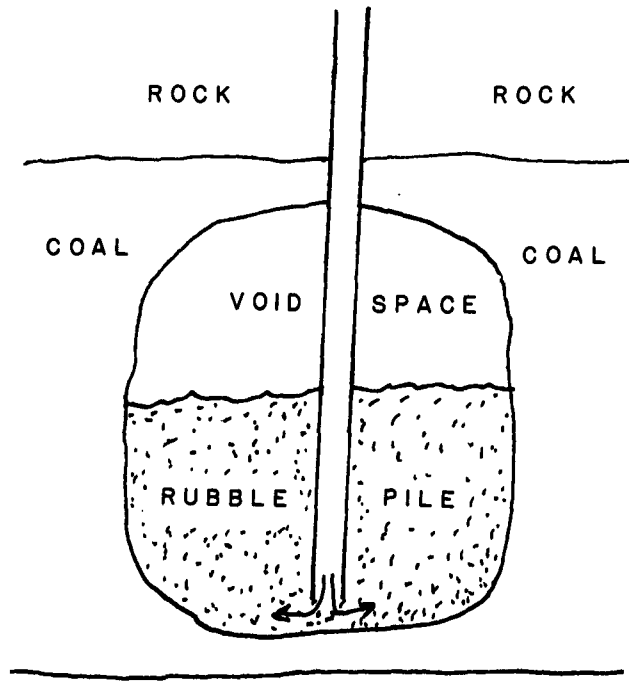

Figure 2. Cavity Configuration for Injection at the Bottom of the Rubble Pile

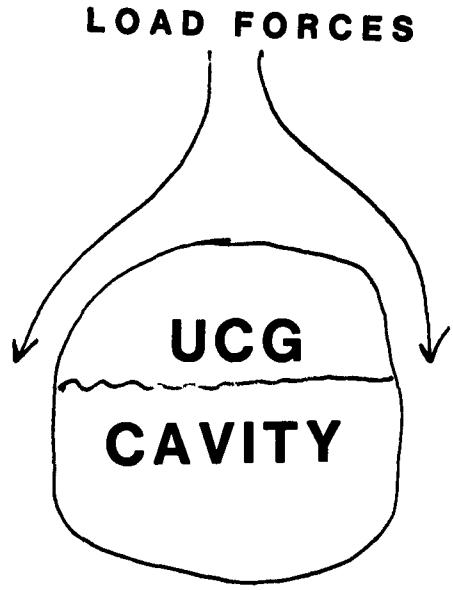

Figure 3. Side Wall Loading Caused by the Cavity

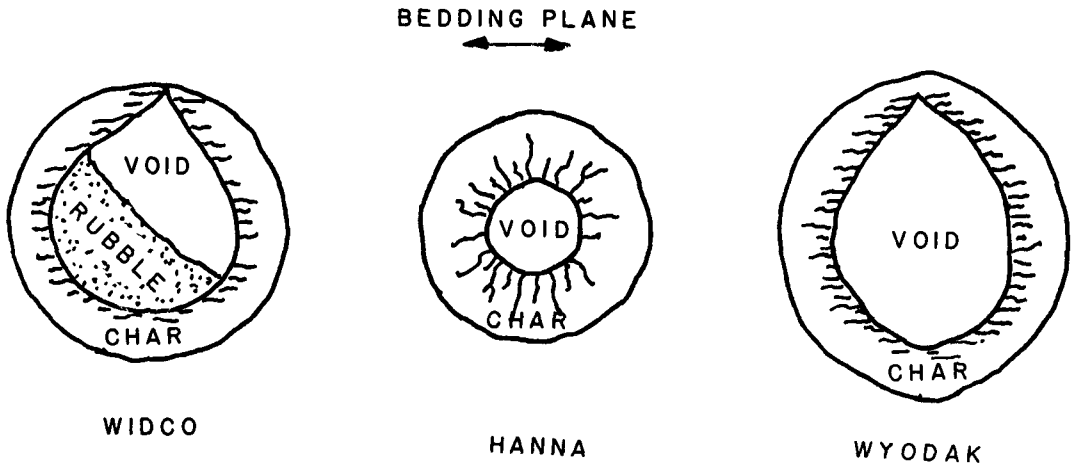

Figure 4. General Cross-Sections Observed at the End of Barrel Tests

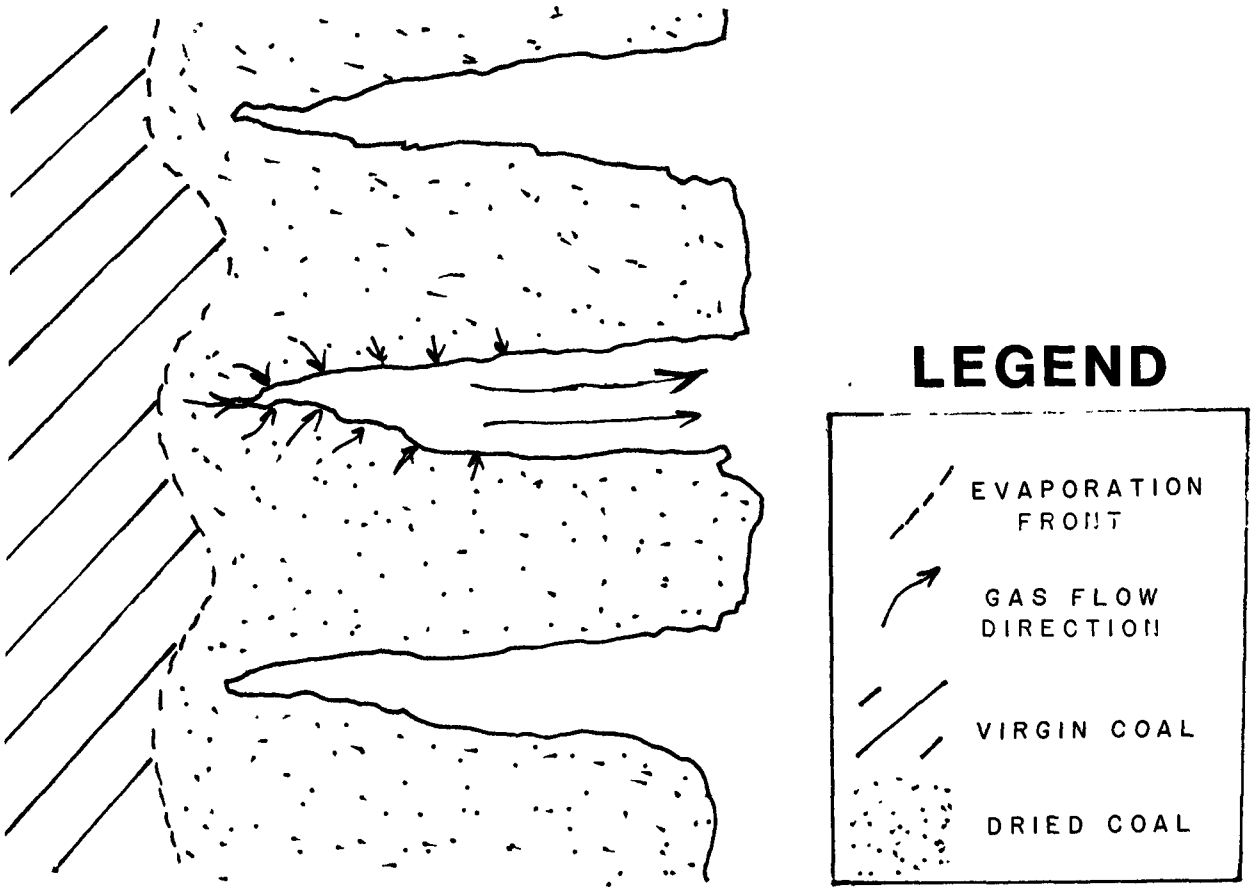

Figure 5. Side View of Altered Coal on the Side Wall

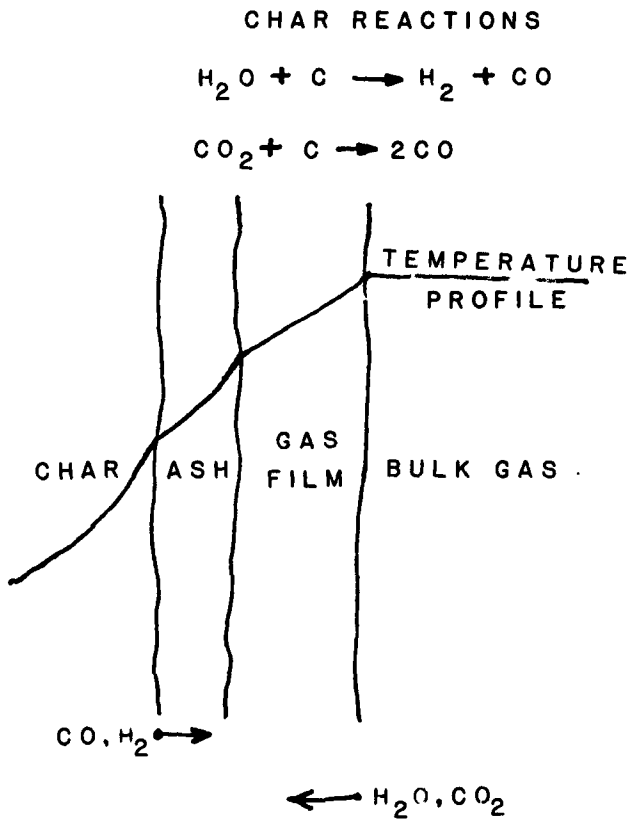

Figure 6. One-Dimensional Description of Thermally Driven Gasification

Figure 7. Cylinderically Symmetric UCG Cavity Model

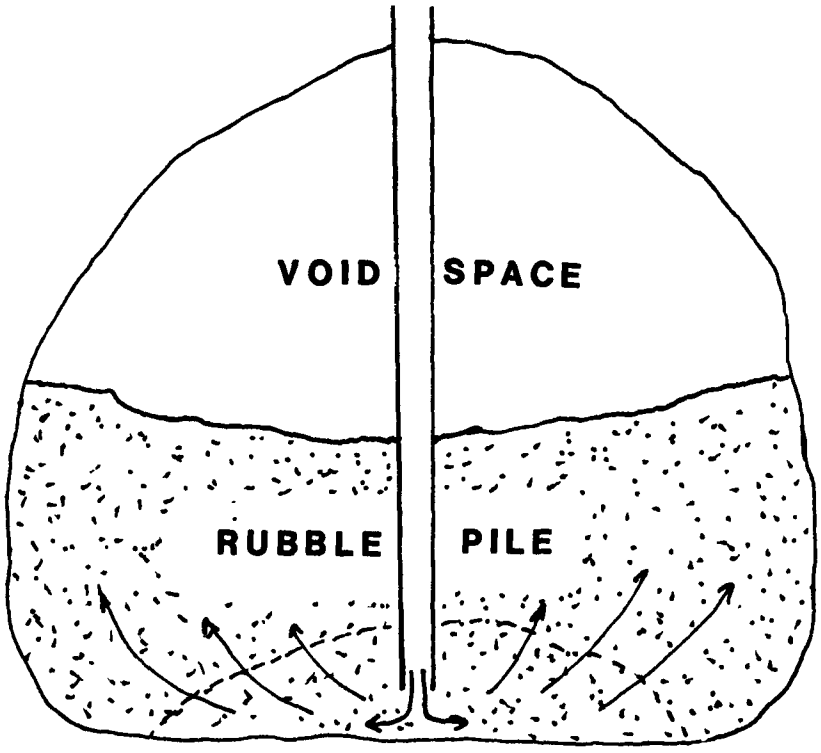

3.3 THERMAL STABILITY OF COAL CAVITIES

by

H. R. Mortazavi 1/
A. F. Emery 1/
R. C. Corlett 1/
P. A. McMurtry 1/

ABSTRACT

Temperature and thermal and moisture stress calculations are reported for different cavity shapes in which the walls are subjected to short time perturbations of surface thermal boundary conditions. The stress field found by adding these perturbation stresses to the overburden stresses are then used to estimate the probability of surface cracks penetrating into the cavity walls, leading to surface spalling and cavity growth. The paper discusses some preliminary results for tensile failure due to heat sources located on the cavity floor or in a central plume. Directions of future studies are also described.

INTRODUCTION

Because the intent of UCG is to abstract energy from coal which cannot be mined by conventional methods, it is clear that its use is rarely well defined. That is, the physical processes which are involved in the injection of air or air/steam, the reverse combustion, and the resulting production of gas are difficult to quantify and to predict. During the past several years, substantial efforts have been made to resolve many of the questions. These efforts can be conveniently divided into three categories: 1) full scale experiments, such as those at Hanna, Hoe and Rawlins with in-situ sensors and post-mortem examinations; 2) small laboratory experiments to study particular aspects of the process, such as the 55 gallon experiments at LLNL (1), and the coal block burning at the University of Washington (2) to study the kinetics of surface combustion and extinction limits of reverse combustion: 3) numerical modeling of all or selected portions of the UCG, such as those of Advani(3), Hsu(4), Harloff(5), Travis(6), Jegbefume(7), Langland(8), Levie(9), and Glass(10).

From a predictive point of view, the results of categories 2 and 3 are of particular interest. The experiments performed by Creighton(1) were designed in conjunction with numerical simulations to determine which features of the flow were most important to the process and what data must be known in order that the simulation be accurate. These small scale experiments and 2-D simulations indicated that the vortex nature of the flow at the injection well needs to be simulated if a correct description of the cavity growth is to be obtained. 2-D and 3-D computations were made by Travis(6) to study the dynamics of the dewatered regions. Unfortunately such 3-D modeling is usually so difficult and expensive that, although advisable, it is not practical. Most modeling will continue to be based upon 2-D flow and thermal fields. With this in mind, the primary advantages of the 3-D simulations are to clarify the differences between 2 and 3-D calculations in order to determine any critical differences and to provide means by which estimates based upon the 2-D analyses might be improved.

1/ Dept. of Mechanical Engineering
University of Washington FU-10
Seattle, WA 98195

The 2-D analyses of Advani(3), Harloff(5), Jegbefume(6), Langland(8), and Hsu(4) have emphasized the cavity growth history. Some of the approaches are based upon observations, such as the spalling-enhanced-drying models in which the details of the growth mechanism are neglected in favor of the semi-quantitative approach of using measured regression rates in coal and rock and assuming a growth shape in which only the roof, not the side walls, experiences regression. Although this model can be used as an aid to ensure the production of a constant energy gas, it depends upon previously measured regression rates and the assumed cavity shape. For previously unstudied UCG burns, the method is useful in a post-mortem sense to explain other observed features. If either the regression rates or the cavity growth characteristics change, the model must be modified.

Advani(3), Harloff(5), Glass(10), and others have approached the simulation on an entirely different level. In these studies, finite element or finite difference codes are employed to predict the temperature distributions in both coal and rock. From these temperatures and a knowledge of the overburden stresses and initial cavity shapes, one can predict the stresses in the region of interest. Given these stresses and some postulated failure mechanisms, it is possible to estimate how the material fails and the time history of the cavity growth. Hsu(4) has studied the formation of linkage paths by explosive charges with subsequent cavity growth and roof subsidence using dynamic material moduli, stress intensity factors and statistical failure models.

In general, failure is presumed to occur by tensile fracture, creep, charring, and compressive collapse. The predictions are extremely sensitive to the thermal and mechanical properties, the fracture strengths, and the proposed mechanisms of failure. Such mechanisms, although based upon continuumn theory, can be regarded as nearly microscopic effects in comparison to the empirical spalling models. In contrast to the latter, these microscopic approaches treat all parts of the cavity alike, in the sense that the cavity growth is a result of local failure and does not take place in a preferential or predetermined direction, and both roof and sidewall collapse are considered.

Advani's model is based upon the traditional rock mechanic fracture, but including creep effects. Hsu's approach is based upon linear fracture mechanics in which local stress intensity factors are compared to the critical values for coal. In contrast to these simulations in which the stresses are primarily induced by the thermal effects, Glass has proposed a model in which the dominant effects are those of drying with its consequent shrinkage. For diffusion controlled drying, the appropriate modelling equations are

$$\frac{\partial}{\partial x}(D_x \frac{\partial w}{\partial x}) + \frac{\partial}{\partial y}(D_y \frac{\partial w}{\partial y}) = \rho \frac{\partial w}{\partial t} \qquad (1)$$

with boundary conditions of

$$-D_n \frac{\partial w}{\partial n} = h_w (w - w_\infty) \qquad (2)$$

Heating is modelled by:

$$\frac{\partial}{\partial x}(k_x \frac{\partial T}{\partial x}) + \frac{\partial}{\partial y}(k_y \frac{\partial T}{\partial y}) + Q_{comb} = \rho c \frac{\partial T}{\partial t} \qquad (3)$$

with boundary conditions of

$$-k_n \frac{\partial T}{\partial n} = h(T - T_\infty) + h_r (T^4 - T_\infty^4) \qquad (4)$$

If the chemical reaction term in the thermal equation is neglected, and the boundary conditions are linearized it is seen that the two equations are similar and both drying and heating can be predicted in the same way. For low temperatures, or for overburdens in which there are no chemical reactions, and for cavity gases with unit Schmidt number ($\nu/D=1$) this means that the moisture content and the temperature can be estimated, one from the solution to the other.

For the combusting coal, this is not the case. However, since the vapor pressure of water is uniquely related to its temperature, we may still relate $w=f(T)$. For most materials, the shrinkage associated with drying can be expressed in the form

$$\frac{\Delta \ell}{\ell} = -\beta \Delta w \qquad (5)$$

and given that w=f(T), we may write

$$\frac{\Delta \ell}{\ell} = -\beta \frac{\partial w}{\partial T} \Delta T = \bar{\alpha} \Delta T \qquad (6)$$

where $\bar{\alpha}$ is a pseudo thermal expansion coefficient which is negative. The drying model thus gives rise to large tensile stresses in the surface layers, leading to cracks.* These cracks then permit invasive flow of the hot gases and easy escape of the water, which effectively moves the thermal boundary inwards of the true surface.

Which of these two models is more correct is not yet known. However it should be noted that the thermal effects, particularly those of creep and plastic flow, are of a much longer time scale than those of drying. Both processes are strongly affected by coal combustion, but if such combustion is restricted to the cavity surface, the computations are still tractable. Derickson and Emery(11) studied the irregular roof subsidence history of a coal mine to determine the relative effects of changing ventilation air temperatures and moisture content. For the mesh shown in figure 1, the thermal effects were found to be small in comparison to the tensile stresses induced by changes in moisture. By combining the thermal and moisture analyses with the stress field due to roof fracture, the correspondence shown on figure 2 was obtained.

CURRENT RESEARCH

In the above described modelling studies, the computations have been carried out for times comparable to those used in the actual burns and the predictions compared to estimated cavity shapes to judge the accuracy of the simulations. In Advani's model, the roof tensile failure is associated with the long term cooling (of the order of 1 year) which occurs after the burn has ceased. The cavity growth computed by Hsu is due to dynamic stress waves produced by the explosive charge located at the base of the injection well.

In our studies, we are concerned with a different aspect of the cavity growth. We assume that cavity growth is strongly affected by sidewall collapse which takes place at short times due to local variations in the thermal sources. Because of the size of the cavities, of

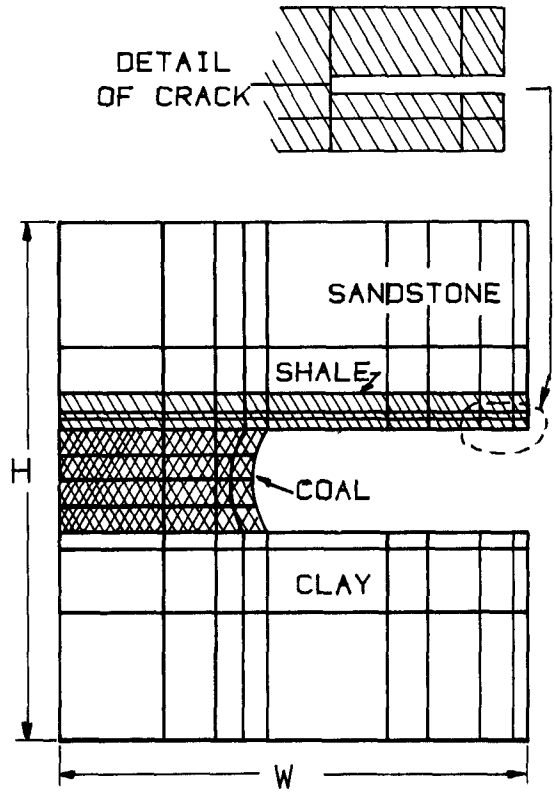

FIGURE 1 Schematic of a Mine with a Crack in the Roof Bedding Plane

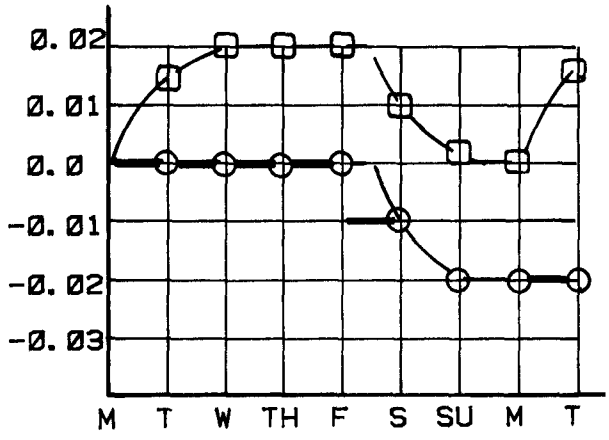

FIGURE 2 Measured (—) and Predicted (□,○) Roof Subsidence (inches) as a Function of Time
□- Without Crack Growth
○- With Crack Growth

* See note at end of paper

the order of tens of meters, and because of the very low thermal diffusivities of the coal and rock, the thermal penetration depths are extremely small and may be regarded as being confined to a very narrow layer near the surface. Since we are not sure whether the shrinkage or the thermal expansion is the cause of the failure, we have studied both effects, albeit only in an introductory sense.

In a real cavity, the thermal loading of the material is due to convection by the hot gases and radiation from the walls and from combustion occurring in the coal which has dropped to the cavity floor. At this point in our study, we have not postulated the mechanisms by which the spalling occurs. In addition, because the thermal diffusion in the coal is so slow, we are concerned only with short time effects, i.e., of the order of hours, rather than days or months. We assume that the cavity has several different shapes, illustrated in figure 3, along with the depicted different thermal boundary conditions. Because of the shape of the side walls, the different thermal source perturbations, and the radiant view the walls have of the source, a temperature gradient will exist along the wall surfaces, causing a gradient of stress, which under certain conditions may lead to local failure by tensile fracture or compressive crushing.

The simulations have been made by assuming that the moisture profiles are similar to the temperature profiles and that the shrinkage stresses can be computed from the temperature through the use of a "negative coefficient of thermal expansion". Different edge crack flaw depths have been postulated to observe the effects of the surface stresses upon the time history of failure by crack extension.

THE SIMULATION

The thermal simulation is carried out with a finite element thermal analyzer using 9 node isoparametric elements. Previous studies have shown that 4 node elements are inaccurate when computing thermal streses and 8 node elements yield inexact transient temperature fields. The program capability includes temperature and time dependent thermal and mechanical properties and heat sources and non-linear boundary conditions for convection and radiation. Although the thermal properties of coal are strongly temperature dependent, the use of such a dependence was not felt to be necessary during these introductory studies which are intended to provide a qualitative understanding of the problem. Property data were taken from reports of Hsu, Derickson and Glass. Surface heat transfer coefficients were taken from studies by McMurtry et. al. (12).

In these calculations, combustion and chemical reactions are ignored because of the short times considered and the assumption that burning occurs only at the coal surface. The computed temperatures and overburden stresses are used as input to a finite element stress analyzer from which local internal and surface stresses, stress intensity factors, and statistical probability of failure were determined.

Ignoring combustion and temperature dependent properties will underestimate the thermal penetration and thus the size of the affected zones, thereby underestimating the possibilty of failure due to drying and compressive stresses and overestimating the reverse effects which occur when the heat source perturbations cease and the coal returns to its original thermal state.

One of the major difficulties in analyzing short time effects is the extremely low thermal diffusivity of the coal and rock. With thermal penetration distances of only cm/hour, an accurate thermal stress analysis, which requires at least 1 element and preferably 2 within the penetration depth, will call for such a dense finite element mesh that computations are not economically reasonable. However, because the penetration distance is so small, and the temperature rises occur so rapidly, the problem is effectively a surface skin analysis and it is not necessary to thermally model the structure in depth. On the other hand, since changes in the surface stresses affect stresses at substantial depths, a relatively large region must be mechanically modelled. In these computations, we have assumed that these effects are confined to a thin surface layer and do not strongly affect the original overburden stresses. This assumption is valid as long as the deformations are sufficiently small that stress relief does not occur. Use of this

assumption then implies that fracture along the bedding planes does not occur and that surface cracks are sufficiently far apart or shallow enough so that the high stresses in the surface zone are not markedly reduced.

A second problem is the chronology of drying. Experiments with paper and wood drying, and numerical simulation of these processes(13) have shown that the short time effects of the increased surface temperatures are a local increase in vapor pressure with a consequent diffusion of water to the interior and increased internal wetting. Longer time effects of pressure driven vapor and capillary action reverse this inward flow and yield subsequent drying. In general the problem cannot be linearized and it is important that the short time effects of heat source perturbations be determined in conjuntion with the long time average thermal conditions. However, if the base temperature profile has existed for a sufficiently long period, the drying mechanism will have stabilized and subsequent perturbations in the moisture and thermal boundary conditions may be linearly superimposed.

RESULTS

Thermal source perturbations were assumed to be of two forms: a) a change in the floor temperature; b) a sudden plume of hot gases rising along the cavity centerline to a height of 60% of the cavity height. For the different cavity configurations shown in figure 3, the radiation viewfactors from the cavity walls to the heat sources were computed and transient temperatures calculated. For cavity shapes 1-5, the cavity wall temperatures increased and thermal expanson effects led to increased compressive stresses, thus compacting the material and reducing the possibility of spalling but increasing the probability of compressive crushing. At the same time, drying was enhanced, with a consequent shrinking of the surface material and the introduction of tensile stresses. The intensity of the thermal perturbations was assumed to be such that the radiant flux would give a maximum 400 C surface temperature change. Figure 4 illustrates typical computed temperatures and Figure 5 shows the corresponding stress profiles for 2 of the cases, one hour after the additional heat source was presumed to become effective. Regions of significant incremental stresses parallel to the surface are easily identified. These zones of high stress are also regions susceptible to failure by random internal failure, comparable to the statistical failure effects found in brittle ceramics. Values of failure probability will be computed at a future date.

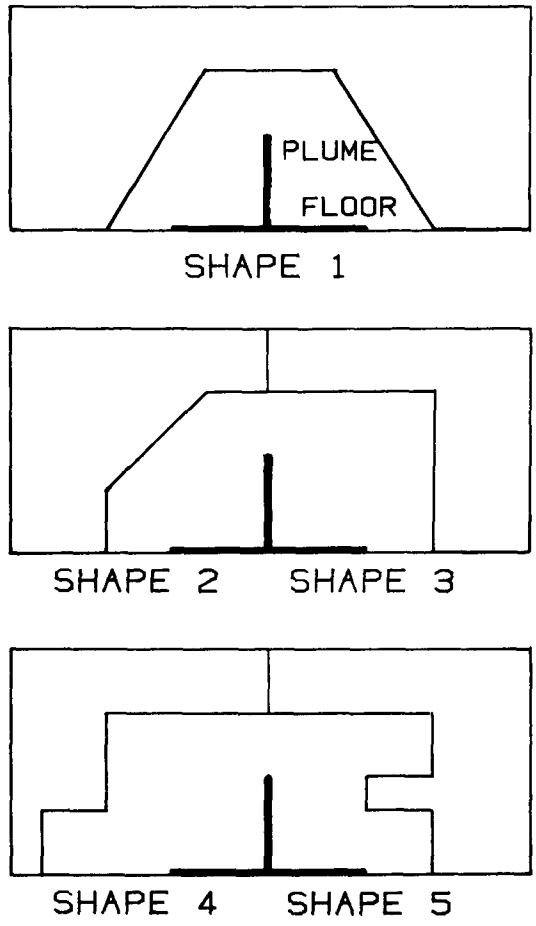

FIGURE 3 Different Cavity Shapes Considered Showing the Locations of the Heat Sources

Configuration 5, with its upper surface partially shielded from the radiant source is cooler and wetter than the lower surface, thus giving bending at the root with high local stresses and possible failure. For this configuration, because of the absence of an initial overburden stress, only the stresses due to the perturbed thermal source exist and affect failure.

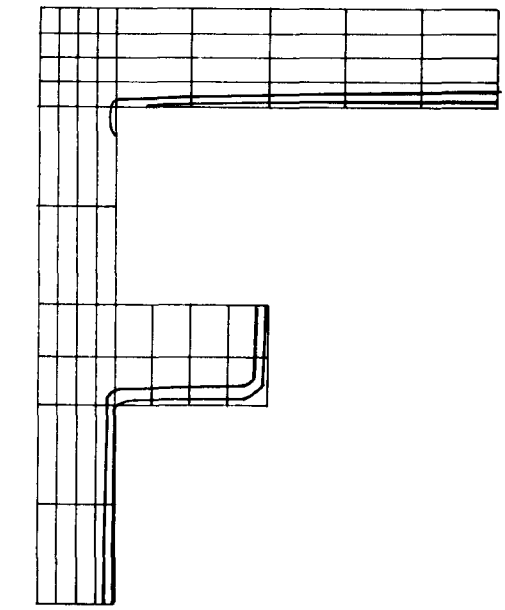

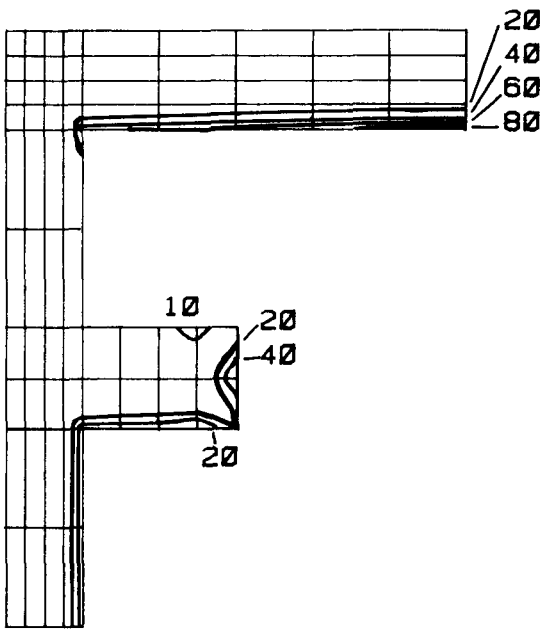

FIGURE 4 Contours of Temperature Changes (at 33%, 66% of surface temperature change) for Two of the Cavity Shapes due to a Heat Source at the Floor after 1 Hour of Exposure

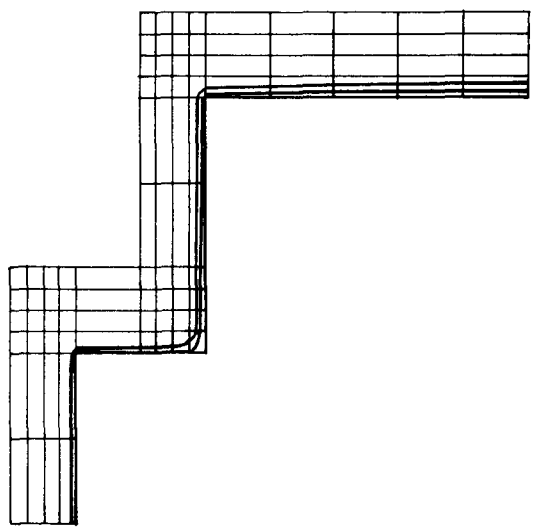

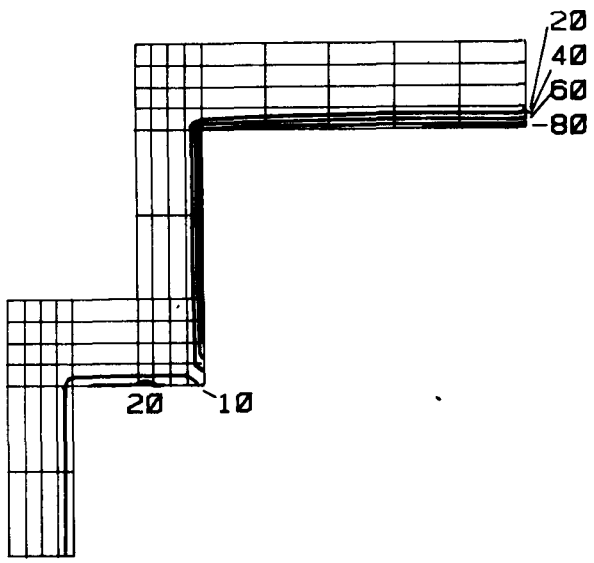

FIGURE 5 Contours of Incremental Tensile Stresses (due to drying) Parallel to the Cavity Surface (% of σ_{max})

Using these stress profiles, it is possible to estimate the tendency for surface cracks to penetrate into the coal. For shallow surface cracks, the stress intensity factor, K, is high due to the large tensile stresses near the surface. As the crack extends into the area where the stresses are compressive, the crack extension ceases. Figure 6 illustrates the temporal effect of the stresses for very shallow cracks. For h = infinity, the surface temperature and moisture content come to immediate equilibrium. As time progresses, the stress field diffuses inward and the tendency for crack extension increases. For lower surface heating and drying rates, h < infinity, the surface temperature continues to rise while the thermal effect diffuses inward. This causes a slower rise of the stress intensity factor and crack extension. Even at longer times the inhibiting effect of the finite surface heat transfer coefficient remains as evidenced by the substantially reduced values of K. Figure 7 depicts regions of high stress intensity factors for cavity shape 2. The high values of K at the center of the roof are due to the overburden stresses. However, the two regions on the side wall are due only to the thermal source, suggesting that the protruding corner will spall. If the incremental stresses are compressive, the marked side regions are susceptible to compressive crushing.

Under these thermal stresses, if the surface defect is an angular or rounded notch, rather than a sharp edge crack, there will be considerable difference in the crack extension history if the notch surface is not exposed to the thermal loading. This is most likely to occur with radiant heating of the side walls from the floor or of the roof from a plume. In these cases, the maximum stresses and stress intensity factors are approximately 15% less and delayed in time (14) in comparison to those observed if the notch surface is directly exposed to the thermal conditions. Calculations for these cases did not show significant differences in the size or location of the possible failure regions.

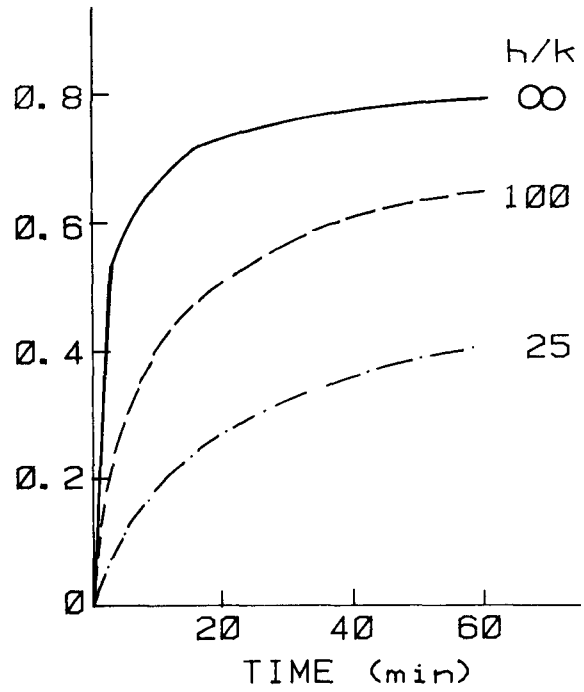

FIGURE 6 Effect of a Finite Surface Heat Transfer Coefficient (h) on the Stress Intensity Factor $K/\alpha E(T - T_{initial})$ as a Function of Time

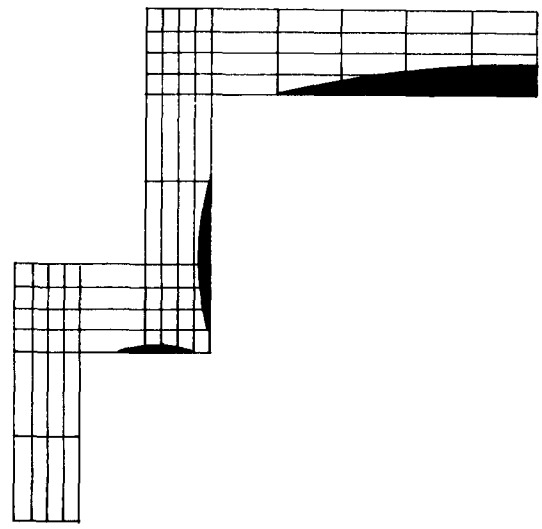

FIGURE 7 Areas of High Stress Intensity Factor due to the Combined Overburden and Moisture Stresses for a Floor Heat Source after 1 hour of Exposure

CONCLUSIONS

These introductory simulations were made to gain some qualitative understanding of the stresses due to thermal perturbations. Substantially more work is needed to include the effects of combustion, charring, a more precise description of moisture transport, and the effects of local surface spalling with the consequent exposure of new surfaces. It is our intent to couple these computations with concurrent studies of the thermophysical reactions taking place in the coal and in the gases within the cavity(12). The aim of the complete study is to provide a method for predicting the response of the cavity walls to temporally and spatially random fluctuations in the thermal boundary conditions. By using concepts of fracture mechanics and statistical failure models, it should be possible to provide a technique to estimate both the history of the cavity growth and of the formation of, and the size of the rubble which is expected to form from large portions of spalled surface material.

ACKNOWLEDGEMENT

The work reported in this paper was supported in part by U.S. Department of Energy/University of Washington contract DE-AS20-82LC10884.

REFERENCES

1. Creighton, J. R.,"Effects of Gas Flow Patterns on Cavity Shape", Proc. Seventh Underground Coal Conversion Symposium, Conf. No. 810923 (1981)

2. Corlett, R. C., and Shearer, D. R.,"The Channel Flow Flame Region of Borehole Reverse Combustion", ibid.

3. Advani, S. H., Lee, J. K., and Min, O. K., "Formulations, Simulations, and Evaluations Associated with Thermo-mechanical and Poro-elastic Models for Underground Coal Conversion", ibid.

4. Hsu, T. R., Fracture and Thermal Conditioning of Canadian Coals, Interim Report 2, Coal Research Group, University of Manitoba, Winnepeg, Canada, 1982

5. Harloff, G. J., "A Two-Dimensional Model of Underground Coal Gasification and Cavity Growth with Application to the Canadian Forestburg Test of 1976", Proc. Seventh Underground Coal Conversion Symposium, Conf. No. 810923 (1981)

6. Travis, B. J., and Nuttall, H. E., "An Analysis of Preburn Three-Dimensional Flow Patterns in Underground Coal Conversion", ibid.

7. Jegbefume, E. U., and Thompson, T. W., "The Use of the Finite Element Method to Predict Roof Collapse and Subsidence Resulting From The Underground Gasification of Coal", ibid

8. Langland, R. T. and Trent, B. C., "Computer Models To Support Investigations of Surface Subsidence and Associated Ground Motion Induced by Underground Coal Gasification,", ibid.

9. Levie, B. F. and Krantz, W. B., "A Model for Roof Spalling and its Application to Predicting Cavity Shapes for the Hanna III UCG Field Test", Proc. Eighth Underground Coal Conversion Symposium, SAND82-2355, 1982

10. Glass, R. E., The Effect of Thermal and Mechanical Properties on Initial Cavity Growth, SAND81-1063, Sandia National Laboratory, 1981

11. Derickson, L. W. Jr. and Emery, A. F., "The Effect of Moisture and Temperature upon the Behavior of an Unsupported Coal Mine Roof", Proc. 20th U. S. Symposium on Rock Mechanics, 1979

12. McMurtry,P. A. ,et. al., "Comprehensive Numerical Model of Forward Combustion Along a Channel", to be presented at the Ninth Underground Coal Conversion Symposium, 1983

13. Dorri, B., Emery, A. F. and Malte, P. C., "Drying Rate of Wood Particles with Longitudinal Mass Transfer", to be presented at the 2nd International Conference on Numerical Methods in Heat Transfer, Seattle, 1983

14. Emery, A. F., Williams, J. A., Avery, J., "Thermal Stress Concentration Caused by Structural Discontinuities", SESA J. Exp Mech, pp 558-564, December 1969

Note: In this paper, thermal stresses should be taken to mean any stresses caused by a positive coefficient of thermal expansion. Likewise, moisture stresses should be taken in representative of stresses associated with the negative coefficient of thermal expansion.

3.4 AN UNDERGROUND COAL GASIFICATION CAVITY SIMULATOR WITH SOLID MOTION

by

C. B. Thorsness[1/]
R. J. Cena[1/]

ABSTRACT

The prediction of cavity growth and product composition have long been major goals in the development of underground coal gasification (UCG). Lawrence Livermore National Laboratory (LLNL) is developing a UCG cavity growth model which incorporates many of the key features observed during our recent large block (LBK) tests conducted at the WIDCo mine at Centralia, Washington, in which early cavity growth and product yield were studied. Postburn excavation following the tests revealed oval-shaped, rubble-filled cavities with significant void space under the cavity roof. The bottom portion of the cavity contained ash and slag, with an overlying rubble region of coal, char, and ash. A void space existed between the rubble pile and the cavity roof which was generally flat with square corners, a result of the apparent breaking away and falling in of the roof material.

The model divides the cavity into three zones consisting of ash, rubble, and void, with provision for movement of solids between zones. In the model, the cavity roof and walls regress at rates dependent on fluid velocities and temperatures within the cavity. The fluid velocities are determined by the geometry of the cavity in conjunction with the calculated temperatures and injection rates, assuming Darcy flow in a non-isotropic permeable medium. The fluid velocities along with the rubble-forming rates are input to a chemical/thermal model which determines product composition and cavity temperatures.

In this paper, basic features of the model are described and a number of preliminary runs are documented. These runs include matching of the LBK data, studies of sensitivity to variations in model parameters and operational parameters, and calculations of possible performance of the upcoming Centralia partial-seam CRIP test.

INTRODUCTION

In the past ten years or so, a number of models have been developed to describe the underground coal gasification (UCG) process. The models can be grouped into two categories:

- Those incorporating detailed physics aimed at specific aspects of UCG.
- Those containing general or composite physics aimed at the overall UCG process.

The models in both categories have their merits. Those looking at specific details of the UCG process often are able to elucidate important physics which may not be clearly discerned in a more general model. In addition, the models are often verifiable from first principles or via simple laboratory measurements. However, since these models do not deal with the overall process, care must be exercised in their use to avoid misleading

[1/]Lawrence Livermore National Laboratory, Livermore, CA 94550.

conclusions outside the range of global material-balance and energy-balance constraints. The overall or composite models, on the other hand, are generally built around material-balance and energy-balance constraints which are implicitly satisfied. However, to make the physics tractable, the models generally incorporate many simplifying assumptions which may or may not encompass the true physics controlling the UCG process. Furthermore, the composite models often depend on parameters that are difficult to measure or estimate, and thus the calculated results have been to a large extent unverifiable, making model validation an extremely difficult task.

Our renewed interest in composite models, despite their apparent drawbacks, comes as a result of five large block (LBK) tests conducted by LLNL at the WIDCo mine near Centralia, Washington. Detailed process information,[1] coupled with extensive excavation mapping[2] of the five LBK burn cavities, has provided us with a reasonably clear picture of cavity growth behavior during the early stages of UCG. The LBK results have provided us with the necessary data base for testing and evaluating composite UCG models in terms of (1) their physics, (2) their parameters, and (3) their results. Of course, validation of the model is limited to early cavity growth at the LBK site; however, we feel the basic physics of the model will prove applicable to larger cavities and other coals, with additional tests planned to aid in the verification process.

Excavation of the LBK tests mapped the burn cavities using vertical slices or cross sections perpendicular to the horizontal borehole connecting injection and production points in each test. Some representative examples of the cavities found are shown in Fig. 1. From these and other data, we have drawn the following conclusions concerning growth of burn cavities at the WIDCo site:

- The burn cavities in general can be described as elliptical cylinders symmetric about the borehole with more vertical than horizontal growth and very little downward growth.

- The cylinders are largest in the vicinity of the injection point, with gradual tapering in both the upstream and downstream directions.

- Most importantly, the cavities are filled with char rubble containing a void region at the top and an ash sublayer below. In addition, the ash sublayer generally demarks the region of active cavity growth.

We feel, from these observations, that the physics of early cavity growth at the WIDCo site includes the following features:

- Oxygen consumption of the char rubble causes settling of the bed, which creates void space at the top of the developing cavity and an ash sublayer at the bottom.

- Rubbling of roof and wall material into the void space via several mechanisms (e.g., gravity, mechanical interaction, heat attack) causes cavity growth and replenishment of the rubble pile.

- A roof rubbling rate that is more rapid than the wall rubbling rate causes somewhat elliptical cavity growth.

Using the above physics, we have undertaken to construct a global model of UCG which, unlike our earlier work,[3] explicitly incorporates solid motion as the key mechanism for cavity growth. It also differs from our earlier work and from a number of other UCG models in that cavity shape (coal recovery) and gas composition are considered in one integrated model.

The criteria used in formulating and implementing the model included the following:

- It must calculate all the important process parameters: gas flow rate, temperatures and pressures, gas composition, and cavity shape.

- It must be efficient enough that many different calculations can be performed with a limited amount of computer resources.

- The model physics must be general enough to determine the influence of important operating parameters such as injected gas flow rate, composition, and pressure.

- Complexity would be included or added only if dictated by available data.

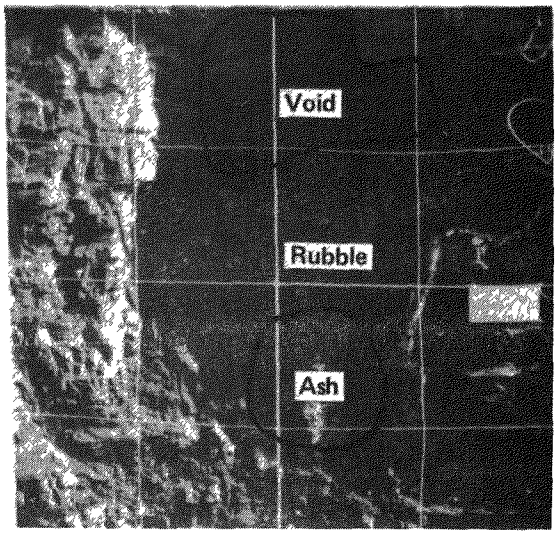

(a) LBK-4, slice 4.

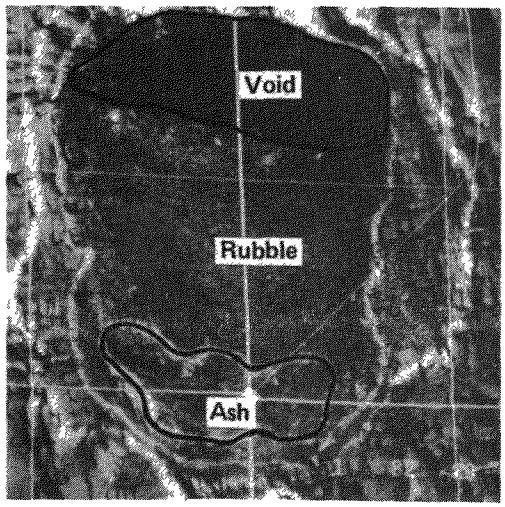

(b) LBK-1, slice 13.

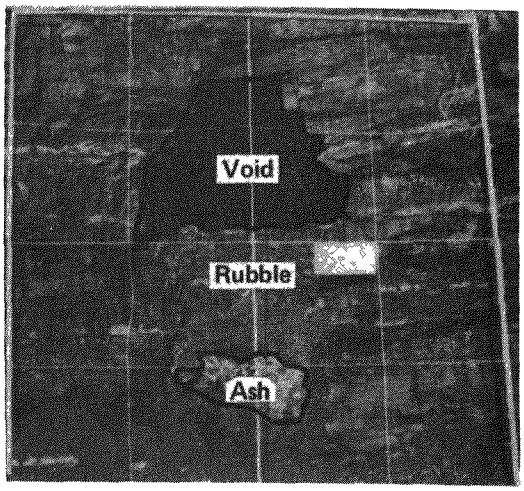

(c) LBK-4, slice 3.

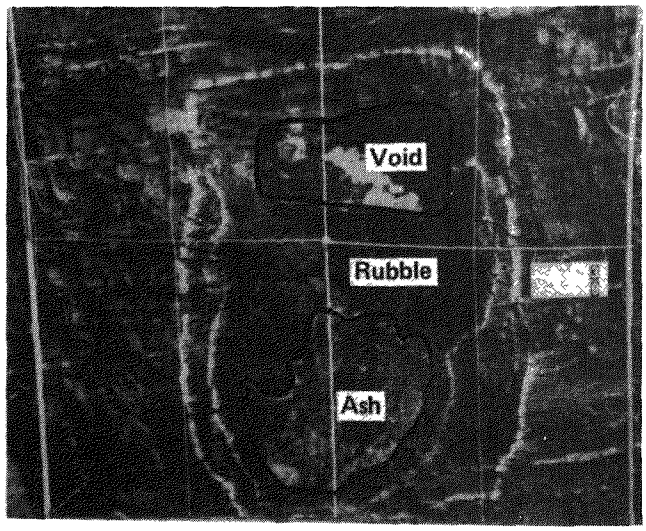

(d) LBK-3, slice 9.

Fig. 1. Typical cavities observed during excavation of the LBK tests (grid lines 1 meter apart).

- It must be compatible with the LBK test data.

In the following, we first briefly describe the model. Then we describe our fit of the LBK tests with particular emphasis on the LBK-1 results. Using the LBK-1 fit as a base case, we then outline the influence of model and process parameters on the calculated results, elucidating features of the model physics. Finally, we show model calculations for our upcoming partial-seam CRIP test scheduled to be fielded in the fall of 1983.[4]

MODEL DESCRIPTION

Any model of the UCG process requires certain simplifying assumptions in order to make the problem tractable. The first simplification we employed was to assume the system could be broken down

into three separate submodels: (1) a fluid flow model, (2) a cavity growth model, and (3) a thermal/chemical model. These are coupled together to model the overall process. Each of these major submodels, in turn, employs additional simplifying assumptions which are discussed below. The model is based on a three-dimensional view of the underground system. We define the x-coordinate by a line connecting the injection and production points of the system. The y-coordinate represents the vertical dimension, and the z-coordinate is the width.

The fluid flow model works primarily on the x,y plane, with the width (the z-coordinate) accounted for in an approximate fashion. The cavity growth and thermal/chemical models deal primarily with slices perpendicular to the x-coordinate in the y,z plane. These slices are then coupled together along the x-coordinate to complete the 3-D picture.

The model recognizes a number of species and compositions. The fluid flow and cavity growth models deal with ash, char rubble, void, coal, and gas. The thermal/chemical model further divides the gas and solids. The gas is divided into 14 species: argon, nitrogen, oxygen, hydrogen, methane, carbon monoxide, carbon dioxide, ethane, ethylene, H_2S, C_6, H_{10}, tar and water vapor. The C_6 and H_{10} species represent pseudo compounds that account for measured light hydrogen species not listed, while tar accounts for the heavy hydrocarbon species. Coal is assumed to be composed of water, ash, and dry coal (consisting of carbon, hydrogen, oxygen, sulfur, and nitrogen). Up to 21 separate species of char are defined, dependent on temperature, consisting of varying amounts of the same elements as dry coal.

Two additional materials, not yet fully implemented in the model, are mobile water and rock. These materials are important when water influx or overburden interaction becomes significant.

Flow Model

The flow submodel is built upon the simplified picture of the underground system shown in Fig. 2, representing the x,y plane of the system. Two separate calculations are performed. First, the general flow field throughout the entire cavity is solved for, followed by a convective/dispersive solution to determine oxygen concentrations within the ash sublayer. As the figure implies, the flow path is primarily within the ash or char rubble. For this reason we have chosen to solve for the velocity field assuming Darcy flow in an anisotropic permeable medium. The flow solution accounts for variations in temperature, pressure and gas source terms throughout the cavity. The solution is basically two-dimensional, with the effect of the third dimension (the cavity width) accounted for in determining the cross-sectional areas for flow.

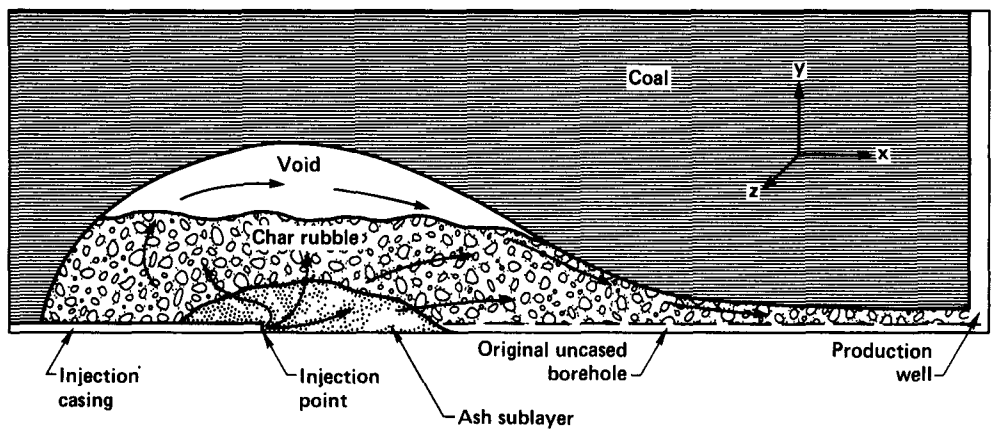

Fig. 2. Darcy flow model in an anisotropic permeable medium. (Longitudinal vertical cross section of cavity.)

Permeabilities of the various regions are input to the model. The two most important are the ash and char rubble permeabilities, with the coal set several orders of magnitude lower and the void set several orders of magnitude higher than either of these two. In addition, a vertical-to-horizontal anisotropy factor may be assigned to each region in the model, and the model also provides a mechanism to enhance permeability at the coal/rubble-pile interface.

After obtaining the average velocity field throughout the cavity using Darcy flow, we solve a convective/dispersive equation to determine oxygen fluxes within the ash sublayer, assuming zero oxygen concentration along the boundary. The oxygen flux is assumed to be primarily convective, with a small amount of dispersion included proportional to the local velocity.

The calculated oxygen flux along the ash/char boundary is the primary result of this submodel and is the driving function for the thermal/chemical submodel. In addition, the calculated velocities throughout the cavity provide input to the cavity growth submodel.

Cavity Growth Model

This submodel calculates the cavity growth and determines, within the system, the location of all material interfaces: (1) ash/char, (2) char/void or char/coal, and (3) void/coal. The basic geometry assumed in the model is shown in Fig. 3, which represents a typical y,z planar slice perpendicular to the x-coordinate. The original borehole connecting the injection and production points is indicated by a small cross in the figure.

The cavity growth model assumes two basic growth mechanisms: (1) roof growth, which occurs in the void region, and (2) wall growth, which occurs in the char rubble region. A third growth, downward, is assumed to occur by the same mechanism, but at a fraction of the wall growth rate. We typically assume the fraction to be zero.

The roof growth in the model takes the form:

$$R_r = a + bw + cw^2,$$

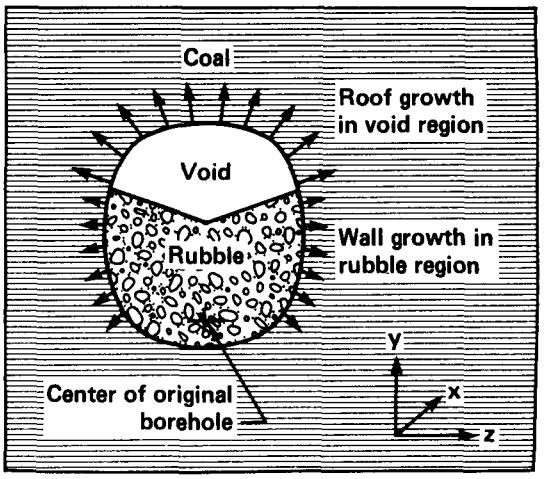

Fig. 3. Cavity growth model showing regions of roof and wall growth. (Transverse vertical cross section of cavity.)

where w is the cavity width (z-coordinate) at the void/rubble interface. In addition, when the cavity temperature falls below a prescribed temperature, T_w, the roof rate is reduced linearly by a simple factor. In keeping with our philosophy of simple physics when possible, to date we have assumed no width dependence in the roof rate (i.e., b = c = 0), which adequately matches the LBK results.

The wall growth rate in the rubble zone is assumed to be proportional to a temperature difference and the local gas velocity. The hypothesis used to obtain this relation is the following. First, we assume the attack on the wall is primarily thermally driven; that is, the rate of growth of the rubble zone depends on the rate of energy arrival at the coal/rubble interface. In addition, it is assumed that the rubble bed is constantly settling as char is consumed, setting up a shear stress at the coal/rubble interface. This shear is capable of dislodging char from the wall and incorporating it in the rubble bed once the coal or char is sufficiently weakened as a result of drying and pyrolysis. The strength of the forming char is further assumed to be directly related to the local char temperature. We define a parameter T_w as the temperature at which this sufficiently weak state has been reached. We currently assume T_w = 500°C. The heat transport to the effective cavity wall is then modeled after a simple

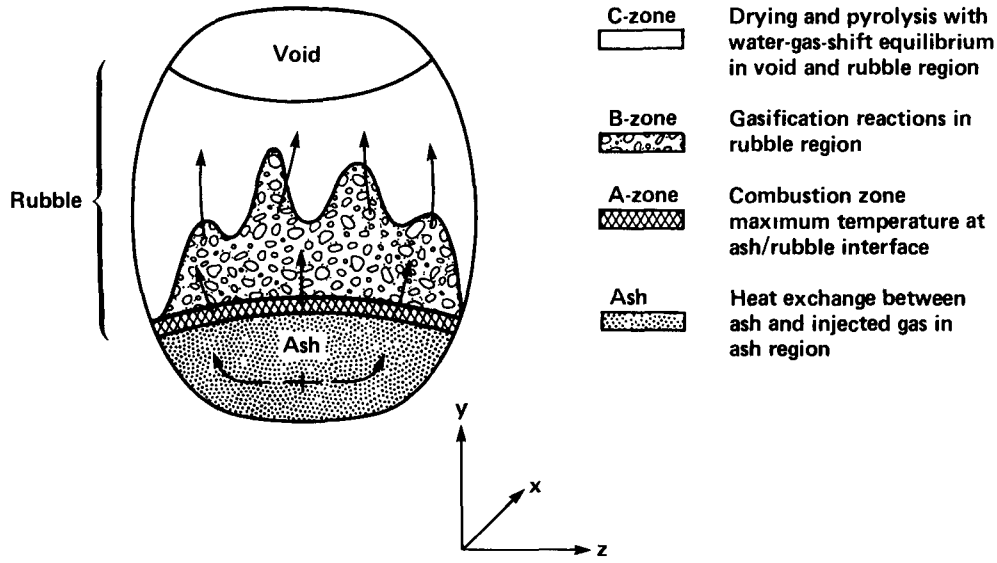

Fig. 4. Chemical/thermal model showing four zones: ash, A, B, and C zones. (Transverse vertical cross section of cavity.)

packed bed concept. This ultimately leads to a relation for wall growth given by

$$R_w = k_w V^{0.8} (T_g - T_w),$$

where k_w is a constant which may depend on coal properties and rubble properties, V is the local average gas velocity, and T_g is the gas temperature in the slice.

We have found that this simple division of growth into wall and roof rate is able to generate a variety of cavity shapes. These shapes depend on the relative magnitude of the wall and roof growth rates and the amount of void present. Among those shapes generated are ones that are quite similar to those observed at the LBK tests.

The calculated interface movement and coal rubbling rate are the primary results of this submodel. The coal rubbling rate is a primary input to the thermal/chemical submodel, while the interface changes affect the fluid flow submodel.

The cavity growth submodel includes several additional features. There is a provision for allowing the bed surface to take on a prescribed shape. Different shapes can be imposed on the cross-sectional view shown in Fig. 3 and on the longitudinal view shown in Fig. 2. Also, some amount of smoothing of the growth rates in both these two views is employed. Finally, a limit to growth of the cavity is placed on regions where char is only being created and not consumed. This is accomplished by letting the char rubble density increase above its base value and smoothly reducing the wall growth rate and eventually setting it to zero when char rubble density reaches a prescribed level.

Chemical/Thermal Model

The chemical/thermal submodel is formulated based on the cross-sectional view of the cavity shown in Fig. 4, representing the y,z plane. Four zones are shown in the figure: the ash zone, previously defined, and the A, B, and C subzones of the chemical/thermal model. Since the model is zero-dimensional, the size and shape of the A, B, and C zones have no significance except in visualizing the elements of the model. The solution is performed on a slice-by-slice basis, proceeding from the far upstream end of the cavity to the downstream production point. The gas flow is visualized as flowing up from the ash into the A zone, then to the B zone, and finally into the C zone. The ash zone is seen as continuous in the x-direction (i.e., in and out of the plane of the figure), as is the C zone. As a result, flow moves up and downstream in these

zones. No up or downstream flow is incorporated into the A zone, because it is assumed to be very thin, nor into the B zone, because it is assumed to be encompassed by the C zone. These four zones then form the basis for writing the thermal/chemical relations for the system.

The A zone, a very thin zone lying at the ash/char interface, represents the initial contact of the injected gases with the char. We employ this zone to estimate maximum temperatures within the underground system. Our estimates to date are based on an equilibrium model which requires complete equilibrium between the gas species: CO, CO_2, H_2O, and H_2 and char. This allows plausible estimates of temperatures for low steam/oxygen ratio systems and air gasification systems, but for higher steam/oxygen ratios (e.g., 2/1, 3/1) the computed temperatures are so low that the assumption of equilibrium is certainly incorrect. We hope to improve the performance of this zone in the future by implementing a different, possibly rate-based model.

Zone B is where the bulk of the gasification is assumed to occur. On the basis of our previous work,[3] we have chosen a very simple specification for this zone.This simple specification appears to capture enough of the physics to allow gas compositions to be estimated adequately and at the same time requires a minimum of computational effort and detailed information. The basic assumption made is that in the B zone, the gasification reactions

$$C + H_2O \rightarrow CO + H_2,$$

$$C + CO_2 \rightarrow 2CO$$

occur and at the same time the gas remains in water-gas-shift equilibrium,

$$CO + H_2O \rightleftarrows CO_2 + H_2.$$

The premise for the model is that the extent of the endothermic gasification reactions is thermally limited, proceeding only as long as the temperature remains sufficiently high. As they proceed, the temperature declines to a point where the rates become so slow that the reactions essentially shut off. At this point we assume the water-gas-shift kinetics are still sufficiently rapid to maintain equilibrium.

With the above premise, we need only specify the temperature, T_c, at which the gasification reactions become slow, which, in conjunction with material and energy balances and the water-gas-shift equilibrium assumption, completely specifies the gas composition and char consumption within zone B.

The char consumed in reaction zone B must come from outside sources. Either or both of the following two extremes may exist: (1) all char enters zone B after it is preheated (dried and pyrolyzed) in zone C, and (2) all char enters zone B directly in the form of wet coal. The adjustable parameter, β, has been implemented in the model to specify any combination of these two cases.

For $\beta = 0$, the quasi one-dimensional case, all of the coal passes through zone C prior to entering B. In this case, the entire heat load required to dry and pyrolyze the coal comes from the sensible heat of the gas leaving zone B. This leads to very low zone C temperatures and extremely efficient gasification (with a minimum heat load on B), both of which are inconsistent with the LBK results. For $\beta = 1$, the well-mixed case, all of the coal enters B directly, which places a maximum heat load on B, reducing the efficiency of gasification while raising zone C temperatures. This case seems more consistent with the LBK results, with $\beta = 0.8$ producing a good match.

We have attempted to implement one β value for all slices and all times as the simplest physics. However, on occasion no solution is possible at the desired β due to insufficient or excess quantities of gas or solids. In these cases, the model adjusts β in the ranges of 0 to 1 in an attempt to obtain a solution. To some extent this is an expedient method to allow the solution to proceed, but it does in many cases reflect the physical reality of the active gasification zone expanding and contracting in response to the reactants present.

From the B zone the gas flows into the C zone. In the C zone we assume all the coal that was not consumed directly in the B zone is dried and pyrolyzed. The gas is assumed to be in water-gas-shift equilibrium if the temperature exceeds T_s (the temperature at which

the water-gas-shift reaction becomes too slow) and all the hydrocarbon products produced by pyrolysis maintain their identity. If the heat balance imposes a temperature below T_s, then only a fraction of the gas is maintained at water-gas-shift equilibrium, with simple mixing occurring therafter. The gases produced in the current slice are mixed with those of upstream slices. Zone C encompasses most of the cavity and includes the bulk of the char rubble and all of the void.

Gas production, temperatures, and char consumption are the primary results of this submodel. The temperatures and char consumption results are input to the cavity growth submodel, and the gas production and temperatures are input to the flow submodel.

The only source of hydrocarbons in the current formulation of the model are those produced by pyrolysis of coal. We handle pyrolysis in the following manner. When the coal is heated, it forms gas, tar, water, and char, the amount of each being a function of the temperature to which the coal is heated. In the model we discretize temperature levels for purposes of calculating pyrolysis products. We do this with a table, based on experimental measurements, that includes the products and char composition at each of the prescribed temperature levels. When the model heats coal, it uses this table to liberate the proper gas components and form the proper char. We assume that incremental heating from one level to the next will release gases and cause char composition changes consistent with the table. The model allows char to cool but does not allow reverse pyrolysis to occur, so that new gases are released and the char composition is changed only if the char is heated to a level it has not encountered before. Finally, the model assumes that all hydrocarbons liberated in the B zone are destroyed. Only those liberated in the C zone are allowed to continue on downstream.

The adequacy of such a simple model is certainly suspect. In particular, we have good reason to believe that additional methane beyond that available from simple pyrolysis is generated and that much of the tar produced is ultimately cracked or coked. We hope to ultimately incoporate these processes into the model, probably by defining a set of secondary pyrolysis reactions which act on the hydrocarbon species and convert them from one form to another, based on some simple rate expressions.

The ash zone represents the final region considered explicitly by the thermal/chemical model. There is no chemistry performed in this zone, only a thermal balance. This balance involves the injected gas stream and the hot ash created in the A and B zones. Since gas, in general, is only injected at one point and then flows in the ash toward both ends of the cavity, the model employs a solution scheme for the ash zone which involves proceeding in two directions from the injection point.

Implementation

The model is currently embodied in a FORTRAN computer code running on a Cray-1 computer. Approximately 150,000 words of memory are required for a typical run. The running time for the average size problem is about 0.5 to 1 second per time step, and approximately 100 to 200 time steps are required for a full simulation. The typical problem is discretized into 27 variable-width slices. The coding is such that redimensioning is simple and problem size specifications are easily changed.

A number of special cases often are encountered for brief periods during the course of a given simulation. These cases involve situations in which the underlying assumptions on which the model was formulated break down. A discussion of the methods employed in these situations is beyond the scope of the present report but will be dealt with in a later one.[5]

MODEL FIT OF LBK RESULTS

The LBK tests[1,2] provide extensive evidence of cavity growth and system performance during the early stages of UCG (at least at one site). The test results provide the necessary framework for development and testing of the model physics during this early cavity growth period. Although successful comparison of model and field results does not necessarily validate the model, the opposite is definitely true; i.e., an unsuccessful comparison is certainly the result

of wrong or incomplete model physics. During the fitting process, the model physics was developed as needed to overcome observed deficiencies. Our approach was to keep the physics as simple as possible while obtaining an adequate comparison. Also, when more complicated physics was indicated, the reasonableness of any additions was analyzed in light of the extensive LBK results.

All of the LBK tests showed similar behavior in both product yield and excavation attributes. The LBK-1 test was selected for detailed model comparison because it was relatively free from the complications of gas losses and uncertain injection locations experienced during the other tests.

LBK-1 Process Data

The model comparison focuses on two main areas: (1) general cavity dimensions and compositions, and (2) cumulative product yields. Extensive process instrumentation provided accurate measurement of cumulative product yields, while less precise excavation results mapped the general cavity dimensions.

For the LBK-1 comparison two times are noteworthy. The first, 58 hours, is the total time from the beginning of the test during which a normal fast-flow schedule was maintained using 3/1 steam/oxygen injection. This is the best time for comparison of cumulative product yields. The second time, 68 hours, is the total time that gas was injected into the main LBK-1 cavity (end of pre-CRIP period), but incorporates a period of erratic gas injection. This later time is best for comparing cavity dimensions. After 68 hours, a CRIP maneuver was performed, moving the injection point back 7 meters with an additional 28% of injection occurring. Comparisons of cavity shapes and volumes assume that the original cavity was relatively unaffected by the post-CRIP gasification phase of the experiment.

Excavation Data

Each of the LBK tests was excavated in slices perpendicular to the borehole connecting the horizontal injection lance and the vertical production well. Each slice was of sufficient cross section to map the entire area of activity with approximately 12 slices per experiment (2-meter intervals). Visual and chemical analysis of the slices provided a record of the extent of cavity growth, as well as the amount of ash, rubble, and void present. Samples of rubble were analyzed and found to contain varying amounts of coal, modified coal (char), and ash. Average densities of the ash and rubble regions were measured, allowing estimates of material masses to be calculated. Because of the varied nature of the rubble pile, error bars must be placed on the composition and amount of char left in the underground system.

Based on the slice results, a longitudinal cross section of each of the LBK tests can be constructed, which when coupled with the slice profiles provides a complete picture of the final burn cavities. Although accurate, these actual longitudinal cross sections can be misleading due to slice variations. Thus, to aid in the model comparison, we employed a fitting process to smooth the slice profiles while maintaining the volumetric information. The procedure was to fit each slice area with an ellipse of equal area. Ellipses were chosen from the overall appearance of the excavated cavities. A single elliptical aspect ratio was used for each test, determined from the volume-weighted average aspect ratio of the slices. The longitudinal cross section for LBK-1 resulting from this fitting procedure (shown in Fig. 5) is the one used in the model comparisons.

In Fig. 5, the injection point is shown at the 6-meter mark; the production point is at 20 meters, off the figure to the right. Note the significant upstream growth of the ash layer along with a downstream tail extending past the 12-meter mark. A relatively flat char/rubble zone is shown, along with a void region which is entirely contained within the region of ash growth. The rubble to the right of the figure necks down rapidly to form an exit channel approximately 2/3 of a meter in diameter which extends to the production well.

Model Parameters

The physical properties of coal, char/rubble, and ash were measured to determine densities, permeabilities, and

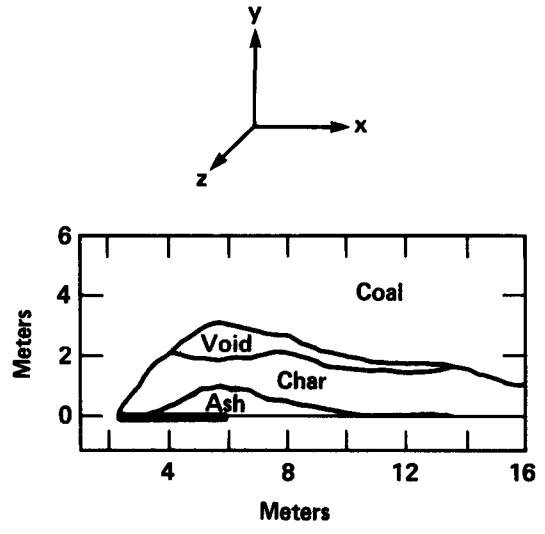

Fig. 5. Longitudinal vertical cross section of the LBK-1 pre-CRIP burn based on excavation data. The wide horizontal line at the bottom of the graph running to the 6-meter mark is the injection lance.

chemical composition. The measured densities and compositions were used directly in the model, while the sample permeabilities were used merely as a yardstick since they may not resemble those of the undisturbed system. One of the key parameters of the model is the rate at which the roof breaks up and falls onto the rubble pile. Table 1 explores the assumption of a constant rubbling rate for each of the five LBK tests by dividing the maximum observed cavity height by the total forward gasification time. Quite good agreement is shown among the tests, with the average of 1.1×10^{-5} m/s close to the 1.06×10^{-5} m/s used in the model.

Permeability contrasts between the ash and char were examined in an attempt to match the LBK-1 results. The first runs assumed the simplest case of equal permeability, which produced rapid short-circuiting of oxygen in the injection slice. The general pattern was for the ash zone to grow rapidly upward, consuming rubble and intersecting the void very quickly. The resultant cavity was localized near the injection slice with little or no upstream ash growth. Decreasing the ash permeability showed no improvement, and although increasing the ash permeability did promote more downstream growth, the upstream ash growth was unaffected.

Since simple permeability contrasts were unsuccessful in matching the LBK-1 data, our next level of complexity was to introduce a vertical-to-horizontal anisotropy factor, defined as a permeability ratio, k_y/k_x. Using equal horizontal permeability for the ash and char and an anisotropy factor of 0.1 in the ash produced cavities with significant upstream and downstream growth, similar to the LBK-1 excavation results (Fig. 5). Such an apparent anisotropy may be the result of the original horizontally drilled borehole or possibly the effect of slagging at the ash/char interface, which was observed during excavation.

Two parameters were introduced into the model to alleviate specific problems. First, the crack factor was introduced to account for a region of enhanced permeability at the coal/rubble interface. The

Table 1. Roof rubbling rate for the five LBK tests, calculated as the total observed cavity height divided by the total forward gasification time.

LBK expt. number	Cavity height (meters)	Time (days)	Roof rubbling rate (μm/s)
1	3.1	2.9	12.0
2	2.4	3.0	9.3
3	3.8	4.6	9.6
4	3.0	2.5	14.0
5	2.9	2.7	12.0
		Average	11.0

execavation results indicated the existence of such a region, which probably carried much of the exit gas flow. Hence the crack factor was added to the model to simulate the presence of this region. The second parameter, leveling, was introduced to overcome the problem of rubble-pile peaks and valleys which tended to form in the model. Since no evidence of an irregular rubble pile surface was detected in the field, we chose to smooth the peaks and valleys using a leveling criterion, stating a maximum slope above which leveling occurs.

The model employing the parameters discussed thus far produced cavities similar to those mapped in the field. Once this general match was obtained, several other parameters were adjusted to improve the match of the LBK-1 results. The first one, the wall growth parameter (k_w), strongly influenced the amount of rubble (and void) within the cavity. This parameter was adjusted until the amount of char rubble and void approximated the estimate for the LBK-1 test.

Two parameters primarily influencing the cumulative product yield were adjusted to match the LBK-1 product gas results. The first, T_c, is the minimum temperature at which the gasification reactions are assumed to occur. Preliminary runs tended to calculate more efficient gasification than experienced in the field. By increasing T_c, the carbon-carrying capability of the gas is reduced, which tends toward less efficient gasification. The second parameter, β, is the fraction of coal dried and pyrolyzed in the gasification zone B. Increasing this fraction puts a higher heat load on the B zone, which also tends to produce less efficient gasification. Adjustment of these two parameters allowed us to achieve a reasonably good match to the LBK-1 process results.

A third parameter, T_s, the minimum temperature at which water-gas-shift equilibrium is allowed, was not adjusted in the matching process since cavity temperatures were well above any reasonable estimates of this temperature cutoff.

Field gasification generally produced hydrocarbon yields different than would be predicted by simple coal pyrolysis, primarily more CH_4 and less tar. Undoubtedly some hydrogenation and tar cracking and coking occurs during UCG to account for these discrepancies. The model is being developed with a pyrolysis submodel to accommodate secondary reactions; however, the details of its implementation have not yet been worked out. In the interim, we have arbitrarily adjusted the pyrolysis reaction to produce excess CH_4 and no tar in order to match reasonably well the production of these species.

The parameters listed in Table 2 produced the best match of the LBK-1 data. Using these parameters, the model produced the longitudinal cross sections (x,y plane) and slice profiles (y,z plane), versus time, shown in Figs. 6 through 8. Comparison of Figs. 8 and 5 shows the shape similarities between the model and excavation results. The overall shape agreement is quite good, the most notable exception being that the extent of upstream char growth is somewhat less in the model. Since the final cavity shape may have been altered slightly by the CRIP portion of the LBK-1 test, closer matching between model and experiment seems unwarranted.

Table 3 compares cavity volumes and cumulative product yields between model and test. Agreement of the major product species, processing ratios, and cavity volumes is quite satisfactory.

As stated earlier, the pyrolysis portion of the model was adjusted to approximately match CH_4 and the other hydrocarbons. Further work is needed to obtain closer agreement of these species.

Due to the wide variation in slice profiles found in the field, direct comparison with the model profiles is not easy. However, the model profiles are in general agreement with the rough elliptical shapes of the field data.

For completeness, the model-calculated velocity profile at the end of the experiment and plots of the important operating parameters versus time are shown in Figs. 9 through 12. It is interesting to note that the trend in the relative amounts of CO and CO_2 in Fig. 12 is similar to that recorded in the field.

Table 2. Model parameters used to fit the LBK-1 data.

Density (kg/m^3):	
Coal (wet, with ash)	1384
Char rubble	540
Ash	580
Permeability (m^2)[a]:	
Coal	1.5×10^{-12}
Char rubble	1.5×10^{-8}
Ash	1.5×10^{-8}
Void	1.5×10^{-4}
Permeability ratio,[a] k_y/k_x	
Coal	1.0
Char rubble	1.0
Ash	0.1
Crack factor[a] (m)	3×10^{-4}
Leveling slope, y/x	0.1
Roof rubbling rate (m/s)	1.06×10^{-5}
Wall rubbling rate parameter,[a] k_w	1.8×10^{-6}
Gasification cutoff temp,[a] T_c (°K)	1373.
Water-gas-shift cutoff temp, T_s (°K)	773.
β factor[a]	0.8

[a]Values altered in parameter sensitivity studies.

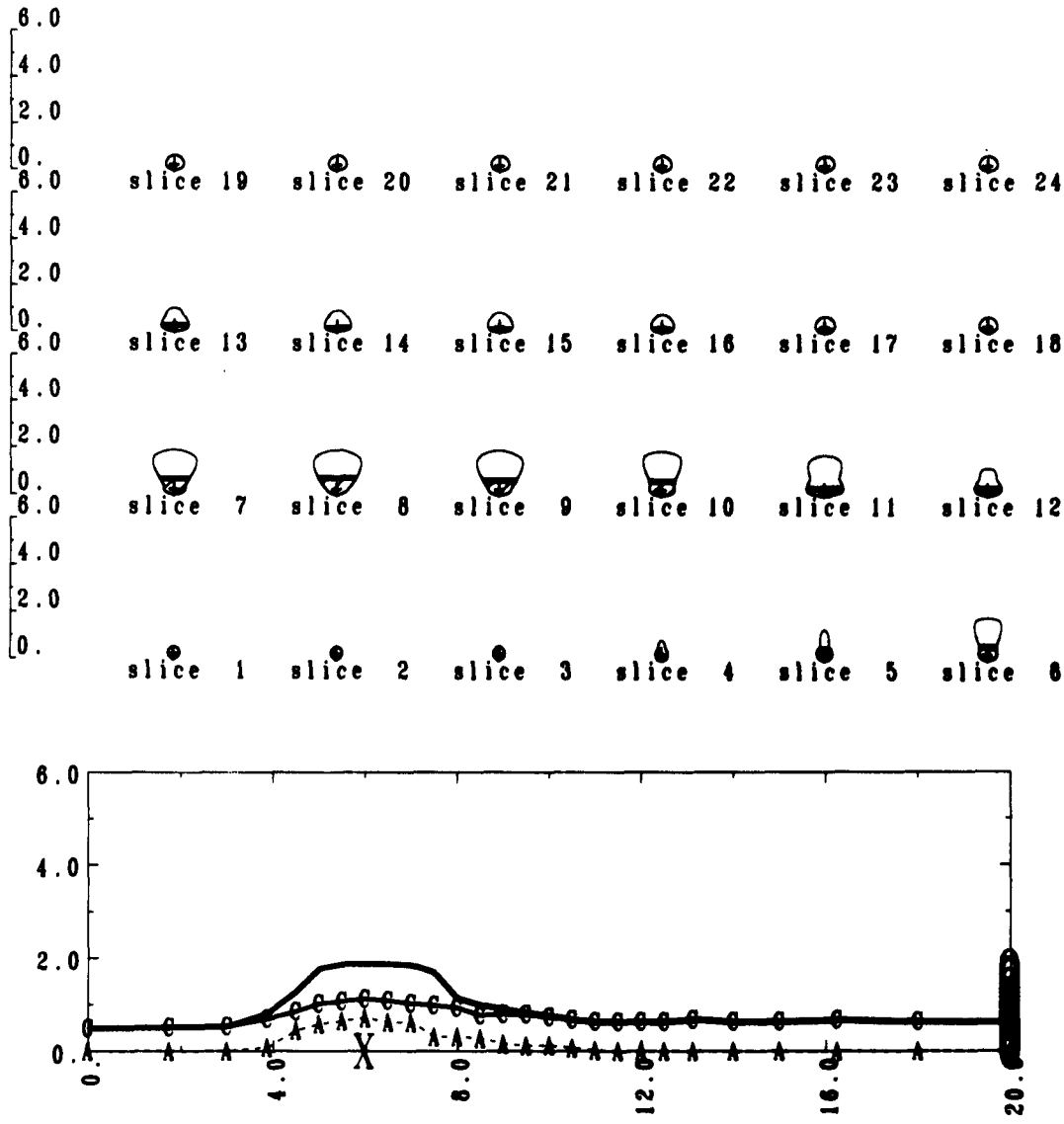

Fig. 6. Calculated longitudinal cross section and slice profiles at 36 hours (0.18 Mmol of O_2 injected) for the LBK-1 test. Slices 25-27 not shown. Injection point at slice 8 is indicated by X. Production is indicated by vertical stack of circles at far right of system.

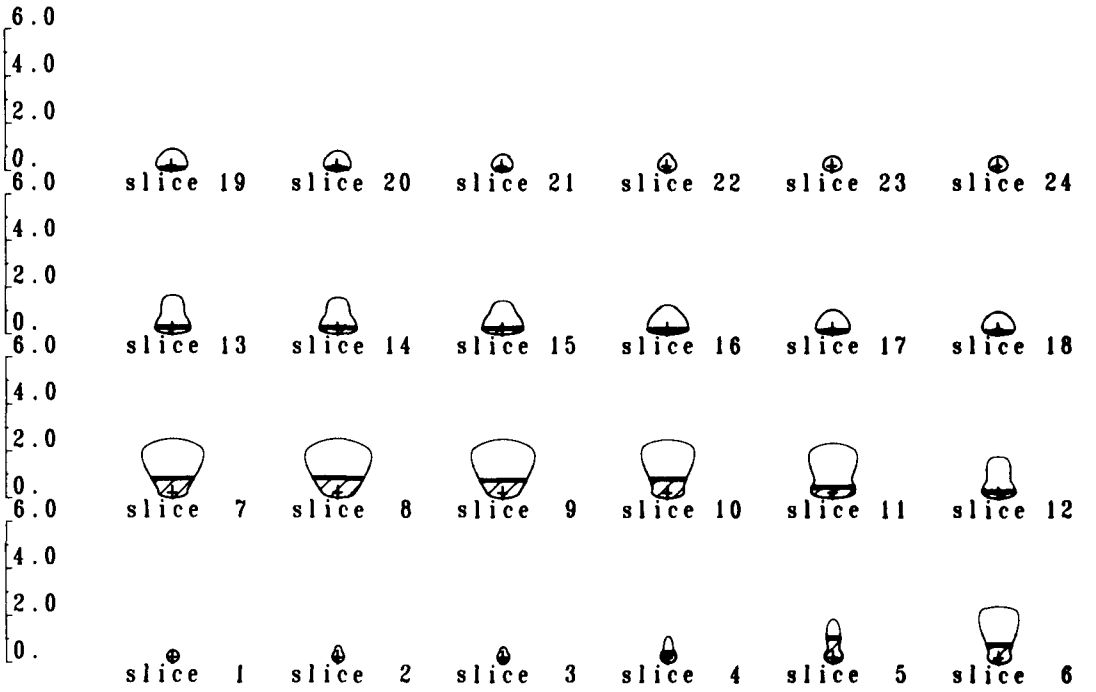

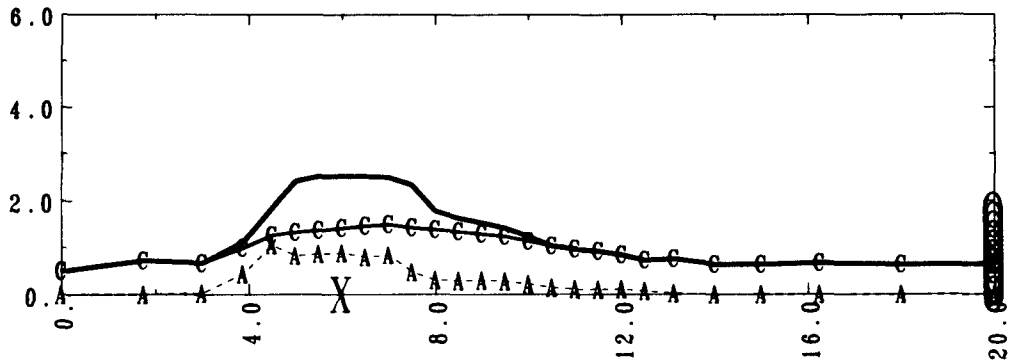

Fig. 7. Calculated longitudinal cross section and slice profiles at 53 hours (0.38 Mmol of O_2 injected) for the LBK-1 test.

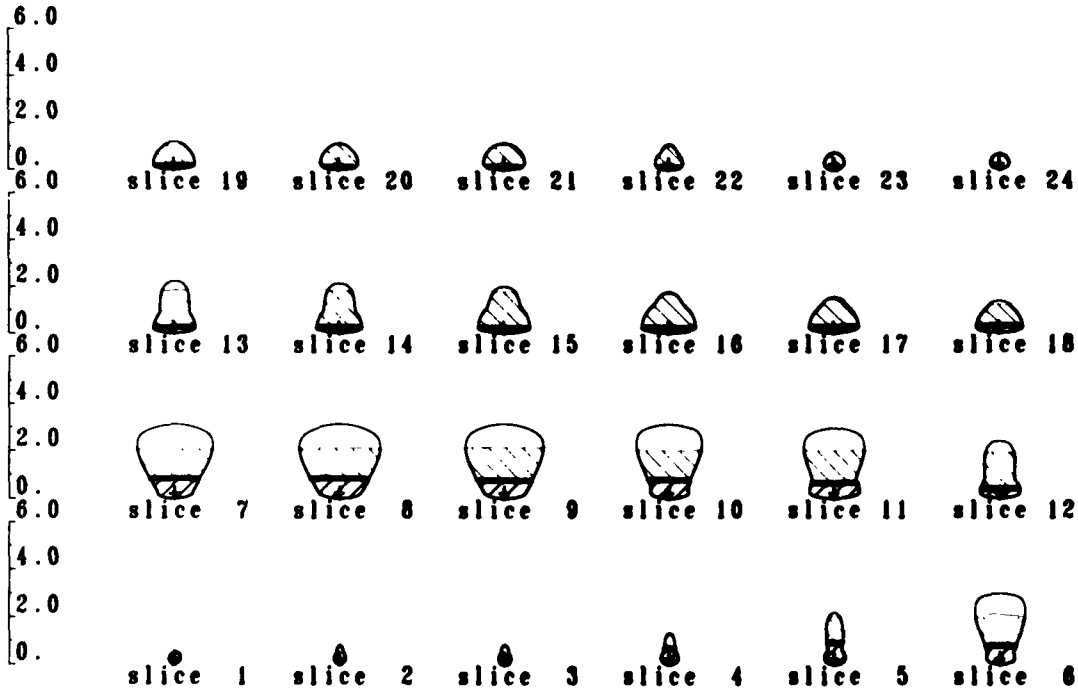

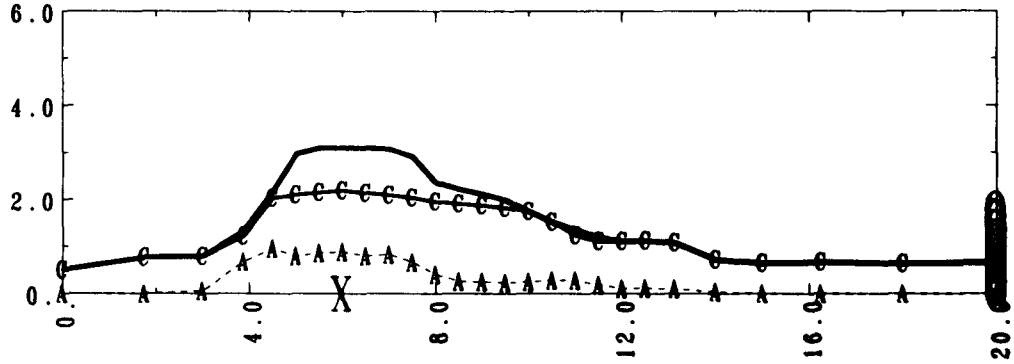

Fig. 8. Calculated longitudinal cross section and slice profiles at 68 hours (0.58 Mmol of O_2 injected) for the LBK-1 test.

Table 3. Comparison of model calculations with LBK-1 test results. All values are for an experimental time of 58 hours, except the volumes, which are for 68 hours.

	LBK-1 test data	Model results
Dry product gas composition (mole fraction):		
N_2	0.004	0.004
H_2	0.42	0.44
CH_4	0.035	0.026
CO	0.25	0.22
CO_2	0.28	0.30
C_2H_4	0.0039	0.00016
C_2H_6	0.0011	0.0010
C_6	0.0008	0.0005
H_{10}	0.0019	0.0006
H_2S	0.0018	0.0020
Produced H_2O/dry gas (mol/mol)	1.10	0.89
Produced carbon per mole injected O_2 (mol/mol)	2.2	2.1
Dry product gas per mole injected O_2 (mol/mol)	3.8	3.8
Product heat of combustion (dry, tar-free; kJ/mol)	230.	220.
Product heat of combustion per mole injected O_2 (kJ/mol)	890.	820.
Total O_2 injected (Mmol)	0.48	0.45
Cavity volumes in active zone (m^3):		
Void	8.	7.
Char	19.	21.
Ash	6.	6.
Total	33.	33.

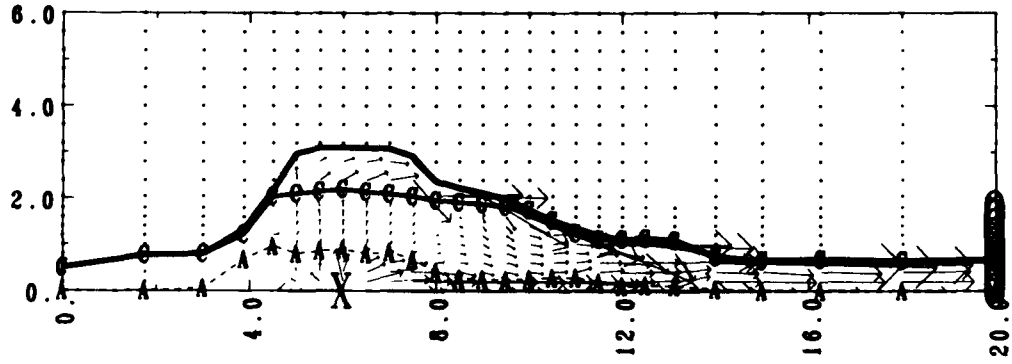

Fig. 9. Calculated velocity field at 68 hours for the LBK-1 test. Vector length is proportional to the local velocity, vector location is approximate.

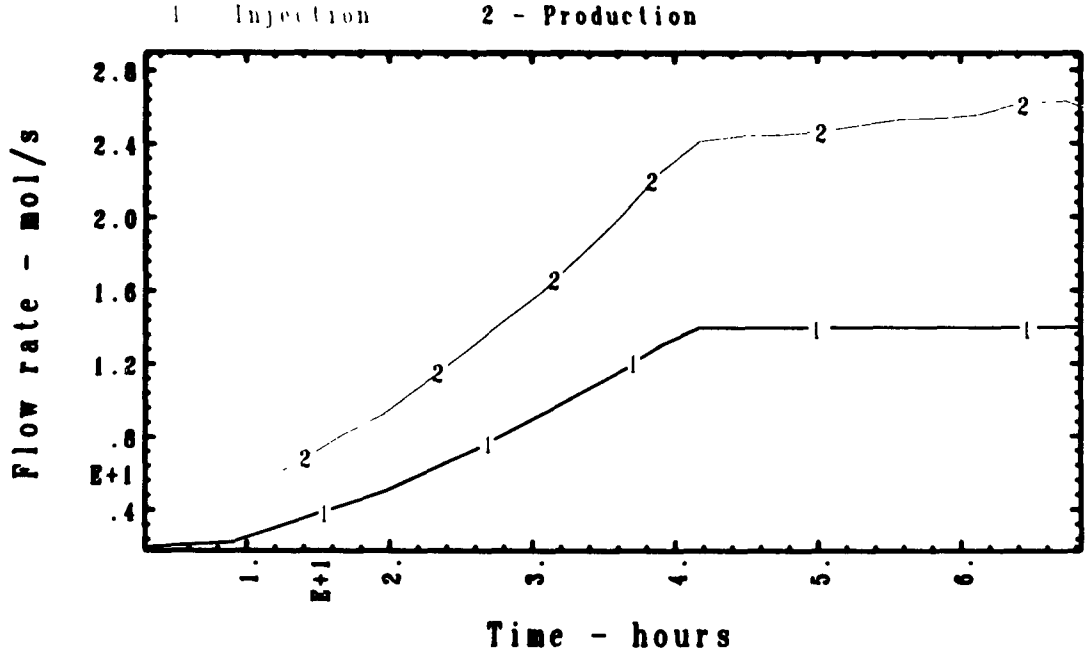

Fig. 10. Injection flow (curve 1) used in the model match of the LBK-1 test. Product flow (curve 2) was calculated by the model.

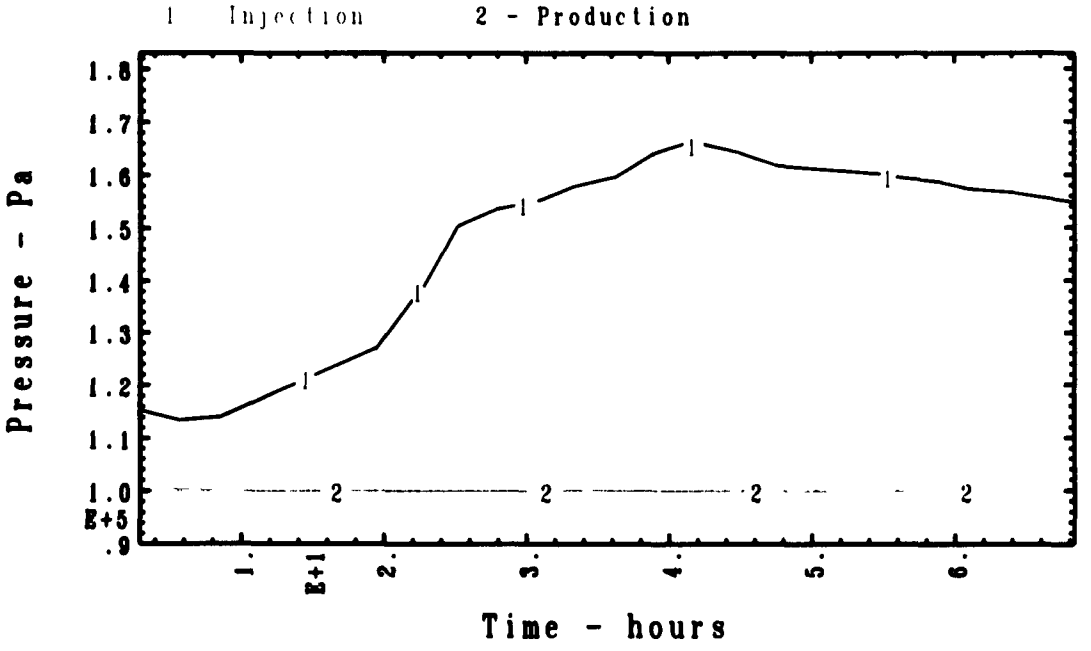

Fig. 11. For the model match of the LBK-1 test, the injection pressure was calculated by the model assuming the constant production pressure maintained in the test.

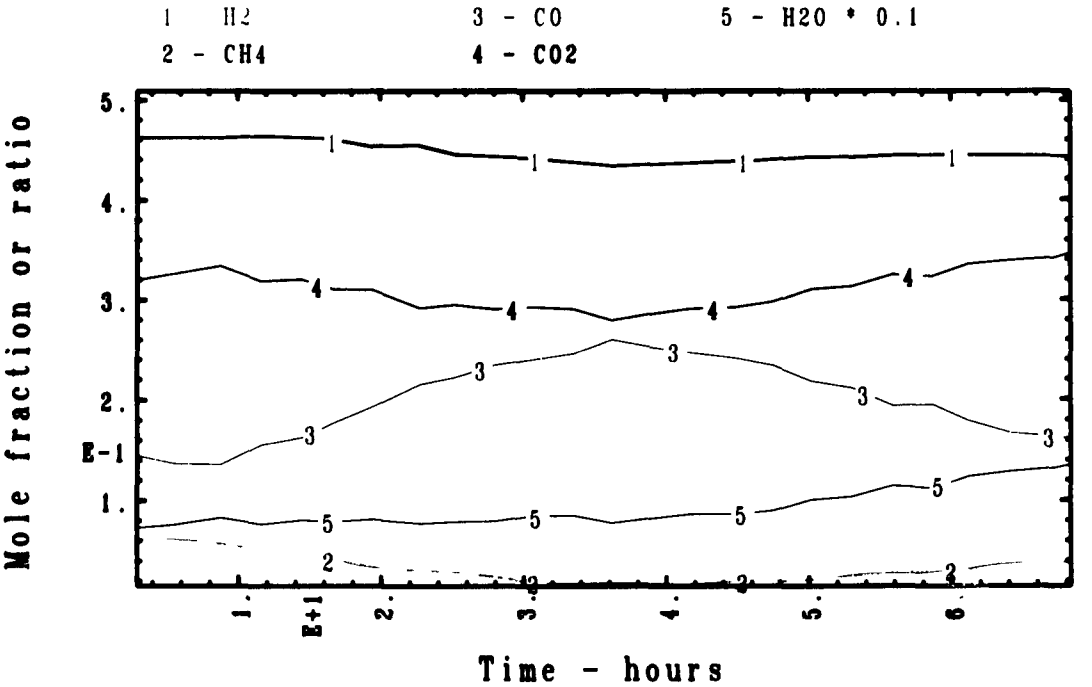

Fig. 12. Product gas composition as calculated by the model for the LBK-1 test match. Dry-gas mole fractions for H_2, CH_4, CO, and CO_2 are included, as well as the water-to-dry-gas mole ratio of the product (curve 5).

EFFECTS OF VARYING THE MODEL PARAMETERS

The parameters used to fit the LBK-1 results are listed in Table 3. To more fully elucidate the model physics, it is instructive to show the model's sensitivity to perturbations in this base set of parameters.

Tables 4 through 6 and Fig. 13 summarize the results of the comparisons. All of the cases were compared at 36 hours (to minimize computing costs), and to improve readability the vertical dimension in Fig. 13 was expanded by a factor of 2.

The sensitivity of the model to permeability contrasts is explored first. The base case of equal horizontal permeability for ash and rubble, with vertical/horizontal anisotropy of 0.1 in the ash, is compared with two other cases in Table 4 and Fig. 13(a)-(c). The first case assumes no anisotropy with equal ash and rubble permeability, and the second case assumes no anisotropy with the ash permeability ten times higher than that of the rubble. The results show severe retardation of upstream ash growth and a marked reduction in the amount of rubble in both cases. The case of lower ash permeability (not shown) also shows this same trend. Since upstream growth was consistently observed for the five LBK tests, the anisotropy factor was retained in the model. Comparison of cumulative product yields (Table 4), especially the ratios of carbon and dry product gas produced to oxygen injected, shows the insensitivity of the model to these permeability contrasts. This is reasonable since in the model the permeability contrasts merely change where the cavity grows,

Table 4. Parametric comparisons with LBK-1 base case run: (1) Equal ash and rubble permeability, no anisotropy. (2) Ash permeability 10 times that of rubble, no anisotropy. (3) No bed leveling.

	LBK-1 base	(1)	(2)	(3)
Dry product gas composition (mole fraction):				
N_2	0.004	0.004	0.004	0.004
H_2	0.45	0.44	0.44	0.45
CH_4	0.035	0.026		
CO	0.21	0.23	0.23	0.21
CO_2	0.30	0.29	0.29	0.30
Produced H_2O per mole dry gas (mol/mol)	0.80	0.77	0.78	0.84
Produced carbon per mole injected O_2 (mol/mol)	2.2	2.2	2.2	2.2
Dry product gas per mole injected O_2 (mol/mol)	4.1	4.0	4.0	4.0
Product heat of combustion (dry, tar-free; kJ/mol)	220.	220.	220.	220.
Product heat of combustion per mole injected O_2 (kJ/mol)	910.	890.	890.	880.
Product temperature (°K)	1260.	1340.	1330.	1260.
Total O_2 injected (Mmol)	0.18	0.17	0.18	0.18
Time (hr)	36.	36.	36.	37.
Cavity volumes (m^3):				
Void	3.6	4.3	4.1	3.4
Char above active ash zone	4.3	1.2	2.1	4.7
Ash upstream of injection node	0.64	0.04	0.01	0.76

Table 5. Parametric comparisons with LBK-1 base case: (1) No crack factor. (2) Doubled wall rubbling rate parameter, k_w. (3) Altered pyrolysis reaction components.

	LBK-1 base	(1)	(2)	(3)
Dry product gas composition (mole fraction):				
N_2	0.004	0.004	0.004	0.004
H_2	0.45	0.45	0.45	0.45
CH_4	0.031	0.037	0.038	0.031
CO	0.21	0.19	0.18	0.21
CO_2	0.30	0.31	0.32	0.30
Produced H_2O per mole dry gas (mol/mol)	0.80	0.89	0.94	0.80
Produced carbon per mole injected O_2 (mol/mol)	2.2	2.2	2.1	2.2
Dry product gas per mole injected O_2 (mol/mol)	4.1	4.0	3.9	4.1
Product heat of combustion (dry, tar-free; kJ/mol)	220.	220.	220.	220.
Product heat of combustion per mole injected O_2 (kJ/mol)	910.	890.	870.	910.
Product temperature (°K)	1260.	1240.	1260.	1270.
Total O_2 injected (Mmol)	0.18	0.17	0.18	0.18
Time (hr)	36.	36.	36.	36.
Cavity volumes (m^3):				
Void	3.6	2.5	2.2	3.6
Char above active ash zone	4.3	7.3	7.1	4.3
Ash upstream of injection node	0.64	0.35	0.41	0.50

without a major impact on the chemical physics. Of course, under more severe conditions (i.e., the lack of any available rubble), the impact on the chemistry would be much more pronounced.

Next, the effect of bed leveling is explored. Leveling was introduced into the model to smooth the peaks and valleys of the rubble bed. The solution without leveling is shown in Fig. 13(d). Comparison with the leveled base case clearly shows the leveling effect. Again, the effect of this parameter on cumulative product yields is shown to be very minor (Table 4).

In the same vein as leveling, the crack factor was introduced into the model to account for a region of high permeability at the coal/rubble interface observed in the field. The minor effect this has on both the cavity shape and product yield is shown in Fig. 13(e) and Table 5.

Increasing the wall growth parameter, k_w, produces wider cavities. The sensitivity of the model to a doubling of this factor is shown in Fig. 14, where slice profiles are compared to the base case. As expected, the higher wall growth widens the cavity walls, with little effect on roof growth. The longitudinal cross section, in Fig. 13(f), shows the increased amount of char rubble supplied by wall growth, as compared with the base case. Even with the amount of rubble increased by 65%, the effect on cumulative product yields is shown (Table 5) to be relatively minor.

The parameters discussed thus far primarily affect cavity shape, with little impact on the chemical physics (except in extreme cases). By constrast,

Table 6. Parametric comparisons with LBK-1 base case run: (1) Reduce T_c by 200°K. (2) Reduce β to 0.3. (3) Reduce β to 0.

	LBK-1 base	(1)	(2)	(3)
Dry product gas composition (mole fraction):				
N_2	0.004	0.004	0.004	0.004
H_2	0.45	0.48	0.45	0.44
CH_4	0.031	0.023	0.045	0.052
CO	0.21	0.21	0.21	0.21
CO_2	0.30	0.28	0.29	0.28
Produced H_2O per mole dry gas (mol/mol)	0.80	0.53	0.53	0.46
Produced carbon per mole injected O_2 (mol/mol)	2.2	2.6	2.8	3.0
Dry product gas per mole injected O_2 (mol/mol)	4.1	5.1	5.1	5.4
Product heat of combustion (dry, tar-free; kJ/mol)	220.	220.	240.	245.
Product heat of combustion per mole injected O_2 (kJ/mol)	910.	1140.	1210.	1330.
Product temperature (°K)	1260.	1090.	1120.	1040.
Total O_2 injected (Mmol)	0.18	0.18	0.17	0.17
Time (hr)	36.	36.	36.	36.
Cavity volumes (m^3):				
Void	3.6	5.1	5.5	6.2
Char above active ash zone	4.3	2.3	2.3	1.7
Ash upstream of injection node	0.64	1.0	1.0	1.2

the following parameters deal primarily with the chemistry and have little impact on the cavity shape physics. The importance of the assumed pyrolysis reaction on hydrocarbon species has already been stated. However, to demonstrate the insensitivity of the model to changes in the distribution of H_2, CO, CO_2, and H_2O, we changed the pyrolysis reaction to produce primarly CO and H_2O with less H_2 and no CO_2. The resultant cavity shape remained unchanged and, as shown in Table 5, the product yields remained virtually identical.

Next, the effect of lowering the gasification shutoff temperature, T_c, by 200°C is explored. Lowering this temperature increases the efficiency of gasification by increasing the carbon-carrying capability of the gas and reducing sensible heat losses. The results of the reduced T_c are shown in Table 6. Interestingly, this change had little effect on the dry gas composition; however, the table shows increases in the ratios of (1) produced carbon to oxygen, (2) dry product gas to oxygen, and (3) heat of combustion of dry product gas to oxygen, all three of which are measures of the efficiency of gasification. Increasing the carbon-carrying capability of the gas also is shown to decrease the volume of rubble and increase the void volume within the cavity.

Finally, the effect of changing β, the fraction of coal dried and pyrolyzed in the active gasification zone, is explored. As explained earlier, coal can

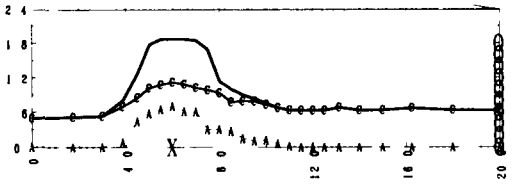

(a) LBK-1 base case.

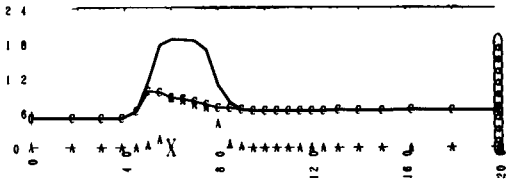

(b) Equal ash and char permeability (no anisotropy).

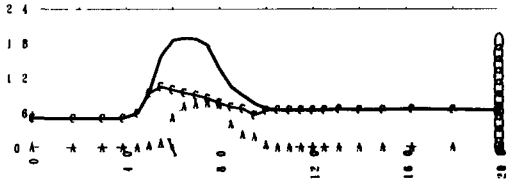

(c) Ash permeability 10 times that of char (no anisotropy).

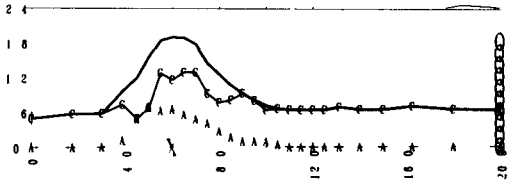

(d) No rubble-bed leveling.

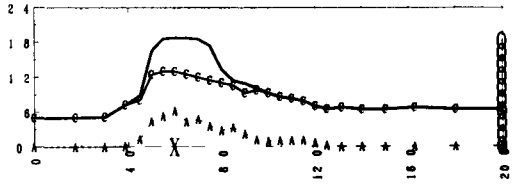

(e) No crack factor.

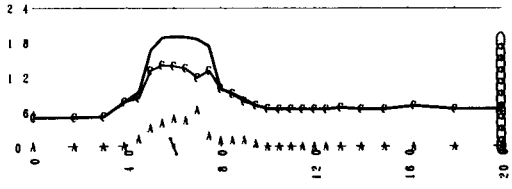

(f) Wall growth factor twice that of base case.

Fig. 13. Parametric comparisons with LBK-1 base case run (longitudinal cross section).

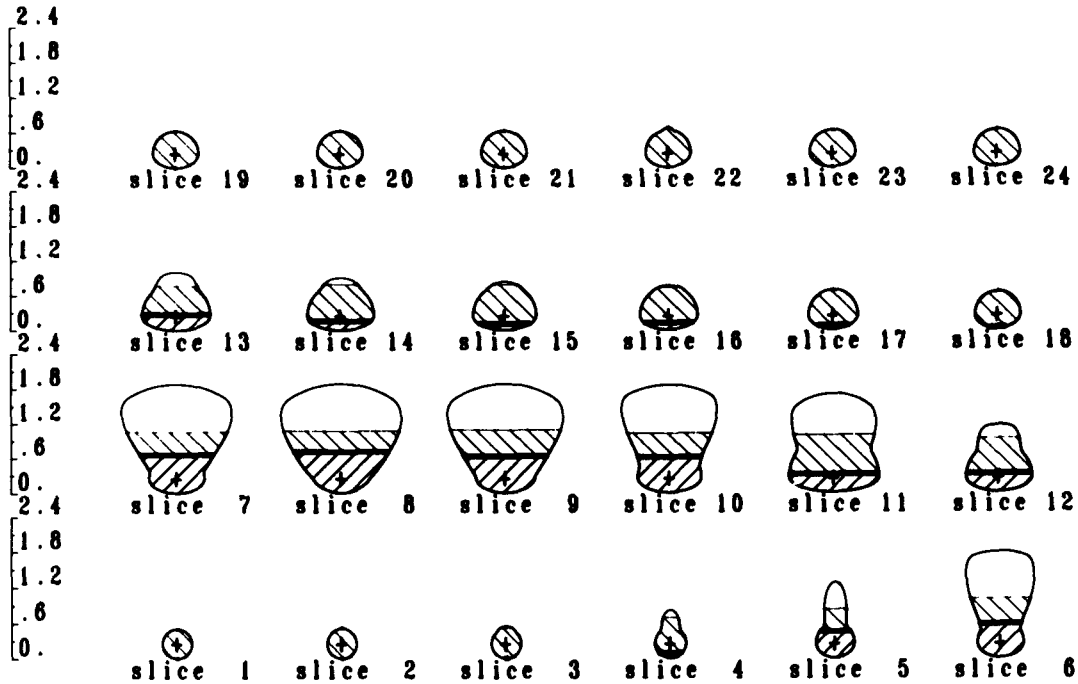

(a) LBK-1 base case run.

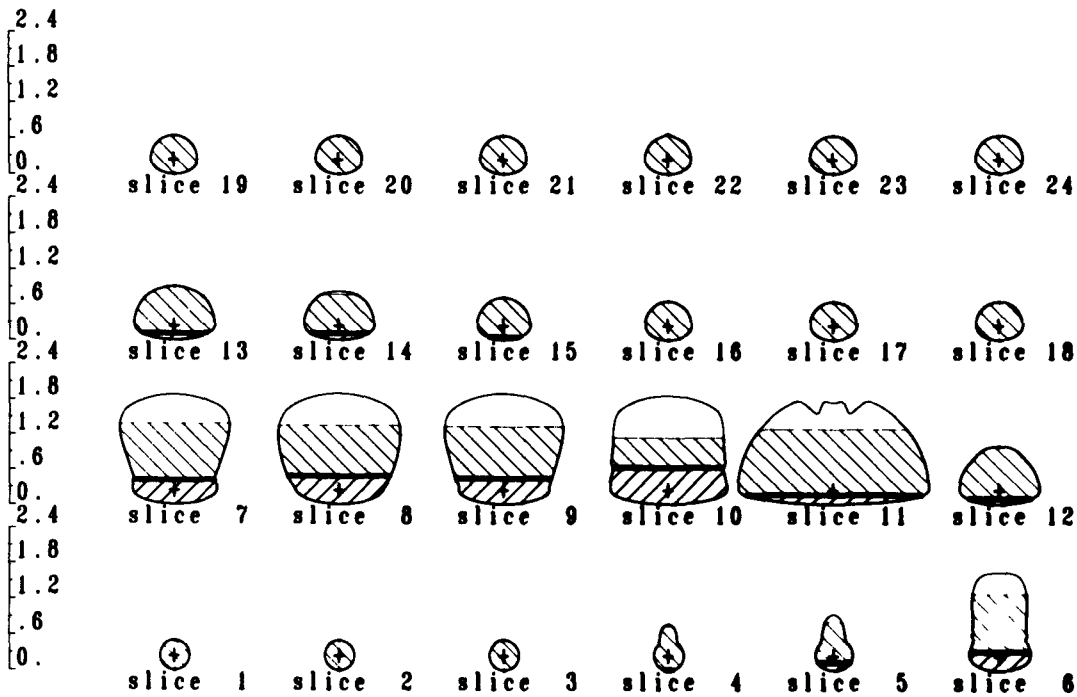

(b) Wall growth rate twice that of base case.

Fig. 14. Parametric comparison of wall growth rate (transverse cross section).

be dried (and pyrolyzed) in two distinct zones in the model. If drying occurs entirely in the mixing zone ($\beta = 0$), this applies a minimum heat load on the gasification zone. As seen in Table 6, lowering β has a similar effect to lowering T_c: the gasification efficiency is increased while the dry gas composition remains relatively constant.

OPERATING PARAMETER COMPARISONS

The five LBK field tests explored the influence of injected gas composition and flow rate schedule on early cavity growth and product yield. Although a detailed comparison of field and model results is beyond the scope of this paper, it is interesting to explore the influence of some of these same parameters on model results.

The influence of injected gas composition is studied first using three compositions: (1) 1/1 steam/oxygen, (2) 3/1 steam/oxygen, and (3) air. Model results are summarized in Table 7 and Figs. 15-17.

The three runs are compared at oxygen injection totals equivalent to that injected during each of the LBK tests (0.58 Mmol). In terms of cavity shape, the controlling parameter among the runs seems to be the wall growth rate. Since this factor depends on velocity to the 0.8 power, we would expect similar wall growth between the 3/1 stream/oxygen and air cases (due to similar velocities), with less overall wall growth of the 1/1 steam/oxygen case. This effect is clearly shown in the figures. Comparison of product yields in Table 7 indicates that the 1/1 steam/oxygen case most efficiently utilizes the injected oxygen, with air gasification being the least efficient. This trend in efficiency is consistent with the LBK field results.

The influence of flow schedule on model results was explored using 3/1

Table 7. Comparison of model calculations assuming three different injected gas compositions, but with the same oxygen injection flow schedule. Comparisons are made at a total oxygen injection equivalent to that in the LBK tests.

	3/1 steam/oxygen	1/1 steam/oxygen	Air
Dry product gas composition (mole fraction):			
N_2	0.004	0.004	0.55
H_2	0.44	0.43	0.16
CH_4	0.027	0.020	0.014
CO	0.21	0.35	0.16
CO_2	0.31	0.19	0.10
Produced carbon per mole injected O_2 (mol/mol)	2.0	2.4	1.9
Dry product gas per mole injected O_2 (mol/mol)	3.7	4.2	6.7
Product heat of combustion (dry, tar-free; kJ/mol)	220.	240.	110.
Product heat of combustion per mole injected O_2 (kJ/mol)	800.	1030.	720.
Total O_2 injected (Mmol)	0.58	0.58	0.58
Cavity volumes (m^3):			
Void	7.2	12.0	5.7
Char	24.2	18.2	25.7
Ash	6.5	8.1	5.9
Total	37.8	38.3	37.3

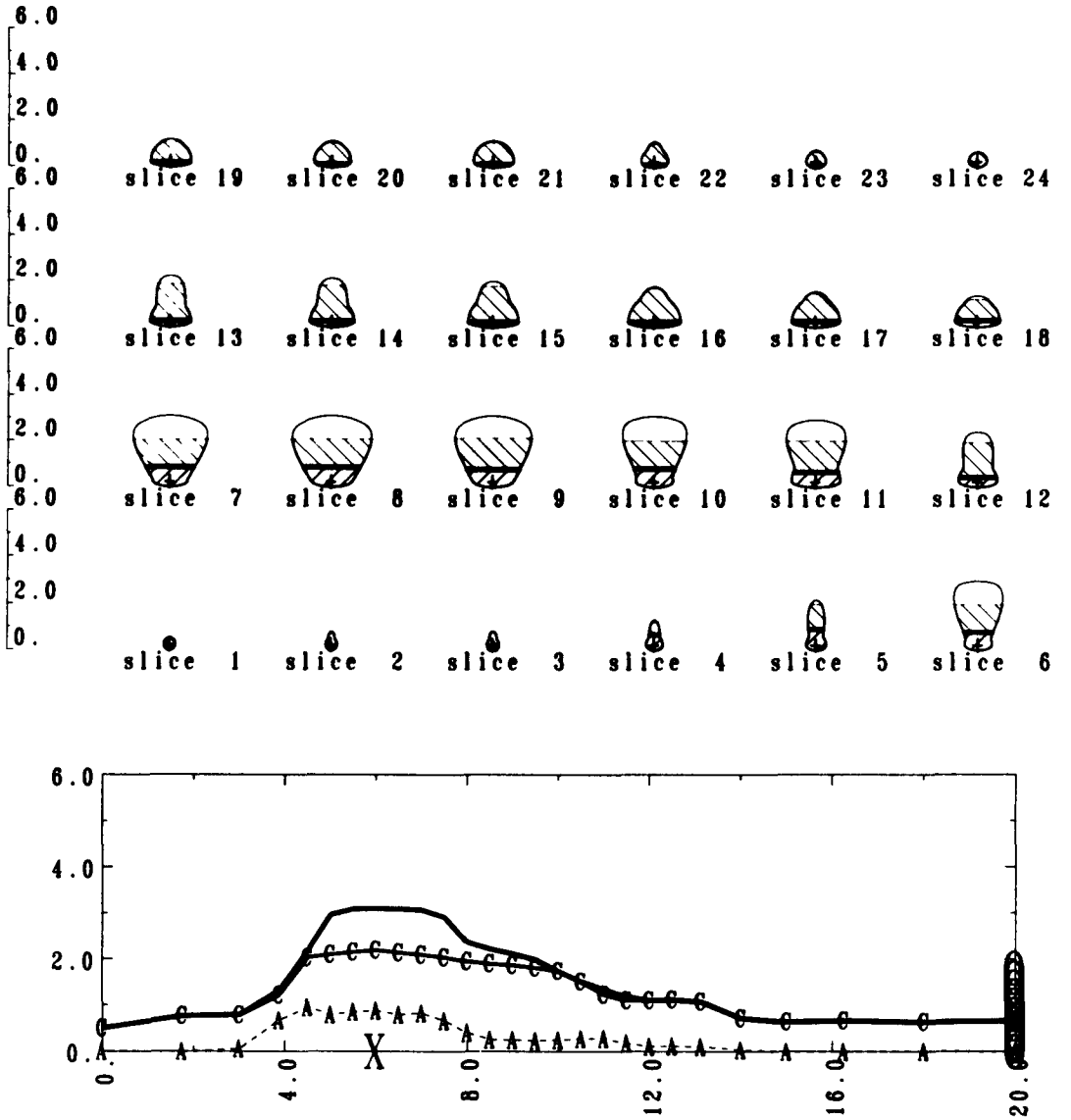

Fig. 15. Calculated longitudinal cross section and slice profiles at 68 hours for the base flow schedule and 3/1 steam/oxygen ratio.

steam/oxygen injection with the same time-squared flow dependence used during the LBK tests:

$$\text{Flow (mol/s)} = kt^2,$$

where t is time in seconds and k is a constant. Three values of k were tested: (1) fast ($k = 3.4 \times 10^{-10}$ mol/s^3), (2) medium ($k = 1.7 \times 10^{-10}$ mol/s^3), and (3) slow ($k = 4.3 \times 10^{-11}$ mol/s^3). Again the runs are compared at equal oxygen totals (0.08 Mmol), with the time to total injection a function of the flow schedule. The results are summarized in Table 8 and Figs. 18-20, where the vertical scale has been increased by a factor of 2 for readability. The model calculates very similar product yields under these circumstances, even though cavity shapes are shown to vary widely. The lack of product sensitivity to flow schedule was also noted during the LBK tests, and the slow flow tests did tend to produce more elongated cavities, similar to the model results.

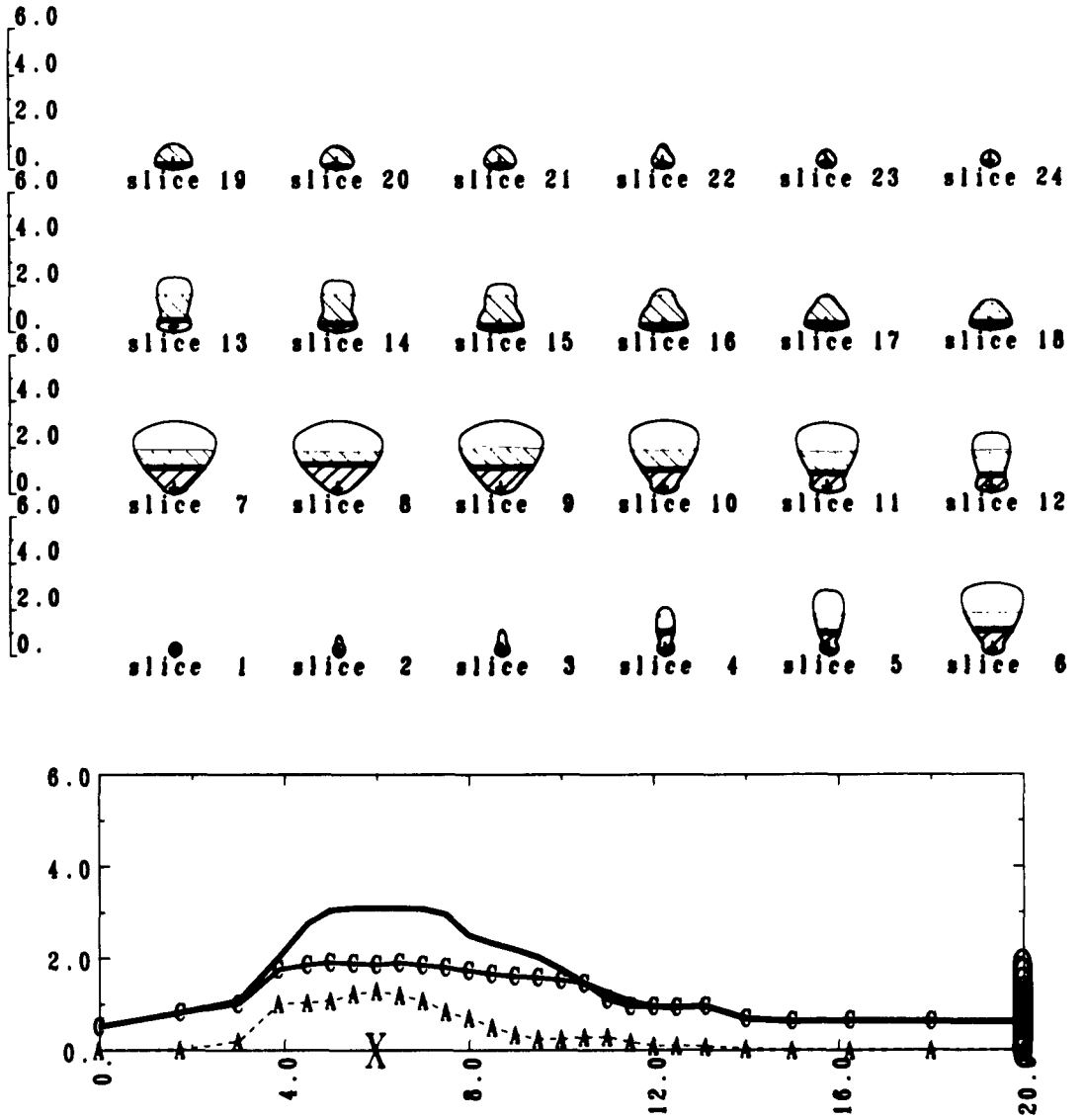

Fig. 16. Calculated longitudinal cross section and slice profiles at 68 hours for the base flow schedule and 1/1 steam/oxygen ratio.

The strong influence of flow rate schedule on cavity shape in the model is a direct result of the model physics. The assumption of constant roof growth (in the presence of void) coupled with a velocity-dependent wall growth results in less wall growth at comparable times and enhanced roof growth at comparable oxygen totals for the slow flow case.

The similarity in product yield despite the differences in cavity shape again shows that the chemical physics is not generally concerned with where the burn takes place, as long as sufficient reactants are present.

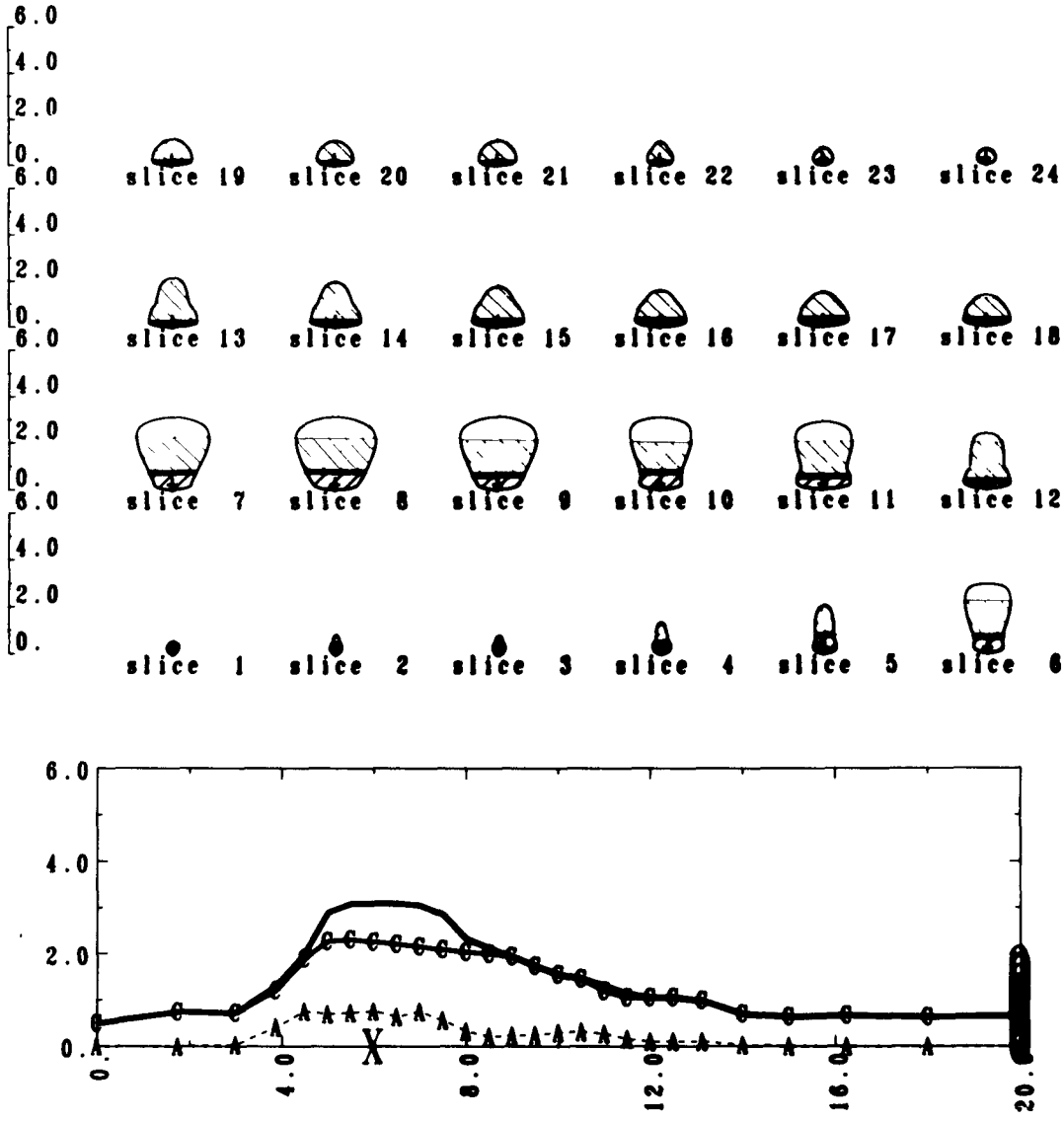

Fig. 17. Calculated longitudinal cross section and slice profiles at 68 hours for the base flow schedule and air injection.

Table 8. Comparison of model calculations assuming three different flow rate schedules for a 3/1 steam/oxygen system. Comparisons are made at similar total oxygen injection.

	Fast	Medium	Slow
Dry product gas composition (mole fraction):			
H_2	0.46	0.46	0.46
CH_4	0.043	0.049	0.059
CO	0.18	0.17	0.14
CO_2	0.31	0.32	0.33
Produced carbon per mole injected O_2 (mol/mol)	2.4	2.3	2.3
Dry product gas per mole injected O_2 (mol/mol)	4.4	4.2	4.2
Product heat of combustion (dry, tar-free; kJ/mol)	230.	230.	240.
Product heat of combustion per mole injected O_2 (kJ/mol)	1000.	970.	990.
Total O_2 injected (Mmol)	0.083	0.083	0.079
Time (hr)	25.	47.	68.
Cavity volumes (m^3):			
Void	1.7	1.2	0.7
Char	6.8	8.0	9.2
Ash	1.1	1.0	0.9
Total	9.6	10.2	10.8

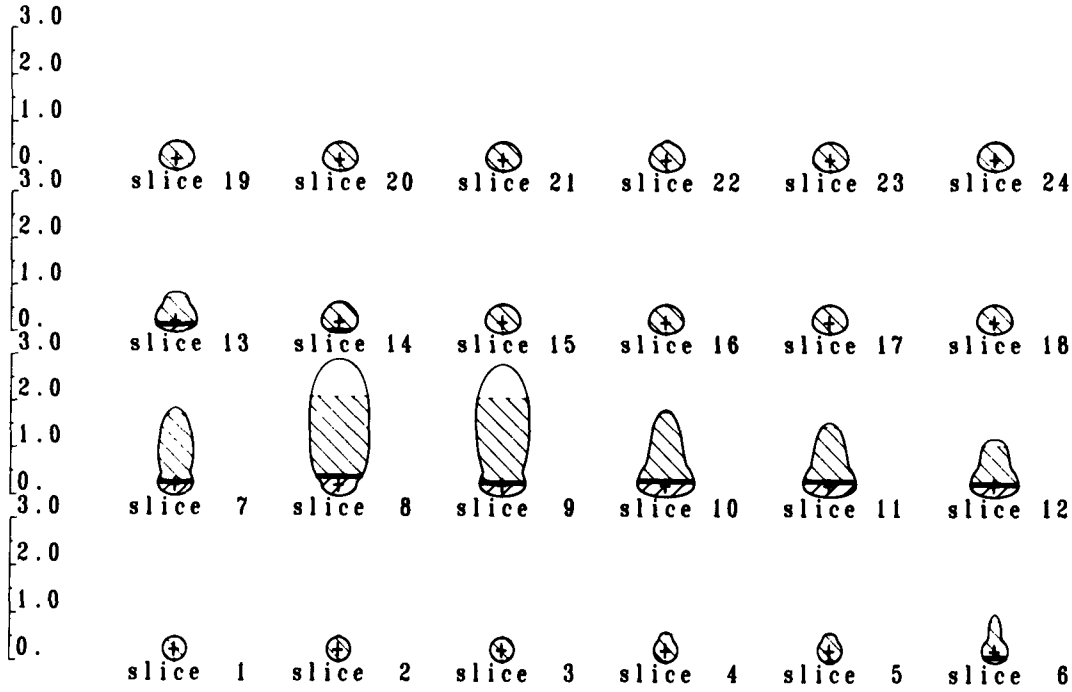

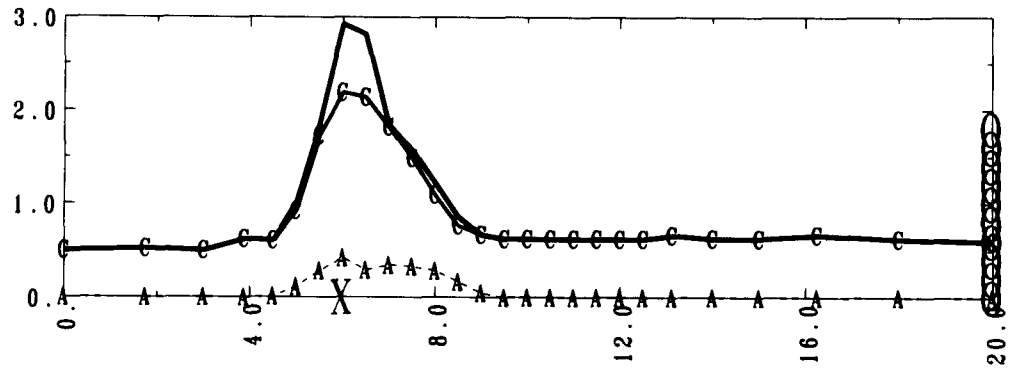

Fig. 18. Calculated longitudinal cross section and slice profiles at 68 hours (0.079 Mmol of O_2 injected) for the slow flow schedule and 3/1 steam/oxygen injection. Note: the vertical scale is expanded by a factor of two over the horizontal scale.

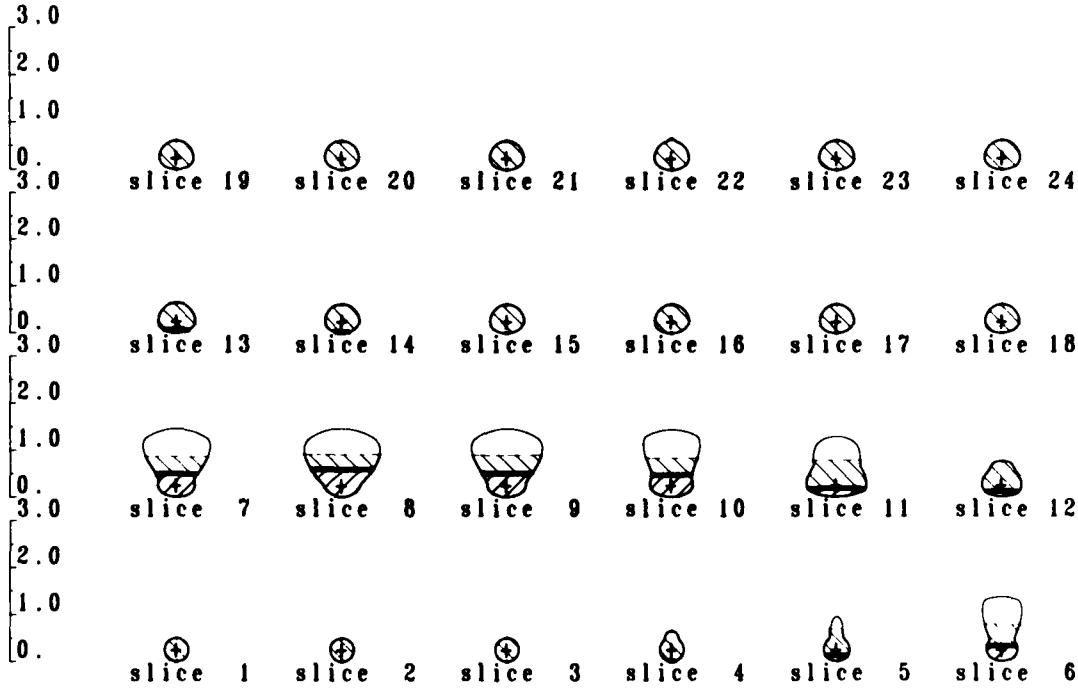

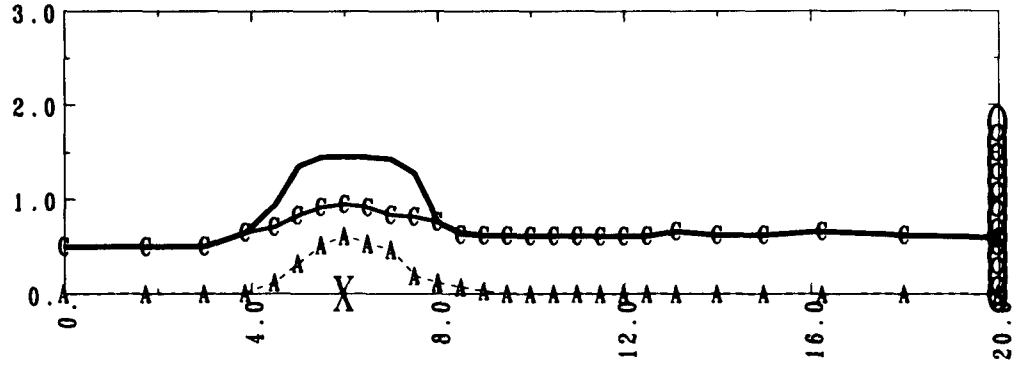

Fig. 19. Calculated longitudinal cross section and slice profiles at 25 hours (0.083 Mmol of O_2 injected) for the fast flow schedule and 3/1 steam/oxygen injection. Note: the vertical scale is expanded by a factor of two over the horizontal scale.

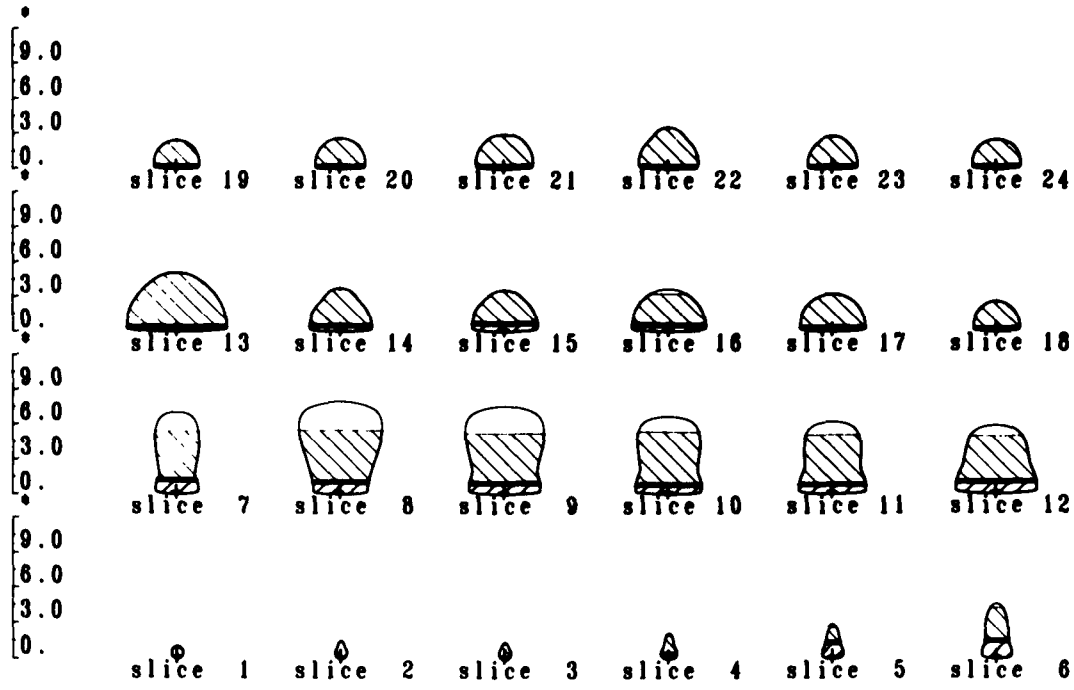

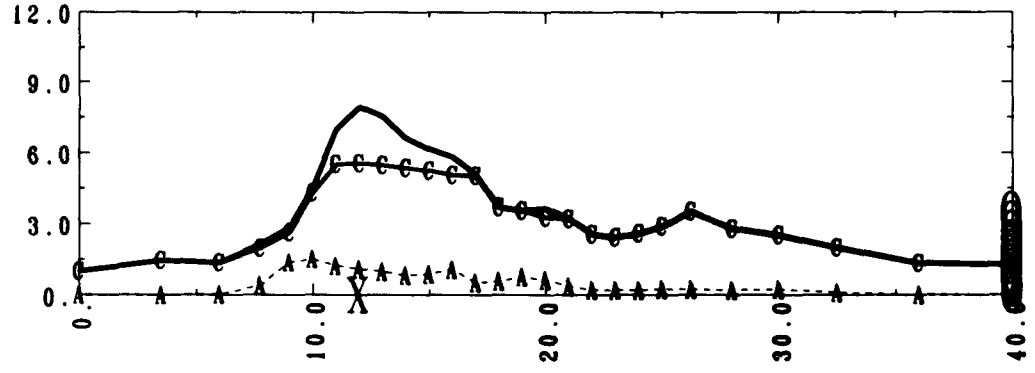

Fig. 21. Calculated longitudinal cross section and slice profiles for the half-seam CRIP experiment at 7.8 days (6 Mmol of O_2 injected), using a fast flow schedule and 3/1 steam/oxygen injection.

detrimental in terms of lost injection lances and ash slagging. Therefore the 3/1 steam/oxygen ratio was selected for the test.

It is interesting to note the remarkable similarity among the runs in terms of total cavity volume, irrespective of differences in operating parameters and calculated cavity shapes. The result would at first seem to be inconsistent with the cavity physics of constant roof growth. However, since this mechanism is postulated to operate only when void space is present, we see that the the amount of char removed also plays an important role in determining total cavity volume. Thus, since the three runs were compared at equal cumulative oxygen totals, with similar char removal efficiencies, similar total cavity volumes resulted.

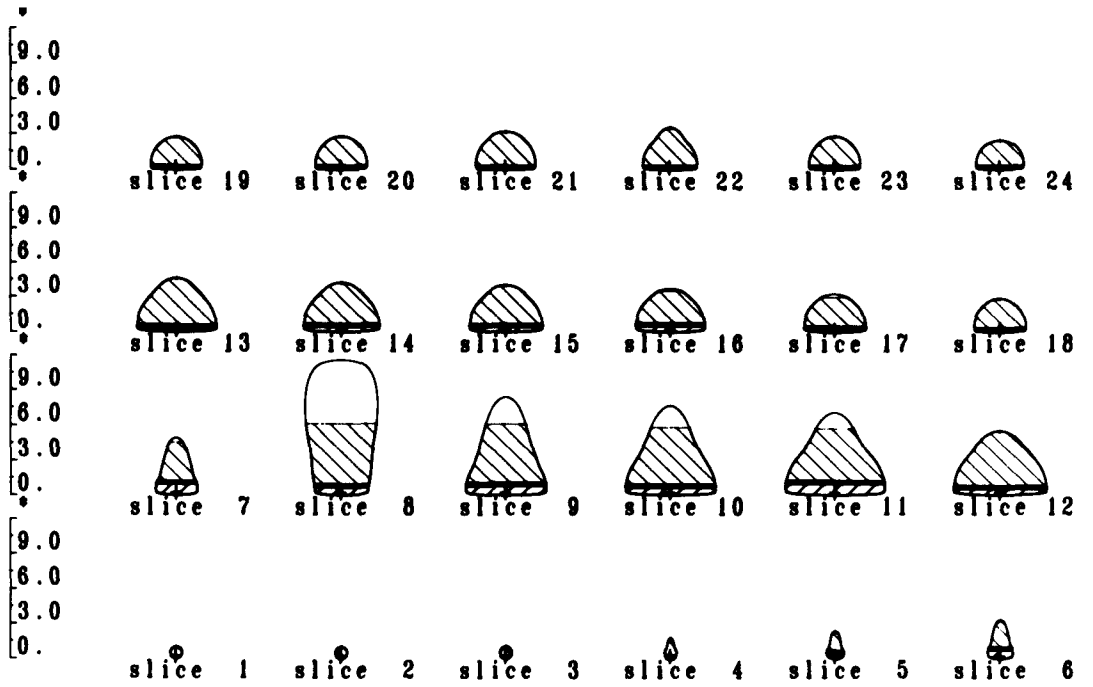

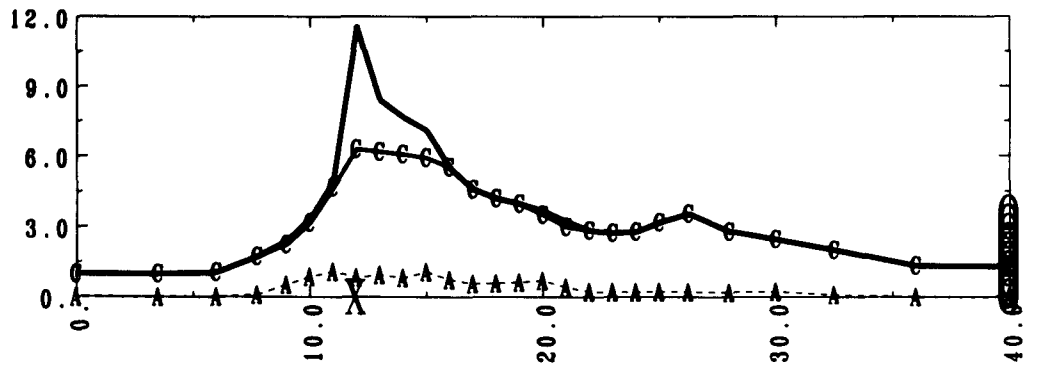

Fig. 22. Calculated longitudinal cross section and slice profiles for the half-seam CRIP experiment at 13.7 days (6 Mmol of O_2 injected), using a slow flow schedule and 3/1 steam/oxygen injection.

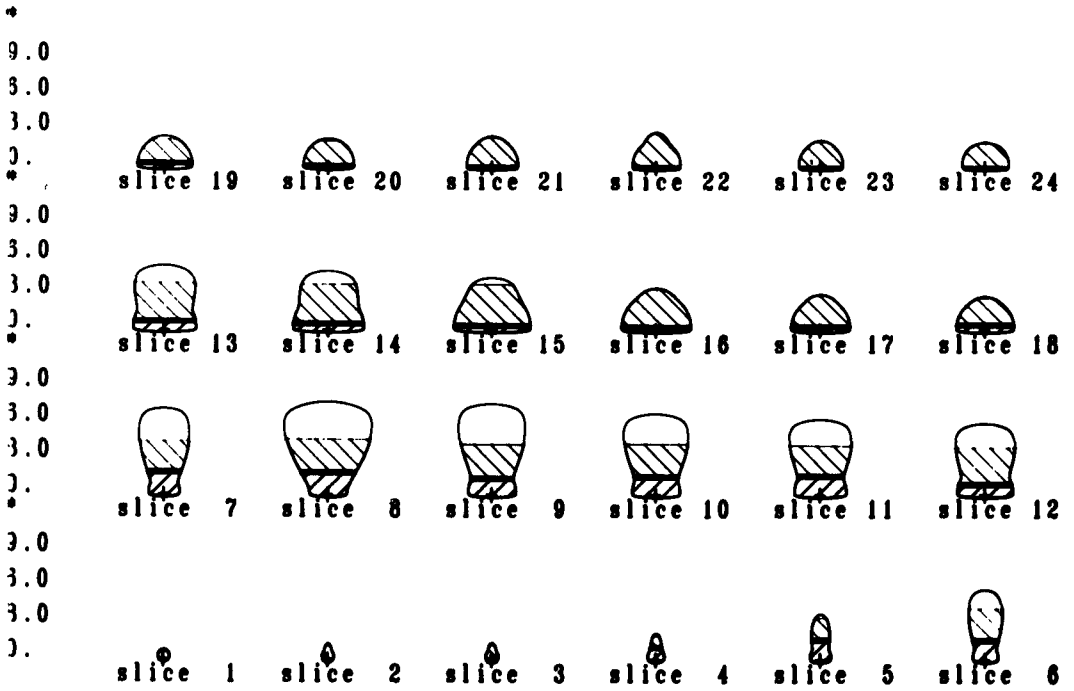

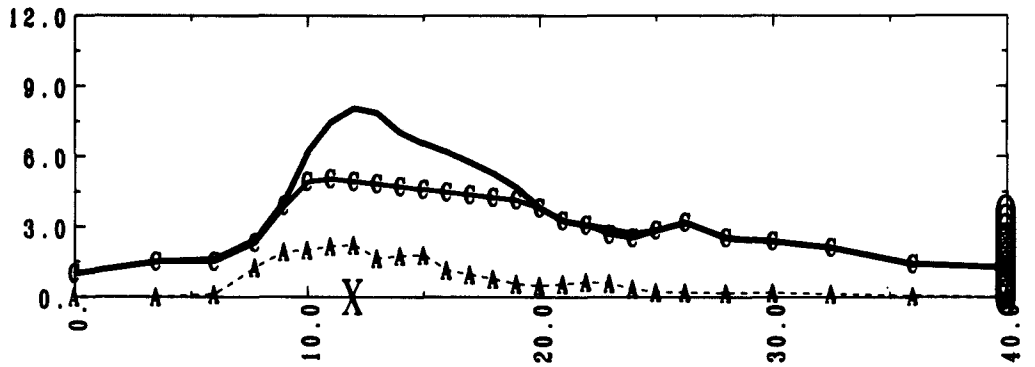

Fig. 23. Calculated longitudinal cross section and slice profiles for the half-seam CRIP experiment at 7.8 days (6 Mmol of O_2 injected), using a fast flow schedule and 1/1 steam/oxygen injection.

SUMMATION

A global model of underground coal gasification with solid motion has been presented. The model is based on early cavity growth behavior as derived from the excavations and process information obtained in the five LBK tests conducted by LLNL at the WIDCo mine near Centralia, Washington. A key element of the model is the movement of solid materials in the ash, rubble, and void regions of the burn cavity resulting from the gasification process. Evidence supporting the model physics was presented along with an explanation of model parameters used to satisfactorily fit the LBK-1 field results. Parameter sensitivity of the model was explored to elucidate the model physics and explain parameter selection. The effect of operating conditions and prediction of the upcoming partial-seam CRIP test were presented.

Model results showed the following:

- The LBK-1 field results could be satisfactorily matched. The fit required anisotropy of the ash, since no simple permeability contrast between ash and rubble matched the data.
- Insensitivity of total cavity volume to operating parameter changes.
- Sensitivity of overall cavity shape to operating parameter changes.
- Gasification efficiencies, not dry gas composition, are good indicators of varying process physics.

Futher work is required to:

- Improve the pyrolysis submodel to account for secondary reactions.
- Implement mobile water and rock physics to handle water influx and overburden interaction.
- Improve zone A to estimate maximum underground temperatures for tests with high steam/oxygen ratios.
- Explore more fully the apparent need for anisotropy in the model.
- Test the model against longer lasting field tests and different coal seams.

ACKNOWLEDGMENTS

The authors thank R. W. Hill of LLNL for extensive consultation concerning the interpretation of the LBK excavation results, and E. Grens of the University of California, Berkeley, for developing the cavity growth submodel discussed in this report. The work was done under the auspices of the U.S. Department of Energy by Lawrence Livermore National Laboratory under Contract No. W-7405-Eng-48.

REFERENCES

1. R. W. Hill and C. B. Thorsness, Summary Report on Large Block Experiments in Underground Coal Gasification, Tono Basin, Washington: Vol. 1. Experimental Description and Data Analysis, Lawrence Livermore National Laboratory, Livermore, Calif., UCRL-53305 Vol. 1 (1982).

2. A. L. Ramirez, D. G. Wilder, and G. A. Pawloski, "Examination of UCG Cavities for the Large Block Test, Centralia, Washington," presented at the Eighth Underground Coal Conversion Symposium, Keystone, Colorado, August 15-19, 1982. Also Lawrence Livermore National Laboratory, Livermore, Calif., UCRL-87978 Preprint (1982).

3. C. B. Thorsness and R. J. Cena, "In Situ Coal Gasification Modeling," presented at AIChE Meeting in Houston, Texas, April 1-4, 1979. Also Lawrence Livermore National Laboratory, Livermore, Calif., UCRL-82269 Preprint (1979).

4. R. W. Hill and C. B. Thorsness, The Partial Seam CRIP Test: Preliminary Design, Lawrence Livermore National Laboratory, Livermore, Calif., UCID-19610 (1982).

5. C. B. Thorsness and R. J. Cena, A UCG Cavity Simulator: The Method Behind the Model, Lawrence Livermore National Laboratory, Livermore, Calif., report in preparation (1983).

3.5 STRESS MEDIATED RESPONSES ASSOCIATED WITH UCG CAVITY AND SUBSIDENCE PREDITION MODELING

by

S. H. Advani [1/] J. K. Lee [1/]
O. K. Min [2/] B. L. Aboustit [1/]
S. M. Chen [1/] S. C. Lee [1/]

ABSTRACT

Recent progress on a DOE sponsored program on thermo-mechanical and poro-mechanical investigations associated with UCC is reported. Various model formulations including moving boundary, thermo-elasto-plastic consolidation, and thermo-visco-elastic representations are discussed. Numerical results, employing these specialized finite element codes, are presented for selected field simulations. In addition, a predictive strategy based on experimentally determined overburden material property data is outlined for the design of UCC experiments from a structural vantage point.

INTRODUCTION

The principal objective of the U.S. Department of Energy program on Underground Coal Conversion (UCC) is to demonstrate the reliable and environmentally acceptable extraction of energy from potentially unminable coal reserves. The various integrated UCC R&D activities, via field and laboratory experiments aligned with the model simulations, have demonstrated the commercial viability of this in situ process. Significant results obtained from the various DOE sponsored programs have been summarized by Stephens [1] and detailed in the Annual Symposia on UCC. Privately sponsored UCC tests have included experiments conducted by Basic Resources, Inc., Texas A and M University, and ARCO Coal Company. Currently, WIDCO is conducting UCC experiments near Centralia, Washington in conjunction with LLNL. A cooperative thin seam UCC experiment between Belgium and West Germany is also underway.

Several fundamental efforts in the areas of reaction kinetics, fluid flow, combustion, spalling-enhanced-drying, and structural response modeling [2,3,4,5,6,7] have been conducted to elucidate governing process mechanisms, perform parameter sensitivity prediction studies, and provide comparisons with field or laboratory data. In this paper, formulations for moving boundary, thermo-elasto-plastic consolidation, and thermo-visco-elastic models are discussed and results from pertinent field simulations are presented. In addition, the role of structural modeling in the context of UCC site selection on the basis of stress mediated roof collapse and subsidence is reviewed.

UCC MODEL FORMULATIONS

The general field equations and finite element methodology associated with UCC response prediction have been given in Reference [8]. Here, extensions of this research related to moving boundary evaluations, thermo-elastic and thermo-plastic consolidation, and thermo-visco-elastic modeling are reported.

Moving Boundary Analysis: Governing equations, formulations, and finite element investigations of moving boundary thermo-mechanical responses have been

1/ Dept. of Engineering Mechanics, The Ohio State University, Columbus, Ohio 43210
2/ Dept. of Mechanical Engineering, Yonsei University, Seoul, 120, Korea

detailed by Min [9]. The energy generated by coal combustion at the burn front is quantitatively introduced in the heat conduction equation. The gasification chamber configuration is defined by a reference front isotherm. Thermo-elastic or thermo-elasto-plastic material properties along with failure criteria are used to define the structural response. The burn front propagation and collapse of failed overburden zones defines the overall gasification chamber and coupled subsidence response. Temperature dependent material properties are used to account for property changes. The methodology for the thermo-mechanical response prediction is illustrated in Fig. 1.

Thermo-elastic and Thermo-plastic Consolidation Analysis: The general theory for thermo-elastic consolidation is presented in Reference [10]. The elasto-plastic analysis for thermal consolidation has been detailed by Aboustit [11]. Here, the plastic strain increment due to thermo-mechanical loading is obtained in accordance with Prager's theory of non-isothermal plastic deformations [12] and the total strain increment is written according to Nagdhi [13]. The inverse incremental relation for stress in terms of strain is deduced along with results specialized to the case of non-isothermal yield surfaces. The field equations for equilibrium, stress-strain, Darcy's flow, continuity, energy, and imposed boundary conditions are employed in their incremental form and a modified iterative incremental scheme is used in the formulation [11]. In this scheme, the heat conduction equation is decoupled from the equilibrium and continuity equations since the effect of the displacements on the temperature profile is negligible. For each increment, the temperature solution is obtained directly from the energy equation and the incremental displacement and pressure solutions are sought with the temperature contribution considered as a forcing term. Stiffnesses are allowed to change during each increment with the proviso that constant stiffnesses be maintained at the onset of the loading as well as prior to failure if a perfectly plastic model is adopted to avoid ill conditioning. The number of iterations is reduced by modifying the load vector to account for plastic loading, i.e., the initial load method in elasto-plastic analysis.

Thermo-visco-elastic Response Analysis: The governing equilibrium, energy, strain-displacement, constitutive equations and associated boundary conditions for uncoupled linear thermo-visco-elasticity have been presented in [8] using the thermorheological simple material (TSM) assumption. In addition, it is assumed that creep occurs only for the deviatoric components while the volumetric behavior is elastic.

The finite element discretized heat conduction equation along with pertinent approximations for the creep strain rate in terms of the compliance and implicit time step incremental solution algorithm for the displacements and stresses are employed in the analysis. In the proper time step selection, the one step Euler's method is applied to the incremental creep strain terms which are susceptible to sharp variations with increasing time and/or temperature. This work is applicable to problems with time dependent temperature boundary conditions, temperature-time dependent thermo-mechanical properties, and temperature dependent failure criteria [14].

NUMERICAL EXPERIMENTS

Results from numerical simulations for the moving boundary, thermo-elasto-plastic consolidation, and thermo-visco-elastic responses are presented. Prior to the field evaluations, the developed finite element codes were validated against pertinent solutions dealing with frost front propagation, one dimensional isothermal consolidation, thick cylinder isothermal elasto-plastic response and thick cylinder themo-visco-elastic response [9,11,14].

Moving Boundary Simulations: Model simulations for Hanna II, Hoe Creek II and III have been previously reported [8]. The selected vertical cross-section idealization of the Rawlins I experiment with the air injection well (AIW) and the production gas well (PGW) is illustrated in Fig. 2a with the corresponding finite element mesh shown in Fig. 2b. The model dimension is 200m x 140m and quadrilateral linear elements are employed in the simulations, with the total number of elements and nodes numbering 594 and 644, respectively. The selected nominal values for thermal properties, control parameters, and temperature dependent

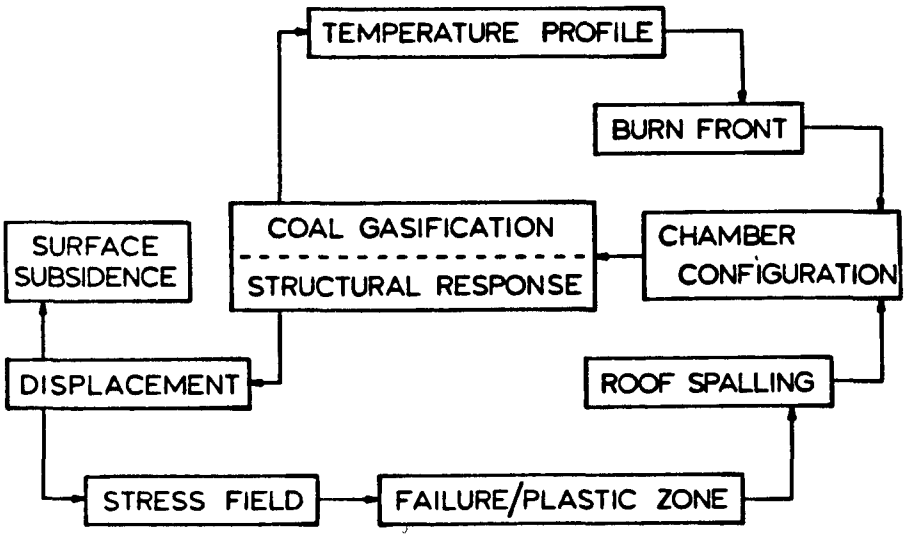

Figure 1. Methodology for Moving Boundary UCC Thermo-Mechanical Response Evaluation

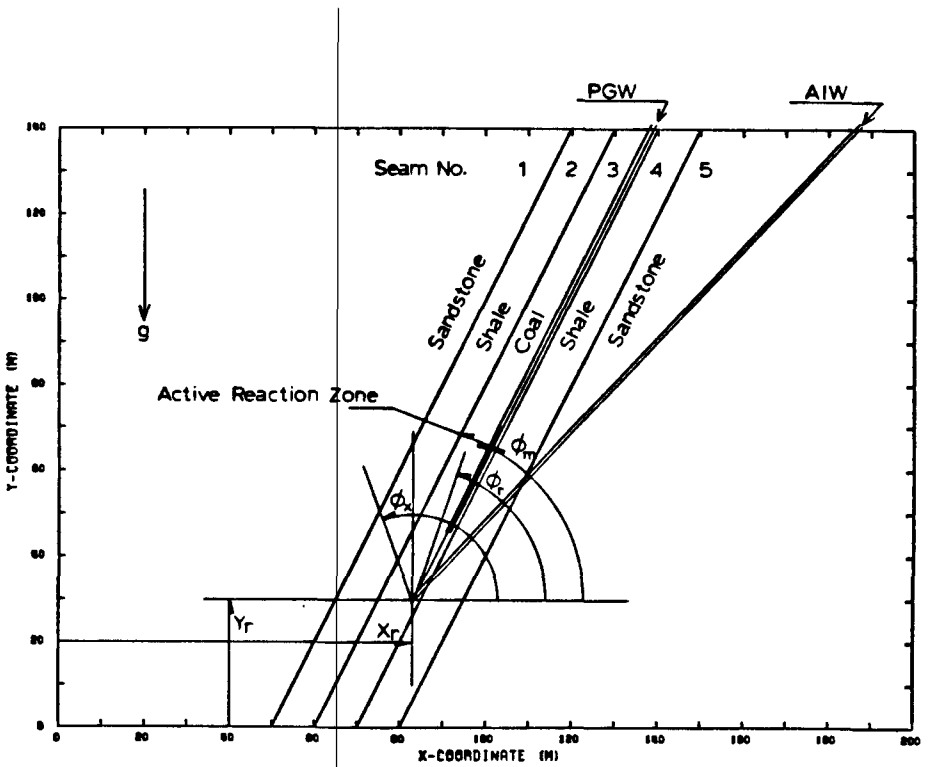

Figure 2a. Assumed Stratigraphy for Rawlins Test No. 1 Simulation

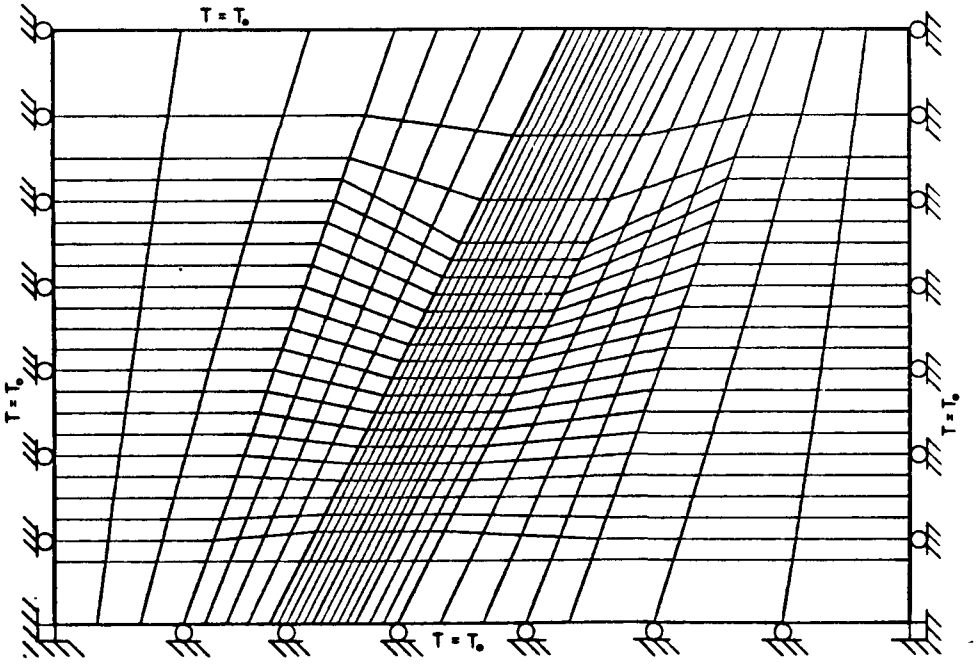

Figure 2b. Selected Finite Element Mesh for Rawlins Test No. 1 Simulation

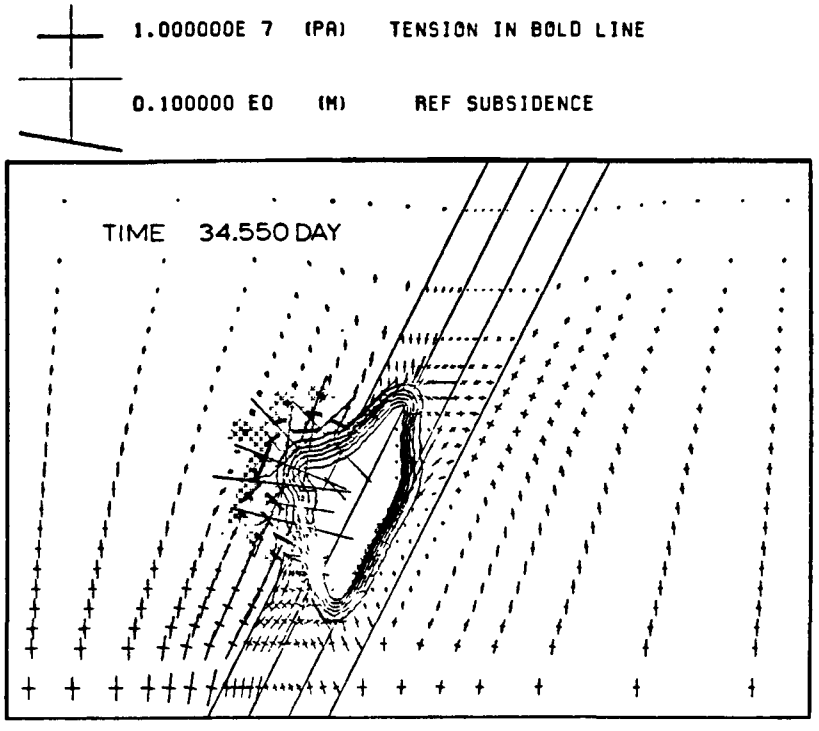

Figure 3. Computed Results for Rawlins Test No. 1 Simulation at t=34.55 days: Temperature Contours (600°C inside in 100°C decrement), Stress Field, Failed Zone (hatched), and Chamber Configuration (inside contour).

material property scaling factors have been presented by Min [9]. An intermediate gasification configuration, computed from an initially selected isotherm, is illustrated in Fig. 3. The stress fields for this steeply dipping coal seam qualitatively reveal a different pattern compared to the horizontal seam results. The arching phenomenon is not as predominant and the failure boundary of the overburden shale and sandstone is approximately parallel to the seam inclination. The computed surface subsidence magnitudes are negligible. With the selected model parameters, the final gasification chamber configurations are compared with the results of post-burn drilling in Fig. 4.

A similar evaluation of the Rawlins II experiment has been conducted using the previous model parameters. Figure 5 illustrates a computed intermediate burn configuration and a comparison of the computed cavity, failure front and post-burn evaluations are shown in Fig. 6.

Figures 7a and 7b detail the idealized stratigraphy and finite element mesh for the Hanna III experiments. Evaluation of an intermediate burn configuration is shown in Fig. 8 with corresponding comparisons in Fig. 9.

Thermo-elasto-plastic Consolidation Simulations: Several calibrative thermo-elastic consolidation and isothermal elasto-plastic simulations have been previously conducted for code validation [11]. Figure 10 illustrates the assumed finite element mesh, strata description, and time dependent cavity for the Centralia site. Computed surface settlement histories corresponding to the elastic and elasto-plastic analyses are presented in Fig. 11. The estimated progression of plastically deformed zones is also presented in this figure. It is noteworthy that the plasticized zones of particular consequence are those in the vicinity of the cavity roof because of their propensity for block caving. Surface consolidation magnitudes appear to be small for the assumed cavity size.

Thermo-visco-elastic Response Simulations: Post-burn thermo-visco-elastic response simulations for Hoe Creek II have been conducted [14]. The selected stratigraphy, assumed boundary conditions with time dependent cavity temperature and finite element discretizations, are illustrated in Fig. 12. The coal (layers 3 and 5) and clay/siltstone (layer 4) and sand/siltstone strata (layer 2) are assumed to obey the thermo-rheological simple material assumption and suitable four parameter discrete models (Burger's models) are adopted for the analysis. Figures 13a and 13b reveal the time dependent subsidence profiles and principal stresses with designated failed element zones at t=0 and 10 years, respectively. In the thermally altered visco-elastic zones, a progression of element failure in the vicinity of the cavity has been determined. With elapsed time, the transition from higher to lower compressive stresses is a result of material softening and the cavity appears to stabilize for longer durations.

DISCUSSION AND CONCLUSIONS

The developed thermo-elastic moving boundary, thermo-elasto-plastic consolidation, and thermo-visco-elastic finite element models provide a sophisticated base for predicting the thermo-mechanical or hygrothermal *in situ* responses associated with UCC. As previously indicated, the accuracy of these codes has been verified by benchmark calibrations against problems with known solutions prior to the evaluation of field cases.

The moving boundary thermo-elastic code realistically characterizes the stress mediated cavity responses associated with the Rawlins I and II and Hanna III experiments. Previous studies have demonstrated the applicability of this code to the Hanna II, Phase 2, Hoe Creek II, and Hoe Creek III experiments. Transient cavity configurations, failure zones, and surface subsidence response are dominated by the selected overburden thermo-mechanical properties and initially assumed cavity shape.

The thermo-elasto-plastic consolidation simulations reveal the potential failure zones and settlement characteristics of the Centralia gasification UCC site. This model has the capability of evaluating the temperature, pore pressure, displacement, and stress responses associated with geotechnical problems. On the other hand, the thermo-visco-elastic evaluations illustrate the impact of time-temperature dependent creep phenomenon of overburden media with emphasis on progressive cavity failure and subsidence.

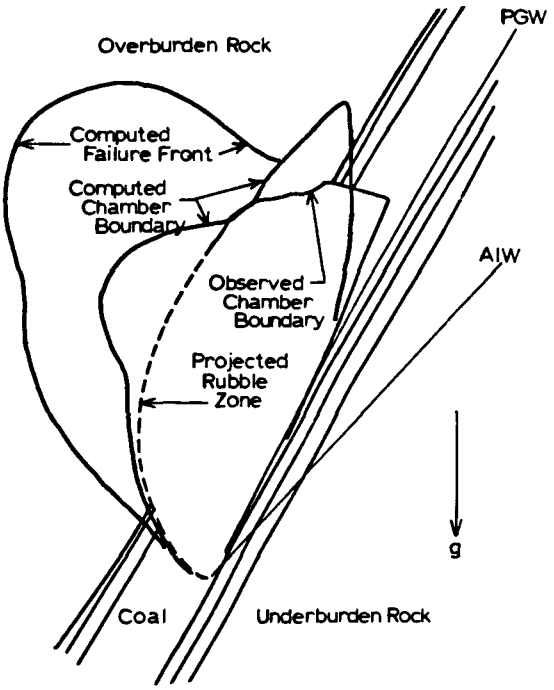

Figure 4. Comparison of Computed Results and Post-burn Study for Rawlins Test No. 1 Simulation.

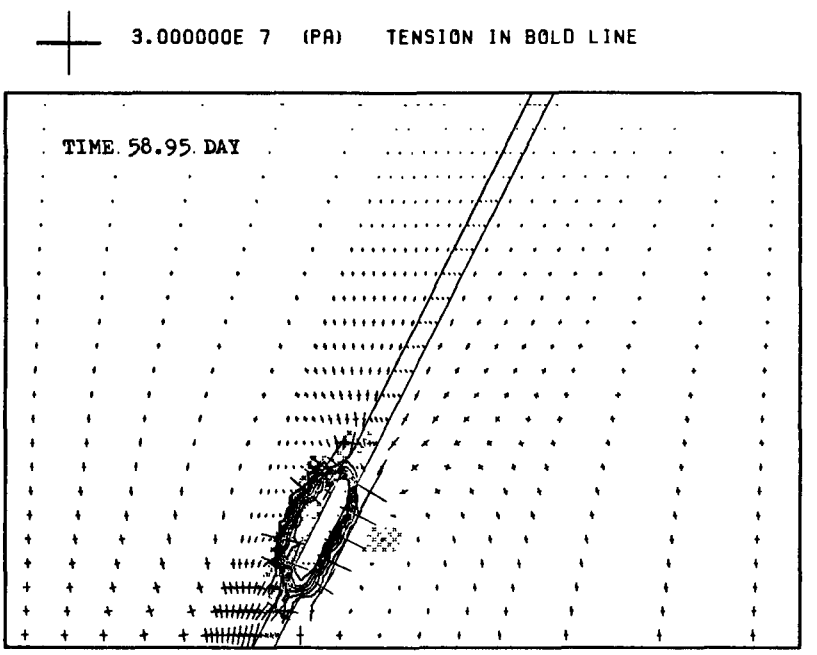

Figure 5. Computed Results for Rawlins Test No. 2 Simulation at t=58.95 days: Temperature Contours (600°C inside in 100°C decrement), Stress Field, Failure Zone (hatched), and Chamber Configuration (inside contour).

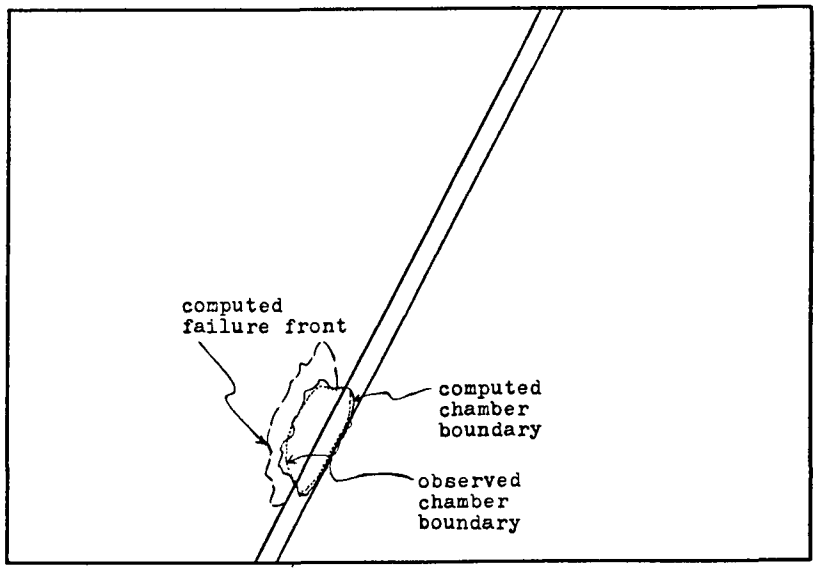

Figure 6. Comparison of Computed Results and Post-burn Study for Rawlins No. 2 Simulation.

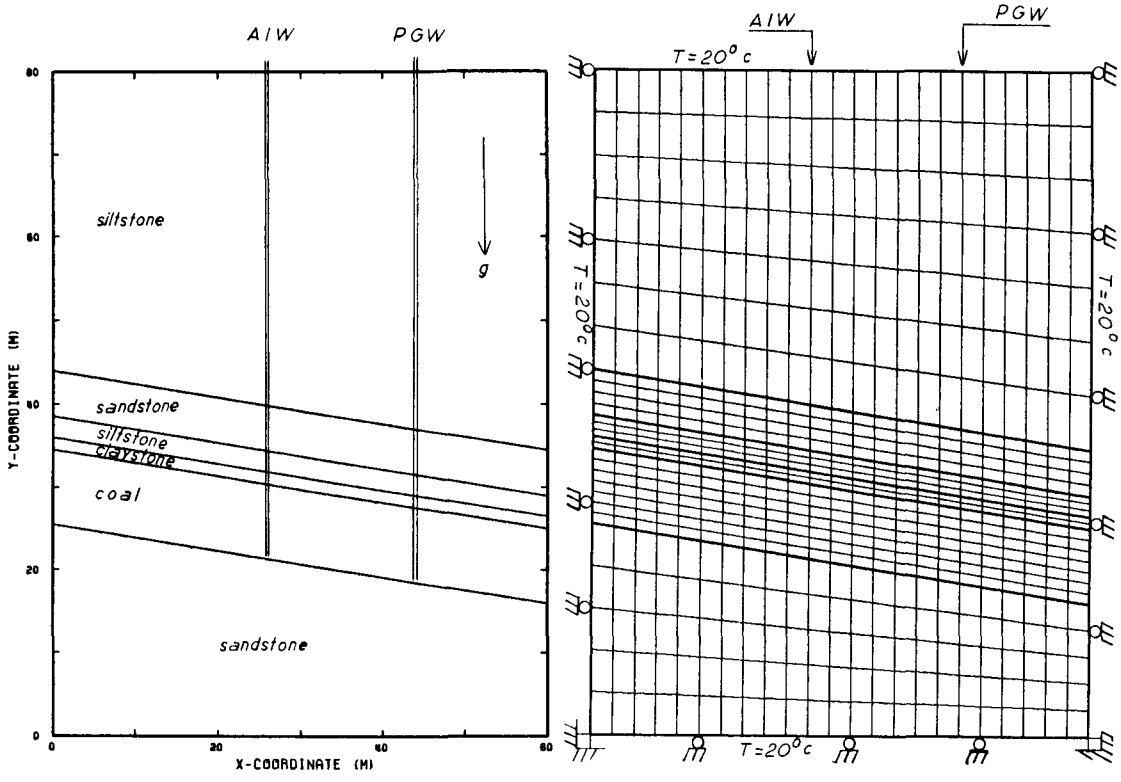

Figures 7a,b. Assumed Stratigraphy and Finite Element Mesh for Hanna III Simulation

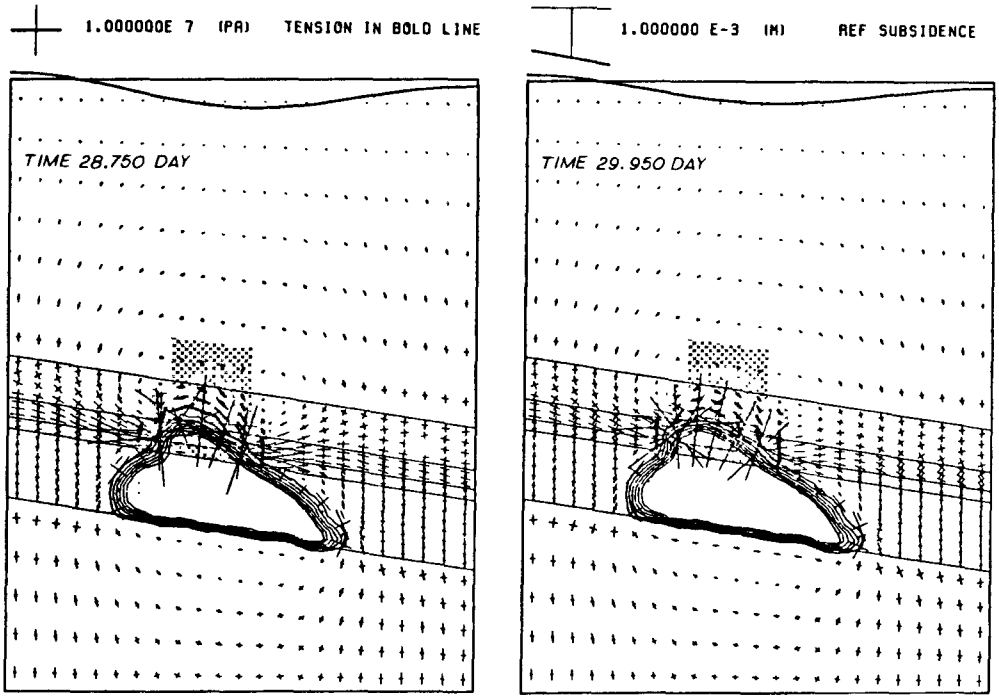

Figures 8a,b. Computed Results of Hanna III Simulation at t=28.75, 29.95 days: Temperature Contours (600°C inside in 100°C decrement), Subsidence, Stress Field, Failed Zone (hatched), and Chamber Configuration (inside contour).

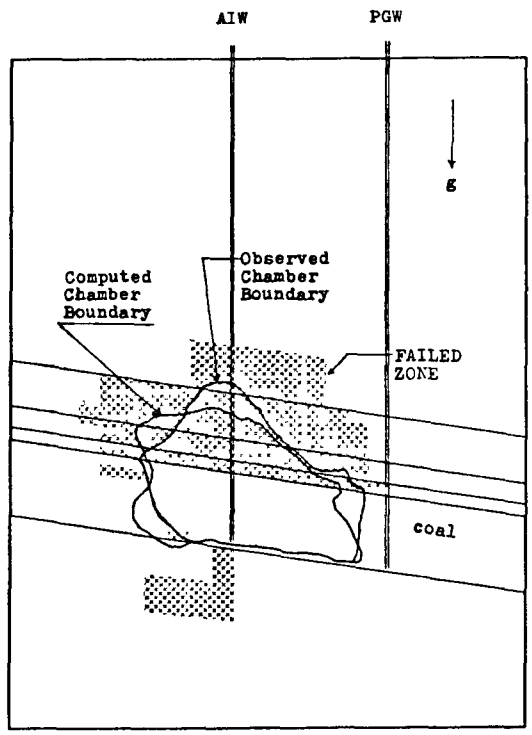

Figure 9. Comparison of Computed Results and Post-burn Study for Hanna III Simulation.

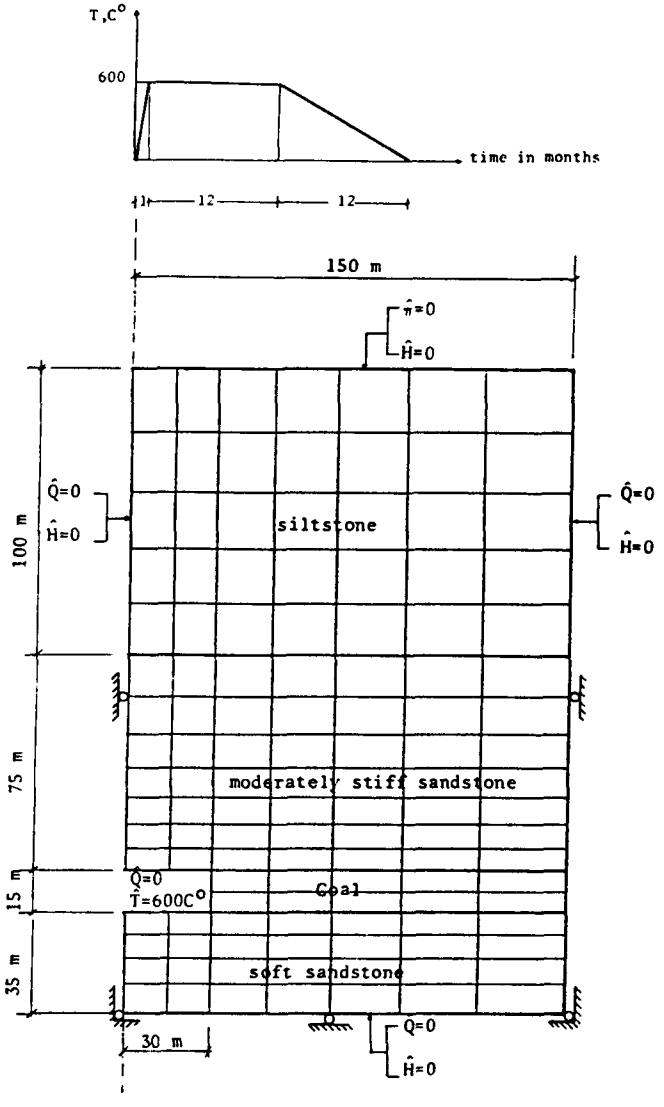

Figure 10. Finite Element Mesh, Strata Description, and Boundary Conditions for Centralia Coal Gasification.

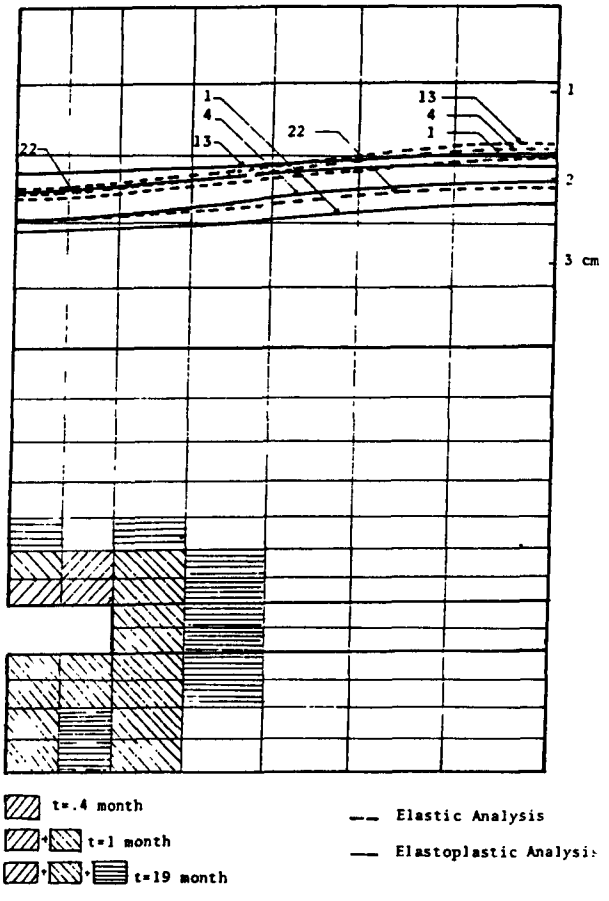

Figure 11. Surface Settlement History and Progression of Plastic Zones, Centralia Coal Gasification (Hatched Area implies Yielded Elements).

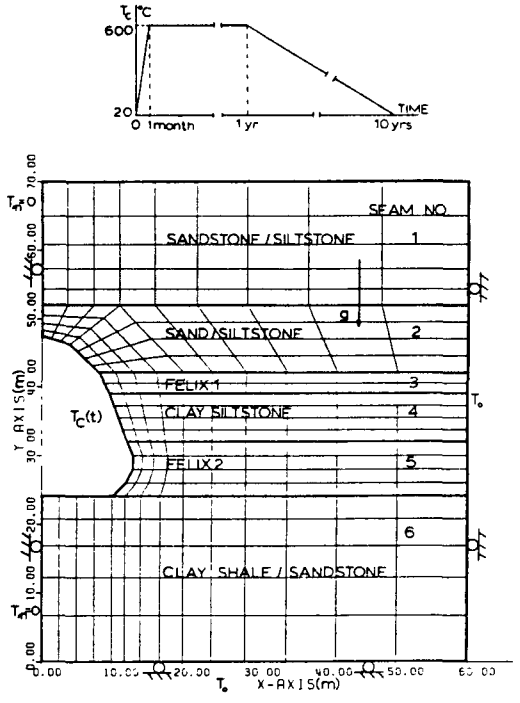

Figure 12. Two-Dimensional Stratigraphy, Assumed Boundary Conditions, and Corresponding FEM Model for Hoe Creek II Post Burn Thermo-Visco-Elastic Simulation.

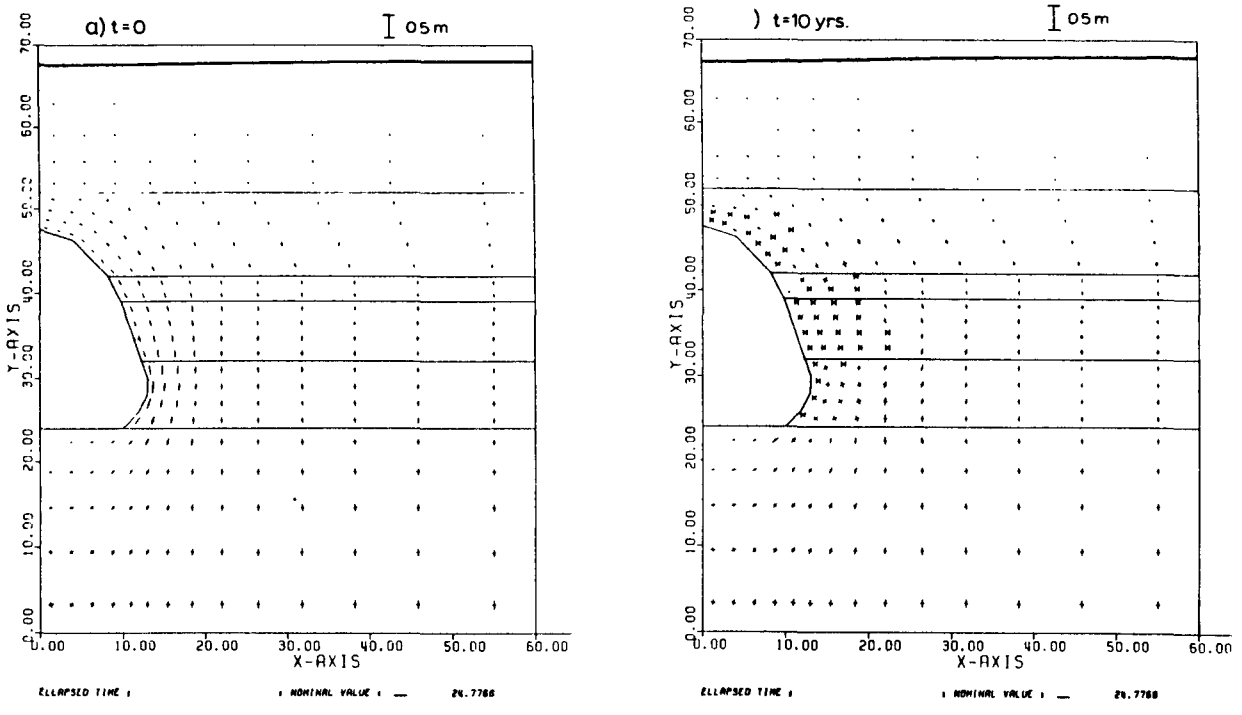

Figures 13a,b. Computed Results at t=0, 10 years for Hoe Creek II Post-Burn Simulation: Subsidence, Principal Stresses ($x10^5$Pa; Boldline for Tension) and * Designates Failed Element.

It is recommended that UCC structural response studies, using the preceding formulations and simulations, be introduced in the design of future experiments. Prior to the implementation of these codes, thermo-mechanical property data from cores is necessary for incorporation in the model. The moving boundary, thermo-elasto-plastic, and thermo-visco-elastic codes can be used for parameter sensitivity investigations to determine ranges of cavity shape, roof collapse, subsidence, pore pressure, and creep response.

Continuation of the preceding investigations is in progress with follow-on studies in the areas of the establishment of equivalence scaling relations between 2D and 3D response models and development of design recommendations for a priori UCC site selection using the determined overburden properties.

ACKNOWLEDGMENTS

This research was supported by the U.S. Department of Energy under Contract No. DE-AS20-82LC10886. Computational facilities were provided by IRCC at The Ohio State University.

REFERENCES

1. D.R. Stephens, "An Introduction to Underground Coal Gasification," Lawrence Livermore National Laboratory UCID - 18801, 1980.

2. C.B. Thorsness and R.F. Cena, "In Situ Coal Gasification Modeling," Lawrence Livermore Laboratory Report No. UCRL - 82269, February, 1979.

3. R.D. Gunn, and D.L. Whitman, "An In Situ Coal Gasification Model (Forward Mode) for Feasibility Studies and Design," Laramie Energy Research Center Report, Laramie, Wyoming, 1976.

4. B.A. Kashiwa et al., "Kinetics of Subbituminous Coal Drying, Proceedings 5th UCC Symposium, pp. 409-418, DOE CONF 790630, 1979.

5. S.H. Advani, Y.T. Lin, "Subsidence and Roof Response Studies Related to Underground Coal Gasification," Proceedings 3rd Annual UCC Symposium, DOE CONF 770652, pp. 422-429, 1977.

6. J. Massaquoi and J.B. Riggs, "Qualitative Study of Flow Patterns in a Laboratory UCC Model," Proceedings 7th UCC Symposium, DOE CONF 810923, pp. 723-729, 1981.

7. B.E. Levie, et al., "A Model for Roof Spalling and Its Application to Predicting Cavity Shape for the Hanna III UCG Field Test," Proceedings 8th UCC Symposium, SAND 82-2355, pp. 321-333, 1982.

8. S.H. Advani and J.K. Lee, "Structural and Fracture Mechanics Modeling Associated with Underground Coal Conversion," Final Report on Contract No. DE-AS20-80LC10335, Department of Engineering Mechanics, The Ohio State University, June, 1982.

9. O.K. Min, "Finite Element Modeling of Thermo-Mechanical Responses Associated with Underground Coal Conversion," Ph.D. Dissertation, The Ohio State University, 1982. Also published as Report No. DOE/LC/10335-T1, Technical Information Center, US DOE, February, 1983.

10. B.L. Aboustit et al., "Finite Element Evaluations of Thermo-Elastic Consolidation," Issues in Rock Mechanics, 23rd U.S. Symposium on Rock Mechanics, AIME, Chap. 60, 587-595, 1982.

11. B.L. Aboustit, "Finite Element Investigations of Thermo-Elastic and Thermo-Plastic Consolidation, Ph.D. Dissertation, The Ohio State University, 1983.

12. Prager, W., "Non-Isothermal Plastic Deformation," Koninklijke Nederland Akademie Van Wetenschappen Te Amsterdam Proceedings of the Section of Sciences, Ses. B, 61, 1958.

13. Nadghi, P.M., Stress-Strain Relations in Plasticity and Thermoplasticity, Plasticity Proc. of the 2nd Symposium of Naval Structural Mechanics, Pergamon Press, 121-169, 1960.

14. Lee, S.C., Ph.D. Dissertation, The Department of Engineering Mechanics, The Ohio State University, Pending, 1983.

3.6 DETERMINATION OF UNDERGROUND COAL GASIFICATION BURN TEMPERATURES USING THERMAL METAMORPHISM OF COAL MACERALS AS A GEOTHERMOMETER

by

A. D. Youngberg[1/]
F. J. Rich[2/]

ABSTRACT

Samples of coal were obtained from the Hanna No. 1 coal at DOE's Hanna underground site. Each sample was heated in a helium atmosphere for one hour, with alteration temperatures begining at about 23 degrees Centigrade, and increasing at 50 degree increments between 50 degrees and 600 degrees Centigrade. The process is believed to have duplicated conditions at certain locations within an underground coal gasification reactor. A method of determining gasification reaction temperatures by relating visible changes in coal macerals with known temperatures of alteration was developed. Macerals were identified using white and blue-ultra violet incident light. A semi-mobile flourescing maceral, exudatinite, was found to be unusally abundant in all samples and displayed a steadily decreasing abundance as heating progressed. Significant changes began between 250-300 degrees Centigrade when reaction vesicles developed due to exudatinite and exinite destruction. Above that temperature, increased cracking and vesicularization of the coal matrix was accompanied by extinction of fluorescence at 400 degrees Centigrade. The devolatization of exudatinite and other Liptinites is among the earliest of conversion reactions. Vitrinite reflectivity increased as temperatures increased. Liptinites are the most useful geothermometer below 400 degrees Centigrade, and vitrinite reflectivity is the best geothermometer above 400 degrees Centigrade.

1/ Laramie Projects Office, Laramie, Wyoming 82071
2/ South Dakota School of Mines and Technology, Rapid City, South Dakota 57701

INTRODUCTION

The United States Department of Energy has conducted a number of underground coal gasification (UCG) experiments at a site near Hanna, Wyoming. The Hanna No. 1 coal seam was used for the experimental work. The Hanna No. 1 coal seam lies within the Paleocene Hanna Formation and is confined to the Hanna Coal Basin of Wyoming (Figure 1). The Hanna No. 1 coal has been classified as a high-volatile C bituminous coal (1).

Various approaches have been used to improve the efficiency of the UCG process at the Hanna site. One of these approaches includes the need for a complete understanding of the coal itself. Through careful analysis of the coal, improved systems for conversion to high quality gaseous fuel might be designed. Various types of analyses have been performed on samples of altered and unaltered coal and carbonaceous shales from the Hanna site. This report details some results from an analysis of the petrographic constituents of the Hanna No. 1 coal.

PURPOSE OF THE STUDY

The purpose of the study is to construct a geothermometer based upon visible thermal alterations in the macerals found in the Hanna No. 1 coal bed. It was determined that a correlation might be made between alteration temperatures and unique petrographic compositions produced by alteration. If such a correlation could be made,

then samples of coal taken from the Hanna UCG site could be observed microscopically and determinations made as to the maximum temperatures to which the coal had been subjected. Samples were heated in the laboratory at various temperatures and the macerals were observed, described, and quantified as changes occurred in their appearances during heating at progressively higher temperatures.

LABORATORY METHODS

Sample Preparation

Crushed bulk samples of unaltered coal were used in the study. Core Hole Number 170, which was drilled ten feet east of the Hanna II, Phase 2 experimental site, was sampled. One sample from the 277-278 feet depth interval and one sample from the 284.2-285.2 feet depth interval were chosen for petrographic study.

Five gram samples were placed in a previously weighed crucible, and their combined weight was recorded. The furnace was heated to the desired temperature and flushed with helium. Helium was chosen because it is inert and would probably not cause chemical alterations in the samples. Heating was done at 50 ^{o}C intervals between room temperature ($\sim$20 ^{o}C) and 600 ^{o}C.

After being heated for one hour, the crucible was removed from the furnace as quickly as possible and weighed to record any weight change. Each sample was mixed immediately with a low viscosity epoxy-type embedding medium which is commonly used for coal pellet preparation. The mixture of coal and epoxy was divided between two steel 1-inch inside diameter steel molds, and compressed at 7000 psi for two minutes. After each sample hardened (18 hours) it was labeled, then ground and polished on a Jarret Automatic Grind-Polisher.

Sample Analysis

Methods of analyzing polished pellets, or briquettes of coal are fairly well established. Stach (2) presents a concise review of techniques. The method of microscopic analysis employed in this study involved incident illumination of polished pellet surfaces and observation at 500 X magnification in oil immersion. Blue-light (actually blue and ultraviolet wavelengths) was employed. Incident blue-light causes liptinite macerals (waxes, resins, spores) to flouresce brightly, especially in low-rank coals. As the liptinites fluoresce they can be easily identified and quantified.

A particular type of liptinite, exudatinite, is unusually common in the Hanna coal samples. Exudatinite is a mobile or semi-mobile oil or resin-like liptinite which has been recognized only in recent years (3). It occupies open spaces within the coal, and therefore tends to be found in fractures or the lumens of coalified cells. Exudatinite in the Hanna samples is especially common in structured woody tissue (telinite) and fungal bodies (sclerotinite). Inasmuch as exudatinite is rather mobile, and may acutally migrate out of samples into the immersion oil (4), it was decided to emphasize exudatinite analyses for this study. The rationale was that, if any substances in the Hanna samples would react quickly to thermal alteration, exudatinite would certainly be among them. Exudatinite is confidently identified only in blue-light, as it fluoresces brightly, but it is nearly invisible in "white" light. In view of these facts, blue-light analyses were emphasized.

Two pellets from each sample interval were counted to determine relative abundances of macerals. Five hundred points were counted per pellet, and both pellets per sample were observed, providing 1000 points per sample.

THERMAL METAMORPHISM OF MACERALS

Tables 1 and 2 illustrate several of the changes which took place during heating of samples from the 277-278 and 284.2-285.2 foot levels respectively. The following observations may be made:

1) There was a gradual decrease in percentages of total liptinites as temperatures increased.

2) Fluorescence essentially ceased at 400^{o}C.

3) Reaction vesicles developed within vitrinite particles between 250-300^{o}C. Vitrinite which contained spores or pollen, resin bodies, etc., became especially vesicular. Exudatinite showed distinct reactivity with consequent evacuation from sclerotinite bodies and interstices among crystals in pyrite framboids. Cracks developed in vitrinite.

4) Between 300-350 °C vitrinite became obviously cracked and vesicular. Resinites clearly showed alteration rims as they reacted.

5) Between 350-400 °C vitrinite became increasingly vesicular, with vesicle size and abundance increasing. Glassy or pitchy appearing deposits occurred in many vesicles. Exudatinite and resinite nearly vanished.

6) Within the 400-500 °C range reflectivity of vitrinite particles appeared to be much more uniform. Resinite, exinite, cutinite, etc., were no longer visible in either "white" or blue light.

7) At 500-600 °C, every coal particle developed a multitude of vesicles, and many were intensely cracked, almost brecciated. Coal particles were of uniform color and composition except for the vesicles and cracks.

Figure 2 shows the liptinite transformations that occurred at low temperatures. It appears from the data that exudatinite, exinite, and resinite are thermally altered to form bituminite. The apparent increase in relative abundance of liptinites between 150°C and 300°C is thus explained. Bituminite is fairly mobile, and as it forms at the expanse of the more solid liptinites, it saturates more of the matrix of the coal. At 400°C, bituminite breaks down too, and literally disappears, along with all the other liptinites. The liptinite "death line" at 400°C is shown in Figure 3. This "death line" coincides with a reflectivity of 1.27 which, incidentally, coincides with medium volatile bituminous ranks and the transition from oil to gas genesis in sediments (2).

CHANGES IN VITRINITE REFLECTIVITY

A vitrinite reflectance analysis was performed on twelve coal pellets that had been heated at various temperatures ranging from 50°C to 600°C. Figure 4 presents the results of those analyses. At temperatures of 50°C to 300°C there is a gradual increase in vitrinite reflectivity. A sharp jump in reflectance occurs between 300°C to 350°C. The reflectance continues to rapidly increase up to 600°C. Thus, vitrinite reflectance is a good geothermometer because the reflectance increases as the temperatures increase.

DISCUSSION AND CONCLUSIONS

Distinct petrographic changes did take place in the Hanna No. 1 samples as they were heated. Decreasing abundances of fluorescent macerals, increasing vesicularity and cracking in vitrinites, and eventual elimination of all macerals except vitrinite can be correlated with temperature ranges. It should, then, be feasible to take samples of coal from the Hanna UCG experimental sites and determine the thermal gradiant away from the sites.

This work has also shown that macerals in the Hanna No. 1 bed coal react at quite different rates when heated. Liptinites are altered before vitrinites and intertinites, though eventually all the macerals become involved in the physical alterations. The fact that liptinites react earlier than vitrinites may carry important implications as far as maintaining optimum gas composition and production are concerned.

Liptinites, for example, are enriched in hydrogen as compared to the other maceral groups. As liptinites decompose thermally, one would expect gases with a high hydrogen/carbon ratio to be produced. In a coal such as the Hanna No. 1, which contains an abundance of easily altered liptinites, conversion of coal to gas could occur at a comparatively low temperature and yet yield a gaseous product enriched in hydrogen. On the other hand, coals which do not have such an abundance of liptinites might require higher conversion temperatures which would involve more vitrinite in the conversion reactions in order to produce gases with a high hydrogen content.

An additional observation is that at higher temperatures, i.e., 400°C and above where particles become vesicular and fractured the reactive surface area within coal fragments is much greater than at cooler temperatures. The abundance of vesicles and the eventual brecciation of the particles should allow the coal to react more readily with hot gases within the gasification chamber. Brecciated coal particles would, of course, also allow product gases to move more readily through the coal bed than if the coal fragments were less extensively broken.

We believe the results of the work show that the most successful UCG operations will be those where careful consideration has been given to the petrographic composition of the coals. Petrography can be used both as a geothermometer and as a technique to predict coal reactivity during underground gasification.

Visible changes in macerals can be correlated with known temperatures of alteration. Liptinite content decreases as temperatures increase. Vitrinite reflectivity increases as temperatures increase. Exudatinite, exinite, and resinite become altered with heat and form bituminite. Liptinites vanish at 400°C.

REFERENCES

1. Youngberg, A. D., 1981, Petrographic Analysis of Unaltered and Thermally Metamorphosed Coal from the Hanna, Wyoming, Gasification Area: Seventh Underground Coal Conversion Symp., Fallen Leaf Lake, CA, Sept. 8-11, pp. 402-415.

2. Stach, E., 1975, Coal Petrology: Gebruder Borntraeger, Berlin, 428 p.

3. Teichmuller, M., 1974, Uber neue Macerale der Liptinit-Gruppe und die Entstehung des Micrinits: Fortschr. Geol. Rheinld. u. Westf., v. 24, pp. 37-64.

4. Spackman, W., A. Davis, and G. D. Mitchell, 1976, The Fluorescence of Liptinite Macerals: Brigham Young Univ. Geol. Studies, v. 22, pt. 3, pp. 59-75.

TABLE 1

CHANGES IN LIPTINITE COMPOSITION FOR
SAMPLES FROM 277-278 FEET INTERVAL

Temperature°C	% Liptinites	# Exudatinite	# Liptodetrinite & Bituminite	# Exinite
19	4.4	10	17	10
50	4.9	12	22	8
100	3.6	14	14	4
150	2.8	8	8	5
200	3 .7	9	22	5
250	4.0	5	17	5
300	2.8	1	13	6
350	1.0	1	7	0
400	0.0	0	0	0

TABLE 2

CHANGES IN LIPTINITE COMPOSITION FOR
SAMPLES FROM 284.2-285.2 FEET INTERVAL

Temperature°C	% Liptinites	# Exudatinite	# Liptodetrinite & Bituminite	# Exinite
21	7.7	1	58	10
50	8.5	3	67	9
100	11.5	4	87	12
150	9.3	7	68	14
200	8.3	4	69	5
250	8.5	2	67	7
300	5.2	1	38	8
350	0.8	0	6	2
400	0.0	0	0	0

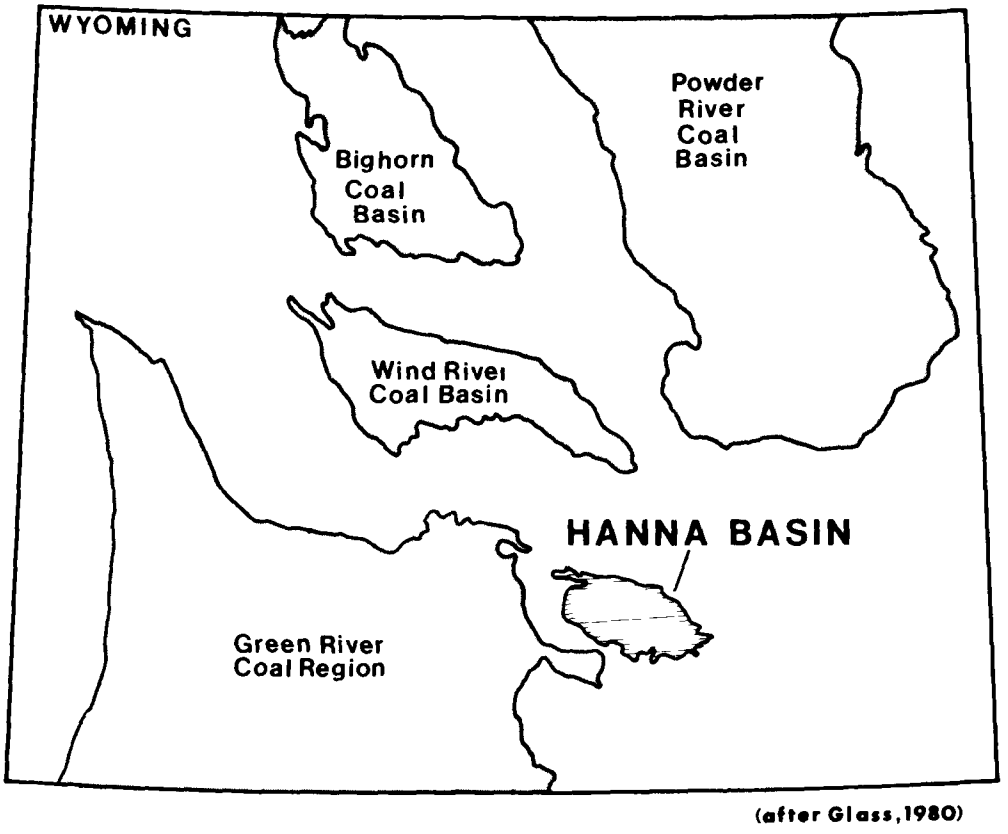

Figure 1
Location of the Hanna Basin With Respect To Other Coal Bearing Areas of Wyoming

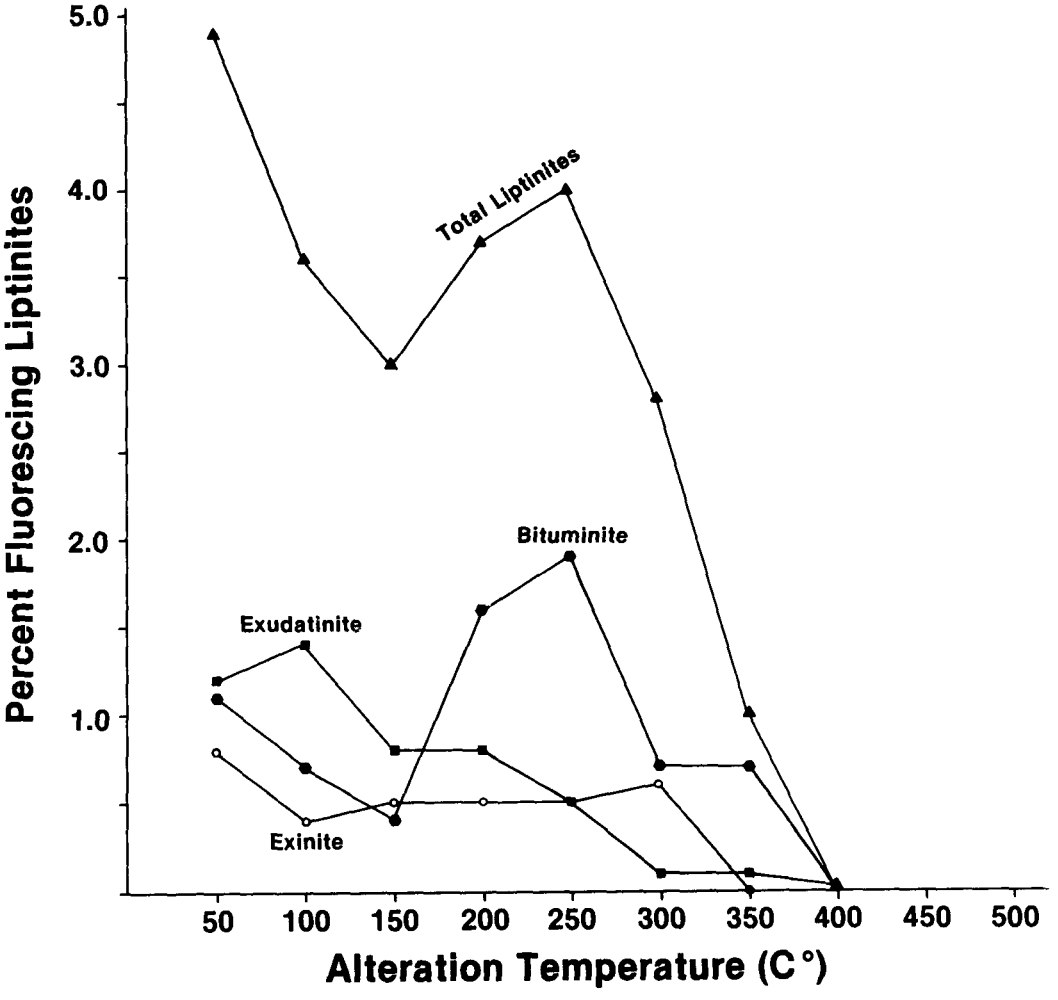

Figure 2
Relative Abundances of Some Liptinites in a Hanna Coal Sample From 277-278 Feet, as a Function of Temperature

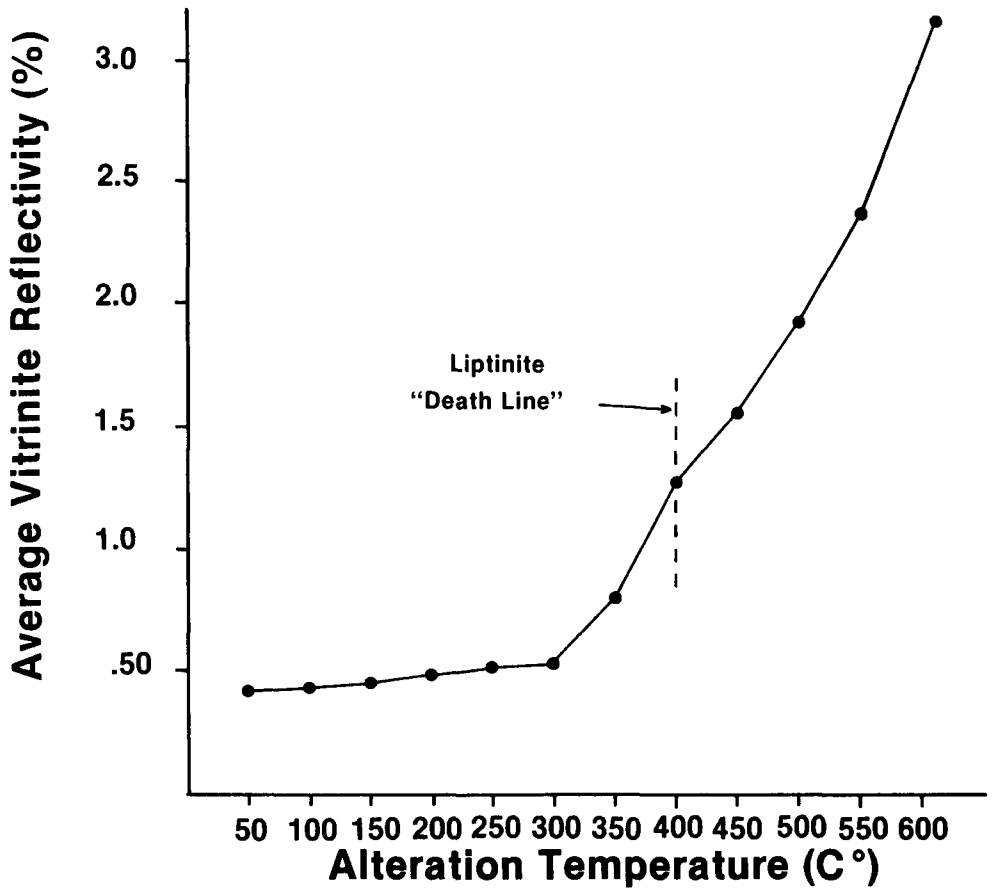

Figure 3
Vitrinite Reflectivity as a Function of Alteration Temperature, Hanna Sample 277-278

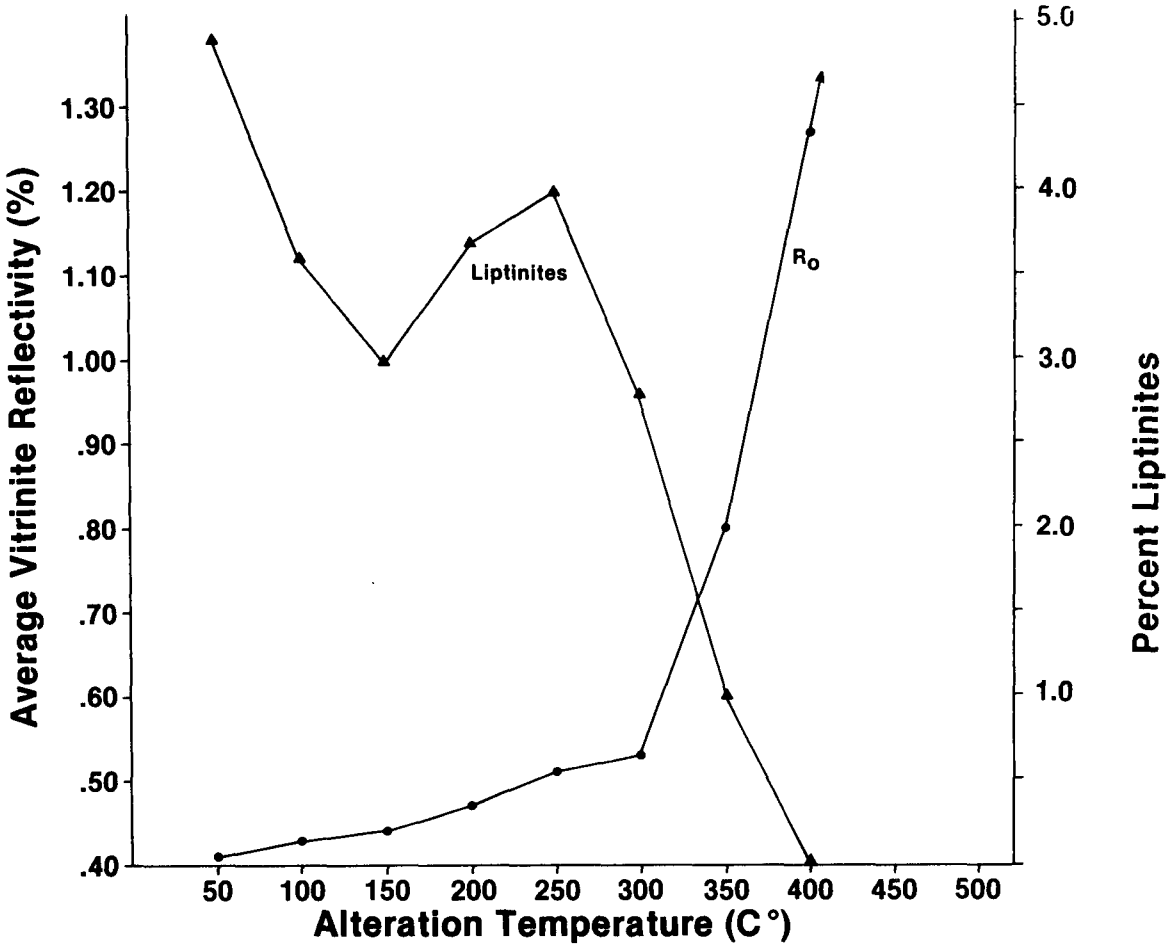

Figure 4
Petrographic Alterations in a Hanna Coal Sample as a Function of Temperature

SESSION IV: POSTER PRESENTATIONS

Proceedings of the Ninth Annual Underground Coal Gasification Symposium, August, 1983

3.7 THE EFFECT OF THERMAL AND STRUCTURAL PROPERTIES ON THE GROWTH OF AN UNDERGROUND COAL GASIFICATION CAVITY

by

Robert E. Glass

ABSTRACT

In field and laboratory studies of underground coal gasification, the growth of the cavity about the initial link has varied from the approximately circular cross section observed in the Hanna Basin coals, to cavities with 2:1 ratios of vertical to horizontal growth as has been observed in the Powder River Basin coals. A model based on the thermal and structural behavior of coal has indicated that these shapes are dependent on the site specific properties of the coal.

In this study, the properties of coal samples taken from the Big Seam near Centralia, Washington, are used in the model to examine the cavity growth in that seam. Due to the high variability of these properties, sensitivity studies are included to determine a range of probable shapes. The results obtained from the model are then compared with field data. The result of the study is a prediction that the vertical-to-horizontal growth ratios will vary from 1:1 to 1.4:1 in underground tests in the Big Seam.

INTRODUCTION

In September, 1983, an Underground Coal Gasification (UCG) test to determine the feasibility of the controlled retracting injection point (CRIP) method is going to be conducted in the upper 4.5 m of the Big Seam near Centralia, Washington.[1] This partial seam test will provide an opportunity to determine the predictive capability of the thermostructural cavity growth model[2] being developed at Sandia. The modeling results will be compared with thermocouple and controlled source audio-frequency magnetotelluric (CSAMT) data as it becomes available to determine the accuracy of the prediction as well as to indicate directions for further refinement of the model.

Since the model, which has been previously discussed,[2] calculates the stress field in the coal based on lithostatic and thermal loads, an essential element of the effort is the determination of the thermal and structural properties of the virgin coal. In a previous study of a Hanna Basin coal,[3] a series of temperature and orientation dependent properties were determined. These data were compared with the results of other studies of thermal[4-7] and structural[8-11] coal properties to determine what additional properties needed to be determined to characterize the thermal and structural response of the Big Seam coal.

The necessary tests include (1) specific heat determination to 275°C, (2) orientation dependent thermal conductivity to 500°C, (3) orientation dependent thermal expansion to 500°C,

Sandia National Laboratories
Albuquerque, New Mexico 87185

and (4) uniaxial compression and indirect tension (Brazil) tests at ambient temperature. Since previous results[3,5,8] indicated that the coal had little load carrying ability at 500°C, this temperature is used as an upper limit in properties studies aimed at examining the structural response of the coal.

These properties are used in a thermal and structural model of cavity growth to predict the growth of the cavity as well as to study the influence that varying lithostatic loads and properties have on the growth pattern. This latter consideration is especially important in a coal whose properties are as variable as those in the Big Seam. The results obtained from the model are in qualitative agreement with the cavity growth patterns seen during the Large Block tests.[14] The final result of this study is a prediction of the cavity growth that will be observed during the test.

COAL PROPERTIES

The specific heat of the virgin coal samples was measured to 275°C to examine the effect of moisture content. This test was conducted using a differential scanning calorimeter with the sample sealed in an aluminum pan to prevent the escape of evolved gases. The data which is presented in Figure 1 shows the endothermic reaction of moisture phase change occurring from 110°C to 240°C. The important aspect of the endothermic reaction is not the temperature range, which is heating rate and pressure dependent, but the total energy involved. The total energy is 3.5 x 10^5J/kg. The proximate analysis of the coal[12] indicates a moisture content of 22% which would require a heat of vaporization of 5.0 x 10^5J/kg. This difference indicates some loss of moisture during sample preparation as well as natural variability in water content from sample to sample. The results of this test and others[5] indicate that an ambient temperature specific heat corrected to account for moisture phase change will adequately specify the temperature dependent specific heat to 275°C. To extend the temperature range above 275°C requires a knowledge of the devolatilization properties of the coal. Since calculations of temperature profiles indicated low sensitivity to variations in the specific heat in the devolatilization temperature range, these tests were not performed on Big Seam coal samples.

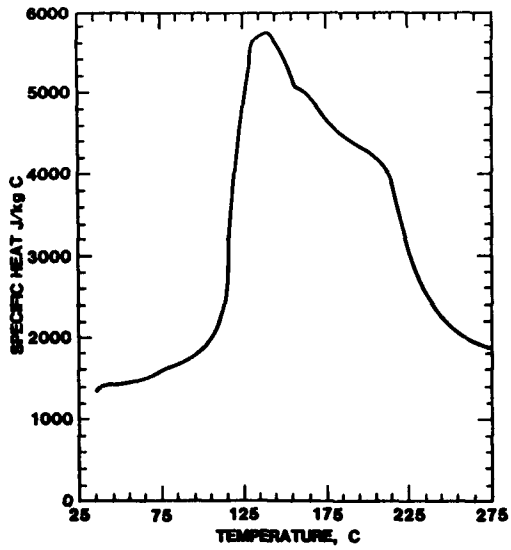

FIGURE 1. Specific heat as measured for the Big Seam coal.

The second thermal property determined was the thermal conductivity. These tests determined the temperature dependence to 500°C and the extent, if any, of anisotropy. The results are summarized in Figure 2, which shows the data obtained from tests on eight samples. As can be seen, there is no appreciable difference due to bedding plane orientation.

The thermal stresses that exist in the coal result from thermal expansion. The property was measured using a single pushrod dilatometer with nominal one-inch long specimens heated at 4°C/min to 500°C. Shown in Figure 3 are the results of four tests with expansion measured perpendicular to the bedding planes. Figure 4 shows the results of four tests with expansion measured parallel to the bedding planes. The most significant aspect

of the thermal expansion data is the shrinkage this coal undergoes upon heating. This indicates that during in situ coal gasification, tensile stresses may be induced in the vicinity of the hot cavity.

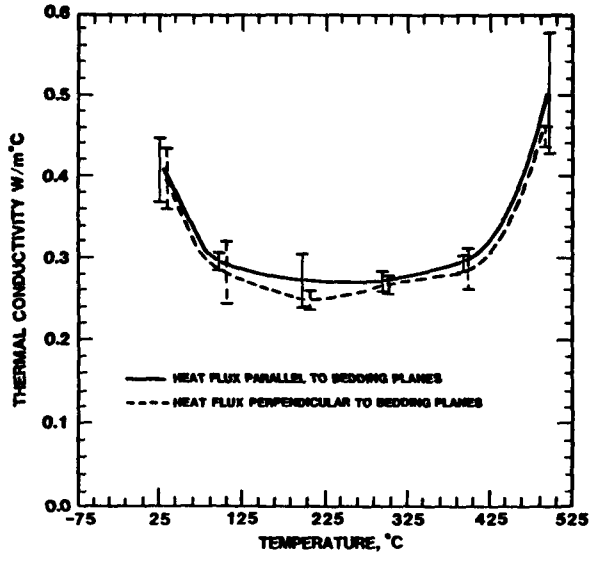

FIGURE 2. The results of thermal conductivity tests indicating that the variability between samples is greater than any anisotropy.

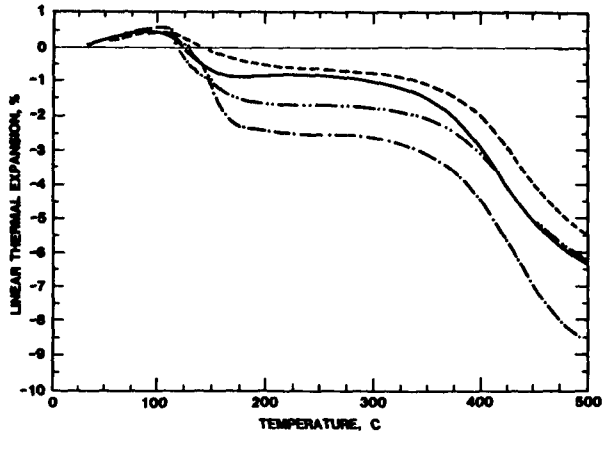

FIGURE 3. The results of thermal expansion tests on four samples from the Big Seam with expansion measured perpendicular to the bedding planes.

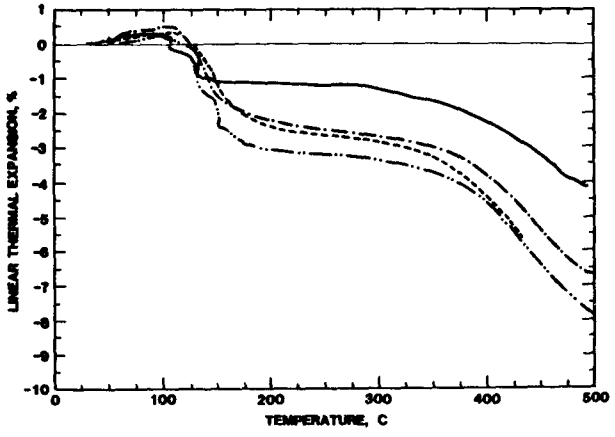

FIGURE 4. The results of thermal expansion tests on four samples from the Big Seam with expansion measured parallel to the bedding planes.

The properties that remain to be determined to specify the elastic response of the coal are the Poisson's ratios (ν), the elastic moduli (E), and the failure criteria. The shear modulus (G) can be approximated by

$$G_{rz} = \frac{E_z}{2(1 + \nu_{rz})}$$

which is exact for the isotropic case, but only approximates orthotropic behavior. These properties were measured at ambient temperature and are shown in Table 1.

The calculation of thermal stress requires values for the elastic moduli up to 500°C. These are obtained using the data shown in Figure 5, which consist of average values for coals determined in other studies[3,8] normalized to their ambient temperature values. These curves are used with the measured ambient temperature values of the elastic moduli to yield the temperature dependent elastic moduli.

In the cavity growth model, the calculation of the thermal and lithostatic stresses is followed by determining which elements have failed. To

do this, it is necessary to define a failure criteria for the coal. The first step in defining the failure criteria is to measure the tensile strengths of the coal.

is perpendicular to the bedding planes. The results of 36 tests are summarized in Table 2. The average tensile strengths which are used as

TABLE 1. UNIAXIAL COMPRESSION TEST RESULTS

SAMPLE ORIENTATION	DENSITY (gm/cm^3)	ELASTIC MODULUS (GPa)	POISSON'S RATIO
Perpendicular	1.38	1.4	0.38
Perpendicular	1.40	2.4	0.40
Perpendicular	1.39	1.4	0.35
Parallel	1.48	1.2	0.41
Parallel	1.40	1.2	0.54
Parallel	1.45	1.2	0.56

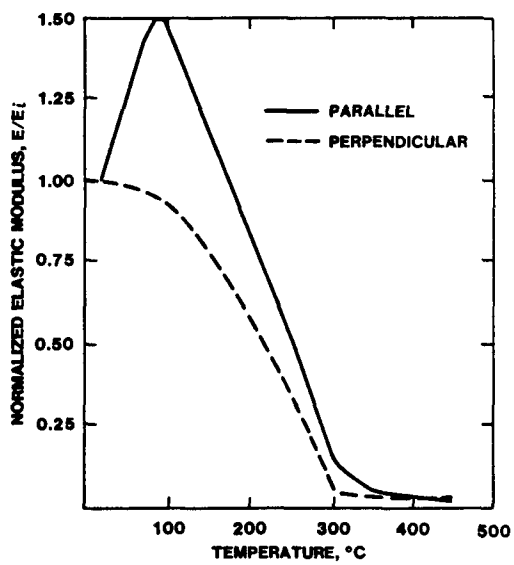

FIGURE 5. The normalized moduli used to determine the temperature dependent elastic moduli for the Big Seam coal.

The tensile strengths were measured by using the Brazil test. The three sample configurations are shown in Figure 6. Configurations A and C result in the failure stress being parallel to the bedding planes while in configuration B the failure stress

the initial failure criteria are lowest when the tensile stress is perpendicular to the bedding plane. The data also indicates significant variability as measured by the standard deviation.

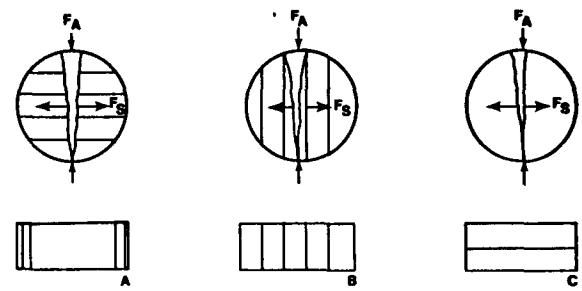

FIGURE 6. The three configurations used for testing the tensile strength of the coal are shown. The orientation of the applied compressive force (F_A) and the resulting tensile failure stress (F_S) are shown with respect to the orientation of the bedding planes.

ANALYSIS

To use the coal properties in a predictive model of cavity develop-

ment, two factors affecting the outcome must be considered. These are (1) the properties, as measured, represent competent rock properties and may vary substantially from the jointed rock mass behavior, and (2) within the measured properties, some coals such as that found in the Big Seam, exhibit high sample-to-sample variability. These factors will be addressed by varying properties to account for greater influence of jointing and fracturing and by varying the properties over the range of values presented in the preceding discussion.

TABLE 2. BRAZIL TEST RESULTS

SAMPLE ORIENTATION*	A	B	C
Number of Samples	13	4	19
Average Tensile Strength (MPa)	1.06	0.84	1.21
Standard Deviation (MPa)	0.36	0.19	0.58
Maximum Strength (MPa)	1.71	1.01	2.12
Minimum Strength (MPa)	0.42	0.65	0.50

*Refer to Figure 6 for more detail.

The base case analysis uses the average of the properties presented to date and summarized in Table 3. The failure criteria to be used is based on observed behavior of the coals. The laboratory studies of the Big Seam[13] coal indicated that the dominant fractures during small scale gasification ran parallel to the bedding planes. This indicates that the failure occurs due to stresses applied perpendicular to the bedding planes and that the failure strength in that direction is the primary component of the failure criteria.

In selecting a value for the tensile failure strength, three options are available. These include (1) averaged strength, (2) weakest observed strength, or (3) zero strength. The first option is discarded based on the assumption that the testing includes very competent coal samples which would not fail when surrounded by weaker neighbors. The third option is not selected since cohesion and friction along flaws will result in a non-zero tensile strength. This leaves the second option, which is to examine the data and select a strength based on probable flawed coal. Four Brazil tests were conducted with stress perpendicular to the bedding planes. The results of these tests were strengths of 1.01, 1.00, 0.72, 0.65 MPa. This indicates that the competent coal has a minimum tensile strength of 1.0 MPa, while a flawed coal has a maximum tensile strength of 0.7 MPa. Further, it indicates that those flaws are common enough to be the primary regions of failure.

An additional component of the failure criteria is based on the temperature dependent elastic moduli. As can be seen in Figure 5, the load carrying ability of the coal is greatly reduced at 400°C; therefore 400°C is used as the second component of the failure criteria. The resulting simplified base case failure criteria consist of a tensile strength perpendicular to the bedding plane of 0.7 MPa and a failure temperature of 400°C. If either of these limits are exceeded, the element has failed. These considerations result in a base case consisting of average properties and the failure criteria. The results

TABLE 3. TEMPERATURE DEPENDENT STRUCTURAL PROPERTIES (BASE CASE PROPERTIES)

TEMPERATURE (°C)	ELASTIC MODULI (GPa) $E_{r\theta}$	E_{rz}	COEFFICIENT OF EXPANSION $\alpha_r \times 10^6$	$\alpha_z \times 10^6$
25.	1.2	1.7	0	0
75.	1.7	1.6	33.	47.
100.	1.8	1.5	33.	44.
170.	1.2	1.2	-119.	-77.
250.	0.6	0.6	-95.	-59.
350.	0.08	0.04	-81.	-56.
450.	0.02	0.02	-116.	-118.

of the base case study are presented in Figure 7.

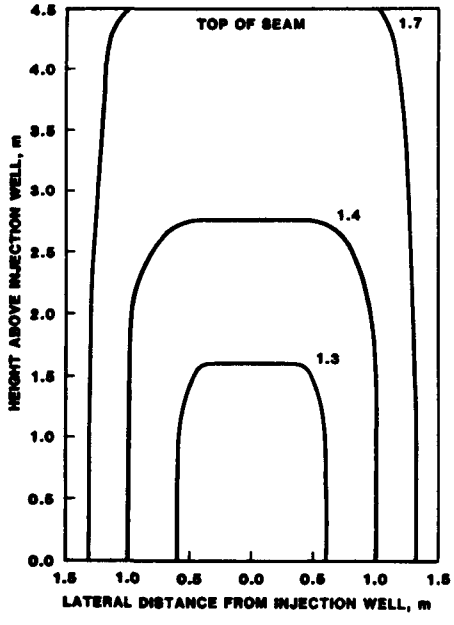

FIGURE 7. Vertical cross sections of the calculated cavity growth based on the base case properties. Numbers indicate the vertical-to-horizontal growth ratios.

The results reported for the Large Block tests[14] indicate a vertical-to-horizontal growth ratio that varies from 1.3:1 to 1.7:1. The results as seen in the model also show a vertical-to-horizontal growth ratio that varies from 1.3:1 to 1.7:1, as can be seen in Figure 7. The ratios start at the lower end and increase with the width of the cavity. This will tend to lead to ever larger blocks of coal falling into the cavity as the lateral width increases. This increasing block size was observed during the Large Block tests.[15]

The calculated results compared with a typical cavity of the Large Block tests[14] for cavities of equal lateral extent are shown in Figure 8. Note the model as previously discussed[2] assumes injection at the bottom of the coal seam to prohibit downward growth of the cavity and hence, only the cavity above the injection point is included. The uncertainty involved in all rock properties measurements are such that any modeling effort must include sensitivity studies to determine the effect of variations in measured properties. The first factor to be considered is the difference between competent rock behavior and jointed rock behavior. It should be noted that the earlier discussion on choice of failure strength had attempted to recognize the probable failure along existing flaws as opposed to failure of a competent rock. Other possible effects of a fractured region of rock include a softer and weaker response of the

rock to applied stress.[16] To model this behavior, changes are made in the properties. The elastic moduli are reduced to one half of their measured values, and the tensile strength is reduced to zero. The results of the first changes are shown in Figure 9. The resultant cavity growth shows a vertical-to-horizontal growth ratio of less than one.

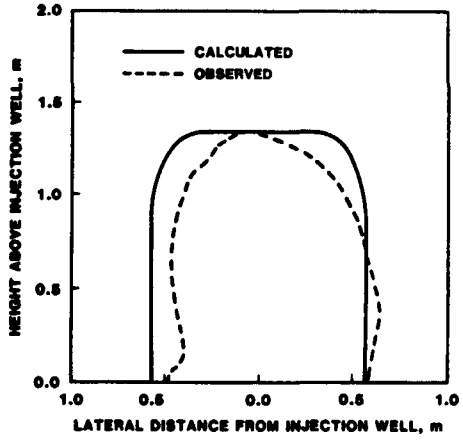

FIGURE 8. Comparison of cavity growth observed during Large Block Tests[14] with calculated results.

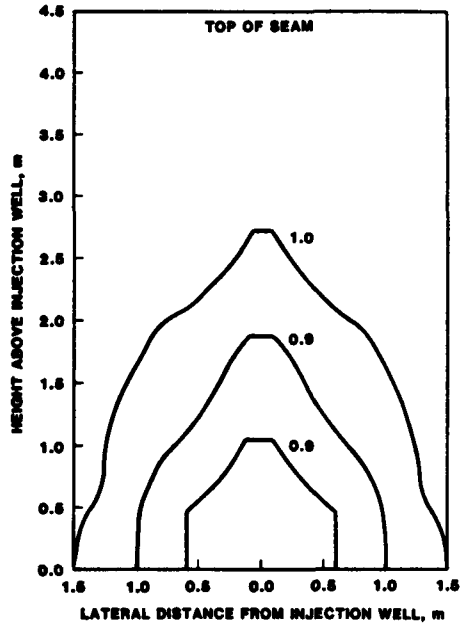

FIGURE 9. Vertical cross sections of the calculated cavity growth using elastic moduli with one-half the base case value. Numbers indicate the vertical-to-horizontal growth ratios.

This calculation indicates that change based solely on a softening of the coal will result in a wider and rounder cavity. Adding zero tensile failure strength to the softened coal results in the cavity growth shown in Figure 10. This cavity exhibits greater vertical-to-horizontal growth ratios ranging from 1.5:1 to 1.9:1, indicating that weakening of the coal due to fracturing will tend to reduce the resource recovery. The variation from observed growth ratios indicate that these are not realistic properties for the Big Seam coal and that previous considerations in determining the failure criteria are adequate for determining the rock mass behavior of the Big Seam coal.

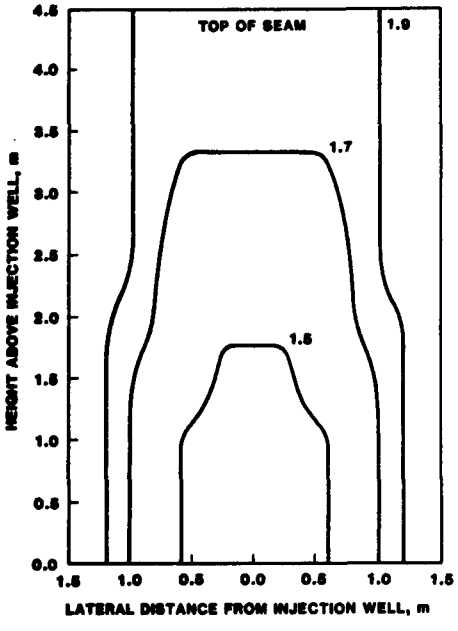

FIGURE 10. Vertical cross sections of the calculated cavity growth using elastic moduli of one-half the base case value and zero tensile strength. Numbers indicate the vertical-to-horizontal growth ratios.

The next change to consider is the high variability in the thermal coefficient of expansion. To examine its effects, the model was run using the highest (most tensile) and the lowest (least tensile) coefficients of expansion as represented by the curves in Figures 3 and 4.

The results of calculations with the high coefficient of thermal expansion are shown in Figure 11. The vertical-to-horizontal growth ranges from 1.6:1 to 2:1. This is due to the greater thermal stresses induced in the coal. It should be noted that these values are also too high to represent the growth observed in Large Block tests. The calculations using the lowest thermal coefficient of expansion are shown in Figure 12. As expected, these showed a lower vertical-to-horizontal growth ratio due to the lower thermal stresses induced.

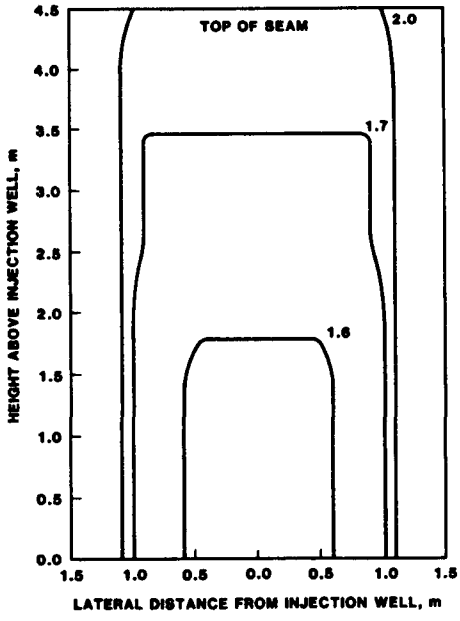

FIGURE 11. Vertical cross sections of the calculated cavity growth using the highest (most tensile) measured coefficients of expansion. Numbers indicate the vertical-to-horizontal growth ratios.

The general agreement between the observed and the calculated cavity growth for the base case and the unfavorable changes resulting from variations gives additional confidence in the ability of the model to predict the underground cavity growth using the base case properties and failure criteria.

The next step is to predict the cavity growth that will be observed

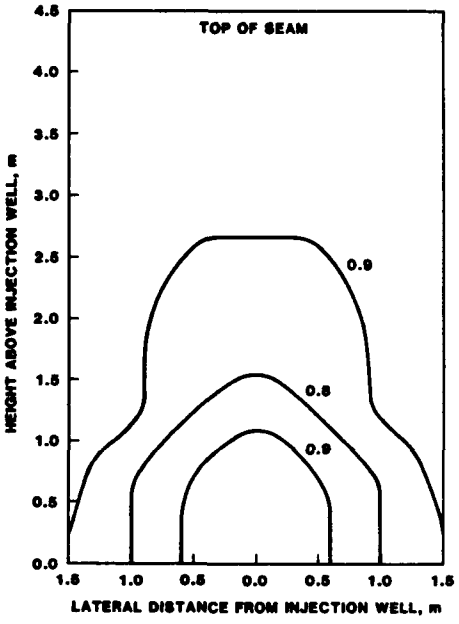

FIGURE 12. Vertical cross sections of the calculated cavity growth using the lowest (least tensile) measured coefficients of expansion. Numbers indicate the vertical-to-horizontal growth ratios.

during the partial seam test. The only factor that needs to be added to the base case study is the lithostatic load. The effect of sixty meters of overburden is added to the model with the resultant cavity growth as shown in Figures 13 and 14. Figure 13 represents a vertical slice of the cavity through the injection point and Figure 14 is a three dimensional view based on axisymmetric growth about a vertical line through the injection point. The final vertical-to-horizontal growth ratio is 1.4:1, which will result in a cavity with a maximum lateral extent of 3.2 m for 4.5 m of seam height. It is anticipated that the subsequent growth will extend most rapidly along the roof of the seam. This latter growth results in lower product quality and reduces resource recovery below the active cavity.

The results of this study were used in determining the placement of some of the thermal instrumentation for the partial seam test. The data from that instrumentation will be com-

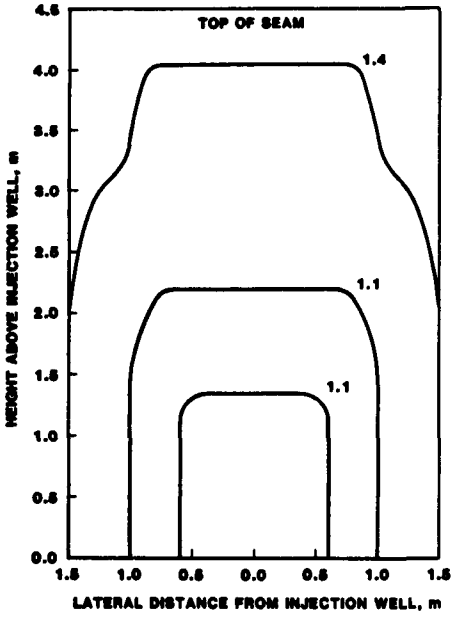

FIGURE 13. Vertical cross sections of the calculated cavity growth at a depth of 60 meters. Numbers indicate the vertical-to-horizontal growth ratios.

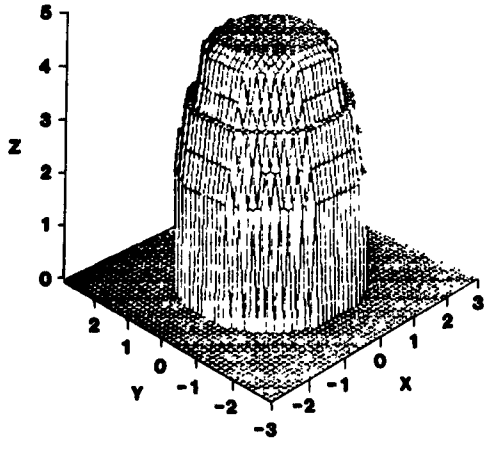

FIGURE 14. Three dimensional view of the calculated cavity as the roof of the Big Seam is reached. The view is the injection point.

pared with the modeling results to determine if further development of the model is required.

CONCLUSION

This study has produced a prediction of the early cavity growth that will be observed in an Underground Coal Gasification test in the Big Seam coal. The prediction is based on a thermal and structural behavior model of the coal and has been shown to agree with results obtained during the Large Block tests.

In addition to the cavity prediction, the analysis has shown that the thermal coefficients of expansion, the elastic moduli and the failure strength are the main factors in determining the vertical-to-horizontal growth ratios. These properties interact such that any change that results in a lower tensile stress state relative to the tensile failure strength, also reduces the vertical-to-horizontal growth ratio and thereby improves initial resource recovery.

This analysis does leave open the question of cavity growth rate. While previous work has included simple calculations based on empirical oxygen consumption rates, a more realistic model should include a lateral coal consumption rate based on heat and mass transfer rates as well as on chemical reactions. These same processes should also yield an ability to predict the elongation of the cavity along the product flow path.

REFERENCES

1. Hill, R. W., C. B. Thorsness, "The Centralia Partial Seam CRIP Test Preliminary Design", UCID-19610, November 1982.

2. Glass, R. E., "Thermomechanical Cavity Growth Modeling", Proceedings of the Eighth Underground Coal Conversion Symposium, August 1982.

3. Glass, R. E., "The Thermal and Structural Properties of a Hanna Basin Coal", Sandia National Laboratories report, SAND 83-0051.

4. Badzioch, S., D. R. Gregory, M. A. Field, "Investigation of the Temperature Variation of the Thermal

Conductivity and Thermal Diffusivity of Coal", Fuel, Vol. 43, July 1964, pp 267-280.

5. Singer, J. M., and R. P. Tye, "Thermal Mechanical and Physical Properties of Selected Bituminous Coals and Cokes", Bureau of Mines RI-8364, 1979.

6. Lee, C. K., J. M. Singer, R. F. Chaiken, "Coal Pyrolysis at Fire-Level Heat Flux", Combustion Science and Technology, 1977, Vol. 16, pp 205-213.

7. Clendenin, J. D., K. M. Barclay, H. J. Donald, D. W. Gilmore, and C. C. Wright, "Thermal and Electrical Properties of Anthracite and Bituminous Coals", the Pennsylvania State College Mineral Industries Experiment Station, "Technical Paper 160, 1949.

8. Shoemaker, H. D., "Mechanical Properties of the Pittsburgh Coal at Elevated Temperatures", Doctoral Dissertation, West Virginia University, 1976.

9. Evans, I., "The Tensile Strength of Coal", Colliery Engineering, October 1961, pp 428-434.

10. Berenbaum, R. and I. Brodie, "Tensile Strength of Coal", J. Inst. Fuel, 1959, Vol. 32, pp 320-327.

11. Heard, H. C., B. P. Bonner, M. S. Costanino, R. N. Schock, and H. C. Weed, "Mechanical Response of Saturated Kemmerer Coal to 4 GPa", UCRL-52063, May 1976.

12. Hill, R. W. and C. B. Thorsness, "The Large Block Tests", UCRL-87611, May 1982.

13. Thorsness, C. B., Hill, R. W., "Coal Block Gasification Experiments: Laboratory Results and Field Plans", Proceedings of the Seventh Underground Coal Conversion Symposium, 1981, Conf.-810923.

14. Stephens, D. R., Clements, W., "LLNL Underground Coal Gasification Project Quarterly Progress Report - April through June 1982", UCRL-50026-82-2, August 1982.

15. Personal communication with R. W. Hill and C. B. Thorsness.

16. Goodman, R. E., Methods of Geological Engineering, West Publishing Company, 1976.

3.8 THE CAVITY PRODUCED BY GASIFYING THIN DEEP SEAMS

by

I H C Wilks[1/]

ABSTRACT

Recent trials in the USA have confirmed that UCG operating under the right thermochemical conditions can produce a medium CV gas. However if UCG is to be economic in deep coal in the UK then at least 50,000 tonnes of coal must be converted to cover the cost of constructing a pair of process wells to access deep seams. Because UK seams are relatively thin, both large well spacings and wide cavities will be required. This paper describes a mathematical model which predicts the size and shape of the cavity formed between a pair of process wells as a function of seam thickness and depth.

The model assumes that the cavity grows radially about the input well during the initial gasification and that the cavity soon fills with collapsed roof strata. Lithostatic pressure packs the collapsed strata tightly everywhere except in a narrow region at the edge, where the relatively high permeability encourages gas to flow along the coal face to the product well rather than the shorter path through the tightly packed strata. The subsequent growth of the cavity is determined using D'Arcy's law to calculate the pattern of gas flow and the proportion of input gas meeting each part of the coal face. Results indicate that large cavities could be burned out and that over 100,000 tonnes of coal could be converted from a pair of wells 200 metres apart in a 2 metre seam at a depth of 1,000 metres.

1/ National Coal Board, Mining Research and Development Establishment, Burton-on-Trent, Staffs. UK.

The views expressed in this report are those of the author and not necessarily those of the National Coal Board.

1. INTRODUCTION

This paper presents a model for the development of a gasifier between widely spaced wells in a thin seam where the cavity is filled with collapsed roof strata. The seam is assumed to have a weak shale roof and be at a depth where the lithostatic pressure over a wide cavity is sufficient to collapse the roof; this will be true for most UK seams below 500 m, though a sandstone roof may remain intact at much lower depths.

The gasifier proposed for deep coal in the UK will operate at 50 bar[1]. The maximum velocity at which gas from such a gasifier can enter a 500 metre, 3½" ID product well has been calculated to be 60 m/s, which restricts the velocity through the cavity to less than 5 cm/s. This implies that the pressure drop across the cavity, even if filled with caved strata, is very small and throughout this work the gas is assumed to be incompressible.

2. ROOF COLLAPSE IN UCG

The cavity is expected to behave in a similar way to the waste behind a fully caved longwall face; in both cases the coal face advances slowly and the horizontal dimensions are much greater than the seam thickness.

The roof of a UK coal seam is usually weak and in longwall mining below 500 metres the lower strata in the roof collapse up to the line of the face supports. The voids formed in the caved strata increase their effective displacement by about 50 per cent, corresponding to a bulking factor (the ratio of bulked to solid volume) of 1.5, and the height of the caved strata is about three times the seam thickness. The higher strata are supported by this caved strata and they do not fail, though in the absence of vertical load they may de-laminate.

As the longwall face advances it gives less support to the strata above the waste and these deform elastically to re-compact the failed rock; measurements of surface subsidence suggest that the bulking factor may be reduced to as little as 1.05. In the region just behind the face supports the rock breaks away at an angle α (often known as the caving angle) and loose rock may only partially fill this region.

If the gasifier is assumed to behave similarly there will be progressive caving around the advancing boundary; this region may be loosely filled with caved strata or there may be an open channel. The deformation of the roof will re-compact the caved strata in the inner region and this will have a much lower permeability than the loosely packed rock next to the coal face. This will be highly permeable because a local bulking factor of about 2 is required to fill this region completely; and if an open channel exists it will offer virtually no resistance to the gas. In either case the gas will be encouraged to flow from the input well outwards to the coal face and thence to the product well, rather than along the shorter path through the tightly packed inner region.

The velocity of the gas through the cavity will be of the order of cms/sec and the drop in pressure less than 0.1 bar[1] and therefore the pattern of gas flow will be determined by the ratio of the permeabilities in the two regions. In order to assess this ratio the permeability of caved strata must be investigated.

3. THE PERMEABILITY OF CAVED STRATA

It is assumed that the flow of gas through caved strata satisfies D'Arcy's law for permeable media: if V is the volume of gas crossing unit area in unit time (the drift velocity) then

$$\eta V = -k\frac{dp}{dx}$$

where η is the viscosity of the gas, k the permeability of the medium and dp/dz the pressure gradient.

The permeability of a porous solid depends mainly on the proportion of empty space (or porosity) in the medium and the area of exposed surface where friction impedes the flow; the following relation between permeability, porosity (P) and the exposed surface area per unit volume ($\mathcal{A}$) is assumed:

$$k \propto P^5/\mathcal{A}^2$$

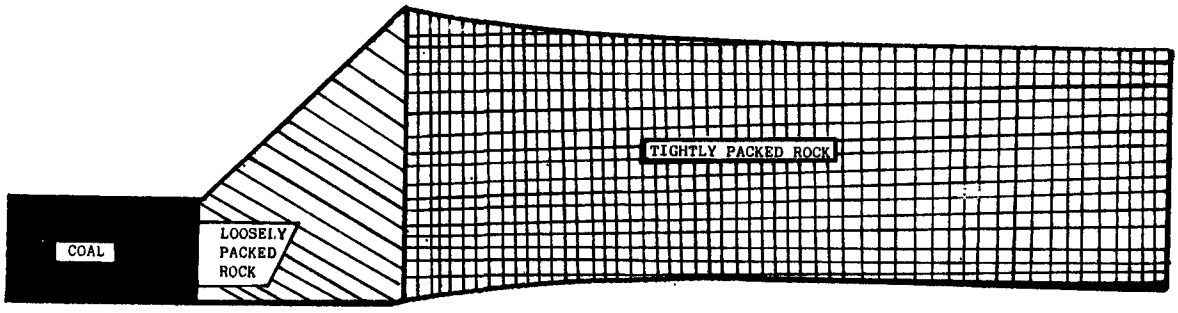

Fig 1. Compaction of Waste in Gasifier

To find α and β consider the flow of gas through a slice of the porous medium, together with the following assumptions:

(i) The pressure gradient is uniform across the slice.

(ii) The slice is perforated by many small identical pores of uniform cross-section.

(iii) One-third of these pores run longitudinally through the slice and the remainder which run transversely do not carry any flow.

(iv) The diameter of the pores is much greater than the mean free path of the gas and so the gas behaves as a Newtonian fluid.

Consider the flow through any one of the longitudinal pores. The velocity varies over the cross-section but must be zero on the walls of the pore. If the z axis is chosen parallel to the flow the velocity will be a function of x and y given by the Navier-Stokes equation:

$$\frac{\partial^2 v}{\partial x^2} + \frac{\partial^2 v}{\partial y^2} = \frac{1}{\eta} \cdot \frac{dp}{dz}$$

This implies that v is proportional to $1/\eta \cdot dp/dz$ and furthermore if a is a typical diameter of the pore then v is also proportional to a^2. The volume discharged by the pore in unit time is $\lambda a^4/\eta \cdot dp/dz$, where λ is a geometric factor depending only on the shape of the cross-section. If there are N pores through a slice of unit area then the longitudinal ones discharge gas at this rate and the total volume crossing unit area in unit time is

$$V = \frac{\lambda N a^4}{3\eta} \cdot \frac{dp}{dz}$$

Comparing this expression with D'Arcy's law implies that the permeability $k = \lambda N a^4/3$, but how do N and a relate to the bulk properties of the medium, P and Σ?

The porosity of the solid is equal to the total cross-section area of the pores perforating a slice of unit area and so $P \propto Na^2$. Similarly the exposed surface area is equal to the total circumference of these pores, and therefore $\Sigma \propto Na$. Substituting for P and Σ in the proposed formula and comparing the two expressions for permeability gives

$$k \propto \frac{(Na^2)^\alpha}{(Na)^\beta} \propto Na^4$$

$$\therefore k = \mu \frac{P^3}{\Sigma^2}$$

μ can be estimated by assuming that the cross-section of the pores is an equilateral triangle of side a, which gives $\mu = 1/5$. If the porous medium consists of closely packed particles with a surface to solid volume ratio S then $\Sigma = (1-P)S$ and the result is Kozeny's[2] equation:

$$k = \frac{1}{5} \frac{P^3}{(1-P)^2 S^2}$$

If the bulking factor of the caved strata is B then $P = 1-B^{-1}$ and Kozeny's equation becomes:

$$k = \frac{1}{5} \frac{(B-1)^3}{S^2 B}$$

If there is no open channel in the coal face region then the caved strata must have a bulking factor 2; let the tightly packed caved strata in the inner region have a bulking factor B_1. If all the waste is of a similar sized solid then the ratio of permeabilities in the two regions is

$$K = \frac{k_2}{k_1} = \frac{B_1}{2(B_1-1)^3}$$

This ratio varies inversely to the cube of (B_1-1) if the inner region is tightly packed ($B_1 \simeq 1$), for example if $B_1 = 1.2$ then $K = 75$ but if $B_1 = 1.1$ $K = 550$. Therefore the coal face region will offer a much lower resistance to the gas flow even if the caved waste extends right up to the coal face. The existence of any open channel will greatly enhance the permeability ratio, but for the remainder of this work the less favourable case of complete filling is assumed.

The roof of a UK coal seam is usually weak and in longwall mining below 500 metres the lower strata in the roof collapse up to the line of the face supports. The voids formed in the caved strata increase their effective displacement by about 50 per cent, corresponding to a bulking factor (the ratio of bulked to solid volume) of 1.5, and the height of the caved strata is about three times the seam thickness. The higher strata are supported by this caved strata and they do not fail, though in the absence of vertical load they may de-laminate.

As the longwall face advances it gives less support to the strata above the waste and these deform elastically to re-compact the failed rock; measurements of surface subsidence suggest that the bulking factor may be reduced to as little as 1.05. In the region just behind the face supports the rock breaks away at an angle α (often known as the caving angle) and loose rock may only partially fill this region.

If the gasifier is assumed to behave similarly there will be progressive caving around the advancing boundary; this region may be loosely filled with caved strata or there may be an open channel. The deformation of the roof will re-compact the caved strata in the inner region and this will have a much lower permeability than the loosely packed rock next to the coal face. This will be highly permeable because a local bulking factor of about 2 is required to fill this region completely; and if an open channel exists it will offer virtually no resistance to the gas. In either case the gas will be encouraged to flow from the input well outwards to the coal face and thence to the product well, rather than along the shorter path through the tightly packed inner region.

The velocity of the gas through the cavity will be of the order of cms/sec and the drop in pressure less than 0.1 bar[1] and therefore the pattern of gas flow will be determined by the ratio of the permeabilities in the two regions. In order to assess this ratio the permeability of caved strata must be investigated.

3. THE PERMEABILITY OF CAVED STRATA

It is assumed that the flow of gas through caved strata satisfies D'Arcy's law for permeable media: if V is the volume of gas crossing unit area in unit time (the drift velocity) then

$$\eta V = -k\frac{dp}{dx}$$

where η is the viscosity of the gas, k the permeability of the medium and dp/dz the pressure gradient.

The permeability of a porous solid depends mainly on the proportion of empty space (or porosity) in the medium and the area of exposed surface where friction impedes the flow; the following relation between permeability, porosity (P) and the exposed surface area per unit volume (Σ) is assumed:

$$k \propto P^{\alpha}/\Sigma^{\beta}$$

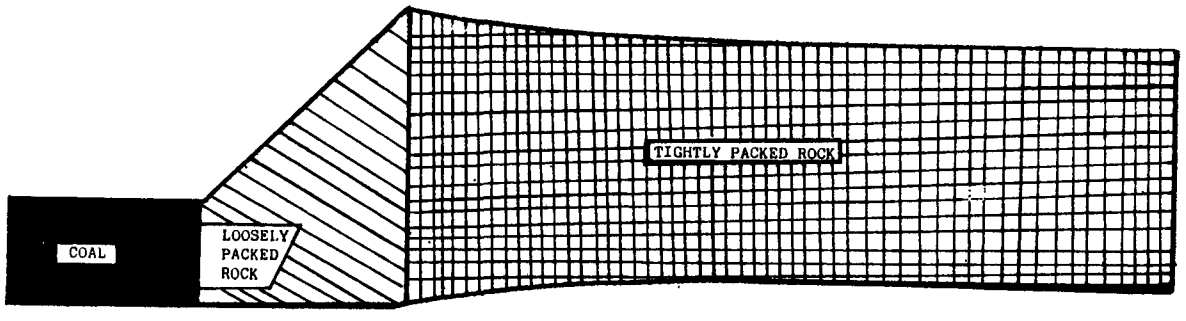

Fig 1. Compaction of Waste in Gasifier

in unit time then

To find α and β consider the flow of gas through a slice of the porous

surface area is equal to the total

Proceedings of the Ninth Annual Underground Coal Gasification Symposium, August, 1983

$$\frac{d\epsilon}{dt} = \dot{A}\, F(\phi;t)$$

where the volume of coal gasified from C is assumed to be proportional to the volume of fresh input gas meeting C.

5. GAS FLOW THROUGH THE CAVITY

The caved strata are assumed to fill the cavity and be tightly packed everywhere except in a narrow region next to the coal face. Within each of these regions the caved strata are assumed to have constant permeability: k_1 in the tightly packed region (called region I) and k_2 in the loosely packed region (II). The pattern of gas flow within the cavity can then be determined using D'Arcy's law and the further assumptions:

(i) The pressure variation is small and the gas behaves as an incompressible fluid.

(ii) The product well remains in region II.

(iii) Gas flow through region along radial streamlines from the input well. This approximation will be valid through most of region I if $k_1 << k_2$; and any small deviations near the boundary shall be neglected.

(iv) Input gas is immediately converted to product gas on entering region II. This assumes a low drift velocity compared to the rate of reaction.

(v) Region II is a narrow channel represented by the boundary curve $r = R(\phi)$.

(vi) The velocity of the product gas through region II does not vary over the cross-section.

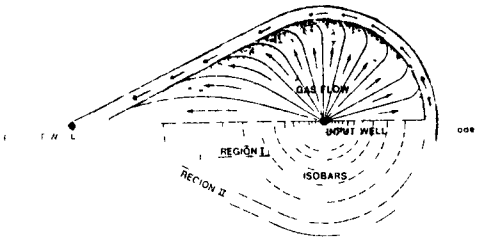

Fig 2. Gas Flow Pattern Within Cavity

(a) Flow Through Region I

Using polar co-ordinates to describe the radial flow through the tightly packed region, the velocity of input gas $\underline{u}$ becomes $u.\hat{\underline{r}}$. The equation of continuity $\mathrm{div}\,\underline{u} = 0$ and D'Arcy's law $\eta_1 \underline{u} = k_1 \,\mathrm{grad}\, p$ then reduce to:

$$\frac{d(ru)}{dr} = 0 \;;\quad \frac{dp}{dr} = -\frac{\eta_1}{k_1} u$$

Integrating the equation of continuity yields $u = \lambda/r$ where λ is an integration constant. This can be determined by substituting $u = \lambda/r$ into D'Arcy's equation, and then integrating from the outside of the input well $r = R_i$ to the cavity boundary $r = R(\phi)$. The drop in pressure (Δp) across the radial streamline from the input well to a point $C(R(\phi),\phi)$ on the coal face then becomes

$$\Delta p = \frac{\lambda \eta_1}{k_1} \ln[R(\phi)/R_i]$$

The velocity of the input gas meeting the coal face at $C(R(\phi),\phi)$ is therefore:

$$u = \frac{k_1 \Delta p}{\eta_1 R(\phi) \ln[R(\phi)/R_i]}$$

The flow rate of gas meeting a small element of the coal face, length δl, which subtends $\delta\phi$ at the input well is

$$u.R(\phi)h\delta\phi$$

where h is the height of the cavity. Substituting for u, dividing by δl then the letting $\delta l \to 0$ gives the volume flow

of input gas per unit length meeting the coal face at C.

$$V(\phi) = \frac{kh(d\phi/dl)\Delta p}{\eta_1 \ln[R(\phi)/R_i]} \quad (5.1)$$

Therefore the distribution of input gas to the coal face, which determines the growth of the cavity, depends not only on known geometric factors $R(\phi)$ and $d\phi/dl$ but also on the unknown drop in pressure (Δp) from the input well to various points on the coal face. Because the product gas in region II flows towards the product well Δp must be a maximum here and fall to a minimum at the opposite end, the gasifier node. The variation can be determined by considering the flow of gas through the narrow boundary region

(b) Flow Through Region II

Because the flow in region II is one-dimensional it varies only with the distance l along the boundary from the gasifier node; l is a more convenient parameter for the flow in region II than ϕ.

When input gas enters region II it is assumed to be immediately converted to product gas and its volume increases by a factor ξ owing to the gasification of coal and the rise in temperature. This gas then joins the main stream of product gas flowing with velocity $v(l)$ towards the product well.

Consider the flow of gas through a small element of region II of length δl at a distance l from the node. Product gas enters with velocity $v(l)$ and leaves with velocity $v(l+\delta l)$; in addition a small volume $\xi V(l)\delta l$ is produced from the input gas. If the area of the cross-section of II is A then the conservation of mass for an incompressible fluid implies that

$$Av(l+\delta l) = Av(l) + \xi V(l)\delta l$$

This is true for all elements except the one containing the gasifier node because the flow is symmetric about this point, gas must flow out of both ends and

$$Av(o+\tfrac{1}{2}\delta l) + Av(o-\tfrac{1}{2}\delta l) = \xi V(o)\delta l$$

Taking the limit as $\delta l \to o$ of these last two expressions gives

$$\frac{dv}{dl} = \frac{\xi}{A} V(l) \; ; \; v(o) = o. \quad (5.2)$$

The velocity of gas through II must also satisfy D'Arcy's law:

$$\frac{d\Delta p}{dl} = \frac{\eta_2}{k_2} v(l) \quad (5.3)$$

Differentiating 5.3 and eliminating v and V using 5.1 and 5.2 leads to a second order equation in Δp .

$$\frac{d^2\Delta p}{dl^2} = g(l)\Delta p \; ; \; \Delta p'(o) = o \quad (5.4)$$

$$g(l) = \frac{\xi h(d\phi/dl)}{KA\ln[R(\phi)/R_i]} \; ; \; K = \frac{\eta_1 k_2}{\eta_2 k_1}$$

where the permeability ratio (K) has been adjusted to take account of the increase in viscosity when the input gas is converted to product gas.

The single initial condition $\Delta p'(o) = o$ is not sufficient to solve the equation uniquely; a second may be contrived by introducing the function $y(l) = \Delta p(l) \div \Delta p(o)$ which satisfies the following equations uniquely.

$$y'' = g(l)y \; ; \; y(o) = 1 \; ; \; y'(o) = o. \quad (5.5)$$

Equations of this type can be solved approximately using the Cowell-Numerov method[3].

(c) Distribution of Input Gas to the Coal Face

The volume of gas meeting unit length of coal face is given by 5.1; comparing this equation with the definition of $g(l)$, 5.4 gives

$$V(l) = \lambda\, g(l)\, y(l).$$

where λ is just a collection of constant factors. Because all the input gas eventually meets the coal face, the proportion per unit length meeting C is

$$F(\ell) = g(\ell)y(\ell) \div \int_0^L g(\ell)y(\ell)d\ell ,$$

where L is the semi-perimeter of the gasifier. The integral can be evaluated using 5.3;

$$\int_0^L g(\ell)y(\ell)d\ell = \int_0^L y'd\ell = y'(L) .$$

$$\therefore \quad F(\ell) = \frac{g(\ell)y(\ell)}{y'(L)} .$$

6. PREDICTED CAVITY SHAPE

The model has been used to predict the development of a gasifier with two wells 200 m apart in a 1,000 m deep, 2 m thick seam. The remaining input parameters were as follows:

Height of cavity	h = 6 m
Caving angle	α = 45°
Cross-section of II	A = 16 m^2
Permeability ratio	K = 100
Increase in volume	ξ = 4

The caved strata will start to be packed about the input well when the cavity is 8 m wide and the shape then is assumed to be an elongated version of the Hoe Creek 2 cavity (Figure 3).

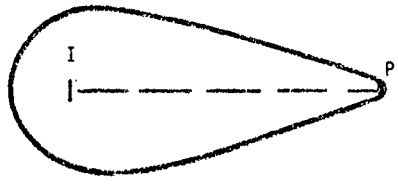

Fig 3. Hoe Creek 2 Cavity

The growth of the cavity was then determined using the method outlined in Section 5 until the width about the product well had grown to 8 m, after which both wells are assumed to be surrounded by tightly packed rock. The choice of 8 m is not critical because until the final stage there is negligible growth about the product well - as can be seen from Figure 4 which shows six stages in the development of the gasifier.

The final shape encloses an area of 53,000 m^2, corresponding to the gasification of 138,000 tonnes of coal.

Figure 5 shows the distribution of coal/gas contact time at the various stages of gasification. The curves are independent of gasification rate but the time scale corresponds to a rate of 250 tonnes/day (6,000 SCF/min of input gas). Even at the final stage, 99% of the gas sees coal for more than 1,000 seconds which is much longer than the estimated reaction time of about 10 seconds[1]. This is consistent with the initial assumption that $t_0 << L/v$.

7. SCALING OF GASIFIER DEVELOPMENT

The model requires the input of many parameters as well as a suitable initial cavity shape in order to predict the development of a gasifier. The experience of many computer runs has shown that the choice of the initial shape does not greatly influence the later development and it is now assumed that all gasifiers start from an elongated Hoe-Creek 2 cavity. The cross-section and height of the cavity are based on observations in longwall mining. Previous work on the thermodynamics and chemistry of UCG[1] has indicated that, independent of gasifier geometry, the volume ratio of product to input gas is about 4. This leaves three parameters which will vary for different gasifiers: the permeability ratio (K), the well spacing (S) and the seam thickness (τ).

If it is assumed that all gasifiers are geometrically similar initially, then those gasifiers with similar patterns of gas flow will have similar development. The patterns of gas flow within similar cavities will now be shown to be approximately similar if the cavities also have the same value of $J = K\tau/S$.

If α = 45°, h = 3τ and ξ = 4 are substituted into 5.4 then the equation determining the gas flow becomes

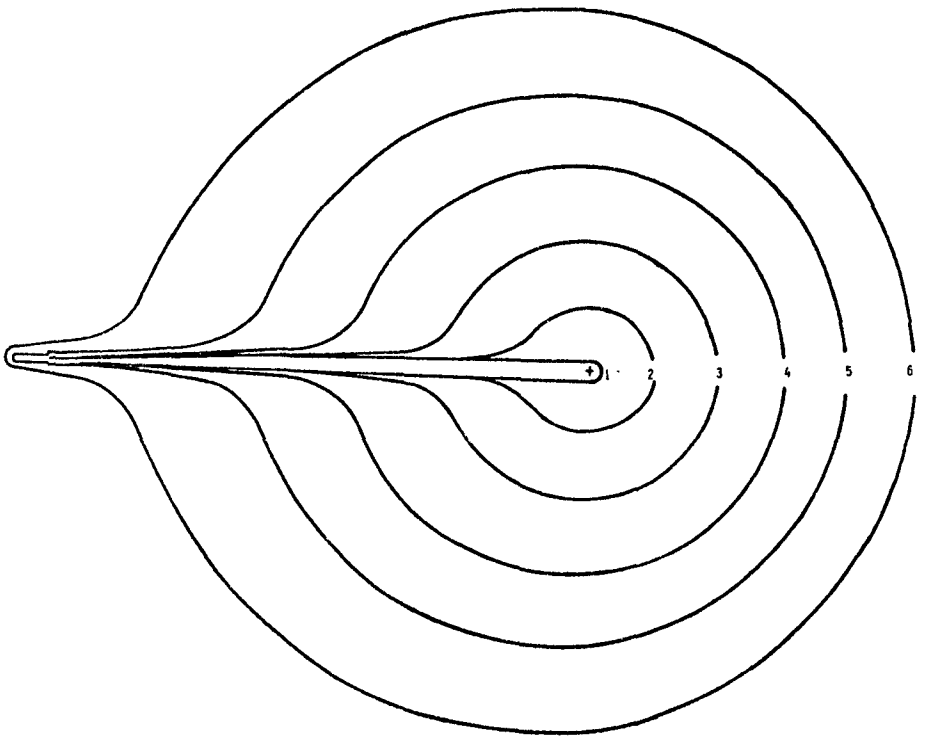

Fig 4. Predicted Development of Gasifier in Section 6

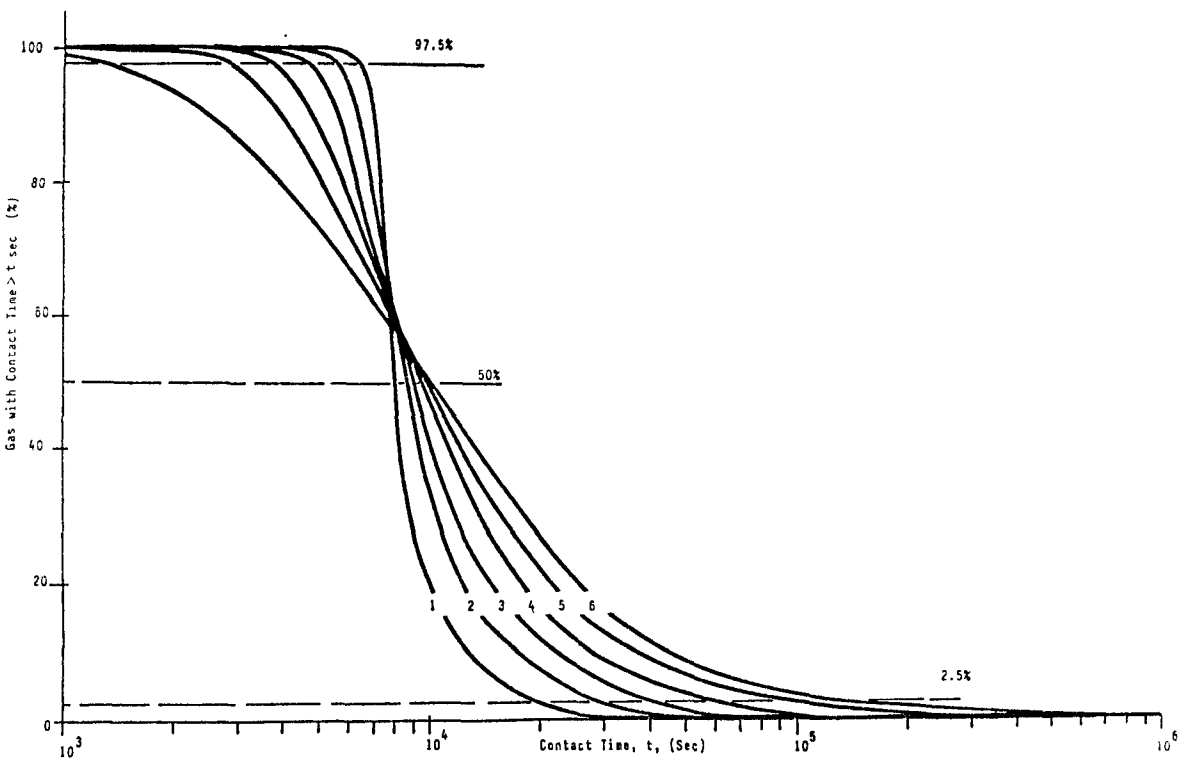

Fig. 5 Proportion of Input Gas Seeing Coal for More Than t Seconds, at Each Stage of Fig 4

$$\frac{d^2y}{dl^2} = \frac{3\, d\phi/dl}{Kt \ln[R(\phi)/R_i]} \quad ; \quad 0 \leq l \leq L.$$

The functions $d\phi/dl$ and $\ln[R(\phi)/R_i]$ depend on the geometry of the gasifier, but because $R_i << R(\phi)$ the logarithmic functions varies so slowly it can be replaced by its average value $\langle \ln R \rangle$. Introducing the dimensionless variable $x = 3l/Kt\langle \ln R \rangle$ reduces the equation to:

$$\frac{d^2y}{dx^2} = \frac{d\phi}{dx} \cdot y \quad ; \quad 0 \leq x \leq 3L/Kt\langle \ln R \rangle$$

The derivative $d\phi/dx$ will be identical for similar cavities and the semi-perimeter L will be proportional to S. Therefore similar cavities with the same value of $S/Kt\langle \ln R \rangle$ will exhibit similar gas flow patterns. However the variation of $\langle \ln R \rangle$ is much less than that of S and may be neglected; and therefore gasifiers with the same number $J = Kt/S$ will have approximately similar development.

The gasifier in Figure 4 corresponds to J = 1, whilst those in Figure 6 are for J = 0.25 and 0.06.

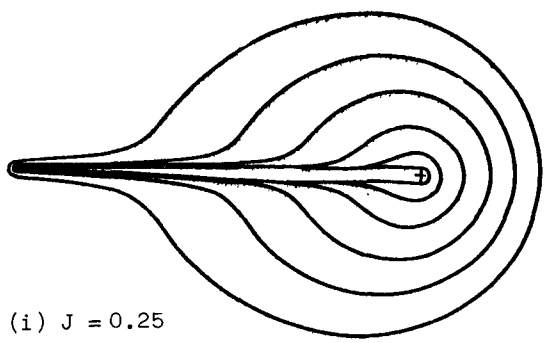

(i) J = 0.25

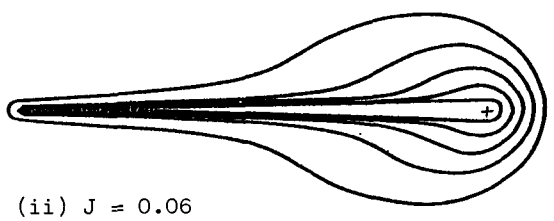

(ii) J = 0.06

Fig 6. Predicted Development for
(i) J = 0.25
(ii) J = 0.06

The developments have been terminated when the growth at the product well became significant and in general the volume of coal burned out is $f(J).L^2t$. where $f(J)$ is plotted in Figure 7.

8. ACKNOWLEDGEMENTS

The author wishes to thank the NCB Director of Mining Research and Development for his permission to present this paper.

9. REFERENCES

1 CHAPPELL, R S and WILKS, IHC. "A Theory for the Underground Gasification of Deep Coal Using the Linked Vertical Well Method", MRDE Report 1983.

2 KOZENY, J. SB Akad Wiss Wien, Abt IIa, 136, 271 (1927).

3 CHURCHHOUSE, R F. Handbook of Applicable Mathematics, Vol 3, Wiley, New York 1981.

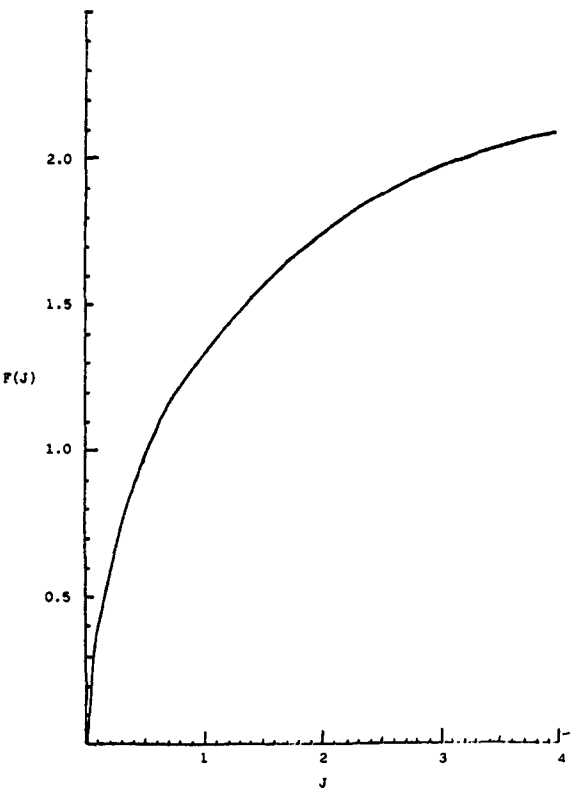

Fig 7. Ratio of Mean Width to Well Spacing of a Fully Developed Gasifier

3.9 MODELING UCG WITH STEAM AND OXYGEN INJECTION IN PRICETOWN-TYPE COAL FIELDS

by

James F. Avery 1/
Donald L. Logston 2/

ABSTRACT

The side wall burn model of underground coal gasification (UCG) in Eastern, swelling coals that was developed at West Virginia University (WVU), has been extended to include steam and oxygen injection during forward gasification. This model is based on the Pricetown I geometry in which the injection well is separated from the first production well by 60 feet and the second production well by 105 feet. The same char region that existed before forward gasification began at Pricetown I is assumed to exist initially in the present study.

With this new model, cavity growth as well as bulk gas temperatures and cavity wall temperatures can be determined for various amounts of steam and oxygen injection. Different total injected flow rates with mass fractions of steam varying between 0 and 40% have been investigated. Cavity shapes at burnthrough or after 12 days and bulk gas and cavity wall temperatures are presented for various amounts of oxygen and/or steam injection.

1/ West Virginia University, Morgantown, West Virginia
2/ USAF, Norton AFB, California

INTRODUCTION

The modeling effort presented in this study is a continuation of the efforts of many investigators at West Virginia University (WVU) since the seventies. Specifically, the forward gasification, cavity model presented at the 6th Underground Coal Conversion Symposium by Schwartz, Eddy and Nielsson (1) has been extended to include steam and oxygen injection. The Schwartz model includes a complex energy balance with convective heat transfer between the wall reaction zone and the bulk or gas zone as well as wall to wall radiation.

During underground coal gasification (UCG), it is essential to keep the reactor hot to prevent tars from condensing and thereby plugging or reducing flow in the cavity. Cooling of the reaction products is especially severe once the burden is exposed since the burden acts as a heat sink. Burning pure oxygen instead of air will increase bulk gas temperatures since no diluent (N_2) is present and the oxidation processes are exothermic.

Steam is injected to increase the water-gas reaction and thus the consumation of coal and production of carbon monoxide. Since the water-gas reaction is endothermic, care must be taken that too much steam is not injected which might quench the reactions or plug the flow passages via tar condensation. Consequently, it is desired to optimize the production of combustible gases without prematurely ending the gasification process.

The following discussion is divided into four sections: 1) a brief review of the model being used, 2) a description of the effect on cavity shape of injecting various flow rates of pure oxygen, 3) a description of the effect on cavity shape of various amounts of water reacting with the coal, and 4) a description of the effect on cavity wall temperatures and bulk gas temperatures of increasing amounts of water reacting with the coal.

BRIEF MODEL DESCRIPTION

The side wall burn, UCG cavity model used in this study is based on the model of Schwartz, Eddy and Nielsson (1). The model was modified to include steam and oxygen injection (2). This necessitated the inclusion of terms representing mass transfer of steam to the reaction zone (wall) and was done completely analogous to the existing scheme for mass transfer of oxygen to the wall. In addition, minor changes in the energy balance equations were made which seemed not to alter the results too significantly.

The growth of the cavity during forward gasification is modeled by finite spatial steps, as explained by Eddy, Raju and Schwartz (3). Each of the finite steps consists of three zones or control volumes. (1) These zones are the coal zone, the wall or reaction zone, and the gas zone. All three zones in the present study are identical to the definitions of Schwartz et al. except for the following: 1) ground water seepage was ignored in the present study, 2) steam and oxygen are injected into the gas zone instead of air, and 3) steam and oxygen are transferred from the gas zone to the reaction zone instead of just oxygen. When energy balances are written for the three zones, a system of two nonlinear equations in two unknowns, cavity wall temperature and bulk gas temperature, results. (1)

The chemical reactions, based on oxygen and steam reaching the wall, are assumed to be (4):

$$C + \tfrac{1}{2}O_2 \longrightarrow CO$$
$$H_2 + \tfrac{1}{2}O_2 \longrightarrow H_2O$$
$$S + O_2 \longrightarrow SO_2$$
$$H_2O + C \longrightarrow H_2 + CO$$

The first three equations will be referred to as the oxidation/reduction reactions and the last as the water-gas reaction. The carbon, sulfur and hydrogen that are reactants in these stoichiometric equations come from the coal and can be related to the coal consumption by the ultimate analysis. (4) The oxygen comes from that "bound" in the coal plus that injected and transferred to the wall.

As was done in previous studies, (5) it is assumed that, under normal conditions, the pyrogenetic water formed from the "bound" oxygen and hydrogen in the coal consumed during the oxidation/reduction process and the oxidation of the remaining "bound" hydrogen in this portion of the coal participate in the water-gas reaction. In addition, injected steam that is transferred to the wall also participates in the water-gas reaction. On the other hand, it is assumed that the pyrogenetic water formed from the "bound" oxygen and hydrogen in the coal consumed during the water-gas reaction and the remaining hydrogen do not react any further and leave the reaction zone.

The above assumptions, however, are not entirely true in the case of the Pricetown I burn. Analysis of that burn revealed that the mass ratio of coal consumed to oxygen supplied, $R_{c/o}$, was 0.92. (6) This ratio, $R_{c/o}$, can be related to the ratio of the mass of water reacting to coal consumed, γ_R, using the ultimate analysis of coal by the following equation (1):

$$\gamma_R = 1.5y_C \left[1 - \frac{1}{R_{c/o}(1.33y_C + 8y_H + y_S - y_O)} \right]$$

where y_C, y_H, y_S and y_O are the mass fraction of carbon, hydrogen, sulfur and oxygen in the coal. The result gives a value of $\gamma_R = 0.202$ for the Pricetown I burn. If the water at Pricetown I had reacted as outlined above, the value for γ_R would have been 0.316. This means that even without steam injection and ignoring ground water seepage, not all of the water that was expected to react in the water-gas reaction did so. This result will be discussed further in a later section.

After modifying the UCG program of Schwartz et al. (1), the data for the

Pricetown I burn was run and compared to known facts of that burn. Figure 1 shows the cavity profile at the time of burnthrough to the production well, P/I-2. The dashed cavity indicates the char zone that existed prior to forward gasification. (6) The solid cavity is the predicted burn cavity. Injection occurred at well P/I-1 and production was obtained at well P/I-2. The model predicted burnthrough to occur in approximately 12 days and indicates that the burn zone had reached thermocouple M3 and was approaching thermocouple M2. These three facts compare very closely with the observations of the Pricetown I burn. (7) This agreement was taken as confirmation that the basic forward gasification model was sufficiently accurate to proceed with the steam/oxygen injection studies.

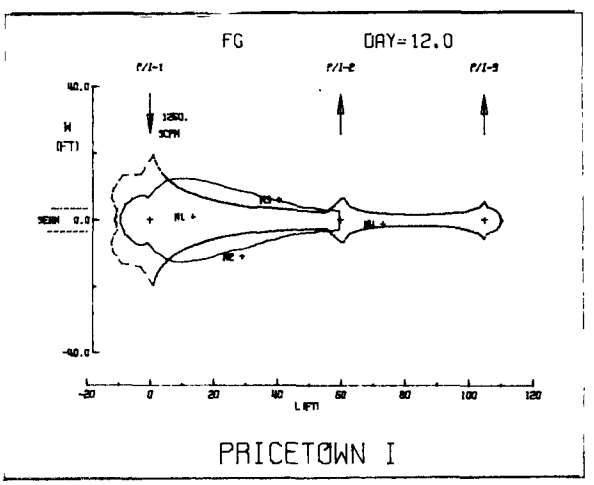

Figure 1. Forward Gasification Cavity of Pricetown I at Burnthrough with Air Injection: $\dot{m}_{tot}$ = 93.8 lbm/min, γ_R = 0.202, $R_{c/o}$ = 0.92, β = 0.0

EFFECT ON CAVITY SHAPE OF OXYGEN INJECTION

Injection of pure oxygen without any steam was investigated first and compared to the results of air injection. As explained previously, not all the water that was available to react, even without steam injection, reacted in the Pricetown I, forward gasification burn. For that reason, initial simulations with pure oxygen being injected were done with the same inherent ratio of water reacted to coal consumed, γ_R = 0.202. Figure 2 shows the cavity shape at burnthrough for pure oxygen in which the volumetric flow rate is equal to that of air during the Pricetown I burn. Comparison of the cavity shapes shows the cavities to be nearly identical in appearance. The major difference is that with pure oxygen, burnthrough occurred in 2.5 days compared to 12 days with air. The ratio of these burnthrough times is approximately equal to the ratio of mass flow of oxygen in the two cases. Thus, at the same total flow rate and amount of water reacting, the burnthrough time is a direct function of the mass flow rate of oxygen.

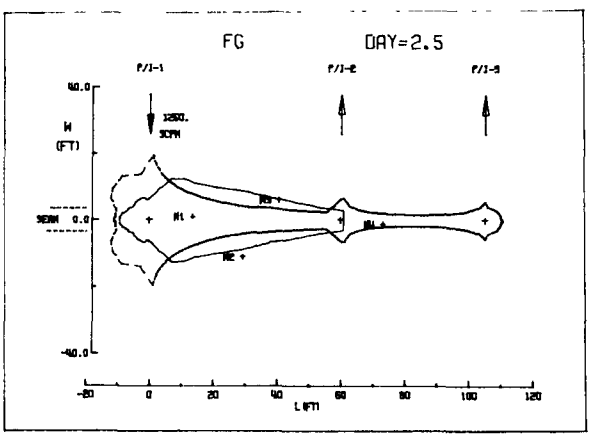

Figure 2. Forward Gasification Cavity at Burnthrough with Pure Oxygen Injection: $\dot{m}_{tot}$ = 98.8 lbm/min, γ_R = 0.202, $R_{c/o}$ = 0.92, β = 0.0

As the mass flow rate of injected oxygen is decreased, the burn cavity increases perpendicular to the cavity walls (longitudinally) and decreases along the axis between the injection and production wells (axially). This is because the residence time of the oxygen in a given finite difference element is much greater, due to the decreased flow rate. Consequently, more oxygen is transferred to the wall where it reacts. Figure 3 shows the forward gasification, burn cavity at burnthrough for an injected oxygen flow rate of 59.3 lbm/min (compared to 98.8 lbm/min for Figure 2) and γ_R = 0.202. It can be seen that burnthrough took seven days and the longitudinal spread of the cavity is much greater than at the higher flow rate.

Thus, it can be seen that burnthrough time and longitudinal spread of the burn cavity are inversely dependent upon flow rate.

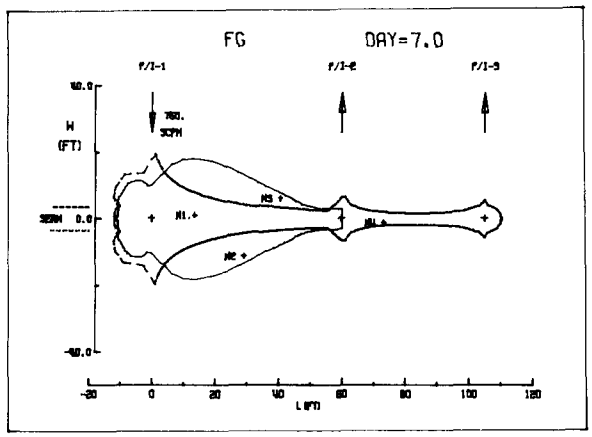

Figure 3. Foward Gasification Cavity at Burnthrough with Pure Oxygen Injection: $\dot{m}_{tot}$ = 59.3 lbm/min, γ_R = 0.202, $R_{c/o}$ = 0.92, β = 0.0

EFFECT ON CAVITY SHAPE OF VARIOUS AMOUNTS OF WATER REACTING

One of the assumptions inherent to the modeling of the forward gasification process with steam injection is that all the water bound in the coal plus that formed during reaction, with one exception, takes part in the water-gas reaction. As explained previously, the one exception is the pyrogenetic water formed from the coal consumed in the water-gas reaction. If one calculates the expected ratio of water reacted to coal consumed, γ_R, for the coal at Pricetown, using the foregoing assumption, a value of 0.316 for γ_R is obtained. Thus, for the present study, it was assumed that with zero steam injection, γ_R would be equal to 0.316. It was also assumed that any steam that was injected, reacted in the water-gas reaction. Thus, with steam injection, γ_R would have to be greater than 0.316.

Figure 4 shows the cavity shape at burnthrough for injection of oxygen only (no steam injection) at a mass flow of 59.3 lbm/min with γ_R equal to 0.316. Comparison with Figure 3 shows that the reaction of the additional water increased the breakthrough time to 9.3 days. In addition, the cavity spread considerably more in the direction perpendicular to the walls.

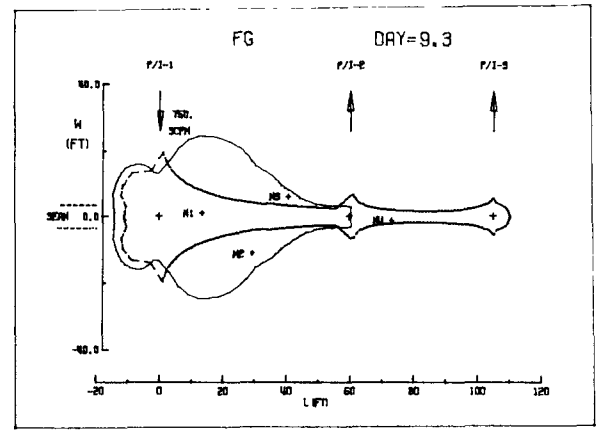

Figure 4. Forward Gasification Cavity at Burnthrough with Pure Oxygen Injection: $\dot{m}_{tot}$ = 59.3 lbm/min, γ_R = 0.316, $R_{c/o}$ = 0.92, β = 0.0

Figure 5 shows the cavity shape at burnthrough with the same total mass flow rate as Figure 4, but with the mass ratio of steam injected to oxygen injected, β, equal to 0.1. Again, the additional water reaction (γ_R = 0.378) increased the burnthrough time (to 12.0 days) and increased the spread of the cavity in a direction perpendicular to the walls.

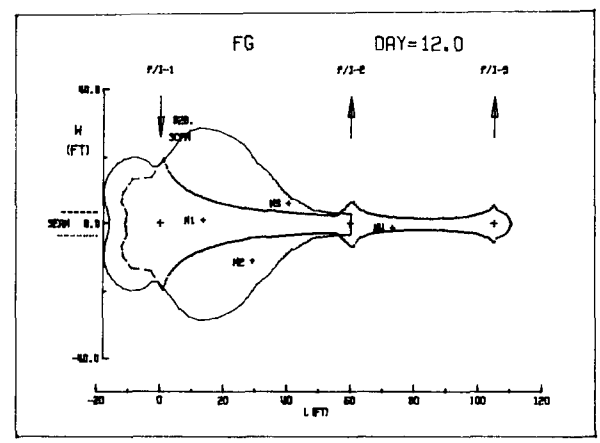

Figure 5. Forward Gasification Cavity at Burnthrough with Pure Oxygen Injection: $\dot{m}_{tot}$ = 59.3 lbm/min, γ_R = 0.378, $R_{c/o}$ = 1.150, β = 0.1

Figures 6 and 7 show the cavity shape after 12 days of forward gasification with a total injected mass flow rate of 59.3 lbm/min and $\beta = 0.2$ ($\gamma_R = 0.430$) and $\beta = 0.4$ ($\gamma_R = 0.514$) respectively. The same trends of decreased axial growth (or increased burnthrough time) and increased longitudinal spread of the cavity with β are observed.

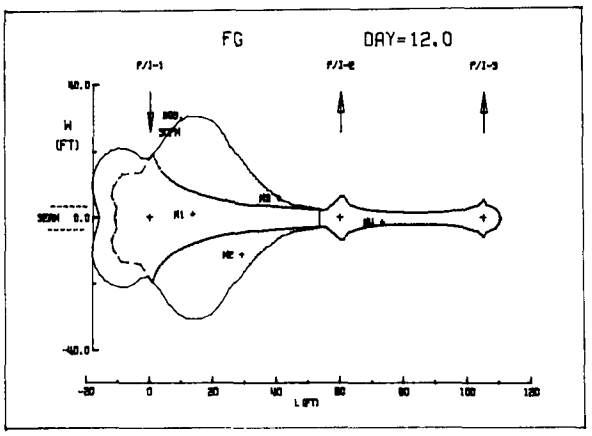

Figure 6. Forward Gasification Cavity After 12 Days with Steam/Oxygen Injection: $\dot{m}_{tot} = 59.3$ lbm/min, $\gamma_R = 0.430$, $R_{c/o} = 1.242$, $\beta = 0.2$

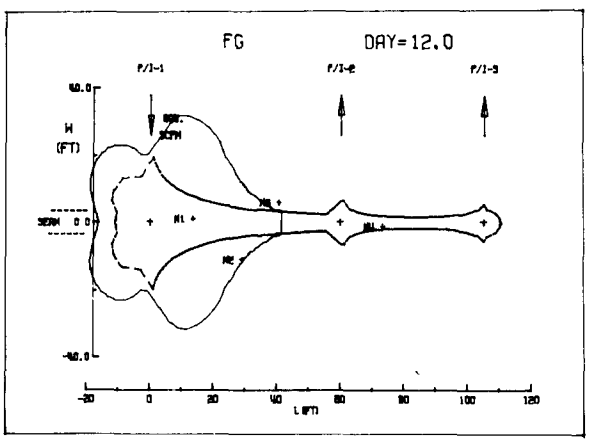

Figure 7. Forward Gasification Cavity After 12 Days with Steam/Oxygen Injection: $\dot{m}_{tot} = 59.3$ lbm/min, $\gamma_R = 0.514$, $R_{c/o} = 1.426$, $\beta = 0.4$

EFFECT ON TEMPERATURES OF INCREASED WATER REACTION

From the foregoing cavity profiles it appears that it would be desirable to increase the amount of water reacting to increase the amount of coal consumed before burnthrough occurs. Unfortunately, since the water-gas reaction is endothermic, increased water reacting means decreased cavity wall and bulk gas temperatures. This effect is so pronounced that without very carefully limiting the amount of water injection, quenching of the combustion and/or tar formation with its resultant plugging of the flow field is probable.

Figure 8 is a plot of the bulk gas temperature, in degrees Rankine, versus axial position, in feet, downstream of the injection well at the end of 1, 4, 6, 8, 10 and 12 days. This is for a mass flow rate of pure oxygen of 59.3 lbm/min in which the ratio of water reacting to coal consumed, γ_R, is equal to 0.202 (the value calculated for the Pricetown I burn). The temperatures shown are high enough that condensation of tars should not occur.

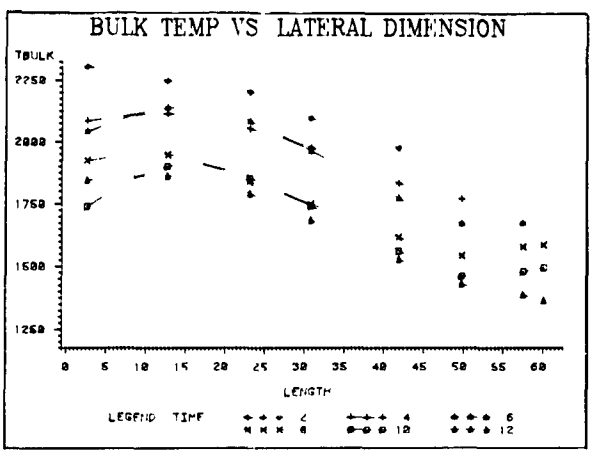

Figure 8. Bulk Gas Temperature (^{o}R) vs. Distance Downstream of Injection Well (ft), Time in Days: $\dot{m}_{tot} = 59.3$ lbm/min, $\gamma_R = 0.202$, $R_{c/o} = 0.92$, $\beta = 0.0$

Assuming all the available water reacts (except the pyrogenetic water from the water-gas reaction), increases γ_R to 0.316 as explained previously. This amount of water reaction is possible without steam injection. Figure 9 is the same

plot as Figure 8 except that γ_R has been increased to 0.316 from 0.202. Notice that the temperatures have decreased although they are, for the most part, high enough to prevent condensation of tars.

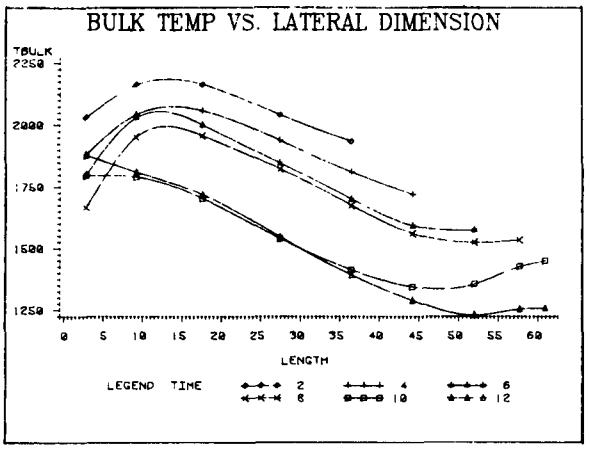

Figure 9. Bulk Gas Temperature (^{o}R) vs. Distance Downstream of Injection Well (ft), Time in Days: $\dot{m}_{tot}$ = 59.3 lbm/min, γ_R = 0.316, $R_{c/o}$ = 1.057, β = 0.0

Increasing the amount of water reacting beyond γ_R = 0.316 is accomplished by steam injection. Figure 10 shows the same information as Figures 8 and 9 except that 10% of the total injected flow ($\dot{m}_{tot}$ = 59.3 lbm/min) is composed of steam (β = 0.1). The value for γ_R in this case is 0.378. As expected, a further decrease in bulk gas temperatures is obtained because of the increased endothermic reaction. Still, however, tar condensation should not be too severe of a problem.

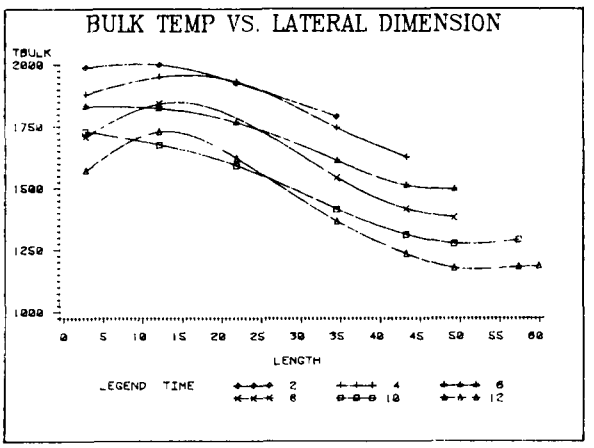

Figure 10. Bulk Gas Temperature (^{o}R) vs. Distance Downstream of Injection Well (ft), Time in Days: $\dot{m}_{tot}$ = 59.3 lbm/min, γ_R = 0.378, $R_{c/o}$ = 1.150, β = 0.1

Further increases in the amount of steam injected and thus the amount of water-gas reaction results in lower bulk gas temperatures and finally condensation of tars. Figure 11 shows what would happen if 40% of the total injected flow ($\dot{m}_{tot}$ = 59.3 lbm/min) was composed of steam (γ_R = 0.514). In this case condensation of tars would be a major problem and would most likely terminate the UCG process.

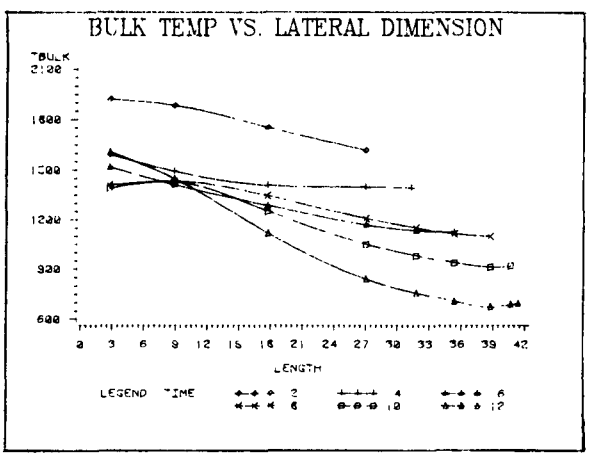

Figure 11. Bulk Gas Temperature (^{o}R) vs. Distance Downstream of Injection Well (ft), Time in Days: $\dot{m}_{tot}$ = 59.3/lbm/min, γ_R = 0.514, $R_{c/o}$ = 1.426, β = 0.4

The effect of increased water reaction on the cavity wall temperature shows the same trends as its effect on bulk gas temperatures. Figure 12 is for the same flow conditions as Figure 10. The difference is that cavity wall temperature is plotted on the ordinate instead of bulk gas temperature. The surprising result is that the wall temperatures shown are less than the corresponding bulk gas temperatures. The opposite would be expected since the reaction (and heat source) occurs at the walls. Although not shown in Figure 12, the initial wall temperatures near the injection well are greater than the corresponding gas temperatures. The temperature difference, however, decreases with time even near the injection well. The only explanation for the reversal in temperatures downstream of the injection well is that the radiation heat transfer model causes this to occur. The radiation model being used assumes that heat is radiated only from wall to wall ("optically thin" case) (8). In other words, the gas is nonparticipating. Cooling of the walls could occur by radiation to the exposed underburden/overburden, which would act as a radiation heat sink. For the flow conditions in Figure 12, the burden is exposed during the first day of forward gasification. Although the "optically thin" assumption has given better results in the past (9), it may be necessary to include an absorbing emitting bulk gas model ("optically thick" case). This is particularly true when steam is injected since water vapor is a strong absorber of radiation in certain wavelength bands.

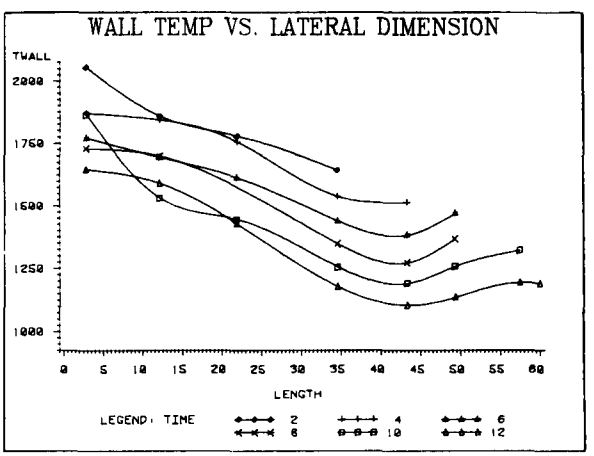

Figure 12. Cavity Wall Temperature (^{o}R) vs. Distance Downstream of Injection Well (ft), Time in Days: $\dot{m}_{tot}$ = 59.3 lbm/min, γ_R = 0.378, $R_{c/o}$ = 1.150, β = 0.1

SUMMARY

Results of the present study dealing with steam and/or oxygen injection showed the following trends:

1) Increasing O_2 concentration of air/O_2 injection at a constant flow rate decreases the time for burnthrough (increases rate of growth of cavity in axial direction) but does not greatly change the cavity shape.

2) Decreasing the injected flow rate of oxygen or air, (without steam) increases the burnthrough time and increases the cavity spread in a direction normal to the walls.

3) Increasing the amount of water reacting at a constant injected mass flow rate increases the burnthrough time (decreases axial growth of the cavity) and increases the spread of the cavity in a direction normal to the walls.

4) Increasing the amount of water reacting at a constant injected mass flow rate decreases both the resulting cavity wall and bulk gas temperatures.

5) The percent of steam in the injected flow must be limited to prevent condensation of tars and the resultant plugging of the flow passage.

REFERENCES

1. S. H. Schwartz, T. L. Eddy, and G. E. Nielsson, "A Simple UCG Cavity Model with Complex Energy Balance," Proceedings of the 6th Underground Coal Conversion Symposium, Afton, OK, pg. III-69, 1980.

2. D. L. Logston, "A Numerical Model of UCG with Steam/Oxygen Injection," M. S. Thesis, West Virginia University, 1983.

3. T. L. Eddy, C. L. Raju and S. H. Schwartz, "An Improved Side Wall Burn Model for Cavity Growth in Underground Coal Gasification," Petroleum Division of ASME, presented at the Energy-sources Technology Conference & Exhibition, New Orleans, LA, Feb. 3-7, 1980.

4. S. H. Schwartz, T. L. Eddy, K. H. Mehta, S. A. Lutz, and M. Binaie-Kondolojy, "Cavity Growth Mechanisms in UCG with Side Wall Burn Gasification," Society of Petroleum Engineers of AIME, Paper Number: SPE 7525, 1978 .

5. S. H. Schwartz and T. L. Eddy, "Two-Dimensional Thermodynamic Model (Second Stage) of In-Situ Underground Coal Gasification of Eastern Thin-Seam Coals," Final Report, DOE Contract EY-77-C-21-8087, Task Order No. 17/Mod. No. 2, 1980.

6. T. L. Eddy, W. H. Ford, Jr., G. J. Morris, S. Thynell, "3-D Thermodynamic Model of Underground Coal Gasification in Eastern Thin Seam Coals," Final Report, DOE-METC Contract DE-AT21-79MC11284, DOE/MC/11284-1160 (DE 84202525), December 1981.

7. T. L. Eddy, W. H. Ford, Jr., S. Thynell, "The UCG Link Zone and Cavity Development at Pricetown I," Proceedings of the 6th Underground Coal Conversion Symposium, Afton, OK, pg. VIII-79, 1980.

8. G. E. Nielsson, T. L. Eddy, and S. H. Schwartz, "Radiation Heat Transfer in Underground Coal Gasification," West Virginia University Report, (METC, DOE Contract No. EY-77-C-21-8087) December, 1979.

9. T. L. Eddy, T. R. Gibbs, C.-M. Jong, T. X. Phouc and W. H. Ford, Jr., Evaluation of the Final Data for the Pricetown I UCG Field Test Via Existing Thermodynamic Models," Final Report, DOE Contract DE-AC21-81MC16477, December, 1982.

This study was sponsored by the West Virginia Energy Research Center under Project Number: ST82-CC7-1.

3.10 KINETICS OF COAL OXIDATION FOR INVESTIGATION OF SPONTANEOUS IGNITION

by

Jae-Ou Choi[1]
H.W. Gudenau[2]
F.H. Franke[3]
R.D. Gunn[4]

ABSTRACT

A flow reactor and a method have been developed to determine the rate of heat evolution from coal due to low temperature oxidation. This information is essential for an improved understanding of spontaneous ignition during the reverse combustion linking phase of UCG. Laboratory tests are performed at pressures up to 80 atmospheres through a temperature range of 40-300°C with 45 cc charges of powdered coal in the flow reactor. The time rate of temperature rise in the coal sample and the CO-, CO_2-concentration in the product gas are monitored continuously. From these data, the kinetic parameters associated with spontaneous ignition can be determined.

INTRODUCTION

To enhance the permeability of the coal layer, it is necessary to link the injection and production wells before gasifying. This can be executed by reverse combustion, directional drilling, electro-linking and hydraulic fracturing. Reverse combustion has been used widely and successfully in the U.S. field tests (1).

However, coal permeability at the depth of 1000 m or more is extremely low. Therefore, higher operating pressures are required for reverse combustion, and this leads to spontaneous ignition on the air injection side where pressure is highest. The reverse combustion link cannot be completed once spontaneous ignition has occurred because condensation of tars formed in the combustion zone block the air flow in cooler regions of the coal seam. Moreover, ignition near the injection well depletes the oxygen so that reverse combustion may not proceed.

During the field test in Thulin, Belgium, spontaneous ignition caused many operating problems. Spontaneous ignition occurred in 3-4 days in the 870 m deep hard coal seam with initial temperatures of 45°C and natural permeability of the coal to N_2-gas of 0.28 millidarcy. The air injection pressure was 230 bars and the flow rate 500 m^3_N/h (2).

With an understanding of physical and chemical processes associated with spontaneous ignition, it may be possible to prevent or control this troublesome problem. Methods to calculate the spontaneous ignition time are available (3,4). It is necessary to know first the characteristics of heat evolution by oxidation of coal with different gas mixtures because the oxidation reactions may be inhibited by gases such as CO_2 at high pressures. Injection of water into the coal seam has not proved an effective method for suppressing spontaneous ignition at the Thulin field test site in Belgium.

1/ Technical University of Aachen, West Germany
2/ Technical University of Aachen, West Germany
3/ Deutsche BP AG, West Germany
4/ University of Wyoming, Laramie, Wyoming

THEORETICAL

The method of determining the rate of heat evolution of coal with oxygen containing gas-mixtures is based on a heat balance in the coal sample as shown by Sebastian and Mayers (5). The heat balance in a differential volume of coal is formulated in one dimension as follows (6).

$$\frac{\delta}{\delta t}(\rho_s H_s + \phi \rho_g H_g) = \frac{\delta}{\delta x}(\lambda_s \cdot \frac{\delta T}{\delta x}) - \frac{\delta}{\delta x}(\dot{m}_g \cdot H_g) + \dot{q} \qquad (1)$$

where

H_g = enthalpy of gas, kJ/kg
H_s = enthalpy of solid, kJ/kg
$\dot{m}_g$ = mass flux of gas, kg/m²·h
$\dot{q}$ = heat generation function, kJ/m³·h
t = time, h
T = coal temperature, K
x = distance coordinate, m
λ_s = thermal conductivity of solid, kJ/h·m·K
ρ_g = density of the gas, kg/m³
ρ_s = density of solid, kg/m³
ϕ = porosity, dimensionless

For our experiments in a small cylindrical flow reactor, equation (1) can be integrated over the whole volume of the coal sample. Heat conduction in the direction of gas flow is assumed negligible.

$$\dot{q}_i = \rho_m C_m \frac{\delta T}{\delta t_i} + \frac{\dot{m}_g \cdot C_g}{L} \Delta T_{g,i} \qquad (2)$$

where

$\rho_m C_m = \rho_s \cdot C_s + \phi \rho_g C_g$

$\Delta T_g = T_{g,out} - T_{g,in}$

"i" = crossing point (see Fig. 1)

If the cylindrical reactor is heated from the outside, equation (2) is only valid at the crossing point when the coal temperature is the same as the sample wall temperature. At these conditions, no radial heat conduction is present.

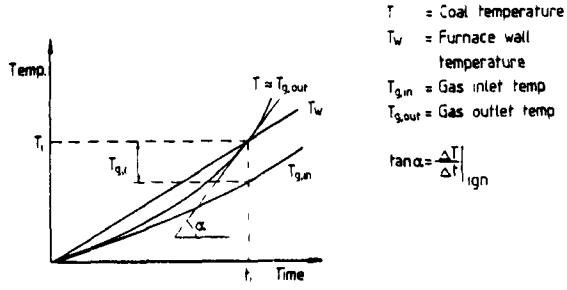

Fig. 1: Typical Temperature-Time Curves

T = coal temperature
T_W = furnace wall temperature
$\Delta T_{g,i}$ = difference of gas temperature at ignition point

A plot of the coal temperature, furnace wall temperature and gas in- and outlet temperatures are shown schematically in Fig. 1. "$\delta T/\delta t$" in equation (2) is the slope or the tangent to the curve representing coal temperature at the crossing point. The rate of heat evolution from the oxidation of the coal can be determined from a plot such as that shown in Fig. 1 along with gas temperature measurements and the physical properties of the coal. The heat generation function can be stated in the form of the product of a temperature function and the oxygen concentration.

$$\dot{q}_i = K(T) \cdot CO_2 \qquad (3)$$

It is assumed in equation (3) that the rate of heat evolution increases linearly with the increase of oxygen concentration in the gas. The temperature function K(T) can be correlated by the Arrhenius equation for the dependence of heat evolution on temperature:

$$K(T) = K_o \cdot \mathrm{Exp}\,(-\frac{E_a}{RT}) \qquad (4)$$

where

T = absolute temperature, K
R = gas constant, kJ/kmol K
K_o = frequence factor, kJ/kmol s
E_a^o = activation energy, kJ/kmol

The kinetic parameters K_o and E_a can be determined, if the logarithms of the temperature functions are plotted against the inverse absolute temperature.

APPARATUS AND PROCEDURE

The apparatus shown in Fig. 2 consists of a corundum heating tube in an autoclave.

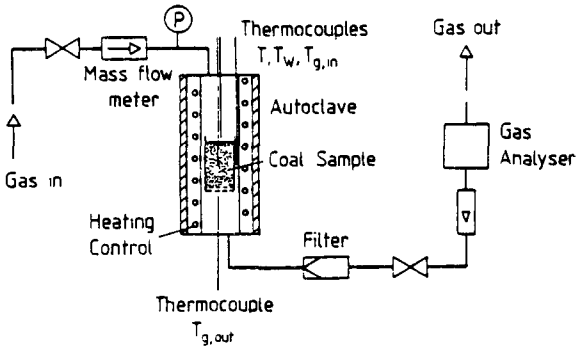

Fig. 2: Schematic of the Apparatus

The quartz glass reaction tube has a diameter of 2.7 cm, and includes a 45 cc coal sample resting on a ceramic filter. The tip of the first thermocouple extends into the center of the coal sample. The second thermocouple is placed between the heating tube and the reaction tube at the same height as the first one. Two other thermocouples taking gas in- and outlet temperatures are immediately above and under the coal sample.

Gas enters the higher end of the reaction tube and flows downward through the coal sample. The gas flow is kept constant with the aid of two needle valves and a mass flowmeter. The pressure in the autoclave is also kept constant. The product gas leaving the autoclave is filtered and dried. The CO- and CO_2-concentrations in the product gas are monitored continuously with the aid of a "Dräger-Polymeter" used for the determination of the mean value of gas concentration.

RESULTS

The first set of experimental data has been completed; however, reduction of these data was not complete by publication time. The data can be obtained from the authors.

LITERATURE

(1) D.R. Stephens, C.B. Thorsness, R.W. Hill, D.S. Thompson, Technical Underground Coal Gasification Summation: 1982 Status, UCRL - 87689, Preprint for the 8th UCC Symposium, Keystone, Colorado, August, 1982

(2) I.D.G.S. Technischer Jahresbericht - 1982 Belgisch-Deutsches-Experiment zur in Situ Vergasung

(3) J. Breuning, personal information

(4) C. Gadelle, M. Pottier, J.F. Raffoux Major problems, First results and projects of underground gasification of deep coal in France. A communication by the technical committee of G.E.G.S.

(5) J.J.S. Sebastian, M.A. Mayers Coke reactivity. Industrial and Engineering Chemistry Vol. 29, No. 10 (1937)

(6) M.D. Kotowski, R.D. Gunn Theoretical aspects of reverse combustion in the underground gasification of coal, Technical information center, ERDA, USA, LERC/RI-76/4 (1976)

3.11 COMPREHENSIVE NUMERICAL MODEL OF FORWARD COMBUSTION ALONG A CHANNEL

by

P. A. McMurtry 1/
R. C. Corlett 1/
A. F. Emery 1/
H. R. Mortazavi 1/

ABSTRACT

Conservation equations of mass, energy and major species are solved by finite difference techniques to describe forward combustion in a circular channel. This model is designed as a numerical experiment to facilitate derivation and quantitative adjustment of relatively simple, phenomenological models intended as components of system models of rubble burnout and cavity evolution.

Input variables include inlet mass flow, oxygen and water/steam mass fractions, and coal moisture, volatile matter, ash and transport properties. The primary outputs are channel enlargement, temperature distributions in solid and gas domains, and major species concentrations along the channel.

The channel flow is treated as quasi-one-dimensional. Mass and energy transfer between the gas and the solid surface is described by appropriate engineering theory and correlations. In the coal, temperature-dependent drying and devolatilization are calculated, with corresponding heat sink effects accounted for. The volatile matter is treated as a pseudo- species of unique heating value. At the coal-gas interface, carbon reactions with steam and oxygen are included. Provision is made for mass transfer resistance due to ash buildup.

Example results are presented for a baseline case of a bored channel in virgin coal, emphasing the small-time (up to 5 hr), incipient cavity phase. These results suggest that transient heat conduction exerts only minor influence on channel growth and channel flow temperature. However, an ash layer of even modest thickness dramatically distorts both of these performance characteristics.

INTRODUCTION

This paper describes a mathematical model of forward combustion in an open channel through coal. The flow is considered as quasi-one-dimensional. The energetics of this flow are coupled with transient heat conduction in the surrounding solid, which is calculated by finite differences.

The model is intended for underground coal gasification (UCG) research applications. One application is calculation of the gasification behavior in a bored channel with or without pretreatment by reverse combustion. Of course, this model fails to apply if the channel widens to such an extent that the flow is no longer quasi-one-dimensional.

Another application is rubble burnout under circumstances where oxidizer gas can be forced through the rubble bed. Then, forward combustion must occur in an ensemble of irregular channels which eventually interact with one another through heat conduction and material depletion. The present model treats only a single uniform channel in a medium of unlimited extent. It is, however, a starting point for more general models which will be statistically interpreted in rubble burnout problems.

1/ Dept. of Mechanical Engineering
University of Washington FU-10
Seattle, WA 98195

A number of investigators have reported models of forward combustion; see Kunselman, Fausett and Mones [1] for a review. Only a minority of these models explicitly consider an open flow domain. Of those that consider an open flow domain, most, e.g., Eddy and Schwartz [2] and Harloff [3], are directed at evolution of open cavities, emphasizing internal circulation induced by forced or free convection.

The general existence of large open cavities in UCG has not been demonstrated by field data. The theoretical arguments, pro or con, are beyond the scope of this paper. Suffice it to remark that, for small time, at least, a bored channel would be expected to predominately exhibit quasi-one-dimensional, as opposed to internally circulating, flow. Moreover, it can be speculated that rubble accumulation prevents large-scale internal recirculation, so that quasi-one-dimensional flow should prevail indefinitely during the gasification process, either in a relatively constricted open channel above the rubble or along multiple passageways within the rubble.

Only one research group has previously published analyses of quasi-one-dimensional flow in UCG forward combustion. Dinsmoor, Galland and Edgar [4] at the University of Texas have reported a quasi-one-dimensional flow model which predicts channel growth, temperatures at the solid surface and in the gas, and gas composition. In that work, the effect of heat conduction in the solid is included as a consequence of an arbitrary, albeit physically reasonable, assumption of a fixed conduction length. Release of volatiles due to conductive heating is ignored.

In the present work, the evolving temperature distribution in the coal is calculated by extension of methods developed by Kashiwa and Harlow [5,6] for studying coal drying. Of note is their technique for handling the phase discontinuity at the drying front.

In reality, mass transport between gases flowing along the channel and charred coal must be impeded to some extent by the existence of a surface ash layer where regression occurs. The importance of this mass transfer resistance obviously depends on the extent to which ash is removed by flow or other mechanisms. To our knowledge, no previous efforts have been made to include this ash resistance in coal channel forward combustion analyses, presumably because its magnitude has not been quantified in terms of relevant variables. In the present model, a phenomenological description of ash resistance is included.

Philosophically, the model reported here is considered a research tool rather than a performance predictive tool for direct aplication to UCG design or process control. The transient heat conduction feature, in particular, is quite costly to compute. It is therefore important to delineate conditions under which transient heat conduction must be accounted for. In a similar spirit, an understanding of the effect of ash resistance is needed to guide new research aimed at suitable characterization of that resistance.

THE MODEL

In this paper, the main features of the model are outlined. A detailed description, including a listing and all permanent data insertions, is presented elsewhere [7].

The model incorporates a chemical scheme essentially the same as that of [4]. However, direct oxidation of carbon monoxide and hydrogen is presently omitted. An additional feature is the treatment of volatiles released from the solid coal into the channel flow. These are allowed to oxidize completely, with stoichiometry and kinetics per Gunn and Whitman [8].

In the solid domain, the transient, axi-symmetric heat conduction equation, with variable thermal conductivity k_c and specific heat density $\rho_c c_c$, and with appropriate source terms for water vaporization and release of volatiles, is solved by finite differences in t-x-r space (t: time, r: radius, x: downstream distance). In the channel flow domain, the convective energy equation is solved in t-x space; i.e., the temperature and various concentrations are local bulk values. These two energy equations are coupled by an energy balance including

convective transport driven by the difference between local bulk flow and wall temperatures, heat conduction into the solid, source terms corresponding to surface reactions (carbon/oxygen and carbon/steam yielding carbon monoxide and hydrogen), and steam flux from the solid. Fluxes of steam and volatiles from the solid into the channel flow are determined by appropriate radial (fixed-x and -t) integrals; i.e., transport through the coal to the channel is considered instantaneous, and axial transport of vapors released by coal heating is excluded. In the channel flow domain, x-t mass balances of carbon monoxide and dioxide, water vapor and hydrogen are maintained.

Thermophysical properties are obtained from several sources. Some of these may vary with coal type, and thermal history prior to calculated forward combustion. The following are embodied in the version of the model used for the example calculations presented later. For coal, the dependence of k_c on moisture content and temperature below 500° C is taken from Westmoreland, Forrester and Gibson [9]. Equations for k_c at higher temperature and for c_c at all temperatures are taken from Tsang [10]. The coal is assumed to have a temperature dependent retained volatiles fraction, numerically that of [8]. This thermophysical description should be reasonably representative of a subbituminous coal, uncharred prior to forward combustion.

Surface reaction rates are calculated in the manner described in [4], using reaction rate constants estimated per Frank-Kaminetskii [11] and Wen and Lee [12] and values of mass transfer coefficient L from the engineering correlations. In the example, the flow is turbulent and L is developed from Treybal [13].

Ash layer resistance is included in the model by formally substituting for L a modified coefficient L_{eff} given by

$$1/L_{eff} = 1/L + \delta/D_{eff}$$

where δ is the ash layer thickness and D_{eff} is an effective diffusion coefficient. The quantity D_{eff} is obtained from the molecular gas diffusion coefficient, and the tortuosity and porosity of the ash layer using conventional ideas for slow flow through porous media; see Szekely, Evans and Sohn [14].

The governing equations are solved in a sequence of operations outlined as follows. All reaction rates and thermophysical properties are evaluated using concentrations and temperatures from the end of the preceding time step. With these quantities fixed, new values of concentrations and temperatures are solved for each cell along the flow channel. New reaction rates are calculated and then a new surface temperature is solved from the surface energy balance. The the heat conduction is solved for new temperatures, considering separately the regions of (1) char, (2) devolatilizing coal, (3) drying coal, and (4) wet coal. In region (2), the rate of volatiles released is obtained from the retained volatiles fraction and the rate of temperature rise. In region (3), the rate of water vaporization is solved to maintain constant temperature.

In this model, δ is assumed much smaller than the channel radius r_o. Hence it is unambiguous to compute the growth of r_o from the rate of the carbon-consuming surface reactions. The ash layer thickness δ is allowed to grow proportionally to the amount of carbon regression until a prescribed limiting value is reached. Thereafter δ is held constant at the limiting value.

In the present form of the program, the computational grid is fixed in the x (streamwise) direction but is periodically adjusted in the r (radial) direction to reflect channel growth. Although, to date, only small-time ($t < 10$ hr) runs have been executed, experience to date suggests that a single fixed streamwise grid is adequate for much longer times. Moreover, for channel flow forward combustion over very large times, the characteristic streamwise length scale would be expected to increase so that a suitably longer x-domain with a proportionally increased x-grid size should suffice.

EXAMPLE RESULTS AND DISCUSSION

As an example, the following conditions are assumed. The inlet gas stream has

oxygen and steam mole fractions 0.3 and 0.2, respectively, with balance nitrogen. The flow rate is initially 13.0 gm/sec and is step-increased 4 gm/sec at the end of each hour. The coal has an initial water volume fraction of 0.1 and volatiles mass fraction 0.325 . Ash mass fraction is 0.1 . The initial cavity radius is 2.5 cm .

Calculations are carried out with ash layer neglected and with an ash layer of limiting thickness δ = 0.25 cm, porosity 0.9 and tortuosity 2.0 accounted for in the mass transfer resistance. It is recognized that there exists no direct evidence for δ of such magnitude in field operations. However, is is virtually self evident that gravity removal of ash could not reduce δ much less than this magnitude. The actual value of δ must be controlled by the resistance of the ash to flow shear at the channel wall. It is remarked that ash layers of this and, sometimes, substantially greater values of δ have been observed in the laboratory to resist flow shear by Corlett and Shearer [15], in laminar reverse combustion experiments with virgin subbituminous coal, and by Corlett and Harloff [16], in forward combustion experiments with reconstituted subbituminous coal at high laminar Reynolds numbers.

It is of interest to consider first the importance of coupling of transient heat conduction in the solid with the channel flow energetics, with ash layer neglected. Figure 1 shows the evolution of channel radius growth. The figure shows that the length of the effected portion of the channel soon stabilizes 3 - 4 m and that channel radius at a persistent but slowly declining rate up to 5 hr . Figure 2 shows the radial temperature gradient in the solid at the channel wall. This quantity is proportional to the local wall conduction flux. It enters into the physics of forward combustion in two ways; First, it contributes to the energy balance which couples the flow and solid energy equations. Second, it drives heating of the coal at depth which releases steam and volatiles to the channel. The magnitude of this gradient rapidly declines as t increases from 0.5 to 5 hr. It is noted that the gradient length scale assumed in [4]

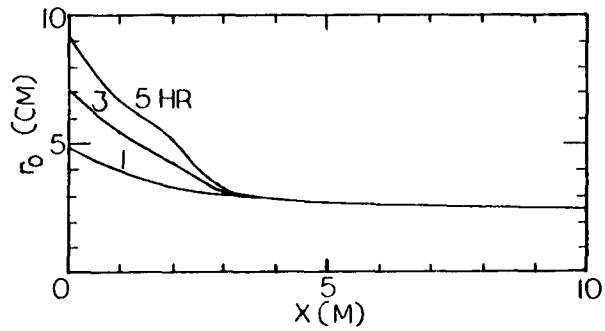

Figure 1 - Growth of channel radius r_o, ash layer neglected.

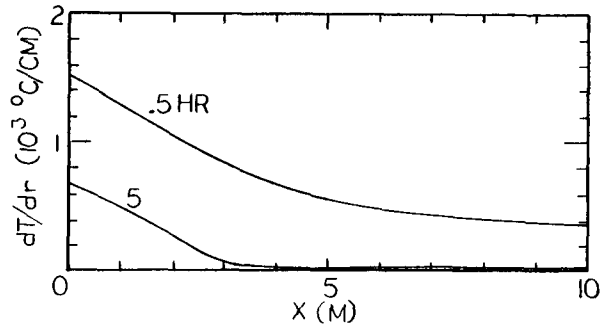

Figure 2 - Conductive radial temperature gradient at wall, at .5 and 5 hr, ash layer neglected.

implies gradient values < 100 on the scale of Figure 2. Figure 3 shows comparative calculations of channel radius r_c vs x at t = 5 hr: with transient conduction per Figure 1; with the conduction term removed from the energy balance but release of steam and volatiles computed on the basis of conduction implied by the calculated wall temperature; and with all effects of heat conduction ignored. The channel growth is little effected by mechanisms controled by heat conduction. The most noteworthy effect is a slight lengthening of the widened portion of the channel when release of volatiles and steam is excluded. This is physically reasonable in view of the facts that absence of volatiles provides less competition for oxygen, and absence of steam results in higher temperature.

We hasten to add that not enough work has been done to allow general conclusions respecting the importance of transient conduction. Such generalization will require consideration of a comprehensive spectrum of coal

types and a full matrix of specifying physical parameters.

Figures 4, 5 and 6 show the effects of ash resistance on channel radius growth, wall temperature, and bulk oxygen fraction, respectively, at t = 5 hr . These figures all point to the conclusion that the ash layer rapidly builds up to the assumed 0.25 cm limiting thickness δ , and that, thereafter, wall reaction rates are substantially depressed; in consequence, oxygen is available for reaction much further downstream than would otherwise be the case.

The implications of the preceding paragraph are clear. It is straightforward enough to compute the effect of ash resistance if the physical characteristics of the retained ash layer are known. The characteristic most important and, unfortunately, subject to worst uncertainty is the mean limiting thickness δ . Until experimental measurement of δ as a function of a reasonable range of wall roughness, flow rate and diameter and for a set of representative coal types is accomplished, calculation of forward combustion performance will be of severely limited value.

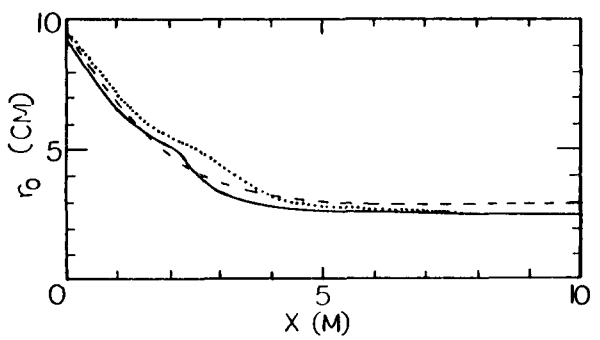

Figure 3 - Channel radius at 5 hr, ash layer neglected. Solid curve is result of full calculation. Dashed line is result with heat conduction ommitted from channel flow/solid coal energy balance. Dotted line is result with all solid coal heat conduction omitted.

ACKNOWLEDGEMENT

The work reported in this paper was supported in part by U.S. Department of Energy/University of Washington contract DE-AS20-82LC10884.

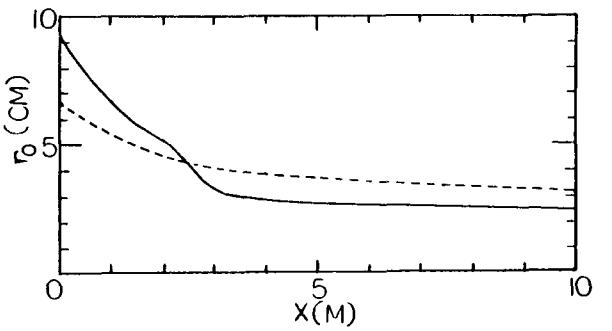

Figure 4 - Effect of ash layer on growth of channel radius to 5 hr. Solid curve per Figure 1; dashed curve includes resistance to ash layer.

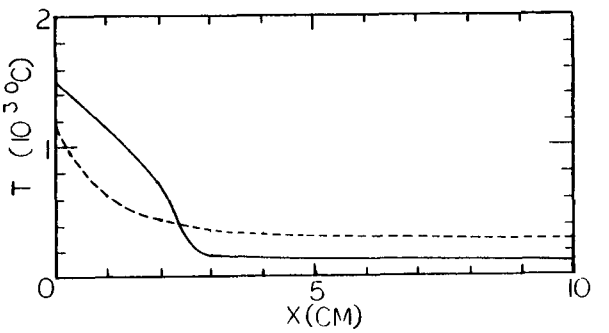

Figure 5 - Effect of ash layer on channel surface temperature, curves per Figure 4.

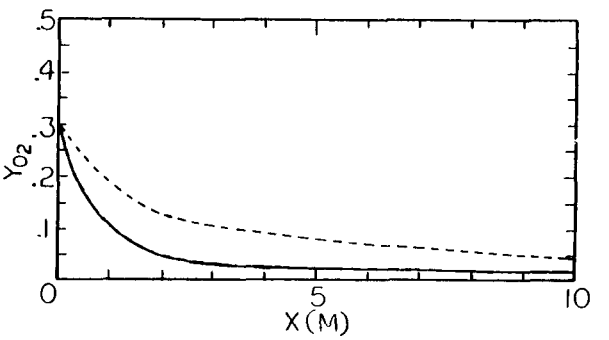

Figure 6 - Effect of ash layer on bulk oxygen concentration in channel, curves per Figure 4.

REFERENCES

1. L.V. Kunselman, D.W. Faucett, and C.G. Mones, "A Comparison of Forward Combustion Models", Proc. Eigth Underground Coal Conversion Symposium, SAND82-2355 (1982).

2. T. Eddy and S.H. Schwartz, "A Sidewall Burn Model Of Cavity Growth In Underground Coal Gasification", J. Energy Res. Tech. Vol. 105 (1983).

3. G.J. Harloff, "A Two-Dimensional Model of Underground Coal Gasification Cavity Growth With Application to the Canadian Forestburg Test of 1976", Proc. Seventh Underground Coal Conversion Symposium, CONF. NO. 810923 (1981).

4. B. Dinsmoor, J.M. Galland, and T.F. Edgar, "The Modeling Of Cavity Formation During Underground Coal Gasification", J. Pet. Tech. (May, 1978).

5. B.A. Kashiwa and F.H. Harlow, "Hot Gas Drying Calculations For A Coal Seam Channel", Proc. Sixth Underground Coal Conversion Symposium, CONF NO. 800716 (1980).

6. B.A. Kashiwa and F.H. Harlow, "An Investigation of Simultaneous Heat And Mass Transfer In Subbituminous Coal", Proc. Fifteenth Intersociety Energy Conversion Conference, Seattle, WA (1980).

7. P.A. McMurtry, "CFFC-1: A Computer Code For Forward Combustion In A Coal Or Char Channel", Report Under US DOE/University of Washington Contract DE-AS20-82LC10884 (in preparation).

8. R.D. Gunn and D.L. Whitman, "An In-Situ Coal Gasification Model (Forward Mode) For Feasibility Studies and Design", LERC/RI-76/2, US ERDA Laramie Energy Research Center, Laramie, Wyoming (February 1976).

9. P.R. Westmoreland, R.C. Forrester, and J.B. Gibson "Pyrolysis and Physical Properties Of Coal Blocks", ORNL/TM-7313 Oak Ridge National Laboratory (June, 1981).

10. T.H. Tsang, "Modeling Of Heat And Mass Transfer During Coal Block Gasification", Ph.D Dissertation, University of Texas at Austin (May, 1980).

11. D.A. Frank-Kamenetskii, Diffusion And Heat Exchange In Chemical Kinetics, Princeton University Press (1955).

12. C.Y. Wen and E.S. Lee, Coal Conversion Technology, Addison-Wesly Publishing Co. (1977).

13. R.E. Treybal, Mass Transfer Operations, McGraw-Hill Book Co., Inc. (1955).

14. J.Szekely, J.W. Evans, and H.Y. Sohn, Gas-Solid Reactions, Academic Press, N.Y. (1976).

15. R.C. Corlett and D.M. Shearer, "Reverse Combustion Along Fissures in Shrinking Coals", Proc. Fourth Underground Coal Conversion Symposium, SAND 78-0941 (1978).

16. G.J. Harloff and R.C. Corlett, "Analysis of Results on Laboratory Simulation of Underground Coal Gasification", Proc. ASME-JSME Thermal Engineering Joint Conf., Vol. 2 Honolulu, Hawaii (1983).

3.12 COMBUSTION TUBE STUDIES ON THE INFLUENCE OF WATER INFLUX ON STEAM OXYGEN GASIFICATION OF LIGNITE

by

W. Min[1/]
T. F. Edgar[2/]

ABSTRACT

Experimental studies to characterize the influence of water influx on steam-oxygen gasification of lignite have been performed using a fixed-bed reactor. Water was directly injected from the upstream side of combustion front and the time span of water injection ranged between 15 minutes and 270 minutes. The variations of product gas composition, heating value, and temperature are discussed. The response of the gasification system to water influx is categorized by three distinct types of transient behavior, depending on the intensity of the disturbance by water influx.

INTRODUCTION

One of the most important variables affecting the success of underground coal gasification process is the rate of water influx into the active gasification zone. Most of the previous research related to water influx in UCG, however, has been limited to analyzing the mechanism of underground water influx [1,2]. Using equilibrium models other investigations [3,4] have focused on the effects of water influx on gasification efficiency, namely the static response of product gas composition and thermal efficiency to the water intruding into the active gasification zone. Up to this time no systematic studies have been made on the transient behavior of the gasification process after water intrudes into the active reaction zone and how such a local event affects the overall gasification process.

Although the above-mentioned equilibrium models have proved to be quite satisfactory in predicting the product gas composition of underground coal gasification process as well as fixed-bed gasifiers operated at steady state conditions, those models are inadequate for predicting the transient behavior of the gasification system disturbed by water influx; at best, their applicability is limited to predicting the static responses of the system output to water influx.

This research is aimed at experimentally investigating the influence of water influx on the steam-oxygen gasification system using a laboratory fixed-bed reactor. While such a fixed-bed gasifier does not exactly represent the actual geometry of UCG, which is essentially three-dimensional, it does represent a starting point to identify the controlling mechanisms in the dynamics associated with underground water influx. In this work, we report data taken on the dynamic response of a steam-oxygen gasification system to water influx using a one-dimensional fixed-bed gasifier. In future work we plan to compare the data obtained here with a one-dimensional transient model to be developed.

EXPERIMENTAL APPARATUS

The layout of the water-injected steam-oxygen gasification system is depicted in Figure 1. The experimental system consists of the following components:

1/ Dept. of Chemical Engineering
The University of Texas
Austin, TX 78712

2/ Dept. of Chemical Engineering
The University of Texas
Austin, TX 78712

1. Gasification reactor with multilayer insulations
2. Pressure vessel
3. Steam generator
4. Water injection system
5. Condensate removal system
6. Gas drying system
7. On-line gas analyzers (CO, CO_2 and O_2)
8. Gas chromatograph
9. Product gas metering device
10. Temperature and pressure measuring system

Reactor

Figure 2 shows the components of the gasification reactor. The reactor used in this experiment is a 2 inch Schedule 40 Croloy 600 pipe, 36 in. in length and 2 1/16 in. in inside diameter. The ends of the pipe are welded to 4 1/2 in. flanges which connect the reactor to the upper and bottom unions by replaceable copper gaskets. The reactor is placed coaxially in a 6 in. Schedule 40 304 stainless steel pipe casing. The outside of the reactor is lined with 0.3 in. thick high-alumina castable refractory and the refractory lining is wrapped with two layers of Fiberfrax ceramic paper 970 of 1/8 in. thickness. The inside of the stainless steel casing is also lined with three layers of Fiberfrax ceramic paper leaving about 1/4 in. of air gap between the two linings.

The design of the reactor and its insulation system, where no guard heaters are used to compensate for the radial heat loss, is based on that the purpose of this research is to investigate the dynamic behavior of the steam-oxygen gasification system disturbed by water influx rather than performing simple steam-oxygen gasification experiments. There is no doubt that supplying heat to the reactor to compensate for the radial temperature gradient, thereby minimizing the resulting heat loss, is more desirable for achieving near-adiabatic conditions. However, such a guard heater system, which has been used by other investigators [5-7], could produce distorted results in water-injected gasification runs, since the significant heat loss to the intruding water is partially offset by the heat supplied by the guard heater system. In addition, the dynamics of the heater response would be coupled to the response of various reactor variables.

Steam Generator

The steam generator is a 15 in. long stainless steel pipe with 1 1/8 in. I.D. and 3/16 in thickness. It is directly mounted on the reactor and connected to the upper union by a bolted flange. A 1/8 in. stainless tube, 11 ft. long coiled on a 1 in. mean diameter and having 39 turns, is placed in the steam generator. A positive displacement diaphragm pump using a 1/8 in. piston pumps water through this coil. The steam generator is heated by 2 half sections of electric heaters capable of delivering up to 720 watts per half section at 120 V. The heater carries a current of 8 amps and delivers enough heat to support a superheated mixture of steam and oxygen for gasification. The heaters are insulated using ceramic paper of 1/8 in. thickness.

Temperature Measurement

The temperature of the center portion of the reactor is measured using 8 fixed center-line K-type thermocouples which are housed in two 1/4 in. inconel 600 tubes. Four 1/16 in. K-type thermocouples (0.01 in. diameter thermocouple wires with MgO insulation) are placed in each of thermowells, and another 1/8 in. thermocouple which is introduced through the top of the steam generator measures the ignition temperature. The center-line thermowells are attached to the upper and bottom unions. The spacing between the center-line thermocouples is 3.5 inches.

Experimental Procedure

The lignite sample used in the experiments was taken from Butler Brick Company's Elgin strip mine in Elgin, Texas. The coal sample, crushed on-site, was partially dried while being transported in a 55-gallon drum. The crushed coal was sorted to a narrow range of particle size - caught on top of U.S. no. 20 sieve (sieve opening 0.841mm) with U.S. no. 16 sieve (sieve opening 1.19mm) above - and stored in airtight polyethylene vessels.

The experimental procedure involves the following basic steps:

1. System check-up
2. Coal loading
3. Steady-state operation with steam and oxygen after ignition
4. Initiation of water injection
5. Termination of water injection
6. End of run at oxygen-breakthrough point
7. Ash and condensate collection
8. System clean-up

The system check-up procedure involves the installation of the upper and bottom unions to the reactor and the pressure vessel by bolted flanges and subsequent leak test of the entire system. During the installation, the center-line thermowells which are attached to the two unions are aligned so that the tip of each thermowell is in contact with each other.

Once the flanges are secure and the system shows no leaks when pressurized at 20 psig, a mixture of 5/8 in. ceramic raschig rings and 1/4 in. ceramic balls is loaded in the reactor to about 10cm above the bottom of the reactor. There is a perforated stainless steel disk on the top of the bottom union to support the beds of the ceramics and coal. Approximately 1150 g (2.5 lb) of lignite is loaded into the reactor without physical compaction to make the depth of the coal bed about 76cm (30 in.) typically.

The coal bed is ignited by a nichrome wire coil which rests on the top surface of the coal bed and is connected to an autotransformer by a pair of copper wires. The insulation between the copper wires and the reactor is provided by ceramic insulating tubes housed in a pair of 1/4 in. stainless tubes which are perpendicularly attached to the upper union. After the coal bed is ignited, the copper wires are forced into the inside of the upper union and the 1/4 in. stainless tubes are connected to a pressure transducer and bourdon gage for reaction pressure measurements.

At the time of ignition, only oxygen is supplied. When the coal at the top is heated to around 900 C, the pump starts delivering water to the steam generator and the steam-oxygen gasification run is carried out. It takes about 30 minutes for the product gas composition to stabilize.

The water injection is initiated about 10 minutes after the temperature measured by the center-line thermocouple, which is located at the same level as the water discharge point, reaches a peak. The water is delivered through one of the two 1/8 in. stainless steel tubes embedded near the reactor wall. Another positive displacement diaphragm pump delivers water, and the direction of water injection at the discharge point is perpendicular to the direction of the combustion front propagation.

Temperature and pressure measurements are continuously recorded on 6-channel graphic display/strip chart recorder. The CO and CO_2 mole fractions in the product stream are continuously monitored with infrared on-line gas analyzers, and the O_2 concentration is measured by an on-line oxygen analyzer. The sample gas is valve-injected every 30 minutes into a gas chromatograph which has been calibrated with six calibration gases containing H_2, N_2, CH_4, CO, CO_2, C_2H_4 and C_2H_6. The cumulative volume of the product gas stream is measured every 10 minutes with a dry test meter.

The experiment is terminated when oxygen is detected in the product gas stream. The run time ranges between 9 to 11 hours depending on the water injection rate and the time span of water injection. After the run is terminated by cutting off the oxygen and steam supply, the reactor is allowed to cool; then the ash and condensate are collected to determine their weight and volume as well as the carbon content of the ash.

RESULTS

The results of 12 gasification experiments are presented in this paper. The experimental conditions are summarized in Table 1. Run #8 was carried out without water injection (steam and oxygen only). In runs #10 through #14, water injection was performed twice with the water discharge points 14 inches apart. For the remaining runs, only a single period of water injection was used. The water discharge point of runs #5 through #9 was located roughly in the middle of the reactor, while the water discharge point of runs #15 and #16 is the same as the first of the two discharge points of runs #10 through #14. A fixed steam/O_2

molar ratio of 3 was used with oxygen feed rate of 1.2 scf/hr (568 scc/min). The pressure drop was negligible due to the low gas flow rate, and the gasification was carried out isobarically at 20 psig. The proximate and ultimate analyses of the coal used in the experiments are given in Table 2.

Table 3 summarizes the experimental results for 12 runs. The variation of dry product gas composition is represented by two average values: (a) the time-averaged value between ignition and the initiation of water injection (for runs in which two water injections are made, the first water injection time is taken) and (2) the time-averaged value between the initiation of (the first) water injection and the oxygen breakthrough point. The heating values are based on volume-averaged gas compositions produced either before and after the water injection period. Of course the averaged results shown here are not as informative as time-dependent variations which will be presented in later figures. However, the results shown in Table 3 provide some insight concerning the effects of water influx.

The results of runs #12 and #13 show that despite the doubled total water influx the outputs of the two runs were not much different from each other. Table 4 shows the content of carbon and hydrogen in the product gas for both runs as well as a case with no water influx (#8); it indicates that the conversion of coal and water was little affected in spite of the significantly increased water influx. The injected moisture did not participate in the gasification reactions and simply increased the water content of the product stream.

The small water influx of run #11 resulted in a substantial increase in the H_2 mole fraction as well as an increase in the heating value of the product gas. The water influx of run #9, in which about the same amount of water was injected as run #11 but at a much lower rate, also resulted in favorable outputs compared with those of run #8, where no water injection was carried out. In run #16, the water injection rate was not much higher than run #9 but the time span of water injection was much longer. Such an increase in total water influx resulted in a substantial increase in the CO_2 mole fraction and a decrease in CO mole fraction. The H_2/CO ratio of run #16 shifted to about 3.0 after water influx, whereas the H_2/CO ratio in runs #9 and #11 remained unchanged from the pre-water-influx level. This level closely matches that of run #8, in which the H_2/CO ratio remained relatively constant at about 2.

The peak temperatures following the square-pulse-type water influx (high rate for a short time span) as in runs #10 through 14 tend to become lower with increasing water influx rate.

Effect of water influx on product gas composition and production rate of each component

Over the range of water influx rates used in this work, the dynamic behavior of the product gas composition (H_2, CO, CO_2) in response to water influx may be categorized as follows:

type 1: Shift to a new quasi-steady state product gas composition

type 2: Momentary increase in H_2 and decrease in CO_2 while water influx persists but after termination of water influx slow return to the original product gas composition

type 3: A momentary increase in H_2 and subsequent oxygen breakthrough after going through a rapid increase in CO_2 mole fraction

The transient behavior of type 1 occurs for a relatively small water influx as in the case of run #16. The variation of the dry product gas composition for run #16 is shown in Figure 3. The immediate changes in H_2 and CO_2 mole fractions after the termination of water influx first imply that gas compositions may be controlled by chemical equilibrium. In order to verify this hypothesis, we attempted to fit the data with equilibrium models developed at Lawrence Livermore National Laboratory [3],[8]. However, this attempt was not successful. The simulation results, which are not presented here, indicated that the response of the mole fraction of each component to the termination of water influx was quite different from the

results shown in Figure 3, both in the direction of change and in magnitude. The predictions made by the LLNL equilibrium model yield variations in the CO and CO_2 mole fractions which were almost equal in magnitude and opposite in direction, while the H_2 mole fraction remained relatively constant. The magnitude of the variations was quite insensitive to the assumed reaction zone temperature.

The validity of the water-gas-shift equilibrium assumption, which has proved to be quite satisfactory in predicting the product gas composition for surface gasifiers as well as for UCG systems [4,9,10,11], seems to be rather questionable in interpreting the transient results shown here. For a coal gasification system where a small amount of water decomposition occurs, the water-gas-shift equilibrium reaction would be far from equilibrium, as pointed out by Johnson [12]. The shifts in the product gas composition shown in Figure 3, therefore, are considered to be mainly due to the changes in reaction rates resulting from the changes in feed conditions associated with water influx rather than equilibrium shift. Also, those cases where the quasi-steady state was maintained during the water injection period implies that the reaction zone temperature was little affected by water influx, as indicated by the peak temperatures which were not much different from the pre-water-injection level (see Table 3).

Figure 4 shows the variations of the production rate of each component during water injection for run #16, and the change in the H_2 production rate is slightly more sensitive to the presence of water influx. The total gas production rate is substantially increased after water influx is initiated and gradually decreases as water influx continues, indicating that the reaction zone temperature is decreasing, when the water influx is terminated, the H_2 production rate rapidly drops at a significantly higher rate than other species. Such a change in the H_2 production rate after termination of water influx is reflected in the product gas composition, yielding variations in H_2 and CO_2 mole fractions which are almost symmetrical, that is, equal in magnitude and opposite in direction.

The response of the product gas composition of the second type occurs for a high water influx rate persisting for a relatively short period of time. The changes in the product gas composition and the gas production rate are much more drastic than type 1. Figures 5 and 6 show the transient behavior of the product gas composition of runs #5 and #12, respectively. The H_2 mole fraction is suddenly increased after water influx is initiated, then rapidly drops during the water influx periods. Such a rapid drop in H_2 mole fraction continues even after water influx is terminated. The CO_2 mole fraction changes in the opposite direction to H_2 with magnitude of the sum of changes in H_2 and CO mole fractions, since the CH_4 mole fraction does not show any significant change in response to water influx. The CO mole fraction always decreases during the course of water influx.

Figures 7 and 8 show the changes of the production rate of each component for runs #5 and #12. These results were obtained by combining the dry test meter readings taken every 10 minutes and the average concentration for that time span. The H_2 production rate, as in the case of run #16, shows a substantial increase during the early period of water influx. However, such an increase in H_2 production rate, unlike the case of small water influx, is maintained only for a short period of time. It then undergoes a drastic decrease, which is a direct result of the reduced overall reaction rate due to the heat loss to water intruding into the reaction zone. The production rate of CO_2, in contrast, tends to remain relatively constant despite the significantly reduced overall gas production rate. The relatively constant CO_2 production rate is thought to be mainly due to the change in the combustion reaction. The formation of CO_2 over CO is favored by the drop of the combustion temperature according to the correlation proposed by Arthur [13]:

$$r_{CO} / r_{CO_2} = k \exp(-E/RT)$$

Figure 9 shows the variation of dry product gas composition of run #13. The variation of the gas composition shown in Figure 9 has essentially the same characteristics of the type 2 transient behavior as in runs #5 and #12. In this case, however, the second water injection

period resulted in oxygen breakthrough (type 3), which was preceded by rapid changes of CO_2 and H_2 mole fractions near the termination of water injection.

What happened during the second water injection may be explained by the penetration of oxygen into the gasification (steam-char reaction) zone. The water intrusion near the combustion zone causes a drastic heat loss in the gasification system via heat of vaporization of water, and the oxygen consumption pattern, which is determined by the temperature profile and the carbon conversion profile of the char bed, is greatly altered. Depending on the rate of water influx, the combustion zone, which is characterized by a sharp temperature gradient and complete depletion of oxygen, could change markedly. In that case, there exists no distinctive boundary between the combustion zone and the gasification zone, and oxygen will penetrate into the gasification zone. Gas-phase oxidation reactions (of CO and H_2) will possibly take place. If the oxygen consumption rate, either by heterogeneous or homogeneous reactions, is not sufficient, the oxygen will penetrate further downstream and lead to oxygen breakthrough.

Even though the water influx of run #13 did yield almost the same carbon and steam conversions as run #12, as shown earlier, such an oxygen penetration into the gasification zone will have a highly detrimental effect on the operation of the gasification system. Furthermore, with increasing oxygen flow rate, the water influx will have a much more pronounced influence on the product gas composition, since the above-mentioned oxygen penetration into the gasification zone is much more likely than lower oxygen flow rate.

Figure 10 shows the variation of the production rate of each component of run #13. The increase in the H_2 production rate is significantly higher than run #12, which is responsible for the larger increase in H_2 mole fraction during the water influx. Again, the production rate of CO_2 remains relatively constant as in the case of run #12.

Effect of Water Influx on H_2/CO Ratio

The H_2/CO molar ratio is an important variable in utilizing the synthesis gas produced via underground coal gasification process. Since the water influx strongly affects the gas composition and the production rate of each component as discussed previously, the influence of water influx on the H_2/CO molar ratio is also expected to be quite significant.

Figures 11 and 12 show the variations of H_2/CO molar ratios of runs #5 and #12, respectively. We can see the H_2/CO ratio, unlike the corresponding changes in the mole fractions (Figures 5 and 6) and the production rates of CO and H_2 (Figures 7 and 8), recovers to the pre-water-influx level quickly once the water influx is terminated. Such a result indicates that the change in H_2/CO molar ratio depends more strongly on the change of the feed composition than on the change of the gasification zone temperature. The significance of this result is two-fold. First, the H_2/CO ratio is quite stable in spite of the greatly disturbed gasification zone properties after water influx. In this regard, the effect of water influx on H_2/CO ratio is not that detrimental compared with its effect on other system outputs such as production rate, heating value, etc. Second, the H_2/CO ratio may serve as a good water-influx indicator for UCG; water influx is usually determined by an indirect method such as hydrogen balancing. The change in the H_2/CO ratio is significant only for the period of water influx.

The results for the effect of water influx on the H_2/CO ratio are summarized in Table 5 for different water injection rates. There seems to be no distinctive correlation between the magnitude of the maximum deviation of H_2/CO ratio from the steady state value and the water injection rate, even though the magnitude of deviation in general increases with increasing water injection rate.

Effect of water influx on heating value and thermal efficiency

The product gas heating value is shown to vary in a very similar manner to the total gas production rate. The variations of the total gas production rate and the product gas heating value of run 13, as shown in Figures 13 and 14, are strikingly similar. This indicates that the decrease in the product

gas heating value is closely related to the decreased gasification intensity of the reaction zone due to the water influx, or vice versa.

The water influx into the active gasification zone also drastically changes the thermal efficiency of the gasification system. In this work, the effect of water influx on the thermal efficiency is considered in terms of cold gas thermal efficiency which is defined as the ratio of the higher heating value of the product gas to the higher heating value of the coal.

The gasification reactor used in this experiment yields a rather poor thermal efficiency compared with adiabatic gasifiers used by other workers [5-7]. The reasons for such an inherent low thermal efficiency are due to the following:

1. No guard heater system is employed, thus radial heat loss is higher than adiabatic gasifiers.

2. Methane mole fraction in the product gas is low because of the relatively low operating pressure.

3. Axial heat transfer through the reactor wall is not negligible.

Due to the inherent limitations described above, the thermal efficiency of the system is relatively low. The typical cold-gas efficiency obtained in this work is about 45%, which is approximately 10% lower than the Exxon adiabatic gasifier [5], with no water injection. Tars and oils account for about 20% of the heat balance, and ambient heat loss is estimated to be 15 to 20%. The remainder is sensible heat of the product gas. The cold gas efficiency of the Exxon gasifier is estimated to be about 55% with operating pressure ranging between 100 and 500 psig which yields higher methane mole fraction (9-15%) in the product gas.

Due to the low methane concentration, the main contribution to the heating value of the product gas is from CO and H_2 (the contribution by CH_4, C_2H_4, C_2H_6 is typically around 20% of total heating value). Also, the variation in the methane mole fraction with water influx is negligibly small compared with the major three components (CO, H_2 and CO_2). Thus, the variation of cold gas efficiency with composition change can be represented by a triangular diagram of CO, H_2 and CO_2 for this lignite, as shown in Figure 15. The dotted lines in Figure 15 represent the lines of constant cold gas efficiency. Because the higher heating values of H_2 and CO (68.3 kcal/gmol vs. 67.6 kcal/gmol) are very similar, the lines of constant cold gas efficiency are roughly parallel to lines of constant CO_2 mole fraction (cold gas efficiency changes 10% for CO_2 mole fraction change 0.15). The constant cold gas-efficiency lines have been drawn based on the percent of the heating value of the product gas having the normalized composition on $CO-H_2-CO_2$ triangular diagram and fixed mole fractions of CH_4, C_2H_4 and C_2H_6 to the heating value of coal. The fixed mole fractions of the three hydrocarbons are taken as 3.5%, 0.1% and 0.3%; the volume of product gas per lb of coal is based on the data of run #8; the heating value of the coal sample is 8500 Btu/lb (dry).

The effect of the amount of water influx on the overall cold gas efficiency is given in Table 6 for runs with dual water injections. The results shown in Table 6 indicate that a small water influx of run #11 does not adversely affect the overall cold gas efficiency compared with run #8 (no water influx). With an increasing amount of water influx, the cold gas efficiency drops considerably, which is an expected result. However, the detrimental effect of water influx on the cold gas efficiency tends to level off with increasing amount of water influx. Further increase in water influx, however, could lead to oxygen breakthrough, which is considered to be more detrimental to the overall gasification process than decrease in the cold gas efficiency.

Effect of water influx on reaction zone temperature

Figure 16 shows the variations of the four center-line temperatures of run #5 after water influx. The temperature near the water injection point (thermocouple No. 5) drops immediately to about 250 F after water injection is initiated. Also, the combustion front velocity is

decreased considerably (from 0.28 ft/hr to about 0.20 ft/hr) after water influx.

During the first two hour period after water influx, there appears to be no distinctive combustion front. Even though the exact axial temperature profile cannot be determined with the fixed thermocouples used in this experiment, the temperature profile when T/C #6 reaches the peak is expected to be very flat. In fact, the time corresponding to the peak of T/C #6 gives the lowest heating value and the highest CO_2 mole fraction, as shown in Figure 5.

The variation of temperature shown in Figure 16 provides a good illustration of how the properties of the reaction zone change during and after water influx.

CONCLUSIONS

A fixed-bed gasifier has been used to study the influence of water influx on the steam-oxygen gasification of lignite. Results show that the variation of dry product gas composition are strongly dependent on the rate of influx, and the variations are caused by the change of reaction rates rather than by the shift in equilibrium.

The effect of water influx on the cold gas efficiency tends to level off with increasing total amount of water influx. The H_2/CO molar ratio is shown to be very stable, and deviates from the steady state level only for the period of water influx. The response of the gasification system can be categorized by three different types of transient behavior, depending on the severity of the disturbance by water influx.

REFERENCES

1. Camp, D.W., "A Model of Water Influx for Underground Coal Gasification," M.S. thesis, University of Colorado, Boulder, 1980.
2. Krantz, W.B., Camp, D.W. and Gunn, R.D., "A Water Influx Model for UCG," Proc. Sixth UCC Symposium, Shangri-La, Oklahoma, III-21, July, 1980.
3. Natarajan, R., Edgar, T.F. and Savins, J.G., "Prediction of Product Gas Composition for UCG," Proc. Sixth UCC Symposium, Shangri-La, Oklahoma, III-15, July, 1980.
4. Thorsness, C.B. and Cena, R.J., "In Situ Coal Gasification Modeling," Lawrence Livermore Laboratory, UCRL-82269, February, 1979.
5. Rodgers, M.E. and Rajan, R., "Pressurized Combustion Tube Gasification of Texas and Wyoming Coals," Proc. Sixth UCC Symposium, Shangri-La, Oklahoma, IV-21, July, 1980.
6. Bell, G.J. and Gunn, R.D., "Adiabatic Coal Gasification Tube Experiments - Forward Combustion," Proc. Sixth UCC Symposium, Shangri-La, Oklahoma, IV-31, July, 1980.
7. Rozsa, R.B. and Thorsness, C.B., "Lawrence Livermore Laboratory Coal Gasification Program: Underground Reaction Modeling and Laboratory Combustion Tube Experiments," Paper LE-3 presented at the Second Annual Underground Coal Gasification Symposium, Morgantown, WV, August, 1976.
8. Hill, R.W. and Thorsness, C.B., "Summary Report on Large Block Experiments in Underground Coal Gasification, Tono Basin, Washington," Lawrence Livermore Laboratory, UCRL-53305, Vol. 1, July 9, 1982.
9. Yoon, H., Wei, J. and Denn, M.M., "A Model for Moving-Bed Coal Gasification Reactors," AIChE J., 24, 885, 1978.
10. Cho, Y.S. and Joseph, B., "Heterogeneous Model for Moving-Bed Coal Gasification Reactors," Ind. Eng. Chem. Proc. Des. Dev., 20, 312, 1981.
11. Stephens, D.R. and Miller, D.G., "Thermodynamic Equilibrium for Wyoming Coal: New Calculations," Lawrence Livermore Laboratory, UCID-17044, February, 1976.
12. Johnson, J.L., "Kinetics of Coal Gasification," pp. 147, John Wiley & Sons, 1979.
13. Arthur, J.R., "Reactions between Carbon and Oxygen," Trans Faraday Soc., 47, 164, 1951.

Table 1. Experimental Conditions

Run No.	Water Inj. rate (g/min)	Water Inj. period (min)
5	2.56	60
6	3.32	108
7	1.42	120
8	0.0	0
9	0.54	135
10	2.56	60
11	2.56	30
12	4.73	60
13	4.73	120
14	4.73	60
15	2.06	120
16	0.63	270

O_2 feed rate for all runs = 568 scc/min = 1.2 scf/hr
Steam feed rate (all runs) = 1.27 g/min (3.0 molar ratio steam/O_2)
Operating pressure = 20 psig
Particle size = 16 - 20 U.S. mesh (0.84 - 1.19 mm)
Water injection mode : step increase
Number of water injections : 1 (run #5 - run #9, run #15, #16) or 2 (run #10 - run #14)

Table 2. Proximate and ultimate analyses of Butler Brick lignite

Proximate analysis (wt. %)		Ultimate analysis (wt. %)	
	Dry		Dry
Ash	27.97	Ash	27.97
Volatile	39.06	Sulfur	1.59
Fixed C	32.97	Nitrogen	0.93
Total	100.00	Carbon	49.95
		Hydrogen	3.98
		Oxygen	15.58
		Total	100.00

as-received moisture content = 15.89%

Heating value of coal (Btu/lb)

As received	Dry	Mineral ash free
7136	8485	11779

Table 3. Summary of results before and after water injection

Run	Heating value (Btu/scf)		Gas composition (mole %)								Peak temperature range (°F)	
			Before				After					
	Before	After	H_2	CO	CH_4	CO_2	H_2	CO	CH_4	CO_2	Before	After
5	201	149	32.0	17.5	3.4	46.8	24.2	10.5	2.8	62.3	1540-1750	950-1580
6	180	167	29.7	13.6	3.4	53.0	28.6	9.4	2.3	59.3	1530-1720	1060-1070
7	209	169	32.8	19.3	3.5	44.1	27.5	9.7	2.4	60.2	1650-1800	1350-1450
8	195	-	31.5	15.2	3.6	49.5					1650-1850	
9	186	212	30.4	14.6	3.5	51.3	36.3	14.8	3.3	45.4	1630-1770	1400-1650
10	194	180	30.8	17.9	3.6	47.5	30.3	12.5	3.5	53.6	1630-1800	1350-1750
11	187	204	29.8	16.2	3.7	50.0	33.3	17.1	3.8	45.8	1650-1750	1700-1900
12	198	176	30.0	18.8	3.9	47.0	29.6	10.8	3.6	55.8	1600-1650	1330-1900
13	206	168	33.3	18.1	3.6	44.7	27.0	10.3	3.0	59.6	1630-1700	1000-1950
14	207	172	31.7	18.7	3.7	45.5	27.1	11.2	3.3	58.3	1630-1650	1150-1950
15	197	179	30.5	18.5	3.7	47.0	29.2	11.9	3.4	55.5	1600-1650	1350-1950
16	204	187	30.7	18.7	3.8	46.5	33.9	11.8	3.6	50.7	1620-1750	1630-1690

Table 4. Carbon Conversion

	Run #12	Run #13	Run #8
Total carbon in product gas (g)	343	336	372
Total carbon in coal charge (g)	473	460	472
C in dry gas / C in coal	72.5%	73.0%	79.5%
Total hydrogen in product gas (g)	32	32	37

Table 5. Effect of water injection rate on the maximum deviation of H_2/CO ratio from steady state level

Run No.	Water inj. rate(g/min)	Steady state H_2/CO ratio	Maximum dev. from s.s.
5	2.56	1.9	1.4
6	3.32	2.3	1.5
7	1.42	2.0	0.7-1.2
8	0.0	2.2	-
9	0.54	1.8	0.5-1.0
10	2.56	1.9	1.1
11	2.56	2.2	1.0
12	4.73	1.9	2.4
13	4.73	1.9	2.4
14	4.73	1.7	2.0
15	2.06	1.8	1.9
16	0.63	1.8	0.4-1.5

Table 6. Effect of amount of water influx on overall cold gas efficiency

Run No.	Injection rate (g/min)	Injection period (min)	Number of water inj.	Total water influx (g)	Cold gas efficiency (%)	Run time (hr)
8	0	0	0	0	44.3	10.0
11	2.56	30	2	77	44.9	9.33
10	2.56	60	2	156	39.9	10.17
12	4.73	60	2	284	35.8	9.67
13	4.73	120	2	568	37.0	9.33

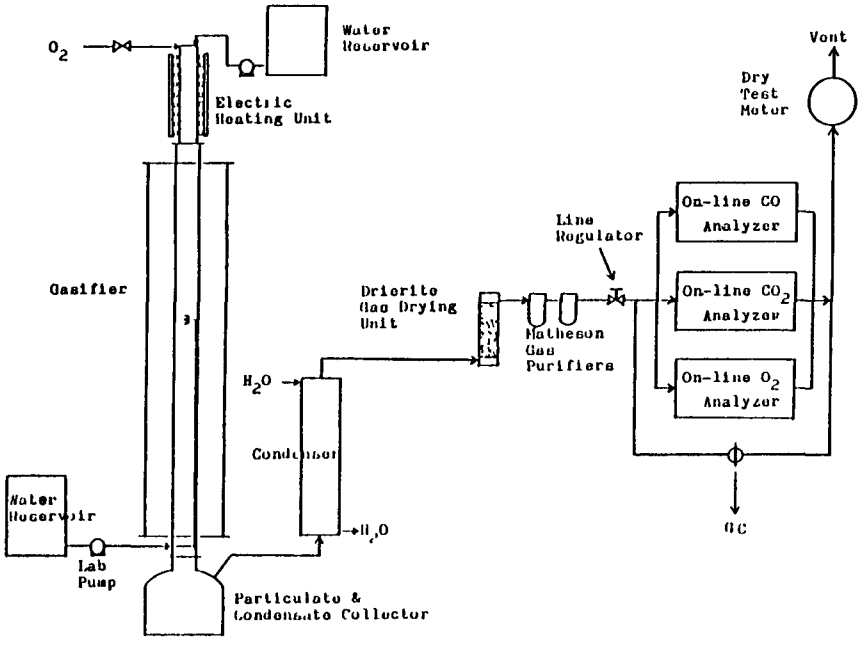

Figure 1. Laboratory equipment flow diagram

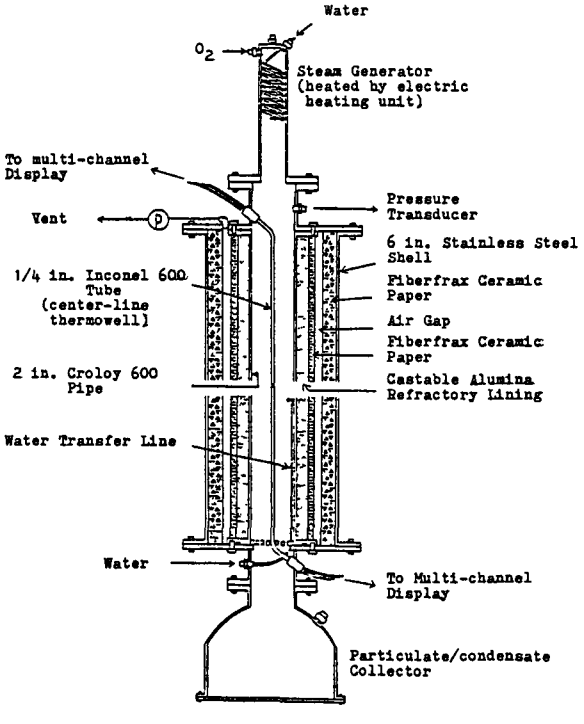

Figure 2. Combustion tube with water injection and steam generator

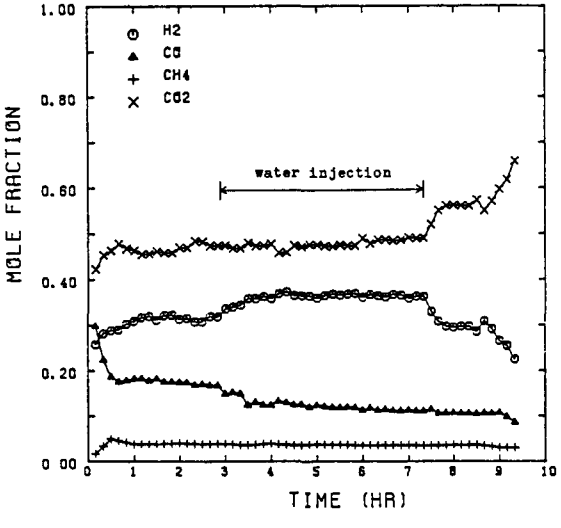

Figure 3. Dry product gas composition, Run No. 16

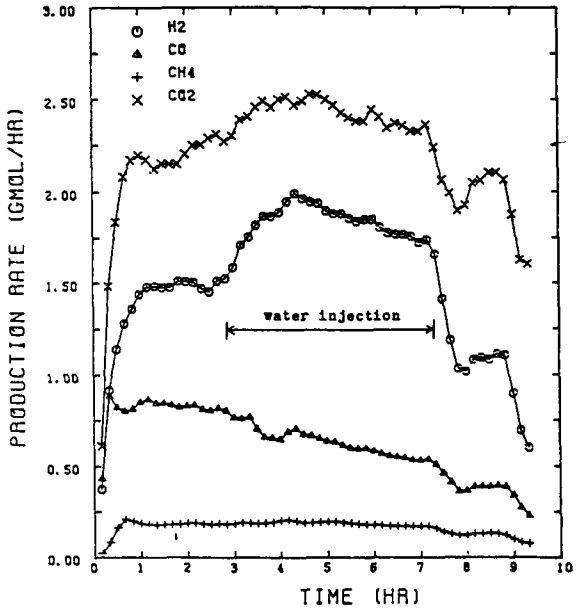

Figure 4. Production rate of each component, Run No. 16

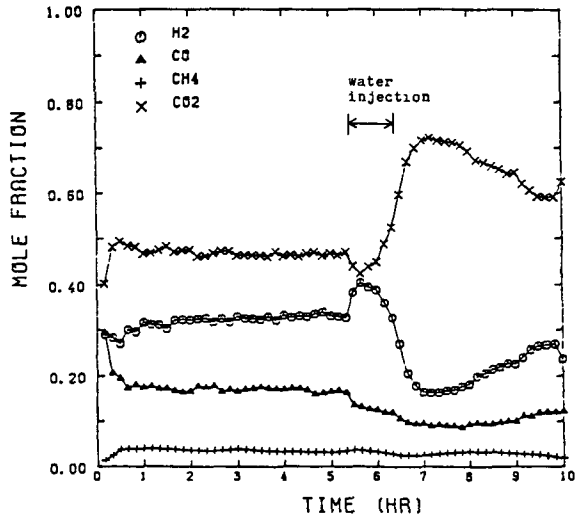

Figure 5. Dry product gas composition, Run No. 5

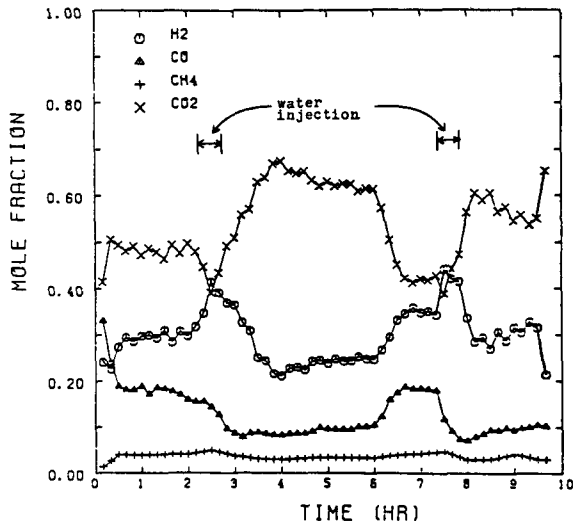

Figure 6. Dry product gas composition, Run No. 12

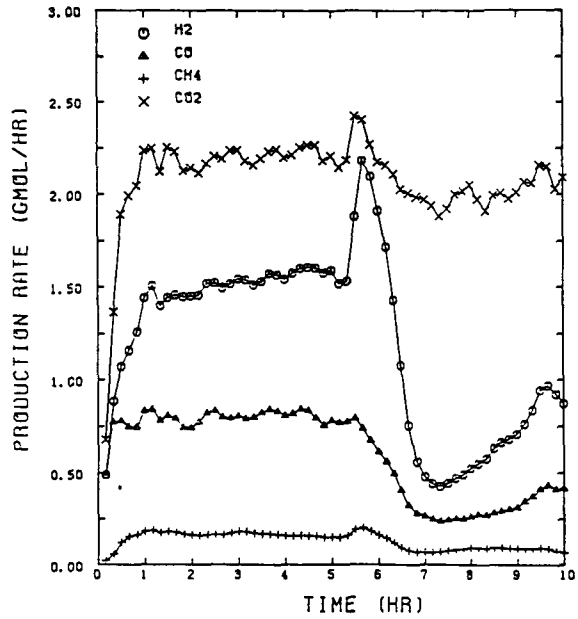

Figure 7. Production rate of each component, Run No. 5

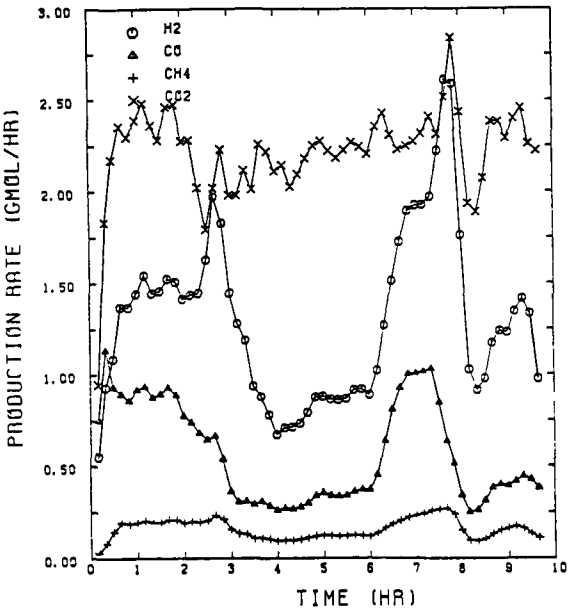

Figure 8. Production rate of each component, Run No. 12

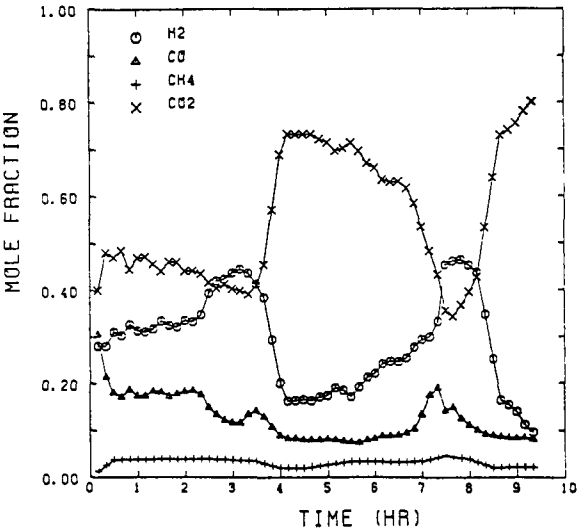

Figure 9. Dry product gas composition, Run No. 13

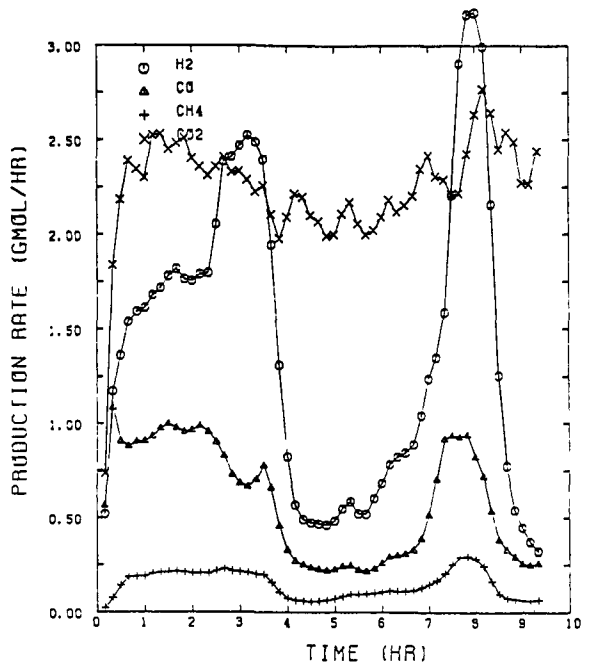

Figure 10. Production rate of each component, Run No. 13

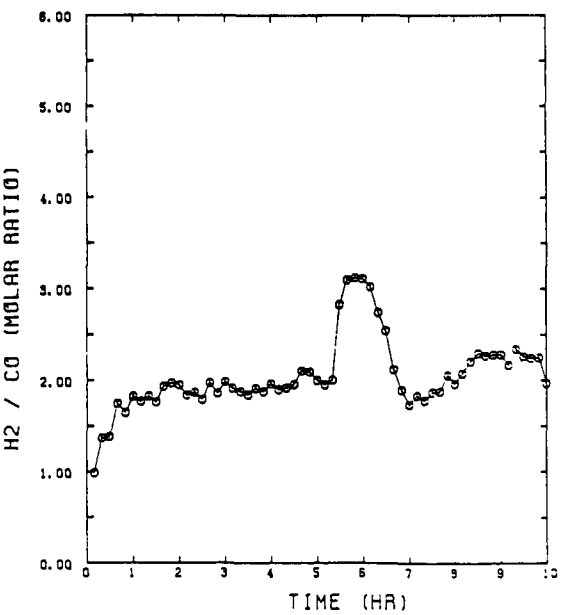

Figure 11. Variation of H_2/CO molar ratio, Run No. 5

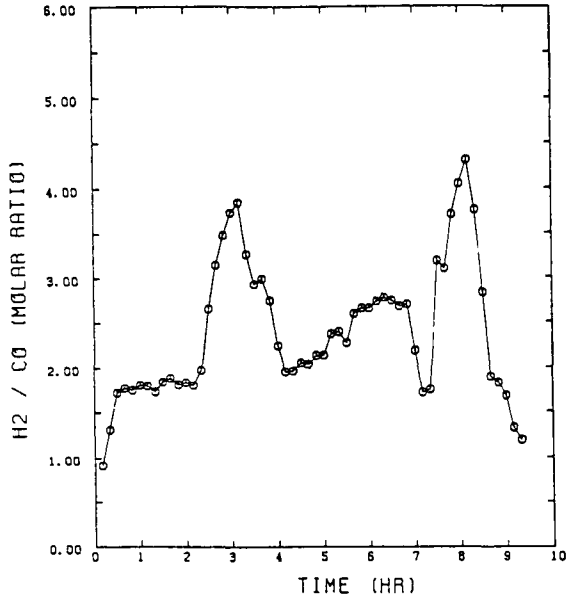

Figure 12. Variation of H_2/CO molar ratio, Run No. 12

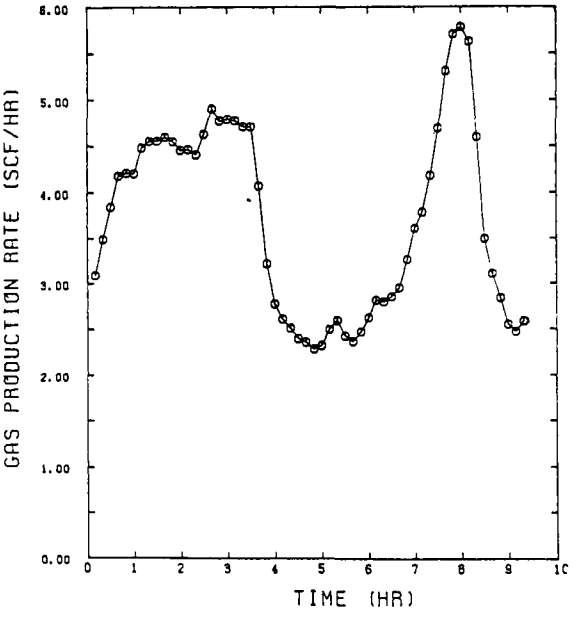

Figure 13. Total gas production rate, Run No. 13

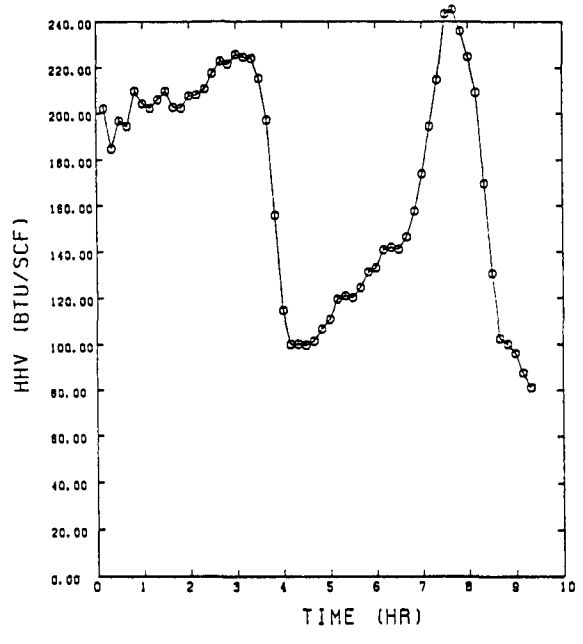

Figure 14. Heating value of product gas, Run No. 13

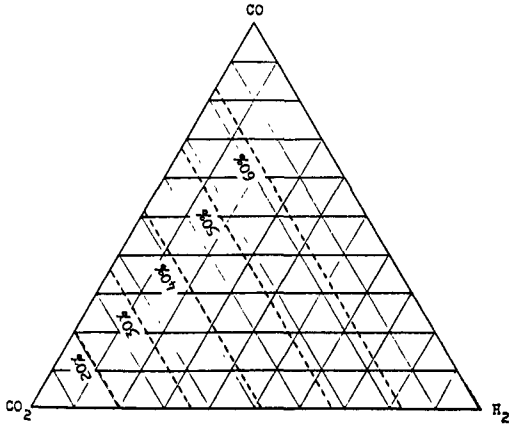

Figure 15. Cold gas efficiency vs. mole fractions of H_2, CO and CO_2

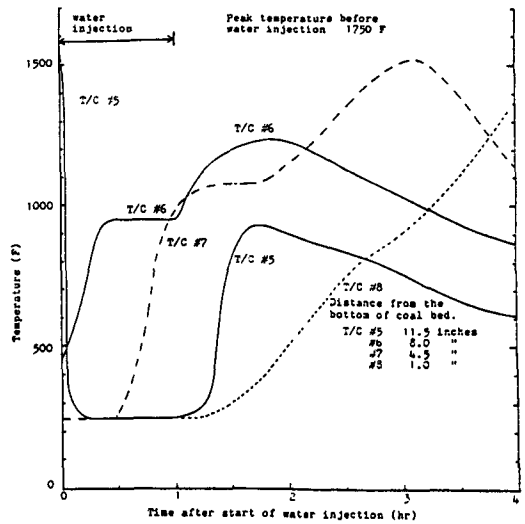

Figure 16. Variation of center-line temperature, Run No. 5

3.13 ANALYSIS OF COAL PYROLYSIS AND DRYING HISTORY FOR VARIOUS COAL GEOMETRIES*

by

Sang-Wook Kang[1]
Linda Ott[1]

ABSTRACT

A simplified analysis of time-dependent coal pyrolysis and drying phenomena was developed for various coal geometries such as spheres and semi-infinite coal slabs. The conservation equations were solved numerically by adapting general purpose computer solution packages. The results demonstrate sizable effects of surface temperature and physical dimensions on the heat transfer, pyrolysis and drying histories.

INTRODUCTION

The impetus for the present work stems largely from the need to determine dominant physical parameters involved in underground coal gasification phenomena. In particular, our purpose is to generate a simple computational tool that yields the heat-transfer history of spherical, cylindrical, and slab coal of various sizes during coal pyrolysis and drying processes. To this end a simplified coal gasification model is constructed consisting of wet-coal drying and primary pyrolysis (no secondary reactions). The derived mathematical equations are then solved by adaptation of existing general-purpose solution algorithms for partial differential equations (PDEs), thus obviating the need for expending considerable time and effort in developing a new solution scheme. In what follows, details of the formulation and computational approach will be presented.

ANALYSIS

For generality we study a time-dependent, one-dimensional (spherical, cylindrical, Cartesian) "flow" problem with lumped-parameters and convective mass and thermal fluxes in the flow field of interest. The lumped physical parameters, such as thermal conductivity, need not be constant, but may vary with temperature - and therefore with time and space - and with pressure, etc. The governing equations, describing the moving-front phenomena, are conservation equations of the global mass, the constituent mass components, the momentum, and the

*This work performed under the auspices of the U.S. Department of Energy under contract No. W-7405-Eng-48.

[1]Lawrence Livermore National Laboratory
Livermore, CA 94550

thermal energy with appropriate boundary conditions (transient or steady). The system of N-partial differential equations that can be solved, using the chosen PDE solver, is expressed in the following generalized structure.

$$\frac{\partial F_j}{\partial t} = f_j \left\{ t,\ r,\ F_1,\ldots F_N,\ \frac{\partial F_1}{\partial r},\ldots,\ \frac{\partial F_N}{\partial r},\ \frac{1}{r^e}\frac{\partial}{\partial r}\left(r^e D_{j,1}\frac{\partial F_1}{\partial r}\right),\ldots,\ \frac{1}{r^e}\frac{\partial}{\partial r}\left(r^e D_{j,N}\frac{\partial F_N}{\partial r}\right)\right\} \quad (1)$$

with $a \leq r \leq b$, $t \geq t_0$, and j = 1 to N. The term F_j signifies a dependent variable function in the field such as density, temperature, etc., r the spatial coordinate, and t the time. The functions $D_{j,\lambda}$ for j, λ = 1 to N may be functions of t, r, $F_1,\ldots,F_N$. The constant e may be 0, 1, 2, depending on whether Eq. (1) is posed in Cartesian, cylindrical, or spherical coordinates, respectively. As sample equations, we show a specific system of partial differential equations utilized in the spherical coal drying and pyrolysis study. For the present, we introduce the following approximations: constant overall pressure inside the coal, unimportant viscous effects; negligible small timewise variations in the densities of water vapor and coal gas compared to the production rates and the convective mass flux effects of these species. The resulting conservation equations are in a form consistent with the requirements of the PDE solver, i.e., Eq. (1), in the spherical coordinate system [1,2].

$$\frac{\partial \rho_1}{\partial t} = -\phi_1 \quad (2)$$

$$\frac{\partial \rho_2}{\partial t} = -\phi_2 \quad (3)$$

$$\rho c\ \frac{\partial \theta}{\partial t} = \frac{1}{r^2}\frac{\partial}{\partial r}\left(r^2 k \frac{\partial \theta}{\partial r}\right) - \left(\Sigma_i \dot{m}_i c_i\right)\frac{\partial \theta}{\partial r} + \Sigma_i \phi_i Q_i \quad (4)$$

The subscripts 1 and 2 denote respectively the liquid water and pyrolyzing coal (solid). The term ρ_i signifies the density of species i, ϕ_i the species production rate, $\dot{m}_i$ the convective mass flux of species i, r the spherical radius, t the time, $\theta = T - T^\circ$, T the absolute temperature, T° the reference temperature, C_i the specific heat of species i, k the mean thermal conductivity, and Q_i the latent heat of phase change of component i. The production rate ϕ_i is expressed in the form $\phi_i = \exp(W_i - B_i/T)$, where W_i and B_i are constants. We also note that the diffusion term is neglected in the component conservation equation as being small in comparison to the convective flux and the species generation effects in the present moving-front problem.

The nonlinear partial differential equations (2)-(4) have been solved by applying the numerical method of Sincovec and Madsen [3], embodied in the general PDE solver. Briefly, the scheme involves a finite-difference method, with centered differencing in the spatial variable for time-dependent nonlinear PDEs, giving a semidiscrete system of nonlinear ordinary differential equations (ODEs) which are then solved using one of the recently developed ODE integrators. The software interface along with an ODE integrator will discretize the problem, select the time step and order, solve the nonlinear equations (checking for convergence, etc.), and automatically maintain a user-specified time integration accuracy. Details of the method are included in Ref. 5 and in the solution package by Madsen [4].

In solving the present mathematical system of non-linear PDEs the equations were recast in dimensionless form for greater generality and applicability to other fluids and situations. For example, the time term is nondimensionalized by dividing it by L^2/α, where L is the characteristic length and α the thermal diffusion coefficient, and the terms ρ_i are divided by their respective density terms and then are expressed in logarithmic form, i.e., $\ln(\rho_i/\rho_I)$. This scheme proved useful when dealing with the case when $\rho_i \to 0$ in applying Madsen's solution algorithm. The resulting equations were then solved on the LLNL-Cray computer. Typical run time is approximately 5×10^{-4} sec per unit mesh zone per unit integration time step.

RESULTS AND DISCUSSION

Results have been obtained for the pyrolysis and drying history of a spherical coal and a semi-infinite coal slab under various conditions such as the surface temperature, sphere size, liquid water content level, thermodynamic properties, etc. We describe here only the salient features of the results obtained for spherical coal, since this is the case of greater current interest.

Figure 1 presents a typical time-wise temperature distribution inside a spherical coal block. The surface temperature in this case was 1000°C and the sphere radius was 0.2m. The temperature penetration rate is roughly proportional to $t^{1/2}$, a trend corresponding to the pure conduction case. However, due to pyrolysis and drying inside the coal the temperature distribution deviates from the pure conduction case. Because of the high surface temperature maintained at the surface, the liquid water level decreases as a result of a "drying" process, as seen in Figure 2. The time-wise movement of the drying front is clearly observed. In addition, the pyrolysis front is generated at the surface and is seen to be also moving inward from the hot coal surface (Fig. 3), though at a slower velocity than that for the drying front. We note that the present analysis is capable of calculating the genesis of these two fronts, i.e., pyrolysis and drying, at the surface and can describe their subsequent movement inside a spherical coal. It should be remarked, however, that the effort consumed considerable amount of programming and travail in manipulating the values of W_i and B_i to assure smooth movement of these fronts. We additionally note that we have not considered spalling or the secondary reactions, such as water and char, CO_2 and char, coking, cracking, etc., in the present analysis, due to the uncertainty in the kinetics and the great complexity of details involved in the system [5,6]. We emphasize, however, that the present approach is valid as a limiting case such as at low temperatures where secondary reactions are negligible.

When calculations are performed on a semi-infinite coal slab, simulating an underground wet coal whose surface is exposed to heating, the results show that the penetration depth of the drying front is about 3 cm from the hot surface when the penetration rate is 10^{-5} m/sec. Here the penetration rate is defined to be the ratio of the penetration depth of the dry front to the elapsed time. This rate is an empirically obtained penetration rate based on LBK experiments [7]. The observed sizes of the falling coal particles include pieces much larger than 3 cm, suggesting that these falling coal pieces are wet, not dry. Therefore these particles will act as a source of heat-sink in the course of removing the liquid water contained in the coal chunks. We note here that the results of the present analysis are consistent with experiments [8].

The effects of the coal size (sphere) are shown on the heat transfer history in Fig. 4, where the amount of heat transferred to a spherical coal particle is plotted as a function of time for particle sizes ranging from $R_0 = 0.05$m to $R_0 = 0.4$m. For convenience the amount is normalized with respect to the total amount of thermal energy that the particles can absorb with infinite time. The results show that a larger fraction of heat is

absorbed by smaller particles for a given amount of time. For instance, at $t = 1.8 \times 10^3$ s, the fraction is 0.74 for $R_0 = 0.05$m, whereas it is merely 0.13 for $R_0 = 0.4$m. In absolute terms the heat transfer is greater for larger particles for a given time. This is a physically reasonable result as the surface area is much larger and the temperature gradient is steeper for larger particles.

The results also show that eighty percent of the heat transfer have been absorbed by the coal by the time the dry front reaches the spherical core. This time is approximately collelated to be $10^6 R_0^2$, where t is in seconds, R_0 in m, for the cases where $\Delta T = 1000°C$, $\alpha = 4.6(10^{-7})$ m^2/sec, and $0.05m \leq R_0 \leq 0.4m$. Thus bulk of heat transfer will take place in a matter of 40 min for $R_0 = 0.05$m, about 3 hrs for $R_0 = 0.1$m and only 11 hrs for $R_0 = 0.2$m. In other words, coal particles of $R_0 = 0.2$m or less will undergo an almost complete heating process in a matter of hours. Because the coal particles observed to-date in the LBK tests have been $R_0 = 0.15$m or smaller, we conclude that the falling coal pieces, unless they are much larger than $R_0 = 0.2$m, will not act as a heat-sink for the duration (on the order of days) of the coal gasification process.

Figure 5 shows the relative influences of the various physical parameters on thermal transport history. It may be seen from the curves that the endothermic term, i.e., the "heat sink" term involving vapor production, predominates over those of the convective vapor and pyrolyzed coal fluxes. In particular, the curve (A) corresponds to a pure conduction case with no drying or pyrolysis inside the coal. It is seen from the figure that the thermal effects generated at the surface have already reached the core of the sphere. These results agree well with the analytic solution given in Carslaw and Jaeger [9]. In order to determine the additional effects of convective thermal fluxes on the temperature history inside the coal, the PDEs were solved with only the conduction and the convective effects included in the energy Eq. (4). The results obtained are shown in Fig. 5, curve (B). The convective flux (both mass and thermal) effects arise from the water vapor and the pyrolyzed coal gas being convected outward from their respective reacting fronts and thus oppose the thermal flux effects moving inward through conduction. From the figure we observe a noticeably lower temperature distribution than the pure conduction case (A) and conclude that the convective flux effects must be accounted for in the analysis. We now consider the endothermic effects: the third term on the right-hand side of Eq. (4). When this "heat sink" term, representing a thermal flux produced by vaporization of the liquid water, is taken into account along with the conduction term in the wet coal, the temperature distribution displays even greater effects of this source of heat absorption at the drying fronts, curve (C). From the particular examples calculated here, then, the curves (B) and (C) demonstrate that the effect of heat absorption from coal drying is greater than that of convective fluxes on the temperature distribution and, therefore, the heat-transfer processes. When all of these effects are combined, i.e., conduction, convection, and heat sink, the resulting temperature distribution is like curve (D) in Fig. 5. For the specific case computed here, their combined effects differ little from case (C). However, solutions obtained from other conditions, not included in the present paper, demonstrate that the convective flux effects are by no means negligible and should be accounted for in coal gasification studies.

CONCLUDING REMARKS

The coal pyrolysis and drying history has been analyzed by formulation of physical models for various geometries (spherical, cylindrical, and cartesian), and by solution of the equations through adaptation of existing numerical codes. The formulation assumes time-dependent, one-dimensional flow for the thermal, mass and momentum characteristics within the coal. Conservation equations for the pyrolyzing coal, the inert coal, and the liquid water content inside the

coal are then derived. In solving these partial differential equations, readily available PDE solution packages were utilized by recasting the equations in a form suitable for the code computations.

Numerical results were obtained for pyrolysis and drying history of spherical coal blocks and semi-infinite coal slabs under typical underground coal gasification conditions. The results display both the pyrolysis front and the drying front moving inward from the surface as a function of time, generating two concurrent vapor masses within the coal, i.e., the water vapor at the drying front and the pyrolyzed coal gas at the pyrolysis front. The results also demonstrate that the falling pieces of coal - observed to be typically R_0 = 0.15m or smaller - can provide heat transfer activity with the hot coal bed for only a few hours, and therefore are not likely to act as viable heat sinks during the long coal gasification processes. The results also show that the effects of "heat sink" due to vaporization of water and pyrolysis of coal on the thermal and pyrolysis behavior predominate over those due to the convective vapor-mass fluxes inside the coal.

REFERENCES

1. R. B. Bird, W. E. Stewart, and E. N. Lightfoot, Transport Phenomena (John Wiley and Sons, New York, 1960).

2. C. B. Thorsness, E. A. Grens, and A. Sherwood, "A One-Dimensional Model for In-Situ Coal Gasification," Lawrence Livermore National Laboratory, Livermore, Calif., UCRL-52523 (1978).

3. R. F. Sincovec and N. K. Madsen, "Software for Nonlinear Partial Differential Equations," ACM Trans. on Math. Software, Vol. 1, No. 3 (Sept. 1975), pp. 232-260.

4. N. K. Madsen, "PDEPACK User's Guide," Lawrence Livermore National Laboratory, Livermore, Calif., UCIR-1027 (1975).

5. J. B. Howard, W. A. Peters, and M. A. Serio, "Coal Devolatilizaton Information for Reactor Modeling, - Assessment of Data and Apparatus Availability with Recommendations for Research," EPRI Report AP-1803 (1981).

6. Chemistry of Coal Utilization, M. A. Elliott, ed., 2nd. Supplementary Volume (John Wiley and Sons, New York, 1981).

7. R. W. Hill and C. B. Thorsness, "Summary Report on Large Block Experiments in Underground Coal Gasification, Tono Basin, Washington: Vol. 1. Experimental Description and Data Analysis," Lawrence Livermore National Laboratory, Livermore, Calif., UCRL-53305 Vol. 1 (1982).

8. B. A. Kashiwa and F. H. Harlow, "An Investigation of Simultaneous Heat and Mass Transfer in Subbituminous Coal," Proc of 15th Intersociety Energy Conversion Engineering Conf., Seattle, WA, August 1980.

9. H. S. Carslaw and J. C. Jaeger, Conduction of Heat in Solids, Second Edition (Oxford University Press, 1973).

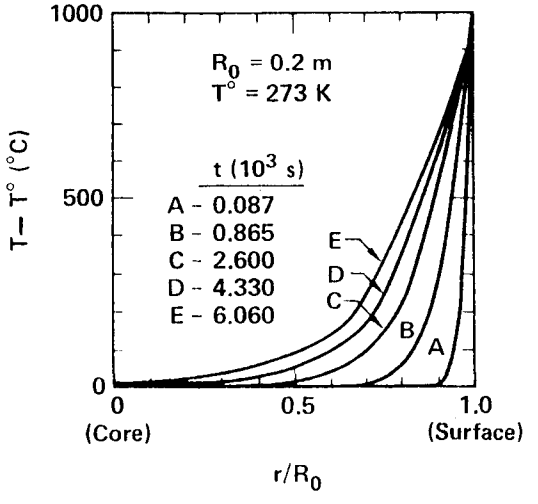

Fig. 1. Temperature distributions during pyrolysis and drying inside a spherical wet coal.

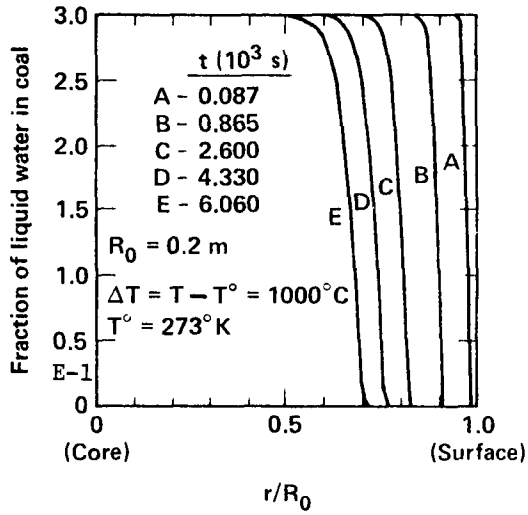

Fig. 2. Liquid water content distributions during pyrolysis and drying inside a spherical wet coal (initially 30% water).

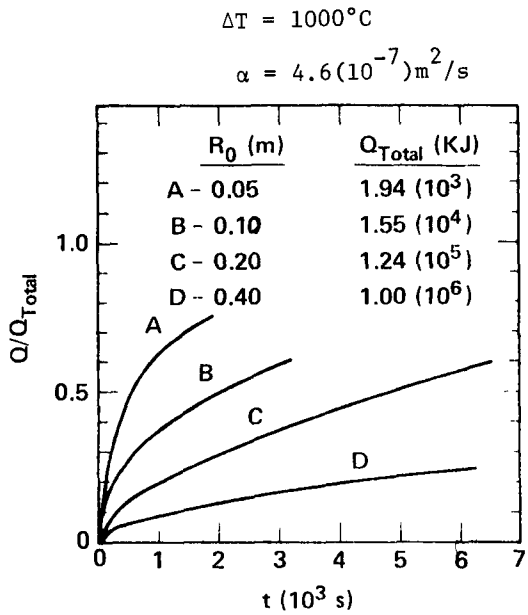

Fig. 4. Heat-transfer history of spherical coal drying and pyrolysis.

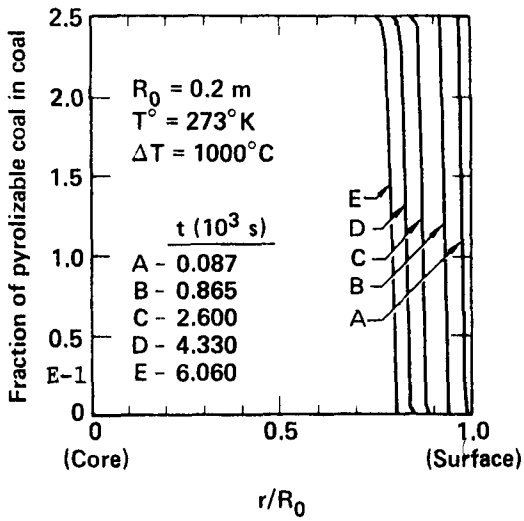

Fig. 3. Pyrolyzable coal distributions during pyrolysis and drying inside a spherical wet coal (initially containing 25% volatiles).

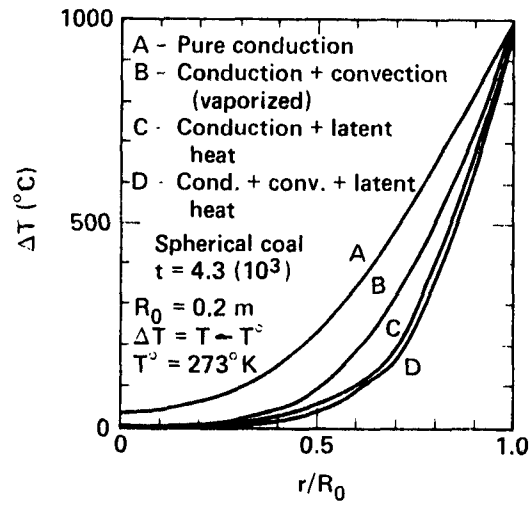

Fig. 5. Effects of various physical parameters on temperature distribution during spherical coal drying and pyrolysis.

3.14 THE PERMEABILITY OF BITUMINOUS COAL AT TEMPERATURES UP TO 700°C AND SIMULTANEOUS PRESSURES P_1 UP TO 70 BAR

by

H. J. Schloemer 1/
J. Wagner 2/

ABSTRACT

Up to this day temperature dependent permeability behavior of compact coal wasn't researched at simultaneous pressures. First of all the term "absolute" permeability is defined as it is ment in this report. Some theoretical foundations follow. Permeability constants are calculated by Darcy' s law and the so called Klinkenberg-correction was applied. A method to avoid gas slip-effects is introduced. Coal preparation and the embed of coal samples is described. Results of permeability tests show that at UCG-conditions several gas barriers are built up within a coal seam, streamed by a gas. The greatest barrier is the plastified coal. Nearly no connected pores exist at this mashed state. Another obstacle is caused by transport of water and tar. It is built up in the cold area of a seam.

1/, 2/ Universität des Saarlandes
6600 Saarbrücken
Technische Mineralogie
West-Germany

PREFACE

In the presented paper the temperature-dependent viscous permeability of compact coal is researched. At that, question is to put whether there is a constant or a variable increase or decrease of the permeability at raising temperature. It also could be that there exist special ranges where remarkable changes will take place.

No doubt, numerous investigations on coal permeability exist but they are exclusive due to the behavior of coal at low temperature conditions. Merely G.E.Foxwell (1) already made some investigations on the gas-permeability behavior of poured coal-granules in the plastic zone in 1924. That is to say his investigations didn't deal with compact coal.

Moreover one can find an interesting work of W.Terschüren, 1978 (2), who indeed was engaged with the behavior of compact coal but because of his autoclave plant he had to recool the coal samples before measuring. In the university of Saarbrücken now for the first time we are able to measure

the gaspermeability of compact coal at insitu-conditions by multiple-purpose autoclave plant. The results of these researches ought to approach the real conditions in UCG and have essential importance to a successfull carrying-out.

THEORETIC FOUNDATION

When gas is streaming through a permeable medium different kinds of flow occur. Beside of viscous flow there is flow with slip-effect, molecular flow and finally surface-diffusion. On the other hand principally you have to distinguish turbulent and laminar flow.

In this report Darcy's law for calculating permeability constants was applied. After the application of the equation of state of an ideal gas Darcy's law can be used in the following form:

$$k = \frac{2\, q_2\, \eta_m\, p_2\, l}{(p_1^2 - p_2^2)\, F}$$

k: permeability constant, [md]
q_2: gas volume at the outlet of the sample, cm^3/s
p_2: pressure at the outlet of the sample
η_m: viscosity, cp
F: square measure of the coal face, cm^2

Approximation to "absolute" permeability values within a temperature range of 20 to 700°C is following. A method to avoid gas slippage and to attain an absolute permeability constant is to influence the mean free path of the gas molecules. The mean free path of gas molecules changes with temperature and pressure. As soon as the mean free path is identical to the pore diameter or the wideness of the fissures in coal gas slippage-effects add to viscous flow. Thus, if the mean free path is small in comparison with the pore diameter, this effect doesn't exist any more.

This is the case in a high permeable media being flowed by a gas. W.H.Somerton et al (3) pointed out that the so called Klinkenberg-effect disappears at about 20 md or little more.

Other investigations (4) prooved, that also at high pressures - e.g. with the reduction of mean free path - gas slippage-effect becomes negligible and the apparent permeability values draw near the absolute values.

Because of the low permeability of coal samples - mostly less than 20 md - you have to eliminate gas slip by an increase of the outlet pressure p_2 and accordingly to that by an increase of the mean pressure $\bar{p}$. If you are able to keep constant the pressure drop Δp within a complete phase of heating up the sample one can create "pseudo-steady-state conditions" to certain extent. The flow sheet of the experimental scheme is to be seen in fig. 1.

Starting at the gas-supply station (1) gas is passing the pre-heater and the main-heater (4,5), a tube system to be heated (6), then it comes into the reactor (16). Afterwards it is flowing through different separating- and filtersystems (9,10). After having

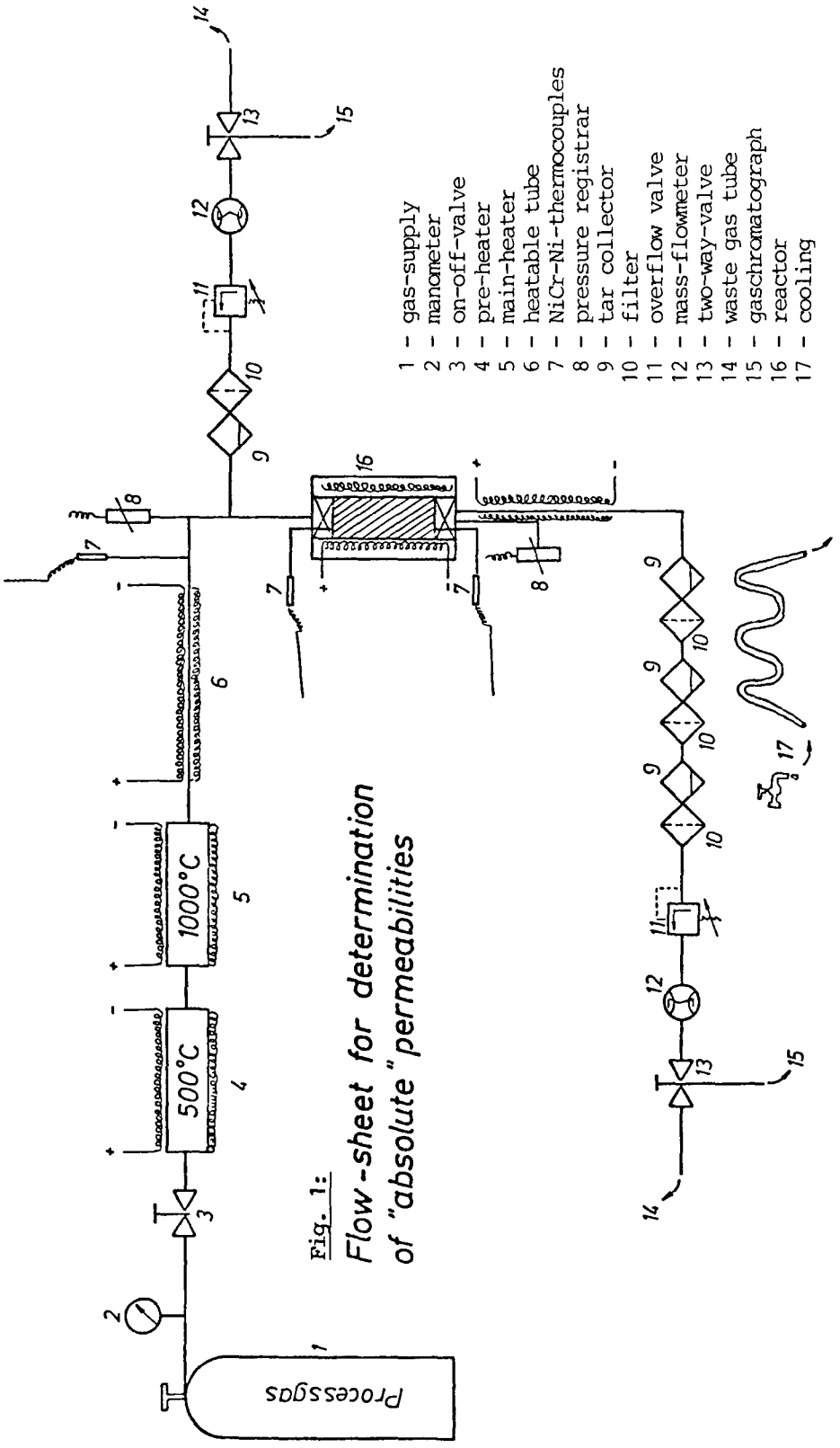

Fig. 1:
Flow-sheet for determination of "absolute" permeabilities

Fig. 2: Time-dependent ways of flow for a gas streaming within the plant

a) start and end of the run

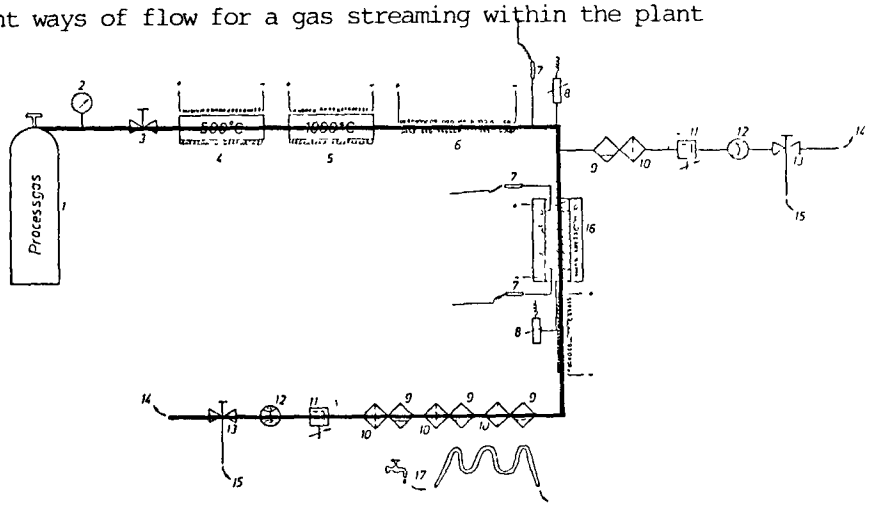

b) absolute sealing of the sample

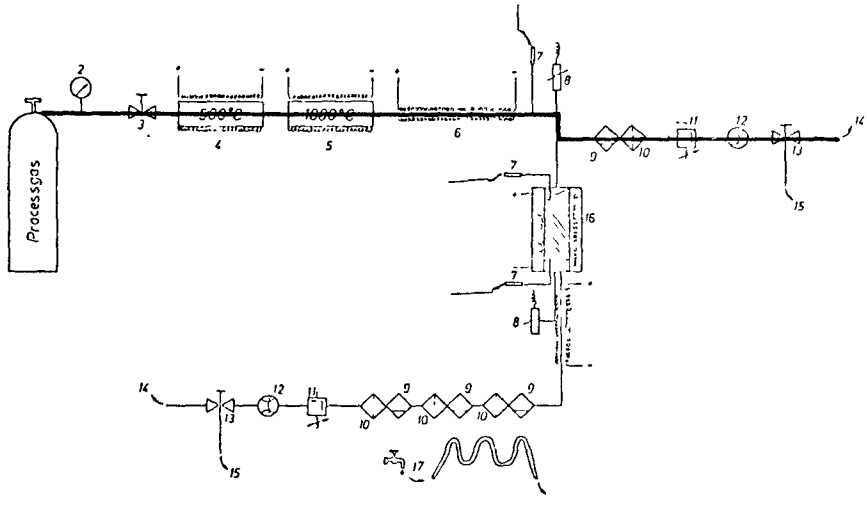

c) start of plastic range

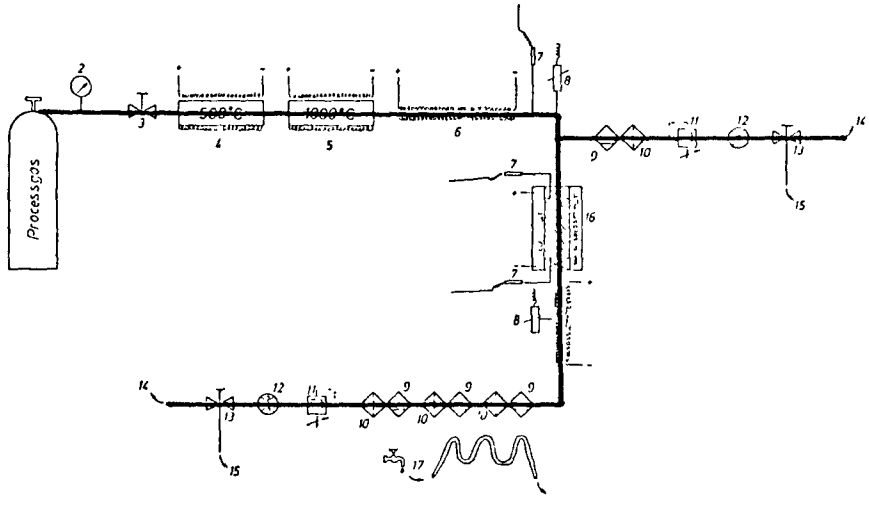

passed an overflow valve (11) it is arriving at a mass-flowmeter (12), wherefrom you can lead it either in a gaschromatograph (15) or in a waste-gas tube (14).
Beside of different cooling systems ($-21^{o}C$) the plant is fit out with heatings, thermocouples (7), pressure registrars (8) and so on which deliver their dates to a register-board.
At a constant flow rate into the plant first the pressure drop Δp is adjusted by means of the valves position 13 in front and behind the receptacle. By use of the valve pos. 3 mean pressure $\bar{p}$ is given. The inlet pressure p_1 is chosen in a manner which indeed allows the large quantity of the gas to flow through the sample (accordingly to the greater pressure drop $\Delta p_a = p_1 - p_2$ in comparison with the smaller pressure drop $\Delta p_b = p_1 - p_x$.
p_x is the maximum overflow-pressure of the valve pos. 13 to be adjusted. A smaller quantity for the present can flow through the high pressure-sided fitting.
The experiment operates with fixed p_1, p_2, Δp and $\bar{p}$ while coal is heated. Flow rates are registered and the variations evaluated. With reference to the phase of the attempt different ways of flow for the gas exist. This is shown in fig. 2.

The meaning of the term "permeability" in the following text must be explained: Own experiments show that when you heat 1 kg of high bituminous coal up to $900^{o}C$ nearly 180 litres of gas are produced by the coal. If you fancy a coal core was split up into an infinite number of segments and is streamed by a gas under gazification conditions it is understandable, that in the first segment only processgas is flowing and the part of the productgas is zero. At the end of the last segment the whole amount of the produced gas passes the coal face. It would be wrong to assume, that the quantity of the gas measured at the end of the sample had flown through all of the core. On the contrary the composition of gas alternates within the axial direction of the sample also does the gas quantity and the pressure.

In particular those facts have to be observed within the plastification range. Therefore, theoretically every single coal segment permits the calculation of a different permeability value at which further there is the difficulty of the disintegration of the bituminous substance to a great number of different gases. Accordingly, a multiple phase fluid system exists, which should be described by a relative permeability value.

Generally it should be pointed out, that under these conditions the evaluation of an absolute permeability is not possible if the exact definition of this term is taken into consideration. To mention some points: for example the calculation of a permeability constant k means, that you have to find out a material constant. This constant is valid to one single sample at which the geometric dimen-

sions (length, diameter, inner surface, pore distribution, porosity,...) have to be fixed. That fixation of the geometric behavior is not to be applied to temperature treated coal at all.

Strictly speaking, at every temperature we have to deal with an other specimen because of the continious changes of the coal. Moreover the calculated permeability constant of a coal at a certain temperature is not time-independent however, this is required by definition. So you have to realize, that in the further text the term "absolute permeability" is just an approachment to a fictive value.

At UCG one can describe several temperature zones, characterized by typical chemical reactions. Referring to K.Engin and H.Goergen (5) we devide the coal seam into the following temperature zones (also look at fig. 3):

1. "cold-seam-area"
   virgin rock; up to about 60°C; assuming a geothermic gradient of 3°C/100 m those temperatures can be found in the surrounding of deep layered coal (below 1500 m).
2. "drying-area"
   from 60°C up to the softening point of the coal. The softening point itself depends on pressure, kind of gas, kind of coal.
3. "smoulder-area"
   the temperature limits of this area are identically with the temperatures of the softening point and the resolidification point.
4. "semicoke- and coke-area"
   temperatures above those at the resolidification point.

In literature the temperature areas 2 and 3 do not exist but one can find them drawn together in the term "pyrolysis-zone". We define two areas, because at temperatures above the softening point after a while pseudo-steady-state conditions are achieved.

Those conditions make possible to calculate absolute permeability constants. However, within the plastic range the consistence of the coal is continiously changing. The process of dilatation can't be stopped, even when the heating is switched off. Thus, properly speaking it is impossible to evaluate an absolute permeability by usual methods.

EXPERIMENTAL LABORATORY WORK

The following types of coal are examined:

1. a low volatile bituminous coal, e.g. a non-baking coal of the Aachen-region/W-Germany and another one of Northwest France.
2. a medium volatile bituminous coal of the Ruhr-region and another one of the Saar-basin, W-Germany.
3. two different high volatile bituminous coals of the Saar-region, namely of the seam Elisabeth and Lummerschied, W-Germany.

Coal preparation, embed of the samples, stickers: The basic supposition to succeed in measuring absolute permea-

bilities is to avoid a bypass of gas in the reactor. The existence of a bypass would suggest much higher permeabilities.

Big dimensioned coal cores were put in a rubber sleeve similar to the system of a Hassler cell. The organic material is temperature-resistant up to 300°C.

Other partly very small samples had to be drilled or cut into prisms by diamond tool. After that they were sticked in the steel-inliner of the reactor. The sticker consists of two components: resin and hardener. Temperature resistance of the mixed glue is also limited to 300°C. The proper permeability of the organic rubbers and gluers is negligible.

With higher temperatures only inorganic materials are suitable to avoid gas bypass. The inorganic stickers have to fullfill high demands: they must be resistant to high temperatures as well as to aggressive media. They must be low permeable and have great adhesive power to coal and to steel; their thermic dilatation has to be on the same level than that of steel and finally they must have a viscosity which allowes to pour the ready mixed gluer into a narrow ring-shaped split.

Among a great number of purchasable ceramic materials there is none which can fullfill all demands.

One ceramic gluer possesses excellent properties. It is named "Thermoguß 2000" and is offered by W. Fritzke GmbH, Düsseldorf/W-Germany. The only handicap is that its adhesive power to coal is very low. This is shown in fig. 4, where it can be seen, that there is a fissure between the coal surface and the ceramic material. Only some adhesive bridges pretend a measurable adhesive power. They can be defined as epitactic pillars. This situation can be considered in fig. 5 and fig. 6 on the next page.

So the coal surface has to be treated by an other ceramic gluer, which has excellent adhesive power to coal as well as it has to Thermoguß 2000. Its name is "Autostic". It is offered by Carlton Brown and Partners Ltd., Elford/GB. Autostatic has to be put on the coal core surface in form of a thin layer by handling the brush.

Results of permeability tests:

As it will be shown several obstacles and barriers exist in a coal seam at UCG-conditions. The first obstacle is a natural one. It is the utmost low permeability of a coal seam in the rock surrounding at overburden pressure. The rate of gas flow is very low because of permeability constants at a level of at best some millidarcy or even microdarcy. Labor measurements demonstrate that with increasing coalification and at the same time with a decrease of pore space there is a very clear superposition of the possibly lower permeability by other more important influences. In particular one should mention those factors, which are characteristic to one specific sample only, such as there is the tectonic

Fig. 3:

Characteristic temperature zones of a coal seam at underground gasification conditions

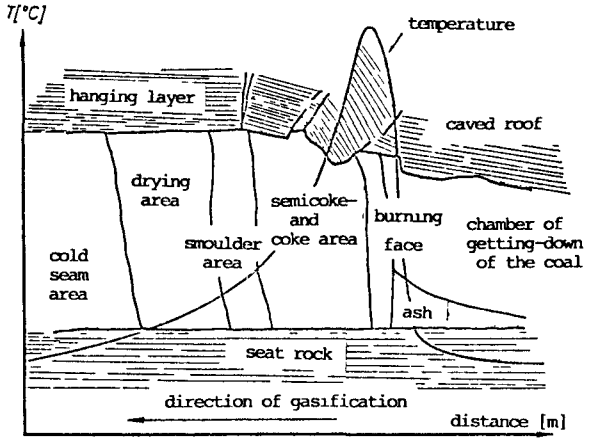

Fig. 4:

Photograph of the interface Thermoguß/ coal made by scanning electron microscope (magnification: 2200)

Fig. 5:

Adhesive bridge of Thermoguß 2000 on coal surface; photo made by scanning electron microscope (magnification: 200)

Fig. 6:

Siliceous Thermoguß-pillars showing epitactical intergrowth with coal-minerals (magnification: 1600)

stress or the mechanical stress during core extraction and, as a direct connection to that, the fissures in the sample.

The permeability constants of cold coal cores also depend on the petrographic consistence. Beside of the main ways for a gas flowing through a sample - the fissures and the cleat-system - there is great importance to the existence of fusite. Not the whole hollow space of single fusite cells is filled by organic or inorganic material. Thus, fusite doesn't create high resistence to a gas flowing through it. On the opposite vitrite has nearly no pore system and therefore creates high resistence to a streaming gas.

Table 1 shows the apparent constants of the two microlithotypes.

An other great advantage of fusite is that it keeps its high permeability also at high temperatures while that of vitrite decreases. The evolution of the permeability within the cold seam area and the drying area is shown in fig. 7.

The reason for the increase of the gaspermeability generally is a loss of water which is fixed so strongly that only high temperatures and simultaneously flowing gas can remove it. The decrease of the constants is attached with first dissolution phenomenons of the bituminous substance and with deposition of first tar products within the pore space.

Table 1: apparent permeability constants of fusite and vitrite (T=22°C)

fusite			vitrite		
p_1 [bar]	q_2 [cm³/s]	k_a [md]	p_1 [bar]	q_2 [cm³/s]	k_a [md]
0,4	4,9	5,0	40	1,8	0,081
			70	2,2	0,033

Fig. 7: temperature-dependent absolute permeability constants within the drying area

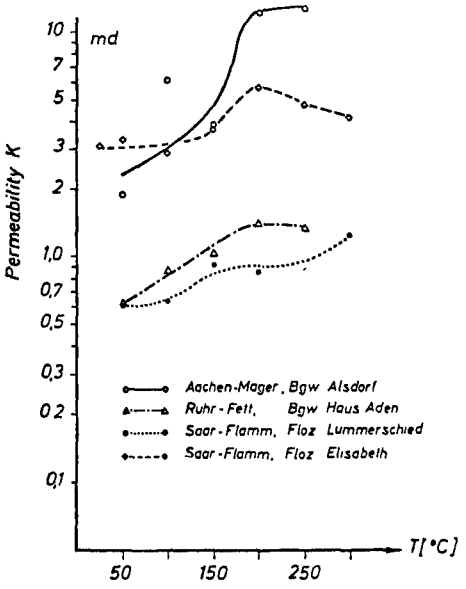

Fig. 8: absolute permeabilities within a temperature range of 50 to 700°C

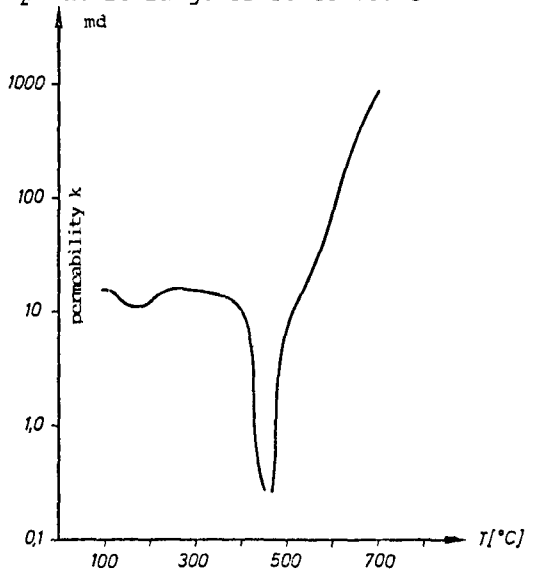

The next great barrier for the gas is an artificial one, which is built up simultaneously with the rise of plastification. The cause of the existence of this barrier and the extraordinary decrease of permeability is a "liquification" of the coal, that is to say a condition where the bituminous substance becomes liquified and at the same time movable. At this state coal also produces a great amount of gases and liquids.

The graph in fig. 8 shows the evolution of temperature de pendent permeability of a coal sample. The gaseous media was Nitrogen.

In table 2 the k-values of a coal measured with air are represented. This gas barrier only exists in high bituminous coal. There it makes the seam nearly impermeable within a temperature range of 300 to 450 ^{o}C.

No problems will exist if people will succeed in creating a coke. The permeability constants of coke are fit to gasify the seam at that state without great problems. Look at table 3.

Practicing the UCG by filter-method and uniflow conditions there is the second barrier at low temperatures of about 100^{o}C. At gasification conditions mineral loaded water and tar products are transported by the gas stream and deposited again in the pore space of the cold coal. There they accumulate and plug the pore system. As a result permeability decrease can be measured. The permeability constants shrink four to thirty times.

Table 2: absolute permeabilities within a temperature range of 100 to 515^{o}C (process-gas: air)

temperature [^{o}C]	permeability [md]
100	23,9
150	23,5
200	25,2
300	26
385	16,5
410	0,9
470	144
515	800

Table 3: absolute permeabilities of different semicoke- and coke-samples

temperature [^{o}C]	permeability [md] sample 1	sample 2	sample 3
500	205	96	115
550	440	170	285
600	590	430	530
700	690	710	660

(1): G.E.FOXWELL:"The Plastic State of Coal", Fuel III (3), 1924

(2): W.TERSCHÜREN:"Zur Gasdurchlässigkeit von Sedimentgestein des Oberkarbons"; Diss., Aachen 1978

(3): W.H.SOMERTON, J.M.SÖYLEMEZOGLU, R.C. DUDLEY:"Effect Stress on Permeability of Coal"; Int.J.Rock Mech. Min.Sci.& Geomech. Abstr., Vol 12, Pergamon Press 1975

(4): J.WAGNER:"Das Gasdurchlässigkeitsverhalten kompakter Steinkohlen unter währenden erhöhten Temperaturen und Drücken"; Diss. Saarbr. 1982

(5): K.ENGIN,H.GOERGEN:"Verfahrèn der UT-Vergasung"; Glückauf-Forschungshefte 34, 1973, Heft 5

3.15 THE MOBILITY OF FLUID/SOLID PHASES OF BITUMINOUS COAL SUBSTANCES AT HIGH PT-CONDITIONS

by

H. J. Schloemer 1/
B. Dernbecher 1/
K. Palz 1/

ABSTRACT

UCG of compact bituminous coal is accompanied by a mobility of tar, plastic mass and even by dead rocks. The plastic behavior was examined at insitu-conditions of static and dynamic pressures of N_2, CO_2 and air at temperatures up to the resolidification point. The results show a very different behavior dependent on the conditions used but specially different to the behavior of standard tested pulverized pressed coal samples.

Due to the plastic mobility of bituminous coal in front of the gasification zone a barrier is caused for the permeability of gas. The same is to be said for dead bands, which in a mixture of air with steam above 800°C are recrystalizing far from the place of origin. Accumulated in dependence of time of UCG the newly built crystals will be a barrier for the gasflow, too.

1/ Universität des Saarlandes
6600 Saarbrücken
Technische Mineralogie
West-Germany

INTODUCTION

Investigating the mobility of fluid and solid phases of coal substances in appliance to underground-gasification there is special interest for the transport and for the space needed of compact coal blocks dependent on high pressure and high temperature. Especially, our research programm deals with the behavior of bituminous coals in deep seated layers beneath about 1500 m or even deeper. In such depth we expect an overburden rock-pressure of about 360 bar and a temperature of about 55°C.

Of course, it's useless telling that coal consists of very different components, e.g. primary gas, bitumen and solids. All of them are of different composition from locality to locality, even from place to place in a very near vicinity. Of the previously mentioned components everywhere primary gas mainly consists of methane but both bitumen-contents and solids may vary considerably.

Especially the solids of coal have

to be differentiated very much, not only on account of differently built up carbonaceous materials (macerals) but also because of very differently composed dead rock bands.

MOBILITY OF FLUID PHASES

Those bitumen-contents behave very different dependent on both the amount within the coal present and the temperature exposed to.

Relative to temperature a range exists, within which high mobility of bitumen is to be observed. Of course, the carbonaceous solid material serves and determines the gasification process, the dead rock bands, naturally, cannot be gasified. But in presence of water their components are being mobilized at high pT-conditions. Therefore, the mineral constituents will take part in the gasification process, too.

In table 1 the criteria of the bituminous coal used for the discussed investigation is shown.

Table 1:

Bituminous coal of Saar-basin, FRG
Volatile matter: 36-39 % in vitrinite
Water content: 2-6 %
Swelling index: 1,5-4,0

First, let us deal with the mobility of the fluid phases, which mostly are part of the bitumen components. The thermal cracking followed by release of low volatile carbonhydrogens (alcane, alcene, acethylene) starts at about 250°C.

Pulverized pressed test samples of bitumineous coal used for the runs soften at about 375°C. At this point and at normal atmospheric pressure the coal swells, blows out and rises. A further thermal cracking of carbon-hydrogen results. All this is accompanied by a slow moving process of dilatation, which causes a moderate increase of plasticity within the coal.

At high pressures, which are necessary for UCG at deep seated seams, the plastic behavior and therefore the mobility - called dilatation - in advance of the burning front in the seam is very different from the one of the pulverized pressed coal. The extent of the plastic mobility of bitumineous coals used is mainly determined by pressure. Several runs show that one has to distinguish referring to the pressure used between static and dynamic pressures. Not only that at high pT-conditions the coal body moves with the direction of the gasflow introduced into the seam, in contrary it also moves against the gasflow and consequently a drive-pressure is being built up.

In an UCG-simulating reactor the different appearance of plastic coal is shown mobilized simultaneously into the same direction with the gasflow used (fig. 1) and in contrast even at higher pressures the coal mass moves against the direction of the impressed gasflow (fig. 2).

Fig. 1:
Plastic dilatation of bitumineous coal with the direction of gasflow of N_2; p=20 bar, T=400°C.

Further there is a considerable influence of the atmosphere, e.g. N_2, CO_2 or air. The plastic behavior is also dependent upon the water content, which may be adsorbed on the surface of different cleavage systems or filled in closed pores.

Fig. 2:
Plastic dilatation of bituminous coal against the direction of gasflow; p=40 bar, T=400°C.

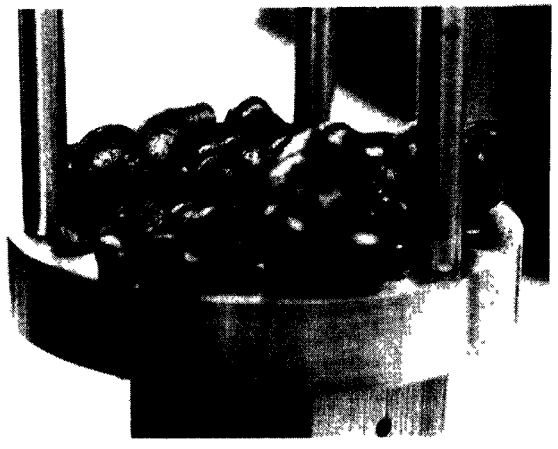

While the plastic range of dry coal samples at high static air pressures of about 30 bar stretches over a range of 200°C, at dynamic conditions a plastic move can only be registered over a range of about 45°C. Fig. 3 represents the results of numerous runs with compact bituminous coals of the Saar-basin both at static and dynamic air conditions showing the softening (lower line) and the resolidifying (upper line) of the coal.

Fig. 3:
Comparison of plastic range of dried bituminous coal samples of the Saar-basin at static and dynamic air pressures

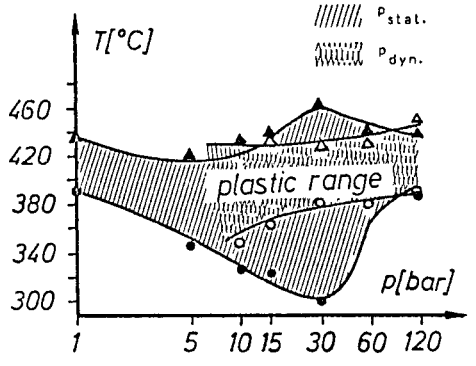

Besides the knowledge that up to 30 bar the plastic range widens it is of interest that at even higher static pressures the temperature range, at which the coal samples become plastic, is shrinking again to about 50°C. This temperature range corresponds to determinations made on pressed pulverized test samples. Further, it shall be noticed, that the mobility of the plastic coal mass at 30 bar already starts at 300°C.

It is unnesessary to say that the mobility of coal components is of highest importance maintaining a necessary gas transport - may it be processgas or productgas - required to keep the UCG-process going. The softening of coal at low temperatures causes an early move and creates a dilatation, which will lead to a barrier for the gas permeability that hardly can be overturned.

The amount of dilatation at the resolidification point at different atmospheres of N_2, CO_2 and air is shown in fig. 4.

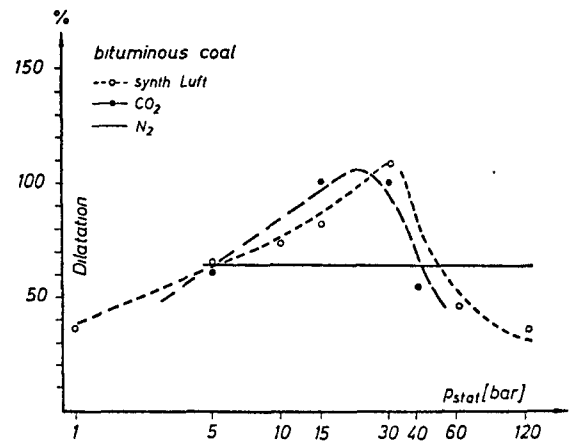

Fig. 4:
Dilatation of compact coal samples at different atmospheres of static N_2-, CO_2-, air-pressures.

As one can see the dilatation achieves twice the space of the original size at CO_2 or air pressures. The maximum of dilatation is reached at the same pressure as the plastic temperature range has attained the most extension. In presence of CO_2-atmosphere bituminous coal already yields a maximum dilatation 10 bar lower than with air. The presence of nitrogen, thereagainst, shows no alteration in dilatation dependent on static pressures.

As already said discussing the comparison of plastic behavior at static and dynamic pressure conditions the volumetric behavior at both pressure-relations is different, too. The results of comparing investigations are demonstrated in fig. 5.

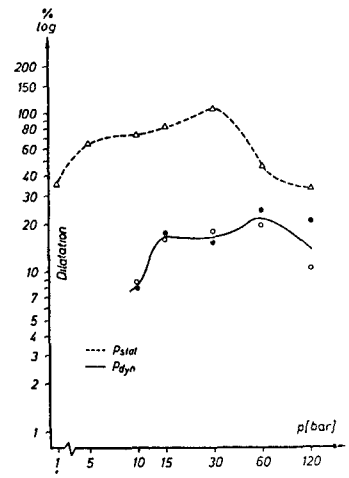

Fig. 5:
Comparison of dilatation of dried coal samples at static and dynamic air pressures.

As can be seen at 30 bar static pressure an increase of dilatation of 100 % is obtained, whereas those samples at dynamic conditions only attain a raise of less than 25 %.

In contrast to dried samples water-saturated coal monoliths have - on account of their relatively high water content - an additional reaction potential at their disposal. Of course, at static conditions it is to be expected that the mobility of coal will increase within the plastic temperature range.

Dried samples we have recognized at

raising dynamic pressures rather show constant mobility, at least a reduction compared to static conditions. Will the behavior be the same with water saturated samples? The results of numerous runs measured at insitu conditions answer the question in fig. 6.

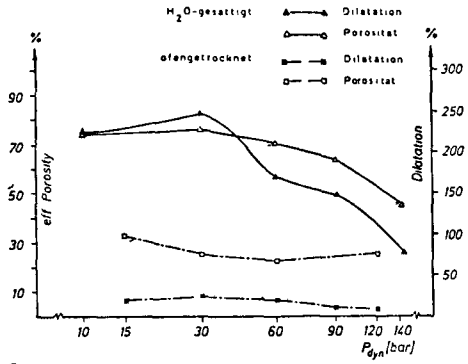

Fig. 6:
Relation between dilatation maximum and effective porosity of bituminous coals of the Saar-basin at dry and water saturated conditions dependent on dynamic air pressures.

Thermally conditioned dilatation of solids after fall of temperature may regressive or remain stable. In cases, in which such volumetric changes become stable, they are caused either by phase transformations, chemical reactions or by origin of porespace. In bituminous coals such extensions are not regressive. They are accompanied by changes within the coal body and they are the results of fluid components, which are as well exposed to chemical reactions as to changes of place.

The coal having passed the plastic range will resolidify attaining the semi-coke state. At fall of temperature to room conditions the new volumetric state may be measured by means of porometric determinations. This has been done with samples treated like shown in fig. 6. Therefore, in this figure relations between dilatation maxima and effective porosities of those coal samples are compared. Expectedly they show a very similar course dependent on dynamic pressures but the development of such a high dilatation of about 250 % at water saturated conditions is yet rather surprising.

Dry coals reach in analogy to the volumetric behavior low porosities. Water saturated bituminous coals create semi-cokes with extremely high porosities of about 75 %. For the gaspermeability, of course, the high porosity above the resolidification point is really favourable, but beyond this point the permeability will become almost zero, because every burning front at UCG possesses a temperature range, within which the mobility of fluid phases creates some kind of dilatation that ends any gasflow.

But, not only the mobility of dissolved fluid phases of thermobitumen products gives rise to a barrier for the gasflow, the mobility of solid phases may possibly cause an other barrier, too.

MOBILITY OF SOLID PHASES

Admittedly, if for UCG only air is used, no transportation of solid phases can be observed. The same is done when the transport-medium consistsof

a mixture of air and steam at temperatures below 800°C. However, mobilisation exists in considerable amount at temperatures of more than 800°C, pressures of 30 bar and higher and in presence of air and steam.

In fig. 7 a scheme of 4 reactors placed one after the other is shown. Cores of underground bored cylindrical compact coals were put into the 1st reactor so that it was filled nearly 70 %.

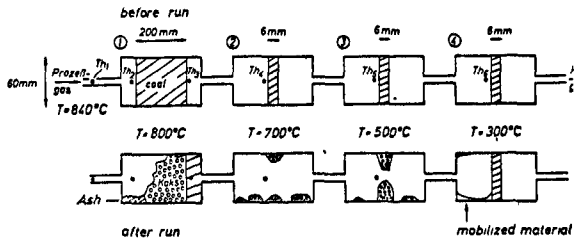

Fig. 7: Scheme for runs of UCG in a serie of 4 reactors at decreasing temperatures and at dynamic pressures of $\bar{p}$ = 40 bar.

After the 1st container three other receptacles were filled with thin slices of coal. The average amount of dirt rocks within selected coal-cores was about 25 %. The mineral composition has been determined of slices of both ends of the core used by means of x-ray phase analysis. The result is shown in table 2. Each reactor was run at a certain temperature. At Th_1=840°C processgas consisting of 75 % respectively 25 % steam by weight was introduced. After about 35 min in the 1st reactor 40 % of the coal body has been gasified, leaving a rest of semi-coke, partially dissolved dirt rock bands and ash. Within the rock bands SEM-pictures demonstrate newly built sanidine, $KAlSi_3O_8$, and mullite, $Al_6Si_2O_{13}$-crystals in a residual matrix of quartz, muscowite- and chlorite-layers (fig. 8). The x-ray analysis showed yet traces of cristobalite, too.

Fig. 8: SEM-photograph of residual dirt rock bands of bituminous coal of Saar-basin; T=800°C, p=60 bar, M: 2000.

An artificially made increase of temperature in reactor 2 and 3, however, has caused a decline of the coal-slices converting them to semi-coke; besides tar-products no mineral-phases could be proven. In contrast, reactor 4 had collected about 1.2 g of mobilized material, which consisted of 4 % talc and corundum and 96 % tar products. The crystallisation of talc, $Mg_3Si_4O_{10}(OH)_2$ and corundum has exceptionally to be ascribed to the dissolution of chlorite, $Mg_3Fe_2Al(AlSi_3O_{10})(OH)_8$. The amount of 4 % of mineral components within the tar mass in the 4th reactor corresponds to a mobility of about 0.05 % related to the amount of dirt rock in the core of reactor 1. The

precipitation of such quantities of mineral components seems to be small, but being transported over a path of 3 m in 35 min one should consider it.

The further investigations were continued in the same manner as discussed before, but in addition the mixture air:steam was enriched with respect to the amount of water and the flowrate of the processgas was put in at D_1=1 kg/h and D_2=2 kg/h.

Because of the decline of the coal-slices in the 2nd and 3rd receptacle at 700° or 500°C the containers remained empty and the fall of temperature was changed to 600°, 300° and the last one at 130°C. The altered scheme is shown in fig. 9.
The results of numerous runs are a bit different compared with the ones discussed before.
The amount of solids is composed of parts of inorganic materials and parts of soot. Both of them have been examined separately. Both are embedded in large mass of tar. The tar products, which in all runs represent the main mobilized materials (60-85 %) show a different behavior or dependent on both flowrates.

In fig. 10 the transport of tar-products dependent on flowrates of processgas and of air/steam-mixtures is shown. While at a flowrate of 1 kg/h already in reactor-cell A3, 600°C, an amount of 10-15 % of tar is present, at doubled rate only in cell A4, 300°C, tar can be registered.

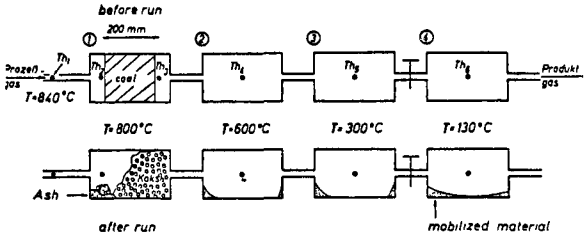

Fig. 9: Scheme of 4 reactor-cells for UCG connected in series, of which the first only is filled with a compact coal core.

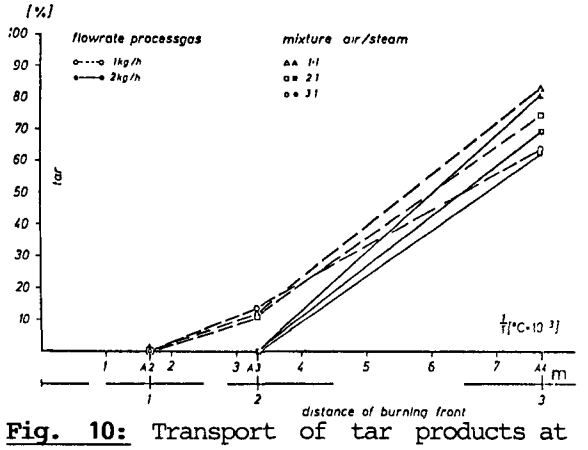

Fig. 10: Transport of tar products at fall of temperatures dependent on flowrates of processgas and of air/steam-mixtures.

The cause seems to be that the precipitation at a temperature of 300°C is de pendent on more time needed for moving, which at a higher flowrate is not given. The different air/steam-mixtures seem not to be of great importance.

An interesting behavior show the solids soot and the inorganic components. In relation to the whole amount of mobilized material they represent

15-40 %, of which soot takes part with 3-6 %. The rest has to be accounted to inorganic materials, of which most is of crystalline character. Ref erring to the behavior of soot there is some analogy to the one of tar, if one considers the dependence upon the gasflow. But, in contrast to the mobility of tar soot already precipitates at a smaller flowrate 1 kg/h in the first cell A2, 600°C, after the gasification reactor, whereas at doubled flowrate in this cell no soot is found yet. Fig. 11 demonstrates the transport of soot dependent on fall of temperature at UCG-like condition.

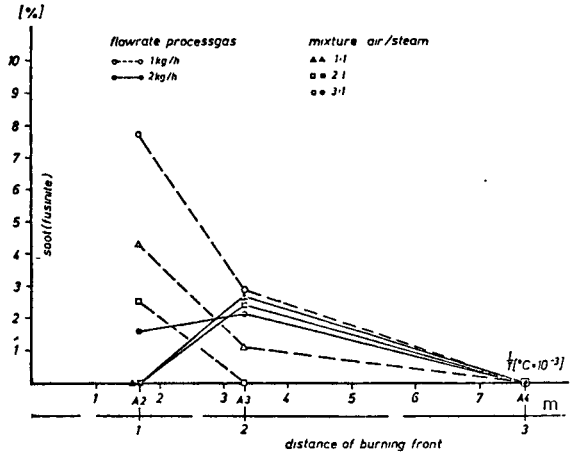

Fig. 11: Mobility of soot dependent on fall of temperature, $\bar{p}$=40 bars.

At a flowrate of 2 kg/h most of soot is found in cell A3, 300°C. The last cell always is off of soot.

The comparison of the transport behavior af tar with the one of soot and also of inorganic materials, which specially will be discusses afterwards, shows that the large mass of tar, though in a fluid state, does not be regarded a transport medium.

The most attention is paid to the behavior of the inorganic components mobilized by UCG. The inorganic materials consist partly of unordered solids, which by means of x-ray analysis cannot be identified. The amount of unordered materials only has been determined, which resembles an average part of 20-25 % related to all of the precipitated solids. By means of SEM the unordered composition is distributed mostly on silica compounds with large amounts of Fe_2O_3, medium parts of Al_2O_3 and smaller ones of CaO, MgO and K_2O. In addition it must be said, that the Fe_2O_3 content does not come from the inliner of the reactors because those contained as much as none Fe.

About 75-80 % of the inorganic solids are crystallized but x-ray analysis shows that one has to distinguish between newly built crystals "far from the place of UCG" and minerals built "at the place of UCG", which are found as so called flue ash together with minerals, which came from the dirt bands of the coal core.

The first called "far from the place of UCG" precipitated phases have been determined:

Mohrite $(NH_4)_2Fe(SO_4)_2 \cdot 6H_2O$
Mascagnite $(NH_4)_2SO_4$
Salmiak NH_4Cl
Magnetite Fe_3O_4

The second called phases coming from

"the place of UCG" found in the cells A2, A3, A4 are:
Anhydrite $CaSO_4$
Dolomite $CaMg(CO_3)_2$
Quartz SiO_2

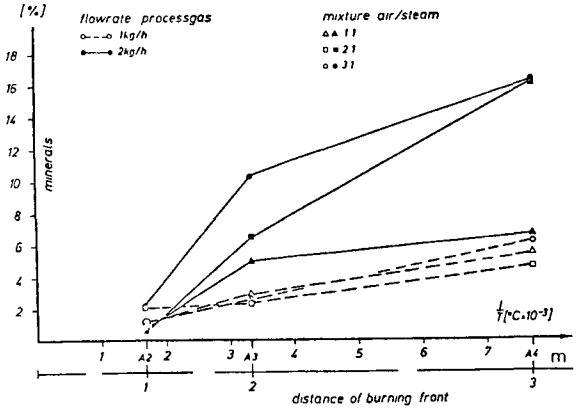

Fig. 12: Mobility of inorganic crystallized solids dependent on fall of temperature at UCG, $\bar{p}$=40 bars.

Of the last mentioned phases anhydrite, dolomite and quartz only anhydrite has to be considered as newly built crystals, dolomite and quartz already are constituents of the dirt rocks and have been transported as flue dust.

Of all the above mentioned phases only magnetite could be detected by SEM. Fig. 13 demonstrates one of the best built crystals.

The results of the quantitative phase analysis show that there is an increase of mineral deposits dependent on fall of temperature and simultaneously more distant from the coal gasification of the 1st reactor. The amount of precipitated solids is significantly determined by the flowrate of the processgas mixture.

Fig. 13: SEM-photograph of newly built idiomorphic magnetites at UCG-like conditions: flowrate 2 kg/h, air/steam-mixture 1:1, T=600°C, $\bar{p}$=40 bars.

While the whole mass transport with a flowrate of 1 kg/h lies at about 4-6 %, the flowrate of 2 kg/h raises the precipitates to about 16 %. One cannot relate this high amount of newly built solid to the amount of minerals of the dirt rock, because most of the solids consist of ammonium phases combined with sulfates or chlorine.

The sulfates are coming from the corroded pyrite, the chlorine comes out of the public water reservoires.

But it can be said, that the average relation of the ammonium phases is about 4:1. Referring to this relation the mobility of parts of the dirt bands lies at about 0.08 %.

Proceedings of the Ninth Annual Underground Coal Gasification Symposium, August 1983

3.16 COAL PYROLYSIS AND METHANE DECOMPOSITION IN THE PRESENCE OF A HOT CHAR BED

by

P. E. Peters[1/]
S. W. Kang[1/]
C. B. Thorsness[1/]

ABSTRACT

The products of coal pyrolysis can have a significant impact on the ultimate products produced from underground coal gasification (UGG) systems, especially the hydrocarbons. As a result, some type of pyrolysis submodel is necessary to successfully model a UCG system. Due to the lack of data, we have in the past used the results of powder pyrolysis experiments for modeling purposes. Although these data represent a well-defined system, they probably are not analogous to the underground system. Unlike the powder pyrolysis experiments, the underground system produces pyrolysis products characteristic of all temperature regimes simultaneously and continuously. In addition, these products undoubtedly are in contact with hot gas, char, and/or ash for a much longer time than is typical in the powder experiments.

With this in mind, we are performing a series of experiments to provide an alternate set of pyrolysis data. In these experiments coal is continuously fed onto a hot bed of char. The pyrolysis products are swept down through the hot char before being removed from the reactor. In this paper we describe the results of these experiments, which have to date been performed at temperatures of 500-900°C and pressures of 100-600 kPa. The data show that methane production reaches a peak near 800°C and that the influence of the modest pressure change from 100 to 600 kPa is small.

In conjunction with these lumped experiments we are also looking at the reactions of methane with hot char and gas, partly as a model compound for the pyrolysis process and partly because of methane's importance as a UCG product. We have conducted a variety of experiments using homogeneous reactors and reactors packed with char. The data from these experiments are presented and an engineering rate expression is derived for methane decomposition. The derived expression is consistent with the increased hydrogen production and decreased methane production seen in the continuous feed experiments for temperatures above 800°C. We find the methane decomposition expression predicts that for typical UCG processes, methane cannot exist in the presence of char for more than 1.5 minutes at 900°C or for more than 30 seconds at 1000°C.

INTRODUCTION

Over the past several years, a number of models for estimating the produced gas compositions from underground coal gasification (UCG) systems have been developed. In general, most of these models deal quite adequately with the major components H_2, CO_2, CO, N_2, and H_2O, but are less successful in dealing with the hydrocarbon species. This is primarily due to the complexity of reaction pathways which lead to the hydrocarbon products, the lack of sufficient experimental data, and the failure of simple thermodynamic considerations, which work so well for the major nonhydrocarbon species, to yield any useful estimates.

The pyrolysis of coal is the ultimate source of nearly all the hydrocarbons produced in the UCG process. As a result, a

[1/]Lawrence Livermore National Laboratory, Livermore, CA 94550.

model for this process is required if we are to make significant improvements in UCG gas compositional models. Much work has been done to understand the fundamentals of coal pyrolysis in simple systems. However, due to the complexity of the UCG process, it is unlikely that a definite model will be available in the near term for predicting pyrolysis yields during UCG.

Due to a lack of fundamental understanding, the modeling of UCG pyrolysis must utilize results obtained experimentally. To date we have relied on the work of Campbell,[1,2] who studied primary pyrolysis via ramped heating of powdered coal. Although Campbell's data are a consistent set of data, they were obtained under idealized conditions where, unlike the UCG system, secondary reactions are minimized.

To provide an alternate set of data, we have designed an experimental apparatus where secondary reaction effects are maximized. The experimental apparatus we have used consists of a bed of hot char onto which coal is continuously dropped. This results in a composite sample of primary pyrolysis products being continuously introduced to a reactive hot char bed. We are generating a consistent set of pyrolysis data with this setup which may serve, along with the powder data, to bound the possible pyrolysis behavior in a UCG system.

In conjunction with the continuous feed experiments, we have also measured batch pyrolysis yields obtained while preparing the char bed. Products produced in this manner may be compared to the powder pyrolysis data to show the influence of size and heating rate on pyrolysis yield.

In addition to the lumped pyrolysis experiments, we are performing experiments which single out methane for special consideration. The motivation here is that methane is the most important hydrocarbon present in a UCG system. We are interested in quantifying its generation and destruction in a UCG process. Unfortunately, the sources of methane in the system are many (e.g., secondary reactions of any number of pyrolysis products, primary pyrolysis, or hydrogenation of the intermediate metachar produced during pyrolysis). The current level of effort is not up to tackling this complex problem. However, the destruction of methane, at least in an engineering sense, is a much simpler problem. Methane is destroyed in a UCG system primarily by combustion and pyrolysis. The combustion question is mainly one of whether oxygen is available, and it is outside the scope of this report. The destruction of methane by coking is, on the other hand, a matter which is subject to relatively simple experimental investigation. Past work has led to an adequate description and rate expression for methane decomposition in the homogeneous gas phase, and has indicated that the decomposition may be considerably enhanced by the presence of char.[3-5] An adequate rate expression is not available, however, for methane decomposition in the presence of char. For this reason we have performed a series of experiments aimed at developing an engineering rate expression for the thermal decomposition of methane in the presence of hot char.

In this report we first describe the experimental apparatus and procedures used to generate the batch pyrolysis, continuous feed pyrolysis, and methane decomposition data. The data obtained to date is then presented, and the pyrolysis data is compared with the powder data of Campbell. Finally, a tentative methane decomposition rate expression is developed and is shown to be consistent with methane data from the continuous feed pyrolysis experiments.

EXPERIMENTAL DETAILS

Four basic types of experiments have been performed. Two types of pyrolysis experiments, the batch and continuous feed experiments, were done in a large reactor, 3 in. (7.6 cm) in diameter and 36 in. (91 cm) long. Methane decomposition experiments were performed in this same large reactor and in a smaller one that was 1 in. (2.5 cm) in diameter and 6 in. (15 cm) long.

The Large Reactor

The large reactor is shown schematically in Fig. 1. The basic components were a 3-in.-diameter Inconel tube surrounded by heaters, a coal feed hopper for the continuous feed experiments, and a tar/water trap at the exit of the reactor. Four thermocouples were located

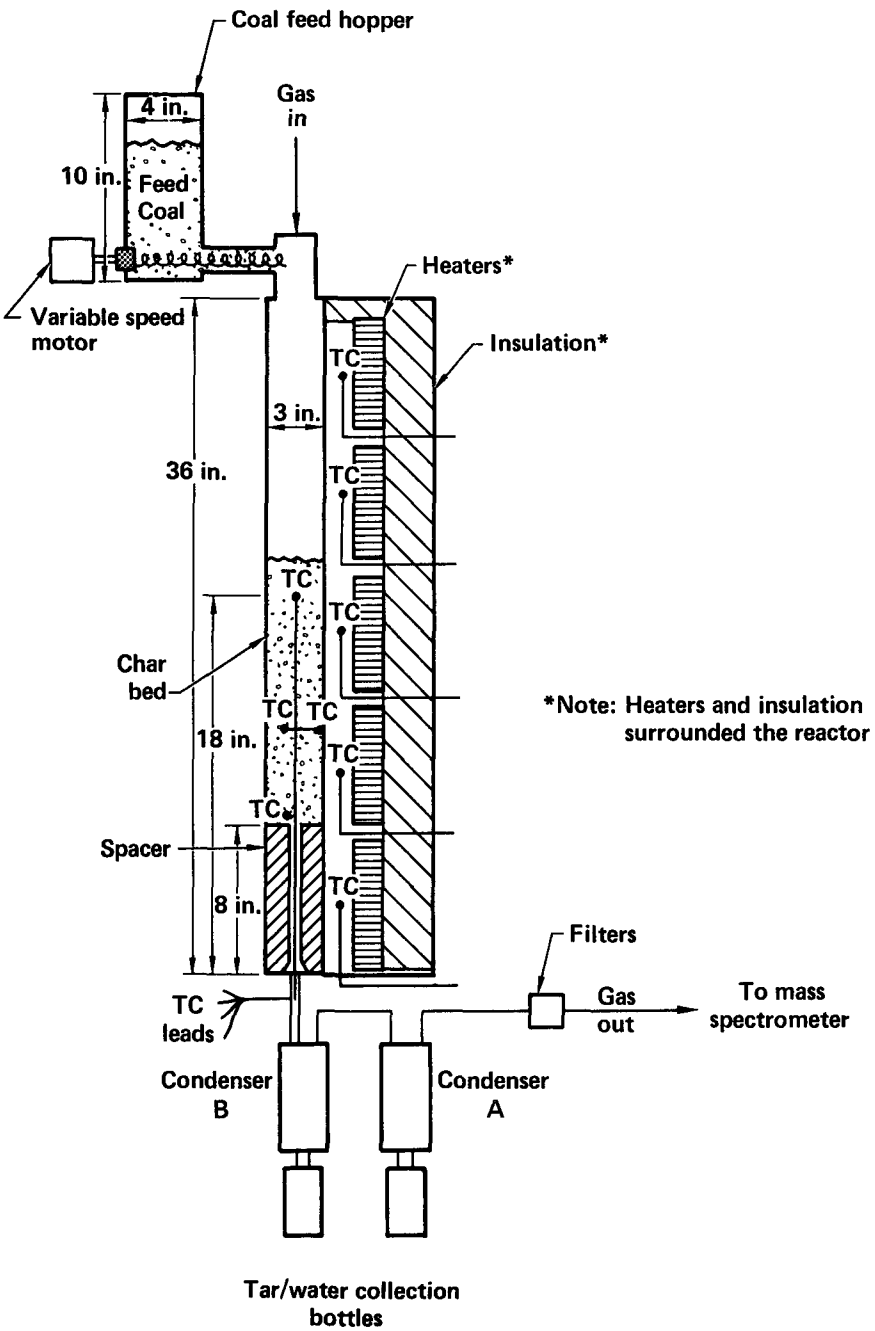

Fig. 1. The large reactor system with coal feeder.

inside the reactor tube to monitor the temperature of the char bed. An additional five thermocouples outside the tube were used for feedback control for the heaters. The top of the reactor was secured by bolts and was removed to load the coal into the main reactor. At the bottom end of the reactor a stainless steel plug with a central hole was used to support the char bed. During the methane decomposition experiments a plunger arrangement, not shown, was used at the top of the reactor to remove the dead space above the char bed.

Provisions were made to meter flow injected into the reactor. The injected gas during the pyrolysis experiments was

argon, which was used as a tracer and sweep gas; during the methane decomposition runs the injected gas was a mixture of argon, methane, and sometimes hydrogen.

The produced gas exits the reactor and passes through a condenser system used to trap tars and water. The dry gas is filtered and then sent on for analysis by an on-line time-of-flight mass spectrometer. The tar/water trap underwent modifications over the course of the experiments. Initial experiments were carried out with a single condenser and then later a second condenser was added as shown in Fig. 1. In our last run we changed the trap to a system in which the exit gas was bubbled through an organic solvent, methylene chloride. We feel this latter system will allow us to clean the gas up better and to obtain a more quantitative measurement of the produced tar.

The hopper assembly was only present for the pyrolysis experiments. Through the use of a variable speed motor attached to an auger device it was used to feed coal into the main reactor for the continuous feed experiments. We were able to obtain a well-controlled constant feed rate with this arrangement.

As stated above, the large reactor was used to perform three types of experiments: batch pyrolysis experiments, continuous feed experiment, and methane decomposition experiments. The batch pyrolysis experiments were really just the char bed preparation phase of the other two experiments. They consisted of loading the main reactor with sized coal 1/4-1/2 in. (0.6-1.3 cm). This was about 5 lb (2 kg) of coal, which created a bed about 15 in. (40 cm) high. Argon flow was turned on at about 2 mmol/s. The heaters were then turned on to give a temperature of 250-300°C, which was used to dry the coal. The drying process took about 2-3 hours. After drying, the tar/water traps were emptied and the heaters were turned up to raise the temperature to the first desired plateau temperature. This plateau temperature was held until the gas evolution was essentially complete. The time a temperature was held varied somewhat but averaged about 4 hours. Before increasing the temperature to the next plateau, the tar/water traps were emptied. Depending on the particular run, anywhere from two to five temperature plateaus were used in a given experiment. The final plateau was always chosen to be near 900°C.

The contents of the tar/water traps corresponding to each of the temperature plateaus was divided into an aqueous and organic phase. The organic phase was called tar and the aqueous phase water for the purposes of these experiments. Most of the data was obtained by using toluene as a solvent for the tar and to assist in the separation. The nature of this separation, the possibility of loss of toluene, and the difficulty in trapping all the tar make the tar numbers obtained subject to considerable uncertainty. We believe these uncertainties were reduced in the last experiment (PYR-8), where the methylene chloride bath was used as the tar/water trap. The trapping of tar appeared to be more efficient and the tar number was obtained by evaporating the methylene chloride (boiling point 40°C).

At the end of batch pyrolysis or bed preparation, a continuous feed or methane decomposition experiment was performed. For the continuous feed experiments, the char bed in the reaction was first brought to the desired temperature and then the coal feed was turned on. The coal was fed into the main reactor for about four hours. This resulted in about 0.5 kg of total coal feed. At the end of the feed period, the tar/water trap was emptied and the coal left in the hopper measured so that the exact amount of feed could be determined. A sample was dried in a vacuum oven to determine the moisture content. The coal placed in the hopper was partially dried to allow it to flow freely. This led to a variability in the moisture content of the coal from run to run. For the last run, the coal feed was dried in a vacuum oven at 110°C overnight. The tar/water trap contents were analyzed in the same way as in the batch phase.

For the methane decomposition experiments, the hopper was not present. At the end of the char preparation phase, the char bed was brought to the desired temperature and then a 5%-by-volume mixture of methane in argon was fed into the reactor at a prescribed flow rate. On several experiments, flow rates and bed temperatures were changed during the course of the run. Single runs lasted up to 8 hours.

Small Reactor

The small reactor is shown schematically in Fig. 2. It was composed of a 1-in. Inconel tube surrounded by heaters and an

Inconel coil for preheating the gas feed. Three thermocouples were placed inside the reactor to monitor the char temperature. An additional thermocouple was positioned outside the reactor to be used for heater control. The top of the reactor tube was secured by a threaded cap.

Char from previous pyrolysis experiments and from batch preparation was loaded into the reactor under argon. The reactor was then heated to the desired experimental temperature with a continuous argon purge flow through the reactor tube. The range of experimental temperatures was from 751°C to 928°C. After establishing the desired experimental temperatures, mixtures of argon, methane, and hydrogen were fed through the reactor, and the extent of decomposition was determined by mass spectrographic analysis of the reactor exit gas. Flow rates, pressures, and temperatures were held constant during the course of each run. The duration of an individual run averaged about 5 hours once methane decomposition had commenced.

The batch char preparation consisted of heating the coal particles to a temperature of 935°C at a rate of 5°C/min, and then holding the temperature at 935°C for 2 hours. Argon was fed to the coal/char continuously during the heating process. No products were collected.

The Coal

The coal used in all the experiments reported here was subbituminous coal from the Wyodak mine located in the Powder River Basin. The first step in the coal preparation was the grinding and sizing of the coal into two fractions--a 1/4-1/2 in. (0.6-1.3 cm) size for use in the large reactor char bed, and a smaller size fraction 1/8-1/4 in. (0.3-0.6 cm) for the coal feeder and for the small reactor experiments. The proximate and ultimate analyses for the coal are shown in Table 1.

RESULTS

Batch Pyrolysis Results

The data from eight char bed preparation steps have been reduced and represent what we call here the batch pyrolysis data. Typical gas evolution data is shown in Fig. 3 for one of the runs. Here for simplicity only the produced dry gas mole

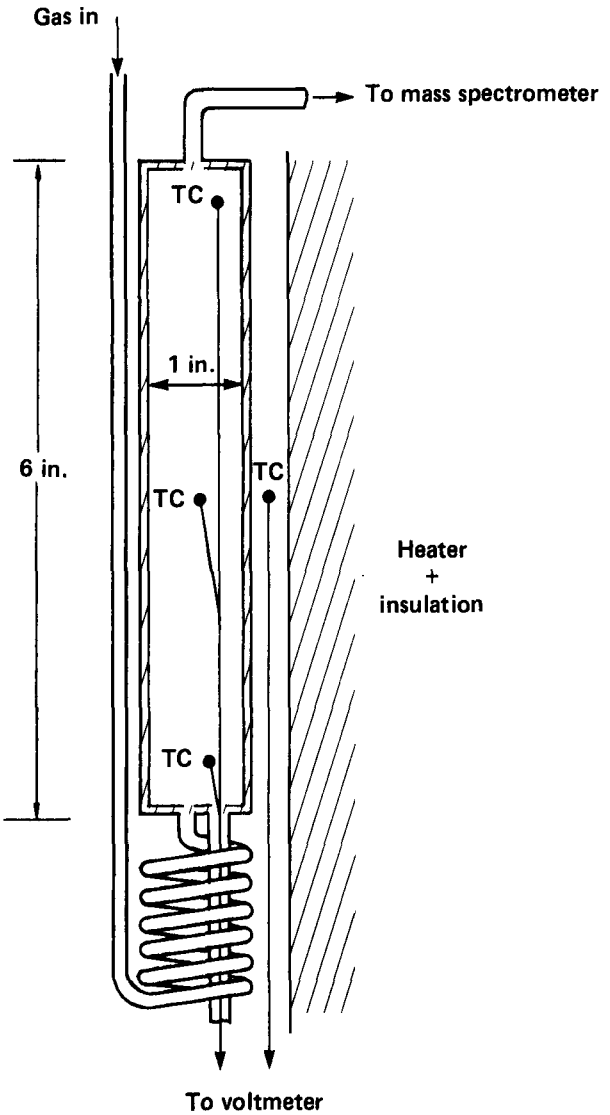

Fig. 2. The small reactor system.

Table 1. Coal composition (wt%).

	Feed coal (3.2-6.4 mm)	Batch coal (6.4-12.7 mm)
Proximate analysis:		
Moisture[a]	24.8	29.3
Ash	7.6	4.3
Volatile	28.9	29.9
Fixed carbon	38.7	36.5
Ultimate analysis (dry):		
Ash	10.2	6.1
Sulfur	0.6	0.5
Nitrogen	1.1	1.0
Carbon	63.8	66.3
Hydrogen	4.5	4.6
Oxygen	19.9	21.6

[a]Equilibrium moisture.

fractions of hydrogen and methane are shown. Also shown is the thermal history for this run. In Fig. 4, this data has been combined with flow rate information to give the total species production as a function of time. In all these runs a 1.5- to-2-mmol/s argon gas sweep was maintained, and the pressure was maintained near 130 kPa.

In Figs. 5-10, the data for the eight runs are shown. Here the species production per unit of dry, ash-free coal as a function of temperature is given. For the gas species, the unit of coal is a one-carbon-basis coal pseudo-molecule, while for the water and tar the weight of char coal is used. The number of data points varies for each experiment because of the difference in the number of temperature plateaus used. The data is for the total production at the end of a temperature plateau period. Also shown on the figure is the more continuous data from the ramped temperature pyrolysis experiments of Campbell[1,2] on essentially the same coal.

It is interesting to note that the data indicate the relative path independence of the final product yields. We see no clear evidence that the number of intermediate temperature plateaus between one temperature level and another influence the product yields significantly.

In addition to the gases shown in Figs. 5-10, we did obtain data on total ethane evolution. The data indicated all the ethane was evolved by 600-700°C and the final yield averaged 0.4 mole/mole coal. These results are consistent with the powder data.

Comparing the batch data and the powder data, we see that the shapes of the species production curves are generally similar. Both are monotonically increasing functions of temperature. The batch data precedes the powder data by about 100°C. This is probably a result of the temperature plateaus built into the batch experiments which are not present in the powder experiments. The powder experiments used a continuously increasing (3°C/min) temperature ramp. The batch data indicated more CO and H_2 production and slightly less CH_4. We attribute these changes to the increased possibility of secondary reaction in the batch geometry resulting from the greater contact with hot char and the longer residence times in the heated zone.

The tar data, Fig. 10, show some scatter. In particular, the results from the PYR-1 experiment seem inconsistent with the other data and probably should be disregarded. The results for the PYR-8 experiment show a slightly higher tar production than the other runs. This, we

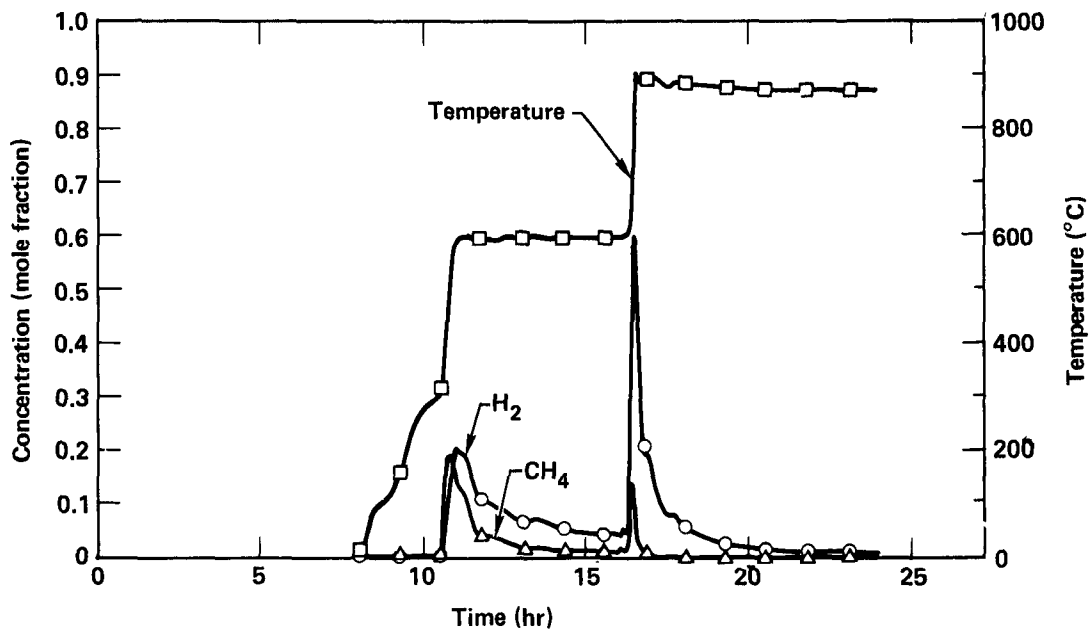

Fig. 3. Typical data for a batch pyrolysis experiment (PYR-5).

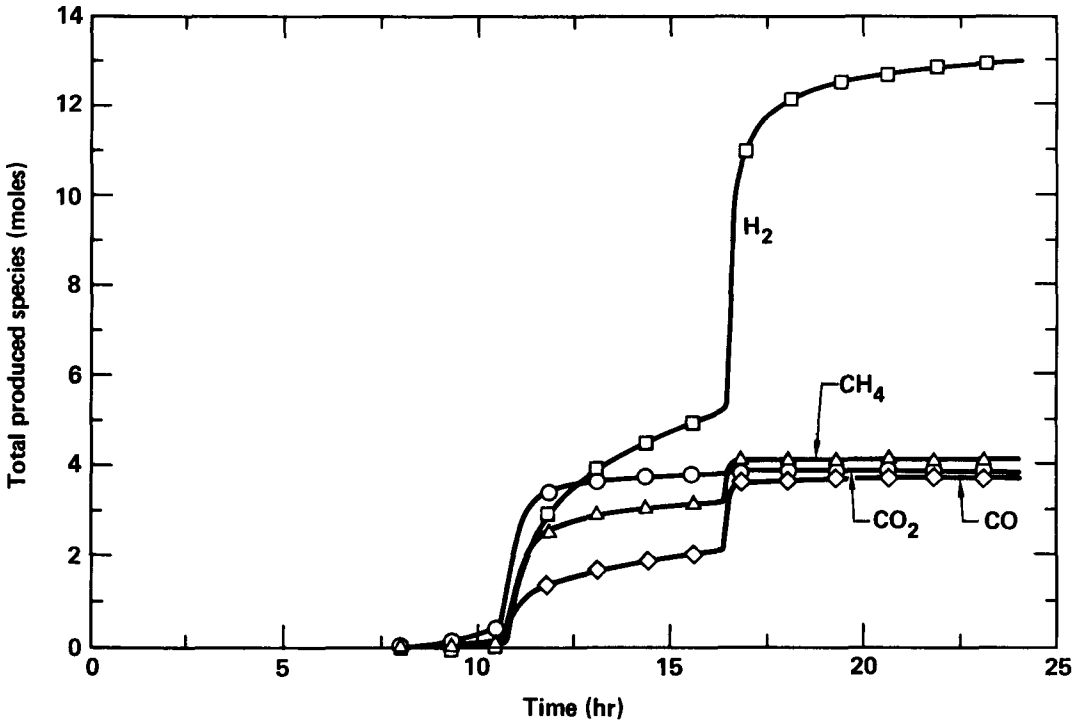

Fig. 4. Total produced species for a typical batch pyrolysis experiment (PYR-5).

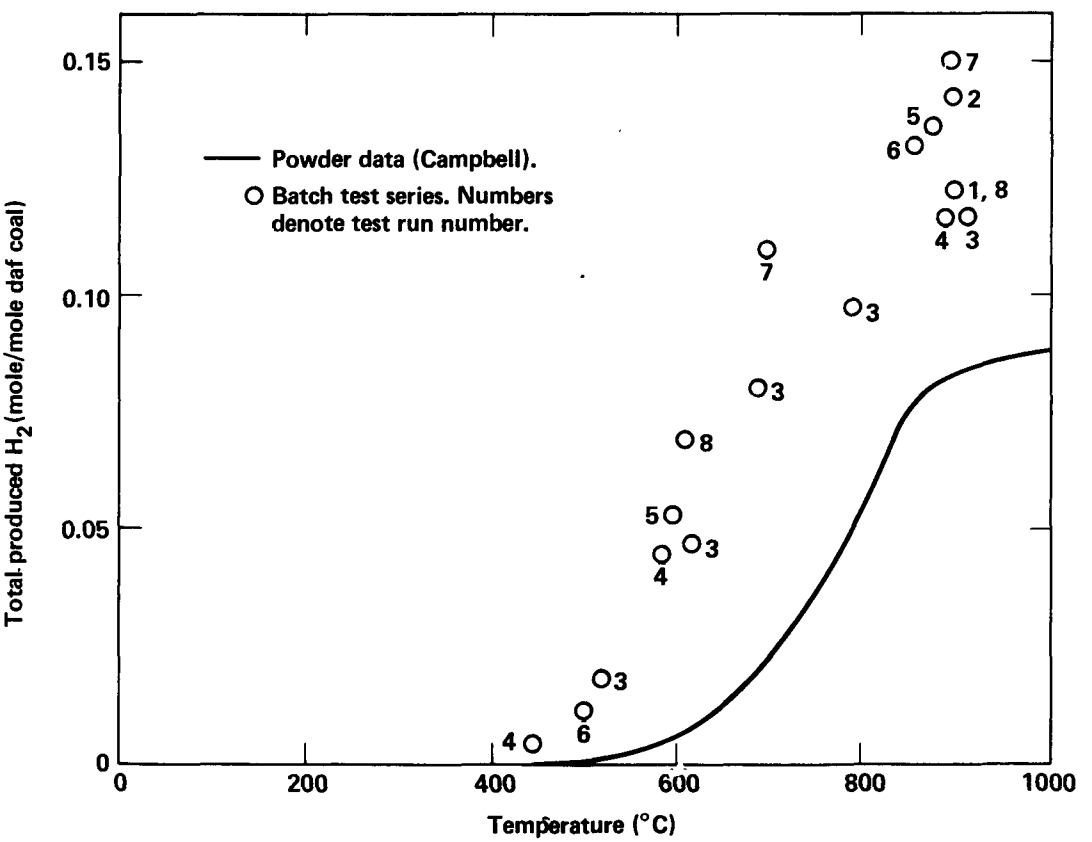

Fig. 5. Total produced H_2 in batch tests and comparison with powder data.

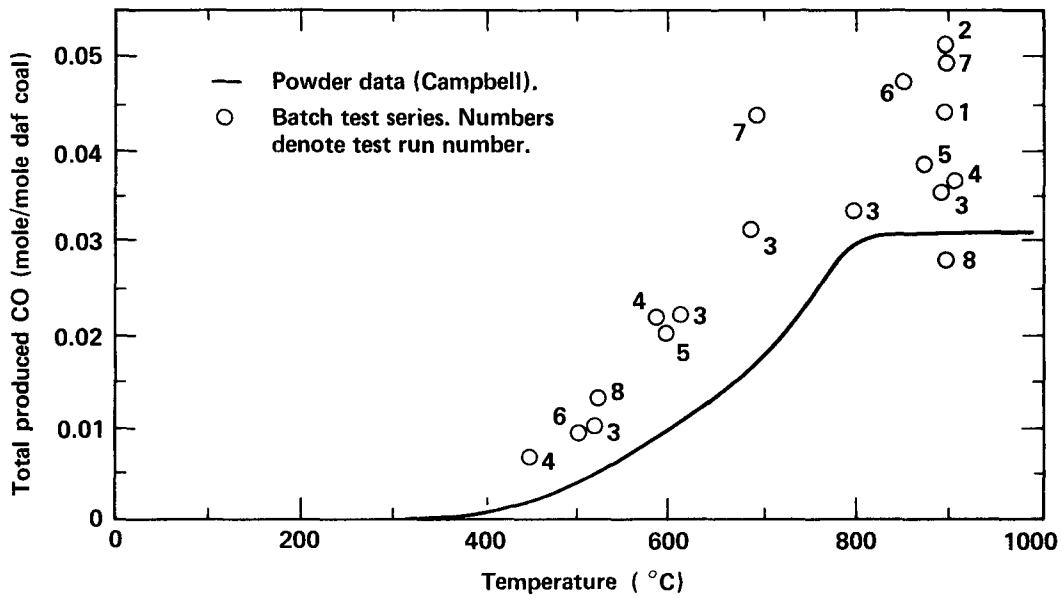

Fig. 6. Total produced CO in batch tests and comparison with powder data.

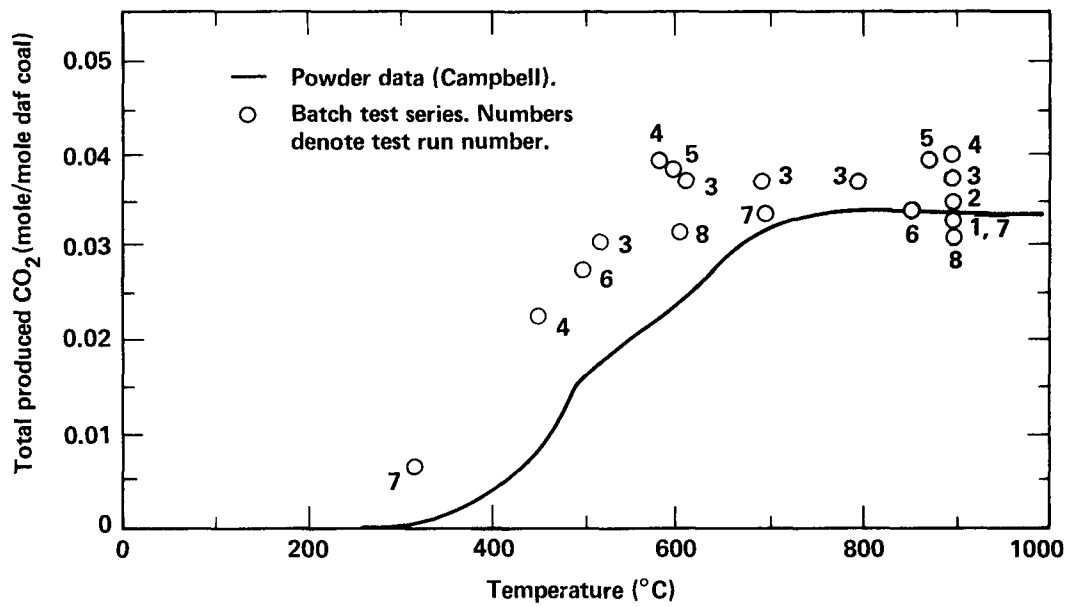

Fig. 7. Total produced CO_2 in batch tests and comparison with powder data.

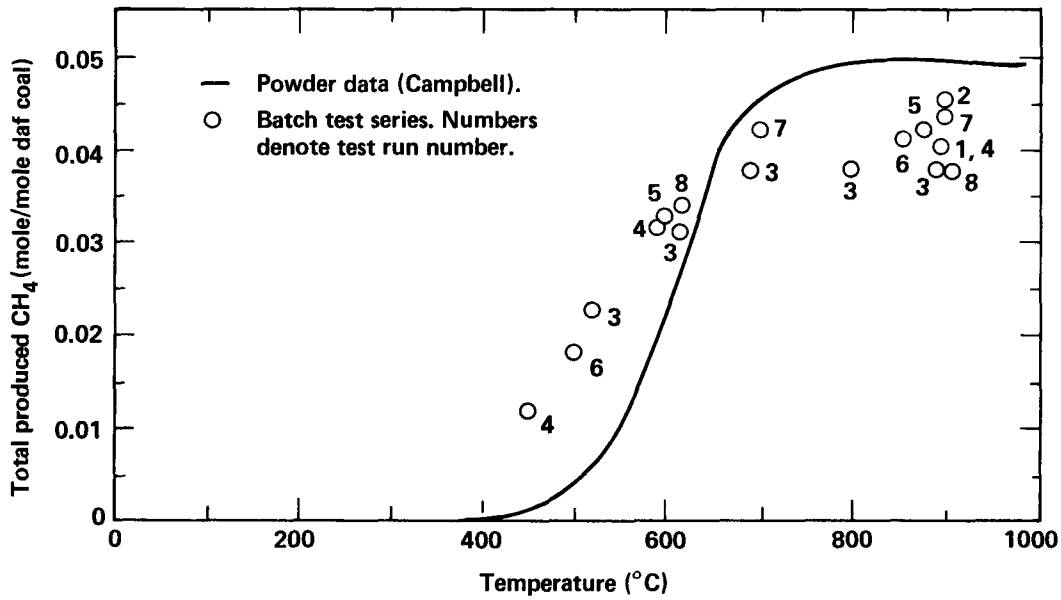

Fig. 8. Total produced CH_4 in batch tests and comparison with powder data.

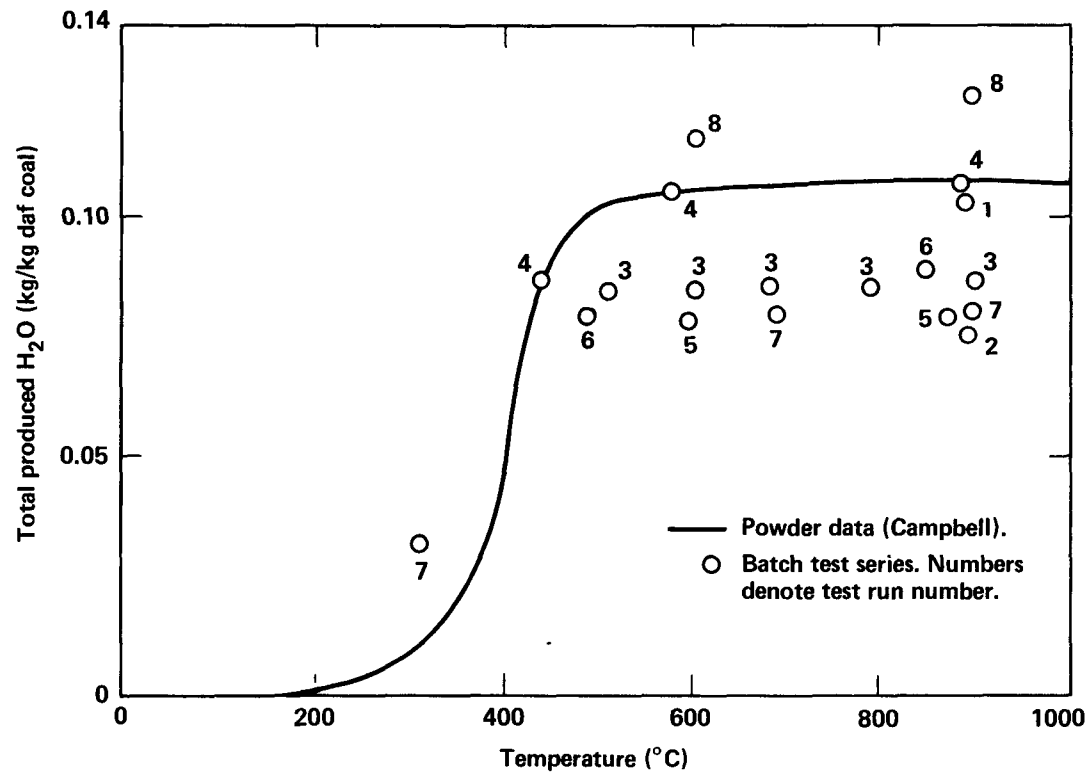

Fig. 9. Total produced water in batch tests and comparison with powder data.

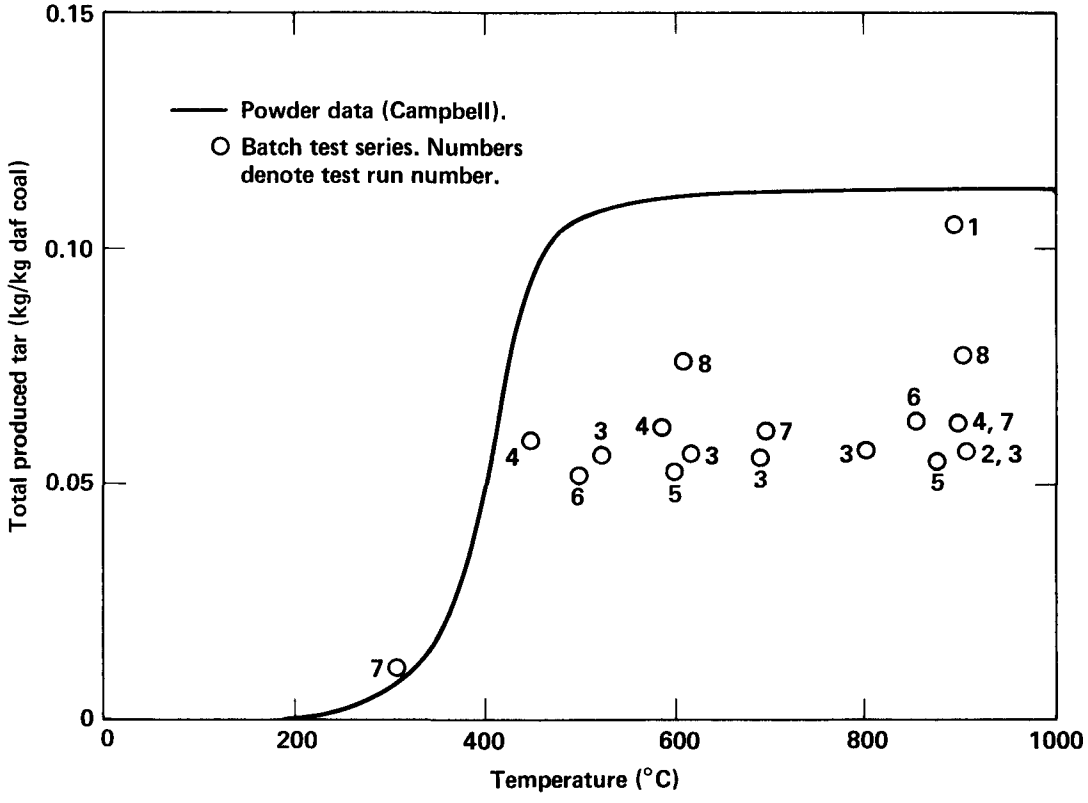

Fig. 10. Total produced tar in batch tests and comparison with powder data.

believe, is not a result of the pyrolysis itself, but of the change to what we hope is a better tar collection system. Nevertheless, the produced tar levels appear to be only 50-70% of those of the powder experiments. We believe this difference is probably significant and is a result again of the increased secondary reaction, coking and cracking, occurring in the batch geometry.

The batch water data, Fig. 9, also shows some scatter and perhaps a lower value than the powder data. Because of the scatter and difficulty of measuring the tar/water split, we do not think the differences are significant.

It would appear that the use of either the powder data or the batch data in an overall gasification model would yield very similar results, with the possible exception of the amount of tar produced.

Continuous Feed Pyrolysis Results

To date we have run eight continuous feed experiments (PYR-1 through PYR-8). Temperature levels of approximately 500, 600, 700, 800, and 900°C were used. In all these experiments except 6 and 7, an argon gas sweep rate of 2 mmol/s and a near atmospheric pressure of 19 psia (130 kPa) were used. In experiments 6 and 7, a pressure of 87 psia (600 kPa) was maintained. The argon flow rate for the bulk of experiment 6 was 9.3 mmol/s, and for experiment 7 it was 3 mmol/s.

In order for the coal to be fed smoothly into the reactor by the hopper-screw-feeder assembly it was necessary that no moisture be on the coal particle surfaces. This required drying of the feed coal. However, to maintain a more representative gas atmosphere we did not fully dry the feed coal in experiments 1-7. We

had hoped to maintain a reasonably consistent moisture content by using similar partial drying procedure. As indicated in Table 2, we were unable to accomplish a consistent partial drying. This uncontrolled variation in water content is not desirable when other parameters (e.g., temperature) are also being varied. Consequently, in the last experiment we fully dried the coal and expect to continue to do this in future experiments, reintroducing the undried coal when other parameters of interest have been investigated.

Typical gas evolution data for the continuous feed experiments is shown in Fig. 11. Notice that after an initial start-up transient, a reasonably steady period of gas evolution is reached. In some cases modest long-term trends were noted, but the dominant feature remained the consistency of produced gas composition. In reducing and analyzing the data we have used this steady period along with the coal feed rate to arrive at values of gas evolution per unit of coal feed. Since the tar and water collection are integral in nature, this same procedure could not be used with them, and the entire feed period including the start-up period was used.

Table 2. Moisture content of coal used in the continuous feed experiments.

Experiment	Moisture (wt%)
PYR-1	14.9
-2	14.9
-3	14.5
-4	9.1
-5	2.6
-6	9.1
-7	2.6
-8	0.0

The influence of the moisture content of the feed coal can be seen by examining the data for experiments 3 and 8 shown in Table 3. In these runs, a similar reactor temperature was used but the coal for PYR-8 was completely dried before loading it into the feed hopper. There is a significant difference in the H_2, CO, CO_2, and H_2O production. The qualitative differences are easy to understand. The higher water content leads to more char/steam reaction, creating more CO and H_2. The

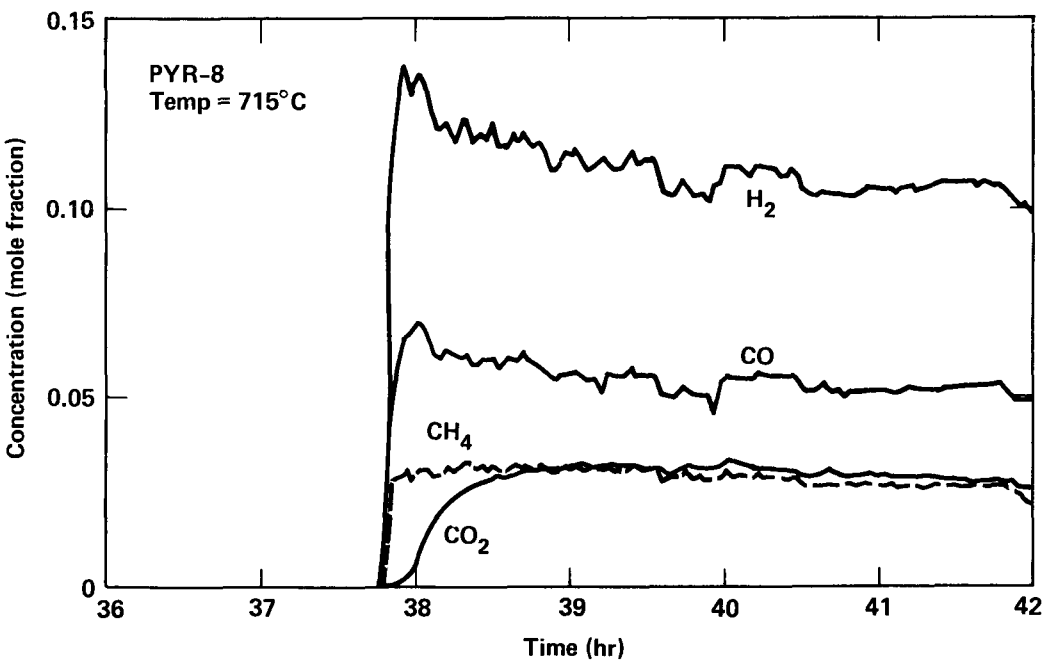

Fig. 11. Product gas composition for a typical continuous-feed pyrolysis experiment.

higher water content also leads to a greater shifting of CO to CO_2 via the water-gas-shift reaction. The two effects lead to more H_2 and CO_2 and less CO in the higher water case. We note that this explanation is not quantitative, indicating additional complications are present. As stated earlier, we are not concerned with a detailed and extremely accurate description of H_2, CO, CO_2, and H_2O evolution from pyrolysis, since when one looks at the total UCG system, the production of these species is seen to be dominated by other considerations. We are primarily interested in the methane and tar production. The data in Table 3 indicate that methane production is apparently not influenced by the presence of additional water. A comparison of tar production for the two runs is difficult because of the low amounts produced and the difficulty in collection. We feel that the difference shown in Table 3 is more a reflection on the tar collection method than on any differences resulting from moisture content.

Gas production data for all the continuous feed experiments are shown as a function of the char bed temperature in Figs. 12-15. For reference, a line representing a fit of the batch data is given. The feed and batch data have similar shapes only at the lower temperatures. This is a result of the varying importance of secondary reactions of the final product yields. At the lower temperatures in the feed experiments, the primary pyrolysis products are formed and then swept out, undergoing only modest secondary

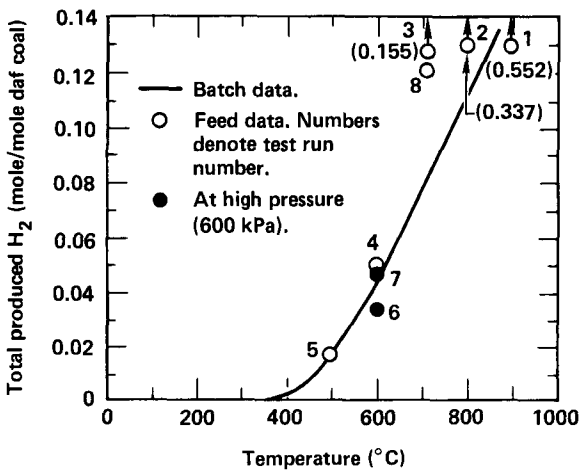

Fig. 12. Total produced H_2 in continuous feed tests and comparison with batch data.

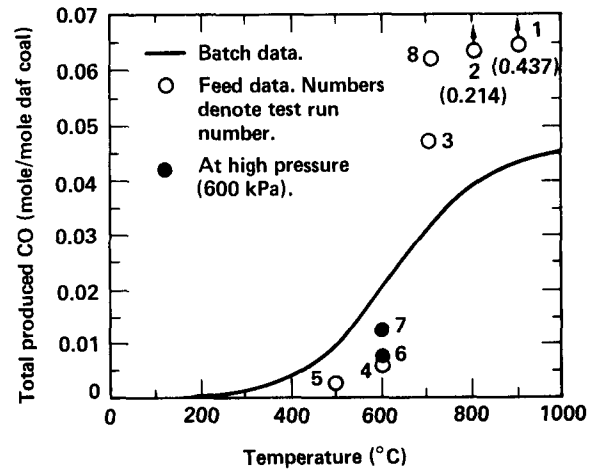

Fig. 13. Total produced CO in continuous feed tests and comparison with batch data.

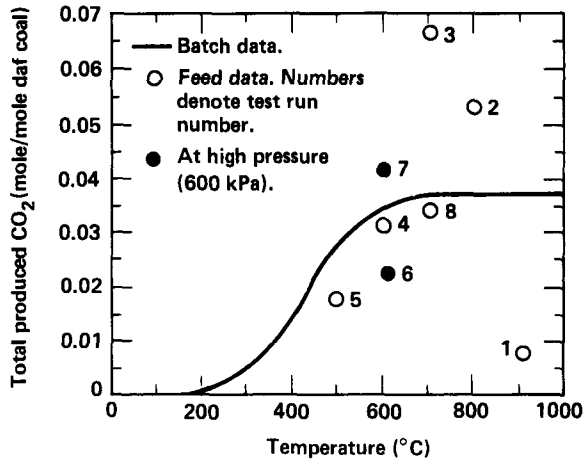

Fig. 14. Total produced CO_2 in continuous feed tests and comparison with batch data.

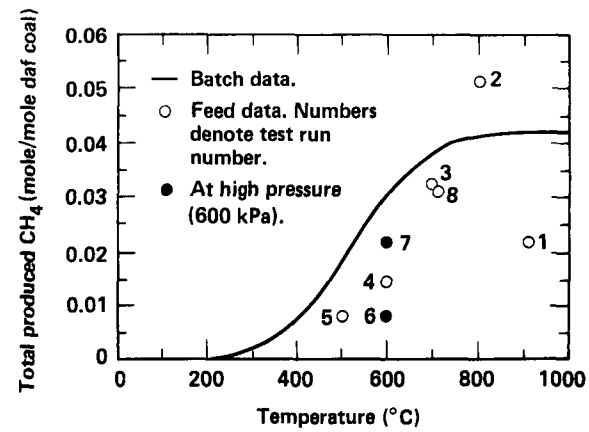

Fig. 15. Total produced CH_4 in continuous feed tests and comparison with batch data.

Table 3. Influence of water content on the continuous feed pyrolysis results.

	Experiment	
	PYR-3	PYR-8
Water in coal (wt%)	14.5	0
Char bed temperature (°C)	700	715
Steady state gas products (mol gas/mol coal):		
H_2	0.155	0.118
CO	0.048	0.058
CO_2	0.066	0.032
CH_4	0.033	0.031
Condensibles (kg/kg coal):		
H_2O	0.13	0.04
Tar	0.031[a]	0.011

[a]This number has a large error bound.

reactions. At higher temperatures, the secondary reactions begin to dominate and the batch and feed data diverge. The feed data show very large values for CO and H_2 at temperatures above 700°C, and are monotonically increasing over the entire temperature range. The CO_2 data, on the other hand, has its highest values near 700°C and low values at either temperature extreme. The data scatter near 700°C is a result of the variability of water content of the feed coals, particularly those of runs 3 and 8. At 900°C, nearly all of the CO_2 is converted to CO, most likely through the action of the water-gas-shift reaction.

The methane from the feed experiments shows a peak near 800°C. The rise up to the 800°C point is controlled by the increased formation of methane from primary and perhaps secondary reactions as temperature increases. However, above 800°C the methane decomposition reaction becomes important and begins to reduce the total methane yield. From this limited data it appears that unless the methane production peak is very sharp, there is only a modest increase in methane production above that of the batch data, and this is limited to a narrow range near 800°C.

The produced ethane concentrations were low enough so that a quantitative measurement was beyond the capacity of the mass spectrometer system used. However, the data obtained shows the same general character as the methane data in that at the higher temperatures, above 800°C, the amount of production was greatly reduced.

Two experiments, 6 and 7, whose data is shown in Figs. 12-15, were run at elevated pressure, 600 kPa. Experiment 6 was performed so that the gas residence time in the reactor was similar to the low pressure runs, while experiment 7 was run with a lower argon flow and a residence time (37 s) about three times greater than that of experiment 6. Comparing the data from 6 and 7 to that of the lower pressure runs indicates that pressure, at least at these modest levels, does not play an important role. The data of 6 and 7 do indicate, however, that residence time does influence the gas production to some extent. For all the gases, the amount produced is greater for the longer residence time, experiment 7. This is true even though the feed coal for experiment 7 had less moisture than that for experiment 6. Also the methane production, which appears to be roughly independent of moisture content, for experiment 7 is twice that obtained in experiment 8. However, this methane production level is only 50% greater than that of experiment 4, which was run at low pressures and for a residence time similar to that of experiment 6. This discrepancy may be related in some manner to the pressure levels. However, the high argon flows of experiment 6 caused the mole fractions of the produced

gases to be low (less than 0.01) and at the limit of our measurement capability.

Tar and water data were also collected for each of the experiments. The water data is, of course, influenced by the water content of the feed coal. Thus a pure dependence on char bed temperature is somewhat clouded. The data is scattered, with a range between 0.0 and 0.14 kg/kg-daf-coal ("daf" stands for dry, ash-free). However, the data do clearly indicate the importance of the char/steam reaction above 800°C, since little or no water was collected for the two runs with char bed temperatures of 800 and 900°C.

The data for tar production indicate that tar production at all temperatures was much below that of the batch tests. Due to measurement problems, no clear trend with temperature is apparent. The tar production runs from 0.0 to 0.031 kg/kg-daf-coal, with an average value of 0.01 kg/kg-daf-coal. This average is very similar to the 0.011 kg/kg-daf-coal obtained in the PYR-8 experiment, in which an improved tar collection system was used. The average value is 1/10 that of the powder data and 1/6 of that of the batch results.

The feed experiments have shown that the system is one in which secondary reactions are very important and, as a result, the produced products are different from those of the batch test. Also, the influence of average temperature is clearly apparent. The experiments to date have concentrated on temperature as the primary parameter. Other parameters which may influence the results include:

- Coal type.
- Residence time.
- Gas environment.
- Pressure.
- Char bed preparation temperature.
- Particle size.

In several of the experiments we have taken an initial look at pressure and residence time and found that, of these, residence time is the more important, but neither is as important as temperature. A very preliminary conclusion related to the gas environment is the insensitivity of methane production to modest increases in steam and H_2 levels. We have not explored particle size or coal type dependence at all. We believe, based on the work of others, that particle size will be unimportant in our system, but coal type may be of considerable importance. In the future we hope to explore further the residence time, gas environment, and pressure. In addition, we hope to look briefly at the influence of char bed preparation temperature and to utilize other coals of current interest to the UCG community.

Methane Decomposition Results

The data from both the small reactor (numbers 1 through 10) and the large reactor (numbers 11 through 23) are presented in Table 4. There are more sets of data than runs for the large reactor because the experimental conditions were altered during the course of the run for some of the large reactor experiments. Data set 7 appears to be inconsistent with set 6 because it shows a decrease in conversion for a corresponding increase in residence time. Data set 7 was not used in the kinetic analysis.

All of the experiments showed the reactivity of the char to be a decreasing function with respect to the duration of the experiment.[5] Figure 16 is a plot of the apparent first order rate coefficient vs the total amount of carbon deposition from the decomposition of methane. The logarithm of the apparent first order coefficient appears to be linear with respect to carbon deposition for most of the duration of the experiment; however, the reactivity of the char appears to approach a steady state value toward the end of each experiment. The steady state conversions for these experiments were subjected to more detailed analysis.

A comparison of data set 21 with data set 22 clearly shows that the methane decomposition's dependence on methane concentration is definitely not first order. This can partially be explained by product inhibition from the adsorption of hydrogen.

If Langmuir-Hinshelwood kinetics are assumed for the heterogeneous contribution to the decomposition, and then combined with the homogeneous expression (Ref. 3) the following rate expression is obtained:

$$\frac{-d}{dt}[CH_4] = \frac{K_1[CH_4]}{1 + K_2[CH_4] + K_3[H_2]} + K_0[CH_4], \quad (1)$$

Table 4. Char gasification data for the asymptotic char reactivity.

#	temperature (K)	[H2]Ø (gmol/cm**3)	[CH4]Ø (gmol/cm**3)	Conversion	Space Time (sec)
1	1Ø24.Ø	Ø.ØØØØe+ØØ	7.937Øe-Ø7	Ø.274ØØØØØØØ	1.64ØØe+ØØ
2	1Ø76.Ø	Ø.ØØØØe+ØØ	7.55ØØe-Ø7	Ø.4Ø6ØØØØØØØ	1.51ØØe+ØØ
3	1Ø76.Ø	Ø.ØØØØe+ØØ	7.55ØØe-Ø7	Ø.363ØØØØØØØ	1.17ØØe+ØØ
4	1Ø76.Ø	3.Ø2ØØe-Ø6	7.55ØØe-Ø7	Ø.Ø41ØØØØØØØ	1.17ØØe+ØØ
5	1123.Ø	2.9ØØØe-Ø6	7.237Øe-Ø7	Ø.Ø66ØØØØØØØ	1.12ØØe+ØØ
6	1174.Ø	2.77ØØe-Ø6	6.92ØØe-Ø7	Ø.Ø46ØØØØØØØ	9.5ØØØe-Ø1
7	1173.Ø	2.77ØØe-Ø6	6.93ØØe-Ø7	Ø.Ø36ØØØØØØØ	1.Ø7ØØe+ØØ
8	12Ø1.Ø	2.71ØØe-Ø6	6.77ØØe-Ø7	Ø.Ø75ØØØØØØØ	1.35ØØe+ØØ
9	1153.Ø	5.64ØØe-Ø6	7.Ø5ØØe-Ø7	Ø.Ø3ØØØØØØØØ	9.9ØØØe-Ø1
1Ø	11Ø9.Ø	5.86ØØe-Ø6	7.33ØØe-Ø7	Ø.Ø15ØØØØØØØ	1.51ØØe+ØØ
11	1192.Ø	Ø.ØØØØe+ØØ	1.157Øe-Ø5	Ø.Ø73ØØØØØØØ	2.7ØØØe+ØØ
12	11Ø7.Ø	Ø.ØØØØe+ØØ	1.23ØØe-Ø5	Ø.Ø37ØØØØØØØ	1.35ØØe+ØØ
13	1137.Ø	Ø.ØØØØe+ØØ	1.274Øe-Ø5	Ø.Ø165ØØØØØØ	1.42ØØe+ØØ
14	1136.Ø	Ø.ØØØØe+ØØ	1.265Øe-Ø5	Ø.Ø28ØØØØØØØ	2.9ØØØe+ØØ
15	1186.Ø	Ø.ØØØØe+ØØ	1.241Øe-Ø5	Ø.Ø55ØØØØØØØ	2.8ØØØe+ØØ
16	1237.Ø	Ø.ØØØØe+ØØ	1.199Øe-Ø5	Ø.112ØØØØØØØ	2.75ØØe+ØØ
17	1186.Ø	Ø.ØØØØe+ØØ	6.66ØØe-Ø7	Ø.Ø9ØØØØØØØØ	1.51ØØe+ØØ
18	1186.Ø	Ø.ØØØØe+ØØ	7.33ØØe-Ø7	Ø.Ø6ØØØØØØØØ	1.342Øe+ØØ
19	1140.Ø	Ø.ØØØØe+ØØ	6.721Øe-Ø7	Ø.23ØØØØØØØØ	2.61ØØe+ØØ
2Ø	1141.Ø	Ø.ØØØØe+ØØ	6.716Øe-Ø7	Ø.11ØØØØØØØØ	1.22ØØe+ØØ
21	1Ø64.Ø	Ø.ØØØØe+ØØ	3.1Ø9Øe-Ø6	Ø.245ØØØØØØØ	5.98ØØe+ØØ
22	1Ø65.Ø	Ø.ØØØØe+ØØ	7.823Øe-Ø7	Ø.119ØØØØØØØ	1.32ØØe+ØØ
23	1Ø64.Ø	Ø.ØØØØe+ØØ	7.43ØØe-Ø7	Ø.165ØØØØØØØ	2.48ØØe+ØØ

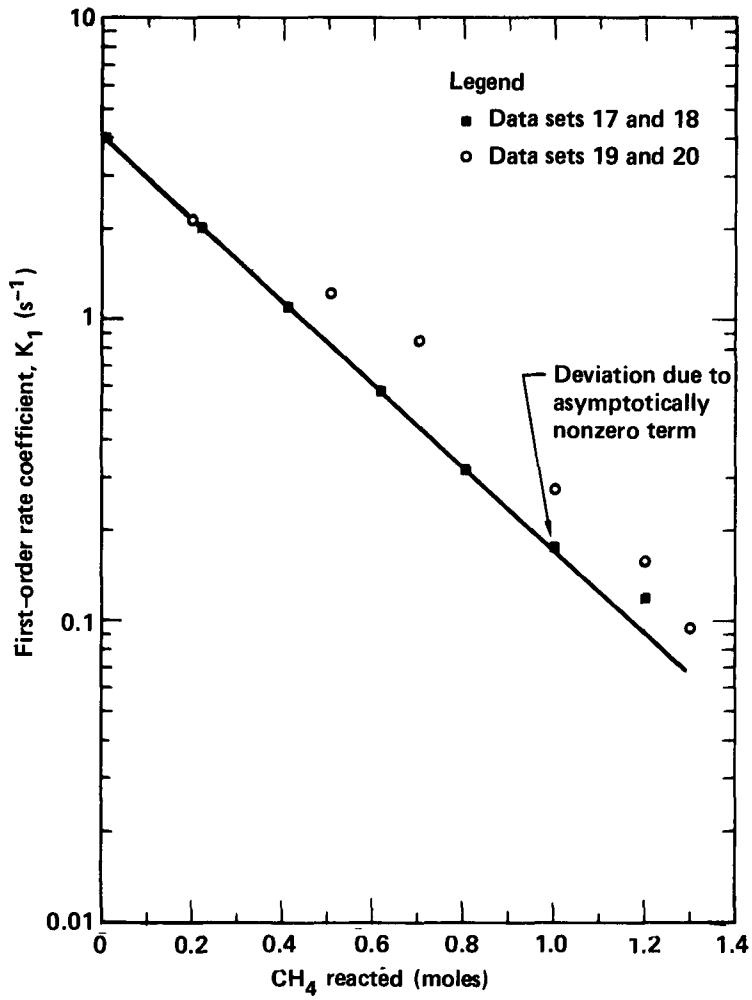

Fig. 16. Apparent first-order coefficient vs total carbon deposition.

where K_0 is the homogeneous decomposition rate constant. If the 1 in the denominator of the heterogeneous term is assumed to be negligible, the following simplification can be obtained:

$$\frac{-d}{dt}[CH_4] = \frac{K_A}{1 + \frac{[H_2]}{K_B \cdot [CH_4]}} + K_0[CH_4]. \quad (2)$$

Equation (2) was integrated and fitted to the asymptotic conversion data with the following results:

$K_A = 4.5 \times 10^{-7}$ mole/cm^3 • s,

$K_B = 2.6 \times 10^4 \exp [-2.5 \times 10^4/RT]$.

A comparison between the predicted residence times and the experimental residence times is presented in Table 5. The majority of these predicted times are within a factor of 2 of the actual times. The engineering rate expression presented here is limited by its assumed form, but is still useful for estimating the magnitude of the decomposition of methane in the presence of hot char for temperatures well below those at which the homogeneous reaction is insignificant. Even at the highest temperature investigated here, the homogeneous reaction alone can at best only account for 11% of the observed conversion (see Table 5).

In addition to hydrogen, it seems reasonable to assume that the heterogeneous reaction may also be inhibited by the presence of CO_2 and CO, both of which are present in an underground gasification process. More experimentation is needed to determine the effect of these gases on methane decomposition. A more comprehensive look at the influence of pressure is also needed in order to ascertain the correct form of the rate expression with respect to methane concentration.

SUMMARY AND CONCLUSIONS

The results of the batch pyrolysis experiments indicated that batch pyrolysis is similar to powder pyrolysis. The continuous feed data show lower tar production, presumably resulting from secondary pyrolysis reactions (coking and cracking) taking place in the hot char bed. The continuous feed data show no substantial increase in methane over batch data. The additional methane produced from secondary pyrolysis reactions appears to be decomposed by a heterogeneous reaction in the char bed. The methane decomposition experiments have shown that the decomposition is greatly enhanced by the presence of char at temperatures between 750 and 925°C. It has also been shown that the heterogeneous methane decomposition reaction is inhibited by the presence of

Table 5. Predicted time and homogeneous contribution.

#	Space time actual	Space time calculated	Conversion a actual	Conversion b homogeneous	Ratio b/a
1	1.6400e+00	1.8426e+00	0.27400000	0.00000305	0.0000111
2	1.5100e+00	2.4563e+00	0.40600000	0.00002561	0.0000630
3	1.1700e+00	1.9686e+00	0.36300000	0.00001984	0.0000546
4	1.1700e+00	1.3753e+00	0.04100000	0.00001984	0.0004840
5	1.1200e+00	1.3662e+00	0.06600000	0.00011730	0.0017773
6	9.5000e-01	5.7505e-01	0.04600000	0.00060815	0.0132206
7	1.0700e+00	--	0.03600000	--	--
8	1.3500e+00	7.5894e-01	0.07550000	0.00211610	0.0280278
9	9.9000e-01	8.4790e-01	0.03000000	0.00030664	0.0102215
10	1.5100e+00	6.6389e-01	0.01500000	0.00009344	0.0062298
11	2.7000e+00	2.0242e+00	0.07300000	0.00315175	0.0431747
12	1.3500e+00	1.0412e+00	0.03700000	0.00133686	0.0361314
13	1.4200e+00	4.8383e-01	0.01650000	0.00024843	0.0150569
14	2.9600e+00	8.3868e-01	0.02800000	0.00049938	0.0178350
15	2.8000e+00	1.6066e+00	0.05500000	0.00268027	0.0487323
16	2.7500e+00	2.9427e+00	0.11200000	0.01332436	0.1189675
17	1.5100e+00	1.5283e-01	0.09000000	0.00144632	0.0160703
18	1.3420e+00	1.4721e-01	0.08000000	0.00128551	0.0160689
19	2.6100e+00	5.6708e-01	0.23000000	0.00050881	0.0022122
20	1.2200e+00	2.1023e-01	0.11000000	0.00024658	0.0022416
21	5.9800e+00	4.3086e+00	0.24500000	0.00006210	0.0002534
22	1.3200e+00	3.4595e-01	0.11900000	0.00001428	0.0001200
23	2.4800e+00	5.3831e-01	0.16500000	0.00002575	0.0001560

hydrogen, and that the reactivity of the char is reduced by the deposition of carbon. An engineering rate expression is presented that is useful for estimating the asymptotic magnitude of the methane decomposition reaction for temperatures between 750°C and 925°C. This expression predicts that 99% of the methane produced under typical UCG conditions would be decomposed at 900°C in approximately 1.5 min and at 1000°C in approximately 30 s.

ACKNOWLEDGMENT

Work done under the auspices of the U.S. Department of Energy by Lawrence Livermore National Laboratory under Contract No. W-7405-Eng-48.

REFERENCES

1. J. H. Campbell, Pyrolysis of Subbituminous Coal as It Relates to In Situ Gasification (Part 1: Gas Evolution), Lawrence Livermore National Laboratory Report UCRL-52035 Part 1 (1976).

2. J. H. Campbell, Pyrolysis of Subbituminous Coal as It Relates to In Situ Gasification (Part 2: Characterization of Liquid and Solid Products), Lawrence Livermore National Laboratory Report UCRL-52035 Part 2 (1976).

3. V. Kevorkian, C. E. Heath, and M. Boudart, J. Phys. Chem., 64, 1960, p. 964.

4. P. R. Westmoreland, R. C. Forrester, and J. B. Gibson, Pyrolysis and Physical Properties of Coal Blocks, Oak Ridge National Laboratory Report ORNL/TM-7313 (1981), p. 65.

5. M. Kamishita, O. P. Mahajan, and P. L. Walker, Fuel, 56, 1977, p. 444.

3.17 GAS QUALITY IMPROVEMENTS THROUGH HIGH AMPLITUDE PRESSURE OSCILLATION

by

K. Gunterman[1]
M. Kurth[1]
H.W. Gudenau[1]
R.D. Gunn[2]

ABSTRACT

Coal gasification with high amplitude pressure oscillation is a promising method enhancing gas quality in deep, relatively impermeable coal beds. A simplified theory shows qualitatively low pressure swinging improves gas quality. Compared with constant pressure gasification, experimental data show at 200 to 300% increase in gas heating value and a large increase in thermal efficiency for the variable pressure experiments.

INTRODUCTION

Much interest currently centers on the gasification of deep-lying seams of bituminous coal because these are an untapped resource of great size and importance in areas such as Northern Europe and Appalachia in the United States. Economic gasification of such coal seams, however, poses many problems. At great depths, the drilling and completion of operating wells become increasingly costly; and, consequently, well spacing must be as large as possible and the recovery of coal between wells must be maximized.

Unfortunately, bituminous coal is rather impermeable, and overburden pressure reduces this permeability still further. Under these conditions, it appears improbable that UCG can be operated as a permeation process. Presumably, the low coal permeability will restrict the flow of air or oxygen primarily to the linking channel. As the side walls of the linking channel burn farther and farther apart, water vapor and oxygen will increasingly bypass the reacting coal face; and gas quality will decrease accordingly. Unlike a permeation or packed bed process, a simple channel gasification process cannot provide the large reacting surface area necessary for efficient reaction.

High amplitude pressure oscillation is a promising method for at least partially overcoming this deficiency of channel gasification. This paper describes an experimental and theoretical investigation of pressure oscillation during coal gasification.

THEORY

A reasonably rigorous mathematical model for coal gasification under conditions of oscillating pressure would apparently be very complicated. At this stage of development, it is believed that simpler models give a much better understanding of the process even though such models may be at best semi-quantitative in accuracy. This is the approach adopted here.

Because of the proximity of confining walls on all sides, a model for a laboratory test differs from a model for a field experiment where confining walls in the lateral direction are generally not present. In addition, it is very difficult to simulate the effects of

1/ Institut fur Eisenhuttenkunde, Technischen Hochschule, 5100 Aachen, West Germany
2/ Department of Chemical Engineering, University of Wyoming, Laramie, Wyoming 82071

overburden pressure on the coal in the laboratory gasification experiment. Therefore, the models presented here are adapted specifically for the laboratory work. It can be shown that this is the worst case and that the lack of confining walls actually enhances the favorable influence of pressure oscillation.

Figure 1 shows the type of apparatus to be modeled. A large autoclave encloses a smaller tube containing the coal sample. The tube is open on one end so that air from the autoclave can enter freely. At the top of the tube along its entire length, a channel has been cut away. The tube is closed at the right hand end so that exhaust gases must exhaust through the small line shown. At the beginning of a cycle, the valve in line 2 closes while air continues to enter the autoclave through line 1. Thus the pressure begins to increase until it reaches its maximum value, and the valve in line 2 opens and exhausts combustion gases until the pressure has dropped to its minimum desired value. At this point, the valve in line 2 closes again; and a new cycle begins.

The process by which pressure oscillation improves gas quality is relatively simple. The pressure upswing portion of the cycle forces the reactant gases into the fine pore structure of the coal where there is a large reactive surface area and reaction is far more complete than in the main channel. During the pressure downswing, the product gases flow from the pores back into the main channel enriching the incompletely reacted gases there.

A simple material balance leads to the following approximate equation for the composition of gas produced at the exit of the apparatus during the gas production or pressure downswing portion of the cycle.

$$y_{iE} = y_{iCh} f + y_{iP} (1 - f) \qquad (1)$$

where,

$$f = \frac{1}{n_E} \left[n_o + \left(\frac{V_D}{RT_D} + \frac{V_{Ch}}{RT_{Ch}} \right) \frac{dP}{dt} \right] \qquad (2)$$

$$1 - f = \frac{V_S \phi}{n_E R T_P} \qquad (3)$$

(1-f) is the fraction of gas flowing at the exit which comes from the pores in the coal and f is the fraction of gas flowing at the exit which has never entered the coal pore structure. Equations (1) through (3) are at best very approximate and time dependent because both y_{iCh} and y_{iP} vary in time. The more important assumptions are:

1) Average values of y_{iCh}, y_{iP}, T_{Ch}, T_P and ϕ can be used although these quantities actually vary along the length of the channel.

2) The time scale for unsteady flow in the porous coal is short compared to the time scale for pressure oscillation, that is, the function dP/dt is nearly the same in the pore structure as it is in the channel.

3) The mole fraction y_{iCh} has the same value under pressure oscillation as for simple channel gasification at the same instantaneous flow rate and pressure.

4) Interactions between y_{iCh} and y_{iP} may be ignored.

In spite of the approximations, Equations (1) through (3) still preserve the major features of pressure oscillation. Equation (1) shows that pressure oscillation enhances gas quality by blending a high quality gas from the pores with the lower quality gas which has only flowed along the open channel. Therefore, two methods exist for improving gas quality: (1) Minimize the fraction of gas which has not permeated the coal pore structure. (2) Maximize the fuel content of gas from the pores. Equation (2) shows that the first method can be achieved by reducing the dead volume and by cutting off air flow, n_o, into the autoclave during the exhaust or pressure downswing portion of the cycle. Both of these methods are effective in laboratory apparatus such as that depicted in Figure 1.

In a field test, however, dead volume is normally small whereas the channel volume, V_{ch}, becomes quite large as the coal is gasified. Therefore,

there is no good procedure for reducing V_{Ch}. However, V_P can be substantially increased relative to V_{Ch}. In a laboratory apparatus, the volume of coal, V_S, is fixed; and the pore structure of this rapidly fills with the reacting gases. In a field test, however, there are no confining walls in the coal; thus a larger volume of coal can be permeated with gaseous reactants. It is only necessary to use a longer time cycle to accomplish this.

Another model is needed to study methods for increasing the fuel content of gas from the pores. A material balance within the pore structure of the coal produces the following differential equation:

$$\frac{\partial y_i}{\partial \tau} = -\frac{1}{N_{Th}^2}\frac{\partial^2 y_i}{\partial z^2} + \frac{N_o \cos \omega \tau}{1 + A \sin \omega \tau}\frac{\partial y_i}{\partial z} - y_i \qquad (4)$$

Equation (4) can be integrated to determine the gas composition, y_{iP}, at the entry from the pore structure into the open channel. Equation (4) is based on the same four assumptions listed for Equations (1) to (3). For convenience, a first order reaction and a sinusoidal pressure cycle have also been assumed although these assumptions can be easily changed. In addition, it has been assumed that temperature is uniform along the length of a pore. Although this last assumption is incorrect, Equation (4) still provides valuable qualitative information.

N_{Th} is the Thiele modulus, a well known quantity in chemical reactor design. It is a measure of the extent that diffusional resistance inhibits reactions taking place within a porous body. The Thiele modulus has an important influence on coal gasification because water vapor, oxygen and carbon dioxide must diffuse to the surfaces of the porous coal in order to react with it. It should be noted, however, that there is an additional diffusional resistance, that is, diffusion resistance across the boundary layer between the channel and the solid coal. Pressure oscillation, therefore, increases gas quality during coal gasification by augmenting diffusional transport with fluid flow within the pores and across the boundary layer. Thus, pressure oscillation becomes increasing important as the second term on the right hand side of Equation (4) becomes increasingly important. In other words, the following ratio should be as large as possible.

$$\frac{N_o}{1/N_{Th}^2} = N_o N_{Th}^2 = \frac{A \omega L^2}{D} = \frac{\pi L^2 \Delta P}{P_a D t_o} \qquad (5)$$

In the experimental work described in this work, the ratio given by Equation (5) was typically on the order one. Thus, during the pressure oscillation experiments, diffusional transport was about as important as flow or forced convection. As Equation (5) shows, pressure oscillation yields increasingly favorable results by overcoming diffusional resistance through increases in any of the following quantities: amplitude of the pressure cycle, P; depth of the pores, L; frequency of the time cycle, $2\pi/k\ t_o$. Absolute pressure has little effect in Equation (5) because the quantity DP_a is physically nearly constant except at extreme pressures and low temperatures.

A different limit of considerable interest arises if the depth, L, of pores penetrated is large and if the cycle time, t_o, is very long. Then, both $1/N_{Th}^2$ and N_o become negligibly small; and Equation (4) simplifies to

$$\frac{d y_i}{d \tau} = - y_i \qquad (6)$$

Integration of Equation (6) gives the following result for a reactant:

$$y_i = y_{io} e^{-kt} \qquad (7)$$

Equation (7) is identical to the equation for a first order irreversible reaction in a batch reactor. This shows that for long cycle times the pores in the coal act as a batch reactor whose contents are periodically discharged into the gasification channel. As shown later, this limit is approached in the experimental work described later.

EXPERIMENTAL EQUIPMENT

All experimental work has been carried out in a large autoclave designed for simulating UCG. The apparatus is described more fully elsewhere (Mohtadi et al., 1981A). The autoclave accepts coal samples four meters in length and 0.32 meters in diameter. The equipment has a maximum operating pressure of 60 bars. The apparatus is shown in Figures 2 and 3. A variety of reactants, hydrogen, stream, air or oxygen can be used as feed gases. Temperature, pressure, compositional and flow measurement are recorded on strip charts, and in addition a microcomputer (Gunterman et al., 1982) averages the various signal readings and computes mass and energy balances. Temperatures are measured at 45 locations within the coal sample, massflow is measured at three locations and gas analysis at five locations.

For gasification experiments, unbroken subbituminous coal samples are taken from a deep mine in the Ruhr District. These samples are encased in steel tubes during the coring operation at the mine, and several of these steel tubes are welded together to produce a four meter long sample. An artificial channel equal to 10% of the coal cross section is cut away at the top of the sample.

DESCRIPTION OF THE TESTS

Portions of the experimental work have been reported previously (Mohtadi et al., 1981B; Kurth et al., 1982). A total of nine experiments are recorded here, five experiments operated with high amplitude pressure oscillation on a 20 minute cycle and four operated at constant pressure as controls. Experiments 8, 9, 12 and 19 operated with pressure oscillations between 7.5 and 12.5 bars. Experiments 7, 10 and 20 operated at constant pressure of 10 bars but at conditions comparable otherwise to the preceding experiments. Experiments 21 and 22 are respectively steady pressure and oscillating pressure experiments conducted at an average pressure of 20 bars. All tests were operated with an air feed rate of a nominal 30 kg/hr except for tests 19 and 20 which were conducted at a somewhat lower air flow rate. Table 1 summarizes the data for all nine experiments.

A number of general conclusions can be reached concerning the effects of pressure oscillation on gas quality. With pressure swinging more methane and hydrogen are produced than during constant pressure conditions. This suggests that there is less combustion of pyrolysis gas in the open channel; however, the strong dependence of methane production on pressure suggests that some of the methane is generated by methanation reactions as well as by devolatilization. Both the hydromethanation of coal char and the hydrogenation of coal tars to produce methane are favored by high pressures according to Le Chatelier's Principle.

The mass ratio of CO/CO_2 produced increases from about 25% at constant pressure to 50% for pressure oscillation. Steam converted increases from 20% to 40%. This shows that the gasification reactions are enhanced as indicated in the theoretical discussion.

The average heating value of gas for constant pressure tests was 1800 to 2500 kJ/m^3. The pressure swinging tests produced gas with average heating values of 3200 to 5500 kJ/m^3 which is an improvement by a factor or 2 to 3 compared with the constant pressure controls. Thermal efficiency (heating value of gas produced/ heating value of coal consumed) approached 95% for the better pressure oscillation tests. This more efficient gasification is reflected in a higher rate of carbon consumption; and, consequently, a shorter duration for the experiments.

At a nominal 10 bars, the amplitude A of the pressure change was 0.25 and at 20 bars it was 0.125. As discussed under theory, a reduction in amplitude should lead to a lower gas quality because the beneficial effect of convective mass transport is reduced at lower amplitudes. This may explain the lower heating value for experiment 22 compared with experiments 8, 12 and 19. Natural coal variability also has an important influence. Experiment 9 shows by comparison rather poor results. Examination of the coal sample after completion of this experiment showed the presence of a large stone and also a very high ash content in the vicinity of the stone; and presumably these circumstances led to the low average heating value for the test.

The high thermal efficiency for the better pressure oscillation tests indicates near optimum results. This should occur if residence time in the poor structure of the coal is sufficiently long for the gasification reactions to approach completion in which case Equations (6) and (7) are most applicable. Calculations show that N_o is on the order of 1/10 or less confirming that Equations (6) and (7) are roughly applicable. Depending on the reaction in question, k has values in the range of 0.05 to 1.0 sec^{-1}, and the average residence time in the pores was 300 seconds. Substitution of these values into Equation (7) shows that the coal gasification reactions should go nearly to completion for the values given above. Thus, for the pressure oscillation experiments the thermal efficiency was very high.

CONCLUSIONS

High amplitude pressure oscillation has been shown to bear great promise as a method for improving gas quality during UCG of low permeability coal. In laboratory experiments, gas quality improved by a factor of 2 or 3 compared with constant pressure experiments, and thermal efficiency was excellent. These experimental findings are completely consistent with qualitative theoretical predictions.

ACKNOWLEDGMENT

One of the authors gratefully acknowledges financial support for this work through grant No. 5081-260-0570. Neither GRI, members of GRI, nor any person acting on behalf of either: (1) Make any warranty or representation, express or implied with respect to the accuracy, completeness, or usefulness of the information contained in this report; or (2) Assumes any liability with respect to the use of, or for damages resulting from the use of, any information, apparatus, method, or process disclosed in this report.

NOMENCLATURE

A = amplitude of the pressure oscillation, $\Delta P/2P_a$

f = fraction of gas flow not from the coal pores

D = diffusivity

k = reaction rate constant

L = thickness of the coal sample

n_E = gas molar flow rate at the exit of the experimental apparatus

n_o = gas molar flow rate at the entrance of the experimental apparatus

N_{Th} = Thiele modulus, $L\sqrt{k/D}$

N_o = dimensionless number, $\frac{\pi \Delta P}{k P_a t_o}$

P = pressure

P_a = average pressure

ΔP = maximum pressure change during cycle

R = universal gas constant

t = time

t_o = duration of one cycle

T_{Ch} = average gas temperature in channel

T_D = average gas temperature in dead volume

T_P = average gas temperature in coal pores

V_{Ch} = channel volume

V_D = dead volume

V_S = volume of coal sample

y_i = mole fraction i in gas phase

y_{iCh} = average mole fraction i in gas phase in channel (constant pressure experiment)

y_{iE} = mole fraction i gas produced from the experimental apparatus

y_{io} = initial concentration of reactant i

y_{iP} = average mole fraction i in gas leaving coal pores

Z = dimensionless distance perpendicular to the channel

ϕ = porosity

τ = dimensionless time, kt

ω = dimensionless frequency, $2\pi/kt_o$

REFERENCES

1. K. Guntermann, G. Suhens, M. Kurth and F.H. Franke: "Measurement and Evaluation of a Simulated Underground Coal-Gasification-Experiment by a Microprocessor System". Proceedings of the 1982 Symposium on Instrumentation and Control for Fossil Energy Processes, Houston, Texas, 1982

2. M. Kurth, F. Fuhrmann, K. Guntermann and W. Wenzel: "The Influence of Pressure-Swinging on the Simulation of Underground Coal Gasification", Proceedings of the 8th UCC Symposium, Keystone, CO, 1982

3. M. Mohtadi, F.H. Franke, W. Wenzel, H.W. Gudenau and M. Kurth: "A Pilot Plant to Simulate In-Situ Gasification", Proceedings of the 1981 Symposium on Instrumentation and Control for Fossil Energy Processes, San Francisco, CA, 1981A

4. M. Mohtadi, M. Kurth, F. Fuhrmann and F.H. Franke: "Simulation of the UCG-Process under Constant Pressure and Pressure Change Conditions in a Large Autocalve Plant". Proceedings of the Seventh Underground Coal Conversion Symposium, Fallen Leaf Lake, CA, 1981B

Table 1
RESULTS OF THE LABORATORY EXPERIMENTS

		Constant Pressure Experiments				Pressure Oscillation Experiments				
Experiment No.		7	10	20	21	8	9	12	19	22
Test Duration (h)		39	51	60,7	51,2	24	54	30,8	53,8	45,5
Operating Pressure (bar)		10	10	10	20	7,5-12,5	7,5-12,5	7,5-12,5	7,5-12,5	17,5-22,5
Gasification Agent Supply (kg/h)	air	30,0	30,0	22,5	30,0	30,5	30,5	30,6	22,5	31,7
	steam	8,15	6,00	4,5	7,8	5,8	6,2	6,00	4,5	5,5
Product Gas (kg)	H_2	4,75	8,5	6,53	6,42	10,57	8,49	11,3	11,2	12,5
	CH_4	10,4	26,77	25,44	28,04	46,95	32,09	58,1	61,44	90,75
	CO	53,4	100,87	71,55	124,70	100,39	143,8	136,3	126,6	155,8
	CO_2	276,7	341,68	350,9	369,10	155,54	381,9	238,1	255,8	429,7
Mass Ratio CO/CO_2		0,19	0,3	0,204	0,338	0,65	0,38	0,57	0,495	0,61
Converted Steam (%)		22,3	20,2	19,75	12,97	45,7	25	39,8	30,9	27
Carbon Conversion (kg)		106,14	156,57	145,4	175,1	120,6	189,75	166,9	170,1	252
Converted Carbon Per Hour (kg/h)		2,72	3,06	2,4	3,4	5,03	3,45	5,4	3,2	5,5
Heat Losses (%)		30,56	24,73	44,7	44,8	2,0	21,55	2,7	4,48	15,0
Thermal Efficiency (%)		50,41	68,2	63,6	58	95,0	69,7	94,6	94	83
Gasification Efficiency (%)		29,5	50,57	35,2	38	86,55	52,6	90,2	87,8	79
Maximum Heating Value (kJ/m^3 i.N.)		2400	2800	3500	5250	10200	5450	9300	8000	11098
Average Heating Value (kJ/m^3 i.N.)		1800	2300	2292	2492	5400	3200	5200	5495	4250
Average Output (KW)		11,6	18,4	12,7	18,6	53,6	20,2	50,7	29,5	46,6

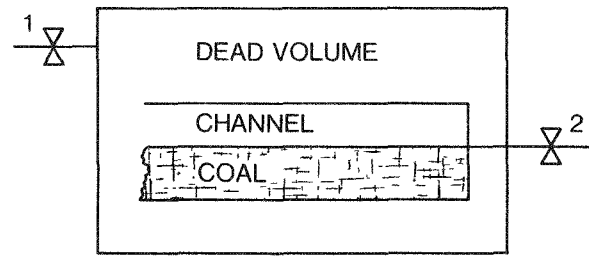

Figure 1. Sketch of an apparatus for pressure oscillation UCG experiments.

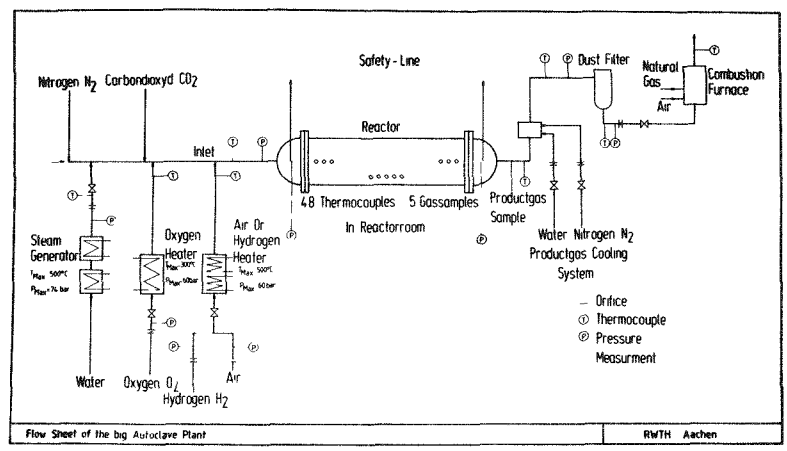

Figure 2. Sketch of experimental equipment used.

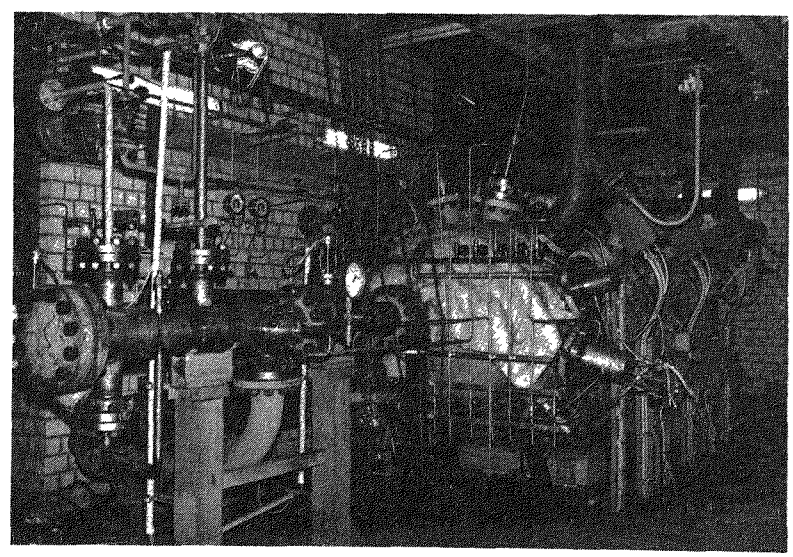

Figure 3. Photograph of the experimental autoclave and accompanying equipment.

3.18 A PROCESS MODEL FOR THE INITIAL STAGES OF ELECTROLINKING

by

W. B. Krantz [1/]
R. K. Tidball [1/]
B. Dautresme [2/]
R. D. Gunn [2/]

ABSTRACT

Electrolinking is a promising means for enhancing coal permeability along one or more narrow linkage channels prior to underground gasification. This linking technique may be particularly advantageous for UCG at great depths where other linking methods may be ineffective or uneconomic. A mathematical model is developed for the initial stages of electrolinking during which the number and size of the electrolink channels are determined. The propensity for electrolinking to channel is shown to arise from the inherent instability of the radially expanding carbonization front. Limited laboratory and field test studies are shown to support the model predictions. A method for improving the reliability of electrolinking and the subsequent resource recovery during gasification is suggested based on the model predictions.

INTRODUCTION

Due to the low natural permeability of coal, it is necessary to carry out a permeability enhancement, or linking step, prior to gasification of the coal. Linking can be accomplished in principle by reverse combustion, directional drilling, hydraulic fracturing, and electrolinking. Although reverse combustion linking has been used successfully in several relatively shallow U.S. field tests, the recent modeling studies of Britten et al. (1) suggest that this technique may not provide sufficient permeability enhancement for deep UCG operations due to the decrease in linkage channel diameter with increasing pressure. The difficulties encountered with reverse combustion linking in the 900 m deep Belgian-German UCG field test support this prediction of Britten et al. Directional drilling may prove to be too costly for linking at great depths. Hydraulic fracturing is only effective if the resulting fractures can be propped, which is difficult to do in coal seams. Electrolinking is a promising method for enhancing the permeability of both shallow and deep coal seams because the electrolinking process should not be affected significantly by depth.

Electrolinking creates small diameter channels of enhanced permeability in coal by carbonizing the coal along these channels via resistance heating. In the simplest configuration, this is accomplished by establishing a potential difference of typically 1000 to 3000 V between cylindrical electrodes placed in the injection and production well bores. Typical power requirements for electrolinking are in the range of 100 to 300 kw. A distinction is made here between "electrolinking," which refers to the generation of the initial small diameter linkage channels, and "electrocarbonization," which refers to the subsequent enlargement of the electrolink channels.

Unfortunately electrolinking is a very poorly understood process. The most extensive studies of this technology were performed in the Soviet Union from the late 1930's into the mid-1950's and are reported by Bondarenko et al. (2). Laboratory and field scale experiments as well as modeling studies were carried out, although the latter were directed

1/ University of Colorado, Boulder, Colorado 80309
2/ University of Wyoming, Laramie, Wyoming 82071

primarily towards electrocarbonization rather than electrolinking. The U.S. efforts in electrolinking began with Forrester and Sarapuu's (3) laboratory and field test studies in 1947 at the Tiger Mine in Hume, Missouri. Electrolinking was subsequently used by the U.S. Bureau of Mines between 1951 and 1954 during the UCG field test at Gorgas, Alabama (4). Much of the current negativism concerning the merits of electrolinking undoubtedly stems from its association with the unsuccessful Gorgas field test. Laboratory and small-scale field test studies of electrolinking were carried out by Wilson et al. (5). Our uncertainties concerning electrolinking are evidenced by the fact that Wilson et al. report that only 16 of 32 field tests of electrolinking conducted under comparable conditions were successful. Nonetheless, there is considerable motivation for development of electrolinking since the Soviets reported that it was faster and less expensive than reverse combustion linking in tests at their lower Moscow field station (6).

This paper reports the results of initial modeling efforts of the authors directed towards enhancing our understanding of the electrolinking process in the hope that it can be developed into a reliable and predictable linking technique applicable to both shallow and deep UCG operations. In particular, this paper addresses the following questions:

- What are the underlying physics of the electrolinking process which control the manner in which the carbonization front propagates?
- Which process parameters control the electrolinking process and how is their influence exerted?
- What controls the number and diameter of the electrolinks which are formed?
- How can the available laboratory and field test results be explained in view of the model predictions?
- How can electrolinking be made a more reliable process?

PHYSICAL CONSIDERATIONS OF ELECTROLINKING

For the "source-sink" electric field generated between two relatively long cylindrical electrodes, the equipotential lines in the immediate vicinity of each electrode are radially symmetric about each electrode. This implies that the heat generation per unit volume is inversely proportional to the square of the radial coordinate directed outward from the axis of the electrode. Hence, the electrical heat generation initially will be greatest in the immediate vicinity of each electrode. This implies that electrolinking is initiated by carbonization of the coal surrounding each electrode.

The subsequent propagation of the carbonization front separating the uncarbonized from the carbonized coal is strongly influenced by the electrical resistivity of the coal which is a strong function of temperature. Uncarbonized coal at ambient temperature typically has an electrical resistivity of 10^3 $\Omega \cdot m$. However, the resistivity increases markedly to a maximum value in the range 10^5 to 10^8 $\Omega \cdot m$ at a temperature of approximately 200°C due to the loss of moisture in the coal. Continued heating of the coal at progressively increasing temperatures causes a pronounced decrease in the resistivity such that the electrical resistivity is only 1 $\Omega \cdot m$ at approximately 700°C at which temperature the coal can be considered to be nearly fully carbonized. This suggests that nearly the entire voltage drop and the bulk of the resistance heating will be confined to the relatively thin zone in which the electrical resistivity is large.

Hence, electrolinking propagates as a moving boundary which originates at the electrode. However, the carbonization front cannot propagate purely radially over any great distance because of the asymmetry of the equipotential lines. This suggests that an electrolink forms in response to the increased density of electric-field lines in the region along the line-of-centers between the electrodes. However, if this explained electrolink channel formation, one would expect a single relatively large diameter electrolink to form. The electrolinks initially generated, however, are known to have diameters which are typically less than that of the electrode; in addition, multiple electrolinks have

been reported (7). This suggests that the number and diameter of the electrolinks which are generated are determined by factors other than the asymmetry in the electric field. In fact, it will be shown in this paper that the number and diameter of the electrolinks are governed by the unstable nature of the radially propagating carbonization front in an electric field. That is, electrolinking is an unstable displacement process much like reverse combustion which was shown to be unstable by Gunn and Krantz (8,9). The unstable nature of the electrolinking process implies that a radially expanding carbonization front will tend to deform into one or more electrolink channels in response to minute perturbations in the process parameters or relevant physical properties.

In view of the above considerations, the authors contend that several important characteristics of the electrolinking process are determined during the initial stages of electrolinking when the carbonization front is expanding radially about the electrodes. Hence, a model is developed here for this initial phase of electrolinking and the stability of this process is analyzed in order to determine some of the characteristics of the electrolinks which are formed. The principal steps in the mathematical analysis leading to the desired relationships given by eqs. (10) and (24), which describe the carbonization front velocity and electrolink channel characteristics as a function of the process parameters, are outlined in the next two sections. The interested reader desiring the complete details of this analysis is referred to the thesis of Tidball (10).

RADIALLY EXPANDING ELECTROLINKING MODEL

Figure 1 shows a schematic of the initial stages of electrolinking consistent with the physical considerations discussed in the preceding section. The carbonized zone extends from the electrode radius, R_E, to the instantaneous carbonization front radius, R_F. The electrode and the fully carbonized zone are assumed to be at a constant maxiumum temperature, T_F. The entire electrical heat generation is assumed to occur in a thin zone of thickness ΔR across which the temperature drops from T_F to the ambient coal temperature, T_O.

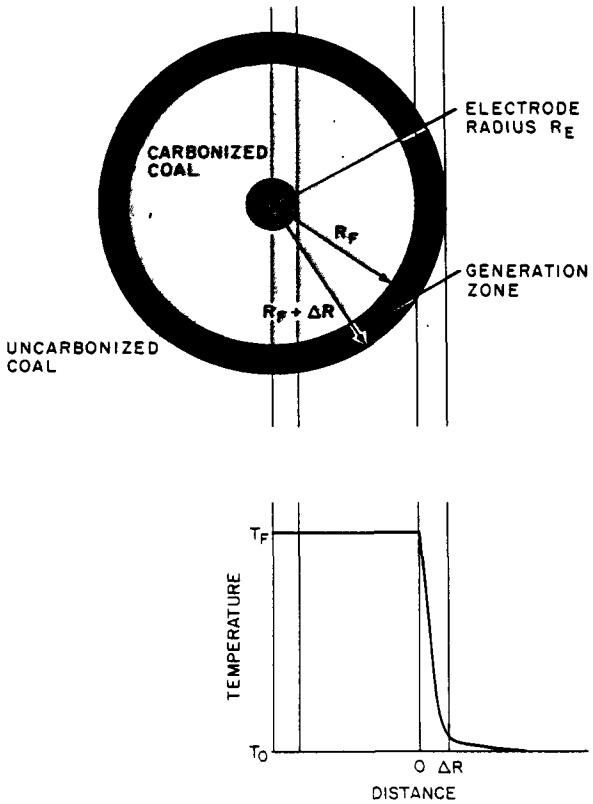

Figure 1. Idealized Electrolinking Process and Corresponding Dimensionless Temperature Profile.

The propagation of the carbonization front is described by the solution to the coupled electric field and thermal energy equations which are given in cylindrical coordinates by the following:

$$\nabla\cdot[\rho_E\nabla\bar{V}] = \frac{1}{r}\frac{\partial}{\partial r}\left(\frac{r}{\rho_E}\frac{\partial\bar{V}}{\partial r}\right) = 0 \qquad (1)$$

and

$$\rho C_p\frac{\partial\bar{T}}{\partial t} = \frac{k}{r}\frac{\partial}{\partial r}\left(r\frac{\partial\bar{T}}{\partial r}\right) + \frac{1}{\rho_E}\left(\frac{\partial\bar{V}}{\partial r}\right)^2 \qquad (2)$$

where $\bar{V}$ is the electric potential (V), $\bar{T}$ is the temperature (K), ρ_E is the electrical resistivity ($\Omega\cdot$m), ρ is the mass density (kg/m^3), C_p is the heat capacity (J/kg$\cdot$K), and k is the thermal conductivity (J/kg$\cdot$m$\cdot$K).

The solution to the above equations is complicated because the electrical resistivity, ρ_E, is a highly nonlinear function of temperature which exhibits a

maximum at approximately 200°C. Since the goal of these initial modeling studies was to discern the mechanism whereby electrolink channels form, several simplifying assumptions were made in order to obtain an analytical solution to eqs. (1) and (2). First, a constant effective electrical resistivity $\bar{\rho}_E$ was defined such that it would result in the same total amount of heat generation as ρ_E; that is,

$$\frac{1}{\bar{\rho}_E}\int_{R_F}^{R_F+\Delta R}\left(\frac{\partial \bar{V}}{\partial r}\right)^2 r\,dr = \int_{R_F}^{R_F+\Delta R}\frac{1}{\rho_E}\left(\frac{\partial \bar{V}}{\partial r}\right)^2 r\,dr \quad (3)$$

Secondly, the voltage and temperature profiles were assumed to exhibit quasi-steady-state behavior in a coordinate system convected at the carbonization-front velocity, $\bar{v}$. Finally, all the electrical heat generation was introduced via heat conduction at the carbonization front rather than appearing as a homogeneous generation term as in eq. (2). This approximation is analogous to the infinitesimally thin flame sheet approximation invoked in combustion problems. This heat conduction term is determined as follows. An overall energy balance on the system shown in Figure 1 yields

$$\rho C_p (T_F - T_0) R_F \frac{dR_F}{dt} + \frac{d}{dt}\int_{R_F}^{R_F+\Delta R} \rho C_p (\bar{T} - T_0) r\,dr$$

$$= \int_{R_F}^{R_F+\Delta R}\frac{1}{\rho_E}\left(\frac{\partial \bar{V}}{\partial r}\right)^2 r\,dr \quad (4)$$

The second term in the above represents the accumulation of energy in the generation zone which is zero under the quasi-steady-state assumption. If this term is expanded via Leibnitz' rule and the result simplified using eqs. (2) (without the generation term) and (4), one obtains

$$kR_F\left.\frac{\partial \bar{T}}{\partial r}\right|_{R_F} = -\int_{R_F}^{R_F+\Delta R}\frac{1}{\rho_E}\left(\frac{\partial \bar{V}}{\partial r}\right)^2 r\,dr \quad (5)$$

The equation above, along with the following boundary conditions, permits an analytical solution to the simplified forms of eqs. (1) and (2):

$$\bar{V} = V_w,\ \bar{T} = T_F \quad \text{at} \quad r = R_F \quad (6)$$

$$\bar{V} = 0,\ \bar{T} = T_0 \quad \text{at} \quad r = R_F + \Delta R \quad (7)$$

where V_w is one-half the potential difference applied between the two electrodes. These four boundary conditions along with eq. (5) determine the four integration constants and the unknown carbonization front velocity $\bar{v}$. It can be shown that in eq. (7) $T = T_0$ is satisfied whenever the generation zone thickness ΔR is equal to at least five characteristic conduction lengths, that is, $\Delta R = 5k/\rho C_p \bar{v}$.

The resulting solutions for the potential and temperature distributions are given by

$$\frac{\bar{V}}{\bar{V}_w} = \frac{\ell n\left[\dfrac{x + N_1}{N_1 + 5}\right]}{\ell n\left[\dfrac{N_1}{N_1 + 5}\right]} \quad (8)$$

$$\frac{\bar{T} - T_0}{T_F - T_0} = 1 - N_1\int_0^x \frac{\exp(-z)}{(z + N_1)}\,dz \quad (9)$$

in which x is a dimensionless distance coordinate defined by $x = (r - R_F)\bar{v}\rho C_p/k$, and N_1 is the dimensionless carbonization front velocity given by

$$N_1 \equiv \frac{\bar{v} R_F \rho C_p}{k} = \left[N_4 \ell n\left(\frac{N_1 + 5}{N_1}\right)\right]^{-1} \quad (10)$$

where N_4 is the electrolinking properties group defined by

$$N_4 \equiv \bar{\rho}_E k (T_F - T_0)/V_w^2 \quad (11)$$

The quantity N_4 is the dimensionless group which characterizes the electrolinking process and is a measure of the ratio of heat conduction to electrical heat generation.

ELECTROLINK CHANNEL DEVELOPMENT

Equations (8), (9), and (10) are only of value in describing the propagation of electrolinking during its initial stages when the carbonization front is expanding symmetrically about the electrode. We now seek to determine whether this radial expansion is a stable process or whether it will degenerate into one or more electrolink channels in response to minute perturbations in the electric-field strength, physical properties, etc. That is, electrolink channel development is hypothesized to arise from the inherent instability of a purely radially expanding carbonization front.

In order to determine if the radially expanding carbonization front is stable, small perturbations of V', T' and ξ' are imposed on the dependent variables $\overline{V}$, $\overline{T}$, and R_F which were determined above. The appropriate form of the electric field and thermal energy equations which the perturbation variables must satisfy are determined by substituting $V = \overline{V} + V'$, $T = \overline{T} + T'$, and $R = R_F + \xi'$ into these equations, linearizing these equations in V', T' and ξ', which are assumed to be infinitesimally small, and canceling those terms which satisfy eqs. (1) and (2) identically. The resulting equations are

$$\frac{1}{r}\frac{\partial}{\partial r}\left(r\frac{\partial V'}{\partial r}\right) + \frac{1}{r^2}\frac{\partial^2 V'}{\partial \theta^2} + \frac{\partial^2 V'}{\partial z^2} = 0 \qquad (12)$$

$$\rho C_p \frac{\partial T'}{\partial t} = k\left[\frac{1}{r}\frac{\partial}{\partial r}\left(r\frac{\partial T'}{\partial r}\right) + \frac{1}{r^2}\frac{\partial^2 T'}{\partial \theta^2} + \frac{\partial^2 T'}{\partial z^2}\right] \qquad (13)$$

In arriving at the above, we have invoked the same simplifying assumptions as were used to simplify eqs. (1) and (2). Note that the angular (θ) and axial (z) coordinate derivatives enter into the above since the perturbations in general will cause variations in the potential and temperature fields in all three coordinate directions. The time derivative remains in eq. (13) even though the quasi-steady-state (QSS) assumption is being invoked since the QSS applies only to the unperturbed state; the perburbation variables V', T' and ξ' will grow or decay in time depending on whether the system is unstable or stable.

The appropriate forms of the boundary conditions described by eqs. (5), (6), and (7) which are satisfied by the perburbation variables are developed in the same way as described above for the field equations and are given by

$$-kR_F\left[\frac{\partial T'}{\partial r} + \xi'\frac{\partial^2 \overline{T}}{\partial r^2}\right] - k\xi'\frac{\partial \overline{T}}{\partial r} = \int_{R_F}^{R_F+\Delta R} 2\left(\frac{\partial \overline{V}}{\partial r}\right)\left(\frac{\partial V'}{\partial r}\right) r\,dr - \left(\frac{\partial \overline{V}}{\partial r}\right)^2 R_F\xi' \quad \text{at} \quad r = R_F \qquad (14)$$

$$V' = -\xi'\frac{\partial \overline{V}}{\partial r}, \quad T' = -\xi'\frac{\partial \overline{T}}{\partial r} \quad \text{at} \quad r = R_F \qquad (15)$$

$$V' \to 0, \quad T' \to 0 \quad \text{as} \quad r \to \infty \qquad (16)$$

These boundary conditions, which must be applied at $r = R_F + \xi'$, are expressed in terms of conditions at $r = R_F$ by expanding in a Taylor series about $r = R_F$ and linearizing the result in the perburbation variables. Since the upper limit of integration in eq. (5) becomes $R_F + \xi'$ when perturbed, the additional term on the right-hand-side of eq. (14) is obtained.

Equations (12) and (13) subject to the boundary conditions given by eqs. (15) and (16) have solutions of the form

$$V' = \hat{V}(x)\exp(ik_\theta\theta)\cdot\exp(ik_z z)\cdot\exp(\beta t) \qquad (17)$$

$$T' = \hat{T}(x)\exp(ik_\theta\theta)\cdot\exp(ik_z z)\cdot\exp(\beta t) \qquad (18)$$

where

$$\hat{V}(x) = -\left[N_1 \ell n\left(\frac{N_1}{N_1+5}\right)\right]^{-1}\xi'\exp(px) \qquad (19)$$

in which

$$p = -\frac{1}{2}N_1^{-1} - \frac{1}{2}\left[N_1^{-2} + 4\alpha^2\right]^{1/2} \qquad (20)$$

$$\alpha^2 = \left(\frac{k_\theta}{N_1}\right)^2 + k_z^2 = \left(\frac{k_\theta}{N_1}\right)^2 + \left(\frac{2\pi n k}{\rho C_p \bar{v} L}\right)^2 \qquad (21)$$

and

$$\hat{T}(x) = \xi' \exp(sx) \qquad (22)$$

in which

$$s = -\frac{1}{2}\left(N_1^{-1} + 1\right) - \frac{1}{2}\left[\left(N_1^{-1} + 1\right)^2 + \left(4\alpha^2 + \beta N_1^{-1}\right)\right]^{1/2} \qquad (23)$$

The parameter β is the amplifcation factor of the three-dimensional perburbation having wave number, α; a wave number corresponding to a positive value of β will increase in amplitude with time, whereas a wave number corresponding to a negative β will decay. Note that a normal mode analysis is assumed whereby a random perturbation is represented by a double Fourier series of normal modes having wave numbers k_θ and k_z in the θ- and z-directions, respectively. Since eqs. (12) and (13) are linear, only a single set of normal modes need be considered in order to determine the behavior of all possible combinations of these modes. Note that k_θ and n in eq. (21) are integers. Since the electrode length, L, is usually much greater than the characteristic conduction length, $k/\rho C_p \bar{v}$, k_z is very small and will be assumed to be zero.

When eqs. (17) and (18) are substituted into eq. (14), the unknown perturbation amplitude of the carbonization front ξ' drops out and a relationship between α, β, and N_4, the electrolinking properties group is obtained:

$$\beta = N_1[N_6 - (N_1^{-1} + 1)^2 - 4\alpha^2]/4 \qquad (24)$$

where

$$N_6 = [2\phi(N_1 N_4)^{-1} + 2] - (N_1 + 1)N_1^{-1}]^2 \qquad (25)$$

and

$$\phi = -\left\{N_1\left[\ell n\left(\frac{N_1}{N_1 + 5}\right)\right]^2\right\}^{-1} \cdot \{2[\exp(5p) - 1] + 1\} \qquad (26)$$

DISCUSSION OF RESULTS

The principal results of this analysis are given by eqs. (10) and (24). The former yields the dimensionless carbonization front velocity N_1 as a function of the electrolinking properties group, N_4, and is plotted in Figure 2. The group N_4 is a measure of the ratio of heat conduction to heat generation. Large values of N_4, corresponding to lower voltages and higher resistivities, imply markedly reduced values of the carbonization front velocity.

An interesting result of this analysis is the estimate obtained for the generation zone thickness, ΔR. The field tests reported by Wilson et al. (5) suggest that for 10 cm electrodes, this was in the range $0.053 \leq \Delta R \leq 0.086$ cm as determined from the measured front velocities. This implies that the zone wherein a significant portion of the heating and voltage drop occurs is extremely thin. Hence, the power requirement for electrolinking should increase less markedly with electrode spacing than would be the case for a medium of constant electrical resistivity for which it would increase as the square of the electrode spacing.

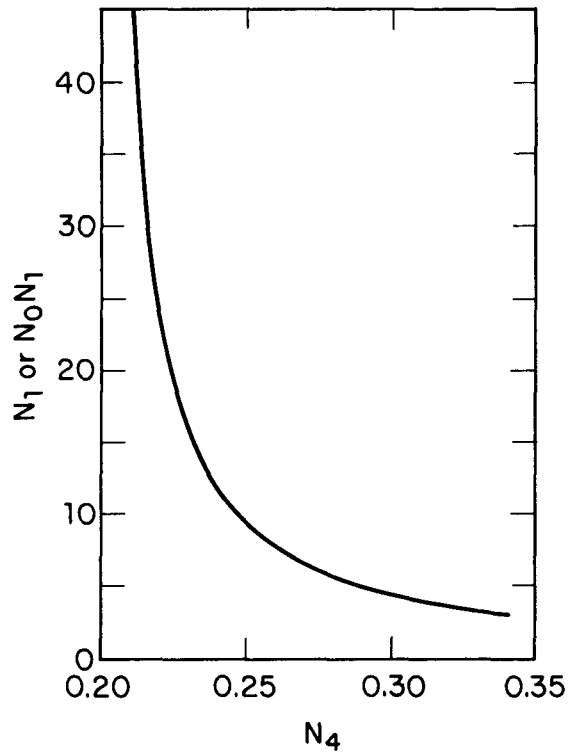

Figure 2. Dimensionless carbonization front velocity as a function of the electrolinking properties group.

Equation (24) can be used to infer the characteristics of electrolink channel formation. For a specified N_4, eq. (24) implies a unique relationship between β, the amplification factor, and α, the channel wave number; this relationship is not continuous, however. Equation (21) relates α to k_θ and k_z, the circumferential and axial wave numbers, respectively. The latter is essentially zero for electrodes whose length is considerably greater than their radius. Hence, eq. (21) implies that physically realizable channel wave numbers correspond to discrete values of α corresponding to $k_\theta = 0,1,2,....$ Only values of α corresponding to positive β's can lead to observable electrolink channels, since as eqs. (17) and (18) indicate, positive β's imply perturbations which will grow. Although positive β's may be found for several values of α, one of these α's will be associated with the largest β for the specified N_4. This α is associated with a $k_{\theta m}$ which is the most probable number of electrolink channels. The minimum number of channels, $k_{\theta \ell}$, corresponds to the smallest physically realizable value of α for which a positive β can be found. The maximum number of channels, $k_{\theta u}$, corresponds to the largest physically realizable value of α for which a positive β can be found.

Table I shows the values of $k_{\theta \ell}$, $k_{\theta m}$, $k_{\theta u}$ and N_1 for selected values of N_4. Table I indicates that as N_4 decreases, or voltage $\overline{V}_w$ increases, both the range of unstable wave numbers as well as the number of electrolinks increases. This implies that the electrolink channel diameter decreases as the electrode voltage increases. Equation (24) predicts that the number of electrolink channels is unbounded at $N_4 = 0.2$. This physically unrealistic prediction results from the fact that eq. (10) predicts that N_1 becomes unbounded at $N_4 = 0.2$. The physically unrealistic predictions at $N_4 = 0.2$ stem from choosing $\Delta R = 5k/\rho C_p \overline{v}$ in eq. (5). It appears that $\rho C_p \overline{v} \Delta R/k$ is in fact a function of N_4 such that $\rho C_p \overline{v} \Delta R/k \to \infty$ as $N_4 \to 0$. However, the first-generation model developed here cannot account for this more complex behavior. Hence, the reader is cautioned not to attach special significance to the limiting value of $N_4 = 0.2$.

Table I: Characteristics of Electrolink Channel Formation as a Function of the Electrolinking Properties Group

N_4	N_1	$k_{\theta \ell}$	$k_{\theta m}$	$k_{\theta u}$
0.205	99.2	18	29	40
0.210	49.2	10	14	19
0.215	32.5	7	9	12
0.220	24.2	6	7	8
0.225	19.2	5	5	6
0.230	15.9	5	5	5
0.231	15.4	S T A B L E		

The predictions shown in Table I suggest that for sufficiently large values of N_4 (>0.230), electrolinking is stable with respect to channel formation. This implies that for specified coal properties, there is a minimum voltage below which electrolink channels will not form. This predicted minimum voltage for channel formation is distinct from the minimum voltage predicted by Bondarenko et al. (2) for electrolinking. The latter corresponds to the minimum voltage required to cause sufficient heating in a narrow zone around the electrode so that electrolinking propagates as a moving boundary process. Hence, the stability model along with the prediction of Bondarenko et al. (2) suggest that there are three theoretically possible regimes for electrolinking. For electrode voltages below the minimum voltage predicted by Bondarenko et al., heat conduction relative to heat generation is sufficiently large to preclude raising the coal temperature to values for which the electrical resistivity is significantly larger than that of the ambient coal. For these low voltages, electrolinking is not practicable since a large amount of coal between the two electrodes is being more-or-less uniformly heated very slowly. If the minimum voltage predicted by Bondarenko et al. is less than that required for channel formation corresponding to $N_4 > 0.230$, then an intermediate regime for electrolinking is possible. Presumably under these conditions, the carbonization front will expand radially about each electrode without electrolink channel formation until the asymmetry of the electric field becomes significant, after which time the large carbonized zone will become skewed towards the line-of-centers between the two electrodes. For sufficiently high electrode voltages such that $N_4 < 0.230$, the model

predicts that electrolink channels will form immediately about each electrode.

The physical explanation for electrolink channel formation can be understood by considering the effect of an increase in N_4 which is seen in Table I to decrease the band of amplified wave numbers and ultimately to stabilize the electrolinking process. That is, heat conduction is a stabilizing influence, whereas heat generation is a destabilizing influence. The manner in which these two mechanisms lead to electrolink channel formation can be understood by referring to Figure 3. This figure shows a radially expanding carbonization front symmetric about the electrode (the circle shown by the dashed line) with the generation of one electrolink in insert a and three channels in insert b (as shown by the shaded region within the outer solid line). These channels arise because more current is channeled to the crests of the links being formed, thus resulting in increased heating near the crests which becomes more pronounced as the number of electrolinks increases. Counteracting this is an increase in heat conduction loss near the crest of each link as the number of links increases. These counterbalancing destabilizing and stabilizing mechanisms imply that only a finite band of discrete wave numbers will be unstable at any specified N_4 corresponding to perturbations in the carbonization front having positive β's which presumably will grow to form electrolink channels.

EXPERIMENTAL EVIDENCE IN SUPPORT OF THESE MODEL PREDICTIONS

This analysis indicates that for voltages such that $N_4 < 0.230$, multiple

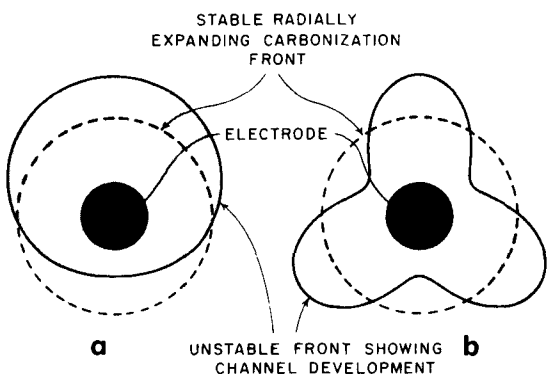

Figure 3. Electrolink formation showing one and three links being generated.

electrolinks can be generated. However, in all the electrolinking experiments reported by Forrester and Sarapuu (3) and by Wilson et al. (5), only one electrolink was observed. This apparent disparity between the model predictions and experimental observations can be explained by the fact that in all the experiments which were excavated in order to determine the number of electrolinks, electrocarbonization was used subsequent to electrolinking in order to enlarge the electrolinks. Electrocarbonization is such that only the first electrolink to break through and establish a high conductance path between the electrodes will be enlarged. Upon excavation, the other non-electrocarbonized channels would be undetected since they would be considerably smaller in diameter. The possibility that multiple electrolinks were generated in the 16 successful electrolinks in the field tests reported by Wilson et al. (5) is supported by the data shown in Table II. This table gives the final electrocarbonized channel radius, $R_{L_{exp}}$, determined by excavation and the predicted final electrocarbonized channel radius, $R_{L_{pred}}$, determined from the model of Bondarenko et al. (2). In nearly all cases the final electrolink radius is predicted to be greater than the experimental value. Since the electrocarbonization model of Bondarenko et al. assumes that the initial radius of the electrolinks is zero, a comparison between the experimental and predicted values in Table II suggests that

Table II: Comparison Between Experimental and Predicted Electrocarbonized Link Radius in Experiments Reported by Wilson et al. (5)

Expt. No.	$R_{L_{exp}}$ (cm)	$R_{L_{pred}}$ (cm)
2	3.7	6.9
6	4.3	8.2
7	3.6	6.3
8	3.8	3.0
9	5.0	1.5
13	3.2	3.3
14	2.9	7.1
15	3.2	5.1
20	5.0	8.2
24	9.6	8.3
26	4.7	7.5
27	6.9	8.9
28	8.0	9.5
29	9.4	9.5
31	9.4	9.4
32	10	7.1

the radius of the electrolink prior to electrocarbonization was negligibly small. Hence, these experiments reported by Wilson et al. suggest that multiple electrolinks may have been generated in many cases, but only the first of these multiple links to break through was subsequently electrocarbonized.

Lessi and Gadelle (7) report the generation of four electrolinks in their laboratory experiments using 0.6 cm electrodes and 3000 V. Four electrolinks could be observed if four or more electrolink channels were generated at each electrode. Those electrolink channels propagating behind each electrode might well die out when the asymmetry of the electric field is felt, such that only those links propagating more-or-less in the direction along the line-of-centers between the electrodes survive and ultimately achieve linkage. Hence, these experiments provide additional support for the model predictions.

MODEL IMPLICATIONS FOR IMPROVING THE ELECTROLINKING PROCESS

The model developed here for the initial stages of electrolinking is highly idealized and represents a first attempt to explain some of the characteristics of electrolinking. The principal result of this model is that it predicts that the electrolinking process can be unstable in that a radially expanding carbonization front about each electrode can give rise to the formation of electrolink channels if the voltage is sufficiently high. Under most practicable operating conditions, electrolinking is probably unstable such that electrolink channels are formed nearly at the initiation of the process. Applying the simplified model developed here to infer how the electrolinking process can be improved is highly speculative. Nonetheless, this model may provide some insight into the problems associated with electrolinking.

Recall that electrolinking was achieved in only 16 of the 32 field test experiments reported by Wilson et al. (5) although in many cases the operating conditions were similar. These results may be explained by the fact that the electrolink channels which were initially generated were quite small as can be inferred from Table II. Small electrolink channels may be more subject to the influence of heterogeneities in the coal which could cause the links to wander along paths which lead to their extinction. The influence of water influx may also be more significant for small links. For cylindrical electrolinks, the ratio of water influx to the heat generated within the link is proportional to ℓ_L/R_L where ℓ_L and R_L are the link length and radius, respectively. This may explain why in some cases small diameter electrolinks cease to propagate as they increase in length.

The question arises as to whether the reliability of the electrolinking process could be improved by making the initial electrolinks larger. The model suggests that larger links might be generated by using larger electrodes or alternatively by operating the electrolinking process initially at voltages below that corresponding to $N_4 > 0.230$. Operating at low voltages might cause the electrocarbonized region to expand radially without electrolink channel formation and thereby enlarge the effective electrode diameter. Once the effective electrode radius has been increased, it might then be possible to generate larger electrolinks by increasing the electrode voltage such that the process becomes unstable to electrolink channel formation. This possibility for creating larger electrolink channels is feasible only if the minimum voltage required for stabilizing the electrolinking process is larger than the minimum voltage predicted by Bondarenko et al. (2) for electrolinking to propagate as a moving boundary process. No information is available to determine if operating in this intermediate regime for electrolinking is possible. A further question is whether larger diameter electrolinks will be less susceptible to heterogeneities in the coal and water influx. An additional potential benefit is that larger electrolinks might obviate the need for enlargement by electrocarbonization. The latter might be particularly advantageous if multiple electrolinks are generated. Field tests employing multiple reverse combustion links suggest that the areal sweep of the gasification process follows the links, and, that multiple links lead to greater resource recovery. This potential improvement in the areal sweep of the coal gasification is lost if electrocarbonization is employed since only one electrolink is enlarged in the electrocarbonization process.

There is no direct confirmation that this suggested improvement in the electrolinking process is feasible. Laboratory experiments are currently being designed to test these concepts. The accuracy of the predictions in this paper is subject to considerable uncertainty due to the simplifying approximations invoked to obtain this first-generation model. Work is underway to refine and extend these model predictions.

ACKNOWLEDGMENTS

The authors gratefully acknowledge financial support from the U.S. Department of Energy (Contract No. DE-AS20-80LC10442) and the Gas Research Institute (Contract No. 5081-260-0570). A portion of this research was completed while one of the authors (WBK) was at Aachen Technical University in West Germany supported by a Fulbright-Hays Senior Research Fellowship and a Faculty Fellowship from the University of Colorado. The authors also acknowledge Ms. Ellen Romig for assistance in typing and preparing the final manuscript.

REFERENCES CITED

(1) J. A. Britten, W. B. Krantz, and R. D. Gunn, "Modeling Studies of Reverse Combustion Linking at High Pressure," Proceedings of the Eighth Underground Coal Conversion Symposium, Sandia Laboratories, Rept. SAND 82-2355, 515 (1982).

(2) S. T. Bondarenko, B. K. Brodskaya, S. N. Lyandres, E. A. Meerovich, V. T. Pan'kovskii, and A. D. Reznikov, "Application of Electric Current for Direct Action on a Seam of Fuel in Shaftless Underground Gasification," G. M. Krzhizhanovskii Power Institute, Academy of Sciences of the USSR (1959); Lawrence Livermore Laboratory, UCRL-TRANS-11050 (1976).

(3) J. D. Forrester and E. Sarapuu, "The Process of Underground Electrocarbonization," University of Missouri, School of Mines and Metallurgy, Technical Series, Bulletin No. 78 (1952).

(4) J. L. Elder, M. H. Fies, H. G. Graham, J. P. Capp, and E. Sarapuu, "Field-Scale Experiments in Underground Gasification of Coal at Gorgas, Alabama--Use of Electrolinking-Carbonization as a Means of Site Preparation," U.S. Bureau of Mines, RI 5367 (1957).

(5) M. W. Wilson, L. L. Hirst, J. L. Elder, J. P. Capp, and J. L. Gentile, "Simulated Underground Gasification for Coal and Electrolinking-Carbonization Method of Preparing Path in a Coal Bed," U.S. Bureau of Mines, RI 5605 (1960).

(6) S. N. Lyandres and A. D. Reznikov, "The Use of Electric Current for Firing Underground Generators," Podzemnaya Gazifikatsiya Uglei, No. 2, 49 (1958); U.S. Bureau of Mines, Translation No. BM-583.

(7) J. Lessi and C. Gadelle, personal communication to W. B. Krantz, Institute Francis du Petrole, Rueil Malmaison, France (1982).

(8) R. D. Gunn, and W. B. Krantz, "Reverse Combustion Instabilities in Tar Sands and Coal," Soc. Pet. Eng. J., 20, 267 (1980).

(9) W. B. Krantz and R. D. Gunn, "Use of Stability Theory in Interpreting UCG Field Test Data," In Situ 5(3), 199 (1981).

(10) R. K. Tidball, "Mathematical Model of Electrolinking," M.S. thesis, University of Colorado, 1983.

3.19 CORRELATION OF LABORATORY-SCALE COAL GASIFICATION DATA WITH THE RAWLINS UNDERGROUND COAL GASIFICATION-STEEPLY DIPPING BED TESTS

by

P. F. Ahner [1]
P. M. Goldberg [1]

ABSTRACT

A laboratory-scale coal gasification reactor has been built and operated to study the effects of process variables (steam/ oxygen ratio, oxygen flux, and pressure) on the yield and composition of the product gas. Results from this study have been compared to data collected during the Gulf-DOE program for UCG-SDB at Rawlins. Many of the trends observed at Rawlins, Test 2, i.e., enhanced methane production at high pressure, and enhanced production at high steam-oxygen ratios have been reproduced in the lab-scale experiments. These studies also contributed to the development of a conceptual UCG reactor which treats the overall reactor as a series of composite reactors each with a different size, a different temperature and different reactants. These reactors are discussed in terms of thermodynamic, kinetic, and catalytic considerations.

INTRODUCTION

The second test in the Rawlins UCG-SDB (Underground Coal Gasification of Steeply Dipping Beds) program was completed in November of 1981 by Gulf Research & Development Company under DOE funding (contract No. DE- AC20-77ET13108). During the operation of Module I, several important correlations were found between operating parameters and product gas composition and yield which were not seen in any other field test.[1,2] Increasing steam/oxygen ratio from 3 to 5 increased product yield (scf dry product/scf oxygen) from 7 to 10 and increased hydrogen concentration. As pressure was increased from 91 psia to 161 psia, methane concentration rose from 18% to 25% and hydrogen decreased from 31% to 26%. A lab-scale gasifier program was initiated to investigate these correlations found during Module I operation further.

COAL GASIFICATION CHEMISTRY

The basic chemistry in UCG is similar to surface gasifiers but some reactions are enhanced due to inherent differences in reactor size and configuration, water influx, and temperature distribution characteristics.

The primary reactions include:

Combustion:

$$C + O_2 = CO_2 + 94.05 \text{ kcal/mole}$$
$$2C + O_2 = 2CO + 26.42 \text{ kcal/mole}$$

Gasification:

$$C + H_2O = CO + H_2 - 31.4 \text{ kcal/mole}$$
$$C + CO_2 = 2CO - 41.2 \text{ kcal/mole}$$

Pyrolysis:

$$\text{coal + heat = char + tar + gases}$$

Secondary reactions include:

Water-gas shift:

$$CO + H_2O = CO_2 + H_2 + 9.8 \text{ kcal/mole}$$

[1] Gulf Research & Development Company
P. O. Drawer 2038
Pittsburgh, PA 15230

Methanation:

$$C + 2H_2 = CH_4 + 17.9 \text{ kcal/mole}$$
$$CO + 3H_2 = CH_4 + H_2O + 59.0 \text{ kcal/mole}$$

Thermodynamic equilibria, kinetics, and catalysis all have a significant effect on the above reactions and therefore control product gas composition and yield (scf dry product gas/scf oxygen injection). Each of these factors is directly affected by temperature, pressure, residence time, concentration of reactants in the reaction zone and the presence of catalysts. In turn, these factors are affected by reactor configuration, size of the reaction zone, coal composition, temperature distribution in the reactor, etc., as shown in Figure 1.

EXPERIMENTAL

The coal gasification reactor, shown in Figure 2, is based on a Lawrence Livermore design.[3] The coal is contained in a 3 in. ID x 30 in. thin-walled, 310 stainless steel sleeve which holds about 5 lb of coal. The stainless steel bellows absorbs the thermal expansion difference between the inner sleeve and the outer pressure vessel. The space between the inner and outer vessels is insulated to decrease heat loss. The outer vessel contains the operating pressure to allow use of a thin-walled sleeve to contain the coal. A thin-walled sleeve is required to minimize the thermal transfer effects along the coal bed axis since excessive heat transfer in this direction significantly alters the combustion characteristics of the coal leading to unrealistic gasification conditions. Thermocouple strings monitor 16 points inside the coal bed itself and 8 points along the reactor skin.

The gasifier flow sheet (Figure 2) allows oxygen, steam, carbon dioxide, nitrogen, and air to be used as injectants. Argon is used to balance the pressure between the inner sleeve and the outer pressure vessel. The products are sent through a tar water knock-out trap and a dry gas flow meter prior to analysis by gas chromatography and venting. Temperature, pressure, and product gas flow data are collected by a data logger.

Subbituminous Rawlins "G" seam coal (the seam in which the field tests were conducted) was used in all runs and, except for the first two runs, was superficially dried in nitrogen at 100°F for 24 h prior to loading. The particle size ranged between 1/16 and 1/8 in. The coal composition is shown below:

Rawlins "G" Seam Coal Composition
(Percent by Weight)

Proximate		Ultimate	
Carbon	74.42	Water	14.62
Hydrogen	5.15	Ash	5.07
Oxygen	19.33	Volatile	35.41
Nitrogen	0.91	Fixed Carbon	44.64
Sulfur	0.23	Sulfur	0.18

NOTE: The analyses is based on the average of 27 as-received core samples. The ultimate analysis is on a moisture ash-free basis.

RESULTS

Discussion of Gasifier Results

A summary of the steam/oxygen runs is given in Table I. Molar steam/ oxygen ratios between 2 and 8 were studied at oxygen flow rates between 2 and 5 scfh. Pressures were varied between 35 and 165 psia. Mass balances (total lb in/ total lb out) remained between 0.86 and 1.10. Channeling of the gasification front through the center of the packed bed was a frequent occurrence during many of the high steam/oxygen ratio runs. Channeling was evidenced by increased burn front progression rate as determined from thermocouple data and through reactor inspection after each run. There are several possible reasons for this trend between progression rate and steam/oxygen ratio.[4] The extreme temperature profile across the diameter of our combustion zone indicates that heat loss was the main reason for channeling in our system. The combustion zone in the center of the bed is >2000°F, but it quickly decreases to around 1000°F at the reactor walls due to heat losses (there are no guard heaters in our system). High steam/oxygen ratios tend to cool the overall reaction zone for two reasons: it promotes the endothermic steam-char reaction and it increases the heat capacity of the injectants. Since the walls of the reactor are cooler than the center, this cooling effect slows the gasification at the walls leaving this coal unreacted and essentially creating a

reactor with a smaller, effective radius. This phenomenon should not therefore have a significant impact on the gasification chemistry and it apparently didn't, considering the very similar effects that ratio had on both the gasifier product and the Rawlins product. The temperature profiles obtained during each run were similar to that obtained by others[3,4,5] and are not shown.

Figures 3 through 10 compare the data obtained from the experiments described above. The products of gasification are presented both as concentrations and as production rates per unit of oxygen injection. This dual presentation is used because data based only on concentrations can be deceiving since large increases in the rate of formation of one product can produce apparent decreases in the concentration of the other products. This production rate per unit oxygen (scfh dry product/scfh oxygen) is defined as product yield. Throughout the plots, trend lines A, B, and C connect data obtained at similar experimental conditions.

Figures 3 and 7 show plots of hydrogen concentration and yield vs steam/oxygen ratio respectively. The strongly increasing trends with steam/oxygen ratio is evident in both figures. Increasing pressure decreases hydrogen (lines A&B) but higher oxygen flows counteract this tendency (line C). Increasing the oxygen flow from 2.2 to 5.1 scfh increases the combustion rate which increases the heat available to the system as evidenced by the average temperature of the reactor skin which rose an additional 220 to 350°F. Although heat losses were higher due to the higher temperatures, most of the additional heat was utilized to promote the endothermic reactions thereby increasing gasification efficiency. The steam/oxygen ratio has a direct effect on hydrogen through two mechanisms: by the steam-char reaction and by the water-gas shift reaction. Increased steam concentration promotes the steam-char reaction as long as sufficient heat is available from coal combustion. If sufficient heat is not available, it tends to cool the system thereby inhibiting gasification. This was evidenced by the decreasing slope of line A at the higher ratios. The overall participation of the steam-char reaction therefore depends on this balance between the available thermal energy and steam concentration. Unlike the steam-char reaction, the water-gas shift reaction is exothermic and occurs in the cooler parts of the reactor. Some of the hydrogen make shown in Figures 3 and 7 is due to this reaction. Increasing steam/oxygen ratio increases steam concentration which drives the shift reaction forward. Increasing the temperature in the hotter zones of the reactor also drives the shift reaction by increasing the concentration of carbon monoxide (formed by the steam-char reaction or the carbon dioxide reduction reaction) which eventually flows through the cooler zones.

The decreasing hydrogen make as pressure is increased is shown by lines A and B. This trend is caused by: consumption of hydrogen due to methanation reactions and increased heat loss due to increased mass and residence time in the reactor. Increased oxygen flow however, increases the overall gasification efficiency and compensates for the consumption of hydrogen by methanation (line C).

Figures 4 and 8 are plots of carbon monoxide concentration and yield vs steam/oxygen ratio, respectively, with the data points being represented as above. Figure 4, reveals an inverse relationship between concentration and steam/oxygen ratio at both oxygen flow rates. This is reasonable since, at low ratios the water-gas shift is suppressed due to the lower steam concentrations in the cooler parts of the reactor. Suppression of the shift reaction allows more of the carbon monoxide which was formed by the gasification reactions in the hotter parts of the reactor to pass through without change. As expected, the runs made at higher oxygen flows (line C vs line B) produce more carbon monoxide due to enhancement of the endothermic steam-char reaction and the carbon dioxide reduction reaction. The interpretation of Figure 8 is not as simple since carbon monoxide yield data (scf carbon monoxide/scf oxygen) is discussed. In this figure the steam/oxygen trend is reversed for Line A. This reversal is simply due to the overall increase in product gas yield as steam/oxygen ratio is increased. This reversal does not hold for the 5.1 oxygen flow runs (Line C), where the heat is sufficient to promote carbon monoxide formation reactions to the extent that these outweigh the increased yield effects of greater steam/oxygen

ratio. As in the case of hydrogen, lines A and B indicate a decrease of both carbon monoxide concentration and yield with pressure. This decrease with pressure is partially due to the enhancement of the water-gas shift reaction at greater pressures, increased heat loss due to increased mass and residence time in the reactor and possibly also due to consumption of carbon monoxide by catalytic methanation. The shift reaction is enhanced at higher pressures because the hydrogen consumption rate is increased due to methanation. Removal of the product hydrogen from the system favors greater shift reaction which consumes more carbon monoxide.

Figures 5 and 9 are plots of methane concentration and yield vs steam/oxygen ratio respectively. Figure 5 shows the strong dependence of methane concentration on pressure (Line B vs Line A); pyrolysis at atmospheric pressure only produces about 4% methane in our particular system. Since the effect of pressure on pyrolysis is minor, significant methanation must be occurring as revealed by the disappearance of hydrogen and possibly carbon monoxide at the higher pressures. Again, increased oxygen flow (Line C vs Line B) produces more methane due to greater gasification efficiencies, (i.e., namely greater steam-char and carbon monoxide production per unit oxygen). Figure 9, shows the same increasing trend with pressure. Here, as in the hydrogen yield plot, the effect of steam/oxygen ratio and oxygen flow is seen. Increasing ratio and/or oxygen flow has a beneficial effect by either adding more reactant and/or energy to the process to obtain a greater conversion efficiency.

Figures 6 and 10 contain plots of carbon dioxide concentration and yield vs steam/oxygen ratio respectively. Carbon dioxide is directly affected by three major reactions: combustion, reduction to carbon monoxide and the water-gas shift reaction. All other reactions which occur decrease carbon dioxide concentration through dilution effects. The most reasonable explanation for the decrease in concentration with ratio is dilution effects due to the steam-char reaction. The shift reaction is also promoted by steam but apparently the dilution effects of the steam-char reaction mask the effects of the shift reaction in this plot. Increasing oxygen flow (Line C) favors carbon dioxide reduction and the steam-char reaction thereby decreasing carbon dioxide concentration by dilution as well as by reaction. As was seen in the 2.1 scfh oxygen runs (lines A and B), increasing the steam/oxygen ratio at the higher oxygen flows lowers carbon dioxide concentration due to dilution effects. Dilution effects are much greater at this higher oxygen flow since more heat is available for the steam-char reaction. The increasing concentration with pressure (Line B vs Line A) is caused by: methanation which consumes hydrogen thereby promoting the shift reaction and greater heat loss due to increased mass and residence time in the reactor. Figure 10 shows the large effect of steam/oxygen ratio on yield. As ratio increases yield increases (line A), thereby increasing carbon dioxide yield since this parameter is the product of carbon dioxide mole fraction and overall product yield. Line C shows the beneficial effects of both ratio and oxygen flow on reducing carbon dioxide yield.

The overall trends seen in this gasifier work can be summarized as follows:

- Increasing pressure dramatically improves methane yield under all the experimental conditions tested. Under milder gasification conditions, i.e., low oxygen flow and low steam/oxygen ratio, carbon monoxide and hydrogen yield decrease with increasing pressure. Under higher oxygen flows and ratios, yields of these components are not affected as much and methane yield increases further. It appears that as long as sufficient heat and steam is available, greater pressures improve gasification efficiency.

- Increasing the steam/oxygen ratio increases the yield of hydrogen and methane by increasing the concentration of reactants in the steam-char, methanation, and the water-gas shift reactions.

- The effects of insufficient reaction heat (i.e., low oxygen flows and high heat losses) was demonstrated as lower product yields of hydrogen, carbon monoxide and methane and greater yields of carbon dioxide. The oxygen flow must be maintained at

a level to overcome heat loss effects and supply additional energy to maximize the endothermic gasification reactions.

Comparison of Lab Gasifier and Rawlins 2 Module I Data

The gasifier data supports the three major trends seen during Rawlins Test 2, Module I operation; namely, the strong relationships between methane yield and pressure, between overall product yield and steam/oxygen ratio, and the effects of steam/oxygen ratio on product composition. Quantitative comparison between the two processes cannot be made, however, since the UCG-SDB reactor has a configuration which makes it more thermally efficient, enhances reaction kinetics, and forms a much larger reactor (see section below).

Plots of methane concentration vs pressure are shown in Figure 11. Overall the gasifier produces much less methane than the UCG-SDB reactor for the reasons discussed in Section V but the dramatic effect of pressure on methane concentration is apparent. Both studies also indicate that pressure enhances overall product yield presumably by increasing residence time in the reaction zones.

Assuming for the moment that methanation is minor at atmospheric pressure and that pyrolysis is not enhanced appreciably by catalysis or pressure, an idea of the methane coming from pyrolysis and the size of the pyrolysis zone can be obtained by extrapolating these plots back to 15 psia. Rawlins 2, Rawlins 1 (adjusted to a N_2-free basis), and gasifier methane yields are 12%, 9.5%, and 4%, respectively, indicating that the pyrolysis zone of Rawlins 2 is about three times larger than the gasifier (relatively speaking). There is no reason to doubt that the other reactors in the UCG conceptualization below share this same scale-up factor. This albeit simplified conclusion "fits in" with the extremely large conceptual UCG reactors described in Section V below and is one of several reasons for the high product yields seen at Rawlins. It also agrees with the post-test coring program conducted on Module I which revealed a large zone of rubblized coal above the firepit.[22] Figure 12 shows a plot of dry product gas yield vs steam/oxygen ratio using both the gasifier and Module I data. The same increasing trend between yield and ratio is evident for both systems. The high heat losses associated with the gasifier masked this trend somewhat, but it can still be seen. Heat losses hinder the steam-char reaction and leads to decreased utilization of injected steam and lower dry product gas yield. Only 8-12% of the injected steam was utilized in the gasifier, whereas 50% was utilized during Module I. The steam utilization factor of other UCG field tests was around 20%, which demonstrates the high thermal efficiency achieved at Rawlins. The effects of insufficient reaction heat or the deleterious effects of pressure on product yield were not seen during Module I operation as they were in some of the gasifier runs. The heat and reactor size available during Module I operation was enough to maintain product yield, even during high-pressure operation.

The same general trends between product distribution and operating conditions were seen in the gasifier and the Rawlins 2 data. Hydrogen and carbon monoxide decreased and methane increased with increasing pressure. Higher steam/oxygen ratios favored increased hydrogen, etc.

A CONCEPTUAL UCG REACTOR

Considering the above studies and the Rawlins results, a conceptual UCG reactor was developed which could account for the data. A UCG reactor must be treated as a series of smaller reactors each run at a different set of experimental conditions which promote different reactions. Figure 13 illustrates a conceptual UCG reactor with its train of smaller reactors. Figure 14 applies these concepts to a UCG-SDB reactor. The concept shown in Figure 13 is idealized since it treats each reactor as a separate entity. In a real system these reactors form a single continuum with no definite boundaries and subsequently there is much gray area where overlap exists between reactors. Surface packed bed reactors also have the same configuration but, due to cost and temperature limitations, they cannot approach the size of the reduction zones attained in UCG or achieve the same thermal efficiencies.

Starting at the left hand side of Figure 13 oxygen, steam, and char enter

4. Bell and Gunn, "Adiabatic Coal Gasification Tube Experiments - Forward Combustion," Sixth UCC Symposium, Afton, Oklahoma, July 1980.

5. Rodgers, M.E., et.al., "Pressurized Combustion Tube Gasification of Texas and Wyoming Coals," Sixth UCC Symposium, Afton, Ok, July, 1980.

6. Gunn, R.D. and Whitman, D.L., "An In Situ Coal Gasification Model (Forward Mode) for Feasibility Studies and Design," LERC/RI-76/2, February, 1976.

7. Stephens, D.R. and Miller, "Thermodynamic Equilibrium for Wyoming Coal: New Calculations," UCID-17044, February 24, 1976.

8. Stephens, D.R., "Thermodynamic Equilibria for Wyoming Coal," UCID-16094, August 4, 1972.

9. Institute of Gas Technology Research Bulletin 2, January 1948.

10. Channabasappa, K.C. and Linden, H.R., Ind. Eng. Chem., 50, 637-44 (1958).

11. Key, A., Gas Research Board Commun. No. 40 (1948).

12. Zielke, C.W. and Gorin, E., Ind. Eng. Chem., 49, 396-403, 1957.

13. Blackwood, J.D., Coke and Gas, 22, 190-4, 218 (1960).

14. Lessard, R.R., Reitz, R.A., "Catalytic Gasification, an Emerging Technology for SNG," 9th Energy Technology Conference, Washington, D.C., February, 1982.

15. Lang, Robert J. and Neavel, R.C., "Behaviour of Calcium as a Steam Gasification Catalyst," Fuel, 1982, Vol. 61, July, 1982.

16. Somorjai, G. and A. Cabrera, Chem. Eng. News, 59, #43:17, October 26, 1981.

17. Walker, P.L., et al., Int. Fundamental Catalytic Coal and Carbon Gasification Symposium, Amsterdam (9/27-29/1982), Fuel, 62, #2140-49, February 1983.

18. Goring, G.E., et al, "Mechanism of Interaction of Low Temperature Char and Steam-Hydrogen Mixtures at 1600°F," Ind. Eng. Chem., Vol. 45, No. 11, p .2586.

19. Goring, G.E., et al, "Effect of Pressure and Carbon Burnoff on Interaction of Low Temperature Char with Steam-Hydrogen Mixtures at 1600°F," Ind. Eng. Chem., Vol. 44, No. 5, p. 1057.

20. Johnson, G.L., "Kinetics of Coal Gasification," Institute of Gas Technology, John Wiley and Sons, 1979.

21. Bienstock, D. et al, "Pilot Plant Development of the Hot Gas Recycle Process for the Synthesis of High BTU Gas," Bureau of Mines, RI #5841, 1961.

22. Avasthi, J.M., "Underground Coal Gasification Cavity Definition for Rawlins Test 2," presented at the Ninth UCC Symposium, Bloomingdale, Illinois, August 7-10, 1983.

TABLE I

RESULTS OF GASIFIER RUNS

Run No.	O_2 SCFH	S/O Ratio	Pressure psia	% H_2	% CO	% CH_4	% CO_2
1	2.2	4.7	35	39.0	19.6	5.4	35.4
2	2.2	8.5	95	37.0	15.1	7.5	39.4
3	2.2	6.3	95	37.1	16.1	6.8	39.1
4	2.2	6.7	165	30.6	13.8	10.3	43.8
5	2.2	2.5	95	31.3	18.4	7.4	41.6
6	4.4	3.1	95	32.5	27.3	7.8	31.1
7	2.2	2.4	165	25.2	15.1	9.6	48.2
8	5.1	2.1	165	30.5	23.3	10.2	33.2
9	5.1	5.3	165	38.5	21.0	12.7	25.2
10	5.0	2.5	35	36.8	26.0	4.8	30.5

FIGURE 1 FACTORS AFFECTING UCG GASIFICATION REACTIONS

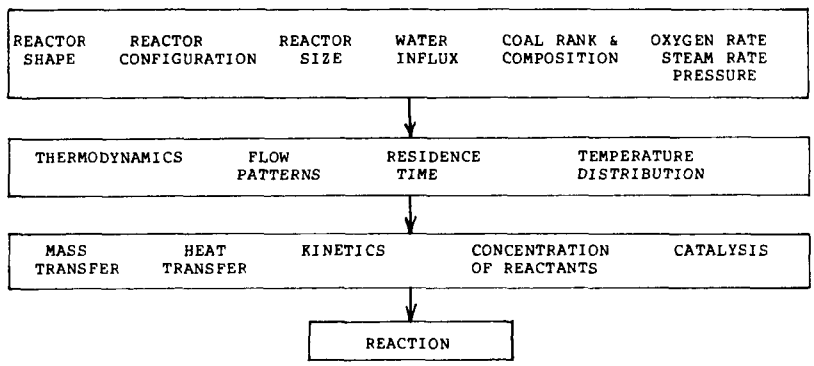

FIGURE 2. LAB GASIFIER FLOWSHEET

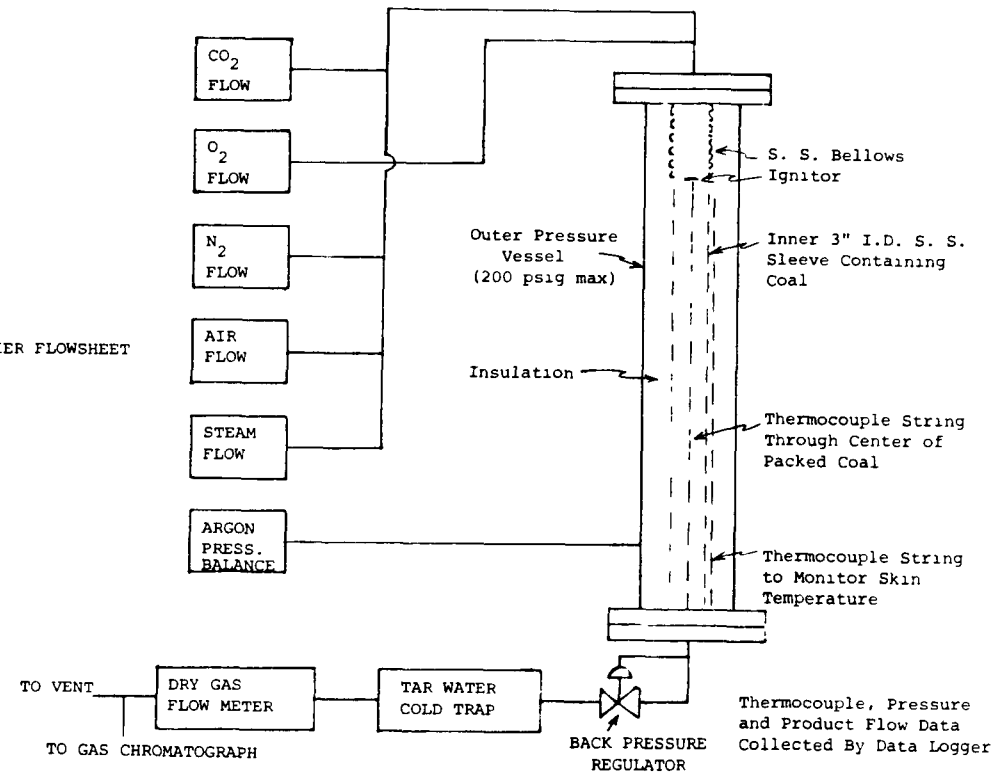

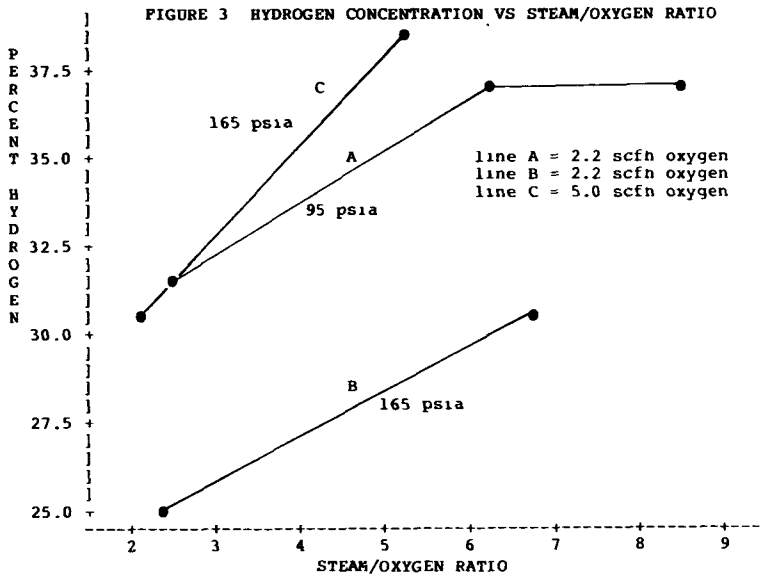

FIGURE 3 HYDROGEN CONCENTRATION VS STEAM/OXYGEN RATIO

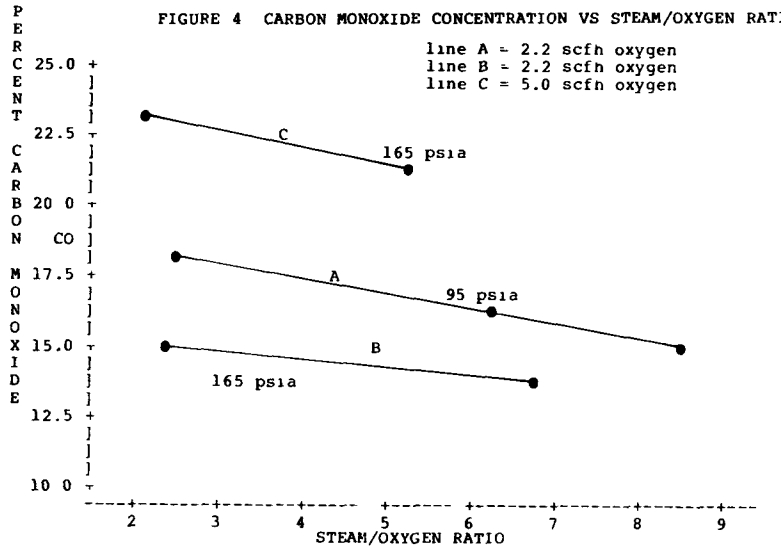

FIGURE 4 CARBON MONOXIDE CONCENTRATION VS STEAM/OXYGEN RATIO

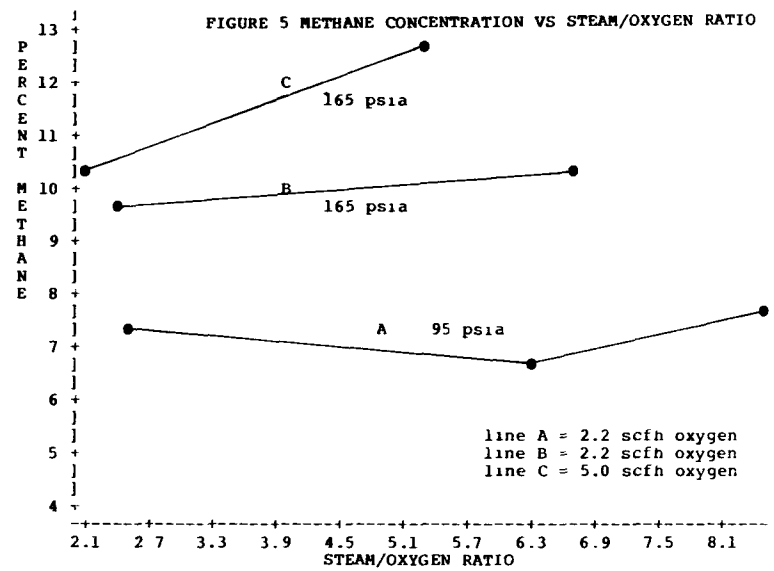

FIGURE 5 METHANE CONCENTRATION VS STEAM/OXYGEN RATIO

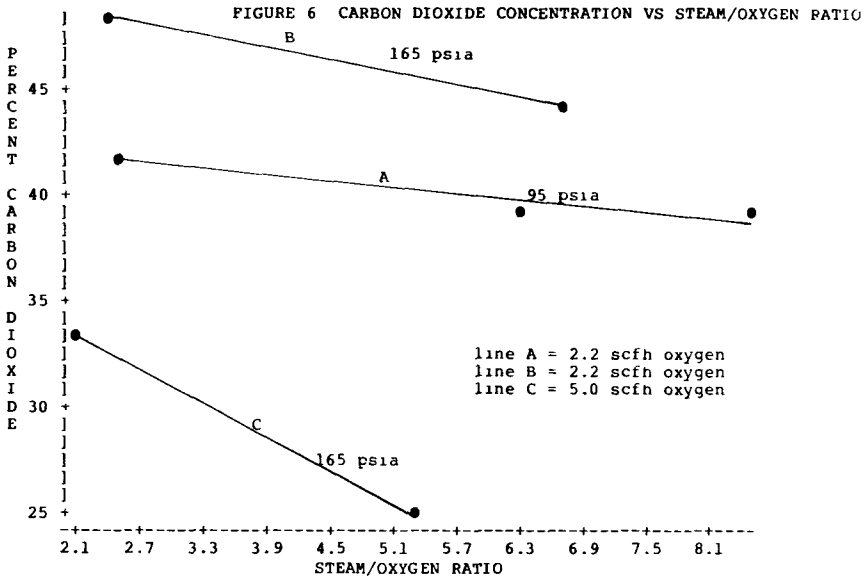

FIGURE 6 CARBON DIOXIDE CONCENTRATION VS STEAM/OXYGEN RATIO

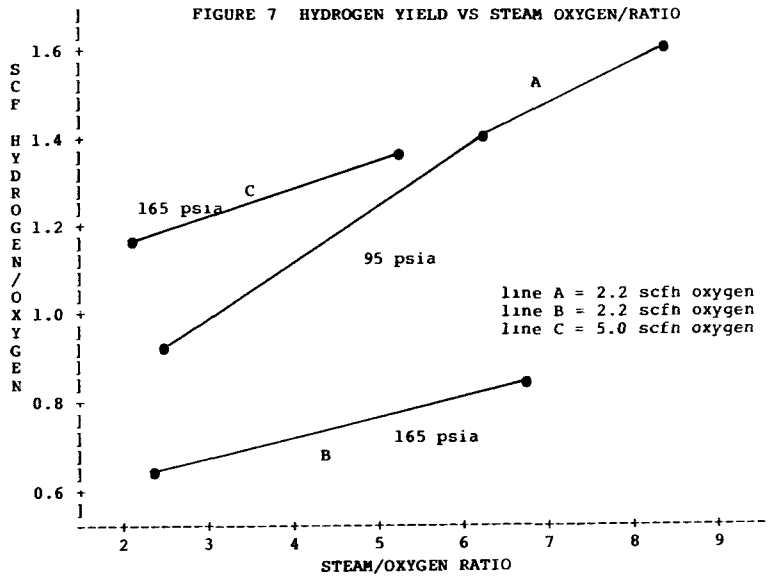
FIGURE 7 HYDROGEN YIELD VS STEAM OXYGEN/RATIO
SCF HYDROGEN/OXYGEN
1.6
1.4
1.2
1.0
0.8
0.6
A
C
165 psia
95 psia
B
165 psia
line A = 2.2 scfh oxygen
line B = 2.2 scfh oxygen
line C = 5.0 scfh oxygen
2
3
4
5
6
7
8
9
STEAM/OXYGEN RATIO

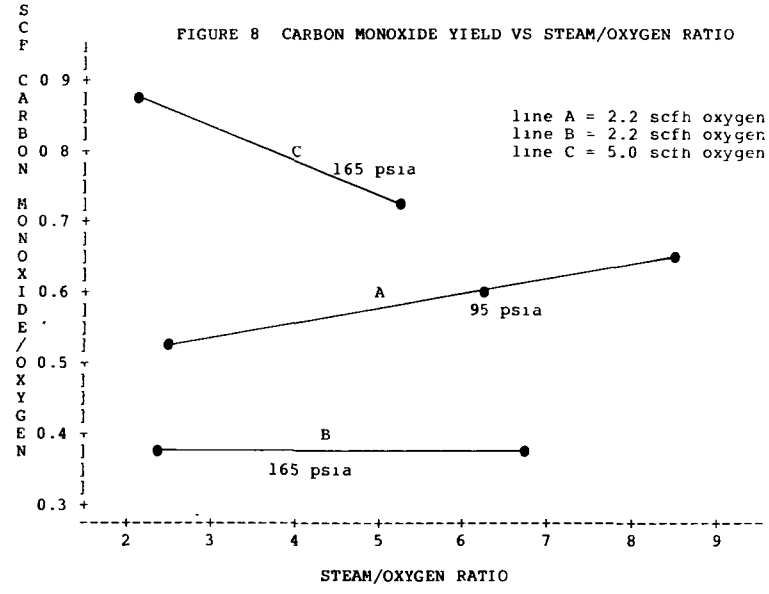
FIGURE 8 CARBON MONOXIDE YIELD VS STEAM/OXYGEN RATIO
SCF CARBON MONOXIDE/OXYGEN
0.9
0.8
0.7
0.6
0.5
0.4
0.3
C
165 psia
A
95 psia
B
165 psia
line A = 2.2 scfh oxygen
line B = 2.2 scfh oxygen
line C = 5.0 scfh oxygen
2
3
4
5
6
7
8
9
STEAM/OXYGEN RATIO

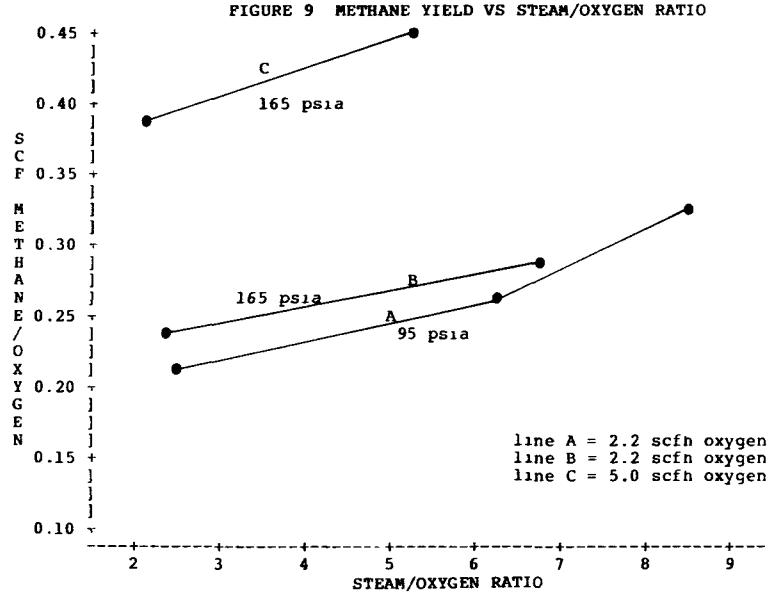
FIGURE 9 METHANE YIELD VS STEAM/OXYGEN RATIO
SCF METHANE/OXYGEN
0.45
0.40
0.35
0.30
0.25
0.20
0.15
0.10
C
165 psia
B
165 psia
A
95 psia
line A = 2.2 scfh oxygen
line B = 2.2 scfh oxygen
line C = 5.0 scfh oxygen
2
3
4
5
6
7
8
9
STEAM/OXYGEN RATIO

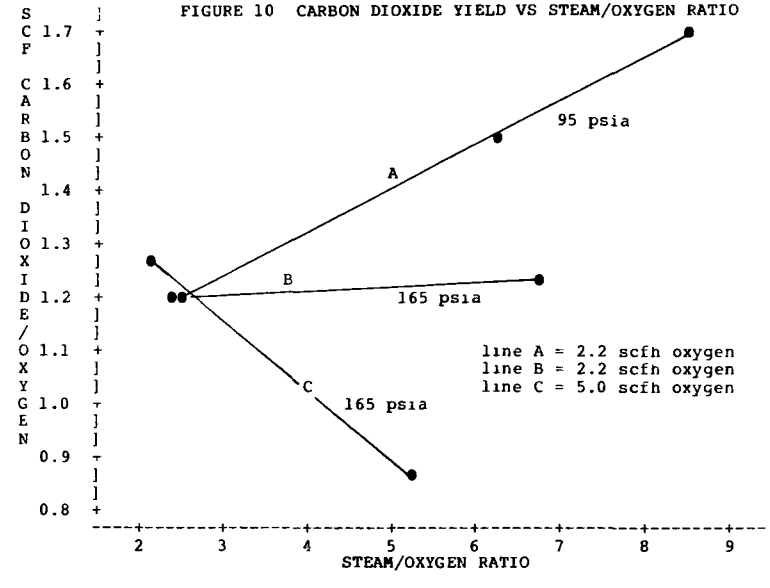
FIGURE 10 CARBON DIOXIDE YIELD VS STEAM/OXYGEN RATIO
SCF CARBON DIOXIDE/OXYGEN
1.7
1.6
1.5
1.4
1.3
1.2
1.1
1.0
0.9
0.8
95 psia
A
B
165 psia
C
165 psia
line A = 2.2 scfh oxygen
line B = 2.2 scfh oxygen
line C = 5.0 scfh oxygen
2
3
4
5
6
7
8
9
STEAM/OXYGEN RATIO

FIGURE 11 COMPARISON OF METHANE CONCENTRATION VS PRESSURE FOR RAWLINS 2 AND GASIFIER DATA

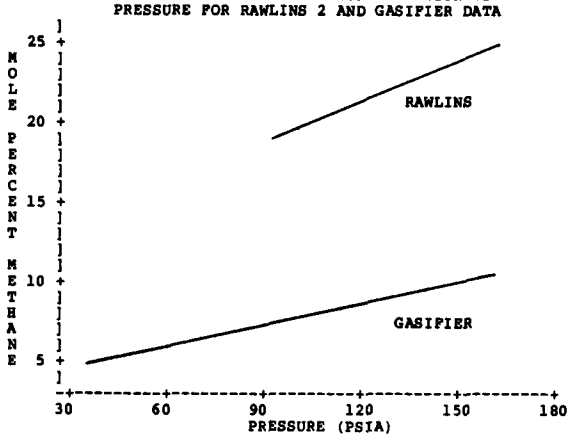

FIGURE 12 COMPARISON OF PRODUCT YIELD VS STEAM/ OXYGEN RATIO FOR RAWLINS 2 AND GASIFIER DATA

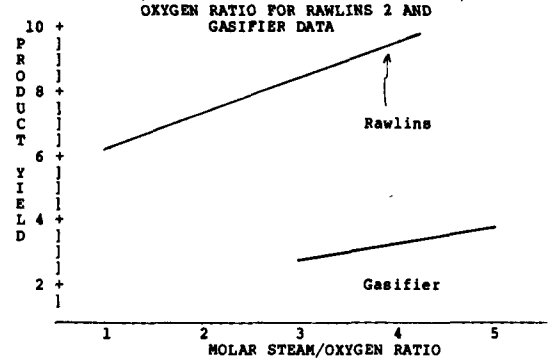

FIGURE 13 A CONCEPTUAL UCG REACTOR

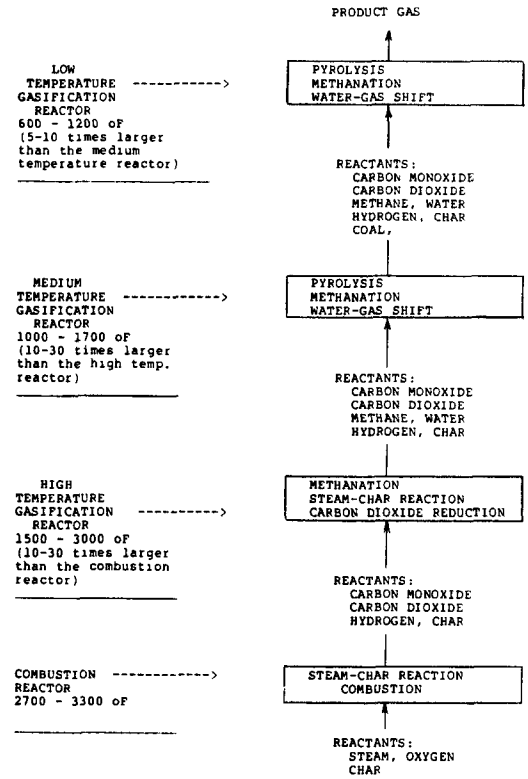

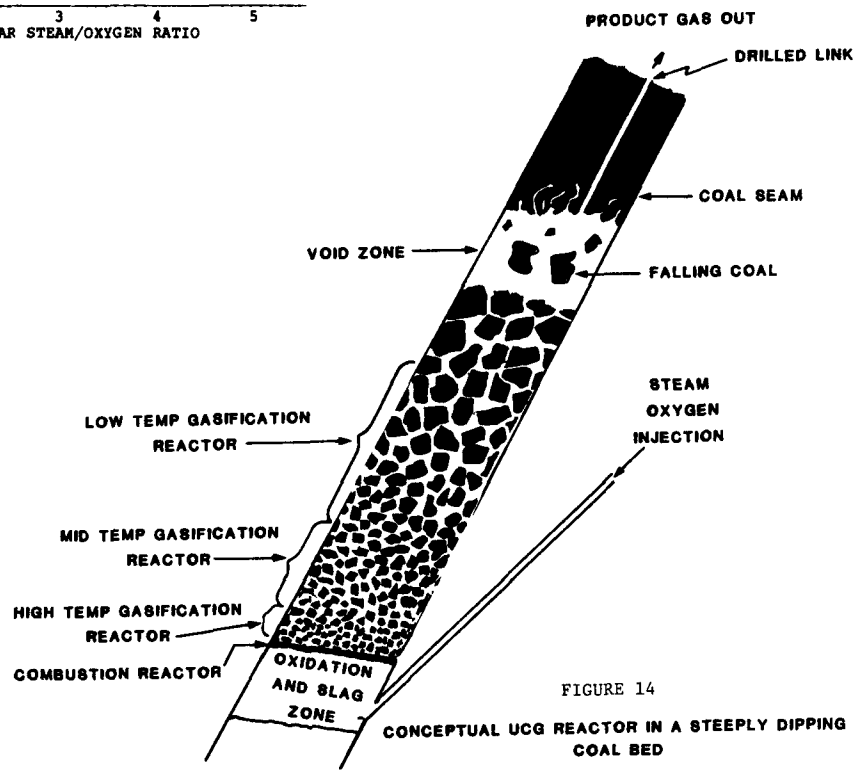

FIGURE 14

CONCEPTUAL UCG REACTOR IN A STEEPLY DIPPING COAL BED

3.20 GASIFYING DUTCH COALS

by

H.H. Boswinkel [1/]

INTRODUCTION

In spite of the large coal deposits in Holland interest in exploiting these reserves revived only recently. Since then a 30 million Dfl exploration programme has been started aiming at an inventory of the coal in some parts of the Netherlands. Simultaneously a number of small scale investigations on advanced extraction methods have been initiated.

The results presented in this paper are part of a technical and economical assessment study of UCG in the Netherlands. The study is being performed under a governmental contract. The first results of a second Dutch investigation [1] aiming at an optimalization of the gasification process also will be presented at this symposium.

In figure 1 a gasification system which produces gas to be utilized in blending high energetic natural gas is illustrated. In this system high pressure air is fed into the thin (1-2 m) Dutch coal seams at depth of approximately 1000 m.

Though short term gasification of thin bituminous coal seams can be considered technically feasible during the study it was experienced that models which describe the economically important long term behaviour of the underground gasifier are not available. In the next pages therefore a suitable model is developed. The model contains a number of assumptions which have to be verified in future development work prior to the execution of field tests in deep lying seams.

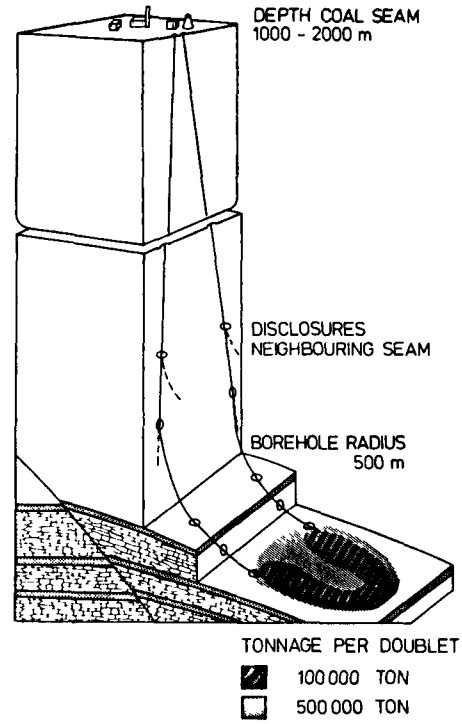

FIG 1 A GASIFICATION DOUBLET

1. DISCLOSING THE COAL SEAM

A boundary condition for commercial UCG is: the cost of disclosing the coal for underground gasification may not exceed the cost of purchasing and coalhandling at a surface gasification plant. To the disclosing costs already belong royalties and reservations for the conse-

1/ Energy Study Centre of the Netherlands Energy Research Foundation, Westerduinweg 3, Postbox 1, 1755 ZG PETTEN, The Netherlands.

quences of subsidence at the surface. This means that especially in Western Europe with its deep lying and thin seams the usual vertical wells would have to be spaced widely apart in order to get access to an economically attractive amount of coal. It is doubtfull whether those wells several hundreds of meters apart ever can be linked by the linking techniques currently available or under development. The only solution to this problem can be found in directionally drilled wells with inseam holes of several hundred meters.

As has been revealed by several authors, for instance, Siegel [2] directional drilling is under development on behalf of the oil companies and conventional mining (degasing) and may become available independent from UCG developments. For the moment the accuracy of inseam drilling depends on the hardness of the surrounding strata but to our opinion undulations in the well path leaving the seam can be tolerated since those sections at least will be pyrolysed during gasification.
In Western Europe a good experience in directional drilling has been gained by the French firms Topservices and Elf-Aquitane [3]. Based on the turbodrilling techniques it seams reasonable to expect that the cost to disclose the coal in a commercial gasifier can be kept below 50 Hfl/ton. The costs of a completed well for a field test at a depth of 500 m have been estimated at 2×10^6 Hfl.

Additional reasoning in favour of directional drilling may be found in:

- The restricted surface area which is required. Especially in Europe it is hard to believe that spatial planning will allow the exploitation of seams from the surface by wells drilled 500 meters apart.
- The orientation of the gasifiers. The mechanical drilling technique permits a free choice in orientation independent from directional variations in coal properties.
- Reliability. Directional drilling is a predictable activity by which even small disturbances in the seam as for instance washouts can be overcome. By the application of directional drilling the vulnerable injection and production channels can be kept out of the subsidence region.

2. THE SHAPE OF THE GASIFIER

In the selected system gasification starts in a drilled hole. Quite soon the initial circular shape of the gasifier will develop into a truncated cone. Within the next week base and cap rock will already be exposed, phase II in figure 2, thus adding to the gasification chamber a widening box of which two walls only consist of char. The width of the box depends on the fracking behaviour of the hot cap rock and the subsidence of the overlying strata.
Phase II gasification is the critical stage in the gasification process. While the box is broadening turbulent mixing decreases and dependent on the Reynolds number gasification at the sidewalls finally may stop [4]. If stage II has been overcome by the fracking and setting mechanisms one or two different flow paths remain hydraulicly separated by an inert packed bed, phase III in figure 2. Essentially no geological mechanism, but the already existing folds and large displacements in the strata, can impede the further expansion of the gasifier in lateral direction. Physical processes as override, ash and slag deposition on sloping char fronts and oxygen bypassing through the inert central bed may hamper the sweep of the gasification.

If on the contrary no process would limit the width of the gasification chamber then as a consequence it would be possible to gasify an economically attractive amount of coal already from a small boreholesystem, with a length of approximately 50 meters. Till further notice a sweep efficiency of 100 m will be assumed.

The wedgeshaped gasification chamber described above will not remain empty. Apart from falling cap rock which forms the central bed:

Thermal stresses and spalling effects [5] will at least cause char rubble preferential at the end of the wedge thus forming an effective fixed bed gasifier [6].

Broken char from the protruding swelling coal seam will also enter the gasification chamber.

On a time scale of days partly depending on the generating power the exposed coal front downstream of the restricted oxidizing zone will be coated with an in thickness growing char layer.

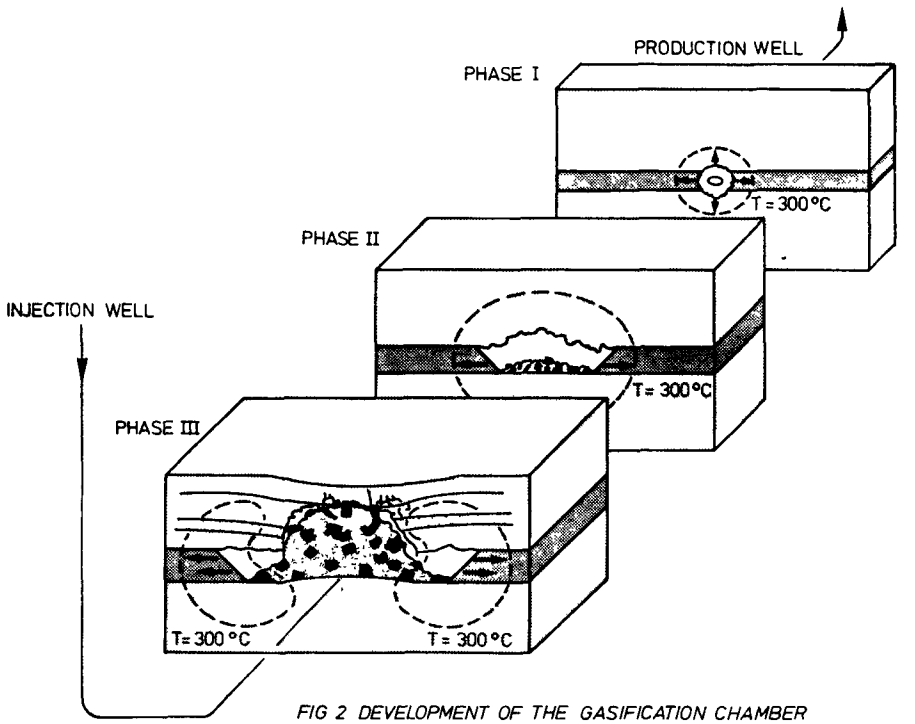

FIG 2 DEVELOPMENT OF THE GASIFICATION CHAMBER

Along this coating in downstream direction reduction of the gases will take place. In lateral direction the wedge is surrounded by layers consisting of respectively cracked char, dry coal and steam forming coal. Evidence has been found [7] of tar migration to dry coal.

In a time span of approximately 5 years for a 10 MW_{th} doublet the wedgeshaped gasifier moves along the original borehole leaving a gasified "horseshoe" (fig. 1) in the underground. Gasification ends with oxygen breakthrough. The amount of coal gasified and converted into char will be more then 100.000 ton assuming a thickness of 1.2 m and a sweep of 100 m. It may be possible to enlarge this amount by back-filling of the burned-out zone [8].

3. THERMAL EFFECTS

A specific feature of underground gasification is the existing lack of feeling for the magnitude of the thermal effects along long and hot flow paths. Though some experience has been gained in the development of geothermal energy systems and also in secundary oil recovery, the temperatures in these systems are still far below the temperatures in gasification and therefore the time dependent effects during gasification can not be extrapolated from this experience.

In our system compressed air at 90 bar and 200 °C is fed into the injecting well. According to calculations 1/ performed to overcome this lack of feeling the air in an 10 MW doublet enters the gasification chamber at varying temperatures. After two weeks the temperature is 100 °C and climbs till 140 °C in approximately two years. The heat losses in the injection well are neglectable compared to those in the gasification chamber and production well.
For the calculation of the temperature profiles in the gasifier a maximum temperature of 1000 °C has been assumed (see also section 4 on the composition of the gas). This maximum temperature is practically independent from changes in temperature in the injection gas. It must be expected that amongst others due to the

1/ Time dependent one dimensional calculations applying an analytical solution for the radial heat losses have been performed [9]. For one case this method has been compared succesfully, within 3%, with the results of a run with a 2 dimensional finite element code.

heat capacity of the gases only 25% of the increase in temperature in the injection gas is added to the maximum temperature [10]. This also means that the economics of preheating must be seriously considered: the reduced benefits in the reaction rates and equilibrium constants may not balance the efforts of preheating.
The temperature of the gas leaving the coal seams varies between two weeks and two years from 480 till 760 °C. At the mouth of the production well these temperatures are respectively 280 and 550 °C.

For the 10 MW high pressure system in which the product gases leave the well at 80 bar this means that after one week the amount of steam produced during the first week of production leaves the well in a small time interval. The surface plant must be designed to accommodate this steam pulse. The temperature range around 300 °C at which tars reach the mouth of the production well happens to occur between 2 weeks and 3 months after the start of the production phase. The seriousness of this tar production must be considered taking into account the tars condensed on the cracks in the dried coal and rock surrounding and downstream of the gasification chamber, which may level off the pulse.

There is some sensitivity for the heat conductivity in the data mentioned above. In table I is shown that doubling the conductivity of the rocks leads to a time delay and therefore to an aggrevation of the effects of tar and steam pulses. It can also be concluded from this table that due to tar condensation plugging of the flow path is likely to occur at low powers.

Heat losses and sensible heat averaged over the lifetime of a doublet as a function of generating power are displayed in figure 3. The bandwith of the curves in this figure is caused by uncertainties in the values for heat conductivity. Figure 3 illustrates clearly that even for thin coal seams heat losses are small at an economically attractive generating power. If we realise that heat recuperation from the burned out coal seam to the injection gases has been neglected in the calculations then this conclusion may be considered as a conservative one.
The sensible heat of the product gases which sharply increases around 10 MW must be exploited commercially for steam production.

	1 MW	10 MW λ rock = .8 $Wm^{-1} K^{-1}$	10 MW λ rock = 1.6 $Wm^{-1}K^{-1}$	50 MW
Averaged conductive losses in MW	.36	1.6	2.3	1.73
in % generated power	36%	16%	23%	35%
Averaged sensible heat in MW	0	2.9	1.3	17.1
in % generated power	< 10%	29%	13%	34%
Occurrence steampulse	> 5 yr	< 4 d	7 wks	< 4 d
Occurrence tarpulse	> 5 yr	< 4 d	1 yr	< 4 d
Length reduction zone > 100 m	> 5 yr	< 4 d	2 wks	< 4 d
Lifetime gasification doublet	50 yr	5 yr	5 yr	1 yr

Table I Thermal characteristics of doublets

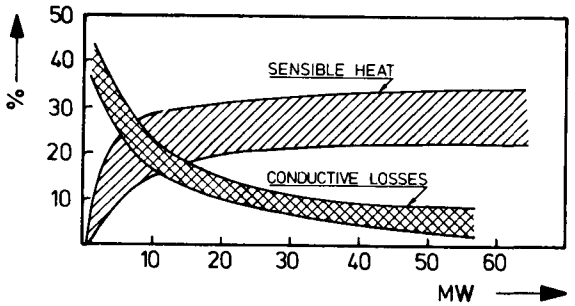

FIG 3 SENSIBLE HEAT (t > 15°C) AND CONDUCTIVE HEAT LOSSES AS A PERCENTAGE OF PRODUCED POWER

Unlike gasification in a surface plant in UCG the gases produced flow through a borehole section of considerable length coated with char which still is at relatively high temperatures. This leads to an extension of the "normal" reduction zone which may influence the composition of the product gases.
Because a lot of uncertainties exist in the rate of the various chemical reactions the reduction zone in the calculations is defined as the channel in which the temperature of the char is above 850 °C. (The temperatures of the gas are about 20 °C higher.) In accordance with UCG field tests the oxidizing zone is considered to be small.

The reduction zone growths with time. Its growthrate depends on the power of the doublet (table I, figure 4).
At the end of the lifetime of a doublet the length becomes limited by the end of the inseam borehole.
In most cases, with the exception of that in which the production well has to be cooled down, the reduction zone is throughout time followed by a hot channel in which an equilibrium between the various gascomponents will be established.

4. THE COMPOSITION OF THE PRODUCT GAS

The shape of the gasifier and the thermal effects discussed above make clear that a large discrepancy must exist in the processes occurring in gasifiers located at the surface and in those located in the underground.
The residence times are in the order of respectively 10 and 1000 seconds. The reactant surface is either concentrated in a few cubic meters or extended along several hundreds of meters. However this simple classification will be disturbed

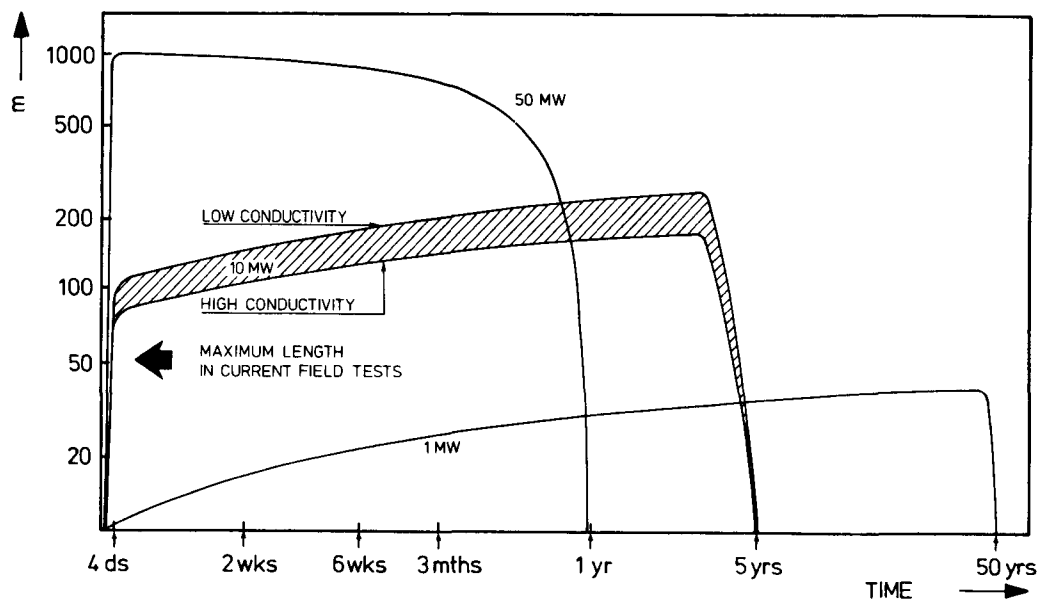

FIG 4 TIME DEPENDENT LENGTH OF THE REDUCTION ZONE (T_{char} > 850°C)

by fixed bed gasification zones which preferentially occur at the end of the wedgeshaped gasifier.
The underground gasifier is not only fed with the injection gases but also with hydrogen and methane from pyrolysis in the surrounding coal, water from drying rock and coal and eventually dependent on the operational pressure with the methane dissolved in the surrounding coal and rock formations.
The temperature profiles discussed in section 3, essentially are not as flat as has been supposed on behalf of the calculations. A further complication of the UCG processes is caused by the concentration gradients of the gas components which exist both in radial and axial direction.

Two effects play an important role in underground gasification:

- The pyrolysis products set free downstream of the oxidizing zone will no longer be subjected to high temperature equilibrium constants and therefore may contribute significally to the caloric value of the product gas.
- The long residence time of the gas in the neighbourhood of cooling but still hot char (length of the reduction zone several hundred meters, gas velocity in the order of 1 m/s in our 10 MW doublet) may cause a complete shift in gas composition from the commonly accepted equilibrium temperature of 1000 °C to a lower value of 800-850 °C.

Those features of UCG may be responsible for the fact that the results of runs with global equilibrium combustion/gasification codes 1/ differ from those obtained with UCG codes [13] for instance in the effect of temperature on energy content of the gases.

The detailed codes developed for UCG thus far [14] have not been designed for the processes occurring in thin seam gasification. Most of them have been designed to interprete and sometimes to predict the results of specific tests. Their forecasting value for the gas composition of larger field tests will remain limited.

1/ A few runs with the Nasa SP-273 code [11] in combination with a heat and mass balance section compiled by Stanford University [12] have been executed.

As a consequence of the notes above forecasts of gas qualities which are needed in economical assessments can not be obtained from experience with surface gasifiers or existing codes.
The only way to obtain a quantitative impression is to extrapolate from field tests in thin bituminous coal seams. The only well documented suitable test, though restricted in duration and in length, which can be used as a data base for the extrapolation has been performed by METC in Pricetown. The 6 MW test Pricetown I has been extensively reported on in the previous UCG symposia. LLNL made a data base [15] available.

The stationary character of Pricetown I is illustrated in figure 5. The higher heating values in the startup phase can be attributed to an enhanced pyrolysis or degasification effect. Considering the oxygen content of the product gases it can be concluded that the combined effect of reaction rates and length of the reduction zone enabled an effective gasification.

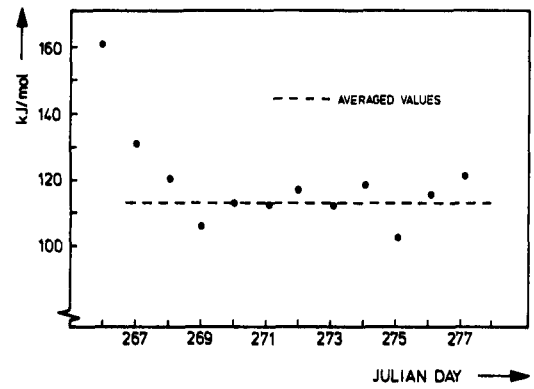

FIG 5 ENERGY CONTENT OF THE PRICETOWN I GAS

In comparison with Pricetown I our standard gasifier with a power of 10 MW will certainly deliver a higher gas quality because:

- The operating pressure of 85 bar theoretically is in favour of a higher methane content.
- The large reduction zone will stimulate the approach of low temperature equilibrium.

As long term deterioration effects as increased heat losses and oxygen breakthrough already have been dealt with the only effect recognised which remains to be discussed is increased water influx. The water from exposed aquifiers might give rise to quenched combustion phenomena. Though the influx of water can not be excluded the amount of water in the undisturbed carboniferous in the Netherlands is limited. Often the hydrostatic head is determined by the distance to the top of the carboniferous which in those areas is covered by watertight clay formations. In this situation collapse of the overlying roof and sagging of the strata may lead to communication and equalization of the pressure with aquifiers and consequently to the influx of water. But if the pressure in the gasifier is higher than the hydrostatic head of the water the influx is limited.
The gasification conditions in Holland at least are better than those at Lisichansk [16] where a low pressure, low power gasifier remained in operation during 13 months.

Excessive gas losses are not expected: the lithostatic pressure at the coal seams of interest is about 200-300 bar.

In analogy with Pricetown the following chemical reaction for the gasification of a typical Dutch coal has been adopted: 32 mol coal + 3.5 mol H_2O + 75 mol air → 100 mol product gas.

The composition of a typical Dutch coal is as follows:

moisture (as rcvd)	%	5
ash (dry)	%	6
volatile matter (dry)	%	30
fixed carbon (dry)	%	64
calorific value (dry)	MJ/kg	35

Pseudo coal molecule: $CH_{.732}O_{.046}S_{.004}N_{.013}$

Molecular weight : 13.78

Density :1400 kg/m^3

Table II

The resultant composition of the dry product gas is as follows:

N_2	59.2
H_2S	0.1
CO_2	9.0
H_2	8.6
CO	18.2
CH_4	3.8

+ traces higher hydrocarbons, pollutions

Table III

The product gas contains traces of NO_x, HCN, NH_3, COS, chloride and 36 mg dust per m^3. The energy content of the gases is 100 kJ/mol.

It is felt that the conservatism applied in the establishment of caloric value must be maintained untill appropriate field tests deliver more accurate information.

5. THE SURFACE PLANT

A preliminary design of the surface installation for a 50 MW_{th} Technical Demonstration Facility has been made by Comprimo BV, a Dutch engineering and contractor firm.
In fig. 6 the "Christmas trees" of 7 doublets with a nominal capacity of 10 MW_{th} each can be recognised in the background. The central building contains the air compressors. Via a pipeline system the product gas passes cyclones for dust removal and enters the gas treatment and cleaning plants. A ground flare will be used for off-gases during normal operation. Due to the projected application of the low BTU gas: blending high energy North Sea gas to standard pipeline gas at a pressure of 70 bar, thorough cleaning and desulphurization are necessary.
The investments in the surface plant have been estimated at 80.10^6 Hfl. The annual running costs are approximately 17×10^6 Hfl including a staff of 58 men.

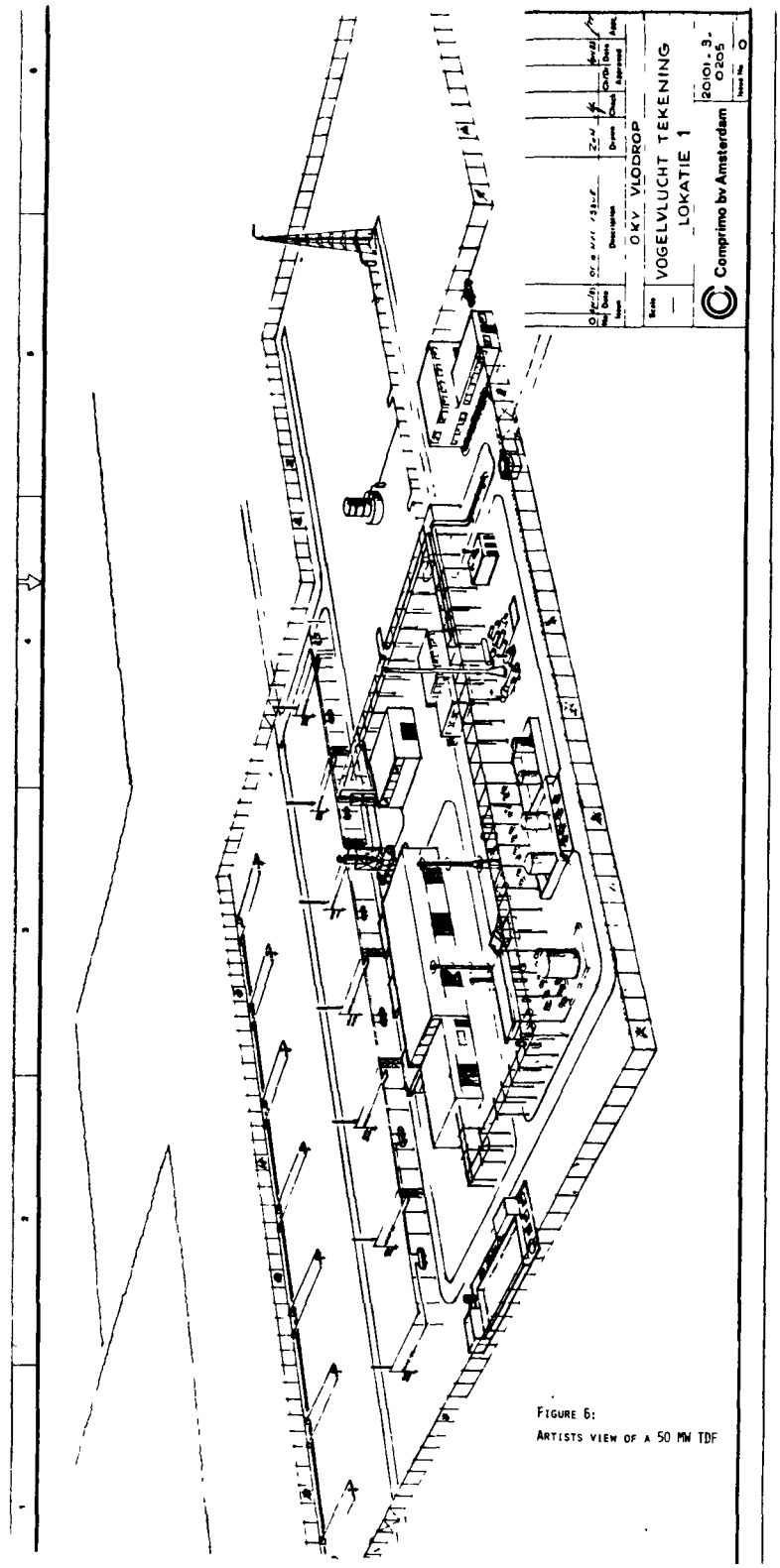

FIGURE 6:
ARTISTS VIEW OF A 50 MW TDF

6. CONCLUSIONS

From the ongoing study on the feasibility of UCG in the Netherlands it can be concluded that:

- Directionally drilled holes are a necessity in crowded countries, in addition, they give an outlook on attractive economics by the exploitation of thin deep lying seams. The disclosure costs per ton of coal probably can be kept low. The long hot char zone may improve significantly the gas quality.
- Commercial gasification of thin seams is totally dominated by the sweep efficiency; the gasification of coal around the initial linkage path is of no economic value.
- Conductive heat losses in thin seams can be kept sufficiently low at generating powers above 10 MW per couple of boreholes.
- Increasing the power above 10 MW brings down the necessary lifetime of a doublet to acceptable values. Plugging of the initial flow paths by condensing tars needs not to be expected at those powers. This is also true for startup problems due to delayed steam and tar ejection.

In the paper technological uncertainties have been revealed also. These must be investigated in future development work. Considering the development costs of deep-lying, thin seam, bituminous coal international co-operation seems fruitful.

Acknowledgements

The work described here has been initiated by an Advisory Committee (BINK) of the Dutch Government and was made possible by a grant from the Dutch Coal Research Programme (NOK).
Mr. S. Cervenka and mr. L. Schoots are acknowledged for their valuable contributions to this paper.

References

[1] UCG with liquid water and air of the deep and thin coal layers in the Netherlands.
J. Bruining et.al. Paper to be presented at the ninth UCG symposium.

[2] Directional drilling as a means of creating gasification flow paths in UCG.
M.M. Siegel; C.C. Chambers proc. 8 UCG symposium SAND 82-2355.

[3] Three horizontal wells in France and Italy.
A. Jourdan et.al. Pétrole Informations april 15, 1982.

[4] The modelling of cavity formation during UCG.
B. Dinsmoor et.al. Journal of Petroleum Technology, may 1978.

[5] A model of roof spalling and its application to predicting cavity shape for the Hanna III UCG field test.
B.E. Levie; W.B. Krantz proc. 8°UCG symposium SAND 82-2355.

[6] The large block tests.
C.B. Thorsness; R.W. Hill proc. 8° UCG symposium SAND 82-2355.

[7] Pricetown post test core analysis.
R.E. Zielinski et.al. proc. 7° UCG symposium Conf.-810923.

[8] UCG in thin dipping seams.
A novel method of cavity backfilling.
A.W. Grupping et.al. proc. 7° UCG Conf.-810923.

[9] L. Schoots priv. comm.
Energy Study Centre, Postbox 1, 1755 ZG PETTEN, The Netherlands.

[10] S. Cervenka priv. comm. Netherlands Energy Research Foundation, Postbox 1, 1755 ZG PETTEN, The Netherlands.

[11] Computer programm for calculation of complex chemical equilibrium compositions, Rocket performance etc.
B.J. Mc Bride et.al. Nasa SP-273, 1976, Rev.

[12] High temperature Gasdynamics Laboratory.
K.D. Annen; T. Nakamura priv. comm.
Stanford University, Palo Alto, 1981.

[13] High pressure gasification of deep coal.
R.S. Chappel. Proc.symp. Heerlen, The Netherlands, march 1980.
Mededelingen Rijks Geologische Dienst vol. 33-1/10.

[14] A comparison of forward combustion gasification models.
L.V. Kunselman proc. 8° UCG symposium SAND 82-2355.

[15] Underground coal conversion data base.
R.J. Cena et.al., november 1982
UCID-19169 Rev.1.

[16] Study of the gasification process at 300-400 meter depths at the Lichansk UCG station.
S.P. Golger UCRL-trans-10811.

3.21 COMPARATIVE ECONOMICS OF SUBSTITUTE NATURAL GAS PRODUCTION BY UNDERGROUND COAL GASIFICATION AND SURFACE GASIFICATION OF WESTERN COAL

by

B. W. Gash(1/)
M. M. Siegel(2/)
J. H. Nienaber(3/)
V. L. Hill(4/) and J. I. Rosenberg(4/)

ABSTRACT

The economics of medium Btu gas production from a deep, thick subbituminous coal using underground coal gasification (UCG) technology and conversion of the medium Btu gas into substitute natural gas (SNG) using conventional aboveground technology were investigated. The levelized constant dollar (LCD) price to produce approximately 255 MMSCFD of SNG via UCG was determined to be $4.74/MMBtu (fourth quarter 1982 dollars). When a process development allowance is included to account for anticipated real cost growth associated with developing technologies, the LCD price for SNG production via UCG is $5.19/MMBtu. The LCD price for SNG production via UCG is from 10 to 20% less than the LCD price for SNG via surface gasification.

INTRODUCTION

Williams Brothers Engineering Company was contracted by Amoco Production Company, Gas Research Institute (GRI) and Hunt Oil Company, jointly, to perform an economics study of the use of underground coal gasification (UCG) technology to produce a medium Btu gas which would in turn be converted to substitute natural gas (SNG). Williams Brothers Engineering Company (WBEC) was also a full participant. The three man-year study[1] consisted of designs and cost estimates for a UCG field system and the surface facilities necessary to clean and to convert the raw gas into SNG.

Prior to this study, engineering estimates available in the literature for the cost of SNG produced via UCG were either conducted before recent U.S. UCG field tests[2,3] or were based on calculations using process models.[4] Furthermore, the economic assumptions used in these estimates varied from study to study so that clear comparisons to advanced surface gasification technologies were not possible.

This study was conducted in accordance with guidelines devised by GRI.[5] The GRI guidelines allow economic comparison of various alternative coal gasification technologies on a consistent basis. Use of the GRI guidelines in this study results in the following:

1. The UCG technology upon which the field system was designed employed a combination of open literature Soviet methodology, and U.S. field test and design data.

2. The design of the surface facilities, i.e., oxygen plant, gas clean-up and conversion, was based on state-of-the-art technology. It was assumed there would be no improvements in such technology which could lower investments or operating costs.

1/ Amoco Production Company, P. O. Box 591, Tulsa, OK 74102
2/ Williams Brothers Engineering Co., 6600 S. Yale Ave., Tulsa, OK 74136
3/ Hunt Oil Company, Minerals Division, P. O. Box 1317, Denver, CO 80201
4/ Gas Research Institute, 8600 W. Bryn Mawr Ave., Chicago, IL 60631

3. Except for ammonia and sulfur, no byproduct credits were taken. Thus, no revenue was generated from byproduct N_2 and CO_2.

4. Costly sparing due to the first-of-a-kind nature of the facility were included to provide a 90% onstream factor. Later plants should be less costly.

FIELD SYSTEM PROCESS DESIGN

The field system design basis assumed a flat-lying subbituminous coal seam 70 ft thick at a depth of 700 ft in the Powder River Basin of Wyoming (Table 1). Wells were slant drilled based on published Soviet technology.[6] Reverse combustion linking with 75.2% CO_2, 24.3% O_2, and 0.5% argon was used. During forward gasification 50% O_2 and 50% steam were injected.

The field system, as illustrated in Fig. 1, was composed of two unequal areas laid out on either side of a central gas processing plant. The smaller area was used last, permitting the reuse of main line pipe from the larger initial field. The field system was divided into 147 generators of equal size. Each generator was composed of a rectangular grid of 105 wells with seven wells per row and fifteen wells per channel. The wells were spaced on 75-ft centers.

Thirty-four of the 147 generators must be in operation at one time to produce sufficient raw gas to result in approximately 255 MMSCFD of SNG. This requires drilling an average of 766 wells each year or a total of 15,435 wells to maintain production at specified levels for the twenty year lifetime of the project.

The field system is operated from the farthest extremity toward the processing facility. As a result, parts of the main lines can be relocated to the second field area once the extremities of the field have been gasified and the gasified areas can be restored with a minimum of interference from operating pipelines. A restoration fund of $5 million per operating year has been included in the economic analysis.

CENTRAL GAS PROCESSING PLANT DESIGN

The central gas processing plant converts raw gas from the UCG field system into SNG. The process steps in sequence include:

1. Quench and Electrostatic Precipitation
2. First Stage Compression and Shift
3. Acid Gas Removal and Sulfur Recovery
4. Methanation
5. Second Stage Compression and Dehydration

Each of these process steps are discussed in the text which follows. Figure 2 is a block flow diagram of the central gas processing plant.

All atmospheric environmental discharges meet best available control technology (BACT) requirements and there is zero discharge of aqueous waste in the design.

The assumed raw gas composition including trace constituents is given in Table 2. The UCG raw gas composition used in this study is typical of the results obtained from UCG field tests in the U.S. (Fig. 3).[7] These tests have all been conducted in thinner coal seams and at more shallow depths than assumed in this study. The thickness and depth of the coal seam used in the study were assumed not to affect the produced gas composition.

Quench and Electrostatic Precipitation

The raw gas is first cleaned in gas quench towers, designed such that the bulk of the particulates and heavier tars are removed in the lower sections of the towers while the heat is removed in the upper sections. The gas exiting the top of the quench towers is further cooled by using it to preheat a boiler feed water stream. In order to achieve the low particulate levels required to prevent fouling of the shift reactor beds, the vapor-liquid stream is separated prior to compression and any remaining particulates in the gas stream

are removed in a high pressure electrostatic precipitator.

Shift

The main gas stream exits the quench unit and is compressed. About one-half of the main gas stream enters the shift converter which contains a sulfur resistant shift catalyst. The shifted gas exits the converter and is blended with the bypassed gas stream (nonshifted gas) resulting in a H_2/CO ratio of 3:1.

Acid Gas Removal and Sulfur Recovery

The main gas stream is then treated in a two stage SELEXOL unit for the selective removal of hydrogen sulfide and carbon dioxide. The hydrogen sulfide in the main gas stream is reduced to less than 1 ppm in the first stage. The second stage of the SELEXOL unit reduces the carbon dioxide content of the main gas stream to 0.5% CO_2. The CO_2 removed from the main gas stream is split into two vent streams. Part of the higher pressure carbon dioxide stream is compressed, blended with oxygen, and used as linking gas for the field system. The remainder is vented in a unit stack at sufficient velocity to assure adequate dispersion in air. The lower pressure stream is routed to the boiler stacks where it is blended with boiler flue gases prior to discharge.

The sulfur recovery area uses a direct oxidation process to recover sulfur from a feed stream with a low hydrogen sulfide concentration (9% in this case). Including the sulfur from the sour water stripper, the total sulfur produced is about 76 long tons per day. The tail gas from the sulfur plant is burned in the steam boilers where the sulfur compounds are converted to sulfur dioxide prior to flue gas scrubbing.

Methanation

The main gas stream exits the SELEXOL unit with 1 ppm H_2S which is removed prior to methanation.

The methanation unit design has three trains of primary reactors and a third stage clean-up reactor after water removal. After methanation, the product gas contains 95% CH_4, 1.9% N_2 and 2.5% Ar (Table 2). This composition satisfactorily meets the requirements of the A.G.A. Research Bulletin Number 36 on Interchangeability of Other Fuel Gases with Natural Gas.[5]

Second Stage Compression and Dehydration

The main gas stream is compressed ahead of the glycol dehydration unit where the moisture content of the SNG is reduced to a pipeline specification of 7 lb/MMSCF. Plant site delivery pressure is 1015 psia.

UTILITIES AND OFFSITES DESIGN

The Utilities and Offsites include facilities to produce and/or compress streams of steam, oxygen, carbon dioxide and water for use in the field system as well as the more typical functions associated with the requirements of the Central Gas Processing Plant.

Units to be discussed briefly in the following text are listed below:

1. Oxygen Plant
2. Steam Plant
3. Water Supply
4. Water Treatment

Oxygen Plant

The oxygen requirement is 15,000 T/D and is supplied at 98% purity by six 2500 T/D commercially available oxygen plants.

The oxygen storage system consists of two 300,000 gallon cryogenic tanks, normal transfer pumps and vaporizer.

Steam Plant

Five 1 million lb/hr boilers are provided to supply approximately 3.9 million lb/hr of steam. One boiler is used as a spare.

Water Supply

Water is assumed to be obtained from a reservoir located approximately 50 miles away. Only 300 gpm of make-up water are required due to the extensive

recycling of water and the maximizing of air-fin cooling. A pipeline and pumping facilities are included in the costs estimates.

Process Water Treatment

Provision is made for process water treatment. As shown in Figure 2, the process water treatment design consists of the following sections:

1. Oils/Water/Solids Separation
2. Phenols Removal
3. H_2S and NH_3 Stripping
4. Biological Treatment

In addition, provisions were included for boiler feedwater treatment and condensate stripping and filtration.

ECONOMIC CALCULATION SUMMARY

The most common method of assessing the merits of a capital investment is the use of discounted cash flow (DCF) analysis. One common method of DCF is the estimation of all cash flows (i.e., costs and revenues) for a facility which are then discounted at the firm's cost of capital compounded each year over its lifetime. The resulting sum is called net present value (NPV), a measure which is commonly used to rank alternative investment opportunities.

Two difficulties arise from using this type of DCF approach to evaluate alternative energy technologies. First, estimation of future SNG revenues requires explicit assumptions about expected future energy prices which are both very uncertain and which will differ greatly depending upon actual years of facility operation projected. Second, any DCF analysis that uses NPV as a comparative measure of economic merit will result in a technology ranking biased toward larger capacity plants (i.e., larger facilities are more likely to exhibit greater absolute net revenues, even though unit costs may be lower in other plants).

Given the uncertainties regarding the extent of cost reduction from plant scale-up, as well as possible capital constraints which may limit SNG plant size, GRI uses an economic evaluation method which is based on the unit costs of production. This method is more suitable for comparative economic analysis among systems of different sizes and capital intensities, as well as for alternative sources of energy.

Comparative economic merit among SNG options considered by GRI is based on calculation of what is called a levelized constant dollar (LCD) cost-of-service price. The LCD price provides a cost-based, inflation-adjusted measure of the required SNG selling price over a plant's lifetime, based on historical real returns on invested capital earned by the regulated natural gas industry. An LCD price is defined as the constant dollar per unit of output that, if charged for each unit over the plant lifetime, would yield the same discounted present value of revenues as would the actual cost-of-service price. Although this method is based on tax and accounting procedures applicable to federally regulated interstate pipeline companies, it should yield similar results to those of a non-regulated energy company, provided that the same capital structure, real rates of return, and discount rate are applied to the investment under each type of plant ownership. The theory and derivation associated with LCD price calculation and some detailed examples are provided in GRI's "Gas Cost Guidelines"[5] and a recent GRI staff paper.[8]

The economic evaluation data from the GRI guidelines[5] are summarized in Table 3. The plant life is 20 years. The construction period is 4 years; production begins in 1986. The plant service factor is 90%. The inflation for byproducts, construction costs, and operating costs is 6%. The capital structure includes 65% debt, 30% common equity, and 5% preferred equity. The weighted average rate of return on capital during the plant lifetime is 10.8%, including inflation. The result is a real or constant dollar weighted average return on capital of 4.5%.

Investments are summarized in Table 4. With a 15% contingency, contractor's overhead, and engineering design costs, the total construction investment is $1,543.6 million. In addition, initial catalysts-chemicals, start-up costs, and other miscellaneous

costs bring the total plant investment to $1,635.9 million.

The annual operating costs and byproduct credits are given in Table 5. The annual operating costs are $232 million. The total byproduct credit from sulfur and ammonia is $6.8 million.

The various contributions to the levelized constant dollar cost-of-service price for SNG are shown in the right-hand column of Table 6 and in Figure 4. Expressed in fourth quarter 1982 dollars, the LCD price is $4.74/MMBtu. To account for anticipated real cost growth associated with developing technologies, GRI also calculates a process development allowance (PDA) based on the stage of process development for key facility subsystems. For this UCG facility, the total PDA, which may account for possible unforeseen cost factors associated with UCG's status as an emerging technology, was estimated at up to 45¢ per MMBtu. It should be stressed that this amount is over and above the 15% project contingency applied to initial capital investment. Thus, the LCD price for this UCG system is $5.19/MMBtu when the PDA is included.

COMPARISON WITH SURFACE GASIFICATION

An economic comparison of UCG/SNG with two surface coal gasification processes estimated by C. F. Braun Co.[9], also designed for the western U.S., is shown in Fig. 4 and Table 6. The basis for the economic analysis among these three systems is the same, with all levelized cost-of-service components adjusted to fourth quarter 1982 dollars. The LCD price for SNG production from UCG is estimated to be considerably less than the price of SNG production from both first and second generation surface gasification facilities.

The potential costs for UCG range from 15% to 20% less than the dry bottom Lurgi process, and from 10% to 15% less than the Westinghouse fluidized bed process. The range in each case is based on whether or not PDA's are added to each system's cost. The lower required price for SNG from UCG is due almost entirely to the cheaper cost assumed in this study for coal used in UCG relative to mined and delivered coal for surface gasification. There is little difference among the three processes in the contributions to the LCD prices due to capital investments or operating costs.

CONCLUSIONS

1. The levelized constant dollar (LCD) price to produce approximately 255 MMSCFD of SNG via UCG is estimated to be $4.74/MMBtu (fourth quarter 1982 dollars). When a process development allowance is included to account for anticipated real cost growth associated with developing technologies the LCD price for SNG production via UCG is $5.19/MMBtu.

2. The LCD price for SNG production from UCG is from 10 to 20% less than the LCD price for surface gasification due to lower coal costs.

REFERENCES

1. Williams Brothers Engineering Company, "Assessment of Underground Coal Gasification in Wyoming Subbituminous Coal for Production of SNG," prepared for Amoco Production Co., Gas Research Institute, Hunt Oil Co., and Williams Brothers Engineering Company, February 1983.

2. Buder, M. K., McCone, A. I., Fascher, R. A., and Terichow, O. N., "Factors Influencing the Economics of Large-Scale In Situ Coal Gasification Operations," 2nd Symposium on Underground Coal Gasification, Morgantown, West Virginia, August 10-12, 1976, p. 145.

3. Garon, A. M., "An Economic Evaluation of Underground Coal Gasification," 2nd Symposium on Underground Coal Gasification, Morgantown, West Virginia, August 10-12, 1976, p. 155.

4. Bruggink, P. R. and Davis, B. E., "Economic Comparison for UCG Processes," 8th Symposium on Underground Coal Conversion, August 15-19, 1982, p. 213.

5. "Guidelines for Evaluation of Commercial Fossil Fuel Gasification Concepts," GRI-83/0003, March 1983.

6. Olness, Delores, "The Angrenskaya Underground Coal Gasification Station," Lawrence Livermore Laboratory, UCRL-53300, June 17, 1982.

7. Gash, B. W. and Hunt, E. B., "A Review of Produced Gas Compositions in UCG Field Tests in the United States," 9th Symposium on Underground Coal Conversion, Bloomingdale, Illinois, August 7-10, 1983.

8. Rosenberg, J. I., Ashby, A. B., and Sellin, J. O., "The Economic Potential for Coal Gasification," presented at the AIChE National Meeting, Houston, Texas, March 27-31, 1983.

9. C. F. Braun Co., Fossil Fuel Gasification, Technical Evaluation Services: Final Report, GRI-81/0135, May 1983.

TABLE 1

ASSUMED FIELD SYSTEM PROCESS DESIGN BASIS

RESOURCE	
Source	Powder River Basin, Wyoming
Coal Seam Depth	700 ft
Coal Seam Thickness	70 ft
Coal Analysis	Typical Subbituminous
Water Table	200 ft
PROCESS	
Link Technique:	Reverse Combustion
Link Reactant Composition:	75.2% CO_2, 24.3% O_2, 0.5% Ar
Forward Gas Reactant Composition:	50% O_2, 50% H_2O (stm)
Forward Burn Reactant Injection Rate Per Well:	1167 SCFM O_2
Product Gas Loss:	5%
Cold Gas Efficiency (without char):	77%*
Sweep Efficiency:	65%
Total Raw Gas Production Rate:	815.6 MSCFM**

* Percentage of energy in affected coal as chemical energy in raw gas brought to surface.

** 100% on-stream factor.

TABLE 2

ASSUMED OVERALL MATERIAL BALANCE
CENTRAL GAS PROCESSING PLANT

STREAM NO.	1	2
COMPONENT DESCRIPTION	Wellhead Gas To Processing Plant MPH	SNG To* Pipeline MPH
H_2	46,531.70	52.52
N_2	539.38	539.28
Ar	692.87	691.80
CO	28,886.66	2.00
CH_4	7,266.90	26,671.07
CO_2	43,902.15	52.52
C_2	297.19	--
C_2+	210.23	--
H_2S	243.90	--
NH_3	371.44	--
MSCFM (Dry)	815.54	177.16
MSCFM (Wet)	1,201.50	177.18
HHV, BTU/SCF (Dry)	254.7	966.1
Particulates, LB/HR	519	--
CS_2, PPM	10	--
COS, PPM	300	--
HCN, PPM	10	--
Oils/Tars, GPM	126.8	--
Phenols, LB/HR	2,823	--
Temperature °F	360	125
Pressure, PSIA	241	1015

* Standard US Pipeline Specifications

TABLE 3

ECONOMIC EVALUATION DATA
FROM GRI GUIDELINES

Book Life, years (BL)	20
Tax Life, years (TL)	10
Construction Period, years (CP)	4
Byproduct Escalation Rate, current dollars (e_b)	0.06
Construction Cost Escalation Rate, current dollars (e_c)	0.06
Fuel Cost Escalation Rate, current dollars (e_f)	0.08
Variable Operating and Maintenance cost (VOM) Escalation Rate, current dollars (e_m)	0.06
Inflation Rate (inf)	0.06
Base Year for Cost Estimation (t_b)	1982
Year of Initial Operation (t_o)	1986
Combined State and Federal Tax Rate	0.50
Depreciation Method (SYD)	Sum-of-Years Digits
Services Factor (SF)	0.90
Working Capital Factor (WCF)	0.15
Debt as Fraction of Capital (f_d)	0.65
Common Equity as Fraction of Capital (f_{ce})	0.30
Preferred Stock as Fraction of Capital (f_{pe})	0.05
Equity as Fraction of Capital (f_e)	0.35
Weighted Average Current Dollar Cost of Capital, before tax (r_b)	0.156
Rate of Return to Debt, current dollars (r_d)	0.092
Rate of Return to Common Equity, current dollars (r_{ce})	0.145
Rate of Return to Preferred Stock, current dollars (r_{pe})	0.092
Average Cost of Capital (after tax on equity, before tax return on debt), current dollars (R)	0.108
Rate of Return (AFUDC)	0.108
Discount Rate, current dollar (d)	0.108
Weighted Average Cost of Capital, current dollar, after tax (r_a)	0.078
Constant Dollar Discount Rate (d_c)	0.045

TABLE 4

TOTAL PLANT INVESTMENT AND
WORKING CAPITAL

($MM Fourth Quarter 1982)

ONSITE FACILITIES CONSTRUCTION INVESTMENT*	568.2
OFFSITE FACILITIES CONSTRUCTION INVESTMENT*	881.8
CONTRACTOR'S OVERHEAD AND PROFIT	46.8
ENGINEERING AND DESIGN COSTS	46.8
	1,543.6
INITIAL CHARGE OF CATALYSTS AND CHEMICALS	23.9
START-UP COSTS	46.4
MISCELLANEOUS	22.0
TOTAL PLANT INVESTMENT	1,635.9
WORKING CAPITAL FOR CONSUMABLES AND SPARE PARTS	37.7

* Includes 15% contingency

TABLE 5

ANNUAL OPERATING COSTS AND BYPRODUCT CREDITS

($MM Fourth Quarter 1982)

FUEL	30.8
SITE RESTORATION FUND	5.0
RAW MATERIALS	9.9
DIRECT OPERATING LABOR AND OVERHEAD	123.3
MAINTENANCE MATERIALS	38.5
LOCAL TAXES AND INSURANCE	24.5
ANNUAL OPERATING COST	232.0
BYPRODUCTS CREDIT (Sulfur and Ammonia)	6.8

TABLE 6

ECONOMIC COMPARISON AMONG 20-YEAR
SNG FACILITIES IN THE WESTERN U.S.

(Levelized Costs in $/MMBtu Fourth Quarter 1982)

	Dry Bottom Lurgi[a]	Westinghouse[a]	UCG[b]
Depreciable Capital Investment	2.07	1.98	1.79
Variable Operating & Maintenance Cost	2.46	2.16	2.49
Fuel Cost	1.30	1.26	0.44
By-Product Credit	(0.20)	(0.10)	(0.08)
Working Capital (Consumable & Spare Part)	0.07	0.06	0.07
Specific Working Capital (Net Accounts Receivable)	0.03	0.03	0.03
Levelized Constant Dollar (LCD) Cost-of-Service Price	5.73	5.39	4.74
Process Development Allowance (PDA)	0.23	0.35	0.45
LCD Price with PDA	5.96	5.74	5.19

a Based on "Fossil Fuel Gasification Technical Evaluation Services: Final Report," prepared for GRI by C. F. Braun & Co., May 1983. Cost estimates were updated to 4th quarter 1983 dollars using the Chemical Engineering Plant Cost Index.

b Based on "Assessment of Underground Coal Gasification in Wyoming Subbituminous Coal for Production of SNG," prepared for Amoco Production Co., Hunt Oil Co., and GRI by Williams Brothers Engineering, February 1983.

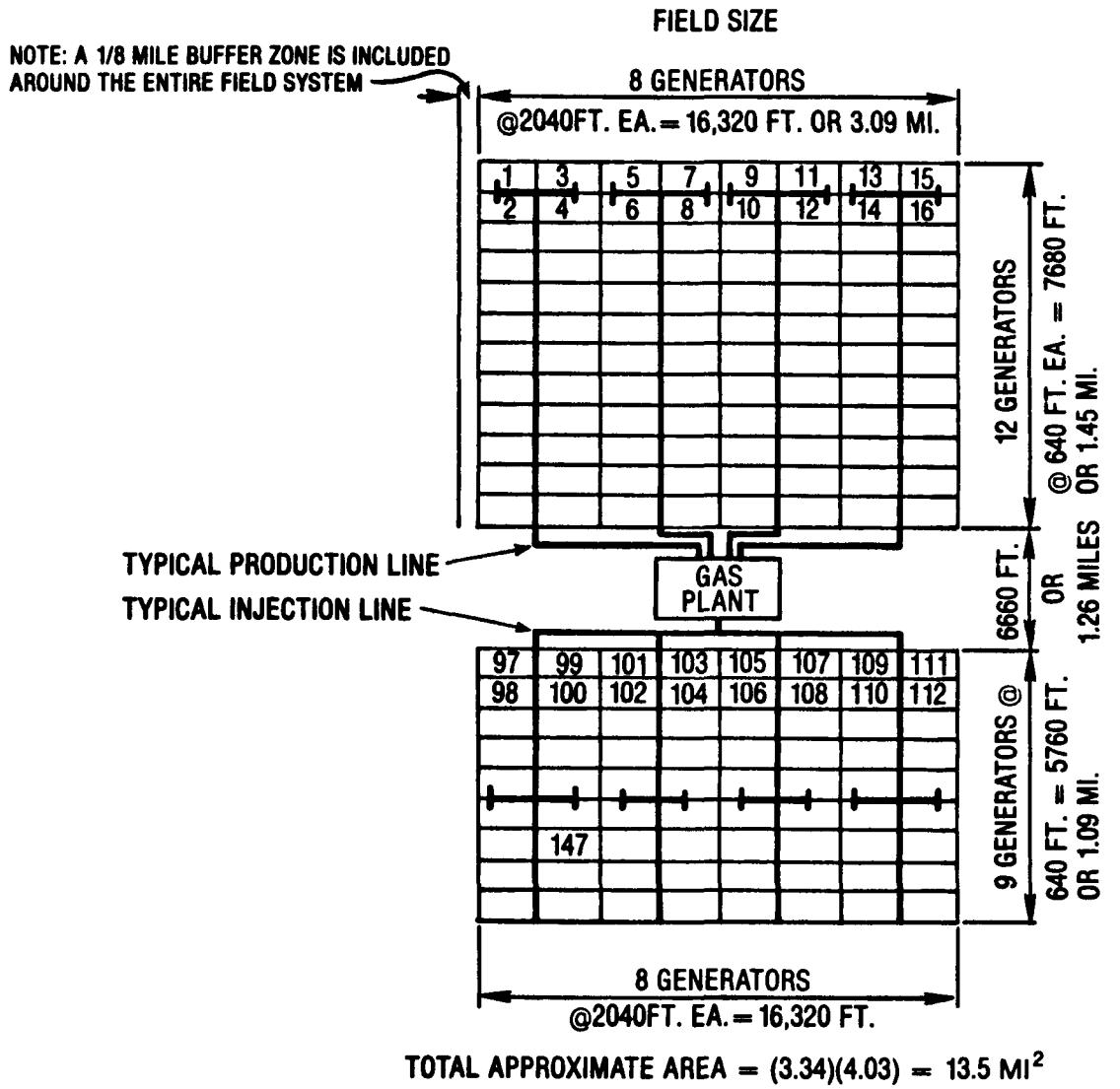

Figure 1. Field System Plot Plan

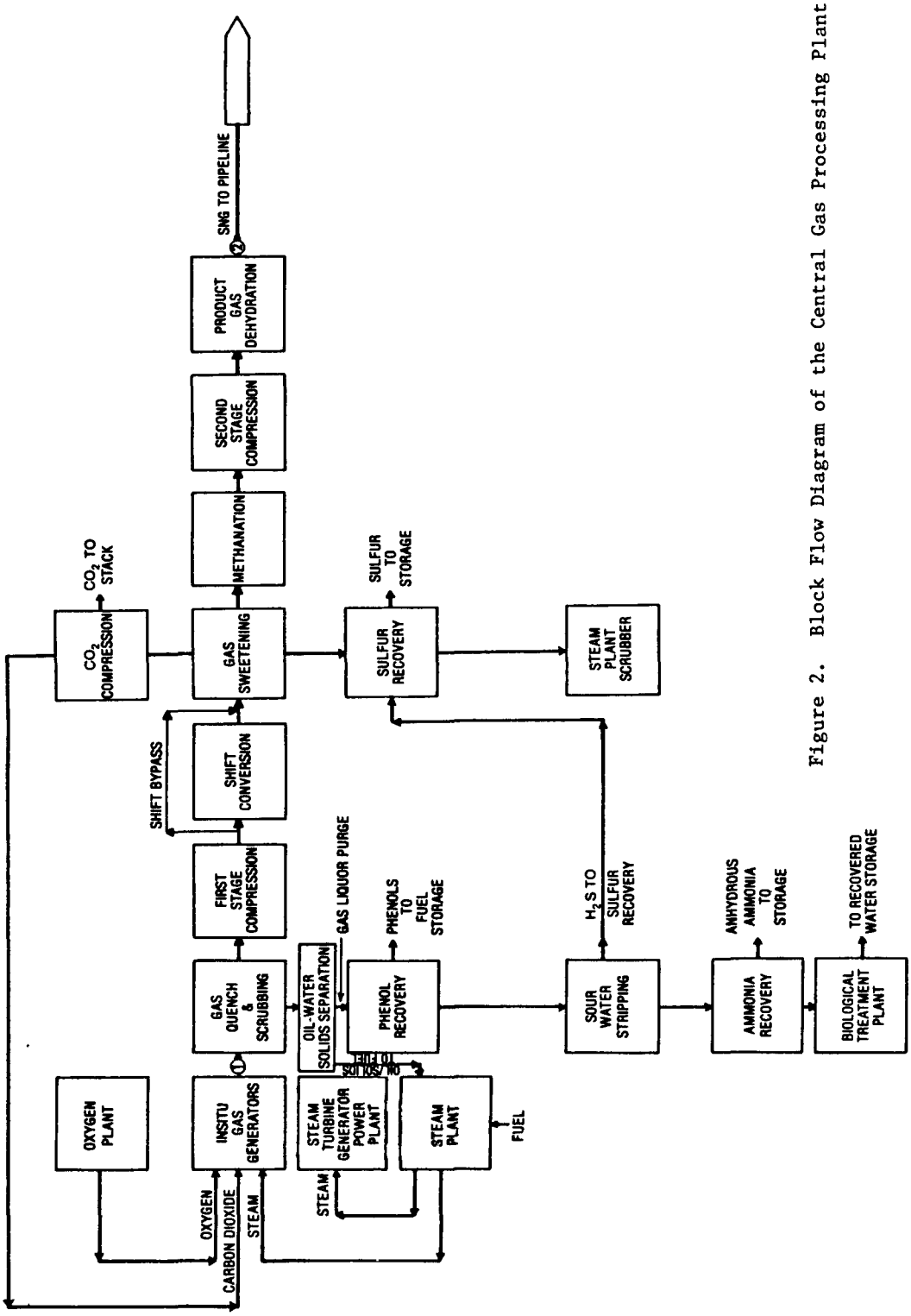

Figure 2. Block Flow Diagram of the Central Gas Processing Plant

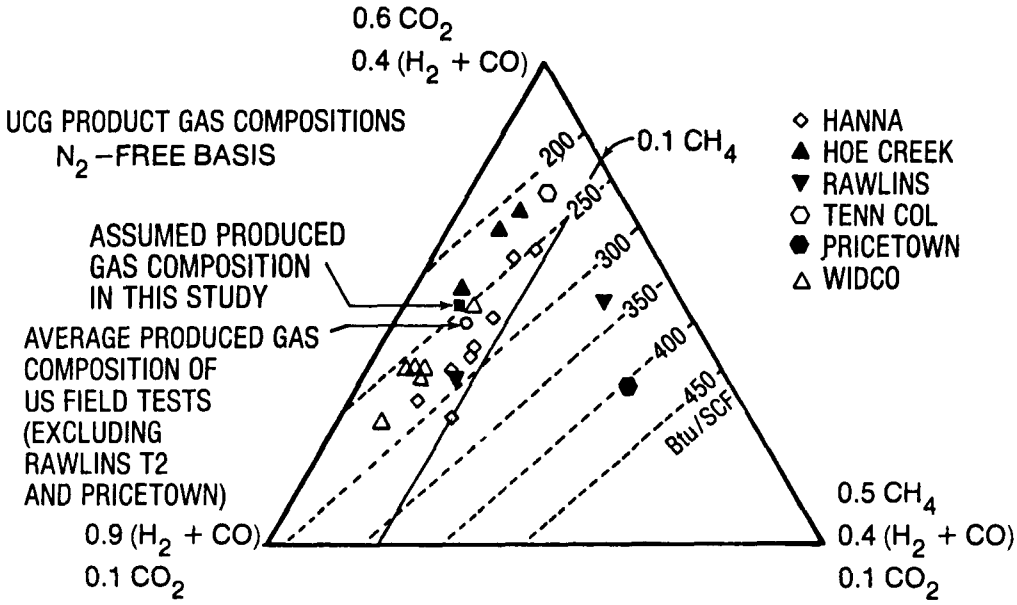

Figure 3. Comparison of the Produced Gas Composition Assumed in this Study with Produced Gas Compositions from US UCG Field Tests

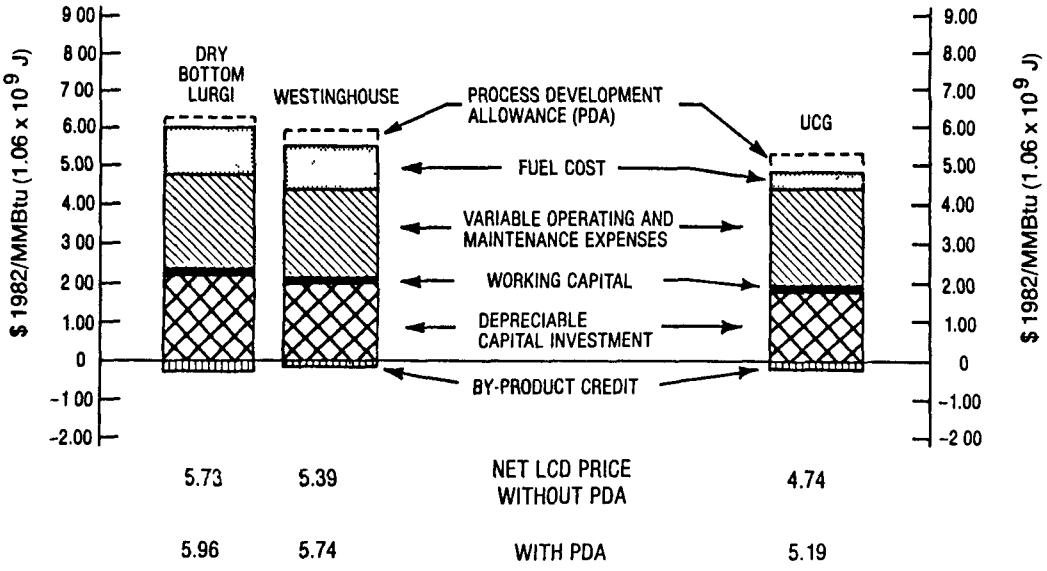

Figure 4. Comparison of the Levelized Constant Dollar (LCD) Price for UCG and Surface Gasification of Coal

4.0 ENVIRONMENTAL

SESSION V: ORAL PRESENTATIONS

4.1 BIOTREATMENT OF UCG WASTEWATER CONDENSATE

by

Michael J. Humenick[1/]
Rodney Brauer[2/]
Timothy Caire[3/]
Desmond F. Lawler[4/]

ABSTRACT

The process of underground coal gasification (UCG) generates a wastewater stream during the cooling and processing of the product gas. The wastewater stream is of large enough volume and contains a wide array of pollutants to pose a significant water pollution problem. The character of UCG condensate is similar to that produced by above-ground gasifiers although some differences are apparent.

The treatment options studied during this laboratory experimental project were activated sludge treatment of raw condensate, activated sludge treatment of stripped condensate, and activated sludge with powdered activated carbon (PAC) addition for treatment of stripped condensate.

The condensates used in the laboratory study were obtained from large-scale field tests in Wyoming. Design and kinetic information for the various activated sludge options are presented along with detailed performance and kinetic data.

Major variables among the treatment options were the amount of dilution water needed to achieve stable operation, the degree of treatment achieved by each option, and the stability of the biological reactor.

1/Professor of Civil Engineering, The University of Wyoming, Laramie, WY 82071
2/Graduate Student, Department of Civil Engineering, University of Wyoming, Laramie, WY 82071
3/Graduate Student, Department of Civil Engineering, University of Texas, Austin, TX 78712
4/Assistant Professor, Department of Civil Engineering, University of Texas, Austin, TX 78712

INTRODUCTION

The energy problems that have developed in the United States during the previous decade have made it necessary to examine new methods of utilizing lignite and sub-bituminous coals present in large quantities in the western United States. One possible alternative is the use of underground coal gasification (UCG).

The objective of the Department of Energy UCG Program is to evaluate the use of UCG for the production of liquid and gaseous hydrocarbon fuels from domestic coal reserves that are considered unsuitable for recovery by conventional mining techniques (1). While UCG is recognized as being one of the most promising methods to produce clean fuels from coal, there are environmental impacts that should be evaluated.

Underground coal gasification is a process in which coal is ignited and gasified within the existing coal seam. The coal is gasified by injecting air or steam/oxygen into the ignited reaction zone through previously completed boreholes. The hot gases are removed at the production well, where they are cleaned and upgraded for use. Cooling of the hot production gases produces oil and water condensates (2). The condensed oils produced can be evaluated for by-product recovery, while the water phase must be treated prior to reuse or discharge.

Organic and inorganic characterization of the oil and water condensates produced in the in-situ coal gasification test at the Hanna IVB site, near Hanna, Wyoming, has been completed (2). Pheno-

lics accounted for the largest fraction for both oil and water condensates. Polynuclear aromatic and heterocyclic hydrocarbons were found to make up the majority of the remaining organics identified in the water sampled, which ranged between 4,000 and 11,000 ppm (2). Tar and water condensates from two lignite gasification sites in Texas were analyzed by Humenick and Mattox (6) for characterization of organic pollutants by gas chromatography-mass spectrometry. The composition of the Texas lignite condensates was very similar to those produced at the Hanna IVB site.

Wastewater produced during the above ground gasification of coal also contains substantial concentrations of organic substances. Chemical oxygen demand (COD) on the order of 10,000 to 40,000 mg/l, and total organic carbon concentrations (TOC) of 5,000 to 10,000 mg/l have been reported for these wastewaters (4,5,7). Wastewaters produced during above ground gasification of coal can be very similar in concentration and proportions to UCG condensate wastewater. Variations in character depend on the specific gasification process employed.

Only a limited number of studies have been completed on the treatment of wastewater produced by above ground coal gasification (5,7,8,9,10,11,12,13,14). This is one of the first reported studies to obtain basic engineering data for the design of biological treatment facilities for UCG condensate water. Aerobic biological processes appear to be the focal point of any overall scheme for treating coal conversion wastewater.

The objectives of this research were to determine the ability of the activated sludge process to treat condensate from UCG and establish design and operating conditions. Several treatment options were studied. They were: Option 1 - treatment of raw condensate by activated sludge; Option 2 - treatment of ammonia-stripped condensate by activated sludge; and Option 3 - treatment of stripped condensate by activated sludge with addition of powdered activated carbon (PAC) to the activated sludge reactor.

MATERIALS AND METHODS

Biological Kinetics

Kinetic models for substrate removal, cell growth, and oxygen utilization in continuous, steady-state, completely-mixed activated sludge systems have been established for some time (15,16). The equations are summarized as follows. Equation (1) relates the mean cell retention time, θ_c, to the yield coefficient, Y, the substrate utilization rate, U, and a decay coefficient, k_d.

$$\frac{1}{\theta_c} = YU - k_d \qquad (1)$$

θ_c is in days, Y has units of mass of cells formed per mass of substrate utilized, U is in terms of mass of substrate utilized per day, per mass of cells, and k_d is in days^{-1}.

Equation (2) relates substrate utilization, U, to effluent substrate concentration, S_e, for low values of S_e.

$$U = k\, S_e \qquad (2)$$

Here, k is a simple proportionality coefficient between substrate utilization and substrate concentration.

Equation (3) relates the oxygen utilization of the biomass, R_r, to substrate utilization, and biomass concentration.

$$R_r = a'U + b' \qquad (3)$$

Here, R_r is in mass of O_2 used per day per mass of biomass, a' is an oxygen utilization coefficient in mass O_2 used per mass substrate removed, b' is an oxygen utilization coefficient for endogenous activities of biomass in mass O_2 used per day per mass of biomass.

Continuous Reactors

To accomplish the objectives of the research, continuous flow, bench-scale reactors were constructed of plexiglass (Fig. 1) and operated at various mean cell retention times and hydraulic retention times. Each reactor had a volume of about 9 liters, which was controlled by an adjustable overflow pipe in the clarification section which comprised about 25 percent of the reactor. Throughout the study, θ_c was held between ten and forty days by appropriate sludge wasting, and hydraulic retention times were held constant for each of the three options studied.

Aerobic conditions were maintained by bubbling compressed air through diffusors located near the bottom of the aeration chamber. Influent was fed to the reactors from refrigerated storage by variable speed peristaltic pumps.

Settled effluent was collected from the overflow tube, analyzed and/or composited daily. Reactors were maintained at room temperature, which did not vary much from 22°C.

Biomass used for acclimation to condensate treatment was obtained from the Gulf Coast Wastewater Authority in Houston, Texas, for Option 1 studies. For Options 2 and 3, the biomass was obtained from the CF & I Steel Co. in Pueblo, Colorado.

Powdered activated carbon used for the study was Filtrasorb 500 which was ground to less than 300 mesh. Carbon was fed directly to the aeration chambers, batchwise, on a daily basis.

Wastewater

The wastewater used in the study was obtained from the Laramie Energy Technology Center's refrigerated cold storage facility in Laramie, Wyoming. The condensate originated from the Hanna IVB UCG field test where approximately 2000 gallons were collected, composited, and stored in 30-gallon (113-liter) drums (2). A partial analysis of the composited condensate used in this study is shown in Table I.

TABLE I

Hanna IVB Aqueous Condensate

Parameter	mg/l or Units
COD	17,000
BOD	5,000 - 6,000*
TOC	4,700
Phenols	5,230
NH_3-N	3,800
Alkalinity	11,000
SCN^-	25
Conductivity	13,000
pH	8.9

Hot Air Stripping

Feed used for Options 2 and 3 was pretreated by hot air stripping before entering the activated sludge units. The 50 mm I.D. stripping column contained about two meters of 0.25 in. (0.6 cm) ceramic intalox saddles and operated at a gas rate of 28 liters/min., with a liquid rate of 7.5 liters/hr., temperature = 95°C, and pressure of 15 psig (103 kPa).

Analytical Procedures

A large array of analyses were performed during the course of this research. These analyses included total organic carbon (TOC); chemical oxygen demand (COD); biochemical oxygen demand (BOD); volatile and suspended solids for quantification of biomass and PAC concentrations; ammonia nitrogen; total Kjeldahl nitrogen; alkalinity; phenols; thiocyanate; phosphorous; nitrate; pH; dissolved oxygen; sludge settleability; pH, phenol, ortho, meta, and para cresol.

Details of the analytical and operating procedures used are found in References 17 and 18.

EXPERIMENTAL RESULTS

For all three options studied, it was found, during preliminary experimentation, that phosphorous had to be added to the wastewater as a biological nutrient. Therefore, all feed was prepared to contain 10 mg/l of phosphate as P. It was also determined that the raw or pretreated condensate could not be treated in the activated sludge units without dilution. Thus, for Option 1 (raw condensate) a 10:1 dilution was required, and for Options 2 and 3 (stripped condensate) a 2:1 dilution (50 percent strength) was required. Tap water was used for dilution in Option 1. Distilled water was used for Options 2 & 3.

Option 1

Option 1 consisted of feeding raw condensate directly to the three activated sludge reactors at a 10:1 dilution. The reactors were controlled at mean cell retention times (sludge age) of 13.3, 20, and 40 days for reactors R-1, R-2, and R-3. Hydraulic retention time was constant for all reactors at 2.5 days. Data was obtained continuously for a period of time greater than 200 days. Average reactor operating conditions for the best steady-state period indicated substrate utilization rates of 0.430, 0.344, and 0.291 mg COD removed/day - mg mixed liquor volatile suspended solids (MLVSS); MLVSS of 1,130, 1,400, and 1.640 mg/l,

S_e of 302, 350, and 362 mg/l COD for reactors R-1, R-2, and R-3, respectively.

Performance.--Percent removal of various wastewater quality parameters during periods of steady operation did not vary much between the three reactors. COD removal was between 85 to 90 percent, thiocyanate removal was 40 to 50 percent, and ammonia removal was about 50 percent. Phenol, m + p - cresol, and o - cresol were measured by gas chromatography using a 2m x 2mm I.D. glass column packed with one percent SP-1240-DA on 100/120 Supelcoport. Removal of these specific compounds was greater than 99 percent. It was noted that about 70 percent of the influent COD is attributed to these simple compounds, which corresponds to the observed COD removal

The pH of the reactors tended to be in the range of 5 to 6, which was attributed to the production of organic acids, nitrification, and the high dilution of influent. This pH may be unfavorable for removal of ammonia and thiocyanate which should improve at pH in the range of seven to eight, which was observed for Option 2 and 3 operations.

Kinetic Coefficients.--Periods of stable operation were used to obtain the kinetic coefficients for Eq. (1). Fig. 2 shows the average data for reactors 1, 2, and 3 which were operated at steady state for 34, 58, and 58 days, respectively. The plot indicates values of 0.35 mg volatile suspended solids (VSS) produced per day per mg COD removed for the yield coefficient, Y, and 0.075 day^{-1} for the decay coefficient, k_d.

It was found that the kinetic model for substrate removal (Eq. 2) could not be applied to the data. This result was attributed to the fact that the reactors were operated so that removal of substrate was very high. Thus, effluent biodegradable substrate was so low that the functionality as given by Eq. 2 could not be shown. Other researchers have obtained similar results (7).

Option 2

During Option2operation, stripped condensate was diluted by 50 percent with distilled water before being fed to the activated sludge reactors. Pretreatment by stripping removed ammonia, alkalinity, H_2S, and volatile organics from the wastewater. Removal of stripped material allowed operation at much lower dilutions as compared to Option 1. It was not an objective to study gas stripping as part of this project. Thus, a reasonable operating condition was chosen to give about 90 percent removal of ammonia in the stripper.

The three activated sludge reactors were operated at nominal sludge ages of 10, 20, and 30 days. Hydraulic retention time was constant for all reactors at eight days.

Performance.--Table II shows the performance and operating conditions for the three reactors during the study of Option 2. Removal of most measures of pollution was quite high. For example, removals of COD, TOC, BOD_5, phenols, ammonia, SCN^-, and TKN were about 88, 90, 95, 99+, 40, 50, and 40 percent, respectively. It was noted that reactor R-2, which operated at θ_c of 20 days, performed in a more stable manner than R-1 or R-3. Also, each reactor required the removal of foam from the surface of the aeration chamber once a day.

TABLE II

Operating and Performance Data[1], Option 2

Parameter	R-1	R-2	R-3
θ_c Days	10.0	20.4	31.2
θ_h	7.4	7.9	7.7
MLVSS	1,100	1,490	2,090
U[2]	0.52	0.38	0.30
U[3]	0.19	0.14	0.11
O_2 Use[4]	0.143	0.188	0.096
SVI[5]	18.2	21.5	35.0
COD In	4,450	4,450	4,450
COD Out	546	528	512
TOC In	1,580	1,580	1,580
TOC Out	156	153	141
BOD_5 In	2,250	2,250	2,250
BOD_5 Out	100	80	160
Phenols In	1,385	1,385	1,385
Phenols Out	0.64	0.63	0.63
Alkalinity In	1,030	1,030	1,030
Alkalinity Out	466	378	437
pH In, Units	8.9	8.9	8.9
pH Out, Units	8.1	8.0	8.1
NH_3-N In	320	320	320
NH_3-N Out	200	180	190
NO_3-N Out	47	45	74
SCN^- In	11.6	11.6	11.6
SCN^- Out	5.6	5.3	0
TKN[6] In	365	365	365
TKN Out	230	200	230

TABLE II, Continued

[1]All concentrations in mg/l, except as noted.
[2]Mg COD Removed/day-mg MLVSS
[3]Mg TOC Removed/day-mg MLVSS
[4]Mg O_2 used/day-mg MLVSS
[5]Sludge-Volume Index, ml/gram
[6]Total Kjeldahl Nitrogen

Kinetic Coefficients.--Figures 3 and 4 show the plot of steady state data to obtain the yield and decay coefficients for Eq.(1). Average values are plotted. From the figures, a yield coefficient of 0.69 mg VSS produced/mg TOC removed and 0.25 mg VSS produced/mg COD removed are obtained. Respective decay coefficients are 0.038 and 0.040 mg VSS destroyed/day-mg MLVSS. The correlation coefficient for both plots is 0.89.

A plot of the data, according to Eq. (2) was not particularly useful because the effluent substrate concentrations were so close to each other. However, it was possible to estimate that the nonbiodegradable portion of the TOC and COD were about 120 and 460 mg/l, respectively.

A plot of the data, according to Eq. (3), was made, and oxygen utilization coefficients a' and b' were obtained. They were 0.145 mg O_2 used/mg COD removed and 0.105 mg O_2 used/day-mg MLVSS.

Option 3

During Option 3, stripped condensate diluted to 50 percent strength was fed to activated sludge reactors, along with powdered activated carbon (PAC), at doses of 500, 1,000, and 1,500 mg/l for reactors R-1, R-2, and R-3, respectively. The results from Option 2 indicated that a θ_c of 20 days provided the most stable operation; therefore, all reactors were operated at θ_c = 20 days for Option 3. Hydraulic retention time, θ_h, was also held constant at about eight days.

Performance.--The operating characteristics of Option 3 were significantly better than those for Options 1 and 2. Reactor stability and consistent effluent quality were key factors. Table III lists the operating and performance data for Option 3. The only independent variable during Option 3 was the PAC dose. The table indicates that the sludge developed during Option 3 was more active than that for Option 2 as indicated by higher oxygen uptake rates and MLVSS concentrations. Apparently, the PAC prevents inhibitory material from affecting the biomass.

TABLE III

Operating and Performance Data. Option 3[1]

Parameter	R-1	R-2	R-3
Carbon Dose	500	1,000	1,500
θ_c, Days	19.3	19.9	19.8
θ_h, Days	7.9	7.5	7.8
MLSS	3,180	4,240	4,840
MLVSS	1,600	2,280	2,340
O_2 Use[2]	0.360	0.173	0.134
SVI[3]	34.8	18.5	17.5
COD In	5,840	5,840	5,840
COD Out	383	292	239
TOC In	1,700	1,700	1,700
TOC Out	92.9	65.7	44.6
BOD_5 In	3,080	3,080	3,080
BOD_5 Out	139	129	162
Phenols In	1,130	1,130	1,130
Phenols Out	0.92	0.85	0.33
Alkalinity In	1,180	1,180	1,180
Alkalinity Out	410	491	410
pH In, Units	8.6	8.6	8.6
pH Out, Units	8.0	8.0	7.9
NH_3-N In	520	520	520
NH_3-N Out	297	333	257
NO_3-N Out	66	86	99
SCN^- In	13.7	13.7	13.7
SCN^- Out	4.8	0	8.0
TKN In	439	439	439
TKN Out	220	230	220

[1]Units of mg/l, except as noted.
[2]mg O_2 used/day-mg MLVSS
[3]ml/gram

Figure 5 shows the data for oxygen uptake according to Eq. (3). O_2 uptake was higher than that for Option 2, which supports the idea that PAC removed inhibitory substances. Values of a' and b' were 2.04 mg O_2 used/mg COD removed and -0.485 mg O_2 used/day-mg MLVSS. The data is unusual, however, in that at zero O_2 uptake, COD removal occurs. This can be interpreted as removal due to the PAC.

Sludge settleability was excellent for R-2 and R-3, which had the higher doses of PAC. Foaming was slightly lower than for Option 2, although removal was still required.

Percent removal of key parameters were generally higher than for Options 1 and 2. Removals of COD, TOC, BOD_5, Phenols, ammonia, thiocyanate, and total Kjeldahl Nitrogen were about 95, 96, 96, >99, 40,

50, and 50 percent, respectively.

SUMMARY

It was apparent that all three options provided good treatment of the condensate. The economics and water balance for a specific operating site and process will probably dictate which option is the most advantageous. The authors prefer Option 3 on the basis of ease and consistency of operation, along with the fact that the effluent will be the most highly treated of the options studied.

CONCLUSIONS

Specific conclusions of the research are as follows.

1. Raw, unstripped UCG condensate (Option 1) can be treated by activated sludge at ten percent strength with a hydraulic retention time of 2.5 days, sludge ages between ten to 40 days, and substrate removal ratio between 0.29 to 0.43 mg COD removed/day-mg MLVSS. COD removal was about 90 percent.

2. Yield and decay coefficients for Option 1 were found to be 0.35 mg VSS produced/mg COD removed and 0.075 day^{-1}, respectively.

3. Hot air stripped UCG condensate can be treated by activated sludge at 50 percent strength (Option 2) with a hydraulic retention time of eight days, sludge ages between ten and thirty days, and substrate removal rates of 0.30 to 0.52 mg COD removed/day-mg MLVSS. COD, TOC, BOD_5, and phenols were removed in excess of 90 to 95 percent.

4. Yield and decay coefficients for Option 2 were found to be 0.25 mg VSS produced/mg COD removed and 0.040 day^{-1}, respectively.

5. Useful relationships between substrate removal and substrate concentration could not be found for Options 1 and 2 for the operating conditions studied.

6. Pretreatment by hot air stripping allowed treatment of UCG condensate at lower dilutions.

7. The additon of powdered activated carbon to the activated sludge system (Option 3) significantly improved operating and performance characteristics of the treatment system as compared to Options 1 and 2. Treatment with removals of pollutants in excess of 95 percent was achieved with PAC doses of 500 to 1,500 mg/l, hydraulic retention time of eight days, and a sludge age of 20 days.

8. All options studied showed that phenol, o and m + p cresol were removed in excess of 99 percent.

9. Nitrificacion was observed for all options. Ammonia removal was about 50 percent.

10. Phosphorus addition at 10 mg/l of phosphate-P was required for biological nutrient supplement for all options.

11. Oxygen requirements for Options 2 and 3 were found to be between 0.13 to 0.36 mg O_2 used per day per mg MLVSS. Oxygen uptake was greater for Option 3, which was attributed to the removal of inhibitory substances by the PAC.

12. Foam removal from the activated sludge aeration chambers was required for Options 2 and 3.

13. Option 3 showed the best operating characteristics and performance of the options studied.

ACKNOWLEDGMENTS

The authors wish to express their appreciation to the project sponsor, The U.S. Department of Energy, Laramie Energy Technology Center, for supplying project funding and wastewater used in the study. Also, the large amount of work would not have been possible without the aid of laboratory help from Frank Hulsey at the University of Texas, and Dean Logan at the University of Wyoming.

REFERENCES

1. Bartke, T. C., "The DOE Underground Coal Conversion Program Field Test Activities in 1979 and 1980," Draft of U.S. DOE Report of Investigations.

2. Humenick, M. J., and Mattox, C. F., "Characteristics of Condensates Produced during Underground Coal Gasification," In-Situ, 6:1, 1982.

3. Singer, P. C., et al., "Treatability and Assessment of Coal Conversion Wastewaters: Phase I," U.S. Environmental Protection Agency, EPA-600/7-7-248, 1979.

4. Forney, A. J., et al, "Analysis of Tars, Chars, Gases, and Water in Effluents from the Synthane Process," U.S. Bureau of Mines Technical Progress Report 76, Pittsburgh Energy Research Center, Pittsburgh, PA, 1974.

5. Johnson, G. E., et al., "Treatability Studies of Condensate Water from Synthane Coal Gasification," U.S. Dept. of Energy, PERC/RI-77/13, Pittsburgh Energy Research Center, Pittsburgh, PA, 1977.

6. Mattox, C. F., and Humenick, M. J., "Organic Groundwater Contaminants from UCG," Paper presented at the 5th UCG Symposium, Alexandria, VA, 1979.

7. Luthy, R. G., et al, "Treatment of Coal Coking and Coal Gasification Wastewaters," Jour. Water Poll. Control Fed., 53:3, 325, 1981.

8. Sack, W. A., "Biological Treatability of Gasifier Wastewater," U.S. Dept. of Energy, METC/CR-79/24, June, 1979.

9. Luthy, R. G., et al., "Biological Treatment of Grand Forks Energy Technology Center Slagging Fixed Bed Coal Gasification Process Wastewater," U.S. Dept. of Energy, FE-2496-42, Mar., 1979.

10. Neufeld, R. G., et al., "Biokinetics of Activated Sludge Treatment of Synthane Fluidized Bed Gasification," U.S. Dept. of Energy PERC/RI-77/13, 1979.

11. Luthy, R. G., and Tallon, J. T., "Biological Treatment of Coal Gasification Process Wastewaters," Water Res. (G.B.), 14:1269, 1980.

12. Luthy, R. G., and Tallon, J. T., "Experimental Analysis of Biological Oxidation Characteristics of Hygas Coal Gasification Wastewater," U.S. Dept. of Energy, FE-2496-27, July, 1978.

13. Sack, W. A., and Bokey,, W. R., "Biological Treatment of Coal Gasification Wastewater," Proc. 33rd Purdue Ind. Waste Conf., 278, Lafayette, IN, 1979.

14. Luthy, R. G., et al., "Biological Treatment of Synthetic Fuel Wastewater," Jour. Envir. Engr. Div., Proc. ASCE, 106:609, 1980.

15. Metcalf and Eddy, Inc., Wastewater Engineering, McGraw-Hill, Second Edition, Chapter 9, 1979.

16. Eckenfelder, W. W., Jr., Water Quality for Practicing Engineers, Barnes and Noble, Inc., New York, NY, 1970.

17. Caire, T. P., Biological Treatability of an Underground Coal Gasification Wastewater, Master's Thesis, The University of Texas at Austin, May, 1983.

18. Brauer, R. G., Activated Sludge and Powdered Activated Carbon - Activated Sludge Treatment of UCG Condensate, Master's Thesis, The University of Wyoming, August, 1983.

FIGURES

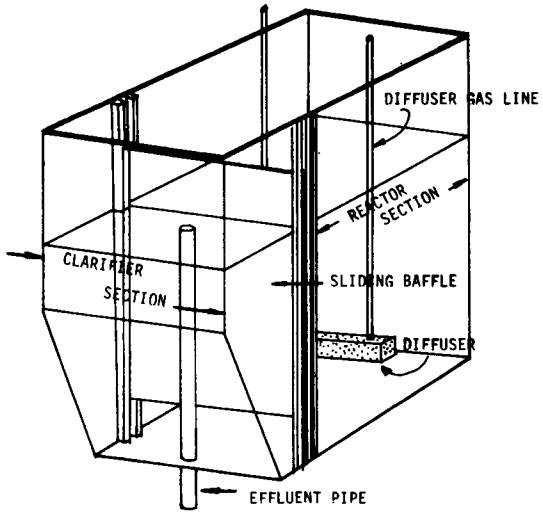

Fig. 1. Reactor/Clarifier

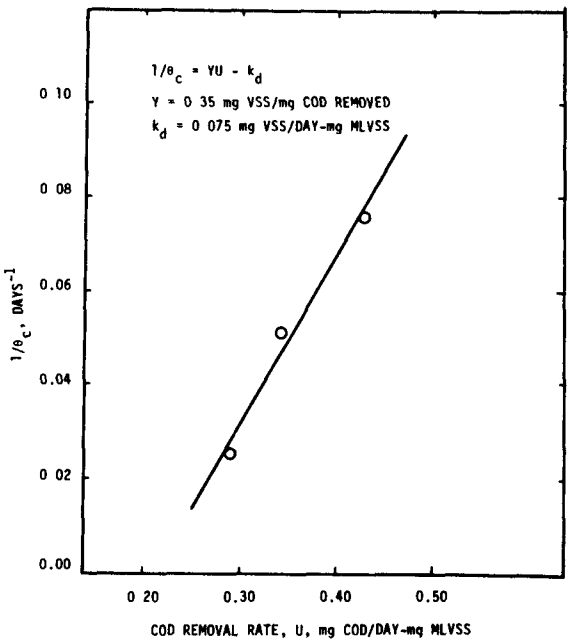

Fig. 2. Yield and Decay Coefficients, Option 1.

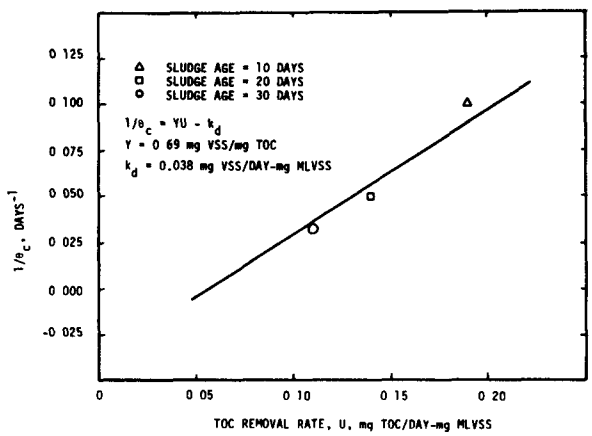

Fig. 3. Yield and Decay Coefficients, Option 2.

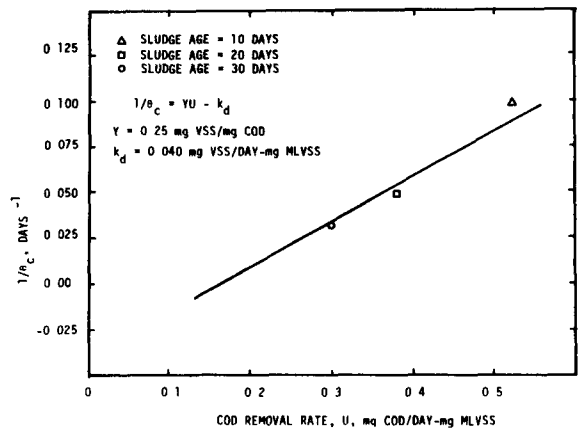

Fig. 4. Yield and Decay Coefficients, Option 2.

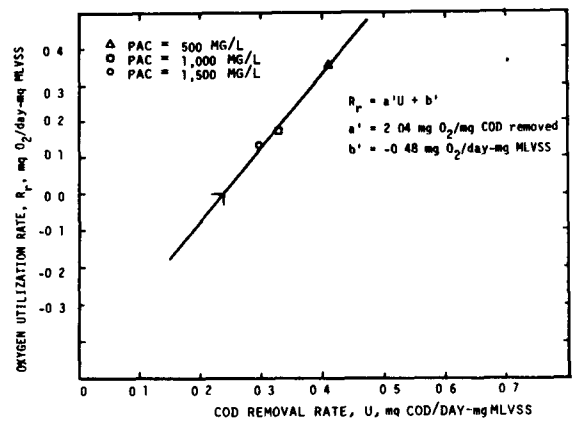

Fig. 5. Oxygen Utilization, Option 3.

4.2 TREATMENT OF UCG CONDENSATES BY ACTIVATED CARBON ADSORPTION

by

Lora S. Johnson[1]
William F. McTernan[2]

ABSTRACT

Condensates from an underground coal conversion experiment performed near Hanna, Wyoming were evaluated for treatability by activated carbon adsorption. Three different carbons were tested in batch operations with the best of these further evaluated in continuous flow mode for their ability to reduce organic contamination.

Equilibrium curves were established for each carbon at a select dosage. Isotherm testing followed at three temperatures together with data fitting to accepted models. Experimental efforts concluded with evaluations of continuous flow adsorption in bench scale packed bed columns operated in a downflow mode.

Depending upon carbon dose and type, pollutant removals based upon TOC varied from thirty to over ninety percent at equilibrium. Additional data will be presented showing phenol and COD removal at the corresponding configurations. There were significant differences noted in adsorption between carbons and between modes of operation. It appears that coal based carbons outperform those derived from lignites. The paper closes with a discussion of the applicability of these research data to field or commercial scale treatment effort.

1/ Post graduate appointee, Associated Western Universities, Salt Lake City, Utah 84111
2/ Senior Research Engineer, University of Wyoming Research Corporation, Laramie, Wyoming 82071

INTRODUCTION

The treatment of wastewaters produced during the underground gasification of coal has importance from industrial as well as environmental perspectives. Industrially, these waters represent potentially valuable commodities which can be reused after treatment to satisfy some inplant water needs. Environmentally, these waters are significant in that they are often highly polluted and can produce major environmental degradation if introduced into receiving surface or groundwater drainages.

Further, those waters transported to the land's surface with, and subsequently condensed from the produced gases are equivalent to materials left in UCG caverns at the instant of combustion cessation. These waters form one component in a mass balanced pollutant loading to regional groundwater systems. The ultimate treatment or mitigation of pollutant plumes which might form after UCG is somewhat conditional upon the information base generated relative to these condensate waters.

The reported research, therefore, has two objectives. These are:

- The determination of the feasibility of adapting a single physical-chemical treatment approach to condensate clean-up.
- The collection of operating parameters to define adsorption capacities and kinetics

as a first step in overall environmental mitigation.

RESEARCH STRATEGY

This effort utilized waters produced during the second phase of the Laramie Energy Technology Center's (LETC) fourth Hanna, Wyoming field gasification experiment. This work has been adequately described elsewhere (1,2,3) but briefly in a coal seam approximately 33 feet thick at an average depth of 323 feet, 1525 tons of coal were gasified to produce approximately 15 MBTU.

Condensate waters were separated from produced gas streams by initially cooling them by means of a 60° C heat exchanger. These condensed fluids were collected in a baffled knock down tank and subsequently pumped to a vertical separator to effectuate gravity induced tar-water separation. Collected waters were then composited in a large recirculating holding tank to ensure homogeneity (4). These waters were barreled and transported to Laramie, Wyoming to be stored at 4° C until used. Table 1 presents the water quality analyses describing these waters.

The research approach taken with this phase of the treatability effort was to evaluate the adsorptive potential of select constituents and parameters found in these waters onto activated carbon surfaces. For this portion of the research no pretreatment was attempted before adsorption. Batch and continuous flow adsorptive systems were developed for this project. Table 2 itemizes the research approach employed.

RESULTS

Figure 1 presents the equilibrium uptake curve determined for Filtrasorb 400 activated carbon at a carbon dosage of 50,000 mg/l. An equilibrium time of four hours was achieved for this system with a residual unadsorbed TOC concentration of approximately 200 mg/l. Similar analyses were performed for the Hydrodarco 4000 and Darco H 90+ systems. The Darco 90+ activated carbon achieved an equilibrium TOC concentration of about 250 mg/l in four hours while the Hydrodarco 4000 system has a 500 mg/l TOC concentration after 22 hours. A twenty-five percent increase in equilibrium time was added to each system to ensure reaction completion and a series of isotherm evaluations were determined for each system. Three constant temperatures and eight carbon dosages were attempted in this initial effort. The resultant data were fitted to a Freundlich isotherm equation (6). This equation has the form:

$$\frac{X}{M} = KC^{1/N} \qquad (1)$$

where:
- X = amount of solute adsorbed (mass units)
- M = weight of the adsorbent (mass units)
- C = concentration of the solute remaining in solution after adsorption is complete (concentration units)
- K and N = constants to be evaluated for each solute and temperature

This equation can be rewritten in a linear form by taking the log of both sides. The equation becomes:

$$\text{Log}\left(\frac{X}{M}\right) = \text{Log } K + 1/N \text{ Log } C \qquad (2)$$

A plot of log X/M versus log C yields a straight line for those data which follow the Freundlich theories of adsorption.

Figure 2 presents the results of this evaluation for the Filtrasorb 400 system at 25° C, while Table 3 presents the data for this figure and the same configuration at 5° C and 50° C. Also included in this table are the corresponding data for the Darco 4000 and Darco H 90+ systems. The information included in this table labeled ultimate capacity is the theoretical, maximum loading for each of the individual activated carbon systems. This value represents the equilibrium value of adsorbed mass and is useful to compare carbons for batch treatability as well as performing preliminary sizing for continuous flow systems. Figures 3 and 4 present the Freundlich isotherm plots for the Darco HD 4000 and Darco H 90+ adsorption data at 25° C, while Tables 4, 5 and 6 present the equilibrium data collected during these isotherm studies at each tempera-

ture for each activated carbon dose. These data clearly show that the coal derived activated carbons are superior to the lignite based system. Ultimate capacities for the coal based carbons were approximately 0.40 while the lignite system was less than 0.20. These values are moderate to high when compared to other wastewaters (7, 8), but it must be remembered that ultimate capacity is a function of wastewater strength as well as the affinity of the material for the activated carbon. The stronger a given waste the higher the ultimate capacity will be if all other factors remain constant. This term can be used to compare activated carbon performance. Temperature did not play a key role in either of the coal based adsorption systems. The lignite system did show a higher degree of adsorption at lower temperature. This follows theory but does not play an important role in these considerations (8).

Figure 5 presents the breakthrough data derived from a five column continuous flow study using Filtrasorb 400 as the adsorbent, at a surface loading rate of 1.6 gpm/ft^2, (66.5 lpm/m^2) and a total of 0.41 lb/column (186.6 g). These curves were graphically integrated at the point of exhaustion to calculate the dynamic ultimate capacity (9). It was determined that 0.34 mass of TOC is adsorbed per an equal mass of adsorbent. At an arbitrarily acceptable effluent level equal to twenty percent of the influent TOC a value of 0.21 was calculated for this capacity term. While either value is acceptable for treatability consideration, the steep, immediate slope associated with breakthrough for each column indicates that a treatment system which only employs activated carbon will not be as acceptable as other configurations for treating this wastewater. Activated carbon appears to be most appropriate in an emergency cleanup mode, in a small batch type process for limited waste volumes or in a sequence of unit processes where specific compound removal could be enhanced.

Figure 6 and 7 present the four point Freundlich isotherms for the sum of the phenol and ortho, meta and para cresol and for those components exhibiting a chemical oxygen demand (COD). These figures are for the Filtrasorb 400 system at 25° C. The corresponding data for these figures as well as for the HD 4000 and H 90+ systems are contained in Tables 7 and 8 respectively. These data reinforce the hypothesis that adsorption of materials found in UCG condensate water is favored in coal based activated carbons (FS 400 and H 90+). Further, even though TOC components comprise a substantial portion of the COD load in these wastes, the adsorptability of each parameter varies. This appears due, in part, to relatively high concentrations of oxidizable inorganic materials in these waters. Unmeasured in the TOC test, they can form a significant amount of COD.

Figures 8 and 9 present the Freundlich plots for the ortho cresol and the combined meta and paracresol adsorption. Tables 9 and 10 contain the data used to generate these figures. The trends noted in the other adsorption studies continue. That is, the performance of the coal based activated carbons greatly exceeds that of the lignite carbons. Calculated ultimate capacities for these systems were 0.04, 0.04 and 0.02 for orthocresol adsorption on the H 90+, Filtrasorb 400 and the HD 4000 respectively. Ultimate adsorption of the combined meta and paracresol on these same surfaces was 0.12, 0.14 and 0.06. The equivalent values for the phenol alone were 0.12, 0.11 and 0.05 respectively.

DISCUSSION AND CONCLUSIONS

The ability of various activated carbon systems to adsorb total organic carbon, chemical oxygen demand, phenols and select cresols was evaluated in batch studies under isothermal conditions. The adsorptive capacities of two coal based carbons, Filtrasorb 400 and Darco H 90+ were approximately equal and greatly exceeded the adsorptive capacity of a lignite derived activated carbon, Darco HD 4000. Although not reported in this study, the kinetics of adsorption for these two carbons were approximately equal.

Continuous flow adsorption was evaluated on a TOC basis for a Filtrasorb 400 system. A surface loading rate of 1.6 gpm/ft^2 produced steep, immediate breakthrough curves as well as a bleeding of residual tars. The carbon capacity at breakthrough approached the ultimate

capacities calculated from batch studies indicating that the breakthrough noted was a function of adsorptive mechanisms rather than hydraulically mediated.

Higher adsorptive capacities were noted for the meta and paracresols as well as the phenols than were seen for the orthocresol fraction. In no case however did concentrations of any constituent go below the ppm range at equilibrium. Substantial contamination still existed even after contact with exceptionally large activated carbon dosages. Based upon the residual material left following adsorption, the almost immediate breakthrough of tars in the flow through system and the overall steepness of the slopes associated with column operation, additional pre and possibly post treatment is required to optimize activated carbon adsorption. At this time, it appears that batch systems with a carbon regeneration step if warranted would be preferable to column operation.

ACKNOWLEDGEMENTS

The authors wish to thank Dr. Richard E. Poulson for the chromatography analyses he performed for phenol and cresol determination.

SELECTED REFERENCES

1. Bartke, T. C., L. Docktor, T. E. Sterner, J. E. Virgona and L. F. Wojdak, 1978. Status Report on the Hanna III and Hanna IV Underground Coal Gasification Experiments. Proceedings Fourth Annual Underground Coal Conversion Symposium, Steamboat Springs, Colorado.

2. Covell, J. R., L. F. Wojdac, F. A. Barbour, G. W. Gardner, R. Glass and P. J. Hommert, 1980. Results of the Fourth Hanna Field Test. Proceedings Sixth Annual Underground Coal Conversion Symposium, Shangri-La, Oklahoma.

3. L. F. Wojdac and T. C. Bartke, 1979. Hanna IV Operational Difficulties - An Evaluation. Proceedings Fifth Annual Underground Coal Conversion Conference, Alexandria, Virginia.

4. _____ 1980. Statement for Hanna IVB Water Samples. Department of Energy, Laramie Energy Technology Center, Laramie, Wyoming.

5. _____ 1980. Analysis Statement for Hanna IVB Water Samples. Department of Energy, Laramie Energy Technology Center, Laramie, Wyoming.

6. Weber, Walter J. Jr., 1972. Physiochemical Processes for Water Quality Control. Wiley Interscience, New York, New York.

7. Fair, Gordon Maskew, J. C. Geyer and D. A. Okun 1971. Elements of Water Supply and Wastewater Disposal. Second Edition. John Wiley and Sons Inc., New York, New York.

8. Giusti, D. M., Conway, R. A. and Lawson, C. T. 1974. Activated Carbon Adsorption and Petrochemicals. Journal Water Pollution Control Federation 46.5:947.

9. Humenick, Michael J. Jr. 1977. Water and Wastewater Treatment Calculations for Chemical and Physical Processes. Marcel Decker Inc., New York, New York.

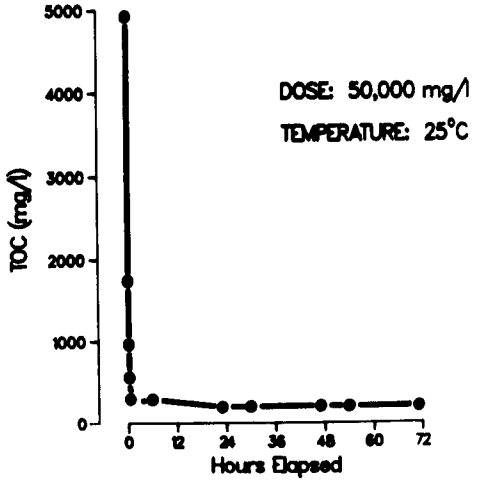

FIGURE 1. Equilibrium uptake curve for Filtrasorb 400.

Table 1
Example Water Quality Analyses
Hanna IVB Underground Coal Gasification Experiment

Parameter (mg/l) except where noted	
Sodium	6.7
Magnesium	4.6
Chloride	38.0
Fluoride	2.8
Nitrate	1200.0
Sulfate	290.0
Carbonate	1200.0
Bicarbonate	8600.0
Nitrogen (NH_3)	3800.0
Oil & Grease	180.0
Total Alkalinity (as $CaCO_3$)	9070.0
pH (standard pH units)	8.9
Conductivity	13000.0
Chemical Oxygen Demand	17000.0
Total Organic Carbon	4707.0
Total Inorganic Carbon	1659.0
Boron (Total)	10.0
Copper (Total)	0.5
Iron (Total)	4.1
Selenium (Total)	0.27
Thiocyanate	10.0
Thiosulfate	41.0
Zinc	0.11

Source: LETC (5)

Table 2
Research Configurations
Activated Carbon Adsorption
Hanna IVB Condensate Water

Carbon Type	Equilibrium Uptake	Isotherm	Multicolumn Breakthrough
Filtrasorb 400	*	*	*
Hydrodarco 4000	*	*	
Darco H 90+	*	*	
Carbon Dosage (mg/l)			
500		*[1]	
1000		*[1]	
2000		*[1]	
3025		*[2]	
5000		*[1]	
10,000		*[1 2]	
17,100		*[2]	
21,800		*[3]	
22,725		*[2]	
25,000		*[1]	
29,090		*[3]	
30,000		*[2]	
36,365		*[3]	
50,000	*	*[1 3]	
100,000		*[1]	
Temperature (C)			
5		*	
25	*	*	*
50		*	
Analytics			
Total Organic Carbon	*	*	*
Chemical Oxygen Demand		*	
Phenols		*	

1. TOC isotherms all carbons
2. TOC, COD, phenol isotherms FS 400, DH 90+
3. TOC, COD, phenol isotherms HD 4000

Table 3
Adsorption Data for Three
Batch Activated Carbon Systems
Hanna IVB Condensate Water

Carbon Type	Temperature (°C)	Ultimate Capacities (mass/mass)	K	N
Filtrasorb 400	5	0.33	0.003	1.67
	25	0.40	0.005	1.96
	50	0.40	0.002	1.60
H 90+	5	0.27	0.009	2.44
	25	0.41	0.004	1.85
	50	0.45	0.003	1.70
HD 4000	5	0.21	0.003	1.96
	25	0.15	0.012	3.33
	50	0.16	0.008	2.86

Table 4
Equilibrium Total Organic Carbon Values
for Varying Activated Carbon Dosages
in Isothermal Conditions for
Hanna IVB Condensates
Five Degree Celsius

Carbon Type	Activated Carbon Concentrations (mg/l)								
	0	500	1000	2000	5000	10000	25000	50000	100000
	Equilibrium Total Organic Carbon Concentrations (mg/l)								
Filtrasorb	3366	3090	3090	2950	2260	1480	318	164	142
Darco H 90+	4404	4303	4129	3935	3127	2128	425	181	140
Darco HD 4000	4181	3980	3831	3793	3240	2935	1640	381	158

Table 5
Equilibrium Total Organic Carbon Values
for Varying Activated Carbon Dosages
in Isothermal Conditions for
Hanna IVB Condensates
Twenty-Five Degrees Celsius

Carbon Type	Activated Carbon Concentrations (mg/l)								
	0	500	1000	2000	5000	10000	25000	50000	100000
	Equilibrium Total Organic Carbon Concentrations (mg/l)								
Filtrasorb 400	4736	4501	4365	4125	3282	2129	523	201	146
Darco H 90+	4645	4379	4253	4009	3171	2193	582	190	117
Darco HD 4000	4878	4900	4743	4600	4184	3480	1894	498	216

Table 6
Equilibrium Total Organic Carbon Values
for Varying Activated Carbon Dosages
in Isothermal Conditions for
Hanna IVB Condensates
Fifty Degrees Celsius

Carbon Type	Activated Carbon Concentrations (mg/l)								
	0	500	1000	2000	5000	10000	25000	50000	100000
	Equilibrium Total Organic Carbon Concentrations (mg/l)								
Filtrasorb 400	4765	4538	4350	4227	3236	2258	648	475	193
Darco H 90+	4680	4443	4143	4012	3228	2180	511	222	174
Darco HD 4000	4810	4857	4660	4510	4120	3360	1860	546	275

Table 7
Equilibrium Chemical Oxygen Demand Values
for Varying Activated Carbon Dosages
in Isothermal Conditions for
Hanna IVB Condensates
Twenty-five Degrees Celsius

Carbon Type	Activated Carbon Concentrations (mg/l)								
	0	10000	17100	21800	22725	29090	30000	36365	50000
	Equilibrium Chemical Oxygen Demand Concentrations (mg/l)								
Filtrasorb 400	16200	7595	4050		2278		1266		
Darco H 90+	16200	7595	4304		2532		1772		
Darco HD 4000	16200			7850		5316		4305	2025

Table 8
Equilibrium Phenol Concentration
for Varying Activated Carbon Dosages
in Isothermal Conditions for
Hanna IVB Condensates
Twenty-five Degrees Celsius

Carbon Type	Activated Carbon Concentrations (mg/l)								
	0	10000	17100	21800	22725	29090	30000	36365	50000
	Equilibrium Phenol Concentrations (mg/l)								
Filtrasorb 400	4818	2351	1115		555		205		
Darco H 90+	4818	2290	1263		590		216		
Darco HD 4000	4818			2383		1721		1332	322

Table 9
Equilibrium Ortho Cresol Values
for Varying Activated Carbon Dosages
in Isothermal Conditions for
Hanna IVB Condensates
Twenty-five Degrees Celsius

Carbon Type	Activated Carbon Concentrations (mg/l)								
	0	10000	17100	21800	22725	29090	30000	36365	50000
	Equilibrium Ortho Cresol Concentrations (mg/l)								
Filtrasorb 400	488	143	37		15		3		
Darco H 90+	488	149	57		19		6		
Darco HD 4000	488			157		89		68	9

Table 10
Equilibrium Para and Meta Cresol Values
for Varying Activated Carbon Dosages
in Isothermal Conditions for
Hanna IVB Condensates
Twenty-five Degrees Celsius

Carbon Type	Activated Carbon Concentrations (mg/l)								
	0	10000	17100	21800	22725	29090	30000	36365	50000
	Equilibrium Meta and Para Cresol Concentrations (mg/l)								
Filtrasorb 400	1580	498	142		54		16		
Darco H 90+	1580	491	186		66		19		
Darco HD 4000	1580			526		292		214	32

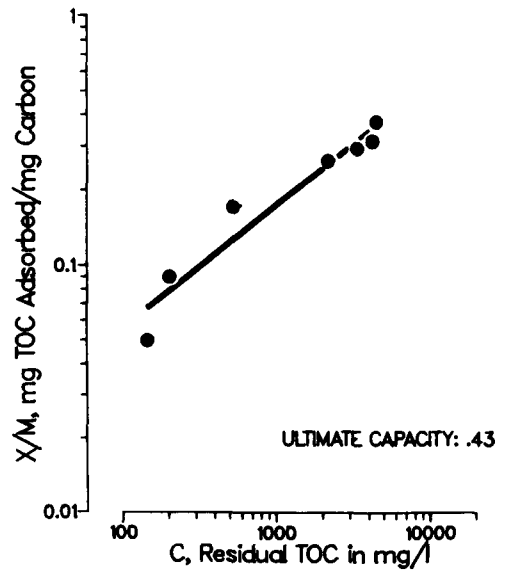

FIGURE 2. Freundlich isotherm for Filtrasorb 400 at 25° Celsius

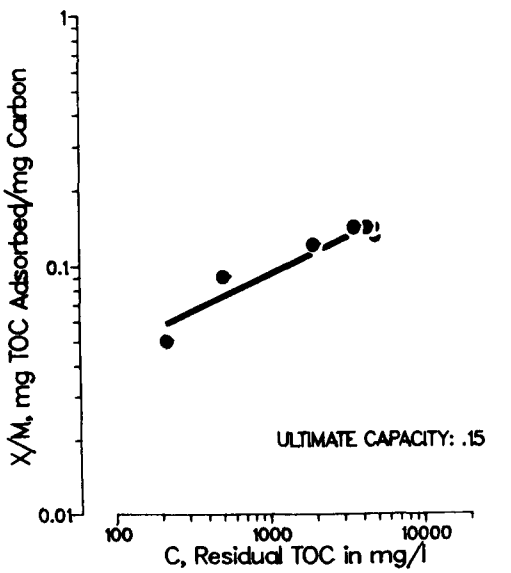

FIGURE 3. Freundlich isotherm for Darco HD 4000 at 25° Celsius

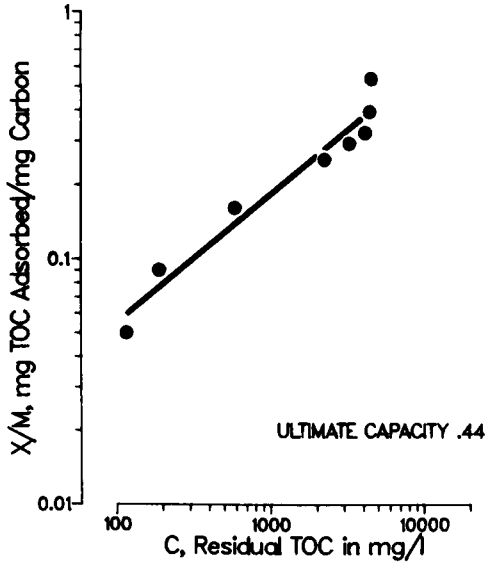

FIGURE 4. Freundlich isotherm for Darco H 90+ at 25° Celsius

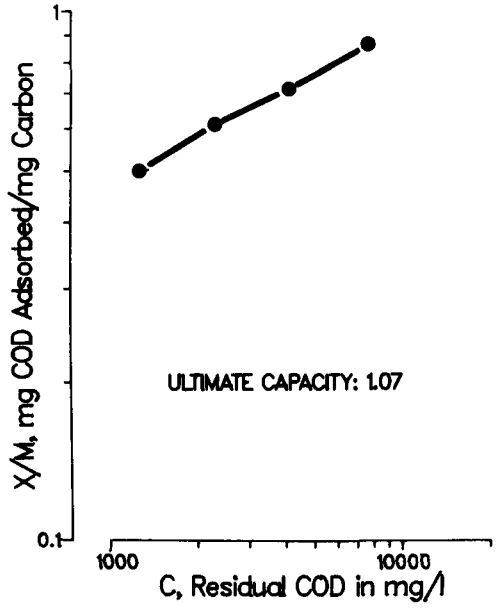

FIGURE 6. Freundlich isotherm for Filtrasorb 400 at 25° Celsius

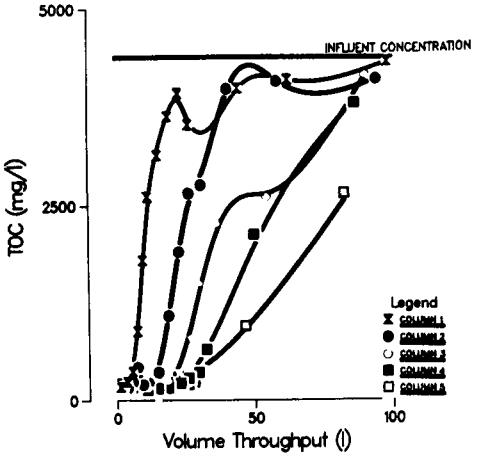

FIGURE 5. Breakthrough curves for Filtrasorb 400 continuous flow system

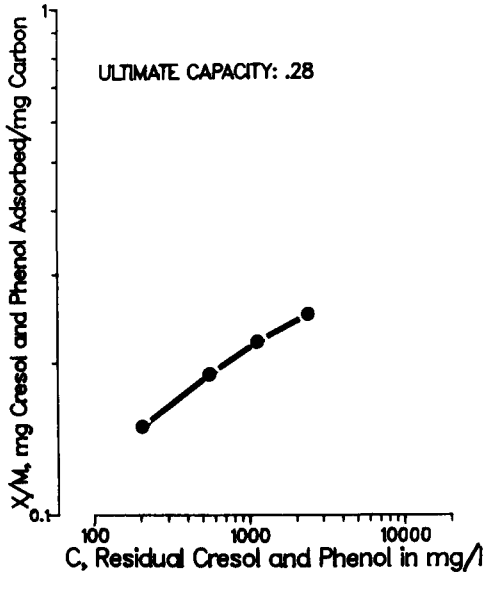

FIGURE 7. Freundlich isotherm for Filtrasorb 400 at 25° Celsius

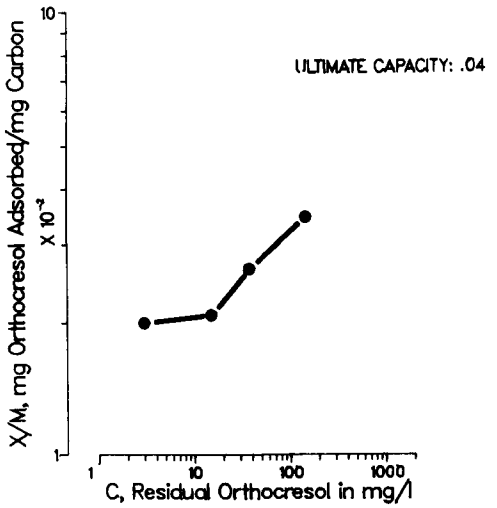

FIGURE 8. Freundlich isotherm for Filtrasorb 400 at 25° Celsius

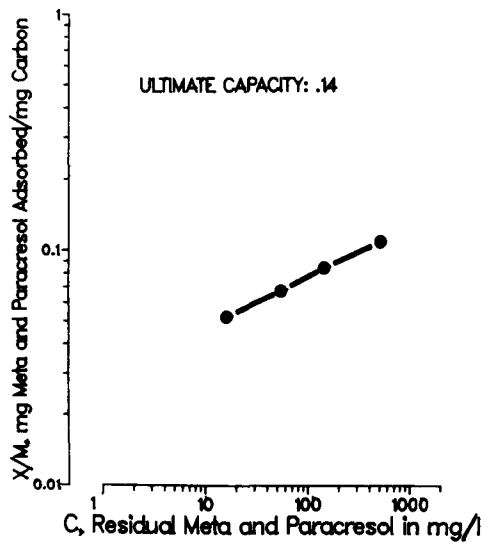

FIGURE 9. Freundlich isotherm for Filtrasorb 400 at 25° Celsius

4.3 THE SORPTION OF LEAD, CADMIUM, ARSENIC, AND SELENIUM BY COAL, CHAR, AND ASH

by

James E. Park 1/
Linda J. McGowan 2/
Patricia Snyder Fair 2/

ABSTRACT

There are several environmental concerns resulting from the in-situ gasification of coal; among them being subsidence, air emissions and groundwater pollution. All of these are important considerations, but this study focused on the potential contamination of groundwater by volatile trace elements. The objective was to assess through laboratory studies the sorptive capacities of the surrounding environment for the contaminants lead, cadmium, arsenic and selenium.

Column and batch studies were performed in order to evaluate the retention of these trace elements on coal, char and ash. Solutions of lead were fed through columns of coal; and lead, cadmium, arsenic and selenium in solution were fed through columns of coal, char and ash. Batch tests examined solutions of the four trace elements individually and together in contact with coal, ash and char.

The movement of the contaminants (Pb, Cd, As and Se) down through the columns was monitored by sampling at 15.2 cm (6") intervals along each column. This data was used to estimate the amount of contaminant sorbed, by weight, by the coal, ash and char. Generally, the amounts sorbed by the three materials in the columns were greater than the sorption shown in the batch tests.

The movement of the trace elements through the columns with respect to the total liquid movement was also studied. Simplified calculations compared the velocity of a trace element's concentration front (in cm/day) determined from the breakthrough curves, with the linear velocity of the flow of the solutions through the columns. The comparisons indicate that for the concentrations and flow rates studied, the retention of trace elements is more a function of concentration than the rate of flow through the materials.

INTRODUCTION

Underground coal gasification (UCG) offers the potential to utilize vast reserves of coal which are not economically accessible by conventional mining techniques. Technology for this process is progressing, but there are still many technical, economic and environmental questions regarding the UCG process.

The environmental concerns of UCG fall into three categories: air pollution, subsidence and water pollution (1). This study focused on one aspect of the water pollution concerns, i.e., the mobilization of trace elements resulting

1/ University of Cincinnati, Cincinnati, OH 45268
2/ U.S. EPA, Cincinnati, OH 45268

from UCG. Temperatures present during an UCG burn are sufficient to volatilize trace elements such as arsenic, cadmium, lead and selenium. These elements are found in most coals, in a variety of concentrations (2). If released during a burn, they could potentially dissolve in the groundwater as it seeps back into the burned cavity, and they may then be transported to adjoining aquifers.

Adsorptive materials are used extensively for pollution control; this study focused on the most abundant adsorptive materials present at an UCG site: coal, char and ash. The objective was to determine the sorptive characteristics of coal, char and ash for the trace elements arsenic, cadmium, lead and selenium. The sorptive characteristics were determined using both column and batch tests. Similar studies have been performed by others using smaller diameter columns and higher concentrations of feed constituents (3, 4).

EXPERIMENTAL PROCEDURE

The coal used in this study consisted of fines obtained from a mine in Kentucky. It was a sub-bituminous variety with approximately 17% ash content. The particle size distribution of the coal, determined using standard ASTM (5) procedures, is shown in Figure 1.

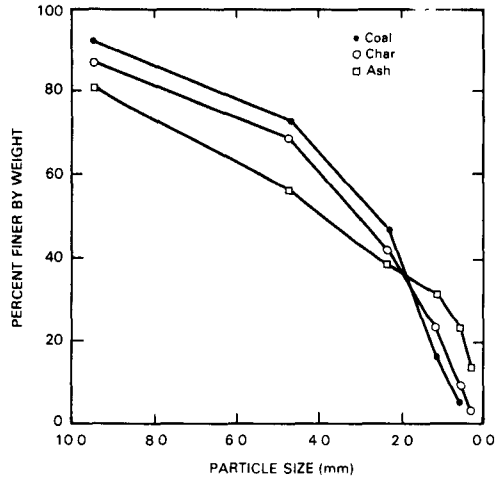

Figure 1 Particle Size Distribution of Coal Char and Ash

The char was prepared from the coal by slowly raising the temperature of the coal to 500-800°C in a muffle furnace. Ash was prepared by increasing the final temperature to at least 1000°C. The particle size distribution of the char and ash were also determined by ASTM (5) procedures and are shown in Figure 1.

Column Studies

Plexiglass columns (14.6 cm I.D.) were constructed for the dynamic studies. Sampling ports were placed at 15.2 cm (6") intervals down each column. The columns were filled with either coal, char or ash which was weighed prior to placing it in the column. Table 1 lists the weights and heights of the materials placed in the columns.

The first two experimental runs studied the sorption of lead on coal. In the next experiment, solutions containing As, Cd, Pb and Se were gravity fed through the coal columns. The final run consisted of char and ash columns with one feed solution containing As, Cd, Pb and Se flowing through them. There were four column studies in all.

The feed solutions were prepared from stock solutions of As_2O_3, $CdSO_4$ or Cd_2NO_3, $Pb(NO_3)_2$, and H_2SeO_3. The stock solutions were added to tapwater acidified with HNO_3 (pH=3) in order to obtain feed solutions in appropriate concentrations. Table 2 lists the feed concentrations.

The flow of the feed solutions through the columns was measured daily. A summary of the flow data is shown in Table 1.

The concentration of the solutions flowing through the columns was measured by daily sampling at the ports on each column. The aqueous samples from each sample port were acidified with HNO_3 to a pH<2 and analyzed for As, Cd, Pb and Se by atomic absorption spectroscopy.

TABLE 1. Background Data for Column Sorption Experiments

Run#/Column#	Material	Height (cm)	Weight (kg/cm)	Average Flow (ml/min)	Porosity
1/1-6	Coal	90-145	.143	1.00-1.26 ±.5	.184-.264
2/1-4	Coal	152-154	.146-.150	.95-1.68 ±.8	.177-.261
3/1-4	Coal	155	.147-.150	.75- .94 ±.4	.234-.312
4/3-5	Ash	54- 58	.089-.098	.69- .87 ±.4	.130-.137
4/4-6	Char	61	.087-.098	.60- .70 ±.3	.225-.230

TABLE 2. Trace Element Concentrations (mg/l) in Feed Solutions for Column Sorption Experiments

Run#/Element	Odd#Columns	Even#Columns
1/Pb	36 ± 8	25 ± 4
2/Pb	105 ± 7	69 ± 4
3/As	.20 ± .01	.098 ± .006
3/Cd	3.26 ± .07	4.8 ± .1
3/Pb	19.9 ± .5	14.9 ± .6
3/Se	.12 ± .02	.20 ± .02
	All Columns	
4/As	.51 ± .05	
4/Cd	9.4 ± .9	
4/Pb	49.5 ± .7	
4/Se	.46 ± .05	

The porosity of the material in the columns was determined for each sorption experiment. Each column was filled to the top of the material, then drained and the volume of water measured. This filling and draining process was repeated until consistent measurements were obtained. The resulting measurements (Table 1) represent the actual volume of water that was in contact with the column material as a percentage of the total volume of the column.

Batch Studies

Batch tests were performed by contacting 20g of material (coal, char or ash) with 100 ml of solution of varying trace element (As, Cd, Pb or Se) concentration. The four trace elements were studied individually. A shaker table was used to thoroughly contact the test material and solution for each 90 minute experiment.

Batch tests contacting varying weights of coal, char or ash with the feed solutions used in the column studies were also performed as a check on the column studies.

The solutions from the batch tests were filtered through 0.45 μm membrane filter paper, acidified with HNO_3 to pH<2, and then analyzed for the trace element(s) of interest by atomic absorption spectroscopy.

RESULTS

Column Studies

Sorptive Capacities. Each column was sampled at six inch intervals down through the column. A series of breakthrough curves, each based on 20 to 50 data points, was calculated for each trace element (As, Cd, Pb and Se) as it moved through the column. The curves (for each column sampling port) were constructed by plotting normalized trace element concentrations vs. normalized flow volume. The concentration was normalized by dividing the sample concentration by the average feed concentration. In the same manner, the total volume of solution which flowed through each column was used to normalize the flow data. Figure 2 shows a series of breakthrough curves for As as the element moved through a column of char. The ports are the five sampling points down the char column with port 5 as the top and port 1 at the bottom of the column.

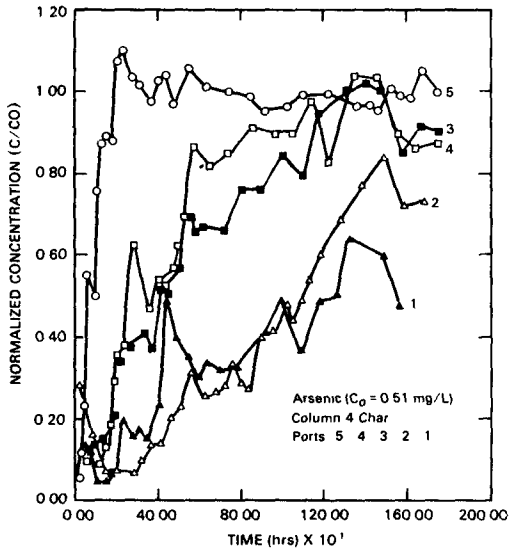

Figure 2 Breakthrough Curves for Arsenic in Char Column

The best fit polynomial equation was calculated for each breakthrough curve. Each curve represents the concentration of a trace element at a column sample port over time and the amount of flow through the column. The area under each curve represents the percentage of the feed constituent (As, Cd, Pb or Se) which was not sorbed by the material (coal, char or ash) above that sampling port.

The total weight (mg) of As, Cd, Pb and Se sorbed between each sampling port was calculated by finding the area between the breakthrough curves. This data was divided by the weight of the sorbing material (coal, char or ash) to determine the amount sorbed per unit weight of sorbent. An average amount sorbed per unit weight of sorbent was calculated for each column. A summary of this sorptive capacity data is given in Table 3.

TABLE 3. Sorptive Capacities of Coal, Char and Ash for Arsenic, Cadmium, Lead and Selenium Based on Column Sorption Experiments

Element/Feed Concentration (mg/l)	mg sorbed / kg material	meq sorbed / kg material
	Coal Columns	
Pb*/105	321	3.1
Pb*/ 69	207	2.0
Pb*/ 36	207	2.0
Pb*/ 25	259	2.5
Pb/ 19.9	265	2.6
Pb/ 14.9	190	1.8
As/ .20	1.88	.08
As/ .098	1.14	.05
Cd/ 3.26	24.2	.43
Cd/ 4.8	44.5	.83
Se/ .12	1.22	.06
Se/ .20	2.00	.10
	Char Columns	
As/ .51	4.6	.18
Cd/ 9.4	18.3	.32
Pb/ 49.5	440.4	4.2
Se/ .46	6.1	.41
	Ash Columns	
As/ .51	8.8	.35
Cd/ 9.4	60.8	1.08
Pb/ 49.5	802.8	8.38
Se/ .46	9.2	.47

*Pb was the only element added to the feed solution in these experiments.

Element Movement-Retention Factors. The velocity at which each trace element moved through the column materials was calculated as another measure of how well the element was sorbed by the coal, char and ash. To calculate element movement, the time corresponding to .20 and .40 (.10 and .20 for Se) of the normalized concentration was determined from each breakthrough curve. These two points were chosen because they were located on the portion of the curve representing the greatest change in concentration per unit time. The two times from each curve were averaged and converted to days. Using the breakthrough curve for port 5 on Figure 2 as an example, .20 corresponds to 30 hours and .40 corresponds to 60 hours. The average time equals 1.9 days.

The distance (in cm) from the top of the coal, char or ash to each sampling port was determined. The element movement at each sampling port was calculated by dividing the distance traveled by the average time. An average element velocity was then determined for each column.

Figures 3 to 6 show the element velocity for each column plotted as a function of the linear flow velocity through the column. Linear flow velocity is the velocity at which the feed solution was moving through the columns. The feed solution concentrations are included on the figures and points obtained using the same feed are connected with a line.

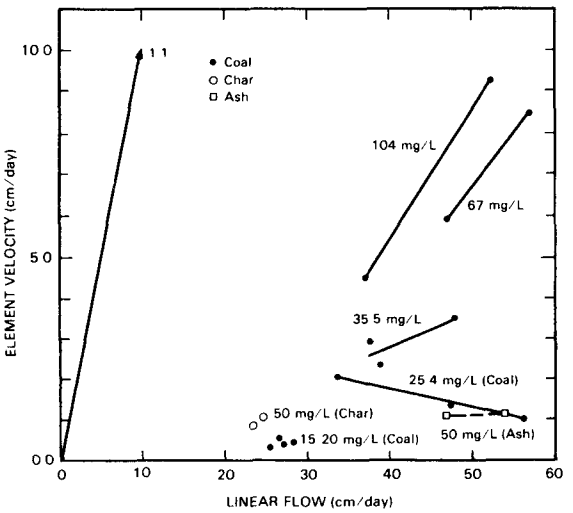

Figure 3 Movement of Lead Through Columns

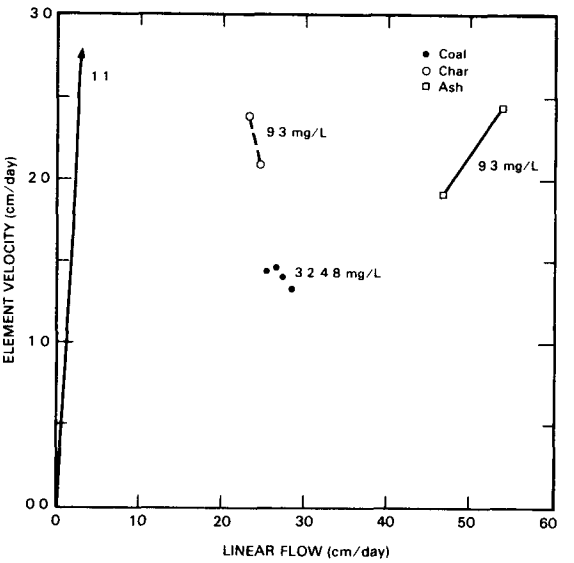

Figure 4 Movement of Cadmium Through Columns

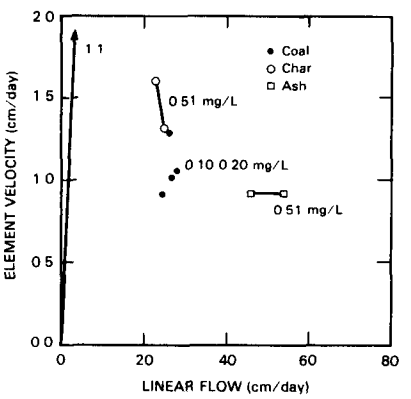

Figure 5 Movement of Arsenic Through Columns

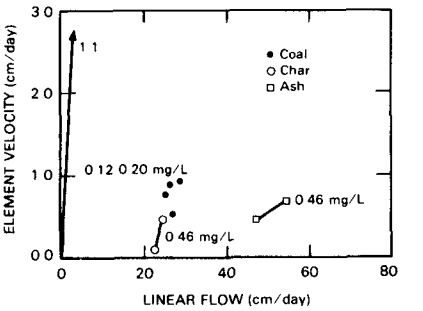

Figure 6 Movement of Selenium Through Columns

The vectors labeled 1:1 on Figures 3 to 6 are present as a reference. If the elements moved through the columns at the same velocity as the feed solution is moving, then there would be no retention by the column and all of the points would lie on this vector. To determine the relative retention of two materials, vectors can be drawn from the origin to any point or cluster of points on the graph. Retention increases clockwise from the 1:1 vector.

Retention factors were obtained by dividing the element velocity by the average linear flow velocity. Retention is inversely proportional to the retention factor. Table 4 summarizes the retention factors for the four elements as a function of feed concentration and sorbing material.

Batch Tests

The results of the batch tests are shown in Figures 7 to 10. The initial solution concentrations are plotted against the milliequivalents adsorbed per kilogram of coal, char and ash. The curves show the relationship between the sorptive capacity of each material and the initial trace element concentration.

Figures 7 and 8 also show the results of contacting the feed solutions used in the column studies with 20g of coal, char or ash. The points are labeled "sorbent + feed" to distinguish them from the batch tests which studied the individual elements. The results of contacting the feed solution with the coal, char and ash for arsenic and selenium were on the curves but they were too low to plot conveniently in Figures 9 and 10.

TABLE 4. Retention Factors of Coal, Char and Ash for Arsenic, Cadmium, Lead and Selenium Based on Column Sorption Experiments

Element/Feed Concentration (mg/l)	Retention Factor
Coal Columns	
Pb*/105	.149
Pb*/ 69	.137
Pb*/ 36	.062
Pb*/ 25	.036
Pb/ 19.9	.019
Pb/ 14.9	.014
As/ .20	.042
As/ .098	.037
Cd/ 3.26	.053
Cd/ 4.8	.052
Se/ .12	.031
Se/ .20	.026
Char Columns	
As/ .51	.059
Cd/ 9.4	.093
Pb/ 49.5	.038
Se/ .46	.010
Ash Columns	
As/ .51	.018
Cd/ 9.4	.042
Pb/ 49.5	.022
Se/ .46	.010

*Pb was the only element added to the feed solution in these experiments.

As a basis for comparing the batch test and column test results, the average adsorptive capacities of the columns for each of the trace elements are also plotted in Figures 7 to 10. The points are labeled "columns" so they will not be confused with the batch test data.

DISCUSSION

Qualitative comparisons of the sorption of the four elements of each material (coal, char and ash) can be made. Similarly, the material's sorptive capacities for each element can be compared. Both types of comparisons were made using the data from this study.

In the comparisons among the elements, the equivalent weights of the elements were used as a basis of comparison. Because sorption occurs at the ionic/molecular level, comparing actual weights of ions with different valences is tenuous.

Based on the sorptive capacities of each column material for the four trace elements (Table 3), in general, the order from best to least sorbed by weight of sorbing material is Pb > Cd > Se > As. Char sorbed Se slightly better than Cd. The general order is consistent with the sorptive capacities determined from the batch studies.

Even though the three sorbing materials showed the same general preference for the four elements, the actual amount sorbed per unit weight was not the same. The ash sorbed more than the char and the coal less than both. These results were not entirely unexpected, since ash contains the highest fraction of inorganic matter of the three materials. One study has indicated that in-

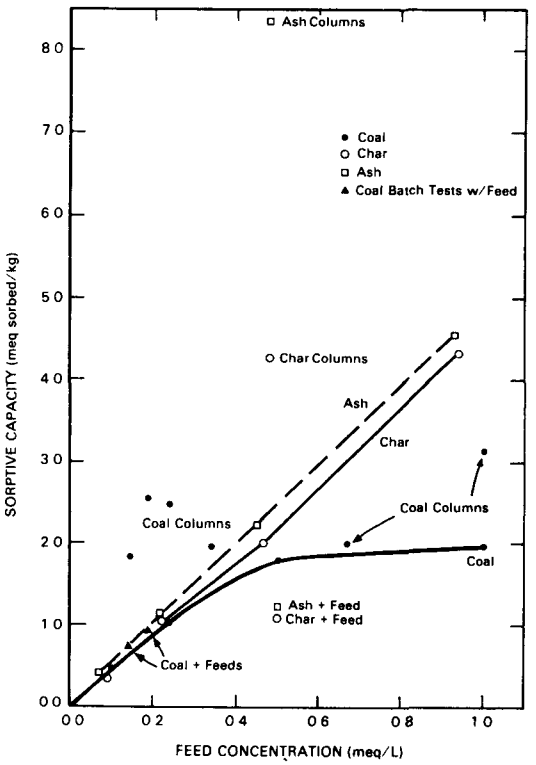

Figure 7 Batch Test Results Lead

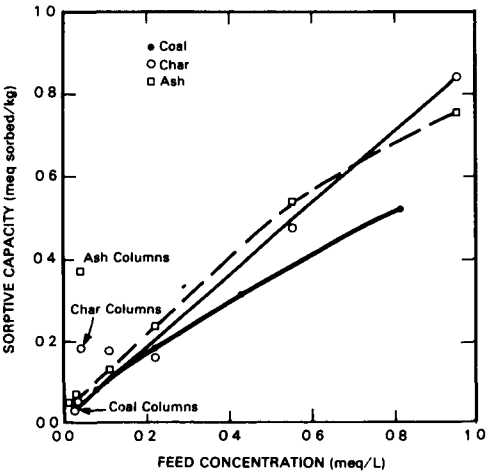

Figure 9 Batch Test Results Arsenic

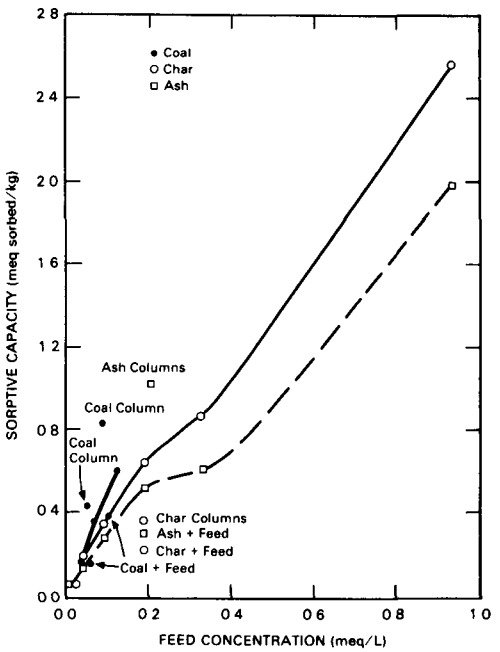

Figure 8 Batch Test Results Cadmium

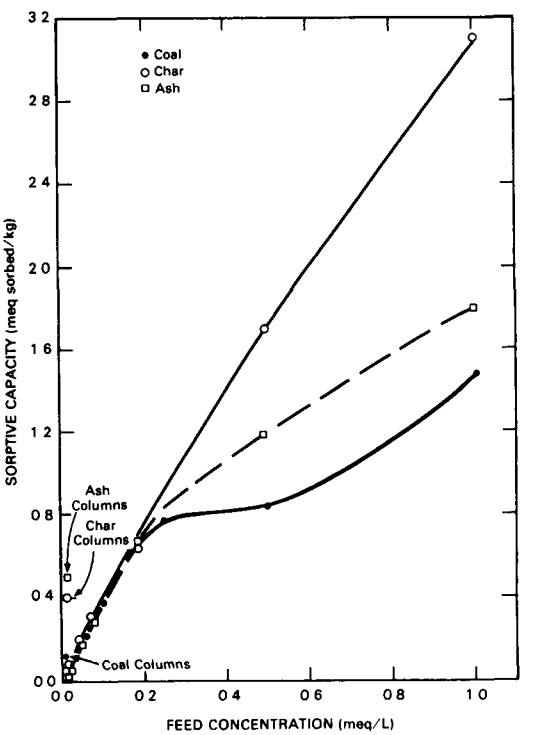

Figure 10 Batch Test Results Selenium

organic matter accounts for 95% of the sorption and carbonaceous matter accounts for 5% of the sorption (6). Additionally, during the formation of ash, mineralogical phase changes occur. These phase changes would be from a high to low order which would generally produce more available sorption sites.

When Figures 3 to 6 are used to compare the relative retention of each element on coal, char and ash, we see that ash retains As, Cd, Pb and Se better than char. Since the feed concentrations of the four elements were not the same for the coal column studies, a direct comparison of coal retention with that of ash and char cannot be made. However, Figure 3 seems to indicate that lead is least retained by coal.

The ranking order of sorption based on retention factors is different from that based on sorptive capacities. Table 4 shows that for ash, the order from best to least retained was Se > As > Pb > Cd. For the char, the order was Se > Pb > As > Cd and for coal it was Pb > Se > As > Cd.

The differences in sorption orders based on sorptive capacities and retentions was in part a result of the higher concentrations of Cd and Pb used in the experiments as compared with As and Se. It may also be indicative of sorptive strength. Cadmium and lead may be selectively sorbed over As and Se, but they may also be less tightly held. Generally, ions with higher charges, such as As^{+3} and Se^{+4}, are better held on sorbents, especially on the clay minerals found in coal (7).

Additionally, sorptive capacity is based on the portion of the total sorbed in a section of a column with a known weight. Retention factors are based on consistent, but arbitrarily chosen, points on the breakthrough curves and their associated times. Retention does not account for the weight of the materials or the feed concentration differences.

The effect of concentration and flow rate on sorption were examined in the early phases of this study. The concentration of lead flowing through coal columns was varied from 15 mg/l to 104 mg/l. The linear flow rate was studied over the range of 25 to 57 cm/day. Figure 3 indicates that concentration had more impact on retention than flow rate. Lead was retained more at the lower concentrations. Flow rate seemed to have little impact on retention.

The behavior of the elements alone and in combination with the others can be compared using Figures 7 to 10. Both lead and cadmium seemed to be affected by the presence of the other elements. The char and ash sorptive capacities for Pb and Cd were larger when the elements were alone in the contacting solution. The coal sorptive capacity for Cd was also larger when Cd was the only element present in the contacting solution.

Cadmium showed another interesting characteristic in the column studies. The concentration of Cd in the columns increased to as high as twice that of the feed concentration. The point at which the concentration of Cd rose above the feed concentration coincided with the appearance of measurable concentrations of lead in the column. It is possible that Pb was replacing Cd on the sorptive sites and forcing it back into solution. This effect was noticed in the coal, char and ash columns and can also be seen in Cd batch test results.

One final comment can be made regarding the results of this study. Figures 7 to 10 show the results of the column studies as well as the batch tests. By comparing the column data with batch test data obtained in the same concentration range, we see that the column data indicate more sorption than would be expected based on batch tests. This means that studies utilizing one method or the other cannot be directly compared.

REFERENCES

1. Edgar, T. F., Technical, Economic and Environmental Evaluation of In-Situ Coal Gasification. In-Situ 1(1), 75-102 (1977).

2. Ruch, R. R., Gluskoter, H. J., and Shimp, N. F., "Occurrence and Distribution of Potentially Volatile Trace Elements in Coal". EPA 650/2-74-054 (1974).

3. Dalton, V. A. and Campbell, J. H., Laboratory Measurements of Groundwater Leaching and Transport of Pollutants Produced During Underground Coal Gasification. In-Situ 2(4), 295-328 (1978).

4. Wang, F. T., "The Sorptive Property of Coal". LLNL Preprint (1980).

5. ASTM D410-38, "Standard Method of Sieve Analysis of Coal" (1976).

6. Walters, E. A. and Niemczyk, T. M., "The Effects of Underground Coal Gasification on Groundwater", U.S. EPA/IERL-Ci Draft Document (1982).

7. Grim, R. E., Clay Minerology, 2nd ed. McGraw Hill (1968).

4.4 EFFECTS OF THE RAWLINS UCG/SDB TESTS ON GROUNDWATER COMPOSITION AND MIGRATION

by

Paul F. Ahner[1/]
Mary A. Bloomstran[2/]

ABSTRACT

The Department of Energy UCG/SDB program (Underground Coal Gasification of Steeply Dipping Beds) has been completed. The program, conducted by Gulf Research & Development Company, ran from 1977 to 1982 and included two field tests. An important goal of this program was to minimize the effects of UCG on the groundwater quality and flow characteristics in the area of the field tests. To achieve this objective, an extensive hydrological characterization program was established and implemented. A five year groundwater monitoring program was conducted to determine the effectiveness of the site selection criteria. Data from the program are presented and relationships are drawn from various UCG site activities such as well pressurization, reverse burnlinking, and test termination.

INTRODUCTION

An essential part of the UCG technology is the ability to understand and limit adverse process effects on groundwater flow and quality. The impact of the process on the geologic systems can be significant since the process involves operation of a georeactor at high temperatures.

1/ Gulf Research & Development Company
P.O. Drawer 2038
Pittsburgh, PA 15230

2/ Gulf Research & Development Company
Suite 610
1341 Union Blvd.
Lakewood, CO 80228

Groundwater composition can be affected by UCG in three ways:

- migration of by-products into the water,
- dissolution of thermally altered minerals into the water, and
- establishment of communication between water-bearing strata.

UCG by-products include coal tars (benzenes, nitrogen bases, phenols, and condensed aromatics), ammonia, and cyanide. Phenols are the dominant organic contaminants due to both their concentration and solubility in water. Ammonia and cyanides are also found in significant levels in the groundwater from UCG reactors.[1-4] During the gasification process, the reactor will reach temperatures in excess of 2700°F (1500°C), causing thermal alteration of certain mineral forms and create new compounds with the sulfur dioxide and carbon dioxide produced in the process. Some of these new minerals are soluble in water and can migrate away from the reactor into the bordering strata. The third way that UCG can affect groundwater composition is by allowing mixing to occur between two or more water-bearing strata. Water-bearing strata can be confined by the presence of nonpermeable zones such as shales and mudstones. Therefore, the water compositions and hydraulic pressure heads produced by confined formations do not have to be identical. Since UCG creates a void with subsequent roof fall into it, communicaton between the coal and overlying water-bearing strata can be established.[5] The combined waters may be a simple blend of the original waters or in some cases the waters may undergo

changes in composition due to precipitation of certain ionic species.

In addition to altering groundwater composition, UCG can alter the flow direction and the piezometric surface of the groundwater. Both are influenced by gravity, pumping, pressure changes, and the directional permeability of the formation. The piezometric surface is an areal portrayal of groundwater depth. It is obtained by extrapolating the pressure head data from a series of wells over an area. The intercommunication of confined water-bearing zones caused by UCG can change the pressure head characteristics and therefore the piezometric surface in the area.

The water-bearing formations at the Rawlins site (down to 700 ft) are all aquicludes and will be referred to as such throughout this report. The most productive water-bearing formation (about 5 gal/day) is the sandstone over the G coal seam. This strata is separated from the coal seam by a 15 to 20 ft carbonaceous shale layer that is highly impermeable to water flow.

Data on water composition and water levels from various monitoring wells have been collected at the Rawlins site since 1978. Interpretation and discussion of the hydraulic head data and water composition from the hydrology wells and the effects of the Rawlins UCG tests on the groundwater is presented.

WELL DESCRIPTION AND HISTORY

The Rawlins hydrology wells consist of the hydrology characterization wells, the Test 1 Hydrology Wells, and the Test 2 Hydrology Wells. The locations of the wells relative to Tests 1 and 2 are shown in Figure 1. A description of each well is shown in Table 1. Some wells were recompleted in the sandstone to monitor the sandstone which is a more significant water-bearing formation than the coal. The hydrology well completion plan is shown in Figure 2.

Rawlins Test 1 was conducted between October 28, 1979 and December 5, 1979, and consumed approximately 28,000 cubic ft of coal. By the summer of 1980, groundwater had filled the cavity and remains stable at the characteristic head of the overlying sandstone (6,770±25 ft). The reactor is at atmospheric pressure.

The second test at Rawlins was conducted between August 22, 1981 and November 11, 1981 and consumed approximately 190,000 cubic feet of coal. The cavity is not yet filled with water. Water levels cannot be measured since the level is still below the coal and sandstone rubble present in the cavity. The sandstone and coal rubble was discovered through post-burn coring conducted by the Laramie Energy Technology Center (LETC). The reactor is at atmospheric pressure.

HYDROLOGY WELL WATER LEVELS

Plots of the water elevations for the hydrology wells are shown in Figures 3 through 12. Water elevation is calculated as the surface elevation of the well minus the water level depth. Analysis of the elevations showed characteristic heads for the coal and the sandstone overburden to be 6,490 to 6,540 ft and 6,740 to 6,800 ft, respectively. The characteristic head for the shale below the coal as determined from well H-13 is about 6,300 ft. This shale is of minor consequence since it is essentially impermeable (i.e., recharge rate of 0.054 gal/day).

Hydrology Characterization Wells

As shown in Figure 3, the immediate effects of Test 1 on the groundwater level appears negligible. This lack of response is due to the 450 ft distance between Test 1 and P-1 and the very low permeability of the coal seam. Lab testing on coal cores revealed a permeability on the order of 0.5 millidarcy.[6] P-1 recharge is about 1 ft/day (0.80 gal/day) or less. The steady increase in water level after Test 1 and prior to Test 2 can be ascribed to:

- communication of the more productive upper sandstone to the less productive coal, resulting from the Test 1 cavity,
- a fracturing incident during the drilling of the nearby Test 2 process wells,
- the intentional hydraulic fracturing conducted between the nearby Test 2 process wells, and
- the conduct of the Test 1 air communication tests and the operation of Test 1 itself.

The sudden drastic drop in P-1 level after Test 2 was due to the draining of the coal seam water into the Test 2 cavity. The Test 2 cavity is continuing to draw water.

Well H-11 shows the same general trends as P-1 and is shown in Figure 4. The trends are not as dramatic because of the higher hydraulic conductivity (permeability) of the sandstone where H-11 is completed. The H-11 recharge rate is approximately 6 ft/day (4.6 gal/day). The drop in water level after Test 1 is probably due to the draining of water into the Test 1 cavity. After filling the cavity, the water level in H-11 returned to its initial head. As in P-1, the water level began falling after Test 2, indicating drainage of the overburden water into the unfilled cavity.

Well H-13 (Figure 5) shows the same general trend as P-1; the initial fluctuation, the gradual rise after Test 1, and a sudden drop after Test 2. The termination of Test 2 caused the level in H-13 to drop, indicating drainage into the cavity. The lag time between the termination of Test 2 and a drop in water level is much longer due to the low permeability of the shale.

Test 1 Hydrology Wells

Well H-18 (Figure 6) is used as a reference well since it intercepts the water prior to entering the cavity and therefore provides unaffected coal groundwater samples. The abnormally high water level (for a well completed to the coal) draws suspicion to this well. There is a 200 ft difference in head between the coal seam and the well. This indicates that either the well is plugged or is in communication with the sandstone overburden. The decreasing head indicates that drainage is still occurring.

Well H-17 water level is shown in Figure 7. This well showed little fluctuation prior to the Test 2 activities. The effects of drainage into the Test 1 cavity were negligible. This lack of response is most likely due to the cavity recharge water being supplied by the much more productive sandstone formation rather than the coal seam. As in the other wells, Test 2 termination caused an immediate drop in head, followed by a more gradual drainage rate into the cavity which is continuing.

Figure 8 shows water levels in well H-16 which was recompleted in the sandstone. The recompletion explains the unusual head measurements. The rise in water level as of June, 1981 is attributed to two factors:

- recompletion of H-16 into the more productive sandstone above the coal and
- the pre Test 2 and Test 2 activities which subjected the strata to the various pressurizations discussed earlier.

Due to the recompletion, the water level continued to rise after Test 2 and has since been affected by drainage into the T-2 cavity and the water level is continuing to drop.

Test 2 Hydrology Wells

The repeated filling of the Test 2 hydrology wells for various reasons and the low permeability of the strata has masked the characteristic coal and sandstone water heads in these wells. This repeated altering of the water heads has also precluded meaningful water levels from being taken before, during or after the test. Some meaningful conclusions can still be drawn.

Water levels in reference well H-21 from February, 1982 to present are shown in Figure 9. Since Test 2 was conducted and terminated prior to this date, the immediate response to Test 2 is not known. The slowly falling water level is indicative of drainage into the Test 2 cavity in addition to possible drainage of the water into the coal to its characteristic head. This drainage can occur because the wells were initially filled up to 6,800 ft, which is above the pressure head of the coal. Wells H-19 and H-20 are shown in Figures 10 and 11, respectively. Both wells show the same decreasing water level. The wells have been bailed to the characteristic coal elevation to more accurately determine the effects of the cavity on water level.

Well H-22 water level (Figure 12) shows that drainage into the cavity is more pronounced from 2/82 to 4/82 compared to the other wells and that the head is slowly increasing. The slowly increasing level indicates that the sandstone is

attempting to restore itself by draining water from a wider area (increasing area of influence). Upon termination of the test, the water level is postulated to have dropped drastically as pressure was relieved in the cavity and water influx began.

OVERALL EFFECTS OF THE RAWLINS TESTS ON GROUNDWATER FLOW AND HYDRAULIC HEAD

Figure 13 shows a cross-sectional view of the confined coal and sandstone aquicludes prior to UCG activities. The sandstone is at its undisturbed, equilibrated head level of approximately 6,740 ft and the coal at its head of 6,540 ft. The groundwater is in its typical undisturbed S 88 W flow direction. The shale zones between the coal and sandstone keep the aquicludes confined from one another.

Figure 14 shows a cross-sectional view of these aquicludes immediately after UCG test termination. Since UCG has removed a large amount of coal from the seam, roof fall of the upper sandstone into the gasified zone occurs and hydraulic communication with the sandstone is established. The unpressurized cavity begins to drain the surrounding formations, thereby changing the direction of water flow toward the cavity. Since the upper sandstone is much more productive than the coal or the underburden, most of the water to fill the cavity comes from this formation, thereby lowering water level in the sandstone around the cavity. This "cone of depression" formed in the coal or underlying shale is much less drastic due to the impermeable nature of these strata.

Figure 15 shows a cross-sectional view after the UCG cavity has filled. The drainage into the cavity has stopped. The relative permeabilities and characteristic heads of the sandstone, coal, and shale cause the following to occur. The sandstone returns to its head of 6,740. The water head on the cavity equalizes with the sandstone head because of their communication with one another and the much lower permeability of the coal. The coal and the underlying shale may experience a slightly higher head in the immediate cavity area after a while due to the higher cavity pressure, but these effects will be slight and highly localized. The 200 ft difference in head (about 90 psi) between the sandstone and the coal is not enough to promote significant migration into the low permeability coal. Conversely, entry of coal seam water into the sandstone is prevented by the higher head in the sandstone. The net result is that, even though UCG caused communication between confined aquicludes to occur, the changes to water quality, piezometric surface, and groundwater flow direction are temporary and insignificant.

WATER COMPOSITIONAL EFFECTS

An in-depth groundwater compositional study for about 50 components was made on samples from numerous wells at various locations prior to Test 1 with the intention of determining "characteristic" groundwater compositions for each strata that might be affected by UCG. These characteristic compositions could then be compared to compositions obtained during and after the field tests to better determine the effects of UCG. The variability of the stratum composition with location and the extremely slow movement of water through the stratum, however, made the water compositions from well to well extremely variable and prevented any correlation of a water composition to a particular stratum. Even the water composition from the same well as a function of time changed significantly. This discussion, therefore, only deals with the ten water quality parameters listed below:

- pH
- conductivity
- temperature
- Eh
- alkalinity
- ammonia
- cyanide
- phenol
- Total Dissolved Solids (TDS)
- Total Organic Carbon (TOC)

In spite of the above-mentioned variability, additional reference or baseline compositions from wells which should not be affected by UCG were still sought. The hydrology characterization wells were chosen for this function because of their respective completions into the overburden, underburden, and coal and their location. Their location almost precludes them from encountering a plume of contaminated water from the reactors because of their distance and primarily because their upstream location relative to the reactors.

Hydrology Characterization Well Compositional Effects

The water compositions from Well P-1 are shown in Table 2. TOC and phenol concentrations are somewhat erratic and it is extrememly difficult to determine whether UCG had any effect on these parameters. Pretest TOC is in the 144 to 240 ppm range and post-test values range from 280 to 412 ppm (until 10/2/82). Pretest phenol ranges from 0.009 to 0.42 ppm and post-test values are in the 0.178 to 0.767 ppm range. The erratic values obtained on both of these parameters led to having identical samples analyzed at two labs (see table). The large difference in the TOC and phenol concentrations is being investigated further. Considering the distance of P-1 from the Test 2 cavity, the movement of groundwater into the cavity, and the direction of groundwater flow, the TOC and phenol are probably very low, as reported by one of the labs.

Well H-11 water analyses are shown in Table 3. UCG apparently has not affected the groundwater composition in this well. All values, except for TOC, are within the normal data scatter range.

The H-13 water analyses are shown in Table 4. This well has such a slow recharge rate (0.067 ft/day or approximately 12 times less than P-1) that, as described in the P-1 discussion, its water composition changed considerably for the first 1-2 years until "consistent" samples were obtained. This trait can be seen by the dramatic change in conductivity, alkalinity, TOC, and TDS from 12/78 to 9/79. There is still some question whether a baseline composition was obtained prior to the UCG tests, since sampling from this well was halted between 9/79 and 2/82 because of its extremely low yield. The only increases seen after the UCG tests have been in phenols and alkalinity. Alkalinity increased from 320 ppm to 717 ppm. Whether these increases were caused by UCG is highly uncertain because of the distance from the cavities, the direction of groundwater flow, and the almost impermeable properties of this stratum.

Test 1 Hydrology Wells

Water samples from reference Well H-18 are shown in Table 5. Water in this well showed no significant changes throughout the monitoring period. This well is updip of the Test 1 cavity and intercepts the water prior to entering the Test 1 cavity.

Water data from Well H-17 are shown in Table 6. Phenol increased from 0.090 to 4.68 ppm after Test 1 and dropped to 0.18 ppm. TDS has been decreasing from 9570 ppm before Test 1 to the present 5,830 ppm. TOC increased from 34 to a maximum of 52 after Test 1, but this difference is within typical scatter. TOC is presently at 40 ppm. UCG effects on well H-17 consisted of a phenol excursion which quickly returned to below baseline concentration.

The analyses from well H-16 are shown in Tables 6 and 7. H-16 shows a definite response to Test 1 as exhibited by phenol and TOC. Signs of "return to baseline conditions" were evident prior to recompletion of this well. The recompletion of H-16 into the upper sandstone was imperative since this stratum is more transmissive and plays a more active role in the hydrology of the area. There are no significant changes in well H-16 parameters as a result of Test 2.

Test 2 Hydrology Wells

The water initially present in these wells is not water from the strata, but rather good quality purchased water. As a result, a strict "before and after Test 2" comparison cannot be made. The water level history of these wells does indicate that the purchased water is being replaced by groundwater since drainage into the Test 2 cavity is occurring. That is, groundwater is not flowing away from the cavity to the well but rather from the well to the cavity. This water could still show UCG contaminants in it, however, since they could be transported out of the cavity a short distance during the test by natural groundwater flow and is now being drawn back in.

Well H-21 is the reference well, and being upstream of the cavity, should be the least affected. Table 9 shows that TOC increased from 20 to 73 ppm, indicating that some contamination did occur as a result of UCG or that the analysis is erroneous as in Well P-1. Phenol fluctuates from 0.001 to 0.009 ppm with no general trends shown.

Table 10 contains the data from well H-19. Reverse plume movement may be occurring due to the drainage effects of the Test 2 cavity. During Test 2 operations some UCG contaminants could conceivably have been transported out of the reactor a short distance by natural groundwater flow and formed a plume of affected water. After the test the groundwater began draining into the cavity, thereby reversing plume flow back through the Test 2 hydrology wells. Well H-19 intercepted this plume around April and June, 1982 as shown by higher TOC and phenol values. These values decrease in October, 1982, indicating that the plume is receding into the cavity.

Well H-20 shows the same reverse plume movement as H-19 regarding phenol and TOC. Water compositions for this well are shown in Table 11.

The composition data from well H-22 are shown in Table 12. The trend in phenol shown in wells H-19 and H-20 is seen here, indicating that the same mechanisms hold for the overburden as well as the coal. The TOC excursion was not seen. Samples were submitted for duplicate analyses and, as can be seen, the reproducibility is not very good.

Test 1 Cavity Water

This section highlights the findings of a paper previously written by A. Behi[7] regarding the effects of Test 1 on groundwater. Table 13 contains the compositional analysis data from samples of water taken from the Test 1 cavity. These data indicate that, except for sulfate and ammonia, all the significant parameters are within the normal range of values obtained from all other wells on site. The TOC and phenol concentrations are even lower in the cavity water than in the surrounding waters in many cases, indicating that adsorption by the coal and/or char in the cavity has occurred. This effect has been seen in lab studies.[8] It was impossible to sample the water before it flowed into the cavity to allow comparison to the present cavity water because most of this water was from the upper sandstone. Samples were not available at the time. The cavity water has a much higher ammonia content (14 mg/l vs 2-3 mg/l in the surrounding wells) and sulfate content (3270 mg/l vs 100-1500 mg/l).

The response of the hydrology wells to this large supply of higher sulfate, higher ammonia content water right beside them has been very slight (if any). Perhaps some sulfate diffusion out of the cavity occurred since the sulfate concentration from Well H-16 (completed to the upper sandstone) is 1900 mg/l. This is a factor of 2-3 greater than the sulfate concentrations from other wells. Water compositional data from the sandstone in this area are not available to confirm whether this is a true excursion, however. No accompanying inordinately high ammonia concentration is present in any of the wells. Low ammonia concentrations contradict the excursion theory. These data, along with the conclusion reached when discussing the water levels, support the conclusion that widespread movements and contamination of cavity water is not going to occur.

CONCLUSIONS

- The Rawlins field tests had a minor impact on groundwater composition and on the well water levels.
- The hydrology associated with the Test 2 cavity is still changing. This partially empty cavity is still filling with water by draining the surrounding formations. As a result, it is drawing the water which was contaminated and transported a slight distance out from the cavity during the test back into itself, effectively retracting its own contaminant plume. This plume was characterized by higher TOC and phenol concentrations. The water passing through these wells has returned to baseline. With time, this cavity will also fill, thereby greatly diluting the contaminants which are not adsorbed by the coal and the surrounding strata. The lower TOC and phenol found in the Test 1 cavity indicates that organics will be adsorbed. After filling, slow outward diffusion of water from the cavity may occur, but extensive migration is not expected based on the observations of the Test 1 cavity. Extensive communication between aquicludes is unlikely due to the impermeable nature of the water-bearing formations and their differences in hydraulic head. The piezometric surface will return to its baseline contours.

- There is no indication of significant groundwater contamination. Test 1 emitted a temporary plume of higher TOC and phenol content water. The water from the Test 1 hydrology wells has returned to baseline. The Test 1 cavity has filled with water and its composition has stabilized. The cavity water has a compositional makeup similar to the surrounding waters except for higher sulfate and ammonia concentrations and generally lower TOC and phenol concentrations. Outward migration of this water from the cavity is slight if any at all.

- Pretest and test activities affected the piezometric surface. Drilling operations, fracturing of the strata to increase permeability, air communication testing, and reverse burn linking all involve pressurizations of the strata with various fluids and were shown to temporarily alter the water levels in nearby wells.

- The upper and lower formations, which bound the gasified coal and the coal itself, are confined aquicludes and contain water of low quality (Class IV as per Chapter VIII "Quality Standards for Wyoming Groundwaters," 1980). The water quality is too poor for agriculture or livestock. The upper sandstone formation, which is the most productive, only recharges at about 4 to 5 gal/day. The coal and the underlying shale recharge are 6 and 100 times smaller, respectively. These aquicludes are "confined" because they exhibit different hydraulic heads. Different heads indicate that they are separated from one another by impermeable strata such as shale. The Rawlins site is characterized by many shale stringers which can effectively isolate water-bearing zones. The characteristic heads of the sandstone and coal are 6,770 ft (±25 ft) and 6,520 ft (±25 ft), respectively.

- The water composition varies significantly from well to well, regardless of the aquiclude being monitored. The water, because of its extremely slow movement through the formation, is in chemical equilibrium with its immediate matrix. The variation in water composition from well to well therefore indicates that the mineral composition of the matrix around each well varies significantly. This variation prevented grouping the waters obtained from the wells into three characteristic categories; namely, upper sandstone waters, coal waters, and underlying shale waters. Each well should be treated as a separate entity and the data from each one should be interpreted on an individual basis.

OVERALL CONCLUSION

Selection of a UCG site with low permeability, low groundwater yield and quality, and strong roof rock greatly reduces the potential for significant groundwater impact.

REFERENCES

1. Campbell, J.H. and Washington, H., "Preliminary Laboratory and Modeling Studies on the Environmental Impact of 'In Situ' Coal Gasification," Proceedings of the Second Annual Underground Coal Gasification Symposium, Morgantown, West Virginia, 1976, pp. 119-139.

2. Humenick, M.J. and Mattox, C.F., "Groundwater Pollutants from Underground Coal Gasification," Water Resources Res., 12:463-472, 1978.

3. Mattox, C.F. and Humenick, M.J., "Organic Groundwater Contaminants from UCG," Proceedings of the Fifth Underground Coal Conversion Symposium, Alexandria, Virginia, 1979, pp. 281-294.

4. Wang, F.T., Mead, S.W., and Stuermer, D.H., "Water Quality Monitoring at the Hoe Creek Test Site: Review and Preliminary Conclusions." paper presented at the 1982 Spring National Meeting of the AICHE, June 7-10, Anaheim, CA, Lawrence Livermore National Lab Reprint UCRL-87650, May 20, 1982.

5. Stone, R., Raber, E., and Winslow, A.M., "Effects of Aquifier Interconnection Resulting from Underground Coal Gasification," prepared by Lawrence Livermore National Laboratory, April 11, 1983.

6. "Site Qualification Studies of the UCG-SDB Site, North Knobs, Wyoming," prepared by Gulf Research & Development Company under DOE Contract No. DE-AC03-77ET13108.

7. Behi, A.M. and Ahner, P.F., "Effects of UCG on Groundwater: A Study of Cavity and Surrounding Groundwater."

8. Humenick, M. J., Britton, L.N., and Mattox, C.F., "Natural Restoration of Ground Water in UCG," In Situ, 6(2), pp. 107-125, 1982.

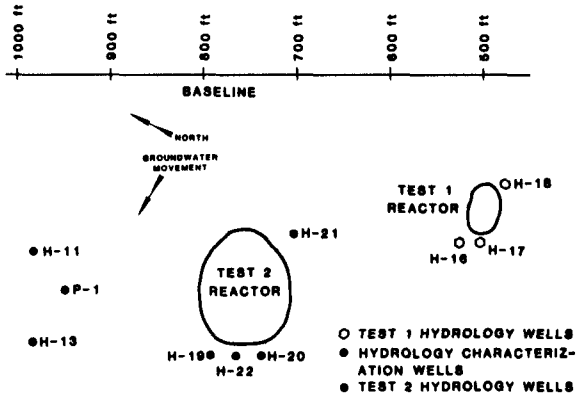

PLAN VIEW OF HYDROLOGY WELL FIELD AND ITS ASSOCIATED UCG REACTORS
FIGURE 1

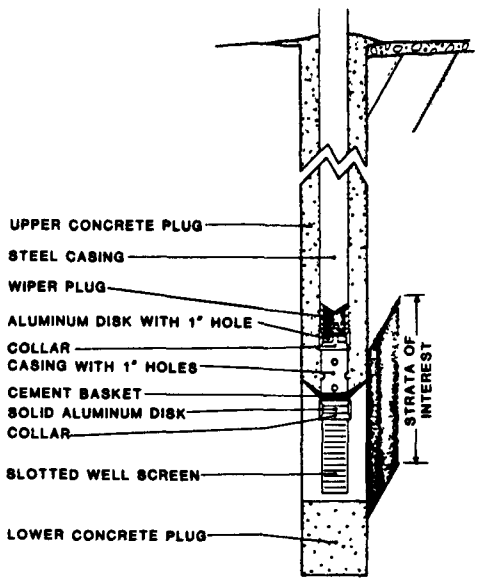

WELL COMPLETION PLAN FOR HYDROLOGY TESTING WELLS AND TEST 1 HYDROLOGY WELLS
FIGURE 2

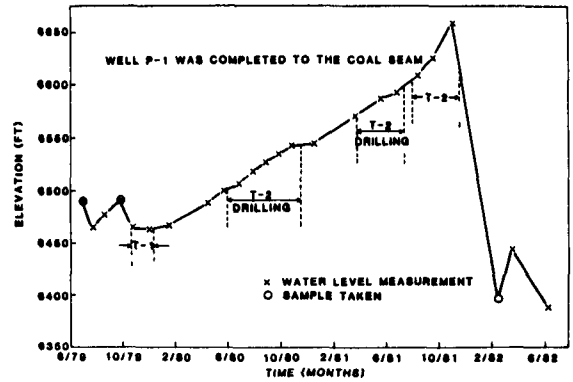

FIGURE 3

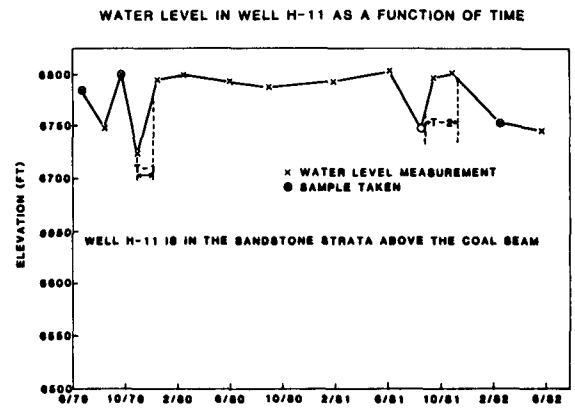

FIGURE 4

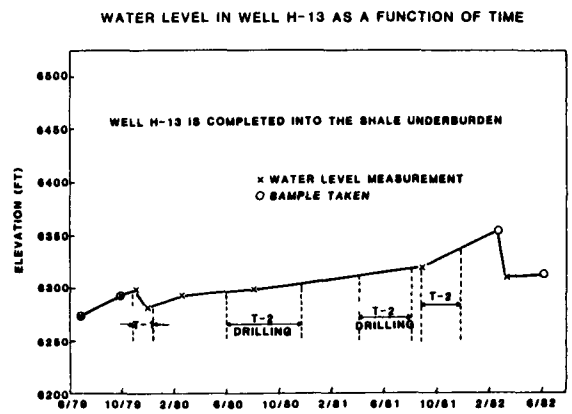

FIGURE 5

WATER LEVEL IN WELL H-16 AS A FUNCTION OF TIME

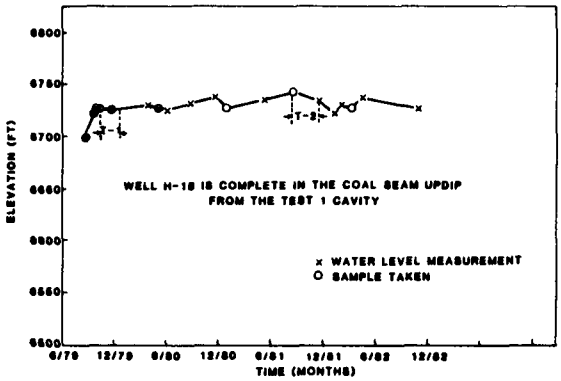

FIGURE 6

WATER LEVEL IN WELL H-17 AS A FUNCTION OF TIME

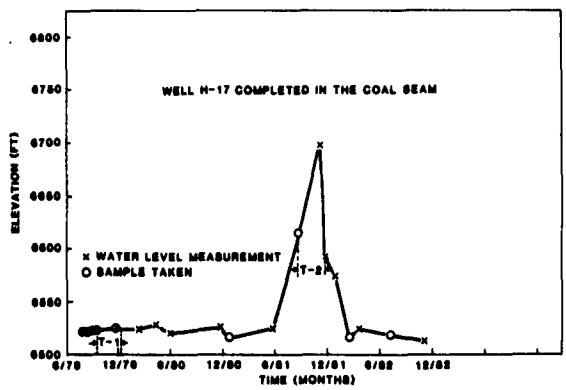

FIGURE 7

WATER LEVEL IN WELL H-18 AS A FUNCTION OF TIME

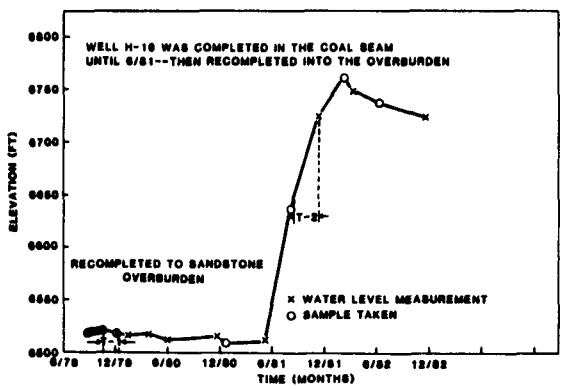

FIGURE 8

WATER LEVEL IN WELL H-21 AS A FUNCTION OF TIME

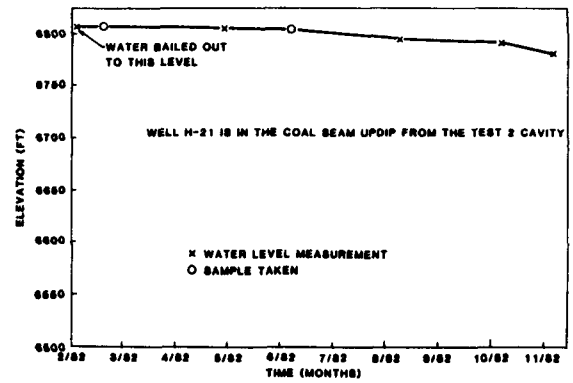

FIGURE 9

WATER LEVEL IN WELL H-19 AS A FUNCTION OF TIME

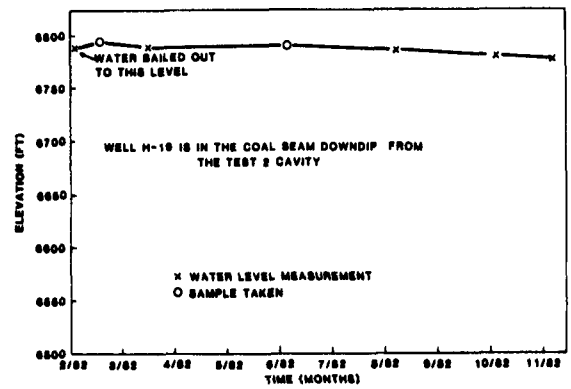

FIGURE 10

WATER LEVEL IN WELL H-20 AS A FUNCTION OF TIME

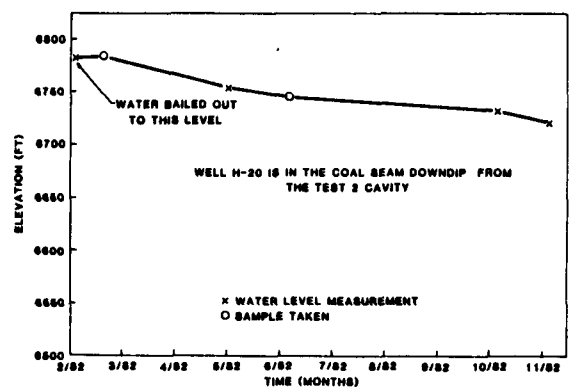

FIGURE 11

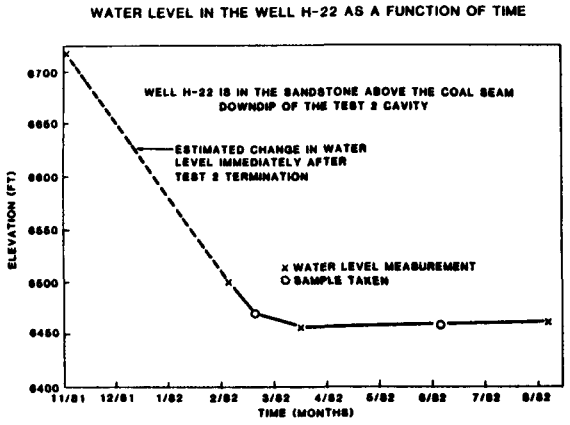

FIGURE 12

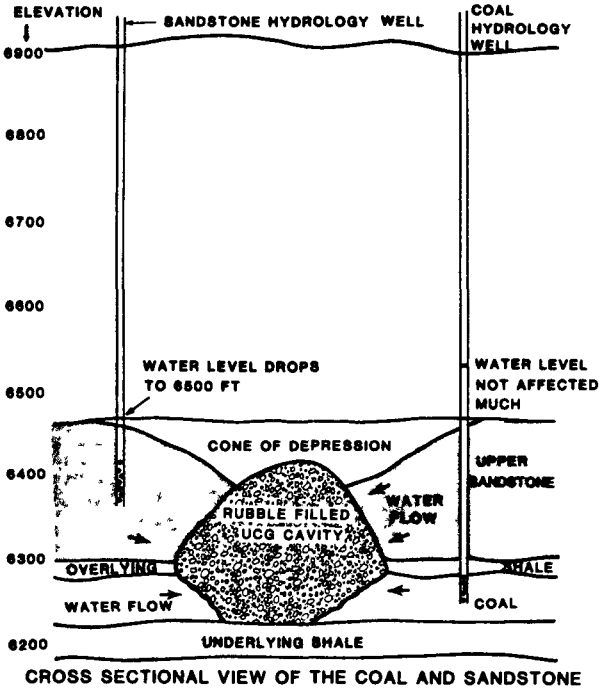

CROSS SECTIONAL VIEW OF THE COAL AND SANDSTONE AQUICLUDES IMMEDIATELY AFTER UCG TERMINATION

FIGURE 14

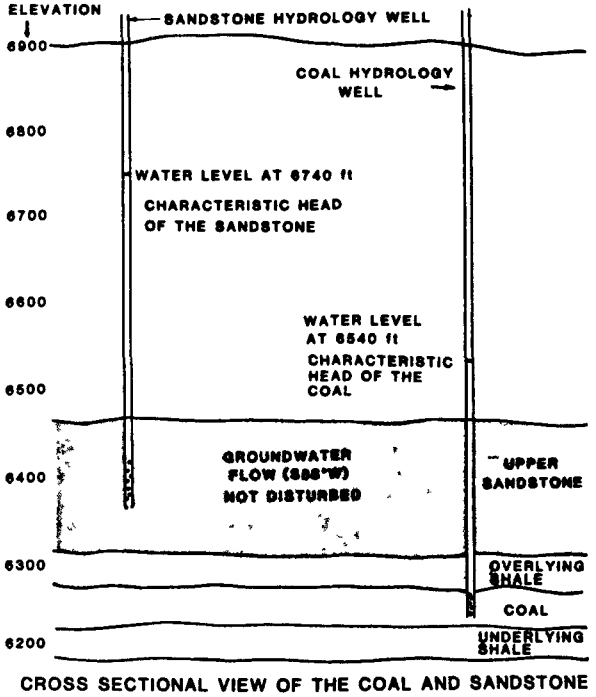

CROSS SECTIONAL VIEW OF THE COAL AND SANDSTONE AQUICLUDES PRIOR TO UCG OPERATIONS

FIGURE 13

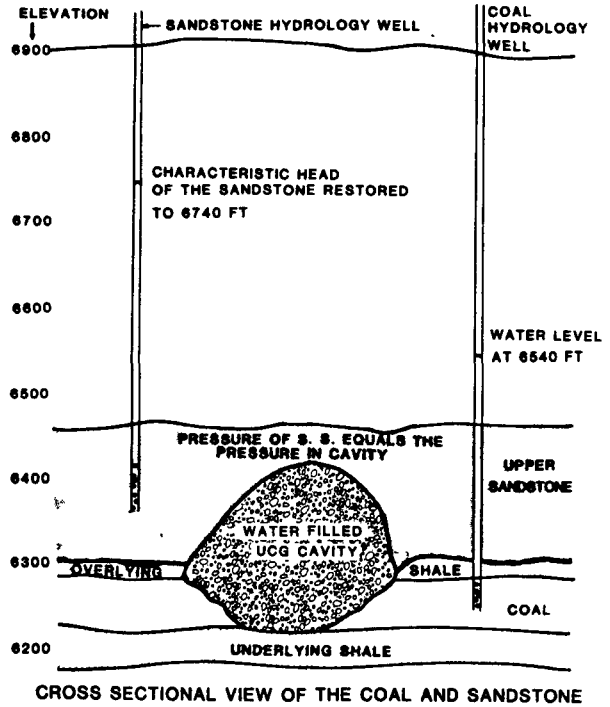

CROSS SECTIONAL VIEW OF THE COAL AND SANDSTONE AQUICLUDES AFTER THE UCG CAVITY HAS STABILIZED

FIGURE 15

Table I Description of Hydrology Wells

Type of Well	Name	Drilling Date	Completion	Purpose
Characterization	P-1	1978	coal seam	pump well
Characterization	H-11	1978	Sandstone above coal	water sampling
Characterization	H-13	1978	Shale below coal	water sampling
Test 1 Hydrology	H-16	1979	* coal seam downdip	water sampling
Test 1 Hydrology	H-17	1979	coal seam downdip	water sampling
Test 1 Hydrology	H-18	1979	coal seam updip	reference water sampling
Test 2 Hydrology	H-19	1980	coal seam downdip	water sampling
Test 2 Hydrology	H-20	1980	coal seam downdip	water sampling
Test 2 Hydrology	H-21	1980	coal seam updip	reference water sampling
Test 2 Hydrology	H-22	1980	*coal seam downdip	water sampling

* later plugged and completed in sandstone above coal

TABLE 2 WATER ANALYSES FROM WELL P-1

DESCRIPTION Well P-1 is completed to the coal seam It is in the hydrology characterization well pattern

SAMPLING DATE	12/7/78	4/5/79	6/27/79	9/25/79	2/17/82	4/27/82	6/3/82	10/02/82	
LABORATORY(a):	WAL	GEOCO	GEOCO	GEOCO	WAL	WAL	WAL	WAL	RMAL
PARAMETER									
pH	12 1	11 4	11 5	10 8	8 1	---	8 8	8 8	
Conductivity (umhos)	---	31900	28500	23500	4950	---	4510	4550	
Temperature (degrees F)	---	48	49	48	46	---	49	49	
Eh (mv)	---	---	---	---	-20	---	-275	-260	
Alkalinity (mg/L)	1320	---	1510	1320	1224	---	1080	844	---
Ammonia (mg/L)	1 0	---	---	---	1.51	---	<1	0 553	---
Cyanide (mg/L)	<0 010	<0 010	<0 010	<0 010	<0 010	---	<0 010	<0 010	---
Phenol (mg/L)	0 009	0 081	0 15	0 42	0 178	---	0 767	0 704	0 014
TDS (mg/L)	23200	28400	23900	19670	5010	---	4820	4750	---
TOC (mg/L)	<1	240	176	144	406	280	412	338	8 5

a WAL=Wyoming Analytical Laboratory; GEOCO Laboratory is now called EDA Instruments Inc ; RMAL=Rocky Mountain Analytical Laboratory

Note Test 1 was conducted between 10/28/79 and 12/5/79; Test 2 was conducted between 8/17/81 and 11/11/81

TABLE 3 WATER ANALYSES FROM WELL H-11

DESCRIPTION Well H-11 is completed to the sandstone immediately above the coal seam It is located in the hydrology characterization well pattern

SAMPLING DATE	12/7/78	4/5/79	6/27/79	9/25/79	8/11/81	2/17/82	10/02/82	
LABORATORY(a)	WAL	GEOCO	GEOCO	GEOCO	WAL	WAL	WAL	RMAL
PARAMETER								
pH	11 9	11 7	10 0	9 4	9 6	11 2	10 1	
Conductivity (umhos)	---	>50000	9500	4520	3600	5150	3550	
Temperature (degrees F)	---	48	50	51	---	43	49	
Eh (mv)	---	---	---	---		-45	+100	
Alkalinity (mg/L)	696	---	602	925	708	809	615	---
Ammonia (mg/L)	0 4	---	---	---	0 9	1 25	0 553	---
Cyanide (mg/L)	<0 010	<0 010	<0 010	<0 010	<0 010	<0 010	<0 010	---
Phenol (mg/L)	<0 001	0 003	0 022	0 018	0 012	0 012	0 001	---
TDS (mg/L)	4680	---	7580	400	2400	3950	2360	--
TOC (mg/L)	<1 0	14	8	15	7	4	37 7	---

a WAL=Wyoming Analytical Laboratory GEOCO Laboratory is now called EDA Instruments Inc , RMAL=Rocky Mountain Analytical Laboratory

Note Test 1 was conducted between 10/28/79 and 12/5/79; Test 2 was conducted between 8/17/81 and 11/11/81

TABLE 4 WATER ANALYSES FROM WELL H-13

DESCRIPTION Well H13 is completed to the shale immediately below the coal seam It is the hydrology characterization pattern

SAMPLING DATE:	12/7/78	4/5/79	6/27/79	9/25/79	2/17/82	4/27/82	6/3/82	10/02/82	
LABORATORY (a)	WAL	GEOCO	GEOCO	GEOCO	WAL	WAL	WAL	WAL	RMAL
PARAMETER									
pH	11 0	10 9	10 5	10 4	10 3	---	12 3	12 2	
Conductivity (umhos)	---	>50000	750000	33000	7700		11050	11000	
Temperature (degrees F)	---	48	50	49	49	---	54	54	
Eh (mv)	---	---	---	---	-325	---	-300	-240	
Alkalinity (mg/L)	186	---	<2	320	772	---	946	717	---
Ammonia (mg/L)	0 2	---	---	---	6 70	7 23	8 21	6 20	---
Cyanide (mg/L)	<0 010	<0 010	<0 010	<0 010	<0 010	---	<0 010	<0 010	---
Phenol (mg/L)	0 014	0 011	0 057	0 024	0 028	---	0 154	0 14	0 13
TDS (mg/L)	1840	65100	63450	29410	15800	12200	9260	9560	---
TOC (mg/L)	27	36	115	232	123	375	292	235	200

a WAL=Wyoming Analytical Laboratory GEOCO Laboratory is now called EDA Instruments Inc RMAL=Rocky Mountain Analytical Laboratory

Note Test 1 was conducted between 10/28/79 and 12/5/79, Test 2 was conducted between 8/17/81 and 11/11/81

TABLE 5 WATER ANALYSES FROM WELL H-18

DESCRIPTION Well H18 is completed to the coal seam but appears to be in communication with the upper sandstone It is located immediately updip of the Test 1 cavity

SAMPLING DATE	8/29/79	9/12/79	9/26/79	11/07/79	5/08/80	12/18/80	8/12/81	2/17/82	6/03/82	10/02/82	
LABORATORY(a)	GEOCO	GEOCO	GEOCO	GEOCO	GEOCO	GEOCO	CDM	WAL	WAL	WAL	RMAL
PARAMETER											
pH	11 5	10 5	10 9	10 0	---	10 0	9 4	10 0	9 9	10 0	
Conductivity (umhos)	4700	4500	4300	3190	---	3600	3400	3010	2500	2700	
Temperature (degrees F)	50	47	50	47	---	---	---	49	51	50	
Eh (mv)	---	---	---	---	---	---	---	+400	+120	+105	
Alkalinity (mg/L)	580	2060	545	848	960	618	1020	567	1060	775	---
Ammonia (mg/L)	---	---	---	---	---	---	1 6	1 91	1 91	1 45	2 1
Cyanide (mg/L)	<0 010	<0 010	<0 010	<0 010	---	0 022	<0 010	<0 010	<0 010	<0 010	---
Phenol (mg/L)	0 14	0 14	0 085	0 069	0 10	0 66	0 015	0 006	0 032	0 020	0 027
TDS (mg/L)	3460	3600	530	3100	2640	2316	2080	1860	2100	2010	---
TOC (mg/L)	50	47	49	45	51	---	35	27	106	58	33

a WAL=Wyoming Analytical Laboratory GEOCO Laboratory is now called EDA Instruments Inc RMAL=Rocky Mountain Analytical Laboratory

Note Test 1 was conducted between 10/28/79 and 12/5/79 Test 2 was conducted between 8/17/81 and 11/11/81

TABLE 6 WATER ANALYSES FROM WELL H-17

DESCRIPTION Well H-17 was completed to the coal seam It is immediately down dip of the Test 1 cavity

SAMPLING DATE	8/29/79	9/12/79	9/26/79	11/07/79	5/08/80	12/18/80	8/12/81	2/17/82	6/03/82	10/02/82	
LABORATORY(a)	GEOCO	GEOCO	GEOCO	GEOCO	GEOCO	GEOCO	CDM	WAL	WAL	WAL	RMAL
PARAMETER											
pH	12 2	10 0	12 0	12 0	---	12 5	12 0	12 8	12 8	12 8	
Conductivity (umhos)	13400	11800	11200	11000	---	12600	18000	7200	7900	8000	
Temperature (degrees F)	50	49	50	47	---	---	---	48	50	50	
Eh (mv)	---	---	---	---	---	---	---	+250	+80	+100	
Alkalinity (mg/L)	2730	830	2040	1950	2640	2436	2390	2552	2420	1960	---
Ammonia (mg/L)	---	---	---	---	---	---	2 7	3 02	2 83	2 15	3 5
Cyanide (mg/L)	<0 10	<0 10	<0 10	<0 10	---	0 058	<0 010	<0 010	<0 010	<0 010	
Phenol (mg/L)	0 090	0 31	0 39	0 66	1 5	4 68	0 034	0 062	0 206	0 053	0 18
TDS (mg/L)	9570	9740	7140	7210	7060	6840	6530	5540	5830	5960	
TOC (mg/L)	29	33	34	42	52	---	45	41	51	40	

a WAL=Wyoming Analytical Laboratory; GEOCO Laboratory is now called EDA Instruments Inc RMAL=Rocky Mountain Analytical Laboratory

Note Test 1 was conducted between 10/28/79 and 12/5/79 Test 2 was conducted between 8/17/81 and 11/11/81

TABLE 8 WATER ANALYSES FROM WELL H-16 WHEN COMPLETED IN THE COAL OVERBURDEN

DESCRIPTION Well H-16 is immediately downdip of the Test 1 cavity It was originally completed to the coal but recompleted to the upper sandstone in 6/81 This table covers the time that H-16 was completed to the upper sandstone

SAMPLING DATE	8/12/81	2/17/82	4/27/82	6/03/82	10/02/82	
LABORATORY(a)	CDM	WAL	WAL	WAL	WAL	RMAL
PARAMETER						
pH	8 7	8 9	---	9 5	9 4	
Conductivity (umhos)	5200	3000	---	3750	3650	
Temperature (degrees F)	---	47	---	50	49	
Eh (mv)	+310	+310	--	+95	+120	
Alkalinity (mg/L)	757	955	---	745	590	---
Ammonia (mg/L)	2 3	1 85	2 19	2 02	1 70	3 3
Cyanide (mg/L)	0 095	0 016	0 013	0 021	<0 010	0 09
Phenol (mg/L)	0 023	0 006	---	0 137	0 020	---
TDS (mg/L)	4020	3660	---	3790	3860	---
TOC (mg/L)	10	10	---	73	16 6	11 0

a WAL=Wyoming Analytical Laboratory GEOCO Laboratory is now called EDA Instruments Inc RMAL=Rocky Mountain Analytical Laboratory

Note Test 1 was conducted between 10/28/79 and 12/5/79 Test 2 was conducted between 8/17/81 and 11/11/81

TABLE 7 WATER ANALYSES FROM WELL H-16 WHEN COMPLETED INTO THE COAL SEAM

DESCRIPTION Well H-16 is immediately downdip of the Test 1 cavity It was originally completed to the coal but recompleted to the upper sandstone in 6/81 This table covers the time that H-16 was completed to the coal

SAMPLING DATE	8/29/79	9/12/79	9/26/79	11/07/79	5/08/80	12/18/80
LABORATORY(a)	GEOCO	GEOCO	GEOCO	GEOCO	GEOCO	GEOCO
PARAMETER						
pH	11 2	10 2	11 6	11 8	---	8 08
Conductivity (umhos)	1900	7500	4800	1700	---	6750
Temperature (degrees F)	50	48	49	48	- -	---
Eh (mv)	---	---	--	-	---	---
Alkalinity (mg/L)	203	1030	1060	1160	1120	124
Cyanide (mg/L)	<0 010	<0 010	<0 010	<0 010	---	<0 010
Phenol (mg/L)	0 023	0 22	0 22	0 53	0 068	3 0
TDS (mg/L)	1530	4920	4510	4870	4850	4308
TOC (mg/L)	13	46	57	73	130	100

a GEOCO Laboratory is now called EDA Instruments Inc ;

Note Test 1 was conducted between 10/28/79 and 12/5/79 Test 2 was conducted between 8 17/81 and 11 11/81

TABLE 9 WATER ANALYSES FROM WELL H-21

DESCRIPTION Well H-21 is completed to the coal seam immediately updip of the Test 2 cavity It is our reference well

SAMPLING DATE	8/12/81	2/17/82	6/03/82	10/02/82	
LABORATORY(a)	CDM	WAL	WAL	WAL	RMAL
PARAMETER					
pH	---	8 5	8 6	8 7	
Conductivity (umhos)	2800	2250	2300	2200	
Temperature (degrees F)	---	45	49	49	
Eh (mv)	---	-45	+20	+20	
Alkalinity (mg/L)	42	163	124	98	---
Ammonia (mg/L)	0 8	0 918	<1 0	0 581	---
Cyanide (mg/L)	<0 010	<0 010	<0 010	<0 010	---
Phenol (mg/L)	0 005	0 002	0 008	0 001	---
TDS (mg/L)	2100	---	2070	1920	---
TOC (mg/L)	20	14	41	73 4	- -

a WAL=Wyoming Analytical Laboratory RMAL=Rocky Mountain Laboratory
CDM=Camp Dresser, McKee Laboratory

Note Test 1 was conducted between 10/28/79 Test 2 was conducted between 8/17/81 and 11/11/81

TABLE 10 WATER ANALYSES FROM WELL H-19

DESCRIPTION Well H-19 is completed to the coal seam immediately downdip of the Test 2 cavity

SAMPLING DATE	8/12/81	2/17/82	4/27/82	6/03/82	10/02/82	
LABORATORY(a)	CDM	WAL	WAL	WAL	WAL	RMAL
PARAMETER						
pH	7 4	6 5	---	6 5	6 5	
Conductivity (umhos)	2100	2100	---	2400	2400	
Temperature (degrees F)	47	47	---	49	49	
Eh (mv)	-80	-80	---	+110	+100	
Alkalinity (mg/L)	46	1067	---	1050	656	--
Ammonia (mg/L)	<0 5	0 257	---	<1 0	0 087	---
Cyanide (mg/L)	<0 5	<0 010	---	<0 010	<0 010	---
Phenol (mg/L)	0 021	0 098	1 06	0 437	0 454	0 37
TDS (mg/L)	2400	2840	---	2500	2090	---
TOC (mg/L)	13	52	---	120	47 5	37 0

a WAL=Wyoming Analytical Laboratory RMAL=Rocky Mountain Laboratory
CDM Camp, Dresser, McKee Laboratory

Note Test 1 was conducted between 10/28/79 Test 2 was conducted between 8/17/81 and 11/11/81

TABLE 11 WATER ANALYSES FROM WELL H-20

DESCRIPTION W-ll H-20 is completed to the coal seam immediately downdip of the Test 2 cavity

SAMPLING DATE	8/12/81	2/17/82	4/27/82	6/03/82	10/02/82	
LABORATORY(a)	CDM	WAL	WAL	WAL	WAL	RMAL
PARAMETER						
pH	7 3	6 5	---	6 4	6 4	
Conductivity (umhos)	2300	2300	---	2400	2450	
Temperature (degrees F)	47	49	---	51	51	
Eh (mv)	-50	-100	---	-140	-100	
Alkalinity (mg/L)	35	1820	---	1070	85	---
Ammonia (mg/L)	0 7	0 493	---	<1	0 029	---
Cyanide (mg/L)	<0 010	<0 010	---	<0 010	0 010	---
Phenol (mg/L)	0 017	0 180	---	0 751	0 704	0 30
TDS (mg/L)	3000	3500	---	3690	2920	---
TOC (mg/L)	19	191	250	231	167	140

a WAL=Wyoming Analytical Laboratory RMAL Rocky Mountain Laboratory
CDM=Camp, Dresser McKee Laboratory

Note Test 1 was conducted between 10/28/79 Test 2 was conducted between 8/17/81 and 11/11/81

TABLE 12 WATER ANALYSES FROM WELL H-22

DESCRIPTION Well H-22 is completed to the sandstone immediately above the coal It is downdip of the Test 2 cavity

SAMPLING DATE	8/12/81	2/17/82	4/27/82	6/03/82	10/02/82	
LABORATORY(a)	CDM	WAL	WAL	WAL(b)	WAL	RMAL
PARAMETER						
pH	10 8	9 8	---	9 6	9 6	
Conductivity (umhos)	2750	1825	---	1700	1750	
Temperature (degrees F)	---	49	---	55	54	
Eh (mv)	---	-220	---	85	+100	
Alkalinity (mg/L)	579	538	---	385 389	264	---
Ammonia (mg/L)	5 4	1 74	2 44	2 1 1 62	0 640	---
Cyanide (mg/L)	0 852	0 026	<0 010	0 014 0 011	0 010	0 020
Phenol (mg/L)	0 344	0 136	---	0 569 0 677	0 387	0 14
TDS (mg/L)	1660	1300	---	1210 1890	1050	
TOC (mg/L)	94	67		69 59	63	29

a WAL=Wyoming Analytical Laboratory RMAL Rocky Mountain Laboratory
CDM Camp Dresser McKe Laboratory

b Double entries are analyses done on diplicate samples

Note Test 1 was conduct l between 10 28/79 Test 2 was conducted between 8 17 81 and 11/11/81

TABLE 13 WATER ANALYSES FROM THE TEST 1 CAVITY

DESCRIPTION: This water was obtained from wells drilled into the Test 1 cavity during the post-burn coring program

SAMPLING DATE	9/23/80	10/20/80	01/08/81	08/11/81
LABORATORY:	GEOCO	GEOCO	CDM	CDM
PARAMETER				
pH	7 99	7 45	---	7 8
Conductivity (umhos)	4200	6000	---	5600
Temperature (degrees F)	---	---	---	---
Eh (mv)	---	---	---	-
Alkalinity (mg/L)	97	---	50	104
Ammonia (mg/L)	---	---	13	14
Cyanide (mg/L)	<0 010	<0 010	---	<0 010
Phenol (mg/L)	<0 001	<0 001	0 02	0 004
TDS (mg/L)	5698	6200	4360	4540
TOC (mg/L)	10 4	5 0	6 0	14 0
Calcium (mg/L)	352	545	305	320
Sulfate (mg/L)	3500	4000	2850	3270

a GEOCO Laboratory is now called FDA Instruments Inc ; CDM=Camp Dresser McKee Laboratory

Note: Test 1 was contacted between 10/28/79 and 12/5/79; Test 2 was contacted between 8/17/81 and 11/11/81

4.5 AN EVALUATION OF THE MAGNITUDE OF GROUNDWATER CONTAMINATION AT THE U.S. DOE HOE CREEK UCG EXPERIMENTAL SITE

by

George Saulnier[1/]

Elizabeth M. McTernan[2/]

Theodore C. Bartke[3/]

ABSTRACT

The U.S. Department of Energy Hoe Creek Underground Coal Gasification Experimental Site has been the subject of many environmentally directed investigations. To date, these investigations have focused primarily on identification and quantification of contaminants in the groundwater at the site as a result of these UCG experiments, and on the possible mechanisms of that contamination in monitoring wells on the northern and eastern boundaries on the site, indicating the possibility of a contaminant plume resulting from the Hoe Creek II burn. State of Wyoming DEQ authorities have requested immediate steps be taken to verify the extent of the contamination and evaluation of methods of containment and restoration of groundwater to baseline quality.

Plots of the concentration of key organic (phenol) and inorganic constituents with distance and areal mapping of phenol concentration shows that contamination in the Felix 1 coal seam, the upper seam which was not a primary gasification target, is spreading radially from the Hoe Creek I, II, and III burn cavities. The most severe effects are noted in the east-southeast direction, the apparent direction of local groundwater flow. The distribution of phenol indicates that some organic constituents were probably transported in a gaseous state during the Hoe Creek II burn and are found up to 400 feet from the cavity at concentrations of tens to hundreds of parts per billion. Concentrations in the Felix 2 seam, the object of the experiment, are orders of magnitude lower and have returned to background levels in some observation wells. Sulfate concentration patterns in both seams indicate an in situ reducing environment has developed within 50 feet of the cavity and may be enlarging.

The general hydrologic flow pattern is that of west-northwest to east-southeast flow with head potential increasing with depth. Because of subsidence over the cavity, all zones are interconnected creating a "short-circuit" in groundwater flow which aids in distributing leached contaminants through the coal seams, and possibly limiting the extent of contamination in the overlying unconsolidated sand.

Full characterization of the nature and extent of contamination requires (1) additional observation wells on and off the experiment site to get better areal and vertical data distribution; (2) sampling at more consistent times and with better spatial distribution; and (3) more detailed analysis of the present and future data, including possible transport and geochemical modeling studies and more relevant experiments concerning natural attenuation and retardation.

Potential treatment methods are the subject of on-going research and may include air-stripping, carbon adsorption and possibly in situ biological degradation. Treatment of the groundwater will be costly and could require 5 to 10 years.

1/ TRW Energy Development Group
2/ University of Wyoming Research Corporation
3/ USDOE, Laramie Project Office

INTRODUCTION

Lawrence Livermore National Laboratory (LLNL) conducted three underground Coal Gasification (UCG) tests at the 80-acre Hoe Creek site 20 miles south of Gillette, Wyoming, in 1976, 1977 and 1979. The tests, designated Hoe Creek I, II, and III, respectively, were targeted at the 25 foot thick Felix 2 coal seam at depths of 115-165 feet. Table 1 summarizes the operating parameters for each burn.[1] A review of this data reveals significant information relative to groundwater contamination. Important factors affecting groundwater contamination are lost gas during the burn and the operating pressure.

The Felix 2 coal seam is overlain by a 14-18 foot thick siltstone-claystone-sandstone bed; the 10-12 foot thick Felix 1 coal seam; a 35 foot thick poorly consolidated channel sandstone with a discontinuous 5-10 foot thick basal siltstone; and 95 feet of poorly consolidated siltstones claystones and then sands. A pretest hydrologic investigation established the following: hydrologic head decreased with depth to the Felix 2 (Figure 1), three water bearing zones with horizontal conductivities of 0.5 to 3.3 ft/day were present in the channel sand, the Felix 1, and the Felix 2; and that the general flow direction in all three zones is northwest to southeast.[2] The flow direction is oriented normal to the direction of maximum hydraulic conductivity indicating that any contaminant plumes would be broad. The fracture permeability in the coal seams indicates that contaminant migration might not always proceed along linear paths but could take circuitous paths depending on fracture zone length and intensity.

A limited number of water quality samples were collected and analyzed prior to the UCG tests. The samples indicate that a sodium bicarbonate water type was present in Felix 2 before testing, but true baseline samples were not collected from the Felix 1 or the channel sand. Later samples indicate that a more sulfate dominated water probably existed in these units prior to testing. A more detailed discussion of baseline parameters is given below.

The LLNL sampling and analysis of water quality at the Hoe Creek facility indicated that phenol contamination of the three water bearing zones occurred after the Hoe Creek UCG experiments. This contamination became wide spread and reached concentrations well above baseline after the Hoe Creek II experiment. Higher than background concentrations of phenol were observed near the east and north boundaries of the Hoe Creek facility prompting the Department of Energy to request a comprehensive overview of the nature and extent of the organic contamination. Because of the immediacy of the potential offsite contamination from the Hoe Creek II experiment, this area was the main focus of this paper.

Contaminant Generation

During the UCG experiments the Hoe Creek II and Hoe Creek III reactors grew vertically and the reactor cavities and subsequent subsidence established hydrologic communication of all three water bearing zones. This hydrologic connection has caused major changes in the local hydraulic head potential. Groundwater was allowed to move downward in the cavity from the channel sand and out into the Felix 1 and Felix 2 coal seams. Potential for ground water flow from the Felix 1 to the Felix 2 has also occurred. The majority of flow seems to have moved into the Felix 1, which has a higher permeability than the Felix 2. This flow scheme was supported by hydrologic modeling studies by LLNL. Figure 2 (3) is a map of the head potential in the Felix 2 in 1979, and shows the mounding effect of downward flow in the cavities. Measurements in 1982 show that head has equalized between Felix 1 and the channel sand, and the head in the Felix 2 is about 10 feet lower. The nearly equal water levels in the Felix 1 and the channel sand shows that these formations have hydraulically adjusted to the disturbance in the potential field caused by subsidence at the cavity, and that, in the area east of the cavity, the silt layer between the two units is a poor confining bed and that a very leaky connection exists between the Felix 1 and the channel sand.

Figure 3 (4) presents the monitor well network designed to measure water levels and collect quality samples in the three zones of interest. The wells were initially sampled quarterly, but recently sampling has been semi-annual to annual. Not every well has been sampled with the same frequency or analysis schedule.

A general comparison of pre and post-burn concentrations indicates that significant hydrologic and water quality changes

have taken place as a result of the experiments. LLNL column studies (5) and other UCG work have identified the following as key chemical parameters in assessing contamination: dissolved phenol, dissolved organic carbon, calcium, sulfate, boron, total dissolved solids, ammonium, fluoride, iron, pH, and Eh. These parameters reflect the chemical environmental parameters most affected by burning, leaching, and gas escape into the water bearing formations. These parameters were reviewed and assessed using distance-concentration plots, water typing, and iso-concentration maps.

The following factors are believed responsible for affecting water quality changes during and after the gasification experiments: 1) gas transport during the overpressuring stage. Potential chemical species include sulfur and nitrogen compounds and possibly potassium sodium, lithium, fluorine, and chlorine; 2) leaching of the solids in the ash produced during the burn; 3) mixing of groundwater of different qualities due to growth of the reactor and subsidence above the cavity; and 4) overburden material which falls into the cavity during subsidence.

The ash from the burn is the principal cause of high total dissolved solids increases and pH changes as water refloods the reactor and reacts with common ash products such as calcium oxide, magnesia, calcium sulfate, calcium hydroxide, and reduced iron forms (perhaps iron monosulfide). Overburden material is another source of leachate as the increase in surface area caused by the rockfall generates increases in total dissolved solids until this material achieves chemical equilibrium with groundwater.

Contaminant Detection

Table 2 (4) lists the baseline data for key constituents as determined by LLNL. The data are from U.S.G.S. analyses of a single set of water samples obtained before any testing was carried out. The channel sand has essentially no baseline data. The areas north and especially west of Hoe Creek II are not well represented. The data for the Hoe Creek III experiment appears to show the influence of Hoe Creek II on the quality of both Felix 1 and Felix 2 water quality. Well M-2 at the northwest corner of the site was intended to sample the channel sand in an area presumeably unaffected by the burns. However, samples showed higher concentrations of phenol than expected and left unresolved the true nature of the baseline in the channel sand.

The baseline water quality data was used to type the groundwater chemically using triangular plots of equivalents per million of the major constituents in the method of Piper.(6) Based on this typing analysis the following was determined:

- Felix 2 - The baseline data for Felix 2 plots is a sodium bicarbonate water with one sample in the sodium sulfate category.
- Felix 1 - The sample set classed as baseline for Felix 1 plots as a sodium-sulfate water type in a close cluster. This data was collected after Hoe Creek I, but the close spacing indicates it may be true baseline data but this cannot be confirmed.
- Channel Sand - Essentially no baseline data was collected for the channel sand. The sample from the M-2 well plots as a mixed cation-sulfate water type, but because of its phenol concentration it is unclear whether this data is true baseline.

Phenol - The phenol concentration of dissolved phenol associated with the Hoe Creek II site have been reported in samples collected from observation wells closest to the burn cavity. Distance-concentration plots of phenol concentration in the Felix 1 and Felix 2 are shown in Figures 4 and 5. Figure 4 shows that concentrations of phenol 100 times background are found in well WS-14 at the site's east boundary 400 feet east of the cavity. Because this sample point is near the site boundary and because the elevated concentrations have persisted from 1977 to the present, there is a strong likelihood that contaminated groundwater may have moved offsite. Without offsite data this possibility of offsite transport cannot be explored.

Phenol concentrations in the Felix 2 are generally an order of magnitude lower than those found in the Felix 1 at similar distances. For example, the August 1982 phenol concentration at WS-13 (in Felix 2), adjacent to WS-14 (in Felix 1) at the eastern boundary of the site was 2 parts per billion (ppb), whereas the phenol concentration in WS-14 was 77 and 100 ppb in split samples. Elevated phenol concentrations do not appear to have traveled as

far from the cavity in the Felix 2 as in the Felix 1. Phenol concentrations above the Felix 1 and 2 background are also observed in the channel sand. The elevated concentration of phenol in well M-2 is puzzling. The well was installed after all three burns in an attempt to get an unaffected "baseline" sample from the channel sand. Unfortunately, the first sampling, in 1980, showed a phenol concentration of 19 ppb, whether this level of phenol was due to the UCG tests, drilling contamination, analytical or sample collection errors, or represented baseline in the channel sand is not known at this time.

Analyses of the distance-concentration data indicates that two pulses of phenol contamination appear to have occurred. First, as speculated by LLNL, gas loss and transport as a result of overpressurization may have deposited organic contamination in the coal seams at large distances from the cavity (400-950 feet). Second, a major pulse of phenol contamination has been generated from leaching of cavity material and char and tar deposited near the cavity by the burn. The peak phenol concentration in Felix 1 was 44,000 ppb adjacent to the cavity in well WS-10 in October 1979. This peak was then observed in WS-12 in May 1980 at 30,000 ppb. Because of the well spacing, it is unclear whether this peak is moving or degrading in place. Travel time estimates ranging from 50 to 170 feet per year can be estimated under various assumptions, and based on the 1982 sampling, the slower figures appear to be more appropriate.

The shape of the contaminant plume is illustrated by Figure 6 which shows the Felix 2 configuration in March 1981. The plume is broadly developed and appears to be spreading laterally as much as down gradient, probably because the maximum hydraulic conductivity is not in the direction of regional flow.

Sulfate - Sulfate shows a large increase in concentration in one well close to the cavity (WS-26) but shows a progressive decrease in concentration with time in samples from the cavity and from wells up to 125 feet from the cavity in both the Felix 1 and Felix 2 coal seams. Figures 7 and 8 show distance concentration plots of sulfate in the Felix 1 and Felix 2. Sulfate is a by-product of the burn and the reduction of concentrations to as low as 10 ppm since the test indicates a strong reducing environment has developed in the area around the cavity where high phenol concentrations are noted. Hydrogen sulfide and black water has been observed during pumping of the cavity wells.

Other Inorganic Constituents - Two distinct trends in inoragnic constituent concentrations are noted in the sample analyses around the Hoe Creek II cavity, one of increase in concentration and one of decrease in concentration. The two inorganic constituents showing a progressive increase in concentration are boron and fluorides. The concentration of boron has increased by about 1 order of magnitude up to 125 feet from the cavity, especially in the Felix 2. The maximum observed concentration is less than 1 ppm, but it is higher than baseline and has increased with each sampling. Very high to high concentrations of fluoride are noted in both Felix 1 and Felix 2 in wells up to 100 feet from the cavity. The observed concentrations are greater than Public Health standards for drinking water and exist in an area of lowered calcium concentration, a condition which allows fluoride to remain in solution. Calcium, iron, magnesium, sodium and total dissolved solids all show lower than baseline concentrations in the wells up to 125 feet from the cavity. Calcium was expected to be one of the ions with an increased concentration as a result of the burn but the concentration of calcium is only high in WS-26. There is a possibility that calcium is involved in precipitation reactions in the same area as the sulfates reduction. The overall reduction in total dissolved solids could be due to either precipitation of minerals or to an influx of recharge water lower in dissolved solids. The growth of the cavity now encompasses an area above the water table which could allow precipitation recharge to more quickly enter the channel sand. (7) The water flow in the cavity would distribute this recharge to the formations accordingly. This pattern is not in agreement with the observed increase in fluoride and boron or with the development of a stratified body of water with a well developed reducing environment, such as exists in the cavity.

Water Types - All water analyses were tested for ionic balance and those with correct balance were plotted on Piper diagrams to discern whether any post-burn pattern or distinctions could be observed.

The Felix 2 groundwater can be generally classified as a sodium-bicarbonate water with occasional high percentages of sulfate. Year by year plots show that after the burn, the Felix 2 water showed an increase in sulfate, but with time the water as returned to a sodium bicarbonate water.

The Felix 1 groundwater is a mixed-cation-bicarbonate to calcium-carbonate water. The water in well WS-26 is a calcium sulfate water reflecting a high input of ash leachate. Wells WS-24 and WS-14 plot as calcium carbonate waters and may reflect the more normal water type of Felix 1 water, as they are farthest from the experiment.

A limited number of samples is available from the channel sand and most plot as calcium bicarbonate waters. However, wells WS-17 and WS-19 has a magnesium bicarbonate water in samples collected in June 1981, and well WS-20 has a calcium sulfate water. These wells appear to demonstrate inorganic water quality types indicating communication with Felix 1 water having ash leachate products. Another possibility for the high magnesium proportion could be calcium mineral precipitation leaving the groundwater richer in magnesium.

Water typing for samples collected from the cavity well show a progressive change from a sodium sulfate water to a calcium bicarbonate water (Figure 9). This change reflects potential sulfate reduction and stratification of the water in the cavity space. The initial high sulfate was contributed from ash leachate.

Chemical Reactions

Groundwater in the Felix 1 and Felix 2 shows a reduction with time in the amount of sulfate up to 125 feet from the Hoe Creek II cavity. The sulfate concentration in the Felix 2 has dropped as low as 10 ppm. This pattern indicates an active sulfate reduction may be taking place. Incomplete data from field measurements shows -121 millivolts in May 1979, another indication of reducing activity.

A likely reaction that may be taking place is sulfate reduction in the presence of organic materials such as tar, phenol, and other by-products of the UCG experiment. The reaction is:

$$\text{(organic material)} + SO_4^{2-} \longleftrightarrow H_2S + \text{carbonate species}$$

The sulfide may remain as H_2S gas (as noted for the cavity well), or may combine with iron to form iron monosulfide. It is possible that the reaction is catalyzed or associated by sulfate reducing bacteria or anaerobic hydrocarbon digesting bacteria. As the sulfate reduction region is the same region where phenol concentrations have been lowering with time the two reactions may be proceeding together. Future sampling should include culturing for the presence of these bacteria.

The decrease in sulfate and total dissolved solids (TDS) concentrations noted for the cavity and near cavity groundwater is also accompanied by an up to an order of magnitude decrease in calcium and magnesium concentrations. The sulfate reduction reaction can lead to an increase in carbonate concentration which will help precipitate alkaline earth and metallic carbonate such as aragnite, siderite, or magnesium calcite. Lattice substitutions in the minerals also allow amounts of strontium, barium and zinc to precipitate. The reaction will lead to a lowering of TDS concentration and a change to a more sodium carbonate water type.

Another potential precipitation reaction, as noted above, is the formation of iron monosulfide (FeSO), the predecessor to pyrite. The kinetics of pyrite precipitation are quite slow but are faster and more common for FeS, which forms a fine black precipitate, which forms H_2S when treated with acid. Distance-concentration plots for iron are not conclusive but suggest a lowering of iron concentration in this zone up to 125 feet from the cavity.

Initial laboratory testing had suggested that the coal would act like an activated carbon filter for organic contamination. However, even though some phenol concentrations have been reduced by an order of magnitude in samples from some wells, the shape of the peak and subsequent experiments have shown that adsorption is not significant, most likely due to the low surface area in contact with the waters. Diffusion and organic decay in chemical reactions appear to contribute the most significant improvement in organic water quality.

Containment Treatment

Reduction of phenol concentration to the baseline values of 0-1 ppb may require a large investment in time and money. Most commercial treatments are designed for much higher concentration tolerances and their cost goes up as the final concentration limit goes down.

Based on the levels of organic contamination shown by the groundwater sampling program, several treatment techniques have been selected for consideration for treatability studies. These include activated carbon adsorption, polymeric resin adsorption, chemical oxidation and biological treatment.

In addition to treatment methods, consideration must be given to methods for removal of contaminated water from the water bearing zones for treatment and a method of disposing of the treated water, whether through reinjection or surface discharge. Complete installation of such a withdrawal system will require additional hydrologic testing and modeling to plan well spacing and pumping rates to withdraw all the contaminated water. The low permeability of the formations will require a large number of wells and possibly offsite spacing to locally deverse the regional gradient of flow and change the direction of movement of the contaminated water.

Summary and Conclusion

In summary, major organic contamination has taken place at Hoe Creek II as a result of underground coal gasification experiments. Contamination appears to have been generated by gas transport during the burn and from leaching of ash, tar and char after reflooding of the experiment site. Large scale effects on water quality have been observed up to 130 feet from the cavity. A major peak appears to have passed the 130 foot mark but has not yet been observed at greater distances, partly due to the well spacing and sampling frequency. Natural processes appear to be at work reducing the effects of inorganic contamination but more study is needed to determine if adsorption, oxidation-reduction, or biological action are helping to remove organic contamination.

REFERENCES

1. Lawrence Livermore Laboratory, 1976-1981 Quarterly Progress Reports, In Situ Gasification Program; Four Reports Annually; UCRL-50026.

2. R. F. Stone and D. F. Snoeberger. "Evaluation on of the Native Hydraulic Characteristics of the Felix Coal (Eocene, Wasatch Formation) and Associated Strata, Hoe Creek Site, Campbell County, Wyoming". Lawrence Livermore National Laboratory, Report UCRL-51992, Rev. 1, 1976.

3. U.S. Department of Energy, "Permit to Mine Application, Hoe Creek III Site", 1978.

4. U.S. Department of Energy, "Groundwater Quality Data for the Hoe Creek UCG Site", 1982.

5. V. A. Dalton and J. H. Campbell. "Laboratory Measurements of Groundwater Leaching and Transport of Pollutants Produced During Underground Coal Gasification". Lawrence Livermore National Laboratory, UCRL-80884, 1978.

6. A. M. Piper. "A Graphic Procedure for the Geochemical Interpretation of Water Analyses". Transactions, American Geophysical Union, V. 25, pp. 914-923, 1944.

7. H. Ganow. Lawrence Livermore National Laboratory, Written Communication, 1983.

Table 1. - Forward Gasification Parameters for Hoe Creek Experiments

	HC-I	HC-II	HC-III
Depth (ft)			
Top of Felix 1	98	100	
Top of Felix 2	123	126	
Duration of Test (days)	10.8	58.5	54.1
Average Pressure (psig)	12.0	24.6	25.2
Maximum Sustained Pressure (psig)		51.9	36.2
Total Dry Gas Production (MM scf)	13	194	188
Product Gas Recovery (%)	93	80	82
Average Dry Gas Composition (% by volume)			
N_2	55	56	9.6
H_2	17	14	34
CH_4	1.6	2.3	4.7
CO	8.8	7.7	11
CO_2	16	18	40
Tar	0.2	0.2	0.1
Coal Consumed (10^3 ft^3)	2.9	47	83

Table 2. - Baseline Conditions at the Hoe Creek Site (from LLL data base)

Parameter	Units	Hoe Creek I Felix 2	Hoe Creek II Felix 2	Hoe Creek III Felix 1	Hoe Creek III Felix 2
Ammonium	(ppm)	0.67	0.71	1.32	0.59
Phenol	(ppb)	0.80	.2	1.8	10.7
TDS	(ppm)	681	769	1872	1058
Sulfate	(ppm)	121	250	1022	357
DOC	(ppm)	7.7	2.7	8.04	7.8
Boron	(ppb)	76	60	160	98
Calcium	(ppm)	33	37	176	83

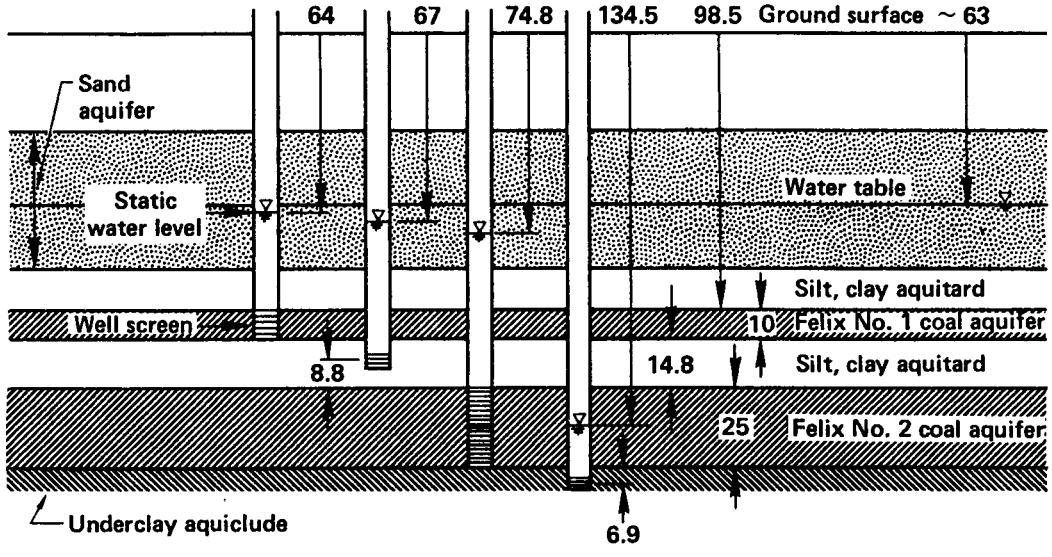

Figure 1. Preburn Hydrologic Head in the Sand Aquifer and Felix 1 and 2 Coal Seams.

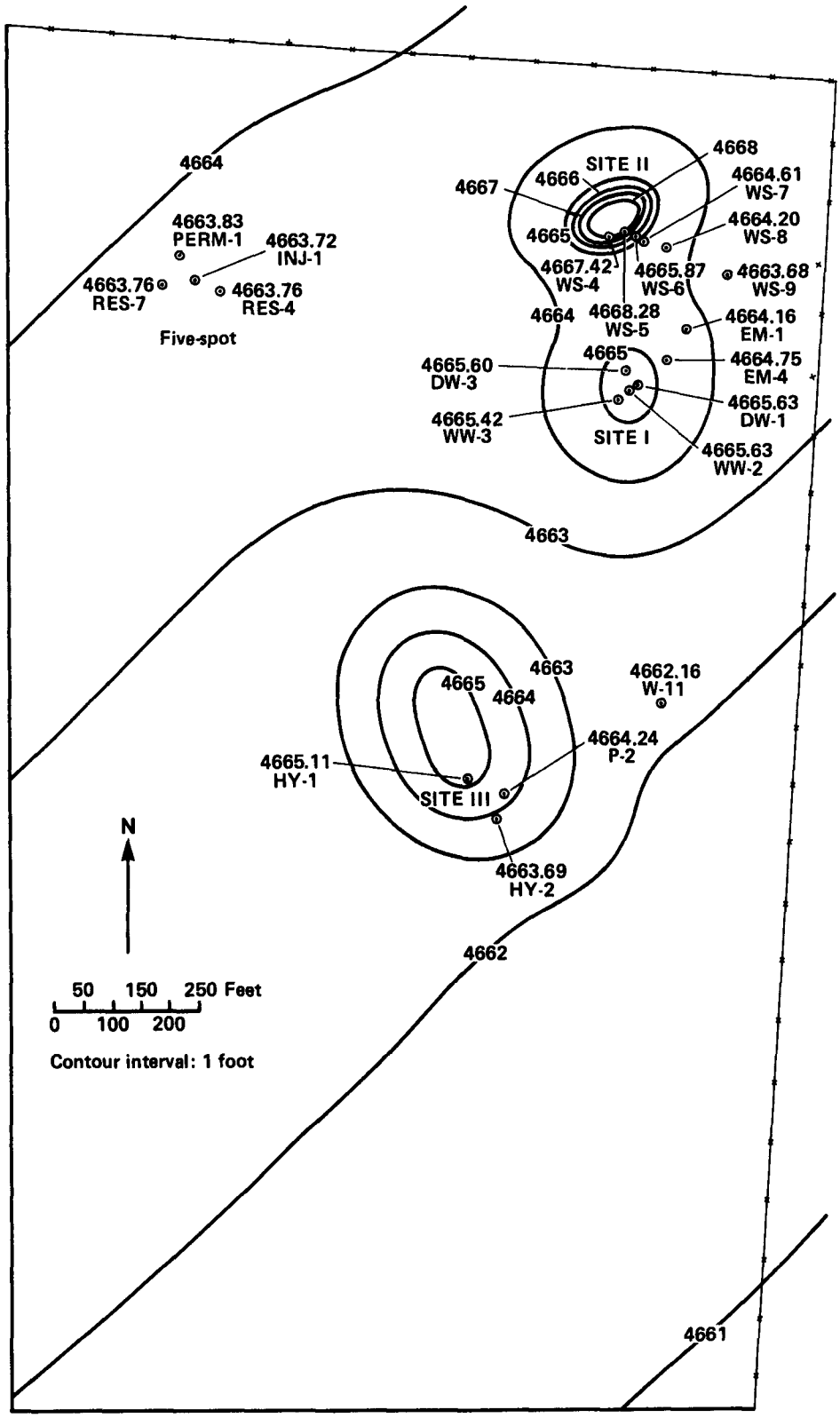

Figure 2. Hydraulic Head Potentiometric Surface Felix No. 2 Coal (1978-1979)

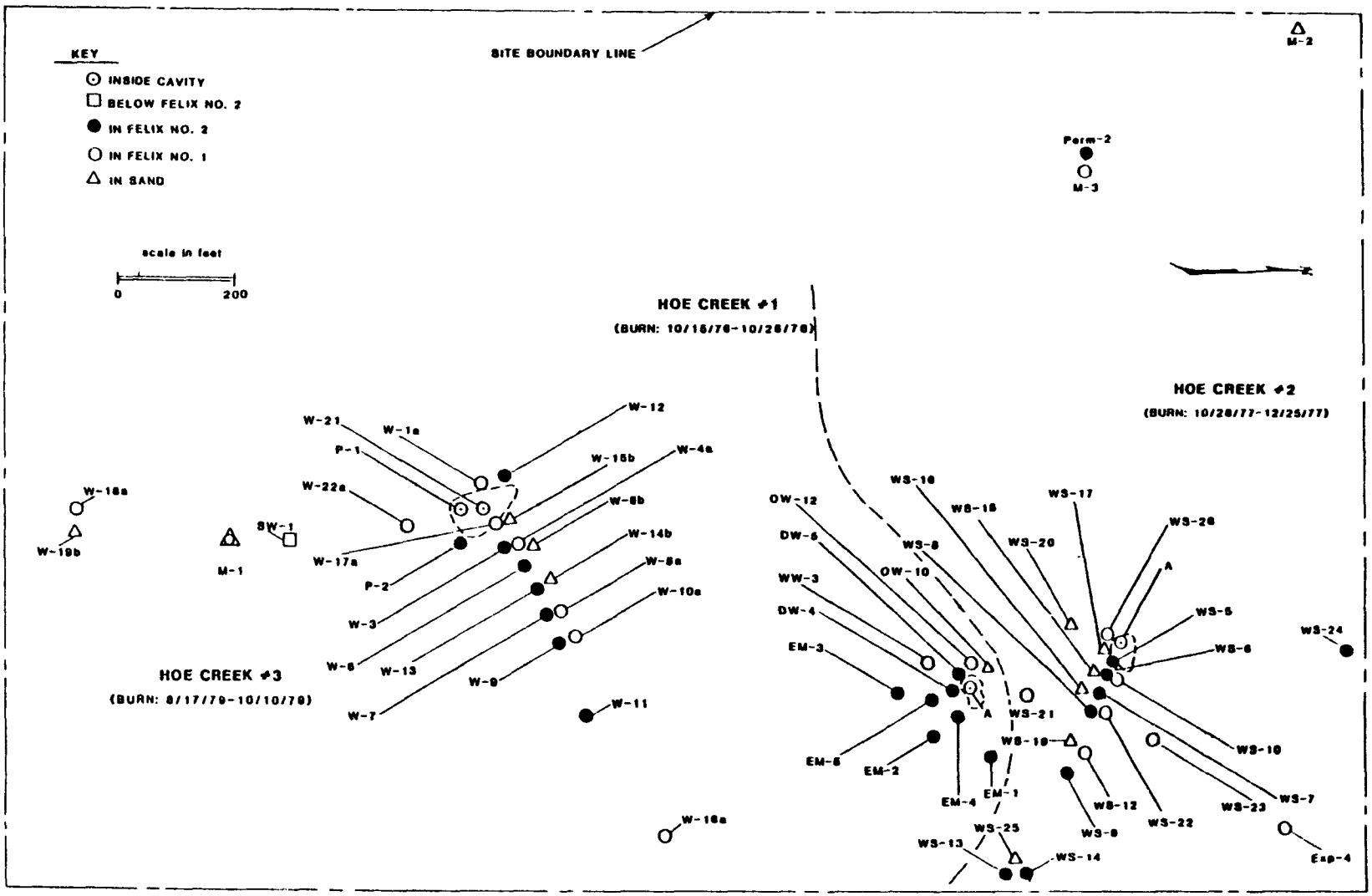

Figure 3. Location of Water Sampling Wells at the Hoe Creek Site.

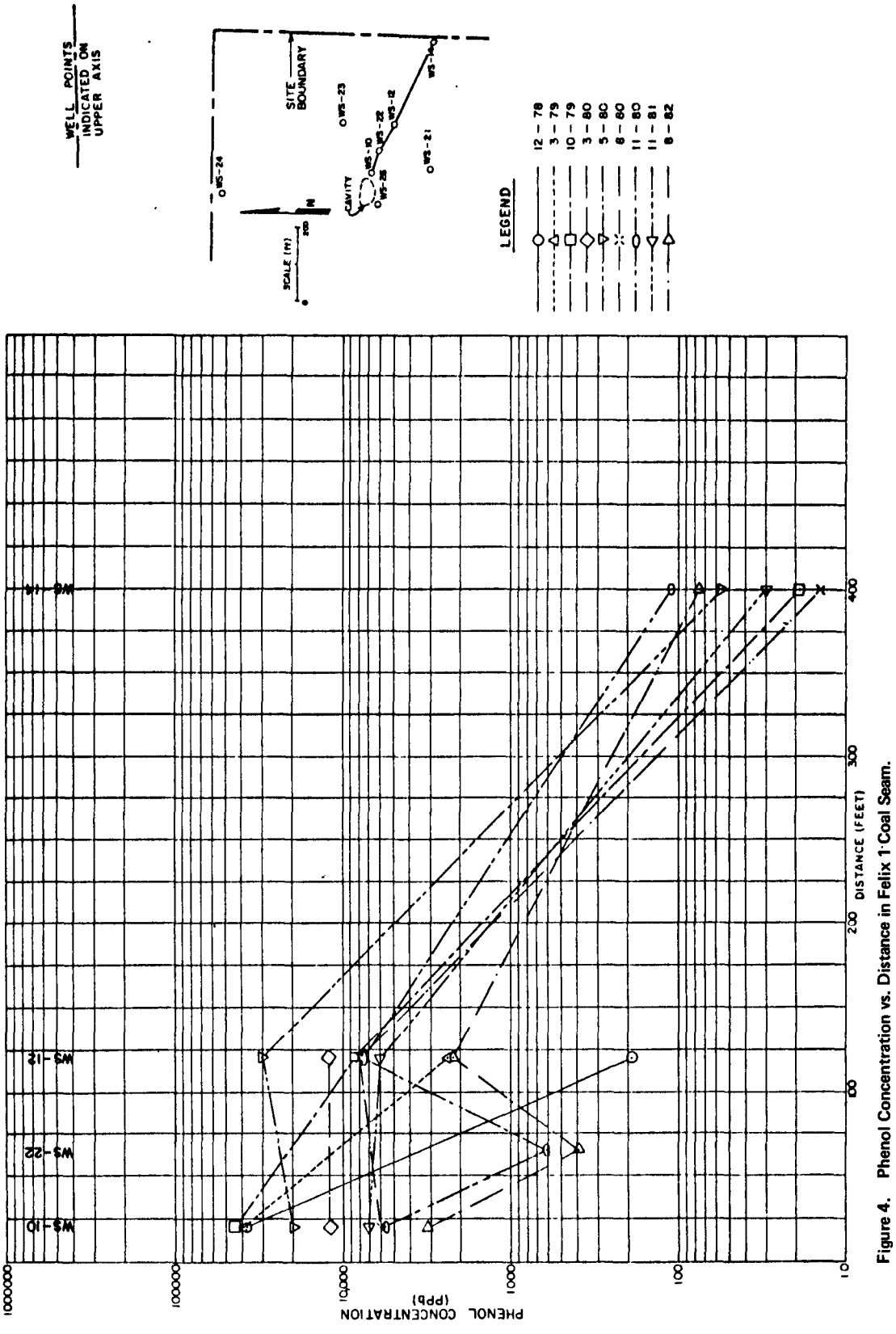

Figure 4. Phenol Concentration vs. Distance in Felix 1 Coal Seam.

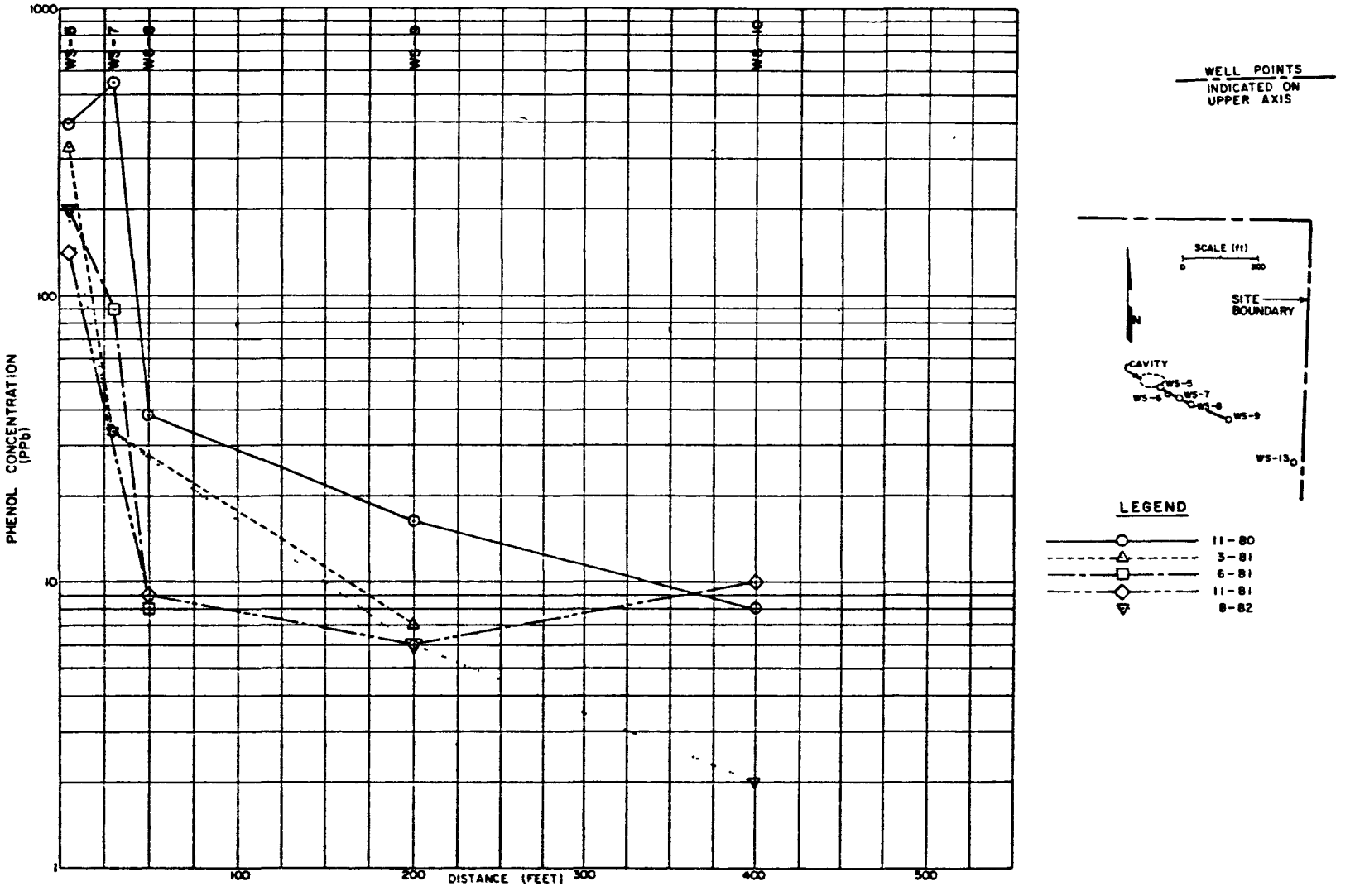

Figure 5. Phenol Concentration vs. Distance in the Felix 2 Coal Seam.

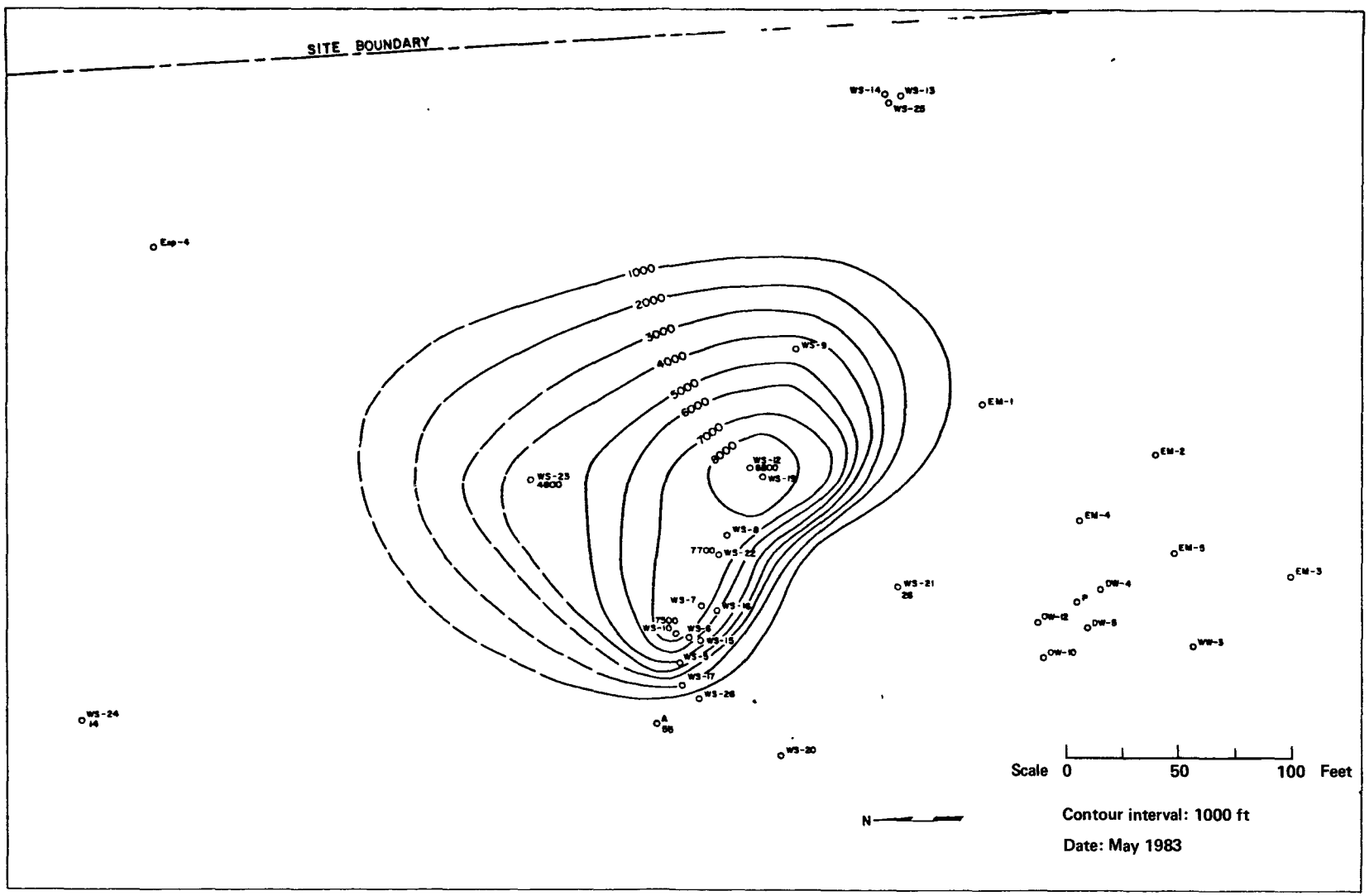

Figure 6. Map of Phenol Concentration in the Felix 1 Coal Seam, 3/81.

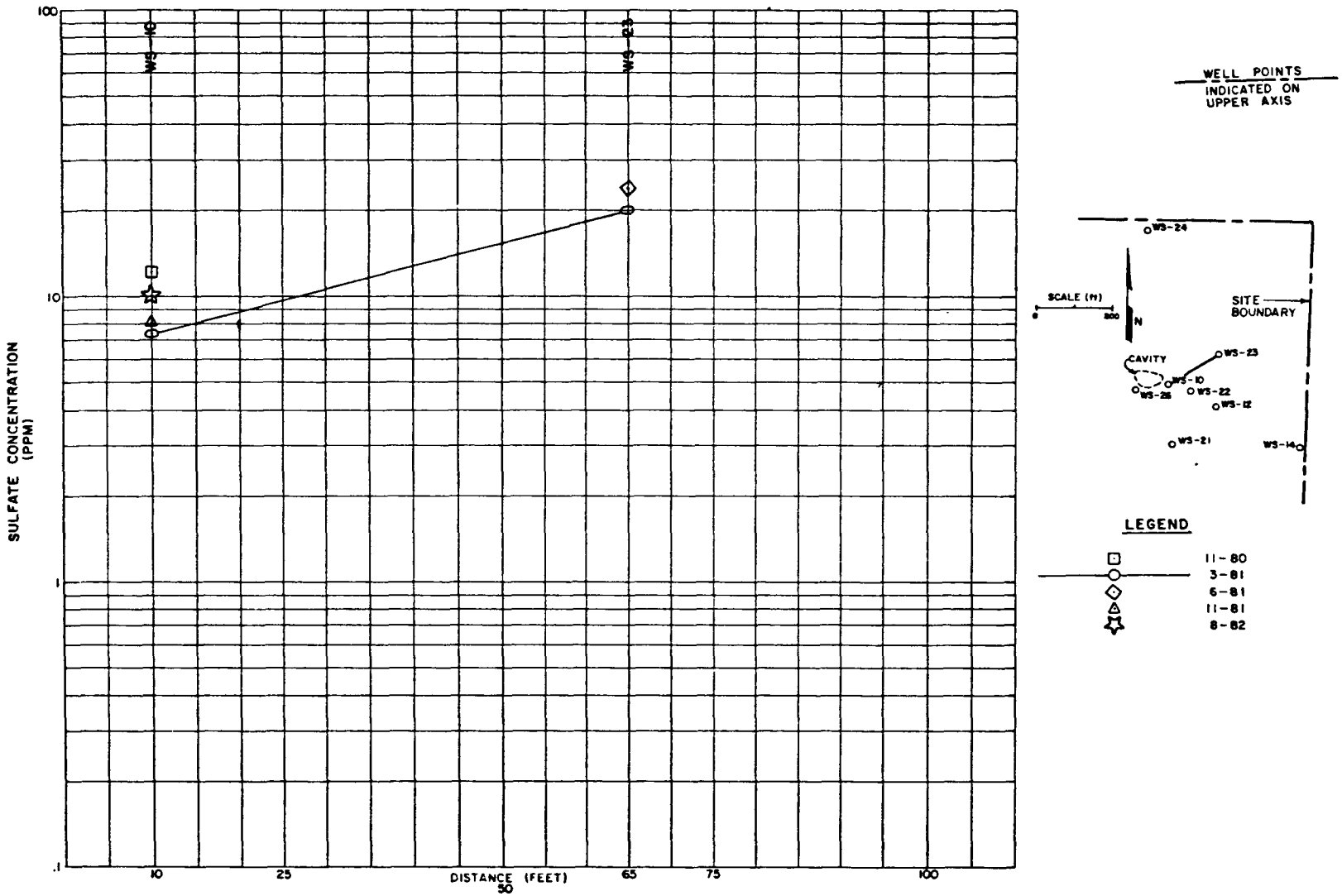

Figure 7. Sulfate Concentration vs. Distance in the Felix 1 Coal Seam.

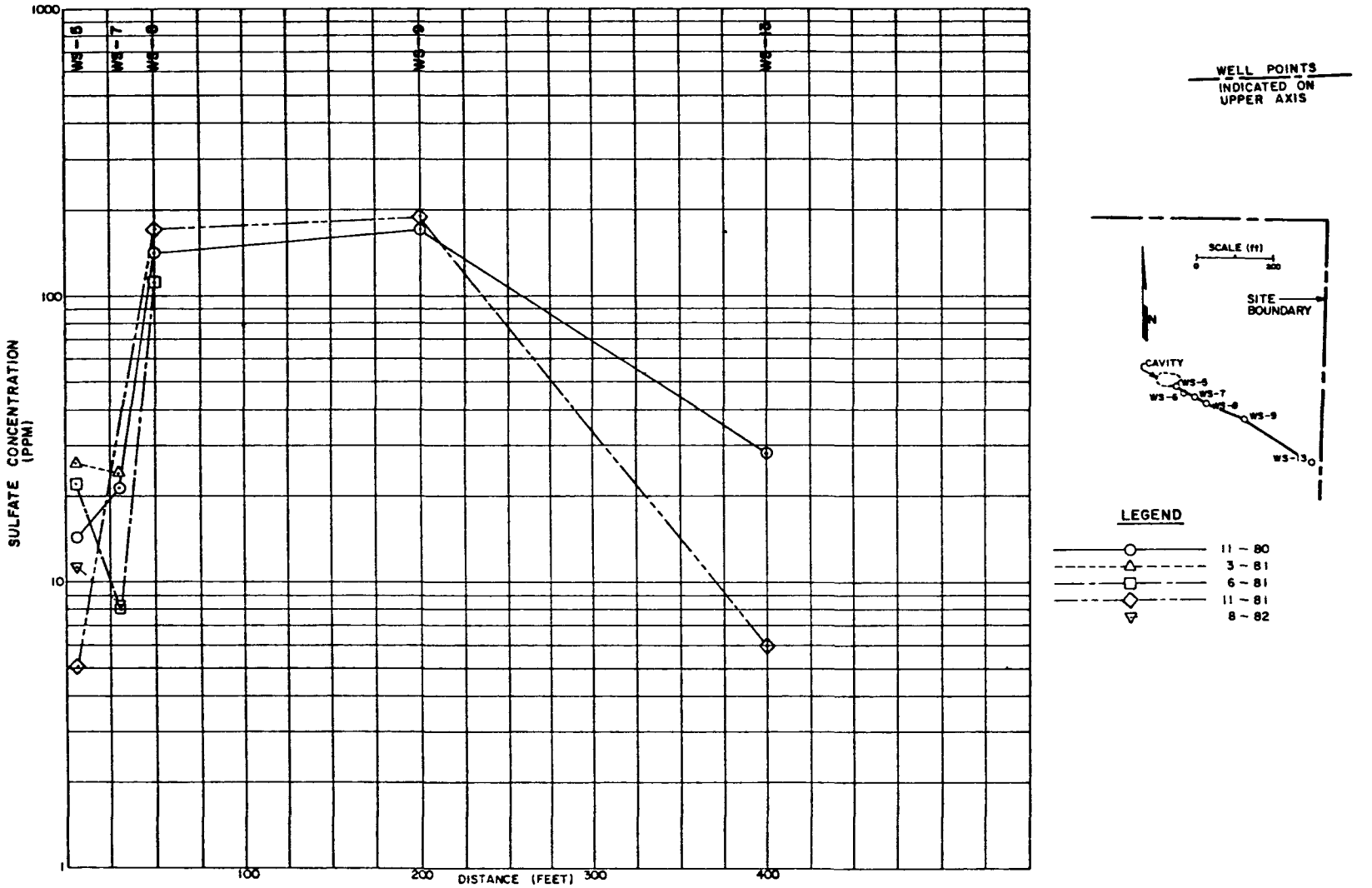

Figure 8. Sulfate Concentration vs. Distance in the Felix 2 Coal Seam.

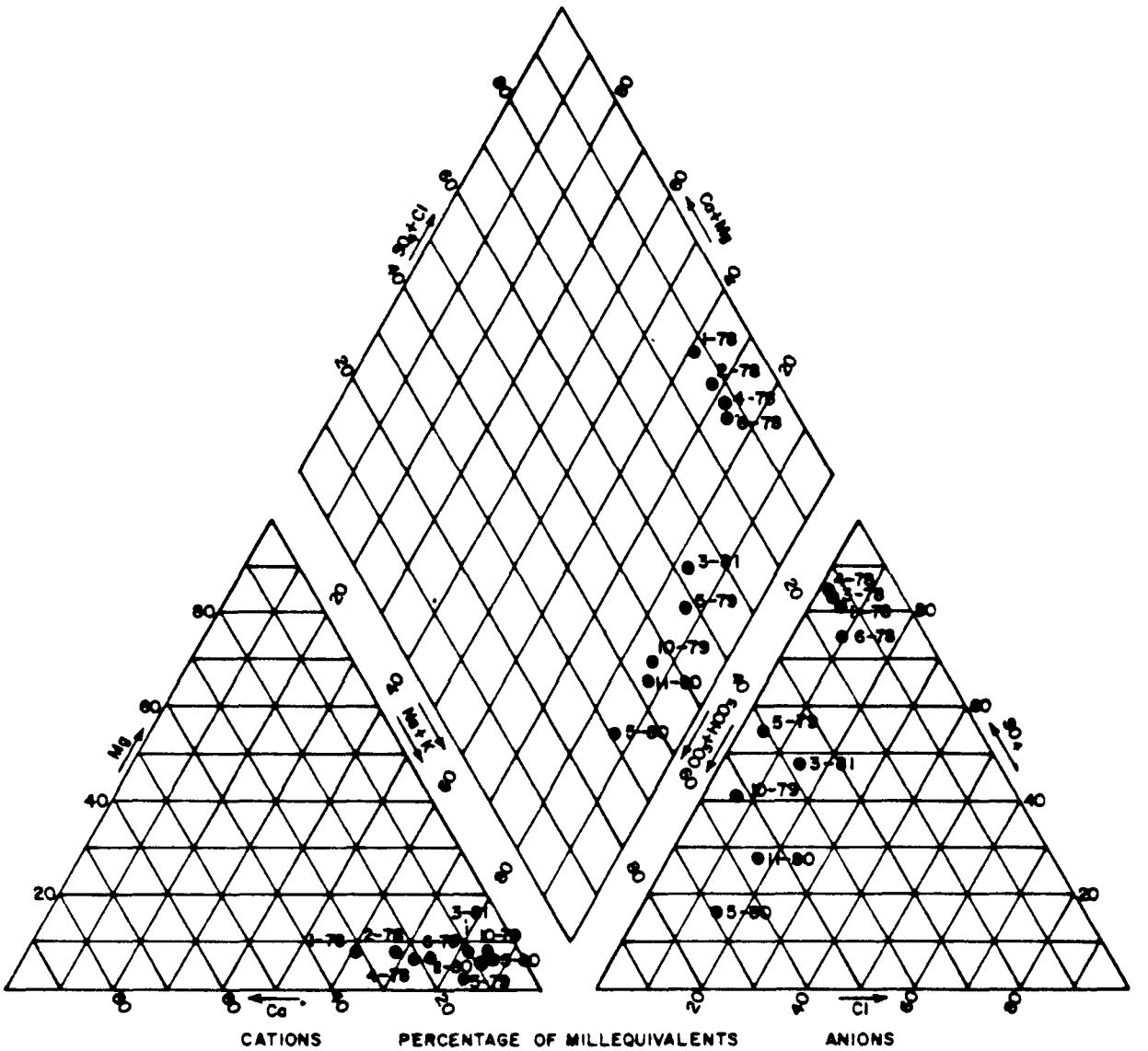

Figure 9. Piper Diagram for Cavity Well A.

Proceedings of the Ninth Annual Underground Coal Gasification Symposium, August, 1983

4.6 SIMULATION OF GROUNDWATER FLOW REGIMES IN A COAL SEAM WITH UCG CAVITIES USING A FINITE ELEMENT MODEL

by

Dr. Dinshaw N. Contractor[1]
Stephen C. Davidson[2]

University of Wyoming Research Corporation, Laramie, Wyoming

ABSTRACT

A two-dimensional finite element groundwater flow model is used to study the flow into and out of large cavities created by underground coal gasification (UCG) burns in a coal seam. The model uses linear triangles to discretize the coal seam in plan and can handle unsteady flows, anisotropic media and the time-dependent boundary conditions imposed by the cavities. After a cavity is created the groundwater begins to flow into the cavity and raises the water level in it, until it fills up. During this phase, the boundary condition imposed is one of constant head at the boundary nodes of the cavity. When the cavity is filled, groundwater flows through the cavity into the coal seam, with the conductivity in the cavity much larger than that in the seam. Either before or after the filling of the cavity, new cavities may be created by UCG burns in adjacent locations of the seam. The program is designed to handle any number of successive burns that may occur. The model has been applied to the UCG burns at the Hanna site in Wyoming. Maps of constant piezometric head in the coal seam simulated by the model at different times have been prepared and compared with similar maps of measured piezometric head.

INTRODUCTION

This paper deals with the simulation of groundwater flow in a coal seam with several cavities created in it by successive UCG burns. This activity in the coal seam alters the natural groundwater flow regime and simulation of the changes can determine the extent of the alteration and how long it would take to return to pre-burn conditions. During the burn, a cavity is formed, that is lined with pyrometamorphic char and filled mostly with rubble (1, 2). At the end of the burn, the cavity will generally be dry because of high temperatures. And the water in the coal seam adjacent to the cavity will drain into it, picking up pollutants as it moves through the char zone. The cavity will gradually fill and it is desirable to estimate how long it takes to fill. During this time, water may be pumped into the cavity from another source to cool it or the polluted water in the cavity may be pumped out to be treated. These exchanges of water should be taken into account in the simulation. Once the cavity fills up, the pre-burn groundwater regime will be gradually re-established and the water (polluted or otherwise) in the cavity will migrate into the coal seam. Cavities may be created successively and they may interact with one another. Before the water quality aspects of this problem can be modeled, it is necessary to model the water quantity problem as a firm foundation on which to base water quality relationships.

Groundwater flow in a wide variety of aquifers has been modeled in the past (3, 4) using techniques such as finite differences, finite elements and the method of characteristics. The problem associated with UCG sites involves the spatial and time-varying internal bound-

1/ Professor of Civil Engineering, University of Arizona, Tucson, AZ 85721
2/ Associated Western Universities, Salt Lake City, UT 84111

ary conditions using a fixed (time-invariant) mesh or network. The finite element method was able to handle this situation without changing the geometry of the network with the appearance of each new cavity formed. The basic groundwater flow equation given below was solved by the finite element theory using Galerkin's weighted-residual method.

$$\frac{\partial}{\partial x}\left(K_x b \frac{\partial h}{\partial x}\right) + \frac{\partial}{\partial y}\left(K_y b \frac{\partial h}{\partial y}\right) + N + q_p + \frac{K_o}{b_o}(h_o - h) = S\frac{\partial h}{\partial t}$$

where
- h - piezometric head in aquifer
- b - saturated thickness of aquifer
- b_o - thickness of aquitard above aquifer
- h_o - piezometric head above aquitard
- K_x, K_y - Hydraulic conductivities in x, y directions
- K_o - Vertical hydraulic conductivity in aquitard
- N - Vertical recharge to a phreatic aquifer
- q_p - Pump flow rate
- S - Storage coeficient
- t - time

Linear triangles were used to discretize the domain and the piezometric head was assumed to vary linearly in the triangular element. The velocity in each element thus becomes a constant and only varies from one element to another. Boundary conditions on the periphery of the domain could be either specified head or specified flow rates. The computer program that was developed, was checked against an analytic solution and found to be accurate. Finally, the model was applied to the underground coal gasification sites in Hanna, Wyoming.

DESCRIPTION OF COMPUTER PROGRAM

The element equations were derived from equation 1 using the Galerkin weighted residual method. The equations were then assembles to form a global matrix and the matrix solved using a banded Gauss elimination subroutine (LEQT1B) provided in the IMSL package. The program, written in FORTRAN 5, can handle confined or unconfined aquifers and steady or unsteady flows. If the aquifer is confined, a leaky aquitard above the aquifer can be modeled. Any number of pumps can be placed at the nodes of the network. If the aquifer is unconfined, recharge is assumed to be constant in an element but can be varied from element to element. The program will calculate and print out the velocity in each element of the network as well as calculate the location of freshwater toes anywhere in the network. A freshwater toe is located at the intersection of a phreatic surface and a lower impermeable boundary. Beyond the toe, the saturated thickness of the water is not set to zero but to an arbitrarily small value, BTOE. In this way, changes in the location of the toe can be followed within a fixed network.

COMPARISON WITH ANALYTIC SOLUTION

After debugging the program, a theoretical solution to a problem was sought that would test the accuracy of the numerical solution. Such a problem was found in reference (5). This problem is related to the response of a finite-diameter to an instantageous charge withdrawal of water and is similar to the creation of a cavity in an aquifer. For example, a well 150 feet in diameter exists in a horizontal aquifer 30 feet thick as in Figure 1. Initially ($t < 0$), the piezometric head in the aquifer and well is at elevation 100 feet. At $t = 0$, the water level in the well is suddenly reduced to elevation 50 feet, simulating the creation of a cavity. The water from the aquifer begins to flow into the well and raises the water level in the well. This rise in the water level in the well can be simulated by the numerical model and its results compared to the analytic solution. Because of axial symmetry, the numerical simulation considered a pie-shaped element network with a central angle of 30^o (See Figure 2). Figure 3 shows the comparison of the analytic and numeric results. Because of the size of the well, the water rises very slowly, however, the comparison is good.

DESCRIPTION OF HANNA UCG SITES

The Hanna coal seam has a thickness that varies from 22 feet at the northwestern corner to 30 feet at the southeast. The bed dips generally in the northeast direction. Pump tests have indicated that the coal seam is anisotrophic with the maximum principal conductivity lying North 45^o East. This direction was then taken to be the X axis, the

maximum principal conductivity becoming K_x. These and other data were obtained from references (6, 7, 8, 9) and discussions with personnel of the University of Wyoming Research Corporation. Despite the availability of these data, there were still many input parameters to the model that had to be based on judgements. These parameters include the pre-burn piezometric head distribution, the volume of the cavities and the porosity and conductivity of the rubble in the cavity.

RESULTS OF HANNA SIMULATION

The area around the Hanna burn sites was discretized into 918 triangular elements and 486 nodes as shown in Figure 4. Small triangles are used around each burn site where steep piezometric head gradients are expected and large triangles were used where the gradients are low. The sub-routine LEQT1B from the IMSL package takes between 3 and 4 seconds to solve the 486 simultaneous equations on the CYBER 170/760 computer. Before simulating the unsteady flow conditions in the Hanna network, it was necessary to determine the most appropriate value of DT, the time interval, for this network. Large values of DT will result in inaccuracy and it was necessary to determine that value of DT that will result in acceptable errors. Figure 5 shows the piezometric head variation just after the formation of a cavity using different values of DT. It was felt that if a DT of 1 week was used, the resulting accuracy would be satisfactory. Using this value of DT, a simulation run was made for a real time of 1 year starting in March 1974. The output at the end of this run was then used as the input to a simulation run of the next year. This was repeated until the simulation reached the end of 1985.

The results of these simulation runs are presented in Figure 6. There are five major cavities; Hanna I, Hanna II (Phase I), Hanna II (Phase II and III), Hanna III and Hanna IV. The time of formation of each cavity is taken to be the time when the burn was completed. The computer simulation provided the time when the cavities filled and indicated that at the present time Hanna III and IV are still filling; a fact verified by monitoring well observations. The simulation runs projected that Hanna IV will fill in February 1985. Hanna III remained unfilled at the end of the simulation runs (December 1985).

Two computer-generated maps of contours of piezometric head are presented in Figures 7 and 8. In the first map, the Hanna I cavity has filled up, the Hanna II cavities are filling and Hanna III and IV have not formed yet. In the second map, Hanna I and Hanna II (Phase I) cavities are filled and the remaining three cavities were filling. Hanna IV had the most significant drawdown. Hanna II (Phases II and III) was almost full and hence there was very little drawdown around this cavity. Hanna III showed no drawdown at all around it. This anomalous behavior of Hanna III was puzzling until a crossection through this cavity was plotted (Figure 9). The coal seam outcrops on the land to the left of the figure. A freshwater toe is created and the aquifer is partly unconfined with the remaining portion confined. At t=0, the initial piezometric head is shown. When the Hanna III cavity was formed, the water level in the cavity was at the bottom. Water from the aquifer caused the water level to rise and the extent of the unconfined flow can be seen. The free surface profiles, 1 and 8 years after the burn are also shown and it can be seen that the water level eight years after the burn is actually lower than it was one year after the burn. Thus, Hanna III does not show the same kind of piezometric head drawdown as the other cavities.

SUMMARY

1) A finite element model of groundwater flow has been developed that can handle the generation and filling of large internal cavities.

2) The computer code has been checked for accuracy against an analytic solution and found to be satisfactory.

3) Simulation runs of the Hanna site have been made till the end of 1985. The simulations give the time of filling of all the burn sites except Hanna III. This burn is very close to the outcrop and flow in and out of this cavity occurs under phreatric conditions.

REFERENCES

1) G. N. Craig, II, L. K. Burns, F. G. Ethridge, T. F. Laughter, A. D. Youngberg. "Overburden Characterization and Post Burn Study at the Hanna, Wyoming, Underground Coal Gasification Site: Stratigraphy, Depostional Environments and Minerology, Hanna Formation. United States DOE/LC/10496-T1 (DE82009053) March 1982.

2) A. D. Youngberg, J. E. McClurg and J. G. Schmitt. "Depositional Environments, Subsurface Stratigraphy, and Post-Burn Characterization of the Paleocene-Eocene Hanna Formation at the Hanna, Wyoming Underground Coal Gasification Site: Hanna III Experiment. United States DOE/LC/-RI-83-1 (DE83005076) January 1983.

3) D. N. Contractor. "A Two-Dimensional Finite Element Model of Salt Water Intrusion in Groundwater Systems,". Technical Report No. 26, Water and Energy Research Institute of the Western Pacific, University of Guam, Mangilao, Guam, October 1981.

4) H. F. Wang, M. P. Anderson. "Introduction to Groundwater Modeling Finite Difference and Finite Element Methods", W. H. Freeman and Company, San Francisco, 1982.

5) H. H. Cooper, Jr., J. D. Bredehoeft, I. S. Papadopuloo. "Response of a Finite Diamter Well to an Instantaneous Charge of Water", Water Resources Research, Volume 3, No. 1, 1967.

6) Radian Corporation. "Relicensing Application; Appendix D-5 Geologic Assessment, Hanna Experimental In-Situ Coal Gasification Project; Final Report". Austn, Texas, February 1981.

7) Radian Corporation. "Relicensing Application; Appendix D-6 Hydrologic Evaluation of the Hanna Coal Gasification Project, Final Report". Austin, Texas, February 1981.

8) A. D. Youngberg, R. D. Santoro. "Hydrogeologic Evaluation of the Hanna Coal Gasification Site", Proceedings of the Seventh Underground Coal Conversion Symposium, U. S. Department of Energy, September 811, 1981.

9) R. Michael Boyd. "Post-Burn Analysis Techniques Applicable to Underground Coal Gasification", Proceedings of the 2nd Annual Underground Coal Gasification Symposium, Morgantown, West Virginia, August 10-12, 1976.

FIGURE 1

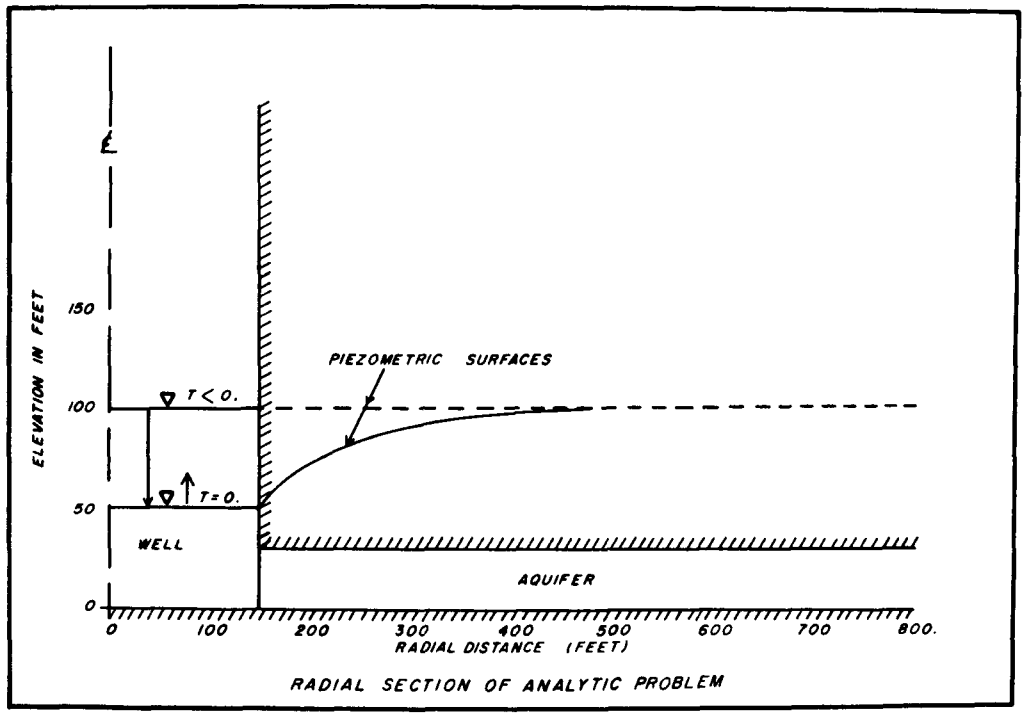

RADIAL SECTION OF ANALYTIC PROBLEM

FIGURE 2

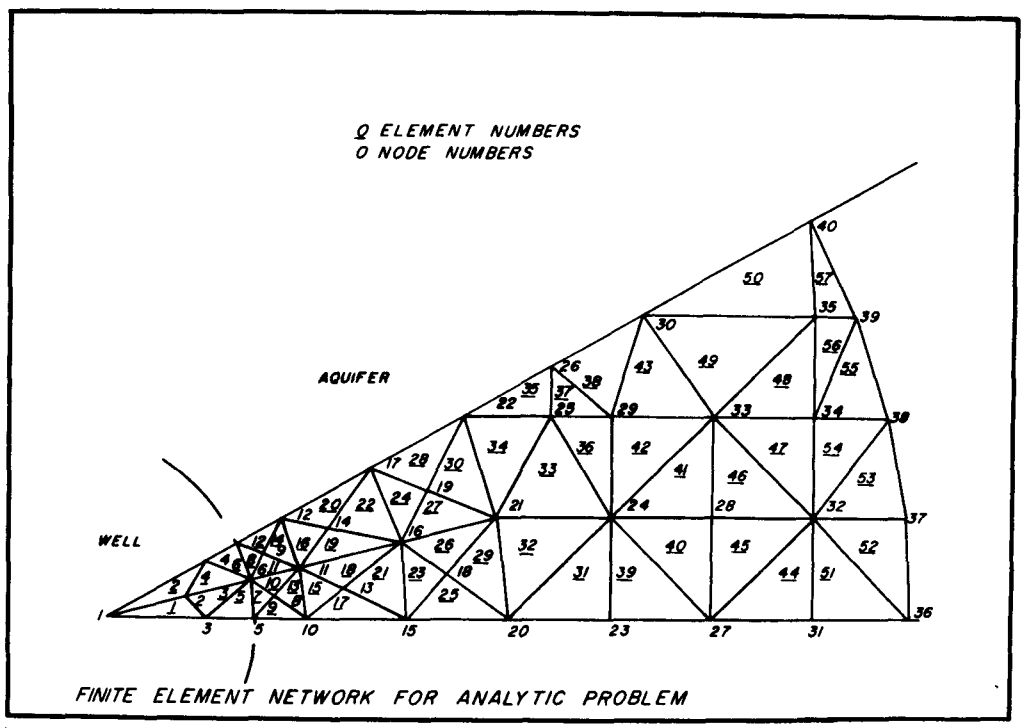

FINITE ELEMENT NETWORK FOR ANALYTIC PROBLEM

FIGURE 3

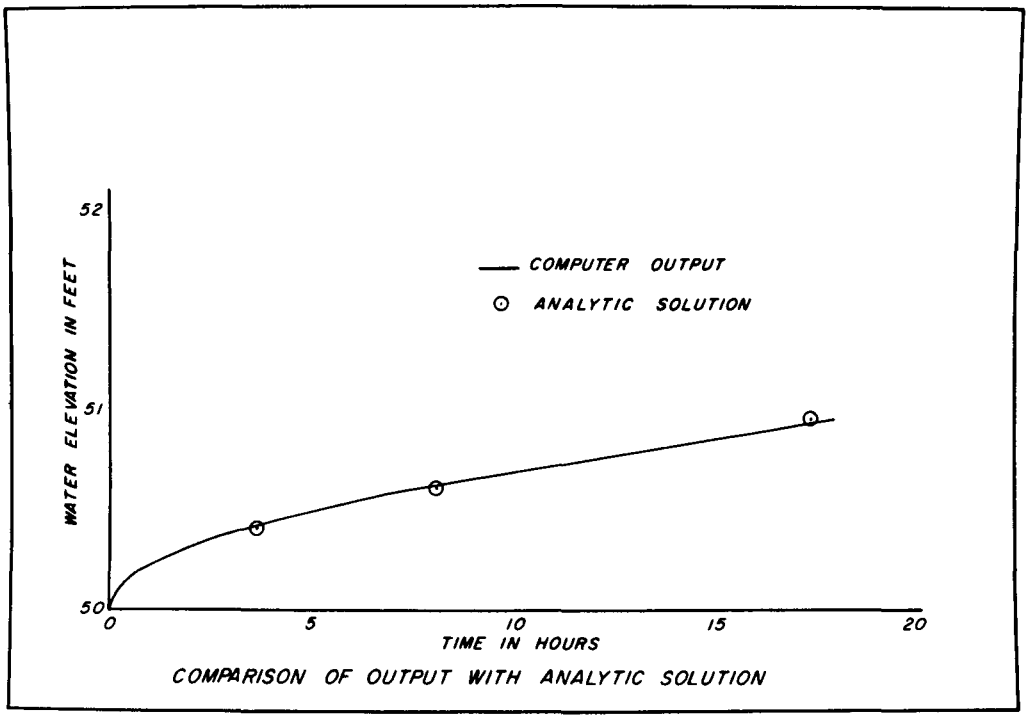

FIGURE 4

Numerical grid distribution
Hanna, Wyoming UCG sites

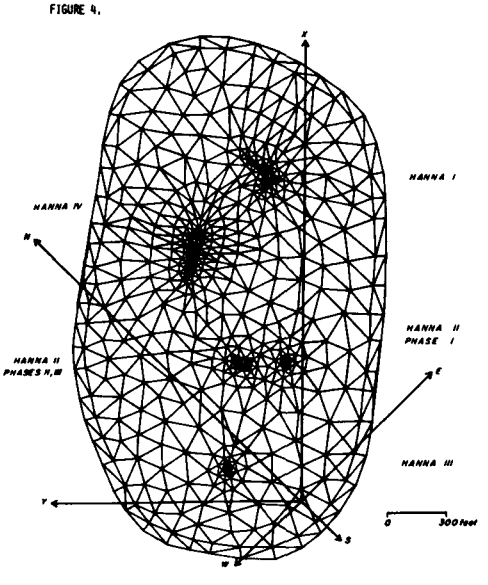

FIGURE 5

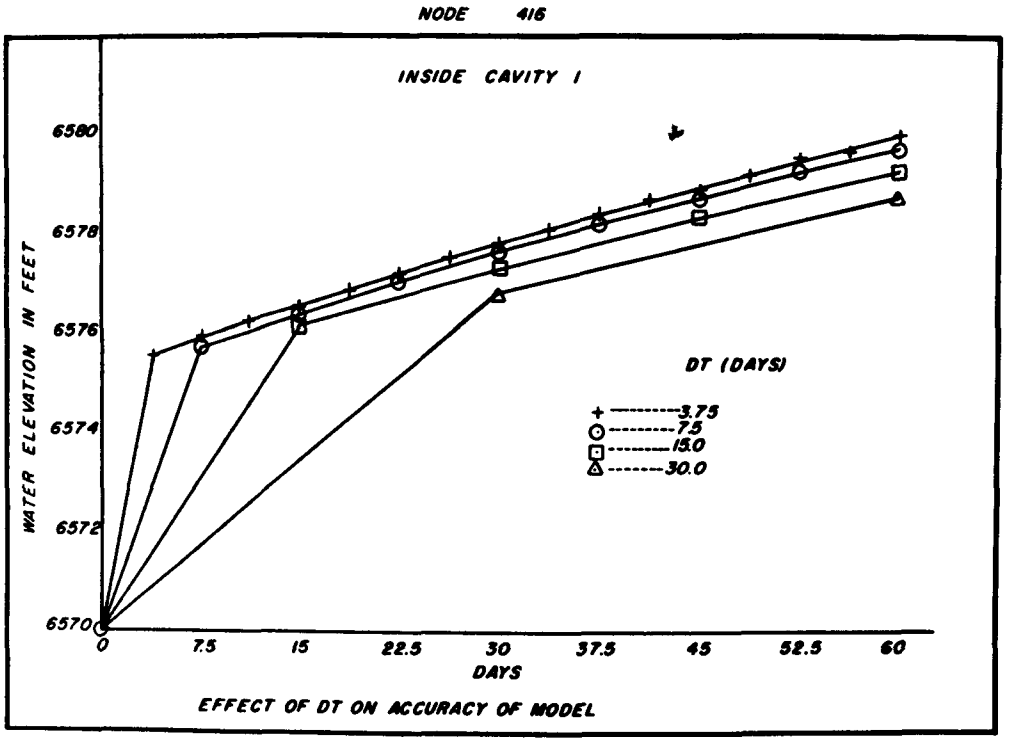

EFFECT OF DT ON ACCURACY OF MODEL

FIGURE 6

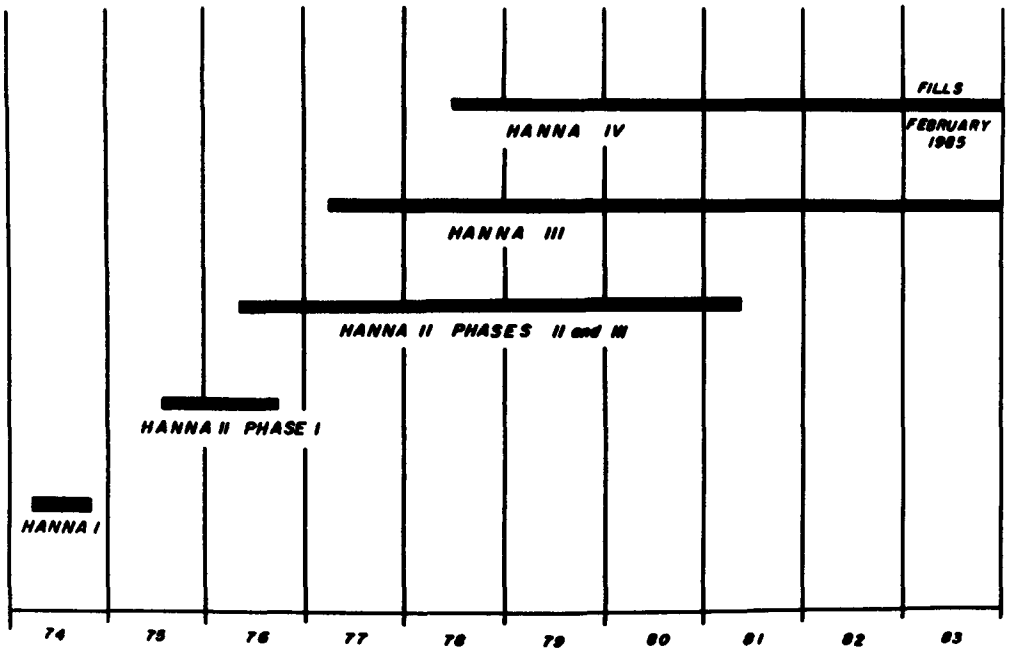

TIME SCALE OF EVENTS IN HANNA SIMULATION

FIGURE 7
Contour Map of Piezometric Head in April 1976

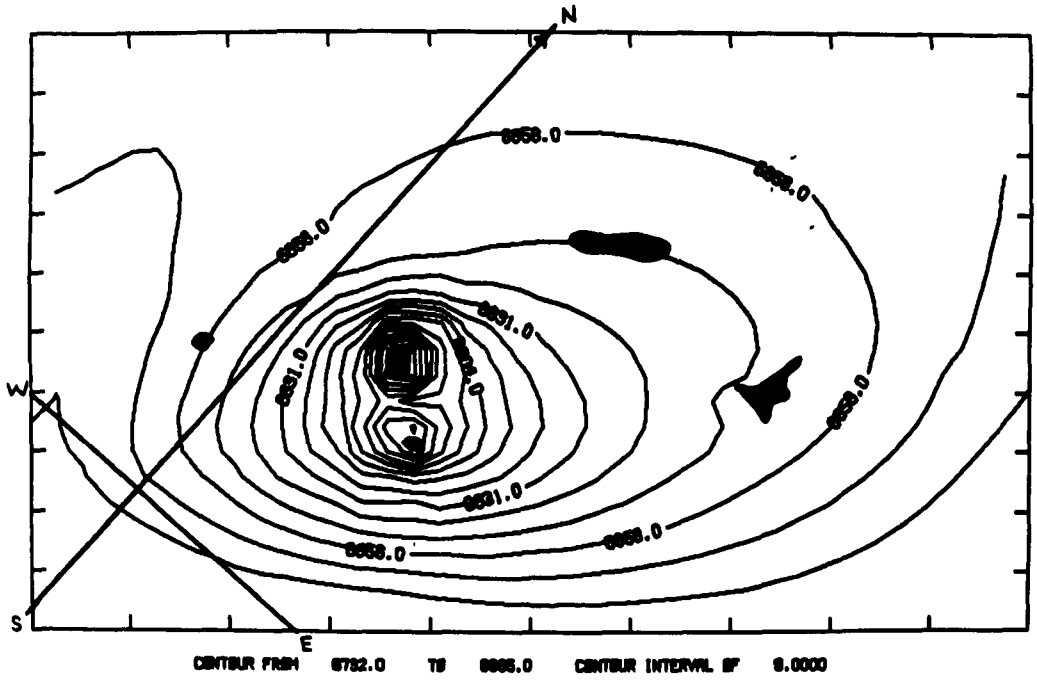

FIGURE 8
Contour Map of Piezometric Head in July 1979

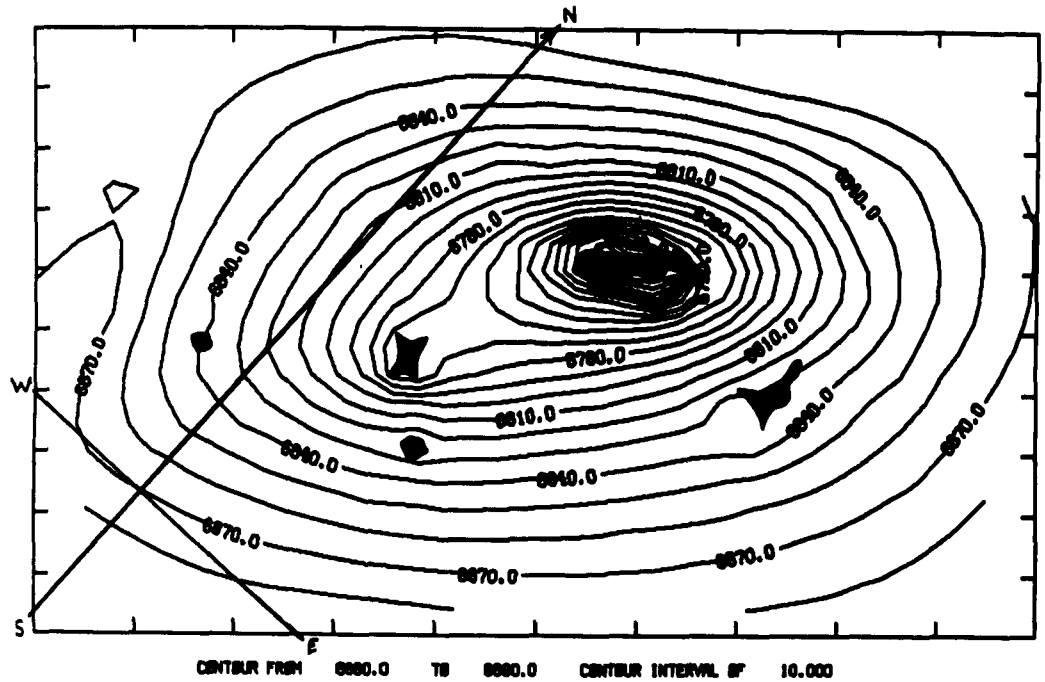

FIGURE 9

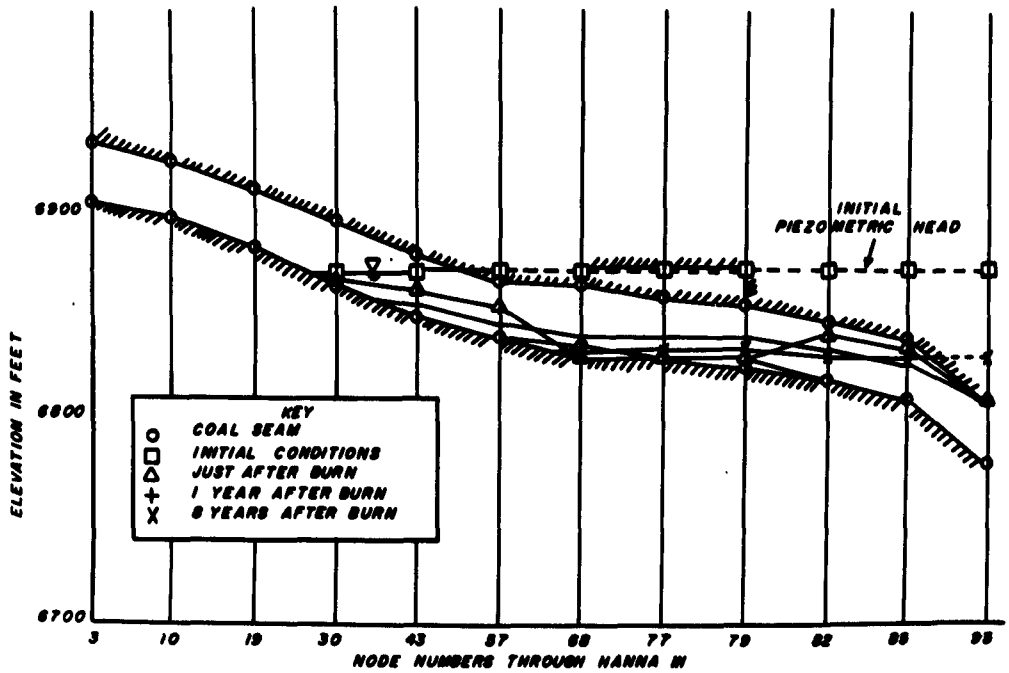

CROSSECTION THROUGH HANNA III

5.1 ECONOMIC BENEFITS FROM BURNOUT OF ABANDONED COAL MINE FIRES

by

Robert F. Chaiken[1/]

INTRODUCTION

Burnout Control of abandoned coal mine fires was developed at the U.S. Bureau of Mines as a means for completely burning out the coal in situ while maintaining control of the heat and fumes produced (1, 2). The control process also enables the thermal energy developed underground to be brought to the surface as high temperature flue gas suitable for powering an on-site waste heat boiler/steam turbine electrical generation plant. Since accelerated coal burning will lead to earlier self-extinguishment of the mine fire after the fuel is totally consumed, Burnout Control offers a means for eliminating a serious environmental problem while at the same time converting a coal waste to a coal resource.

Unlike costly conventional methods of extinguishing abandoned coal mine fires (such as excavation and quenching), Burnout Control through the production and sale of electricity can lead to net revenues which would make the process economically viable. This paper documents some of the cost factors involved in determining the net revenues from Burnout Control. Net cash flow analyses indicate the possibility of sufficient rates of return from relatively low capital investments to attract the interest of private investors.

1/ U.S. Department of the Interior, Bureau of Mines, Pittsburgh Research Center, P.O. Box 18070, Pittsburgh, PA 15236.

BACKGROUND

Burnout Control Process

The control technique for burnout of underground coal mine fires involves exhaust ventilation of the mine at vacuum levels readily obtained with available fan systems (e.g., 35,000 scfm at 60-in H_2O gage). Placing the mine fire at negative pressure relative to one atmosphere induces air flow into the fire zones through strategically placed boreholes to accelerate burning while exhausting produced heat and fumes to the surface. This is depicted in figure 1 which is an artist's rendition of the Burnout Control process without heat utilization. Figure 2 is a photograph of the Burnout Control ventilation system constructed and operated at the site of an abandoned coal mine fire.

In 1982, the Bureau completed a four month continuous controlled burn of a shallow (approximately 35-ft overburden) mine in the Pittsburgh seam (Calamity Hollow Mine Fire Project). Thermal power levels up to 6 MW(t) and exhaust temperatures up to 1,800° F were developed from a one acre fire zone (see figure 3). In total, approximately 1,100 tons of coal were consumed with a time weighted average exhaust output of 3.1 MW(t) at 1,100° F. Some of this work has been reported briefly at previous UCC Symposia (3, 4). Full details of the work have and/or will appear shortly in a five part series of Bureau of Mines' Reports of Investigations (5-9). It is believed that sufficient technical data were developed during the

Calamity Hollow Mine Fire Project to allow examining the economic feasibility of firing small electrical power plants with heat from abandoned coal mine fires.

Applying Burnout Control for Electricity Production

The potential for Burnout Control in eastern United States is believed to be quite large. It has been estimated that there are some 116 million tons of coal endangered by some 64 abandoned coal mine fires in the eastern coal producing states (10). These mine fire sites are undoubtedly dispersed and probably variable in size. These factors call for the use of small mobile power plants (up to approximately 5 MW(e)) which can be relocated as required on a given fire site or to other mine fires. Power plants of this size should be well suited for firing by a single Burnout Control ventilation system, which based on the Calamity Hollow field trial might control as much as 30 acres of fire in underground mine workings. Commercialization of the process is envisioned as one or more Burnout Control/Power Plant modules operating as a mobile surface facility, each interconnecting with the extensive electrical transmission network which covers much of the eastern United States. Sale of electricity into this network would be arranged through individual utility companies - possibly under Section 210 of the Federal Public Utility Regulatory Policies Act (PURPA) of 1978.

ECONOMIC ANALYSIS

This section is devoted to economic analyses of the costs and rates of return to be expected from a single Burnout Control/Power Plant module operating as described previously. The analyses involve net cash flow calculations using various input data for capital costs, operating costs, and expected revenues. Generalizing the treatment of these variables enables a sensitivity analysis to be made of the significance of such factors as power plant size, resource size, price of electricity, etc.

Basic Economic Model

1. Coal Resource, QT BTU (total for single module and location)

An abandoned mine is assumed to contain 50% of the coal originally present in the coalbed. Undergrund heat loss from burnout is assumed to be 10% (11). From bed thickness, area and heating value, QT is readily estimated. The following table gives several examples used in this paper based on a 6-ft thick seam of 13,900 BTU/lb coal:

Acres	Remaining coal, tons	QT, BTU
5	26,000	0.66×10^{12}
10	53,000	1.3×10^{12}
20	110,000	2.6×10^{12}
30	160,000	4.0×10^{12}

2. Gross Earning from Sale of Electricity, EG ($/yr)

It is assumed that the overall conversion efficiency from heat to electricity is 20%, with 95% of electricity produced sold at S, $/KW-hr. The power plant of size K, KW(e) operates 8,000 hrs/yr.

$$EG\ (\$/yr) = 0.95*8{,}000*S*K$$

3. Lifetime of Resource, L (yr)

$$L\ (yr) = \frac{5.86 \times 10^{-5}*QT}{8{,}000 * K}$$

The constant in the numerator is the product of the conversion factor for KW-hr to BTU and the assumed conversion efficiency for heat to electricity.

4. Capital Costs, CC ($)

The cost of the installed Burnout Control ventilation system is assumed to be $500,000 invariant to scaling. The turnkey cost of the power plant scales linearly with size as CP ($/KW).

$$CC\ (\$) = K*CP + 5 \times 10^5$$

5. Operating Costs, OP ($/yr)

It is assumed that OP is invariant with size of power plant since it is controlled primarily by labor costs for a 3 shift/day operation.

6. Profit Before Taxes, BPR ($/yr)

$$BPR\ (\$/yr) = EG - OP$$

7. Tax Calculation, TAX ($) for the Nth year of operation.

$$TAX\ (\$) = TAX*\left[BPR - DPR*CC\right] - TCR*CC$$

where TAX = 0.46, the corporate tax rate
TCR = 0.1, the investment tax credit calculated for N = 1 only, but with any excess credit carried forward to subsequent years until expended
DPR = fractional annual depreciation of capital costs (assumed straight line)

8. Net Annual Profits After Taxes, NPR ($) for Nth year of operation

$$NPR\ (\$) = BPR - TAX\ (\$)$$

9. Payback Period, PB (yr)

After each year of operation, all net profits after taxes can be used to payback capital costs. The time to recoup CC (i.e., the payback period) is then determined by interpolation between years n and n + 1 when the quantity

$$\sum_{n=1}^{N} (NPR)_n - CC$$

changes from a negative to a positive value.

10. Salvage Value, SALV ($)

It is assumed that the salvage value of major equipment after the Nth year of operation is the non-depreciated value of CC less a one time demobilization cost of $100,000 corrected for the tax write-off for that year.

$$SALV\ (\$) = (1-N*DPR)*CC - (1-TAX)*10^5$$

11. Return on Investment, ROI ($)

The total dollar value returned for N years of operation is calculated as:

$$ROI\ (\$) = \sum_{n=1}^{N} (NPR)_n + SALV$$

12. Internal Rate of Return, IRR (dimensionless)

IRR is the effective net annual rate of return from investing CC ($). It is defined through the net cash flows, $(NCF)_n$ by the equation (12):

$$CC = \sum_{n=1}^{N} (NCF)_n\ (1 + IRR)^{-n}$$

where $(NCF)_{n\neq N} = (NPR)_n$

$$(NCF)_N = (NPR)_N + SALV$$

IRR takes into account the present value cost of using capital for n years as well as the effect of taxes on the rate of return. For example, a simple annuity investment of CC dollars paying interest, I of 18% annually will yield after taxes an IRR = (1 - TAX)*I or IRR = 0.54*0.18 = 0.0972

A close but not necessarily exact solution for IRR can be obtained by recognizing that except for n=1, the value of all $(NPR)_n$ will probably have the same or nearly the same dollar value. For n=1, the investment tax credit, TCR is expected to significantly increase the value of NPR over that of subsequent years. As such, it is possible to approximate the equation defining IRR as:

$$CC = (1 + IRR)^{-1}*(NPR)_1 + \overline{NPR} \sum_{n=2}^{N} (1 + IRR)^{-n} + SALV*(1 + IRR)^{-N}$$

where $\overline{NPR} = \frac{1}{N-1}\left[\sum_{n=1}^{N} (NPR)_n - (NPR)_1\right]$,

an average value for years n>1

Since the summation term involving IRR is now merely a geometric series whose value can be expressed as:

$$\sum_{n=2}^{N} (1 + IRR)^{-n} = \frac{(1 + IRR)^N - 1}{IRR*(1 + IRR)^N} - \frac{1}{(1 + IRR)},$$

IRR can be solved for explicity by a numerical iteration technique.

13. Additional Financial Factors

While there would be no difficulty including in the model such additional financial parameters as coal royalties, depletion allowances, pollution abatement and energy tax credits, and interest on loans, they are not considered in the present treatment of economic benefits.

Results and Discussion

The predictive value of the described economic model depends to a large degree on the validity of the assumptions and the values taken for the required input data, many of which will be site selective.

However, reasonable estimates for input data can be made, and their values modified to provide a sensitivity analysis of the parameters. In this manner, a degree of reliability can be ascertained as to the overall economic benefits of the process; for example, does profit depend very strongly on whether a given input exceeds a "reasonable" range of values. Of particular interest in this analysis is the effect of power plant size, resource size, and selling price on the lifetime (L), payback period (PB), and rate of return (IRR).

Figure 4 depicts calculated curves for L and PB for various sized power plants (expressed in megawatts), coal resources, and electricity selling prices, using common cost and depreciation data (i.e., CP = 1000 \$/KW; OP = 6×10^5 \$/yr, DPR = 0.1). The predicted payback periods for a given S apparently fall on a common curve which crosses the lifetime curves. The effect of a change in S is to shift the payback curves either upward (decreasing S) or downward (increasing S). In choosing a coal resource site (i.e., QT), it would be desireable to have a payback period less than the lifetime of the site. At S = .06 \$/KW-hr, this would occur for resources greater than 2.6×10^{12} BTU (i.e., a 20 acre site in a 6-ft coal seam), and power plants less than 4 or 5 MW(e) - values which are conceptually reasonable for applying Burnout Control. While it is not essential to assume the criteria that PB should be less than L, its acceptance will establish limits for acceptable values of QT, K and S. As figure 4 indicates, these limits are probably not overly restrictive for commercial application.

Figure 5 shows how the internal rate of return at S = 0.06 \$/KW-hr is expected to vary with QT and K, using the same common cost data as figure 4. The shape of the curves indicate that power plants in excess of 4 MW(e) would be required to achieve IRR values exceeding 10% (i.e., approximately equivalent to 18% bank interest). These results in conjunction with those in figure 4 and the requirement for mobility suggest that a power plant of 5 MW(e) might be an optimum size. It also suggests that Burnout Control/Power Plant modules might be standardized at this size for general use. Such standardization would be highly beneficial from the viewpoint of design, construction, maintenance and lower capital costs.

Figure 6 depicts how the return on a capital investment of \$5.5. million for a 5 MW(e) module will vary with the selling price of electricity. As expected, both IRR and ROI vary steeply and almost linearly with S, with the internal rate of return ranging from near zero (break even point) at about \$0.025/KW-hr to about 25% at \$0.08/KW-hr. The corresponding return on investment (ROI) ranges from about \$4 million to \$12 million. At S = 0.07 \$/KW-hr, the return would almost double the original investment in the 6 year lifetime of the 4×10^{12} BTU coal resource.

The effects of variations in operating costs, power plant costs and depreciation shcedules on the economics of a 5 MW(e) module were also examined. The specific results and input data are shown in table 1. It is readily seen that the cost of the power plant has a major influence on the expected payback period and rate of return. At CP = 600 \$/KW, which may not be unreasonable for a standardized power plant, the IRR approaches 30%, with a PB of about 3 years. Both these factors should attract the interest of private investors.

Changes in depreciation schedule and operating costs have a measurable but much less significant effect on the economic benefits. Lower values of PB are favored by higher rates of depreciation and lower operating costs, while higher values of IRR are favored by both lower rates of depreciation and lower operating costs. While there would be distinct economic benefits to decreasing OP, the benefits of altering DPR would depend on the degree of importance given to a lower PB as versus a higher IRR.

It is interesting to now use the results generated above to describe an "optimistic" (but still reasonable) case for a fire in the Pittsburgh seam at a site similar to that at Calamity Hollow. The coal resource for this site was estimated to be approximately 9,500 tons/acre with an average recoverable heating value of 12,000 BTU/lb (5). The assumption that 30 acres will constitute a single location for a Burnout Control/Power Plant module yields a value of QT = 6.8×10^{12} BTU. The following input data: K = 5 MW(e); S = 0.06 \$/KW-hr; DPR = 0.05; CP = 600 \$/KW; OP = 4×10^5 \$/yr then yield the calculated results shown in table 2. The economic benefits of this case are self-evident.

CONCLUSIONS

It is clear from the economic analyses that Burnout Control with on-site utiization of recovered heat for electricity production can be highly profitable with relatively small semi-mobile power plant facilities (approximately 5 MW(e)) feeding into the public utility network or supplying third party users.

Calculated returns on investments for a single Burnout Control/Power Plant module at a single fire location appear quite promising, even for "conservative" estimates of input data. For "optimistic" estimates, net internal rate of returns of about 33% with a payback period of 3 years might be expected.

The re-use of modules at more than one fire site was not considered explicity in the present analysis. However, it can be inferred from the calculated sensitivity of economic benefits to power plant costs, that even more attractive profits would accrue from longer term repeated use of the Burnout Control/Power Plant modules.

REFERENCES

(1) R. F. Chaiken, "Controlled Burnout of Wasted Coal on Abandoned Coal Mine Lands", U.S. Bureau of Mines RI 8478 (1980) 23 pp.

(2) R. F. Chaiken, "Method for Controlled Burnout of Abandoned Coal Mines and Waste Banks", U.S. Patent No. 4387655 (June 14, 1983).

(3) R. F. Chaiken, L. E. Dalverny, M. C. Irani and I. A. Zlochower, "Burnout Control of Fires in Abandoned Coal Mines and Waste Banks by In Situ Combustion", Proceedings of the Seventh Underground Coal Conversion Symposium, Fallen Leaf Lake, California (Sept. 8-11, 1981), sponsored by the U.S. Department of Energy (CONF-810923) pp. 380-394.

(4) R. F. Chaiken, "Controlled Burnout at an Abandoned Coal Mine Fire", Proceedings of the Eigth Underground Coal Conversion Symposium, Keystone, Colorado (August 15-19, 1982), sponsored by the U.S. Department of Energy (SAND 82-2355) pp. 511-514.

(5) M. C. Irani, R. F. Chaiken, L. E. Dalverny, G. M. Molinda, and K. E. Soroka, "Calamity Hollow Mine Fire Project (In Five Parts) 1. Development and Construction of the Burnout Control Ventilation System", U.S. Bureau of Mines RI 8762 (1983) 29 pp.

(6) R. F. Chaiken, L. E. Dalverny, E. F. Divers, A. G. Kim, and K. E. Soroka, "Calamity Hollow Mine Fire Project (In Five Parts) 2. Operation of the Burnout Control Ventilation System", U.S. Bureau of Mines RI (in preparation).

(7) L. E. Dalverny, R. F. Chaiken, and K. E. Soroka, "Calamity Hollow Mine Fire Project (In Five Parts) 3. Instrumentation for Combustion Monitoring, Process Control and Data Recording", U.S. Bureau of Mines RI (in preparation); also see Paper 83-HT-46 presented at the ASME-AIChE National Heat Transfer Conference, Seattle, Washington (July 24-28, 1983).

(8) R. F. Chaiken, E. F. Divers, A. G. Kim, and K. E. Soroka, "Calamity Hollow Mine Fire Project (In Five Parts) 4. Quenching the Fire Zone", U.S. Bureau of Mines RI (in preparation).

(9) K. E. Soroka, R. F. Chaiken, L. E. Dalverny, and E. F. Divers, "Calamity Hollow Mine Fire Project (In Five Parts) 5. Excavation and Evaluation of the Fire Zone", U.S. Bureau of Mines RI (in preparation).

(10) W. Johnson and G. C. Miller, "Abandoned Coal- Mined Lands- Nature, Extent, and Cost of Reclamation", BuMines Spec. Pub. 6-79 (1979) 29 pp.

(11) R. F. Chaiken, "Heat Balance in In Situ Combustion", U.S. Bureau of Mines RI 8221 (1977) 11 pp.

(12) L. D. Schall and C. W. Haley, "Introduction to Financial Management", McGraw-Hill Book Co., New York (1977) pp. 214-223.

TABLE 2. - Economic Benefits for "Optimistic" Case of a Burnout Control/ Power Plant Module Operating in Pittsburgh Seam
($QT = 6.8 \times 10^{12}$ BTU; K = 5 MW(e), S = 0.06 $/KW-hr; DPR = .05; CP = 600 $/KW; $OP = 4 \times 10^5$ $)

n, yr	1	2	3*	4	5	6	7	8	9	10*
CC 10^6 $	3.5	0	→	→	→	→	→	→	→	→
EG 10^6 $	2.28	→	→	→	→	→	→	→	→	→
OP 10^6 $	.40	→	→	→	→	→	→	→	→	→
BPR 10^6 $	1.88	→	→	→	→	→	→	→	→	→
DPR 10^6 $	.18	→	→	→	→	→	→	→	→	→
TCR 10^6 $	.35	0	→	→	→	→	→	→	→	→
TAX 10^6 $	.78	→	→	→	→	→	→	→	→	→
NPR 10^6 $	1.45	1.10	→	→	→	→	→	→	→	→
**SALV 10^6 $	3.27	3.10	2.92	2.75	2.57	2.40	2.22	2.05	1.87	1.70
**ROI 10^6 $	4.72	5.64	6.56	7.48	8.40	9.32	10.2	11.2	12.1	13.0
**IRR, %	34.8	31.3	31.2	31.3	31.6	31.8	32.1	32.4	32.6	32.9

*Payback = 2.9 yrs; Lifetime = 10 yrs
**Values shown for year n refer to results if operation were terminated after year n.

CC = capital cost
EG = gross earnings
OP = operating cost
BPR = profit before taxes
DPR = depreciation
TCR = investment tax credit
NPR = profit after taxes
SALV = salvage value
ROI = return on investment
IRR = internal rate of return

TABLE 1. - Sensitivity Study for 5 MW Power Plant with Selling Price of $.06/KW-hr

QT 10^{12} BTU	CP $/KW	OP 10^5 $/yr	DPR frac/yr	Payback yrs	IRR frac/yr	ROI 10^6 $
0.66	1000	6	0.10	-	0.20	6.6
1.3				-	.15	7.2
2.6				-	.15	8.4
4.0				4.3	.16	9.7
8.0				4.3	.20	13.3
4.0	600			2.9	.28	8.1
	800			3.6	.21	8.9
	1000			4.3	.16	9.7
	1200			4.8	.13	10.4
	1000	4		3.9	.19	10.3
		5		4.1	.18	10.0
		6		4.3	.16	9.7
		7		4.5	.15	9.3
		6	0.05	4.8	.18	10.5
			.10	4.3	.16	9.7
			.12	4.1	.16	9.3
			.17	3.7	.14	8.4

QT = coal resource
CP = cost of power plant
OP = operating costs
DPR = depreciation
IRR = internal rate of return
ROI = return on investment

TABLE 2. - Economic Benefits for "Optimistic" Case of a Burnout Control/ Power Plant Module Operating in Pittsburgh Seam (QT = 6.8 x 10^{12} BTU; K = 5 MW(e), S = .06 $/KW-hr; DPR = .05; CP = 600 $/KW; OP = 4 x 10^5 $)

n, yr	1	2	3*	4	5	6	7	8	9	10*
CC 10^6 $	3.5	→	→	→	→	→	→	→	→	→
EG 10^6 $	2.28	→	→	→	→	→	→	→	→	→
OP 10^6 $	.40	→	→	→	→	→	→	→	→	→
BPR 10^6 $	1.88	→	→	→	→	→	→	→	→	→
DPR 10^6 $	.18	→	→	→	→	→	→	→	→	→
TCR 10^6 $	.35	0	→	→	→	→	→	→	→	→
TAX 10^6 $	.78	→	→	→	→	→	→	→	→	→
NPR 10^6 $	1.45	1.10	→	→	→	→	→	→	→	→
**SALV 10^6 $	3.27	3.10	2.92	2.75	2.57	2.40	2.22	2.05	1.87	1.70
**ROI 10^6 $	4.72	5.64	6.56	7.48	8.40	9.32	10.2	11.2	12.1	13.0
**IRR, %	34.8	31.3	31.2	31.3	31.6	31.8	32.1	32.4	32.6	32.9

*Payback = 2.9 yrs; Lifetime = 10 yrs
**Values shown for year n refer to results if operation were terminated after year n.

CC = capital cost
EG = gross earnings
OP = operating cost
BPR = profit before taxes
DPR = depreciation
TCR = investment tax credit
NPR = profit after taxes
SALV = salvage value
ROI = return on investment
IRR = internal rate of return

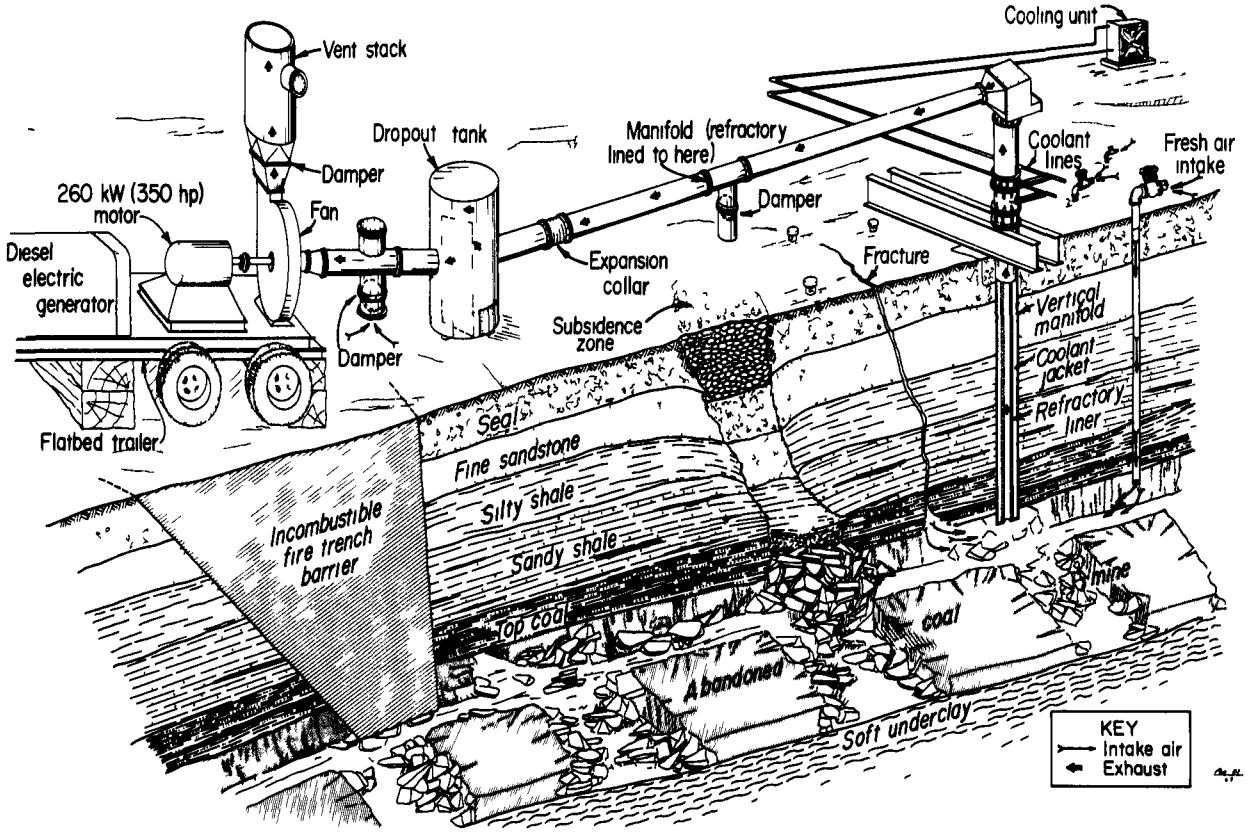

FIGURE 1. - Artist drawing of Burnout Control Process

FIGURE 2. - Photograph of Burnout Control Ventilation System at Calamity Hollow

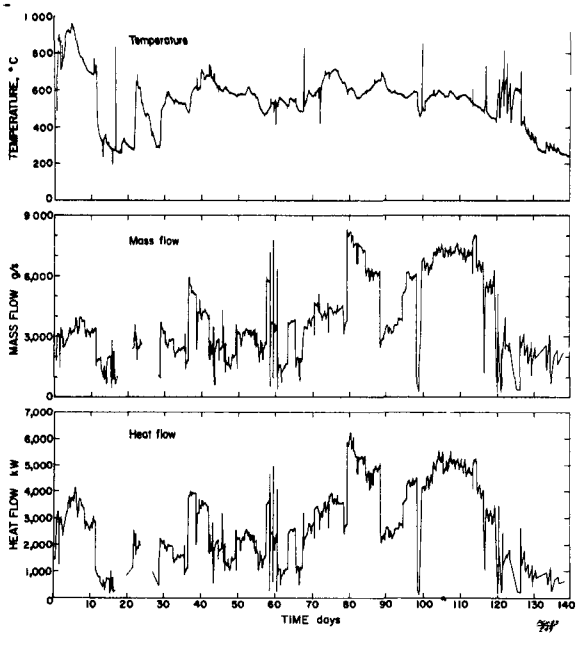

FIGURE 3. - Temperature, mass flow, and thermal power (station 1). Data from Calamity Hollow Mine Fire Project.

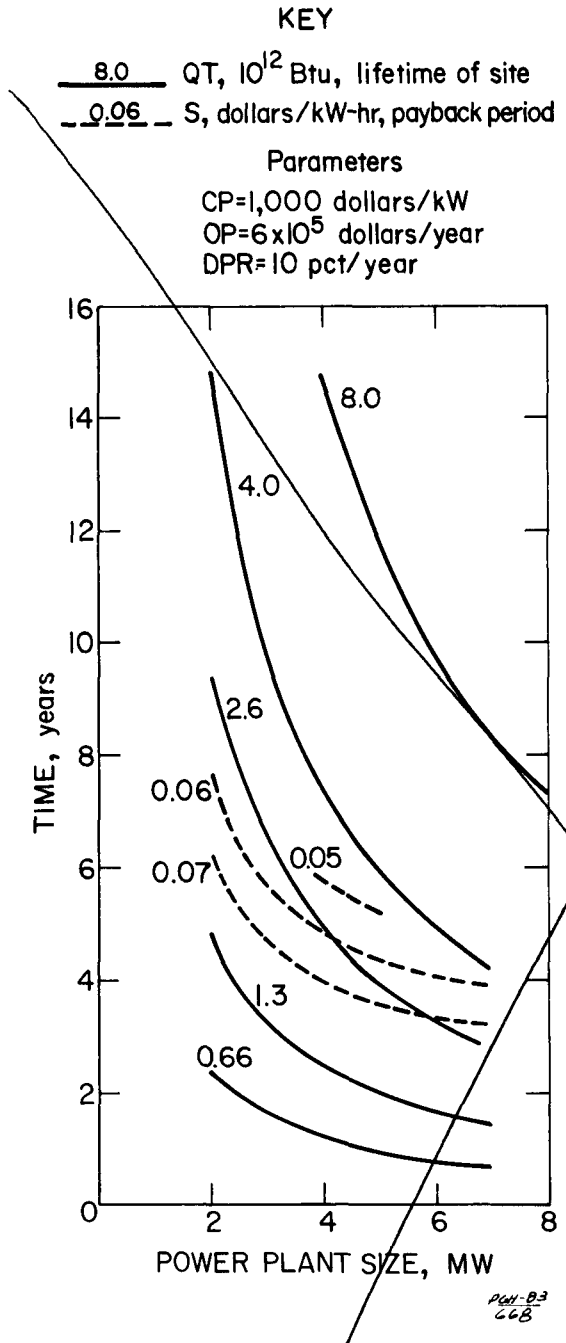

FIGURE 4. - Calculated relationship between power plant size, coal resource, lifetime, payback and selling price.

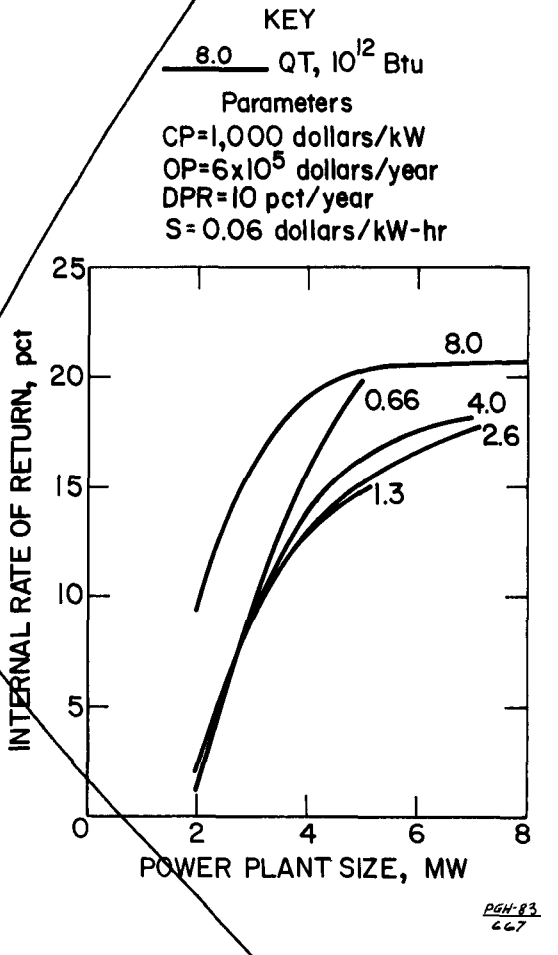

FIGURE 5. - Calculated Relationship between internal rate of return, power plant size, and coal resource.

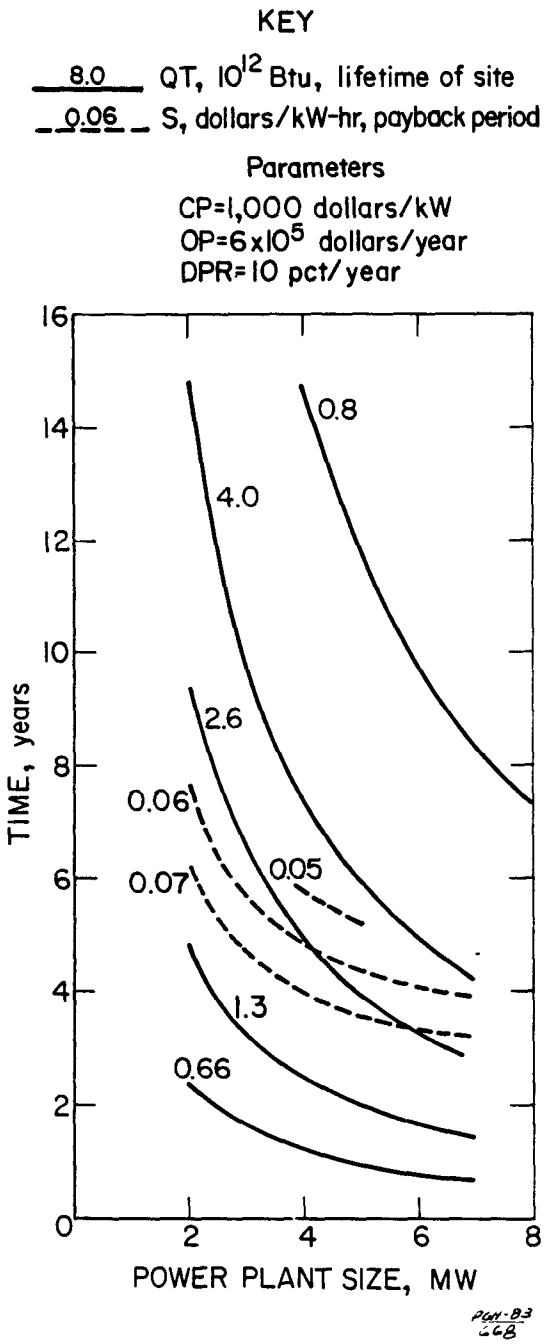

FIGURE 4. - Calculated relationship between power plant size, coal resource, lifetime, payback and selling price.

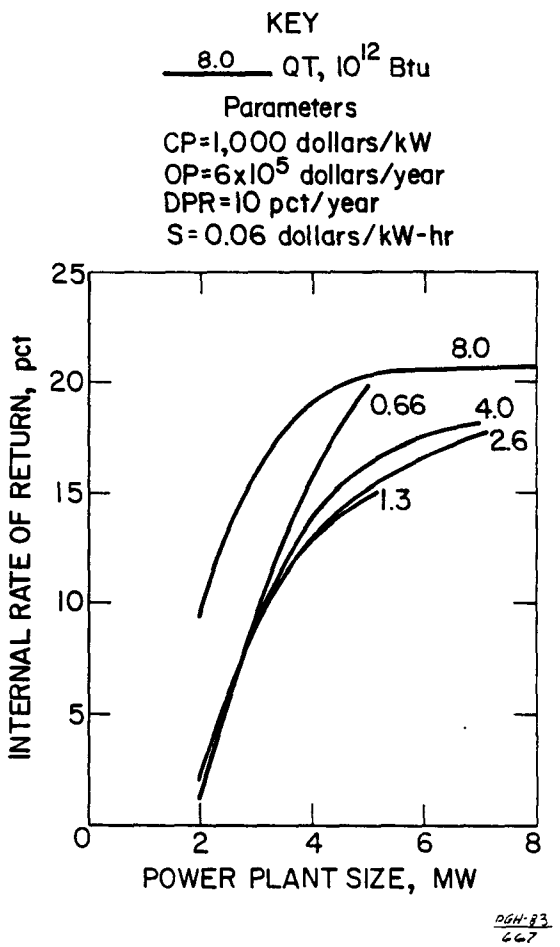

FIGURE 5. - Calculated Relationship between internal rate of return, power plant size, and coal resource.

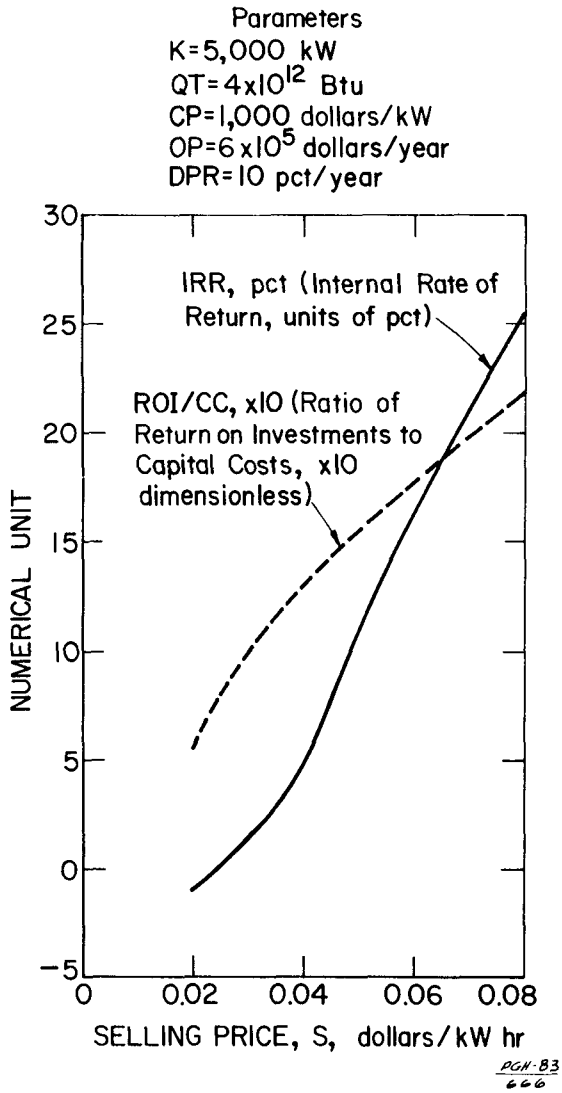

FIGURE 6. - Effect of Electricity Selling Price on Rate of Return and Return on Investment.

5.2 ECONOMIC FACTORS IN PROCESSING HIGH-METHANE CONTENT UCG-DERIVED GAS

by

A. James Moll
Earl D. Oliver
Dale R. Simbeck
Synthetic Fuels Associates, Inc.

ABSTRACT

Methane contents in fuel gas derived from underground coal gasification (UCG) as high as 25% have been reported in some field tests. High methane content appears to be a mixed blessing. On the positive side it indicates low oxygen consumption and decreased volume of gas to be processed per unit of fuel value. However, projected demands are stronger for liquids fuels and chemicals than for pipeline gas. Methane acts as a diluent in the carbon monoxide-hydrogen synthesis gas for purposes of reacting the mixture to make liquid products.

There are numerous options for processing high methane content synthesis gas streams depending on the product or products made. Three general product categories of product options are covered in this paper: production of methane (SNG) alone, co-production of SNG and a synthesis gas product such as methanol, and production of methanol alone. Process choices to be made in all categories include sulfur-tolerant or sulfur-free shift conversion, acid gas removal method, and sulfur recovery method. The all-SNG category also requires selection of a methanation heat removal method. The co-production category requires choice of cryogenic methane recovery or methanation of synthesis reactor purge gas. Forcing all-methanol production requires a decision on the process chosen for methane destruction, what stream to apply methane destruction, and whether to concentrate the methane by cryogenic separation.

The various process options are reviewed and the economic factors affecting the decision among options are discussed. The advantages and disadvantages of the process options are examined. The implications of the process choice to the viability of UCG are reviewed.

INTRODUCTION

High methane content in UCG-derived fuel gas indicates that the gasification process is probably efficient in terms of fuel yield and oxygen usage. The high methane content is highly desirable if methane (SNG) is the desired product. However, methane is an inert diluent if carbon monoxide-hydrogen synthesis gas is the desired product. Numerous process options are available to convert the methane to carbon monoxide and hydrogen, but at the price of increased investment and reduced energy efficiency.

UCG-derived gas is not unique among coal gasification processes in producing some methane. In fact only entrained processes produce essentially no methane. The commercialized Lurgi gravitating bed process typically produces a raw gas containing about 9% methane. Table 1 compares a typical UCG gas composition with those representative of surface gasification processes. Field experimental data show that the methane content of UCG-derived gas from steeply dipping seams can be much higher than from any surface gasifier.

DISCUSSION

Overall Process Options

The processing of UCG-derived gas for the production of methane (SNG) as the sole product is depicted in Figure 1. Two alternative flow schemes are shown depending on whether "clean" or "dirty" conditions for carbon monoxide shift conversion is used. "Dirty" shift conditions refers to carrying out the shift conversion reaction on sulfur-containing gas while "clean" shift means that the sulfur compounds have already been removed from the gas.

The high methane content expected in UCG-derived gas is a definite advantage for the production of SNG. The methane formed during gasification does not lead to high consumption of oxygen as carbon oxides do. Moreover, methanation requirements, including recycle gas cooling and compression, are reduced. Still the production of SNG requires considerable exothermic methanation with attendant increased costs and reduced energy efficiency.

The main advantage of the dirty shift option is that the gas stream can remain saturated in water vapor at the waste heat recovery outlet temperature. The remaining water vapor reduces the need for steam addition. An additional advantage is that only one stage of acid gas removal is required. On the other hand the sulfur-resistant shift catalyst needed for dirty shift may be somewhat more expensive than clean shift catalysts.

The co-production of SNG and methanol is a promising alternative to minimize investment and maximize fuel value of the products. One method of SNG methanol co-production is to direct some or all of the methane-rich methanol synthesis purge gas to a methanation reactor. Both clean and dirty shift options may be used in this configuration. Another method of co-production is to cryogenically separate the methane from the purified gas stream. Figure 2 shows both the purge gas and cryogenic separation methods, each using the dirty shift option. It is seen that there are numerous interdependent process choices to be made for SNG-methanol co-production.

The natural gas surplus in recent years has suggested to some observers that liquid fuels (usually methanol) or chemicals via synthesis gas are the most advantageous products from coal gasification. For the case of no SNG production the number of process options becomes even more numerous. Two of the process options are shown in Figure 3. One option is to cryogenically separate methane from the methanol purge gas and convert it to synthesis gas by autothermal reforming. Another option is sending the entire dirty gas stream through partial oxidation. However, more oxygen is required to partially oxidize the entire gas stream than only the methane content. It is noted that this option is equivalent to sending the output of a Lurgi gasifier to partial oxidation. The number of process options is even larger for all methanol production than for SNG production or for SNG-methanol co-production. For example, in addition to the two options in Figure 3 the methanol synthesis purge gas could be partially oxidized or cryogenic separation could be used on the entire gas stream and the clean shift configuration could be used with any option.

Comparison of Process Options

Unfortunately, most of the process choices cannot be made independently of each other. The options need to be carefully compared, with each option being completely defined. Evaluations of the process economics of the various cases need to be performed on a realistic and consistent basis. No final answers can be given to questions concerning the most attractive process options until such comparisons are made.

However, several qualitative observations can be made to reduce the number of cases needing to be evaluated. The question of dirty versus clean shift is crucial in determining other process steps. A qualitative comparison of the utilities requirements of the two approaches indicates the effect of this choice on energy efficiency and the product cost. First of all it appears obvious that the steam requirements are less for dirty shift since much of steam remains in the partially cooled raw gas.

In clean shift the gas is cooled to ambient temperature for gas absorption. During gas cooling a large amount of low level heat is recovered. However, high level steam is needed subsequently for shifting. The utility requirements for acid gas removal will also be much higher for the clean shift option because of higher absorbent circulation rates needed for two discrete stages. Intuitively, "dirty" shift seems to be more promising although system conditions including gas analysis and gas pressure will have considerable influence.

The use of cryogenic separation of methane from synthesis gas is not now commercial but appears entirely feasible. The sharpness of the methane-carbon monoxide separation would be the limiting factor. Efficient commercial cryogenic systems have been engineered for air separation and natural gas liquefaction. Extremely sharp separations are not necessary for the options in this paper.

Partial oxidation, steam reforming, and autothermal reforming are all commercial processes for producing synthesis gas from hydrocarbons. Each process has a different range of applicability in terms of feedstock and outlet gas composition. Partial oxidation can convert a wide range of high sulfur feedstocks into a synthesis gas with a low ratio of hydrogen to carbon monoxide. Steam reforming converts natural gas and light liquids into a hydrogen-rich gas containing considerable unconverted methane. Autothermal reforming converts low-sulfur feedstocks into synthesis gas of intermediate composition.

Sulfur recovery is yet another operation with many options (and problems). Considerations include handling of sulfur compounds other than H_2S and Claus-type versus oxidative-type (Stretford) processes. In general Claus units are preferred when the concentration of H_2S in the acid gas is sufficiently high. Stretford units have been applied extensively and successfully in a wide variety of applications, but have problems if the carbon dioxide partial pressure in the gas stream is too high.

Choice of Product

The choice of product or products to be made in a UCG is very important to avoid excessive capital requirements. Here perhaps the best rule to follow is "fit the product to the coal and the technology." Thus if UCG of a steeply dipping seam of coal produces gas with a methane content of 20% it appears to be economical to co-produce SNG along with higher valued synthesis products such as methanol. However, the forced conversion of the methane content into methanol would be equivalent to producing methanol from expensive natural gas. One may choose to make only synthesis products from UCG gas if it contains only 3% methane, for example. The manufacture of SNG as the sole product from high-methane content gas may be indicated if the natural gas supply-demand situation changes and pipeline gas is again considered a premium value fuel. Of course transportation cost of the product to market will be an important consideration.

Implications to UCG Viability and Outlook

It is important to achieve three goals for UCG to be viable:

- reliable operation
- capital cost competitive with surface gasification
- high fuel yield (energy efficiency) per unit capital cost.

The problems of processing high-methane content synthesis gas are similar for UCG-derived gas and gas from a surface coal gasifier. However, UCG-derived gas has additional problems including:

- low gas pressure
- variable composition
- a remote site necessarily adjacent to coal location.

The selection of an appropriate gas processing scheme for a UCG project can essentially equalize gas processing costs with surface gasification and allow full advantage to UCG for the avoidance of mining, coal and ash handling, and gasification vessels.

CONCLUSIONS

- A variety of process technologies are available to accomplish the various steps involved in converting high-methane containing UCG-gas to saleable products.

- The selection of the process scheme will affect the required plant investment, the energy efficiency, and therefore the cost of the product. More information is needed about UCG to specify the optimum process scheme.

- Specific process conclusions include:
  - -It is likely that cryogenic separation will be an economical method of methane recovery.
  - -Dirty shift reaction is indicated to be more efficient than clean shift reaction.
  - -Partial oxidation of raw UCG gas is likely to be too expensive in terms of oxygen usage and waste heat recovery.
  - -Co-production of both SNG and methanol appears to be desirable if the raw UCG gas contains an appreciable amount of methane.

Table 1

REPRESENTATIVE COMPOSITIONS OF RAW GAS
PRODUCED BY UCG AND SURFACE COAL GASIFIERS

Gas Composition mol % (dry)	UCG Steeply Dipping	UCG Flat Seam	Lurgi (Fixed Bed)	Westinghouse (Fluidized Bed)	Texaco (Entrained)
Methane	13-25	3-7	10	3	0.2
Other Hydrocarbons	0.5-1.0	0.2-0.5	1	-	-
Hydrogen	29-33	30-45	42	34	34
Carbon Monoxide	11-22	10-25	18	51	48
Carbon Dioxide	32-42	12-45	29	11	16
Hydrogen Sulfide	0.2-1.0	0.2-1.0	0.2	0.2	0.3
Nitrogen/Argon	0.2-0.5	0.2-0.5	0.2	0.8	1.5

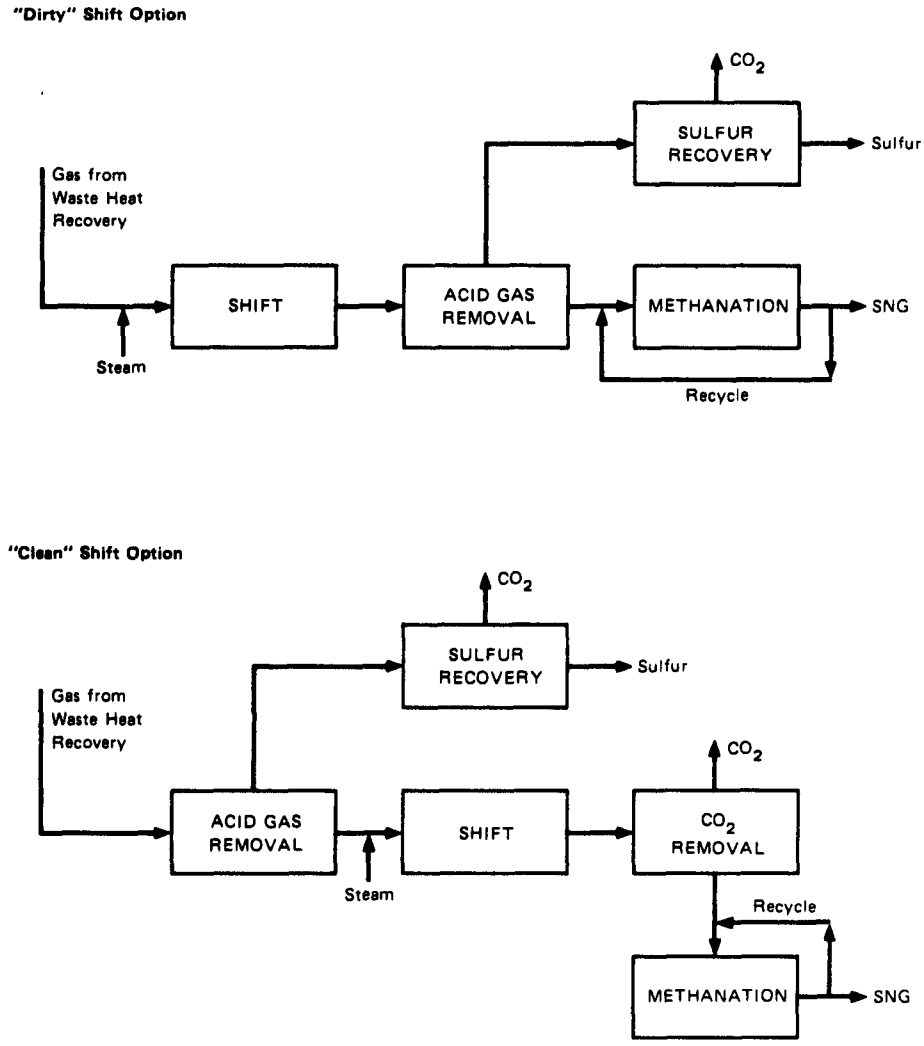

FIGURE 1 TYPICAL PROCESS OPTIONS FOR PRODUCING SNG FROM HIGH-METHANE CONTENT SYNTHESIS GAS

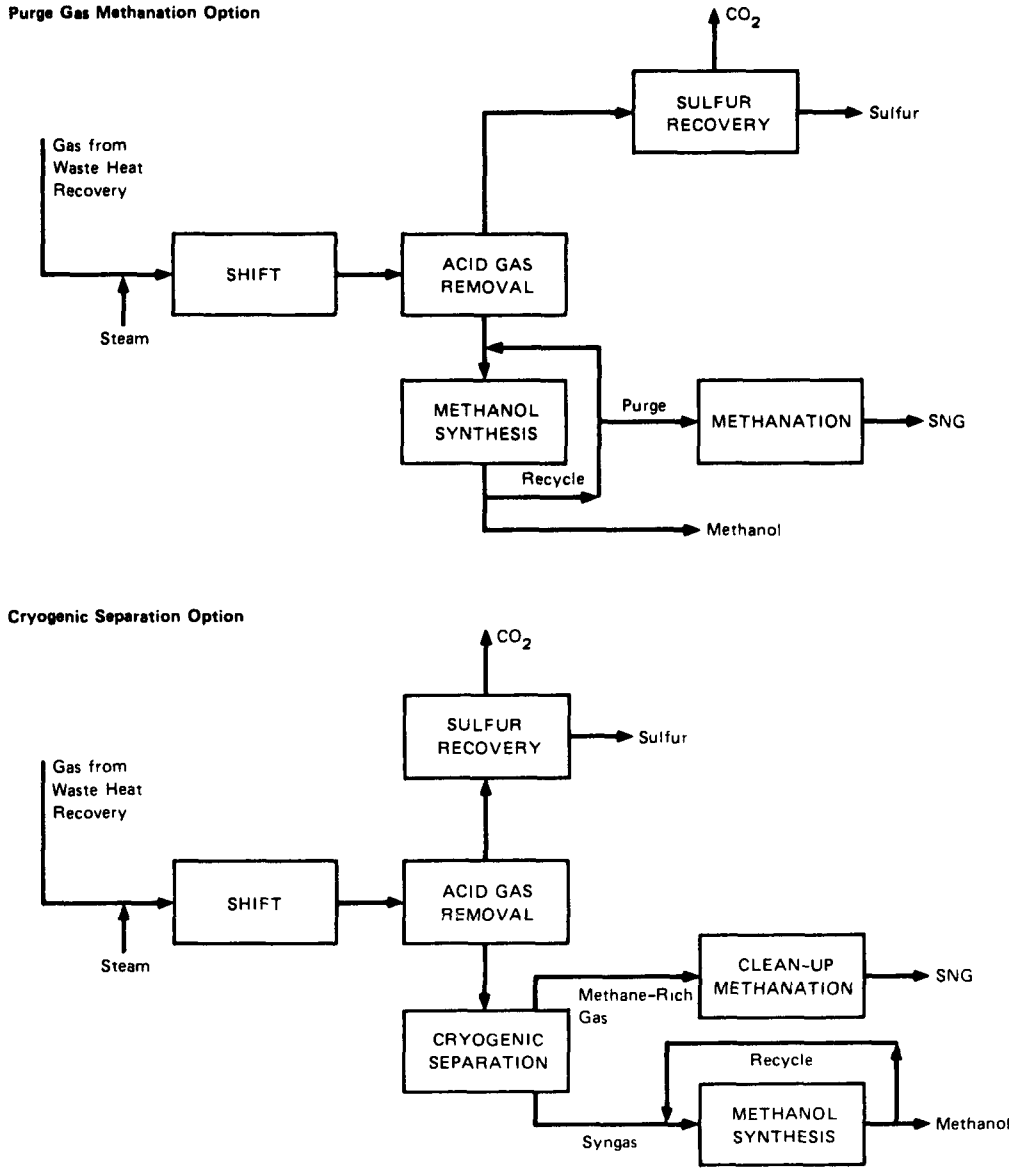

FIGURE 2 TYPICAL PROCESS OPTIONS FOR CO-PRODUCING SNG AND METHANOL FROM HIGH-METHANE CONTENT SYNTHESIS GAS

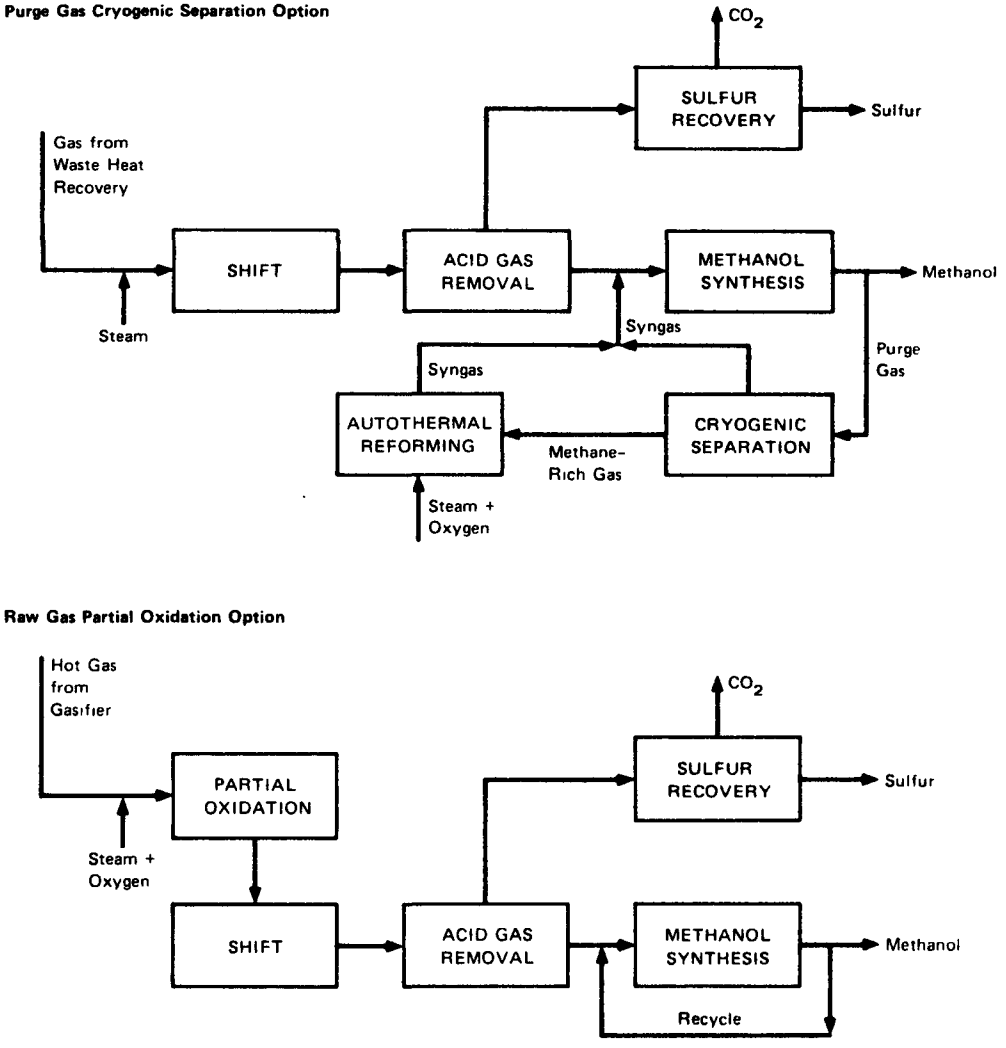

FIGURE 3 TYPICAL PROCESS OPTIONS FOR PRODUCING METHANOL AS SOLE PRODUCT FROM HIGH-METHANE CONTENT SYNTHESIS GAS

5.3 UCG WITH LIQUID WATER AND AIR OF THE DEEP AND THIN COAL LAYERS IN THE NETHERLANDS

BY

J.Bruining, B.C.A.M. van Beurden, D.N. Dietz, W.H.P.M. Heynen and A.P.E. Maljaars

Delft University of Technology, Department of Mining Engineering, Mijnbouwstraat 120, 2628 RX Delft, and Department of Chemical Engineering, Julianalaan 136, 2628 BL Delft, The Netherlands

Coal in the Netherlands occurs in thin layers (~ 1 m) and at great depths (~ 1500 m). As a result in situ gasification may suffer great heat losses. If steam would be injected as gasification agent, most of this steam would condense before it has reached the bottom of the well. Therefore we focus our attention on the injection of liquid water in addition to air as gasification agent. With an experimental sep up built to perform gasification experiments, it is shown that part of the heat that is released to the adjacent rocks by the hot product gas returns to the pay zone to generate steam from the cold injection water.

INTRODUCTION

The amount of coal beneath the Netherlands is equivalent to a multiple of the world gas reserve[1]. The coal occurs in thin layers (~ 1 m) and a large part is located at depths below 1500 m. Therefore this coal cannot be mined economically with conventional means. A research programme is being carried out to investigate the possibility to utilizing this coal by underground gasification[2].

As a result of the occurrence of coal in deep and thin layers, heat losses are important.[3] If steam would be injected as gasification agent, most of this steam would condense before it has reached the bottom of the well.

Consider for example one unit as a square part of a coal layer of 140x140 m^2 with an injection well in the center and four production wells at the corners (fig.1). Table I presents some general data including an estimate of the amount of steam that can be injected as gasification agent. Approximately all the (100 bar) steam, considered in this example (Table I) i.e. 43.6 tons per day, will condense in the injection well[4]. Therefore we focus our attention on the injection of liquid water instead of steam.

Liquid water injection was proposed by D.N. Dietz[5] as a method of heat recuperation. Part of the heat that is released to the adjacent rocks by the hot product gases is recuperated by the cold injection water and reintroduced in the process zone. Optimal heat recuperation depends on the liquid water/air injection ratio. Two gasification modes can occur, depending on this liquid water/air injection ratio[6] :

a) Normal wet gasification. This occurs for relatively low water/air injection ratio's. The reaction zone is displaced at a speed determined by the fuel consumption rate.

b) Partially quenched gasification. This is an entirely different process and from a theoretical point of view more similar to reverse combustion. It occurs for high water/air injection ratio's.

For the study of the heat recuperation effect in these modes we have built an experimental set up that allows gasification experiments at high pressure. Equipment and experiments are discribed in section I. In section II we present a simple method to calculate the outlet composition and temperature in the reaction zone, which is derived from existing gasification models[7,8].

The heat recuperation effect can be elucidated from a discussion of the experiments in terms of these adiabatic models (section III).

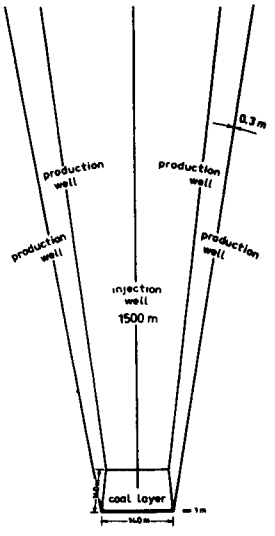

Fig.1.
Model of underground gasification to illustrate the peculiar relationship between the occurrence of Dutch coal in thin layers and its production from great depth. Thickness of the coal layer is 1 m.

Tabel I.
Estimate of amount of steam to be injected as gasification agent and the rate of steam condensation in the injection well.

Content of a injection/production unit of the coal layer = 140x140x1 = 19600 m^3

Weight of coal (density 1.4 g/cm^3) = 1.4x19600 = 27440 ton

Project time = 500 days

Coal consumption rate = 54.9 tons/day

Steam injection rate = 41.2 tons/day

Air injection rate = $1.4\ 10^5$ nm^3/day

$4C + O_2 + 4N_2 + 2H_2O\ (g) \rightarrow 4CO + 2H_2 + 4N_2$

Energy density of coal = 25 GJ/m^3

Power at 100% efficiency 11.3 MW/unit

Steam condensation rate 43.6 tons/day

at 100 bar in 1500 m injection well[4].

Section I - Experimental

Gasification experiments have been carried out to show that part of the heat lost to the cap and base rock can be recuperated and reintroduced into the process zone by cold water injection (fig. 6).

§1 Equipment

A schematic flow diagram of the equipment has been shown in fig.2. The gasification takes place in the reactor (1). Some experiments were carried out in a non-deformable (inner) steel tube with a diameter of 114 mm and a wall thickness of 2 mm (114x2 mm^2) and other experiments were performed in a deformable steel foil tube (120x0.5 mm^2), protected on the inside with a nickel foil tube (119x0.2 mm^2). All tubes had a length of 1 m. A deformable tube made of steel foil or a tube made of nickel foil alone were not capable of withstanding the process conditions.

The inner tube is mounted inside an outer steel tube (323.8x21.4 mm^2), with a length of 2 m. This tube can withstand high pressures (100 atm) at somewhat elevated temperatures (250°C). Temperatures on the outside have not exceeded 70°C.

The annular space (filled with nitrogen and dry sand) is overpressurized with respect to the process pressure inside the inner tube. Thus the inner tube is deformed and squeezed on the carbon. In this way spurious short circuit streams of air can be avoided and underground behaviour can be simulated. The behaviour of one of the foil tubes is shown in figure 3. No leakage occurred.

In the center of the tubes we have mounted eight Pt/Pt(Rh) 10% thermocouples at distances of 25,35,45,55,60,65,70 and 75 cm from the inlet point. Temperature data acquisition has been effected with a DAI-microcomputer. Temperatures are accurate within 5°C.

The inner tube is filled with activated carbon grains (diameter = 2.5 mm). We have used carbon instead of char in order to perform reproducible experiments and for the ease of interpretation of the experimental data. To prevent the grains from blocking the outlet, we have covered the bottom of the tube with a layer of sand (18 cm). On top of the carbon grains we poured another layer of sand (~ 18 cm). The experiments have been carried out with the reactor in vertical position.

The gasification agents (air and water) have been injected from above. Automatic controls are used to achieve constant air and water injection rates of 1-10 nm^3/hr and 0.5-5 l/hr respectively. Flows are measured by calibrated pressure difference cells. High pressure gases are supplied by cylinders. High pressure water is displaced from a vessel with nitrogen. The product gas leaves the reactor at the bottom at a constant pressure, which is adjusted by a specially designed pneumatically controlled reducing valve[9]. A small part of the product gas is cooled, dried and analyzed. Two gaschromatographs equiped with activated carbon columns alternate to measure the gas composition (H_2, N_2, CO, CH_4 and CO_2) every 15 minutes. Pressures at the inlet and outlet side of the reactor are read from a manometer.

§ 2 Experiments

Before ignition, air (1 nm^3/hr) flows through the carbon bed at a pressure of 4 ata. The carbon grains are heated indirectly by a 750 W heating wire (used at 500 W) mounted near the injection side around the outside of the inner tube. Ignition occurs after one-two hours.

When a heated zone of sufficient length has been established water and air injection rates are set to constant values. In this way a quasi steady state will be attained (fig.5).

A few tentative experimental runs were carried out. These runs were all characterized by steady outlet compositions. We could only measure steady state temperature profiles in one experiment due to teething troubles.

In this experiment we were able to maintain steady state process conditions for nearly three hours. The experiment was carried out in a non-deformable tube and will be reported in more detail (fig. 4).

As the experiments are run presently with the reactor in vertical position, no spurious short circuit streams will occur. In fig.4 we have plotted the outlet compositions, the temperatures, the air and water injection rates and the pressures measured at the inlet and outlet side of the reactor, versus time. The outlet compositions are constant during the steady state period (fig.4a). Some product compositions have been summarized in Table II.

All temperatures measured by the thermocouples mounted inside the reactor show qualitatively similar behaviour. We can look upon the temperature data in fig.4b as temperature profiles when we read this figure from the injection side (right) to the production side (left). From the right to the left we observe a very gradual increase from 20-140 °C. Then a very steep increase occurs to temperatures around 1000 °C. The wiggling occurred only for high water/air injection ratio's possibly due to unsteady water evaporation. Downstream of the maximum the temperature drops sharply to about 850 °C. Then the temperature decreases more gradually to a few hundred degrees before it drops to temperatures around 100 °C, which were observed almost immediately after the start of the experiment.

During the steady state period the air and liquid water injection rates were maintained at 2.41 Nm^3/hr and 0.84 l/hr respectively (see fig.4c). This corresponds to a liquid water/air injection ratio of 0.47 mol/mol. The injection and outlet pressures were read from manometers every 10 minutes. The pressures remained constant in the first part of the steady state period but increased in the last hour due to clogging.

Section III compared the experimental data at times between 210 and 225 minutes (see fig.4) with the theory.

Section II - Theory

§ 1 Simplified calculation of the outlet composition and temperature of the product gas from existing one-dimensional adiabatic gasification models.

The gasification process in a porous medium can be described by Darcy's equation and the heat and mass balance equations[7,8]. These partial differential equations have been solved with finite difference methods[7].

Thus one can find the non-steady temperature and concentration profiles in the porous medium. Gunn[8] mentions that the gas composition (and other variables) in field tests and combustion tube experiments stabilize in about an hour in the same way as we have found here. Unfortunately steady state behaviour in the strict sense of the word does not occur. The general procedure is to consider the coal bed from the injection to the produc-

tion well as composed of parts for which the steady state approach can be adopted 8,10,11 (see fig.5). We shall focus our attention on the reaction zone. The steady state assumption means here that the reaction zone travels at a speed v_1. In other words the temperature and concentration (etc.) profiles in the reaction zone remain unchanged in a system that travels at a speed v_1, from the injection to the production point. In this system the partial differential equations can be reduced to ordinary differential equations[8].

As part of the solution one finds the steady state temperature and concentration profiles in the reaction zone. Such a temperature profile has been shown in fig.5. From the injection to the production side one observes here that, in the adiabatic case, the temperature slopes steeply to a temperature of about 1000°C and subsequently declines to approach asymptotically to a value of 850°C. From a practical point of view, however, we are interested in :

II-1

a) The product composition of the gas as it leaves the reaction zone;
b) The amount of fuel converted to product gas;
c) The downstream temperature of the gas as it leaves the reaction zone;

rather than in the temperature and concentration profiles within the reaction zone. Therefore we shall show under which conditions the variables of interest (II-1) can be found without solving the differential equations.

Consider the overall reaction (see fig.5).

II-2

$$\text{content pores}(T_1)+\text{ash}(T_1)+(m+n+r+z)C+O_2+qN_2+\sigma H_2O \xrightarrow{\Delta H=0} \text{ash}(T_o)+mCO+nCO_2+sH_2+rCH_4+tH_2O+q'N_2+zC+\text{content pores}(T_o)$$

The terms with the content of the pores will be disregarded, which is justified at low pressures.
From this equation one derives from a mass balance for oxygen, hydrogen and nitrogen:

II-3 - oxygen : $2+\sigma = m+2n+t$

II-4 - hydrogen : $\sigma = s+2r+t$

II-5 - nitrogen : $q = q'$

In the moving coordinate system gases move from the cold injection to the hot production side, but solids (carbon + ash) move in the opposite direction at the reaction zone velocity v_1. In other words cold injection gases react with hot coal (and hot ash) to form hot product gases and cold fuel (and cold ash). The reaction enthalpy (ΔH) must be zero for adiabatic (no heat losses) gasification :

ΔH = enthalpy (hot product gas) + enthalpy (cold product solids) - enthalpy (cold reactant gas) - enthalpy (hot reactant solids) $\overset{\text{def}}{=\!=} H_{pr}(T_1)+H_s(T_o)-H_r(T_o)-H'_s(T_1)=0$

From this equation one can derive an implicit equation for the temperature T_1 of the gases as they leave the reaction zone :

$$\text{II-6} \quad \int_{T_o}^{T_1} C_p^{\text{prod}}\,dT = (H_r(T_o)-H_{pr}(T_o))+(H_s(T_1)-H_s'(T_o))$$

Equation II-6 uses the notation C_p^{prod} for the specific heat of the product gases. The prime in $H_s'(T_o)$ serves as a reminder that the consumption of fuel must be incorporated in this enthalpy term. The temperature T_1 is the temperature of the product gases as it leaves the reaction zone. The compositions and temperature (T_o) of the injection gases are usually known. The amount of ash participating in the process can be inferred from the ash content in the coal layer. There are, however, eight unknowns namely :

a) six stoichiometric coefficients (m,n, s,r,t,q);
b) the final temperature T_1 of the product gas as it leaves the reaction zone;
c) the stoichiometric coefficient z which indicates the amount of fuel left unburnt.

We have already found four equations i.e. equations II-3, II-4, II-5 and II-6, which are valid when a steady state is attained. This means that there are still four variables that need to be determined. We shall distinguish the following three cases (A,B,C).

A) The composition of the product gas as it leaves the reaction zone is known experimentally

When the product composition is known all the stoichiometric coefficients (a), can be calculated. This means that equations II-3/5 are satisfied. The two remaining variables, the temperatures T_1 and the stoichiometric coefficient z which indicates the amount of fuel left unburnt, must still be determined. We shall distinguish two possibilities :

1) For low water/air injection ratio's no fuel will be left unburnt. In other words (see II-2) :

II-7 z=0 for low water/air injection ratio's.
With equations II-6 and II-7 all quantities of interest (II-1) can be calculated. This case will be applied in section III.

2) For high water/air injection ratio's some fuel may be left unburnt and z is not equal to zero. The value of z is determined by the interplay of convective and conductive heat transport and the oxidation reaction rate. In this case the gasification is called partially quenched[6]. This gasification mode is similar to reverse combustion from a theoretical point of view. The unfortunate consequence is that z can only be found either from a complete solution of the ordinary differential equations, or from the experimental data. In other words :

II-8 z < experimentally determined / obtained from solution of ordinary differential equations

With equations II-6 and II-8 all quantities of interest (II-1) can be calculated.

B,C) Conditions for steady state behaviour

The compositions can be obtained from theoretical model calculations. In these models one assumes steady state behaviour in the reaction zone. A steady state can only occur if the reaction rate becomes or approaches zero at the (far) downstream part of the reaction zone. Otherwise the outlet composition changes as the distance between the reaction front and drying front increases (see fig.5) during the gasification process and further reaction occurs. The reaction rates drop to zero when equilibrium compositions are obtained (B) or when the temperatures have attained very low values (C).

B) The outlet product gas has an equilibrium composition

It is not clear to us whether an equilibrium can be achieved and maintained in practice. If it occurs it will be for low water/air injection ratio's. We have chosen the following three independent equilibrium reactions (any other choice leads to the same result) :

II-9 $C+CO_2 \rightleftharpoons 2CO$ $\quad K_p^{I}=p_{CO}^2/p_{CO_2}$

II-10 $C+H_2O \rightleftharpoons CO+H_2$ $\quad K_p^{II}=p_{CO}p_{H_2}/p_{H_2O}$

II-11 $C+2H_2 \rightleftharpoons CH_4$ $\quad K_p^{III}=p_{CH_4}/p_{H_2}^2$

The partial pressures p_i (i = CO, CO_2, etc.), can be calculated from the stoichiometric coefficients

$$p_{CO} = \frac{m}{m+n+s+r+t+q} P_{tot}$$

Where P_{tot} is the total pressure at which the gasification is carried out. The equilibrium constants K_p can be calculated from thermodynamic data[12,13] For the low water/air injection ratio's no fuel will be left unburnt (z=0) and from equation II-7, II-3/6 and II-9/11 all variables of interest can be calculated. This case will be applied in section III to show that the experimentally observed composition is completely different from the equilibrium composition.

C) The temperature of the product gas as it leaves the reaction zone is so low that the reaction rates are negligible

This has occurred for the water/air injection ratio's that we have applied here. In this case it turns out that

the characteristics (II-1) can only be found from a complete solution of the differential equations. The scope for variation is, however, small particularly when no fuel is left unburnt (z=0). The outlet temperature T_1 can be estimated as the temperature for which the reaction rates become negligible irrespective of the reaction rates upstream. In other words

II-12 T_1' = temperature for which reaction rates become negligible

Apart from equations II-7 and II-12 the equations II-3/6 are also valid. Therefore there are only two degrees of freedom that depend on the gasification process in the entire reaction zone.

§ 2 Non-adiabatic case : Heat losses may lead to a more efficient process!

What happens to the sensible heat of the product gases leaving the reaction zone? Downstream drying occurs. near the drying front (see fig.5.). The reaction and drying front move (usually) further apart as time proceeds. Between the reaction and drying front heat is lost to the cap and base rock. The sensible heat of the gases would have been lost in the 1500 m long production well if no heat loss had occurred in the coal layer. Part of the heat can be recuperated if it was stored in the cap and base rock[14]. The cap and base rock were initially heated by the hot gases. When the reaction front moves further downstream cold injection gases encounter the heated cap and base rock and the lost heat flows back into the reaction zone. This effect has been illustrated schematically in figure 6.

If heat losses occur, the temperature does not become constant in the downstream part of the reaction zone but decreases more or less linearly (see fig.7.). Heat loss terms must be included in the enthalpy balance equation. From figure 5 one observes that these heat loss terms (H_{loss}) consist of a loss (+) term due to conduction to cap and base rock and conduction in the flow direction downstream and a "gain" (-) term owing to recuperation upstream. The enthalpy balance equation becomes (see eq II-6)

$$\text{II-13} \quad \int_{T_0}^{T'} C_p^{prod} dT = H_r(T_0) - H_{pr}(T_0) + H_s(T_1') - H_s'(T_0) - H_{loss}$$

We shall define the temperature T_1' as the temperature which occurs in the reaction zone when the reaction rates just become negligible. This part of the reaction zone where chemical reactions occur will be called the process zone. The temperature T_1' is lower than the temperature T_1 calculated from equation II-6, if more heat is lost than gained in the process zone. The temperature T_1' is higher than T_1 if heat gain is dominant. In that case heat losses lead to a more efficient process!

Section III - Results and discussion

Hot gases leave the reaction zone. These gases give off heat to the cap and base rock. As the reaction front moves further downstream part of this heat is recuperated. This section illustrates the heat recuperation effect by the experimental data and its comparison to the theory in two ways :

I Temperatures rise gradually to steam temperatures upstream of the reaction front.

II The temperature T_1 (see fig.5.), calculated from the experimental composition, is lower than the experimentally observed value T_1' (see section II, § 2).

ad I. In figure 7 we have shown the experimental temperature profile (at 210 minutes) in the tube, with the help of the temperature data as given in figure 4b. We have made use of the known reaction zone velocity to put in some detail near the reaction front. Upstream of this front the temperature rises gradually to steam temperatures. Convective heat transport tends to make the temperature slope steeper. The gradual behaviour is also observed for lower water/air injection ratio's where no wiggling of the temperature occurs.

ad II. Table II compares experimental composition data with theoretically obtained

values. These theoretical values are obtained from an equilibrium model[12] (see section II, case B). One observes that the experimental composition is very different from the equilibrium composition. The experimental composition remained constant during the steady state period. Therefore the temperature T_1' (see figure 7) attains such a low value that the reaction rates become negligible (see section II, case C). Table II also compares the experimental efficiency of the gasification process with the value obtained from the equilibrium model. The efficiency is defined as the latent heat of the gas divided by the heat of combustion of the carbon necessary to produce the gas.

The experimental efficiency is high and differs only marginally from the value calculated by the adiabatic equilibrium model.

From the experimental composition and the liquid water/air injection ratio the temperature T_1 (see figure 5, section II; case A, § 1) can be calculated. The calculated temperature (T_1^w = 683°C) is drawn in figure 7. This temperature T_1^w must be compared with the temperature T_1', defined as the temperature at which the reaction rates become negligible in the non-adiabatic case (see section II, §2). It is difficult to determine the temperature T_1' experimentally from figure 7. When the reaction rates are non zero the temperature slopes more steeply (from 1010-850°C) than at lower temperatures where the temperature decline is due to heat losses only. From figure 7 one observes that the temperature T_1' is higher than the adiabatic temperature T_1^w. This indicates that more heat is recuperated than lost in the process zone (see section II, § 2). In an extreme case of heat recuperation all the water has been converted to steam before entering the reaction zone.

Again one can calculate from the experimental composition and the steam/air injection ratio, the adiabatic temperature T_1^{st} (see section II, case A), which attains a value of 1076°C (see figure 7). This temperature is higher than any temperature observed during the steady state period of the experiment. Therefore one concludes that heat recuperation has caused partial evaporation of water.

The heat recuperation effect must be quantified and optimized with further experiments.

Conclusion

The advantage of steam as gasification agent is that it leads to high process temperatures and thus to favourable reaction rates. Unfortunately the steam injected in a deep layer will largely condense before it has reached the bottom of the injection well unless very high injection rates can be applied. More often one can equally well inject liquid water. In that case the injection of steam is a waste of energy.

Cold water recuperates part of the heat that was released to the adjacent rock by the hot gas, is converted to steam and reintroduces this heat to the process zone (fig.6.).

Application of thermodynamic reasoning to the experimental data shows that the heat recuperation effect indeed contributes to the efficiency of the gasification process. Heat loss from the process zone where the endothermic reactions occur, however, is expected to have a negative effect on the efficiency inspite of the recuperation effect. Heat loss downstream of this zone is partly reintroduced in the process zone and has only a positive effect. A shorter process zone, which occurs at higher pressures, will exhibit the positive effect of heat loss in the layer more clearly. Heat recuperation is more effective for thin layers.

The heat recuperation effect cannot be quantified with the experimental data presently available. More experiments with thermocouples mounted in the sand in the annulus are necessary to quantify and optimize.

REFERENCES

1. M.J.M. Bless and N. de Voogd "Exploration of coal in the Netherlands". Meded,Rijks Geol.Dienst, 33 (3), (1980), 17-32
2. J.J. Dozy ed. "Research on the coal beneath the Netherlands". Geologie en Mijnbouw, 61, (1982), 355-395
3. D.N. Dietz and J. Bruining "Underground combustion of heavy oil; Implications for coal gasification". Meded.Rijks Geol.Dienst, 33 (3), (1980), 72-80
4. A. Satter "Heat losses during flow of steam down a well bore". SPE Reprint Series No.10, (1972), p.55
5. D.N. Dietz Patent application 7303779, (March, 19th, 1973)
6. D.N. Dietz and J. Weydema "Wet and partially quenched combustion" SPE Reprint Series No.10, (1972), 216
7. C.B. Thorsness and R.B. Rosza "In situ coal gasification program : Model Calculations and Laboratory experiments". SPEJ 18, (1978), 105-116
8. R.D. Gunn, D.L. Whitman and D.D. Fischer "A permeation theory for in situ gasification". SPEJ 18, (1978), 300-314
9. W.H.P.M. Heynen "Pneumatisch bediend reduceer-ventiel voor drukregeling in proefbuis t.b.v. ondergrondse steenkoolvergassing". In Dutch, Delft TH-report, June (1980)
10. H.L. Beckers and G.J. Harmsen "The effect of water injection on sustained combustion in a porous medium". SPE Reprint Series, No.10, (1972), 231
11. K. Dziunikowski "Underground gasification of coal by air : Interpretation of physico-chemical principles". J.Inst. Fuel, July 1960, 337
12. C.B. Thorsness and A.E. Sherwood "Moving equilibrium front model for in situ gasification". U.C.R.L.-52524, Lawrence Livermore Laboratory Report, U. of California, Livermore (1978)
13. See for example, W.J. Moore "Physical Chemistry", Longmans (1963)

REFERENCES

14. J. Bruining and D.N. Dietz "Heat exchanges between a layer and the adjacent rocks during underground combustion of oil or coal : Implications for "conventional" underground coal gasification". TH-report, July (1980)

ACKNOWLEDGEMENTS

The work described here was part of the research programme "Nederlands Onderzoekprogramma Kolen"(BEOP) and was made possible by financial support from EZ.

We are indebted to Professor R.D. Gunn for many useful discussions and to Dr. C.B. Thorsness for the use of his computer programmes.

We thank W. Brabander for welding the combustion tubes.

LIST OF SYMBOLS

C_p^{prod}	heat capacity of product gas
ΔH	overall reaction enthalpy (see equation II-2)
$H_{pr}(T_1)$	enthalpy of product gas at temperature T_1
$H_r(T_o)$	enthalpy of reactant gas at temperature T_o
$H_s(T)$	enthalpy of fuel and ash at temperature T
H_{loss}	netto conductive heat loss from production zone
K_p^I	equilibrium constant for $C+CO_2 \rightleftharpoons 2CO$
K_p^{II}	equilibrium constant for $C+H_2O \rightleftharpoons CO+H_2$
K_p^{III}	equilibrium for $C+2H_2 \rightleftharpoons CH_4$
m	stoichiometric coefficient for CO
n	stoichiometric coefficient for CO_2
p_i	partial pressure of component i ($i=O_2,N_2,H_2,CH_4,CO,CO_2\ H_2O$)
P_{tot}	total pressure
q	stoichiometric coefficient for injected nitrogen

LIST OF SYMBOLS

q'	stoichiometric coefficient for produced nitrogen	v_1	velocity of reaction zone (see fig.5)
r	stoichiometric coefficient for methane	v_2	velocity of drying front (see fig.5)
s	stoichiometric coefficient for hydrogen	v_3	velocity of steam condensation front (see fig.5)
t	stoichiometric coefficient for water	z	stoichiometric coefficient for amount of fuel left unburnt
T_o	injection temperature	σ	stoichiometric coefficient for injection water
T_1	temperature at which produced gas leaves reaction zone (see fig.5 and section II, cases B and C)		

Table II.
Comparison of experiments to equilibrium models[12] at a pressure of 3.2 ata and a water/air ratio of 0.472 mol/mol

	Experimental		Equilibrium	
	(210')	(225')	No CH_4	CH_4
Composition N_2 (%)	47.5	47.2	46.0	46.2
H_2O (%)	18.4	18.8	10.6	9.2
H_2 (%)	8.5	7.8	16.9	15.0
CH_4 (%)	0.7	0.9	0	1.7
CO (%)	16.4	15.9	11.7	12.6
CO_2 (%)	8.3	9.1	14.8	15.2
Temperature T_1^w (^oC) (see fig.7)	672	693	650	652
Temperature T_1^{st} (^oC) (see fig.7)	1066	1086	--	--
Heating value (kJ/nm^3)	3782	3748	3723	4146
Efficiency (%)	74	73	78	81

Theoretcal equilibrium compositions and experimental compositions for a liquid water/air injection ratio of 0.472 mol/mol at an absolute pressure of 3.2 ata. The experimental compositions were taken respectively at 210 and 225 minutes (see fig.4). The heating value of the gas includes the condensation heat of water.
The efficiency of the experiments is high inspite of heat loss effects. The adiabatic temperatures of the product gas for liquid water injection T_1^w and steam injection T_1^{st} have been included in the Table (see text).

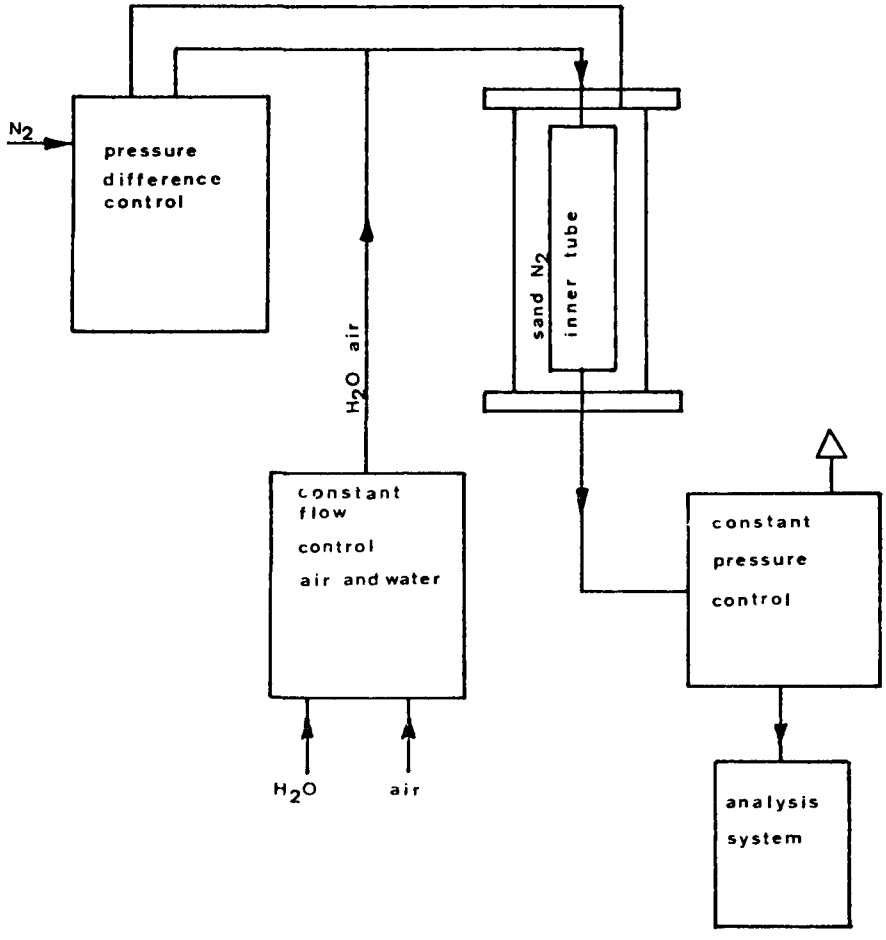

Fig.2. Schematic flow diagram of equipment for coal gasification experiments

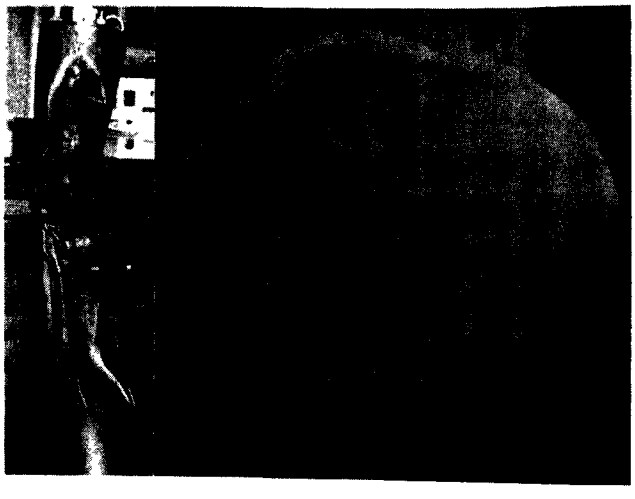

Fig.3. Behaviour of one of the deformed foil tubes

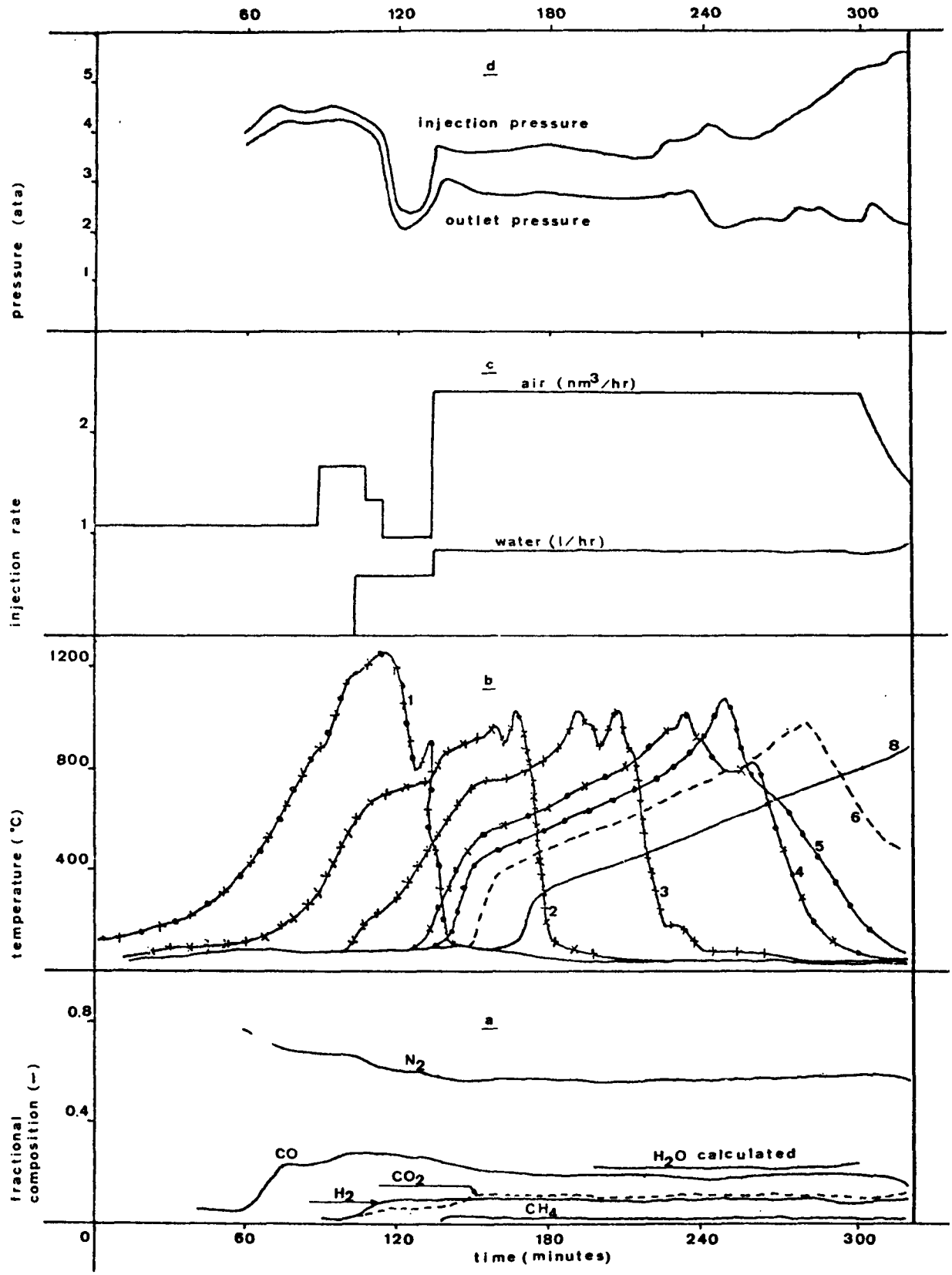

Fig.4. Experimental outlet compositions (a), temperatures (at 1=25 cm, 2=35 cm, 3=45 cm, 4=55 cm, 5=60 cm, 6=65 cm and 8=75 cm from the injection point)(b), injection rates (c) and pressures (d), as function of time.

5.0 GENERAL SUBJECTS

SESSION VI: ORAL PRESENTATIONS

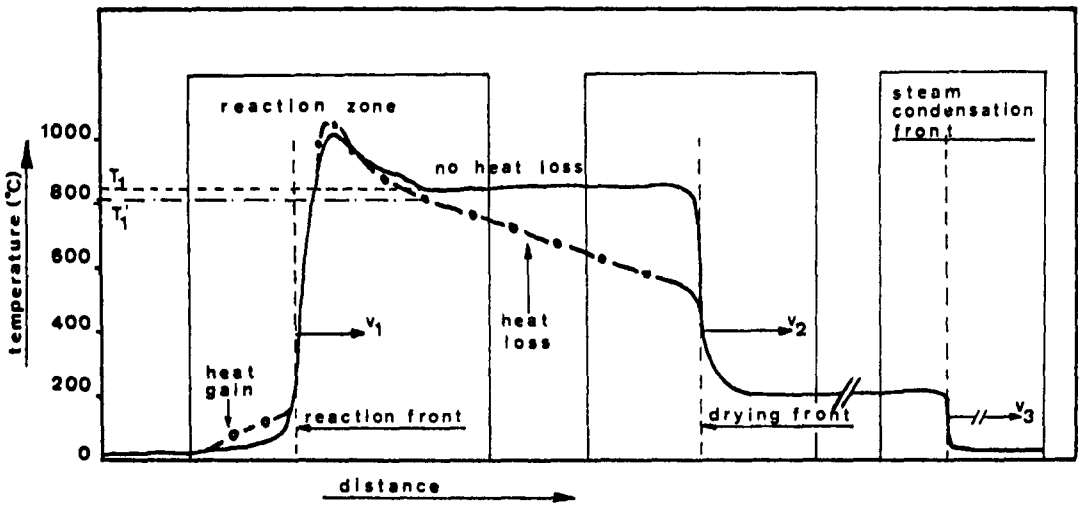

Fig.5. The bed from the injection to the production point is considered as composed of parts for which the steady state approach can be adopted[10,12]. These parts, indicated as rectangles in the figure, travel each with their characteristic velocity $v_1 < v_2 << v_3$.

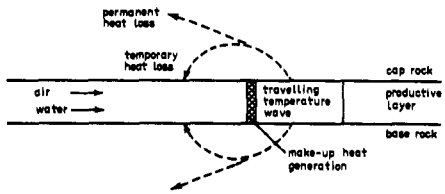

Fig.6. Compensation for heat losses from a temperature wave

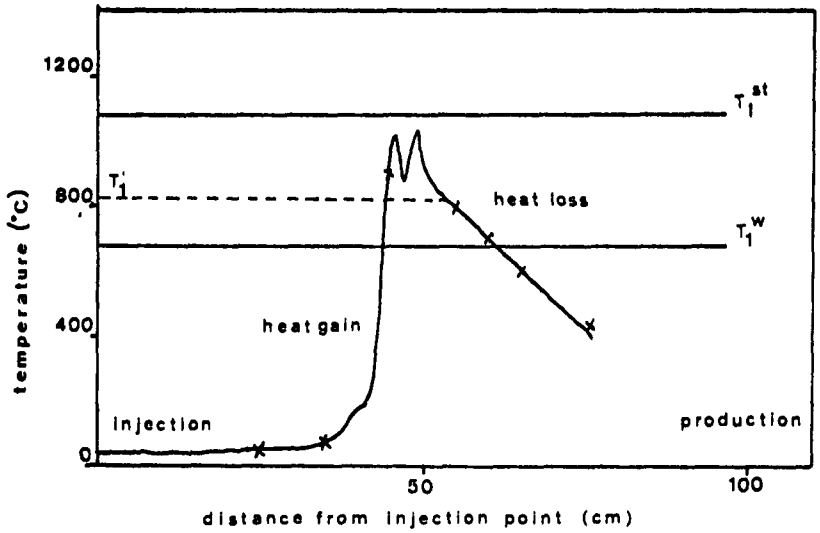

Fig.7. Temperature profile obtained from fig.4b at 210 minutes. Measured points are indicated as x. Some detail has been put in near the reaction front, which is calculated from the known reaction zone velocity. The temperatures T_1' calculated from the experimental composition for liquid water injection (T_1^w) and steam injection T_1^{st} have been indicated in the figure (see text).

6.0 KEYNOTE ADDRESS

6.1 WORLD ENERGY PERSPECTIVE

by

Bernard S. Lee 1/

I thought I would share a few thoughts on how one person looks at world energy. My thoughts may or may not agree with yours, but at least it comes with sincerity. I am not going to talk about Btu's heating values or tonnages of resources which you know much more about than I do. Instead, I would like to look at world energy from the perspective of people.

If you take a look at what has been going on and what will be coming in the future, I think you realize that there are a few mismatches in the world energy situation. The first important mismatch is the mismatch in the amount of resources and the use of these resources in the world. Three-fourths of the fossil energy resources in this world is in the form of a solid, specifically coal. Eighty percent of the energy contained in the United States is in the form of coal. Yet, 70 percent of the energy consumed in the world today is in the form of liquid and gas. So we have an imbalance between what we have the most of and what we use the most.

If you look at the picture further, there is another mismatch, and that is the mismatch between where energy is consumed and where it is produced. It turns out that places where energy is in great demand because they are densely populated, more often than not, are places where there are not too many choices for energy. Turned around the other way, the high energy producing parts of the world are sparsely populated. Because people consume energy, it would be nice if we had lots of people in places where there is lots of energy, and then, maybe everybody would not fight about it so hard. But, that is not the way the world was created.

If you look at oil production in the world, Russia leads the hit parade producing the largest amount of oil. Russia is followed by the United States, then Saudi Arabia, Mexico, and China. So Russia and the United States, with large populations, do not come out too badly. But, there are not too many people in Saudi Arabia. China, on the other hand, is the fifth largest oil producer as a country. There are, also, lots of people.

If you look at natural gas, the largest producers are the United States of America and Russia, followed by Canada, The Netherlands, and the United Kingdom. Again, the United States and Russia happen to have a lot of people, so that is not too far out of line. We have about 230 million people in this country. There are about 270 million people in Russia. In comparison, China has a billion people, and India has 700 million people. China has a fair amount of energy resources but certainly not in proportion to its population.

Then you look at the energy rich countries in the Persian Gulf. Iran has 40 million people, Iraq has 14 million people, and Saudi Arabia

1/ Institute of Gas Technology, Chicago, IL 60616

has less than 10 million people. Of the smaller countries, Kuwait has only 1.5 million people, the United Arab Emirates has less than 1 million people, and Qatar with .25 million people. If you have the opportunity to go out to that part of the world, you begin to ask yourself, "If it was not for all the oil and gas, that area is desert-like and really is not good for anything but a very small concentration of the population." Right now the population concentration is brought about strictly because of the wealth generated by the oil and gas business. But, you have a feeling that is not going to last very long, because there does not seem to be any other resources.

To me, people are the most important factor in determining the shape of the world in the future. Taking another view, the Iran/Iraq war has been going on for over 3 years. If they are at a fighting standstill, a 40 million population country fighting against a 14 million population country, all things being equal, the larger country can wear out the smaller country and still have a lot of people left over. That is the way the war of attrition goes on, and I think that is the way energy resources will be allocated in the future.

Taking a look at wealth distribution, it is certainly an increasing mismatch as time goes on. We have in this world a tremendous number of developing countries. A nice name is LDC's. These countries are less fully developed than the highly industrialized countries of the world. They are the ones with the largest increase in population, not only because of greater birth rates, but because of better health care. Even if you keep the birth rate down, longevity and elimination of diseases are causing the population to increase to the point where it becomes a very important consideration. More LDC's have difficulty making payments on their loans. Part of their loans are for energy imports. People have to have energy to better themselves. I think, it is humanitarian and civilized to help people become better situated, yet there is no way they can pay back the loans. Refinancing pushes this back further and further, but eventually there has to be an accounting of some sort. A small company can go bankrupt by filing a Chapter 11 and start again somewhere. I do not see how a country can go bankrupt. What happens to that country? Letting it go bankrupt would not solve the basic problem. It is a very trying problem. I do not really know what the world leaders are going to do.

There have been many suggestions by the producing countries and the OPEC countries to pool their resources together to help LDC's finance themselves. I do not know what LDC's without natural resources and with growing populations can do in the long run. That is a long-term fundamental problem that needs to be faced by the world at large, and energy is a very important aspect. What this says to me is that because of wealth distribution and location, geopolitics will be a central aspect of the world energy situation, not only today and in the past, but more and more as time goes. There is no doubt that geopolitics will determine energy policy, the direction of energy research, and the implementation of new energy results more so than strict technical developments and technical innovation.

Perhaps, we should take a couple of minutes and look at some of the world's major producers and users. The USSR, for example, is the largest producer of crude oil. Its production, based on the information we have, is at a peak. There is some debate as to whether there is a downward slope or not. One statistic that is interesting is that, in 1980, it was estimated the Soviet Union needed to drill somewhere around 1 million meters of new wells to generate a net addition of 1 million metric tons of oil per year. A million metric tons of oil per year is not a whole lot. It translates to something like 20,000 barrels per day. The same million ton production in 1985 is estimated to require the drilling of 7 million meters of additional wells, a seven-fold

increase in 5 years. What this says is that Soviet oil fields are being depleted and will become more and more depleted as time goes on. For the moment, the USSR has a tremendous deposit of natural gas that they are tapping to generate foreign exchange and subsidize their relatively inefficient economy. But, this can only go on for so long. There is no doubt that a country that large and a country dedicated to taking a leadership position in the world will be looking at energy rich areas. All you have to do is look at the globe and see how close the Soviet Union is to the Middle East. Certainly, this is not new to anyone. It is not without intention that events in Afghanistan have been going on for several years. Looking at what might go on in Iran, the largest populated country in the Middle East area with 40 million people (more than all of the other Gulf countries added together) their encroachment into that area is something I am very concerned about.

In the Middle East, we are talking about the greatest concentration of crude oil in the world. In 1982, the production figures show that with the cutback in the world energy consumption and more conservation in a stagnant world economy, the production out of the Middle East is a little less than 13 million barrels of oil per day. Of that 13 million, 2 million is produced by Iran and 1 million by Iraq. Both of them are killing each other day by day, bombing each other, and disrupting each other's supplies. Once the war is over and their oil wells are fixed up, the resources are there for each of the two countries to triple their production as a whole. Instead of producing 13 million barrels, they could produce over 20 million barrels per day of oil. But, I feel that in this area there is a strong sentiment about oil being a once only divine gift. They do not look upon the oil as a resource that needs to be tapped and sold quickly but as an inheritance that needs to be managed prudently so that it would not run out in one generation but will last for many generations. In the future, there will be a shift in the attitudes of people in that area. They will not double their production even if it is possible from a geologic sense. Their national policy would not allow them just to produce oil for the short-term satisfaction of the world energy supply. Production from the Middle East will be held down not by so-called economic factors but by national feelings. Once the oil and gas are gone, that area will just go back to desert. There is not enough infra-structure being established to maintain a stable, industrialized country for the long-term. Therefore, I do not see, by and large, a viable, long-term buildup of an industrialized center in the Gulf area. I am not quite as optimistic as some others.

Well, let us look at a more pleasant side, and move to North America. I have always looked at the energy situation from a North American focus. I believe that the United States needs to look at its neighbor to the North, Canada, and its neighbor to the South, Mexico, and treat the three countries as one unit. It is symbiotic and synergistic to have all three preserve each other as good neighbors. In the United States, our total energy consumption in 1982 is down to 71 quads, which is significantly below the peak of 79 quads reached in 1978. For a highly industrialized nation, this is quite an accomplishment, and it will be interesting to watch as the economy picks up to see how well we will do in keeping the total energy consumption down to a manageable level. It is encouraging to know that oil imports have dropped from a peak of 8.69 million barrels a day in 1977 to a year end figure of 4.2 million barrels and may drop a little lower than that. But, again, how long this will continue we do not know. If we do not develop alternative energy sources, the only swing fuel in the world is oil; and, of course, its use has got to go up. It is encouraging to look at the United States and see the refinery acquisition cost of crude being down to the level of somewhere around $30 a barrel from its high point of about $35 a barrel. This reflects the stable world oil situation. The Saudi marker price

of $29 a barrel is holding firm. Other prices, like the Egyptian price and the Russian price, have all picked up so the world oil situation seems to have stabilized.

One of the thoughts expressed is that as soon as the economy perks up, the Saudi's will crank up their oil production, because they need funds for industrialization. As I said earlier, I do not believe that is going to take place. Not that they would not spend a lot of money to industrialize, but I just do not think it will be to the same degree.

The anomaly in this country is natural gas prices, which are following the oil price because of regulation. Gas prices have gone up since 1981 from $2/million Btu's to $2.60 at the start of this year. Now, I think, this will slow down eventually when we get the regulatory barriers out of the way. In the long-term in the United States, from an oil and gas standpoint, I think, we must react to the world oil situation, and we must not slacken our pace with developing alternative energy resources. Our oil production has peaked; our gas production has a lot further to go, much like the Russian situation. And, that is all we need to consider in the three nation bloc, the North American bloc, to deal with each other. I am always very encouraged to see that our Government has taken a friendly but firm attitude as trading partners with Canada and Mexico. We are their most logical customer, and we supply equipment back to them. It is good for our people, and it is good for their people.

Now, let me swing over to Asia -- that is the area with the greatest concentration of people, half of the population of the world. People speak glowingly in reports about exploration along the coast of China, and finding oil deposits, and the resulting oil export from this region. To me, that is another pipe-dream. For a billion people, any small incremental improvement in living standards and any small increment in personal luxuries would require a tremendous amount of production and a tremendous increase in energy consumption. Today, China exports approximately 200,000 bbl/day or about 10 percent of its total national production. The huge potential domestic demand would, in my judgment, soon wipe out China's role as a possible major exporter of petroleum.

Moving to western Europe, natural gas from the Soviet Union now supplies 12 percent or 1 quad of the annual gas needs of western Europe. When the Yamal pipeline, which was the subject of so much controversy between the United States and its western allies, starts to flow gas late this year and with full flow by 1986, the delivery of natural gas from the Soviet Union would double, thus, providing about one-quarter of the gas supply of western Europe.

The western European nations realize that excessive dependence on the Soviet Union is not desirable. They need flexibility and look for a diversity of supply sources. Therefore, in addition to natural gas being brought in from North Africa via the underwater pipeline from Tunisia to Sicily, another pipeline is being studied from North Africa to Spain across the Mediterranean. Western European nations are looking to further development of the North Sea for additional production. They look to a wider range of coal supplies from Australia, South Africa, and Poland, as well as the United States. Western European nations realize they do not have indigenous energy supplies sufficient for a stable future so they are doing the next best thing, namely, working to establish a wide variety of sources for imports while, at the same time, developing their indigenous sources to the maximum extent possible.

It is, therefore, clearly apparent from examination of the various regions of the world that geopolitics will become ever more central to the future of world energy supply and demand. Geopolitics has always been a dominant theme in history, especially as related to the acquisition of natural resources. With the

burgeoning world population, the geopolitical forces that impact national decisions will be even stronger. In this context and during this period, our national posture regarding energy must be centered on two elements. Regarding imports, we must broaden and diversify our sources of imports to make us flexible. This requires not only the maintaining of stability in the Persian Gulf regions but also the development of strong mutual trading agreements with our North American neighbors. Domestically, we must devote our full attention to the development of indigenous resources that would allow us to be potentially self-sufficient in energy. As the pressure mounts in the world from its growing population and growing demand for energy to improve living standards, we have no time to lose to put these policies into practice in order to establish a sound national posture for a stable future.

APPENDIX A

Ninth Annual Underground Coal Gasification Symposium Agenda

AGENDA

Sunday, August 7, 1983

1:00 p.m. - 7:00 p.m.	Registration, Main Lobby
6:30 p.m.	Welcome Reception Port of Call Theme Poolside (Inclement Weather -- Apache Room)
	The Kansas Room will be available to all conferees on a 24-hour basis from August 7-10 for group meetings of 8 or less. Please schedule your groups with the UCG registration desk.

Monday, August 8, 1983

7:00 a.m. - 8:15 a.m.	Registration, Main Lobby
7:00 a.m.	Briefing Breakfast Speakers, Poster Presenters, Chairpersons Blackhawk Room
7:45 a.m.	Continental Breakfast All Participants Fireplace Lounge
8:30 a.m.	Symposium Commences

MONDAY, AUGUST 8, 1983
SESSION I
FIELD WORK

Session Chairman -- Edward L. Burwell,
U.S. Department of Energy, Headquarters

Apache Room

8:30 a.m.	Welcome -- Paul R. Wieber, Director, Extraction Projects Management Division, Morgantown Energy Technology Center
8:45 a.m.	Opening Remarks -- Cleve Benedict, Deputy Assistant Secretary for Oil, Gas, Shale, and Coal Liquids, U.S. DOE
9:00 a.m.	"The Department of Energy's Underground Coal Conversion Program for 1983," Edward L. Burwell, Laramie Project Office
9:25 a.m.	"The Centralia Partial Seam CRIP Test," R. W. Hill, Lawrence Livermore National Laboratory
9:50 a.m.	"An Industrial Perspective of Underground Coal Gasification," Alan Singleton, Gulf Research and Development Company
10:15 a.m.	BREAK -- Fireplace Lounge
10:30 a.m.	"First Results of Belgian-German UCG-Test at Great Depth," Robert Gunn, Institution Pour Le Developpement De La Gazeification, Souterraine, Belgium
10:55 a.m.	"Underground Gasification of Deep Coal Electrolinking Experiments," J. Lessi, French Institute of Petroleum, France
11:20 a.m.	"A Review of Produced Gas Compositions in UCG Field Tests in the United States," B. W. Gash, Amoco Production Company
11:45 a.m.	"Underground Coal Gasification -- The Leading Source for Lower Priced Gas," Frederick W. Hammesfahr, Hammesfahr, Winter, and Associates, Inc.
12:10 p.m.	FREE TIME

MONDAY, AUGUST 8, 1983
SESSION II
FIELD WORK-POSTER

Session Chairman -- Vernon L. Hill,
Gas Research Institute

Apache Room

7:00 p.m. "Numerical Modeling: A Site Selection Tool for In Situ Gasification of Texas Lignite," J. E. Russell, Texas A&M University

"Underground Coal Gasification Cavity Definition for Rawlins Test 2," J. M. Avasthi, Gulf Research and Development Company

"Subsidence Prediction for the Forthcoming TONO UCG Project," H. J. Sutherland, Sandia National Laboratory

"Monitoring of the TONO Project Partial Seam CRIP UCG Experiment Using the CSAMT Technique," Lewis C. Bartel, Sandia National Laboratory

"Application of Remanent and Rock Magnetic Properties to Thermal Alteration of Overburden at Hanna, Wyoming, UCG Site," Rob Oliver, Laramie Project Office

"Geotechnical Studies of the Overburden and Pyrometamorphic Rocks from the Rawlins T-2 UCG Site," Lary K. Burns, Colorado State University

"Potential for Development of UCG in the Bituminous Coal Resource," Joseph W. Martin, Charles W. Byrer, and Allen C. Brummert, Morgantown Energy Technology Center

"Electroenhanced Underground Coal Gasification," Erich Sarapuu, Electrofrac Corporation

"Field Testing of a Cornering Water Jet Drill," Bruce P. Engler and David L. Shirey, Sandia National Laboratory

"A Comparison of Forward Combustion Gasification Models-II," Charles G. Mones and L. John Fahy, University of Wyoming Research Center

"Conclusions from Modeling the Final Data of Pricetown I," Ronald T. Gibbs, Georgia Institute of Technology

"Reclamation of Rawlins UCG Site," Paul F. Ahner, Gulf Research and Development Company

10:00 p.m. Adjourn

TUESDAY, AUGUST 9, 1983
SESSION III
MODELING/EXPERIMENTAL

Session Chairman -- William Krantz,
University of Colorado

Apache Room

8:30 a.m.	"Unexpected Aspects of Reverse Combustion: Effects of Pressure, Volatility, and Chemical Reactivity," Ronald Glaser, University of Wyoming Research Corporation
8:55 a.m.	"Assessment of Lateral Cavity Growth Mechanisms," James B. Riggs, West Virginia University
9:20 a.m.	"Thermal Stability of Coal Cavities," Richard C. Corlett, University of Washington
9:45 a.m.	BREAK -- Fireplace Lounge
10:00 a.m.	"A UCG Cavity Simulator with Solid Motion," C. B. Thorsness, Lawrence Livermore National Laboratory
10:25 a.m.	"Stress Mediated Responses Associated with UCC Cavity and Subsidence Prediction Modeling," Sunder H. Advani, Ohio State University
10:50 a.m.	"Determination of Underground Coal Gasification Burn Temperature Using Thermal Metamorphism of Coal Macerals as a Geothermometer," Rob Oliver, Laramie Project Office
11:15 a.m.	LUNCH -- Blackhawk Room

TUESDAY, AUGUST 9, 1983
SESSION IV
MODELING/EXPERIMENTAL-POSTER

Session Chairman -- Richard C. Corlett,
University of Washington

Cheyenne Room

1:30 p.m. "The Effect of Thermal and Structural Properties on the Growth of an Underground Coal Gasification Cavity," Robert E. Glass, Sandia National Laboratory

"The Cavity Produced by Gasifying Thin Deep Seems," Ivan Wilkes, National Coal Board, Mining Research and Development Establishment, United Kingdom

"Modeling UCG with Steam and Oxygen Injection in Pricetown-Type Coal Fields," James F. Avery, West Virginia University

"Kinetics of Coal Oxidation for Investigating Self-Ignition," Jae-Ou Choi, Technical University of Aachen, West Germany

"Comprehensive Numerical Model of Forward Combustion Along a Channel," Richard C. Corlett, University of Washington

"Combustion Tube Studies on the Influence of Water Influx on Steam-Oxygen Gasification of Lignite," T. F. Edgar, University of Texas

"Analysis of Coal Pyrolysis and Drying History for Various Coal Geometries," S. W. Kang, Lawrence Livermore National Laboratory

"The Permeability of Bituminous Coal at Temperatures Up to 700°C and Simultaneous Pressures Up to 70 Bar," J. Wagner, The University of Saarlandes, West Germany

"The Mobility of Fluid/Solid-Phases of Bituminous Coal Substances at High pT-Conditions," H. J. Schloemer, The University of Saarlandes, West Germany

"Coal Pyrolysis and Methane Decomposition in the Presence of a Hot Char Bed," C. B. Thorsness, Lawrence Livermore National Laboratory

"Gas Quality Improvements Through High Amplitude Pressure Oscilation," K. Guntermann, Technical University of Aachen, West Germany

"A Process Model for the Initial Stages of Electrolinking," Bertrand Dautresme, University of Colorado

TUESDAY, AUGUST 9, 1983
(Continued)

"Correlation of Laboratory-Scale Coal-Gasification Data with the Rawlins Underground Coal Gasification -- Steeply Dipping Beds Tests," Paul F. Ahner, Gulf Research and Development Research Company

"Gasifying Dutch Coals," H. H. Boswinkel, Dutch Energy Research Foundation (ECN), The Netherlands

"Comparative Economics of Substitute Natural Gas Production by UCG and Surface Gasification of Western Coal," B. W. Gash, Amoco Production Company

5:00 p.m. Adjourn

6:00 p.m. SOCIAL HOUR -- Mohawk Room

7:00 p.m. DINNER -- Mohawk Room

Master of Ceremonies -- Paul R. Wieber, Director
Extraction Projects Management Division
Morgantown Energy Technology Center

Address -- "World Energy Perspective"
Bernard S. Lee, President, Institute of Gas Technology

WEDNESDAY, AUGUST 10, 1983
SESSION V
ENVIRONMENTAL

Session Chairpersons -- William F. McTernan and Elizabeth M. McTernan, University of Wyoming Research Corporation

Apache Room

8:30 a.m. "Biotreatment of Underground Coal Gasification Wastewater Condensate," Michael J. Humenick, University of Wyoming Research Corporation

8:55 a.m. "Treatment of UCG Condensates by Activated Carbon Adsorption," Lora S. Johnson, University of Wyoming Research Corporation

9:20 a.m. "The Sorption of Lead, Cadmium, Arsenic, and Selenium by Coal, Char, and Ash," James E. Park, University of Cincinnati

9:40 a.m. BREAK -- Fireplace Lounge

10:05 a.m. "Effects of the Rawlins UCG-SDB Tests on Groundwater Composition and Migration," M. A. Bloomstran, Gulf Research and Development Company

10:30 a.m. "An Evaluation of the Magnitude of Groundwater Contamination at the U.S. DOE Hoe Creek UCG Experimental Site," George Saulnier, TRW Energy Development Group

10:55 a.m. "Simulation of Groundwater Flow Regimes in a Coal Team with UCG Cavities Using a Finite Element Model," Dinshaw N. Contractor, University of Arizona

11:25 a.m. LUNCH -- (on own)

WEDNESDAY, AUGUST 10, 1983
SESSION VI
GENERAL SUBJECTS/SUMMARY

Session Chairman -- Burl E. Davis,
Gulf Research and Development Company

Apache Room

1:30 p.m. "Economic Benefits from Burnout of Abandoned Coal Mine Fires," Robert F. Chaiken, U.S. Bureau of Mines

1:55 p.m. "Economic Factors in Processing High-Methane Content UCG Derived Gas," A. James Moll, Synthetic Fuels Associates

2:20 p.m. "A UCG with Liquid Water and Air of the Deep and Thin Layers in the Netherlands," J. Bruining, Delft Technical University, The Netherlands

2:45 p.m. BREAK -- Fireplace Lounge

3:00 p.m. Session Summaries/Roundtable Discussions

4:00 p.m. Adjourn

APPENDIX B

Ninth Annual Underground Coal Gasification Symposium Participants List

NINTH ANNUAL UNDERGROUND COAL GASIFICATION SYMPOSIUM
August 7-10, 1983
Participants List

Sunder H. Advani
Professor and Chairman
Ohio State University
209 Boyd Laboratory
155 West Woodruff
Columbus, OH 43210
(614) 422-2731

Paul F. Ahner
Senior Research Chemist
Gulf Research and Development Company
P.O. Drawer 2038
Pittsburgh, PA 15230
(412) 665-5914

Bob Arora
Staff Engineer
P.O. Box 1700
EDC
Houston Lighting and Power
Houston, TX 77001

Luis E. Arri
Amoco Production Company
Research Center
P.O. Box 591
Tulsa, OK 74102
(918) 660-3981

Jitendra M. Avasthi
Research Engineer
Gulf Research and Development Company
P.O. Drawer 2038
Pittsburgh, PA 15230
(412) 665-2776

Ralph A. Avellanet
Program Manager
Underground Coal Gasification
U.S. Department of Energy
Fossil Energy
FE-33
Washington, DC 20545
(301) 353-2918

James P. Avery
Assistant Professor
West Virginia University
315 Engineering Sciences Building
Morgantown, WV 26506
(304) 293-3111

Wayne Bahr
State of Illinois
Department of Energy and
Natural Resources
325 W. Adams
Room 300
Springfield, IL 62706
(217) 785-2015

Lewis C. Bartel
Sandia National Laboratory
P.O. Box 5800
Organization 1541, Building 823
Albuquerque, NM 87185
(505) 844-6902

S. P. Barone
Gas Research Institute
8600 West Bryn Maur Avenue
Chicago, IL 60631

Theodore C. Bartke
UCG Program Manager
Laramie Project Office
P.O. Box 3395, University Station
Laramie, WY 82071
(307) 721-2375
FTS 328-4375

Greg Bell
Gas Research Institute
8600 W. Bryn Mawr Avenue
Chicago, IL 60631

Cleve Benedict
U.S. Department of Energy
FE-30
1000 Independence Avenue, SW
Washington, DC 20585

Mary A. Bloomstran
Chemical Engineer
Gulf Research and Development Company
134 Union Boulevard, Suite 610
Lakewood, CO 80228
(303) 988-8140

Hans H. Boswinkel, IR
Stichting Energieonderzoek
Centrum Nederland (ECN)
Hoofdkantoor Scheveningseweg
112 Den Haag
Postbus 80404, 2508 GK's-Gravenhage
Petten, The Netherlands 1755 ZG
02246-6262

Charles Brandenberg
Gas Research Institute
Program Manager
Coal Bed to Methane
8600 W. Bryn Mawr Avenue
Chicago, IL 60631

Eugene C. Bredeson
Burlington Northern
704-1st Northwest Bank Center
175 North 27th Street
Billings, MT 59101

Roger Broeker
Foster-Wheeler
110 S. Orange
Livingston, NJ 07039

J. Bruening
Delft Technical University
Department of Mining Engineering
Mijnbouwstratt 120
Delft, The Netherlands 2628 RX

Allen C. Brummert
U.S. Department of Energy
Morgantown Energy Technology Center
P.O. Box 880
Morgantown, WV 26505

Kenneth Burnham
Gas Research Institute
8600 West Bryn Maur Avenue
Chicago, IL 60631

Lary K. Burns
Colorado State University
College of Forestry and Natural
Resources
Department of Earth Resources
Fort Collins, CO 80523
(303) 491-6378

Edward L. Burwell
Program Manager for Gas
U.S. Department of Energy
FE-33, D-122
Germantown, MD 20545
(301) 353-2978
FTS 233-2918

Charles W. Byrer
U.S. Department of Energy
Morgantown Energy Technology Center
P.O. Box 880
Morgantown, WV 26505
(304) 291-4547

Robert Chaiken
P.O. Box 18070
Bureau of Mines
Pittsburgh, PA 15236

Marc Chelemer
Union Carbide
P.O. Box 444
Tonawanda, NY 14151-0044
(716) 879-2594

Joe-Ou Choi
Technical University of Aachen
Institut für Eisenhuttenkunde
Intzestrabe 1
D-5100 Aachen
West Germany
0241-805843

Dinshaw N. Contractor
Department of Civil Engineering
University of Arizona
Tucson, AZ 85721

Richard Corlett
University of Washington
Department of Mechanical Engineering
FU-10
Seattle, WA 98195

Al Couper
Amoco Oil
Box 400
Naperville, IL 60566
(312) 420-4843

George F. Dana
Manager, Geology and Geochemistry,
Division of Physical Sciences
University of Wyoming Research Corporation
Box 3395, University Station
Laramie, WY 82071
(307) 721-2236
FTS 328-4236

Jerry H. Daniel
Staff Engineer
Gulf Research and Development Company
134 Union Boulevard, Suite 610
Lakewood, CO 80228
(303) 988-8140

Bertrand Dautresme
Research Assistant
Department of Chemical Engineering
University of Colorado
Campus Box 424
Boulder, CO 80309

Stephen Davidson
AWU Post Masters Participant
Environmental Sciences Division
University of Wyoming Research Corporation
P.O. Box 3395, University Station
Laramie, WY 82071
(307) 721-2431

Burl E. Davis
Director of Special Projects
Gulf Research and Development Company
P.O. Drawer 2038
Pittsburgh, PA 15230
(412) 665-2769

Leroy Dockter
Laramie Project Office
P.O. Box 3395
University Station
Laramie, WY 82071

Thomas F. Edgar
Professor
Department of Chemical Engineering
University of Texas
Austin, TX 78712
(512) 471-3080

Bruce P. Engler
Electronics Staff Assistant
Sandia National Laboratories
In Situ Technologies -- Division 9747
Albuquerque, NM 87185
(505) 846-3599

L. John Fahy
Research Engineer
University of Wyoming Research
Corporation
P.O. Box 3395, University Station
Laramie, WY 82071
(307) 721-2348
FTS 328-4348

John Forrest
Product Manager
PLEXCO
3240 N. Mannheim Road
Franklin Park, IL 60131
(312) 455-0600

Bruce W. Gash
Staff Research Engineer
Amoco Production Company Research Center
P.O. Box 591
Tulsa, OK 74102
(918) 660-3949

Glen Garelek
Discover Magazine
Time & Life Building
Room 17B
Rockefeller Center
New York, NY 10020

Adolf W. Gessner
U.S. Synthetic Fuels
2121 K Street, NW
Washington, DC 20586
(202) 822-6558

Ronald Gibbs
Georgia Institute of Technology
Atlanta, GA 30332

Ronald R. Glaser
Research Assistant/Graduate Student
Department of Chemical Engineering
University of Wyoming
Laramie, WY 82071
(307) 766-3170

Robert E. Glass
Technical Staff Member
Sandia National Laboratories
In Situ Technologies -- Division 9747
Albuquerque, NM 87185
(505) 844-2254

Joe Grant
Basic Resources, Incorporated
Suite 1420
717 North Harwood Street
Dallas, TX 75201

Robert D. Gunn
Professor
Department of Chemical Engineering
University of Wyoming
Laramie, WY 82071
(307) 766-3170

Klaus Gunterman
Technical University of Aachen
Institut fuer Eisehuttenkunde
Intzestrabe 1
D-5100 Aachen
Germany, F.R.
0241-805843

Joseph H. S. Haggin
Associate Editor
Chemical and Engineering News
176 West Adams Street, Suite 1433
Chicago, IL 60603
(312) 326-7325

Mr. Frederic W. Hammesfahr
President
Hammesfahr, Winter and Associates, Incorporated
P.O. Box 536
Bernardsville, NJ 07924
(201) 766-1133

Dr. Ing Gunter Hewing
Studiengesellschaft Kohlegewinnung Zweite Generation e.V.
Franz-Fischer-Weg 61
D-4300 Essen 13
Germany
(0201) 1059673

Richard W. Hill
Section Leader, Chemical Engineering
Lawrence Livermore National Laboratory
P.O. Box 808, L-365
Livermore, CA 94550
FTS 532-7316

Vernon Hill
GRI
8600 West Bryn Maur Avenue
Chicago, IL 60631

Michael J. Humenick
Professor
Department of Civil Engineering
The University of Wyoming
1017 Sheridan
Laramie, WY 82070
(307) 766-3201
FTS 766-3201

Alan E. Humphrey
President
World Energy, Incorporated
P.O. Box 925
Laramie, WY 82070
(307) 742-8361

Lora S. Johnson
University of Wyoming Research Corporation
P.O. Box 3395, University Station
Laramie, WY

William B. Johnson
Fish Engineering and Construction
1990 South Post Oak Road
Houston, TX 77056
(713) 621-8830, x645

Babu Joseph
Washington University
Department of Chemical Engineering
Campus Box 1198
St. Louis, MO 63130

Sang Wook Kang
Physicist
Lawrence Livermore National Laboratory
P.O. Box 808
Livermore, CA 94550
(415) 422-4978

W. E. H. King
Head of SNG Engineering
British Gas Corporation
326 High Holborn
London WCIV 78T
United Kingdom

Christian W. Knudson
Technical Director
Scientific Design Company
6750 West Loop South
Bellaire, TX 77401
(713) 669-9900

William B. Krantz
Professor of Chemical Engineering
University of Colorado
Campus Box 424
Boulder, CO 80309
(302) 492-7050

George Larsen
Thunder Basin Coal Company
P.O. Box 406
Wright, WY 82732
(307) 939-1300

Bernard S. Lee
President
Institute of Gas Technology
3424 South State Street
Chicago, IL 60616

Jacques Lessi
Institut Francais du Petrole
B. P. 311
92 506 Rueil Malmaison Cedex
1 et 4 avenue de Bois-Preau, France
33-1--749.02.14

Bob Lindquist
State of Illinois
Department of Energy and
Natural Resources
325 W. Adams
Room 300
Springfield, IL 62706
(217) 785-2015

L. C. Marchant
Research Coordinator
University of Wyoming Research
Corporation
P.O. Box 3395, University Station
Laramie, WY 82071
(307) 721-2203
FTS 328-4203

Joseph W. Martin
U.S. Department of Energy
Morgantown Energy Technology Center
P.O. Box 880
Morgantown, WV 26505
(304) 291-4447

Elizabeth M. McTernan
Scientist/Engineer II
University of Wyoming Research
Corporation
Box 3395, University Station
Laramie, WY 82071
(307) 721-2372
FTS 328-4372

William F. McTernan
Senior Research Scientist
University of Wyoming Research
Corporation
Box 3395, University Station
Laramie, WY 82071
(307) 721-2251
FTS 328-4251

A. James Moll
Syn Fuels Associates
444 Castro Street, Suite 920
Mountain View, CA 94041
(415) 969-8876

Charles G. Mones
Research Engineer
University of Wyoming Research
Corporation
P.O. Box 3395, University Station
Laramie, WY 82071
(307) 721-2319
FTS 328-4319

Rob Oliver
University of Wyoming
Research Corporation
P.O. Box 3395
University Station
Laramie, WY 82071

Janet Owen
Business Development Representative
Bechtel Group, Incorporated
50 Beale Street
San Francisco, CA 94105
(415) 768-9916

James E. Park
Research Associate
University of Cincinnati
Department of Civil and Environmental
Engineering
U.S. EPA T&E Facility
1600 Gest Street
Cincinnati, OH 45268

Roger Paul
WIDCO
1015 Big Hanaford Road
Centralia, WA 98531
(206) 736-2831

Lynn Peay
University of Wyoming
Research Corporation
P.O. Box 3395
University Station
Laramie, WY 82071

Jack L. Peterson
Sr. Vice President
DM International, Incorporated
P.O. Box 721900
Houston, TX 77272
(713) 498-5995

Slawomir Piatnicki
Estado Do Rio Grande
Do Sul Porto Alegre
R. Washington LU12, 675
C. Postal, 1864
Brazil

Rajen Puri
Amoco Production Company Research
Center
P.O. Box 591
Tulsa, OK 74102
(918) 660-3984

James B. Riggs
Associate Professor
Texas Tech University
Lubbock, TX 79409

Ken Robinson
Director
Coal Utilization Projects
Standard Oil
200 E. Randolph Drive
P.O. Box 5910-A
Chicago, IL 60680
(312) 856-2302

Joseph Rosenburg
Gas Research Institute
8600 West Bryn Mawr Avenue
Chicago, IL 60631

Cyril Ruane
Maverick Exploration
13472 West 70th Place
Arvada, CO 80004
(303) 832-9500

James E. Russell
Brockett Professor
Texas A&M University
Department of Petroleum Engineering
College Station, TX 77843
(409) 845-2284

Erich Sarapuu
Manager
Electrofrac Corporation
Penntower Building
3100 Broadway, Suite 307
Kansas City, MO 64111

George Saulnier
TRW Energy Development Group
200 Union Boulevard, Suite 201
Lakewood, CO 80228

H. Schloemer
Professor
University of Saarland
Saarbrucken
W. Germany 6600
681-302-2912

Urban E. Sharum
Research Chemist
Laramie Project Office
P.O. Box 3395
Laramie, WY 82071
(307) 721-2430
FTS 328-4430

David L. Shirey
Technical Staff Member
Sandia National Laboratories
In Situ Technologies -- Division 9747
Albuquerque, NM 87185
(505) 844-8795

Alan Singleton
Gulf Research and Development
P.O. Box 2038
Pittsburgh, PA 15230

Paul E. Soister
Chief Geologist
Maverick Exploration Company
4901 South Franklin Street
Englewood, CO 80110
(303) 789-3590

Douglas R. Stephens
Project Director
Lawrence Livermore National Laboratory
P.O. Box 808-L-367
Livermore, CA 94550
(415) 422-7330
FTS 532-7330

David Stopek
Senior Chemical Engineer
Science Applications, Incorporated
918 Chestnut Ridge Road, Suite 8
Morgantown, WV 26505
(304) 599-9696

Herbert J. Sutherland
Technical Staff
Sandia National Laboratories,
Division 9752
P.O. Box 5800
Albuquerque, NM 87185

Lee Taylor
Technical Staff Member
Sandia National Laboratories
P.O. Box 5800
Albuquerque, NM 87185
(505) 844-2866

Dr. Charles Thorsness
Lawrence Livermore National Laboratory
P.O. Box 808-L-367
Livermore, CA 94550
(415) 422-8124
FTS 532-8124

Richard K. Traeger
Manager, Geo Energy Technology
Department II -- 6240
Sandia National Laboratories
P.O. Box 5800
Albuquerque, NM 87185
(505) 844-2055

J. Wagner
Professor
University of Saarland
Saarbrucken
W. Germany 6600
681-302-2912

Heiner Wempe
Geologist
P.O. Box 1913
5170 Julich
W. Germany
02461-614859

Warren H. Westphal
President
Spruce Creek Energy Company
5650 South Syracuse Circle, Suite 212
Englewood, CO 80111

Paul R. Wieber
U.S. Department of Energy
Morgantown Energy Technology Center
P.O. Box 880
Morgantown, WV 26505
(304) 291-4109

Ivan Wilks
National Coal Board, Mining Research
and Development Establishment
Ashby Road, Stanhope Bretby,
Burton-On-Trent
Staffs, United Kingdom DE15 OQD
0283-216161, x647

Thomas Wood
Bechtel Group
P.O. Box 3965
San Francisco, CA 94119

*U.S. GOVERNMENT PRINTING OFFICE: 1984--759-088/8